RIKEN Accelerator Progress Report 2013

vol. 47

独立行政法人理化学研究所　仁科加速器研究センター
RIKEN Nishina Center for Accelerator-Based Science

RIKEN Accelerator Progress Report 2013

vol. **47**

独立行政法人理化学研究所　仁科加速器研究センター
RIKEN Nishina Center for Accelerator-Based Science
Wako, Saitama, 351-0198 JAPAN

This complete version of APR can be downloaded from our website.

http://www.nishina.riken.jp/researcher/APR/index_e.html

GRAVURE & HIGHLIGHTS OF THE YEAR

« Selection process of gravure and highlights »

Gravure and highlights will be selected by two-steps process. In the first step, referees will recommend manuscript for gravure or highlight. With the above recommendation, the editors will then give secondary recommendation.

After the following 1 and 2 are comprehensively considered, the editor-in-chief will draft a manuscript idea which will be thoroughly discussed by the editors for the final decision:

1. Approval based on the editor's judgment as an expert/non-expert in the field (thereby agreeing with the referee's recommendation)
2. Additional recommendation based on the editor's expertise.

Extending the Nuclear Chart, Expanding our Wisdom

The BigRIPS separator is a new-generation superconducting in-flight fragment separator at the Radioactive Isotope Beam Factory (RIBF). Since 2007, the BigRIPS has produced a wide range of radioactive isotope (RI) beams at unprecedented intensities. It is characterized by large ion-optical acceptances, a two-stage structure, and high resolving power for particle identification (PID).

The large acceptances (±40 and ±50 mrad in the horizontal and vertical directions, respectively, and ±3% in momentum) allow efficient production of RI beams using not only projectile fragmentation, but in-flight fission of a ^{238}U beam with wide kinematical distribution as well.

The two-stage structure enables flexible operations, e.g. separator-spectrometer and separator-separator modes, and reduces demands for tagging detectors in the second stage. The latter point results in higher particle identification capability when combined with a high resolving power of the ion-optical system (see page v for details).

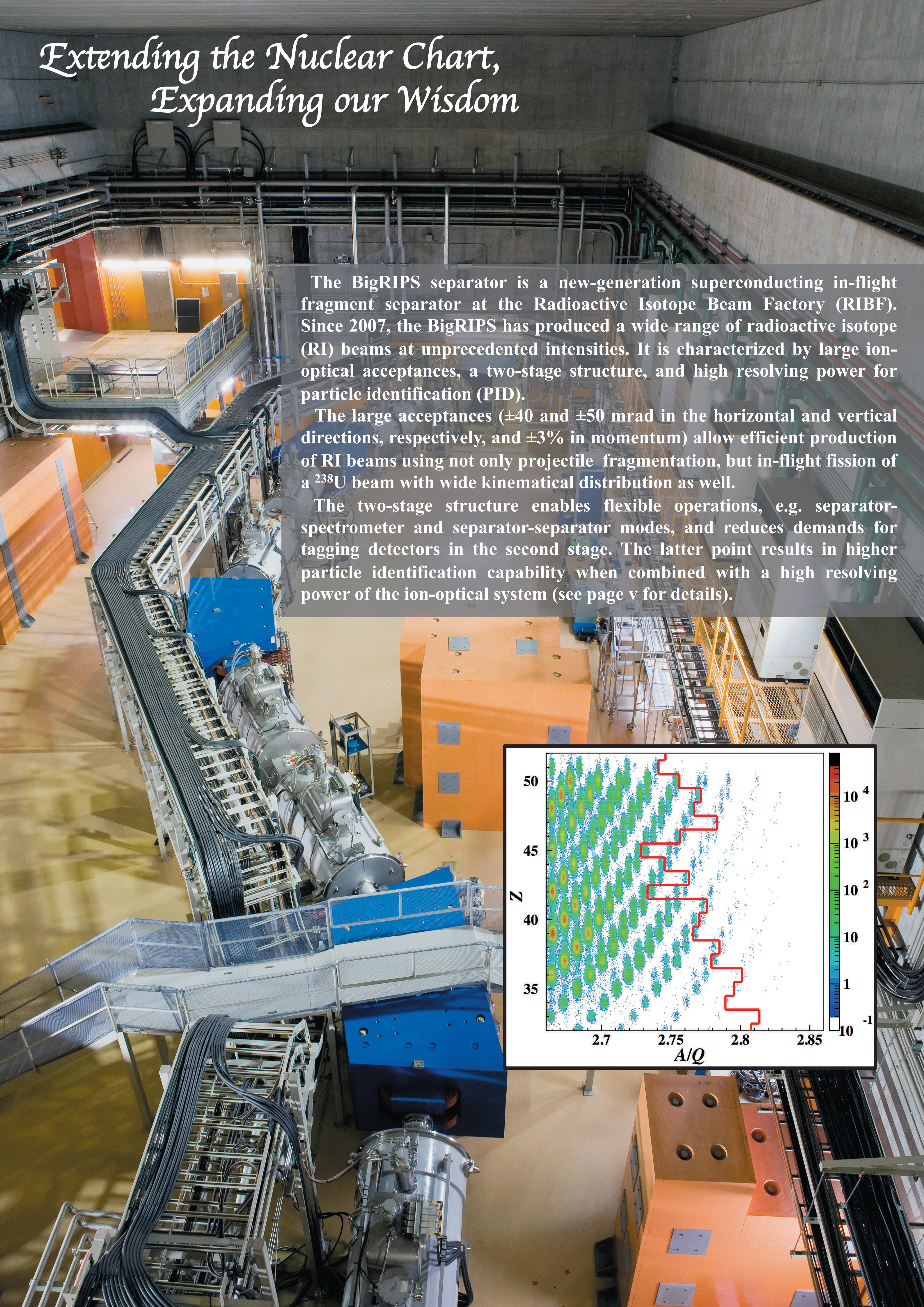

RI Beams & New Isotopes for Science

Since 2007, 317 RI beams have been supplied to nuclear physics experiments at the RIBF. The isotopes are produced from primary beams of ^{238}U, ^{124}Xe, ^{70}Zn, ^{48}Ca, and ^{18}O, as shown with red circles in Fig. 1 (see page iv for details).

At the same time, yields and production cross sections have been measured for a total of 877 rare isotopes (light blue squares). Among them 47 (blue squares) and 4 (green squares, proton-rich side) new isotopes produced from the ^{238}U and ^{124}Xe beams are included. The total number of new isotopes produced at RIKEN, since Nishina's discovery of ^{237}U, is 87. This number is still increasing and preliminary results of 69 new isotopes will be reported soon.

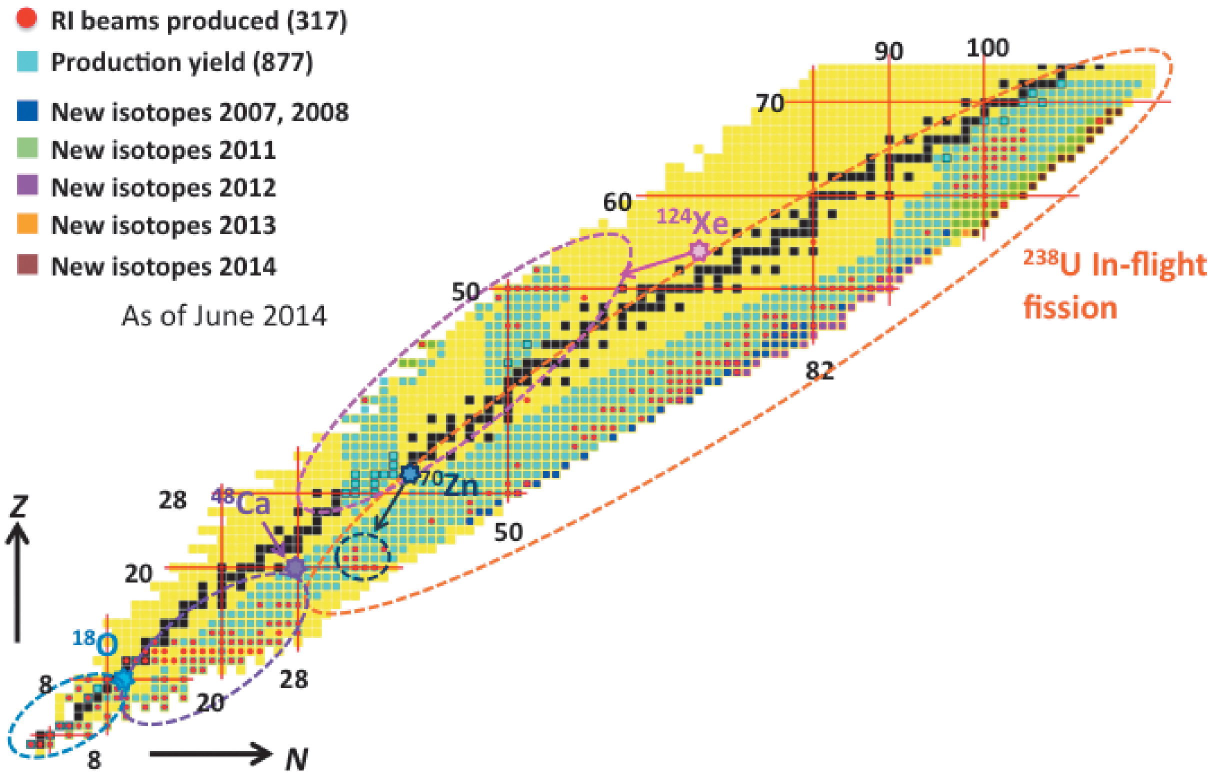

New Isomers

~ Indications of new aspects of nuclear structure ~

We have discovered 18 and 25 new isomers in the new isotope search experiments performed in 2008 and 2011, respectively (see D. Kameda et al., Phys. Rev. C **86**, 054319 (2012) for details). The existence and properties of new isomers provide us with information on the structure of the relevant nuclei that is otherwise unavailable.

The newly discovered isomers are of practical importance too. The characteristic γ-rays from the isomers enable unambiguous particle identification (PID) and can serve as an irreplaceable calibration standard for TOF-Bρ-ΔE PID. A good example is ^{117}Ru shown in the figure on the right. The isomeric states discovered in 2008 have already been used for PID in RI beam production in the EURICA experiments.

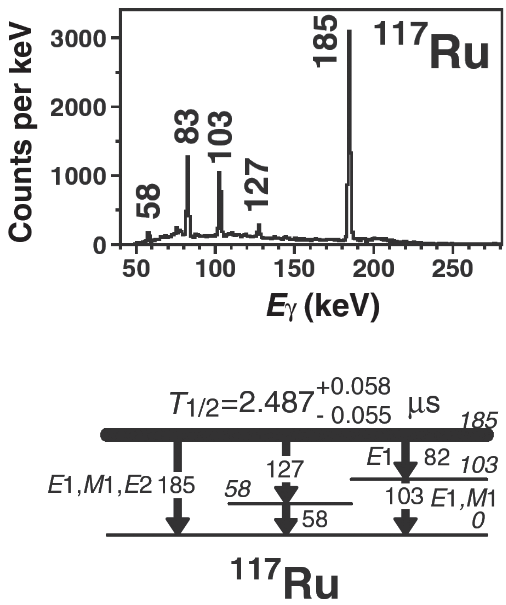

Cross Section and Production Yields of Rare Isotopes

~Baseline of RI-beam science~

Cross section and production yields of rare isotopes are critical in designing RI-beam experiments. The measured production yields and cross sections are useful to improve our understanding of the reaction mechanism of RI production and refine the theoretical models.
(see pages vi—viii for details)

In figure (a) on the right, the measured production rates from the ^{238}U+Be fission are compared with the LISE++ calculations (version 8.4.1) which employs the abrasion fission (AF) model for the nuclear fission.

The comparison clearly shows a large disagreement in the region of $Z > 50$.

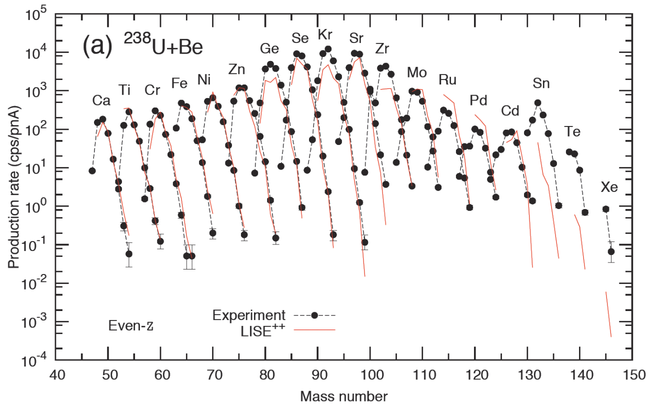

The RI production cross sections by the fragmentation of the ^{124}Xe, ^{70}Zn, ^{48}Ca, and ^{18}O primary beams are compared with predictions of the EPAX3.01 and EPAX2.15 models. EPAX2.15 is found to give better predictions for the ^{48}Ca beam, as shown in the figure (b) on the right, while EPAX3.01 produces successful predictions for the ^{124}Xe primary beam.

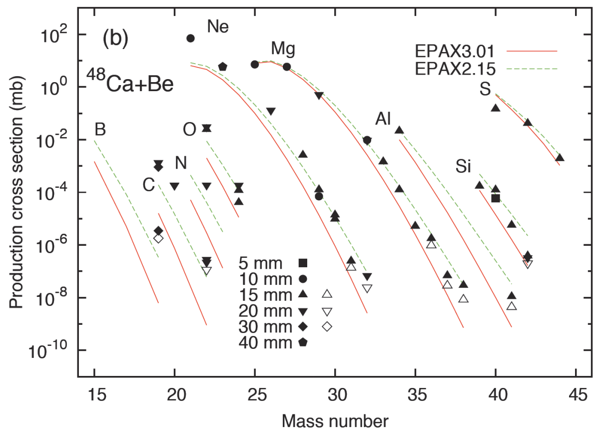

These yield and cross section data are available at
http://www.nishina.riken.jp/RIBF/BigRIPS/intensity.html.

Future work

Primary-beam intensities at the RIBF are increasing every year. At the same time, the demand for RI beams with higher Z and/or with higher intensity is increasing.

Recently, several trials were successful in increasing the limits of the counting rate for the detectors and improving A/Q resolution for RI beams with high Z where many charge states are mixed; introduction of Ag electrodes to the parallel plate avalanche counters resulted in better rate duration, i.e. stable operation up to 70 kcps even for RI beams with $Z > 60$. A new mechanism to shift plastic-scintillator positions, with respect to the beam position, helps us to avoid deterioration of time resolution due to radiation damage by heavy-ion irradiation. New ion-optics is found to be useful in improving the A/Q resolution, where Bρ resolution at the second stage is designed to be doubled compared with the previously used optics.

The BigRIPS team continues to make efforts to provide RI beams with higher intensities and higher qualities.

Hiroshi Suzuki for the BigRIPS team

RI beam production at BigRIPS since its commissioning in 2007

N. Inabe,*[1] N. Fukuda,*[1] H. Takeda,*[1] D. Kameda,*[1] H. Suzuki,*[1] Y. Shimizu,*[1] H. Sato,*[1] D. Murai,*[1] D. S. Ahn,*[1] T. Ohnishi,*[1] K. Kusaka,*[1] Y. Yanagisawa,*[1] A. Yoshida,*[1] K. Tanaka,*[1] M. Ohtake,*[1] K. Yoshida,*[1] and T. Kubo*[1]

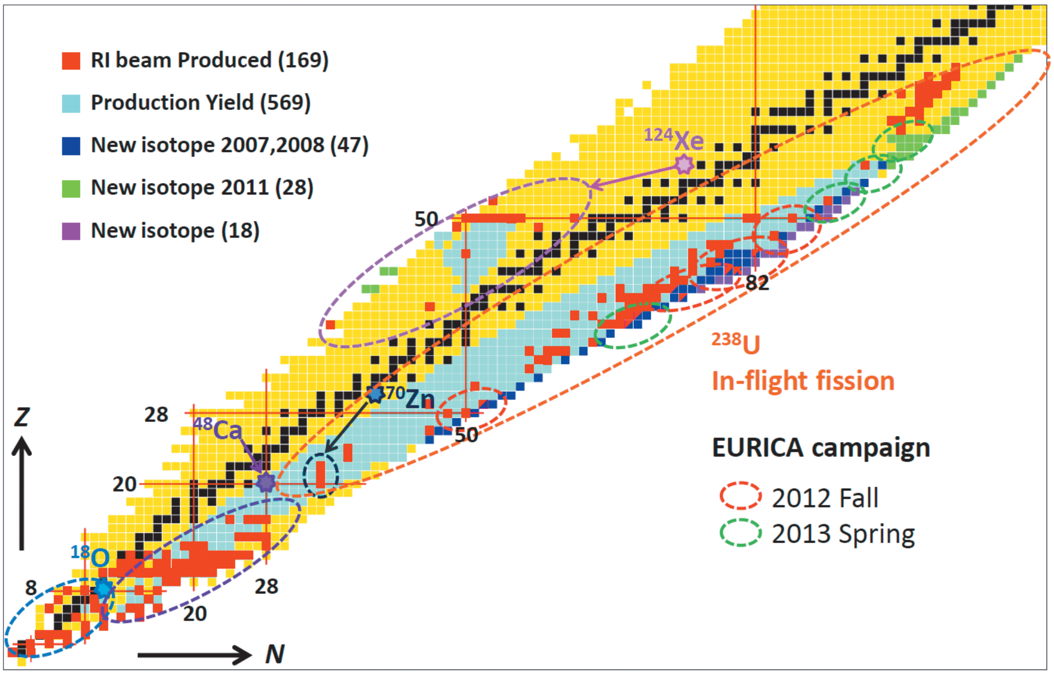

Fig.1 RI's produced at BigRIPS from March 2007 to July 2013.

Since the commissioning of the BigRIPS separator[1)] in March 2007, a variety of RI beams have been produced at the BigRIPS and used for experiments. Figure 1 shows the nuclear chart in which all isotopes produced at the BigRIPS from March 2007 to July 2013 are indicated in different colors. Red indicates isotopes used for experiments and light blue indicates isotopes whose production yields and cross sections were measured. New isotopes are shown in different colors according to the year in which they were discovered: blue in 2007 and 2008, green in 2011, and purple in 2012. Light isotopes with $Z < 25$ were produced using projectile fragmentations of ^{18}O, ^{48}Ca, and ^{70}Zn beams. The projectile fragmentation of ^{124}Xe is used for proton rich isotopes, and the in-flight fission of ^{238}U for medium and heavy (Z = 20~68) isotopes. The production yields were measured for 569 isotopes. A total of 169 RI beams were used in the experiments. 89 new isotopes were discovered by the in-flight fission of ^{238}U and 4 new isotopes were discovered by the projectile fragmentation of ^{124}Xe.

The number of experiments performed using RI beams for various primary beams in each year is summarized in Table 1. Before 2010, RI beams were mainly produced using the ^{238}U beam with low intensity and ^{48}Ca. In December 2011, proton rich RI beams including ^{100}Sn were produced from the accelerated ^{124}Xe beam for the first time. In 2012, RI beams around ^{78}Ni, ^{115}Nb, ^{123}Rh, ^{128}Pd, and ^{136}Sn including new isotopes discovered in 2008 were produced from the ^{238}U beam with increased intensity (~10 pnA) and delivered to EURICA. Another 18 new isotopes were discovered at this time.

In April 2013, ^{16}C was delivered to ESPRI and ^{16}C and ^{12}C were delivered to SAMURAI. Heavy RI beams around ^{142}Te, ^{150}Ba and ^{158}Nd and middle ones around ^{104,108}Y, ^{108}Zr, and ^{72}Fe from ^{238}U were delivered to EURICA in May and June 2013. Very proton rich RI beams of ^{100}Sn and ^{73}Sr from ^{124}Xe were also delivered to EURICA in June 2013.

Production yields and cross sections of isotopes produced in 2013 are currently being analyzed.

Table1. Number of experiments performed using RI beams in each fiscal year.

	^{238}U	^{124}Xe	^{86}Kr	^{70}Zn	^{48}Ca	^{18}O	^{14}N	^{4}He	Tot
'07	4		1						5
'08	2				4				6
'09	3				3		3	1	10
'10					10	1	2		13
'11	4	2				2			8
'12	6	3		1	4	6			20
'13	4	2				3			9
Tot	23	7	1	1	21	12	5	1	71

References

1) T. Kubo: Nucl. Instr. Meth. **B 204**, 97 (2003).

*1 RIKEN Nishina Center

Identification and separation of radioactive isotope beams by the BigRIPS separator at the RIKEN RI Beam Factory†

N. Fukuda,[*1] T. Kubo,[*1] T. Ohnishi,[*1] N. Inabe,[*1] H. Takeda,[*1] D. Kameda,[*1] and H. Suzuki[1]

We have developed a method for achieving excellent resolving power for in-flight particle identification of radioactive isotope (RI) beams, which is routinely used with the BigRIPS fragment separator[1)] at the RIKEN RI Beam Factory (RIBF)[2)]. In the BigRIPS separator, RI beams are identified by their atomic number Z and mass-to-charge ratio A/Q, which are in turn deduced from the measurements of time of flight (TOF), magnetic rigidity ($B\rho$), and energy loss (ΔE). Such in-flight particle identification is essential for delivering tagged RI beams, making it possible to perform various types of experiments including secondary reaction experiments. Since the total kinetic energy is not measured in this scheme, and consequently A and Q cannot be determined independently, the resolution of A/Q must be adequately high to identify the charge state Q of RI beams. This is achieved in the Z versus A/Q particle identification plot as demonstrated in Fig. 1, where fully stripped and hydrogen-like peaks are very closely located.

We achieved a high A/Q resolution by precisely determing the $B\rho$ and TOF values. Precise $B\rho$ was determined by the trajectory reconstruction method for which ion-optical transfer matrix elements were experimentally determined up to the third-order. The significant improvement in A/Q resolution by our trajectory reconstruction technique is clearly seen in Fig. 2, where comparion of the A/Q resolution among three different transfer matrix elements in the trajectory reconstruction is shown. Precise TOF was determined by the slew correction method for TOF signals. We iteratively carried out the derivation of transfer matrix elements and slew correction such that the A/Q resolution was best optimized. Furthermore we completely removed background events to enhance the reliability of particle identification.

The excellent particle identification thus achieved allows us to supply tagged RI beams to a variety of experiments at RIBF. Furthermore it helps us to reliably identify new isotopes from a very small number of events. Such enhanced capability of the BigRIPS separator is significantly advancing the research on exotic nuclei at RIBF.

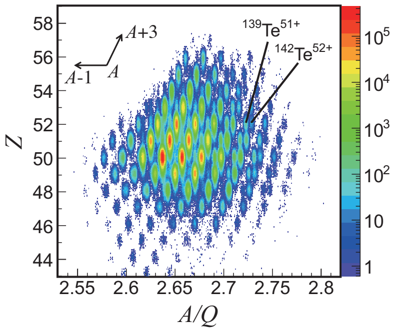

Fig. 1. Z versus A/Q particle identification plot for fission fragments produced in the ^{238}U + Pb reaction at 345 MeV/nucleon. The experimental conditions and BigRIPS setting are given in the G3 Setting section in Ref.[3)].

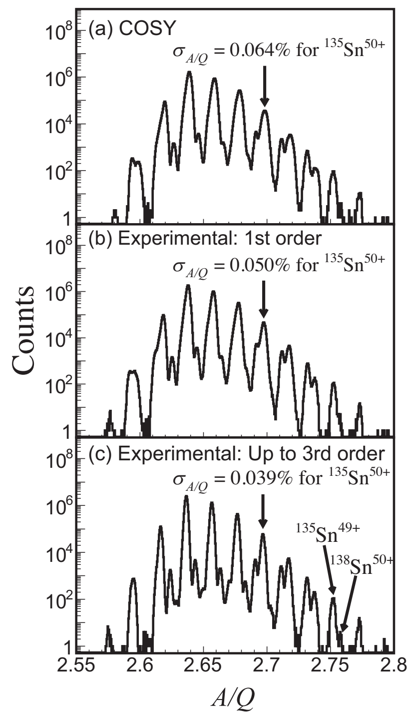

Fig. 2. Comparison of the A/Q resolution among three different transfer matrix elements used in trajectory reconstruction. The comparison is shown for Sn isotopes produced by in-flight fission of a ^{238}U beam at 345 MeV/nucleon. The experimental conditions and BigRIPS settings are the same as those in Fig. 1.

References
1) T. Kubo: Nucl. Instr. Meth. **B 204**, 97 (2003).
2) Y. Yano: Nucl. Instr. Meth. **B 261**, 1009 (2007).
3) T. Ohnishi et al.: J. Phys. Soc. Jpn. **79**, 073201 (2010).

† Condensed from the article in Nucl. Instr. Meth. **B 317**, 323 (2013)

*1 RIKEN Nishina Center

Production cross section measurements of radioactive isotopes by BigRIPS separator at RIKEN RI Beam Factory†

H. Suzuki,*1 T. Kubo,*1 N. Fukuda,*1 N. Inabe,*1 D. Kameda,*1 H. Takeda,*1 K. Yoshida,*1 K. Kusaka,*1 Y. Yanagisawa,*1 M. Ohtake,*1 H. Sato,*1 Y. Shimizu,*1 H. Baba,*1 M. Kurokawa,*1 T. Ohnishi,*1 K. Tanaka,*1 O. B. Tarasov,*1,*2 D. Bazin,*1,*2 D. J. Morrissey,*1,*2 B. M. Sherrill,*1,*2 K. Ieki,*1,*3 D. Murai,*1,*3 N. Iwasa,*1,*4 A. Chiba,*1,*4 Y. Ohkoda,*1,*4 E. Ideguchi,*5 S. Go,*1,*6 R. Yokoyama,*6 T. Fujii,*6 D. Nishimura,*1,*7 H. Nishibata,*1,*8 S. Momota,*1,*9 M. Lewitowicz,*10 G. DeFrance,*10 I. Celikovic,*10 and K. Steiger*11

We have measured the production rates and production cross sections for a variety of radioactive isotopes which were produced from ^{124}Xe, ^{48}Ca, and ^{238}U beams at an energy of 345 MeV/nucleon using the BigRIPS separator[1)].

Proton-rich isotopes with atomic numbers Z = 40-52 were produced by projectile fragmentation of the ^{124}Xe beam on a Be target, during which we also measured their momentum distributions. We found that the exponential tails at the low-momentum region fall off faster than those of the LISE^{++}[2)] calculation with the original parameterization. The EPAX3.01 cross-section formula[3)] agreed fairly well with the experimental cross sections. Furthermore, we have discovered four new isotopes on the proton-drip line, ^{85,86}Ru and ^{81,82}Mo. Figure 1 (a) shows a two-dimensional plot of Z versus mass-to-charge ratio (A/Q) in the ^{85}Ru setting. The four new isotopes were clearly identified on the left side of the solid lines, which indicate the limits of known isotopes. In the ^{105}Te setting, ^{103}Sb was not observed in our measurement, as shown in Fig. 1 (b). We obtained clear evidence that ^{103}Sb is particle-unbound with a half-life upper limit of 49 ns.

Neutron-rich isotopes with Z = 5-16 were produced by the projectile fragmentation of the ^{48}Ca beam on Be targets. The EPAX2.15 formula[4)] reproduces the experimental cross sections fairly well.

Neutron-rich isotopes with Z = 20-59 were produced by in-flight fission of a ^{238}U beam on Be and Pb targets. The measured production rates were compared with the LISE^{++} calculations, in which the abrasion fission (AF) model and the AF + Coulomb fission model were used for the ^{238}U+Be and ^{238}U+Pb cases, respectively. In the former case, the LISE^{++} calculations reproduced the experimental production rates well for the $Z < 50$ region but underestimated them for $Z > 50$. In the latter case, the LISE^{++} predictions reproduce them fairly well overall.

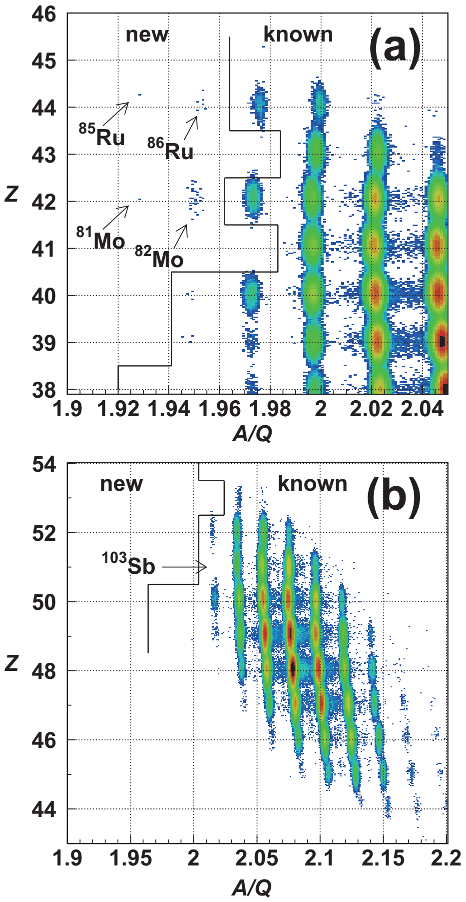

Fig. 1. (a)Enlarged two-dimensional PID plot of Z vs. A/Q for ^{85}Ru setting. ^{85,86}Ru and ^{81,82}Mo are the new isotopes. (b)PID plot for ^{105}Te setting.

† Condensed from the article in Nucl. Instrum. Meth. Phys. Res., **B 317**, 756 (2013)

*1 RIKEN Nishina Center
*2 National Superconducting Cyclotron Laboratory, Michigan State University
*3 Department of Physics, Rikkyo University
*4 Department of Physics, Tohoku University
*5 Research Center for Nuclear Physics, Osaka University
*6 Center for Nuclear Study, University of Tokyo
*7 Department of Physics, Tokyo University of Science
*8 Department of Physics, Osaka University
*9 School of Environmental Science and Engineering, Kochi University of Technology
*10 Grand Accelerateur National d'Ions Lourds
*11 Physik Department, Technische Universität München

References
1) T. Kubo et al.: Nucl. Instrum. Meth. Phys. Res. **B 204**, 97 (2003).
2) O.B.Tarasov and D.Bazin: LISE^{++} site, http://lise.nscl.edu, Michigan State University.
3) K. Sümmer: Phys. Rev. C **86**, 014601 (2012).
4) K. Sümmer and B. Blank: Phys. Rev. C **61**, 034607 (2000).

Comparison of production yields of neutron-rich nuclei between Be and W targets by in-flight fission of ^{238}U beam

D. Murai,[*1,*2] T. Kubo,[*1] N. Inabe,[*1] D. Kameda,[*1] N. Fukuda,[*1] H. Takeda,[*1] H. Suzuki,[*1] K. Yoshida,[*1] K. Kusaka,[*1] K. Tanaka,[*1] Y. Yanagisawa,[*1] M. Ohtake,[*1] T. Ohnishi,[*1] H. Sato,[*1] Y. Shimizu,[*1] H. Baba,[*1] M. Kurokawa,[*1] K. Ieki,[*1,*2] D. Nishimura,[*1,*3] E. Ideguchi,[*4] S. Go,[*1,*5] R. Yokoyama,[*5] T. Fujii,[*1,*5] N. Iwasa,[*1,*6] T. Yamada,[*6] A. Chiba,[*1,*6] S. Momota,[*1,*7] H. Nishibata,[*1,*8] O. B. Tarasov,[*1,*9] D. J. Morrissey,[*1,*9] B. M. Sherrill,[*1,*9] Y. Satou,[*1,*10] S. Kim,[*1,*10] J. W. Hwang[*1,*10] and G. Simpson[*11]

We have measured production yields by the in-flight fission of a ^{238}U beam at 345 MeV/nucleon with a Be target and a W target, and investigated the suitability of the targets for the production of neutron-rich nuclei with atomic numbers Z ranging from 57 to 69. The isotopes were produced and identified using the BigRIPS separator. Particles were identified by the $B\rho$-TOF-ΔE method to determine Z and the mass-to-charge ratio A/Q.

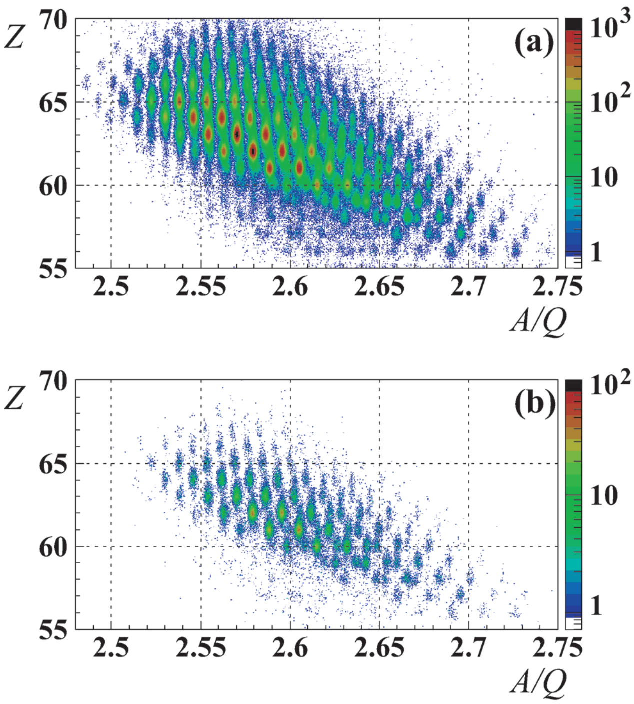

Fig. 1. Particle identification plot of Z versus A/Q obtained with (a) the Be target and (b) the W target.

*1 RIKEN Nishina Center
*2 Department of Physics, Rikkyo University
*3 Faculty of Science and Technology, Tokyo University of Science
*4 Research Center for Nuclear Physics, Osaka University
*5 Center of Nuclear Study, University of Tokyo
*6 Department of Physics, Tohoku University
*7 School of Environmental Science and Engineering, Kochi University of Technology
*8 Department of Physics, Osaka University
*9 NSCL, Michigan State University
*10 Department of Physics and Astronomy, Seoul National University
*11 LPSC-IN2P3

The target thicknesses were 5 and 0.7 mm for the Be and W targets, respectively; these thickness were energy-loss equivalent. The BigRIPS setting was the same as the ^{168}Gd setting in the new-isotope-search experiment.[1] The total rates were 79.9 counts/particle nA and 51.5 counts/particle nA for the Be and W targets, respectively. Figure 1 shows the Z versus A/Q plots for the Be and W targets. The resolutions of A/Q and Z are typically 0.045% and 0.45%, respectively. Figure 2 shows the production yield for each target. The squares and circles show the experimental data obtained with the Be and W targets, respectively. The result indicate that the production yield with the Be target is larger than that with the W target in the region where $Z > 62$.

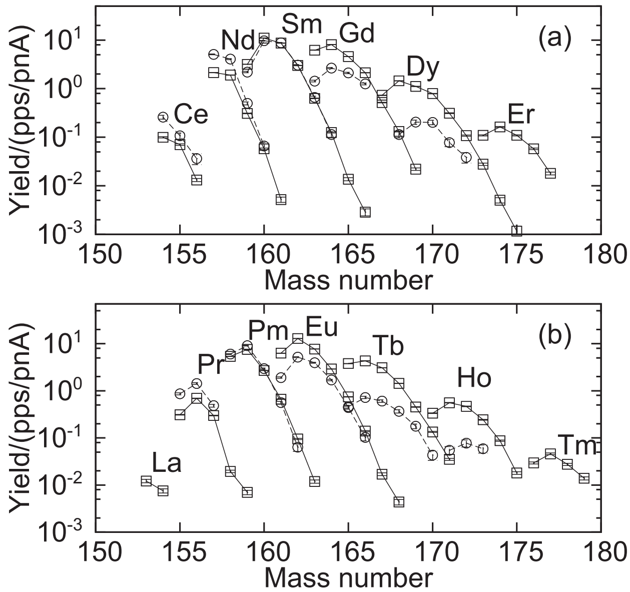

Fig. 2. Measured production yields with the Be (squares) and W (circles) targets. (a) Results for even-Z isotopes. (b) Results for odd-Z isotopes.

The transmission of the BigRIPS separator is not taken into consideration in these results. We are proceeding with the analysis to deduce the production cross sections.

References

1) D. Kameda et al.: RIKEN Accel. Prog. Rep. **45**, 117 (2012).

Production rates of new neutron-rich rare-earth nuclei via in-flight fission of a 345 MeV/nucleon ^{238}U beam

D. Kameda,[*1] T. Kubo,[*1] N. Fukuda,[*1] H. Takeda,[*1] H. Suzuki,[*1] K. Yoshida,[*1] K. Kusaka,[*1] K. Tanaka,[*1] Y. Yanagisawa,[*1] M. Ohtake,[*1] N. Inabe,[*1] H. Sato,[*1] Y. Shimizu,[*1] H. Baba,[*1] M. Kurokawa,[*1] D. Nishimura,[*1,*2] T. Ohnishi,[*1] N. Iwasa,[*1,*3] A. Chiba,[*1,*3] T. Yamada,[*1,*3] E. Ideguchi,[*4] S. Go,[*1,*5] R. Yokoyama,[*5] T. Fujii,[*5] H. Nishibata,[*1,*6] K. Ieki,[*1,*7] D. Murai,[*1,*7] S. Momota,[*1,*8] Y. Satou,[*9] J. W. Hwang,[*1,*9] S. Kim,[*1,*9] O. B. Tarasov,[*1,*10] D. J. Morrissey,[*1,*10] B. M. Sherrill,[*1,*10] and G. Simpson[*11]

The reaction mechanism of in-flight fission is not clear yet due to the complexity of the abrasion fission process, in which many kinds of fissile nuclei can contribute to the production of fission fragments. The measurement of the production rates of various fission fragments is useful not only to plan various experiments but also to understand such a reaction mechanism. In 2011, using a 345 MeV/nucleon ^{238}U beam with a Be target, we searched for new isotopes and isomers whose atomic numbers roughly range from 56 to 68.[1)] Here, we report on the production rates of new isotopes, in addition to the improvements in particle identification (PID) compared to our previous report.[2)]

Fission fragments were separated and analyzed using the BigRIPS separator. We adopted two settings that targeted the regions of nuclei around ^{159}Pr and ^{168}Gd. The mass-to-charge ratio (*A*/*Q*) was deduced from the time of flight (TOF) and magnetic rigidity measurements obtained using BigRIPS. The atomic number (*Z*) was deduced from the TOF and energy losses, which were measured using a stack of Si detectors in the focal plane. The PID plot in the region of ^{159}Pr is presented in Fig. 1. Since our previous report,[2)] we have modified the gate conditions to remove background events and improved the resolutions of *A*/*Q* and *Z* by carrying out detailed analysis. As a result, in the two settings, we identified a total of 26 new isotopes: ^{153}Ba, ^{154,155,156}La, ^{156,157158}Ce, ^{156,157,158,159,160}Pr, ^{162,163}Nd, ^{164,165}Pm, ^{166,167}Sm, ^{169}Eu, ^{171}Gd, ^{173,174}Tb, ^{175,176}Dy, ^{177}Ho, and ^{179}Er.

The production rates of fully stripped fragments are presented in Fig. 2 along with the LISE++ calculations.[3)] Here, for the LISE++ abrasion fission (AF) model, we adopted the same parameters as those used in the previous experiment.[4)] This AF model reproduced the production rates in the region of Z = 20 to 49 fairly well.[4,5)] In the present region of Z = 56 to 65, however, the calculations are orders of magnitudes smaller than the measured rates. This difference might be due to the AF model parameters, which were optimized to reproduce limited cross-section data for Z = 20 to 46.[3)] Further systematic studies are now in progress.

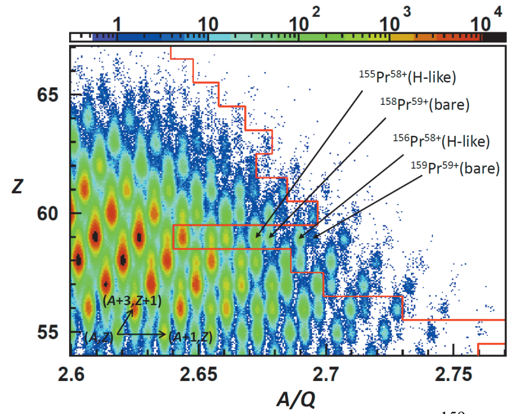

Fig. 1. Z versus A/Q PID plot in the region of ^{159}Pr. The red lines indicate the known limits of neutron-rich isotopes.

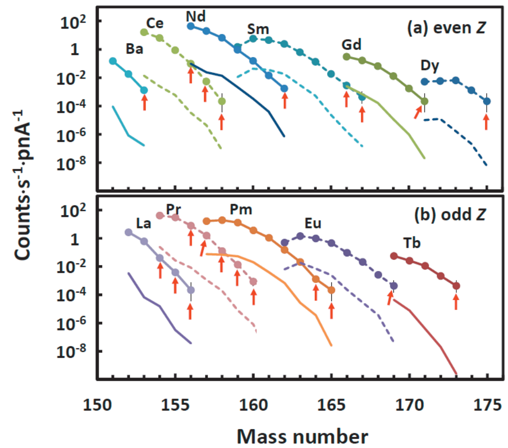

Fig. 2. Measured production rates of (a) even-Z and (b) odd-Z isotopes in the region of ^{159}Pr. The red arrows indicate the production rates of new isotopes. The LISE++ calculations are denoted by the dashed or solid curves without circles (see text).

*1 RIKEN Nishina Center
*2 Department of Physics, Tokyo University of Science
*3 Department of Physics, Tohoku University
*4 Research Center for Nuclear Physics, Osaka University
*5 Center for Nuclear Study, University of Tokyo
*6 Department of Physics, Osaka University
*7 Department of Physics, Rikkyo University
*8 School of Environmental Science and Engineering, Kochi University of Technology
*9 Department of Physics and Astronomy, Seoul National University
*10 National Superconducting Cyclotron Laboratory, Michigan State University
*11 LPSC-IN2P3

References

1) D. Kameda et al.: RIKEN Accel. Prog. Rep. **45**, 117 (2012).
2) D. Kameda et al.: RIKEN Accel. Prog. Rep. **46**, 20 (2013).
3) O. B. Tarasov and D. Bazin: Nucl. Instr. Meth. B **266**, 4657 (2008) and references therein.
4) T. Ohnishi et al.: J. Phys. Soc. Jpn. **79**, 073201 (2010).
5) H. Suzuki et al.: Nucl. Instr. Meth. B **317**, 756 (2013).

Evidence for a new nuclear ‘magic number’ in ^{54}Ca[†]

D. Steppenbeck,[*1] S. Takeuchi,[*2] N. Aoi,[*3] P. Doornenbal,[*2] M. Matsushita,[*1] H. Wang,[*2] H. Baba,[*2] N. Fukuda,[*2] S. Go,[*1] M. Honma,[*4] J. Lee,[*2] K. Matsui,[*5] S. Michimasa,[*1] T. Motobayashi,[*2] D. Nishimura,[*6] T. Otsuka,[*1*5] H. Sakurai,[*2*5] Y. Shiga,[*7] P.-A. Söderström,[*2] T. Sumikama,[*8] H. Suzuki,[*2] R. Taniuchi,[*5] Y. Utsuno,[*9] J. J. Valiente-Dobón,[*10] and K. Yoneda[*2]

Over recent years, the evolution of nuclear shell structure in exotic, neutron-rich nuclei has attracted much attention on both the experimental and theoretical fronts. In the neutron-rich fp shell, the onset of the $N = 32$ subshell closure is well established from the structural characteristics of ^{52}Ca[1,2], ^{54}Ti[3,4] and ^{56}Cr[5,6]. This subshell gap is reproduced successfully by numerous theoretical predictions. In the framework of tensor-force-driven shell evolution[7], the onset of the $N = 32$ subshell closure results as a direct consequence of a sizable $\nu p_{3/2}$–$\nu p_{1/2}$ gap, which presents itself as the $\nu f_{5/2}$ orbital shifts up in energy owing to a weakening of the attractive $\pi f_{7/2}$–$\nu f_{5/2}$ interaction as protons are removed from the $\pi f_{7/2}$ orbital. Another important manifestation of some theories is the prediction of a large subshell gap at $N = 34$, which develops if the $\nu f_{5/2}$ orbital lies sufficiently high in energy above the $\nu p_{1/2}$ orbital. It has already been shown that no significant $N = 34$ subshell gap exists in ^{56}Ti[4,8] or ^{58}Cr[6,9] and, therefore, the size of the energy gap in ^{54}Ca is an important structural characteristic that requires experimental input. Moreover, the single-particle states of ^{53}Ca should also reflect the nature of the $N = 34$ subshell closure in isotopes far from stability.

The structures of ^{54}Ca and ^{53}Ca were investigated using in-beam γ-ray spectroscopy at the RIBF to address this issue. A primary beam of ^{70}Zn^{30+} ions at 345 MeV/u was used to create a radioactive beam containing ^{55}Sc and ^{56}Ti, which was focused on a 10-mm-thick

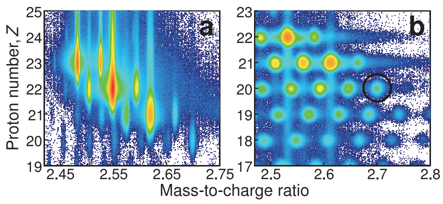

Fig. 1. (colour) Particle identification plots measured by (a) the BigRIPS separator and (b) the ZeroDegree spectrometer. The black circle indicates ^{54}Ca events.

† Condensed from the article in Nature **502**, 207 (2013).

*1 Center for Nuclear Study, University of Tokyo.
*2 RIKEN Nishina Center.
*3 RCNP, University of Osaka.
*4 Center for Mathematical Sciences, Aizu University.
*5 Department of Physics, University of Tokyo.
*6 Department of Physics, Tokyo University of Science.
*7 Department of Physics, Rikkyo University.
*8 Department of Physics, Tohoku University.
*9 Japan Atomic Energy Agency.
*10 Laboratori Nazionali di Legnaro.

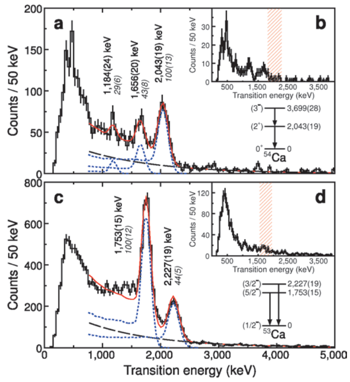

Fig. 2. (colour) Doppler-corrected γ-ray energy spectra for (a) ^{54}Ca and (c) ^{53}Ca. Insets (b) and (d) indicate γ rays in coincidence with the 2043- and 1753-keV lines.

Be reaction target located inside the DALI2 γ-ray detector array at F8. Reaction products were identified with the ZeroDegree spectrometer (see Fig. 1).

The energy spectra for ^{54}Ca and ^{53}Ca deduced in the present work are presented in Fig. 2. The most intense peak in the ^{54}Ca spectrum, the line at 2043(19) keV, is assigned as the $2^+_1 \to 0^+$ ground-state transition. Several other weaker lines are also reported. The relatively high energy of the 2^+_1 state reflects the doubly magic nature of ^{54}Ca and provides direct experimental evidence for the onset of a sizable subshell closure in $N = 34$ isotones far from stability. Shell-model calculations adopting a modified GXPF1B Hamiltonian indicate that the strength of the $N = 34$ subshell gap in ^{54}Ca (the $\nu p_{1/2}$–$\nu f_{5/2}$ SPO energy gap) is in fact comparable to the $N = 32$ subshell gap in ^{52}Ca (the $\nu p_{3/2}$–$\nu p_{1/2}$ SPO energy gap) (see original Letter for details). In the ^{53}Ca spectrum, the 1753(15)-keV transition is reported for the first time, while the line at 2227(19) keV is consistent in energy with a transition previously measured in a decay study[10].

References

1) A. Gade et al., Phys. Rev. C **74**, 021302(R) (2006).
2) F. Wienholtz et al., Nature **498**, 346 (2013).
3) R. V. F. Janssens et al., Phys. Lett. B **546**, 55 (2002).
4) D.-C. Dinca et al., Phys. Rev. C **71**, 041302(R) (2005).
5) R. Chapman et al., Nucl. Phys. A **119**, 305 (1968).
6) A. Bürger et al., Phys. Lett. B **622**, 29 (2005).
7) T. Otsuka et al., Phys. Rev. Lett. **95**, 232502 (2005).
8) S. N. Liddick et al., Phys. Rev. Lett. **92**, 072502 (2004).
9) J. I. Prisciandaro et al., Phys. Lett. B **510**, 17 (2001).
10) F. Perrot et al., Phys. Rev. C **74**, 014313 (2006).

First physics data of the J-PARC E15 Experiment

Y. Sada,[*1,*2] M. Iwasaki,[*1,*3] Y. Ma,[*1] H. Ohnishi,[*1] F. Sakuma,[*1] M. Sato,[*1] M. Tokuda,[*1,*3] Q. Zhang,[*1]
for the J-PARC E15 Collaboration

1 Introduction

The K̄N interaction has been determined to be strongly attractive through extensive measurements of the kaonic hydrogen atom and low-energy K̄N scattering. As a consequence of strong K̄N interaction, there are many theoretical predictions of the deeply bound K-nuclear states. In particular, an extensive study on the simplest K-nuclear bound system, K̄NN, has been in progressed on both the theoretical and experimental[1)] sides. Since available experimental information is limited, interpretations of the results are controversial. To completely understand the K̄N interaction, we require more experimental results on various interactions for formation of the K̄NN bound state. The E15 experiment at the K1.8BR beam-line aims to search for the K̄NN bound state[2)] with the in-flight ^{3}He(K$^-$, N) reaction at 1.0 GeV/c. Such measurement allows us to investigate the K̄NN bound state in terms of both its formation via missing-mass spectroscopy and its decay via invariant-mass spectroscopy.

2 Experimental setup

The experimental setup consists of three parts: a high-precision beam-line spectrometer, a cylindrical detector system (CDS) that surrounds a liquid ^{3}He target system, and forward particle TOF detectors. The kaon beam at a momentum of 1.0 GeV/c is identified using an aerogel Cherenkov counter. The kaon beam momentum is analyzed by the beam-line spectrometer, which has a momentum resolution of 2.2 MeV/c at 1.0 GeV/c. The CDS is placed around the target in order to detect decay particles from the K̄NN bound state. The CDS consists of a solenoid magnet, a cylindrical drift chamber (CDC), and a cylindrical detector hodoscope (CDH). The decay particles from the target are detected by the CDS, which has a solid angle coverage of 59% of 4π. With the CDS, we can perform particle identification and track reconstruction (momentum resolution is 5% at 600 MeV/c). A neutron TOF counter (NC), placed 15 m downstream from the center of the target at 0 degrees with respect to the beam direction, measures forward-going neutral particles. The TOF resolution is determined to be 150 ps (σ) using a gamma-ray data sample. The missing-mass resolution of the ^{3}He(K$^-$, n) reaction is estimated to be 9 MeV/c^2 at the region of interest ($P_n \sim 1.2$ GeV/c). The details of the spectrometer system can be found in another paper[3)].

*1 RIKEN Nishina Center
*2 Department of Physics, Kyoto University, Japan
*3 Department of Physics, Tokyo Institute of Technology, Japan

3 First physics data

The first physics run of the E15 experiment was carried out in May 2013. By irradiating 5×10^9 kaons on the helium-3 target, 3×10^5 forward neutrons were successfully recorded.The accumulated data corresponds to 1% of the statistics requested in the original proposal. Fig 1 shows the missing mass of the ^{3}He(K$^-$, n) reactions measured by the NC. One or more charged tracks are required in the CDS to reconstruct the reaction vertex.

In the spectrum, a peak from the quasi-free reaction $K^-N \to \bar{K}N$ on ^{3}He is clearly seen. The spectrum with K_s^0 tagged in the CDS is superimposed on the figure, in which the excess below the K̄NN threshold (2.37 GeV/c^2) is not observed. Therefore the excess below the K̄NN threshold in the semi-inclusive ^{3}He(K$^-$, n) spectrum is barely explained by the detector responses and the quasi-free reaction. Further analysis is in progress to understand the observed spectrum.

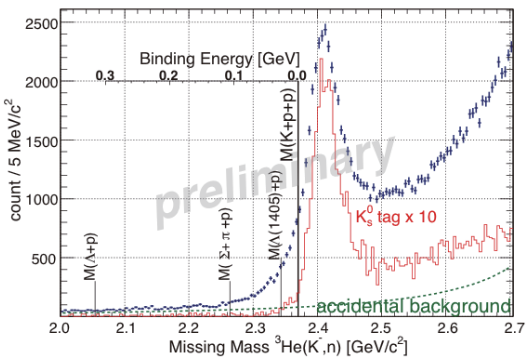

Fig. 1. Missing masses of the ^{3}He(K$^-$, n) reactions.

References
1) M. Agnello, *et al.*, Phys. Rev. Lett 94, 212303 (2005).; T. Yamazaki, *et al.*, Phys. Rev. Lett 104, 132502 (2010).; L. Fabbietti, *et al.*, Nucl. Phys. A 914, 60 (2013).; A. O. Tokiyasu, *et al.*; Phys. Lett. B 728C, 616-621 (2014).
2) M. Iwasaki, *et al* (E15 collaboration), J-PARC E15 proposal, (http://j-parc.jp/NuclPart/pac 0606/pdf/p15-Iwasaki.pdf).
3) K. Agari, et al., Prog. Theor. Exp. Phys. 02B011 (2012). 5

Measurement of the $^{248}Cm + ^{48}Ca$ fusion reaction products at RIKEN GARIS

K. Morita,[*1,*2] K. Morimoto,[*1] D. Kaji,[*1] H. Haba,[*1] Y. Wakabayashi,[*1] M. Takeyama,[*3,*1] S. Yamaki,[*4,*1] K. Tanaka,[*5,*1] H. Hasebe,[*1] M. Huang,[*1] J. Kanaya,[*1] M. Murakami,[*6,*1] A. Yoneda,[*1] A. Yoshida,[*1] T. Yamaguchi,[*4] F. Tokanai,[*3] T. Yoshida,[*3] Z. Gan,[*7] L. Ma,[*7] H. Geissel,[*8] S. Hofmann,[*8] Y. Maurer,[*8] K. Fujita,[*2] Y. Narikiyo,[*2] T. Tanaka,[*2] S. Yamamoto,[*2] M. Asai,[*9] and K. Katori[*1]

The reaction, $^{248}Cm + ^{48}Ca \rightarrow ^{296}Lv^*$(Livermorium, Z = 116), has been studied at the RIKEN Linear Accelerator (RILAC) Facility using a gas-filled recoil ion separator GARIS. Although this reaction was intensively studied at the Flerov Laboratory of Nuclear Reaction (FLNR), Russia[1,2)], and GSI, Helmholtzzentrum für Schwerionenforschung, Germany[3)], the number of observed events is still very small because of the small production cross sections. The first aim of the present study is to observe more events in the region of superheavy nuclei and possibly to obtain new spectroscopic information of those nuclei. The second aim is to examine the performance of the GARIS facility using the relevant reaction for a future project with the ^{50}Ti beam, instead of the ^{48}Ca beam, to search for new heaviest nuclei. Because of the limitation of target nuclear species, one needs to use beams heavier than ^{48}Ca for further investigation of superheavy nuclei.

A ^{48}Ca beam was accelerated by RILAC at 262 MeV, and it irradiated ^{248}Cm targets prepared by electro deposition of $^{248}Cm_3O_8$ on titanium foils. Eight targets were mounted on a wheel rotating at 1000 rpm. The diameter of the wheel is 10 cm. The average thickness of $^{248}Cm_3O_8$ was 0.290 mg/cm^2, which contained 0.265 mg/cm^2 ^{248}Cm, and that of titanium foils was 0.903 mg/cm^2. The energy of the beam at half depth of the target was estimated to be 250 MeV by using a range-energy table. Reaction products were separated from beam particles and from unwanted particles by GARIS and then implanted in a position-sensitive semiconductor detector (PSD), which covered 60 mm × 60 mm, set on the focal plane of GARIS. Four side detectors (SSDs) of the same size were set in a box arrangement to detect the decay products (alpha particles or spontaneous fission (SF) fragments) emitted at backward angles from the PSD. Time-of-flight counters consisting of micro-channel plates (MCPs) were set upstream of the PSD. The average beam intensity was 0.8 particle μA. In a beamtime of 10days, 4.3×10^{18} ^{48}Ca ions irradiated the targets. The Bρ value of the GARIS was set to 2.21 Tm.

We observed five correlated events during the experiment, all of which terminated by spontaneous fission (SF). Decay characteristics of those events agreed well with previous studies[1,2,3)]. Although it is difficult to identify the nuclides of the products only from the present experimental study, we could state that two of the events were attributed to the decays of ^{293}Lv (3 n evaporation channel) and three of them to the decays of ^{292}Lv (4 n evaporation channel) by referring to the assignments in the previous studies. The two events attributed to the ^{293}Lv decay consisted of three consecutive alpha decays followed by SF. The two events attributed to the ^{292}Lv decay consisted of two alpha decays followed by SF. One of the events we tentatively assigned to the decay of ^{292}Lv consisted of three alpha decays followed by SF. The tentative assignment is based on the decay characteristics of the decay energies and decay times of ^{292}Lv and ^{288}Fl (Flerovium, Z = 114) and the decay time of ^{284}Cn (Copernicium, Z = 112). Because an alpha decay of ^{284}Cn has not been observed, this possibly involves a new decay mode of ^{284}Cn and new isotope ^{280}Ds decays by SF. The production cross sections of ^{293}Lv and ^{292}Lv were deduced to be $2.1^{+2.9}_{-1.4}$ pb and $3.1^{+3.0}_{-1.7}$ pb, respectively, by assuming the transmission of GARIS to be 0.35. Observed events are summarized in Table I.

Further analysis is now in progress.

Table I Observed decay events, energies, and time intervals of the events. Bottom row indicates the possible assignments of nuclei

Chain 1	Chain 2	Chain 3	Chain 4	Chain 5
10.79 MeV 0.032 s	10.47 MeV 0.253 s	2.77 MeV$^+$ 0.0020 s	10.66 MeV 0.0041 s	7.76 MeV^{++} 0.032 s
9.89 MeV 0.548 s	9.89 MeV 3.97 s	9.99 MeV 0.243 s	0.83 MeV+ 0.0090 s	9.72 MeV 0.666 s
232 MeV 0.065 s	2.46 MeV$^+$ 7.76 s	182 MeV 0.832 s	9.09 MeV 0.282 s	1.64 MeV$^+$ 7.56 s
	195 MeV 19.8 s		163 MeV 0.0096 s	221 MeV 4.63 s
^{292}Lv	^{293}Lv	^{292}Lv	$^{292}Lv^{+++}$	^{293}Lv

$^+$ escape energies (partly measured using PSD)
$^{++}$ energies measured only using SSD. $^{+++}$ tentative

*1 RIKEN Nishina Center
*2 Department of Physics, Kyushu University
*3 Department of Physics, Yamagata University
*4 Department of Physics, Saitama University
*5 Department of Physics, Tokyo University of Science
*6 Department of Chemistry, Niigata University
*7 Institute of Modern Physics, Lanzhou
*8 GSI Helmholtzzentrum für Schwerionenforschung
*9 Advanced Science Research Center, Japan Atomic Energy Agency

References

1) Yu. Ts. Oganessian et al.: Phys. Rev. C**63**, 011301(R) (2000).
2) Yu. Ts. Oganessian et al.: Phys. Rev. C**70**, 064609 (2004).
3) S. Hofmann et al.: Eur. Phys. A**48**, 62 (2012).

Operational test of micro-oven for ^{48}Ca beam†

K. Ozeki,[*1] T. Kageyama,[*1] M. Kidera,[*1] Y. Higurashi,[*1] and T. Nakagawa[*1]

In order to supply a high-intensity and stable ^{48}Ca beam from the 18-GHz electron cyclotron resonance ion source (ECRIS),[1)] we have been conducting operational tests of a micro-oven for the ^{48}Ca beam.

The structure of the micro-oven and the method to produce the ^{48}Ca beam are described in Ref. 2.

In these test experiments conducted at the 18-GHz ECRIS, the material used was the element ^{40}Ca. The beam intensity was measured using a Faraday cup installed at the exit of the analyzing magnet. Figure 1 shows the charge distribution of Ca ions when the beam intensity of 60 electric μA was obtained for Ca^{11+}. In the test experiment from which this spectrum was obtained, a hot liner was installed into the plasma chamber, and a negative voltage bias was not applied to the micro-oven (both cases are mentioned below).

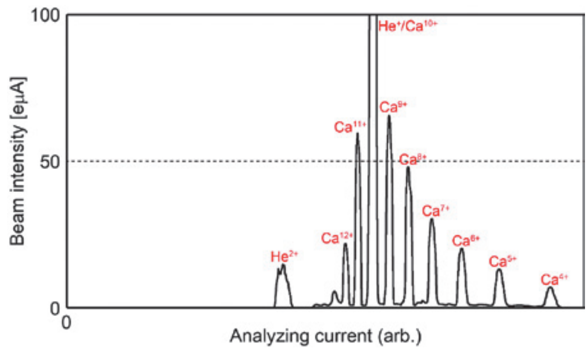

Fig. 1. Charge distribution of calcium ions.

For the supply of metallic beams, several facilities use a so-called "hot-liner"[3, 4)] to reduce the material consumption rate. In this method, the inner surface of the plasma chamber is thermally decoupled from the cooling water jacket. The inner surface is heated by the plasma to enable the metallic atoms to re-evaporate from the inner surface. Fig. 2 shows the results of one of the long-term experiments in the cases in which the hot liner was not installed (without the hot liner) and installed (with the hot liner) in the plasma chamber. The beam intensities for Ca^{11+} are shown. In the case without the hot liner, the beam intensity was not maintained at a constant value. In the case with the hot liner, the beam intensity was maintained at 30 electric μA. The amounts of calcium placed in the crucible and subsequently consumed were 252 mg and 230 mg, respectively, for the case without the hot liner, and 246 mg and 105 mg, respectively, for the case with the hot liner. The consumption rates without and with the hot liner were estimated to be 0.88 mg/h and 0.44 mg/h, respectively.

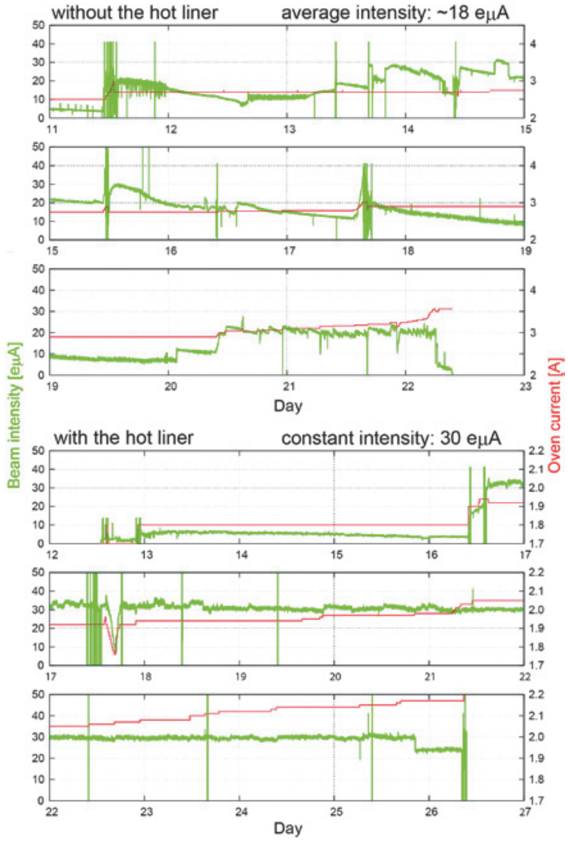

Fig. 2. Long-term experiment results when the hot liner was not installed and when it was installed in the plasma chamber.

One method to enhance the beam intensity is the "biased disk" method.[5)] In this method, a negatively biased metal disk is installed in the plasma chamber. We investigated the effect of a negative bias applied to the micro-oven itself under the various oven positions. Beam intensity enhancement of up to 20% was observed. An effect similar to a biased disk was confirmed.

References

1) T. Nakagawa: Nucl. Instrum. Methods B **226**, 392 (2004).
2) K. Ozeki et al.: RIKEN Accel. Prog. Rep. **46**, 128 (2013).
3) V. B. Kutner et al.: Rev. Sci. Instrum. **71**, 860 (2000).
4) P. Lehérissier et al.: Rev. Sci. Instrum. **73**, 558 (2002).
5) G. Melin et al.: Proc. 10th Int. Workshop on ECR Ion Sources, Ork Ridge, 1991, p. 1.

† Condensed from the article in Rev. Sci. Instrum. **85**, 02A924 (2014)

*1 RIKEN Nishina Center

Current status of RI beam production at electron-beam-driven RI separator for SCRIT (ERIS)

T. Ohnishi,[*1] S. Ichikawa,[*1] M. Togasaki,[*1,*2] K. Kurita,[*1,*2] Y. Haraguchi,[*1,*3] and M. Wakasugi[*1]

The electron-beam-driven RI (Radioactive Isotope) separator for SCRIT (ERIS) at the SCRIT electron scattering facility[1)] consists of a RI generator and an ISOL-type RI separator employed to produce low-energy RI beams used for the electron scattering of unstable nuclei. In ERIS, the photofission of uranium driven by an electron beam is used for RI production. Details of ERIS were reported in Ref. 2. During the present year, uranium-carbide target was prepared, and the RI production has been started. In this paper, we report the first result of the RI production at ERIS.

For the RI production, we prepared uranium-caribide disks. Uranium carbide was obtained by the carbothermal reduction of uranium oxide in presence of carbon around 1800 °C. First, uranyl nitrate was mixed with 20μm graphite grains, after which uranyl nitrate was oxidized to UO_3 under air flow by heating to 500 °C. Next, UO_3 powders with graphite were manually ground, and they were formed into a disk without a binder at 180-MPa compression. The obtaind disk was 20 mm in a diameter and around 2 mm in a thickness. It was heated to 1000 °C in a vaccum for outgassing, and the reduction reaction $UO_3 \rightarrow UO_2$ proceeded. The finished disk consisted of about 0.7-g grahpite and 1.9-g UO_2 powders. Mass concentration of uranium in the disk was estimated as 1.9 g/cm^3. In total, 20 disks were prepared. The sum of the thicknesses of 20 disks was almost 50 mm, and the total amount of uranium was about 30 g. Finally, all uranium-oxide disks were converted into uranium carbide at around 1800°C by using the heating system in ERIS.

The prepared uranium-carbide disks were irradiated with electron beams accelerated to 150 MeV by RTM [1)]. The electrom beam power was nearly 10 W. Tantalum disks with a thickness of 5 mm and a diameter of 20 mm were inserted in front of the production target to increase the production of γ rays. The target temperature was around 2000 °C. Produced RIs were accelerated to 20 kV and mass-separated by the analyzing magnet. They were transported to the particle identification system for ERIS (PIE) located at the exit of ERIS. PIE consists of a rotating Al disk and a Ge detector, and it measures γ rays corresponding to the decay of the RIs stopped inside the rotating disk.

Figure 1 shows the rate of Sn and Xe isotopes at PIE. These rate are estimated from the observed γ-ray yield using the efficiency of the Ge detector and the half-life of each isotope. By comparing with the expected production rate inside the target, the overall efficiency can be estimated. Here, the overall efficiency includes the efficiency of release from the target, ionization in the ion source, and efficiecy of transport from ion source to PIE. For example, the measured rate for ^{137}Xe is 1.1×10^5 atoms/s and the expected production rate is about 1.6×10^8 atoms/s. The overall efficiency for ^{137}Xe is estimated to be 0.07%. In this experiment, the overall efficiency of stable xenon with a calibrated gas flow was measured to be 1%. Since the stable xenon was introduced into the ionization chamber through a gas inlet, the measured overall efficiency of stable xenon includes only ionization and transport efficiencies. The release efficiency of ^{137}Xe is estimated as 7% from these results. In the case of ^{132}Sn, the measured and expected production rates are 6.0×10^3 and 2.6×10^7 atoms/s, respectively. The release efficiency of ^{132}Sn is evaluated as 2.3% using the same ionization and transport efficiencies as those of Xe. This assumption is supported by the results obtained at ALTO[3)]. The release efficiency of Sn at ERIS is lower than that of Xe. One of the reasons is the inadequate conditions of the adsorption process at ERIS, such as temperature.

Further studies concerning the target fabrication and the optimization of the target and ion source conditions are in progress to increase the release efficiency.

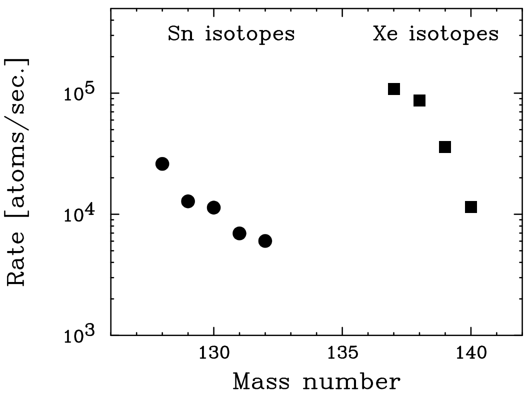

Fig. 1. Rate of Sn and Xe isotopes at the particle identification system of ERIS. The electron beam power was almost 10 W during the measurement. These rates are estimated on the basis of the observed γ-ray yield.

References
1) M. Wakasugi et. al: Nucl. Instr. Meth. B**317**, 668(2013).
2) T. Ohnishi et. al: Nucl. Instr. Meth. B**317**, 357(2013).
3) M. Cheikh Mhamed et. al: Nucl. Instr. Meth. B**266**, 4092(2008).

*1 RIKEN Nishina Center
*2 Department of Physics, Rikkyo University
*3 Department of Electrical Engineering, Nagaoka University of Technology

In-beam validation of the MINOS device at HIMAC

C. Santamaria,[*1,*2] A. Obertelli,[*1,*2] N. Aoi,[*3] L. Audirac,[*1] H. Baba,[*2] D. Beaumel,[*2,*4] S. Boissinot,[*1] D. Calvet,[*1] F. Château,[*1] A. Corsi,[*1] A. Delbart,[*1] P. Doornenbal,[*2] A. Giganon,[*1] A. Gillibert,[*1] Y. Kondo,[*2,*5] Y. Kubota,[*6] C. Lahonde-Hamdoun,[*1] V. Lapoux,[*1] J. Lee,[*2] C.S. Lee,[*6] M. Matsushita,[*6] J.-Ph. Mols,[*1] T. Motobayashi,[*2] T. Nakamura,[*2,*5] M. Kurata-Nishimura,[*2] S. Ota,[*6] H. Otsu,[*2] A. Peyaud,[*1] E.C. Pollacco,[*1] G. Prono,[*1] H. Sakurai,[*2] M. Sasano,[*2] E. Takada,[*7] H. Tokieda,[*6] T. Uesaka,[*2] K. Yoneda[*2] and J. Zenihiro[*6]

MINOS[1)] is a new device aimed at the in-beam spectroscopy of very exotic nuclei by proton-knockout at the RIBF facility. It is composed of a thick liquid hydrogen target[2)] (10-20cm) to maximize the luminosity surrounded by a cylindrical Time Projection Chamber equipped with a bulk-Micromegas[3)] pad detection plane. The latter allows to track the recoiled protons and thence apply a Doppler correction to the gamma rays measured by a gamma array such as DALI2[4)] at RIBF. As a final phase in the development of MINOS, a full in-beam test of the TPC and of its electronics system was performed at HIMAC in October 2013.

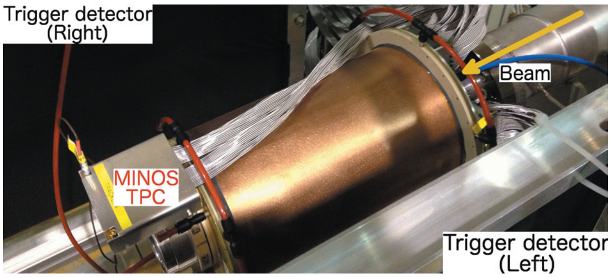

Fig. 1. MINOS experimental setup during the in-beam test using the PH2 course in HIMAC facility.

In this experiment, fragmentation reactions including $(p,2p)$ were produced using a beam of ^{20}Ne at 350 and 180 MeV/u impinging on 0.5 mm thick CH_2 or C targets placed inside the beam pipe instead of the LH_2 target. Beam detectors were placed upstream and downstream for both tracking and trigger purposes. As no particle identification was provided after the detector, two layers of plastic scintillators were placed on the left and right of the MINOS TPC to select events with charged particles passing through the device. A picture of the experimental setup is shown in Fig. 1.

The MINOS detector composed of about 4864 channels was for the first time read out with the electronics system constituted of front-end cards from the T2K experiment equipped with AFTER chips and of the newly-developed Feminos cards. The MINOS data acquisition was also successfully coupled to the RIBF data acquisition[5)] which handled the triggers and beam detectors information.

The use of two different gas mixtures ($Ar+5\%C_4H_{10}$ and $Ar+3\%C_4H_{10}+15\%CF_4$), several TPC voltages and two distinct detection pad geometries during this test also enabled a characterization of the TPC with track dispersion, gain as well as drift velocity changes on experiment-like data.

Eventually, this experiment tested the TPC vertex position resolution and its efficiency. The development of a tracking software for MINOS was carried out with the use of Hough filters, first to select the two-particle-like events in the two-dimensional detection plane and then to filter off the noisy signals in the tracks in three dimensions, before fitting the final tracks to obtain the vertex position. A full-width-half-maximum resolution around 5 mm in the beam direction was obtained with the ^{20}Ne beam at 350 MeV/u and the CH_2 targets, as shown on the right side of Fig. 2.

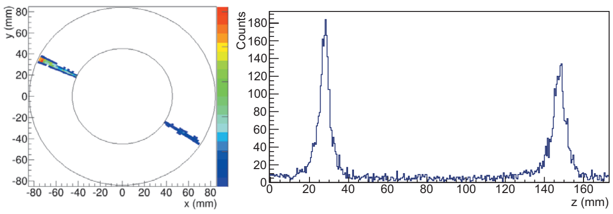

Fig. 2. (Left) Two-proton-like event. (Right) Reconstructed vertex position in the beam direction for a ^{20}Ne beam at 350 MeV/u and two 0.5 mm thick CH_2 targets separated by 124 mm.

Full-scale GEANT4 simulations are also being carried out for comparison to experiment in terms of efficiency as the final step in the validation of MINOS [6)]. This in-beam measurement at HIMAC opens the way to the upcoming physics experiments foreseen in Spring 2014 with the first physics results of the MINOS detector.

References
1) A. Obertelli et al: Eur. Phys. J. A **50** 8 (2014).
2) A. Obertelli et al.: Eur. Phys. J. A **47** 105 (2011).
3) I. Giomataris et al.: Nucl. Instr. Meth. A **376**, 29 (1996).
4) S. Takeuchi et al.: RIKEN Accel. Prog. Rep. **36**, 148 (2003).
5) H. Baba et al.: Nucl. Instr. Meth. A **616**, 65 (2010).
6) C. Santamaria et al., in preparation.

*1 CEA Saclay, IRFU/Service de Physique Nucléaire
*2 RIKEN Nishina Center
*3 RCNP, Osaka University
*4 IPN Orsay
*5 Tokyo Institute of Technology, Department of Physics
*6 CNS, The University of Tokyo
*7 NIRS-HIMAC

Seniority isomer in ^{128}Pd[†]

H. Watanabe[*1,*2] and EURICA U-beam collaboration in 2012

The level structure of the very neutron-rich nucleus ^{128}Pd has been studied for the first time. Neutron-rich nuclei below ^{132}Sn were produced using in-flight fission of a $^{238}U^{86+}$ beam at 345 MeV/nucleon impinging on a 3-mm-thick beryllium target. The primary beam intensity ranged from 7 to 12 pnA during the experiments. The nuclei of interest were separated by the BigRIPS separator and the following ZeroDegree spectrometer. The identified particles were implanted into a highly segmented active stopper named WAS3ABi[1)], which consisted of eight double-sided silicon-strip detectors (DSSSD) stacked compactly. Each DSSSD had a thickness of 1 mm with an active area segmented into sixty and forty strips (1-mm pitch) on each side in the horizontal and vertical directions, respectively. The DSSSDs also served as detectors for electrons following β-decay and internal conversion processes. Gamma rays were detected by the EURICA spectrometer[2)], which consisted of twelve Cluster-type detectors, each of which contained closely packed seven HPGe crystals.

Figure 1 shows a γ-ray energy spectrum measured in delayed coincidence with ^{128}Pd ions. Four γ rays at energies of 75, 260, 504, and 1311 keV have been unambiguously observed. These γ rays are found to be in mutual coincidence and exhibit consistent time behavior. Therefore, we conclude that they proceed through a single cascade originating from one isomeric state. A least-squares fit of the summed gated time spectra of the isomeric-decay transitions yields $T_{1/2} = 5.8(8)$ μs half-life, as shown in Fig. 1. The relative intensities of these isomeric γ rays are in agreement within experimental errors, except for the 75-keV transition that is expected to be highly converted. The total internal conversion coefficient for the 75-keV transition derived from a comparison with the 1311-keV γ-ray intensity is 2.6(17), which is consistent with the theoretical value of 3.88 for an $E2$ multipolarity.

On the basis of the above arguments on the observed γ transitions, the level scheme of ^{128}Pd is proposed as displayed in Fig. 1, where the spin and parity of the 5.8-μs isomeric state at 2151 keV is assigned as $J^{\pi} = 8^{+}$. The spin-parity assignment for the levels and the ordering of the transitions between the isomer and the ground state are based on a close resemblance to the yrast level energies below the analogous 8^{+} isomers in ^{130}Cd[3)] and ^{96}Pd ($N = 50$)[4)]. A transition strength of $B(E2; 8^{+} \rightarrow 6^{+}) = 0.22(3)$ W.u. can be obtained from the measured half-life of the 2151-keV isomeric state.

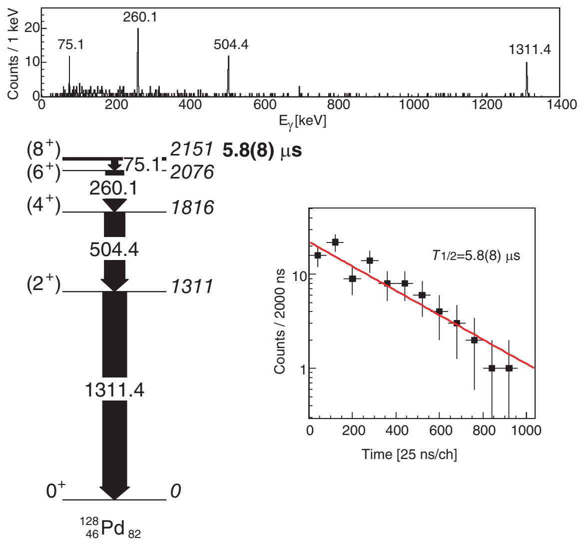

Fig. 1. Gamma-ray spectrum measured in coincidence with ^{128}Pd ions within $0.15 - 25$ μs (top), level scheme of ^{128}Pd (bottom left), and sum of time distributions of the 260-, 504-, and 1311-keV γ rays in ^{128}Pd (bottom right).

The excitation energies of the $J^{\pi} = 2^{+} - 8^{+}$ states in ^{128}Pd are comparable to those in ^{130}Cd[3)]. The constancy of level energies is characteristic of the seniority scheme, where seniority υ counts the number of nucleons that are not in pairs coupled to spin zero. In the case of an n-particle (or n-hole) system in a single-j shell, the level energies with identical J^{π} and υ are independent of n. Such energy properties are also visible for the even $N = 50$ isotones from Mo ($Z = 42$) to Cd ($Z = 48$), in which the yrast $J^{\pi} = 2^{+} - 8^{+}$ levels consist of the same multiplet that involves predominantly valence protons in the $\pi g_{9/2}$ orbital with $\upsilon = 2$. Since the single-proton levels in the $Z = 28 - 50$ shell are nearly identical in the ^{132}Sn and ^{100}Sn regions, it is expected that the level properties exhibited by the $N = 82$ isotones are similar within the valence proton space to those in the case of $N = 50$. Therefore, the excited states in ^{128}Pd can be interpreted in terms of the $\upsilon = 2$ configuration of the $\pi g_{9/2}$ subshell.

References

1) S. Nishimura: Prog. Theor. Exp. Phys. 03C006 (2012).
2) P.-A. Söderström et al.: Nucl. Instrum. Methods B 317, 649 (2013).
3) A. Jungclaus et al.: Phys. Rev. Lett. 99, 132501 (2007).
4) W. Kurcewicz et al.: Z. Phys. A 308, 21 (1982).

† Condensed from the article in Phys. Rev. Lett. **111**, 152501 (2013)
*1 IRCNPC, School of Physics and Nuclear Energy Engineering, Beihang University
*2 RIKEN Nishina Center

Evolution of collectivity in neutron-rich Ru nuclei[†]

P.-A. Söderström,[*1] G. Lorusso,[*1] H. Watanabe,[*2] S. Nishimura,[*1] P. Doornenbal,[*1] G. Thiamova,[*3] F. Browne,[*1,*4] G. Gey,[*1,*3,*5] H.S. Jung,[*6] T. Sumikama,[*7] J. Taprogge,[*1,*8,*9] Zs. Vajta,[*1,*10] J. Wu,[*11] Z.Y. Xu,[*12] H. Baba,[*1] G. Benzoni,[*13] K.Y. Chae,[*14] F.C.L. Crespi,[*13,*14] N. Fukuda,[*1] R. Gernhäuser,[*16] N. Inabe,[*1] T. Isobe,[*1] A. Jungclaus,[*9] D. Kameda,[*1] G.D. Kim,[*17] Y.-K. Kim,[*17] I. Kojouharov,[*18] F.G. Kondev,[*19] T. Kubo,[*1] N. Kurz,[*18] Y.K. Kwon,[*17] G. Lane,[*20] Z. Li,[*11] A. Montaner-Pizá,[*21] K. Moschner,[*22] F. Naqvi,[*23] M. Niikura,[*12] H. Nishibata,[*24] A. Odahara,[*24] R. Orlandi,[*25] Z. Patel,[*26] Zs. Podolyák,[*26] H. Sakurai,[*12] H. Schaffner,[*18] G. Simpson,[*3] K. Steiger,[*16] H. Suzuki,[*1] H. Takeda,[*1] A. Wendt,[*22] A. Yagi,[*24] and K. Yoshinaga[*27]

One of the central features in our understanding of the atomic nucleus is the appearance of magic numbers. Isotopes in their proximity can be described in terms of single-particle interactions with an inert core. Most nuclei, however, lie sufficiently far from magic numbers for collective behaviour to dominate over the single particle structure. In the prolate-oblate transition regions comparable energy minima corresponding to different shapes can lead to shape coexistence and to stable intermediate shapes with different deformations on each axis, so called triaxial nuclei.

An experiment was carried out using at RIBF using a ^{238}U beam with an energy of 345 Mev/u, and an average intensity of $\sim$ 10 pnA and a 555 mg/cm^2 beryllium target. After the target, BigRIPS and ZeroDegree were used for separation and tagging of the nuclei of interest. The secondary beam was implanted into the WAS3ABi silicon detectors. The β-delayed γ-rays were detected with the EURICA[1)] detector array.

The β-delayed γ-ray spectra associated with ^{116}Tc and ^{118}Tc were analysed and interpreted in terms of observables of collectivity[2)]. The energy ratio $R(4/2) = E(4_1^+)/E(2_1^+)$ is one such observable, ranging approximately from the minimum at $R(4/2) = 2$ for spherical nuclei and the maximum $R(4/2) = 3.33$ for rigid rotors. The trends of this ratio as a function of N for Mo, Ru and Pd chains, shown in Fig. 1, indicate that these elements are well deformed in this region. The Pd chain exhibits a relatively stable value around the transitional limit, $R(4/2) = 2.5$, while the Mo chain is closer to the deformed limit and the Ru chain lies in between the former. For the most neutron-rich Ru isotopes the beginning of a shape transition towards sphericity can clearly be seen.

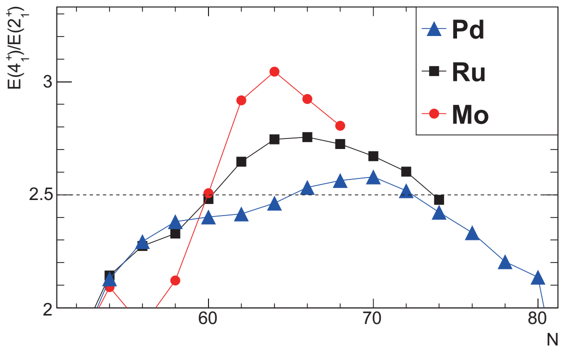

Fig. 1. Experimental $R(4/2)$ ratios. In addition to what was shown in[2)], recent data from[3,4)] have been added to the Pd chain.

Calculations were also carried out for the even-even $^{108-118}$Ru isotopes with the interacting boson model and the algebraic collective model. The conclusions are that the very neutron-rich nuclei still show many features associated with triaxial γ-soft nuclei, represented by the O(6) symmetry, but are approaching a spherical structure, the U(5) symmetry, with increasing neutron number towards the $N = 82$ shell closure.

[†] Condensed from the article in Phys. Rev. C, **88**, 024301 (2013)

[*1] RIKEN Nishina Center
[*2] Department of Physics, Beihang University
[*3] LPSC, Université Grenoble-Alpes, CNRS/IN2P3
[*4] University of Brighton
[*5] ILL, Grenoble
[*6] Department of Physics, Chung-Ang University
[*7] Department of Physics, Tohoku University
[*8] Universidad Autónoma de Madrid
[*9] CSIC, Spain
[*10] Atomki, Debrecen
[*11] School of Physics, Peking University
[*12] Department of Physics, University of Tokyo
[*13] INFN Sezione di Milano
[*14] Department of Physics, Sungkyunkwan University
[*15] Dipartimento di Fisica, Università di Milano
[*16] Technische Universität München
[*17] Institute for Basic Science, Rare Isotope Science Project
[*18] GSI Helmholtzzentrum für Schwerionenforschung
[*19] Nuclear Engineering Division, Argonne National Laboratory
[*20] Australian National University
[*21] CSIC, University of Valencia
[*22] Universität zu Köln
[*23] Wright Nuclear Structure Laboratory, Yale University
[*24] Department of Physics, Osaka University
[*25] Instituut voor Kern en Stralingsfysica, University of Leuven
[*26] Department of Physics, University of Surrey
[*27] Department of Physics, Tokyo University of Science

References

1) S. Nishimura: Prog. Theor. Exp. Phys., **2012**, 03C006 (2012)
2) P.-A. Söderström et al.: Phys. Rev. C, **88**, 024301 (2013)
3) H. Wang al.: Phys. Rev. C, **88**, 054318 (2013)
4) H. Watanabe al.: Phys. Rev. Lett., **111**, 152501 (2013)

Isomer spectroscopy of neutron-rich Nd isotopes

Mn. Tanaka,[*1] E. Ideguchi,[*1] G. Simpson,[*2] R. Yokoyama,[*3] S. Nishimura,[*4] P. Doornenbal,[*4] G. Lorusso,[*4] P.-A.Söderström,[*4] Z.Xu,[*20] J.Wu,[*4,*12] N. Aoi,[*1] H. Baba,[*4] F.Bello,[*5] F. Browne,[*4,*6] R. Daido,[*7] Y. Fang,[*7] N. Fukuda,[*4] G. Gey,[*2,*4,*8] S. Go,[*3,*4] N. Inabe,[*4] T. Isobe,[*4] D. Kameda,[*4] K. Kobayashi,[*9] M. Kobayashi,[*3] T. Komatsubara,[*10] T. Kubo,[*4] I. Kuti,[*11] Z. Li,[*12] M. Matsushita,[*3] S. Michimasa,[*3] C.-B. Moon,[*13] H. Nishibata,[*7] I. Nishizuka,[*14] A. Odahara,[*7] Z. Patel,[*4,*15] S. Rice,[*15] E. Sahin,[*5] L. Sinclair,[*4,*16] T. Sumikama,[*14] H. Suzuki,[*4] H. Takeda,[*4] J. Taprogge,[*17,*18] Zs. Vajta,[*11] H. Watanabe,[*19] and A. Yagi[*7]

Prolate-deformed nuclei are found to appear in the neutron-rich part of the nuclear landscape around $Z = 60$ and beyond $N = 90$, after the systematic studies of excited states. In strongly deformed nuclei, quantum number K is known to be a good quantum number. Since transitions with large changes in K are suppressed, many nuclei in this region have isomeric states. In addition to the quadrupole deformation, appearances of higher-order deformations such as octupole and hexadecupole deformations have been predicted[1]; however, they are not yet understood well. Isomer spectroscopy is a useful method to gain information on such structures of these nuclei.

Neutron-rich $_{60}$Nd isotopes have been investigated by means of isomeric γ-ray spectroscopy. Such isotopes were produced by the in-flight fission of ^{238}U at RI Beam Factory in RIKEN Nishina Center, and were selected and identified by using the BigRIPS separator. The identification of the nuclei was performed on the basis of the ΔE-TOF-$B\rho$ method, which allows an event-by-event determination of their atomic number and the mass-to-charge ratio, where ΔE, TOF, and $B\rho$ denote energy loss, time of flight, and magnetic rigidity, respectively. The identified particles were implanted into passive and active stoppers. A passive stopper made of Cu was used for the measurement at a high count rate, while the WAS3ABi[2] active stopper consisting of five double-sided silicon strip detectors was used for the β-γ spectroscopy. Delayed γ rays were detected by the germanium cluster detector array EURICA[3]. Gamma rays previously known from the 5^- K-isomeric state of ^{156}Nd[4] were observed, and new K-isomeric states of heavier isotopes were discovered.

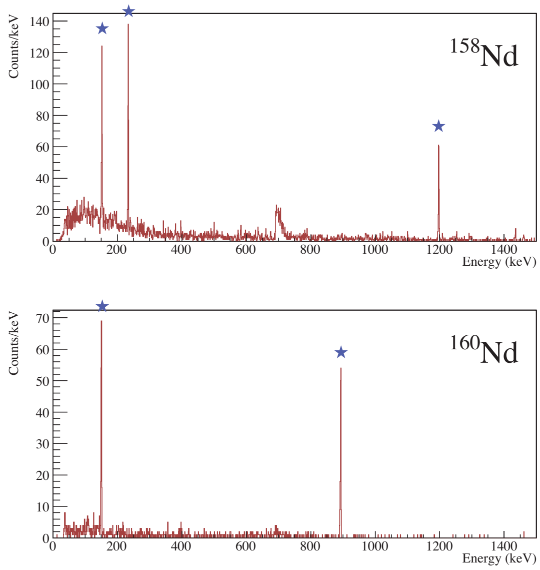

Fig. 1. Gamma-ray energy spectra for $^{158}_{60}$Nd$_{98}$ and $^{160}_{60}$Nd$_{100}$. Marked peaks are the γ rays identified newly. The spread peak at $\sim$ 700 keV comes from (n,n$'$) reaction with Ge.

Figure 1 shows the γ-ray energy spectra of ^{158}Nd and ^{160}Nd using both the passive and active stopper data. We have observed three strong peaks at 151.6, 233.4, and 1198.2 keV for ^{158}Nd, and two strong peaks at 150.2 and 893.0 keV for ^{160}Nd. In both ^{158}Nd and ^{160}Nd, the half-lives of γ rays were preliminarily obtained as 0.339(20) μs and 1.63(21) μs, respectively. From the systematics of Nd isotopes, the energy of the first 2^+ states will be around 70 keV. However, such low-energy γ transition is highly converted, and accordingly, the 70-keV peaks could not be observed. Further analysis to make spin-parity assignments based on the decay pattern and coincidence relations is now in progress.

*1 Research Center for Nuclear Physics, Osaka University
*2 LPSC, Université Grenoble-Alpes, CNRS/IN2P3
*3 Center for Nuclear Study, The University of Tokyo
*4 RIKEN Nishina Center
*5 University of Oslo
*6 The University of Brighton
*7 Department of Physics, Osaka University
*8 ILL, 38042 Grenoble Cedex
*9 Department of Physics, Rikkyo University
*10 University of Tsukuba
*11 MTA Atomki
*12 Peking University
*13 Hoseo University
*14 Department of Physics, Tohoku University
*15 The University of Surrey
*16 University of York
*17 Instituto de Estructura de la Materia, CSIC
*18 Universidad Autónoma de Madrid
*19 Beihang University
*20 Department of Physics, The University of Tokyo

References

1) P. Möller et al.: Atomic Data and Nuclear Data Tables **59**, 185 (1995).
2) S. Nishimura et al.: RIKEN Accel. Prog. Rep. **46**, 182 (2013).
3) S. Nishimura: Prog. Theor. Exp. Phys. 03C006 (2012).
4) G. S. Simpson et al.: Phys. Rev. C **80**, 024304 (2009).

Proton scattering of ^{16}C at 300 MeV/nucleon

S. Terashima,[*1] T. Baba,[*2,*3] Y. Matsuda,[*2,*4] J. Zenihiro,[*2] H. Sakaguchi,[*2,*4] M. Dozono,[*2] T. Furuno,[*2,*3] S. Gotanda,[*2,*5] C.L. Guo,[*1] Y. Kanaya,[*2,*5] T. Kawabata,[*3] Y. Maeda,[*5] H.J. Ong,[*4] S. Ota,[*6] H. Otsu,[*2] W.W. Qu,[*1] H. Sakurai,[*2] M. Tsumura,[*2,*3] T. Uesaka,[*2] J.C. Yang,[*1] and G.L. Zhang[*1]

Neutron-rich carbon isotopes can provide opportunities to study the evolution of nuclear structure up to the neutron drip line. Even-even carbon isotopes have been extensively studied so far. ^{16}C was identified as an exotic structure using lifetime measurement for the first time at RIKEN[1)]. Then, the lifetime of the 2^+ state in ^{16}C was remeasured using different methods including more neutron-rich carbon isotopes, ^{18}C and ^{20}C [2–4)]. The existence of the anomalous behavior of ^{16}C is still under discussion. Proton elastic and inelastic scattering can provide unambiguous optical potential and shape information of the ground state via the coupled channel effect with the deformation parameter $\beta_{pp'}$. In addition, ^{16}C is a first step to develop a neutron skin or neutron halo up to ^{22}C. The angular distribution of elastic scattering is expected to provide us with density distribution information that includes not only the radius but also surface diffuseness.

In April 2013, an experiment the so-called Elastic Scattering of Proton with RI beam (ESPRI) setup was performed at the RIKEN Nishina Center. The ^{16}C beam with an intensity more than 10^5 Hz at approximaately 300 MeV/nucleon was produced in BigRIPS using an ^{18}O primary beam at 345 MeV/nucleon. The incident ^{16}C with a purity of 95% was selected with a set of narrow slits setting ($\pm$2 mm) at F1 and F2, and then, it was transported to the F12 area. The size of the beam spot was $\sigma = 3$ mm (5 mm) in the horizontal (vertical) direction on the secondary solid hydrogen target named SH TRICK (Solid-Hydrogen Target for Recoil detection In Coincidence with INVERSE Kinematics)[5)]. The use of para-H_2 was critical in operating it safely during this experiment for one week.

Further, beam particle identification was perfermed using the energy deposit(ΔE) of a plastic scintillator and beam trajectory using beam tracking detectors at F12. The thickness and effective diameter of the secondary target that was tilted to 45∘ at target center was 1 mm and 20 mm, respectively. The recoil protons were identified using time-of-flight(TOF)-ΔE-E technique by plastic scintillators and NaI(Tl)s; the scattering angle (θ_p) and energy (T_p) of the recoil proton were reconstructed using the tracking detectors, position detectors, total energy calorimeters, and energy loss calculation in passive materials.

Figure 1 shows a kinematical correlation between θ_p and T_p, and the expected kinematical curves of elastic and inelastic scattering (6 MeV). The two strong loci are observed clearly. A line at most intense locus is the ground state, which includes the first excited state. Another line corresponds to a higher inelastic channel. Figure 2 shows an angler distribution of the elastic channel and theoretical calculation using relativistic impulse approximation(RIA) and relativistic Hartree density[6)] as reference. Detailed data analysis for angular distribution of elastic and inelastic channels are currently in progress.

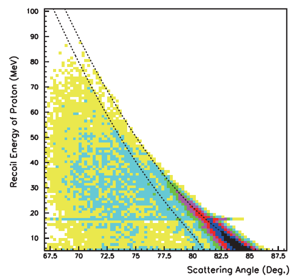

Fig. 1. Kinematical correlation of the p(^{16}C,p) reaction. Dashed lines represent expected kinematical curves of elastic and inelastic scattering.

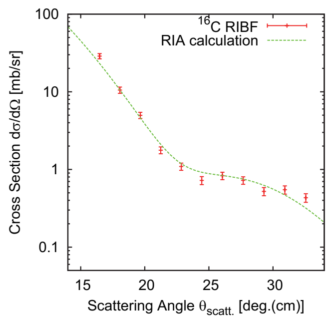

Fig. 2. Preliminary result of angular distribution of elastic channel p(^{16}C,p) with the theoretical calculation using RIA and the relativistic Hartree density[6)].

References
1) N. Imai et. al.: Phys. Rev. Lett. **92**, 062501 (2004).
2) H.J. Ong et. al.: Phys. Rev. C **78**, 014308 (2008),
3) M. Wiedeking et al.: Phys. Rev. Lett. **100**, 152501 (2008),
4) M. Petri et al.: Phys. Rev. Lett. **86**, 044329 (2012).
5) Y. Matsuda et al.: Nucl. Intr. Meth. **A643**, p6 (2011).
6) C.J. Horowiz and B.D. Serot: Nucl. Phys. **A368**, p503 (1981).

*1 School of Physics and Nuclear Energy Technology, Beihang Univeristy, Beijing
*2 RIKEN Nishina Center
*3 Department of Physics. Kyoto University
*4 Research Center for Nuclear Physics, Osaka University
*5 Department of Applied Physics, Faculty of Engineering Miyazaki University
*6 Center for Nuclear Study, University of Tokyo

Structure of ^{19}C studied by one-neutron knockout at SAMURAI

J.W. Hwang,[*1,*2] Y. Satou,[*1] S. Kim,[*1,*2] N. A. Orr,[*3] T. Nakamura,[*4,*2] Y. Kondo,[*4,*2] N. L. Achouri,[*3] T. Aumann,[*5] H. Baba,[*2] F. Delaunay,[*3] P. Doornenbal,[*2] N. Fukuda,[*2] J. Gibelin,[*3] N. Inabe,[*2] T. Isobe,[*2] D. Kameda,[*2] D. Kanno,[*4,*2] N. Kobayashi,[*4,*2] T. Kobayashi,[*6,*2] T. Kubo,[*2] S. Leblond,[*3] J. Lee,[*2] F. M. Marques,[*3] R. Minakata,[*4,*2] T. Motobayashi,[*2] D. Murai,[*7] T. Murakami,[*8] K. Muto,[*6] N. Nakatsuka,[*8] T. Nakashima,[*4,*2] A. Navin,[*9] S. Nishi,[*4,*2] S. Ogoshi,[*4,*2] H. Otsu,[*2] H. Sato,[*2] Y. Shimizu,[*2] H. Suzuki,[*2] K. Takahashi,[*6] H. Takeda,[*2] S. Takeuchi,[*2] R. Tanaka,[*4,*2] Y. Togano,[*10,*13] A. G. Tuff,[*11] M. Vandebrouck,[*12] and K. Yoneda[*2]

The structure of light nuclei near the neutron drip line has been studied extensively over the past decades. With development in experimental technology, heavier nuclei have emerged as a major focus, and a large number of relevant experiments for neutron-rich carbon or more massive nuclei have been conducted. The present work aims to expore neutron-unbound states of ^{19}C by one-neutron knockout. A study exploiting in-beam γ-ray spectroscopy for ^{19}C concluded that $3/2_1^+$ and $5/2_1^+$ states are bound.[1)] A recent report on the inclusive measurement of one-neutron knockout cross section, however, argued that the experimental knockout cross section from ^{20}C to ^{19}C did not support the existence of the $5/2_1^+$ state below the threshold.[2)] In this reserach, the invariant mass measurement in inverse kinematics was carried out, which allows us to elucidate the issue of boundedness of the $5/2_1^+$ state.

The experiment was performed at RIBF. BigRIPS produced a ^{20}C secondary beam with an energy of 280 MeV/nucleon. The beam intensity was 170 cps at the target position with a momentum acceptance of $\Delta P/P = \pm 3\%$. The beam impinged on a carbon target with a thickness of 1.8 g/cm^2, which produced ^{19}C via the one-neutron knockout. The trajectory of the beam was determined with two drift chambers (BDCs). Charged fragments from the reaction were separated using SAMURAI[3)], and their energy loss and time of flight were measured using a hodoscope, which is an array of plastic scintillators. Their momenta were reconstructed from their trajectories with two drift chambers (FDCs) placed before and after the magnet. Momenta of decay neutrons were measured with NEBULA using the TOF method.[4)] The experimental scheme is identical to that of Ref.[5)].

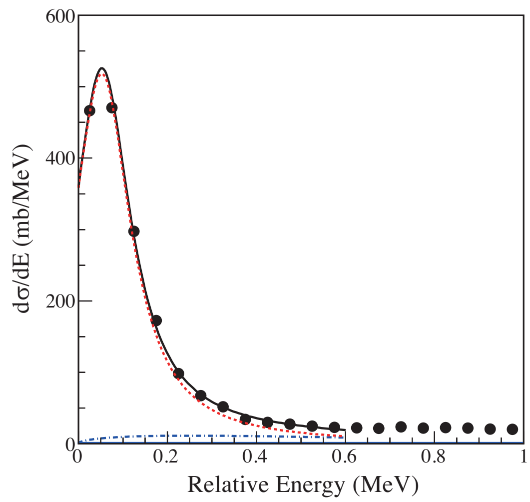

Fig. 1. Relative energy spectrum for the $^{18}\mathrm{C}+n$ unbound system (filled circles). The black solid line is the result of the fit; the blue dash-dot line is the assumed background; the red dashed line is the extracted resonance.

A preliminary spectrum for the relative energy of the C(^{20}C,$^{18}\mathrm{C}+n$) reaction is shown in Fig. 1. Geometrical acceptance was estimated with a Monte-Carlo simulation. The observed resonance close to the threshold is consistent with the result of Thoennessen et al.[6)] A preliminary value for the cross section populating this state was derived, which seems to corroborate the argument that the $5/2_1^+$ state is unbound. A quantitative analysis will be carried out to obtain (1) the position of the resonance and (2) the angular momentum of the knocked-out neutron by examining the parallel momentum distribution of the knockout residue.

*1 Department of Physics and Astronomy, Seoul National University
*2 RIKEN Nishina Center
*3 LPC-Caen, ENSICAEN, Université de Caen, CNRS/IN2P3
*4 Department of Physics, Tokyo Institute of Technology
*5 Institut für Kernphysik, Technische Universität Darmstadt
*6 Department of Physics, Tohoku University
*7 Department of Physics, Rikkyo University
*8 Department of Physics, Kyoto University
*9 GANIL, CEA/DSM-CNRS/IN2P3
*10 ExtreMe Matter Institute (EMMI) and Research Division, GSI
*11 Department of Physics, University of York
*12 Institut de Physique Nucléaire, Université Paris-Sud, IN2P3-CNRS
*13 Present address:Department of Physics, Tokyo Institute of Technology

References

1) Z. Elekes et al.: Phys. Lett. B **614**, 174 (2005).
2) N. Kobayashi et al.: Phys. Rev. C **86**, 054604 (2012).
3) T. Kobayashi et al.: Nucl. Instr. Meth. B **317**, 294 (2013).
4) Y. Kondo et al.: RIKEN Accel. Prog. Rep. **45**, 131 (2012).
5) Y. Kondo et al.: RIKEN Accel. Prog. Rep. **46**, 6 (2013).
6) M. Thoennessen et al.: Nucl. Phys. A **912**, 1 (2013).

Exploration of cluster structure on neutron rich nuclei ^{16}C with SAMURAI magnetic spectrometer

H. Otsu,[*1] M. Kurata-Nishimuira,[*1] Y. Togano,[*3] Y. Shimizu,[*1] H. Sato,[*1] T. Isobe,[*1] H. Baba,[*1] M. Sasano,[*1] S. Takeuchi,[*1] P. Doornenbal, [*1] N. Fukuda,[*1] K. Kusaka,[*1] J. Ohnishi,[*1] K. Yoneda,[*1] T. Motobayashi,[*1] J. Zenihiro,[*1] J. Lee,[*1] H. Liu,[*1] H. Sakurai,[*1] T. Kobayashi,[*2] K. Sekiguchi,[*2] N. Chiga,[*2] T. Sumikama ,[*2] K. Muto,[*2] Y. Wada,[*2] Y. Kondo,[*3] R. Minakata,[*3] S. Ogoshi,[*3] T. Nakamura,[*3] Y. Satou,[*4] J. Hwang,[*4] Y. Matsuda,[*5,*14] T. Murakami,[*5] N. Nakatsuka,[*5] T. Kawabata,[*5] J. Gibelin,[*6] S. Leblond,[*6,*1] N. Kobayashi,[*7] M. Niikura,[*7] M. Matsushita,[*8,*1] E. Yu. Nikolskii,[*9,*1] S. Sakaguchi,[*10] D. Beaumel,[*11,*1] A. Navin,[*12] V. Lapoux,[*13] and M. Itoh[*14]

The highly excited states in weakly bound unstable nuclei have been attracting considerable interest recently. In particular, an important question is whether alpha-cluster degree of freedom emerges near the threshold in unstable nuclei as in stable nuclei. For stable nuclei, the Ikeda diagram predicts such threshold cluster states, and many experimental evidences have been reported[1]. However, this threshold-rule has not been examined for unstable nuclei.

The present study is aimed at searching cluster states in the neutron-rich nucleus ^{16}C through α inelastic scattering at incident energy of 200 MeV/nucleon. Such a technique has been successfully applied on various stable isotopes[2].

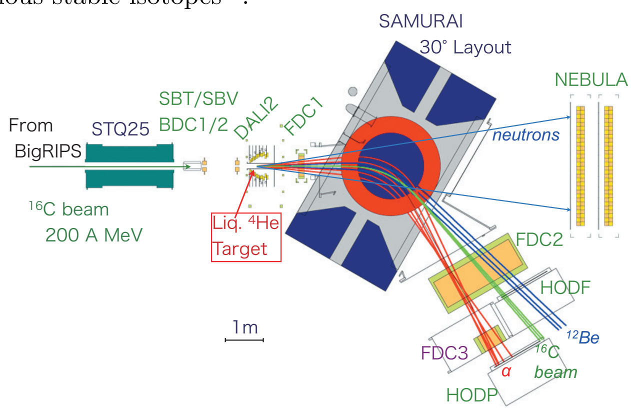

Fig. 1. Experimental setup. Detectors on the SAMURAI focal plane are arranged for α + residual particle detection.

A secondary beam of ^{16}C at 200 MeV/u and an intensity of 2×10^5 Hz is impinged on a 7 mm thick cryogenic liquid ^{4}He target[3]. The experiment was performed by using the SAMURAI spectrometer[4]. The large momentum acceptance property enables us to detect A/Z=3 particle and A/Z=2 particle including α simultaneously. The experimental setup is shown in Fig.1. The setup is similar to that used for the SAMURAI Day–one experiments[5]. The A/Z=2 particles were detected using A/Z=2 arm consisting of FDC3 and HODP. The A/Z=3 particles were detected using FDC2 and HODF (A/Z=3 arm). The correlation between ΔE and detector ID of HOD gated by the α particle in the A/Z=2 arm is shown in Fig.2, where ^{11,12}Be arising from the breakup of ^{16}C can be clearly identified.

From the measured four momenta of α particle and the corresponding Be isotopes, the invariant mass of ^{16}C* will be reconstructed. For such a purpose, multiple track reconstruction techniques on drift chambers have been developed[6]. The analyses of the data are in progress.

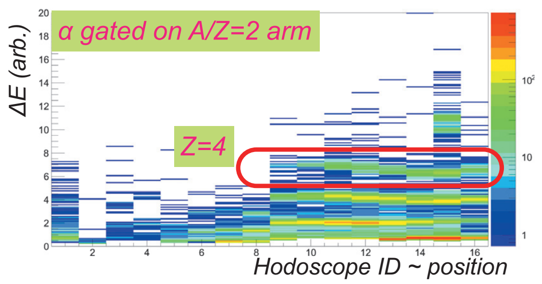

Fig. 2. Particle identification on SAMURAI focal plane. $Z=4$ particles are identified on A/Z=3 arm in coincidence with α particles, which are gated on the A/Z=2 arm.

In summary, we first measured the α dissociation channel on excited ^{16}C using the SAMURAI spectrometer. Our future scope will focus on sd shell neutron rich nuclei such as $^{26-30}$Ne.

*1 RIKEN Nishina Center
*2 Department of Physics, Tohoku University
*3 Department of Physics, Tokyo Institute of Technology
*4 Department of Physics, Seoul National University
*5 Department of Physics, Kyoto University
*6 LPC Caen
*7 Department of Physics, The University of Tokyo
*8 CNS, The University of Tokyo
*9 National Research Centre "Kurchatov Institute"
*10 Department of Physics, Kyushu University
*11 Institut de Physique Nucl'eaire d' Orsay, IN2P3/CNRS
*12 GANIL, CEA/DSM-CNRS/IN2P3
*13 CEA, Saclay
*14 CYRIC, Tohoku University
*15 RCNP, Osaka University

References

1) M. Freer, Rep. Prog. Phys. 70 (2007) 2149.
2) T. Kawabata et. al., Phys. Lett B 646, 6(2007).
3) M. Kurata-Nishimura, et. al., RIKEN Accel. Prog. Rep. 46(2013)165.
4) T. Kobayashi, et. al., Nucl. Instr. and Meth. B317(2013)294.
5) Y. Kondo, et. al., RIKEN Accel. Prog. Rep. 46(2013)6.
6) M. Kurata-Nishimura, et. al., RIKEN Accel. Prog. Rep. 47, this volume.

Structure study of ^{10}He by ^{11}Li(d,^{3}He) transfer reaction

A. Matta,[*1,*2] D. Beaumel,[*1,*3] H. Otsu,[*3] V. Lapoux,[*4] N.K. Timofeyuk,[*2] N. Aoi,[*3] M. Assie,[*1] H. Baba,[*3] S. Boissinot,[*4] R. Chen,[*3] F. Delaunay,[*5] N. de Sereville,[*1] S. Franchoo,[*1] P. Gangnant,[*6] J. Gibelin,[*5] F. Hammache,[*1] C. Houarner,[*6] N. Imai,[*7] N. Kobayashi,[*8] T. Kubo,[*3] Y. Kondo,[*8] Y. Kawada,[*8] L.H. Khiem,[*9] M. Kurata-Nishimura,[*3] E.A. Kuzmin,[*10] J. Lee,[*3] J.F. Libin,[*6] T. Motobayashi,[*3] T. Nakamura,[*8] L. Nalpas,[*4] E. Yu. Nikolskii,[*3,*10] A. Obertelli,[*4] E.C. Pollacco,[*4] E. Rindel,[*1] Ph. Rosier,[*1] F. Saillant,[*6] T. Sako,[*8] H. Sakurai,[*3] A. Sanchez-Benitez,[*11,*12] J-A. Scarpaci,[*1] I. Stefan,[*1] D. Suzuki,[*1] K. Takahashi,[*8] M. Takechi,[*3] S. Takeuchi,[*3] H .Wang,[*3] R. Wolski,[*13] K. Yoneda[*3]

All studies in which ^{10}He has been populated by proton removal from ^{11}Li and observed in invariant-mass spectroscopy agree that E $\sim$ 1.2-1.6 MeV[1–4]. Recently, the analysis of the missing-mass spectrum from the transfer reaction ^{8}He(t,p)^{10}He[5] lead to a sizeably higher value, E $\sim$ 2.1 MeV.

Our experiment, performed in July 2010 at the RIKEN RIPS facility, used a secondary beam of ^{11}Li at 50 AMeV on a CD_2 target. At forward angle, a wall of four MUST2 telescopes[6] were coupled with four 20 μm thick silicon detectors in order to perform an E-ΔE identification of the light particles, and separation of ^{4}He and ^{3}He. At zero degree, a fifth MUST2 telescope and a two stages plastic detector were used for identification of heavy residues of reaction in coincidences. In addition a ^{9}Li beam at 50 A.MeV was used to perform a reference experiment populating the ground state of ^{8}He.

The final excitation spectrum of the unbound ^{10}He, reconstructed in coincidence with ^{8}He decay products (Fig.1), exhibits two clean resonances located respectively at 1.3(3) MeV and 6.3(6) MeV above the two neutron threshold, with natural widths of 1.1(6) MeV and 2.7(7) MeV respectively. The associated differential cross sections have been extracted. They are about one order of magnitude smaller than those predicted in standard DWBA calculations. The implication of this reduction and possible explanations, such as the influences of different neutron binding energies, are explored and put into perspective with the measured cross section of the ^{8}He ground state via the ^{9}Li(d,^{3}He) reaction.

The spectrum obtained in coincidence with the ^{6}He decay products (Fig.1) is showing a preferred decay to the ^{6}He+4n channel when possible. This could be inferred to the important role played by the ^{8}He(2+) excited state in the ^{10}He structure, arguing for the development of models beyond the three-body approach.

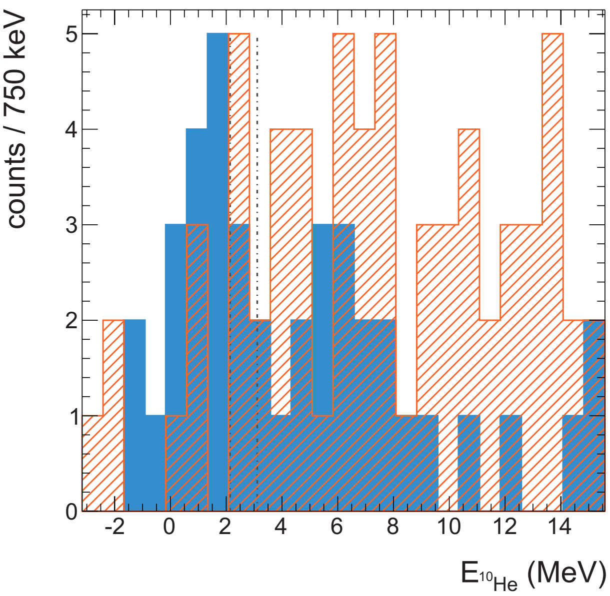

Fig. 1. The ^{10}He spectrum measured from ^{11}Li(d,^{3}He) reaction data in coincidences between ^{3}He and ^{8}He *(solid blue)* and ^{6}He *(dashed orange)*. The two vertical dashed lines indicate the positions of the ^{6}He+4n and ^{4}He+6n thresholds.

References
1) A. Korsheninnikov *et al*, Phys. Lett. B 326, 31-36 (1994)
2) A. Ostrowski *et al*, Phys. Lett. B 338, 13-19 (1994)
3) T. Kobayashi *et al*, Nucl. Phys. A 616, 223-230 (1997)
4) H. Johansson *et al*, Nucl. Phys. A 847, 66-88 (2010)
5) M. Golovkov *et al*, Phys. Lett. B 672, 22 29 (2009)
6) E. Pollacco *et al*, Eur. Phys. Jour. A 25, 287-288 (2005)

*1 Institut de Physique Nucléaire, IN2P3-CNRS
*2 Department of Physics, University of Surrey
*3 RIKEN Nishina Center
*4 CEA, Centre de Saclay, IRFU/Service de Physique Nuclaire
*5 LPC Caen, ENSICAEN, Universit de Caen, CNRS/IN2P3
*6 GANIL, CEA/DSM - CNRS/IN2P3
*7 IPNS,KEK
*8 Tokyo Institute of Technology,O-okayama,Tokyo
*9 Center of Nuclear Physics, Institute of Physics, Vietnam Academy of Science and Technology
*10 National Research Centre “Kurchatov Institute”
*11 Departamento de FA, Universidad de Huelva
*12 Centro de Física Nuclear da Universidade de Lisboa
*13 Institute of Nuclear Physics PAS

New isotope candidates, ^{215}U and ^{216}U

Y. Wakabayashi,[*1] K. Morimoto,[*1] D. Kaji,[*1] H. Haba,[*1] M. Takeyama,[*1,*2] S. Yamaki,[*1,*3] K. Tanaka,[*1,*4] K. Nishio,[*5] M. Asai,[*5] M. Huang,[*1] J. Kanaya,[*1] M. Murakami,[*1,*6] A. Yoneda,[*1] K. Fujita,[*7] Y. Narikiyo,[*7] T. Tanaka,[*7] S. Yamamoto,[*7] and K. Morita[*1,*7]

Theory[1]) predicts that nuclei with $N = 126$ exist up to Fm($Z = 100$) because of the appearance of the fission barrier originating from the ground-state shell correction. The heaviest $N = 126$ nuclei reported so far is ^{218}U($Z = 92$). In this paper, we attempt to produce heavier nuclei such as ^{220}Pu. In our experiment, we observed a new isotope, ^{216}U, which is the daughter nucleus of ^{220}Pu.

We performed an experiment at the RIKEN Linear Accelerator (RILAC) facility. We used ^{82}Kr beams of 372 and 387 MeV to bombard a rotating $BaCO_3$ target foil having a thickness of approximately 400 μg/cm^2. To determine the efficient reaction for the production of ^{216}U, we studied the reaction ^{82}Kr + ^{136,137,138}Ba leading to the same nucleus ^{216}U with different neutron evaporation channels. Each ^{136,137,138}BaCO$_3$ target was prepared by sputtering on 0.8–2.3-μm-thick aluminum foils, and they were also covered with 40 μg/cm^2 of aluminum by sputtering. Several 0.8-μm- and 1.1-μm-thick aluminum foils were prepared as the degraders. The beam energies at the center of the target were changed from 344 to 374 MeV by combining backings and degraders to obtain the excitation function. Evaporation residues (ERs) were separated from the beam particles and other reaction products using a gas-filled recoil ion separator (GARIS), and they were implanted into a position-sensitive strip detector (PSD; 58 × 58 mm^2) at the focal plane. Two timing detectors were set in front of the PSD to determine the time-of-flight (TOF) of the ERs. Time information was also used to distinguish between the α-decay events in the PSD and the recoil implantations. A Ge-detector was placed 6 mm behind the PSD for the α-γ coincidence measurement. In this experiment, 1.7×10^{17} and 2.7×10^{17} beam doses were accumulated at 372 MeV and 387 MeV, respectively.

Isotope identification was performed by using an α-decay chain with the help of known α-decay properties (energies and half-lives) of the descendants and the position correlations between the implanted ERs in the PSD and the subsequent α-decays. Figure 1 shows an α-α correlation spectrum obtained in this experiment. In Fig. 1, the candidates of the new isotopes, ^{215}U and ^{216}U, were observed. These α-decay properties and the obtained cross sections are summarized in Table 1. The decay energies and half-lives of these descendants agree well with those of the references. In the future, an additional irradiation experiment will be performed to confirm the production of ^{215}U and ^{216}U.

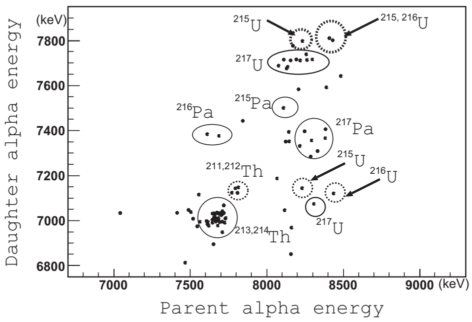

Fig. 1. α-α correlation spectrum. The time difference between the implanted ERs and the parent α-decay, and between the parent and the daughter α-decays were within 150 ms and 2.2 s, respectively. The horizontal and vertical position windows in the PSD were within the same strip (~3.6 mm width) and ±1.5 mm, respectively.

Table 1. α-α correlated events of ^{215}U and ^{216}U. The time and position difference between the implanted ERs and the α-decay are ΔT and ΔX, respectively. E$_{beam}$ represents the ^{82}Kr beam energy at the center of the target.

	E_α (keV)	ΔT	ΔX (mm)	Reaction (E_{beam}) Cross section
^{216}U	8408	6.98 ms	0.15	^{137}Ba+^{82}Kr (365)
^{212}Th	7811	43.4 ms	0.12	→ ^{216}U + 3n
^{208}Ra	7144	2.23 s	1.12	$0.19^{+0.44}_{-0.16}$ nb
^{204}Rn	6424	34.7 s	0.14	
^{215}U	8436	5.82 ms	1.02	^{136}Ba + ^{82}Kr (374)
^{211}Th	7807	29.1 ms	0.72	→ ^{215}U + 3n
^{207}Ra	7124	773 ms	0.36	$0.34^{+0.49}_{-0.22}$ nb
^{203}Rn	6474	45.6 s	2.71	
^{215}U	8230	635 μs	0.35	
^{211}Th	7799	59.9 ms	0.99	
^{207}Ra	7145	1.06 s	0.39	

	E_α (keV) ref.	$T_{1/2}$ ref.	α-decay branch
^{212}Th	7802±10	30^{+20}_{-10} ms	99.7%
^{208}Ra	7133±5	1.3±0.2 s	95%
^{204}Rn	6418.9±0.4	74.4±1.8 s	72.4%
^{211}Th	7792±14	37^{+28}_{-11} ms	~100%
^{207}Ra	7131±4	1.2±0.1 s	≤100%
^{203}Rn	6.499±2	44±2 s	66%

*1 RIKEN Nishina Center
*2 Department of Physics, Yamagata University
*3 Department of Physics, Saitama University
*4 Tokoy University of Science
*5 Japan Atomic Energy Agency
*6 Department of Chemistry, Niigata University
*7 Department of Physics, Kyushu University

References

1) H. Koura and T. Tachibana: Butsuri (in Japanese), 60, 717 (2005).

Production of ^{262}Db in the ^{248}Cm(^{19}F,5n)^{262}Db reaction and decay properties of ^{262}Db and ^{258}Lr[†]

H. Haba,[*1] M. Huang,[*1] D. Kaji,[*1] J. Kanaya,[*1] Y. Kasamatsu,[*2] Y. Kikutani,[*2] H. Kikunaga,[*3] Y. Komori,[*2] H. Kudo,[*4] Y. Kudou,[*1] K. Morimoto,[*1] K. Morita,[*1] M. Murakami,[*1] K. Nakamura,[*2] K. Nishio,[*5] K. Ozeki,[*1] R. Sakai,[*1] A. Shinohara,[*2] T. Sumita,[*1] A. Toyoshima,[*5] K. Tsukada,[*5] Y. Wakabayashi, [*1] and A. Yoneda[*1]

We have been developing a gas-jet transport system coupled to GARIS as a novel technique for superheavy element chemistry.[1)] So far, isotopes of element 104, ^{261}Rf, and element 106, ^{265}Sg, have been produced for chemical studies in the ^{248}Cm(^{18}O,5n) and ^{248}Cm(^{22}Ne,5n) reactions, respectively.[1,2)] In this work, we produced element 105, ^{262}Db in the ^{248}Cm(^{19}F,5n) reaction and investigated its decay properties in detail for future chemical studies of Db.

$^{248}Cm_2O_3$ targets with thicknesses of 230, 290, and 330 µg cm^{-2} were prepared by electrodeposition onto a 2-µm Ti foil. The $^{19}F^{6+}$ or $^{19}F^{9+}$ ion beam was extracted from RILAC. The beam energies were 103.1 and 97.4 MeV at the middle of the target, and the typical beam intensity was 4 particle µA. The evaporation residues (ERs) separated by GARIS were guided into the gas-jet chamber through a 0.5-µm-thick Mylar window, which was supported by a grid with 84% transparency. Several magnetic rigidities were investigated in $B\rho$ = 1.73–2.09 Tm at a He pressure of 33 Pa; the optimal collection efficiency for ^{262}Db was 8.1 ± 2.2% at $B\rho$ = 1.89 Tm. The ERs were then transported by a He/KCl gas jet to the rotating-wheel apparatus MANON for α/SF spectrometry. In MANON, aerosol particles were deposited on a Mylar foil of 0.5-µm thickness, 40 of which were set on the periphery of a rotating wheel. The wheel was stepped at 15.5 s intervals to position the samples between 15 pairs of Si PIN photodiodes.

We searched for time-correlated α_1-α_2 event pairs in the time window of 58.5 s and in the energy range of 8.0 MeV ≤ E_α ≤ 9.0 MeV. As a result, 71 and 4 α_1-α_2 pairs were found at 103.1 and 97.4 MeV, respectively. By referring to the α-particle energies (E_α) and half-lives ($T_{1/2}$) adopted for ^{262}Db and its daughter ^{258}Lr,[3)] 74 α_1-α_2 were reasonably assigned to ^{262}Db → ^{258}Lr →. One exceptional α_1-α_2 pair at 103.1 MeV was ^{261}Db → ^{257}Lr → *via* the ^{248}Cm(^{19}F,6n) reaction. No α_1-α_2 pair on ^{263}Db produced in the ^{248}Cm(^{19}F,4n) reaction (^{263}Db → ^{259}Lr →) was observed. We also observed two SF events that correlated with the α decays with energies and decay times of ^{262}Db. This suggests that small SF and/or EC branches exist in ^{258}Lr; the EC decay daughter of ^{258}Lr, ^{258}No, is a short-lived SF decaying nuclide with $T_{1/2}$ ≈ 1.2 ms and b_{SF} = 100%.[3)] On the basis of the semi-empirical systematics of nuclear mass and half-lives, the EC decay would be favored in ^{258}Lr next to the α decay.[4)]

The observed decay patterns of ^{262}Db and ^{258}Lr are shown in Fig. 1. The α-particle energies of E_α = 8.46 ± 0.04 (α intensity I_α = 70 ± 5%) and 8.68 ± 0.03 MeV (30 ± 5%) were determined for ^{262}Db, though three energies of E_α = 8.45 (75%), 8.53 (16%), and 8.67 (9%) had been adopted.[3)] The half-life of ^{262}Db was measured to be $T_{1/2} = 33.8^{+4.4}_{-3.5}$ s, and this agrees well with $T_{1/2}$ = 34 ± 4 s in Ref.[3)] In this work, the SF activity with $T_{1/2}$ = 30.2 ± 6.1 s was also assigned to ^{262}Db with a SF branch of b_{SF} = 52 ± 4%. This is larger than the currently adopted b_{SF} = ~33%.[3)] On the other hand, the α-particle energies of ^{258}Lr range from E_α = 8.43 to 8.73 MeV and the average α energy of E_α = 8.61 MeV agrees well with E_α = 8.605 MeV deduced from the α energies and intensities of ^{258}Lr in Ref.[3)] The half-life of ^{258}Lr, $T_{1/2} = 3.54^{+0.46}_{-0.36}$ s also agrees with that in Ref.[3)] ($T_{1/2} = 3.9^{+0.4}_{-0.3}$ s). The EC branch in ^{258}Lr was first determined to be b_{EC} = 2.6 ± 1.8%. The cross sections for the ^{248}Cm(^{19}F,5n)^{262}Db reaction were 2.1 ± 0.7 nb at 103.1 MeV and $0.23^{+0.18}_{-0.11}$ nb at 97.4 MeV, while those for the ^{248}Cm(^{19}F,4n)^{263}Db reaction were the upper limits of ≤ 0.064 nb at 103.1 MeV and ≤ 0.13 nb at 97.4 MeV.

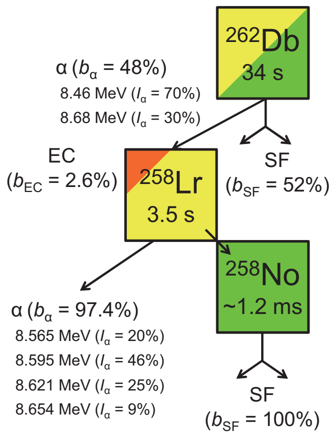

Fig. 1. Observed decay patterns for the chain ^{262}Db → ^{258}Lr → (^{258}No →). The α-particle energies and intensities (I_α) of ^{258}Lr and all decay data of ^{258}No are taken from Ref.[3)]

† Condensed from the article in Phys. Rev. C **89**, 024618 (2014).

*1 RIKEN Nishina Center
*2 Graduate School of Science, Osaka University
*3 Research Center for Electron Photon Science, Tohoku University
*4 Department of Chemistry, Niigata University
*5 Advanced Science Research Center, JAEA

References

1) H. Haba et al.: Chem. Lett. **38**, 426 (2009).
2) H. Haba et al.: Phys. Rev. C **85**, 024611 (2012).
3) R. B. Firestone and V. S. Shirley: *Table of Isotopes, 8th ed.* (John Wiley & Sons, New York, 1996).
4) H. Koura: private communication.

Beta-decay properties of neutron-rich Zr isotopes studied by the Skyrme energy-density functional method†

K. Yoshida*1

The study of unstable nuclei has been a major subject in nuclear physics for a couple of decades. The collective mode of excitation emerging in the response of the nucleus to an external field is a manifestation of the interaction among nucleons. Thus, the spin-isospin channel of the interaction and the spin-isospin part of the energy-density functional (EDF), which is crucial for understanding and predicting the properties of unstable nuclei and asymmetric nuclear matter, have been studied in much detail, especially through Gamow-Teller (GT) strength distributions.

The GT strength distribution has been extensively investigated experimentally and theoretically not only because of interest in the nuclear structure but also because β-decay half-lives set a time scale for the rapid-neutron-capture process (r-process), and hence determine the production of heavy elements in the universe. The r-process path is far away from the stability line, and involves neutron-rich nuclei. They are weakly bound and many of them are expected to be deformed according to the systematic Skyrme-EDF calculation[1)].

Recently, β-decay half-lives of neutron-rich Kr to Tc isotopes with $A \simeq 110$ located on the boundary of the r-process path were newly measured at RIBF[2)]. The ground-state properties such as deformation and superfluidity in neutron-rich Zr isotopes up to the drip line have been studied by employing the Skyrme-Hartree-Fock-Bogoliubov (HFB) method, and it has been predicted that Zr isotopes around $A = 110$ are well deformed in the ground states[3)].

To investigate the GT mode of excitation and β-decay properties in the deformed neutron-rich Zr isotopes, we construct a new framework of the deformed HFB + proton-neutron QRPA employing the Skyrme EDF self-consistently in both the static and dynamic levels. Furthermore, the HFB equations are solved in real space for a proper description of the pairing correlations in weakly bound systems and coupling to the continuum states.

The $T = 0$ pairing interaction is effective for the GT excitation in systems where the ground states have the $T = 1$ pairing condensates. In the neutron-rich Zr isotopes under investigation, we find that the $T = 0$ pairing interaction enhances the low-lying GT strengths. The low-lying GT strength distribution strongly affects the β-decay rate. Thus, we can clearly see the effect of $T = 0$ pairing in the β-decay life time. We can calculate the β-decay half-life $T_{1/2}$ with Fermi's golden rule by using the GT strength distributions microscopically obtained in the self-consistent pnQRPA framework.

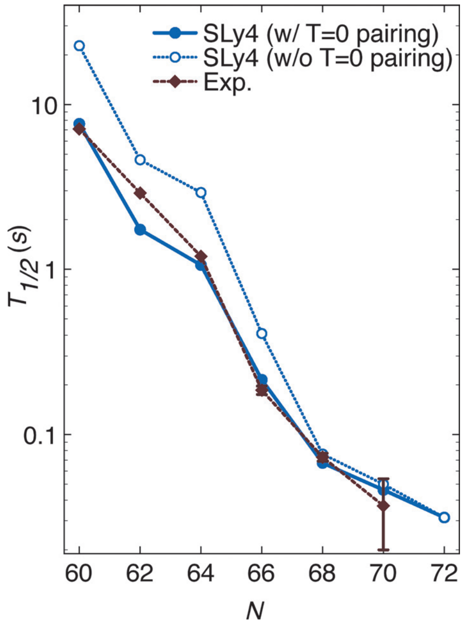

Fig. 1. Experimental and theoretical β-decay half-lives of the Zr isotopes, calculated by employing the SLy4 EDF combined with and without the $T = 0$ pairing interaction.

Figure 1 shows the β-decay half-lives of the Zr isotopes calculated with the SLy4 EDF combined with and without the $T = 0$ pairing interaction. We see that the attractive $T = 0$ pairing interaction substantially shortens the β-decay half-lives. β-decay rates depend primarily on the Q_β value, the residual interactions in both the p-h and p-p channels, and the shell structures. The framework developed here self-consistently treats these key ingredients on the same footing. Once the strength of the $T = 0$ pairing interaction is determined so as to reproduce the observed β-decay half-life of ^{100}Zr, our calculation scheme well produces the isotopic dependence of the half-lives up to ^{110}Zr as was recently observed at RIBF.

† Condensed from the article in Prog. Theor. Exp. Phys. (2013) 113D02

*1 Graduate School of Science and Technology, Niigata University

References

1) M. V. Stoitsov et al.: Phys. Rev. C **68**, 054312 (2003).
2) S. Nishimura et al.: Phys. Rev. Lett. **106**, 052502 (2011).
3) A. Blazkiewicz et al.: Phys. Rev. C **71**, 054321 (2005).

Heavy-quark measurement using distance of closest approach analysis

R. Akimoto,[*1,*2] Y. Akiba,[*1] H. Asano,[*1,*3] T. Hachiya,[*1] M. Kurosawa,[*1] M. Shimomura,[*4] and the PHENIX VTX group

Heavy quarks (charm and bottom) can be used as probes to study the interaction between partons and a quark-gluon plasma (QGP). Heavy quarks are created by initial hard scattering, and thus, the changes intheir properties when passing through the QGP can be clearly extracted from their final states.

Separate measurements of modifications for charm and bottom quarks are informative because the dependence of the modification on the quark mass can be evaluated. The separation of charm and bottom quarks can be achieved by the analysis of the distances between the tracks and the beam collision vertex (DCA). The DCA distributions of bottomed hadrons are wider than those of charmed hadrons because the lifetimes of bottomed hadrons are considerably longer than those of charmed hadrons.

In this study, electrons and positrons from heavy-quark decay were measured[a], and the yields of charm and bottom quarks were evaluated by fitting the DCA distribution in the XY plane[b]. We updated the following items from the previous results reported in ref.[1]:

- Optimization of cut parameters for the isolation cut, which is explained in ref.[1].
- Evaluation of contributions of electrons from heavy quarkonia such as J/ψ.
- Evaluation of a systematic error from uncertainties of transverse momentum (p_T) distributions of charm and bottom quarks.

Owing to the optimization, the purity of heavy-quark electrons in inclusive electrons is increased to more than 50% where p_T is larger than 1 GeV/c. The left panel of Fig. 1 shows the S/N ratio, which is defined as the yield of heavy-quark electrons divided by that of the others. The solid and open circles represent the S/N ratios as a function of electron p_T with and without the isolation cut, separately. The contribution from heavy quarkonia was evaluated by using their cross sections[2]. The right panel of Fig. 1 shows the yield fractions of electron components in inclusive electrons. The brown points represent the contributions of heavy-quarkonium decay. The contribution of heavy quarkonia is ~15% in inclusive electrons at $p_T > 3$ GeV/c. The systematic error from the uncertainties of p_T distributions of charm and bottom quarks was evaluated using the distributions obtained from a PYTHIA simulation and FONLL calculation[3] and was found to be ~50% for all p_T ranges.

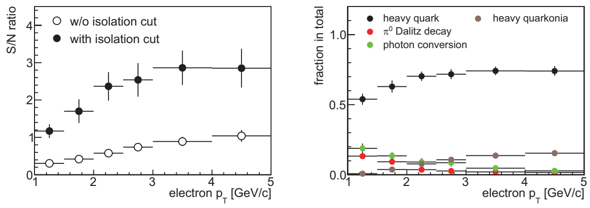

Fig. 1. S/N ratio (left) and yield fractions of electron components in inclusive electrons (right). The black, red, green, and brown points in the right panel represent the fractions of heavy-quark electrons, electrons from π^0 Dalitz decay, electrons from photon conversion, and electrons from decay of heavy quarkonia, respectively.

Figure 2 shows a comparison of the bottom fractions in heavy-quark electrons as a function of electron p_T before and after the updates for p+p collisions with $\sqrt{s}$ = 200 GeV. The open and solid circles indicate the fractions before and after the updates, respectively. The result after the updates is consistent with that before the updates. The increase in the systematic error is due to the error from the uncertainties of p_T distributions of charm and bottom quarks.

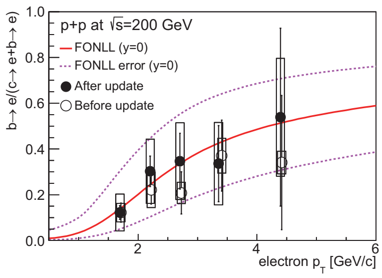

Fig. 2. Bottom fractions in heavy-quark electrons. The open and solid circles indicate the fractions before and after the updates. The bars and squares represent statistical and systematic errors, respectively. The solid line indicates the result of FONLL calculation at rapidity $y = 0$, and the dashed lines indicate the boundaries of the error band for the calculation.[3]

*1 RIKEN Nishina Center
*2 Center for Nuclear Study, Graduate School of Science, University of Tokyo
*3 Kyoto University
*4 Iowa State University

a) Electrons and positrons from heavy-quark decay are called heavy-quark electrons.

b) The XY plane is defined as the plane perpendicular to the beam axis, and the Z direction is defined as the direction along the beam axis.

References

1) R. Akimoto *et al.*: RIKEN Accel. Prog. Rep. **46**, 60 (2012).
2) A. Adare *et al.*: Phys. Rev. D **85**, 092004 (2012).
3) M. Cacciari *et al.*: Phys. Rev. Lett. **95**, 122001 (2005).

Search for a dark photon in π^0 Dalitz decays by PHENIX experiment at RHIC

Y. Akiba*[1] and Y. Yamaguchi*[2] for PHENIX Collaboration

Several models of dark matter suggest the existence of a "dark photon," an $U(1)$ gauge boson in the dark matter sector that mixes with an ordinary photon[1]). In these models, a dark photon is responsible for annihilation of a pair of dark matter particles into an e^+e^- pair. Such annihilation can explain the positron excess observed by PAMELLA, FERMI, and AMS-2 satellite experiments. A dark photon can also explain the 3 σ level deviation of the anomalous magenetic moment of the muon (muon $g-2$) from the Standard Model calculation.

In the simplest version of these models, a dark photon U mixes with a QED photon γ with a very small mixing term of the Lagrangian

$$\mathcal{L}_{\rm mix} = -\frac{\epsilon}{2} F^{\rm QED}_{\mu\nu} F^{\mu\nu}_{\rm dark},$$

where ϵ is the mixing parameter.

The dark photon can have a small mass M_U. If M_U is greater than twice the electron mass m_e, it can decay into an e^+e^- pair. In the natural version of the model, this is the only decay mode. This means the following:

(1) A dark photon can be produced in any process that can produce virtual photon with a small fraction ϵ^2.
(2) Once produced, it decays exclusively into an e^+e^- pair.
(3) The decay width of dark photon is very narrow and practically zero due to the small coupling ϵ^2

Therefore, if the mass of the dark photon is less than that of π^0, a clear signal of dark photon should show up as a narrow peak in e^+e^- pair mass spectrum of π^0 Dalitz decays $\pi^0 \to e^+e^-\gamma$.

We searched for the signal of dark photon in π^0 Dalitz decay data measured by PHENIX experiment at RHIC. PHENIX is very well suited for this search since it has a very good electron identification capability, a high mass resoluiton of low mass e^+e^- pairs, and a high statistics data sample of π^0 Dalitz decay. We used the data set of $p+p$ collision in 2006 run and d+Au collisions in 2008 run, both at $\sqrt{s_{NN}}$ = 200 GeV. We analyzed approximately 1.3 million e^+e^- pairs for the search.

We did not find any significant peak in the Dalitz pair mass spectrum. Thus, we set the upper limit on the mixing parameter ϵ^2 as a function of dark photon mass M_U from our null search result. In setting the upper limit, we employed the CLs method, a statistical method now widely used by the LHC experiments for new particle searches.

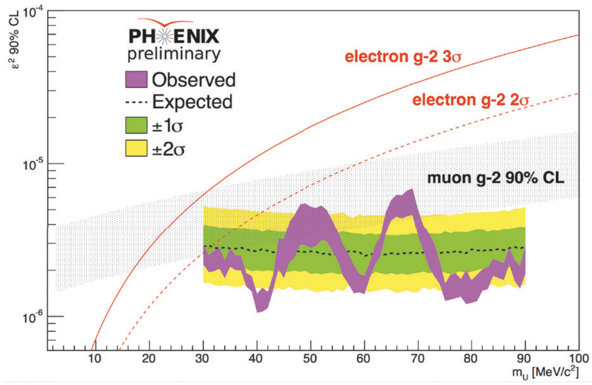

Fig. 1. Limit on the dark photon mixing parameter ϵ^2 as a function of dark photon mass. See the text for details.

The preliminary results of the search is shown in Fig.1. The magenta band shows the observed 90 % CL upper limit on ϵ^2. The width of the band represents the systematic uncertainty of the limit. The fluctuation of the limit is due to statistical fluctation of the background continuum, i.e., Dalitz pair mass spectrum. If the background e^+e^- mass spectrum fluctuate up (down), the upper limit on the dark photon becomes higher (lower). The dashed curve represents the "expected level" of the upper limit if there is no such statistical flucutation. The green and yellow bands are expected statistical fluctuation of the upper limit at 1σ and 2σ level, respectively. The fluctuation of the observed limit is within approximately 2σ level.

The gray band in the figure shows the 90 % CL region that can explain the muon $g-2$ deviation. The dashed curve shows the upper limit on ϵ^2 from electron $g-2$ at 2σ level. Together with the limit from electron $g-2$, our results have excluded almost all region of the muon $g-2$ band.

We are now working to finalize the data. We will publish the final results soon.

References

1) Nima Arkani-Hamed et al., Phys. Rev. D79: 015014 (2009).

*1 RIKEN Nishina Center
*2 CNS, University of Tokyo

Primordial spectra from sudden turning trajectory†

T. Noumi*1 and M. Yamaguchi*2

Inflation is strongly supported by recent observations of cosmic microwave background (CMB) anisotropies.[1,2] In particular, single field slow-roll inflation predicts almost adiabatic, Gaussian, and scale invariant primordial curvature perturbations, and these predictions well fit the observational results. On the other hand, high energy theories such as supergravity and superstring theory generically predict additional scalar fields other than inflaton. To reconcile such a generic prediction of theories with recent observations, it may be suggested that only one light field plays a role of inflaton while the others are heavy. In fact, effects of such heavy fields are generically suppressed by their mass and the inflationary dynamics can be well approximated by single field inflation.

While such a scenario can explain the current observational results well, it would be quite interesting if we could detect some deviation from single field slow-roll inflation in the current and future observational experiments: such a deviation would be useful as a probe of high energy physics. In this report, we would like to investigate a possibility that heavy fields can affect inflationary dynamics and imprint some features on primordial spectra.

One typical situation heavy fields matter is the case when heavy fields are excited by the sudden turn of the potential and oscillates with high frequency.[3–7] In general, oscillations of heavy fields generate the following two significant effects: the modification of the Hubble parameter and the conversion effect, that is, the mixing between adiabatic and isocurvature (heavy field) modes. We investigate these effects in detail and evaluate the power spectra and bispectra of the primordial curvature perturbations in two-field inflationary models with the canonical kinetic terms and a sudden turning potential.

Suppose that the background trajectory is first along the bottom of the potential (the slow-roll direction). The trajectory starts oscillating at the turning point and such a heavy field oscillation induces a deviation from single field slow-roll inflation. The primordial power spectrum of scalar curvature perturbations can then be calculated as

$$\mathcal{P}_\zeta(k) = \frac{H_{\rm sr}^2}{8\pi^2 M_{\rm sr}^2 \epsilon_{\rm sr}} \left[1 + \mathcal{C}_{\rm Hubble}(k) + \mathcal{C}_{\rm conv}(k)\right], \quad (1)$$

where the first term represents the almost scale-invariant power spectrum in single field slow-roll inflation. The last two terms are the scale-dependent deviation originated from the heavy field oscillations.

† Condensed from the article in JCAP 1312 (2013) 038

*1 RIKEN Nishina Center

*2 Department of Physics, Tokyo Institute of Technology

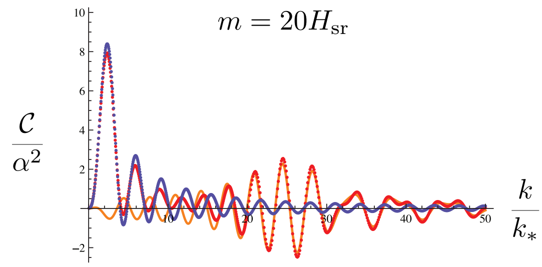

Fig. 1. Deviation in the primordial power spectrum. The orange/red/blue are $-\mathcal{C}_{\rm Hubble}$, $\mathcal{C}_{\rm conv}$, and $\mathcal{C} = \mathcal{C}_{\rm Hubble} + \mathcal{C}_{\rm conv}$, respectively. Free parameters of our model are the heavy field mass m, the turning angular α, and the turning scale k_*. Here we used $m = 20_{\rm sr}$ and assumed that α is small enough, say $\alpha \sim \mathcal{O}(0.1)$.

The deviation $\mathcal{C}_{\rm Hubble}$ is from the Hubble deformation effect and $\mathcal{C}_{\rm conv}$ is from the conversion effect. As depicted in Fig. 1, the parametric resonance amplification occurs from both of the two effects and the peak at the turning scale arises from the conversion effect. It is, however, explicitly shown that resonance effects from the two effects accidentally cancel each other out for the case with the canonical kinetic terms. As a consequence, the peak at the turning scale becomes clear and this feature characterizes this class of models with heavy field oscillations.

We also evaluated primordial bispectra, whose main source comes again from the Hubble deformation effect and the conversion interaction. We find resonance and peak features in the bispectra as in the case of power spectra. Although the size of bispectra is not necessarily large, our results may be useful for probing these effects observationally.

In this work, we discussed two-field models with a sudden turning potential as a phenomenological toy model, and clarified features of heavy field oscillations. It would be interesting to investigate more realistic models with heavy field oscillations e.g. based on string theory. It must be important to discuss their detectability in the current and future observations.

References

1) G. Hinshaw *et al.*: arXiv:1212.5226.
2) P. A. R. Ade *et al.*: arXiv:1303.5082.
3) X. Chen: JCAP **1201**, 038 (2012).
4) G. Shiu and J. Xu: Phys. Rev. D **84**, 103509 (2011).
5) S. Cespedes, V. Atal and G. A. Palma: JCAP **1205**, 008 (2012).
6) A. Achucarro, J. -O. Gong, S. Hardeman, G. A. Palma and S. P. Patil: JHEP **1205**, 066 (2012).
7) X. Gao, D. Langlois and S. Mizuno: JCAP **1210**, 40 (2012).

Sudden termination of high-energy γ rays detected from thunderclouds before lightning[†]

H. Tsuchiya,[*1,*2] T. Enoto,[*1,*3] K. Iwata,[*4] S. Yamada,[*1] T. Yuasa,[*5] T. Kitaguchi,[*1] M. Kawaharada,[*5] K. Nakazawa,[*6] M. Kokubun,[*5] H. Kato,[*1] M. Okano,[*1] T. Tamagawa,[*1] and K. Makishima[*6,*7]

Observations of prolonged γ rays emitted from thunderclouds are important for understanding how relativistic electrons are produced there. Recently, the Gamma Ray Observation of Winter Thunderclouds (GROWTH) experiment, successfully operated mainly by RIKEN and the University of Tokyo at the Kashiwazaki-Kariwa nuclear power plant since December 2006, has been conducting an increasing the number of prolonged γ-ray observations. Here we report one particular event wherein γ-ray emission suddenly terminated immediately before a lightning flash.

At ~13:30 universal time (UT) on December 30, 2010 (22:30 local time), the GROWTH system of daq0 and daq1, consisting mainly of NaI counters, detected γ-ray increases lasting for ~3 min. Figure 1 shows the enhancements, together with those obtained by radiation monitoring posts (MPs) operated by the Tokyo Electric Power Company. The observed duration is consistent with previous GROWTH events[1,2]. Importantly, only three MPs located within ~1 km of the GROWTH system clearly detected the radiation bursts, while the remaining MPs (1–6) observed no increases with statistical significance $>2\sigma$. This means that the horizontal extent of γ-ray emission on the ground was within ~1 km at most.

A lightning event was recorded by our optical sensor and electric field mill at 13:35:55 UT (dashed line in Fig. 1). It is noted that a γ-ray termination seemingly coincided with the lightning occurrence. Interestingly, the Japan Lightning Detection Network system (Franklin Japan Co. Ltd.) registered no lightning within 5 km of our site between 13:05 and 14:05 UT. Thus, the termination is thought to be related to lightning that occurred >5 km away from the site.

As shown in Fig. 2, a notable feature of this event is that the γ-ray termination occurred not in an exact coincidence with the lightning, but 800 ms prior to it. In addition, it is obvious that only >3 MeV γ-ray radiation ceased before the lightning. This finding indicates that production of relativistic electrons to emit >3 MeV γ rays would stop 800 ms before the lightning.

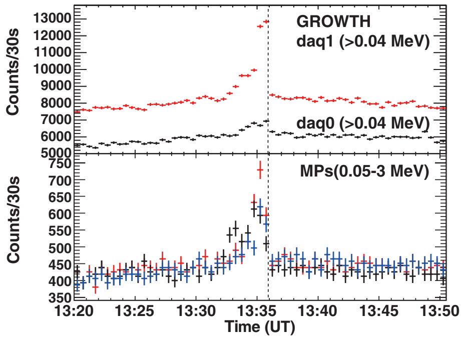

Fig. 1. Count histories per 30 s of the present event, obtained during 13:20–13:50 UT. (Top) The NaI count rates of daq0 and daq1. (Bottom) The NaI count rates of MPs 9 (black), 8 (red), and 7 (blue). The vertical dashed line indicates the lightning occurrence time.

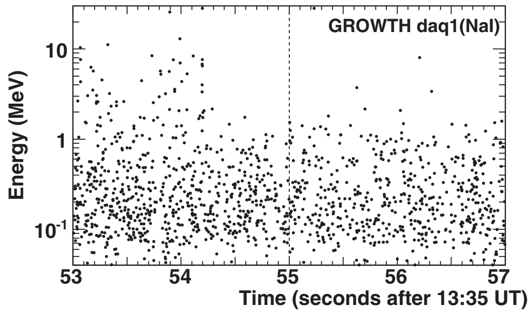

Fig. 2. Photon energies recorded during 13:35:53-13:35:57 UT. The time resolution is 0.1 ms.

Using an aircraft-onboard detector, Mcarthy and Parks[3] observed a similar termination event that follows an x-ray (5–110 keV) increase lasting for ~10 s, and estimated a source length of ~1 km by considering the duration, the aircraft velocity, and an attenuation length of 150 m for 100 keV x rays. It is certain from the present and these results that a local electric field in thunderclouds is enhanced, in a few seconds to minutes, to accelerate electrons and initiate lightning.

In summary, the present event shows that relativistic electrons were continuously produced in a limited acceleration region 800 ms before lightning.

† Condensed from the article in Phys. Rev. Lett., Vol. 111, 015001 (2013)

*1 RIKEN Nishina Center
*2 Japan Atomic Energy Agency
*3 Goddard Space Flight Center, NASA
*4 Shibaura Institute of technology
*5 Department of High Energy Astrophysics, Institute of Space and Astronautical Science, JAXA
*6 Department of Physics, University of Tokyo
*7 MAXI team, RIKEN

References
1) H. Tsuchiya et al.: Phys. Rev. Lett. **99**, 165002 (2007).
2) H. Tsuchiya et al.: J. Geophys. Res. **116**, D09113 (2011).
3) M. P. McCarthy and G. K. Parks: Geophys. Res. Lett. **12**, 393 (1985).

μSR study of Al-Mg, Al-Si and Al-Mg-Si alloys†

K. Matsuda,*[1,*3] K. Nishimura,*[1,*3] S. Wenner,*[2] R. Holmestad,*[2] T. Matsuzaki,*[3] F. L. Pratt,*[4] and C. D. Marioara*[5]

Al–Mg–Si alloys constitute most of the worldwide aluminium market as they have good mechanical strength and are easily formable into end products. An optimal heat treatment of alloys containing merely 1% solutes (Mg and Si) typically increases the hardness by a factor of 5 from pure aluminium. After the material is formed, an industrial hardening procedure consists of solution heat treatment (SHT), typically at 550 deg., some (unavoidable) storage at room temperature (RT) and artificial aging (AA), typically at 180 deg. Al–Mg–Si alloys quenched from SHT are unstable at RT, and atomic clusters (with Mg and Si at Al-fcc positions) form from the supersaturated solid solution.[1,2] The clusters in general are too small and coherent with the Al matrix to be observed by transmission electron microscopy (TEM).

Muons undergo interstitial diffusion inside solids. In aluminium, they have been shown to be trapped by atoms in substitutional lattice positions and by vacancies,[3-5] yielding a lower apparent muon diffusivity. In this work, we exploit this effect and identify the muon trapping behavior of Mg and Si atoms as well as vacancies in different stages of heat treatment of aluminium alloys. Due to its industrial and scientific interest, we study the ternary Al–Mg–Si system, and we also include the binary Al–Mg and Al–Si alloys mainly to isolate the ternary-specific features in the μSR data. Very dilute alloys have been probed with μSR before, and small additions of Si, Mg and Cu were found to greatly affect the muon kinetics.[6] Our previous work on the Al–Mg–Si system revealed the presence of a muon trapping peak corresponding to clustering/precipitation.[4] The main goal of the current work is to establish a connection between muon trapping rates and the microstructure of Al–Mg–Si alloys as found from TEM studies.

Observed muon spin relaxation spectra in zero-field were compared with those from a Monte Carlo simulation using four fitting parameters: the dipolar width (Δ), the trapping rate (ν_t), detrapping rate (ν_d) and the fraction of initially trapped nuons (p_0), assuming that muon spins relaxed with the single Δ value only when they were trapped. This data analysis is similar to those employed by Sato et al.[7] and Hatano et al.[8] The resulting temperature variation of the muon trapping rate is shown for eight selected samples in Fig. 1

We note the following trapping rate characteristics for Al–Mg: 1) heat treatment does not change the muon behavior much in Al–Mg alloys at temperatures up 120K.

† Condensed from the article in Acta Materialia 61, 6082 (2013)

*1 Department of Materials Science and Engineering, U. Toyama
*2 Department of Physics, NTNU
*3 RIKEN Nishina Center
*4 ISIS Facility, RAL
*5 Materials and Chemistry, SINTEF

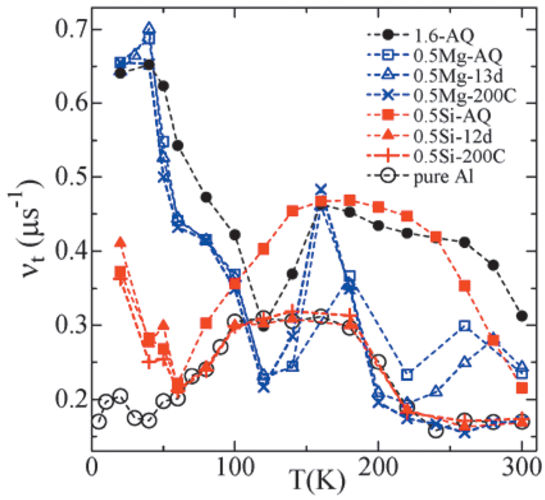

Fig. 1 Muon trapping rates (ν_t) for Al-Mg-Si, Al-Mg, Al-Si alloys and pure Al estimated using simulations.[4,5] The symbol-label of 1.6-AQ denotes the trapping rate with the Al-1.6%Mg_2Si sample quenched after SHT, those of 0.5Mg illustrate the results with the samples of Al-0.5%Mg quenched (0.5Mg-AQ), storage at RT for 13d (0.5Mg-13d), and annealed at 200 deg. for 1000 minutes (0.5Mg-200C), and the same manner used with the samples of Al-0.5%Si. The open circle presents the trapping rate observed with a pure Al (purity is 99.99%).

2) 13d and AQ samples have higher trapping rates than pure Al at temperatures of 240–300 K. This is not the case for the 200C sample. Correspondingly, for Al–Si: 3) the muon behavior in 12d and 200C samples is very similar to that in pure Al, excluding only the lowest temperatures. 4) A significant difference was observed at high temperatures between AQ and 12d (or 200C) samples. 5) The higher trapping rates of 0.5Mg-13d than those of 0.5Si-12d around RT indicate that Mg atoms tend to keep vacancies more than Si atoms.

One of the authors (K. Nishimura) acknowledges JSPS KAKENHI No.25289260.

References

1) K. Matsuda et al., J. Materials Science 35, 179 (2000).
2) S. Kim et al., Materials Transactions 54, 297 (2013).
3) K. W. Kehr et al., Phys. Rev. B26, 567 (1982).
4) S. Wenner et al., Phys. Rev. B86, 104201 (2012).
5) S. Wenner et al., Acta Metrialia 61, 6082 (2013).
6) M. Doyama et al., Hyper. Inter. 17, 225 (1984).
7) E. Sato et al., Hyper. Inter. 17, 203 (1984).
8) T. Hatano et al., Hyper. Inter. 17, 211 (1984).

Investigation of the magnetic states in new spin-tetrahedral $K_4Cu_4Cl_{10}O$[†]

X.G. Zheng,[*1] M. Fujihala,[*1] and I. Watanabe[*2]

Geometrically frustrated magnets, in which localized magnetic moments on triangular, kagome or pyrochlore lattices interact through competing exchange interactions, have recently attracted a lot of interest owing to the diversity in the exotic ground states that they display. Various reports on unconventional magnetic properties provide a challenging and testing ground for theoretical models. Among the several systems reported, the S-1/2 quantum systems have received particular attention.

While much of the kagome and pyrochlore antiferromagnets, which are much more complicated to theoretically model than the triangular lattice, are still not well understood, the isolated spin tetrahedral system with weak inter-tetrahedral couplings has recently attracted attention because it can directly demonstrate the interplay of inter-tetrahedral couplings with the built-in tetrahedral frustration. Of more wide interest, they also represent an interesting class of magnets consisting of weakly coupled magnetic clusters. Till date, the $Cu_2Te_2O_5X_2$ (X = Cl, Br) family and the related compound $Cu_4Te_5O_{12}Cl_4$ have been considered the only real systems of such tetrahedra, but they have remarkable structural anisotropies both inside and outside the tetrahedra, leading to much controversy about their anisotropic magnetic couplings and dimensionality [1-3]. There are several questions that prompt lot of discussion. The most important one is the magnetic dimensionality of the system due to the notable structural anisotropies inside and between the tetrahedra.

Recently, we have synthesized new S-1/2 quantum systems of spin-tetrahedral $K_4Cu_4Cl_{10}O$, where the magnetic moments (Cu^{2+} spins) occupy a three-dimensional tetrahedral lattice, as shown in Fig. 1.

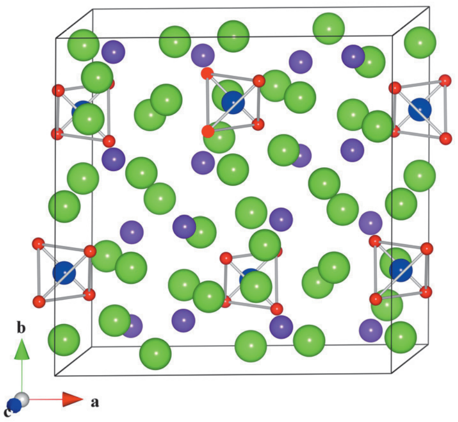

Fig. 1. Tetrahedral lattice in $K_4Cu_4Cl_{10}O$.

The spin-tetrahedral $K_4Cu_4Cl_{10}O$ showed a very broad susceptibility maximum centered around 10 K and a rapid increase below 5 K. μSR measurements for the system were performed at RIKEN-RAL.

For $K_4Cu_4Cl_{10}O$, no change appeared around 10 K, which is consistent with a spin-singlet state theoretically predicted for isolated spin tetrahedral system. Long-range order was observed below 4.4 K (Fig. 2), but with broad distribution in the precession frequency, which is interpreted as evidence for an incommensurate order.

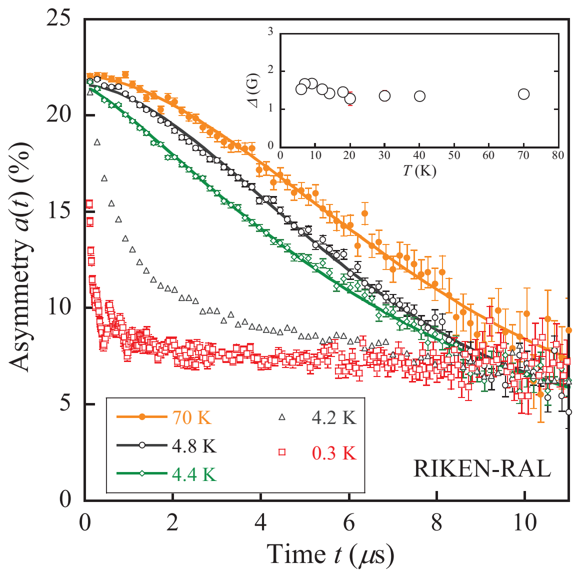

Fig. 2. Zero-field μSR asymmetry spectra at typical temperatures for $K_4Cu_4Cl_{10}O$ obtained from the RIKEN-RAL beam line. The solid lines on the back of the high-temperature data are fitted curves as described in Phys. Rev. B 87, 144425 (2013). The inset plot shows the estimated nuclear field distribution Δ.

Here, our work shows that similar incommensurate ordering also exists in a three-dimensional isolated spin tetrahedral system.

References
1) P. Lemmens, K.-Y. Choi, E. E. Kaul, C. Geibel, K. Becker, W. Brenig, R. Valenti, C. Gros, M. Johnsson, P. Millet, and F. Mila, Phys. Rev. Lett. 87, 227201 (2001).
2) O. Zaharko, A. Daoud-Aladine, S. Streule, J. Mesot, P.-J. Brown, and H. Berger, Phys. Rev. Lett. 93, 217206 (2004).
3) Z. Jagličić, S. El Shawish, A. Jeromen, A. Bilušić, A. Smontara, Z. Trontelj, J. Bonča, J. Dolinšek, and H. Berger, Phys. Rev. B 73, 214408 (2006).

† Condensed from the article in Phys. Rev. B 87, 144425 (2013)

*1 Department of Physics, Saga University
*2 RIKEN Nishina Center

C O N T E N T S

Page

GRAVURE & HIGHLIGHTS OF THE YEAR

4. Hadron Physics

7. Astrophysics and Astro-Glaciology

8. Accelerator

III. RESEARCH ACTIVITIES II (Material Science and Biology)

1. Atomic and Solid State Physics (Ion)

4. Radiation Chemistry and Biology

IV. OPERATION RECORDS

V. EVENTS

VI. ORGANIZATION AND ACTIVITIES OF RIKEN NISHINA CENTER (Activities and Members)

I. PREFACE

Preface

The RIKEN RI Beam Factory has reached its harvest time. From its commissioning in 2006 to 2013, 71 experiments have been performed with ^{238}U, ^{124}Xe, ^{86}Kr, ^{70}Zn, ^{48}Ca, ^{18}O, ^{14}N, and ^{4}He beams from the Superconducting Ring Cyclotron (SRC) and the isotope separator BigRIPS. The SRC recorded its highest ^{238}U current of 25pnA in 2013, a performance far beyond that of any other accelerator facilities in the world. This edition of Accelerator Progress Report highlights the history of RI delivery at the RIBF in its gravure pages. While some are yet unpublished, we should be proud that more than 100 new isotopes have been discovered at the RIBF.

Our RI beams attract many users from all over the world. Following the great success of the EURICA (Euro-Riken Crystal Array) campaign, MINOS, a state-of –the-art setup with a hydrogen target and a vertex detector, arrived from Saclay, France. A large-scale Time Projection Chamber to be installed in the SAMURAI spectrometer has recently arrived from the USA. Furthermore, other detectors like NeuLand (highly segmented neutron time-of-flight counters from Germany) and BRIKEN (hundreds of neutron counters from the USA to surround the target) are to be shipped to the RIKEN RIBF.

To effectively explore new regions in the nuclear chart using such devices, we have introduced a new scheme of experimental proposal, Proposal for Scientific Project. With this new scheme, experimentalists are asked to propose a series of experiments based on common physics interests that uses the same experimental apparatus and targets not just one or two nuclei but a wide region of nuclei.

Under this new scheme, the SEASTAR project employing the MINOS and the DALI2 detectors was established to aim for a systematic search of new 2^+ energies in the wide range of the neutron-rich nuclei accessible with the RIBF's currently available ^{70}Zn and ^{238}U beam intensities. The proposal was approved and the first beam time was already allocated. Somewhat different from our traditional style of proposal, the new scheme requires the experimentalists to form a bigger and tighter collaboration. The Nishina Center appreciates an understanding by all users of the necessity of such an approach, and promises its fair operation to the user community.

As we have now reached the stage to reap the harvest of the RIBF research, many interesting results are being published. In 2013, we issued three press releases on the RIBF experiments, “Discovery of exotic isomers with a magic number”, “Evidence for a new nuclear magic number of 34 --- a key to access a dream region of island-of-stability”, and “Magic numbers’ disappear and expand area of nuclear deformation”. The Nishina Center thanks and congratulates all those involved in these experiments, and is convinced that this trend will continue to grow in the future. It should be noted and appraised that in 2013, prestigious prizes were given to the staffs in our accelerator group for their record-breaking accelerator operation, especially with the gas stripper developments.

Unfortunately, JFY2013 did not close peacefully. The STAP incident, a serious scientific misconduct that occurred at the RIKEN Center for Developmental Biology has affected RIKEN severely. I apologize for any inconveniences you have had to deal with to in complying with RIKEN’s countermeasures. If any similar incident ever occurred at the Nishina Center, the Center would cease to exist. We thus declare that such an incident will never happen in our field.

Hideto En'yo
Director,
RIKEN Nishina Center for Accelerator-Based Science

II. RESEARCH ACTIVITIES I
(Nuclear, Particle and Astro-Physics)

1. Nuclear Physics

Search for isomers in neutron-rich Cs isotopes

A. Yagi,[*1] A. Odahara,[*1] R. Daido,[*1] Y. Fang,[*1] H. Nishibata,[*1] R. Lozeva,[*2] C.-B. Moon,[*3] S. Nishimura,[*4] P. Doornenbal,[*4] G. Lorusso,[*4] P.-A. Söderström,[*4] T. Sumikama,[*5] H. Watanabe,[*6] T. Isobe,[*4] H. Baba,[*4] H. Sakurai,[*7,*4] F. Browne,[*8,*4] Z. Patel,[*9,*4] S. Rice,[*9,*4] L. Sinclair,[*10,*4] J. Wu,[*11,*4] Z.Y. Xu,[*7] R. Yokoyama,[*12] T. Kubo,[*4] N. Inabe,[*4] H. Suzuki,[*4] N. Fukuda,[*4] D. Kameda,[*4] H. Takeda,[*4] D.S. Ahn,[*4] D. Murai,[*13] F.L. Bello Garrote,[*14] J.M. Daugas,[*15] F. Didierjean,[*2] E. Ideguchi,[*16] T. Ishigaki,[*1] H.S. Jung,[*17] T. Komatsubara,[*18] Y.K. Kwon,[*18] S. Morimoto,[*1] M. Niikura,[*7,*4] I. Nishizuka,[*5] T. Shimoda,[*1] and K. Tshoo[*18]

Neutron-rich nuclei in the northeast region of the doubly-magic ^{132}Sn are attracting much attention for the investigation of shape evolution from spherical (single-particle like) shapes to deformed (collective-like) prolate shapes as a function of the neutron number. Additionally, a variety of collective modes, such as the octupole collective mode and so on, is expected to appear in this mass region. As isomers are efficient probes of nuclear structure, we performed an isomer search experiment for the neutron-rich Cs isotopes in the framework of the EURICA project[1)].

The isomers were produced through in-flight fission of a 345 MeV/nucleon ^{238}U beam. The fission fragment separator system of BigRIPS and Zero Degree Spectrometer[2)] was tuned for neutron-rich Sb, Te, I, Xe, and Cs isotopes with A=140−150. The isotopes with a rate of approximatelly 50 pps were implanted into a stack of 5 double-sided Si strip detectors (WAS3ABi)[1)]. The β rays and γ rays emitted from the stopped isotopes were detected by WAS3ABi and EURICA, which consists of 12 cluster-type Ge detectors, respectively. Particle identification was performed on the basis of the information of time-of-flight (TOF), magnetic rigidity ($B\rho$) and energy loss of the fragments to deduce mass-to-charge ratio (A/Q) and atomic number. The particle identification for our $B\rho$ setting is shown in ref. 3. Figure 1 shows the A/Q spectrum of the Cs isotopes deduced using the information of $B\rho$ at F5 and F7 as well as TOF between F3 and F7. The isomers were searched for on the basis of the timing information between the γ ray detected by EURICA and ion passage in the plastic scintillator just upstream of WAS3ABi. The long flight time (approximately 650 ns) limited the half lives of longer than hundreds of nanoseconds.

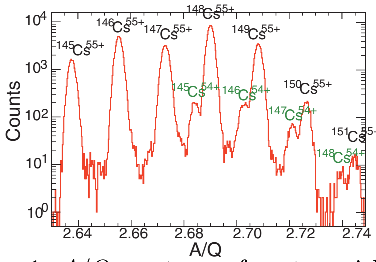

Fig. 1. A/Q spectrum of neutron-rich Cs isotopes.

In this time range, we found new isomers in the nuclei ^{145}Cs, ^{146}Cs, ^{147}Cs, and ^{148}Cs. As an example, a decay curve of the isomer in ^{146}Cs is shown in Fig. 2. The half life and decay scheme obtained in this work for ^{144}Cs were consistent with the results reported in ref. 4. The decay schemes of newly found isomers in $^{145-148}$Cs have been established. The isomers in odd-odd Cs isotopes are caused by the direct low-energy deexcitation from the isomer, which is effected by the proton and neutron interaction. In contrast, the decay pattern of the isomers in the odd-Cs isotopes suggests that these isomers are supposed to be K-isomer candidates.

Systematic studies of the isomers in the Cs isotopes are expected to provide new insights on shape evolution as well as proton-neutron interaction in various deformed systems. Detailed analysis is in progress.

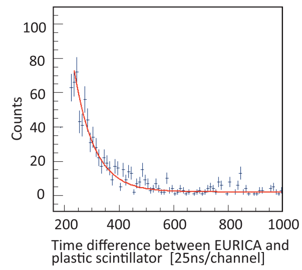

Fig. 2. Decay curve of the newly found isomer in ^{146}Cs.

*1 Department of Physics, Osaka University
*2 IPHC/CNRS and University of Strasbourg
*3 Department of Display Engineering, Hoseo University
*4 RIKEN Nishina Center
*5 Department of Physics, Tohoku University
*6 Department of Physics, Beihang University
*7 Department of Physics, University of Tokyo
*8 CEM, University of Brighton
*9 Department of Physics, University of Surry
*10 Department of Physics, University of York
*11 Department of Physics, Peking University
*12 CNS, University of Tokyo
*13 Department of Physics, Rikkyo University
*14 Department of Physics, University of Oslo
*15 CEA/DAM
*16 RCNP, Osaka University
*17 Department of Physics, University of Notre Dame
*18 IBS

References

1) S. Nishimura *et al.*, Prog. Theor. Exp. Phys. **2012** (2012) 03C006.
2) T. Kubo *et al.*, Prog. Theor. Exp. Phys. **2012** (2012) 03C003.
3) R. Lozeva *et al.*, in this report.
4) T. Rzaca-Urban *et al.*, Phys. Rev. C **80** (2009) 064317.

Decay spectroscopy in the neutron-rich A∼140 region beyond the doubly-magic ^{132}Sn

R. Lozeva,[*1] A. Odahara,[*2] C.-B. Moon,[*3] S. Nishimura,[*4] P. Doornenbal,[*4] G. Lorusso,[*4] P.A. Söderström,[*4] T. Sumikama,[*5] H. Watanabe,[*6] T. Isobe,[*4] H. Baba,[*4] H. Sakurai,[*7,*4] F. Browne,[*8,*4] R. Daido,[*2] Y. Fang,[*2] Z. Patel,[*9,*4] S. Rice,[*9,*4] L. Sinclair,[10*,4] J. Wu,[*11,*4] Z.Y. Xu,[*7*] A. Yagi,[*2] R. Yokoyama,[*12] T. Kubo,[*4] N. Inabe,[*4] H. Suzuki,[*4] N. Fukuda,[*4] D. Kameda,[*4] H. Takeda,[*4] D.S. Ahn,[*4] D. Murai,[*13] F.L. Bello Garrote,[*14] J.-M. Daugas,[*15] F. Didierjean,[*1] E. Ideguchi,[*16] T. Ishigaki,[*2] H.S. Jung,[*17] T. Komatsubara,[*18] Y.K. Kwon,[*18] S. Morimoto,[*2] M. Niikura,[*7] H. Nishibata,[*2] I. Nishizuka,[*5] T. Shimoda[*2] and K. Tshoo[*18]

An isomer and β-decay experiment was performed in the framework of the EURICA project at RIBF[1,2)] aiming at detailed decay spectroscopy and systematical study of the nuclear shape in one of the most interesting, and yet unexplored regions of the nuclear chart, the one beyond the doubly-magic ^{132}Sn. For these nuclei, we may expect gradual change from spherical shape with predominantly single-particle-like structures, to a more deformed, prolate shape with collective-type of excitations, while with the increase of the neutron-number also octupole collectivity may develop. Furthermore, the perturbed shell structure of these nuclei by e.g. sub-shell gaps or intruder high-j orbitals may also cause isomeric states, picturing in turn these exotic systems far off stability.

The experiment was performed using in-flight ^{238}U fission at 345 MeV/u on Be target with a thickness of 2.9 mm. The beam intensity was between 1-5 pnA. The nuclei of interest were transported and selected by BigRIPS and implanted in the active stopper, WAS3ABi, consisting of five Si DSSD detectors[1)]. Twelve Ge Cluster detectors and eighteen $LaBr_3$(Ce) detectors[3)], constituting the EURICA 4π array surrounding the stopper, detected the isomeric- or β-delayed γ-rays. The experimentally obtained particle identification is shown in Fig. 1, where a line indicates the nuclei beyond which no half-lives are known according to[4)]. Our preliminary data analysis of known half-lives for e.g. ^{138,139}Sb nuclei show a very good agreement with the ISOLDE measurement [5)], providing an important input to the nucleosynthesis data around the A = 130 solar-system r-process abundance peak.

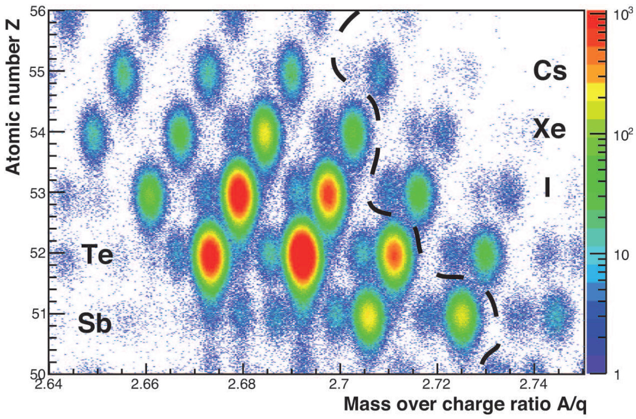

Fig. 1. Particle identification of the exotic nuclear cocktail.

Although the analysis is still in progress, our preliminary results show also several isomeric states before and after a β-decay in e.g. in Sb and I nuclei. Isomers are found also in the very neutron-rich Cs isotopes[6)]. In addition, first excited states e.g. in the produced even-even nuclei with the neutron increase will provide new and vital information for the shell structure and the shape evolution in this region along with the detailed studies of the other exotic isotopes populated in the experiment.

References
1) S. Nishimura et al: RIKEN Accel. Prog. Rep. **45**, L182 (2013).
2) P.-A. Söderström et al: Nucl. Instr. Meth. Phys. Res. B **317**, 649 (2013).
3) Z. Patel et al: in this report.
4) G. Audi et al: Chi. Phys. C **36**, 1157 (2012).
5) O. Arndt et al: Phys. Rev. C **84**, 061307(R) (2011).
6) A. Yagi et al: in this report.

*1 IPHC/CNRS and University of Strasbourg
*2 Department of Physics, Osaka University
*3 Department of Physics, Hoseo University
*4 RIKEN Nishina Center
*5 Department of Physics, Tohoku University
*6 Department of Physics, Beihang University
*7 Department of Physics, University of Tokyo
*8 CEM, University of Brighton
*9 Department of Physics, University of Surrey
*10 Department of Physics, University of York
*11 Department of Physics, Peking University
*12 CNS, University of Tokyo
*13 Department of Physics, Rikkyo University
*14 Department of Physics, University of Oslo
*15 CEA/DAM
*16 RCNP, Osaka University
*17 Department of Physics, University of Notre Dame
*18 IBS

Lifetime measurements of excited states in $^{102,\,104}$Zr with a $LaBr_3$(Ce) array

F. Browne,[*1,*3] A. M. Bruce,[*1] T. Sumikama,[*2] S. Nishimura,[*3] P. Doornenbal,[*3] G. Lorusso,[*3] Z. Patel,[*3,*4] S. Rice,[*3,*4] L. Sinclair,[*3,*5] P.-A. Söderström,[*3] H. Watanabe,[*3,*6] J. Wu,[*3,*7] Z. Y. Xu,[*8] H. Baba,[*3] N. Chiga,[*2] R. Carroll,[*4] R. Daido,[*10] F. Didierjean,[*11] Y. Fang,[*10] N. Fukuda,[*3] G. Gey,[*12,*19,*3] E. Ideguchi,[*10] N. Inabe,[*3] T. Isobe,[*3] D. Kameda,[*3] I. Kojouharov,[*13] N. Kurz,[*13] T. Kubo,[*3] S. Lalkovski,[*14] Z. Li,[*7] R. Lozeva,[*11] I. Nishizuka,[*2] H. Nishibata,[*10] A. Odahara,[*10] Zs. Podolyák,[*4] P. H. Regan,[*4] O. J. Roberts,[*1] H. Sakurai,[*3] H. Schaffner,[*13] G. S. Simpson,[*12] H. Suzuki,[*3] H. Takeda,[*3] M. Tanaka[*10] J. Taprogge,[*15,*16,*3] V. Werner,[*17] O. Wieland,[*18] and A. Yagi[*10]

Developments of novel scintillator materials have offered a step-change in performance characteristics of scintillation detectors for γ ray measurements. In particular, cerium-doped lanthanum tri-bromide ($LaBr_3$(Ce)) has proven to be a promising candidate for measuring lifetimes of low-lying excited nuclear states in the ps-to-ns range. Such information is a powerful tool in extracting, for example, nuclear deformations.

An array of 18 $LaBr_3$(Ce) detectors was installed at the F11 focal plane of the BigRIPS spectrometer, augmenting the existing EURICA array[1)2)]. In order to examine the performance of the $LaBr_3$(Ce) array, the known lifetimes of the 2_1^+ states in $^{102,\,104}$Zr were measured by means of β-γ spectroscopy. The parent nuclei were produced by the in-flight fission of a 345 MeV/A ^{238}U beam on a 555 mg/cm^3 thick ^{9}Be target. The fission fragments were transported through BigRIPS and the ZeroDegree spectrometer before being implanted into the WAS3ABi active stopper (5 highly segmented DSSSDs), which lies between two plastic scintillators (β-plastics). To correlate a β-decay event with an implanted ion, a signal in the same DSSSD pixel to the implant was required. A time condition was placed on the ion implantation to β-decay time to reduce contamination from granddaughter decays.

The level lifetime was obtained by measuring the time difference between the β-plastic, and a signal in the $LaBr_3$(Ce) array. A systematic uncertainty of 10% was added to the measured 2_1^+ lifetimes to account for the lifetimes of higher-lying levels. This was estimated from the time difference spectra for the $4_1^+ \to 2_1^+$ transitions. Figure 1 shows preliminary results of the background subtracted time difference spectra gated on the $2_1^+ \to 0_{g.s.}^+$ transitions, the energies of which are given in Tab. 1 along with the mean lifetime of the levels, which are in good agreement with literature values[3)].

The energy systematics indicate increased collectivity as N increases, however, the dependence of the transition probability on E_γ results in a longer lifetime for the 2_1^+ state in ^{104}Zr than for ^{102}Zr. Future work will concentrate on a more complete characterisation of the low-energy background, the prompt-response function and the contribution of systematic uncertainties. The lifetimes of the 2_1^+ states of more exotic Zr isotopes will also be measured.

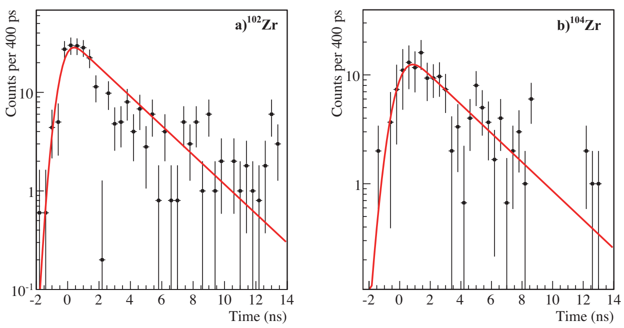

Fig. 1.: Preliminary, background subtracted time difference spectra for, a) ^{102}Zr and b) ^{104}Zr. The extracted mean lifetimes of the 2_1^+ states are listed below.

Table 1.: Comparison between τ values derived in this work and adopted values[3)].

Nuclide	E(2_1^+) [keV]	τ [ns]	ENSDF τ [ns]
^{102}Zr	151.8(1)	2.7(3)	2.6(6)
^{104}Zr	139.3(3)	3.2(3)	2.9(4)

*1 CEM, University of Brighton
*2 Department of Physics, Tohuku University
*3 RIKEN Nishina Center
*4 Department of Physics, University of Surrey
*5 Department of Physics, University of York
*6 Beihang University
*7 Department of Physics, Peking University
*8 Department of Physics, University of Tokyo
*10 RCNP, Osaka University
*11 IPHC/CNRS and University of Strasbourg
*12 LPSC, UJF-INPG-IN2P3, Grenoble
*13 GSI Helmholtzzentrum für Schwerionenforschung GmbH
*14 Department of Physics, Sofia University
*15 Departamento de Física Teórica, Universidad Autónoma de Madrid
*16 Instituto de Estructura de la Materia
*17 Institut fuer Kernphysik, Technische Universitaet Darmstadt
*18 INFN Sezione di Milano
*19 NPP, ILL, Grenoble

References

1) P.-A. Söderström *et al.*, Nucl. Instr. and Meth. **B317**, 649 (2013).
2) Z. Patel *et al.*: In this report.
3) Evaluated Nuclear Structure Data File, http://www.nndc.bnl.gov/ensdf

Progress of study of β-decay of neutron-rich nuclei with $Z \sim 60$

J. Wu,[*1,*2] S. Nishimura,[*1] G. Lorusso,[*1] Z.Y. Xu,[*3] H. Baba,[*1] F. Browne,[*1,*4] R. Daido,[*5] P. Doornenbal,[*1] Y.F. Fang,[*5] E. Ideguchi,[*6] T. Isobe,[*1] Z. Li,[*2] A. Odahara,[*5] Z. Patel,[*1,*7] S. Rice,[*1,*7] G. Simpson,[*8] L. Sinclair,[*1,*9] P.-A. Söderström,[*1] T. Sumikama,[*10] H. Watanabe,[*11] A. Yagi,[*5] R. Yokoyama,[*12] N. Aoi,[*6] F.L. Bello Garrote,[*13] G. Benzoni,[*14] G. Gey,[*7] A. Gottardo,[*15] G.D. Kim,[*16] Y.K. Kim,[*16] K. Kobayashi,[*17] I. Kojouharov,[*18] N. Kurz,[*18] H. Nishibata,[*5] H. Sakurai,[*1] H. Schaffner,[*18] M. Tanaka,[*6] J. Taprogge,[*19] T. Yamamoto[*5] and the EURICA collaboration

Approximately half of the elements heavier than iron are formed by the rapid neutron-capture process (r-process). In the solar r-process abundance distribution, the region of rare-earth elements forms a peak around $A = 160$, which may have a different mechanism of formation compared with the other two distinct peaks at $A = 130$ and $A = 195$ relating to neutron-closed shells at $N = 82$ and $N = 126$, respectively[1]. β-decay half-lives of the elements always play an important role at both the cold and hot r-process paths and will be expected to constrain the conditions in understanding the r-process nucleosynthesis.

To study the rare-earth peak, a β-decay experiment with $Z \sim 60$ was performed at the RIBF facility in June 2013. This experiment was carried out using the in-flight fission of a 345 MeV/nucleon ^{238}U beam colliding with a Be target. The secondary beam, including a cocktail of highly neutron-rich isotopes, was implanted in the β-decay counting system WAS3ABi [2](Wide-range Active Silicon-Strip Stopper Array for Beta and ion detection), which consists of a stack of five highly segmented DSSSDs (Double-Sided Silicon Strip Detectors). With the help of the high-purity germanium detectors (EURICA)[3], γ rays with a high production rate emitted from implanted radioactive isotopes or the daughters nuclei fed through the β decay can be measured. The β-decay half-lives could be determined by fitting the distribution of the time difference between the implantations in the WAS3ABi and the following β-decay events.

In this experiment, approximately 35 half-lives were measured, including approximately 25 new half-lives. Figure 1 displays some preliminary results of four decay curves obtained in this experiment. Daughter half-lives, granddaughter half-lives, as well as the constant background are taken into account by using the Likelihood fitting method. The β-decay half-lives can also be obtained by using β-delayed γ rays detected by the EURICA detector, which can eliminate the uncertainties from the daughter and granddaughter half-lives. Figure 2 shows the β-decay curve of ^{149}La gated the β-delayed γ rays.

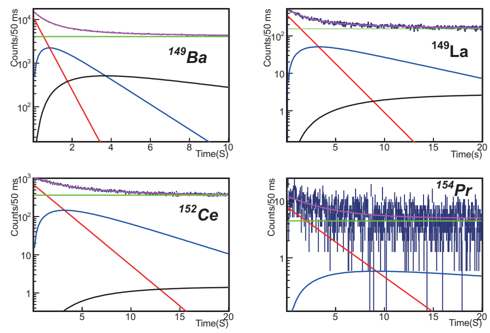

Fig. 1. Decay curves of four kinds of isotopes (^{149}Ba,^{149}La, ^{152}Ce, ^{154}Pr) are displayed. The red lines correspond to parent nuclei. The blue curves, black curves, and green lines correspond to the daughter nuclei, granddaughter nuclei, and a constant background.

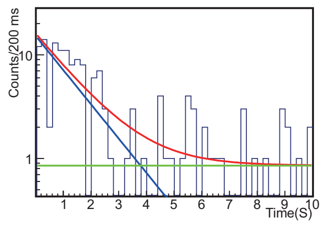

Fig. 2. ^{149}La decay curve obtained gating on the β-delayed γ-ray energy with 245.4keV.

In the latter phases of analysis, further new half-lives will be obtained. Simulation work of r-process will be performed by comparing the theoretical calculations with our experimental results.

*1 RIKEN Nishina Center
*2 Department of Physics, Peking University
*3 Department of Physics, University of Tokyo
*4 University of Brighton
*5 Department of Physics, Osaka University
*6 Research Center for Nuclear Physics, Osaka University
*7 Department of Physics, University of Surrey
*8 LPSC, France
*9 Department of Physics, University of York
*10 Department of Physics, Tohoku University
*11 Department of Physics, Beihang University
*12 Center for Nuclear Study, University of Tokyo
*13 University of Oslo
*14 INFN,Milano
*15 INFN,Legnaro
*16 IBS
*17 Rikkyo University
*18 GSI
*19 Instituto de Estructura dela Materia

References

1) Matthew R. Mumpower et al, Phys. Rev. C 85, 045801 (2012).
2) S.Nishimura, G.Lorusso, Z.Xu et al., RIKEN Accel. Prog. Rep. 46, 182 (2013).
3) P.-A. Söderström et al.: JPS Conf. Proc. 1, 013046 (2014).

Study of the superallowed β-decay of ^{100}Sn

D. Lubos,[*1,*2] M. Lewitowicz,[*3] R. Gernhäuser,[*1] R. Krücken,[*4] S. Nishimura,[*2] H. Sakurai,[*5] H. Baba,[*2] B. Blank,[*6] A. Blazhev,[*7] P. Boutachkov,[*8] F. Browne,[*9,*2] I. Celikovic,[*3] P. Doornenbal,[*2] T. Faestermann,[*1] Y. Fang,[*10,*2] G. de France,[*3] N. Goel,[*8] M. Gorska,[*8] S. Ilieva,[*11] T. Isobe,[*2] A. Jungclaus,[*12] G. D. Kim,[*13] Y.-K. Kim,[*13] I. Kojouharov,[*8] M. Kowalska,[*14] N. Kurz,[*8] Z. Li,[*15] G. Lorusso,[*2] K. Moschner,[*7] I. Nishizuka,[*16,*2] J. Park,[*4] Z. Patel,[*17,*2] M. M. Rajabali,[*4] S. Rice,[*17,*2] H. Schaffner,[*8] L. Sinclair,[*18,*2] P.-A. Söderström,[*2] K. Steiger,[*1] T. Sumikama,[*16] H. Watanabe,[*19] Z. Wang,[*4] J. Wu,[*12,*2] and Z. Y. Xu[*5,*2]

An experiment for studying the superallowed Gamow-Teller decay of the doubly magic nucleus ^{100}Sn was performed in June 2013 at the high-resolution separator BigRIPS of the RIBF at the RIKEN Nishina Center. The β-decay of a $g_{9/2}$-proton in ^{100}Sn to a $g_{7/2}$-neutron in ^{100}In shows the smallest log(ft) $= 2.62^{+0.13}_{-0.11}$ value in the nuclear chart. The Gamow-Teller strength $B_{GT} = 9.1^{+2.6}_{-3.0}$, as deduced from the last experiment at GSI[1]. This value is consistent with the results of B_{GT} calculations as derived from LSSM calculations. However, the uncertainties in the extracted B_{GT} are still dominated by statistics. In particular, the contribution of the β-decay end-point energy $E_{\beta,max}$ amounts to 85% of the B_{GT} uncertainty. In the present experiment, a 4 mm Be target was bombarded with a ^{124}Xe beam of 345 MeV/u at intensities up to 36.4 pnA to produce ^{100}Sn by fragmentation. In total, 2525 ^{100}Sn ions (Fig. 1) were identified during 8.5 days of beamtime. This exceeds the number obtained in the previous experiment at GSI[1] by nearly a factor of 10, and the uncertainties in B_{GT} are expected to be improved by more than a factor of 2. Furthermore, a number of nuclides towards the proton dripline have been newly identified (see Čeliković et al.[2]) and significantly higher statistics for N=Z and N=Z-1 isotopes have been obtained.

In order to observe β- and γ-decays, ^{100}Sn and most of the neighboring nuclei (see Fig. 1) were implanted into the WAS3ABi detector, which is a closed stack consisting of three highly segmented silicon detectors of 1 mm thickness each surrounded by 84 Ge- and 18 LaBr-detectors of the 4π-γ-spectrometer EURICA. This WAS3ABi detector array is expanded by a stack of 10 silicon detectors of the same thickness in order to measure the total energy of the decay positrons accurately. Since $E_{\beta,max} = 3.29 \pm 0.20$ MeV is rather small[1], the decay positrons are stopped in the silicon stack, enabling a high-precision measurement in order to determine $E_{\beta,max}$. We find correlated β-decays by considering decay events occurring within a time window t_C and active detector volume around the implantation. Thus, we can determine the half-lives of β-decays. From β-delayed γ-decays, using the largest data sample on ^{100}Sn, we will be able to distinguish between two scenarios for the β-delayed γ-cascades to confirm a dominantly populated 1^+ state in ^{100}In after β-decay. Furthermore, we are looking for a 6^+ isomeric state in ^{100}Sn, as predicted by Grawe et al.[3] based on LSSM calculations.

After a preliminary energy calibration of the WAS3ABi detectors, one of the most challenging tasks is to determine systematic uncertainties in the β-decay endpoint energy $E_{\beta,max}$ and β-half-life $T_{1/2}$. A small (systematic) error in these quantities affects the B_{GT}, resulting in a large relative uncertainty. Since ^{100}Sn has a long half-life, the background contribution on this measurement is also studied in detail to minimize these systematic uncertainties.

First results indicate a good agreement with known values[1] of both quantities $T_{1/2}(^{100}Sn)$ and $E_{\beta,max}(^{100}Sn)$.

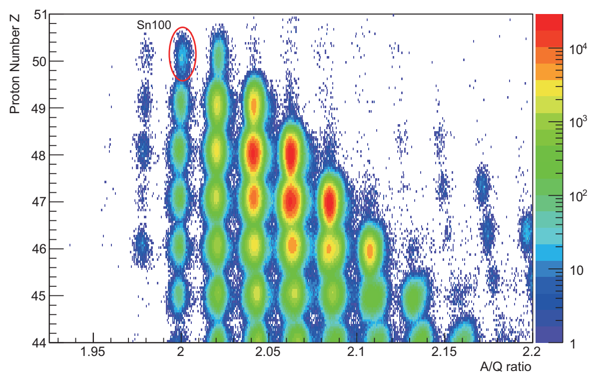

Fig. 1. figure
PID plot in the region of ^{100}Sn. The total number of identified ^{100}Sn nuclei is 2525 (red encircled region).

*1 Physik Department E12, Technische Universität München
*2 RIKEN Nishina Center
*3 GANIL
*4 TRIUMF
*5 Department of Physics, University of Tokyo
*6 CENBG
*7 Institut für Kernphysik, Universität zu Köln
*8 GSI Darmstadt
*9 School of Comp., Eng. and Maths., Brighton University
*10 Department of Physics, Osaka University
*11 Institut für Kernphysik, TU Darmstadt
*12 IES CSIS
*13 Institute for Basic Science
*14 CERN
*15 School of Physics, Peking University
*16 Department of Physics, Tohoku University
*17 Department of Physics, Surrey University
*18 Department of Physics, University of York
*19 Department of Physics, Beihang University

References
1) C. Hinke et al., Nature, **486**, 341 (2012)
2) I. Čeliković et al., RIKEN Acc. Prog. Rep., this volume
3) H. Grawe et al., Eur. Phys. J. A **27**, s01, 257 (2006)

Decay spectroscopy around ^{78}Ni with the EURICA setup

G. Benzoni,[*1] H. Watanabe,[*2,*3] D. Sohler,[*4] E. Sahin,[*5] G. de Angelis,[*6] S. Nishimura,[*2] G. Lorusso,[*2] T. Sumikama,[*7] P. Doornenbal,[*2] Z.Y. Xu,[*8] T. Isobe,[*2] P.A. Söderström,[*2] F. Browne,[*9] J. Wu,[*2,*10] H. Baba,[*2] Z. Patel,[*11] S. Rice,[*11] L. Sinclair,[*12] R. Yokoyama,[*13] R. Daido,[*14] Y. Fang,[*14] M. Niikura,[*8] R. Avigo,[*1,*15] F.L. Bello Garrote,[*5] N. Blasi,[*1] S. Ceruti,[*1,*15] F.C.L. Crespi,[*1,*15] M.-C. Delattre,[*16] Zs. Dombradi,[*4] A. Gottardo,[*6] I. Kuti,[*4] K. Matsui,[*8] B. Melon,[*17] D. Mengoni,[*18] T. Miyazaki,[*8] V. Modamio-Hoybjor,[*6] S. Momiyama,[*8] A.I. Morales,[*1,*15] D. Napoli,[*6] R. Orlandi,[*19] H. Sakurai,[*2,*8] R. Taniuchi,[*8] J. Taprogge,[*20,*21] Zs. Vajta,[*4] J.J. Valiente-Dobòn,[*6] O. Wieland,[*1] A. Yagi,[*14] M. Yalcinkaya[*22]

Exotic nuclei play an important role in nuclear shell structure studies since they allow to search for possible modifications of magic numbers with increasing N/Z ratio. The tensor force, one of the non-central components of the effective nucleon-nucleon interaction, is expected to modify the relative single particle energies owing to an increased attraction for orbitals with anti-parallel spin configuration and a repulsion for orbitals with parallel spin configuration. In such contest, nuclei at Z=28, N=50 shell gaps are particularly interesting since they are good candidates to reveal changes into the shell structure. Astrophysical implications also involve the discussion on neutron-rich nuclei, since they are expected to dominate the nuclear composition throughout the collapse of massive stars.

In this view an experiment aiming at studying decay spectroscopy in the region close to ^{78}Ni, i.e. in the isotopic chains of Cu, Ni, Co and Fe, was performed at RIKEN in May 2013 as part of the EURICA campaign at the Radioactive-Isotope Beam Factory (RIBF) facility.

The wanted species were produced by means of inflight fission of a ^{238}U beam at a bombarding energy of 345 MeV/u. The resulting fragments were separated in the BigRIPS separator, by the use of degraders at the intermediate dispersive foci[1)]. The cocktail beam was transported in the ZeroDegree spectrometer down to the final focal plane F11. The beam was then slowed down in an Al degrader to ensure the implantation of the wanted species in the 5 silicon detectors of the WAS3ABi array[2)]. This silicon array was surrounded by the EURICA spectrometer consisting of 12 EUROBALL cluster detectors[3)]. $LaBr_3$ scintillator detectors were also mounted in clusters to allow fast-timing measurements. The experiment collected data for an equivalent time of 3 days with an average primary beam intensity of 10pnA. The total count rate at the final focal plane F11 was limited to 100pps to ensure ion-β correlations. In Figure 1 a particle identification (PID) plot is shown. The plot does not include the full statistics of the experiment. The Bρ setting of the separator was set in order to transport ^{71}Fe in its central trajectory.

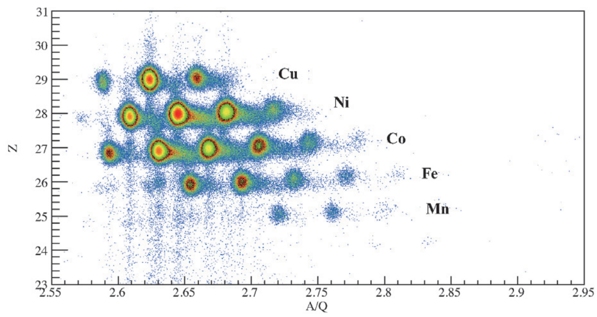

Fig. 1. PID plot of the cocktail beam implanted in the WAS3ABi array.

The study of isomeric γ transitions and β-delayed transitions in the populated nuclei is ongoing. The same reaction was also exploited to perform Coulomb excitation reaction to study the first excited states in $^{73-75}$Ni isotopes[4)].

*1 INFN
*2 RIKEN Nishina Center
*3 Beihang University
*4 MTA Atomki
*5 University of Oslo
*6 LNL-INFN
*7 Tohoku University
*8 University of Tokyo
*9 University of Brighton
*10 Peking University
*11 University of Surrey
*12 York University
*13 CNS, University of Tokyo
*14 Osaka University
*15 Universitá degli Studi di Milano
*16 IPNO Orsay
*17 INFN sezione di Firenze
*18 Universitá degli Studi di Padova
*19 Instituut voor Kern- en StralingsFysica/K.U. Leuven
*20 Consejo Superior de Investigaciones Cientificas
*21 Universidad Autnoma de Madrid
*22 University of Instambul

References
1) T. Kubo: Nucl. Instr. Methods Phys. Res. Sect. **B204**, 97 (2003).
2) S. Nishimura: Prog. Theor. Exp. Phys. **2012**, 03C006 (2012).
3) P.-A. Söderström et al., Nucl. Instr. and Meth. **B317**, 649 (2013).
4) A. Gottardo, this report.

Structure of neutron-rich Zr and Mo isotopes

T. Sumikama,[*1,*3] F. Browne,[*2,*3] A. M. Bruce,[*2] I. Nishizuka,[*1,*3] S. Nishimura,[*3] P. Doornenbal,[*3] G. Lorusso,[*3] Z. Patel,[*3,*4] S. Rice,[*3,*4] L. Sinclair,[*3,*5] P.-A. Söderström,[*3] H. Watanabe,[*3,*6] J. Wu,[*3,*7] Z. Y. Xu,[*3,*8] A. Yagi,[*3,*9] H. Baba,[*3] N. Chiga,[*1] R. Carroll,[*4] R. Daido,[*3,*9] F. Didierjean,[*10] Y. Fang,[*3,*9] G. Gey,[*3,*11,*12] E. Ideguchi,[*13] N. Inabe,[*3] T. Isobe,[*3] D. Kameda,[*3] I. Kojouharov,[*14] N. Kurz,[*14] T. Kubo,[*3] S. Lalkovski,[*15] Z. Li,[*7] R. Lozeva,[*10] N. Fukuda,[*3] H. Nishibata,[*3,*9] A. Odahara,[*9] Zs. Podolyàk,[*4] P. H. Regan,[*4] O. J. Roberts,[*2] H. Sakurai,[*3,*8] H. Schaffner,[*14] G. S. Simpson,[*11] H. Suzuki,[*3] H. Takeda,[*3] M. Tanaka,[*3,*13] J. Taprogge,[*3,*16,*17] V. Werner,[*18] and O. Wieland[*19]

Neutron-rich isotopes in the vicinity of ^{110}Zr have attracted much attention, because a shape transition to oblate or triaxial and a tetrahedral-shape isomer may be observed.[1)] The decay spectroscopy of the Zr and Mo isotopes was performed at RIBF at RIKEN Nishina Center to extend the previous experiment[1)] to more neutron-rich region. The neutron-rich nuclei were produced by the in-flight-fission reaction of ^{238}U beam at 345 MeV/u in a 3-mm-thick Be target, and implanted into the double-sided silicon-strip detectors (WAS3ABi), which were placed at the center of the high-purity-germanium detector array (EURICA).[2)] A fast-timing $LaBr_3$(Ce) array was combined with EURICA for a half-life measurement of excited states.

Figure 1 shows the particle-identification (PID) plot of the radioactive-isotope (RI) beam separated by the BigRIPS separator. The β-γ spectroscopy of ^{102,104}Y, and ^{106}Nb was performed individually by using a high-purity-beam setting. Figure 2 shows the PID spectrum of ^{102}Y setting. The purity of ^{102}Y was 46%. A preliminary result of the half-life measurement for ^{102,104}Zr using the fast timing array is given in another report.[3)] The beam setting shown in Fig. 3 is used to search for an isomeric state in ^{110}Mo using a passive Cu stopper. Further analysis is in progress.

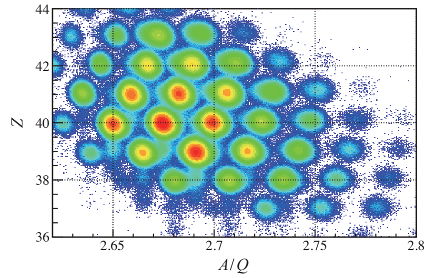

Fig. 1. PID plot of the atomic number Z and the mass to charge ratio A/Q. A wider and more-neutron-rich region than Figs. 2 and 3 was selected by the BigRIPS separator.

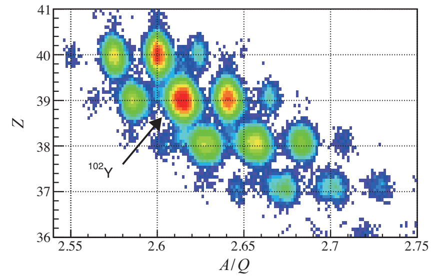

Fig. 2. PID plot of a high-purity-beam setting for the spectroscopic study of β decay from ^{102}Y.

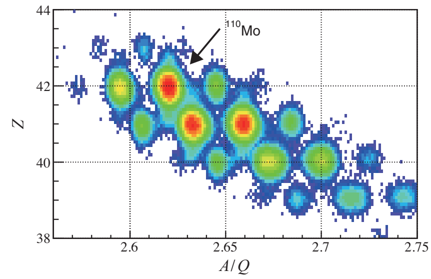

Fig. 3. PID plot of a high-purity-beam setting to search for an isomeric state in ^{110}Mo.

*1 Department of Physics, Tohoku University
*2 School of Physics and Nuclear Energy Engineering, University of Brighton
*3 RIKEN Nishina Center
*4 Department of Physics, University of Surrey
*5 Department of Physics, University of York
*6 School of Computing Engineering and Mathematics, Beihang University
*7 Department of Physics, Peking University
*8 Department of Physics, University of Tokyo
*9 Department of Physics, Osaka University
*10 IPHC/CNRS and University of Strasbourg
*11 LPSC, Universitè Grenoble-Alpes, CNRS/IN2P3
*12 ILL, Grenoble
*13 RCNP, Osaka University
*14 GSI
*15 Department of Physics, Sofia University
*16 Departamento de Física Teórica, Universidad Autónoma de Madrid
*17 Institutode Estructura de la Materia
*18 Department of Physics, Yale University
*19 INFN Sezione di Mirano

References

1) T. Sumikama *et al.*: Phys. Rev. Lett. **106**, 202501 (2011).
2) S. Nishimura: Prog. Theor. Exp. Phys. **2012** 03C006.
3) F. Browne *et al.*: RIKEN Accel. Prog. Rep. **47**, (2014).

Search for K-isomers in neutron-rich Z≈60 isotopes

E. Ideguchi,[*1] G. Simpson,[*2] R. Yokoyama,[*3] Mn. Tanaka,[*1] S. Nishimura,[*4] P. Doornenbal,[*4] P.-A. Söderström,[*4] G. Lorusso,[*4] Z. Xu,[*5] J. Wu,[*4,*6] T. Sumikama,[*7] N. Aoi,[*1] H. Baba,[*4] F. Bello,[*8] F. Browne,[*4,*9] R. Daido,[*10] Y. Fang,[*10] N. Fukuda,[*4] G. Gey,[*2,*4,*11] S. Go,[*3,4] N. Inabe,[*4] T. Isobe,[*4] D. Kameda,[*4] K. Kobayashi,[*12] M. Kobayashi,[*3] T. Komatsubara,[*13] T. Kubo,[*4] I. Kuti,[*14] Z. Li,[*6] M. Matsushita,[*3] S. Michimasa,[*3] C.-B. Moon,[*15] H. Nishibata,[*10] I. Nishizuka,[*7] A. Odahara,[*10] Z. Patel,[*4,*16] S. Rice,[*4,*16] E. Sahin,[*8] L. Sinclair,[*4,*17] H. Suzuki,[*4] H. Takeda,[*4] J. Taprogge,[*18,*19] Zs. Vajta,[*14] H. Watanabe,[*20] and A. Yagi[*10]

The neutron-rich A∼150 region contains a wide variety of shape phenomena, including shape coexistence and possible static octupole and hexadecapole deformations. Although quadrupole deformation has been extensively examined across most of the nuclear chart, both octupole and hexadecupole deformations remain much less well studied in comparison. These higher-order deformations can have a strong influence on gamma-decay rates and the quasi-particle energies of nuclei, and hence, their detailed studies are necessary to test the various differing predictions of several nuclear models. We have performed an experiment to search for μs isomers in the neutron-rich A= 150 ∼160 Nd, Ce, Ba nuclei and to study their β-decay, in order to examine octupole and hexadecupole deformations in this region. These studies have become possible for the first time using the world's highest intensity in-flight RI beams available at RIBF with the high-efficiecy gamma spectrometer, EURICA[1)].

To study the excited levels of these A = 150 ∼ 160 isotopes, we have performed isomer and beta-gamma spectroscopy using EURICA in two different RI beam settings. One setting involves focusing on the Nd region and the other, on the Ba region.

During the experiment for the Nd setting (see Fig. 1), a previously reported isomer in ^{156}Nd[2)] was confirmed and a new isomer in ^{158}Nd was identified. We also succeeded to find some more isomers in neutron-rich Nd isotopes up to ^{160}Nd[3)]. These findings will allow us to study the systematic analysis of isomers in neutron-rich Nd isotopes, and the development of quadruple and hexadecupole deformations as a function of neutron numbers will be investigated. In addition, we have also found several more new microsecond isomeric states in this region[4)]. These data are currently being analyzed.

In the Ba setting run, RI beams of $^{149-151}$Ba, $^{151-153}$La, and ^{154,155}Ce were mainly collected, as shown in Fig. 2. The isotopes were stopped at the active stopper, WAS3ABi,[5)] and beta-gamma spectroscopy of these isotopes was performed using the EURICA setup. All the isotopes indicated above are newly studied with the aim of systematic investigation of octupole correlations, a study that has not been possible so far. Detailed analyses are underway.

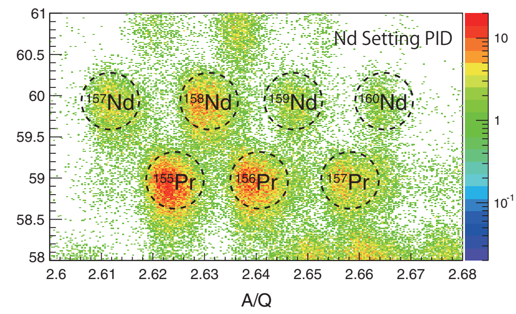

Fig. 1. Particle identification (A/Q vs Z) plot for the Nd setting run.

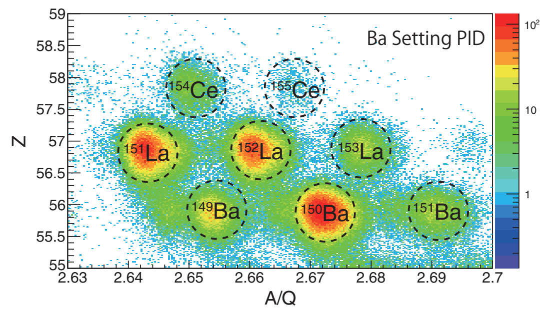

Fig. 2. Particle identification plot for the Ba setting run.

*1 Research Center for Nuclear Physics, Osaka University
*2 LPSC, Université Grenoble-Alpes, CNRS/IN2P3
*3 Center for Nuclear Study, The University of Tokyo
*4 RIKEN Nishina Center
*5 Department of Physics, The University of Tokyo
*6 Peking University
*7 Department of Physics, Tohoku University
*8 University of Oslo
*9 The University of Brighton
*10 Department of Physics, Osaka University
*11 ILL
*12 Department of Physics, Rikkyo University
*13 University of Tsukuba
*14 MTA Atomki
*15 Hoseo University
*16 The University of Surrey
*17 University of York
*18 Instituto de Estructura de la Materia, CSIC
*19 Universidad Autónoma de Madrid
*20 Beihang University

References

1) S. Nishimura: Nucl. Phys. News 22, No. 3 (2012).
2) S. G. Simpson *et al.*: Phys Rev. C 80, 024304(2009).
3) Mn. Tanaka *et al.*, in this report.
4) R. Yokoyama *et al.*, in this report.
5) S.Nishimura, G.Lorusso, Z.Xu et al.: RIKEN Accel. Prog. Rep. 46, 182 (2013).

Isomer study on neutron-rich Pm isotopes using EURICA at RIBF

R. Yokoyama,[*1] E. Ideguchi,[*2] G. Simpson,[*3] Mn. Tanaka,[*2] S. Nishimura,[*4] P. Doornenbal,[*4] P.-A. Söderström,[*4] G. Lorusso,[*4] Z. Y. Xu,[*5] J. Wu,[*4,*6] T. Sumikama,[*7] N. Aoi,[*2] H. Baba,[*4] F. Bello,[*8] F. Browne,[*9,*4] R. Daido,[*10] Y. Fang,[*10] N. Fukuda,[*4] G. Gey,[*3,*4,*11] S. Go,[*1,*4] N. Inabe,[*4] T. Isobe,[*4] D. Kameda,[*4] K. Kobayashi,[*12] M. Kobayashi,[*1] T. Komatsubara,[*13] T. Kubo,[*4] I. Kuti,[*14] Z. Li,[*6] M. Matsushita,[*1] S. Michimasa,[*1] C.-B. Moon,[*15] H. Nishibata,[*10] I. Nishizuka,[*7] A. Odahara,[*10] Z. Patel,[*16,*4] S. Rice,[*16,*4] E. Sahin,[*11] L. Sinclair,[*17,*4] H. Suzuki,[*4] H. Takeda, [*4] J. Taprogge,[*18,*19] Zs. Vajta,[*14] H. Watanabe[*20] and A. Yagi[*10]

It has been known that large prolate deformation develops in neutron-rich $Z \sim 60$ nuclei. This can be seen from the systematics of excitation energies of the first 2^+ states of even-even $Z = 55$ to 66 nuclei as shown in FIG.1 of ref[1]. In this deformed region, many K-isomers with micro second half-lives have been discovered. For example, $K^\pi = 4^-$ isomers are systematically observed in $Z = 62$ to 68, $N = 100$ isotones[2,3]. It is interesting to investigate whether the same kind of isomers exist in lower Z isotones, as this information will be helpful in understanding the deformed shell structure of such highly neutron-rich nuclei.

We performed isomer and β-γ spectroscopy on neutron-rich $Z = 56$ to 61 isotopes at RIBF. The neutron-rich isotopes were produced using in-flight fission of a 345MeV/nucleon ^{238}U beam. Fission fragments were identified by measuring the time-of-flight (TOF) and magnetic rigidity ($B\rho$) in the second stage of BigRIPS and by measuring the energy loss (ΔE) by the ion chamber at the final focal plane, F11. The measurement was conducted in two different setups. In one setup, the beam was implanted into an active stopper, WAS3ABi[4] which consists of five layers of Double-Sided-Silicon-Strip Detectors (DSSSDs) with 40×60 strips, in order to obtain β-γ and isomer data at the same time. In this setup, the total implantation rate was limited up to ~100 cps. In the other setup, a copper stopper was introduced instead of the DSSSD to accept a wide range of nuclides with a high total rate, in order to optimize the isomer search. The γ rays from the isomeric states were detected by EURICA[5], which is an array of 12-cluster Ge detectors. Each cluster consists of seven crystals that enable adding back Compton-scattered events in the neighboring crystals.

*1 Center for Nuclear Study, The University of Tokyo
*2 Research Center for Nuclear Physics, Osaka University
*3 LPSC, Université Grenoble-Alpes, CNRS/IN2P3
*4 RIKEN Nishina Center
*5 Department of Physics, The University of Tokyo
*6 Department of Physics, Peking University
*7 Department of Physics, Tohoku University
*8 Department of Physics, University of Oslo
*9 School of Computing Engineering and Mathematics, University of Brighton
*10 Department of Physics, Osaka University
*11 ILL, Grenoble
*12 Department of Physics, Rikkyo University
*13 Department of Physics, University of Tsukuba
*14 MTA Atomki
*15 Department of Display Engineering, Hoseo University
*16 Department of Physics, University of Surrey
*17 Department of Physics, University of York
*18 Instituto de Estructura de la Materia, CSIC
*19 Departamento de Física Teórica, Universidad Autónoma de Madrid
*20 Department of Physiscs, Beihang University

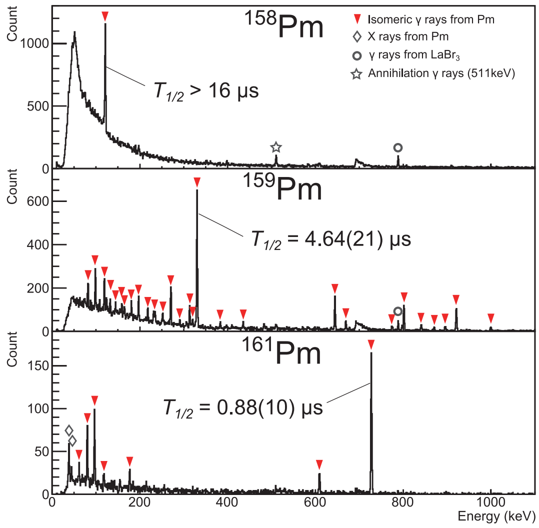

Fig. 1. Preliminary γ-ray energy spectra of ^{158}Pm, ^{159}Pm and ^{161}Pm. The time windows of ^{158}Pm is up to 16μs and that of ^{159}Pm and ^{161}Pm are up to 5μs. Events close to the timing of the beam implantation are excluded. Half-lives of ^{159}Pm and ^{161}Pm are obtained from the 330 and 728keV γ ray respectively.

After the analysis of the data, isomers were found in Pm isotopes with $A = 158$, 159, and 161. Fig. 1 shows the preliminary energy spectra of the delayed γ rays for the Pm isotopes. Many new γ rays were observed for them. Half-lives of ^{159}Pm and ^{161}Pm were obtained by fitting the timing spectra gated by the γ-ray energy. ^{158}Pm was found to have a half-life much longer than the 16μs time window. Further analysis of the γ-γ coincidence and relative intensities are in progress to construct the level schemes. β-γ analysis will also be performed to obtain more information on the low-lying states of these nuclei.

References

1) R. F. Casten *et al.*: Phys. Rev. Lett. 47, 1433 (1981)
2) G. D. Dracoulis *et al.*: PRC 81, 054313 (2010)
3) S. Go *et al.*: RIKEN Accel. Prog. Rep. 46, 21 (2013)
4) S. Nishimura *et al.*: RIKEN Accel. Prog. Rep. 46, 182 (2013)
5) S. Nishimura: Nucl. Phys. News 22, No. 3 (2012)

Beta-delayed proton emission of ^{73}Sr and effective lifetime of the rp-process waiting point ^{72}Kr in X-ray bursts environment

L. Sinclair,*1 G. Lorusso,*2 P. Davies,*1 J. Wu,*3 Z.Y. Xu,*4 S. Nishimura,*2 P. Doornenbal,*2 P.-A. Söderström,*2 F. Browne,*5 D. Lubos,*6 Z. Patel,*7 S. Rice,*7 H. Baba,*2 A. Estrade,*8 Y. Fang,*9 J. Henderson,*1 T. Isobe,*2 D. Jenkins,*1 S. Kubono,*2 Z. Li,*3 I. Nishizuka,*10 H. Sakurai,*2 P. Schury,*2 T. Sumikama,*10 R. Wadsworth,*1 H. Watanabe,*2 V. Werner,*11 and the EURICA collaboration

The nuclide ^{72}Kr is a potential waiting point of the astrophysical rp-process. However, its lifetime under conditions of X-ray bursts may significantly be reduced by the two-proton capture reaction ^{72}Kr(p,γ)^{73}Rb(p,γ)^{74}Sr. The rate of this reaction is highly sensitive to the characteristics of the low-energy states of the intermediate nucleus ^{73}Rb and, in particular, to the proton-separation energy, S_p, of ^{73}Rb. No constraints from direct measurements exist, resulting in significant uncertainties in calculations of astrophysical interest.

Nuclear structure in the 70–80 mass-number region is particularly interesting. Rapid shape changes, shape coexistence, and *np*-pairing effects are all expected. This is a challenging region from a theoretical perspective and little experimental data exists for nuclei beyond the N=Z line. This experiment affords an opportunity to access nuclei both at and beyond the N=Z line in this mass-number region.

The nuclei of interest were produced by fragmentation of a 345 MeV/u ^{124}Xe primary beam colliding with a ^{9}Be target. The beam intensity ranged from 30–35 pnA. The secondary beam purification and identification was performed using the BigRIPS fragment separator. The fragments of interest were unambiguously identified, and their subsequent decays were recorded using the WAS3ABi silicon stopper in conjunction with EURICA[1]. Implantations were correlated with their subsequent β-decays on the basis of position and time, enabling measurement of half-lives and β-delayed γ rays.

Two experimental settings were used to access proton-rich isotopes around ^{73}Sr (as shown in the particle-identification (PID) plot in Fig. 1 with ^{73}Sr highlighted). As a first setting, BigRIPS was set for maximum transmission of ^{73}Sr, the number of implanted nuclei predicted by LISE^{++} was 2500 and the requested beam time was 2.5 days. A second setting was optimized for the transmission of ^{74}Sr, and the number of implanted nuclei predicted was 8000 for 0.5 days. The actual total beam time was 45 h for ^{73}Sr and 9 h for ^{74}Sr. The number of implanted ^{73}Sr and ^{74}Sr were 186 and 590, respectively. The discrepancies observed between the expected counts and actual counts is due to the actual production cross-section being lower than that predicted by LISE^{++} calculations.

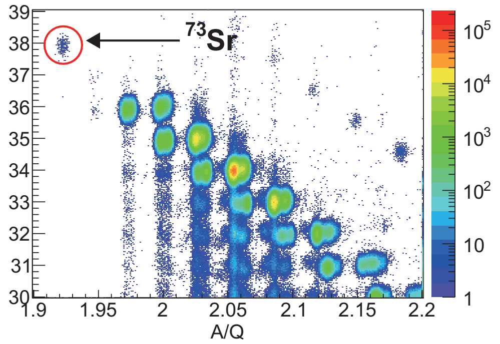

Fig. 1. PID plot of nuclei transmitted through the fragment separator BigRIPS from the ^{73}Sr setting.

Upon the experiment's completion, an energy calibration of WAS3ABi was carried out using 482 and 972 keV conversion electrons emitted from a ^{207}Bi source.

The β^+-decay half-lives of nuclei ^{73}Sr, ^{74}Sr and ^{76}Y have been measured. The accuracy of these measurements were verified by extracting the half-lives of previously studied nuclei and comparing with the literature values.

The isotopes ^{69}Br, ^{72}Rb and ^{73}Rb were observed in BigRIPS, for which there is evidence of implantation and decay events in WAS3ABi. Future analyses will focus on these events, as well as the low-lying structure populated through β^+-decay of exotic nuclei produced around ^{73}Sr. A search for new isomeric states, such as the one found in ^{70}Se, is also being carried out.

This large set of data will provide new half-lives, direct input for rp-process calculations, and new insights into the structure of nuclei in this region.

References

1) P.-A. Söderström et al.: Nucl. Instr. and Meth. **B317**, 649-652, (2013)

*1 Department of Physics, University of York
*2 RIKEN Nishina Center
*3 School of Physics, Peking University
*4 Department of Physics, University of Tokyo
*5 CEM, University of Brighton
*6 Technische Universität München
*7 Department of Physics, University of Surrey
*8 School of Physics and Astronomy, University of Edinburgh
*9 Department of Physics, Osaka University
*10 Department of Physics, Tohoku University
*11 Department of Physics, Yale University

Commissioning of a $LaBr_3$(Ce) array with EURICA at RIBF

Z. Patel,[*1,*2] F. Browne,[*1,*3] A. M. Bruce,[*3] N. Chiga,[*4] R. Daido,[*5] S. Nishimura,[*1] Zs. Podolyák,[*2] P. H. Regan,[*2,*6] O. J. Roberts,[*3] H. Sakurai,[*1] P.-A. Söderström,[*1] T. Sumikama,[*4] and H. Watanabe[*7]

An array of 18 $LaBr_3$(Ce) detectors were introduced to complement the HPGe EURICA (Euroball-RIKEN Cluster Array) detectors for the Spring 2013 campaign at RIBF. These detectors were supplied by The University of Surrey and The University of Brighton to provide fast-timing information on the half-lives of excited states within radioactive nuclei[1)].

$LaBr_3$(Ce) crystals are very fast scintillators with high effective Z and a fast decay time. This makes them superior to other detectors for γ-ray decay time measurements, as they are able to measure half-lives with a picosecond-nanosecond range while also possessing good energy resolution[2,3)].

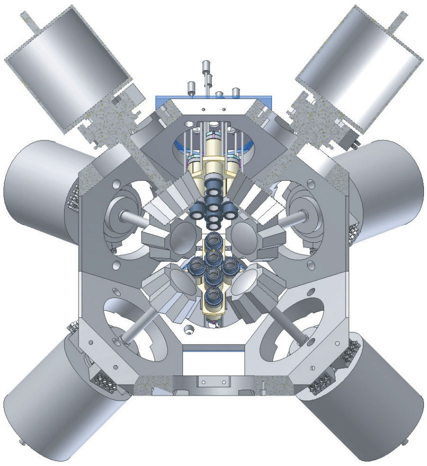

Fig. 1.: A schematic of one-half of EURICA with $LaBr_3$(Ce) detectors, viewed perpendicular to the beam line. The remaining unseen detectors are arranged at the bottom of the array.

Radioactive isotopes were delivered by BigRIPS to the experimental area, where they were implanted into WAS3ABi (Wide Angle Silicon Strip Stopper Array for Beta and ion implantation). The resulting γ rays following the isotope's decay were detected by the surrounding HPGe and $LaBr_3$(Ce) detectors (Fig. 1). Two plastic scintillators were added to WAS3ABi (one upstream and one downstream) to provide a stop signal for the short-range TDC of the $LaBr_3$(Ce) detectors, as the silicon detector's time resolution is too poor at hundreds of nanoseconds.

*1 RIKEN Nishina Center
*2 Department of Physics, The University of Surrey
*3 School of Computing, Engineering and Mathematics, The University of Brighton
*4 Department of Physics, Tohoku University
*5 Department of Physics, Osaka University
*6 Radioactivity Group, National Physics Laboratory
*7 Department of Physics, Beihang University

The $LaBr_3$(Ce) crystals are ∅ 1.5" x 2", each coupled to a H10570MOD Hamamatsu PMT. The crystals have removable 5 mm lead shields to prevent crosstalk between detectors. The configuration can be seen in figure 1. The plastic scintillators measured 45 mm x 150 mm x 2 mm and were placed approximately 3 - 5 mm from the first and last DSSDs.

The PMTs of the $LaBr_3$(Ce) detectors have an anode and a dynode output for timing and energy measurements respectively. The energy signal was taken from the last dynode of the 8-stage PMT and passed to a CAEN N568B shaping amplifier followed by a CAEN V785 ADC. The time signal from the anode is passed to an Ortec 935 CFD and then divided between a CAEN V775 short-range TDC and a CAEN V1190A long-range TDC. A stop signal from the plastic scintillator at F11 ($\sim$ 1 m before WAS3ABi) or from WAS3ABI is used for the long-range TDC. The stop signal for the short-range TDC is taken from the plastic scintillators.

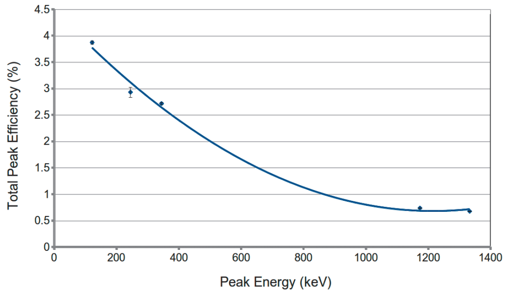

Fig. 2.: Absolute efficiency of the $LaBr_3$(Ce) detectors measured using ^{152}Eu and ^{60}Co sources.

The absolute efficiency of the $LaBr_3$(Ce) array is shown in figure 2. This was measured using ^{152}Eu and ^{60}Co point sources placed inside the WAS3ABi chamber, with the $LaBr_3$(Ce) detectors positioned on average $\sim$ 10 cm from the silicon strip detectors.

Analysis of data taken by the $LaBr_3$(Ce) detectors is in progress: preliminary results from half-life measurements in Zr isotopes can be found in reference 4.

References

1) O. J. Roberts *et al.*, Nucl. Instr. Methods A **748**, 91 (2014).
2) P. H. Regan *et al.*, EPJ Web of Conferences **63**, 01008 (2013).
3) O. J. Roberts *et al.*, EPJ Web of Conferences **63**, 01018 (2013).
4) F. Browne *et al.*, Measurement of Lifetimes of Excited States in ^{102}Zr and ^{104}Zr in this report.

Deuteron Analyzing Powers for *dp* elastic scattering at 250–294 MeV/nucleon and three-nucleon force

K. Sekiguchi,[*1] Y. Wada,[*1] J. Miyazaki,[*1] T. Taguchi,[*1] U. Gebauer,[*1] M. Dozono,[*2] S. Kawase,[*3] Y. Kubota,[*3] Y. Maeda,[*4] T. Mashiko,[*1] K. Miki,[*5] S. Sakaguchi,[*6] H. Sakai,[*2] N. Sakamoto,[*2] M. Sasano,[*2] Y. Shimizu,[*2] K. Takahashi,[*1] R. Tang,[*2] T. Uesaka,[*2] T. Wakasa,[*6] and K. Yako[*3]

The study of three-nucleon forces (3NFs) is essential for clarifying various nuclear phenomena. In addition to the first signals indicating 3NF effects in the binding energies of ^{3}H and ^{3}He, the significance of 3NFs has been recently pointed out for descriptions of discrete states in higher-mass nuclei. Three-nucleon scattering at intermediate energies ($E/A \sim 200$ MeV) is one attractive approach to investigate the dynamical aspects of 3NFs, such as momentum and/or spin dependences. With the aim of clarifying the roles of the 3NFs in nuclei, experimental programs with polarized deuteron beams at intermediate energies are in progress at RIBF. As the first step, we measured a complete set of deuteron analyzing powers (iT_{11}, T_{20}, T_{21}, T_{22}) in deuteron–proton (dp) elastic scattering at 250 and 294 MeV/nucleon (MeV/N).

A schematic diagram of the experimental setup can be found in Ref. (1). Vector- and tensor-polarized deuteron beams were accelerated by the injector cyclotrons AVF and RRC up to 90 (100) MeV/N; subsequently, they were accelerated up to 250 (294) MeV/N by the SRC. Typical values of the beam polarizations were 80% of the theoretical maximum values. The measurement for dp elastic scattering was performed by using a detector system, BigDpol, installed at the extraction beamline of the SRC. Polyethylene (CH_2) of thickness 330 mg/cm^2 was used as the hydrogen target. In BigDpol, four pairs of plastic scintillators coupled with photo-multiplier tubes were placed symmetrically in the azimuthal directions to the left, right, up and down. Scattered deuterons and recoil protons were detected in the kinematical coincidence condition by each pair of detectors. The angles ($\theta_{\mathrm{c.m.}}$) measured in the center-of-mass system are in the range 40°–162°. In the experiment, the deuteron beams were stopped in a Faraday cup, which was installed at the focal plane F0 of the BigRIPS spectrometer.

Here, we report the results of energy dependence of the deuteron tensor analyzing power T_{22}. The angular distribution of T_{22} is shown with open circles, together with the previously reported data at 70 and 135 MeV/N[1)]. The red (blue) bands in the figure are the Faddeev calculations with (without) Tucson–Melbourne'99 (TM99) 3NF[2)] based on the modern NN potentials, namely CDBonn[3)], AV18[4)], Nijmegen I, and Nijmegen II[5)]. The solid lines are the calculations including Urbana IX 3NF[6)] based on the AV18 potential.

The tensor analyzing power T_{22} reveals an energy dependence different from those obtained for the cross section and the other analyzing powers iT_{11}, T_{20}, and T_{21}[1)]. At 135 MeV/N and below, adding 3NFs degrades the description of data in a large angular region. It is contrary to what happens at energies above 250 MeV/N, for which large 3NF effects are supported by the T_{22} data.

In order to obtain a consistent understanding of the spin dependence of 3NFs up to high momenta, we plan to perform deuteron analyzing power measurements at 190 MeV/N.

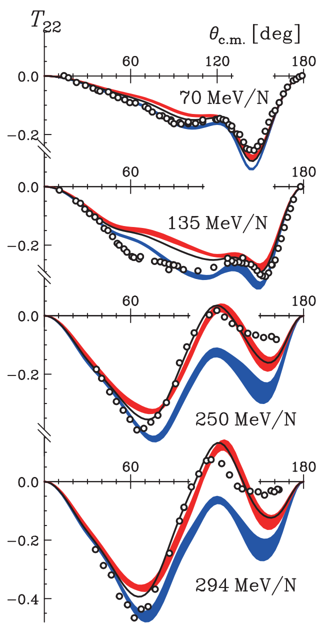

Fig. 1. Tensor analyzing power T_{22} for dp elastic scattering at 70–294 MeV/N.

*1 Department of Physics, Tohoku University
*2 RIKEN Nishina Center
*3 CNS, University of Tokyo
*4 Faculty of Engineering, University of Miyazaki
*5 RCNP, Osaka University
*6 Department of Physics, Kyushu University

References
1) K. Sekiguchi et al.: Phys. Rev. C **83**, 061001 (2011).
2) S. A. Coon and H. K. Han: Few Body Syst. **30**, 131 (2001).
3) R. Machleidt: Phys. Rev. C **63**, 024001 (2001).
4) R. B. Wiringa et al.: Phys. Rev. C **51**, 38 (1995).
5) V. G. J. Stoks et al.: Phys. Rev. C **49**, 2950 (1994).
6) B. S. Pudliner et al.: Phys. Rev. C **56**, 1720 (1997).

Shallow and diffuse spin-orbit potential for proton elastic scattering from neutron-rich helium isotopes at 71 MeV/nucleon[†]

S. Sakaguchi,[*1,*2] T. Uesaka,[*1] N. Aoi,[*3] Y. Ichikawa,[*1] K. Itoh,[*4] M. Itoh,[*5] T. Kawabata,[*6] T. Kawahara,[*1] Y. Kondo,[*7] H. Kuboki,[*1] T. Nakamura,[*7] T. Nakao,[*4] Y. Nakayama,[*7] H. Sakai,[*1] Y. Sasamoto,[*4] K. Sekiguchi,[*8] T. Shimamura,[*7] Y. Shimizu,[*1] and T. Wakui[*5]

Strong spin-orbit coupling in atomic nuclei plays an important role in nuclear structure and reactions. Its manifestation in neutron-rich nuclei has attracted extensive interest, since a number of experimental results suggest a change in the shell structure that could be explained by a reduction in the spin-orbit splitting. On the other hand, there has been no experimental study on how the spin-orbit coupling is modified in nuclear reactions. Spin asymmetry in proton–nucleus scattering is a prominent manifestation of the spin-orbit coupling in nuclear reactions. The spin-orbit term in the optical model potential is generally expressed by a derivative of the density distribution[1–3]. It would be interesting to probe the nature of the spin-orbit potential for a nucleus with a very diffuse surface.

In order to investigate the effect of the exotic density distribution on the spin-orbit potential, we measured the vector analyzing powers for proton elastic scattering from ^{6}He and ^{8}He at 71 MeV/nucleon at RIPS beamline at RI Beam Factory using the solid polarized proton target specially constructed for the RI-beam experiment [4]. To determine the spin-orbit potentials, we performed a phenomenological optical model analysis using the ECIS79 code. For the function of the potential, we used a standard Woods-Saxon form factor with a Thomas-type spin-orbit term. We search for a parameter set that reproduces both the $d\sigma/d\Omega$ and A_y data. Details of the fitting procedure and obtained parameters can be found in Refs.[5,6].

The characteristics of the spin-orbit potential is discussed in terms of the r.m.s. radius of the potential $\langle r_{ls}^2\rangle^{1/2} = \sqrt{\int r^2 V_{ls}(r) d\boldsymbol{r} / \int V_{ls}(r) d\boldsymbol{r}}$ and the amplitude of $rV_{ls}(r)$ at the peak position. Here, r is the distance from the center-of-mass of ^{6,8}He and $V_{ls}(r)$ is the spin-orbit potential. Figure 1(a) shows the mass-number dependence of the $\langle r_{ls}^2\rangle^{1/2}$ values for the spin-zero nuclei. The closed circles show the potentials locally obtained for each nucleus. The dashed and dot-dashed curves represent the global optical potentials[7,8]. We can see that the $\langle r_{ls}^2\rangle^{1/2}$ values of ^{6}He and ^{8}He are remarkably larger than the systematics. Moreover, it is interesting to find a close similarity between the behavior of $\langle r_{ls}^2\rangle^{1/2}$ and the matter radius r_m, plotted as the open squares in Fig. 1(a). This indicates the particular sensitivity of the spin-orbit interaction to the nuclear surface structure.

Figure 1(b) displays the amplitude of $rV_{ls}(r)$ at the peak position. The peak amplitudes for ^{6}He and ^{8}He are considerably smaller than the standard values of 3.5–5.5 MeV fm. From these results, it is concluded that the spin-orbit potentials between a proton and neutron-rich ^{6}He and ^{8}He nuclei are considerably shallower and more diffuse than the global systematics of nuclei along the stability line. This is considered to be a consequence of the diffuse density distribution of these neutron-rich isotopes.

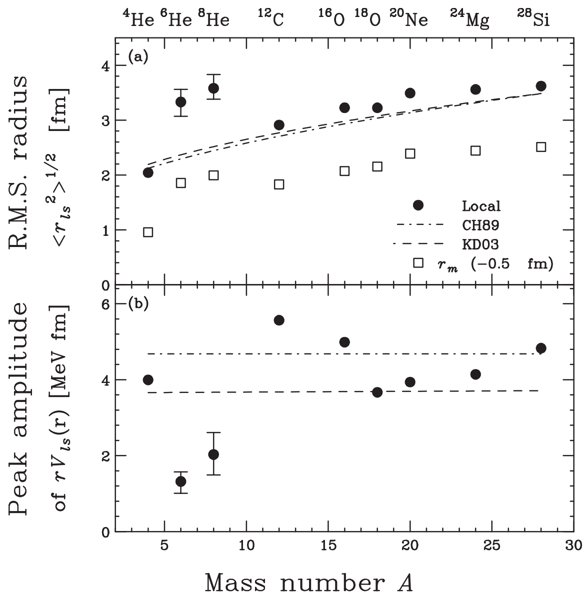

Fig. 1. See text for details. The symbols for r_m are shifted vertically by -0.5 fm to prevent overlap.

† Condensed from the article in Phys. Rev. C **87**, 021601(R) (2013)

*1 RIKEN Nishina Center
*2 Department of Physics, Kyushu University
*3 RCNP, Osaka University
*4 CNS, University of Tokyo
*5 CYRIC, Tohoku University
*6 Department of Physics, Kyoto University
*7 Department of Physics, Tokyo Institute of Technology
*8 Department of Physics, Tohoku University

References
1) C. B. Dover *et al.*: Nucl. Phys. A **190**, 373 (1972).
2) R. R. Scheerbaum: Nucl. Phys. A **257**, 77 (1976).
3) E. Bauge *et al.*: Phys. Rev. C **58**, 1118 (1998).
4) T. Wakui: Proc. of PST2005 (World Scientific, 2007).
5) S. Sakaguchi *et al.*: Phys. Rev. C **84**, 024604 (2011).
6) S. Sakaguchi *et al.*: Phys. Rev. C **87**, 021601(R) (2013).
7) R. L. Varner *et al.*: Phys. Rep. **201**, 58 (1991).
8) A. J. Koning *et al.*: Nucl. Phys. A **713**, 231 (2003).

Study of proton and neutron density distributions observed via proton elastic scattering at 200 and 300 MeV

J. Zenihiro,[*1] H. Sakaguchi,[*2] S. Terashima,[*4] Y. Matsuda,[*2] S. Adachi,[*3] T. Baba,[*3] T. Furuno,[*3] T. Hashimoto,[*2] T. Kawabata,[*2] J. Lee,[*1] Y. Maeda,[*5] K. Miki,[*2] T. Murakami,[*3] H. J. Ong,[*2] A. Tamii,[*2] J. Tanaka,[*2] M. Tsumura,[*3] T. Yamamoto,[*2] and L. Yu,[*4]

A systematic study of the nucleon density distributions of finite nuclei is important for understanding the isospin dependence of the nuclear many-body system. For example, the neutron skin thicknesses are known to be strongly correlated with the density-dependent term of the symmetry energy, and the isospin-dependent term of the nuclear equation of state.

In previous works,[1,2] we have succeeded in extracting the neutron density distributions of stable nuclei such as Sn and Pb isotopes via proton elastic scattering. At the same time we have launched a new project aimed at measuring the Elastic Scattering of Protons with RI beams (ESPRI) with the purpose of the extraction of proton and neutron density distributions of unstable nuclei. We have newly developed and tested unique devices for the ESPRI measurements at NIRS-HIMAC in Chiba and GSI in Germany.[3,4] Finally, we have successfully performed the ESPRI experiment at RIBF in April, 2013.[5]

Unlike the case of stable nuclei, however, we have no information on the nuclear charge densities of unstable nuclei. Thus, we have proposed a new method to extract proton and neutron densities via two-energy proton elastic scattering. This method is based on the large difference between the energy dependences of the p-p and p-n interactions. Recently, we performed an experiment to demonstrate this new method using real data of Zr isotopes. In this report, we show the preliminary results of ^{90}Zr only. For other isotopes (^{92,94}Zr), the analysis is still ongoing.

The experiment was performed at RCNP, Osaka University. Polarized proton elastic scattering from ^{90,92,94}Zr and ^{58}Ni at 200 and 300 MeV was measured by using the Grand Raiden magnetic spectrometer.[6] Figure 1 shows the angular distributions of cross sections ($d\sigma/d\Omega$) and the analyzing powers (A_y) of ^{90}Zr($\vec{p}$,p) at 200 and 300 MeV and of ^{58}Ni($\vec{p}$,p) at 200 MeV. The red lines denote the result of relativistic impulse approximation (RIA) with relativistic-Hartree (RH) densities. The ^{58}Ni data was used to determine the effective interaction at 200 MeV (solid lines). Using the effective interaction, the proton and neutron densities of ^{90}Zr were simultaneously searched and the results are denoted by the solid lines in Fig. 1 and 2. The proton and neutron densities can be separately and simultaneously determined by the new method. The extracted proton and neutron radii of ^{90}Zr are 4.210(20) and 4.300(17) fm, respectively. The extracted proton radius is very consistent with that of 4.198(1) fm, which is derived from the charge radius determined via the combined analysis of electron elastic scattering and muonic atom X-rays data.[7]

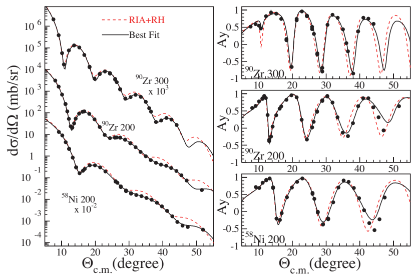

Fig. 1. Obtained data of $d\sigma/d\Omega$ and A_y of ^{90}Zr at 200 and 300 MeV and of ^{58}Ni at 200 MeV. The black solid lines show the fitting results while the red dashed lines are RIA calculations with RH densities.

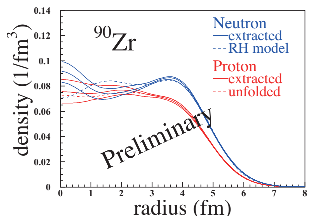

Fig. 2. Extracted proton and neutron densities, denoted by solid red and blue lines, respectively. While upper and lower lines show the error envelopes due to the experimental errors, middle lines are the best-fit results. The red dashed line shows the proton density by unfolding the nuclear charge density. Blue dashed line shows the same by the RH model calculation.

References
1) S. Terashima *et al.*: Phys. Rev. C **77**, 024317 (2008).
2) J. Zenihiro *et al.*: Phys. Rev. C **82**, 044611 (2010).
3) Y. Matsuda *et al.*: Phys. Rev. C **87**, 034614 (2013).
4) S. Terashima *et al.*: GSI Scientific Report, 148 (2010).
5) S. Terashima *et al.*: in this report.
6) M. Fujiwara *et al.*: Nucl. Instr. Meth. A **422**, 484 (1999).
7) I. Angeli: At. Data Nucl. Data Tables **87**, 185 (2004).

*1 RIKEN Nishina Center
*2 RCNP, Osaka University
*3 Department of Physics, Kyoto University
*4 School of Physics and Nuclear Energy Engineering, Beihang University
*5 Department of Applied Physics, University of Miyazaki

Spin-isospin response of the neutron-rich nucleus ^{8}He via the (p, n) reaction in inverse kinematics

M. Kobayashi,[*1] K. Yako,[*1] S. Shimoura,[*1] M. Dozono,[*2] S. Kawase,[*1] K. Kisamori,[*1,*2] Y. Kubota,[*1,*2] C.S. Lee,[*1,*2] S. Michimasa,[*1] H. Miya,[*1,*2] S. Ota,[*1] H. Sakai,[*2] M. Sasano,[*2] and M. Takaki[*1]

Charge-exchange (p, n) reactions at intermediate energies ($E > 100$ MeV) serve as powerful tools to study spin-isospin responses of nuclei; Gamow-Teller (GT) transitions are a particular example of such reactions. In the present work, we focused on the neutron-rich nucleus ^{8}He, which has the largest neutron-to-proton ratio among all known particle-stable nuclei ($N/Z = 3$). It can be described as an α-particle surrounded by four valence neutrons, exhibiting a neutron halo or thick neutron skin. We measured the ^{8}He$(p, n)^8$Li reaction at 190A MeV in inverse kinematics in order to study the spin-isospin response of ^{8}He. This is the first measurement of the charge-exchange reaction on ^{8}He.

The experiment was performed at the RIKEN RI Beam Factory (RIBF). Recoil neutrons with low kinetic energies from the (p, n) reactions were detected by the recently developed neutron detector WINDS.[1)] The residual nucleus ^{8}Li and its decay product ^{7}Li were detected using auxiliary beam line detectors, a plastic scintillator, and a multi-wire drift chamber (LP-MWDC)[2)], installed at FH10, which is downstream from the secondary target at FH9. A superconducting triplet quadrupole (STQ) was installed between FH9 and FH10. The triton decay channel of the excited state in ^{8}Li was not tagged in this measurement.

Double differential cross sections for the ^{8}He$(p, n)^8$Li reaction at excitation energies of 0–20 MeV and neutron energies of 2.0–4.4 MeV, which correspond to momentum transfers of 0.31–0.46 fm^{-1}, were obtained. Figure 1 shows the double differential cross sections for $T_n = 2.0$–2.6 MeV, corresponding to $q = 0.31$–0.35 fm^{-1}. In the spectrum, two peaks were observed at ~ 1 MeV and ~ 8 MeV. The lower peak corresponds to the first excited 1^+ state of ^{8}Li at 0.98 MeV.

The angular distributions of the cross sections for the peaks at ~ 1 MeV and ~ 8 MeV are shown in Fig. 2. In this figure, the differential cross sections were corrected for the transmission efficiencies between FH9 and FH10. They were compared to the results of distorted wave impulse approximation (DWIA) calculations. The angular distribution of the peak at ~ 1 MeV, which is a flat distribution, was reproduced well by the sum of the 0.98-MeV state ($J^\pi = 1^+$) and the ground state ($J^\pi = 2^+$). The cross sections at $q = 0$ for the 0.98-MeV and 8-MeV states were extracted. We then calculated the GT strength B(GT) for the 8-MeV state by using the extracted cross sections at $q = 0$ and the known B(GT) value of 0.24 for the 0.98-MeV state. The obtained GT strength was B(GT) ~ 8 for the neutron decay channel of the 8-MeV state.

*1 Center for Nuclear Study, the University of Tokyo
*2 RIKEN Nishina Center

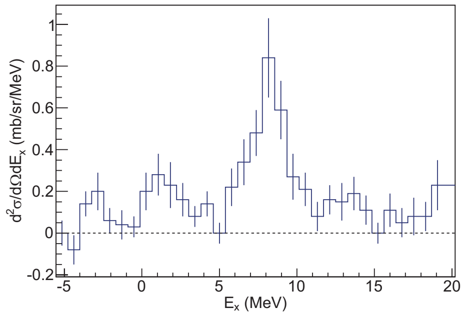

Fig. 1. (Preliminary) Double differential cross sections for $T_n = 2.0$–2.6 MeV.

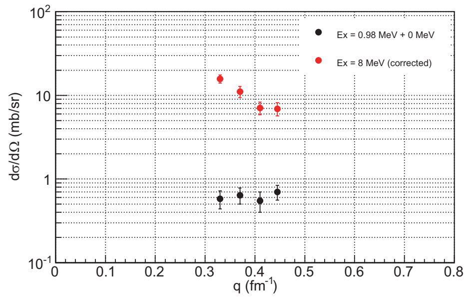

Fig. 2. (Preliminary) Angular distributions of the measured cross section for the 0.98-MeV (black) peak and the 8-MeV (red) peak.

It is known that the excited state at ~ 9 MeV with a large GT strength of B(GT) ~ 5 decays primarily by triton emission.[3,4)] In contrast, we observed, for the first time, a neutron decay channel of the resonance state with a large B(GT) strength. This result suggests that most of the GT strength is concentrated in the resonance state at ~ 8 MeV. The observed state is most likely the Gamow-Teller resonance of ^{8}He. Further analysis is in progress.

References

1) K. Yako *et al.*: RIKEN Accel. Prog. Rep. **45**, 137 (2012).
2) H. Miya *et al.*: Nucl. Instr. Meth. B **317**, 710 (2013).
3) M.J.G. Borge *et al.*: Z. Phys. A **340**, 255 (1991).
4) M.J.G. Borge *et al.*: Nucl. Phys. A **560**, 664 (1993).

New type of spectroscopy via heavy-ion double charge exchange (^{12}C, ^{12}Be(0^+_2)) reaction

M. Takaki,[*1] T. Uesaka,[*2] S. Shimoura,[*1] N. Aoi,[*3] M. Dozono,[*2] S. Gotanda,[*4] T. Hashimoto,[*3] Y. Kanaya,[*4] T. Kawabata,[*5] K. Kisamori,[*1,*2] M. Kobayashi,[*1] Y. Kubota,[*1,*2] Y. Maeda,[*4] M. Matsushita,[*1] S. Michimasa,[*1] K. Miki,[*3] E. Milman,[*2] S. Ota,[*1] M. Sasano,[*2] A. Tamii,[*3] M. Tsumura,[*5] and J. Zenihiro[*2]

One of the most interesting features in atomic nuclei is the variety of spin and isospin responses. The Gamow–Teller (GT) transition is the simplest spin–isospin response within one-phonon excitations, and it has been well studied. In contrast, data on multi-phonon excitations have been scarce. The double GT giant resonance (DGTGR)[1)] is the most basic two-phonon excitation mode. However, DGTGRs have not been observed so far. The discovery of the DGTGR is an essential step in extending the research of the spin–isospin responses to multi-phonon space. Another interest for studying DGTGR relates to its relevance in neutrino physics; the DGT transition is induced by the same transition operator as the $\beta\beta$-decay is , *i.e.*, $\sigma\tau\sigma\tau$. However, the $\beta\beta$-decay has quite small DGT strength. A major part of the DGT strength is concentrated among highly excited states in DGTGR. A promising spectroscopic method to search for DGTGRs is through heavy-ion double charge exchange (HIDCX) reactions, which can induce two-phonon excitations with spin and isospin transfer by two units.

In 2011, we conducted a HIDCX ^{12}C(^{18}O, ^{18}Ne)^{12}Be reaction experiment and found a large cross section of 1.5 μb/sr for the second 0^+ (0^+_2) state in ^{12}Be at 0°[2)]. This is probably because all the initial ^{12}C($0^+_{\mathrm{g.s.}}$), intermediate ^{12}B($1^+_{\mathrm{g.s.}}$), and final ^{12}Be(0^+_2) states are dominated by a $0\hbar\omega$ configuration[3–5)]. This led us to a new idea to use the (^{12}C, ^{12}Be(0^+_2)) reaction as a tool to investigate DGTGRs. In this probe, the excitation energy of target nuclei are measured using a missing–mass technique. Several final states in ^{12}Be can degrade the signal-to-noise ratio of an observed spectrum in the method. The key of this probe is to avoid the contamination by tagging the two 511–keV γ-rays emitted back-to-back from the e^+e^- decay with the mean lifetime of 331 ns[6)]. In order to demonstrate the feasibility of the delayed γ-ray tagging method, we performed the HIDCX ^{18}O(^{12}C, ^{12}Be(0^+_2))^{18}Ne reaction measurement using the Grand Raiden (GR) spectrometer at RCNP, Osaka University. The primary ^{12}C beam at 100A MeV bombarded a 20-mg/cm^2 $H_2{}^{18}O$ ice target. The momenta of outgoing particles were analyzed using GR. The two 511–keV γ-rays from ^{12}Be(0^+_2) were detected using a NaI(Tl) array surrounding a plastic-scintillator stopper at the GR focal plane. Figure 1 shows the GR horizontal position spectra. The position corresponds to the excitation energy of ^{18}Ne. The peak of the spectrum without the γ-ray tagging, which originates from the ^{18}Ne ground state, is rather broad and has a tail. The broadening is probably due to contributions from different final states in ^{12}Be, and the tail originates from accidental coincidence events of ^{9}Li and ^{6}He. On the other hand, in a red spectrum with γ-ray tagging, the peak indicated by a red arrow is narrower, and the background has mostly vanished. The obtained energy resolution was ~3 MeV mainly because of an energy–loss difference in the target, and thus the difference between the peak positions of the two spectra is within the resolution. The result of the test experiment shows the feasibility of the gamma-ray tagging method. Our next step is to apply this method to nuclei exhibiting $\beta\beta$-decay, such as ^{48}Ca.

*1 Center for Nuclear Study, The University of Tokyo
*2 RIKEN Nishina Center
*3 Research Center for Nuclear Physics, Osaka University
*4 Department of Applied Physics, University of Miyazaki
*5 Department of Physics, Kyoto University

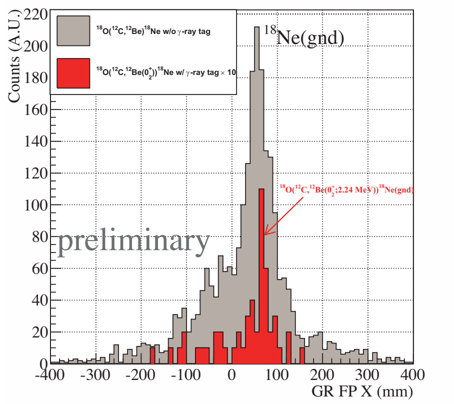

Fig. 1. Horizontal position spectra of the GR focal plane with or without γ-ray tagging. For the red spectrum, detection efficiency of 10% is considered for the NaI(Tl) array.

References

1) D.C. Zheng, L. Zamick, N. Auerbach: Ann. of Phys. **197**, 343 (1990).
2) M. Takaki *et al.*: RIKEN Accel. Prog. Rep. **46**, 29 (2013).
3) F.C. Barker: J. Phys. G **2**, L45 (1976).
4) H. Fortune and R. Sherr: Phys. Rev. C **74** (2006) 024301.
5) R. Meharchant *et al.*: Phys. Rev. Lett. **108** (2012) 122501.
6) S. Shimoura *et al.*: Phys. Lett. B **560** (2003) 31; *ibid* **654**, (2007) 87.

Study of spin-isospin responses via exothermic charge exchange reaction (^{8}He, ^{8}Li)

H. Miya,[*1,*2] S. Shimoura,[*2] K. Kisamori,[*1,*2] M. Assié,[*3] H. Baba,[*1] T. Baba,[*4] D. Beaumel,[*3] M. Dozono,[*1] T. Fujii,[*2] N. Fukuda,[*1] S. Go,[*1,*2] F. Hammache,[*3] E. Ideguchi,[*5] N. Inabe,[*1] M. Itoh,[*6] D. Kameda,[*1] S. Kawase,[*2] T. Kawabata,[*4] M. Kobayashi,[*2] Y. Kondo,[*7] T. Kubo,[*1] Y. Kubota,[*1,*2] C. S. Lee,[*1,*2] Y. Maeda,[*8] H. Matsubara,[*9] S. Michimasa,[*2] K. Miki,[*5] T. Nishi,[*10] M. Kurata-Nishimura,[*1] S. Ota,[*2] H. Sakai,[*1] S. Sakaguchi,[*11] M. Sasano,[*1] H. Sato,[*1] Y. Shimizu,[*1] H. Suzuki,[*1] A. Stolz,[*12] M. Takaki,[*2] H. Takeda,[*1] S. Takeuchi,[*1] A. Tamii,[*5] H. Tokieda,[*2] M. Tsumura,[*4] T. Uesaka,[*1] K. Yako,[*2] Y. Yanagisawa,[*1] and R. Yokoyama[*2]

We performed the exothermic charge-exchange (CE) reaction of (^{8}He, ^{8}Li) at the RIKEN RIBF facility by using the BigRIPS, the High-Resolution Beamline (HRBL), and the SHARAQ spectrometer.[1,2] Missing mass spectra in the ^{4}He, ^{12}C(^{8}He, ^{8}Li) reactions were measured at the beam energy of 190 MeV/nucleon. The spin-isospin response of a spin-dipole transition with the radioactive isotope (RI) beam induced by the CE reaction was studied.

The intensity of the secondary ^{8}He beam, which was produced via a projectile-fragmentation reaction of an ^{18}O beam, was about 2 Mcps at the secondary target position (SHARAQ-S0). The scattered ^{8}Li was momentum-analyzed with the SHARAQ spectrometer. Low-pressure multiwire drift chambers[3] were placed at the foci of the BigRIPS and the HRBL. Cathode readout drift chambers[4] were installed at the final focal plane (SHARAQ-S2) of the SHARAQ spectrometer. The high-resolution achromatic (HRA) transport mode[2] was set to obtain a momentum acceptance of 2%. The detail experimental setup is described in a previous report.[5].

The secondary RI beam has momentum distribution. In order to perform high-resolution missing mass spectroscopy with the RI beam, measurement of the beam momentum (δ) of incoming and outgoing particles at the target is required. At the momentum-dispersive focal planes, δ is correlated with the beam trajectory. In the HRA mode, it is important to measure the trajectory, mainly the horizontal position (x), at the BigRIPS-F6 and the SHARAQ-S2. δ couples with the beam transfer matrix elements of x and horizontal angle (a). The matrix elements should be measured to obtain the missing mass energy in the CE reaction. The ^{8}Li beam was transported to the S2 for checking the matrix elements of $(x|x)$ and $(x|a)$ of the beamline and the SHARAQ spectrometer.

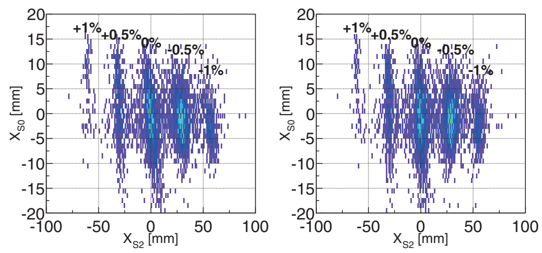

(a) (b)

Fig. 1. Correlation of x_{S0} with x_{S2} (a) before and (b) after correction.The five loci correspond to the particles with δ = -1%, -0.5%, ... ,1%, which were tagged at the BigRIPS-F6.

Figure 1(a) shows the correlations of x_{S0} with x_{S2} for the momentum correction of the ^{8}Li beam. The five loci correspond to the particles with δ = -1%, -0.5%, ... ,1%, which were tagged at the F6. The inclinations of the loci indicate the matrix element of $(x|x)$. The difference in the inclinations for different δ's is due to the effect of the second-order matrix element of $(x|x\delta)$. This defference enables enabled us to obtain the δ at high resolution by correcting the correlation, as shown in Fig. 1(b). The matrix elements of $(x|a)$ and $(x|a\delta)$ were determined to correct the tilt of the focal plane. These higher-order matrix elements of the beamline at F6 were determined by checking the correlation with tagging the beam momentum at S2. The missing mass resolution was evaluated to be 3.2 MeV in FWHM by using the matrix elements and 4.6 MeV in FWHM before the correction. Further analysis of the missing mass and angular distribution is now in progress.

*1 RIKEN Nishina Center
*2 Center for Nuclear Study, The University of Tokyo
*3 Institut de Physique Nucléaire, Orsay
*4 Department of Physics, Kyoto University
*5 Research Center Nuclear Physics, Osaka University
*6 Cyclotron and Radioisotope Center, Tohoku University
*7 Department of physics, Tokyo Institute of Technology
*8 Department of Applied Physics, University of Miyazaki
*9 National Institute of Radiological Sciences
*10 Department of physics, The University of Tokyo
*11 Department of Physics, Kyushu University
*12 National Superconducting Cyclotron Laboratory, Michigan State University

References

1) T. Uesaka et al.: Prog. Theor. Exp. Phys. (2012) 03C007.
2) S. Michimasa et al.: Nucl. Instr. Meth. B **317**, 305-310 (2013).
3) H. Miya et al.: Nucl. Instr. Meth. B **317**, 710-713 (2013).
4) K. Kisamori et al.: CNS Ann. Rep. 2011 (2013).
5) H. Miya et al.: RIKEN Prog. Rep. **46** 25 (2013).

Spectroscopy of single-particle states in oxygen isotopes via $^{A}\mathrm{O}(\vec{p}, pN)$ reaction with polarized protons

S. Kawase,[*1] T. Uesaka,[*2] S. Shimoura,[*1] K. Yako,[*1] S. Ota,[*1] S. Michimasa,[*1] H. Tokieda,[*1] H. Miya,[*1*2] T. L. Tang,[*1] K. Kisamori,[*1,*2] M. Takaki,[*1,*2] Y. Kubota,[*1,*2] C. S. Lee,[*1,*2] R. Yokoyama,[*1] T. Fujii,[*1,*2] M. Kobayashi,[*1] M. Sasano,[*2] J. Zenihiro,[*2] H. Matsubara,[*2] M. Dozono,[*2] H. Sakai,[*2] T. Kubo,[*2] K. Yoshida,[*2] N. Inabe,[*2] Y. Yanagisawa,[*2] H. Takeda,[*2] K. Kusaka,[*2] N. Fukuda,[*2] D. Kameda,[*2] H. Suzuki,[*2] T. Kawahara,[*2,*3] T. Wakui,[*2,*4] S. Sakaguchi,[*2,*5] T. Noro,[*2,*5] T. Wakasa,[*2,*5] J. Yasuda,[*2,*5] T. Fukunaga,[*2,*5] Y. Maeda,[*6] W. Kim,[*7] S. H. Hwang,[*7] S. Stepanyan,[*7] A. Obertelli,[*8] A. Galindo-Uribarri,[*9] E. Padilla-Rodal,[*10] D. Beaumel[*2,*11] for the SHARAQ04 collaboration

The $(\vec{p}, pN)$ reaction is an effective spectroscopic tool to examine single-particle states. One can determine the spin-parity of single-particle states in nuclei from the momentum dependence of the cross section and the vector analyzing power without model dependence.[1)] In this experiment, our goal was to determine the spin-orbit splitting of the 1p spin doublet in oxygen isotopes as a function of their neutron number.

We performed $^{14,22-24}\mathrm{O}(\vec{p}, 2p)$ reaction measurements (SHARAQ04 experiment) with a polarized proton target at RIKEN RIBF to measure single-particle spectra and to determine spin-orbit splitting in $^{14,22-24}\mathrm{O}$. For the experimental setup, see refs.[2,3)]

Figure 1 shows the time-of-flight (TOF)-ΔE correlations for (a) incident and (b) residual particles in $^{14}\mathrm{O}$ runs. The particles are identified via the TOF-ΔE method on an event-by-event basis. For residuals, only their atomic numbers are identified. The proton separation energy (S_p) of the target nuclei can be obtained from the scattering angles and momenta of scattered protons:

$$S_p = (1-\gamma)\, m_p - \gamma\,(T_1 + T_2) + \beta\gamma\left(p_{1\parallel} + p_{2\parallel}\right),$$

where γ and β are the Lorentz factor and the velocity of the beam, respectively; m_p is the proton mass; T_1 and T_2 are the kinetic energies of the scattered protons; and $p_{1\parallel}$ and $p_{2\parallel}$ are the momenta of the scattered protons. In this formula, the momentum of the residual nucleus is ignored because its effect to S_p is negligibly small compared with the resolution of S_p. Figure 2 shows the separation energy spectrum for the $^{14}\mathrm{O}(p, 2p)^{x}\mathrm{N}$ reaction. Some amount of strength can be seen above the separation energy of $^{14}\mathrm{O}$ (4.627 MeV). However, it is difficult to distinguish excited states in the current result because of the small statistics. We intend to continue the analysis of these results by investigating different gating methods that may improve the efficiency, resolution, and S/N ratio.

The analysis for $^{22}\mathrm{O}$ and $^{24}\mathrm{O}$ beams is still ongoing.

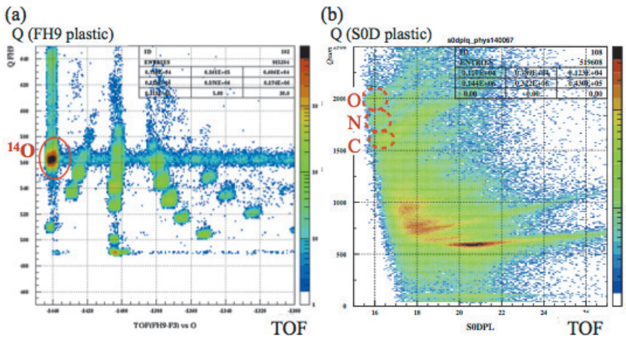

Fig. 1. TOF-ΔE correrations for (a) incident and (b) residual particles in $^{14}\mathrm{O}$ runs. TOF was measured by using plastic scintillators between (a) F3 and FH9 and (b) target position and S0 downstream.

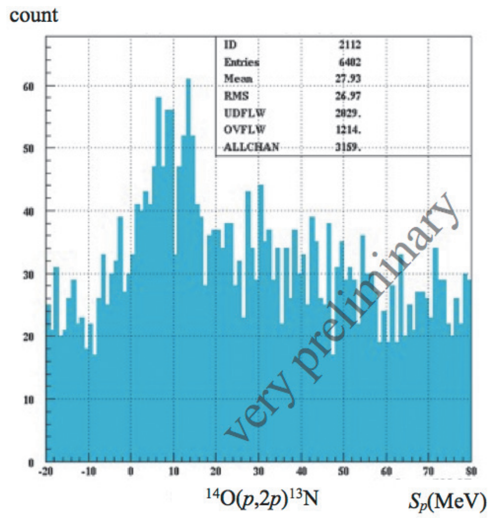

Fig. 2. Separation energy spectrum for $^{14}\mathrm{O}(p, 2p)^{x}\mathrm{N}$.

*1 Center for Nuclear Study (CNS), University of Tokyo
*2 RIKEN Nishina Center
*3 Department of Physics, Toho University
*4 CYRIC, Tohoku University
*5 Department of Physics, Kyushu University
*6 Department of Applied Physics, University of Miyazaki
*7 Department of Physics, Kyungpook National University
*8 CEA Saclay
*9 Oak Ridge National Laboratory
*10 Instituto de Ciencias Nucleares, Universidad Nacional Autónoma de México
*11 Institut de Physique Nucléaire d'Orsay

References
1) G. Jacob, Th. A. J. Maris *et al.*: Nucl. Phys. A, **257**(3), 517 (1976).
2) S. Kawase *et al.*: RIKEN Accel. Prog. Rep. **46** (2013) 30.
3) T. L. Tang *et al.*: RIKEN Accel. Prog. Rep. **46** (2013) 162.

Missing-mass spectroscopy of the 4n system via exothermic double-charge exchange reaction at high beam counting rates

K. Kisamori,[*1,*2] S. Shimoura,[*2] H. Miya,[*1,*2] M. Assie,[*3] H. Baba,[*1] T. Baba,[*4] D. Beaumel,[*1,*3] M. Dozono,[*1] T. Fujii,[*1,*2] N. Fukuda,[*1] S. Go,[*1,*2] F. Hammache,[*3] E. Ideguchi,[*5] N. Inabe,[*1] M. Itoh,[*6] D. Kameda,[*1] S. Kawase,[*2] T. Kawabata,[*4] M. Kobayashi,[*2] Y. Kondo,[*1,*7] T. Kubo,[*1] Y. Kubota,[*1,*2] M. Kurata-Nishimura,[*1] C. S. Lee,[*1,*2] Y. Maeda,[*8] H. Matsubara,[*1] S. Michimasa,[*2] K. Miki,[*5] T. Nishi,[*1,*9] S, Noji,[*10] S. Ota,[*2] S. Sakaguchi,[*1,*11] H. Sakai,[*1] Y. Sasamoto,[*2] M. Sasano,[*1] H. Sato,[*1] Y. Shimizu,[*1] A. Stolz,[*10] H. Suzuki,[*1] M. Takaki,[*2] H. Takeda,[*1] S. Takeuchi,[*1] A. Tamii,[*5] L. Tang,[*2] H. Tokieda,[*2] M. Tsumura,[*4] T. Uesaka,[*1] K. Yako,[*2] Y. Yanagisawa,[*1] and R. Yokoyama[*2]

Since the report on candidates of bound tetra-neutron system[1)], Multi-neutron systems in nuclei have attracted considerable attention on both the experimental and theoretical fronts. On the other hand, later theoretical studies using ab-initio calculations[2)] have suggested that the tetra-neutron cannot exist as a bound system.

We performed missing-mass spectroscopy of the 4n system via an exothermic double-charge exchange reaction ^{4}He(^{8}He,^{8}Be)4n. The purpose of this experiment was to obtain information on few-body forces, such as the T=3/2 three body force, and the correlations between in multi-body scattering states that reflect final state interactions of sub-systems, such as di-neutron correlations. In order to produce the 4n system with a small momentum transfer of less than 20 MeV/c, a secondary beam of ^{8}He with a large internal energy, 190 A MeV, was used.

The experiment was performed at the RIKEN RI Beam Factory (RIBF) using the SHARAQ spectrometer and a liquid He target system. The Be target at BigRIPS-F0 was bombarded by a primary beam of ^{18}O at 230 A MeV to produce the ^{8}He secondary beam. We measured the momentum of the ^{8}He beam at BigRIPS-F6 with the High-Resolution Beamline and also measured the momentum of two alpha particles, which were the decay products of the ^{8}Be ejectile, with the SHARAQ spectrometer.

Because a small cross section was expected for this reaction, it was important to achieve a large yield and good S/N ratio. The highest ^{8}He beam intensity in this experiment was 2×10^6 counts/second, which was produced by the 13.7 MHz AVF cyclotron. The first bunch of triggered particles comprise 14.6 % of the multi-particle event, and the next bunch comprises 12.7 % (the bunch after that comprise 10.6 %). We developed a new analytical framework that contains information of multi particles arranged in a bunch structure as a new dimension. Previous frameworks have assumed that one trigger event corresponds to only one particle.

By reading multi-hit TDCs and assigning bunches in plastic scintillators, we can increase the statistics by 12.1%w. With the multi wire drift chambers(MWDCs) as tracking detectors at the beamline, it is found that other particles in the later bunches of the triggered particle cause tracking errors. By treating the sum of drift times of the planes shifted to the half cell of MWDCs (Fig. 1), we can improve statistics by 10.3% and eliminate multi-particles in each bunch.

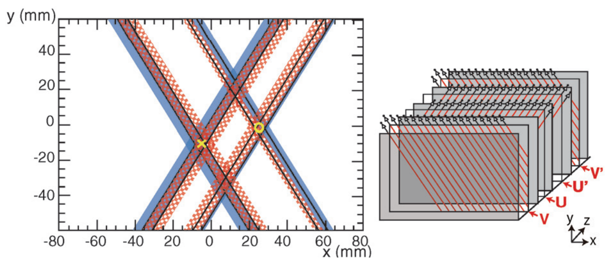

Fig. 1. Example of an event snapshot. The MWDC at F6 consists of 4 planes (U(30°)-U'(30°)-V(60°)-V'(60°)). Solid lines represent hit wires. Blue solid and red meshed bands represent the drift length of U(U') and V(V') planes, respectively. We can track the position (indicated by yellow circle) if there are 4 candidates. The yellow cross denotes the particle in the next bunch of triggered particle.

At the final focal plane of the SHARAQ spectrometer, two-alpha events can be tracked using cathode readout drift chamber[4)] (CRDCs). We identified approximately about a hundred candidate events for the 4n system. We are yet to examine the kinematical conditions and eliminate the background.

*1 RIKEN Nishina Center
*2 Center for Nuclear Study, the University of Tokyo
*3 IPN, Orsay
*4 Department of Physics, Kyoto University
*5 Research Center Nuclear Physics, Osaka University
*6 Cyclotron and Radioisotope Center, Tohoku University
*7 Department of Physics, Tokyo Institute of Technology
*8 Faculty of Engineering, University of Miyazaki
*9 Department of Physics, the University of Tokyo
*10 National Superconducting Cyclotron Laboratory, Michigan State University
*11 Faculity of Science, Kyushu University

References
1) F. Marques *et al.*: Phys. Rev. **C 65**, 044006 (2002)
2) S. Pieper: Phys. Rev. Lett. **90**, 252501 (2003)
3) K. Kisamori *et. al.*: CNS Ann. Rep. 2010 (2012)
4) K. Kisamori *et. al.*: Accelerator Progress Rep. **46** (2013)

Parity-transfer (^{16}O, ^{16}F) reaction for study of pionic 0^- mode

M. Dozono,[*1] T. Uesaka,[*1] M. Sasano,[*1] S. Shimoura,[*2] S. Michimasa,[*2] S. Ota,[*2] H. Matsubara,[*2] Y. Sasamoto,[*2] S. Noji,[*2] H. Tokieda,[*2] H. Miya,[*2] S. Kawase,[*2] L. Tang,[*2] Y. Kikuchi,[*2] K. Kisamori,[*2] M. Takaki,[*2] Y. Kubota,[*2] C. S. Lee,[*2] T. Fujii,[*2] R. Yokoyama,[*2] H. Sakai,[*1] T. Kubo,[*1] K. Yoshida,[*1] Y. Yanagisawa,[*1] N. Fukuda,[*1] H. Takeda,[*1] D. Kameda,[*1] N. Inabe,[*1] K. Yako,[*3] T. Wakasa,[*4] K. Fujita,[*4] S. Sakaguchi,[*4] H. Sagawa,[1,5] M. Yamagami,[*5] and M. Ichimura[*1]

The spin-dipole (SD) 0^- excitation is an important topic in the study of spin-isospin responses in nuclei. Because the 0^- excitation carries the same quantum number as a pion, its strength distribution is expected to reflect pion-like correlations in nuclei such as tensor correlations[1)]. Despite this importance, experimental information on 0^- states is very limited because of a lack of experimental tools that are suitable for 0^- studies.

In a previous report[2)], we proposed a new probe, a parity-transfer (^{16}O, ^{16}F(0^-)) reaction for 0^- studies. The parity-transfer reaction uses $0^+ \rightarrow 0^-$ transition in the projectile to probe 0^- states in a target nucleus. This reaction has unique sensitivity to unnatural parity states, which is an advantage over other reactions used so far.

For the first parity-transfer measurement, we plan to perform a ^{12}C(^{16}O, ^{16}F(0^-))^{12}B experiment at the RIKEN RIBF facility by using a SHARAQ spectrometer. Figure 1 shows the schematic of the experimental setup. A primary ^{16}O beam of 250 MeV/A is transported onto a ^{12}C target. The outgoing ^{16}F are unbound to $^{15}\mathrm{O} + p$. Thus, we perform the coincidence measurements of the decayed $^{15}\mathrm{O} + p$ pairs. These particles are momentum analyzed using the SHARAQ spectrometer. The analyzed ^{15}O are detected with the focal plane detectors of SHARAQ (two cathode readout drift chambers (CRDCs)), while the protons are detected at the low-momentum side of the first dipole magnet. The 0^- state of ^{16}F is identified by reconstructing the invariant mass of the $^{15}\mathrm{O} + p$ pairs.

For this measurement, we have been developing a proton tracking detector system, which consists of two multi-wire drift chambers (MWDCs) and one plastic scintillator (See Fig. 1). Table 1 shows the specifications of the MWDCs. Each MWDC has an effective area of 480 mm^W × 240 mm^H to cover the acceptance for the protons emitted from ^{16}F. The readout electronics and data acquisition (DAQ) system are the same as those described in Ref.[3)].

The performance of the MWDC was tested in the SHARAQ04 experiment. A proton beam with an energy and intensity of 250 MeV and 1 kHz, respectively, was incident on the MWDC. The position resolution was estimated from the residual of $x_{\mathrm{X}} - x_{\mathrm{X'}}$. Here, x_{X} ($x_{\mathrm{X'}}$) is a hit position in the X (X') layer. We also estimated the tracking efficiency, which was defined as the ratio of the number of events with the residual within 3σ to the number of beams measured by using the scintillator at the upstream of the MWDC. The resulting position resolution and tracking efficiency were 270 μm (FWHM) and 96%, respectively, when we applied a voltage of -1.6 kV on the potential wires and cathode planes. This performance is sufficient for the (^{16}O, ^{16}F(0^-)) measurement.

The experiment is scheduled to be conducted in 2014.

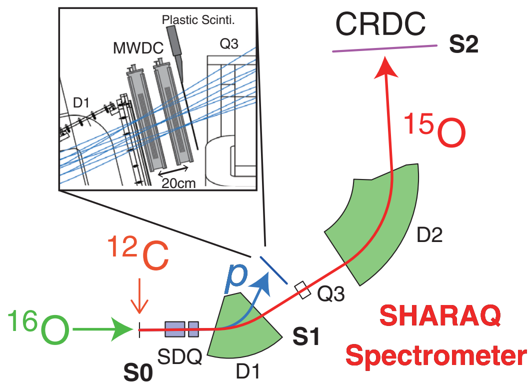

Fig. 1. Schematic of the experimental setup.

Table 1. Specifications of the MWDCs. The X' (Y') plane is offset by half cell from the X (Y) plane.

Configuration	X - X' - Y - Y'
Effective area	480 mm^W × 240 mm^H
Cell size	12 mm^W × 10 mm^t
Numbers of channels	120
Anode wire	Au-W, 20 μm$^\phi$
Potential wire	Cu-W, 80 μm$^\phi$
Cathode plane	Al-Mylar, 2 μm^t
Counter gas	P10 : Ar - CH_4 (90 - 10), 1 atm
Gas window	Al-Mylar, 25 μm^t

References
1) C. L. Bai *et al.*: Phys. Rev. Lett. **105**, 072501 (2010).
2) M. Dozono *et al.*: RIKEN Accel. Prog. Rep. **45**, 10 (2012).
3) H. Miya *et al.*: Nucl. Instr. Meth. B **317**, 701 (2013).

*1 RIKEN Nishina Center
*2 Center for Nuclear Study, University of Tokyo
*3 Department of Physics, University of Tokyo
*4 Department of Physics, Kyushu University
*5 Center for Mathematics and Physics, University of Aizu

Missing mass spectroscopy on carbon isotopes beyond proton drip-line

T. Miyazaki,[*1,*2] H. Otsu,[*2] E. Yu. Nikolskii,[*2,*5] Y. Shiga,[*2,*3] M. Kurata-Nishimura,[*2] S. Takeuchi,[*2] Y. Satou,[*4] M. Kurokawa,[*2] H. Baba,[*2] G. Lorusso,[*2] T. Isobe,[*2] M. Niikura,[*1] E. A. Kuzmin,[*2,*5] A. A. Korsheninnikov,[*2,*5] A. A. Ogloblin,[*2,*5] S. A. Krupko,[*6] M. S. Golovkov,[*6] A. A. Bezbakh,[*6] R. S. Slepnev,[*6] A. S. Fomichev,[*6] S. I. Sidorchuk,[*6] A. V. Gorshkov,[*6] A. G. Knyazev,[*6] P. Papka,[*7] H. J. Ong,[*8] S. Kim,[*4] J. W. Hwang,[*4] S. Choi,[*4] H. Chae,[*4] E. Kim,[*4] Y. H. Kim,[*4] D. Lubos,[*2,*9] D. Beaumel,[*2,*10] P. A. Söderström,[*2] S. Sakaguchi,[*11] S. Kubono,[*2] A. K. Perrevoort,[*2] E. Milman,[*2] S. Chebotaryov,[*2] W. Powell,[*2] T. Motobayashi,[*2] K. Yoneda,[*2] and H. Sakurai[*1,*2]

The ^{8}C nucleus is one of the most proton rich nuclei existing outside of the proton drip-line. While the mass of the ground state and decay modes of ^{8}C[1–4] has been known, the energy and the spin-parity of the excited states have never been measured. Therefore, we investigated the excited states of ^{8}C by using missing mass spectroscopy, which enabled us to search for the unbound nuclei ^{8}C unbiasedly with respect to three-body, four-body, and five-body decay[4].

The experiment was performed at the RIPS facility[5] in RIKEN. A 70 MeV/nucleon ^{12}C primary beam with an intensity of 200 pnA bombarded a ^{9}Be production target with a thickness of 0.5 mm. A 50 MeV/nucleon ^{10}C secondary beam was produced via projectile fragmentation and distributed to a reaction chamber located downstream of the second achromatic plane (F3) of RIPS. Particle identification of the secondary beam was carried out on event by event basis using the time of flight and energy loss, which were measured by two plastic scintillators placed at the first achromatic plane (F2) and F3 of RIPS. Two parallel plate avalanche counters (PPACs)[6] placed at F3 and double PPACs in the reaction chamber were used to measure and adjust the beam position. We obtained the pure ^{10}C beam with an intensity of about 2×10^5 Hz.

The secondary ^{10}C beam was injected into a cryogenic H_2 gas target (CRYPTA)[7]. Temperature and pressure of the H_2 gas were kept around 30 K and 0.4 MPa, respectively. The H_2 gas was sandwiched by two 10-μm-thick Havar[8] foils. The diameter and thickness of the target cell were 30 and 1 mm, respectively.

Recoil deuterons and tritons from the reaction were detected by silicon detectors called a RIKEN telescope[9] and a Dubna telescope, respectively. The double-sided strip detector (DSSD) of the RIKEN telescope was installed at 120.5 mm downstream from the target. The Dubna telescope, which was installed downstream of the RIKEN telescope, consisted of 1-mm-thick DSSD and 16 trapezoid 25-mm-thick CsI(Tl) scintillators with photo-multiplier readouts. The DSSD has 16 sectors in front and 16 rings at the back. The DSSD is circular with a 28 mm ϕ hole, and the active radius ranges from 33 to 84 mm. The DSSD was placed at 300 mm from the target, followed by the CsI(Tl) scintillators at 5-mm intervals. The polar angular coverage of the Dubna telescope is about $3.0^\circ \leq \theta \leq 8.0^\circ$ in a laboratory frame.

Four plastic scintillators were installed at 0 degree, downstream of Dubna telescope. The first two scintillators were used to stop the ^{10}C beam. They identified $Z = 4$ and $Z = 6$ particles from the reactions. The following two scintillators were used as the stopper and separator for lighter particles such as α particles and protons produced by the reactions. Therefore, we selected these scintillators with thicknesses of 2, 5, 2, and 15 mm from upstream.

Trigger sources of the data acquisition were the RIKEN telescope $\otimes$ beam, the Dubna telescope $\otimes$ beam, and the down-scaled beam. Data were taken for 31 hours under the condition with H_2 gas, and 11 hours without H_2 gas.

In the online analysis, the recoil deuterons and tritons detected by the Dubna telescope were well identified. From the energy information of these recoil particles, the excitation energy of ^{8}C and ^{9}C will be deduced by the missing mass method. A detailed analysis is now in progress.

*1 Department of Physics, The University of Tokyo
*2 RIKEN Nishina Center
*3 Department of Physics, Rikkyo University
*4 Department of Physics, Seoul National University
*5 National Research Centre "Kurchatov Institute"
*6 Flerov Laboratory of Nuclear Reactions, Joint Institute for Nuclear Research
*7 Department of Physics, Stellenbosch University
*8 Resarch Center for Nuclear Physics, Osaka University
*9 Technische Universität München
*10 Institut de Physique Nucléaire d'Orsay, IN2P3/CNRS
*11 Department of Physics, Kyushu University

References

1) R. G. H. Robertson et al.: Phys. Rev. Lett. **32**, 1207 (1974).
2) R. E. Tribble et al.: Phys. Rev. C **13**, 1 (1976).
3) R. G. H. Robertson et al.: Phys. Rev. C **13**, 3 (1976).
4) R. J. Charity et al.: Phys. Rev. C **82**, 041304(R) (2010).
5) T. Kubo et al.: Nucl. Instrum. Methods Phys. Res. B **70**, 309 (1992).
6) H. Kumagai et al.: Nucl. Instrum. Methods. Phys. Res. B **317**, 717 (2013).
7) H. Ryuto et al.: Nucl. Instrum. Methods. Phys. Res. A **555**, 1 (2005).
8) http://www.goodfellow.com/E/Havar-High-Strength-Non-Magnetic-Alloy-Foil.html
9) E. Yu. Nikolskii et al.: Phys. Rev. C **81**, 064606 (2010)

Design of experiment for search of ^{10}N resonances with resonant scattering of ^{9}C off polarized proton

E. Milman,[*1,*2] T. Teranishi,[*3] S. Chebotaryov,[*1,*2] N. Imai,[*4] T. Kawahara,[*1] S. Sakaguchi,[*3]
K. Tateishi,[*1] and T. Uesaka[*1]

The ^{9}C+p elastic resonant scattering has been proposed for search of resonances in the unbound ^{10}N nucleus whose structure is almost unknown at present. Theoretically, four low-lying ^{10}N levels are expected as two very broad $2s_{1/2}$ and two very broad $1p_{1/2}$ proton single-particle resonances, each of which has a width much larger than 1 MeV. These resonances overlap each other and may not be clearly identifiable in the ^{9}C+p excitation function. The level information obtained in the experiment is useful for discussing resonances in ^{10}Li because ^{10}N and ^{10}Li are mirror partners that are expected to have similar structures. The ^{10}Li structure provides us with valuable information for constructing the three-body model of the borromean ^{11}Li nucleus.

We proposed to measure analyzing power to resolve these broad resonances[1]. The combined information of the excitation function and an analyzing power spectrum will enable us to impose more strict constraints on analysis of the resonances.

The range of center-of-mass energy was set to 1–5 MeV to cover the ground state of ^{10}N, predicted at around 1.5 MeV, and several excited states (one experimentally observed at 2.6 MeV[2]). For the measurement of analyzing power and excitation function, we considered to adopt the thick-target method in inverse kinematics (TTIK), where the excitation function can be scanned with a single beam energy utilizing the energy loss of the beam particle in the target.

We conducted LISE++ simulation to produce ^{9}C beam on RIPS with a low energy of 5 MeV/A. In the simulation, using a ^{12}C primary beam with 70 MeV/A and 200 pnA, 3.5 mm-thick Be target, and 583 mg/cm^2-thick Al wedge degrader at F1, beam intensity obtained at F2 was ~3.5 × 10^4 pps with a purity of >90%. RF deflector can be used to reduce the rate of contamination because the rate of contaminations such as ^{8}B and ^{7}Be is one order magnitude larger than the simulated value in the proton rich side. We also planned to replace Al wedges with $(CH_2)_n$ wedges to decrease the multiple scattering effect.

Polarized target is required for the measurement of analyzing power. A polarized proton solid target for low-energy beam experiments[3] has been designed based on existing system for intermediate energies[4]. A single crystal of p-terphenyl doped with pentacene molecules with a concentration of 0.05 mol% was chosen as the target material, which allows us to operate the target in vacuum environment at room temperature. Thickness of the target was chosen to be 110 μm to cover the range of the secondary ^{9}C beam. Strength of the magnetic field was chosen to be 0.2 T to maintain the polarization, and this does not severely affect the particle trajectory. The estimated polarization was 15% at this magnetic field. Production and polarization of thin films (7 μm) have recently been realized at Osaka University[5], where the size of the grown single crystal was 3 × 4 mm^2. However, production of large sized single crystals, with a desired diameter of 2 cm, remains a challenge. We designed a technique to grow a crystal between two thin films.

We consider use of silicon detector for detection of protons with energies of 3–18 MeV. Each telescope consists of one 65 μm-thick double sided silicon detector (DSSD) and two 1.5 mm-thick DSSDs with a detection area of 50 mm × 50 mm. Two telescopes are planned to be placed at both left and right sides of the beam line at a laboratory angle of ±22.5◦, where the vector analyzing power is expected to have large absolute values. We plan to place another telescope at 0◦. The distance between the target and the telescopes is 250 mm.

TTIK method allows us to archive an E_{CM} resolution of approximately 76 keV with a proton energy resolution of 120 keV.

$$E_{CM} = \frac{1}{4\,cos^2\,\theta_p}\frac{A+1}{A}E_p \qquad (1)$$

Equation 1 shows dependence of E_{CM} on recoil proton energy, where A= 9 for ^{9}C and θ_p is proton scattering angle in laboratory frame.

In conclusion, we proposed the first low energy RI experiment with polarized proton target. RIKEN polarized proton target has been redesigned for use with low energy RI beam. We plan to construct the target in the next fiscal year.

*1 RIKEN Nishina Center
*2 Department of Physics, Kyungpook National University
*3 Department of Physics, Kyushu University
*4 KEK

References

1) T. Teranishi, S. Sakaguchi, T. Uesaka et al., AIP Conf. Proc. 1525, 552 (2013).
2) A. L´epine-Szily et al., Phys. Rev. C 65, 054318 (2002).
3) S. Sakaguchi et al., Nuclear Instruments and Methods in Physics Research B 317, 679-684 (2013)
4) T. Uesaka et al., Nuclear Instruments and Methods in Physics Research A 526, 186 (2004).
5) K. Tateishi et al., J. Phys. Soc. Jpn. 82, 084005 (2013).

Measurement of alpha elastic scattering on ^{15}O

A. Kim,[*1] K. Y. Chae,[*1] M. S. Gwak,[*1] S. M. Cha,[*1] S. H. Choi,[*2] Y. H. Kim,[*2] H. W. Chae,[*2] K. I. Hahn,[*3] D. H. Kim,[*3] G. W. Kim,[*3] S. Y. Han,[*3] P. S. Lee,[*4] J. Y. Moon,[*5] H. Yamaguchi,[*6] D. Kahl,[*6] and T. Nakao[*6]

The measurement of alpha elastic scattering on ^{15}O for studying the resonance states of ^{19}Ne was performed by using the CRIB (CNS Radioactive Ion Beam separator) at the Center for Nuclear Study, University of Tokyo. Alpha-cluster structures have been an interesting subjects of study. Several investigations of alpha-cluster structures have been conducted on 4N nuclei such as ^{8}Be, ^{12}C, ^{16}O, and ^{20}Ne.[1–3] In the case of ^{19}Ne, because the system of nuclei can be regarded as ^{20}Ne plus one hole, weakly coupled states of the alpha and hole have been studied theoretically in the low-excitation energy region, but limited experimental data are available, till date. Therefore, experimental study of alpha elastic scattering on ^{15}O is very crucial for understanding how alpha clustering is manifested in proton-rich nuclei. Unknown alpha-cluster states of ^{19}Ne from 1^- and 3^- members ($K^\pi = 0^-$ cluster band of ^{20}Ne) as well as 4^+ and 6^+ members ($K^\pi = 0^+$ cluster band of ^{20}Ne) can be identified by performing alpha elastic scattering on ^{15}O. Because the study of alpha cluster states of ^{19}Ne has been carried out theoretically, this experimental result can be used to confirm the alpha-cluster structure of Z>N nuclei of Ne isotopes.[4,5]

Moreover, astrophysically, the ^{18}F$(p,\alpha)^{15}$O reaction is very important because the amount of ^{18}F produced in a nova depends sensitively on the reaction rates of ^{18}F$(p,\alpha)^{15}$O and ^{18}F$(p,\gamma)^{19}$Ne.[6] To date, experimental studies using ^{18}F beams as well as theoretical works have been reported competitively. However, resonance parameters of relevant states above the proton threshold at $E_x = 6.411$ MeV have not been confirmed and remain controversial.[7–9] Therefore, if the resonance properties of ^{19}Ne using ^{15}O$(\alpha,p)^{18}$F are studied, which is a time reverse reaction of ^{18}F$(p,\alpha)^{15}$O, we can expect better results because the ^{15}O + α threshold energy is only 3.53 MeV(E_x of ^{19}Ne).

In this study, the ^{15}O$(\alpha,\alpha)^{15}$O reaction was measured in the energy range $E_{c.m.} = 1.5 - 7.1$ MeV, which corresponds to $E_x = 5.0 - 10.6$ MeV of ^{19}Ne. The primary beam, ^{15}N (7.0 MeV/u, 0.6 pμA), was transported from the AVF cyclotron and impinged on a hydrogen gas target with a thickness of 1.09 mg/cm^2. The secondary beam, ^{15}O, was obtained by the $p(^{15}\mathrm{N},n)^{15}$O reaction. Fig. 1 shows beam identification for ^{15}O and other contaminations on the F2 focal plane. The main contamination of the secondary beam was ^{15}N, the primary beam. ^{15}O beams of 6×10^5 counts/s were collected at the F3 chamber which contains He gas and a Si telescope and the beams were 96 % pure after passing through a Wien filter. The energy of the ^{15}O beam was 34 MeV after the entrance window (Mylar 25 μm-thick) of the F3 chamber.

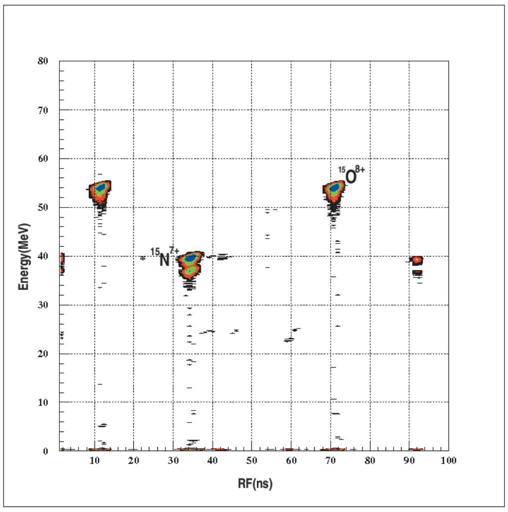

Fig. 1. Secondary beam identification on the F2 focal plane.

For inducing alpha elastic scattering, we filled He gas directly in the F3 chamber without a special gas cell. We installed the one-set telescope of consisting two Si layers (20 μm-thick and 480 μm-thick, respectively) at zero degrees; it was located at a distance of 200 mm from the entrance window of the chamber and the pressure of ^{4}He gas was 760 Torr at room temperature, which is equivalent to that for an effective thickness of 3.33 mg/cm^2. The data are currently being analyzed.

*1 Department of Physics, Sung-Kyun-Kwan University
*2 Department of Physics, Seoul National University
*3 Department of Physics, Ewha Womans University
*4 Department of Physics, Chung-Ang University
*5 RISP, Institute for Basic Science
*6 Center for Nuclear Science, University of Tokyo

References

1) K. Ikeda et al.: Prog. Theor. Phys. Suppl. **68**, 1 (1986)
2) H. Horiuch et al.: Suppl. Prog. Theor. Phys. **192**, 1 (2012)
3) M. Freer : Rep. Prog. Phys. **70**, 2149 (2007)
4) F. Nemoto and H. Bando: Prog. Theor. Phys. **47**, 1210(1972)
5) T. Sakuda and F. Nemoto: Prog. Theor. Phys. **62**, 1274 (1979)
6) M. Hernanz et al.: Astrophys. J. **526**, L97 (1999)
7) D. W. Bardayan et al.: Phys. Rev. C **70**, 015804 (2004)
8) H. Fortune et al.: Phys. Rev. C **73**, 024302 (2006)
9) A. St. J. Murphy et al.: Phys. Rev. C **79**, 058801 (2009)

Study of unbound oxygen isotopes ^{25}O and ^{26}O using SAMURAI

Y. Kondo,[*1,*2] T. Nakamura,[*1,*2] N. L. Achouri,[*3] T. Aumann,[*4] H. Baba,[*2] F. Delaunay,[*3] P. Doornenbal,[*2] N. Fukuda,[*2] J. Gibelin,[*3] J. W. Hwang,[*5] N. Inabe,[*2] T. Isobe,[*2] D. Kameda,[*2] D. Kanno,[*1,*2] S. Kim,[*5] N. Kobayashi,[*1,*2] T. Kobayashi,[*6,*2] T. Kubo,[*2] S. Leblond,[*3] J. Lee,[*2] F. M. Marqués,[*3] R. Minakata,[*1,*2] T. Motobayashi,[*2] D. Murai,[*7] T. Murakami,[*8] K. Muto,[*6] N. Nakatsuka,[*8] T. Nakashima,[*1,*2] A. Navin,[*9] S. Nishi,[*1,*2] S. Ogoshi,[*1,*2] N. A. Orr,[*3] H. Otsu,[*2] H. Sato,[*2] Y. Satou,[*5] Y. Shimizu,[*2] H. Suzuki,[*2] K. Takahashi,[*6] H. Takeda,[*2] S. Takeuchi,[*2] R. Tanaka,[*1,*2] Y. Togano,[*10,*13] A. G. Tuff,[*11] M. Vandebrouck,[*12] and K. Yoneda[*2]

Unbound states of the neutron-rich oxygen isotopes ^{25}O and ^{26}O have been studied by the invariant-mass method by using SAMURAI[1)] with the aim to elucidate the mechanism of the neutron drip line anomaly in oxygen and fluorine isotopes. Another interesting topic is the possible two-neutron radioactivity of the ^{26}O ground state, predicted by a theoretical study.[2)] Experimentally, only the upper limit of the ground-state energy[3,4)] and lifetime with a large error[5)] are currently available.

Details of the experimental setup are described in our previous report.[6)] Figure 1 shows a mass identification plot of outgoing $Z = 8$ charged particles observed in the breakup of ^{27}F on a carbon target. Particle identification is performed by the $B\rho$-ΔE-TOF technique. The magnetic rigidity $B\rho$ is determined by the positions and angles at the entrance and exit of the SAMURAI magnet measured by means of the MWDCs (BDC1,2 and FDC1,2). Combining the $B\rho$ value with energy loss ΔE and TOF measured by a plastic scintillator hodoscope (HODF), outgoing particles can be clearly identified. The mass resolution $\Delta A = 0.18$ (FWHM), corresponding to 13σ separation, is achieved for ^{24}O.

Figure 2 shows a preliminary decay energy spectrum of $^{24}O+n$ observed in the breakup of ^{27}F. The sharp peak near the neutron decay threshold corresponds to the ^{26}O ground state and the peak at approximately 0.8 MeV corresponds to the ground-state resonance of ^{25}O. Since the obtained statistics is much larger than that obtained in the previous experiments,[3,4)] a better constraint on the ^{26}O ground-state energy can be obtained. Analysis is currently in progress.

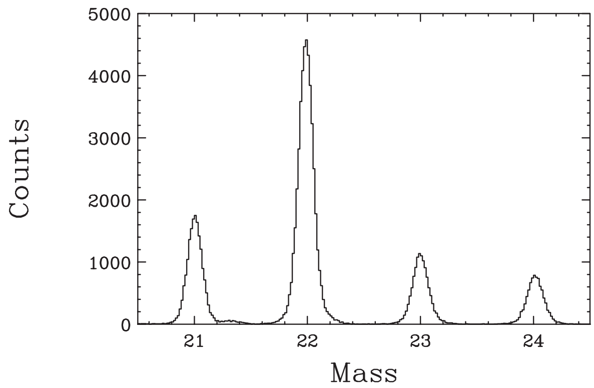

Fig. 1. Mass spectrum of outgoing $Z = 8$ particles in the breakup of ^{27}F.

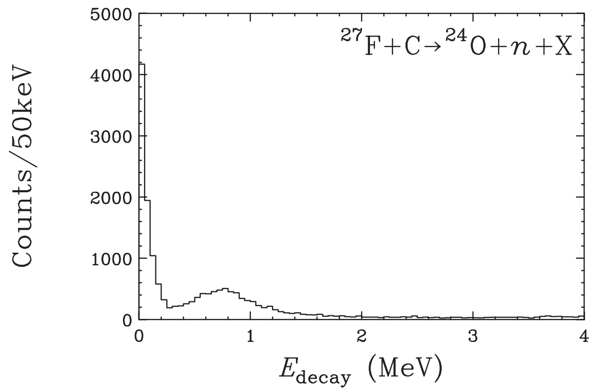

Fig. 2. Decay energy spectrum of $^{24}O+n$ in the breakup of ^{27}F.

*1 Department of Physics, Tokyo Institute of Technology
*2 RIKEN Nishina Center
*3 LPC-Caen, ENSICAEN, Université de Caen, CNRS/IN2P3
*4 Institut für Kernphysik, Technische Universität Darmstadt
*5 Department of Physics and Astronomy, Seoul National University
*6 Department of Physics, Tohoku University
*7 Departiment of Physics, Rikkyo University
*8 Department of Physics, Kyoto University
*9 GANIL, CEA/DSM-CNRS/IN2P3
*10 ExtreMe Matter Institute (EMMI) and Research Division, GSI
*11 Department of Physics, University of York
*12 Institut de Physique Nucléaire, Université Paris-Sud, IN2P3-CNRS
*13 Present address:Department of Physics, Tokyo Institute of Technology

References

1) T. Kobayashi et al.: Nucl. Instr. Meth. B. **317**, 294 (2013).
2) L. V. Grigorenko et al.: Phys. Rev. C. **84**, 021303 (2011).
3) E. Lunderberg et al.: Phys. Rev. Lett. **108**, 142503 (2012).
4) C. Caesar et al.: Phys. Rev. C. **88**, 034313 (2013).
5) Z. Kohly et al.: Phys. Rev. Lett. **110**, 152501 (2013).
6) Y. Kondo et al.: RIKEN. Prog. Accel. Rep. **46**, 6 (2013).

Two-neutron removal reaction from ^{22}C†

N. Kobayashi,[*1,*2] T. Nakamura,[*1] J. A. Tostevin,[*1,*3] Y. Kondo,[*1] N. Aoi,[*4] H. Baba,[*4] S. Deguchi,[*1] J. Gibelin,[*5] M. Ishihara,[*4] Y. Kawada,[*1] T. Kubo,[*4] T. Motobayashi,[*4] T. Ohnishi,[*4] N. A. Orr,[*5] H. Otsu,[*4] H. Sakurai,[*4] Y. Satou,[*6] E. C. Simpson,[*3] T. Sumikama,[*7] H. Takeda,[*4] S. Takechi,[*4] S. Takeuchi,[*4] K. N. Tanaka,[*2] N. Tanaka,[*2] Y. Togano,[*4] and K. Yoneda[*4]

We report the first measurement of the two-neutron removal reaction from a ^{22}C secondary beam at around 240 MeV/nucleon. The experiment was performed at the RI beam factory in 2009, as detailed in Ref.[1]. The extracted quantities are the inclusive cross section of ^{22}C and the momentum distribution for the charged residues of ^{20}C. ^{22}C is known to be the most neutron-rich bound nucleus among C isotopes, whereas ^{21}C is particle unbound. Hence, ^{22}C is pictured as a three-body (^{20}C + n + n) Borromean system, which may be useful in deriving the two-neutron halo formation in ^{22}C.

There is little knowledge about ^{22}C. Until Gaudefroy *et al.* performed the mass measurement of ^{22}C (i.e., $S_{2n}(^{22}\mathrm{C}) = -0.14(46)$ MeV),[2] its experimental mass was never known. Hence, we followed the 2003 mass evaluation,[3] in which the two-neutron separation energy was 0.42(94) MeV. The ground state of ^{21}C was assumed to be produced at a continuum energy of ε^* = 0.30 MeV after neutron removal with a ground-state separation energy $S_{1n}(^{22}\mathrm{C})$ of 0.70 MeV.

Based on the shell model with the WBP effective interaction[4] in a *psd*-model space truncated to allow $0\hbar\omega$ and $1\hbar\omega$ excitations, three final states of ^{21}C are predicted below the ^{20}C first neutron threshold of 2.90 MeV. These states are a $1/2_1^+$ ground state with $C^2S = 1.4$, a $5/2_1^+$ state at $E_x = 1.11$ MeV with $C^2S = 4.2$, and a $3/2_1^+$ state at $E_x = 2.19$ MeV with $C^2S = 0.34$. Using these C^2Ss and an eikonal reaction model,[5,6] the theoretical inclusive cross section is calculated to be 283 mb, which is in agreement with the experimental cross section of 266(19) mb.

The measured and theoretical inclusive ^{20}C parallel momentum distributions (convoluted with the experimental resolution of 27 MeV/c) are compared in Fig. 1. The theoretical distribution (solid curve) corresponds to the inclusive (unbound) ^{21}C momentum distribution, which is calculated as the weighted sum of the momentum distributions to the individual final states. Prior to this sum being calculated, the neutron emission recoil broadening for the ^{20}C residue is included for each final state according to its ε^* value, i.e., $\varepsilon^* = E_x + 0.30$ MeV. The dashed (dot-dashed) curve shows the contribution of knockout via the $1/2_1^+$ ($5/2_1^+$) state of ^{21}C. Each of two states contributes almost half of the inclusive one-neutron removal cross section. The theoretical calculation is in good agreement with the experimental distribution, providing strong support for the weakly bound $\nu 2s_{1/2}$ character for the ^{22}C ground state. This result is consistent with the result of the recent interaction-cross-section measurement and associated analysis presented in Ref.[7], which is suggestive of an extended ^{22}C matter density.

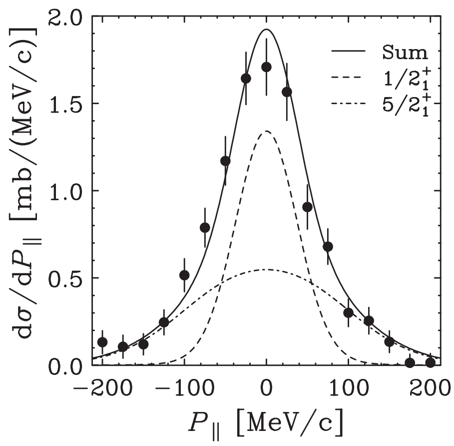

Fig. 1. Comparison of measured and theoretical inclusive parallel momentum distributions of ^{20}C, following two-neutron removal from ^{22}C on a carbon target at 240 MeV/nucleon. See the text for a description of the curves.

References
1) N. Kobayashi *et al.*, Phys. Rev. C **86**, 054604 (2012) and references therein.
2) L. Gaudefroy *et al.*, Phys. Rev. Lett. **109**, 202503 (2012).
3) G. Audi, A. H. Wapstra, and C. Thibault, Nucl. Phys. **A729**, 337 (2003).
4) E. K. Warburton and B. A. Brown, Phys. Rec. C **46**, 923 (1992).
5) P. G. Hansen and J. A. Tostevin, Annu. Rev. Nucl. Part. Sci. **53**, 219 (2003) and references therein.
6) E. C. Simpson and J. A. Tostevin, Phys. Rev. C **79**, 024616 (2009).
7) K. Tanaka *et al.* Phys. Rev. Lett. **104**, 062701 (2010).

† Condensed from the article in Phys. Rev. C. **86**, 054604 (2012)[1].

*1 Department of Physics, Tokyo Institute of Technology
*2 Present address: Department of Physics, University of Tokyo
*3 Department of Physics, University of Surrey
*4 RIKEN Nishina Center,
*5 LPC-Caen, ENSICAEN, IN2P3-CNRS, Université de Caen
*6 Department of Physics and Astronomy, Seoul National University
*7 Department of Physics, Tokyo University of Science

One-neutron knockout reaction of ^{17}C on a hydrogen target at 70 MeV/nucleon[†]

Y. Satou,[*1] J.W. Hwang,[*1] S. Kim,[*1] K. Tshoo,[*1] S. Choi,[*1] T. Nakamura,[*2] Y. Kondo,[*2] N. Matsui,[*2] Y. Hashimoto,[*2] T. Nakabayashi,[*2] T. Okumura,[*2] M. Shinohara,[*2] N. Fukuda,[*3] T. Sugimoto,[*3] H. Otsu,[*3] Y. Togano,[*3] T. Motobayashi,[*3] H. Sakurai,[*3] Y. Yanagisawa,[*3] N. Aoi,[*3] S. Takeuchi,[*3] T. Gomi,[*3] M. Ishihara,[*3] S. Kawai,[*4] H.J. Ong,[*5] T.K. Onishi,[*5] S. Shimoura,[*6] M. Tamaki,[*6] T. Kobayashi,[*7] Y. Matsuda,[*7] N. Endo,[*7] and M. Kitayama[*7]

Much of our knowledge on the quantum nature of atomic nuclei comes from the studies of nuclear reactions. Among the various collision processes, the nucleon knockout reaction is recognized as one of the most sensitive tools for spectroscopy, especially of unstable nuclei. The knockout residue produced by removing a nucleon from a fast-moving beam particle is efficiently observed in inverse kinematics by a detector placed in the forward hemisphere. The removed nucleon(s) will be selected democratically from the valence space, allowing the states with unique, often rarely accessible, configurations to be populated in this process. The final state in the residue is identified by tagging de-excitation γ rays and by observing decay neutrons and constructing the invariant mass. For one-nucleon knockout case, the momentum spread of the residue reflects the Fermi motion of the nucleon suddenly removed, and is sensitive to its orbital angular momentum (the l value). The cross sections leading to the individual final states relate to the occupancy of single-particle orbits, providing a link to understand the details of the nuclear structure.

This study aims at exploring the unbound states in ^{16}C through an application of the one-neutron knockout technique to a ^{17}C beam. This is done by focusing on searching the lowest-lying cross-shell transitions, whose location reflects the shell gap between the p and sd orbits. The experiment was performed at the RIPS facility of RIKEN using the setup given in Refs.[1,2]. The ^{17}C beam was produced from a 110-MeV/nucleon ^{22}Ne beam, which impinged on a Be target. The secondary target was pure liquid hydrogen contained in a cylindrical cell. The average energy of ^{17}C at the middle of the target was 70 MeV/nucleon. The target was surrounded by a NaI(Tl) scintillator array. The fragment was bent by a dipole magnet behind the target, and was detected by a plastic counter hodoscope. The neutrons were detected by plastic scintillator arrays placed ~5 m downstream from the target. The relative energy ($E_{\rm rel}$) of the final system was calculated from the momentum vectors of the charged fragment and the neutron.

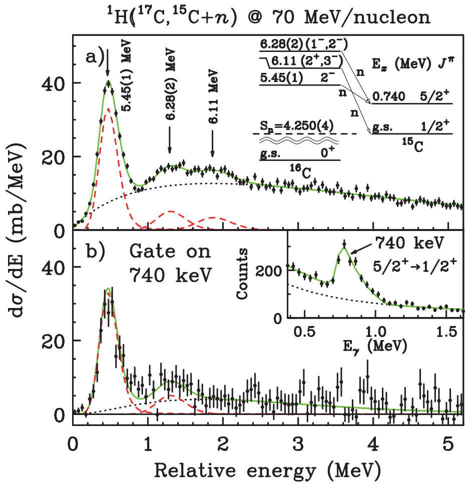

Fig. 1. Relative energy spectra for the (a) ^{1}H(^{17}C,^{15}C+n) and (b) ^{1}H(^{17}C,^{15}C($5/2^+$; 0.74 MeV)+n) reactions.

Fig. 1 shows the $E_{\rm rel}$ spectra for the (a) ^{1}H(^{17}C,^{15}C+n) and (b) ^{1}H(^{17}C,^{15}C($5/2^+$; 0.74 MeV)+n) reactions. Shown in the inset of Fig. 1 (b) is the energy spectrum for γ rays emitted from ^{15}C. Fig. 1 (a) was used in a fitting analysis to extract the resonance parameters.

Two new states at 5.45(1) and 6.28(2) MeV were populated together with a known state at 6.11 MeV. For the 5.45-MeV state, an attempt was made to deduce the l value of the knocked-out neutron from the $p_{||}$ distribution associated with the unbound residue. This, together with a comparison in terms of the measured and calculated knockout cross sections, has led to a spin-parity assignment of 2^- for this state. Possible spins and parities have been suggested for the other states, bringing about an advanced understanding of the level scheme of ^{16}C. The energy of the first 2^- state was adequately reproduced by the standard shell-model calculation using the WBT interaction without invoking modifications to the residual interaction.

† Condensed from the article in Phys. Lett. B **728**, 462 (2014)

*1 Department of Physics and Astronomy, Seoul National University
*2 Department of Physics, Tokyo Institute of Technology
*3 RIKEN Nishina Center
*4 Department of Physics, Rikkyo University
*5 Department of Physics, University of Tokyo
*6 Center for Nuclear Study, University of Tokyo
*7 Department of Physics, Tohoku University

References

1) Y. Satou, et al.: Phys. Lett. B **660**, 320 (2008).
2) K. Tshoo, et al.: Phys. Rev. Lett. **109**, 022501 (2012).

Invariant mass spectroscopy of ^{17}C at SAMURAI

S. Kim,[*1,*2] Y. Satou,[*1] J.W. Hwang,[*1,*2] T. Nakamura,[*2,*3] N. A. Orr,[*4] Y. Kondo,[*2,*3] J. Gibelin,[*4] N. Kobayashi,[*2,*3] R. Tanaka,[*2,*3] R. Minakata,[*2,*3] S. Ogoshi,[*2,*3] S. Nishi,[*2,*3] D. Kanno,[*2,*3] T. Nakashima,[*2,*3] N. L. Achouri,[*4] T. Aumann,[*5] H. Baba,[*2] F. Delaunay,[*4] P. Doornenbal,[*2] N. Fukuda,[*2] N. Inabe,[*2] T. Isobe,[*2] D. Kameda,[*2] T. Kobayashi,[*6,*2] T. Kubo,[*2] S. Leblond,[*4] J. Lee,[*2] F. M. Marqués,[*4] T. Motobayashi,[*2] D. Murai,[*7] T. Murakami,[*8] K. Muto,[*6] N. Nakatsuka,[*8] A. Navin,[*9] H. Otsu,[*2] H. Sato,[*2] Y. Shimizu,[*2] H. Suzuki,[*2] K. Takahashi,[*6] H. Takeda,[*2] S. Takeuchi,[*2] Y. Togano,[*10,*13] A. G. Tuff,[*11] M. Vandebrouck,[*12] and K. Yoneda[*2]

Many properties of nuclei away from the β-stability line are important to better understand nuclear processes that control stellar nucleosynthesis and energy balance. These nuclei often exhibit exotic structures. For example, the appearance of anomalous parity intruder states at a low excitation energy region provides evidence for the shell-gap quenching and/or large nuclear deformation.

The present study focuses on low-lying negative parity states in ^{17}C above the neutron decay threshold. Two β-delayed neutron emission measurements of ^{17}B have reported such states: Raimann et al.[1)] indicated states at 2.25(2), 2.64(2), 3.82(5), and 1.18(1) MeV with no definite spin-parity (J^{π}) assignment. Achieving higher sensitivity for the β-n-γ coincidence yield, Ueno et al.[2)] was successful to locate states at 2.71(2), 3.93(2), and 4.05(2) MeV with the suggested J^{π} values of $1/2^-$, $3/2^-$, and $(5/2^-)$, respectively. This study aimed to populate these states and to examine their properties by the one-neutron knockout reaction of an energetic beam.

The measurement was performed using the SAMURAI spectrometer[3)] during the first physics run of the apparatus. A beam of ^{18}C at approximately 250 MeV/nucleon provided by BigRIPS at RIBF impinged on a carbon target with a thickness of 1.8 g/cm^2. The unbound states in ^{17}C produced by the one-neutron removal processes subsequently decayed into a ^{16}C fragment and a neutron. These decay products were detected in coincidence. There should be some background events by the neutrons arising from the one-neutron removal processes; however, such background is expected to be relatively featureless and would not affect the resonance. The momentum vector of the ^{16}C fragment was determined by (1) position information in the two drift chambers (FDCs) placed at the entrance and exit of the SAMURAI dipole magnet and (2) energy loss and timing information in the plastic scintillator hodoscope (HODF). The momentum vector of the neutron was determined using the position and timing information in the plastic scintillator neutron hodoscope (NEBULA). The energy spectrum of ^{17}C was reconstructed using the invariant mass method involving the momentum vectors of the fragment and neutron.

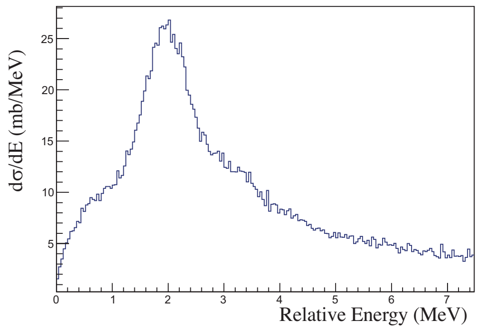

Fig. 1. Preliminary relative energy spectrum of the ^{16}C+n unbound system.

A preliminary relative energy spectrum for the ^{16}C + n system is shown in Fig.1. A clear peak structure was observed at 2 MeV in relative energy, which corresponds to the excitation energy of $E_x = 2.7$ MeV. This energy is close to the energy of the first $1/2^-$ state at $E_x = 2.71(2)$ MeV reported in Ueno et al.[2)]. To examine the identity of these two states, an analysis is being carried out (1) to compare the populating cross section with the theoretical value based on the corresponding shell-model spectroscopic factor together with the Glauber model and (2) to extract the orbital angular momentum of the knocked-out neutron from the parallel momentum distribution. A search for the other reported states will also be performed.

*1 Department of Physics and Astronomy, Seoul National University
*2 RIKEN Nishina Center
*3 Department of Physics, Tokyo Institute of Technology
*4 LPC-Caen, ENSICAEN, Université de Caen, CNRS/IN2P3
*5 Institut für Kernphysik, Technische Universität Darmstadt
*6 Department of Physics, Tohoku University
*7 Department of Physics, Rikkyo University
*8 Department of Physics, Kyoto University
*9 GANIL, CEA/DSM-CNRS/IN2P3
*10 ExtreMe Matter Institute (EMMI) and Research Division, GSI
*11 Department of Physics, University of York
*12 Institut de Physique Nucléaire, Université Paris-Sud, IN2P3-CNRS
*13 Department of Physics, Tokyo Institute of Technology

References
1) G. Raimann et al.: Phys. Rev. C **53**, 453 (1996).
2) H. Ueno et al.: Phys. Rev. C **87**, 034316 (2013).
3) K. Yoneda et al.: RIKEN Accel. Prog. Rep. **45**, i (2012).

Structure of ^{18}B

S. Leblond,*1 S. Ogoshi,*2 R. Minakata,*2 J. Gibelin,*1 F. M. Marqués,*1 N. A. Orr,*1 Y. Kondo,*2 T. Nakamura,*2 R. Tanaka,*2 N. L. Achouri,*1 T. Aumann,*3 H. Baba,*4 F. Delaunay,*1 P. Doornenbal,*4 N. Fukuda,*4 J. W. Hwang,*5 N. Inabe,*4 T. Isobe,*4 D. Kameda,*4 D. Kanno,*2 S. Kim,*5 N. Kobayashi,*2 T. Kobayashi,*6 T. Kubo,*4 J. Lee,*4 T. Motobayashi,*4 D. Murai,*7 T. Murakami,*8 K. Muto,*6 T. Nakashima,*2 N. Nakatsuka,*8 A. Navin,*9 S. Nishi,*2 H. Otsu,*4 H. Sato,*4 Y. Satou,*5 Y. Shimizu,*4 H. Suzuki,*4 K. Takahashi,*6 H. Takeda,*4 S. Takeuchi,*4 Y. Togano,*10 A. G. Tuff,*11 M. Vandebrouck,*12 K. Yoneda*4

The investigation of the light neutron-rich dripline nuclei, including in particular those exhibiting halos, is a central theme of nuclear structure physics. In the present work a series of measurements, aimed at elucidating the structure of the two heaviest candidate two-neutron halo systems, ^{19}B and ^{22}C[1–3], and the associated unbound sub-systems ^{18}B and ^{21}C, the level schemes of which are critical to the defining the ^{17}B-n and ^{20}C-n interactions for three-body models, have been undertaken. In addition to being of direct importance to halo physics, ^{18,19}B and ^{21,22}C are of considerable interest in terms of the evolution of shell-structure far from stability as they span the N=14 and 16 subshell closures below doubly-magic ^{22,24}O.

The measurements were accomplished using the SAMURAI spectrometer[4] coupled to the large area neutron array NEBULA[5] and were performed as part of the first phase of SAMURAI experiments. The analysis to date has concentrated on the fragment+neutron channels and, in particular, ^{17}B+n which is known to exhibit a strongly interacting virtual s-wave threshold state[6]. Beyond the intrinsic physics interest noted above, a well defined threshold state provides an ideal means to validate the calibration and analysis procedures.

In addition to populating ^{18}B via proton removal from ^{19}C (which should populate almost exclusively s-wave strength), the complementary probe of neutron removal from a ^{19}B beam has been investigated. Figure 1 shows the reconstructed ^{17}B+n invariant mass (or relative energy) spectra for the two reactions. As may be clearly seen the proton removal populates a very narrow threshold structure, the form of which is consistent with the s-wave virtual state deduced by Spyrou *et al.*[6]. The neutron removal, however, in addition to the threshold peak shows clear evidence for the population of a state or states in the region of 0.5–1 MeV.

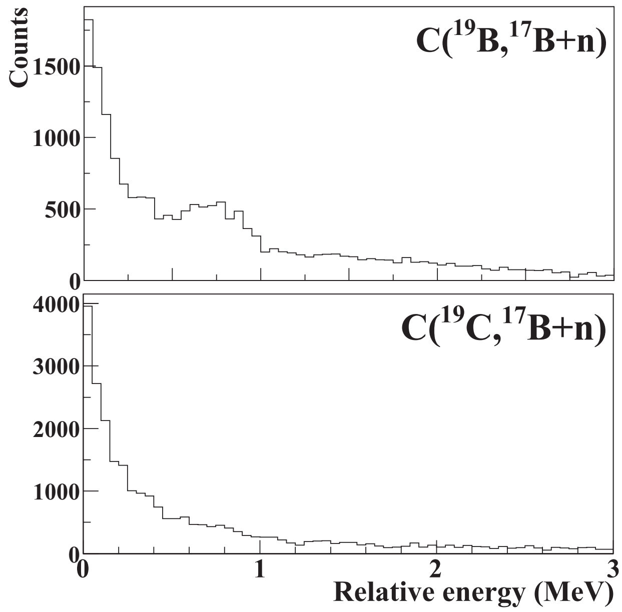

Fig. 1. Preliminary results for the ^{17}B+n relative energy spectra obtained for proton and neutron removal reactions at 240 MeV/nucleon.

The further analysis of these preliminary results is currently underway as are the data sets for the analogue reactions populating ^{21}C.

The research descibed here forms part of the thesis work of S. Leblond who acknowledges the support provided in terms of a 6 month RIKEN Nishina Center IPA fellowship in 2013.

*1 LPC-Caen, ENSICAEN, Université de Caen, CNRS/IN2P3
*2 Department of Physics, Tokyo Institute of Technology
*3 Institut für Kernphysik, Technische Universität Darmstadt
*4 RIKEN Nishina Center
*5 Department of Physics and Astronomy, Seoul National University
*6 Department of Physics, Tohoku University
*7 Departiment of Physics, Rikkyo University
*8 Department of Physics, Kyoto University
*9 GANIL, CEA/DSM-CNRS/IN2P3
*10 ExtreMe Matter Institute (EMMI) and Research Division, GSI
*11 Department of Physics, University of York
*12 Institut de Physique Nucléaire, Université Paris-Sud, IN2P3-CNRS, Orsay

References

1) K. Tanaka *et al.*: Phys. Rev. Lett. **104**, 062701 (2010).
2) N. Kobayashi *et al.*: Phys. Rev. **C83**, 054604 (2012).
3) L. Gaudefroy *et al.*: Phys. Rev. Lett. **109**, 20503 (2012).
4) T. Kobayashi et al.: Nucl. Instr. Meth. B **317**, 294 (2013).
5) Y. Kondo *et al.*: RIKEN Accel. Prog. Rep. **45**, 131 (2012); http://be.nucl.ap.titech.ac.jp/~nebula
6) A. Spyrou *et al.*: Phys. Lett. B **683**, 129 (2010).

Energy dependence of π^- differential cross section in ^{28}Si + In with beam energies of 400, 600, and 800

M. Sako,[*1*2] T. Murakami,[*2] Y. Ichikawa,[*2] K. Ieki,[*4] Y. Ikeda,[*4] S. Imajo,[*2] T. Isobe,[*1] S. Ebesu,[*2] M. Matsushita,[*6] J. Murata,[*4] Y. Nakai,[*1] S. Nishimura,[*1] M. Nitta,[*4] H. Sakurai,[*1*6] R. Sameshima,[*2] E. Takada,[*3] and K. Yoshinaga[*5]

Information on the nuclear equation of state (EoS) within a broad density range is important for understanding the physics of neutron stars. However, the isospin-dependent term in EoS, i.e., the density dependence of the symmetry energy $E_{sym}(\rho)$ has a large model dependence in the supra-normal density region ($\rho > \rho_0$, the saturation density $\rho_0 \cong 0.16 fm^{-3}$). As a result, the relationship between the radius and the mass of a neutron star cannot be reliably calculated. According to a transport model calculation (IBUU04),[1)] detailed studies of the pion yield ratio, $Y(\pi^-)/Y(\pi^+)$, in central nucleus-nucleus collisions at intermediate energies can be conducted to obtain significant constraints on $E_{sym}(\rho)$ in the supra-normal density region.

The IBUU04 predicts that the beam energy dependence of the pion yield ratio is strongly related to the behavior of $E_{sym}(\rho)$ in the supra-normal density region.[1)] We performed a series of experiments using 400, 600, and 800 MeV/nucleon ^{28}Si beams accelerated at the Heavy Ion Medical Accelerator in Chiba (HIMAC) and an In target with a compact centrality filter and a pion range counter(RC)[2)].

The π^+ events can be clearly identified by the $\pi^+ \to \mu^+ + \nu_\mu$ decay after they are stopped at the RC.[3)] The π^- events were selected using ΔE_i-ΔE_j (energy deposition at each layers of RC) correlations obtained experimentally for π^+ events, because in-flight energy depositions are same between the π^+ and π^- events. However, a pionic atom, which is created by the stopped π^- and surrounding nuclei, decays various particles and some of them hit the next counter. Next we estimated a π^- leak rate to the next counter.

The leak rate α at which the decayed particles hit the next elements was estimated with CsI(^{129}Xe,$\pi^\pm$)X experimental data at 90° for which, the statistics is sufficient and the S/N ratio is large. We obtained a typical value of α, $10.83^{+0.81}_{-0.59}$(SYS) %. For obtaining the production cross section of the π^-, the reduction rate by the decay in flight, nuclear reaction, and multiple Coulomb scattering until the π^- reaches the RC from the production point was estimated using Geant4.

The Lorentz-invariant cross sections of the π^- as a function of the kinematic energy of the π^- in a mid rapidity frame E_{mid} (the CM frame of NN) were shown at Figure 1. Further analysis of the π^- and efforts to fix the systematic uncertainties are in progress.

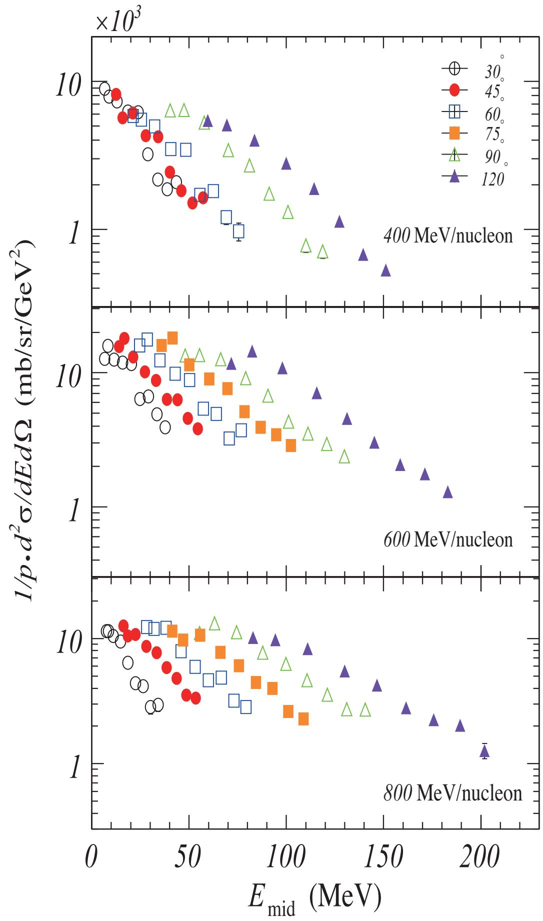

Fig. 1. Lorentz-invariant cross sections of the π^- as a function of kinematic energy in the mid-rapidity frame (E_{mid}) for In(^{28}Si,$\pi^\pm$)X reaction with 400(top part), 600(middle part) and 800(bottom part) MeV/nucleon beam with statistical errors.

References
1) B. A. Li, G. C. Yong, and W. Zuo, Phys. Rev. C **71**, 014608 (2005).
2) T. Murakami et al., Nucl. Phys. A **834**, 593c (2010) (NN2009 proceedings).
3) M. Sako et al., RIKEN Accel. Prog. Rep. **46**,(2013).

*1 RIKEN Nishina Center
*2 Department of Physics, Kyoto University, Kyoto
*3 Department of Accelerator and Medical Physics, NIRS
*4 Department of Physics, Rikkyo University, Tokyo
*5 Department of Physics, Tokyo University of Science
*6 Department of Physics, University of Tokyo

Study of symmetry energy using isospin diffusion process in heavy-ion collision at RIBF

N. Nakatsuka,[*1] R.H. Showalter,[*2] T. Isobe,[*3] J. Winkelbauer,[*2] T. Murakami,[*1] W.G. Lynch,[*2] B. Tsang,[*2] H. Sakurai,[*3] J. Lee,[*3] M. Nishimura,[*3] S. Nishimura,[*3] Y. Nakai,[*3] N. Fukuda,[*3] N. Inabe,[*3] D. Kameda,[*3] T. Kubo,[*3] H. Suzuki,[*3] H. Takeda,[*3] Y. Yanagisawa,[*3] S. Yennello,[*4] A.B. McIntosh,[*4] L. Heilborn,[*4] A. Zarrella,[*4] W. Powell,[*5] J. Sampson,[*5] J. Estee,[*2] L. Fei,[*6] G. Zhang,[*6] A. Chbihi,[*7] A. Galindo-Uribarri,[*8] E.P. Rodal,[*9] B. Hong,[*10] G. Jhang,[*10] W. Reviol,[*11] D.G. Sarantites,[*11] and L.G. Sobotka[*11]

The nuclear equation of state (EoS) is an important information that helps in understanding the astrophysical phenomena such as neutron stars and type-2 supernovae. The EoS shows highest uncertainty on a symmetry energy term, which is proportional to the square of the isospin asymmetry. We strive to improve the remaining uncertainties of constraints on the density dependence of the symmetry energy at subsaturation densities, $\rho/\rho_0 \approx 0.4$-1 in the so called isospin-diffusion process of heavy-ion collisions. The isospin diffusion process has been observed in the experiments performed at NSCL/MSU using stable nuclear beams[1)]. We performed the experiment to measure the isotopic distribution of the projectile residues from the collision of cocktail beams, where the $^{107}_{49}$In and the $^{112}_{50}$Sn beams are on $^{124}_{50}$Sn and $^{112}_{50}$Sn targets at 70MeV/u respectively. The particle identification of projectile residues is performed by the $B\rho$-ΔE-TOF technique using the ZeroDegree spectrometer. The Washington University Microball[2)] was used to obtain the centrality information. We used $B\rho$ settings of 2.41 and 2.52 T·m in order to avoid beam particles with any charge states hitting the detectors at F11. The standard beam tracking and timing detectors at F10 and F11 were used for reconstructing the beam tracks through the spectrometer. Fig#1 shows a preliminary PID plot of Z versus $A = Q$ for the ^{107}In on ^{124}Sn reaction. Isotopes with Z=30-40 are clearly shown separated in the figure. Fig#2 shows a preliminary plot of Z versus multiplicity of the charged particles obtained by the Microball. From the obvious correlation between the multiplicity and the size of the residue, we can determine the collision centrality with the help of a model calculation. In the offline analysis, we will select the data in the ZeroDegree Spectrometer only from the peripheral events using obtained information from the Microball. Then the measured yields of isotopes with $Z = 30 \sim 40$ will be compared with the theoretical predictions to extract a new constraint on the symmetry energy at sub saturation densities.

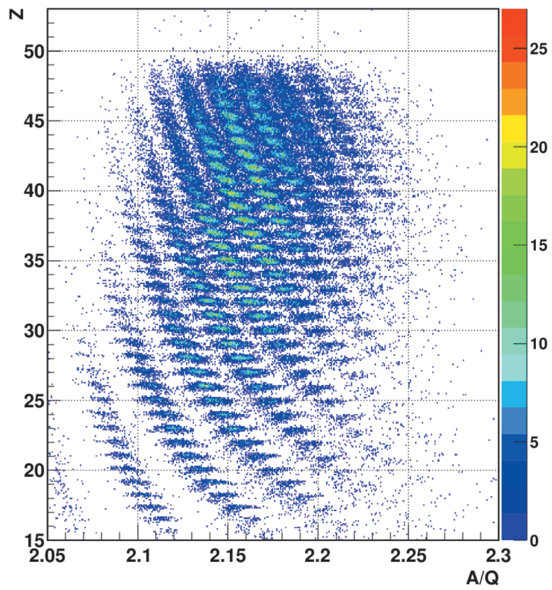

Fig. 1. PID of heavy-ion collision residue performed using ZeroDegree Spectrometer

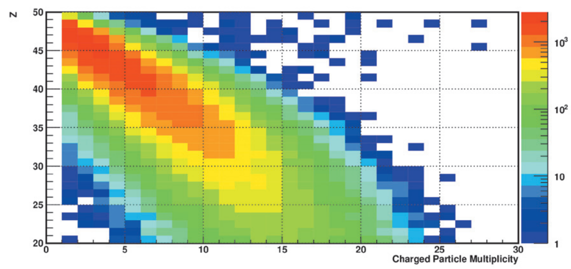

Fig. 2. Correlation between multiplicity and Z of residue using Microball

*1 Department of Physics, Kyoto University
*2 National Superconducting Cyclotron Laboratory, Michigan State University
*3 RIKEN Nishina Center
*4 Cyclotron Institute, Texas A&M University
*5 Department of Physics, University of Liverpool
*6 Chinese Academy of Sciences
*7 Physics Division, GANIL
*8 Physics Division, Oak Ridge National Laboratory
*9 Institute of Nuclear Sciences, National Autonomous University of Mexico
*10 Department of Physics, Korea University
*11 Department of Chemistry, Washington University

References

1) M.B. Tsang et al., Phys. Rev. Lett. **92** (2004) 062701.
2) D.G.Sarantities et al., Nucl. Instrum. Methods Phys.Res., Sec. A **381** (1996) 418.

Simulation study of neutron measurement using NEBULA simulation package for SπRIT project

G. Jhang[*1,*2] and T. Isobe[*2] for the SπRIT Collaboration

Neutron and proton emission is one of many reaction observables that can be used to constrain the density-dependent nuclear symmetry energy[1)], which is important to describe isospin-asymmetric nuclear matter.

In the SπRIT project, we plan to measure the n/p ratio complementary to the t/^{3}He ratio measurement by making use of the TPC and the NEBULA array. In order to investigate the response of the NEBULA array before the actual experiment, we are performing a simulation with the NEBULA simulation package v2.0.5[2)] developed by Nakamura group at Tokyo Institute of Technology on the basis of GEANT4.9.2p02 and ROOT. We are using the Particle and Heavy Ion Transport code System(PHITS)[3)] v2.60 as an event generator to produce collision events with ^{132}Sn projectiles and ^{124}Sn targets. Detailed information on the physics processes used can be found in the link of Ref. 4.

Table 1. Information on generated events

beam energy (AMeV)	neutron events	total events
200	522,665	100,000,000
300	523,058	

In the simulation setup, the NEBULA array is placed 2 m away to the left side of the beam direction so that charged reaction particles having high p_z and beam remnants do not enter the array.

In the distribution of the number of neutrons for each beam energy shown in Fig. 1, lines with "Accepted" in the legend indicate that most of the neutrons generated by the collision are going outside of the acceptance range, and less than 40 neutrons enter the array in our setup.

Figure 2 shows the momentum distribution of neutrons detected by the NEBULA array. The distribution of neutrons with the assumption of 100% detection efficiency(blue) is slightly different from that obtained by taking the time of flight of each neutron's first hit(pink). The difference originates from the exclusion algorithms that excludes some number of scintillator bars near the first detection. This result implies that if we can distinguish the first hit only from the secondary, tertiary, and so on, we can measure most neutrons' momenta with precision. The red line shows the added backgrounds, which should be eliminated to obtain the proper neutron information.

We are building an algorithm to eliminate the background noise, which is about 10 times larger than primary neutron signals as shown in Fig. 2, in order to obtain precise information on as many neutrons as possible. Such information can reveal whether we can distinguish one theoretical model from the others in the actual experiment.

*1 Department of Physics, Korea University
*2 RIKEN Nishina Center

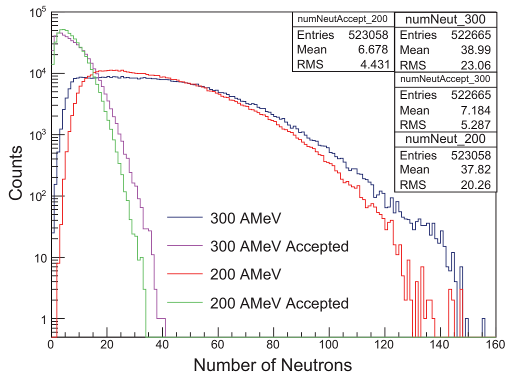

Fig. 1. Number of neutrons in generated events and in accepted the range of the NEBULA array

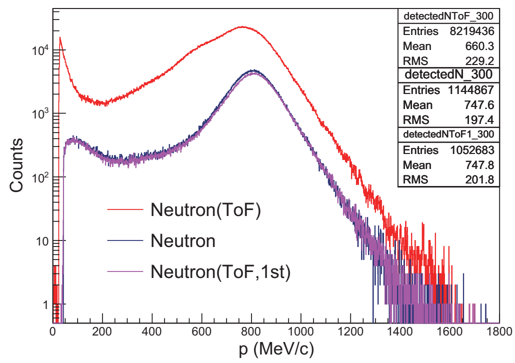

Fig. 2. Momentum distribution of neutrons with beam energy. Blue line is the result with an assumption of 100% detection efficiency of the NEBULA array. Pink line is the result with the time of flight method for the primary reaction. Red line shows the signal plus noise expected in a real experiment without any cut parameter.

References
1) M. A. Famiano *et al.*: Phys. Rev. Lett. **97**, 052701, (2006).
2) NEBULA simulation package: http://be.nucl.ap.titech.ac.jp/˜nebula/index.php
3) T. Sato *et al.*: J. Nucl. Sci. Technol. **50:9**, pp. 913-923, (2013).
4) PHITS(Particle and Heavy Ion Transport code System): http://phits.jaea.go.jp/OvMapOfModels.html

In-beam γ-ray spectroscopy of ^{34,36,38}Mg: Merging the $N = 20$ and $N = 28$ shell quenching[†]

P. Doornenbal,[*1] H. Scheit,[*1,2] S. Takeuchi,[*1] N. Aoi,[*1] K. Li,[*1,2] M. Matsushita,[*1,3] D. Steppenbeck,[*1] H. Wang,[*1,2] H. Baba,[*1] H. Crawford,[*4] C.R. Hoffman,[*5] R. Hughes,[*6] E. Ideguchi,[*7] N. Kobayashi,[*8] Y. Kondo,[*8] J. Lee,[*1] S. Michimasa,[*7] T. Motobayashi,[*1] H. Sakurai,[*1] M. Takechi,[*1] Y. Togano,[*1] R. Winkler,[*9] and K. Yoneda[*1]

The neutron-rich $_{10}$Ne, $_{11}$Na, and $_{12}$Mg isotopes are located within a region known as the "Island of Inversion" and form one of the most notable regions of sudden shell structure change. Abnormally high masses were discovered for ^{31,32}Na, leading to the presumption that the $\nu f_{7/2}$ orbitals intrude into the sd shell orbitals, thereby quenching the $N = 20$ shell gap. Later theoretical works predicted, however, that not the entire orbitals are inverted but $\nu(sd)^{-2}(fp)^2$ $(2\hbar\omega)$ configurations are lowered so much in energy that they form the ground states for $10 \leq Z \leq 12$, $20 \leq N \leq 22$ nuclei instead.

The $N = 28$ magic number is originally formed by the large $\nu f_{5/2}$–$\nu f_{7/2}$ spin-orbit splitting but is also known to vanish, as seen in the large deformation arising for $^{42}_{14}$Si[1,2]. Initially believed to be two isolated regions, we show in this letter that the $N = 20, 28$ shell quenching is interlinked via the neutron-rich magnesium isotopes, thereby forming a new connected large area of deformation in the Segré chart.

Key information on the shape of a nucleus can be obtained for even-even nuclei from the energy of the first excited 2^+ state $E(2^+_1)$, the first 4^+ state $E(4^+_1)$, and their $E(4^+_1)/E(2^+_1)$ ratio, $R_{4/2}$. Previous studies revealed a low excitation energy of 660(6) keV for the 2^+_1 state in ^{36}Mg and suggest that the "Island of Inversion" stretches at least to neutron number $N = 24$ for the magnesium isotopes and thus beyond its originally proposed boundaries[3]. In the present study, the experimental knowledge of the $E(2^+_1)$ and $E(4^+_1)$ is extended to the $N = 26$ nucleus ^{38}Mg via one- and two-proton removal reactions..

A primary beam of ^{48}Ca with an average intensity of 70 particle nA and an energy of 345 MeV/nucleon was impinging on a 15 mm thick rotating Be target located at the BigRIPS fragment separator's entrance. Secondary beams were selected and purified via the $B\rho - \Delta E - B\rho$ method, and identified with the $\Delta E - B\rho -$ TOF method. The rate for ^{39}Al and ^{40}Si isotopes transported through BigRIPS was 75 and 3000 pps, respectively. The secondary beams were incident on a 2.54 g/cm^2 thick carbon secondary target, which was surrounded by the DALI2 spectrometer[4]. Reaction residues from the secondary target were identified by the ZeroDegree Spectrometer, applying again the $\Delta E - B\rho -$ TOF method.

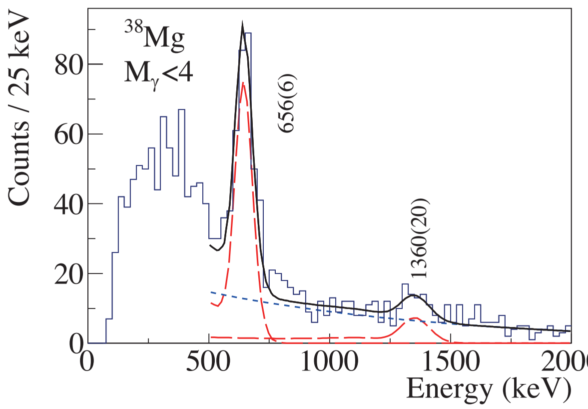

Fig. 1. Doppler corrected γ-ray energy spectrum in coincidence with ^{38}Mg detected in BigRIPS and ZeroDegree.

Two γ-ray transitions were observed in ^{38}Mg from the $1p$ and $2p$ knockout channels after correcting for the Doppler shift, as shown in Fig. 1, which were attributed to the $2^+_1 \rightarrow 0^+_{gs}$ and the $4^+_1 \rightarrow 2^+_1$ decays. In ^{36}Mg, following a different reaction channel, a second transition was observed and attributed to the $4^+_1 \rightarrow 2^+_1$ decays, while for ^{34}Mg known values were determined with higher accuracy[5]. Almost constant $R_{4/2}$ ratios of 3.14(5), 3.07(5), and 3.07(5) were obtained for ^{34,36,38}Mg at $N = 22, 24, 26$, close to the ideal value of 3.33 for a rigid rotor. The values were in agreement with state-of-the art shell model calculations and suggested that the $N = 20$ and $N = 28$ shell quenching merge for the neutron-rich magnesium isotopes.

References

1) B. Bastin *et al.*, Phys. Rev. Lett. **99**, 022503 (2007).
2) S. Takeuchi *et al.*, Phys. Rev. Lett. **109**, 182501 (2012).
3) A. Gade *et al.*, Phys. Rev. Lett. **99**, 072502 (2007).
4) S. Takeuchi *et al.*, RIKEN Acc. Prog. Rep. 36, 148 (2003).
5) K. Yoneda *et al.*, Phys. Lett. B, 233 (2001).

† Condensed from the article in Phys. Rev. Lett. **111**, 212502 (2013)

*1 RIKEN Nishina Center
*2 School of Physics, Peking University
*3 Department of Physics, Rikkyo University
*4 Nuclear Science Division, Lawrence Berkeley National Laboratory
*5 Physics Division, Argonne National Laboratory
*6 Department of Physics, University of Richmond
*7 CNS, University of Tokyo
*8 Department of Physics, Tokyo Institute of Technology
*9 NSCL, Michigan State University

In-beam γ-ray spectroscopy of ^{80}Zn

Y. Shiga,[*1,*2] K. Yoneda,[*1] D. Steppenbeck,[*1,*3] N. Aoi,[*4] H. Baba,[*1] P. Bednarczyk,[*5] P. Doornenbal,[*1] Zs. Dombradi,[*6] Zs. Fulop,[*6] S. Go,[*1,*3] T. Hashimoto,[*4] E. Ideguchi,[*1,*3] K. Ieki,[*1,*2] K. Kobayashi,[*1,*2] Y. Kondo,[*1,*7] J. Lee,[*1] H. Liu,[*1] M. Matushita,[*1,*2] R. Minakata,[*1,*6] T. Motobayashi,[*1] D. Nisimura,[*1] H. Otsu,[*1] H. Sakurai,[*1] D. Sohler,[*6] Y. Sun,[*8] A. Tamii,[*4] S. Takeuchi,[*1] R. Tanaka,[*1,*7] Z. Tian,[*8] Zs. Vajta,[*6] H. Wang,[*1,*8] T. Yamamoto,[*4] X. Yang,[*1] Z. Yang,[*8] Y. Ye,[*8] R. Yokoyama,[*1,*3] and J. Zenihiro[*1]

In-beam γ-ray spectroscopy of nuclei in the vicinity of the doubly-magic nucleus ^{78}Ni was performed. In recent studies, a drastic change of the shell structure was elucidated for the neutron magic number $N = 8$, 20, and 28 in the regions far from stability The energy of the first $I^{\pi} = 2^+$ state $E(2_1^+)$, and the energy ratio of the 4_1^+ state to the 2_1^+ state $E(4_1^+)/E(2_1^+)$ in even-even nuclei are of particular interest, since they are sensitive to the evolution of the shell structure and nuclear deformation. In this study, the systematic energy trend of the low-lying states was investigated for the chain of Zn isotopes ^{74,76,78,80,}Zn which covers the magic number $N = 50$.

In order to produce RI beams around ^{80}Zn, a ^{238}U primary beam with energy of 345A MeV was made to impinge on a 925-mg/cm^2-thick beryllium target. The fragments produced were separated and identified with the BigRIPS[1)] by the $B\rho$-ΔE-ToF method on an event-by-event basis. Then, the RI beams impinged on a 1889-mg/cm^2-thick beryllium target to induce secondary reactions. The de-excitation γ-rays emitted from reaction residues were observed by the NaI(Tl) detector array DALI2[2)], which surrounded the secondary target. The reaction residues were identified using the ZeroDegree spectrometer. Figure 1 shows the particle identification plots for the incoming particles obtained with the BigRIPS (left) and for the outgoing particles obtained with the ZeroDegree spectrometer (right).

Figure 2 shows the Doppler-shift corrected γ-ray energy spectrum obtained for the reaction channel ^{9}Be(^{81}Ga,^{80}Zn) with a restriction of a γ-ray multiplicity M_γ, being equal to 1. In the spectrum, five peaks were observed. The peak at 1492(1) keV[3)] is for the known γ-ray transition corresponding to the $2_1^+ \to 0_{\text{g.s.}}^+$ decay, while the other four transitions are candidates for new levels and are still under analysis for confirmation. Further analysis is on-going to reconstruct the level scheme by γ-γ coincidence, and to identify the spins and parities of the states by the analysis of momentum distribution of the outgoing reaction residues.

*1 RIKEN Nishina Center
*2 Department of Physics, Rikkyo University
*3 Center for Nuclear Study, University of Tokyo
*4 RCNP, Osaka University
*5 IFJ Pan
*6 MTA Atomki
*7 Department of Physics, Tokyo Institute of Technology
*8 School of Physics, Peking University

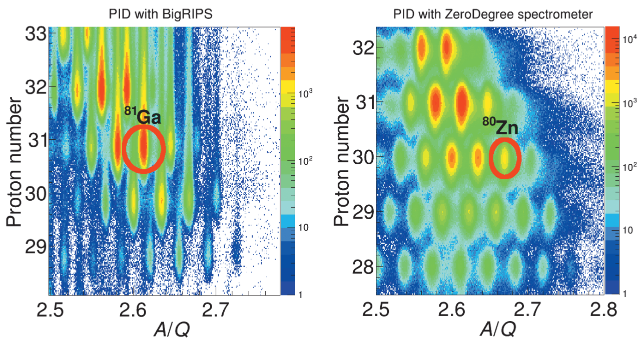

Fig. 1. Particle identification by the BigRIPS (left) and the ZeroDegree spectrometer (right). Plotted is the proton number against the ratio of mass to charge A/Q.

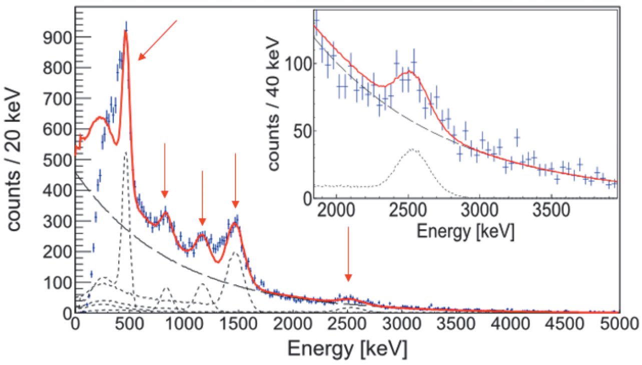

Fig. 2. Doppler-corrected γ-ray energy spectrum for ^{9}Be(^{81}Ga,^{80}Zn) reaction with M_γ=1 condition. The dotted curves are the response function with GEANT4 simulation. The solid curve corresponds to the fitting of five response functions with exponential background taken into account. The spectrum, expanded to around 2500 keV, is also shown in the upper inlet.

References
1) T. Kubo et al.: Prog. Theor. Exp. Phys. 03C003 (2012).
2) S. Takeuchi et al.: RIKEN Accel. Prog. Rep. **41**, 149 (2008).
3) J. Van. de Walle et al.: Phys. Rev. Lett. **99**, 142501 (2007).

Intermediate energy Coulomb excitation of ^{73,74,75}Ni

A. Gottardo,[*1] G. de Angelis,[*1] P. Doornenbal,[*2] G. Benzoni,[*3] J. Lee,[*2] H. Liu,[*2] M. Matsushita,[*4] D. Mengoni,[*5] V. Modamio-Hoybjor,[*1] S. Momiyama,[*6] T. Motobayashi,[*2] D. Napoli,[*1] M. Niikura,[*6] E. Sahin,[*7] Y. Shiga,[*2,*8] H. Sakurai,[*2,*6] R. Taniuchi, [*6] S. Takeuchi,[*2] H. Wang,[*2,*12] J.J. Valiente-Dobòn,[*1] R. Avigo,[*3,*11] H. Baba,[*2] N. Blasi,[*3] F.L. Bello Garrote,[*7] F. Browne,[*2,*10] F.C.L. Crespi,[*3,*11] S. Ceruti,[*3,*11] R. Daido,[*12] M.-C. Delattre,[*13] D. Fang,[*12] Zs. Dombradi,[*14] T. Isobe,[*2] I. Kuti,[*14] G. Lorusso,[*2] K. Matsui,[*6] B. Melon,[*15] T. Miyazaki,[*6] S. Nishimura,[*2] R. Orlandi,[*16] Z. Patel,[*2,*17] S. Rice,[*2,*17] L. Sinclair,[*2,*18] P.A. S¨oderstr¨om,[*2] D. Sohler,[*14] T. Sumikama,[*19] J. Taprogge,[*20,*21] Zs. Vajta,[*14] H. Watanabe,[*2,*22] O. Wieland,[*3] J. Wu,[*2,*19] Z. Y. Xu,[*6] M. Yalcinkaya,[*23] R. Yokoyama[*4]

Doubly magic nuclei located in very exotic regions of the nuclear chart are key elements in nuclear structure studies. The appearance or disappearance of the shell gaps associated with magic numbers in very exotic nuclei is strongly related to the single-particle energies of nucleon orbitals and to the residual interactions among valence nucleons. The ^{100}Sn and ^{78}Ni regions are fundamental in this regard and are the focus of the efforts of many research laboratories worldwide. From the N=Z=50 ^{100}Sn located at the proton drip line to the neutron rich N=50 ^{78}Ni with N/Z=1.78, it is currently possible to access the shell structure of these isotones. This very large excursion in isospin also allows to magnify and probe the isovector part of the nuclear mean field. In particular, the tensor part of the spin-isospin term of the residual interaction has been predicted to modify the single-particle structure, inducing a collective behavior in this region. For the Ni isotopic chain, the filling up of the $g_{9/2}$ neutron orbit is expected to induce a strong core polarization due to the spin-isospin interaction that enhances the B(E2:$2^+ \rightarrow 0^+$), a measure of the quadrupole collectivity. We performed an intermediate energy Coulomb excitation study of the ^{73,74,75}Ni isotopes, in order to fix the seniority-scheme pattern of the B(E2) strength. Neutron-rich Ni isotopes were produced by fission of a ^{238}U beam on a ^{9}Be target at a bombarding energy of 345 MeV/u, with an average intensity of 10 pnA. The resulting fragments were analyzed using the BigRIPS separator[2)] and transported to a secondary natural Pb target for Coulex reactions. After this target, the ions were again analyzed in the ZeroDegree spectrometer and delivered down to the final focal plane. The γ rays from Coulex have been detected by the DALI2 spectrometer[3)] in coincidence with the recoiling ions identified at the focal plane of the ZeroDegree spectrometer. A preliminary γ spectrum, after selection on ^{74}Ni ions, is shown in Fig. 1. The γ peak corresponding to the $2^+ \rightarrow 0^+$ de-excitation at 1024 keV of ^{74}Ni[4,5)] is clearly visible. Decay spectroscopy investigation[6)] with EURICA was performed at the final focal plane in conjunction with the in-beam part.

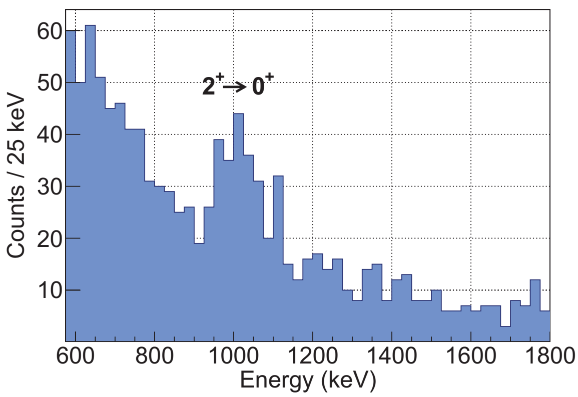

Fig. 1. The γ-ray spectrum detected in DALI2 after selection on ^{74}Ni. The $2^+ \rightarrow 0^+$ transition at 1024 keV is clearly visible.

*1 LNL, INFN
*2 RIKEN, Nishina Center
*3 INFN sezione di Milano
*4 CNS, University of Tokyo
*5 Dipartimento di Fisica, Universitá degli Studi di Padova
*6 Department of Physics, University of Tokyo
*7 Department of Physics, University of Oslo
*8 Department of Physics, Rikkyo University
*9 Department of Physics, Peking University
*10 School of Computing, Engineering and Mathematics, Brighton University
*11 Dipartimento di Fisica, Universitá degli Studi di Milano
*12 Departement of Physics, Osaka University
*13 IPN Orsay
*14 MTA Atomki
*15 INFN sezione di Firenze
*16 Instituut voor Kern- en Stralings Fysica/K.U.
*17 Department of Physics, University of Surrey
*18 Department of Physics, University of York
*19 Department of Physics, Tohoku University
*20 IEM, CSIC Madrid
*21 Department of Physics, Universidad Autònoma de Madrid
*22 Department of Physics, Beihang University
*23 Department of Physics, Istanbul University

References
1) P.-A. Söderström et al.:, Nucl. Instr. Methods Phys. Res. Sect. **B317**, 649 (2013).
2) T. Kubo: Nucl. Instr. Methods Phys. Res. Sect. **B204**, 97 (2003).
3) S. Takeuchi et al.: RIKEN Acc. Prog. Rep. **36**, 148 (2003).
4) C. Mazzocchi et al.: Phys. Lett. **B622**, 45 (2005).
5) N. Aoi et al.: Phys. Lett. **B692**, 302 (2010).
6) G. Benzoni et al.: Riken annual report 2013.

Zeeman resonance spectroscopy of $^{84-87}$Rb in superfluid helium

X.F. Yang,[*1,*2] T. Furukawa,[*1,*3] T. Wakui,[*1,*4] K. Imamura,[*1,*5] T. Fujita,[*1,*6] Y. Mitsuya,[*1,*5] M. Hayasaka,[*1,*7] Y. Ichikawa,[*1] Y. Ishibashi,[*1,*9] H. Shirai,[*1,*8] T. Suzuki,[*1,*8] Y. Ebara,[*3] A. Hatakeyama,[*10] M. Wada,[*1] T. Sonoda,[*1] Y. Ito,[*1] T. Kobayashi,[*11] S. Nishimura,[*1] M. Kurata-Nishimura,[*1] Y. Kondo,[*1,*8] K. Yoneda,[*1] H. Ueno,[*1] T.Shinozuka,[*4] T. Shimoda,[*6] K. Asahi,[*1,*8] and Y. Matsuo[*1,*12]

OROCHI is a newly developed laser spectroscopy method for optical determination of nuclear spins and moments of exotic radioisotopes (RIs)[1)]. It aims to overcome several experimental limitations due to the low yield of RIs and large contaminations in the production of RIs by taking advantages of the characteristic properties of atoms in superfluid helium (He II). Firstly, it utilizes condensed He II as the trapping medium for the RI beam and the matrix of in situ laser spectroscopy of trapped atoms. Subsequently, by measuring the hyperfine and Zeeman splitting energies of atoms using optical pumping and laser microwave (MW)/radiofrequency (RF) double resonance method, nuclear moments and spins of RIs can be determined. Initial studies with the OROCHI method were concentrated in field of the technological research and development with a considerable number of off-line experiments, which confirmed the feasibility of the OROCHI method[1)]. Recently, after extensive tests and calculations, the first on-line experiments with the $^{84-87}$Rb beam have been successfully performed. In this experiment, the primary ^{85,87}Rb and secondary ^{84,86}Rb beams produced from RIPS were precisely trapped in He II. Optical pumping and Zeeman resonance (ZR) for $^{84-87}$Rb and the isomer state ^{84m}Rb have been successfully observed.

Figure 1 shows the measured spectra for $^{84m,84-87}$ Rb isotopes, which are recorded by scanning the applied magnetic field (B_0) with a fixed-frequency RF field. The corresponding beam for each spectrum and isotopes for each observed ZR are marked in Fig. 1. Note that in the case of ^{86}Rb, to reduce the deformation of the observed spectra owing to beam instability, the recording time for one cycle is changed to 1 s (10 s for ^{84,85,87}Rb). The detailed measurement method is explained in an early report[2)]. Conventionally, nuclear spin can be directly deduced from the resonance peaks with the relation (for the ground state of an alkali atom) $I = \frac{\mu_B B}{\nu} - \frac{1}{2}$, where ν is the RF frequency and B is the magnetic field. In practice, the accuracy of the deduced nuclear spin is degraded by the residual magnetic field (B_L). The detailed information about how B_L affects the results can be found in a recent article[3)]. In this work, to eliminate the effects of B_L, we used a combination relation of the Bell-Bloom equation[4)], which describes optical pumping in longitudinal ($B_\parallel$: $B_0 + B_{L\parallel}$ (parallel component of B_L)) and transverse magnetic fields ($B_\perp$: perpendicular component of B_L) (for details, see Yang et al.[3)]) and $I_{LIF} \propto N_{atom}(1 - P_z)$ to fit the peaks at $B_0 = 0$, while the ZR peaks are fitted with the Lorentz function (red curve in Fig. 1).

From the ZR, after eliminating the effect of B_L, nuclear spins were deduced as 1.9(1) for the ^{84}Rb, 6.2(1) for ^{84m}Rb, 2.5(1) for ^{85}Rb, 1.9(2) for ^{86}Rb, and 1.53(6) for ^{87}Rb. The inaccuracy of the B_0 and the estimated $B_L$is supposed to be the main experimental error. In addition, 3.3% of error arises from the field inhomogeneity within the observation region and uncertainty of the observation region (1 mm). Taking all the factors into account, the nuclear spins of $^{84m,84-87}$Rb were correctly deduced within the experimental error, which are consistent with the literature values.

Consequently, we have successfully observed the ZR spectra for $^{84-87}$Rb isotopes and their nuclear spin can be determined with a good accuracy, which directly confirms the feasibility of the OROCHI method. It is worth emphasizing here that the measured spectra were recorded in 30 minutes or less with a beam intensity of $\sim 10^4$ pps. All the results suggest that, after further being developed and improved, the OROCHI method can be established as a promising method to precisely measure nuclear spins and moments of various nuclear species near the drip line with a low yield.

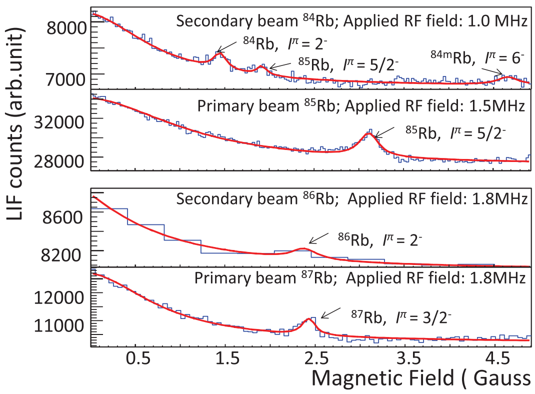

Fig. 1.: Zeeman resonance spectra for $^{84m,84-87}$Rb.

References

1) T. Furukawa et al.: Hyp. Int. **196**, 191 (2010).
2) T. Furukawa et al.: RIKEN. APR. **46**, xi(2013).
3) X.F. Yang et al.: Hyp. Int. **227**, 147 (2014)
4) M. Arndt et al.: Phys. Rev. Lett **74**, 1359(1995)

*1 RIKEN Nishina Center
*2 School of Physics, Peking University
*3 Department of Physics, Tokyo Metropolitan University
*4 Cyclotron Radioisotope Center, Tohoku University
*5 Department of Physics, Meiji University
*6 Department of Physics, Osaka University
*7 Department of Physics, Tokyo Gakugei University
*8 Department of Physics, Tokyo Institute of Technology
*9 Department of Physics, University of Tsukuba
*10 Department of Applied Physics, Tokyo University of Agriculture and Technology
*11 Laser Technology Laboratory, RIKEN
*12 Department of Advanced Science, Hosei University

Study of high-spin states in ^{35}S

S. Go,[*1,*3] E. Ideguchi,[*2] R. Yokoyama,[*3] M. Kobayashi,[*3] K. Kisamori,[*1,*3] S. Michimasa,[*3] S. Shimoura,[*3] M. Niikura,[*4] A. Yagi,[*5] H. Nishibata,[*5] M. Sugawara,[*6] M. Koizumi,[*7] Y. Toh,[*7] T. Shizuma,[*7] A. Kimura,[*7] H. Harada,[*7] K. Furutaka,[*7] S. Nakamura,[*7] F. Kitatani,[*7] Y. Hatsukawa,[*7] D. Suzuki,[*8] I. Matea,[*8] D. Verney,[*8] and F. Azaiez[*8]

Superdeformed rotational bands in the mass 40 region have been discovered in ^{36}Ar,[1)] ^{40}Ar[2)] and ^{40}Ca[3)]. The occurrence of the superdeformed structure in this region is related to the existence of large energy gaps that are formed between the down-sloping $f_{7/2}$ and the up-sloping $d_{3/2}$ and $d_{5/2}$ orbitals, as can be seen in the Woods-Saxon single particle diagram in Fig. 1. The diagram also indicates the superdeformed structure in sulfur isotopes since there is a large energy gap at $Z = 16$. The spin-parity of the superdeformed band heads in odd-mass isotopes could give information about the orbital that drives the superdeformed structure. Therefore, we performed the in-beam gamma-ray spectroscopy to search for superdeformed states in ^{35}S at the Tandem-ALTO facility, Institut de physique Nucléaire d'Orsay.

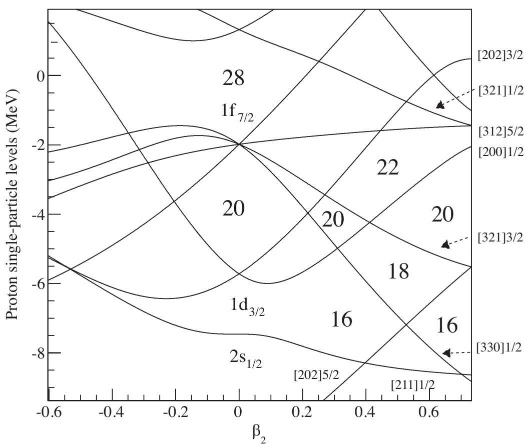

Fig. 1. Woods-Saxon orbitals as a function of the quadrupole deformation parameter β_2. The calculation was performed by the WSBETA code[4)].

High-spin states of ^{35}S were produced by the fusion evaporation reaction, ^{26}Mg(^{18}O, $2\alpha 1n$)^{35}S. ^{18}O beam energies of 75 and 80 MeV were used. The thickness of the ^{26}Mg target was 1 mg/cm^2. Gamma rays were measured using the ORGAM array consisting of EUROGAM germanium detectors[5)]. A total of 13 detectors were installed at 5 different angles. The energy loss of charged particles from compound nuclei was measured by Si-Ball[6)], a 4π array of 11 silicon detectors of 170 μm in thickness.

In order to identify high-spin states of ^{35}S, the gamma–gamma coincidence analysis was performed. For instance, the transitions reported in the previous study[7)] were observed by gating the de-excitation gamma ray from the first excited state at 1302 keV of ^{35}S (see Fig. 2). All possible energy gates were examined to construct the level scheme. Thus, an 1576-keV E2 transition from the excited state at 8.8 MeV was found. The half-life was estimated to be less than a few hundred femto seconds due to the existence of the residual Doppler shift of the transition[8)]. This means the transition has high-collectivity and indicates superdeformed band member in ^{35}S. Further analysis is being carried out.

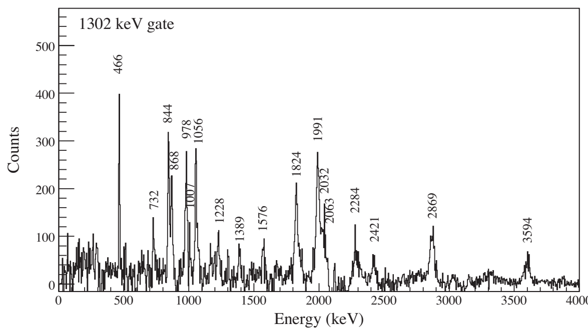

Fig. 2. Gamma-ray energy spectrum of ^{35}S in coincidence with the 1302 keV transition.

References

1) C.E. Svensson et al.: Nucl. Phys. A, **682**, 1 (2001).
2) E. Ideguchi et al.: Phys. Lett. B, **686**, 18 (2010).
3) E. Ideguchi et al.: Phys. Rev. Lett. **87**, 222501 (2001).
4) S. Ćwoik et al.: Comp. Phys. Comm. **46**, 379 (1987).
5) C.W. Beausang et al.: Nucl. Instr. Meth. A, **313**, 37 (1992).
6) T. Kuroyanagi et al.: Nucl. Instr. Meth. A, **316**, 211 (1999).
7) E. Ideguchi et al.: CNS Ann. Rep. 2009, **23** (2011).
8) B. Cederwall et al.: Nucl. Instr. Meth. A, **354** 591 (1995).

*1 RIKEN Nishina Center
*2 Research Center for Nuclear Physics, Osaka University
*3 Center for Nuclear Study, University of Tokyo
*4 Department of Physics, University of Tokyo
*5 Department of Physics, Osaka University
*6 Chiba Institute of Technology, Faculty of Information and Computer Science
*7 Japan Atomic Energy Agency
*8 Institut de Physique Nucléaire d'Orsay

Measurement of ^{41}S spin polarization

H. Shirai,[*1] Y. Ichikawa,[*2] H. Ueno,[*2] Y. Ishibashi,[*2,*3] T. Suzuki,[*1] T. Furukawa,[*4] A. Yoshimi,[*5] Y. Abe,[*2,*3] K. Asahi,[*1] J. M. Daugas,[*6] T. Fujita,[*7] M. Hayasaka,[*8] K. Imamura,[*2,*9] S. Kishi,[*8] S. Kojima,[*1] D. Nagae,[*3] A. Nakao,[*2] Y. Ohtomo,[*1] T. Sagayama,[*8] Y. Sakamoto,[*1] and T. Sato[*1]

Spectroscopic data have indicated the erosion of the $N = 28$ shell gap in several studies[1–4)]. In particular, the isomeric state of ^{43}S at 320 keV is suggested to have a quasi-spherical shape with a spin-parity of $7/2^{-}$[5,6)]. On the other hand, the spin-parity of the ground state of ^{43}S has been neither confirmed nor predicted uniquely[5,7,8)]. In order to investigate the mechanism of the $N = 28$ magicity loss through the determination of the spin parity of the ground state of ^{43}S, we aim to measure systematically the ground state electromagnetic moments for ^{41,43}S.

The electromagnetic moments of nuclei in their ground states are measured by combining the technique to produce spin-polarized RI beams[9)] and the method of β-ray-detected nuclear magnetic resonance (β-NMR). In this scheme, the RIs are stopped in a crystal, which provides spin-lattice relaxation times T_1 that are longer than the β-decay halflife of the RI. In order to find out optimum conditions for the β-NMR measurement, the T_1 measurements were carried out for stopper crystal candidates, such as Si, ZnS, and CaS. In the measurements, an RI beam of ^{41}S, for which a large yield was expected, was used, instead of ^{43}S, to measure the relaxation time T_1.

The experiment was carried out at the RIPS[11)] facility at RIBF. The RI beam of ^{41}S was produced by the fragmentation of ^{48}Ca projectiles at an energy of $E = 63$ MeV/nucleon on a 0.52 mm-thick ^{9}Be target. The intensity of the ^{48}Ca beam at the target was typically 200 pnA. The isotope separation of the ^{41}S beam was conducted by the RIPS beam line, in which the emission angle θ_{F} and momentum p_{F} of the fragment were selected so as to realize ^{41}S spin-polarization. Under the condition of $p_{\mathrm{F}} = p_0 \times (1.015 \pm 0.025)$ and $\theta_{\mathrm{F}} > 1^{\circ}$, where p_0 represents the central momentum of the fragment ^{41}S, the ^{41}S beam was obtained from RIPS with a purity of 47% and an intensity of 1.6×10^4 particles/s.

The ^{41}S beam was then transported to the final focal plane and implanted into a stopper crystal located at the center of the adiabatic field rotation (AFR) device[12)]. The AFR device enables us to extract the asymmetry of β-ray emission without relying on the NMR technique, by only rotating a pair of Nd permanent magnets adiabatically. The β rays emitted from ^{41}S were counted by plastic scintillators, two of which were set above the crystal and two others were set below it. The measurement was conducted according to the following sequence of cycles: beam irradiation for 2,900 ms, rotation of the AFR magnets for 150 ms, waiting time of 200 ms, and the β ray counting for 2,900 ms. The irradiation and counting time periods were chosen to be comparable with the meanlife of ^{41}S. The waiting margin was inserted in order to avoid spurious effects that might arise from a tiny vibration of the magnets following the rotation. The value of AP was deduced from β rays counts obtained in the following four different configurations with the field directions up/down and the magnet rotation true/false (hence, the spin is flipped/not flipped). Here, A and P denote the asymmetry parameter for the β-ray emission and the degree of polarization of ^{41}S, respectively. From the results of the AFR measurement, we obtained $AP = -0.14(4)\%$ with the CaS multi-crystal stopper of 0.5 mm thickness, and T_1 was found to be longer than 4,600 ms in 1σ confidence level.

Following the T_1 and AP measurements, the g-factor search by means of the β-NMR method was carried out using the spin-polarized ^{41}S with $AP = -0.14\%$ and the CaS crystal. Because the range within which the g-factor of ^{41}S is predicted theoretically is quite wide, a fast switching system for changing the tank-circuit frequency[13)] has been used. The results of the NMR measurement are under analysis.

*1 Department of Physics, Tokyo Institute of Technology
*2 RIKEN Nishina Center
*3 Department of Physics, Tsukuba University
*4 Department of Physics, Tokyo Metropolitan University
*5 Research Core for Extreme Quantum World, Okayama University
*6 CEA
*7 Department of Physics, Osaka University
*8 Department of Physics, Tokyo Gakugei University
*9 Department of Physics, Meiji University

References

1) S. Grévy et al.: Eur. Phys. J. **A 25**, 111 (2005).
2) F. Sarazin et al.: Phys. Rev. Lett. **84**, 5062 (2000).
3) R. W. Ibbotson et al.: Phys. Rev. C **59**, 642 (1999).
4) Zs. Dombrádi et al.: Nucl. Phys. **A727**, 195 (2003).
5) L. Gaudefroy et al.: Phys. Rev. Lett. **102**, 092501 (2009).
6) R. Chevrier et al.: Phys. Rev. Lett. **108**, 162501 (2012).
7) F. Nowacki et al.: Phys. Rev. C **79**, 014310 (2009).
8) I. Hamamoto: J. Phys. G: Nucl. Part. Phys. **37**, 055102 (2010).
9) K. Asahi et al.: Phys. Lett. B **251**, 488 (1990).
10) K. Sugimoto et al.: J. Phys. Soc. Jpn. **21**, 213 (1966).
11) T. Kubo et al.: Nucl. Instrum. Meth. B **70**, 309 (1992).
12) Y. Ishibashi et al.: Nucl. Instrum. Meth. B **317**, 714 (2013).
13) N. Yoshida et al.: Nucl. Instrum. Meth. B **317**, 705 (2013).

Offline experiment of high-resolution resonance ionization spectroscopy on Titanium using injection-locked Ti:Sapphire laser system

T. Takamatsu,[*1] H. Tomita,[*1,*2] T. Takatsuka,[*1,*2] Y. Adachi,[*1,*2] Y. Furuta,[*1]
K. Wendt,[*3] V. Sonnenschein,[*4] T. Noto,[*1,*2] T. Iguchi,[*1] T. Sonoda[*2] and M. Wada[*2]

Resonant ionization is useful for precise optical spectroscopy of radioactive isotopes of many elements to investigate the structures of unstable nuclei. We have developed a high-resolution resonance ionization spectroscopy (HR-RIS) combined with a supersonic gas jet system [1,2] in the PArasitic Laser Ion Source (PALIS) system at RIKEN and a narrow bandwidth tunable pulsed laser system, *i.e.*, an injection-locked Ti:Sapphire laser system [3,4]. An offline experiment was performed using this injection-locked Ti:Sapphire laser system.

The experimental setup for HR-RIS on Ti are shown in Fig.1. Titanium atomic vapor was evaporated by resistive heating of a Ti filament in a vacuum chamber called a reference cell. For optical resonance excitation and ionization from the ground state or a thermally populated low-lying excited state using the Ti:Sapphire laser, an ionization scheme shown in Fig.2 (a) was used. The titanium atomic vapor was irradiated using the second harmonics of the injection-locked Ti: Sapphire laser tuned to the first step transition. The second harmonics of a standard Ti: Sapphire laser was additionally used for efficient ionization via autoionization states. Here, an external cavity diode laser (ECDL) was used as a master laser of the injection-locked Ti:Sapphire laser. We achieved a line width of 20 MHz and a 0.4 mJ/pulse at the maximum output of the injection-locked Ti:Sapphire laser operated at a repetition rate of 1 kHz. Titanium ions produced by resonance ionization were accelerated with an electric field and detected by a multi channel plate (MCP) after traversing the field free region. The number of pulses from MCP was obtained from a counter with a timing gate in the time-of-flight of Ti ions.

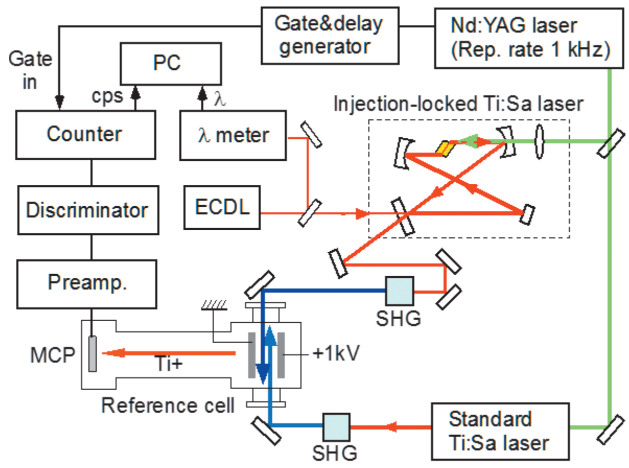

Fig.1 Experimental setup for HR-RIS on Ti

We investigated the Rydberg and autoionization states by scanning of the second step laser from 554800 cm^{-1} to 55600 cm^{-1} for a higher count rate. We identified a strong and broad autoionization state around 55400 cm^{-1} as shown in Fig.2 (a). The optical spectrum of stable Titanium obtained by the frequency scan of ECDL, *i.e.*, the scanning of the first step laser is shown in Fig.2 (b). The line-width in the spectrum was estimated to be approximately 210 MHz, and five peaks corresponding to the ^{46,47,48,49,50}Ti isotopes were clearly resolved in the spectrum. Further, their ratios were in good agreement with the natural abundances of Ti isotopes (^{46}Ti-8.0% ^{47}Ti-7.3% ^{48}Ti-73.8% ^{49}Ti-5.5% ^{50}Ti-5.4%). The isotope shift of the optical transition of ^{46}Ti and ^{50}Ti to ^{48}Ti were evaluated to be approximately 1.7 GHz and 1.6 GHz, respectively. Presently, the particularly narrow hyperfine splitting of ^{47}Ti and ^{49}Ti is not resolved because of the remaining Doppler broadening of the experimental geometry. In the near future, the resolution will be improved by applying the supersonic gas-jet system.

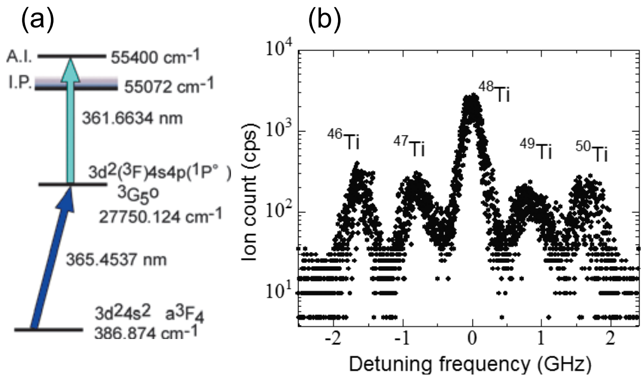

Fig.2 (a) Ionization scheme on Ti (b) Optical spectrum of Ti isotopes.

*1 Department of Quantum Engineering, Nagoya University
*2 RIKEN Nishina Center
*3 Institute of Physics, Johannes Gutenberg-University Mainz
*4 Department of Physics, University of Jyväskylä

References

1) T. Sonoda et al., Hyperfine Interact 216, 103, (2013).
2) T. Sonoda, et al., Nucl. Instrum. Meth. B 295, 1, (2013).
3) T. Takatsuka, et al., Nucl. Instrum. Meth. B 317, 586, (2013).
4) T. Kessler, H. Tomita et al., Laser Physics 18, 842, (2008).

First α-γ spectroscopic study using a Si-Ge detector array installed at the focal plane of GARIS

D. Kaji,[*1] K. Morimoto,[*1] Y. Wakabayashi,[*1] M. Takeyama,[*1,*2] and M. Asai[*1,*3]

A basic study on α-γ spectroscopy was performed using a Si-Ge detector array installed at a focal plane of a gas-filled recoil ion separator GARIS.

The GARIS has been applied for studying production and decay properties of superheavy element (SHE) nuclides produced via Pb/Bi-based fusion reactions (cold fusion); in particular, these studies focused on the search for 113^{th} element on the basis of ^{209}Bi(^{70}Zn,n)^{278}113 reaction from 2003 to 2012[1-3]. In the most of these experiments, the number of identified atoms was limited because of the low production cross section of the SHE nuclides. The nuclide identification method was based on the genetic relation between mother and daughter. It involved measuring the α-decay and spontaneous fission SF. Therefore, a detailed decay scheme including γ-decay could not be obtained. In 2013, we newly installed a Si-Ge detector array, as shown in Fig. 1, at the focal plane of GARIS for studying the production and decay properties of reaction products for ^{248}Cm+^{48}Ca[4]. The Si-Ge array is useful as a probe for detecting prompt γ-ray coinciding with SF[5]. Before the experiment, we calibrated the Si-Ge array by using a ^{207}Pb(^{48}Ca,2n)^{253}No reaction.

Projectiles of ^{48}Ca with a charge state of 11^+ were extracted from the 18-GHz ECR ion source and accelerated up to 218.5 MeV using the RILAC. The intensity of a typical beam incident on a target was 5.2×10^{12} s^{-1} (0.86 pμA). The metallic ^{207}Pb target was prepared by vacuum evaporation on a 60 μg/cm^2 carbon foil. Target thickness was 371 μg/cm^2 for ^{207}Pb (enrichment of 99.59%). Sixteen frames of the sector targets were mounted on a ϕ30 cm rotating wheel, which was rotated at 3300 rpm. The reaction products were separated in-flight from projectiles and other by-products by GARIS, and they were guided into the focal plane detection system after they passed through the time-of-flight detector. The separator was filled with helium gas at a pressure of 73 Pa. The magnetic rigidity $B\rho$ was set to 2.064 T·m for ^{253}No. Gamma rays emitted in prompt coincidence with α-particles registered by a conventional position-sensitive Si detector (PSD box)[1-3] were measured using a planar-type Ge detector for counting low-energy photons (CANBERRA BE6530; active volume: ϕ91.5 mm×31.6 mm^t). The distance between PSD and Ge detector was c.a. 6 mm (3 mm between PSD and 1 mm^t Al window + 2 mm between Al window and Ge detector). The peak efficiency for 122-keV photons was 22.8% at the middle position of the PSD. Figure 2 (a) shows a two-dimensional energy plot of α- and γ-rays observed in prompt coincidence. The energy spectrum of γ-rays observed in prompt coincidence with α-decays is given in Fig. 2 (b). These data were obtained under low-background condition, despite the high beam intensity of 0.86 pμA. Observed α- and γ-transitions due to ^{253}No agree well with previously reported values[6].

The Si-Ge array will be applicable to study α-γ(X) spectroscopy of SHE nuclides.

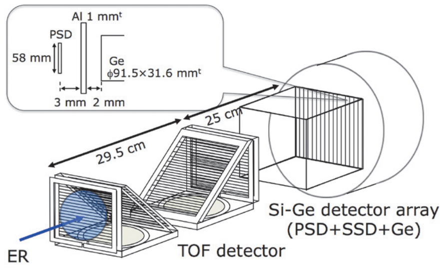

Fig. 1. New focal plane detector including Si-Ge array.

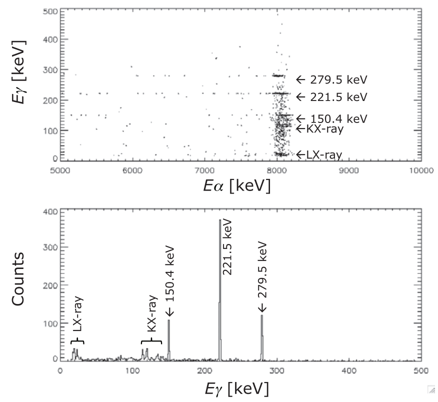

Fig. 2. (a) Two-dimensional plot of α-γ coincidence. (b) Projection of the events onto the γ-energy axis.

References
1) K. Morita et al.: J. Phys. Soc. of Jpn. 73, p.2593 (2004).
2) K. Morita et al.: J. Phys. Soc. of Jpn. 77, p.045001 (2007).
3) K. Morita et al.: J. Phys. Soc. of Jpn. 81, p.103201 (2012).
4) K. Morita et al.: In this report.
5) M. Takeyama et al.: In this report.
6) F. P. Heßberger et al.: Eur. Phys. J. A 48, p.75 (2012).

*1 RIKEN Nishina Center
*2 Department of Physics, Yamagata University
*3 Advanced Science Research Center, JAEA

Experimental study of resonant states in ^{27}P via elastic scattering of ^{26}Si+p †

H.S. Jung,[*1] C.S. Lee,[*1] Y.K. Kwon,[*1] J.Y. Moon,[*1] J.H. Lee,[*1] C.C. Yun,[*1] S. Kubono,[*2] H. Yamaguchi,[*2] T. Hashimoto,[*2] D. Kahl,[*2] S. Hayakawa,[*2] S. Choi,[*3] M.J. Kim,[*3] Y.H. Kim,[*3] Y.K. Kim,[*4,*5] J.S. Park,[*4] E.J. Kim,[*6] C.-B. Moon,[*7] T. Teranishi,[*8] Y. Wakabayashi,[*9] N. Iwasa,[*10] T. Yamada,[*10] Y. Togano,[*11] S. Kato,[*12] S. Cherubini,[*13,*14] and G.G. Rapisarda[*13,*14]

We studied proton resonant states in ^{27}P via elastic scattering to investigate the ^{26}Si$(p,\gamma)^{27}$P reaction, which is an important in the rp-process path for the understanding of the nucleosynthesis in explosive hydrogen burning[1,2]. This reaction is also relevant to the production of ^{26}Al[3]. The knowledge of the structure of ^{27}P is still insufficient because of uncertain resonance parameters, such as resonance energies and spin-parity assignments.

The measurement of the ^{26}Si+p elastic scattering was performed at the low-energy RI beam facility CRIB (CNS Radioactive Ion Beam separator) of the Center for Nuclear Study (CNS), the University of Tokyo[4,5], by bombarding a H_2 gas target with a ^{26}Si radioactive ion beam in inverse kinematics[6] and detecting scattered protons using silicon detectors for a ΔE-E telescope. We applied the thick-target method [7,8] to scan the entire energy region of interest simultaneously. The excitation function was obtained from the scattered proton energy spectrum by a kinematics conversion process. A ^{24}Mg primary beam with an energy of 7.5 MeV/A and an intensity of 1.6 eμA extracted from the AVF cyclotron bombarded a ^{3}He gas target which was at 550 Torr and 90 K. The secondary beam was produced by the ^{3}He(^{24}Mg,^{26}Si)n reaction. Protons elastically scattered to the forward angles in the laboratory frame were detected by a ΔE-E telescope.

By calculating the kinematics, including energy loss in the target, the measured proton energy of each event was converted to a center-of-mass energy. We performed an analysis using the R-matrix calculation code (SAMMY-8.0.0)[9] to deduce resonance parameters such as excitation energy E_x, spin J, parity π, and proton partial width Γ_p of resonance states. Figure 1 shows best-fit results for the excitation function.

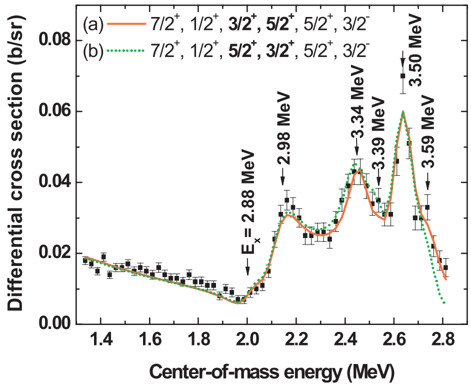

Fig. 1. Final results for the excitation function of ^{26}Si+p as the best fits are shown but without firm spin-parity assignment for the doublet around 3.3 MeV.

Six new resonant states in ^{27}P have been suggested, and we mostly determined their resonance parameters such as resonance energy, width, and spin-parity with the R-matrix calculation. Two small bumps around 3.39 MeV and 3.59 MeV were introduced to improve the fitting because exclusion of these resonances resulted in a less satisfactory fit for near resonant states. Parameters of resonant states in ^{27}P are expected to contribute to the nuclear data for the nuclear reaction network calculation of the rp-process nucleosysnthesis. The previous estimate of the total reaction rate of ^{26}Si$(p,\gamma)^{27}$P, which was evaluated by Iliadis *et al.*[10], should be reanalyzed with the nuclear physics input newly obtained in present work.

† Condensed from the article in Phys. Rev. C. **85**, 045802 (2012)

*1 Department of Physics, Chung-Ang University
*2 Center for Nuclear Study, University of Tokyo
*3 Department of Physics and Astronomy, Seoul National University
*4 Department of Nuclear Engineering, Hanyang University
*5 Institute for Basic Science
*6 Department of Education, Chonbuk National University
*7 Faculty of Sciences, Hoseo University
*8 Department of Physics, Kyushu University
*9 Advanced Science Research Center, JAEA
*10 Department of Physics, Tohoku University
*11 RIKEN Nishina Center
*12 Department of Physics, Yamagata University
*13 Laboratori Nazionali del Sud-INFN
*14 Dipartimento di Fisica e Astronomia, Universita di Catania

References

1) H. Herndl et al.: Phys. Rev. C **52**, 1078 (1995).
2) J. L. Fisker et al.: Astrophys. J. **174**, 261 (2008).
3) R. Diel et al.: Astron. Astrophys. **298**, 445 (1995).
4) S. Kubono et al.: Eur. Phys. J. A **13**, 217 (2002).
5) Y. Yanagisawa et al.: Nuc. Instrum. Methods Phys. Res. Sect. A **539**, 74 (2005).
6) K.P. Artemov et al.: Nuc. Phys. **52**, 408 (1990).
7) W. Galster et al.: Phys. Rev. C **44**, 2776 (1991).
8) S. Kubono: Nuc. Phys. A **693**, 221 (2001).
9) A.M. Lane and R.G. Thomas: Rev. Mod. Phys. **30**, 257 (1958).
10) C. Iliadis et al.: Nuc. Phys. A **841**, 31 (2010).

Study of resonance states in ^{26}Si by elastic scattering of $^{22}Mg+\alpha$

N.N. Duy,[*1] L.H. Khiem,[*1] S. Kubono,[*2] H. Yamaguchi,[*2] D. Kahl,[*2] T. Hashimoto,[*2] S. Ota,[*2] Y. Wakabayashi,[*3] T. Komatsubara,[*4] T. Teranishi,[*5] S. Kato,[*6] N. Iwasa,[*7] T. Yamada,[*7] Y.K. Kwon,[*8] A. Kim,[*9] Y.H. Kim,[*9] J. Song,[*9] J. Hu,[*10] and Y. Ito[*11]

The data of ^{26}Si are important not only in the astrophysics but also in the nuclear structure. The resonance states of ^{26}Si are valuable for investigating the reaction rate of $^{22}Mg(\alpha,p)^{25}Al$ and $^{25}Al(p,\gamma)^{26}Si$ reactions in the Supernovae II and X-ray bursts, which are important in understanding the astrophysical nomalies. In addition, the alpha-cluster structure, above the alpha decay threshold (E_{thr} = 9.164 MeV), is expected to be obtained in the ^{26}Si nucleus because of the alpha-cluster threshold rule. Futhermore, although the energy levels of the mirror nucleus, ^{26}Mg, are well-known, there are many unknown spin-parities. These quantum parameters can be assigned using the ^{26}Si data. There were some experimental efforts for the levels near and above the alpha decay threshold, but the data is still limited. Several resonance states in the energy region considered were obtained by the works in ref.[1, 2], but such states had a large uncertainty because of unknown spin-parities. Therefore, we performed the elastic scattering of the $^{22}Mg(\alpha,\alpha)^{22}Mg$ reaction using a radioactive ion (RI) beam of ^{22}Mg to obtain the experimental data corresponding to the mentioned aims for ^{26}Si at the CRIB facility of RIKEN in October 2011. We performed the experiment of $^{22}Mg+\alpha$ by applying the thick-target method using the active-target detector GEM-MSTPC in inverse kinematics.[3)] The RI beam of ^{22}Mg, which was produced via the $^{3}He(^{20}Ne,^{22}Mg)n$ reaction, with the intensity of 1200 particles/s satisfied the energy condition of E_{cm} = 0.5 – 3.0 MeV in the center-of-mass of the elastic scattering $^{22}Mg(\alpha,\alpha)^{22}Mg$.[4)] Therefore, the energy corresponded to the region of E_x = 9.5 – 12.5 MeV in ^{26}Si. The RI beam was incident on the gas target, which was a gas mixture of $^{4}He+CO_2$ (10%) at 140 Torr at room temperature. The gas was filled in a chamber in which the electrode structures of GEM-MSTPC and arrays of silicon detector telescopes were installed. The trajectory and timing information of the incoming ^{22}Mg were obtained using the beam monitors PPACs for particle identification. The ejectiles coming from the elastic scattering $^{22}Mg(\alpha,\alpha)^{22}Mg$ were distinguished from those due to the $^{22}Mg(\alpha,p)^{25}Al$ reaction based on the ΔE-E method by using the information from the silicon telescopes. The events due to the elastic scattering and the production of the beam contaminants were identified based on the Bragg curves of the outgoing ^{22}Mg and the contaminants determined by GEM-MSTPC.

The data were analyzed event by event. The calculation of the kinematics was carried out by considering the energy loss of the projectile measured by the active-target detector. The energy of alphas was measured by the active-target detector and the silicon telescopes. The excitation function of the cross section of the elastic scattering $^{22}Mg(\alpha,\alpha)^{22}Mg$ could be determined in the forward angles, which related to 0-5 degrees and 5-10 degrees in the laboratory frame. The resonances in the excitation function were applied to the R-matrix analysis performed by the AZURE code[5)] to deduce the quantum quantities of the resonance states of ^{26}Si above the alpha threshold. We could obtain six states, in which three new states (11.245, 11.493, and 11.807 MeV) and three lower states matched well with the results obtained by previous works.[1, 2)] In addition, the spin-parity assignment for the first and sixth states is satisfied with two values, as shown in Table 1.

Table 1. The resonance states above the alpha threshold of ^{26}Si obtained by the elastic scattering of $^{22}Mg(\alpha,\alpha)^{22}Mg$.

Levels	E_r (MeV)	Γ(MeV)	J^{π}
1	10.325 ± 0.071	0.218 ± 0.011	$(2^+, 1^-)$
2	10.678 ± 0.016	0.194 ± 0.006	0^+
3	10.831 ± 0.113	0.186 ± 0.013	1^-
4	11.245 ± 0.028	0.208± 0.027	4^+
5	11.493 ± 0.216	0.292 ± 0.010	3^-
6	11.807 ± 0.117	0.156 ± 0.032	$(0^+, 2^+)$

According to the study in ref.[6)], the first, third, and sixth level in the ^{26}Si nucleus are very close to the three resonances located at 10.300 MeV (0^+), 10.844 MeV (1^-), and 11.828 MeV (2^-), respectively, in ^{12}C. In addition, such states of ^{12}C might have a structure of 3α.[7)] Therefore, the ^{26}Si may exist under alpha cluster as a structure of (p+3α+3α+p).

The direct measurement of alpha elastic scattering was performed for the first time. The data of ^{26}Si is very limited so far. The cluster structure of the isotopes with a number of nucleon nearby the value of 4N (N = 2, 3, 4…) is very uncertain. Hence, we need such type of data significantly more to investigate the structure of ^{26}Si in future.

References

1) A. Matic et al., Phys. Rev. C 84 025801 (2011) 1 - 7.
2) J. C. Thomas et al., Eur. Phys. Jour. A 21, (2004) 419-435.
3) N. N. Duy et al., CNS Ann. Rep. 2011 (2013) 9 - 10.
4) N. N. Duy et al., Nucl.Instrum.Meth A 723 (2013) 99-101.
5) R. E. Azuma et al., Phys. Rev. C 81 045805 (2010) 1-17.
6) F. Ajzenberg-Selove et al., Nuclear Physics A114 (1968) 13-16.
7) L. R. Hafstad et al., Physical Review Vol.54 (1938) 681 – 692.

*1 Institute of Physics, Vietnam Academy of Science and Technology
*2 Center for Nuclear Study, Graduate School of Science, Univ. of Tokyo
*3 Japan Atomic Energy Agency
*4 Department of Physics, University of Tsukuba
*5 Department of Physics, University of Kyushu
*6 Department of Physics, University of Yamagata
*7 Department of Physics, University of Tohoku
*8 Department of Physics, ChungAng University
*9 Department of Physics, Seoul University
*10 Institute of Modern Physics, Chinese Academy of Science
*11 Low Energy Experimental Nuclear Physics Gr., Univ. of Tsukuba

Confirmation of the astrophysically important 6.15-MeV, 1^- state in ^{18}Ne via resonant proton scattering of ^{17}F+p

J. Hu,[*1] J.J. He,[*1] S.W. Xu,[*1] H. Yamaguchi,[*2] P. Ma,[*1] D. Kahl,[*2] J. Su,[*3] H.W. Wang,[*4] T. Nakao,[*2] Y. Wakabayashi,[*5] J.Y. Moon,[*6] T. Teranishi,[*7] H.S. Jung,[*6] T. Hashimoto,[*8] A. Chen,[*9] D. Irvine,[*9] and S. Kubono[*5]

The ^{14}O(α, p)^{17}F reaction is important during the ignition phase of X-ray bursts. However, thus far, the rate of this reaction remains unknown. Therefore, studies on this reaction are of great importance in researching explosive stellar environments in a nuclear astrophysics context. The ^{14}O(α, p)^{17}F reaction is mainly resonant, and its reaction rate depends on the resonant properties of the excited states that are above the α threshold in the compound nucleus ^{18}Ne. A state observed in ^{18}Ne at E_x = 6.15 MeV has been tentatively identified as the important state, which could be dominated at low temperatures.

The experiment was performed using the CNS radioactive ion beam separator (CRIB)[1]. A primary beam of $^{16}O^{6+}$ was accelerated up to 6.6 MeV/nucleon with an average intensity of 560 enA. A D_2 gas target was bombarded with the primary beam, resulting in the production of a secondary beam of ^{17}F via the ^{16}O(d, n)^{17}F reaction in inverse kinematics. The ^{17}F beam, with a mean energy of 61.9 MeV and an average intensity of 2.5×10^5 pps, was then delivered to the F3 experimental chamber where it bombarded a thick H_2 gas target. The recoiled light particles were measured by using three sets of ΔE-E Si telescopes at averaged angles of $\theta_{\rm lab} \approx 3°$, 10°, and 18°, respectively.

The excitation function of ^{17}F+p elastic scattering cross sections at different scattering angle regions are shown in Fig. 1(a)–(b). Five resonances, *i.e.*, at E_x = 6.15, 6.28, 6.35, 6.85, and 7.05 MeV, all of which with the exception of 6.85 MeV had been observed previously in other ways, were analyzed using the multichannel R-matrix calculations.[2] The most probable fitting curves are shown in Fig. 1(a)–(b). As shown in the figure, the fitting results at different scattering angle regions are consistent with each other.

According to our R-matrix analysis, see Fig. 1(c), a dip structure around $E_{\rm c.m.}$ = 2.21 MeV corresponding to the 6.15-MeV level in ^{18}Ne can be fitted as 1^- ($s = 2^+$, $\ell = 1$), Γ = 50 keV very well. The shape of the dip structure is clear, in contrast to the bump shape

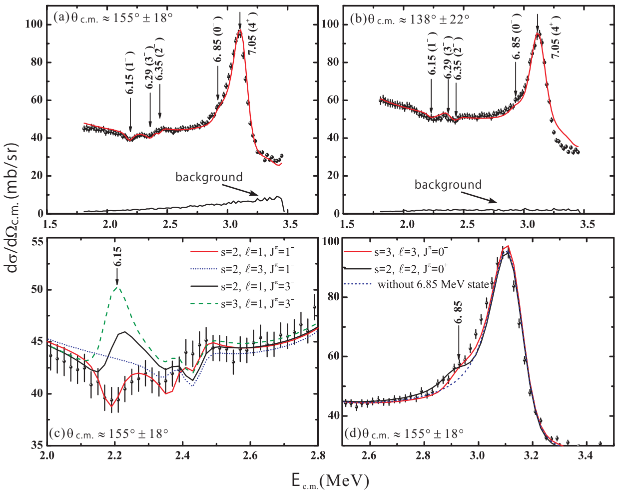

Fig. 1. The center of mass differential cross sections for elastically scattered protons. The curves represent the R-matrix fits to the data.

reported previously.[3] The 1^- assignment with high statistics in this work firmly maintains the significant position of 6.15-MeV state at low temperatures.

Moreover, a shoulder-like structure around $E_{\rm c.m.}$ = 2.93 MeV was observed (Fig. 1(a) and (b)). This may imply that a new state was discovered at E_x = 6.85 MeV in ^{18}Ne. Both 0^-or 0^+ resonances can reproduce the observed shape, as shown in Fig. 1(d). Because of the small energy shift for the negative-parity states in this excitation energy region[4], this new state is possibly the analog state of ^{18}O at E_x = 6.88 MeV (0^-). Another possibility also exists: This new state could be a candidate of the 0^+ state, a band-head state of the six-particle four-hole (6p-4h) band.[5]

A more comprehensive analysis and the inclusion of α particle information are in progress.

References

1) Y. Yanagisawa et al.: Nucl. Instr. Meth. A **539**, 74 (2005).
2) P. Descouvemont: *Theoretical Models for Nuclear Astrophysics* (Nova Science Publishers Inc., New York, 2003).
3) J. Gómez del Campo et al.: Phys. Rev. Lett. **86**, 43 (2001).
4) H. T. Fortune and R. Sherr: Phys. Rev. Lett. **84**, 1635 (2000).
5) H. T. Fortune and R. Sherr: Phys. Rev. C **68**, 034307 (2003).

[*1] Institute of Modern Physics, Chinese Academy of Sciences
[*2] Center for Nuclear Study, the University of Tokyo
[*3] China Institute of Atomic Energy
[*4] Shanghai Institute of Applied Physics, Chinese Academy of Sciences
[*5] RIKEN Nishina Center
[*5] Department of Physics, Chung-Ang University
[*6] Department of Physics, Kyushu University
[*7] RCNP, Osaka University
[*8] Department of Physics and Astronomy, McMaster University

Progress on the ^{16}N beta delayed alpha decay studied using the Center for Nuclear Study Multi Sampling Time Projection Chamber

S. Cherubini,[*1,*2,*5] S. Hayakawa,[*2] A. Di Pietro,[*2,*5] P. Figuera,[*2,*5] M. Gulino,[*2,*3] M. La Cognata,[*2] M. Lattuada,[*1,*2] C. Spitaleri,[*1,*2] H. Yamaguchi,[*4] D.M. Kahl,[*4] T. Nakao,[*4] S. Kubono,[*5] Y. Wakabayashi,[*5] T. Hashimoto,[*6] N. Iwasa,[*7] Y. Okoda, [*7] K. Ushio,[*7] T. Teranishi,[*8] M. Mazzocco,[*9] C. Signorini,[*9] D. Torresi,[*9] J.Y. Moon,[*10] T. Komatsubara,[*10] P. Lee,[*11] K. Chae,[*12] M. Gwak[*12]

The importance of measuring the cross section of the nuclear reaction ^{12}C$(\alpha,\gamma)^{16}$O at astrophysical energies is well known. Despite half a century long efforts to perform this measurement, knowledge regarding this cross section remains unsatisfactory. Direct and indirect approaches have been used in order to determine a reliable estimation of its value, which is buried in the realm of the tenth of femtobarn[1)]. Direct measurements were performed down to a center of mass energy of approximately 1 MeV, however, the goal for the application to astrophysics requires to reach 300 keV. With regards to indirect methods, it has been shown that important pieces of information on the E1 component of the ^{12}C$(\alpha,\gamma)^{16}$O cross section can be derived from the study of the ^{16}N beta delayed alpha decay[2)]. Many attempts were conducted to measure the low energy tail of this latter alpha spectrum and the state of the art on these studies is reported in a paper by Tang and collaborators[3)].

In order to improve the available results on the measurements of the spectrum of the alpha particles emitted in the decay of ^{16}N, we proposed a new experimental approach based on the use of the Multi Sampling Time Projection Chamber (MSTPC) of the Center for Nuclear Study (CNS) of the University of Tokyo. In this new approach the limitations arising from the use of implantation foils adopted in all previous experiments were eliminated, because the chamber itself becomes the implantation material, and the detection efficiency of the decay products is also increased.

The experiment required a long technical development phase. During this phase, two ^{16}N beam production test runs were performed at the CNS Radiocative Ion Beam (CRIB) facility with very good results. The intesities of the ^{16}N beam obtained during these tests reached 10^6 ions per second. A key point in the experiment was the necessity of using MSTPC in pulsed mode: an implantation period, during which the beam is sent and stopped in the middle of the active region of the MSTPC, is followed by a time period in which the beam is stopped before entering CRIB and the ^{16}N decay events are detected and registered by the MSTPC. In order to prevent the destruction of the active devices of the MSTPC, namely two gas electron multipliers, a gating grid was introduced to stop electron multiplication during the ^{16}N beam implantation period. Various timings for the implantation (beam on) and counting (beam off) periods were tested. The final decision was to use an equal duration of 50 ms for these two periods.

Despite the fact that during the experiment the intensities of the beam reached a value that was lower than expected on the basis of the previous tests, the experiment was technically successful and data analysis is being initiated.

References
1) C. E. Rolfs, W. S. Rodney: Cauldrons in the cosmos, The University of Chicago Press, (1988)
2) F. C. Barker: Austr. J. Phys., 24, 777 (1971)
3) X. D. Tang *et al.*: Phys. Rev. C81, 045809 (2010)

*1 Dipartimento di Fisica e Astronomia, Università di Catania
*2 INFN - Laboratori Nazionali del Sud
*3 Università KORE, Enna
*4 Center for Nuclear Study, University of Tokyo, Wako Branch
*5 RIKEN Nishina Center
*6 RCNP, Osaka University
*7 Department of Physics, Tohoku University
*8 Department of Physics, Kyushu University
*9 Dipartimento di Fisica, Università di Padova and INFN-Sez. Padova
*10 Institute for Basic Science
*11 Department of Physics, Chung Ang University
*12 Department of Physics, Sungkyunkwan University

Search for new isotopes near the proton drip-line close to ^{100}Sn

I. Čeliković,[*1,*2] M. Lewitowicz,[*1] R. Gernhäuser,[*3] R. Krücken,[*4] S. Nishimura,[*5] H. Sakurai,[*6] H. Baba,[*5] B. Blank,[*7] A. Blazhev,[*8] P. Boutachkov,[*9] F. Browne,[*5,*10] G. de France,[*1] P. Doornenbal,[*5] T. Faestermann,[*3] Y. Fang,[*11] N. Goel,[*9] M. Gorska,[*9] S. Ilieva,[*12] T. Isobe,[*5] A. Jungclaus,[*13] G. D. Kim,[*14] Y.-K. Kim,[*14] I. Kojouharov,[*9] N. Kurz,[*9] G. Lorusso,[*5] D. Lubos,[*3] K. Moschner,[*8] I. Nishizuka,[*15] J. Park,[*4] Z. Patel,[*16] M. Rajabali,[*4] S. Rice,[*16] H. Schaffner,[*9] L. Sinclair,[*17] P. A. Söderström,[*5] K. Steiger,[*3] T. Sumikama,[*15] Z. Wang,[*4] H. Watanabe,[*18] J. Wu,[*19] and Z. Xu[*6]

The ^{100}Sn nucleus, the heaviest doubly magic and particle-stable nucleus with N=Z, has been the subject of numerous experimental and theoretical studies. It is one of the most important nuclei for testing nuclear structure models.

Prior to the main ^{100}Sn experiment in 2013, we performed a test experiment in December 2011 with the aim of optimizing the configuration settings of the BigRIPS[1)] separator at RIKEN, for the production and selection of ^{100}Sn.[2)] This experiment was subsequently used to set up our main ^{100}Sn experiment, which was performed in June 2013 and was dedicated to the measurement of Gamow-Teller strength in the decay of ^{100}Sn to ^{100}In (see D. Lubos et al.[3)]), to the mapping of the proton drip-line in the region of Te-Ru, and to the study of short-lived isomeric states in this region of the nuclear chart. In this contribution, we report on the search for new isotopes close to the drip-line in the Te-Ru region.

Nuclei around ^{100}Sn were produced by fragmentation of a 345 MeV/nucleon $^{124}Xe^{52+}$ beam impinging on a 4-mm Be target. The average beam intensity was 30 pnA during 203 hours of data taking.

The nuclei were identified on an event-by-event basis through the Bρ - ΔE - TOF method using the standard BigRIPS focal plane detectors. The nuclei of interest were implanted in a stack of 3 double-sided silicon strip detectors called WAS3ABi, followed by a stack of 10 single-sided silicon strip detectors used to measure the total energy of β-particles emitted after the decay of the implanted nuclei. The implantation detectors were surrounded by the EURICA array consisting of 12 seven-element Ge cluster detectors and 18 $LaBr_3$ crystals for the detection of delayed γ-rays.

A confirmation of Z and A/Q identification was achieved by the observation of the characteristic γ-lines of known isomers in ^{98}Cd and ^{96}Pd. The relative r.m.s. Z and A/Q resolutions for the Sn and N=Z isotopes were 0.41% and 0.09%, respectively. Available signals from the PPACs, plastic scintillators, and ionisation chambers were used to apply additional off-line gates, which allows the removal of spurious events from the particle identification plot.

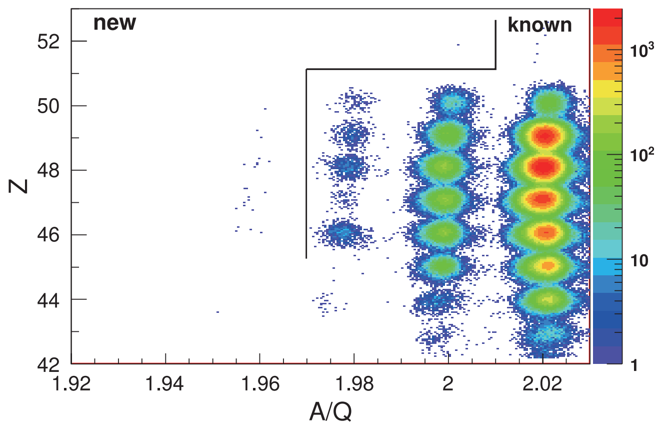

Fig. 1. Particle identification matrix Z vs A/Q around the ^{100}Sn after applying cleaning conditions.

We have discovered 3 new isotopes with more than 3 counts: ^{94}Cd, ^{92}Ag, ^{90}Pd. The consistency of all measured signals of interest for each nucleus has been checked, and the assignment of these new isotopes is unambiguous. We have also tentatively assigned events to ^{104}Te, ^{98}Sn, ^{96}In observed with less than 3 counts. One event was assigned to ^{86}Ru, the identification of which has been recently reported by H. Suzuki.[4)]

References

1) T. Kubo: Nucl. Instr. Meth. Phys. Res. B 204 (2003) 97
2) M. Lewitowicz et al.: RIKEN Acc. Prog. Rep, Vol 45 (2011) p. vi.
3) D. Lubos et al.: RIKEN Acc. Prog. Rep (this volume).
4) H. Suzuki et al.: Nucl. Instr. Meth. Phys. Res. B 317 (2013) 756

*1 GANIL
*2 Institute "Vinča", University of Belgrade
*3 Physik Department E12, Technische Universität München
*4 TRIUMF
*5 RIKEN Nishina Center
*6 Department of Physics, University of Tokyo
*7 CENBG
*8 Institut für Kernphysik, University of Cologne
*9 GSI Darmstadt
*10 School of Computing, Engineering and Mathematics, Brighton University
*11 Department of Physics, Osaka University
*12 Institut für Kernphysik, TU Darmstadt
*13 IEM CSIC, Madrid
*14 Rare Isotope Science Project, Institute for Basic Science
*15 Department of Physics, Tohoku University
*16 Department of Physics, University of Surrey
*17 Department of Physics, University of York
*18 Department of Physics, Beihang University
*19 Department of Physics, Peking University

Identification of 18 new neutron-rich isotopes produced in the EURICA uranium beam campaign

Y. Shimizu,[*1] T. Kubo,[*1] N. Fukuda,[*1] N. Inabe,[*1] D. Kameda,[*1] H. Sato,[*1] H. Suzuki,[*1] H. Takeda,[*1] K. Yoshida,[*1] H. Baba,[*1] F. Browne,[*1,*2] P. Doornebal,[*1] G. Gey,[*1,*3,*4] T. Isobe,[*1] A. Jungclaus,[*5] Z. Li,[*6] G. Lorusso,[*1] S. Nishimura,[*1] G. Simpson,[*3] P.-A. Söderström,[*1] T. Sumikama,[*7] J. Taprogge,[*1,*5,*8] Zs. Vajta,[*1,*9] H. Watanabe,[*1,*10,*11] J. Wu,[*1,*6] and Z.Y. Xu[*12]

The EUROBALL RIKEN Cluster Array (EURICA) collaboration aims to conduct isomer and β-delayed γ-ray spectroscopy of several hundred nuclei far from stability. In 2012, at the RIKEN Nishina Center RI Beam Factory (RIBF), the EURICA uranium beam campaign was been conducted to investigate isomeric decays from very neutron-rich nuclei and their β decays[1-3].

In the EURICA uranium beam campaign, the nuclei of interest were produced by the in-flight fission of 345 MeV/nucleon ^{238}U beam colliding with a 2.92-mm-thick Be target. The primary beam intensity was 8.24 particle nA on average. Table 1 summarizes the two settings used in the EURICA uranium beam campaign. Fission fragments were identified by using the superconducting in-flight separator BigRIPS[4] and the ZD spectrometer. The particle identification (PID) was performed using the ΔE-TOF-$B\rho$ method, which allows the event-by-event determination of the atomic number Z and mass-to-charge ratio A/Q of fragments[5].

Table 1. Summary of the experimental conditions.

Setting	^{136}Sn	^{128}Pd
Target (mm)	Be 2.92	Be 2.92
Bρ ^{a} (Tm)	8.004	7.391
Degrader at F1 (mm)	Al 2.82	Al 2.82
Degrader at F5 (mm)	Al 2.46	Al 2.46
F1 slit (mm)	+43.0/−64.2	+22.0/−64.2
F2 slit (mm)	+12.0/−18.0	+8.0/−12.0
Irradiation time (h)	99.6	102.9

^{a} Values from the magnetic fields of the first dipole magnet.

Figure 1 shows a two-dimensional PID plot of Z versus A/Q for the ^{136}Sn setting. The solid red line indicates the limit of known isotopes. The relative root mean square (rms) Z resolution and the relative rms A/Q resolution achieved were typically 0.38 and 0.037%, respectively, for the ^{136}Sn setting. Thanks to the excellent resolution in A/Q, we have produced and identified the following 18 new neutron-rich isotopes: ^{118}Mo, ^{121}Tc, ^{122}Tc, ^{125}Ru, ^{127}Rh, ^{129,130,131}Pd, ^{132}Ag, ^{134}Cd, ^{136,137}In, ^{139,140}Sn, ^{141,142}Sb, ^{144}Te, and ^{146}I. A detailed analysis is currently in progress.

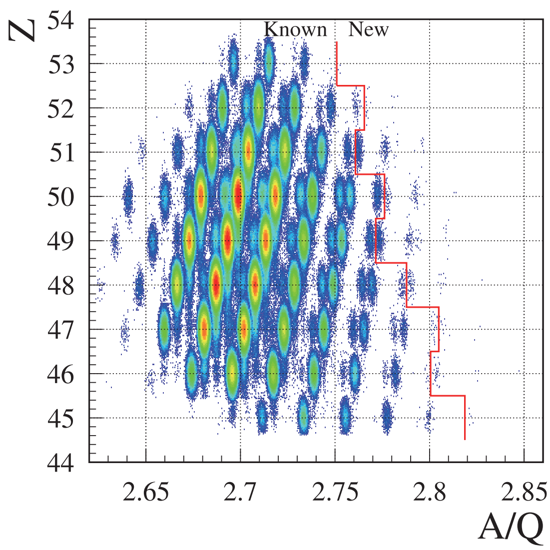

Fig. 1. Two-dimensional PID plot of Z versus A/Q for the ^{136}Sn setting. Red line indicates the limit of known isotopes.

References
1) G. Lorusso *et al.*: RIKEN Accel. Prog. Rep. **46**, x (2013).
2) G.S. Simpson *et al.*: RIKEN Accel. Prog. Rep. **46**, 22 (2013).
3) H. Watanabe *et al.*: Phys. Rev. Lett. **111**, 152501 (2013).
4) T. Kubo *et al.*: Nucl. Instr. and Meth. **B 204**, 97 (2003).
5) N. Fukuda *et al.*: Nucl. Instr. and Meth. **B 317**, 323 (2013).

*1 RIKEN Nishina Center
*2 School of Computing, Engineering and Mathematics, University of Brighton
*3 LPSC, Grenoble
*4 Instituto de Estructura de la Materia
*5 IEM-CSIC, Madrid, Spain
*6 Department of Physics, Peking University
*7 Department of Physics, Tohoku University
*8 Universidad Autónoma de Madrid, Spain
*9 MTA Atomki, Debrecen, Hungary
*10 International Research Center for Nuclei and Particles in the Cosmos, Beihang University
*11 School of Physics and Nuclear Energy Engineering, Beihang University
*12 Department of Physics, University of Tokyo

Charge-state determination for new isotopes near the proton drip-line

Y. Ohkoda,[*1,*3] T. Kubo,[*1] N. Fukuda,[*1] N. Inabe,[*1] H. Takeda,[*1] D. Kameda,[*1] H. Suzuki,[*1] K. Yoshida,[*1] K. Kusaka,[*1] K. Tanaka,[*1] Y. Yanagisawa,[*1] M. Ohtake,[*1] H. Sato,[*1] Y. Shimizu,[*1] H. Baba,[*1] M. Kurokawa,[*1] K. Ieki,[*1,*2] D. Murai,[*1,*2] N. Iwasa,[*1,*3] A. Chiba,[*1,*3] E. Ideguchi,[*4] S. Go,[*1,*5] R. Yokoyama,[*5] T. Fujii,[*5] D. Nishimura,[*1,*6] H. Nishibata,[*1,*7] S. Momota,[*1,*8] M. Lewitowicz,[*9] G. DeFrance,[*9] I. Celikovic,[*9] K. Steiger,[*10] O. B. Tarasov,[*1,*11] D. Bazin,[*1,*11] D. J. Morrissey,[*1,*11] and B. M. Sherrill[*1,*11]

Particle identification (PID) based on the ΔE-TOF-$B\rho$ method, in which atomic number Z and mass-to-charge ratio A/Q are calculated from measured energy loss (ΔE), time of flight (TOF), and magnetic rigidity ($B\rho$), does not work well for isotopes whose A/Z value is close to an integer number, such as 2 or 3. This is because hydrogen-like and fully stripped events are very closely located in a Z versus A/Q PID plot. In these cases, measurement of total kinetic energy (TKE) is additionally needed to identify the charge state. We performed such TKE measurement to calculate the charge state number Q for medium heavy proton-rich isotopes with $A/Z \sim 2$.

The experiment was performed in December 2011 at RIBF using a ^{124}Xe beam at 345 MeV/nucleon. The BigRIPS separator[1)] was used to separate and identify produced isotopes, and was tuned for very proton-rich isotopes with $Z = 30$-45. The PID based on the ΔE-TOF-$B\rho$ method was made at the second stage of the BigRIPS separator.[2)] The TKE measurement was made using a stack of eleven 1-mm-thick silicon detectors, placed downstream of the BigRIPS separator. The energy loss data from the silicon detectors were added to calculate the TKE. We calculated the A value from the TKE and TOF, and the Q value from the A/Q value obtained by the ΔE-TOF-$B\rho$ method.

The relative resolution achieved in the TKE measurement is 0.48% on average. The resulting Q resolution was calculated to be $\sigma = 0.25$ on average, which allows 4.0σ separation for $\Delta Q = 1$ in charge-state identification plot. We observed the dependence of Q resolution on the stopping range in the silicon stack detector. Figure 1 shows the Q resolution as a function of the stopping range of the isotopes, where some deterioration of the Q resolution is observed around a certain value of stopping range. This can be attributed to a thin dead layer on the surface of the silicon detectors. We expect that it is possible to improve the Q resolution by selecting the stropping range according to the $B\rho$ measurement or by using silicon detectors whose dead layer thickness is significantly small.

We can select events of fully stripped isotopes from a Z versus Z-Q plot, where Z-Q gives the number of electrons. Figure 2 shows a Z versus A-$2Q$ PID plot for the fully stripped events (Z-Q = 0). Here, the Z value is obtained from the ΔE-TOF-$B\rho$ method, while A-$2Q$ is calculated using the A and Q values obtained in the present work. Note that for isotopes with $A/Z \sim 2$, the resolution of A-$2Q$ is comparable to the A/Q resolution achieved by the ΔE-TOF-$B\rho$ method, because of the nature of error propagation.

As shown in Fig. 2, the present TKE measurement confirms the identification of four new isotopes, $^{81.82}$Mo and ^{85,86}Ru, which we previously observed using the ΔE-TOF-$B\rho$ method.[2)] This also confirms that the new isotopes are fully stripped.

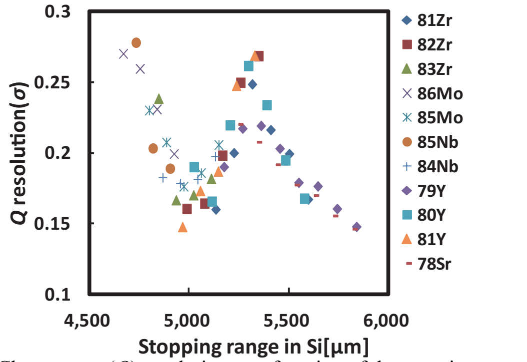

Fig.1 Charge state (Q) resolution as a function of the stopping range

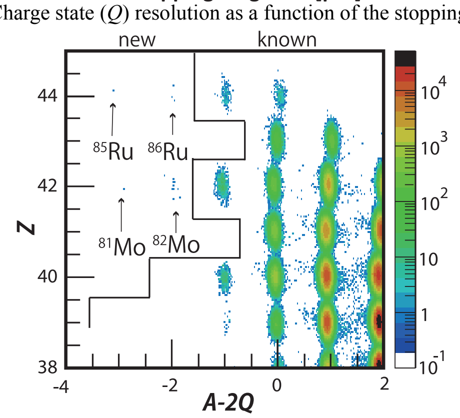

Fig. 2 Z versus A-$2Q$ particle identification plot for projectile fragments produced in the reaction ^{124}Xe+Be at 345 MeV/nucleon.

References

1) T. Kubo et al.: Nucl. Instr. and Meth. **B 204**, 97 (2003).
2) H. Suzuki et al.: Nucl. Instr. and Meth. **B 317**, 756 (2013).

*1 RIKEN Nishina Center
*2 Department of Physics, Rikkyo University
*3 Department of Physics, Tohoku University
*4 Research Center for Nuclear Physics, Osaka University
*5 Center for Nuclear Study, University of Tokyo
*6 Department of Physics, Tokyo University of Science
*7 Department of Physics. Osaka University
*8 Kochi University of Technology
*9 Grand Accelerateur National d'Ions Lourds
*10 Physik Department, Technische Universität München
*11 National Superconducting Cyclotron Laboratory, Michigan State University

2. Nuclear Physics (Theory)

Giant monopole resonances in covariant finite-amplitude method[†]

H. Z. Liang,[*1] T. Nakatsukasa,[*1] Z. M. Niu,[*2] and J. Meng[*1,*3]

During the past decades, the covariant density functional theory has received widespread attention because it has successfully described many nuclear phenomena[1)]. In this report, we mainly focus on the recent progress in the self-consistent relativistic random-phase approximation (RPA) established by using the finite-amplitude method (FAM).

The RPA is one of the leading theories applicable to both low-lying excited states and giant resonances. In the relativistic framework, quantitative RPA calculations were realized after recognizing the importance of the Dirac sea. Subsequently, great efforts on the relativistic RPA have been made. However, most investigations are essentially restricted within spherical symmetry. The conventional RPA calculations in the matrix form face a significant computational challenge when the number of particle-hole (ph) configurations N_{ph} becomes large.

The so-called finite-amplitude method was proposed as a promising solution for this computational challenge[2,3)]. In this method, the effects of residual interactions are numerically evaluated by considering a finite density deviation around the ground state. Thus, the self-consistent RPA calculations become possible with a slight extension of the static Hartree-Fock code. Furthermore, by using the iterative methods, the computation time linearly depends on N_{ph}, instead of N_{ph}^3, in the diagonalization scheme, which is crucial when N_{ph} becomes large.

Work is in progress for developing the self-consistent relativistic RPA by using both the iterative and matrix FAM schemes, i.e., i-FAM and m-FAM, the detailed formalism of which can be found in the original article[†].

In Fig. 1, we show the isoscalar giant monopole resonances (ISGMR) in ^{208}Pb calculated with the relativistic parametrization DD-PC1. The effects of the Dirac sea and the rearrangement terms can be examined by switching on or off the corresponding ph residual interactions.

First, the transition strengths calculated in the m-FAM scheme with and without the Dirac sea are compared in the upper panel. It is found that the Dirac sea shows profound effects on the centroid energy, and the experimental data[4)] is reproduced only when the Dirac sea is taken into account. Although the effects of the Dirac sea cannot be isolated in the coordinate-space representation, it can be clearly seen that the i-FAM results are exactly above the m-FAM results that include the Dirac sea. This confirms that these two FAM schemes are equivalent and the effects of Dirac sea can be taken into account automatically and implicitly.

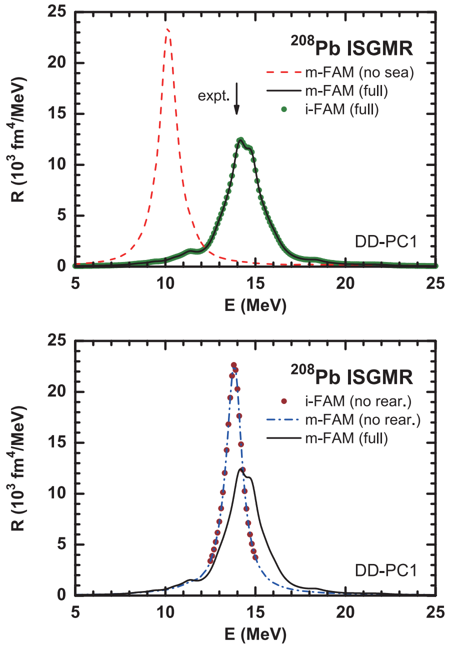

Fig. 1. ISGMR in ^{208}Pb calculated using i-FAM and m-FAM. The results calculated with and without the Dirac sea and the rearrangement terms are compared. The experimental centroid energy[4)] is denoted by the arrow.

It is tedious to calculate the rearrangement terms in the conventional RPA calculations; in contrast, in FAM, these terms can be simply taken into account by re-calculating the coupling strengths with new densities. In the lower panel, the transition strengths of ISGMR calculated using m-FAM with and without the rearrangement terms are shown, together with the i-FAM results calculated without the rearrangement terms. The equivalency of these two FAM schemes is demonstrated once more. It is also found that the rearrangement effects on the centroid energies is quantitatively substantial.

References

1) J. Meng et al.: Prog. Part. Nucl. Phys. **57**, 470 (2006).
2) T. Nakatsukasa, T. Inakura, and K. Yabana: Phys. Rev. C **76**, 024318 (2007).
3) T. Nakatsukasa: Prog. Theor. Exp. Phys. **2012**, 01A207 (2012).
4) D. H. Youngblood et al.: Phys. Rev. C **69**, 034315 (2004).

† Condensed from the article in Phys. Rev. C **87**, 054310 (2013)

*1 RIKEN Nishina Center
*2 School of Physics and Material Science, Anhui University
*3 School of Physics, Peking University

Spin-orbit effects on pseudospin symmetry†

H. Z. Liang,[*1] S. H. Shen,[*2] P. W. Zhao,[*2] S. Q. Zhang,[*2] and J. Meng[*1,*2]

Pseudospin symmetry (PSS)[1,2] was introduced in 1969 to explain the near degeneracy between pairs of nuclear single-particle states with the quantum numbers $(n-1, l+2, j = l+3/2)$ and $(n, l, j = l+1/2)$. They are regarded as the pseudospin doublets with modified quantum numbers $(\tilde{n} = n-1, \tilde{l} = l+1, j = \tilde{l} \pm 1/2)$. Although this concept was introduced for more than 40 years ago, the origin of PSS and its breaking mechanism in realistic nuclei have not been fully understood. Specifically, determining whether its nature is perturbative remains an unsolved problem.

Recently, we used the perturbation theory to investigate the symmetries of the Dirac Hamiltonian and their breaking in realistic nuclei[3], which provides a clear and quantitative way for investigating the perturbative nature of PSS. On the other hand, supersymmetric (SUSY) quantum mechanics can provide a PSS-breaking potential without singularity, and naturally interpret the unique feature that all states with $\tilde{l} > 0$ have their own pseudospin partners except for the intruder states[4]. Then, the similarity renormalization group (SRG) technique fills the gap between the perturbation calculations and the SUSY descriptions by transforming the Dirac Hamiltonian into a diagonal form and keeping every operator Hermitian[5,6].

Therefore, understanding the PSS and its breaking mechanism in a quantitative manner by combining the SRG technique, SUSY quantum mechanics, and perturbation theory is considered promising.

Here, we highlight the PSS-breaking potentials $\tilde{V}_{\rm PSO}(r)$, which are derived from the Dirac equation with the SRG and SUSY transformations.

In the upper panel of Fig. 1, the $\tilde{V}_{\rm PSO}(r)$ obtained without and with the spin-orbit (SO) term are shown for the $\tilde{f}$ orbitals. These potentials show several special features, which are crucial for understanding the PSS: (i) They are regular functions of r. (ii) Their amplitudes directly determine the sizes of reduced pseudospin-orbit (PSO) splittings $\Delta E_{\rm PSO} \equiv (E_{j_<} - E_{j_>})/(2\tilde{l}+1)$ according to the perturbation theory. (iii) Their shape, being negative at small radius but positive at large radius with a node at the surface region, can explain the general tendency of the PSO splittings becoming smaller with increasing single-particle energies.

To identify the SO effects, the $\tilde{V}_{\rm PSO}(r)$ obtained with the SO term is further decomposed into the contributions of the indirect and direct SO effects, because the former one represents the SO effects on $\tilde{V}_{\rm PSO}(r)$ via the superpotentials, while the latter is the SO potential itself. Comparison with the result obtained without the SO term shows that the indirect effect is small and eventually results in less influence due to the cancellation between the inner and outer regions. On the other hand, the SO potential is always positive with a peak at surface. It substantially raises the $\tilde{V}_{\rm PSO}(r)$, in particular for the surface region.

All of these properties are shown in the lower panel of Fig. 1, in which $\Delta E_{\rm PSO}$ are shown as a function of $E_{\rm av} = (E_{j_<} + E_{j_>})/2$. $\Delta E_{\rm PSO}$ match the amplitudes of $\tilde{V}_{\rm PSO}(r)$. The decreasing PSO splittings with increasing single-particle energies is due to the special shape of $\tilde{V}_{\rm PSO}(r)$. The SO term reduces $\Delta E_{\rm PSO}$ systematically, and this effect can be understood now in a quantitative manner.

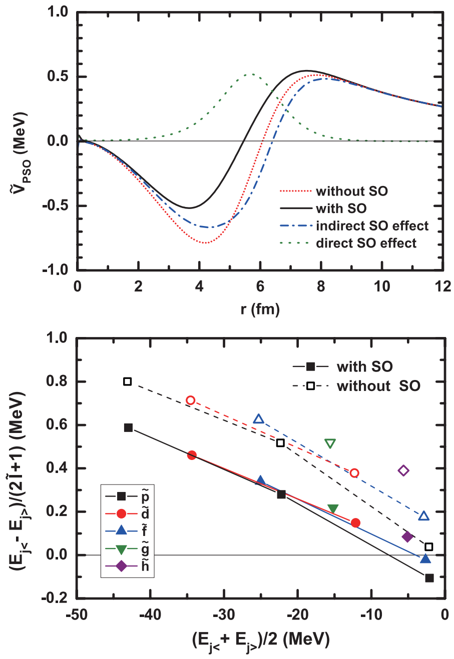

Fig. 1. Upper panel: PSS-breaking potentials $\tilde{V}_{\rm PSO}(r)$ obtained with and without SO term. The former one is decomposed into the indirect and direct the SO effects. Lower panel: $\Delta E_{\rm PSO}$ vs $E_{\rm av}$ with and without the SO term, where $j_<, j_>$ stand for the $\tilde{l} \mp 1/2$ states.

References
1) A. Arima, M. Harvey, and K. Shimizu: Phys. Lett. B **30**, 517 (1969).
2) K. Hecht and A. Adler: Nucl. Phys. A **137**, 129 (1969).
3) H. Z. Liang et al.: Phys. Rev. C **83**, 041301(R) (2011).
4) S. Typel: Nucl. Phys. A **806**, 156 (2008).
5) J.-Y. Guo: Phys. Rev. C **85**, 021302(R) (2012).
6) J.-Y. Guo et al.: Phys. Rev. Lett. **112**, 062502 (2014).

† Condensed from the articles in Phys. Rev. C **87**, 014334 (2013) and *ibid.* **88**, 024311 (2013)

*1 RIKEN Nishina Center
*2 School of Physics, Peking University

Shape evolution of giant resonances in Nd and Sm isotopes †

K. Yoshida*1 and T. Nakatsukasa*2

A giant resonance (GR) is a typical high-frequency collective mode of excitation in nuclei. Effects of nuclear deformation on GRs have been investigated both experimentally and theoretically. Among them, the deformation splitting of the isovector giant dipole resonance (GDR), due to different frequencies of oscillations along the major and minor axes, is well established. Emergence of a double-peak structure of the photoabsorption cross section of ^{150}Nd and ^{152}Sm clearly indicates the onset of the deformation in the ground state. For the GRs with higher multipolarity, although deformation splitting is less pronounced, peak broadening has been observed. The detailed and systematic investigations of GRs would give us unique information on the shape transition in nuclei.

In contrast to low-energy modes of excitation, GRs substantially reflect bulk nuclear properties. Thus, their studies may provide information on nuclear matter. Although various macroscopic models have been applied to GRs, a quantitative description of GRs requires a microscopic treatment of nuclear response. For heavy deformed open-shell nuclei, the leading theory currently for this purpose is the quasiparticle-random-phase approximation (QRPA) based on the nuclear energy-density-functional (EDF) method. The QRPA based on the deformed ground-state configuration with superfluidity can treat a variety of excitations in the linear regime.

We develop a new calculation code of the deformed HFB and QRPA for use in the massively parallel computers to examine the applicability of the Skyrme-EDF-based QRPA to the excitation modes in heavy deformed systems. Using this new parallelized code, the deformation effects on the GRs in Nd and Sm isotopes are investigated. We perform numerical analysis for GRs with a multipolarity $L = 0 - 3$ with both isoscalar (IS) and isovector (IV) characters, and examine the incompressibility and the effective mass both in spherical and deformed nuclei.

Figure 1 shows the strength distributions of IS monopole and quadrupole excitations in the Sm isotopes. We discuss first the giant quadrupole resonance (GQR). With an increase in the mass number, the peak energy of the ISGQR becomes smaller. This is consistent with the experiment on the systematic observation[1),2)]. The K splitting, $E_{K=2} - E_{K=0}$, for the ISGQR is 2.8 MeV in ^{154}Sm. This is consistent with the experimental observation. Since the energy splitting associated with deformation is comparable to the smearing parameter of 2 MeV, the deformation splitting, which is clearly visible in the photoabsorption cross sections does not appear in the ISGQR.

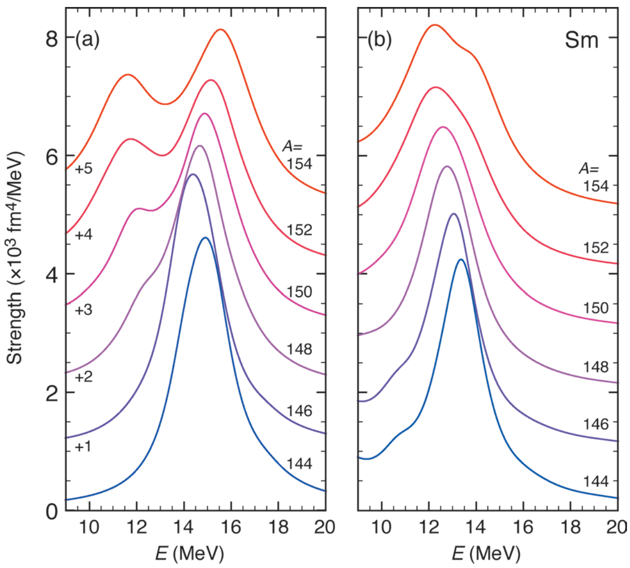

Fig. 1. Strength distributions (shifted) of (a) ISGMR and (b) ISGQR in Sm isotopes.

Next, let us discuss the giant monopole resonance (GMR). In the spherical nuclei, we can see a sharp peak at around 15 MeV which is identified as the ISGMR. The ISGMR in deformed nuclei has a double-peak structure. The higher-energy peak of the IS monopole strength is identified as a primal ISGMR and the lower-energy peak is associated with the coupling to the $K^\pi = 0^+$ component of the ISGQR. The lower peak of the ISGMR around 11 MeV is located at the peak position of the $K^\pi = 0^+$ component of the ISGQR.

For the ISGMR in ^{154}Sm, the SkM* functional gives the excitation energy, which is very close to the observed value[1)]. However, in ^{144}Sm, the SkM* underestimates the observation, and the SLy4 gives the reasonable energy. The present calculation suggests that the nuclear-matter incompressibility corresponds to about 230 MeV, as deduced from the comparison of the GMR excitation energy for ^{144}Sm, and 210 MeV for ^{154}Sm.

References

1) M. Itoh et al.: Phys. Rev. C **68**, 064602 (2003).
2) D. H. Youngblood et al.: Phys. Rev. C **69**, 034315 (2004).

† Condensed from the article in Phys. Rev. C. **88**, 034309 (2013)

*1 Graduate School of Science and Technology, Niigata University
*2 RIKEN Nishina Center

Tensor force and shape evolution of Si isotopes in Skyrme-Hartree-Fock model†

A. Li,[*1] X. -R. Zhou,[*1] and H. Sagawa[*2,*3]

In the present study, we focus on the tensor effect on the shape evolution of Si isotopes. We determined whether the tensor-force-driven deformation is present in neutron-rich Si isotopes, especially ^{30}Si with a possible $N = 16$ subshell, because some models (e.g., the FRDM) predicted a spherical shape for these nuclei[1)] while their large $B(E2)$ values suggested a deformed nature[2)]. For this purpose, we use the deformed Skyrme-Hartree-Fock model (DSHF)[3)] with BCS approximation for the nucleon pairing. We show in Fig. 1 the energy curves of ^{30}Si (left panel) and ^{32}Si (right panel) as a function of the quadruple deformation parameter β_2 using the Skyrme interactions with tensor terms T22, T24, T44, T64, and T66[4)]. The energy minima are indicated with triangles. ^{30}Si is suggested to be deformed, but T22 and T44 with relatively large pairing strengths ($\sim$ 1000 MeV) fail to give deformed energy minima. In contrary, a deformed ground state can be achieved using the T24, T64 and T66 parametrization with a small pairing strength ($\sim$ 800 MeV). Moreover, the predicted oblate shape of these nuclei is consistent with the recent RMF result[5)]. A possibility of achieving a deformed ground state using weak nucleon pairing may stem from a well-known fact that the pairing interaction forms the $J = 0^+$ pairs of identical particles that have spherically symmetric wave functions. As a result, nuclei tend to be more spherical when a strong pairing coupling exists between neutrons and protons as in the cases of T22 and T44; otherwise nuclei are more likely to be deformed, as in the cases of T24, T64, and T66. This suggests that the resulting shape of a nucleus is sensitive to the nucleon pairing in this nucleus, and the experimentally determined deformed shape of ^{30}Si suggests that a relatively weak paring correlation is present in the Skyrme effective forces T24, T64 and T66. We also notice that a large tensor force present in T64 and T66 tends to produce a deep energy surface; i.e., the tensor force exerts a dramatic effect that maintains a deformed ground state in ^{30}Si. The effect of the tensor force is also observed in ^{32}Si as shown in the right panel of Fig. 1. Its shape is predicted to be spherical using T22, T24, and T44 but oblate using T64 and T66 with large tensor forces. The spherical result in the first three cases is obviously not consistent with experiments, and the shape change from spherical to oblate when introducing a large tensor force is intriguing.

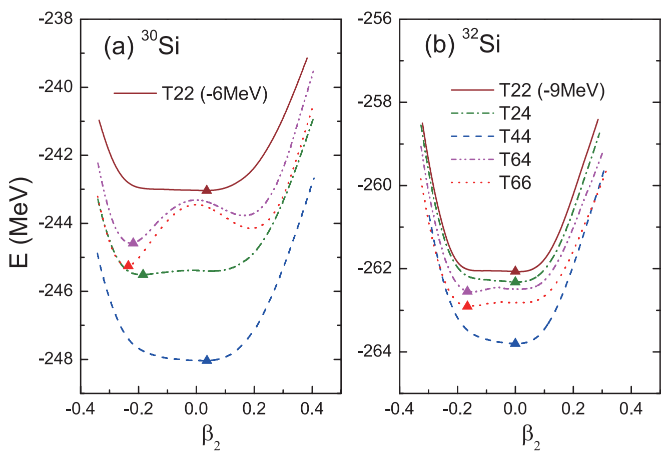

Fig. 1. (Color online) Energy curves of ^{30}Si (left panel) and ^{32}Si (right panel) as a function of the quadruple deformation parameter β_2 using the Skyrme interactions T22, T24, T44, T64, and T66. The energy minima are indicated with triangles.

In summary, we used the DSHF model to investigate the shape evolution of the quadruple deformation of Si isotopic nuclei. We found interesting manifestations of the tensor force and pairing effect in several isotopic nuclei, such as ^{30}Si and ^{32}Si. The effect of tensor force is observed when we compare the predicted shape of ^{32}Si using increasing tensor forces in the HF energy density. The tensor-force-driven deformation in these nuclei should be investigated in more details because it may result in a further improvement of many theoretical models or parameterizations toward a better description of theories on the shell structures of nuclei in general, such as the shell model and SHF model.

References

1) T.R. Werner et al., Nucl. Phys. A**597** 327 (1996).
2) R. W. Ibbotson et al., Phys. Rev. Lett. **80**, 2081 (1998).
3) D. Vautherin, Phys. Rev. C **7**, 296 (1973).
4) T. Lesinski et al., Phys. Rev. C **76**, 014312 (2007).
5) Z. P. Li, J. M. Yao, D. Vretenar, T. Niksic, H. Chen, and J. Meng, Phys. Rev. C**84**, 054304 (2011).

† Condensed from the article in Prog. Theor. Exp. Phys. 063D03(2013)
*1 Department of Astronomy and Institute of Theoretical Physics and Astrophysics, Xiamen University
*2 RIKEN Nishina Center
*3 University of Aizu

Incompressibility in finite fermionic systems: application to stable and exotic nuclei†

E. Khan,[*1] N. Paar,[*2] D. Vretenar,[*2] L.G. Cao,[*3] H. Sagawa,[*4,*5] and G. Colò[*6]

Recently, it has been inferred that the measurement of isoscalar giant monopole resonances (GMRs) may probe the incompressibility of the nucleus in a range below the saturation density, rather than exactly at the saturation density[1]. Recent measurements of isotopic chains[2,3], possibly extended to exotic nuclei[4,5], are therefore relevant for constraining this more general density-dependent incompressibility. The use of isotopic chains also provided opportunities to study pairing and shell effects on incompressibility. It has been shown that one cannot rule out shell and pairing effects on nuclear incompressibility[6,7]. We therefore focus on the nuclear incompressibility along isotopic chains and through magicity.

The calculations following fully microscopic approaches based on the energy density functionals (EDFs) to predict the GMR position are usually performed using the constrained Hartree-Fock-Bogoliubov (CHFB) or the quasiparticle random-phase approximation (QRPA) approaches[8]. In the present study, we calculate the GMR energy for the Skyrme EDF with the CHFB approach. For completeness, results obtained using Skyrme and relativistic functionals are also given using the QRPA approach.

The results obtained using the various methods mentioned above are displayed in Fig. 1 for Sn and Pb isotopic chains. The nuclear incompressibility of a finite nucleus K_A is evaluated using

$$K_A = \frac{2A\langle r^2\rangle^2_{g.s.}}{m_{-1}}, \qquad (1)$$

where m_{-1} is the inverse energy-weighted sum rule and $\langle r^2\rangle_{g.s.}$ is the mean-square radius of the ground state. First, it should be noted that the three microscopic methods provide K_A values that do not differ by more than 10%. The nuclear incompressibility K_A is almost constant at 140 MeV around stable nuclei but changes as a function of A in the case of more exotic nuclei.

The incompressibility of fermionic systems has been studied using several approaches. Analytical relations using simple free Fermi gas and spherical Harmonic Oscillator (HO) models allowed us to show the direct link between the incompressibility and the zero-point kinetic energy T_0, implying that incompressibility is rooted in the localization properties of the constituents of the system. The HO model provides $K_A \simeq 5T_0$, showing that 140 MeV is a sound estimation of the nuclear incompressibility in stable nuclei.

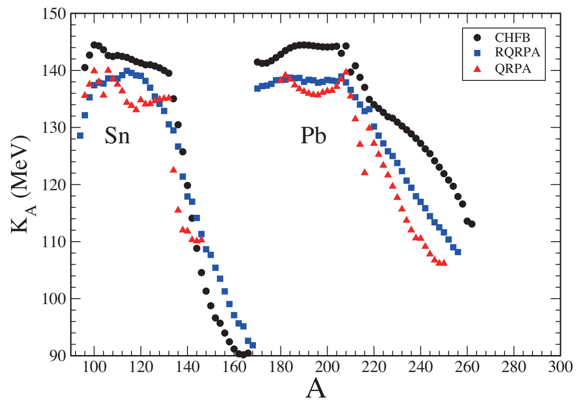

Fig. 1. Nuclear incompressibility in Sn and Pb isotopic chains calculated using the microscopic Skyrme-CHFB method (circles), the Skyrme-QRPA method (triangles) and relativistic QRPA method (squares).

In order to study the evolution of nuclear incompressibility along isotopic chains, several microscopic EDF-based approaches have been used. In the case of exotic nuclei, a decrease in K_A is predicted in all the models because of the emergence of a soft monopole strength. These results confirm the important role of the soft monopole resonance, and attempting to detect it would be useful. More generally, the behavior of the GMR in exotic nuclei and/or beyond magicity should be studied experimentally. Measurements of the GMR around ^{132}Sn and ^{210}Pb would be of interest.

References

1) E. Khan, J. Margueron and I. Vidaña, Phys. Rev. Lett. 109, 092501 (2012).
2) T. Li et al., Phys. Rev. C81, 034309 (2010).
3) U. Garg, *COMEX3 conference*, Mackinac Island (2009).
4) C. Monrozeau et al., Phys. Rev. Lett. 100, 042501 (2008).
5) M. Vandebrouck et al., Exp. E456a performed at GANIL (2010).
6) J. Li, G. Colò and J. Meng, Phys. Rev. C78, 064304 (2008).
7) E. Khan, Phys. Rev. C80, 011307(R) (2009)
8) N. Paar, D. Vretenar, E. Khan and G. Colò, Rep. Prog. Phys. 70, 691 (2007)

† Condensed from the article in Phys. Rev. C. **87**, 064311(2013)
*1 Institut de Physique Nucléaire, Université Paris-Sud, IN2P3-CNRS
*2 Physics Department, Faculty of Science, University of Zagreb
*3 Institute of Modern Physics, Chinese Academy of Science
*4 RIKEN Nishina Center
*5 Mathematics and Physics, University of Aizu
*6 Dipartimento di Fisica, Università degli Studi and INFN Sez. di Milano

Competition between T=1 and T=0 pairing in pf shell nuclei with $N = Z$[†]

H. Sagawa,[*1,*2] Y. Tanimura,[*3] and K. Hagino[*3]

The role of the neutron-proton isoscalar spin-triplet (T=0, S=1) pairing interaction in finite nuclei has been a topic of discussion for long.[1–3] The isoscalar spin-triplet pairing interaction is known to be stronger than the isovector spin-singlet (T=1, S=0) one in nuclear matter.[4] Nevertheless, nuclei favor the spin-singlet T=1 pairing between identical particles. A straightforward explanation for this contradiction is that most stable nuclei have different numbers of neutrons and protons; thus, protons and neutrons occupy different single-particle orbits near the Fermi surface, which leads to the inhibition of T=0 pairing. It was also suggested that the nuclear spin-orbit field largely suppresses the spin-triplet pairing, much more than the spin-singlet pairing.[5,6]

To clarify the role of $T = 0$ pairing, we diagonalize the Hamiltonian with the spin-singlet and spin-triplet pairing terms in pf shell model configurations for nuclei with the same number of protons and neutrons, $N = Z$. The pairing correlation energies of the ($J^\pi = 0^+$, T=1) and ($J = 1^+$, T=0) states are shown in Fig. 1 as a function of the scaling factor f for the $T = 0$ pairing. The lowest energy state with J^π=0^+ for the $l = 3$ case acquires more binding energy than the J^π=1^+ state for the strength factor $f < 1.5$. In the case of strong T=0 pairing, that is, $f \geq 1.6$, the J^π=1^+ state acquires more binding energy than the lowest J^π=0^+ state. These results are largely attributed to the quenching of the T=0 pairing matrix element by the transformation coefficient corrsponding to a change of the scheme from the jj coupling to LS coupling. This quenching never happens for the T=1 pairing matrix element, since the mapping of the two-particle wave function between the two coupling schemes is simply implemented by a factor $\sqrt{j+1/2}$. For the $l = 1$ case, there is a competition between the J^π=0^+ and the J^π=1^+ states as seen in Fig. 1. Because of smaller spin-orbit splitting in this case, the couplings among the available configurations are rather strong, and the lowest J^π=1^+ state acquires more binding energy than the J^π=0^+ state when $f \geq 1.4$. These results are consistent with the spins observed for $N = Z$ odd-odd nuclei in the pf shell, where all the ground states have the spin-parity $J^\pi = 0^+$, except for $^{58}_{29}$Cu. The ground state of $^{58}_{29}$Cu has $J^\pi = 1^+$, because the odd proton and odd neutron occupy mainly the $2p$ orbits, wherein the spin-orbit splitting is expected to be much smaller than in $1f$ orbits.

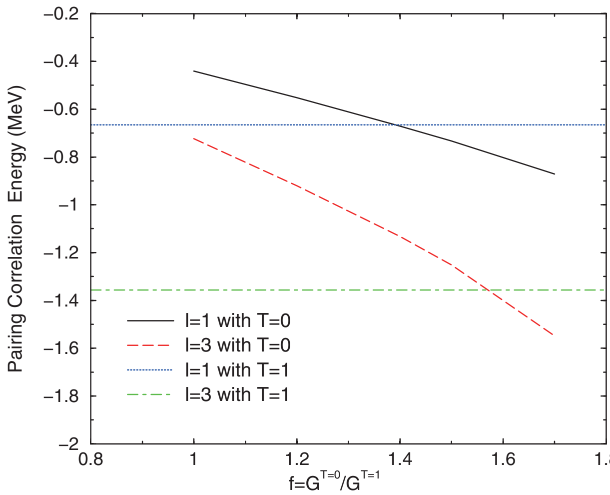

Fig. 1. (Color online) Pairing correlation energies for the lowest ($J^\pi = 0^+$, T=1) and ($J = 1^+$, T=0) states with the $l = 3$ and $l = 1$ configurations as a function of the scaling factor f of the $T = 0$ pairing. The strength of the spin-singlet T=1 pairing interaction is fixed at $G^{(T=1)}$=24/A MeV with mass A=56, while the strength for the spin-triplet T=0 pairing interaction, $G^{(T=0)}$, is varied with the factor f multiplied by $G^{(T=1)}$.

In summary, by diagonalizing the pairing Hamiltonian, we have shown that the spin-triplet pairing correlation energy in the $1f$ shell configuration becomes larger than the spin-singlet pairing energy when the strength of the spin-triplet pairing is larger than that of the spin-singlet pairing by a factor of 1.6 or more. However, for the $2p$ configuration, the spin-triplet pairing correlation becomes dominant even when the factor f is approximately 1.4.

References
1) A. L. Goodman, Nucl. Phys. A186, 475(1972); Phys. Rev. C**60**, 014311(1999).
2) A. O. Macchiavelli et al., Phys. Rev. C**61**, 041303(R)(2000); A. O. Macchiavelli et al., Phys. Lett. B**480**, 1(2000).
3) A. F. Lisetskiy et al., Phys. Rev. C**68**, 034316 (2003).
4) M. Baldo, U. Lombardo, and P. Schuck, Phys. Rev. C**52**, 975(1995); L. G. Cao, U. Lombardo, and P. Schuck, Phys. Rev. C**74**,064301(2006).
5) A. Poves and G. Martinez-Pinedo, Phys. Lett. B**430**, 203(1998).
6) G. F. Bertsch and Y. Luo, Phys. Rev. C**81**, 064320(2010).

† Condensed from the article in Phys. Rev. C **87**, 034310 (2013)

*1 RIKEN Nishina Center
*2 Center for Mathematics and Physics, the University of Aizu
*3 Department of Physics, Tohoku University

Joint project for large-scale nuclear structure calculations

N. Shimizu,[*1] T. Otsuka,[*1,*2] T. Togashi,[*1] N. Tsunoda,[*2] and Y. Utsuno[*1,*3]

A joint project for large-scale nuclear structure calculations has been under way since the year 2001, based on a collaboration agreement between RIKEN Nishina Center and Center for Nuclear Study, the University of Tokyo. We maintain PC servers, one of which has 1TB main memory and is suitable for large-scale nuclear shell-model calculations. In this project, we performed various shell-model calculations of the nuclides that had been measured at the RIKEN RI Beam Factory, such as ^{54}Ca, ^{34}Na, ^{35}Na, ^{37}Mg, ^{50}Ar, and ^{55}Sc, under collaborations with many experimentalists.[1,2] Since these collaborations are presented in other reports, we here introduce two theoretical achievements of this project in 2013: The extended Kuo-Krenciglowa method and the shell-model analysis of Cr isotopes.

Until recently, most shell-model calculations were confined to a single oscillator shell like the sd shell or the pf shell. However, recent interest in nuclei away from the stability line requires larger shell-model spaces. Because the derivation of microscopic effective interactions has been limited to degenerate model spaces, there are both conceptual and practical limits to shell-model calculations that utilize those interactions. We develop a method to calculate effective interactions for a nondegenerate model space, based on the extended Kuo-Krenciglowa method, which is a natural extension of the conventional Kuo-Krenciglowa method.[3,4] We calculated effective interactions within (i) a single oscillator shell (a so-called degenerate model space) like the sd shell or the pf shell and (ii) two major shells (nondegenerate model space) like the $sdf7p3$ shell (sd shell, $0f_{7/2}$ and $1p_{3/2}$) or the $pfg9$ shell (pf shell and $0g_{9/2}$). We also calculated the energy levels of several nuclei that have two valence nucleons on top of an inert core. Our results show that the present method works excellently in shell-model spaces that comprise several oscillator shells as well as in a single oscillator shell. This work is published in 2014.[5]

The experimental observation in odd-mass neutron-rich Cr isotopes revealed that the excitation energy of $9/2^+_1$ state decreases considerably with increasing neutron number.[6] We performed shell-model calculations for these Cr isotopes with $pfg9d5$ model space, which consists of a full pf shell, $0g_{9/2}$, $1d_{5/2}$ orbits, with a certain truncation. We introduced a new Hamiltonian, which is composed of the GXPF1Br effective interaction[1] for the pf shell and V_{MU}[7] for the rest of the model space. The shell-model result agrees adequately with experimental data, as shown in Fig.1. We also discussed the deformation from the potential energy surfaces by the Q-constrained Hartree-Fock calculation.[8]

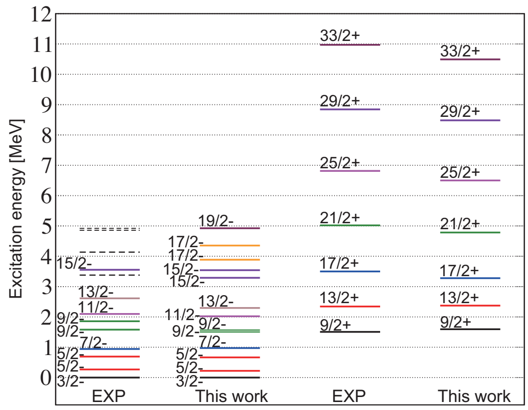

Fig. 1. The level scheme of ^{57}Cr. The columns labeled 'EXP' and 'This work' represent the experimental data and the results of the shell-model calculation, respectively. The dashed lines denote the unassigned spin states.

References
1) D. Steppenbeck *et al.*: Nature **502**, 207 (2013).
2) T. Nakamura *et al.*: Phys. Rev. Lett. submitted.
3) T. T. S. Kuo and E. Osnes: Lecture Notes in Physics Vol. 364 (Springer, Berlin, 1990).
4) K. Takayanagi: Nucl. Phys. A **852**, 61 (2011); *ibid.* Nucl. Phys. A **864**, 91 (2011).
5) N. Tsunoda, K. Takayanagi, M. Hjorth-Jensen and T. Otsuka: Phys. Rev. C, **89**, 024313 (2014).
6) D. E. Appelbe *et al.*: Phys. Rev. C **67**, 034309 (2003), S. J. Freeman *et al.*: Phys. Rev. C **74**, 064301 (2004), A. N. Deacon *et al.*: Phys. Lett. B **622**, 151 (2005).
7) T. Otsuka *et al.*: Phys. Rev. Lett. **104**, 012501 (2010).
8) N. Shimizu *et al.*: Phys. Rev. C **85**, 054301 (2012).

*1 Center for Nuclear Study, University of Tokyo
*2 Department of Physics, University of Tokyo
*3 Japan Atomic Energy Agency

Pairing correlation and quasi-particle resonances in neutron drip-line nuclei

Y. Kobayashi[*1] and M. Matsuo[*2]

In neutron drip-line nuclei, which have an extremely shallow Fermi surface, the pairing correlation is expected to influence low-energy scattering and resonances of a neutron. An interesting phenomenon predicted in the theory of superfluid nuclei is quasi-particle resonance.[1–3)] A scattering neutron can couple to a hole state by creating a Cooper pair and thus resulting in a narrow resonance. The quasi-particle resonance has also been studied for neutron drip-line nuclei.[4–6)] As neutron drip-line nuclei are expected to provide better opportunities for observation of quasi-particle resonance, we study these drip-line nuclei to clarify the properties of quasi-particle resonance. In the present study, we focus on the influence of the pairing on the resonance width.

We use the coordinate space Hartree-Fock-Bogoliubov (cHFB) equation[7)] to describe the scattering wave function of a neutron under the pairing effect. We solve the cHFB equation such that the quasi-particle wave function satisfies the scattering boundary condition:

$$\begin{pmatrix} u_{lj}(r) \\ v_{lj}(r) \end{pmatrix} \rightarrow \begin{pmatrix} \cos\delta_{lj} j_l(k_1 r) - \sin\delta_{lj} n_l(k_1 r) \\ D h_l^{(1)}(\kappa_2 r) \end{pmatrix}, \quad (1)$$

where $k_1 = \sqrt{2m(\lambda + E)}/\hbar$, $\kappa_2 = \sqrt{-2m(\lambda - E)}/\hbar$. Here, m, λ and E are the mass of neutron, Fermi energy and quasi-particle energy, respectively. Next, we calculate the phase shift δ_{lj} and the elastic cross section.

We consider the (^{46}Si+n) system. According to several HFB calculations, ^{46}Si is a neutron drip-line nucleus of Si isotopes. We assume that this nucleus has a spherical shape. Note that ^{46}Si has a weakly bound $2p$ orbit. We use the Woods-Saxon potential as the nuclear potential, and the pair potential is also assumed to have the Woods-Saxon shape. The averaged pairing gap $\bar{\Delta}$ is a strength of the pair potential.

Fig.1 shows the calculated partial cross section. Narrow low-lying peaks seen in $p_{1/2}$ and $p_{3/2}$ are the quasi-particle resonances. These peaks disappear if we switch off the pairing as they are originally weakly bound $2p_{1/2}$ and $2p_{3/2}$ orbits in the Woods-Saxon potential. In order to analyze the effect of pairing on the resonance width, we calculate the width of the $p_{1/2}$ resonance for various pairing strengths $\bar{\Delta}$. We extract the resonance width and resonance energy from the phase shift using a fitting method. The green line in Fig.2 shows the relation between the resonance width and the resonance energy for various values of $\bar{\Delta}$. As the pairing strength increases, both the resonance width and the resonance energy increase. For comparison, we plot the width vs. energy relation for the single-particle potential resonance of the $2p_{1/2}$ state (red line in Fig.2), which is obtained by varying the depth of the Woods-Saxon potential V_0. If we compare these two results at the same resonance energy, we find that the width of quasi-particle resonance is narrower than the width of single-particle potential resonance. We conclude that the pairing has an effect of reducing the resonance width

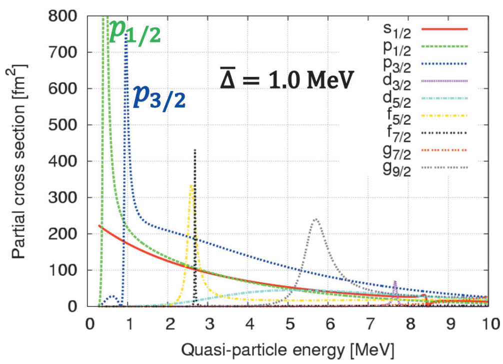

Fig. 1. Partial cross section with $\bar{\Delta} = 1.0$MeV.

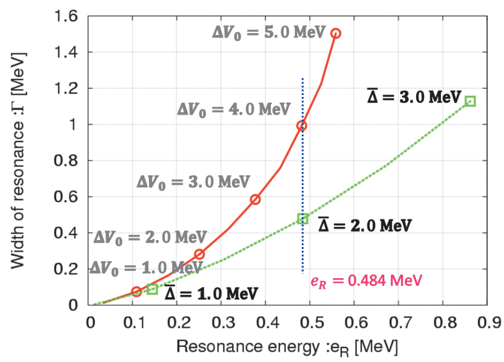

Fig. 2. Comparison of results of resonance width.

References
1) S. T. Belyaev et al.: Sov. J. Nucl. Phys. 45, 783 (1987).
2) A. Bulgac: nucl-th/9907088.
3) J. Dobaczewski et al.: Phys. Rev. C 53, 2809 (1996)
4) M. Grasso et al.: Phys. Rev. C 64, 064321 (2000).
5) I. Hamamoto et al.: Phys. Rev. C 68, 034312 (2003).
6) J. C. Pei et al.: Phys. Rev. C 84, 024311 (2011).
7) J. Dobaczewski et al.: Nucl. Phys. A 422, 103 (1984).

*1 Graduate School of Science and Technology, Niigata University
*2 Department of Physics, Faculty of Science, Niigata University

Di-neutron correlation in pair-addition vibrational mode of the neutron-rich Sn isotopes†

H. Shimoyama[*1] and M. Matsuo[*2]

Recently, two-neutron transfer in unstable nuclei has attracted attention since the experiments using radioactive ion beams became possible[1,2]. Anticipating future experiments, we have been theortically investigating two-neutron transfer modes in heavy-mass neutron-rich nuclei. A good example is of neutron-rich Sn isotopes with $A \geq 132$, for which we predict enhanced pair-addition transfer populating the ground states (pair rotation) or the low-lying 0^+ states (pair vibration) in the neighboring $\Delta N = 2$ isotopes[3]. In this works we analyze in detail the microscopic structure of the two-neutron transfer modes, and we show that di-neutron correlation appears in the pair vibrational mode of the neutron-rich Sn.

We describe the two-neutron transfer using the Hartree−Fock−Bogoliubov (HFB) mean-field theory and the continuum quasiparticle random phase approximation (QRPA)[3,4]. The Skyrme functional with the parameter SLy4 is adopted. For pairing interaction, we choose the density-dependent delta interaction.

We analyze the microscopic structure of the two-neutron transfer modes in the Sn isotopic chain, especially the pair-addition vibrational mode in $^{132-140}$Sn. Within the QRPA theory, one can characterize an excitation mode in terms of forward- and backward-propagating amplitudes $X^{\nu}_{ii'}$ and $Y^{\nu}_{ii'}$ for the two-quasiparticle configuration $ii' = (nlj)\,(n'l'j')$. The index ν is a label for QRPA normal modes, and excitation energy is denoted as $\hbar\omega_\nu$. Concerning the low-lying pair vibration state predicated to appear at $\hbar\omega_\nu = 3.81$ MeV in ^{134}Sn, for example, the main two-quasiparticle configurations ($|X^{\nu}_{ii'}| > 0.1$) are $[3p_{3/2}]^2$, $[1h_{9/2}]^2$, $[2f_{7/2}]^2$, $[2f_{5/2}]^2$, $[1i_{13/2}]^2$, $[3p_{1/2}]^2$, and $[3p_{3/2}][4p_{3/2}]$. These quasiparticle orbits are weakly bound or unbound resonant quasiparticle states. Similarly, the transition density $P^{(\mathrm{ad})}_{\nu L=0}(r)$ for the monopole ($L = 0$) pair-transfer operator can be decomposed as $P^{(\mathrm{ad})}_{\nu 0}(r) = \sum_{ii'} P^{(\mathrm{ad})}_{\nu 0,ii'}(r)$ in terms of the two-quasiparticle configurations. For the main components, the amplitude of these decomposed transition densities are significantly smaller than that of the total transition density. Even if we sum the main decomposed transition densities, it reproduces approximately half of the total transition density. This suggests that the low-lying pair vibration in ^{134}Sn has a some degree of collectivity.

Figure 1 shows the transition density $P^{(\mathrm{ad})}_{\nu 0}(r)$ and the partial sums of the decomposed transition densities, $P^{(\mathrm{ad})}_{\nu 0,l_{cut}}(r) = \sum_{ii',l\leq l_{cut}} P^{(\mathrm{ad})}_{\nu 0,ii'}(r)$, for various values of the angular momentum cut-off l_{cut}. Although the partial sums ($P^{(\mathrm{ad})}_{\nu 0,l_{cut}}(r)$) of each high-l component are very small, the inclusion of these small transition densities is necessary to reproduce the total transition density. The highest orbital angular momentum of the occupied Hartree−Fock single particle orbit in ^{134}Sn is $l_{occ} = 5(1h_{11/2})$. However it is clear that the large value of the orbital angular momentum contributes to the total transition density. The coherent accumulation up to high-l contributions in the pair-addition vibrational mode suggests the di-neutron[5] correlation discussed in the same manner in Ref.[4, 6].

We find that the di-neutron correlation in the low-lying pair vibration of $^{132-140}$Sn is formed by large numbers of weakly bound and unbound continuum quasiparticle states. Therefore, even if the positions of the quasiparticle states are varied for other Skyrme parameter sets, this di-neutron character may be observed in the low-lying pair vibration or pair rotation of the neutron-rich Sn isotopes with $N \geq 82$.

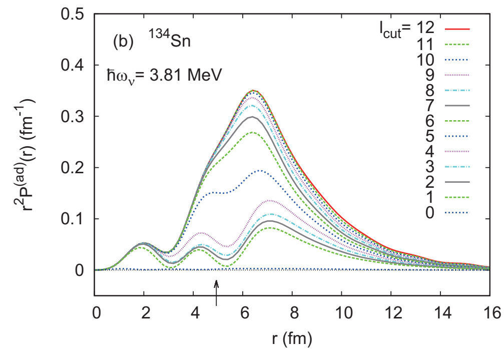

Fig. 1. Decomposition of the pair-addition transition density $P^{(\mathrm{ad})}_{\nu 0,l_{cut}}(r)$ of the pair-addition vibrational mode in ^{134}Sn with respect to the orbital angular momentum cutoff $l_{cut} = 0, 1, 2, \cdots, 12$. The arrow indicates the neutron rms radius $R_{N,rms}(= \sqrt{\langle r_n^2\rangle}) = 4.93$ fm.

References

1) I. Tanihata et al.: Phys. Rev. C **100**, 192502 (2008).
2) K. Wimmer et al.: Phys. Rev. C **105**, (2010).
3) H. Shimoyama and M. Matsuo: Phys. Rev. C **82**, 044317 (2011).
4) Y. Serizawa and M. Matsuo: Prog. Theor. Phys. **121**, 97 (2009).
5) G. F. Bertsch and H. Esbensen, Ann. Phys. (NY) **209**, 327 (1991).
6) M. Matsuo, K. Mizuyama, Y. Serizawa: Phys. Rev. C **71**, 064326 (2005).

† Condensed from the article in Phys. Rev. C **88**, 054308 (2013)

*1 Department of Physics, Faculty of Science and Graduate School of Science and Technology, Niigata University
*2 Department of Physics, Faculty of Science, Niigata University

Angular momentum dependence of moments of inertia due to Coriolis anti-pairing and blocking effects†

K. Sugawara-Tanabe*1 and K. Tanabe*1

In a series of papers,[1,2] we have developed the top-on-top model to systematically describe the level energies, and B(E2) and B(M1) values for in- and out-of-band transitions in the triaxial strongly deformed (TSD) bands in odd-A nuclei. Numerical analysis have been performed for the TSD bands in odd-mass Lu isotopes,[1] ^{167}Ta,[2] and for the odd-odd nucleus ^{164}Lu.[3] Without the angular momentum dependence (I-dependence) of the moments of inertia, the level energies along the TSD bands cannot be reproduced.

In order to investigate how the I-dependence arises, we take into account both the Coriolis anti-pairing (CAP) effect[4] and the blocking effect within the framework of the HFB theory. The cranking effect is described in terms of the second-order perturbation to the cranking term in the HFB equation based on the BCS solution.[7] In dealing with the gap equation, we pay special attention to an integral wherein the finiteness of the system becomes tangible.

For the case of axially symmetric deformation, the moment of inertia J_x is introduced through the constraint for the x-component of angular momentum I_x, i.e., $\langle I_x \rangle = I - I_0 = J_x \Omega_x$, where $\langle\,\rangle$ stands for the quasivacuum expectation value. We have assumed that the system is independent of rotation (i.e., $\Omega_x = 0$) in the band-head state with $I = I_0$. Based on Refs.[5,6], we assume that only large matrix elements of single-particle angular momentum $(j_x)_{\alpha\beta}$ have a common excitation energy of $\delta(= \varepsilon_\beta - \varepsilon_\alpha)$ between two single-particle energy levels. Then, using the closure approximation, we get the relation J_x and the rigid-body moments of inertia $J_x^{\rm rig}$ for both even and odd nuclei.

In order to relate the gap value Δ to the angular momentum I, we need to solve the gap equation for both even and odd nuclei.[7] We apply a technique similar to the one we used for deriving the relation between J_x and $J_x^{\rm rig}$ for both even and odd nuclei. Assuming that Δ is still not too small, relevant summations over the single-particle energies with a level density $\rho\ (= 1/d)$ (d is the average distance between single-particle energy levels) can be replaced by integrals. On the other hand, when Δ is much smaller than d, we carry out the summation without converting it into an integral, because an abnormal enhancement is found when $\Delta \ll d$. We adopt the picket fence approximation for the single-particle energies. The sum is expanded into an asymptotic series, and we derive the formula using a functional value of the Riemann Zeta function and Euler constant.

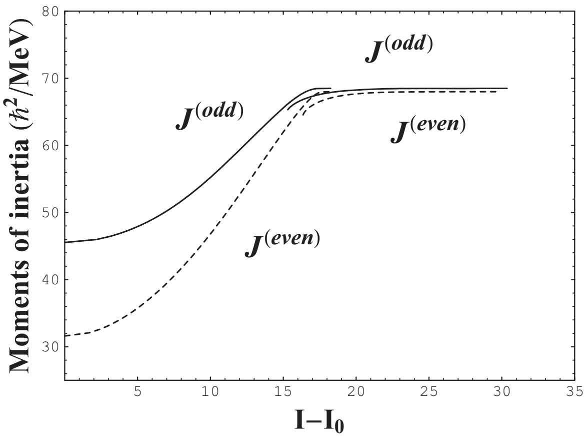

Fig. 1. Angular momentum dependence of moments of inertia for even and odd-A nuclei.

In Fig. 1, we compare $J^{(odd)}$ (solid line) and $J^{(even)}$ (dashed line) for the cases of $\Delta \geq d$ (low-spin part) and $\Delta \ll d$ (high-spin part). We adopt $\delta = 2$ MeV and $J_x^{\rm rig} = 68$ MeV^{-1}; the starting pairing gap Δ is 0.8 MeV for an even nucleus and 0.6 MeV for an odd nucleus, and the last single-particle energy in an odd nucleus is 0.6 MeV based on measurements made from the fermi surface.

As shown in the figure, the increase in the moments of inertia becomes slow in high-spin parts, whereas the gap values continue to decrease, maintaining a finite value. The curve for $J^{(odd)}$ starts from a higher value than $J^{(even)}$ because of the blocking effect, and it increases gradually, showing concave upward, which agrees with the curve for the values adopted in Ref..[3]

References

1) K. Tanabe and K. Sugawara-Tanabe: Phys. Rev. C **73**, 034305 (2006); Phys. Rev. C **77**, 064318 (2008).
2) K. Sugawara-Tanabe and K. Tanabe: Phys. Rev. C **82**, 051303(R) (2010).
3) K. Sugawara-Tanabe, K. Tanabe and N. Yohinaga: preprint (2014).
4) B. R. Mottelson and J. G. Valatin: Phys. Rev. Lett. **5**, 511 (1960).
5) A. Bohr and B. R. Mottelson: *Nuclear Structure* (Benjamin, Reading, MA, 1975), Vol. II.
6) D. Bengtsson and J. Helgessen: Lecture notes in a summer school at Oak Ridge (1991).
7) K. Sugawara: Prog. Theor. Phys. **35**, 44 (1966).

† Condensed from the article presented at Ferench-Japanese Symposium on Nuclear Structure Problems, 30 Sep.- 3 Oct. 2013, Paris, France

*1 RIKEN Nishina Center

Energy-density-functional calculations including proton–neutron mixing[†]

K. Sato,[*1] J. Dobaczewski,[*2,*3] T. Nakatsukasa,[*1] and W. Satuła[*2]

We performed calculations based on the Skyrme energy density functionals that include an arbitrary mixing between protons and neutrons. This is the first step towards the density functional calculation including proton–neutron (p-n) pairing. The p-n pairing is a long-standing open problem in nuclear physics, and its possible relations to various nuclear phenomena have been widely discussed.[2)] However, in spite of several theoretical studies over the years since the late sixties, a consistent theoretical treatment of the p-n pairing is still missing. Our ultimate goal is to develop a consistent symmetry-unrestricted energy-density-functional (EDF) approach including the p-n mixing both in the pairing and particle–hole (p-h) channels. To treat the p-n pairing within the EDF framework, one needs to generalize the quasiparticle states as mixtures of protons and neutrons. In connection with this extension of quasiparticles, one also needs to extend density functionals to those with mixing between protons and neutrons. In this work, as a first step in achieving our goal, we consider an extension of EDFs including the p-n mixing in the p-h channel, with both the rotational and isospin symmetries conserved. We developed a code for the p-n mixing calculation by extending the code "HFODD,"[3)] which solves the nuclear Skyrme–Hartree–Fock(–Bogolyubov) problem by using the Cartesian deformed harmonic-oscillator basis. In this p-n mixing calculation, we performed the so-called isocranking calculation by adding the isocranking term to the Hamiltonian: $\hat{h}' = \hat{h} - \vec{\lambda}\cdot\hat{\vec{t}}$. Here, $\hat{\vec{t}}$ is the isospin operator. The isocranking term is analogous to that used in the standard tilted-axis-cranking calculations for high-spin states. By adjusting the isocranking frequency $\vec{\lambda}$, we can control the size and direction of the isospin of the system. We first performed isocranking calculations for $A = 14$ and $A = 48$ systems with the Coulomb interaction switched off, and we confirmed that our code is correctly implemented. In this case, the total and single-particle energies are independent of the direction of the isospin of the system. Next, we performed calculations with the Coulomb interaction included. In this model, isobaric analog states (IASs) are calculated by adjusting the isocranking frequency. We developed an efficient method for determining the isocranking frequency, with which we successfully calculated the $T \simeq 4$ states in $A = 40 - 56$ isobars.

The isocranking calculation is a simple linear constraint method. We also implemented in our code an improved method for optimization with constraints, known as "the augmented Lagrange method," and employed it for the calculation of the high-isospin states in ^{48}Cr. Such calculations can be used to study the nuclear symmetry energy.

In Fig. 1, we plot the energies of the $I = 0^+, T = 1$ triplet of states in the $A = 14$ isobars calculated using the SkM* EDF. The $T_z = 0$ IAS representing the excited $I = 0^+, T = 1$ state in ^{14}N is calculated by using the isocranking model and is described by a single time-even Slater determinant built of single-particle p-n mixed orbitals. Fig. 1 illustrates that the model is indeed capable of quantitatively describing the excitation energies of the $0^+, T = 1$ IASs. One can see that there is asymmetry between the energy differences $|E(T_z = 0) - E(T_z = -1)|$ and $|E(T_z = 0) - E(T_z = 1)|$, which may be related to charge asymmetry and independence of the NN interaction. To investigate this point, we also started a systematic calculation of the $T = 1$ triplets in the A=10–58 region.

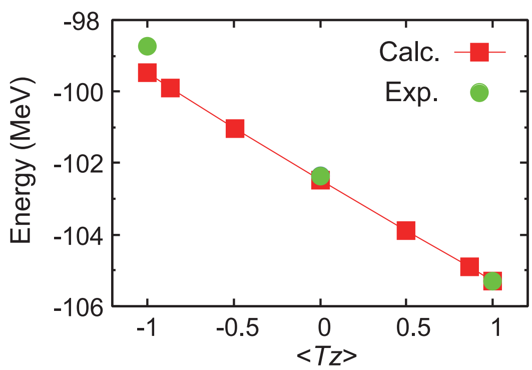

Fig. 1. Energies of $T \simeq 1$ states in $A = 14$ isobars in comparison with the experimental data[4)]. To correct the deficiency of the SkM* EDF, the calculated curve is shifted up by 3.2 MeV.

References

1) K. Sato et al.: Phys. Rev. C **86**, 061301(R) (2013).
2) E. Perlińska et al.: Phys. Rev. C **69**, 014316 (2004).
3) N. Schunck et al.: Comput. Phys. Commun. **183**, 166 (2012); J. Dobaczewski et al. (unpublished).
4) National Nuclear Data Center, Brookhaven National Laboratory, http://www.nndc.bnl.gov/.

† Condensed from the article in Ref. 1)

*1 RIKEN Nishina Center
*2 Institute of Theoretical Physics, Faculty of Physics,University of Warsaw
*3 Department of Physics, University of Jyväskylä

Skyrme-RPA calculation for octupole vibrations of rotating superdeformed nuclei

M. Yamagami, *1 and K. Matsuyanagi*2

The superdeformed (SD) shell structure is significantly different from that of normal deformation. Each major shell at the SD shape consists of about equal numbers of positive- and negative-parity levels. This is a favorable situation for the appearance of negative-parity vibrations. In fact, low-frequency octupole vibrations have been predicted by random phase approximation (RPA) calculations with the Nilsson potential[1)] and discovered in several experiments for SD nuclei in Dy and Hg-Pb regions.

One of the central issues concerning the collective motions of SD nuclei is the octupole instability (appearance of the static shape) depending on angular momentum. Several authors have already demonstrated the importance of the Coriolis force at low-spin band head states of octupole vibrational bands.

Recently, SD bands were discovered in ^{36,40}Ar, ^{40}Ca, and ^{44}Ti. In this mass-number region, we can expect rich experimental information on the collective modes of SD nuclei because the observation of rotational bands starting from the 0^+ state and the linking transition between the SD bands and low-lying normal deformed bands are unique features characterizing the SD states in the region around mass number $A \sim 40$ (for example, see Ref.[2)]).

In this study, we investigate the rotational effect on the ocutpole vibrations of SD states in the $A \sim 40$ region. We have already demonstrated the low-frequency octupole vibrations of the 0^+ SD states through RPA calculations with the Skyrme force (Skyrme-RPA)[3)]. For the excitations from the SD yrast bands, on the other hand, the Skyrme-RPA calculation has not yet been performed owing to computational limitations.

We develop a new framework of the Skyrme-RPA calculation. The single-particle Hamiltonian describing independent-particle motion in the triaxially deformed particle–hole potential that is uniformly rotating with rotational frequency ω_{rot} about the x-axis is adopted; $h' = h - \omega_{rot} j_x$. The Skyrme SkM* interaction is employed for the h. The particle–hole residual interaction is derived from the Skyrme force through the Landau–Migdal approximation:

$$V_{ph}(\mathbf{r}, \mathbf{r}') = N_0^{-1} [F_0 + F_0' \tau \cdot \tau' + (G_0 + G_0' \tau \cdot \tau') \sigma \cdot \sigma'] \delta(\mathbf{r} - \mathbf{r}').$$

The single-particle wave functions φ_k and the two-particle wave functions $\Psi_{kk'} = \varphi_k^\dagger \varphi_{k'}$ are represented by the Fourier-series expansion method in order to effectively treat the configurations involving unbound single-particle states.

We show the isoscalar octupole transition strengths for $K^\pi = 0^-$ and 1^- excitations of the triaxial SD state of ^{44}Ti in Figs. 1 and 2. The results with $\omega_{rot} = 0.0$ and 0.6 MeV/$\hbar$ are compared.

In the $K^\pi = 1^-$ case, an octupole instability of the SD yrast states toward a reflection-asymmetric shape (banana-like shape) is suggested to take place at $\omega_{rot} > 0.6$ MeV/$\hbar$ (corresponding to the total angular momentum $I > 5\hbar$) because of the Coriolis effect.

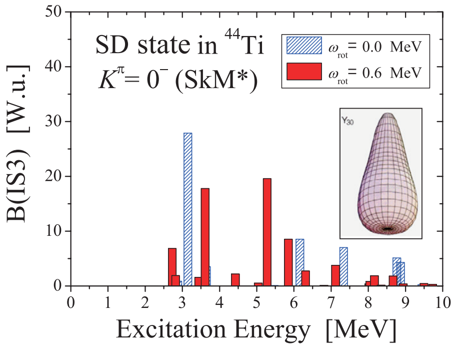

Fig. 1. Isoscalar octupole transition strength for $K^\pi = 0^-$ excitation of the SD state in ^{44}Ti. The results with $\omega_{rot} = 0.0$ and 0.6 MeV/$\hbar$ are compared. The deformation is almost constant at $(\beta_2, \gamma) = (0.58, 9.4°)$ in both cases. $B(IS3)$ is shown in Weisskopf units (W.u.).

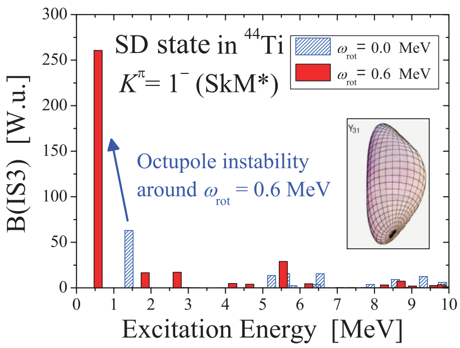

Fig. 2. The same as Fig. 1 but for $K^\pi = 1^-$ excitation.

References
1) T. Nakatsukasa et al.: Phys. Rev. C **53** , 2213 (1996).
2) E. Ideguchi et al.: Prog. Theor. Phys. Suppl. **196**, 427 (2012).
3) T. Inakura et al.: Nucl. Phys. **A768**, 61 (2006).

*1 Department of Computer Science and Engineering, University of Aizu
*2 RIKEN Nishina Center

Di-neutron correlation in asymptotic tail of weakly bound nuclei

Y. Zhang,[*1] M. Matsuo,[*2] and J. Meng[*3]

Neutrons penetrating far outside the nuclear surface often exhibit exotic features of neutron-rich nuclei close to the drip-line. An important question is whether and how neutrons are correlated in the external tail region. The di-neutron correlation in two-neutron halo nuclei, such as ^{11}Li, has attracted attention in this context.[1,2] However, theoretical analyses using the Hartree-Fock-Bogoliubov (HFB) models suggest that the di-neutron correlation also prevails in heavier mass nuclei, including nuclei close to the stability line.[3,4] In the present work, we attempt to clarify the emergence mechanism of the di-neutron correlation by investigating the Cooper pair wave function in the Skyrme HFB model both numerically and analytically, with a focus on its asymptotic behavior at large distances.

We have performed a systematic Skyrme HFB calculation[5] for even-even Ca, Ni, Zr, and Sn isotopes ranging from the stability line to the neutron drip-line. In order to guarantee convergence at large distances, we solve the HFB equation in the radial coordinate representation, using a very large radial cut-off at 100 fm and the orbital angular momentum cut-off at $l = 72$. We then evaluate the neutron pair condensate (equivalent to the pair density and the pairing tensor) $\tilde{\rho}(\boldsymbol{R}) \equiv \langle\Phi_0|\psi(\boldsymbol{R}\uparrow)\psi(\boldsymbol{R}\downarrow)|\Phi_0\rangle = \Psi_{\rm pair}(\boldsymbol{R},\boldsymbol{R})$. Note that the pair condensate is a part of the neutron Cooper pair wave function, defined by $\Psi_{\rm pair}(\boldsymbol{r}_1,\boldsymbol{r}_2) = \langle\Phi_0|\psi(\boldsymbol{r}_1\uparrow)\psi(\boldsymbol{r}_2\downarrow)|\Phi_0\rangle$.

The asymptotics of the pair condensate is characterized by an exponential behavior $\tilde{\rho}(R) \to C\exp(-\tilde{\kappa}R)$, and the exponential constant $\tilde{\kappa}$ is extracted by a fitting to the microscopically calculated $\tilde{\rho}(R)$. As shown in Fig. 1, the extracted exponential constants (solid symbols) follow a universal relation $\tilde{\kappa} = \sqrt{8m|\lambda|}/\hbar$, where λ is the Fermi energy and m is the neutron mass. The result is different from the previous estimate[6,7] $\tilde{\kappa}_{\rm qp} = \sqrt{2m(|\lambda|+E_{\rm qp,l})}/\hbar + \sqrt{2m(|\lambda|-E_{\rm qp,l})}/\hbar$ (open symbols), which relies on the asymptotic behavior of the quasiparticle wave function with the lowest quasiparticle energy $E_{\rm qp,l}$.

The universal relation can be interpreted as the penetration of a di-neutron with mass $M = 2m$ and with the binding energy given by the two-neutron separation energy $S_{2n} = 2|\lambda|$, i.e. $\tilde{\kappa} = \sqrt{2MS_{2n}}/\hbar$. We can justify this interpretation via an analytic and general examination of the HFB theory. It should be noted that in the limit $r_1, r_2 \to \infty$, the following two-particle Schroedinger equation holds for the Cooper pair wave function:

$$(t(1)+t(2)+v(1,2))\Psi_{\rm pair}(\boldsymbol{r}_1,\boldsymbol{r}_2) = 2\lambda\Psi_{\rm pair}(\boldsymbol{r}_1,\boldsymbol{r}_2) \quad (1)$$

where $v(1,2)$ is the nn interaction. As a consequence, the asymptotic form is given in terms of the di-neutron coordinate system $r = |\boldsymbol{r}_1 - \boldsymbol{r}_2|$, $R = |(\boldsymbol{r}_1+\boldsymbol{r}_2)/2|$ as

$$\Psi_{\rm pair}(\boldsymbol{r}_1,\boldsymbol{r}_2) \to C_0^{L=0}\phi_0^{L=0}(r)\exp(-\kappa_{\rm d}R)/R \quad (2)$$

for small r. Here, $\phi_0^{L=0}(r)$ is the wave function of the S-wave virtual state of the nn system, representing the di-neutron, and the exponential constant $\kappa_{\rm d} = \sqrt{2M(2|\lambda|)}/\hbar$ arising from the center of mass motion of the di-neutron.

We also found that the di-neutron asymptotics, Eq.(2), dominates in weakly bound neutron-rich nuclei with a small neutron separation energy or small $|\lambda|$. Conversely, single-particle (quasiparticle) components also contribute to the asymptotics of the Cooper pair in nuclei having a larger neutron separation energy, as the single-particle value (open symbol) and the full value (solid one) coincide in these nuclei. As a corollary, the condition for the dominance of the di-neutron correlation is given as $|\lambda| \lesssim \Delta$ or $S_{2n} \lesssim 2\Delta$.

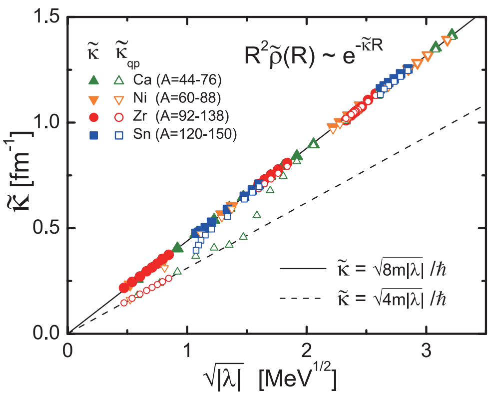

Fig. 1. The asymptotic exponential constant $\tilde{\kappa}$ of the neutron pair condensate $\tilde{\rho}(R)$.

*1 Graduate School of Science and Technology, Niigata University (presently Tianjin University)
*2 Department of Physics, Niigata University
*3 School of Physics, Peking University

References

1) G. F. Bertsch and H. Esbensen: Ann. Phys. (NY) **209**, 327 (1991).
2) T. Nakamura *et al.*: Phys. Rev. Lett. **96**, 252502 (2006).
3) M. Matsuo, K. Mizuyama and Y. Serizawa: Phys. Rev. C **71**, 064326 (2005).
4) N. Pillet, N. Sandulescu, and P. Schuck: Phys. Rev. C **76**, 024310 (2007).
5) Y. Zhang, M. Matsuo, and J. Meng: Phys. Rev. C **86**, 054318 (2012).
6) A. Bulgac, preprint FT-194-1980, Bucharest, 1980, nucl-th/9907088.
7) J. Dobaczewski, W. Nazarewicz, T. R. Werner, J. F. Berger, C. R. Chinn, and J. Dechargé: Phys. Rev. C **53**, 2809 (1996).

Deformed nuclei in the black-sphere approximation

A. Kohama, [*1] K. Iida,[*1,*2] K. Oyamatsu,[*1,*3] and H. Koura[*1,*4]

The size of an atomic nucleus is one of the most fundamental quantities that characterize the bulk properties of the nucleus. It is well known for β stable nuclei in the ground state thanks to systematic measurements of electron and proton elastic differential cross sections. This helps clarify the equation of state of nuclear matter near the saturation point.[1)] When studying the density derivative L of the symmetry energy of nearly symmetric nuclear matter, the total reaction cross section, σ_R, of neutron-rich nuclei is one of the most important observables.

In this work, in order to obtain the value of L, we focus on the empirical data of the interaction cross section, σ_I, measured at ~900 MeV per nucleon,[2,3)] as a first step. Since the data of Ne and Mg isotopes at ~240 MeV per nucleon have already been obtained at the RI Beam Factory of RIKEN,[4)] systematic analyses are necessary. For the analyses, we adopt the black-sphere (BS) model of nuclei.

We have so far systematically analyzed the proton elastic scattering and σ_R data for stable nuclei at a proton incident energy of $T_p \sim$ 800–1000 MeV on the basis of a "black-sphere picture" of nuclei.[5)] We showed that for proton beams incident on stable nuclei, the cross section of a black sphere of radius a, which is determined by fitting the angle of the first elastic diffraction peak calculated for proton diffraction by a circular black disk of radius a to the measured value, is consistent with the measured σ_R.[5)] This finding is also observed for σ_R of nucleus-nucleus reactions down to approximately 100 MeV per nucleon.[6)]

In the model, the absorption cross section is written by $\sigma_{BS} = \pi\left(a_0(\text{proj.}) + a_0(\text{C})\right)^2$, where $a_0(\text{proj.})$ is the BS radius of a projectile. $a_0(\text{C})$ is the BS radius of the target C nucleus obtained using the method mentioned above.[5,6)] For proton incident energies higher than ~ 800 MeV, $a_0(\text{C}) = 2.69 \pm 0.07$ fm.

According to the systematic analysis based on a macroscopic nuclear model, at large neutron excess, the calculated nuclear matter radius increases with L via the L dependence of the nuclear matter saturation density. It is indispensable to duly incorporate such dependence into the BS model for application to the reactions involving neutron-rich nuclei.

The relatively large neutron excess of the isotopes of Ne and Mg is advantageous for studying the value of L. However, nuclear deformation occurs in this region of nuclei. We change the black sphere into a spheroid of the same volume to take nuclear deformation into account before discussing the L dependence. The values of the deformation parameter, β, are taken from microscopic nuclear structure models.[7)] Under the adiabatic approximation, the values of σ_R for deformed nuclei should be evaluated by angle averaging of the cross section values over the deformation direction of nuclei.[8)]

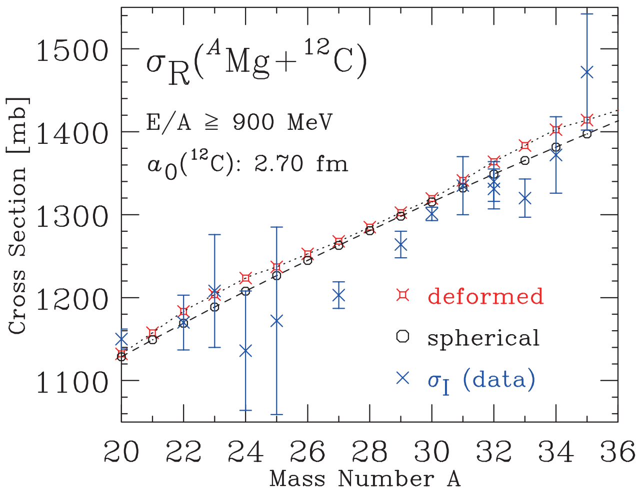

Fig. 1. Effect of nuclear deformation on σ_R as a function of projectile mass number, A, indicated by squares with crosses. The values of β are from SkM*. The spherical cases (○) are obtained by "BS scaling", $a_0(\text{proj.}) \simeq 1.2135A^{1/3}$ fm, in σ_{BS}.[5)] For comparison, we plot the empirical values of σ_I of ^{A}Mg on a carbon target.[2,3)]

The results are shown in Fig. 1. Although we adopt the values of β given by a mean field calculation with the effective interaction SkM*, which tends to offer large deformation, the effect on σ_R is rather small. This is consistent with the work of Christley and Tostevin,[8)] but inconsistent with the work of Horiuchi *et al.*[9)] Before drawing conclusions, we have to examine the interaction dependence by adopting SLy4, KTUY,[7,10)] etc. The study is now in progress.

References
1) K. Oyamatsu *et al.*: Prog. Theor. Phys. **109**, 631 (2003).
2) A. Ozawa *et al.*: Nucl. Phys. A **693**, 32 (2001).
3) R. Kanungo *et al.*: Phys. Rev. C **83**, 021302(R) (2011).
4) M. Takechi *et al.*: Phys. Lett. B **707**, 357 (2012).
5) A. Kohama *et al.*: Phys. Rev. C **72**, 024602 (2005).
6) A. Kohama *et al.*: Phys. Rev. C **78**, 0061601(R) (2008).
7) T. Inakura *et al.*: Nucl. Phys. **A710**, 261 (2002).
8) J. A. Christley *et al.*: Phys. Rev. C **59**, 2309 (1999).
9) W. Horiuchi *et al.*: Phys. Rev. C **86**, 024614 (2012).
10) H. Koura *et al.*: Prog. Theo. Phys. **113**, 305 (2005).

*1 RIKEN Nishina Center
*2 Depart. of Natural Science, Kochi University
*3 Depart. of Human Informatics, Aichi Shukutoku University
*4 ASRC, JAEA

Shell-model description of low-lying states in Rn isotopes

N. Yoshinaga*[1] and K. Higashiyama*[2]

Polonium and radon isotopes below the neutron closed shell at $N = 126$ provide an important region for testing shell-model structure. The isomeric 8_1^+ states in $^{206-214}$Rn were experimentally confirmed to be based on a proton $(0h_{9/2})^4$ configuration[1]. The low-lying near-yrast states were analyzed in terms of the interacting boson model plus two quasiparticles model[2], where one of the bosons is replaced by a pair of nucleons at high spin. A good agreement with experiment was achieved for both the energy spectra and electromagnetic transitions.

In this work, the band structure of the Rn isotopes is studied in terms of the full-fledged shell model. As for single-particle levels, all the six orbitals, $0h_{9/2}$, $1f_{1/2}$, $0i_{13/2}$, $1f_{5/2}$, $2p_{3/2}$, and $2p_{1/2}$, in the major shell between the magic numbers 82 and 126 are considered for both neutrons and protons. The effective interactions comprise single-particle energies and monopole and quadrupole pairing plus quadrupole-quadrupole interactions, whose strengths are adjusted to fit experimental data. The interaction strengths adopted in the present calculations are assumed to be the same for all the nuclei.

In Fig. 1, the measured spectra for even-even Rn isotopes are compared with the shell model results. The even-spin yrast sequences are well reproduced except for the 8_1^+ states, which are lower in energy than the experimental data. For better reproduction of the 8_1^+ states, multipole pairing interactions more than quadrupole might be necessary. Concerning other states, good agreements between theory and experiment are achieved.

In order to investigate the collective behavior at low energies and the effect of the single particle excitations at high spins, the energy spectra in the shell model are compared with those in a pair-truncated shell model (PTSM)[3,4]. The building blocks of this model are angular momenta zero (S) and two (D) collective pairs together with non-collective pairs. The Hamiltonian in this truncated space (PTSM space) is set identical to that used in the shell model. In Fig. 2, the energy levels obtained by the PTSM for ^{208}Rn are compared with those of the shell model. There is a good correspondence between the energy levels of the shell model and those in the PTSM. This means that the model space spanned by the PTSM is sufficient for describing the shell model results.

In search for the microscopic structure of the yrast band, we analyze the expectation values of the numbers of pairs (not shown). It is found that the valence neutron excitation plays an essential role in describing the low-lying states, and the pair of $0h_{9/2}$ protons is indispensable for the states above spin 8.

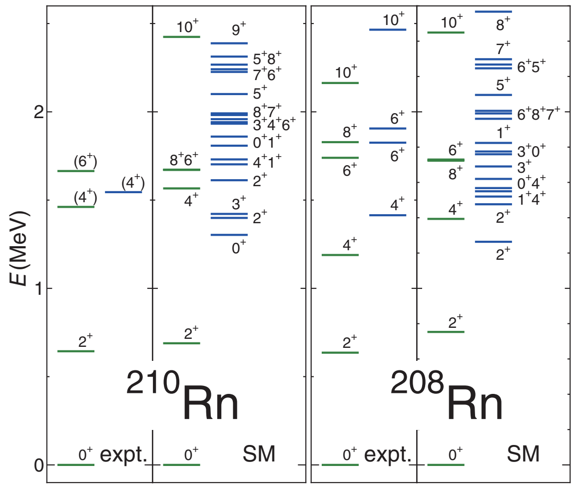

Fig. 1. Comparison of the experimental energy levels (expt.) with those of the shell model (SM) for ^{208}Rn and ^{210}Rn.

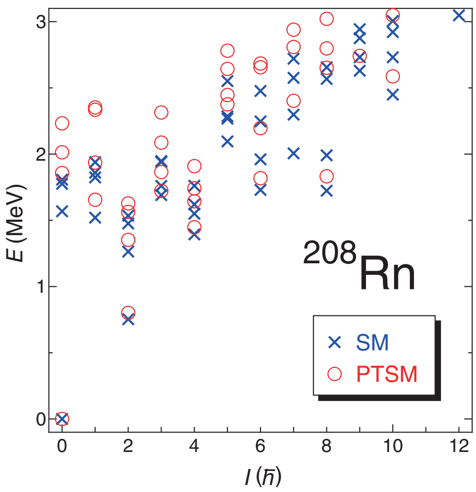

Fig. 2. Comparison of the calculated energy levels in the PTSM (PTSM) and the shell model results (SM) for ^{208}Rn.

References
1) K. H. Maier et al.: Hyperfine Interact. **9**, 87 (1981).
2) A. Zemel and J. Dobes: Phys. Rev. C **27**, 2311 (1983).
3) N. Yoshinaga and K. Higashiyama: Phys. Rev. C **83**, 054309 (2004).
4) K. Higashiyama and N. Yoshinaga: Phys. Rev. C **83**, 034321 (2011).

*1 Department of Physics, Saitama University
*2 Department of Physics, Chiba Institute of Technology

Shell-model study of nuclear structure around ^{100}Sn

M. Honma,[*1] T. Otsuka,[*2,*3,*4] T. Mizusaki,[5] Y. Utsuno,[*6] N. Shimizu,[*3] and M. Hjorth-Jensen[*4,*7]

The nuclear structure around the doubly-magic N=Z nucleus ^{100}Sn has been of great interest from various viewpoints such as the development of shell-structure and the proton-neutron correlations. For a reliable prediction of unknown targets by the shell model, one of our strategies is to minimally modify so-called G-matrix interactions[1)] by fitting the shell-model results to available experimental energy data. In the previous work[2)], we have determined an effective interaction called JUN45 in the model space covering nuclei with $28 \leq N, Z \leq 50$. Also, we have tried the shell-model fits to describe Sn isotopes with N=50$\sim$82 and obtained an effective interaction SNBG1[3)]. Since the ^{100}Sn is located at the end of the model space in both studies, it was impossible to discuss the excitation across the N and/or Z=50 shell closure. In this report, we present another approach along this line, aiming at the description of nuclei including ^{100}Sn.

We take four single-particle orbits $1p_{1/2}$, $0g_{9/2}$, $1d_{5/2}$ and $0g_{7/2}$ for both protons and neutrons assuming a hypothetical "core" $^{76}_{38}$Sr$_{38}$. This choice is motivated by the excellent success of the $(p_{1/2}, g_{9/2})$ model space near the $N\sim50$ lines due to the approximate degeneracy of these orbits around there, as suggested in Fig.1(a). Also, since the $7/2^+$ state comes down rapidly as the proton number is increased towards $Z = 50$ (see Fig.1(b)), the last two orbits $(d_{5/2}, g_{7/2})$ are essential. Based on the information about the dominant configurations obtained with the JUN45 and the SNBG1 interactions, we have selected the experimental data in the range of $47 \leq N \leq 58$ for the fit. In order to reduce the amount of computation for the fitting, we take the t=4 truncated model space, where t stands for the maximum number of nucleons that can excite from the $(p_{1/2}, g_{9/2})$ orbits to the $(d_{5/2}, g_{7/2})$ orbits relative to the naive lowest configuration. Starting from the G-matrix interaction derived from the N^{3}LO interaction[4)], we have carried out a series of iterative fits. We assume the isospin symmetry, and adopt the $A^{-0.3}$ mass-dependence of the two-body matrix element (TBME). In the latest fit, 197 TBMEs and 4 single-particle energies have been determined with a rms error of 231keV for 528 data.

As examples of the fitted results, the energy levels of low-lying states are shown in Fig.1 for odd-mass isotones with N = 50 and 51. It can be seen that the overall trends are reasonably described by the present shell-model calculations. As for ^{100}Sn, using this interaction at the t = 6 truncation level, the excitation energy of the 2^+_1 state is predicted to be 4.8MeV, and the 0p-0h component in the ground-state wavefunction is 71%. The calculated B(E2; $0^+ \to 2^+$)=0.13 e^{2}b^2 with the effective charges e_p=1.5, e_n=0.5 is almost consistent with the shell-model result in a different model space[7)].

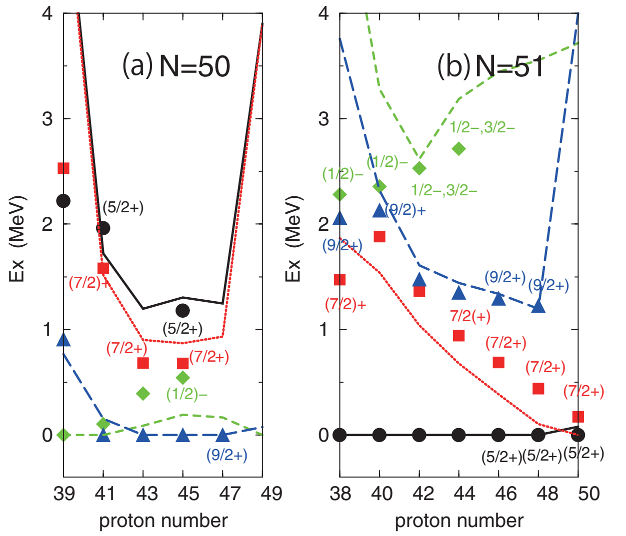

Fig. 1. Energy levels of low-lying states for (a) N=50 isotones with odd-number of protons and (b) N=51 isotones with even-number of protons. Calculated $1/2^-$, $9/2^+$, $5/2^+$ and $7/2^+$ states are shown with dashed, long-dashed, solid and dotted lines, respectively, which are compared with the experimental data denoted by diamonds, triangles, circles and squares, respectively. Experimental data are taken from Ref.[5)], where uncertain spin assignments are explicitly shown. The shell-model results are obtained by using the efficient code MSHELL64[6)].

*1 Center for Mathematical Sciences, University of Aizu
*2 Department of Physics, University of Tokyo
*3 Center for Nuclear Studies, University of Tokyo
*4 National Superconducting Cyclotron Laboratory, Michigan State University
*5 Institute of Natural Sciences, Senshu University
*6 Advanced Science Research Center, Japan Atomic Energy Agency
*7 Department of Physics and Center of Mathematics for Applications, University of Oslo

References

1) M. Hjorth-Jensen *et al.*: Phys. Rep. **261**, 125 (1995).
2) M. Honma *et al.*: Phys. Rev. C **80**, 064323 (2009).
3) M. Honma *et al.*: RIKEN Accel. Prog. Rep. **45**, 35 (2012).
4) D. R. Entem *et al.*: Phys. Rev. C **68**, 041001(R) (2003).
5) Data extracted using the NNDC WorldWideWeb site from the ENSDF database.
6) T. Mizusaki *et al.*: MSHELL64 code (unpublished).
7) G. Guastalla *et al.*: Phys. Rev. Lett. **110**, 172501 (2013).

Giant dipole resonance in ^{88}Mo from phonon damping model's strength functions averaged over temperature and angular momentum distributions[†]

N. Dinh Dang,[*1] M. Ciemala,[*2] M. Kmiecik,[*2] and A. Maj[*2]

Many theoretical and experimental studies in nuclear structure during the last three decades were devoted to the giant dipole resonance (GDR) in highly excited nuclei. The GDR line shape and its full-width at half maximum (FWHM) Γ_{GDR} are experimentally extracted from the statistical calculations by using the Lorentzian strength function to reproduce the γ-ray spectra detected from the decay of the highly-excited compound nucleus (CN) at the excitation energy E^*. They are often compared with the theoretical predictions, which are obtained at a given values of nuclear temperature T and/or angular momentum J.

The extraction of T and J is crucial for a meaningful comparison between experiment and theory because the initial temperature T_{max} and/or angular momentum J_{max} at the first step in the decay of the CN are significantly higher than the mean values $\overline{T}$ and $\overline{J}$, obtained by averaging over all daughter nuclei in the decay process. Moreover, while the theoretical GDR strength function is calculated at a fixed value of T and/or J, its experimental counterpart is extracted by fitting the spectrum, which is generated by a multistep cascade decay, where the nucleus undergoes a cooling down from T_{max} (and/or J_{max}). Because of this mechanism, the authors of Ref.[1] have proposed to incorporate the theoretical strength functions into the full statistical decay calculations and compare the results obtained with the experimental data. This method was applied to test the validity of several theoretical models in Refs.[1,2], including the phonon damping model (PDM)[3], which describes the broadening of the GDR width at finite T and J via coupling of the GDR to non-collective particle-hole (ph), particle-particle (pp) and hole-hole (hh) configurations. However it is not clear if the GDR line shape obtained by averaging the GDR strength functions in the whole interval of T and/or J is equivalent to the GDR strength function obtained at the mean values $\overline{T}$ and $\overline{J}$ in these intervals.

In the present paper the PDM is employed to calculate the strength functions for the GDR in the statistical decays after the fusion-evaporation reaction ^{48}Ti + ^{40}Ca, which produces the CN ^{88}Mo* at various excitation energies E^*[4]. The calculations use the empirical probability distributions for T and J to produce the GDR average strength functions $\overline{S}(\omega, E^*)$ as well as $\overline{T}$ and $\overline{J}$ at each energy E^*. The calculations show that,

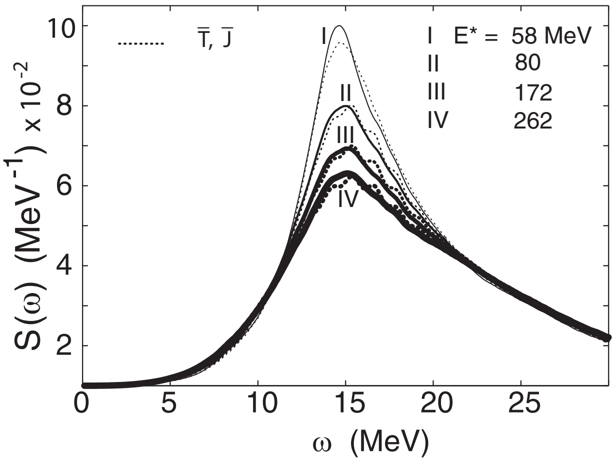

Fig. 1. GDR average strength function $\overline{S}(\omega, E^*)$ for ^{88}Mo at different excitation energies E^* obtained by using the T- and J-probability distributions. The dotted lines are the strength functions $S(\omega, T, J)$ obtained at the corresponding $T = \overline{T}$ and $J = \overline{J}$.

while the GDR width increases with E^*, it approaches a saturation at high $T = 4$ MeV when $J > 50\hbar$. At a larger $J \geq 70\hbar$, the width saturation shows up at any T. The GDR strength function $\overline{S}(\omega, E^*)$ obtained by averaging the individual strength functions $S(\omega, T, J)$ over the empirical T- and J-probability distributions turns out to be almost identical to $S(\omega, \overline{T}, \overline{J})$ calculated at $\overline{T}$ and $\overline{J}$ (Fig. 1). Therefore, once $\overline{T}$ are $\overline{J}$ are known, one may compare the theoretical prediction for the individual strength function $S(\omega, T, J)$ and its width, obtained at $\overline{T}$ and $\overline{J}$, with the data, without the need of generating and averaging the strength functions over the whole T and J distributions.

References

1) G. Gervais, M. Thoennessen, and W.E. Ormand, Phys. Rev. C **58**, R1377 (1998).
2) N. Dinh Dang, K. Eisenman, J. Seitz, and M. Thoennessen, Phys. Rev. C **61**, 027302 (2000).
3) N.D. Dang and A. Arima, Phys. Rev. Lett **80**, 4145 (1998); N. Dinh Dang and A. Arima, Nucl. Phys. A **636** 427, (1998); N. Dinh Dang and A. Arima, Phys. Rev. C **68**, 044303 (2003); N. Dinh Dang, Phys. Rev. C **85**, 064323 (2012).
4) M. Ciemala *et al.*, Acta Physica Polonica B **42**, 633 (2011), M. Ciemala, Ph.D. thesis (in Polish), Niewodniczanski Institute of Nuclear Physics PAN, Krakow, Report No. 2062/PL (2013).

† Condensed from the article in Phys. Rev. C **87**, 054313 (2013)

*1 RIKEN Nishina Center
*2 Niewodniczanski Institute of Nuclear Physics PAN, Kraków

On the importance of using exact pairing in the study of pygmy dipole resonance†

N. Dinh Dang*1 and N. Quang Hung*2

One of the major issues in the theoretical study of the pygmy dipole resonance (PDR) in medium and heavy nuclei is the discrepancy in the predictions of different approaches regarding the strength and collectivity of the PDR. While the relativistic random-phase approximation seems to predict a prominent peak identified as the collective PDR below 10 MeV in heavy nuclei[1,2], the results of calculations including monopole pairing within the quasiparticle RPA (QRPA) do not expose any collective states in the low-energy region of the $E1$ strength distribution[3]. One of the possible sources of such discrepancy may well lie in superfluid pairing, which plays a crucial role in open shell nuclei in the vicinity of the neutron drip line. However all the theoretical calculations of the PDR so far either neglected pairing, such as the relativistic RPA, or adopted the mean-field pairing. The latter is taken into account within the Hartree-Fock-Bogolyubov, Hartree-Fock + BCS formalisms, or coupling of QRPA particle-hole (ph) states to more complicate configurations like the 2p2h ones. Given the progress in the exact solutions of the pairing problem in recent years, it is highly desirable to see how exact pairing affects the PDR as compared to the predictions given by the approaches employing the conventional mean-field pairing gap.

The present paper studied the effect of superfluid pairing on the PDR in light, medium and heavy neutron-rich oxygen, calcium and tin isotopes. Beside the conventional BCS gap, the exact pairing gap obtained by diagonalizing the pairing Hamiltonian with constant parameters G_N and G_Z for neutron and proton pairing interactions, respectively, is also employed to calculate the strength function of the giant dipole resonance (GDR) in these nuclei within the framework of the phonon-damping model (PDM)[4]. The analysis of the numerical calculations allows us to make the following conclusions: 1) Exact pairing decreases the two-neutron separation energy in light nuclei, but increases it in heavy nuclei as compare to that obtained within the BCS theory; 2) Exact pairing significantly enhances the PDR in medium (calcium) and heavy (tin) nuclei, whereas the BCS pairing causes a much weaker effect as compared to the case when pairing is neglected. This observation indicates that BCS pairing might not be sufficient to describe the PDR in medium and heavy neutron-rich nuclei; 3) The significant change in the line shape of the GDR with increasing the mass number A indicates that the values for the model's parameters cannot be kept fixed when the calculations are extended to the nuclei in the vicinity of the neutron drip line. This includes the parameters of the nuclear mean field such as the parameters of the Woods-Saxon potential or the parameters of effective interactions such as various Skyrme types, which are used in microscopic calculations of the GDR and PDR.

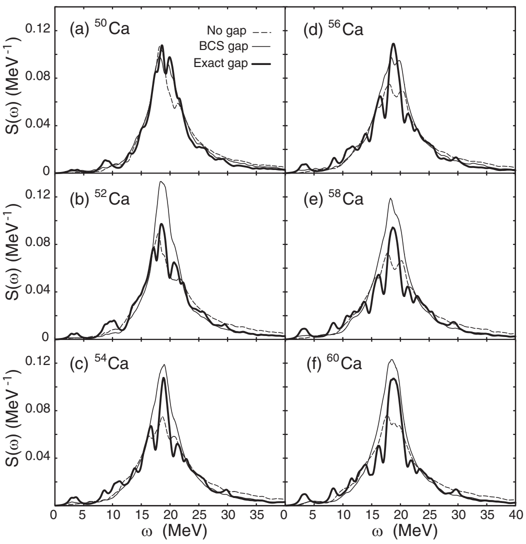

Fig. 1. GDR strength functions for calcium isotopes obtained within the PDM. The predictions without pairing, including BCS pairing and exact pairing are denoted by the dashed, thin solid, and thick solid lines, respectively.

The obtained results may serve as a hint to clarify while several microscopic approaches, mentioned in the Introduction, are in disagreement regarding the strength and fine structure of the PDR. The present paper also emphasizes the necessity of using exact pairing, whenever possible, instead of the BCS one or the HFB average pairing gap in the future study of the PDR.

References

1) D. Vretenar, N. Paar, P. Ring, and G.A. Lalazissis, Nucl. Phys. A **692**, 496 (2001).
2) E. Litvinova, P. Ring, and D. Vretenar, Phys. Lett. B **647**, 111 (2007).
3) D. Sarchi, P.F. Bortignon, and G. Colò, Phys. Lett. B **601**, 27 (2004).
4) N. Dinh Dang, V. Kim Au, T. Suzuki, and A. Arima, Phys. Rev. C **63**, 044302 (2001).

† Condensed from the article in J. Phys. G. **40**, 105103 (2013)
*1 RIKEN Nishina Center
*2 School of Engineering, TanTao University, Long An

Microscopic analysis of fusion hindrance in heavy systems

K. Washiyama[*1]

The interplay between nuclear structures and dynamical effects is crucial for appropriate descriptions of heavy-ion fusion reactions at energies around the Coulomb barrier. Coupled-channels calculations have been widely used to quantitatively describe the entrance channel of fusion reactions in light- and medium-mass systems whose charge product (Z_1Z_2) is less than $1,600$. On the other hand, in heavy systems ($Z_1Z_2 > 1,600$), it is observed that the fusion probability is strongly hindered around the Coulomb barrier, compared with $Z_1Z_2 < 1,600$ systems and with coupled-channels results.[1] This is called fusion hindrance, and the extra energy needed to make such systems to fuse is called extra-push energy.[2] Quasi-fission process, where a colliding system reseparates to projectile-like and target-like fragments before forming a compound nucleus, is considered to be mostly responsible for this hindrance. For a better description of the reaction mechanism in heavy systems, a dynamical diffusion model using a macroscopic Langevin equation has been developed.[3] Moreover, extra-push energies and quasi-fission process have been analyzed using the time-dependent Hartree-Fock (TDHF) model.[4]

Recently, we proposed a method to extract nucleus-nucleus potential and one-body energy dissipation from the relative motion of colliding nuclei to nuclear intrinsic excitations in fusion reactions from TDHF time evolutions.[5] This method relies on the hypothesis that complex microscopic mean-field evolution of head-on collisions can be accurately reduced to a simple one-dimensional macroscopic evolution that obeys a Newton equation including potential and dissipation terms. In the present report, we apply this method to study the property of potential and energy dissipation in heavy systems and to understand the origins of fusion hindrance.

Figure 1 shows nucleus–nucleus potentials V as a function of relative distance R for the ^{96}Zr + ^{124}Sn system ($Z_1Z_2 = 2,000$) obtained with our method for three center-of-mass energies $E_{\rm cm}$. As a reference, we plot by the filled circles the frozen density potential calculated from the same energy density functionals as in TDHF with the density of colliding nuclei frozen to their ground-state one, meaning that no dynamical effects are included during collision. Note that for the case with $E_{\rm cm} = 228.4$ MeV, the relative velocity $\dot{R}$ becomes almost 0 at $R \sim 11.4$ fm, and we stop the extraction of potential at this stage (indicated by the blue filled diamond in Fig. 1). By comparing the obtained potentials in Fig. 1 with those in $Z_1Z_2 < 1,600$ systems in Ref.[5], we find two significant differences:

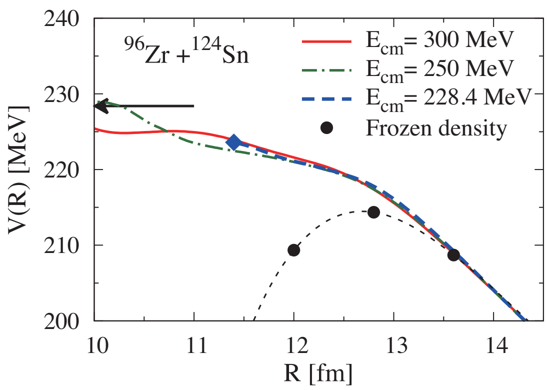

Fig. 1. Nucleus–nucleus potential of the ^{96}Zr + ^{124}Sn system extracted from our method with different $E_{\rm cm}$. Filled circles denote the frozen density potential. The arrow indicates the fusion threshold energy.

(1) Energy dependence of potential, which appears around the Coulomb barrier in $Z_1Z_2 < 1,600$ systems, is less pronounced in heavy systems. (2) While a barrier is observed in the frozen density potential at $R \sim 12.8$ fm, there is no barrier in the obtained potentials, and the potentials monotonically increase as R decreases because of dynamical effects. Furthermore, we analyze the origin of the fusion hindrance from the TDHF trajectory with the fusion threshold energy, $E_{\rm cm} = 228.4$ MeV. Extra-push energy by TDHF can be defined as the difference between the fusion threshold energy and the barrier of the frozen density potential. In this system, this is calculated to be 14 MeV. According to our method of extracting potential, the origin of the extra-push energy can be identified from the sum of the total dissipated energy, increase in potential energy, and remaining kinetic energy. In this case at $R \sim 11.4$ fm, the total dissipated energy and increase in potential energy are 4.0 MeV and 9.2 MeV, respectively. We conclude from this analysis that the main contribution to the extra-push energy is the increase in extracted potential at $R \lesssim 12.8$ fm.

References

1) C.-C. Sahm et al.: Nucl. Phys. A **441**, 316 (1985).
2) W. J. Swiatecki: Phys. Scripta **24**, 113 (1981); Nucl. Phys. A **376**, 275 (1982).
3) Y. Aritomo, K. Hagino, K. Nishio, and S. Chiba: Phys. Rev. C **85**, 044614 (2012).
4) C. Simenel, B. Avez, C. Golabek: Proceedings of the KERNZ08 conference, arXiv:0904.2653; L. Guo and T. Nakatsukasa: EPJ Web Conf. **38**, 09003 (2012).
5) K. Washiyama and D. Lacroix: Phys. Rev. C **78**, 024610 (2008); K. Washiyama, D. Lacroix and S. Ayik: Phys. Rev. C **79**, 024609 (2009).

*1 RIKEN Nishina Center

3. Nuclear Data

Compilation of nuclear reaction data from RIBF

A. Makinaga,*1 V. Devi,*2 M. Aikawa,*1 S. Ebata,*2 N. Furutachi,*1 D. Ichinkhorloo,*2 K. Katō,*1 M. Odsuren,*2 N. Otuka,*3,*4 and K. Tsubakihara*5

Nuclear data, e.g. cross sections, half-lives, and decay radiation properties, can be obtained through scientific investigation of nuclear properties and reactions. The results of experimental measurements of different nuclear reaction data are distributed in various publications and hence are difficult for users to access. Therefore, there is a need to compile the data into a database. One of the database is the EXFOR library, which is maintained by the International Network of Nuclear Reaction Data Centres (NRDC) under the auspices of the International Atomic Energy Agency (IAEA). As one of the NRDC members, the Hokkaido University Nuclear Reaction Data Centre (JCPRG)[1)] has contributed about 10 percent of the data on charged-particle nuclear reactions in the EXFOR library.

JCPRG compiles and accumulates charged-particle data obtained in Japanese facilities in their own database NRDF. The compiled nuclear reaction data is available through the online search system of the NRDF and the EXFOR library[2)]. In addition to the collaboration with the NRDC network, JCPRG established a collaborative research contract with the RIKEN Nishina Center in 2010, to increase the availability of the nuclear reaction data produced at the RIBF. The compiled files of the nuclear data produced at the RIBF are translated to the EXFOR format for the benefit of nuclear data users. We have addressed a smooth and high-quality compilation of the RIBF data as one of the important tasks in this collaboration. This write-up provides a brief overview of the JCPRG compilation activity in 2013 regarding experimental nuclear reaction data produced at the RIBF.

Among the papers compiled in 2013, thirteen contained RIBF data in the compilation scope of the EXFOR library, out of which eight papers[3–10)] published in 2013 had already been registered on the EXFOR library. Five papers published in 2012[11–15)] had also been registered on the EXFOR library in 2013. The data can be easily accessed from the EXFOR search system[2)] by using the accession numbers given in Table 1. The list of RIBF data compiled into the EXFOR library is also available on the JCPRG website[1)] along with additional information.

To ensure a high-quality database, we ask authors to provide the original data plotted in each figure so that the data compiled in the NRDF and the EXFOR library are accurate. If the original data could not be obtained from the corresponding author, we digitized numerical data from the plotted figures using the digitization software GSYS. If we receive the original numerical data in the future, we will replace the digitized data with the original data. We also correspond with the authors about inquiries for data, error, and experiments as necessary. The numerical data for almost all of the EXFOR entries compiled in 2013 were proofread by authors, and a detailed description of the entries has been revised according to the authors' comments.

Table 1. Entry numbers with references compiled in 2013

	2012		2013	
Entries	E2384[11)]	E2416[15)]	E2404[3)]	E2430[7)]
	E2888[12)]		E2405[4)]	E2431[8)]
	E2391[13)]		E2406[5)]	E2434[9)]
	E2401[14)]		E2407[6)]	E2438[10)]
Total	5		8	

As a result of the collaboration for four years, most of the compilation process was well established and is working well as reported above. We are continuously making efforts to improve the completeness and usability of the experimental nuclear reaction data produced at the RIBF. For such improvements, the first JCPRG-RNC joint workshop on nuclear data was held on August 8-9, 2013[16)]. The workshop was helpful for understanding the present and future status of the RIKEN-JCPRG research collaboration and related nuclear data activities.

*1 Faculty of Science, Hokkaido University
*2 Meme Media Laboratory, Hokkaido University
*3 RIKEN Nishina Center
*4 NDS, IAEA
*5 Department of Engineering Science, Osaka Electro-Communication University

References

1) http://www.jcprg.org/
2) http://www.jcprg.org/exfor/
3) M. U. Khandaker et al.: Nucl. Instrum. Methods Phys. Res. B **296** (2013) 14.
4) B. Guo et al.: Phys. Rev. C **87** (2013) 015803.
5) T. Sumita et al.: J. Phys. Soc. Jpn. **82** (2013) 024202.
6) S. Sakaguchi et al.: Phys. Rev. C **87** (2013) 021601(R).
7) A. K. Kurilkin et al.: Phys. Rev. C **87** (2013) 051001.
8) H. Yamaguchi et al.: Phys. Rev. C **87** (2013) 034303.
9) J. J. He et al.: Phys. Rev. C **88** (2013) 012801.
10) M. Murakami et al.: Phys. Rev. C **88** (2013) 024618.
11) K. Tshoo et al.: Phys Rev. Lett. **109** (2012) 022501.
12) K. Morita et al.: J. Phys. Soc. Jpn. **81** (2012) 103201.
13) S. Takeuchi et al.: Phys Rev. Lett. **109** (2012) 182501.
14) N. Kobayashi et al.: Phys. Rev. C **88** (2012) 054604.
15) LI Kuo-Ang et al.: Chin. Phys. Lett. **29** (2012) 102301.
16) M. Aikawa et al.: in this report.

Nuclear data format suitable simultaneously for databases, experimentalists, and users

M. Aikawa,[*1] M. Chiba,[*2] S. Ebata,[*3] T. Katayama,[*4] K. Katō,[*1] A. Makinaga,[*1] H. Noto,[*4] and K. Tsubakihara[*5]

Nuclear reactions are useful in many fields related to nuclear physics, such as astrophysics, nuclear engineering, and radiation therapy. Many experimental studies have been performed worldwide to obtain nuclear reaction data, such as cross sections and product yields. The majority of such data is published in scientific journals, which may apply charges and are accessible only to researchers in the relevant academic fields. In addition, nuclear reaction experiments require enormous cost and huge researcher effort. Therefore, it is desirable to make such data freely available through the Internet.

One such database is the EXFOR database[1)] maintained by the International Network of Nuclear Reaction Data Centres (NRDC) under the auspices of the International Atomic Energy Agency (IAEA). Another is Nuclear Reaction Data File (NRDF)[2)] developed by the Hokkaido University Nuclear Reaction Data Centre (JCPRG)[3)]. JCPRG and RIKEN Nishina Center established a collaborative research contract in 2010 to increase the availability of the nuclear reaction data produced at the RIBF. Under this collaboration, the nuclear reaction data obtained at the RIBF is compiled into the two databases above. However, including state-of-the-art experiments and physical quantities causes problems. For instance, the forthcoming electron scattering data from SCRIT is outside the compilation scope of NRDF and JCPRG on the EXFOR library at the moment. Therefore, we must extend the scope for the RIBF experiments.

In addition, the two databases have their own formats, which were defined more than forty years ago and designed for programming languages prevalent at that time, e.g., Fortran. Therefore, a new format suitable for the current situation and technology is desirable. The format must be applicable for the confirmation process of compiled data performed by experimentalists. It is also desirable for nuclear data users to read and manipulate data in the same format without detailed explanations. The format is now under development using XML technology, which is both human-readable and machine-readable. This feature is a requirement for the next-generation format to enable experimentalists to directly input data into the databases and to enable nuclear data users to retrieve them.

*1 Faculty of Science, Hokkaido University
*2 Sapporo Gakuin University Professor Emeritus
*3 Meme Media Laboratory, Hokkaido University
*4 School of Economics, Hokusei Gakuen University
*5 Department of Engineering Science, Osaka Electro-Communication University

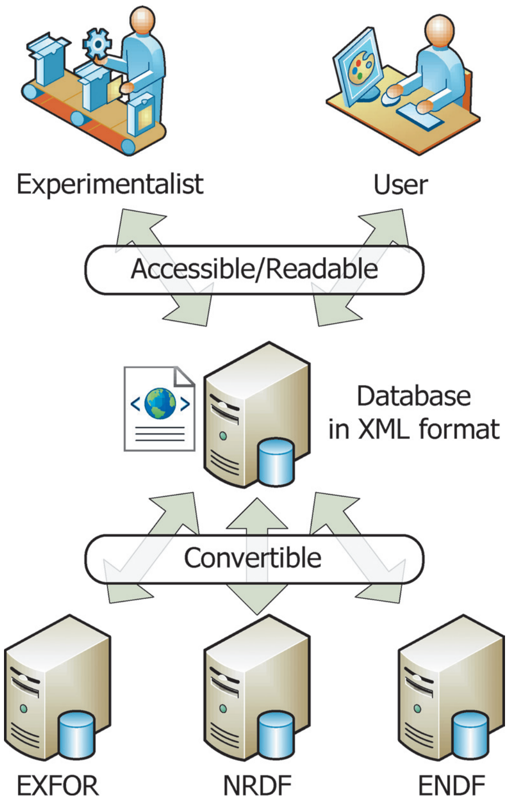

Fig. 1. Schematic of the process of accessing the database with the format under development using XML technology.

Here, we emphasize that this format does not affect other databases. The contents in the two databases above and evaluated libraries in the ENDF format, e.g. JENDL[4)], can be converted one to one nearly equivalently into the new format. Figure 1 shows a schematic of the process of accessing the database with the format under development using XML technology. The format is described in simple terms and abbreviated less for users to understand and express contents correctly. Through this format, experimentalists and users can directly access the database in which contents are converted from the databases and libraries.

References
1) http://www.jcprg.org/exfor/
2) http://www.jcprg.org/nrdf/
3) http://www.jcprg.org/
4) K. Shibata et al.: J. Nucl. Sci. Technol. 48, 1 (2011).

Development of nuclear data application software with “Webble World”

S. Ebata,[*1] A. Makinaga,[*2] and M. Aikawa[*2]

Nuclear reaction data is applicable and considerably important for public societies and various academic communities, e.g., nuclear engineering, radiation therapy, and physics. Moreover, there exists a need for means to utilize this data efficiently and conveniently by individual users. To realize a system capable of utilizing such nuclear data, we are developing application software.

There are several open tools available for searching through data. However, these tools are versatile, and not optimized for individual users. It is difficult to satisfy both universality and optimization of the tools simultaneously. Under such situations, we are motivated to create a tool customizable by “users”. In Hokkaido University Meme Media Laboratory, the IntelligentPad (IP) system has been developed to circulate and manage the knowledge of information[1]. On the IP system, data and functions are treated as objects, which are called “Pads”. Since Pads can be connected to each other, user can combine required Pads and constructs original tools for the suitable to their needs.

In the previous work, we developed a “Nuclear Reaction Data and Handling Tools for the NRDF”[2–5] and the “Charged particle nuclear reaction data retrieval system (CONTIP)”[4,5]. Here in, we plan to introduce “Webble World” to develop the current systems on the Web. If the system can be extended through Webble World, it will be independent of operating systems; it is available through the Internet and can be shared between users. The users can customize and construct an original tool for their own purposes.

The fundamental idea of Webble World is same as that of the IP system. In the Webble World, an object with a function is called a “Webble” (Fig.1), instead of a “Pad”. Webbles connected by users are conserved in the Webble World, and they are used as components for a new Webble. Webble has some slots to connect with others. For instance, if we connect an appropriate slot in the “Text Webble” with the corresponding slot in the “Display Webble” correctly, we can send the text from the former Webble to the latter and view the text on the latter. A user, however, needs to know the basic structure detail of a Webble, which is part of the tasks in the development of a Webble tool.

The proposed new system can be utilized to search, retrieve, and plot nuclear data. As objectives, an appropriate connection between the system and a database and also the plot of the retrieved data are necessary. There have already been Webbles with functions for the purposes as shown in Fig.2. The proposed system is slightly difficulty in terms of intuitiveness. Therefore, we plan to develop simple usage manual to assist in developing the tools, while also considering the needs of nuclear data users.

Hokkaido University Nuclear Data Centre (JCPRG) is developing the system for using nuclear data with Webble World. Work on making set of Webbles for searching nuclear data, and manuals to use these compound Webbles, is progressing. In addition, we are constructing a new data format using XML in order to improve the usability7 of the system.

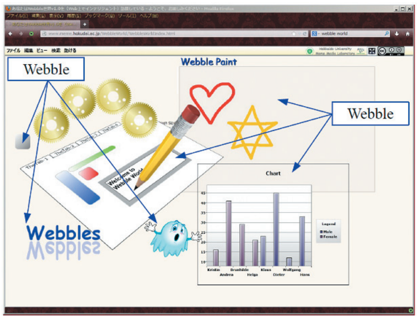

Fig. 1. Many Webbles on Webble World[6]

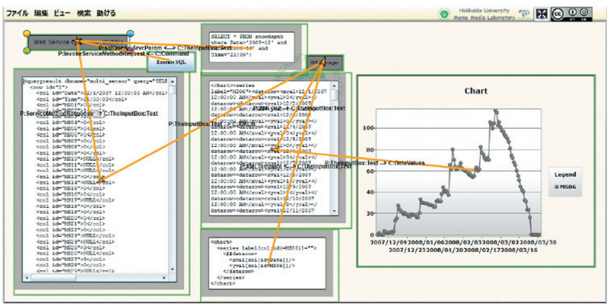

Fig. 2. Compound Webble to read and convert nuclear data, and to subsequently express them on a graph. Yellow lines show the relation between Webbles.

References
1) Y. Tanaka: Proc. of International Conference on Multimedia Information system, 299 (1991).
2) K. Kato: Genshikaku Kenkyu, Vol.39, No.5, 63 (1995).
3) M. Chiba: JCPRG Annual Report Vol.12, 27 (1998).
4) H. Masui: JCPRG Annual Report Vol.12, 56 (1998).
5) Y. Obayashi: JCPRG Annual Report Vol.13, 15 (1999).
6) Webble world, Meme media laboratory, Hokkaido Univ. “ http://cow.meme.hokudai.ac.jp/WebbleWorldPortal/

*1 Meme Media Laboratory, Hokkaido University
*2 Faculty of science, Hokkaido University

Systematic study of nuclear data for nuclear transmutation

A. Makinaga,[*1] M. Aikawa,[*1] K. Katō,[*1] A. Kohama,[*2] H. Otsu,[*2] and H. Sakurai[*2]

Long-lived fission products (LLFPs) are problematic radioactive wastes in spent nuclear fuels. Because LLFPs have long half-lives, special techniques for safe management and disposal are required. A promising way to solve this problem is "nuclear transmutation technology". The basic concept of this technology is to change LLFPs into "short-lived nuclei" or "stable nuclei" by using various kinds of particle beams from accelerators and neutron flux in nuclear reactors. Recently, the use of an accelerator-driven system (ADS) has been studied globally for this purpose. In Japan, J-PARC[1)] plans to establish ADS techniques.

From the viewpoint of nuclear data, various kinds of cross section data for LLFPs are needed to design the nuclear transmutation system reliably. Cross section data of proton, neutron, and photon induced reactions on LLFPs are required to establish more effective procedures and to estimate costs. However, as listed in Table 1, most of the experimental data are still unavailable owing to the difficulty in preparing enriched targets and in handling of activities.

Table 1. Half-lives of LLFPs and the current status of the experimental data of photon, neutron, and proton induced reactions in EXFOR[5)]. Numbers with and without parentheses indicate those of the experimental works and data points of cross sections or maxwellian averaged cross section. "-" means no experimental data in EXFOR.

Nuclei	Half-life	Status of experimental data		
	(year)	photon	neutron	proton
^{79}Se	65,000	-	-	-
^{90}Sr	29	-	5(5)	-
^{93}Zr	150,000	-	3(8)	-
^{99}Tc	210,000	-	16(428)	2(82)
^{107}Pd	6,500,000	-	2(2)	-
^{126}Sn	100,000	-	-	-
^{129}I	16,000,000	1(27)	5(5)	-
^{135}Cs	2,300,000	-	4(4)	-
^{137}Cs	30	-	3(3)	-
^{151}Sm	89	-	4(47)	-

One possible way to access the cross sections is the inverse reaction method. For example, neutron capture cross sections can be estimated with photo nuclear reactions[2–4)]. In addition, unstable LLFP beams at the RIBF facility are strong candidates to produce related nuclear data. In order to promote nuclear transmutation technology, the sharing of knowledge and information among researchers in related fields, e.g., nuclear engineering and nuclear physics, is imperative.

*1 Faculty of Science, Hokkaido University
*2 RIKEN Nishina Center

Simultaneously, management of the experimental nuclear reaction database to survey information, as shown in Table 1, and theoretical evaluations of the cross sections is also essential. Due to the lack of experimental cross sections, we performed theoretical estimation using the calculation code TALYS[6)]. Figure 1 shows the total reaction cross sections induced by protons on LLFPs. We were able to determine the cross sections of the order of barn. The impact of this result must be assessed and the cost of the transmutation of LLFPs must be estimated.

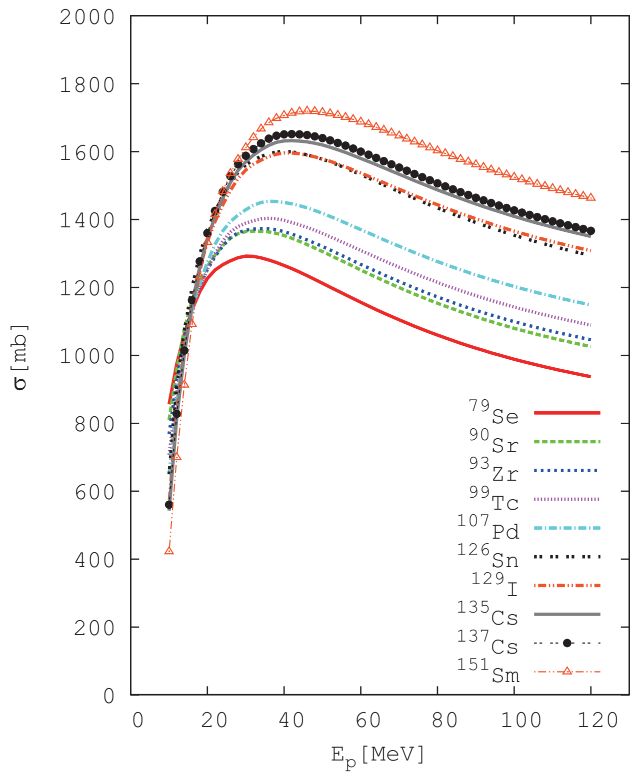

Fig. 1. Calculation of total reaction cross sections induced by protons on LLFPs by using the code TALYS.

References
1) J-PARC (http://j-parc.jp/Transmutation/ja/ads-j.html)
2) H. Utsunomiya et al.: Phys. Rev. Lett. 100, 162502 (2008).
3) A. Kimura et al.: Jour. Nucl. Sci. Technol. 49, 708 (2012).
4) A. P. Tonchev et al.: Phys. Rev. C 82, 054620 (2010).
5) IAEA-EXFOR (https://www-nds.iaea.org/exfor/exfor.htm)
6) A. J. Koning et al.: AIP Conf. Proc. 769, 1154 (2005).

JCPRG-RNC joint workshop on nuclear data

M. Aikawa,[*1] A. Makinaga,[*1] S. Ebata,[*2] K. Katō,[*1] A. Kohama,[*3] H. Otsu,[*3] and H. Sakurai[*3]

The Hokkaido University Nuclear Reaction Data Centre (JCPRG)[1)] and RIKEN Nishina Center established a collaborative research contract in 2010 to increase the availability of the nuclear reaction data produced at the RIBF. Under the collaboration, the data from the RIBF are compiled into two databases, Nuclear Reaction Data File (NRDF) and the EXFOR library. The former is the JCPRG original database and the latter is maintained by the International Network of Nuclear Reaction Data Centres (NRDC) under the auspices of the International Atomic Energy Agency (IAEA).

The major part of the compilation process has been well established during the collaboration period of four years[2)]. Furthermore, we are continuously improving the coverage and usability of the data from the RIBF. For such improvements, the first JCPRG-RNC joint workshop on nuclear data was held on August 8-9, 2013 (Fig. 1). Its purpose was to discuss and share information on the following topics:

(1) Current status and problems of compilation
(2) Experiments at RIBF
(3) Usability of nuclear data
(4) Nuclear data evaluation

In this article, we briefly report on the workshop.

As reported in another article[2)], in 2013, we compiled 13 papers, which include experimental data from the RIBF. In the compilation, however, there still remain some problems such as the compilation scope, format, and author proofs. The compilation scope depends on the purpose of each database. For instance, the incident particles compiled in NRDF and transmitted from JCPRG to the EXFOR library are restricted to charged nuclei, mesons, and photons. Therefore, at the moment, the electron scattering data with SCRIT is outside the scope. Because of its importance, however, extension of the scope to include the SCRIT data was discussed. In addition, we also discussed the necessity to compile papers published in other than peer-reviewed journals such as proceedings and annual reports. Such papers are also important from the viewpoint of completeness, but in some cases, it is risky to include results of the works under progress in the reports.

As for the format, the two databases were initiated more than 40 years ago; hence, it is difficult to format these databases using the present-day state-of-the art experiments and physical quantities. Therefore we discussed the extension of the format for the RIBF experiments. Furthermore, the format must be communicable to authors, as well as readable to nuclear data users. The format is now being constructed using the XML technology, which is both human-readable and machine-readable[3)]. It is necessary to use a human- and machine-readable technology so as to enable the experimentalists in directly inputting the data into the databases and nuclear data users in retrieving the data. Another format for a simulation code PHITS is also requested from a participant.

Fig. 1. Group photo

In addition to the format extension, there is a request to create a new user interface to connect the databases not only with nuclear data users but also with nuclear physics experimentalists. The interface makes it possible for the nuclear data users and the experimentalists to interactively and directly access the databases. We developed an interface using the Webble World technology at the Hokkaido University Meme Media Laboratory[4)].

Nuclear reaction data are useful in many application fields; e.g., nuclear physics, nuclear engineering, and radiation therapy. In the workshop, we focused on two applications, nuclear transmutation and radiation therapy. Two invited talks were devoted to these fields in terms of the nuclear data point of view. We confirm the importance of the fields.

The workshop helped the participants in understanding the present and future status of the RIKEN-JCPRG research collaboration and related nuclear data activities. We continue to exchange valuable information and requests with nuclear data users and experimentalists to improve our activity more effectively.

*1 Faculty of Science, Hokkaido University
*2 Meme Media Laboratory, Hokkaido University
*3 RIKEN Nishina Center

References
1) http://www.jcprg.org/
2) A. Makinaga et al.: in this report.
3) M. Aikawa et al.: in this report.
4) http://cow.meme.hokudai.ac.jp/WebbleWorldPortal/

4. Hadron Physics

Neutral pion production with respect to centrality and reaction plane in Au+Au collisions at $\sqrt{s_{NN}} = 200$ GeV[†]

Y. Aramaki[*1] for the PHENIX Collaboration

The suppression of high transverse momentum (p_T) hadrons in relativistic heavy ion collisions was observed at the Relativistic Heavy Ion Collider (RHIC). The phenomenon is interpreted as the energy loss of a hard-scattered parton in the hot, dense, strongly interacting quark–gluon plasma (QGP) formed in the collisions. The suppression patterns are quantified by the nuclear modification factor R_{AA} of the neutral pion as

$$R_{AA}(p_T) = \frac{1/N_{\mathrm{AA}}^{\mathrm{evt}} d^2/dp_T dy}{\langle T_{AB}\rangle \, d^2\sigma_{pp}^{\pi^0}/dp_T dy}, \qquad (1)$$

where $\sigma_{pp}^{\pi^0}$ is the production cross section of π^0 in $p+p$ collisions, $\langle T_{\mathrm{AB}}\rangle = \langle N_{coll}\rangle/\sigma_{pp}^{\mathrm{inel}}$ is the nuclear overlap function averaged over the relevant range of impact parameters, and $\langle N_{coll}\rangle$ is the number of binary nucleon–nucleon collisions computed using $\sigma_{pp}^{\mathrm{inel}}$. In this paper, the results of π^0 production and R_{AA} and its azimuthal angular dependence are presented. The results are based on the data collected in the 2007 RHIC run. The data sample is four times larger than that of Ref.[1]. Furthermore, the reaction plane detector installed in 2007 improved event-plane resolution.

Firstly, the measured π^0 invariant yields of Au+Au collisions for all centralities and for minimum bias data have been reported. These results are compared to the published η yields[2]. The measured η/π^0 ratios from minimum bias collisions for various data sets and colliding systems are compared. Although the uncertainties vary, the ratios of η/π^0 are consistent with previously published ones and are also consistent with the overlaid PYTHIA-6.131 $p+p$ calculation. The production rate of η/π^0, 0.46±0.01(stat)±0.01(syst), is constant with the centralities at $p_T > 2$ GeV/c for the same collision energy. These observations indicate that at high p_T, the fragmentation occurs outside the medium and the ratio is governed by vacuum fragmentation.

Secondly, the nuclear modification factor R_{AA} of π^0 is compared to the previous result and the charged hadron R_{AA} at the LHC energy. The yields of π^0 are suppressed by a factor of 5, as in earlier measurements; however, with the improved statistical and systematic uncertainties, the significant rise of R_{AA} as a function of p_T with a slope $d\mathrm{R_{AA}}/\mathrm{dp_T}$ of $0.0106\pm^{0.0034}_{0.0029}$ (GeV/c)$^{-1}$ in central collisions has been observed for the first time at the RHIC energy. In comparison with the charged hadron R_{AA} observed in $\sqrt{s_{NN}} =$ 2.76 TeV Pb+Pb collisions at the Large Hadron Collider (LHC) (ALICE experiment)[3], the two data sets for RHIC and LHC appear to be similar for the entire p_T range of 5–20 GeV/c. However, the RHIC and LHC are different in terms of colliding energy, resulting in an approximate increase by a factor of 2 increase in the parton density at the LHC[4]. On the basis of the slope of the p_T distribution and R_{AA}, the average fractional momentum loss ($\mathrm{S_{loss}}$) of π^0 is deduced. If one assumes that the fragmentation function of the parton after energy loss is unchanged, the $\mathrm{S_{loss}}$ can be interpreted as the average fractional energy loss of the initial parton. The calculated $\mathrm{S_{loss}}$ shows a decrease with increasing p_T at central collisions. In comparison with the $\mathrm{S_{loss}}$ value of the ALICE charged hadron measurement ($\mathrm{S_{loss}} \sim 0.3$), the $\mathrm{S_{loss}}$ at the PHENIX π^0 measurement below 10 GeV/c ($\mathrm{S_{loss}} \sim 0.21$) is about 30% lower value.

To study the path-length dependence of the suppression, the π^0 yield is also measured at different azimuthal angles with respect to the event plane; a strong azimuthal-angle dependence of the π^0 R_{AA} is observed. The data are compared to theoretical models of parton energy loss as a function of the path length L in the created medium. While all models considered describe the ϕ-integrated R_{AA} adequately, the pQCD-based calculations, in which the energy loss depends on the path length as L^2, fail to describe the differential $R_{AA}(\Delta\phi)$. The data obtained using a hybrid model[5] that utilizes pQCD for hard interactions and anti-de-Sitter space/conformal field theory[6] (AdS/CFT) for soft interactions is also compared to the measured data, and were able to obtain an adequate fit. Since the energy loss in this model is proportional to L^3, the data require an energy loss with a power greater than 2, as given by models in which the soft interactions with the medium are strongly coupled. Therefore, one is led to the tentative conclusion that strong coupling plays an important role in parton energy loss in the medium.

References

1) A. Adare *et al.* (PHENIX Collaboration): Phys. Rev. Lett. **101**, 232301 (2008).
2) A. Adare *et al.* (PHENIX Collaboration): Phys. Rev. C **82**, 011902 (2010).
3) K. Aamodt *et al.* (ALICE Collaboration): Phys. Lett. B **696**, 30 (2011).
4) W.A. Horowitz and M. Gyulassy: Nucl. Phys. A **872**, 265 (2011).
5) C. Marquet and T. Renk: Phys. Lett. B **685**, 270 (2010).
6) J.M. Maldacena: Adv. Theor. Math. Phys. **2**, 231 (1998).

† Condensed from the article in Phys.Rev.C **87**, 034911 (2013)

*1 RIKEN Nishina Center

Study of medium properties with two particle correlations in d+Au collisions at $\sqrt{s_{NN}} = 200$ GeV at PHENIX

C.-H. Chen *1

Two-particle correlation is a powerful method to study jet-medium interaction and the collective motion of particles. Interesting new results are revealed by LHC data when $p+p$ collisions with two-particle correlations are studied. Upon observing low-multiplicity $p+p$ collisions at 7 TeV, the $\Delta\eta$-$\Delta\phi$ correlation function is, as expected, found to have a single nearside peak at $\Delta\eta \approx 0$ and $\Delta\eta \approx 0$ and an away-side peak at $\Delta\phi \approx \pi$ along $\Delta\eta$. For high-multiplicity $p+p$ collisions at the same energy, an enhancement along $\Delta\eta$ at $\Delta\phi \approx 0$, or a "ridge" structure, is observed [1]. Finally, p+Pb collisions at 5.02 TeV with similar multiplicity selection, exhibit ridge structure as well [2].

This long-range correlation along the $\Delta\eta$ direction at $\Delta\phi \approx 0$ has been observed at RHIC previously. In two-particle $\Delta\eta$-$\Delta\phi$ correlations in central Au+Au collisions, an enhancement along $\Delta\eta$ at $\Delta\phi \approx 0$ has been observed [3]. It has also been found that this long-range correlation extends to as far as $\Delta\eta \approx 4$ [4]. Similar phenomena has been confirmed in Pb+Pb collisions at LHC [5].

This long-range correlation along $\Delta\eta$, or "ridge", was originally believed to exist only in central Au+Au collisions, but now has also been observed in $p+p$ and p+Pb collisions in LHC. The fact that the ridge appears in both system leads to the question of whether the ridge observed in $p+p$ and p+Pb in LHC is the same as that seen in heavy-ion collisions at RHIC.

Triggered by the new results from LHC, it is important to investigate whether a similar effect exists in d+Au collisions at RHIC. Studying d+Au collisions will certainly provide new insights into the p+Pb data at LHC. First, d+Au is collided at 200 GeV, which is considerably smaller than p+Pb at 5.02 TeV at LHC. Further, in d+Au collisions, the two nucleons in the deuteron may make the initial colliding geometry more complicated than in p+Pb collisions.

At PHENIX, it is possible to measure the two particle correlations with a large η gap by correlating a charged hadron in the central arm spectrometer ($|\eta| < 0.35$) and the energy cluster in the Muon Piston Calorimeter (MPC, $3.1 < |\eta| < 3.9$). A large $\Delta\eta$ separation can strongly suppress the non-flow contribution, and thus the remaining correlation should reflect the properties of the produced medium.

Since d+Au is an asymmetric system, in central d+Au collision, the multiplicity distribution, or $dN/d\eta$, is asymmetric along the direction of η [6], where the multiplicity is larger in the Au-going direction than in the d-going direction. Therefore a comparison of the correlation in d+Au to $p+p$, might reveal some new properties in d+Au collisions.

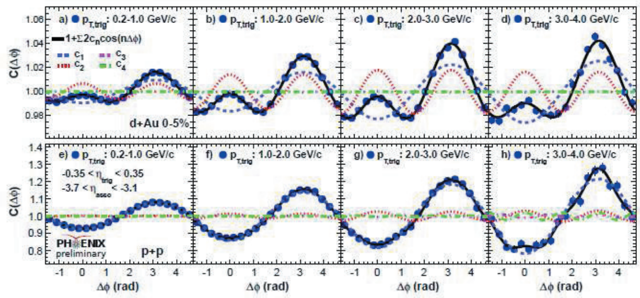

Fig. 1. The unidentified charged hadron in the central arm correlated with energy clusters in MPC in the Au-going direction ($-3.9 < \eta < -3.1$) in d+Au and $p+p$ collisions.

Figure 1 depicts the correlation function of the charged hadron in mid-rapidity correlated with the energy cluster in MPC in the Au-going direction in the most central d+Au collisions (0-5%) for various hadron p_T. This is compared with the same correlation function measured in $p+p$ collisions. In $p+p$ collisions, the correlation function has a local minimum at $\Delta\phi \approx 0$. In the case of d+Au correlation functions, the nearside shape is significantly different from the shape in $p+p$. Instead of showing a local minimum, it is either peaked at $\Delta\phi \approx 0$, or there is a strong correlation at $\Delta\phi \approx 0$.

We further measure the Fourier coefficients of the correlation functions. In $p+p$, the correlation functions are well described by c_1, which could be understood as conservation of momentum with very little contribution from other harmonics. In central d+Au collisions, we observe a significant contribution not only from c_1, but also c_2. This indicates that in central d+Au collisions, something similar to elliptic flow in heavy ion collisions has been seen.

References

1) V. Khachatryan et al., *J. High Energy Phys.* **09** (2010) 091
2) S. Chatrchyan et al., *Phys. Lett. B* **718** (2013) 795
3) B. Abelev et al., *Phys. Rev. C* **80** (2009) 064912
4) B. Alver et al., *Phys. Rev. Lett.* **104** (2010) 062301
5) S. Chatrchyan et al., *J. High Energy Phys.* **07** (2011) 76
6) B. Beck et al., *Phys. Rev. C* **72** (2005) 031901

*1 Riken Brookhaven Research Center, Brookhaven National Laboratory

Status of CuAu flow measurement

H.Nakagomi [*1] for the PHENIX Collaboration

The quark-gluon plasma(QGP) is a phase of matter in quantum chromodynamics (QCD). This phase is predicted to exist at high temperature and high density. Currently at RHIC and LHC, QGP is created by colliding nuclei. In the heavy-ion collistions, azimuthal anisotropy of produced particle emmission exists. Collectively, this anisotropy is a quite important probe to understand the properties of QGP because this collectivity is sensitive to initial collision geometry and early time evolution. The strength of anisotropic flow is expressed as $v_n(n = 1, 2, 3)$ and the azimuthal distribution of emitted particles $dN/d\phi$ is expressed as follows using v_n .

$$\frac{dN}{d\phi} \propto 1 + \sum_{n=1} 2v_n \cos(n[\phi - \Psi_n]), \quad (1)$$

where $v_n =< \cos(n[\phi - \Psi_n]) >$ with $n = 1, 2, 3..., \phi$ is the transverse angle of an emitted particle and Ψ_n is an event plane. The event plane is defined as the average angle of all emmitted particles that are detected. Thus even-order flow(v_2) which is called elliptic flow has been studied. These studies provide initial spatial conditions and the information of specific viscosity η/s of QGP in the hydrodynamic. The anisotropic flow is originated from initial spatial anisotropy. The initial spatial anisotropy lead to anisotropic collectivity in momentumu space. However, the hydrodynamic model does not completely agree with experimental data completly. There is still uncertainty in the theoretical model. Recently, the fluctuation of initial spatial anisotropy was focused upon. The fluctuation of eccentricity can lead to initial spatial triangularity. The initial spatial triangularity from the fluctuation is the origin of v_3 which is triangular flow strength. This Fourier coefficient is important to determine the initial state anisotropy and η/s.

In 2012, Cu+Au collisions were investigated at RHIC. Such asymmetric collisions of heavy nuclei can provide different participant profiles through symmetric collisions of heavy nuclei such as Au+Au and Cu+Cu because of uniqe initial geometry. In symmetric collisions, initial geometry fluctuations lead to odd harmonics. However in Cu+Au collisions such an uniqe initial geometry could lead to non-zero odd harmonics. Cu+Au v_3 could come from such a initial geometrical triangularity, rather than fluctuation. Therefore, the measurement of Cu+Au non-zero harmonics is quite important to determine initial conditions.

In this paper, we report the current status of v_2,v_3 measurement at midrapidity in Cu+Au collisions. In order to measure v_2, v_3, an event-plane method is applied. To apply the event-plane method, the following relation between true v_n^{tr}, Ψ_n^{tr} that could not be measured experimentally and observed v_n, Ψ_n is needed.

$$v_n^{tr} = v_n^{ob} / < \cos(n[\Psi_n - \Psi_n^{tr}]) >, \quad (2)$$

where $< \cos(n[\Psi_n - \Psi_n^{tr}]) >$ correspond to the event-plane resolution. The event plane is determined by

$$Q_{xn} = \sum_{i=1} w_i \cos(n\phi_i), Q_{yn} = \sum_{i=1} w_i \sin(n\phi_i), \quad (3)$$

$$\Psi_n = \tan^{-1}(Q_{yn}/Q_{xn})/n, \quad (4)$$

where Ψ_n is the measure of the event plane and $Q_{x(y)n}$ is the projection of Ψ_n to the x(y) axis. w_i is the weight and ϕ_i is the angle of a particle.

In this analysis, the event plane is determined by beam beam counter(BBC) and a forward silicon vertex detector(FVTX). These detectors are located at foward/backward rapidity. In order to measure v_n precisely, there should be rapidity gap between the regions of measurement of v_n and Ψ_n because if are not separeted these regions, v_n would include a non-flow contribution. This non-flow is a correlation that dose not originate from the event plane. Thus, it is better to choose the detector that is located at forward/backward rapidity as the event plane measrement detector.

Figure1 shows the event plane resoluiton of BBC and FVTX for Ψ_2. In the central region $(0-20\%)$, the resolution of FVTX South resolution is larger than that of FVTX North. This behavior is also found in BBC. This behavior originate from the multiplicity that is used to measure the event plane and strength of v_2. Currently, I have calibrated Ψ_3 and am working on calculating Ψ_3 resolution.

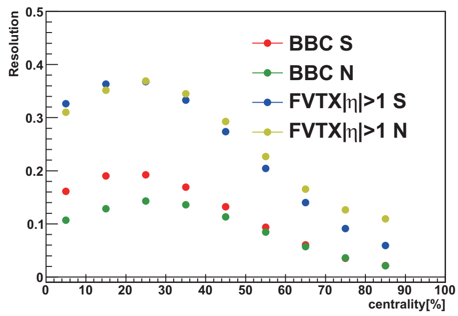

Fig. 1. FVTX/BBC Ψ_2 resolution as a function of centrality.

References
1) PRL 107, 252301 **40**, L1299 (2011).
2) arXiv:1111.5095v1 Lett. **2011**
3) arXiv:1210.5570v2 [nucl-ex] 8 Nov 2012

[*1] Univ. of Tsukuba

Study of direct photon azimuthal anisotropy in $\sqrt{s_{NN}}$=200GeV Au+Au in RHIC-PHENIX experiment

S. Mizuno*1 for the PHENIX collaboration

High energy heavy ion collision experiments have been performed since 2000 at the Relativistic Heavy Ion Collider (RHIC), in order to study properties of quark-gluon plasma (QGP). Direct photon, which includes all sources from various processes except one from hadron decay, has been measured as a powerful tool. It is expected not to interact strongly with QGP, thus providing information on when it is created. Furthermore, because direct photons are created in various processes during the entire space-time history of collisions, they provide different probes from all stages, for example, initial hard scattering, thermal radiation from QGP, and bremsstrahlung from partonic energy loss. Photons originating from various sources are measured inclusively in the experiment, so there are dificulities in measuring photons while identifying their sources. To circumvent the difficulty, we measure the direct photon azimuthal anisotropy.

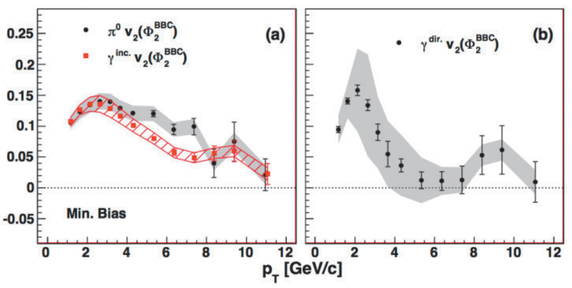

Fig. 1. v_2 as a function of p_T of π^0(Black) and inclusive photon(Red) in the left plots. Direct photon v_2 as a function of p_T is in the right plots.[1)]

Azimuthal anisotropy is defined as a relative amplitude of anisotropic azimuthal distribution with respect to the reaction plane. To quantify the anisotropy, Fourier series is used for the azimuthal distribution of the number of emitted particles.

$$dN/d\phi = N_0[1 + \sum 2v_n cos\{n(\phi - \Psi_n)\}] \quad (1)$$

$$v_n = < \cos\{n(\phi - \Psi_n\} > \quad (2)$$

where ϕ is the azimuthal angle of photons, and v_n and Ψ_n are the strength and direction of the n^{th}-order harmonic azimuthal anisotropy, respectively. The second component (v_2) is referred to as elliptic flow and is measured for various dependences (e.g. p_T, particle species). It provides the collective properties of the high density matter, possibly QGP, that interacts and expands hydro-dynamically under given initial conditions. In addition, v_2 is found to be affected by the initial geometry.

It is found that direct photon v_2 is close to zero in the high p_T region, although π^0 has finite v_2. This is consistent with the expectation that prompt photons from intial hard scattering are dominant at high p_T. It is also found that direct photon v_2 is almost the same as π^0 at low p_T, where thermal photons are thought to be dominant. The precise reason of this large v_2 is not well understood yet.

Higher order azimuthal anisotropy $v_n(n > 2)$ is considered to be more sensitive to initial geometry and QGP shear viscosity η/s (the ratio of shear viscosity *eta* to entropy density s) under expansion. Hence, $v_n(n > 2)$ has been actively studied recently, and it is considered to be important for calculating the initial state model and the viscosity of QGP. The results of $\pi^{\pm}$, $K^{\pm}$, and $p\bar{p}$ are shown in Fig. 2. It is found that $v_n(n > 2)$ also has collective motion.

The ongoing studies on direct photon $v_n(n > 2)$ could help in understanding the puzzle of direct photon v_2.

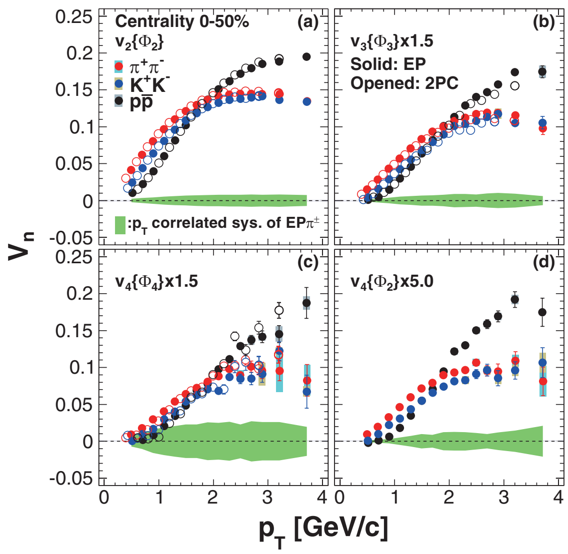

Fig. 2. $\pi^{\pm}$,$K^{\pm}$, and $p\bar{p}$ (a) v_2, (b) $v_3 \times 1.5$, (c) $v_4 \times 1.5$, and (d) $v_4(\Psi_2) \times 5.0$ as functions of p_T. The green band indicates p_T correlated systematic uncertainties.

References

1) A. Adare et al.: P.R.L. 109, 122302 (2012)

*1 University of Tsukuba

Result of the energy scan program at RHIC-PHENIX

Y. Ikeda*1

1 Introduction

According to quantum chromodynamics, quarks and gluons are confined with strong forces in hadrons. It is expected that they are de-confined at a high temperature or high density[1,2]. This is called Quark Gluon Plasma (QGP), which may have existed in the early universe according to the big bang theory or in the core of a neutron star[3,4]. Experimentally, it is formed by relativistic heavy ion collision with a collider. The system geometry is elliptical at the first stage of a non-central collision. The geometrical anisotropy generates the asymmetry in the yield of particles as a function of the azimuthal angle with respect to the event plane of an event. The azimuthal anisotropy indicates an interaction with a short mean free path of partons in a hot dense medium. It also gives information about the initial state and its expansion, possibly through the QGP phase. The magnitude of azimuthal anisotropy of particle emission is measured as the second term of a Fourier series (v_2),

$$dN/d\phi = N(1 + 2v_2 \cos 2(\phi - \Psi)), \quad (1)$$

where N is number of the particle emissions, ϕ is azimuthal angle of the particle emission [rad], and Ψ is the event plane angle [rad].

2 Quark number scaling of hadron v_2

The measured large v_2 of hadrons is an indicator of the small mean free path in the hot dense medium and a hydrodynamic model with a low viscosity reproduces the collective behavior of the particles[5,6]. Meanwhile, the v_2 value scales with the constituent quark number and is independent of the particle mass. It indicates that the flow of hadrons is built up by the flow of quarks in the QGP according to the quark coalescence model. The v_2 of hadrons is the sum of the v_2 of combined partons in the quark coalescence model as follows,

$$v_2^{hadron}(p_T) = n v_2^{parton}(\frac{p_T}{n}), \quad (2)$$

where n is the number of partons in hadrons[7,8]. The experimental result of quark number scaling of v_2 suggests the quark level collectivity in the hot dense matter and the quark coalescence mechanism forms hadrons from quark matter via quark-gluon phase transition in the Au+Au $\sqrt{s_{NN}}$ = 200 GeV collision at RHIC-PHENIX[9].

The study of v_2 with the energy scan of heavy ion collision may provide information about the threshold behavior of collision energy, if the quark number dependency is an indicator of a QGP phase. A new reaction plane detector was installed to measure the v_2 of hadrons with an enhanced event plane resolution at the RHIC-PHENIX experiment[10]. The higher resolution allows us to study v_2 at low energy collisions, which have low statistics of particles.

3 Results of the energy scan program at RHIC-PHENIX

The v_2 of π^+ π^-, K^+, K^-, p, $\bar{p}$ and d were measured in the Au+Au $\sqrt{s_{NN}}$ = 39 and 62 GeV collisions[11]. The number of constituent quark scaling of the v_2 of hadrons is mostly established in these energies (fig.1 shows the results of 39 GeV). Considering this as an indication of the QGP phase, the threshold energy of the QGP-hadron phase transition would be lower than $\sqrt{s_{NN}}$ = 39 GeV. In contrast, particle (especially p) v_2 differs from anti-particle v_2 in these lower beam energy collisions. It could be given by interactions such as p-$\bar{p}$ annihilation in the high baryon density caused by the baryon stopping in the low energy collision.

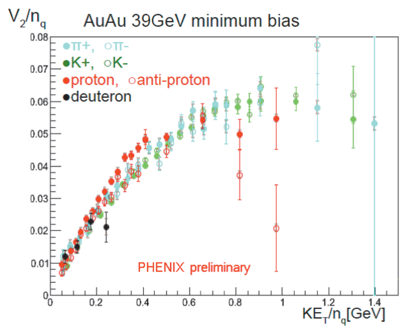

Fig. 1. The scaled hadron v_2 as a function of $KE_T = m_T - m$ with the number of constituents quarks in the Au+Au $\sqrt{s_{NN}}$ = 39. The KE_T scale cancels the p_T shift by the collective behavior.

*1 RIKEN Nishina Center

References

1) F.Karsch: in:Lecture Notes in Physics **583**, 209 (2002).
2) F. Karsch et. al.: Phys. Lett. B **478**, 447 (2000).
3) E.V.Shuryak: Phys. Rep. **61**, 71 (1980).
4) J.C.Collins et. al.: Phys. Rev. Lett. **34**, 1353 (1975).
5) P. F. Kolb: Heavy Ion Phys. **21**, 234 (2004).
6) S. S. Adler et al.: PRL**91**, 182301 (2003).
7) R.J. Fries et. al.: PRL**90**, 202303 (2003).
8) R.J. Fries et. al.: PRC**68**, 044902 (2003).
9) A. Adare et al.: PRC**85** 064914 (2012).
10) E. Richardson et al.: NIM A**636** 99 (2010).
11) Y. Ikeda for the PHENIX collaboration: SQM, Birmingham (2013).

Search for the strong magnetic field via di-electron measurement in heavy-ion collisions at RHIC-PHENIX

T. Hoshino[*1,*2] for the PHENIX collaboration

A strong magnetic field is expected to be created in high-energy heavy-ion collisions. The intensity of the magnetic field created in the collisions at BNL-RHIC is estimated to reach about 10^{14} teslas. The field creation can be considered to be due to the effect of both of collision participants and collision spectators and the field direction is perpendicular to the reaction plane (Fig. 1).

The possibility of field creation was presented first about 35 years ago[1]. In recent years, this began to attract attention because achieving an increase in the field intensity with increasing energy of the collider is well beyond the critical field of an electron ($eB_c = m_e^2$). The time evolution of this field is also calculated based on theories. According to the theoretical calculation, the field intensity decreases rapidly, but maintains for a few fm/c above the critical magnetic field of an electron[2]. Chiral magnetic effects and other interesting effects, such as non-linear QED effects, are discussed based on the theories to be caused by the strong field. From experimental studies, charged particle asymmetry with respect to the reaction plane[3] and direct-photon azimuthal anisotropy[4] suggest the presence of the strong field. However, the field itself is yet to be directly detected experimentally.

Direct detection of the field in high-energy nuclear collisions is a very important issue. Detection of the strongest field in the universe has a major impact in itself. Further, the observation of the field leads to the confirmation of the chiral magnetic effect. Moreover, there is a possibility to verify non-linear quantum electrodynamics effects such as vacuum-birefringence and the decay of real photons.

Direct photons/virtual photons are good candidates for probing the field detection, because they are not affected by the strong interaction and they maintain the initial information. Pi0 decay photons/Dalitz-decay electron pairs are candidates for control probes because they are from the later time. Combinatorial pairs from mixed events could also be used as a control probe.

According to the calculation of photon vacuum polarization in a strong magnetic field, the production rate of di-electrons from virtual photon decay depends on the field direction[5]. Since PHENIX has a good electron-identification capability, we focus on virtual photon decays with a dependence on the magnetic field direction. By using electron pairs from virtual-photon decays as the probe, polarization measurement is possible without the using of a polarimeter.

*1 RIKEN Nishina Center
*2 Department of Physical Science, Hiroshima University

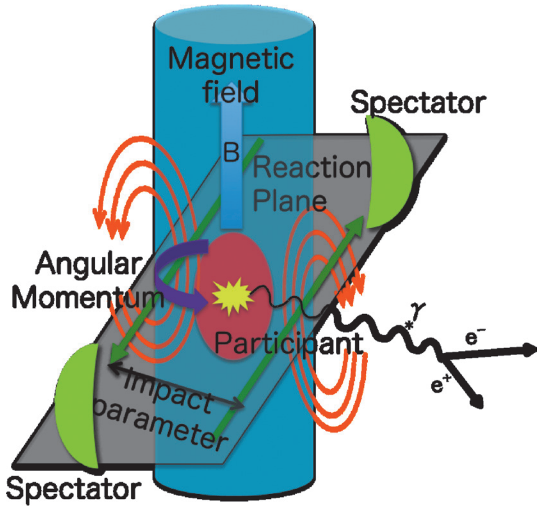

Fig. 1. Schematic image of the magnetic field creation in heavy-ion collision

We are using the $\sqrt{s_{NN}} = 200$ GeV Au+Au collisions data set collected in 2004 at the RHIC-PHENIX. Electrons and positrons are identified by RICH and EMCal, and momentum is decided by Drift Chamber and Pad Chamber. Global variables, z-vertex, centrality and reaction plane, are decided by Beam-Beam Counter.

We select two di-electron invariant-mass region, $0.12 < m_{ee} < 0.3$ GeV/c^2 and $0 < m_{ee} < 0.1$ GeV/c^2. The first region contains virtual photon components, and thus, this region is expected to contain the signal. The second is dominant Dalitz-decay di-electron, which has no-physics effect to polarization. The polarization is measured using the angular distributions of di-electron with a correlation to the reaction plane, as a function of centrality, because it depends on the strength of the created field. Now, we focus on polarizations of Dalitz-dacay pairs and combinatorial pairs, which is important for background subtraction. We discuss what kind of background is included, how to subtract backgrounds, and how to extract the signal.

References

1) B.Muller et al.: Phys. Rev. Lett. 36, 517 (1976)
2) D.E.Kharzeev et al.: Nucl. Phys. A 803, 227 (2008)
3) B.I.Abelev et al. (STAR): Phys. Rev. Lett. 103, 251601 (2009)
4) A.Adare et al. (PHENIX): Phys. Rev. Lett. 109, 122302 (2012)
5) K.Ishikawa et al.: Int. J. Mod. Phys. A28, 1350100 (2013)

High p_T hadron production in Au+Au collisions at $\sqrt{s_{NN}} = 200$ GeV

Y. Akiba,[*1] R. Akimoto,[*1] H. Asano,[*1] S. Bathe,[*1,*2] S. Baumgart,[*1] K. Boyle,[*1] J. Bryslawskyj,[*2] C-H. Chen,[*1] L. Ding,[*3] A. Enokizono,[*4] S. Esumi,[*5] T. Hachiya,[*1] S. Horiuchi,[*5] J. Koster,[*1] K. Kurita,[*4] M. Kurosawa,[*1] A. Lebedev,[*3] M. McCumber,[*6] H. Nakagomi,[*4] R. Nouicer,[*1] C. Ogilvie,[*3] Z. Rowan,[*2] H. Sako,[*1] S. Sato,[*7] A. Shaver,[*3] M. Shimomura,[*1,*3] M. Stepanov,[*8] A. Taketani,[*1] M. Wysocki,[*9] and the PHENIX VTX group

One of the most significant discoveries at RHIC has been the suppression of high p_T hadrons in central Au+Au collisions[1]. In pQCD models, the data constrain the transport coefficient, $\hat{q}$[2].

Currently the best measurement at RHIC is achieved by neutral pions[3]. For charged hadrons, the measurement is limited by a background from photon conversions and random tracks, both mimicking high transverse momentum tracks.

With the recent addition of a Silicon Vertexing Tracker (VTX)[4] to PHENIX, it is possible to significantly reject this background and to extend hadron measurement to a higher p_T. Tracks need to be reconstructed with a small Distance of Closest Approach (DCA) of the track projection on the primary vertex. Real tracks are reconstructed with zero DCA convoluted with the detector resolution, whereas fake tracks can have any DCA.

Figure 1 shows the raw DCA distribution in the transverse plane. A peak is observed around zero DCA, which is dominated by real tracks, above a background of random tracks and weak decays.

Figure 2 shows the transverse momentum distribution of tracks with and without the small-DCA requirement. At high p_T, the spectrum without the DCA requirement appears unphysically flat, whereas the spectrum with the requirement continues to fall. This observed behavior suggests that the DCA requirement successfully suppresses the background.

These plots indicate the potential of this method. Recently, significant progress has been made in rejecting misfunctioning parts of the detector and improving the tracking algorithm. The analysis is still in progress.

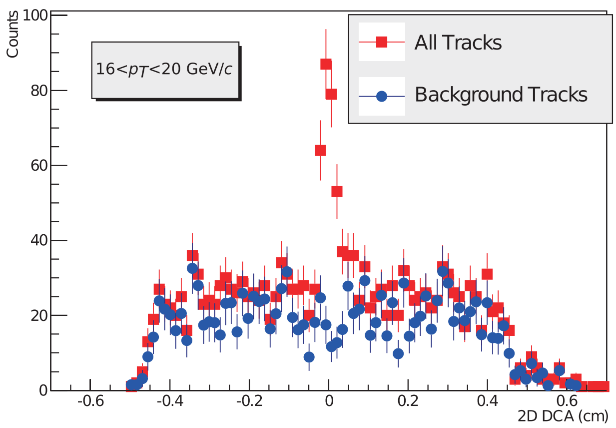

Fig. 1. Raw DCA distribution in the transverse plane. The peak around zero DCA is dominated by real tracks. The underlying background comes from random tracks and weak decays. The fall-off at ± 0.4 cm is an artifact of the tracking algorithm.

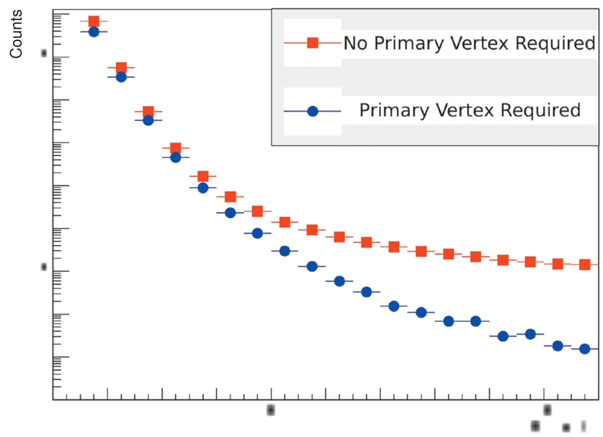

Fig. 2. Uncorrected hadron p_T spectra for different purity cuts. At high p_T, the spectrum without the DCA requirement appears unphysically flat while the spectrum with the DCA requirement continues to fall.

*1 RIKEN Nishina Center
*2 Department of Natural Sciences, Baruch College, CUNY
*3 Department of Physics & Astronomy, Iowa State University
*4 Department of Physics, Rikkyo University
*5 Institute of Physics, University of Tsukuba
*6 Department of Physics, University of Colorado, Boulder
*7 Advanced Science Research Center, Japan Atomic Energy Agency
*8 Physics Department, University of Massachusetts, Amherst
*9 Physics Division, Oak Ridge National Laboratory

References

1) K. Adcox *et al.* [PHENIX Collaboration]; Phys. Rev. Lett. 88, 022301 (2002).
2) A. Adare *et al.* [PHENIX Collaboration]; Phys. Rev. C **77**, 064907 (2008).
3) A. Adare *et al.* [PHENIX Collaboration]; Phys. Rev. C **87**, no. 3, 034911 (2013).
4) A. Taketani *et al.* [PHENIX Collaboration]; Nucl. Instrum. Meth. A **623**, 374 (2010).

Status of the charm and bottom measurement with PHENIX-VTX

T. Hachiya,[*1] A. Adare,[*2] Y. Akiba,[*1] R. Akimoto,[*1] H. Asano,[*1] S. Bathe,[*1] J. Bryslawskyj,[*3] A. Dion,[*4] T. Koblesky,[*2] M. Kurosawa,[*1] M. McCumber,[*5] D. McGlinchey,[*2] T. Moon,[*1] H. Nakagomi,[*1] R. Nouicer,[*6] H. Sako,[*7] S. Sato,[*7] M. Shimomura,[*8] T. Sumita,[*1] A. Taketani,[*1] H. Torii,[*1] and the PHENIX VTX group

Heavy quarks (bottom and charm) are one of the clean probes for studying properties of hot dense medium created in the high energy heavy ion collisions. Due to their large mass, heavy quarks are mainly produced though the initial hard scattering. Once produced, the heavy quarks traverse and interact with the medium. Therefore, the modification of their production yield and emission angle reflects the medium properties.

The PHENIX experiment[1)] installed a silicon vertex tracker (VTX)[2)] and collected a large amount of $p+p$, Au+Au and Cu+Au collision events at $\sqrt{s_{NN}} =$ 200 GeV successfully in the past three years. The VTX provides a clear separation of charm and bottom quarks via measurement of distance of the closest approach of electrons relative to the collision vertex (DCA).

The preliminary results of the fraction of $(b \to e)/(b \to e + c \to e)$ and the azimuthal anisotropy of charms were already reported[3,4)]. In order to improve the DCA measurement, we recently updated the following items in the analysis:

(1) Hot and dead channel status on the sensor:
The bad channels that have extremely higher and lower hit rate were masked. In addition, the unstable channels that changed the hit rate by time were also newly masked. Figure 1 shows the map of the hot and dead channels for a readout chip. The colored channels indicate the bad channels caused by the faulty bump bonding between the sensor and the readout chip.

(2) Parameter tuning of the track association between the VTX hits and the track measured in the central arm:
The angular resolution of tracks measured in the central arm was an input for the χ^2 calculation of the track fitting between VTX hits and the track. This resolution was updated to be realistic (1m rad.). The blue histogram and black curve in Fig. 2 show the χ^2 distribution for the reconstructed proton in simulation and the ideal χ^2 function. The histogram suitably reproduces the ideal curve.

(3) DCA decomposition method:
The charm and bottom yields were obtained by fitting the measured DCA distribution with the DCA templates of charms and bottoms[3)]. The DCA templates are correlated with the shape of their transverse momentum (p_T) distribution since the DCA is determined by convolution of two effects: the decay length of the parent particle and p_T kick relative to the parent momentum. In order to include this effect, we fit both the DCA and p_T distribution of electrons simultaneously. We are testing the several methods to decompose charm and bottom components.

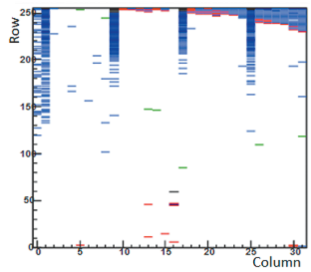

Fig. 1. Hot and dead channels for a readout chip. The colors indicate the bad statuses mostly due to faulty bump bonding.

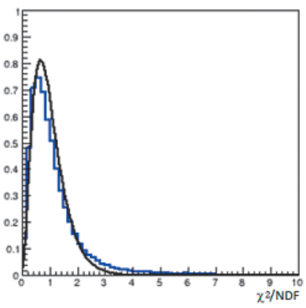

Fig. 2. The χ^2 distribution of proton in simulation. The histogram suitably reproduces the ideal curve.

We are working to complete the Au+Au and $p+p$ analysis for publication. The Cu+Au analysis is also in progress and we aim to show the first Cu+Au result in 2014.

*1 RIKEN Nishina Center
*2 University of Colorado
*3 City University of New York
*4 Department of Physics and Astronomy, Stony Brook University
*5 Oak Ridge National Laboratory
*6 Brookhaven National Laboratory
*7 Japan Atomic Energy Agency
*8 Iowa State University

References
1) K. Adcox et al.: Nucl. Inst. Meth. A **499**, 469 (2003).
2) R. Nouicer et al.: Proc. of Sci. (Vertex2007), 042 (2007).
3) R. Akimoto et al.: RIKEN Accel. Prog. Rep. 46, 60 (2013).
4) M. Kurosawa et al.: RIKEN Accel. Prog. Rep. 46, 61 (2013).

Measurement of D^0 in $p+p$ collisions at $\sqrt{s}$ = 200 GeV using the Silicon Vertex Tracker at RHIC-PHENIX

T. Moon,[*1,*2] A. Adare,[*3] Y. Akiba,[*1] R. Akimoto,[*1,*4] H. Asano,[*1,*5] S. Bathe,[*1] J. Bryslawskyj,[*6] A. Dion,[*7] T. Koblesky,[*3] T. Hachiya,[*1] M. Kurosawa,[*1] M. Mccumber,[*8] D. Mcglinchey,[*3] H. Nakagomi,[*1,*9] R. Nouicer,[*1] H. Sako,[*1] S. Sato,[*1] M. Shimomura,[*10] T. Sumita,[*1] A. Taketani,[*1] H. Torii,[*1] and the PHENIX VTX group

Measurements of the D^0 meson (and its charge conjugate) via the hadronic channel $D^0 \to K^- + \pi^+$ ($\bar{D}^0 \to K^+ + \pi^-$) in $p+p$ collisions provide important information. First, the total cross section of charm production can be obtained and compared with perturbative Quantum Chromodynamics (pQCD) calculations. Second, it provides the baseline measurement of charm production in order to understand the properties of the hot and dense QCD medium, created by heavy ion collisions, by comparing D^0 production in $p+p$ and Au+Au collisions.

Direct reconstruction of the D^0 meson is challenging because of its short decay lengths, $c\tau = 122.9\mu m$, and a very large combinatorial background. However, the Silicon Vertex Tracker (VTX),[1),2)] installed into the PHENIX experiment during the 2011 run, can separate the primary vertex and the $D^0 \to K^- + \pi^+$ decay vertex with high resolution. This can substantially eliminate the combinatorial background.

The strategy to extract D^0 production yield is based on an invariant mass analysis of all the possible pairs of two oppositely charged tracks. The invariant mass, $M_{K\pi}$, is defined as follows.

$$M_{K\pi} = \sqrt{(E_+ + E_-)^2 - (\overrightarrow{p}_+ + \overrightarrow{p}_-)^2} \quad (1)$$

$$E_\pm = \sqrt{m_\pm^2 + \overrightarrow{p}_\pm^2} \quad (2)$$

In the above equations, the subscript + or − indicates the charge of the track. We assigned the mass, $(m_+, m_-) = (m_K, m_\pi)$ or (m_π, m_K).

In the absence of any ion pair selection, the signal to combinatorial background ratio would be too small to extract the D^0 signal in the invariant mass distribution. It is, therefore, mandatory to select tracks on the basis of kinematical and geometrical considerations.

One of the quantities that is useful for track selection is the distance of the closest approach (DCA) of the reconstructed track to the primary vertex in the plane transverse to the beam direction. DCA of the daughter track, K^- or π^+, of the D^0 meson is larger than that of primary track, which comes from the primary vertex. Therefore, we can reject those primary tracks used in the invariant mass analysis by applying a DCA cut.

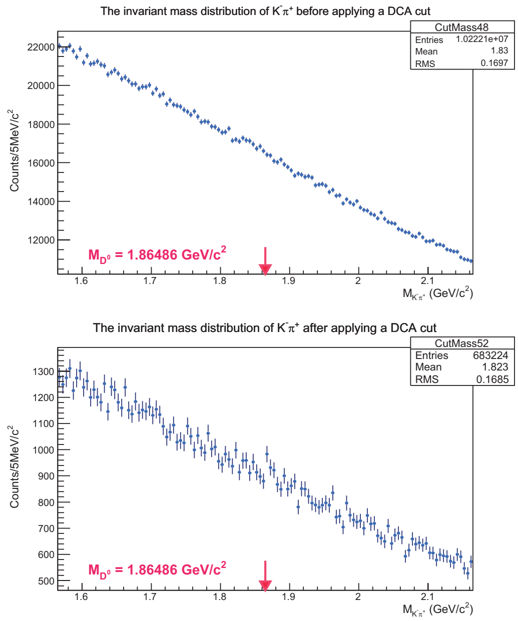

Fig. 1. The invariant mass distribution of $K^-\pi^+$ before and after applying a DCA cut

The intermediate result is shown in Fig. 1, which indicates the invariant mass distribution of $K^-\pi^+$ before and after applying a DCA cut. There is a hint of a small peak at the D^0 mass region in the mass spectrum with the DCA cut (the lower panel). However, there still remains a substantial combinatorial background. Therefore, it is necessary to further reduce the combinatorial background without sacrificing too many D^0 signals, and it is expected to be solved by selecting tracks in accordance with the D^0 decay kinematics using the VTX. We have been developing an analysis code that selects the decay kinematics of D^0 appropriately, leaving room for improving of the signal to background ratio.

References

1) A. Taketani et al. [PHENIX Collaboration]; Nucl. Instrum. Meth. A. **623**, 374, 2010.
2) T. Hachiya et al.: RIKEN Accel. Prog. Rep. **44**, 179 (2011).

*1 RIKEN Nishina Center
*2 Department of Physics, Yonsei University
*3 Department of Physics, University of Colorado
*4 CNS, Univ. of Tokyo
*5 Department of Physics, Kyoto University
*6 Department of Physics, Baruch Colleage, CUNY
*7 Department of Physics, Stony Brook University
*8 Los Alamos National Laboratory
*9 Department of Physics, Univ. of Tsukuba
*10 Department of Physics, Iowa State University

Development of coordinate offset online calibration system at RHIC-PHENIX

H. Asano,[*1,*2] A.Adare,[*3] Y. Akiba,[*2] R. Akimoto,[*4,*2] A. Dion,[*5] S. Bathe,[*6,*2] J. Bryslawskyj,[*6] D.McGlinchey,[*3] T.Koblesky,[*3] T.Moon,[*7,*2] T. Hachiya,[*2] M. Kurosawa,[*2] A. Lebedev,[*8] M. McCumber,[*9] H. Nakagomi,[*10,*2] R. Nouicer,[*11,*2] H. Sako,[*12,*2] S. Sato,[*12,*2] M. Shimomura,[*4,*2] T. Sumita,[*2] H.Torii,[*2] A. Taketani,[*2] and the PHENIX VTX group

The PHENIX experiment in the Relativistic Heavy Ion Collider (RHIC) at Brookhaven National Laboratory has been upgraded by installing a silicon vertex tracker (VTX)[1]. The VTX has been developed for heavy-flavor (charm and bottom) measurements and is dedicated to precise tracking for finding primary and secondary vertices. The first set of physics data including the VTX was recorded for the Au+Au collisions in RUN 11 (RHIC experiment performed in 2011).

The first and second layers of the VTX are comprised of pixel detectors, and the third and the fourth layers of VTX are comprised of stripixel detectors[2], as shown in Fig. 1. Geometrical calibration is important because precise alignment is required in the VTX to identify primary and secondary vertices. To analyze the distance of closest approach (DCA) of tracks to the primary vertex, we require a drift chamber (DC) track is associated with the clusters on the VTX, as shown in Fig. 2.

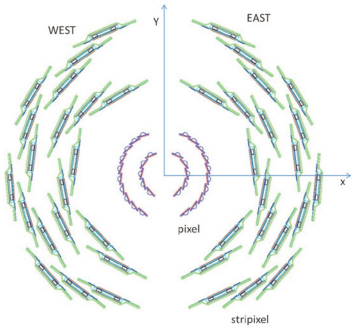

Fig. 1. Cross section of the VTX. The VTX is separated into a west half barrel and an east half barrel.

In the PHENIX apparatus, the west and east half barrels of VTX and DC in the east and west arms are mechanically separated, and their relative positions may shift. After each time we open up the apparatus to access the detectors, we need to calibrate the relative positions of the detectors. We developed an online and automated system to calibrate the coordinate offset between each of the west and east half barrels of VTX and DC in the east and west arms. Once we access the detectors, we always take zero-magnetic-field data in which all tracks from the collision point are assumed to be straight. The online calibration system calculates the beam center position with respect to DC west/east and VTX west/east coordinate system. Once the zero-field data are taken, the online calibration system runs immediately, and its result is submitted to a database. This result is used in the tracking analysis. This module outputs QA plots so that we can confirm that the result is reasonable.

In summary, we developed a coordinate offset online calibration system for RHIC-PHENIX. The system outputs calibration parameters of the coordinate offset of VTX and DC for the tracking analysis with VTX and DC data.

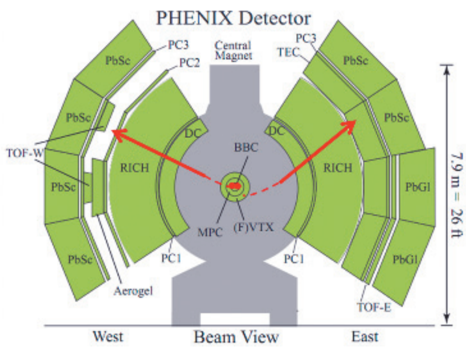

Fig. 2. Cross section of the PHENIX detector. The relative position of VTX west/east and DC west/east can be moved during the experiment.

*1 Department of Physics, Kyoto University
*2 RIKEN Nishina Center
*3 Department of Physics, University of Colorado Boulder
*4 Center for Nuclear Study, Univ. of Tokyo, Japan
*5 Department of Physics and Astronomy, Stony Brook University
*6 Department of Physics, City University of New York
*7 Department of Physics, Yonsei University
*8 Department of Physics and Astronomy, Iowa State University
*9 Los Alamos National Laboratory
*10 Graduate School of Pure and Applied Sciences, University of Tsukuba
*11 Brookhaven National Laboratory
*12 JAEA, Advanced Science Research Center

References

1) M Baker et al, Proposal for a Silicon Vertex Tracker (VTX) for PHENIX Experiment, 2004 BNL72204-2004, Physics Dept. BNL
2) A. Taketani et al., Nucl. Instr. and Meth. A 623 (2010) 374

Status of analysis of longitudinal double helicity asymmetry in π^0 production in $\sqrt{s} = 510$ GeV polarized proton–proton collision by PHENIX central arm

I. YOON[*1,*2] for the PHENIX Collaboration

The final goal of this research is to contrain polarized gluon distribution via measurement of the longitudinal double helicity asymmetry of π^0 production ($A_{LL}^{\pi^0}$) with $\sqrt{s} = 510$ GeV RHIC PHENIX data. Based on the results of EMC experiment and other following experiments, the quark-spin component of a proton is only $0.330 \pm 0.011(Theo.) \pm 0.025(Exp.) \pm 0.028(Evol.)$. [1)2)] The remaining spin might be carried by gluons or orbital momentum. However, the gluon-spin component is poorly measured because polarized gluon distribution has not been measured precisely.[2)] However, measurement with $\sqrt{s} = 510$ GeV RHIC PHENIX data can contribute significantly toward constraining polarized gluon distribution. The gluon-spin component can be measured via $A_{LL}^{\pi^0}$ in polarized proton collisions, which is defined as

$$A_{LL}^{\pi^0}(P_T) = \frac{\sigma_{++}^{\pi^0} - \sigma_{+-}^{\pi^0}}{\sigma_{++}^{\pi^0} + \sigma_{+-}^{\pi^0}} \quad (1)$$

where $\sigma_{++}^{\pi^0}$ and $\sigma_{+-}^{\pi^0}$ denote the π^0 cross section from a collision between same helicity protons and that from a collision between opposite helicity protons, respectively.

Compared to the previous measurement with $\sqrt{s} =$ 200 GeV RHIC data (Run09), the ongoing measurement with $\sqrt{s} = 510$ GeV RHIC data (Run13) will cover a lower momentum-fraction (Bjorken x) kinematic region, where the uncertainty large. The integrated luminosity of Run13 is much higher compared to that of Run09. The figure of merit ($\int L \times P_B^2 \times P_Y^2 dt$) considering beam polarization (P_B and P_Y) is also higher. Table 1 presents a comparison between Run09 and Run13. Thus, this research can contribute toward constraining polarized gluon distribution. The progress of the analysis is presented herein.

Table 1. Measurement with RHIC Run09 and Run13 data

	Run09	Run13
$\sqrt{s}$	200 GeV	510 GeV
Bjorken x region	0.05∼0.2	0.02∼0.08
$\int Ldt$	15 pb^{-1}	145 pb^{-1}
$\int L \times P_B^2 \times P_Y^2 dt$	1.4 pb^{-1}	14.7 pb^{-1}

In this experiment, π^0 is measured via $\pi^0 \to \gamma\gamma$ decays using a highly segmented electromagnetic calorimeter (EMCal) covering $|\eta| < 0.35$ and $\Delta\phi = \pi$.

Thus far, event selection and related low-level study, EMCal warnmap generation, and EMCal TOF tower-by-tower correction have been done.

An EMCal warnmap is a map of abnormal EMCal towers. To reject events from the abnormal towers, a warnmap has been generated wherein noisy, dead and uncalibrated towers are marked. EMCal tower-by-tower TOF correction has been performed. Before the correction, there was tower-by-tower TOF deviation, and the deviation depended on time. After the correction, the TOFs of all towers are well aligned.

For event selection, the shower-shape cut, charge-veto cut and TOF cut are applied to reject hadronic, charged and ghost events, respectively. Clusters in an EMCal can survive up to three bunch-crossings. Clusters from previous crossings are called ghost clusters. For the charge-veto cut and TOF cut, cut parameters are optimized by the signal-to-noise ratio. In addition to the three cuts mentioned above, the conventional minimum energy cut and vertex cut are also applied. After event selection, the statistics for remaining π^0 is 6.97×10^7. The results of the event selection are summarized in Fig. 1.

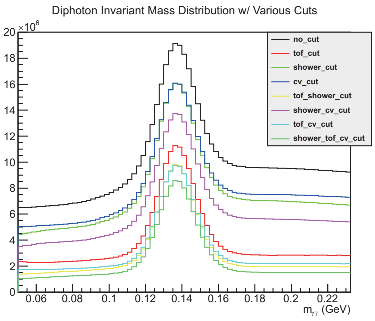

Fig. 1. Diphoton invariant mass distribution with various cuts for all P_T bins. After event selection, 70% of the noise is suppressed, whereas 30% of the signal is lost.

After the completion of event selection, $A_{LL}^{\pi^0}$ calculation has been started. $A_{LL}^{\pi^0}$ calculation is currently in preliminary stage. Estimation of statistical and systematic uncertainties is also being carried on. To validate the analysis, single-spin asymmetry is being calculated.

*1 RIKEN Nishina Center
*2 Department of Physics & astronomy, Seoul National University

References
1) J. Ashman et al.: Phys. Rev. B **206**, 2 (1988).
2) A. Airapetian et al.: Phys. Rev. D **75**, 012007 (2007).
3) D. de Florian and W. Vogelsang: Phys. Rev. D **80**, 034030 (2009).

Status of π^0 pair A_{LL} analysis in RHIC-PHENIX experiment

K.Hashimoto,[*1,*2] R.Seidl,[*1] and Y.Goto[*1] for the PHENIX collaboration

1 Introduction

The proton has a spin of 1/2 that originates from internal quarks and gluons. Results from deep inelastic scattering (DIS) experiments[1)] show that the quark spin contribution to the proton spin is only about 25% . In the PHENIX experiment, the gluon-spin contribution to the proton spin has been studied for more than 10 years. In recent years, double helicity asymmetries, A_{LL}, have been measured in several types production ($\pi^0, \pi^{\pm}$, direct photon, etc). In the case of single inclusive π^0 production, A_{LL} is defined as follow:

$$A_{LL}^{\pi^0} \equiv \frac{\sum_{a,b,c} \Delta f_a \Delta f_b \hat{\sigma}^{ab\to cX} \hat{a}_{LL}^{ab\to cX} D_c^{\pi^0}}{\sum_{a,b,c} f_a f_b \hat{\sigma}^{ab\to cX} D_c^{\pi^0}} \tag{1}$$

where $f_{a,b}$ represent unpolarized parton distribution functions (PDFs) of partons a and b and $\Delta f_{a,b}$ represent polarized PDFs, $D_c^{\pi^0}$ is a fragmentation function (FF) of parton c to π^0, $\hat{\sigma}^{ab\to cX}$ and $\hat{a}_{LL}^{ab\to cX}$ denote the cross section and A_{LL} of the partonic subprocess $ab \to cX$ respectively.

Experimentally, the A_{LL} for π^0 production is determined as

$$A_{LL}^{\pi^0} = \frac{1}{< P_B P_Y >} \frac{N_{++} - RN_{+-}}{N_{++} + RN_{+-}}; R = \frac{L_{++}}{L_{+-}} \tag{2}$$

where $N_{++(+-)}$ is the number of π^0s and R is the relative luminosity between bunches with the same and opposite helicities. $< P_B P_Y >$ are the averaged beam polarizations.

2 Simulation study on kinematics coverage

Bjorken-x is a fraction of a proton's longitudinal momentum. Let us imagine a reaction parton a interacting with parton b and producing jets(or partons) c and d: $parton(a)+parton(b) \to jet(c)+jet(d)$. In this case, Bjorken-x can be determined by using pseudorapidity and the transverse momentum of scatterted partons c and d

$$x_1 = \frac{1}{\sqrt{s}}(p_{T,c}e^{\eta_c} + p_{T,d}e^{\eta_d}) \tag{3}$$

$$x_2 = \frac{1}{\sqrt{s}}(p_{T,c}e^{-\eta_c} + p_{T,d}e^{-\eta_d}) \tag{4}$$

If both partons c and d are produced in the mid-rapidity region, $e^{\eta_{c,d}}$ and $e^{-\eta_{c,d}}$ are similar. Hence, x_1 and x_2 of the dijet production at the mid-rapidity region have a similar value. We can not mesure total energy of scattered partons. We measured the π^0 pair instead of the dijet(or partons). If we select back-to-back hadron pair production at the mid-rapidity region, the Bjorken-x of two incoming partons should be almost balanced. If values of two Bjorken x are not balanced, the produced particles system is boosted, and these particles should move to the exterior of the PHENIX central arm acceptance, where the rapidity region is $|\Delta\eta| < 0.35$. Figure 1 is a result of PYTHIA6.4 simulation. The vertical the horizontal axes are the log of Bjorken-x distribution. The colors denote the number of events. We accepted all events in which the pt of π^0, which decays gamma fire trigger is up to 2.0 GeV and in which the pt of π^0, which is produced in the opposite direction of the triggered π^0 is up to 1.5 GeV. The events in which two Bjorken-x's are similar are selected. The selection of back-to-back hadron pair production at a mid-rapidity region can suppress events in which two Bjorken-x's are Bjorken-x1>>Bjorken-x2 or Bjorken-x1<<Bjorken-x2.

3 Current status of this study

We calculated A_{LL} as well as A_L for π^0 pair production , A_{LL} for the single inclusive π^0 production etc, for cross checking. We determined te our analysis passed these tests. We are also checking for consistency in statistics between experimental data and simulated data with the PYTHIA 6.4 event generator.

This analysis is being preformed at RIKEN-CCJ[2)], and we are grateful for its smooth operation.

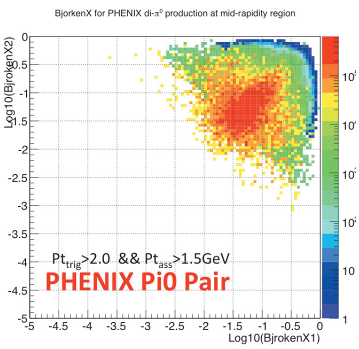

Fig. 1. Bjorken-x distribution for the π^0 pair production.

References
1) http://arxiv.org/abs/hep-ph/0101224v1
2) http://ccjsun.riken.jp/

*1 RIKEN Nishina Center
*2 Department of Physics, Rikkyo University

Measurement of longitudinal double-spin asymmetries of J/ψ production in polarized p+p collisions at $\sqrt{s}$=500 GeV for 2012 run

X. Wang,[*1,*2] H. Yu,[*2,*3,*4] and M. Liu[*4]

Understanding the contribution of polarized gluons to the proton spin is a key step for resolving the proton-spin puzzle. A number of different channels have been used to study gluon polarization, including final state hadrons[1)] and jets[2)]. Some rarer process involving direct photons or heavy-flavor production will allow us to measure the gluon contribution at the leading order, but their significantly lower production rates limit their impact on the ΔG constraints. At Relevistic Heavy Ion Collider (RHIC) energies, heavy-quark production is dominated by the gluon–gluon interaction; thus, measurements of the longitudinal double-spin asymmetry in heavy-flavor production in the polarized p+p collisions will allow us to study the polarized gluon distributions. J/ψ is a bound state of a c and $\bar{c}$ pair. Here, we report the status of longitudinal double-spin asymmetries in J/ψ production in polarized p+p collisions in the PHENIX experiment at the RHIC for data collected during 2012.

In the case of the heavy-quark production at RHIC, the asymmetry is proportional to the gluon polarization at the leading order:

$$A_{LL} \sim \frac{\Delta g(x_1)}{g(x_1)} \times \frac{\Delta g(x_2)}{g(x_2)} \times a_{LL}^{gg \to Q\bar{Q}}, \tag{1}$$

where $\Delta g(x)$(g(x)) is the (un)polarized gluon distribution, and $a_{LL}^{gg \to Q\bar{Q}}$ is the partonic asymmetry.

The J/ψ production have been measured by the PHENIX muon spectrometers at forward and backward rapidities ($1.2 < |\eta| < 2.4$), where two muons go into the same arm.

The longitudinal double-spin asymmetry A_{LL} can be measured according to the following equation:

$$A_{LL} = \frac{1}{P_b P_y} \frac{N^{++} - RN^{+-}}{N^{++} + RN^{+-}}, \tag{2}$$

where P_b and P_y are the beam polarizations for blue and yellow beams, respectively; $N^{++}(N^{+-})$ is the J/ψ yield from the same (opposite) helicity beam collisions; and $R = L^{++}/L^{+-}$ is the relative luminosity measured using beam beam counter (BBC) and zero degree calorimeter (ZDC) at very forward rapidity.

The invariant mass distribution of dimuons is shown in Fig. 1. Invariant mass distribution is fitted using a third-order polynomial and two Gaussian functions. The number of J/ψ is calculated on the basis of he fitting with a 2σ cut. The measured inclusive asymmetry

*1 RIKEN Nishina Center
*2 Department of Physics, New Mexico State University
*3 Department of Physics, Peking University
*4 P-25, Los Alamos National Laboratory

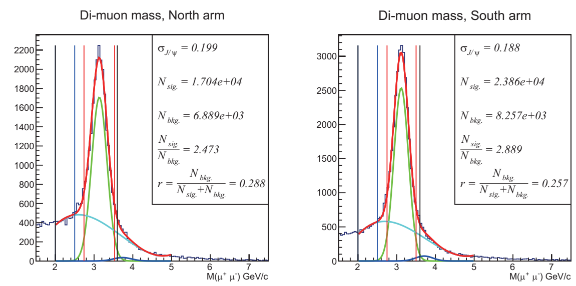

Fig. 1. Invariant mass distribution of dimuons at $\sqrt{s} = 500$ GeV for data obtained during the 2012 run.

A_{LL}^{incl} is related to $A_{LL}^{J/\psi}$ by

$$A_{LL}^{J/\psi} = \frac{A_{LL}^{incl} - r \cdot A_{LL}^{BG}}{1-r}, \tag{3}$$

$$\delta A_{LL}^{J/\psi} = \frac{\sqrt{(\delta A_{LL}^{incl})^2 + r^2 \cdot (\delta A_{LL}^{BG})^2}}{1-r}, \tag{4}$$

where r is the background fraction, and A_{LL}^{BG} is the background asymmetry, which is measured using like-sign dimuons under the J/ψ peak and the side-band unlike-sign dimuons.

Fig. 2 shows the sensitivity of J/ψ A_{LL}^{incl} vs. p_T based on data obtained during the 500 GeV polarized p+p run in 2012. The analysis is in progress and we are working towards preliminary results for J/ψ cross section and its longitudinal double-spin asymmetry.

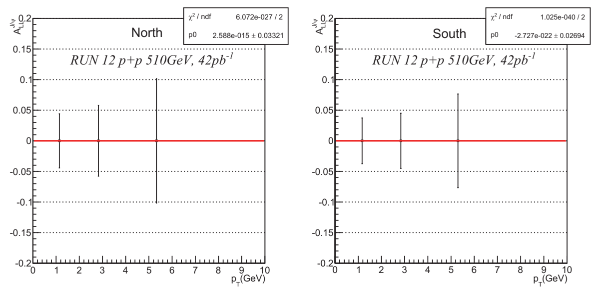

Fig. 2. Sensitivity of A_{LL} vs. p_T in J/ψ production at $\sqrt{s} = 500$GeV for data obtained during 2012.

References

1) PHENIX collaboration: Phys. Rev. D 83, 032001 (2011); Phys. Rev. Lett. 103, 012003 (2009); Phys. Rev. D 79, 012003 (2009); Phys. Rev. D 73, 091102(R) (2006).
2) PHENIX collaboration: Phys. Rev. D 84, 012006 (2011).

PHENIX local polarimetry analysis status

M. Kim,[*4,*1] Y. Goto,[*1] T. Iguri,[*3,*1] Y. Imazu,[*1] C. Kim,[*5,*1] T. Moon,[*6,*1] T. Murakami,[*2] J. Murata,[*3] T. Nagashima,[*3,*1] I. Nakagawa,[*1] S. Park,[*4,*1] R. Seidl,[*1] W. Saito,[*3,*1] K. Tanida,[*4,*1] and I. Yoon[*4,*1]

One of the main goals of the PHENIX experiment at the Relativistic Heavy Ion Collider (RHIC) is to study the proton spin structure through spin asymmetry measurements of production cross sections using various probes from polarized $p+p$ collisions. In 2013, we ran longitudinally polarized $p+p$ collisions at $\sqrt{s} = 510$ GeV. Since the stable polarization direction of proton beams circulating in the ring is perpendicular to the ground, the polarization direction is kept perpendicular except in the experimental hall during longitudinally polarized beam collision runs.

Measuring proton beam polarization along the longitudinal direction at the collision is important in double longitudinal spin asymmetry A_{LL} measurements. The polarization in RHIC is measured by RHIC polarimeters at the position where the spin vector is vertical; however, once the polarization direction is changed to be longitudinal, some transverse component of the beam polarization can remain. This should be accounted as a systematic error in the A_{LL} calculation.

The PHENIX local polarimeter measures the transverse component of proton beam polarization at the collision point with single transverse spin asymmetry A_N in forward neutron production. A large A_N for the neutron production was measured in the PHENIX experiment.[1] For forward neutron production, which has a small transverse momentum p_T, the large A_N cannot be explained by perturbative QCD, but the One Pion Exchange (OPE) models explain it well. In the OPE model, finite A_N is accompanied by the interference of the spin-flip amplitude of pion-exchange and the spin-nonflip amplitude of other Reggeon exchange. A detailed theoretical study is still ongoing.

The PHENIX local polarimeter consists of Zero Degree Calorimeters (ZDCs) and Shower Max Detectors (SMDs) and is located downstream of the beam dipole-bending-magnet outside of the interaction region. ZDC is a hadron calorimeter, and SMD is a hodoscope composed of plastic scintilator strips. The neutron's position is calculated by centroid method using energy deposited in the SMD.

For obtaining the local polarimeter data, a transversely polarized commissioning fill, a longitudinally polarized commissioning fill, and physics fills are used. 81M events were taken for the transverse commisioning fill, and 280M events were taken for the longitudinal commissioning fill. During physics runs, the local polarimeter trigger was used with a prescale, and the scaled trigger rate was about 100-200 Hz.

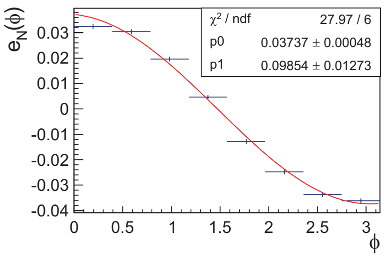

Fig. 1. e_N fitting

Events with 70-300 GeV energy are considered in order to avoid background photons; beam scraping backgrounds from the beam pipe, which deposit low energy in ZDC; and events that directly hit the optical fibers for ZDC readout. Further, only the events with at least two hits in the SMD scintillator strips in both x, y coordinates are considered in order to reject the photon background. A fiducial acceptance cut with radius = 0.5-4.0 cm from the SMD center is applied in order to avoid shower leakage or the smearing effect at the center caused by the SMD with about 1 cm position resolution. After the event selection, 19M events are used for the transverse run analysis.

The measured analyzing power ${A_N}^{measured}$ is defined as

$${A_N}^{measured} = \frac{1}{sin(\phi-\phi_0)}\frac{e_N(\phi)}{p}.$$

e_N is the raw asymmetry calculated with the square root formula,[1] and its values for the south detector (counter-clockwise direction from the collision point) in the transverse run are plotted in Fig.1. Only the statistical error is calculated for the error bars. p is the proton beam polarization, and it is 0.369 ± 0.061 for the yellow beam (beam runs counter-clockwise direction) during the transverse run. The calculated ${A_N}^{measured}$ is 0.101 ± 0.018. For the transverse component calculation, we calculate ${A_N}^{measured}$ of longitudinal runs in the same manner, then divide that by ${A_N}^{measured}$ of the transverse run. The transverse component is about 1% or less during the commissioning run.

Currently, modification of the pedestal and gain parameters for ZDC and SMD is ongoing. After these are finialized, the codes with new parameters will be rerun. Further, the systematic errors will be estimated.

*1 RIKEN Nishina Center
*2 Department of Physics, Kyoto University
*3 Department of Physics, Rikkyo University
*4 Department of Physics and Astronomy, Seoul National University
*5 Department of Physics, Korea University
*6 Department of Physics, Yonsei University

References
1) A. Adare et al. : Phys. Rev. D **88**, 032006 (2013).

Sea quark polarization measurement by $W^{\pm} \to \mu^{\pm}$ in PHENIX 2012

C. Kim,[*1,*2] Y. Goto,[*1] T. Iguri,[*1,*3] Y. Imazu,[*1] M. Kim,[*1,*4] T. Moon,[*1,*5] T. Murakami,[*6] J. Murata,[*3] T. Nagashima,[*1,*3] I. Nakagawa,[*1] S. Park,[*1,*4] W. Saito,[*1,*3] R. Seidl,[*1] K. Tanida,[*1,*4] and I. Yoon[*1,*4]

The leptonic decayed $W^{\pm}$ bosons measurement at RHIC aims to achieve precise constraint of each flvaor-decomposed sea quark's spin contribution to the whole proton spin $\frac{1}{2}$.

The $W^{\pm} \to \mu^{\pm}$ analysis by using the dataset of year 2012 shares the basic strategy set in the 2011 analysis[1)], but also has several advantages such as enhanced statistics and upgraded W trigger for data acquisition. Table 1 shows a few key features of the recent longitudinally polarized pp collisions.

Table 1. Results of recent polarized pp collisions in PHENIX Muon Arms.

Year	$\sqrt{s}$	L (pb^{-1})	P (%)	FoM (LP^2)
2009	500	8.6	39.0	1.3
2011	500	16.7	48.0	3.8
2012	510	31.5	51.9	8.5
2013	510	146.0	55	44.2

The main observable in this analysis is the single spin asymmetry (A_L) calculated by muons decayed from desired W bosons.

The major background source is muons from in-flight decayed low p_T ($p_T \leq 3$ GeV/c) hadrons, which mimic high p_T muons as well as various irreducible muonic backgrounds. Owing to the dominance of these backgrounds in addition to smearing in momentum and charge determination, observing distinct Jacobian peak in $W^{\pm} \to \mu^{\pm}$ measurement in forward rapidity is not expected, unlike the $W^{\pm} \to e^{\pm}$ measurement in mid-rapidity. Therefore, accurate estimation of the S/BG ratio plays an essential role in a reliable signal extraction process.

Table 2. S/BG ratio in Run 12 (preliminary).

Channel	n_{sig}	n_{μ}	n_{had}	S/BG
South μ^-	$88.87^{+16.97}_{-16.28}$	44.42	$177.77^{+19.60}_{-18.60}$	$0.40^{+0.12}_{-0.10}$
South μ^+	$92.48^{+20.55}_{-19.91}$	44.88	$258.74^{+24.38}_{-23.31}$	$0.30^{+0.10}_{-0.08}$
North μ^-	$38.95^{+11.90}_{-11.15}$	42.71	$139.78^{+15.45}_{-14.56}$	$0.21^{+0.09}_{-0.07}$
North μ^+	$72.37^{+15.75}_{-15.04}$	38.67	$185.69^{+18.93}_{-17.98}$	$0.32^{+0.10}_{-0.09}$

To estimate the S/BG ratio properly, we use a partially indirect approach by using likelihood to the W. The procedure for the estimation is as follows. First, calculate the W likelihood by using the data and NLO level Monte Carlo sample. Second, construct the overall probability density function (PDF) for signal and backgrounds by using three types of component PDFs based on W likelihood. Each component PDF corresponds to a signal, muonic backgrounds, and hadronic backgrounds, respectively. Finally, estimate the S/BG ratio via the overall PDF and unbinned max. likelihood fit technique. The estimated S/BG ratio in the preliminary condition is summarized in Table 2. Also, A_L calculated by applying the above S/BG ratio can be seen in figure 1.

*1 RIKEN Nishina Center
*2 Department of Physics, Korea University
*3 Department of Physics, Rikkyo University
*4 Department of Physics, Seoul National University
*5 Department of Physics, Yonsei University
*6 Department of Physics, Kyoto University

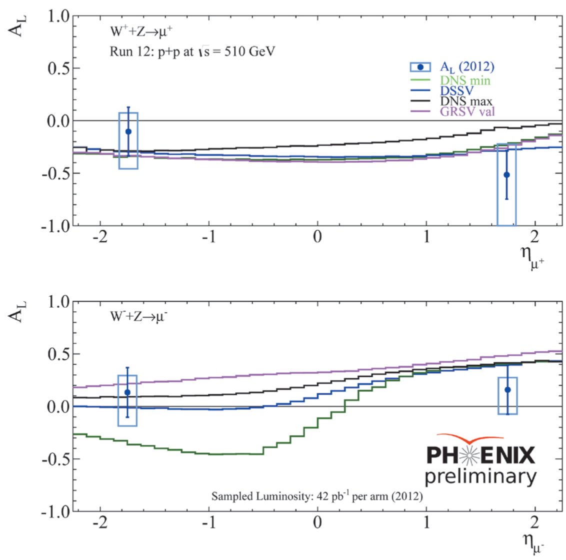

Fig. 1. A_L in Run 12 (preliminary). Empty squared box indicates systematic error by dilution factor.

After the preliminary, various refinements have been made or are underway, such as inclusion of kinematic variables from the Forward Silicon Vertex Detector (FVTX), applying overall trigger efficiency, update in detector efficiency, and further fine tune of hadronic PDF. Among them, inclusion of FVTX variables and fine tune of hadronic PDF are expected to play a significant role in improving statistics in the region of interest (W likelihood ≥ 0.92) as well as reduced errors, which will enable better estimation of the S/BG ratio and A_L.

References

1) H. Oide et al: RIKEN Accel. Prog. Rep. 46 xviii

Study of the dimuon process for PHENIX $W^{\pm} \to \mu^{\pm}$ analysis using 2012 data

S.Park,[*1,*4] Y. Goto,[*1] T. Iguri,[*1,*3] Y. Imazu,[*1] M. Kim,[*1,*4] C. Kim,[*1,*5] T. Moon,[*1,*6] T. Murakami,[*2] J.Murata,[*3] T. Nagashima,[*1,*3] I. Nakagawa,[*1] R. Seidl,[*1] W. Sato,[*1,*3] K. Tanida,[*1,*4] and I. Yoon[*1,*4]

Using the parity violation of weak interactions, we measured the single spin asymmetry of W production in longitudinally polarized p+p collisions. This enables us to access the flavor-separated sea quark polarization in protons[1)]. PHENIX measured the single spin asymmetry A_L^W via lepton decays of W bosons, $W^{\pm} \to e^{\pm}$ at midrapidity ($|\eta| < 0.35$) and $W^{\pm} \to \mu^{\pm}$ ($1.2 < |\eta| < 2.2$) at the center of mass energy $\sqrt{s} =$ 510 GeV at RHIC. After the first measurement in 2011 for the $W^{\pm} \to \mu^{\pm}$ channel, PHENIX collected data at an integrated luminosity of 50 pb^{-1} in 2012 with fully upgraded detectors and a trigger system.[2)]. The preliminary result of A_L obtained using the 2012 data is shown in Fig. 1. The measured asymmetries are consistent with theory models within large uncertainty ranges.

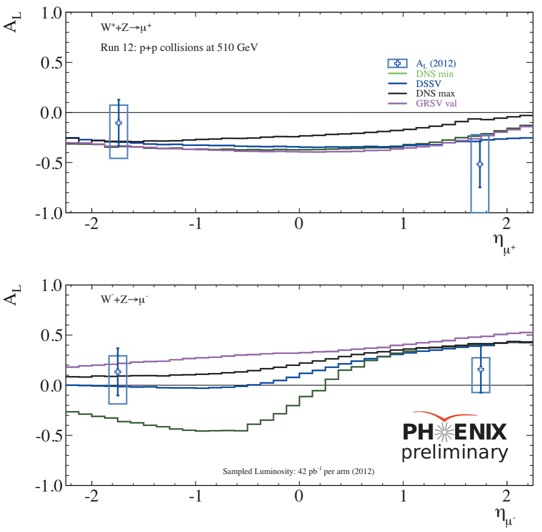

Fig. 1. Preliminary result of A_L for W^+(top) and W^-(bottom) at forward/backward rapidity region with various theoritical predictions.

After the preliminary result was obtained, there have been efforts toward the finalization of the 2012 data analysis. Understanding the background of the W→ μ analysis is one of the most important goals. The major background source is coming from decays of kaons and pions to muons in flight. In addition to this hadron background, there are muon backgrounds from the dimuon process that are open heavy flavor, quarkonia, and Drell-Yan process. Estimating the muon background is one of the essential steps to extract the signal-to-background ratio accurately. We simulate the dimuon processes using the PYTHIA event generator and GEANT4 detector simulation. The cross section of each process can be estimated by comparing the simulated dimuon yield to data. Fig. 2 shows the invariant mass spectrum of dimuon events in the 2012 data. We select unlike-sign muon pairs that travel to the same side of the PHENIX muon arm spectrometer. The discrepancy in the mass spectrum of the two muon arms reflects the difference in trigger efficiency. The simulated dimuon yields that take the trigger efficiency into account are used to extract analytical functions for each process. The scale factor of analytical functions for each process that contributes to the dimuon yields are then determined through simultaneous fit to the data. Currently, the simultaneous fit is being performed, and the result will be finalized shortly.

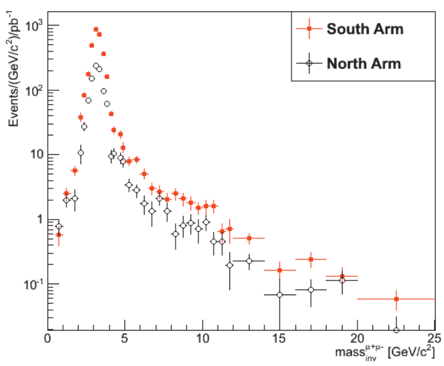

Fig. 2. Invariant mass distributions of dimuon events from data for south (red) and north (black) muon arms.

In addition to the dimuon study, dedicated analysis work is in progress on different fronts. Evaluation of the trigger efficiency and systematic uncertainty estimation are some of the tasks to be carried out. Furthermore, the signal-to-background ratio is expected to be improved through a review of the hadron background.

*1 RIKEN Nishina Center
*2 Department of Physics, Kyoto University
*3 Department of Physics, Rikkyo University
*4 Department of Physics and Astronomy, Seoul National University
*5 Department of Physics, Korea University
*6 Department of Physics, Yonsei University

References

1) H. Oide et. al, RIKEN Accel. Prog. Rep. 46, 18 (2013)
2) S. Park et. al, RIKEN Accel. Prog. Rep. 46, 63 (2013)

PHENIX W→ μ measurements from the 2013 data-taking period

R. Seidl,[*1] Y. Goto,[*1] T. Iguri,[*1,*3] Y. Imazu,[*1] M. Kim,[*1,*4] C. Kim,[*1,*5] T. Moon,[*1,*6] T. Murakami,[*2] J. Murata,[*3] T. Nagashima,[*1,*3] I. Nakagawa,[*1] S. Park,[*1,*4] ,W. Saito,[*1,*3] K. Tanida,[*1,*4] and I. Yoon[*1,*4]

The parity violation of the weak interaction accesses only left-handed particles and right-handed antiparticles. In longitudinally polarized proton-proton collisions one therefore can acess fixed helicities of the quarks and antiquarks involved in the production of real W bosons. Furthermore the charge of the produced W predominantly selects the quark and antiquark flavors involved. W^+ are mostly generated by a u and anti-d quark while W^- are mostly generated by a d and an anti-u quark. The PHENIX experiment has the capabilities to detect Ws inclusively through their electron and muon decays at central and forward rapidities respectively. In the 2013 data taking period RHIC was entirely run with polarized protons at center of mass energies of $\sqrt{s} = 510$ GeV to finish the RHIC W program[1)]. In PHENIX all major muon trigger upgrades installed and commissioned over the last several years as well as the forward vertex tracker FVTX were fully operational for this run. Furthermore PHENIX implemented various improvements in the operation of the detector to increase the data taking efficiency without sacrificing quality. In a limited vertex region (more can be used for the forward W analysis) a total luminosity of about 146 pb^{-1} were accumulated with average longitudinal beam polarizations of 54%, which is close to five times the data accumulated in the previous year with comparable polarizations. The accumulated figure of merit for single spin W asymmetries are displayed in Fig. 1 for the three most recent 500 or 510 GeV data taking periods.

Having developed the $W \to \mu$ analysis already in the previous two years, most of the offline quality assurance is finished and the analysis to the single spin asymmetries relevant to access the sea quark polarizations in the nucleon is close to be available to the public. One aspect relevant in this analysis and in particular the extraction of W production cross sections is the evaluation of the overall trigger efficiency for candidate events found to be likely W signal events in a MC and data based W likelihood calculation. As various muon triggers cover only certain rapidity ranges these trigger efficiencies need to be obatained independently for various rapidity bins, detector arms and muon charges. Fig. 2 shows the total trigger efficiencies after weighting each according to their relative contribution to the final W candidate event sample.

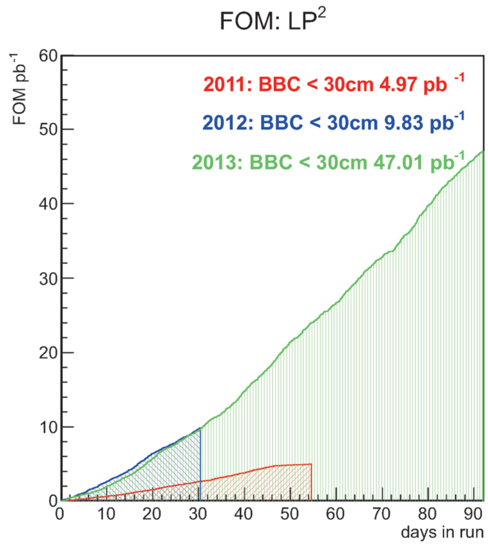

Fig. 1. Figure of merit P^2L accumulated in PHENIX as a function of the day in the run relevant to the forward W analysis. The different colors correspond to the 2011 data taking (red), 2012 (blue) and 2013 (dark green).

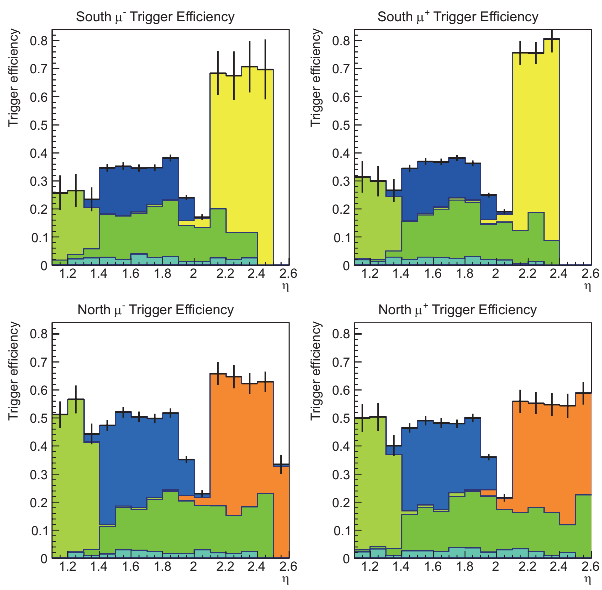

Fig. 2. Overall trigger efficiencies separated by muon arm and charge as a function of rapidity. Various individual trigger contributions are shown as histogram stack.

*1 RIKEN Nishina Center
*2 Department of Physics, Kyoto University
*3 Department of Physics, Rikkyo University
*4 Department of Physics, Seoul National University
*5 Department of Physics, Korea University
*6 Department of Physics, Yonsei University

References

1) E. C. Aschenauer *et al.*, arXiv:1304.0079 [nucl-ex].

Improvement of global alignment of PHENIX muon tracker

T. Iguri,[*1,*2] Y. Goto,[*2] Y. Imazu,[*2] M. Kim,[*2,*4] C. Kim,[*2,*5] T. Moon,[*2,*6] T. Murakami,[*3] J. Murata,[*1] T. Nagashima,[*1,*2] I. Nakagawa,[*2] S. Park,[*2,*4] R. Seidl,[*2] W. Saito,[*1,*2] K. Tanida,[*2,*4] and I. Yoon[*2,*4]

The alignment of tracking chambers is one of the long-standing challenges for nuclear physics experiments. The PHENIX muon system measures the charged-particle momentum using three tracking stations with cathode readout chambers, namely muon tracker (MuTr), implemented in a magnetic field volume[1)]. The precision of the relative alignment between the three tracking chambers directly affects the resolution of momentum measurement. Over the past few years, the PHENIX spin program has been focusing on polarized sea-quark measurements in protons through asymmetry measurements of the W-boson production [2)]. Because of the large mass of W-boson, the muon decayed (which we detect) from the W-boson has a high transverse momentum of $\sim$ 40 GeV/c. Such a high-momentum trajectory is barely bent in the magnetic field, and its sagitta is about a few to several mm in the MuTr volume. The possible misaligment of MuTr chambers will result in further momentum smearing over its intrinsic resolution. The higher the momentum, the more serious the side effect on the charge determination of the traversing particles. The possible charge misreconstruction is a fatal error for the asymmetry measurement, since the opposite charge (either W^+ or W^-) production is predicted to appear in opposite asymmetry. The goal of this study is to achieve the intrinsic resolution of 150 μm as currently, an intrinsic resolution of only $\sim$ 300μm achieved.

We developed a global alignment program that calculates the smallest χ^2 solution of actual hit locations when the straight tracks pass through the three MuTr stations assigning the relative location of chambers as free parameters. In this manner, the program will find the relative alignment of chambers to minimize the residuals. The residual is the distance between the linear interpolation of front- and back-plane hit positions and the actual hit position in the middle plane. The alignment parameters are limited to transverse shifts and rotations. The result of the new alignment demonstrated narrower residual distributions than that previously achieved[3)]; however, it was found that unresolved non linear radial dependences of the residual distributions remain even with the present algorithm.

As a rough quantitative estimate of the misaligment effect, the width of the residual distribution between radial dependent and non-dependent regions were compared. The resulting estimate showed difference of 100 to 500 μm depending on the octants. Note that this indicates a possible room for the improvement of the alignment by fixing the aligment to the radial direction. In order to investigate further problems in the present alignment scheme, of the azimuthal-direction dependence (orthogonal to radial direction) was also checked. Odd dependences were also found in the azimuthal direction. As an overall trend, bad alignment octants are problematic in both radial and azimuthal directions, and thus, a somewhat complicated correlation needs to be addressed. Since there are 16 chamber planes involved simultaneously in the alingment, finding the cause of these dependences is nontrivial. To obtain some hints to disentangle the complication, the local alignment was evaluated. The plane-based local residual was defined using two or three gaps (stations 1 and 2 have three gaps, and station 3 has only two gaps) and two planes (one is a stereo plane; the other is a non-stereo plane). The local residual distributions are again evaluated for radial and azimuthal dependence. Since local residual distributions are independent of other stations, one can expect some localized misalignment in a particular station if the cause of the global misalignment comes from the single plane or station; however, we did not observe that any octant shows such a trend, as shown in Fig. 1. It is interesting to investigate how closely we can reproduce the global residual distribution in comparison with the observed local ones. A toy Monte-Carlo simulation (MC), which includes the multiple scattering effect, is under development. Since the MC assumes perfect alignment, any fraction of the residual width that cannot be explained by the MC can be interpreted as room for the improvement of the alignment.

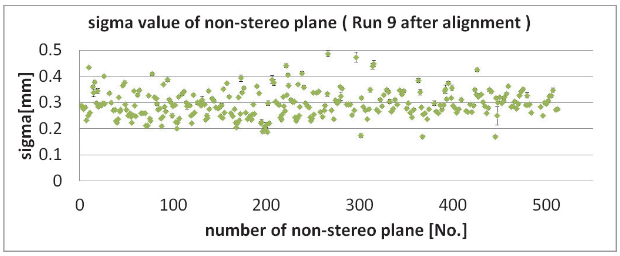

Fig. 1. Standard deviation of local residuals plotted for all non-stereo planes (Run9 after alignment).

*1 Department of Physics, Rikkyo University
*2 RIKEN Nishina Center
*3 Department of Physics, Kyoto University
*4 Department of Physics and Astronomy, Seoul National University
*5 Department of Physics, Korea University
*6 Department of Physics, Yonsei University

References

1) H. Akikawa et.al., NIM **A499**, 537 (2003).
2) H. Oide, RIKEN Accel. Prog. Rep. **45** (2012).
3) K. Watanabe, Thesis, Rikkyo Univeristy (2012).

RIKEN Accel. Prog. Rep. 47 (2014)

Forward spectrometer upgrade of the PHENIX experiment

Y. Goto*1 for the PHENIX Collaboration

The PHENIX experiment proposes substantial detector upgrade for long-term enhancement of major physics programs using full luminosity of the recently upgraded RHIC accelerator.[1] The proposed midrapidity upgrade replaces the present magnet with a solenoid, and removes the large iron yoke at forward rapidity that provides the hadron absorber for the muon detectors. The open geometry of the forward direction of the proposed upgrade will allow for addition of a forward spectrometer covering forward rapidity region, $1 < \eta < 4$, with capability of measuring hadrons, photons, electrons, muons and jets. We have been investigating requirements for detector design and performance of the forward upgrade consisting of charged-particle tracking, particle identification, electromagnetic and hadronic calorimeters as shown in Fig. 1.

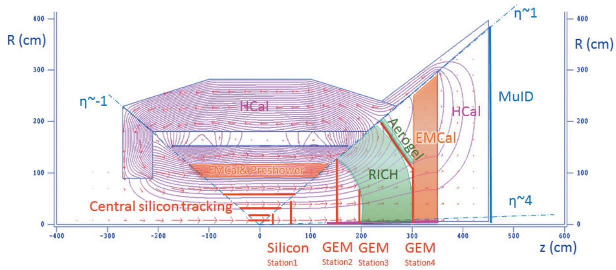

Fig. 1. Conceptual configuration of the forward spectrometer upgrade.

A physics topic regarding the forward upgrade is Cold Nuclear Matter (CNM) effects in proton- and deuteron-nucleus collisions. We aim to measure nuclear gluon distribution, $G_A(x)$, to know initial state of heavy-ion collisions and to understand the strongly coupled Quark-Gluon Plasma. It is important to investigate gluon suppression, or suppression of $G_A(x)$, at small-x and verify the Color Glass Condensation framework, which is an effective field theory for describing saturated gluon.[2] We also aim to know the perturbative-QCD (pQCD) mechanism of the energy loss of partons in the CNM, its relation to transverse momentum broadening, and detailed hadronization and time scales.

Another physics topic is measurements of single transverse-spin asymmetry. The asymmetries have been measured in the Fermilab fixed-target experiment with transversely polarized proton beams[3] and in the RHIC transversely polarized proton collider experiments at much higher energies.[4] pQCD models have been developed to explain the asymmetries. At small transverse momenta, the asymmetries have been explained using transverse-momentum dependent (TMD) factorization framework.[5] They have been explained with correlations between the transverse spin of the target proton and intrinsic transverse momentum of quarks in the initial state, which is called the Sivers effect[6] and described by the Sivers function. They have also been explained with correlations between quark spin and the transverse momentum of hadrons in the final state, which is called the Collins effect[7] and described by the Collins fragmentation function. At larger transverse momenta, higher-twist effect explains the asymmetries with spin-dependent transverse momentum components generated through quark-gluon and multi-gluon correlations using the collinear factorization framework.[8]

The Sivers function contributes with opposite sign to the transverse-spin asymmetries in the semi-inclusive DIS process and the Drell-Yan process due to non-universality of the TMD factorization framework.[9] This is a fundamental QCD prediction based on gauge invariance and its verification is an important milestone in the field of hadron physics. The verification allows testing of non-perturbative aspects of QCD and the concept of factorization. The forward upgrade will enable us to measure the Sivers function in the Drell-Yan process.

The Collins effect will be investigated through an azimuthal anisotropy in the distribution of hadrons in final-state jets with the forward upgrade detectors. The asymmetry of single identified hadrons described by the Collins fragmentation function will give a measurement of quark transversity distribution at large x which will determine the tensor charge of the nucleon.

There is a new possibility in collisions of polarized protons and nuclei. Transverse single-spin asymmetries in $p\uparrow + A$ collisions may have a sensitivity to the saturation scale in the nucleus. This link between the physics of the CNM and spin structure of the nucleon is one of the most interesting recent developments.

*1 RIKEN Nishina Center

References
1) C. Aidala et al.: arXiv:1207.6378 [nucl-ex].
2) F. Gelis, E. Iancu, J. Jalilian-Marian and R. Venugopalan: Ann. Rev. Nucl. Part. Sci. **60** (2010) 463.
3) D. L. Adams et al.: Phys. Lett. B **261** (1991) 201, Phys. Lett. B **264** (1991) 462.
4) L. Adamczyk et al.: Phys. Rev. D **86** (2012) 051101, A. Adare et al.: arXiv:1312.1995 [hep-ex].
5) D. Boer et al.: arXiv:1108.1713 [nucl-th].
6) D. W. Sivers: Phys. Rev. D **41** (1990) 83.
7) J. C. Collins: Nucl. Phys. B **396** (1993) 161.
8) J. Qiu and G. Sterman: Phys. Rev. D **59** (1999) 014004.
9) J. C. Collins: Phys. Lett. B **536** (2002) 43.

Design for an eRHIC detector based on the sPHENIX detector†

K. Boyle*[1] for the PHENIX Collaboration

The PHENIX experiment has recently submitted a plan[1)] for a detector design at eRHIC, a version of the Electron Ion Collider (EIC) planned at Brookhaven National Laboratory (BNL) which makes use of one of the current RHIC hadron rings. The EIC will collide polarized electrons with heavy nuclei and polarized protons, with its primary purpose to explore the gluon (the strong force carrier). eRHIC is expected to turn on in 2025.

A detailed description of the EIC physics case has been laid out in the recent White Paper[2)]. eRHIC is expected to probe through polarized electron-proton collisions the properties of (sea)quarks and gluons in the nucleon, such as spin, orbital motion and spacial distributions. The kinematic coverage of ePHENIX in parton momentum fraction x and 4-momentum transfer Q^2 is compared to that of other measurements in Fig. 1. Measurements of the gluon helicity over a wide kinematic range will allow unprecedented constraints of the gluon polarization, Δg. In Semi-Inclusive scattering, correlations between transverse momentum of gluons and quarks and the proton spin will be fully explored. Through Deeply Virtual Compton Scattering, eRHIC will measure the orbital angular momentum contributions to the proton spin.

As it will also be able to scatter electrons off nuclei, eRHIC will be able to explore the nature of gluons at high density, where the effects of gluon saturation (when gluon splitting and recombination balance) are expected. By varying kinematics as well as the nuclei species, we will be able to vary the path length of a struck quark through the nuclei, and probe the nature of hadronization in and out of nuclear matter.

The ePHENIX detector design is shown in Fig. 2, and makes use of the BABAR solenoid[3)] and the sPHENIX detector upgrade[4)] being planned for later this decade. We plan to add a high resolution electromagnetic calorimeter in the electron-going direction for precision measurement of the scattered electron. GEM based trackers will allow for charged sign identification and hadron rejection based on energy to momentum cuts.

In addition to the sPHENIX electromagnetic and hadronic calorimetry, we plan to add a Time Projection Chamber (TPC) for tracking and a Detector of Internally Reflected Čerenkov radiation (DIRC) for hadron particle identification (PID), based on the BABAR DIRC detector. PID in the central barrel allows for measurements of sea quark spin and transverse momentum distributions at low momentum fraction, x.

In the hadron-going direction, new electromagnetic and hadronic calorimeters are planned, as well as additional trackers and PID detectors. The combination of an Aerogel-based Ring Imaging Čerenkov (RICH) detector for low momentum tracks and a gas-based RICH detector for tracks up to ~ 60 GeV/c will allow for measurements at highest and moderate x over the full available Q^2 range.

ePHENIX will be capable of doing the physics possible with eRHIC. Efforts on fully simulating the detector is currently underway.

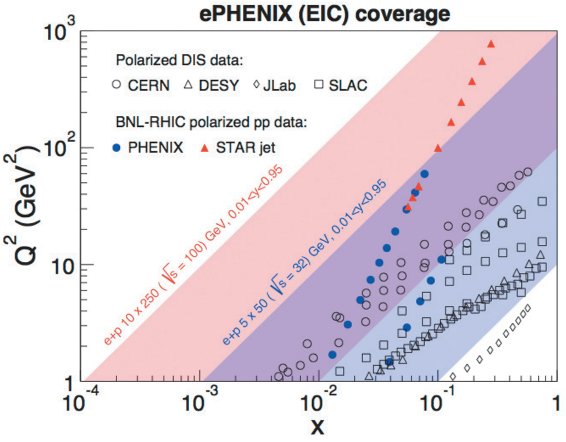

Fig. 1. Kinematic coverage (blue and red bands) expected at eRHIC with the ePHENIX detector for inclusive measurements in electron-proton scattering. Also shown are current world data.

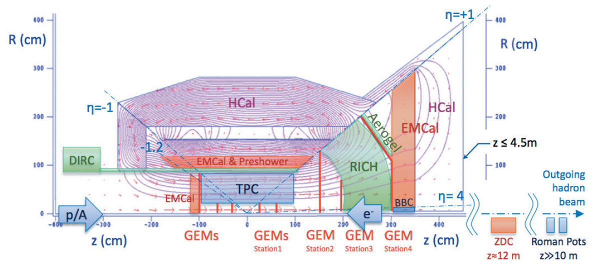

Fig. 2. Design of the ePHENIX detector at eRHIC. The proton/Nuclei beam enters from the left, and the electron beam enters from the right.

References
1) A. Adare *et al.* [PHENIX Collaboration], arXiv:1402.1209 [nucl-ex].
2) A. Accardi, *et al.*, arXiv:1212.1701 [nucl-ex].
3) B. Aubert *et al.* [BaBar Collaboration], Nucl. Instrum. Meth. A **479**, 1 (2002).
4) C. Aidala, *et al.*, arXiv:1207.6378 [nucl-ex].

*1 RIKEN Nishina Center

The Application of Gaussian Process Regression to Background Spectrum Modeling at PHENIX

J. Seele,*1 C. Gal,*2 and A. Deshpande*1,*2

Often in nuclear and particle physics, we need to estimate the area under a peak which sits over an oddly shaped background (see figure 1). Occasionally we are able to perform an analytical first principles calculation to calculate a shape for the background, but more often we are faced with little or no information about what the shape of the background should be. Faced with this, we typically choose a polynomial and fit this functional form to the background. The choice of this polynomial and its fitting leaves an unquantified uncertainty.

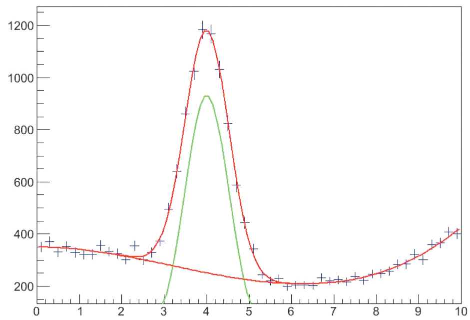

Fig. 1. A sample background (sampled from a known third order polynomial) and Gaussian peak spectrum.

Gaussian processes[1,2] are a mathematical concept that allow for a method of data regression and predictive functional modeling using a minimal set of prior assumptions. A nice feature of this method is that simultaneously with the predictions, uncertainties are provided.

Gaussian processes are a specific type of stochastic process where the variance of each of the random variables comprising the process is Gaussian. An important feature of stochastic processes is that, mathematically, they sample over the space of functions similar to how a random variable samples over a set space of possible outcomes. In defining the variances to be Gaussian, we've narrowed down the space of possible functions and simplified the math needed to specify the process. Specifically, with this requirement of Gaussian uncertainties, the expectation of the process can be defined entirely in terms of a mean function and a covariance function similar to how the Gaussian distribution is defined purely by a mean and a variance.

The specific background spectrum that we are interested in applying this technique to is the background sitting beneath the Jacobian peak, in $W^{\pm}$ production in p+p collisions[4]. This is a steeply falling spectrum that isn't modeled well by using power laws or exponentials. This particular problem requires the extension of the Gaussian process technique to multiscale problems, which required transforming the data[3] and applying the Gaussian process regression in this warped space. Our current application of Gaussian processes to modeling this spectrum can be seen in figure 2.

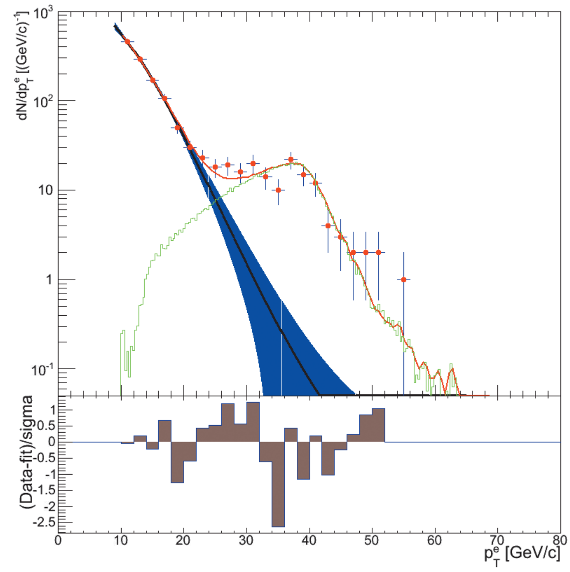

Fig. 2. The W Jacobian peak and background spectra. The black line and blue band represent the Gaussian process best fit and uncertainty band.

The uncertainty band currently encompasses a large space of functions, many of which we don't expect to be physical (e.g. an undulating, falling spectrum). We are currently working to add shape constraints to the Gaussian process modeling by sampling individual, though coarsely grained, functions from the constrained space and then accepting or rejecting those functions based on their individual shapes.

References

1) MacKay, David J. C.: *Information Theory, Inference, and Learning Algorithms* (Cambridge University Press, 2003)
2) Rasmussen, C. E. & Williams, K. I.: *Gaussian Processes for Machine Learning* (The MIT Press, 2006)
3) Snelson, E., Rasmussen, C. E., Ghahramani, Z.: *Warped Gaussian Processes*, NIPS, 2003.
4) Adare, et al. : Phys.Rev.Lett. 106 (2011) 062001

*1 RIKEN Nishina Center
*2 Department of Physics, Stony Brook University

Fragmentation function measurements with the Belle detector

R. Seidl,*1 M. Leitgab,*2 A. Vossen,*3 F. Giordano,*2 N. Kobayashi,*4 M. Grosse-Perdekamp,*2 A. Ogawa,*1 C. Hulse,*5 and G. Schnell*5,*6

The transition of quasi-free, high-energetic partons into confined hadrons cannot be described from first principle QCD as the related parton and hadron masses are typically too low to apply perturbative QCD. The fragmenation functions (FF), describing this transition, therefore need to be measured experimentally, similarly to the parton distribution functions (PDFs) in the nucleon. Their definition is also rather similar as for example the fragmentation function $D_{1,q}^{h}(z,Q)$ describes the number density of producing a hadron h from a parton q with fractional energy $z = E_h/E_q$ and at an energy scale Q. Until recently most data was obtained close to the Z resonance in e^+e^- annihilation, while little data at smaller scales was available and therefore the gluon fragmenation was not well constrained. The Belle experiment at KEK has collected more than a 1 ab^{-1} of luminosity close to the $\Upsilon(4S)$ resonance at $\sqrt{s} = 10.58$ GeV and about 63 pb^{-1} were used to extract unpolarized fragmenation functions in the process $e^+e^- \to hX$ which was published recently[1]. The results can be seen in Fig. 1 as a function of the fractional energy $z = 2E_h/\sqrt{s}$. Before this measurement very little low-energy scale data and almost no high-z data was available. It is expected that this data will soon be used in a global QCD analysis to parametrize the flavor dependence of pion and kaon fragmenation functions. In addition the analysis of unpolarized fragmenation functions continues in Belle with the aim to extract direct flavor information via the use of di-hadrons in opposite hemispheres. In this case the different combinations of favored (eg. $u \to \pi^+$) and disfavored (eg. $u \to \pi^-$) fragmenation functions can be disentangled by the various charge combinations of the two detected hadrons. It is expected that preliminary results will be available soon. Also the extraction of the explicit transverse momentum dependence of fragmenation functions is ongoing which so far is only assumed to be of a certain form in various global fits, but explicit measurements are not available so far.

Furthermore, the published results on the spin dependent fragmentation function measurements[2] are in the process to be augmented to also access the flavor dependence by not only concentrating on charged pions, but also on charged kaons and neutral mesons as well as their transverse momentum dependence. Also

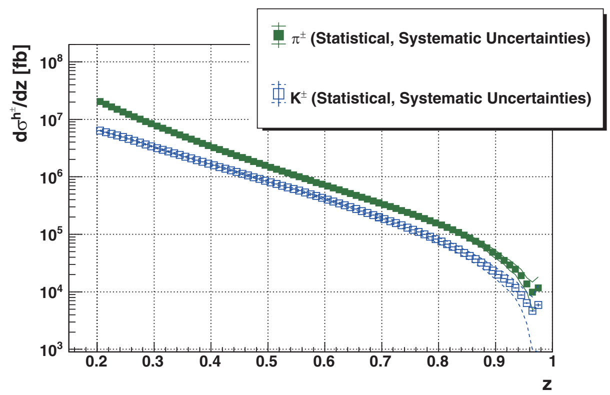

Fig. 1. Charged pion and kaon differential cross sections as a function of the fractional energy z. The error bands describe the total systematic uncertainties.

here the inclusion of various hadron types allows the flavor decomposition of the corresponding spin dependent fragmenation functions. By making use of them, the flavor decomposition of the quark transversity distribution of the nucleon in semi-inclusive deep-inelastic scattering and proton-proton experiments. Also here a QCD gobal transversity analysis for either the Collins function related measurements[3] or the interference related measurements[4] is available with the present data.

References

1) M. Leitgab *et al.* [Belle Collaboration], Phys. Rev. Lett. **111**, 062002 (2013).
2) R. Seidl *et al.* [Belle Collaboration], Phys. Rev. Lett. **96**, 232002 (2006). R. Seidl *et al.* [Belle Collaboration], Phys. Rev. D **78**, 032011 (2008), [Erratum-ibid. D **86**, 039905 (2012)]. A. Vossen *et al.* [Belle Collaboration], Phys. Rev. Lett. **107**, 072004 (2011).
3) M. Anselmino, M. Boglione, U. D'Alesio, A. Kotzinian, F. Murgia, A. Prokudin and S. Melis, Nucl. Phys. Proc. Suppl. **191**, 98 (2009).
4) A. Bacchetta, A. Courtoy and M. Radici, JHEP **1303**, 119 (2013).

*1 RIKEN Nishina Center
*2 Physics department, University of Illinois
*3 Physics department, University of Indiana
*4 Department of Physics, Tokyo Institute of Technology
*5 Department of Physics, University of the Basque Country
*6 Ikerbasque

Probing flavor asymmetry of antiquarks of the proton in the E906/SeaQuest experiment

S. Miyasaka,[*1] Y. Goto,[*2] Y. Miyachi,[*3] K. Nagai,[*1] K. Nakano,[*1]
S. Obata,[*1] F. Sanftl,[*1] S. Sawada,[*2,*4] T.-A. Shibata[*1,*2] for the E906/SeaQuest experiment

E906/SeaQuest is an extension of the earlier Drell-Yan experiments at Fermi National Accelerator Laboratory (Fermilab), such as E772 and E866/NuSea[1)], and it studies the internal structure of the proton at the parton level using the Drell–Yan process. In the leading order, the Drell–Yan process is described by the quark–antiquark annihilation process: $q + \bar{q} \rightarrow \gamma^* \rightarrow \mu^+ + \mu^-$. SeaQuest uses a 120-GeV proton beam extracted from the Fermilab Main Injector.

The ratio $\bar{d}/\bar{u}$ was measured in the Bjorken x range $0.015 < x < 0.35$ in the E866 experiment. The statistically precise part of the data in the range $0.015 < x < 0.2$ tends to agree with several models, such as the meson cloud model. However, the data appear to deviate from these models in the larger x region. SeaQuest will determine the ratio up to $x = 0.45$ more precisely than the E866. The SeaQuest spectrometer consists of four tracking stations. Each station has drift chambers or drift tubes for tracking and hodoscopes for trigger. The Japanese group is in charge of the drift chambers of the third station. Two drift chambers are aligned at the station to cover the large acceptance. SeaQuest completed a two-month commissioning run in spring 2012. After an upgrade, a two-year physics run began in fall 2013.

In the commissioning run, we successfully reconstructed the di-muon mass distribution, and a J/ψ peak was clearly observed (Fig. 1). The mass resolution was $\sim$ 0.3 GeV, which meets the requirement. This proves that the detectors and tracking software work adequately. After the commissioning run, three main hardware upgrades were performed. The first one was an upgrade of the beam quality. During the commissioning run, we observed high-multiplicity events because the beam had high instantaneous intensity. This made the track reconstruction difficult. An improvement of the duty factor was confirmed in the current run. The beam tuning is now ongoing, and we will have a full-intensity beam (10^{12} protons per second) once it is completed. The second main upgrade is the installation of a Cherenkov detector in the beam line to measure the beam intensity at 53 MHz RF frequency. This allows us to determine the absolute cross section of the Drell–Yan process and to generate a veto trigger in order to avoid the high-intensity part of the beam. The last main upgrade is the improvement of the hodoscopes and drift chambers. For hodoscopes, we upgraded the existing PMT bases with a new circuit board to achieve higher rate capabilities. For drift chambers, one new chamber was constructed to ensure a larger acceptance at the third station. The chamber has 5,300 wires, and we manually constructed it in 2012. The chamber was installed at the bottom part of the third station. The construction of another new drift chamber is ongoing. It will be also installed at the first station.

After the current physics run began, we were working on the optimization of every component for stable data accumulation. Our current focus is to optimize the trigger system. The system examines the hit pattern of the hodoscopes to identify the pattern characteristics of the high-mass muon pairs produced from the Drell–Yan process or J/ψ decay. We are now trying to suppress the background as much as possible through the hit-pattern study. The preliminary result of the mass distribution shows a suppression of the background compared to the distribution obtained in the commissioning run. Once the optimization is completed, we will start taking the Drell–Yan data. The data accumulated in the next two years will have a significant impact on our understanding of the internal structure of the proton.

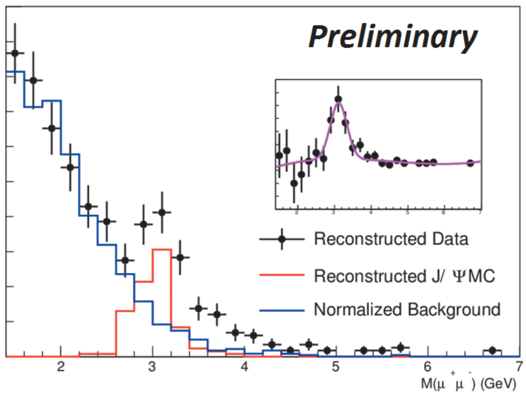

Fig. 1. Di-muon mass distribution reconstructed using the data taken in the commissioning run. The J/ψ peak is clearly observed. The inset shows the mass distribution in which the normalized background is subtracted.

*1 Graduate School of Science and Engineering, Tokyo Institute of Technology
*2 RIKEN Nishina Center
*3 Faculty of Science, Yamagata University
*4 Institute of Particle and Nuclear Studies, KEK

References
1) E.A. Hawker *et al.*, NuSea, Phys. Rev. Lett. **80**, (1998) 3715

Elliptic flow of neutral pion in Pb+Pb collisions at $\sqrt{s_{NN}} = 2.76$ TeV by ALICE experiment

T. Tsuji,[*1,*2] H. Hamagaki,[*2] T. Gunji,[*2] H. Torii,[*1] for the ALICE collaboration

It has been observed in central Pb+Pb collisions at ($\sqrt{s_{NN}}$) = 2.76 TeV at the Large Hadron Collider (LHC) facility at CERN that the yield of charged particles at a high transverse momentum (p_T) is strongly suppressed compared with the expected yield from p+p collisions, assuming scaling with the number of binary collisions. This suppression is attributed to the energy loss of hard-scattered partons within quark-gluon plasma (QGP) created in heavy ion collisions. This phenomenon known as jet quenching. A useful way to quantify the suppression of high-p_T hadrons is to introduce the nuclear modification factor (R_{AA}), where the p+p cross section is scaled with the thickness function $\langle T_{AA}\rangle$ of the two nuclei

$$R_{AA}(p_T) = \frac{1}{< T_{AA} >}\frac{(1/N_{AA}^{evt})d^2N_{AA}/dp_Tdy}{d^2\sigma_{pp}/dp_Tdy}.$$

Experimental data can be well reproduced by using multiple models employing different approaches that are used to calculate the energy loss of hard-scattered partons as they traverse the dense medium. To compare these models, improved experimental control of the path length L is required because the energy loss of a high-p_T parton increases rapidly with increase of the the distance traveled through the medium.[1)] Thus, the measurement of the energy loss with respect to the path length is expected to provide detailed information about the mechanism of the energy loss of the parton. If R_{AA} is measured as a function of centrality ($cent$) and the azimuthal angle ($\Delta\phi$) with respect to the event plane, $R_{AA}(L)$ can be determined. Therefore, the differential observable $R_{AA}(\Delta\phi)$ directly probes the path length dependence of the energy loss.

The $R_{AA}(p_T, cent, \Delta\phi)$ with respect to the azimuthal angle is factorized as

$$R_{AA}(p_T, cent, \Delta\phi) = F(\Delta\phi, p_T)\cdot R_{AA}(p_T, cent),$$

where $F(\Delta\phi, p_T)$ is the ratio of the relative yield, given as

$$F(\Delta\phi, p_T) = \frac{N(\Delta\phi, p_T)}{\int d\phi N(\Delta\phi, p_T)},$$

and $N(\Delta\phi, p_T)$ can be expressed in terms of a Fourier expansion with $\Delta\phi$.

$$N(\Delta\phi, p_T) \propto 1 + 2\sum_{n=1}^{\inf}(v_n\cos(n\Delta\phi)),$$

*1 RIKEN Nishina Center
*2 Center for Nuclear Study, Graduate School of Science, University of Tokyo

where v_n is the magnitude of the n-th order harmonic. The second harmonic, v_2, represents the strength of elliptic azimuthal anisotropy. The anisotropy v_2 at a low p_T is caused by the collective flow, which gives rise to the background in the measurement of $R_{AA}(p_T, \Delta\phi)$ for investigating energy loss.

The values of $\pi^0 v_2$ were calculated. π^0 v_2 was extracted by using the dN/dϕ method. In this method, v_2 is obtained by fitting the azimuthal angular distribution of π^0 with

$$N(\Delta\phi, p_T) = N(1 + 2v_2\cos(2\Delta\phi)).$$

π^0 values are reconstructed by the invariant mass method with reconstructed energy obtained using a photon spectrometer (PHOS) in the ALICE experiment.[2)] Fig.1 shows $\pi^0 v_2$ values as a function of p_T. In

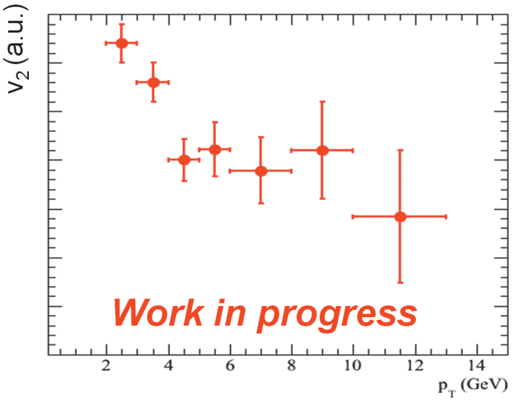

Fig. 1. $\pi^0 v_2$ values as a function of p_T. Bars indicate the amplitude of statistical errors estimated from all data for semi-central triggered events in 2011.

this figure, all data for semi-central triggered events in 2011 are analyzed. Centrality is defined by V0 detectors, which are scintillation detectors, and covers the range from -3.7 to -1.7 and from 2.8 to 5.1 in pseudo rapidity. In this plot, $\pi^0 v_2$ values denote the same tendency of the v_2 values of the charged particles qualitatively.[3)] Calculations of $\pi^0 v_2$ are presently ongoing.

References

1) A. Majumber: J. Phys. G. Nucl. Part. Phys. **34**, S377 (2007).
2) K. Aamodt et al., for the ALICE Collaboration: JINST **3**, S08002 (2008).
3) B. Abelev et al., for the ALICE Collaboration: Phys. Lett. **B719**, 18-28 (2013).

Measurement of high-p_T neutral mesons with a high-energy photon trigger at ALICE

S. Yano[*1] and K. Shigaki[*1]

ALICE, one of the experiments at the Large Hadron Collider (LHC) at CERN, is aimed at studying heavy-ion collisions and the properties of a deconfined state of matter, the quark-gluon plasma (QGP)[1)]. High-p_T particle production is a powerful tool for characterizing the QGP because the interaction of its fast partons depends on the QGP transport properties. The hadron yields in heavy-ion collisions can be quantified by the nuclear modification factor (R_{AA}), which is the ratio of the particle yield in heavy-ion collisions normalized by the number of inelastic nucleon–nucleon collisions to the yield in *pp* collisions. Previous experiments have shown that R_{AA} at high p_T is significantly smaller than 1, which can be explained by the energy loss of fast partons traversing in QGP.

The ALICE experiment has a high-resolution and high-granularity electromagnetic calorimeter called PHOS[1)]. One of the main achievable physics goals by PHOS is the study of the energy loss through the measurement of high-p_T neutral mesons (π^0 and η). Three PHOS modules are installed in the ALICE experiment, which covers azimuthal angles in the range $260° < \phi < 320°$ and pseudorapidity $|\eta| < 0.125$. PHOS provides a photon trigger (PHOS trigger) by requiring the measured energy to be above a threshold. The threshold was set to be 2 and 4 GeV in *pp* collisions at $\sqrt{s} = 8$ TeV and 7 GeV in *p*-Pb collisions at $\sqrt{s_{NN}} = 5.02$ TeV. By using the PHOS trigger, high-p_T neutral mesons can be efficiently measured in the ALICE experiment. This paper discribes the analysis status of neutral-pion production measured with the PHOS trigger and minimum-bias (MB) trigger data in *pp* collisions.

In this analysis, $0.3nb^{-1}$ MB-trigger data and $70nb^{-1}$ PHOS-triggered data in *pp* collisions at $\sqrt{s} = 8$ TeV are used. The PHOS-trigger efficiency as a function of measured photon energy is evaluated with real MB-trigger data. By using this efficiency, the efficiency for a parent particle is estimated through a simulation. For instance, neutral-pion trigger efficiency in *pp* collisions at $\sqrt{s} = 8$ TeV is shown in Fig. 1.

The rejection factor of the PHOS trigger for the MB-trigger data, R, was determined with real data in this analysis. R corresponds to the number of MB-trigger events inspected while one PHOS trigger is issued. It is 150 for 2-GeV threshold in *pp* at 8 TeV, 4800 for 4-GeV threshold in *pp* at 8 TeV, and 6500 for 7-GeV threshold in *p*-Pb at 5.02 TeV.

Fig. 2 shows the invariant raw yield of neutral pions measured with the MB trigger (open circles) and that with the PHOS trigger (closed circles) in *pp* collisions at $\sqrt{s} = 8$ TeV. Only the statistical errors are shown in Fig. 2. Up to 40 GeV/c, neutral pions can be measured with PHOS trigger. No other experiments have successfully measured neutral pions up to 40 GeV/c. At the low-p_T region, MB- and PHOS-trigger results are consistent with each other within statiscical errors.

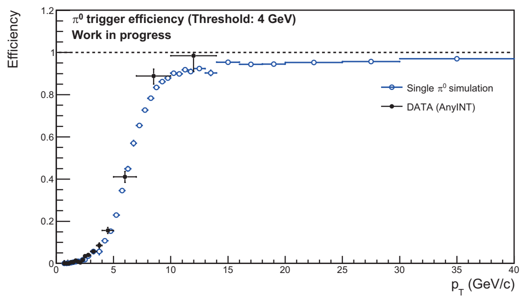

Fig. 1. Neutral-pion trigger efficiency.

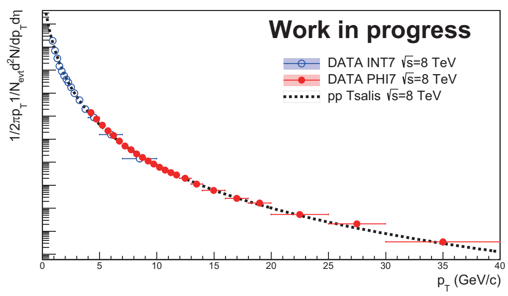

Fig. 2. Invariant raw yield of neutral pions in *pp* collisions at 8 TeV.

In summary, we began investigating PHOS-triggered data and attempting to extract the invariant yield of neutral mesons for the PHOS-triggered data. The final result of the invariant yield up to 40 GeV/c in *pp* collisions is expected to be obtained shortly. Furthermore, $1.6nb^{-1}$ PHOS-triggered data are recorded in *p*-Pb collisions at $\sqrt{s_{NN}} = 5.02$ TeV. Neutral pions above 40 GeV/c can be measured with this data set. The analysis of PHOS-trigger data will extend our understanding of high-p_T particle production beyond the previounsly published result[2)] of MB-tigger data. In Pb-Pb collisions, neutral pions near 40 GeV/c can be measured with data taken in 2011. By analyzing this data set, the extraction of R_{AA} for single particles up to 40 GeV/c will be possible, which is one of the future plans of our data analysis.

References
1) The ALICE Collaboration, JINST 3, S08002 (2008).
2) The ALICE colaboration, Phys.Lett.B 717 (2012), pp. 162 - 172.

*1 Department of Physics Science, Hiroshima University

Azimuthal distributions of jets with respect to high-p_T neutral pion triggers in pp collisions from ALICE

D. Watanabe[*1,*2] and T.Chujo[*2]

Jet measurements play a critical role in probing the hot and dense QCD medium created in heavy-ion collisions. Detailed transport properties of the medium can be extracted through measurements of parton energy loss and medium response with respect to the lost energy.

In general, the energy loss of recoil jets and leading jets depends on the path length in the medium (i.e, creation point and moving direction in the medium). For example, jet pairs with a large energy asymmetry in the final states can be from the surface of the medium,as shown in Fig.1. While leading jets escape the medium from the surface recoil jets traverse in the medium with loss to its energy. We use this surface bias to acquire deeper insight into the medium properties: The stronger the surface bias, the greater is the path length in the dense medium of the recoiling jet at the opposite azimuth. By measuring the full jets in the recoil side rather than measuring high-p_T hadrons, we can perform a more comprehensive and direct study of jet interactions in medium.[1)]

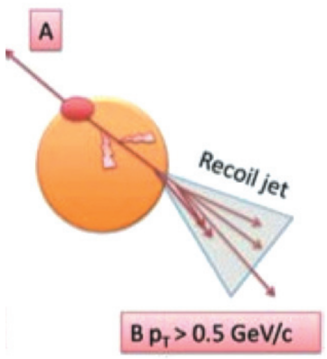

Fig. 1. Simple geometry of hadron-jet correlation with the leading particle in a recoil jet momentum threshold $p_T > 0.5$ (GeV/c)[2)]

In this paper, we report the jet azimuthal distribution with neutral pion triggers in pp collisions at $\sqrt{s}$ = 7 TeV from LHC-ALICE, which is very important as a baseline study for heavy-ion collisions. The ALICE detector was built as a general-purpose detector for measurements of ultra relativistic heavy ion collision at the LHC.[3)] For neutral pion identification, an electromagnetic calorimeter (EMCAL) is used. Jets are measured by a Time-Projection Chamber (TPC) and Inner-Tracking System (ITS).

This analysis used the shower shape and cluster splitting method[4)] to identify high p_T π^0. With this method, high p_T π^0 around 40 GeV/c can be identified with the signal-to-noise ratio of 90%.

Fig.2 shows the azimuthal angular correlation between π^0 and jet in pp collisions, where π^0 p_T is from 8 to 12 GeV/c and the associated jet p_T is higher than 10 GeV/c. From this distribution, two main observables will be discussed as the functions of trigger and associated p_T. One is the away-side yield per trigger yield, and the other is the width of the near-side and away-side correlation. These quantities will be discussed in the future, and similar analysis will be done for p-Pb and Pb-Pb collisions in order to understand the ordinal nuclear matter effects and the properties of the hot and dense medium.

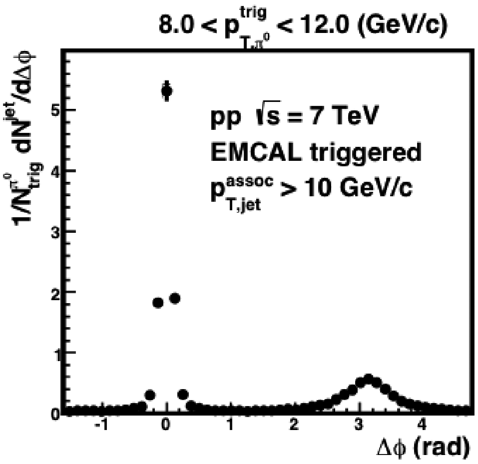

Fig. 2. π^0-jet azimuthal correlation with trigger p_T region of 8-12 GeV/c and associated jet threshold $p_{T,jet} > 10$ GeV/c

References
1) ALICE collaboration, An Addendum to the EMCal Technical Design Report (DCAL), CERN-LHCC-2010-011
2) STAR collaboration, M. Ploskon et al., Nucl. Phys. A830, 255c
3) ALICE collaboration, Performance of the ALICE Experiment at the CERN LHC, arXiv:1402.4476v2
4) ALICE collaboration, X. ZHU, Analysis of the π^0-charged hadron correlations using ALICE EMCAL, https://indico.cern.ch/event/181055/session/37/contribution/451

*1 RIKEN Nishina Center
*2 University of Tsukuba

Measurement of dielectron production in $\sqrt{s_{NN}} = 5.02$ TeV p-Pb collisions at LHC-ALICE

S. Hayashi,[*1] H. Hamagaki,[*1] and T. Gunji[*1]

In high-energy heavy-ion collisions, heavy quarks are primary produced during the initial hard scattering and experience the entire evolution of system. Therefore, they are sensitive to the transport properties of the hot and dense matter created in the collisons. In paticular, the correlation of heavy quark pairs provides key insight into the mechanisms of the energy loss and thermalization[1]. This can be studied through the measurement of dielectron production because correlated electron-positron pairs from semi-leptonic decays of heavy quarks are the dominant source of dielectrons above 1 GeV/c^2. The dielectron measurement around the intermediate-mass region in p-Pb collisions reveals cold-nuclear-matter effects such as gluon shadowing and gluon saturation on the heavy-quark production.

In the ALICE experiment, the Transition Radiation Detector (TRD) has a capability of the online electron identification and provides an electron trigger to enrich the data samples for the study of heavy-flavor electron production. In 2013, ALICE successfully collected data in p-Pb collisions with the TRD trigger ($L_{\rm int} = 1.4$ nb^{-1}) and the minimum bias trigger ($L_{\rm int} = 0.067$ nb^{-1}).

In the central barrel of the ALICE detector, charged tracks are reconstructed with the Inner Tracking System (ITS) and the Time Projection Chamber (TPC)[2]. Electrons are identified using dE/dx obtained in the TPC and time-of-flight measurement with the TOF detector (120ps resolution). TOF is essential to remove

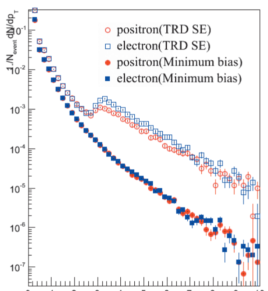

Fig. 1. Single-electron p_T distributions for the minimum-bias trigger and the TRD single-electron trigger.

contaminants such as of kaons, protons and deuterons up to 2 GeV/c. The hadron contaminations can be reduced less than 1% up to 6 GeV/c by the TOF information. Figure 1 shows the single-electron spectrum. A clear enhancement of electron samples by more than 20 times can be observed above 3 GeV/c for the TRD triggered data.

*1 Center for Nuclear Study, Graduate School of Science, the University of Tokyo

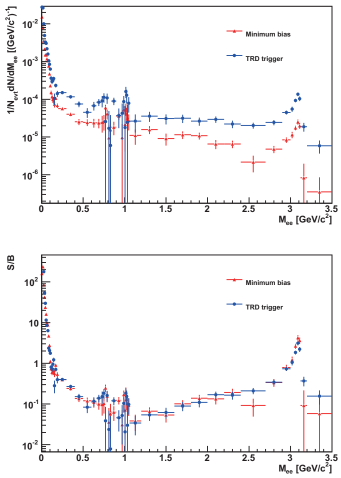

Fig. 2. Upper panel: The dielectron spectrum after background subtraction. Lower panel: the signal to background ratio.

For the estimation of the dielectron background, like-sign pairs in the same-events technique are used. Since the acceptance depends on the sign of charge, acceptance difference between unlike-sign and like-sign pairs is evaluated using mixed unlike-sign and mixed like-sign pairs. Equation 1 is calculated, and the R-factor is corrected to like-sign pairs to estimate the background.

$$R = \frac{N_{+-}|_{mix} + N_{-+}|_{mix}}{N_{++}|_{mix} + N_{--}|_{mix}} \quad (1)$$

where $N_{++}|_{mix}$, $N_{--}|_{mix}$ and $N_{+-}|_{mix}$, $N_{-+}|_{mix}$ are like-sign pairs and unlike-sign pairs in mixed events, respectively. The estimated background is defined as $N_{CB} = 2R\sqrt{N_{++}N_{--}}$, where N_{++}, N_{--} are like-sign pairs in the same event.

Figure 2 shows the inclusive dielectron spectrum after background subtraction, and the signal-to-background ratio. The vector mesons and J/ψ peaks can be seen clearly. The signal-to-background ratio agrees with the result of the pp collisions[3]. in different p_T bins.

References
1) X. Zhu *et al.*, Phys. Rev. Lett 100, 152301 (2008)
2) F. Carminati *et al.*, J. Phys. G: Nucl. Part. Phys. 30 (2004) 1517 1763
3) Markus K. Koehler, arXiv:1302.2049 (2013)

5. Hadron Physics (Theory)

Quark contribution for center domain in heavy ion collisions†

K. Kashiwa*1 and A. Monnai*1

The quark-gluon plasma (QGP) is characterized by large color opacity and near-perfect fluidity in high-energy heavy ion experiments at the Relativistic Heavy Ion Collider (RHIC) and the Large Hadron Collider (LHC). While hydrodynamic analyses have been quite successful in quantitative description of the hot media[1)], there are continuing debates on the origin of fluidity. It is recently proposed that center domain structure can be the key to the problem[2)]. QCD has SU(3) symmetry, and the Polyakov-loop potential has three minima in the QGP phase. Since the color glass condensate, a description of pre-collision state, implies that the typical correlation length on the transverse plane is characterized by the inverse of saturation scale in heavy ion collisions, a domain structure can appear in the hot medium. This indicates a short mean free path as the domains are separated by energy barrier.

In the present work, we introduce quark contribution to the center domain picture[3)]. We consider the gluon and quark perturbative one-loop effective potentials:

$$F_g = \frac{2\pi^2 T^4}{3}\sum_{a,b}\Big(1-\frac{\delta_{ab}}{3}\Big)B_4(|q_a-q_b|_{\mathrm{mod}\ 1}), \quad (1)$$

$$F_f = -\frac{4\pi^2 N_f T^4}{3}\sum_a B_4\Big(\Big|q_a+\frac{1}{2}\Big|_{\mathrm{mod}\ 1}\Big), \quad (2)$$

where T is temperature, a and b are color indices, B_4 is the forth Bernoulli polynomial, N_f is the number of flavors. q_a is defined by the classical part of the time-like component of the vector potential $(A_4^{cl})^{ab} = (2\pi T/g)q_a\delta^{ab}$, where g is the gauge coupling.

The overall effective potential[4)] is shown in Fig. 1. One can see that the three minima have the same free energy in the pure gauge case while imbalance is induced as the number of flavors increases. We label the three states as $\nu = 0$, 1 and 2 corresponding to the fact that Polyakov loop at the minima can be written as $\Phi = \exp(2\pi i\nu/3)$ in the high temperature limit.

The emergence of the stable ($\nu = 0$) and the metastable ($\nu = 1, 2$) states is important because pressure imbalance among the domains can lead to longer mean free path. Schematic pictures of parton scattering with different number of flavors/temperatures are summarized in Fig. 2; (a) In the pure gauge system, the typical mean free path is characterized by the domain size. (b) When the system has small number of flavors, the stable domains expand while the metastable ones shrink, leading to the longer mean free path on average. (c) Domain percolation can occur as the temperature further increases. (d) Finally, the metastable states vanish completely and the system can become weakly coupled above the topological critical temperature defined as $T_{\mathrm{cri}} = T(P_1 = P_2 = 0)$ where P_ν is the pressure. The increase in shear viscosity from RHIC to LHC temperatures is roughly estimated as ∼ 1.5-1.6 in our model, which is in agreement with the hydrodynamic implication from experimental data ∼ 1.7[5)].

We developed a model that can provide a bridge from hydrodynamic to perturbative QCD pictures. A new critical temperature is proposed, which implies that the medium can suddenly lose fluidity in heavy ion collisions of very high energies. Future prospects include investigation on the system size dependence.

† Condensed from the article in Phys. Rev. D 89, 011501(R) (2014)

*1 RIKEN Nishina Center

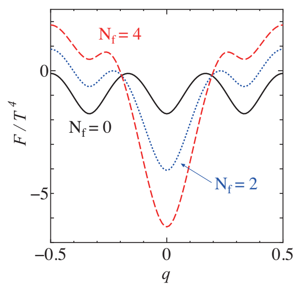

Fig. 1. Dimensionless effective potentials as a function of q for the number of flavors $N_f = 0$, 2 and 4.

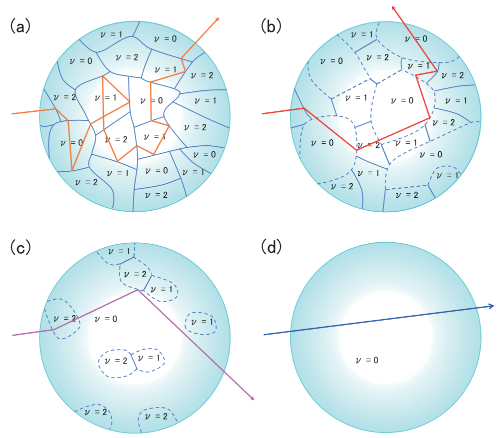

Fig. 2. Schematic pictures of the N_f dependence of the center domain structure and parton scattering.

References

1) B. Schenke *et al.*, Phys. Rev. Lett. **106**, 042301 (2011).
2) M. Asakawa *et al.*, Phys. Rev. Lett. **110**, 202301 (2013).
3) K. Kashiwa and A. Monnai, Phys. Rev. D **89**, 011501(R) (2014).
4) V. M. Belyaev *et al.*, Phys. Lett. B **277**, 331 (1992).
5) C. Gale *et al.*, Phys. Rev. Lett. **110**, 012302 (2013).

Signatures of chiral magnetic wave in heavy ion collisions

H. -U. Yee,[*1*2]

Chiral magnetic wave[1)] is a collective hydrodynamic mode of chiral charge densities in the presence of background magnetic field, as a consequence of underlying triangle anomaly of QCD. It has a longitudinal dispersion relation along the direction of the magnetic field

$$\omega = \pm v_\chi k - i D_L k^2 + \cdots , \tag{1}$$

where the chiral magnetic velocity v_χ is completely fixed by the thermodynamic charge susceptibility χ as

$$v_\chi = \frac{e N_c B}{4\pi^2 \chi} , \tag{2}$$

whereas the sign in front of the first term in the dispersion relation depends on the chirality, that is, left-handed charge fluctuations propagate in the opposite direction to that of the right-handed charge fluctuations. Since off-central heavy ion collisions can create magnetic fields as large as $eB \sim m_\pi^2$ at RHIC and about ten times larger at LHC, they provide an interesting environment where one can potentially test possible experimental signatures of chiral magnetic wave.

One observable that might be affected by the chiral magnetic wave is the elliptic flows of early photons and dileptons, for which the recent experimental data from RHIC indicate a value larger than the current theory estimate without taking into account the presence of magnetic fields. Earlier studies have suggested possible enhancement of the elliptic flows of photons due to the magnetic field, but a proper account of possible effects coming from chiral magnetic wave was first examined in Ref.[2)] in the framework of AdS/CFT correspondence. We observed that the chiral magnetic wave can significantly modify the elliptic flows for the momentum $p < 1$ GeV. Also, the quadrupole to the elliptic flow square ratio, v_4/v_2^2, is largely different from a constant, violating a typical scaling $v_4 \sim v_2^2$ for charged hadrons. We also predicted a distinctive signature in the polarization of photons originating from chiral magnetic wave. Future experiments probing the momentum range $p < 1$ GeV will be interesting to potentially see such behaviors due to chiral magnetic wave.

Another observable of interest is the charge dependent elliptic flows of pions, $\Delta v_2 \equiv v_2(\pi^-) - v_2(\pi^+)$, which was recently measured at RHIC. The QCD plasma formed by heavy ion collisions naturally has a small average positive vector charge density as a remnant of the colliding two positively charged nuclei, but one can also select events with any sign of the net charge that exist via statistical fluctuations. Recalling that $Q_V = Q_L + Q_R$ and $Q_A = -Q_L + Q_R$ where $Q_{V,A}$ are vector (axial) charge densities and $Q_{L,R}$ are left (right)-handed chiral charge densities, the initial vector charge density with average zero axial charge corresponds to having equal amounts of chiral charges Q_L and Q_R. Chiral magnetic wave acting on these chiral charges will move them apart in opposite directions along the magnetic field, which leads to a net vector charge quadrupole moment that is proportional to the initial vector charge density. Based on this, we predicted in Ref.[3)] that this quadrupole moment, in conjunction with the radial flow developed by hydrodynamic evolution, will eventually result in Δv_2 proportional to the initial vector charge density,

$$\Delta v_2 = r A_\pm , \quad A_\pm = \frac{(N_+ - N_-)}{(N_+ + N_-)} , \tag{3}$$

with a positive slope parameter r, which has been confirmed by the experimental analysis of RHIC. The simulation in Ref.[3)] for r to compare with experimental value was crude, neglecting many realistic elements in heavy ion collisions, and in Ref.[4)] we significantly improved the simulation by implementing a realistic 2+1 dimensional hydrodynamic code with isothermal Cooper-Frye freeze out condition, as well as chiral phase transition effect on the chiral magnetic wave. Our result for r and its dependence on the impact parameter compare well with experiments, although our analysis does not exclude other contributions unrelated to triangle anomaly.

In Ref.[5)] we systematically classified possible P and CP odd observables in photon and dilepton emission rates. Since axial charge is P and CP odd, which is a unique characterization of it, these observables must be proportional to event-by-event fluctuations of axial charges in the QCD plasma formed in heavy ion collisions. Our observables are related to spin (helicity) alignments of the photons and dileptons, and we have shown that they probe the imaginary part of the chiral magnetic conductivity of the plasma at finite momenta, which ultimately arises from the underlying triangle anomaly of QCD.

References

1) D. E. Kharzeev and H. -U. Yee: Phys. Rev. D **83**, 085007 (2011).
2) H. -U. Yee: Phys. Rev. D **88**, 026001 (2013).
3) Y. Burnier, D. E. Kharzeev, J. Liao and H. -U. Yee: Phys. Rev. Lett. **107**, 052303 (2011).
4) H. -U. Yee and Y. Yin, Phys. Rev. C **89**, 044909 (2014).
5) K. A. Mamo and H. -U. Yee: Phys. Rev. D **88**, 114029 (2013).

*1 Department of Physics, University of Illinois, Chicago
*2 RIKEN Nishina Center

Dihadron Fragmentation Functions in the NJL-Jet Model†

H. Matevosyan,*1 W. Bentz,*2*3 and A. W. Thomas *1

[QUARK FRAGMENTATION FUNCTIONS]

In order to describe the scattering of high energy electrons on nuclear targets in terms of quark degrees of freedom, the Nambu-Jona-Lasinio (NJL) model is often used as an effective theory of QCD. For example, this model was successfully applied in Ref.[1] to describe quark distribution and fragmentation functions observed in semi-inclusive deep inelastic scattering (SIDIS) processes. Here we extend the model to the description of dihadron fragmentation functions (DiFFs), which are expected to play an important role for extracting the transversity parton distribution functions from SIDIS processes with two final detected hadrons[2].

The unpolarized DiFFs ($D_q^{h_1 h_2}(z, M_h^2)$) for the process $q \to h_1 h_2$ depend on the sum of the light-cone momentum fractions $z = z_1 + z_2$ and the invariant mass squared $M_h^2 = (P_1 + P_2)^2$ of the produced hadron pair. In order to calculate these functions, we use the quark jet picture, with the elementary fragmentation functions for $q \to h$ calculated in the NJL-jet model[3]. The multihadron emissions from a high energy virtual quark (flavor $q = u, d, s$) are described by using Monte-Carlo techniques, averaging over a sufficiently large number of events (10^{10} in the results shown below) and restricting the total number of primary emitted hadrons for each fragmentation chain to a predefined number (equal to eight in the results below). In this study we include the pseudoscalar π, K and vector (ρ, ω, K^* and ϕ) mesons. The strong 2-body and 3-body decays of the primary vector mesons to secondary π and K are also included in the simulations, and are very important to describe the invariant mass spectra of the final π and K pairs.

Fig.1 shows the DiFF for $u \to \pi^+\pi^-$, integrated over z in the region 0.2 to 0.8, for the cases of primary mesons only (dashed line) and the full final states including the decay products of the primary vector mesons (solid line). The ρ^0 peak around $M_h^2 \simeq (0.78\,\mathrm{GeV})^2$, and the enhancement in the region below 0.4 GeV^2 coming from $\omega \to \pi^+\pi^-\pi^0$ with shifted invariant mass due to the unobserved π^0, are clearly seen in the figure. Fig.2 shows the results obtained by performing the Q^2 evolution in leading order (LO), where we assign a typical NJL-jet scale of 0.2 GeV^2 to the model results shown by the solid lines in Figs. 1 and 2. The vector meson decays have an important influence on the shape of the DiFFs even at very high values of Q^2.

The future development of our model will allow us to extract also the so called interference DiFFs by considering the fragmentation of a transversely polarized quark, which also play an important role to extract the transversity distribution functions from measured SIDIS two-hadron asymmetries.

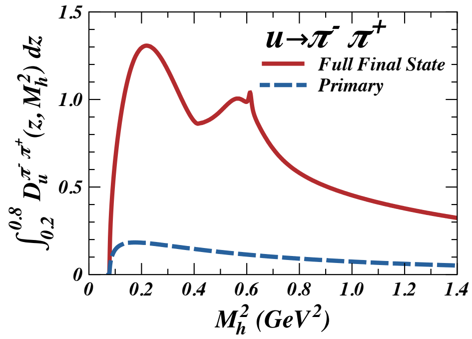

Fig. 1. Fragmentation function for $u \to \pi^+\pi^-$ calculated in the NJL-jet model, including only primary (dashed line) and full (solid line) final states.

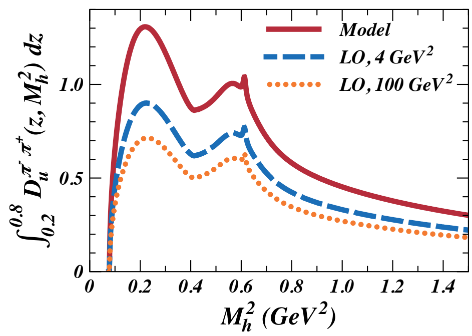

Fig. 2. The solid line is the same as in Fig.1, and the other lines show the results obtained by the Q^2 evolution in leading order (LO) to higher energy scales.

This work was supported by the Australian Research Council (Grants No. FL0992247 and No.CE110001004), the University of Adelaide, and the Japanese Ministry of Education, Culture, Sports, Science and Technology (Kakenhi Grant No. 20168769).

References
1) H. H. Matevosyan, W. Bentz, I.C. Cloët, A.W. Thomas, Phys. Rev. **D 85**, 014021 (2012).
2) R.L. Jaffe, X. Jin, J. Tang, Phys. Rev. Lett. **80**, 1166 (1998).
3) T. Ito, W. Bentz, I.C. Cloët, A.W. Thomas, K. Yazaki, Phys. Rev. **D 80**, 074008 (2009).

† Condensed from an article by H.H. Matevosyan et al, Phys. Rev. **D 88**, 094022 (2013).
*1 University of Adelaide
*2 Department of Physics, Tokai University
*3 RIKEN Nishina Center

Twist-3 fragmentation and transverse single-spin asymmetries†

D. Pitonyak*1

Transverse single-spin asymmetries (TSSAs) in inclusive hadron production (denoted by A_N) have been the subject of intense study since the late 1970s. These are defined as

$$A_N = \frac{d\sigma(\vec{S}_\perp) - d\sigma(-\vec{S}_\perp)}{2\, d\sigma_{unp}}\,, \tag{1}$$

where $d\sigma(\vec{S}_\perp)$ $(d\sigma(-\vec{S}_\perp))$ is the cross section with transverse spin $\vec{S}_\perp$ oriented "up" ("down") and $d\sigma_{unp}$ is the unpolarized cross section. Experiments have measured large effects for these observables (with the most recent results from proton-proton collisions at RHIC[1–3]), which contradict the prediction of the naïve collinear parton model[4]. However, a framework using twist-3 multi-parton correlators can potentially describe these large TSSAs[5–7].

The assumption for many years was that the so-called soft-gluon pole (SGP) piece dominates over the other contributions[7,8]. This part involves the non-perturbative twist-3 Qiu-Sterman (QS) function $T_F(x,x)$[6,7], which was extracted several years ago[8]. However, a later analysis revealed that this extraction of $T_F(x,x)$ does not satisfy the model-independent relation with the Sivers function extracted from semi-inclusive deep-inelastic scattering (SIDIS) off a transversely polarized proton: the two different extractions disagree in sign[9]. This "sign mismatch" crisis has led to a reexamination of whether the QS function is the most significant part of TSSAs in inclusive hadron production — see, e.g., the recent discussion[10]. The focus has now shifted to whether a contribution involving twist-3 fragmentation functions can resolve the "sign mismatch" and provide the dominant effect.

The complete analytic result for the twist-3 fragmentation term in the single-spin dependent cross section for $p^\uparrow p \to hX$ was given for the first time by the present author and A. Metz[11]:

$$\begin{aligned}\frac{P_h^0 d\sigma(\vec{S}_\perp)}{d^3\vec{P}_h} &= -\frac{2\alpha_s^2 M_h}{S}\epsilon_{\perp,\alpha\beta}\, S_\perp^\alpha P_{h\perp}^\beta \\ &\times \sum_i \sum_{a,b,c}\int_{z_{min}}^1 \frac{dz}{z^3}\int_{x'_{min}}^1 \frac{dx'}{x'}\,\frac{1}{x}\,\frac{1}{x'S+T/z} \\ &\times \frac{1}{-x'\hat{t}-x\hat{u}}\, h_1^a(x)\, f_1^b(x')\left\{\left[\hat{H}^c(z) - z\frac{d\hat{H}^c(z)}{dz}\right]S_{\hat{H}}^i\right. \\ &+\frac{1}{z}H^c(z)\, S_H^i \\ &\left.+\, 2z^2\int \frac{dz_1}{z_1^2}PV\frac{1}{\frac{1}{z}-\frac{1}{z_1}}\hat{H}_{FU}^{c,\Im}(z,z_1)\,\frac{1}{\xi}\,S_{\hat{H}_{FU}}^i\right\}. \end{aligned} \tag{2}$$

See the paper[11] for more details. In particular, Appendix A of the aforementioned reference contains the hard scattering coefficients S^i in (2).

The piece in (2) also involves two independent non-perturbative functions: $\hat{H}(z)$ and $\hat{H}_{FU}^{\Im}(z,z_1)$. (The function $H(z)$ can be written in terms of the other two.) In principle one has information on $\hat{H}(z)$ through its relation to the Collins function in SIDIS. One must then parameterize the unknown function $\hat{H}_{FU}^{\Im}(z,z_1)$ and see if a fit to the data[1–3] is possible. We propose the following form for this (3-parton) fragmentation correlator that is consistent with its support properties:

$$\begin{aligned}\hat{H}_{FU}^{\Im}(z,z_1) &= N z^\alpha (z/z_1)^\beta (1-z)^\delta (1-z/z_1)^\gamma \\ &\times D_1(z)\, D_1(z/z_1)\,,\end{aligned} \tag{3}$$

where D_1 is the unpolarized fragmentation function. We are in the process of carrying out a numerical study of A_N in $p^\uparrow p \to \pi X$ using (3). This will be an important step towards solving an almost 40 year problem of what causes large TSSAs in inclusive hadron production from proton-proton collisions.

References

1) I. Arsene *et al.* [BRAHMS Collaboration], Phys. Rev. Lett. **101**, 042001 (2008) [arXiv:0801.1078 [nucl-ex]].
2) L. Adamczyk *et al.* [STAR Collaboration], Phys. Rev. D **86**, 051101 (2012) [arXiv:1205.6826 [nucl-ex]].
3) A. Adare *et al.* [PHENIX Collaboration], arXiv:1312.1995 [hep-ex].
4) G. L. Kane, J. Pumplin and W. Repko, Phys. Rev. Lett. **41**, 1689 (1978).
5) A. V. Efremov and O. V. Teryaev, Sov. J. Nucl. Phys. **36**, 140 (1982) [Yad. Fiz. **36**, 242 (1982)]; Phys. Lett. B **150**, 383 (1985).
6) J.-w. Qiu and G. F. Sterman, Phys. Rev. Lett. **67**, 2264 (1991); Nucl. Phys. B **378**, 52 (1992).
7) J.-w. Qiu and G. F. Sterman, Phys. Rev. D **59**, 014004 (1999) [hep-ph/9806356].
8) C. Kouvaris, J. W. Qiu, W. Vogelsang and F. Yuan, Phys. Rev. D **74**, 114013 (2006) [arXiv:hep-ph/0609238].
9) Z. -B. Kang, J. -W. Qiu, W. Vogelsang and F. Yuan, Phys. Rev. D **83**, 094001 (2011) [arXiv:1103.1591 [hep-ph]].
10) A. Metz, D. Pitonyak, A. Schäfer, M. Schlegel, W. Vogelsang and J. Zhou, Phys. Rev. D **86**, 094039 (2012) [arXiv:1209.3138 [hep-ph]].
11) A. Metz and D. Pitonyak, Phys. Lett. B **723**, 365 (2013) [arXiv:1212.5037 [hep-ph]].

† Condensed in part from the article in Phys. Lett. B, Vol. 723, 365 (2013), whose work was funded by the NSF under Grant No. PHY-1205942

*1 RIKEN Nishina Center, Brookhaven National Lab

Polarized fragmentation functions and electron-positron annihilation†

D. Pitonyak*1

Electron-positron annihilation into (possibly polarized) hadrons, where one or more hadrons are identified, gives one access to fragmentation functions (FFs), which embody the process of a parton forming a hadron, and they contain important information about the strong interaction in the non-perturbative regime. (These are analogous to parton distribution functions (PDFs) that look at partons inside of hadrons.) Such experiments have been run by both the Belle Collaboration at KEK in Japan and the BABAR Collaboration at SLAC in the US. In order to have a complete framework to analyze FFs in electron-positron annihilation, one must write the cross section in a general form involving structure functions, which can then be calculated (for small transverse momentum of the exchanged boson) in terms of twist-2 transverse momentum dependent (TMD) FFs. For the future International Linear Collider (ILC), it is also beneficial to have complete results for polarized leptons including electroweak effects. Given its similarity to Drell-Yan, one should also be able to transcribe such results to that reaction, which would be useful for double-polarized Drell-Yan experiments at RHIC.

Here we extend earlier works[1–5] in order to address these issues. The cross section for the reaction $e^+e^- \to h_a h_b\, X$ is given by

$$4\frac{P_a^0 P_b^0\, d\sigma}{d^3\vec{P}_a d^3\vec{P}_b} = \frac{2\alpha_{em}^2}{q^2}\,(L_{\mu\nu}W^{\mu\nu})_{\gamma\gamma} + \frac{M_Z^4 G_F^2}{64\pi^2 q^2}\,(L_{\mu\nu}W^{\mu\nu})_{ZZ} + \frac{\alpha_{em}\sqrt{2}M_Z^2 G_F}{8\pi q^2}((L_{\mu\nu}W^{\mu\nu})_{\gamma Z} + h.c.)\,, \quad (1)$$

where one has leptonic tensors $L^{\mu\nu}$ and hadronic tensors $W^{\mu\nu}$ for γ-exchange, Z-exchange, and their interference. As the present author, M. Schlegel, and A. Metz discuss in detail[6], one can write down the first term in (1) in terms of 72 structure functions using electromagnetic gauge invariance, hermiticity, and parity (see Eq. (3.21) of [6]). The second and third terms are more involved due to the fact that one no longer has the parity constraint. Nevertheless, one can calculate these terms (as well as the first) within the parton model at twist-2. The result leads to 128 structure functions (see Eqs. (4.34), (4.35) and Appendix A of [6]). Where relevant, we have checked our results with those in[1–4]. Thus, we have for the first time a complete framework for the study of TMD FFs within $e^+e^- \to h_a h_b\, X$ including electroweak terms and the polarization of all particles.

We also note that if we make the replacements $(4P_a^0 P_b^0 d\sigma/d^3\vec{P}_a d^3\vec{P}_b)_{e^+e^-} \longrightarrow (4l^0 l'^0 d\sigma/d^3\vec{l}\, d^3\vec{l}')_{DY}$, $z_a\,(z_b) \to x_a\,(x_b)$, and $N_c \to 1/N_c$, the structure functions associated with unpolarized leptons for the pure electromagnetic case are the same as those given in Drell-Yan[5] with the TMD PDFs replaced by their TMD FF analogues. The only additional change one must remember is that h_a (h_b) in the e^+e^- case has a large minus- (plus-) component of momentum, whereas for Drell-Yan one normally uses the reverse convention. Along the same lines, one can easily transcribe the results in Appendix A of [6] to obtain the relevant expressions for Drell-Yan when one allows the $q\bar{q}$ pair to annihilate into a Z-boson. Thus, we have for the first time full results for double-polarized Drell-Yan that include electroweak effects, which would be needed if such experiments were conducted at RHIC.

We would finally like to highlight a structure function that appears in [6] for first time:

$$G_{UU}^{\cos 2\phi, ew} = \sum_q \mathcal{F}_5^{q-}(s)\, C_{ew}^q\big[w_3\, H_1^\perp\, \bar{H}_1^\perp\big]\,, \qquad (2)$$

where $\mathcal{F}_5^{q-}(s)$ is a prefactor that is nonzero if Z-exchange is included, $C_{ew}^q[\cdots]$ is the convolution of a weight w_3 and the Collins function $H_1^\perp$. One could access (2) at a future ILC and extract the Collins function. This result could then be checked against the Collins function that has been obtained recently from Belle and BABAR data[7]. Given that the ILC would have around two orders of magnitude higher center-of-mass energy than Belle and BABAR, such an analysis would also be an important test of the TMD evolution formalism and its application to phenomenology, which has been of recent interest.

References

1) D. Boer, R. Jakob and P. J. Mulders, Nucl. Phys. B **504**, 345 (1997) [hep-ph/9702281]; Phys. Lett. B **424**, 143 (1998) [hep-ph/9711488].
2) D. Boer, R. Jakob and P. J. Mulders, Phys. Lett. B **424**, 143 (1998) [hep-ph/9711488].
3) D. Boer, Phys. Rev. D **60**, 014012 (1999) [hep-ph/9902255].
4) D. Boer, Nucl. Phys. B **806**, 23 (2009) [arXiv:0804.2408 [hep-ph]].
5) S. Arnold, A. Metz and M. Schlegel, Phys. Rev. D **79**, 034005 (2009) [arXiv:0809.2262 [hep-ph]].
6) D. Pitonyak, M. Schlegel and A. Metz, arXiv:1310.6240 [hep-ph].
7) M. Anselmino, M. Boglione, U. D'Alesio, S. Melis, F. Murgia and A. Prokudin, Phys. Rev. D **87**, 094019 (2013) [arXiv:1303.3822 [hep-ph]].

† Condensed from the article arXiv:1310.6240 [hep-ph] submitted to Physical Review D

*1 RIKEN Nishina Center, Brookhaven National Lab

Spatial Wilson loops in high-energy heavy-ion collisions

A. Dumitru[*1,*2]

Collisions of heavy ions at high energies provide opportunity to study non-linear dynamics of strong QCD color fields[1)]. The field of a very dense system of color charges at rapidities far from the source is determined by the classical Yang-Mills equations with a recoilless current along the light cone[2)]. It consists of gluons characterized by a transverse momentum p_T on the order of the density of valence charges per unit transverse area Q_s^2; this saturation momentum scale separates the regime of non-linear color field interactions at $p_T \lesssim Q_s$ or distances $r \gtrsim 1/Q_s$ from the perturbative regime at $p_T \gg Q_s$.

Right after the impact strong longitudinal chromomagnetic fields $B_z \sim 1/g$ develop due to the fact that the individual projectile and target fields do not commute[3)]. They fluctuate according to the random local color charge densities of the valence sources. Here we show that magnetic loops

$$W_M(R) = \frac{1}{N_c}\left\langle \mathrm{tr}\,\mathcal{P}\exp\left(ig\oint dx^i A^i\right)\right\rangle \tag{1}$$

effectively exhibit area law scaling, $W_M(R) \sim e^{-\sigma\,\pi R^2}$, and we compute the magnetic string tension σ. Furthermore, we argue that at length scales $\sim 1/Q_s$ the field configurations might be viewed as uncorrelated Z(N) vortices. We also compare to the expectation value of the Z(N_c) part of the loop; thus, for two colors we compute

$$W_M^{Z(2)}(R) = \left\langle \mathrm{sgn}\,\mathrm{tr}\,\mathcal{P}\exp\left(ig\oint dx^i A^i\right)\right\rangle \tag{2}$$

where sgn() denotes the sign function.

The field in the forward light cone immediately after a collision[4)], at proper time $\tau \equiv \sqrt{t^2-z^2} \to +0$, is given by $A^i = \alpha_1^i + \alpha_2^i$. In turn, before the collision the individual fields of projectile and target are 2d pure gauges,

$$\alpha_m^i = \frac{i}{g}U_m\,\partial^i U_m^\dagger \quad , \quad \partial^i\alpha_m^i = g\rho_m\ , \tag{3}$$

where $m = 1,2$ labels projectile and target, respectively, and U_m are SU(N) matrices. Note that for a non-Abelian gauge group, the sum A^i of two pure gauges is not a pure gauge, so $W_M \neq 1$.

The large-x valence charge density ρ is a random variable. For a large nucleus, the effective action describing color charge fluctuations is quadratic[2)], $S_{\rm eff} = \rho^a(\mathbf{x})\rho^a(\mathbf{x})/2\mu^2$. The variance of color charge fluctuations determines the saturation scale $Q_s^2 \sim g^4\mu^2$. The brackets in eq. (1) denote an average over the fluctuating color charges $\rho_1(\mathbf{x})$, $\rho_2(\mathbf{x})$ of the two charge sheets corresponding to projectile and target, respectively.

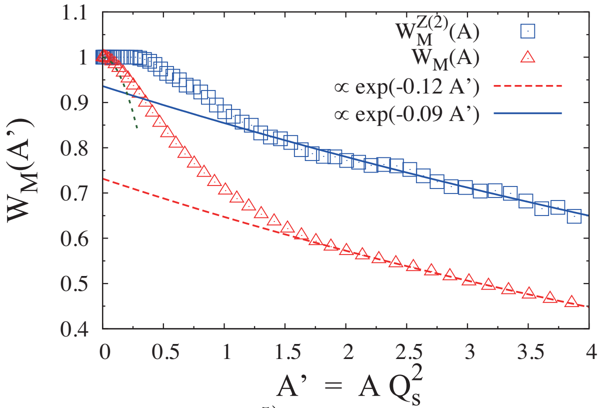

Fig. 1. Expectation value[5)] of the magnetic flux loop right after a collision of two nuclei (time $\tau = +0$) as a function of its area $A' \equiv A\,Q_s^2$. Symbols show numerical results for $SU(2)$ Yang-Mills on a 4096^2 lattice; the lattice spacing is set by $g^2\mu_L = 0.0661$. The lines represent fits over the range $4 \geq A' \geq 2$.

In fig. 1 we show numerical results for W_M immediately after a collision. It exhibits area law behavior for loops larger than $A \gtrsim 2/Q_s^2$. The corresponding "magnetic string tension" is $\sigma_M/Q_s^2 = 0.12(1)$. The area law indicates uncorrelated magnetic flux fluctuations through the Wilson loop and that the area of magnetic vortices is rather small, their radius being on the order of $R_{\rm vtx} \sim 0.8/Q_s$. We do not observe a breakdown of the area law up to $A \sim 4/Q_s^2$, implying that vortex correlations are small at such distance scales. Also, restricting to the Z(2) part reduces the magnetic flux through small loops but σ_M is comparable to the full SU(2) result.

References

1) A. H. Mueller, Nucl. Phys. B **558**, 285 (1999).
2) L. D. McLerran and R. Venugopalan, Phys. Rev. **D 49**, 2233 (1994), Phys. Rev. **D 49**, 3352 (1994); Y. V. Kovchegov, Phys. Rev. **D 54**, 5463 (1996).
3) D. Kharzeev, A. Krasnitz and R. Venugopalan, Phys. Lett. B **545**, 298 (2002); R. J. Fries, J. I. Kapusta and Y. Li, nucl-th/0604054; T. Lappi and L. McLerran, Nucl. Phys. A **772**, 200 (2006).
4) A. Kovner, L. D. McLerran and H. Weigert, Phys. Rev. D **52**, 6231 (1995); Phys. Rev. D **52**, 3809 (1995).
5) A. Dumitru, Y. Nara and E. Petreska, Phys. Rev. D **88**, 054016 (2013).

† Condensed from the article in Phys. Rev. D, Vol. 88, 054016 (2013)
*1 Department of Natural Sciences, Baruch College (CUNY)
*2 RIKEN Nishina Center

Bose-Einstein Condensation in "the very hot"

J. Liao[*1,*2]

In relativistic heavy ion collisions, a highly occupied gluonic matter is created shortly after initial impact, which is in a non-thermal state and often referred to as the glasma. How the glasma evolves quickly toward an emergent hydrodynamic behavior remains a significant challenge for theory as well as phenomenology. Recently there has been important progress in understanding the pre-equilibrium evolution using the kinetic theory description, in a highly overpopulated regime[1–3)] where the system is weakly coupled yet strongly interacting with the possibility of a transient BEC during the course of thermalization.

Inspired by the Color Glass Condensate description of the initial conditions, the gluon distribution in the glasma is schematically given by $f(p \leq Q_s) = f_0$, $f(p > Q_s) = 0$ with Q_s the saturation scale. One may introduce the overpopulation parameter $n\epsilon^{-3/4}$ which is directly related to the ratio between inter-particle distance d and typical de Broglie wavelength λ, i.e. $n\epsilon^{-3/4} \sim (\lambda/d)^{\alpha}$ thus measuring the degrees of quantum coherence: when $n\epsilon^{-3/4} \to \hat{o}(1)$ then $\lambda \to d$ and one expects BEC to occur. In the glasma distribution $n_0\epsilon_0^{-3/4} = f_0^{1/4}\,\frac{2^{5/4}}{3\,\pi^{1/2}}$ and, compared with thermal case $n\,\epsilon^{-3/4}|_{SB} = \frac{30^{3/4}\,\zeta(3)}{\pi^{7/2}} \approx 0.28$, the system becomes *overpopulated* when $f_0 > f_0^c \approx 0.154$. One thus see in the glasma with $f_0 = 1/\alpha_s$, even with rather modest weak coupling $\alpha_s \simeq 0.3$ the system is highly overpopulated and will develop Bose condensate.

So how does the thermalization proceed in such a overpopulated glasma? Numerical solutions reported in [2)] suggest two generic features. First, two cascades in momentum space will quickly develop: a particle cascade toward the IR momentum region that quickly populates the soft momentum modes to high occupation, and a energy cascade toward the UV momentum region that spreads the energy out. As a consequence a high occupation number at IR is quickly achieved, leading to the second interesting feature: an almost instantaneous local "equilibrium" form for the distribution near the origin $\vec{p} \to 0$: $f^*(p \to 0) = \frac{1}{e^{(p-\mu^*)/T^*}-1}$. In the overpopulated case the IR cascade persists to drive the local thermal distribution near $p = 0$ to increase rapidly in a self-similar form (see Fig.1 upper). The associated negative local "chemical potential" is driven to approach zero, i.e. $(-\mu^*) \to 0^+$ and ultimately vanishes in a finite time, marking the onset of the condensation. The approaching toward onset is well described by a scaling behavior: $|\mu^*| = C(\tau_c - \tau)^{\eta}$ with a universal exponent $\eta \approx 1$ for varied values of $f_0 > f_0^c$. Such general link from initial overpopulation to the onset of BEC *in a finite time* with a scaling behavior appears to be very robust against different choices of initial distribution shapes and possible initial anisotropy, including longitudinal expansion, as well as adding finite medium-generated mass.

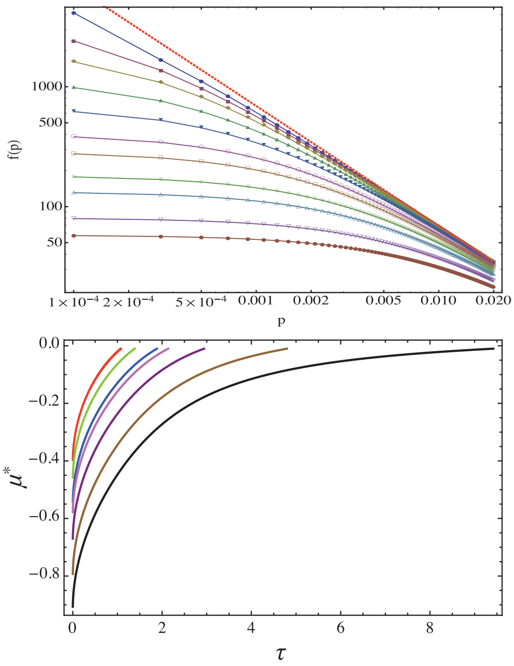

Fig. 1. Local thermal form (upper) of $f(p \to 0)$ and the vanishing of local chemical potential $\mu^* \to 0$ (lower).

There is one particularly important issue related to the role of inelastic processes. One may even wonder if such onset (manifested as the development of an infrared singularity in the kinetic evolution) would happen anymore. To answer this, one needs to study the kinetic evolution including both processes: a first attempt has been done, recently in [3)]. Contrary to usual expectation, it is found that the inelastic process has two effects: globally changing (mostly reducing) the total particle number, while locally at small p always filling up the infrared regime extremely quickly. This latter effect is found to significantly speed up the emergence of local thermal form with vanishing local "chemical potential" and catalyzes the onset of Bose condensation to occur faster (as compared with the purely elastic case) in the overpopulated glasma.

References

1) J. -P. Blaizot, F. Gelis, J. -F. Liao, L. McLerran and R. Venugopalan, Nucl. Phys. A **873**, 68 (2012).
2) J. -P. Blaizot, J. Liao and L. McLerran, Nucl. Phys. A **920**, 58 (2013).
3) X. -G. Huang and J. Liao, arXiv:1303.7214 [nucl-th].

*1 Physics Department and Center for Exploration of Energy and Matter, Indiana University
*2 RIKEN Nishina Center

Out-of-equilibrium chiral magnetic effect at strong coupling†

S. Lin *1 and H-U. Yee*1,*2

The chiral magnetic effect in relativistic heavy-ion collisions has been proposed as a signature of local parity violation in QCD above deconfinement phase transition[1]. The manifestation of the chiral magnetic effect requires both a strong magnetic field and chiral imbalance in fundamental quarks. Despite continuous theoretical efforts in understanding the effect, many quantitative questions remain unanswered. One of them is the value of the chiral magnetic conductivity, which is complicated by the fact that the magnetic field produced by the spectators exists only at the early stage of the collisions, when quark-gluon plasma (QGP) is not yet thermalized. An accurate calculation of the chiral magnetic conductivity should be carried out for QGP in an out-of-equilibrium setting. In this work, we report on our attempt in this direction

We considered chirally imbalanced QGP undergoing thermalization. It can be modeled by a gravitationally collapsing shell in 5D Anti-de Sitter (AdS) space. The shell carries an axial charge density, described by an axial chemical potential μ_A. The end point of the gravitational collapse is the formation of the AdS-Reissner-Nordstrom (AdS-RN) black hole, which is dual to QGP with an axial charge density. The central quantity is the chiral magnetic conductivity in the thermalization process. It is defined for at finite frequencies as the response of the vector current to the external magnetic field

$$\vec{J}_{EM} = \sigma_\chi(\omega)\vec{B}(\omega). \tag{1}$$

This is to be evaluated at different times in the thermalization history. Note that (1) assumes the current response is much faster than the evolution of QGP toward equilibrium, which is not true in the near-equilibrium regime. We restricted our study to the far-from equilibrium regime. We obtained the chiral magnetic conductivity for different frequencies in Fig. 1. The end point QGP has a temperature $T = 300$ MeV and an axial chemical potential $\mu_A = 50$ MeV. We found that in general the chiral magnetic conductivity increases as QGP thermalizes, which is consistent with the expectation that more and more thermalized constituents are available in conducting the current. We also found that the magnitude of conductivity changes only slightly as the frequency of the magnetic field is varied, while increasing the frequency does results in longer delay in the response. We stress that the conventional conductivity has the opposite behavior.

We also studied the chiral magnetic wave in the same thermalization model for QGP with vanishing axial charge density. The chiral magnetic wave rises from a coupled fluctuation of the axial and vector charges in the presence of a background magnetic field. In equilibrium, it has the dispersion $\omega = \mp v_\chi k$, with the wave velocity proportional to the magnetic field and the velocity changes sign when the chirality of the charge is reversed[2]. We found that the dispersion relation is modified to

$$\omega = v_{out}k \mp \Delta\omega(k, B). \tag{2}$$

We see that the frequency splits into two terms: The first term is entirely of off-equilibrium origin: the wave velocity v_{out} vanishes as QGP thermalizes; It is also independent of the chirality of the charge. The second term depends on the chirality, and it is linear in both k and B. It is reminiscent of chiral magnetic wave velocity in equilibrium. This shows that the physical effect of the chiral magnetic wave may be enhanced owing to the out-of-equilibrium effect.

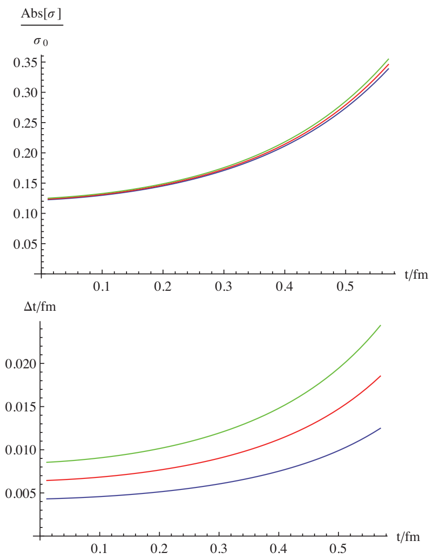

Fig. 1. The chiral magnetic conductivity as a function of thermalization history for frequencies $\omega = 200$ MeV(blue solid), $\omega = 300$ MeV(red dashed) and $\omega = 400$ MeV(green dotted). The left plot shows the magnitude normalized by chiral magnetic conductivity in equilibrium and the right plot shows the time delay of the response.

References
1) D. E. Kharzeev, L. D. McLerran and H. J. Warringa, Nucl. Phys. A **803**, 227 (2008)
2) D. E. Kharzeev and H. -U. Yee, Phys. Rev. D **83**, 085007 (2011)

† Condensed from the article in Phys. Rev. D **88**, 025030 (2013)
*1 RIKEN Nishina Center
*2 Department of Physics, University of Illinois at Chicago

RIKEN Accel. Prog. Rep. 47 (2014)

General conditions ensuring relativistic causality in an effective field theory based on the derivative expansion†

Y. Minami*1 and Y. Hidaka*1

We discuss the general conditions ensuring relativistic causality in an effective field theory based on the derivative expansion. Relativistic causality implies that the Green function vanishes in a space-like region. It is known that a naive derivative expansion violates causality in some cases such as the first-order relativistic dissipative hydrodynamics. We note that the Lorentz covariance and time and space derivatives of equal order do not ensure causality. We derive the general conditions for causality that should be satisfied by any effective theory consistent with special relativity.

Derivative expansion is a useful tool at a low-energy scale and widely used in effective theories. Chiral perturbation theory is a good example of a successful low-energy effective theory in hadron physics[1]. From a modern perspective, hydrodynamics is also a low-enegy effective theory; the leading-order hydrodynamic equations are called Euler equations, and the first-order hydrodynamic equations are called Navier–Stokes equations.

Causality is an important concept in physics. In relativistic systems, the propagation of any information cannot exceed the speed of light (relativistic causality). However, it seems that a low-energy effective theory in medium is incompatible with relativistic causality. For example, in first-order relativistic hydrodynamics, shear and heat flows violate causality because the first-order equation has the form of a diffusion equation[2,3]. We note that the first-order hydrodynamic equation is Lorentz covariant, i.e., the covariance does not ensure the causality. It is argued that the acausality of the first-order hydrodynamics originates from the difference between the order of time- and space-like derivatives in the equation of motion. In the diffusion equation, the time-like derivative is of the first order, while the space-like one is of the second order. However, we note that equality in the order of time- and space-like derivatives does not ensure the causality. For example, let us consider the following equation:

$$\left[\tau(u^\mu\partial_\mu)^2+u^\mu\partial_\mu+\Gamma(\eta^{\mu\nu}-u^\mu u^\nu)\partial_\mu\partial_\nu\right]n(x^\mu)=0,\tag{1}$$

where $n(x)$ is a scalar density, u^μ is a constant time-like vector, $\eta = \mathrm{diag}(-1, 1, 1, 1)$,$\tau$ is the relaxation time, and Γ is the diffusion constant. In this equation, the time-like derivative is of the same order as the space-like one. This equation has the form of the telegraphic equation such that the propagation is restricted in the region defined by $vx_t > x_s$, where $v = \sqrt{\Gamma/\tau}$, $x_t = u\cdot x$, and $x_s = \sqrt{-(\eta^{\mu\nu} - u^\mu u^\nu)x_\mu x_\nu}$. If $\Gamma < \tau$, causality is satisfied because the velocity is smaller than the speed of light, i.e., $v < 1$[3]. However, if $\Gamma > \tau$, the propagation speed exceeds the speed of light. Furthermore, if $\Gamma = 0$, causality is not violated even though the order of the time and space derivatives are different. Therefore, the equal order of space and time derivatives in the equation of motion does not ensure in itself that the Green function is causal.

What ensures the causality in general?

The purpose of this paper is to derive the conditions ensuring relativistic causality in an effective theory based on the derivative expansion. We will consider the retarded Green function in a scalar theory at tree level, i.e., thermal and quantum fluctuations will not be taken into account. In this case, the retarded Green function in the derivative expansion is generally written as a rational function in the momentum space:

$$G_R(\omega,k)=\frac{Q(\omega,k)}{P(\omega,k)},\tag{2}$$

where $P(\omega, k)$ and $Q(\omega, k)$ are polynomials in ω and k:

$$P(\omega,k)= p_n(k)\omega^n + p_{n-1}(k)\omega^{n-1} + ... + p_0(k),\tag{3}$$
$$Q(\omega,k)= q_m(k)\omega^m + q_{m-1}(k)\omega^{n-1} + ... + q_0(k).\tag{4}$$

Here, $n > m$, and $p_j(k)$ and $q_j(k)$ are the polynomials in k. Because we assumed isotropy, the Green function turns becomes a function of $k \equiv |\boldsymbol{k}|$. The relativistic causality implies that the retarded Green function must vanish in the space-like region. Therefore, we derive the general condition ensuring Eq. (2) vanishes in the space-region, which is given by

$$\lim_{k\to\infty}\left|\mathrm{Re}\,\frac{\omega(k)}{k}\right|<1 \text{ and } \lim_{k\to\infty}\left|\mathrm{Im}\,\frac{\omega(k)}{k}\right|<\infty,\tag{5}$$

and the condition that $p_n(k)$ must not depend on k. Here, $\omega(k)$ is a pole of Eq. (2). These conditions ensure causality in effective theories based on the derivative expansion, and they are the main results of our paper.

References

1) S. Weinberg, Phys. Rev. Lett. **17**, 616 (1966); Physica A **96**, 327 (1979).
2) W. Israel and J.M.Stewart, Ann. Phys. (N.Y.) **118** (1979), 341.
3) S. Pu, T. Koide, D. H. Rischke, Phys. Rev. D **81**, 114039 (2010).

† Condensed from the article in arXiv:1401.0006 [hep-ph]

*1 RIKEN Nishina center

Boundary Restoration of Chiral Symmetry†

B. Tiburzi*1

One of the hallmark features of the theory of strong interactions is spontaneous breaking of chiral symmetry. While quark masses explicitly break the chiral symmetry of the QCD action, the lightest quarks (up and down) have masses that can be treated as a perturbation about the symmetric $SU(2)_L \otimes SU(2)_R$ chiral limit. The formation of a chiral condensate by the QCD vacuum in the chiral limit, namely $< \overline{\psi}\psi > \neq 0$, spontaneously breaks the chiral symmetry down to the vector subgroup, $SU(2)_V$. This symmetry breaking pattern along with the explicit breaking due to the quark masses gives an explanation of the lightness of the iso-triplet of pseudo-scalar pions because they must be the emergent Goldstone bosons.

Lattice gauge theory provides a first principles method for solving QCD numerically on finite Euclidean space-time lattices. Strictly speaking, spontaneous symmetry breaking cannot occur in a finite volume. In practice, the formation of a chiral condensate on periodic lattices is determined by the size of the pion Compton wavelength compared to the lattice size[2–4]. In this work[1], we explore a different restoration of chiral symmetry. We consider the fate of chiral symmetry on a Euclidean manifold with three infinite directions, and one compact direction that, unlike the periodic case, has a boundary. Specifically the compact direction is subject to homogeneous Dirichlet boundary conditions (DBCs), as have been utilized recently in various lattice gauge theory computations.

The effect of a boundary on the chiral condensate cannot be ascertained within chiral perturbation theory, because the chiral condensate is determined by the expression

$$< \overline{\psi}\psi(x) > = -\frac{\Sigma}{4} < U(x) + U^\dagger(x) > + \cdots. \qquad (1)$$

Due to the unitarity of the coset manifold, the right-hand side of this relation does not vanish at the boundary in contradiction with the quark boundary conditions satisfied on the left-hand side. A consistent treatment of the chiral condensate in the presence of DBCs necessitates including the dynamics of isoscalar scalar mesons. For this reason, we employ the sigma model which shares the same symmetry breaking pattern as QCD with two light quark flavors, and provides the simplest model of spontaneous chiral symmetry breaking. The parameter Σ in Eq. (1) becomes a field $\Sigma(x)$ satisfying DBCs. The chiral condensate $< \overline{\psi}\psi(x) >$ is determined by minimizing the action to find the vacuum configuration.

† Condensed from Reference[1]

*1 Department of Physics, The City College of New York (CUNY), USA; and RIKEN Nishina Center

An example of our results is shown in Fig. 1, which depicts the effect of DBCs on the volume-averaged value of the chiral condensate, defined by $\overline{< \overline{\psi}\psi >} = \frac{1}{L}\int_0^L dx < \overline{\psi}\psi(x) >$. In the limit of an asymptotically large extent L, the volume-averaged chiral condensate tends to the infinite volume value, however, the approach to asymptopia is slow. The asymptotic condensate can be determined in closed form, and averaged over the compact direction to produce

$$\overline{< \overline{\psi}\psi >} = < \overline{\psi}\psi > \left[1 - \frac{4\log 2}{m_\sigma L} + \cdots\right], \qquad (2)$$

from which we see power-law scaling controlled by the Compton wavelength of the sigma meson.

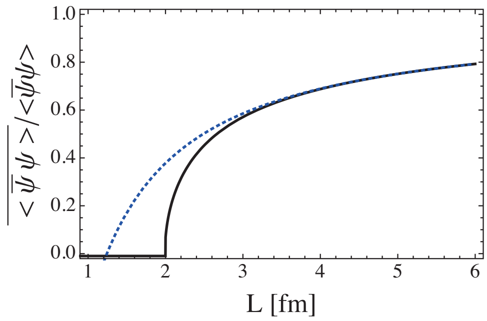

Fig. 1. Ratio of the volume-averaged condensate in the sigma model $\overline{< \overline{\psi}\psi >}$ to the infinite volume condensate $< \overline{\psi}\psi >$ plotted as a function of the finite extent L. The dotted curve shows the asymptotic formula in Eq. (2). Below $L \approx 2\,\mathtt{fm}$, the sigma model vacuum energy is minimized by $< \overline{\psi}\psi(x) > = 0$ for all x, and chiral symmetry is completely restored. The cusp is likely softened by including higher-lying sigma states.

Our sigma model results show that one should be cautious in interpreting results from lattice computations employing DBCs on small lattices. To establish the credibility of lattice computations with Dirichlet boundaries, one requires a lattice computation of the chiral condensate, either locally or volume averaged, which will ultimately reveal the extent to which chiral symmetry is restored in the presence of a boundary. In turn, frustration of the chiral condensate via Dirichlet boundaries may enable us to learn more about the mechanism that underlies spontaneous chiral symmetry breaking.

References

1) B. C. Tiburzi, Phys. Rev. D **88**, 034027 (2013).
2) J. Gasser, H. Leutwyler, Phys. Lett. B **184** (1987) 83.
3) J. Gasser, H. Leutwyler, Phys. Lett. B **188** (1987) 477.
4) J. Gasser, H. Leutwyler, Nucl. Phys. B **307** (1988) 763.

Cutoff effects on lattice nuclear forces†

T. Doi*1

Nuclear forces, the interactions among nucleons, serve as the cornerstone in nuclear physics. While they have been traditionally determined through the scattering experiments, their theoretical understanding by using the fundamental theory, quantum chromodynamics (QCD), has not been established yet. Recently, a novel approach was proposed to determine nuclear forces on a lattice[1,2]. In this approach, now called the HAL QCD method, nuclear forces are directly obtained from Nambu-Bethe-Salpeter wave functions calculated on the lattice. The method has been successfully extended to general hadron interactions such as three-nucleon forces[3]. See Ref.[4] for a recent review.

For the quantitative determination of nuclear forces, systematic uncertainties in lattice simulations should be carefully examined, such as the effect of discretization artifacts. There have been, however, no work that performs the continuum extrapolation on nuclear interactions. The aim of this work is to perform the first systematic study for the lattice cutoff dependence of nuclear interactions.

We employ $N_f = 2$ configurations with clover fermion generated by CP-PACS collaboration[5]. The measurements are performed at three lattice spacings, $a = 0.2150, 0.1555, 0.1076$ fm. The physical lattice size is $L^3 \times T \simeq (2.5\,\text{fm})^3 \times 5\,\text{fm}$, and the hadron masses are $(m_\pi, m_N) \simeq (1.1, 2.2)$ GeV. The computational cost in the Wick and color/spinor contractions is reduced by the unified contraction algorithm[6]. For details about the simulation parameters, see Doi (2013)[7].

In Fig. 1, we plot the nuclear central potential in $^1S_0$ channel for each lattice cutoff. We observe that cutoff dependence is nonnegligible at short distances, while it is suppressed at long distances. This is a natural consequence of the discretization being an intrinsically short-range effect. It is also interesting that repulsive core is enhanced on a finer lattice, which is consistent with the study on the operator product expansion[8].

Although the lattice cutoff dependence on potentials looks sizable at short distances, such effect is expected to be suppressed in physical observables such as phase shifts and scattering length, because of the phase space factor of $\propto r^2$, as is shown in the inset of Fig. 1.

In order to quantitatively study the cutoff effect on physical observables, we fit the potential and solve the Schrödinger equation in infinite volume. In Fig. 2, we show the preliminary results for the scattering length against the lattice spacing a, with only a statistical error. Because the scattering length represents the low-energy phenomena, the cutoff dependence is found to be negligible compared to the statistical errors. Detailed studies for the systematic uncertainties on phase shifts and scattering length are in progress.

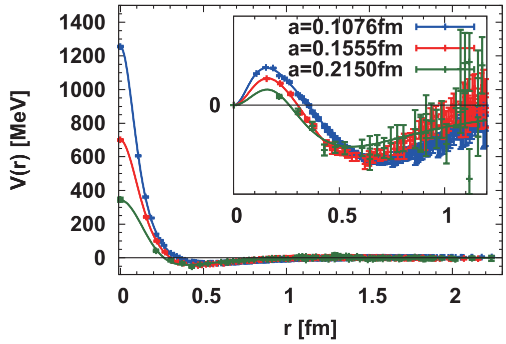

Fig. 1. Central potentials $V_C(r)$ in $^1S_0$ channel. Inset shows $r^2V_C(r)$ to include phase space factor. Solid lines correspond the fit for the potentials.

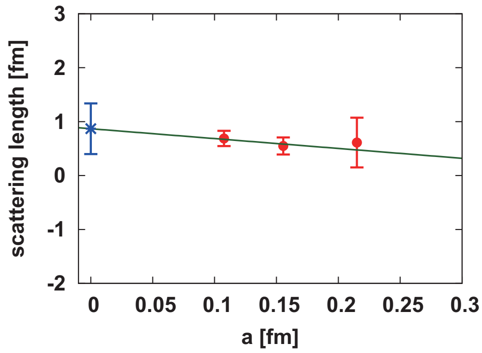

Fig. 2. Scattering length in $^1S_0$ channel against lattice spacing a. Blue point corresponds to the result in the continuum limit obtained by linear extrapolation against a.

† Condensed from the article in PoS LAT2013, 226 (2013)
*1 RIKEN Nishina Center

References

1) N. Ishii, S. Aoki and T. Hatsuda, Phys. Rev. Lett. **99** (2007) 022001 [nucl-th/0611096].
2) S. Aoki, T. Hatsuda and N. Ishii, Prog. Theor. Phys. **123** (2010) 89 [arXiv:0909.5585 [hep-lat]].
3) T. Doi *et al.* [HAL QCD Coll.], Prog. Theor. Phys. **127** (2012) 723 [arXiv:1106.2276 [hep-lat]].
4) S. Aoki *et al.* [HAL QCD Coll.], Prog. Theor. Exp. Phys. **2012** (2012) 01A105 [arXiv:1206.5088 [hep-lat]].
5) A. Ali Khan *et al.* [CP-PACS Coll.], Phys. Rev. D **65** (2002) 054505 [E: D **67** (2003) 059901].
6) T. Doi and M. G. Endres, Comput. Phys. Commun. **184** (2013) 117 [arXiv:1205.0585 [hep-lat]].
7) T. Doi [HAL QCD Collaboration], PoS LAT2013, 226 (2013), arXiv:1311.2697 [hep-lat].
8) S. Aoki, J. Balog and P. Weisz, JHEP **1005** (2010) 008 [arXiv:1002.0977 [hep-lat]].

Nucleon axial charge in lattice QCD with nearly physical pion mass

Y. Aoki,[*1,*2] T. Blum,[*3,*2] T. Izubuchi,[*4,*2] C. Jung,[*4,*2] M.F. Lin,[*4,*2] S. Ohta,[*5,*6,*2] S. Sasaki,[*7,*2] E. Shintani,[*8,*2] and T. Yamazaki[*1,*2]

We report the status of lattice quantum chromodynamics (QCD) calculations of nucleon isovector axial and vector charges using the four recent domain-wall fermions (DWF) ensembles with 2+1 dynamical flavors jointly generated by the RIKEN-BNL-Columbia (RBC) and UKQCD collaborations[1)]: the strange-quark mass is set at physical value and degenerate up- and down-quark mass is varied with the pion mass of about 420, 330, 250 and nearly physical 170 MeV.

Spontaneously broken chiral symmetry drives the axial charge, g_A, of nucleon away from its chiral partner, the vector charge, g_V, to a larger value. The current experimental estimate of the ratio of these charges is $g_A/g_V = 1.2701(25)$[2)]. This ratio is an important quantity that not only determines neutron life time but also the interaction of pion and nucleon through the Goldberger-Treiman relation[3)], and hence nuclear stability, syntheses and abundance. Numerical lattice-QCD calculations underestimate the ratio by about 10 %[4–7)]. The cause of this deficit is not known: insufficient lattice volumes[4,7)] and excited-state contaminations[8)] have been discussed as possible cause.

We have improved the statistical accuracy[7)] of our calculations so the statistical errors now stand at around 4 %. The AMA method[9)] was important in achieving this for the pion mass of about 330 and 170 MeV. With these improved statistics we have now excluded excited-state contamination as the cause of the deficit[7)]. On the other hand, in the two cases with the pion mass of 170 MeV and 330 MeV the ratio has been found to suffer from very long-range autocorrelation[7)]. At 170 MeV the calculated charge ratio, g_A/g_V, starts with a value that is statistically consistent with the experiment at the beginning quarter of the calculation, but then monotonically decreases quarter by quarter to a value drastically low (see Fig. 1.) A similar but less drastic autocorrelation has been observed at 330 MeV as well. This results in the observed deficit, but we are yet to understand what causes this very long-range autocorrelation. We do not find such long-range autocorrelation at 250 and 420 MeV: the autocorrelation for these two cases are much shorter-ranged.

The absence of a long-range autocorrelation at lighter pion mass of 250 MeV in contrast to the presence at heavier 330 MeV suggests this peculiar autocorrelation is related to insufficient lattice spatial volume. The finite-size effect can be parametrized by a dimensionless product, $m_\pi L$, of the calculated pion mass, m_π, and linear spatial extent of the lattice, L[4)]: Indeed the autocorrelation is milder at 330 MeV with $m_\pi L$ of about 4.5 than at 170 MeV with $m_\pi L$ of about 4.0, and absent for 250- and 420-MeV with $m_\pi L$ of about 5.8[7)]. Thus the observed autocorrelations seem consistent with finite-size scaling in terms of $m_\pi L$: the nucleon as seen by its isovector axialvector current or interaction with pion may be much larger than its electric charge distribution indicates.

Though our statistics is still too low to conclude more definitely, we captured an important clue toward understanding the deficit, likely in its relation with the finite-size effect that may scale with $m_\pi L$.

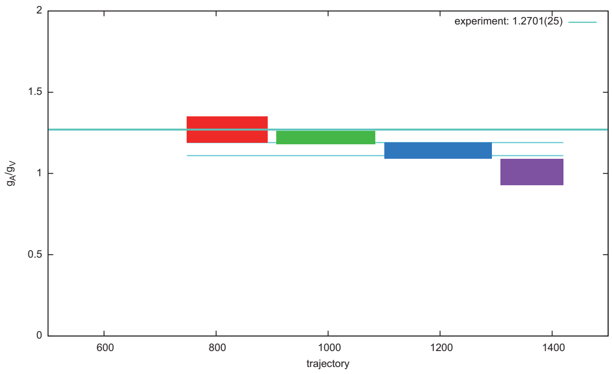

Fig. 1. Unusually long-range autocorrelation is seen in the isovector axial to vector charge ratio, g_A/g_V along the gauge-configuration generation history at $m_\pi = 170$ MeV and $m_\pi L$ of about 4.0, slowly moving from consistent with experiment to drastically low. Similarly long-range autocorrelation has been seen in at $m_\pi = 330$ MeV and $m_\pi L$ of about 4.5 as well, but not at 250 or 420 MeV that share $m_\pi L$ of about 5.8. No other observable shows such a long-range autocorrelation.

*1 Kobayashi-Maskawa Institute, Nagoya University
*2 RIKEN Nishina Center
*3 Physics Department, University of Connecticut
*4 Physics Department, Brookhaven National Laboraotry
*5 Institute of Particle and Nuclear Studies, KEK
*6 Department of Particle and Nuclear Physics, SOKENDAI
*7 Physics Department, Tohoku University
*8 Physics Department, Mainz University

References

1) R. Arthur et al. *Phys.Rev.*, D87:094514, 2013.
2) Particle Data Group, J. Beringer, et al. *Phys. Rev.*, D86:010001, 2012. and 2013 partial update for 2014.
3) M.L. Goldberger and S.B. Treiman. *Phys.Rev.*, 110:1178–1184, 1958.
4) T. Yamazaki et al. *Phys.Rev.Lett.*, 100:171602, 2008.
5) H. Wittig. *PoS*, LATTICE2011:025, 2011.
6) H.-W. Lin. *PoS*, LATTICE2012:013, 2012.
7) S. Ohta. *PoS*, LATTICE2013:274, 2013.
8) S. Capitani et al. *Phys.Rev.*, D86:074502, 2012.
9) T. Blum et al. *Phys.Rev.*, D88:094503, 2013.

Lattice QCD calculation of $n - \bar{n}$ transition amplitudes

M. Buchoff,[*1] C. Schroeder,[*2] S. Syritsyn,[*3] B. Tiburzi,[*3,*4] and J. Wasem[*5]

In searches for physics beyond the Standard Model, violation of baryon number conservation is an essential direction. The absence of experimental data on baryon number violation has no known particle physics principle beneath it and, on the other hand, would be difficult to understand given the observed baryon asymmetry of the Universe. Two important hypothetic processes may signal the baryon number violation, one is the proton decay changing the baryon number by $\Delta B = 1$ and the other is neutron-antineutron oscillation, $\Delta B = 2$. A number of new experiments with stored neutrons and cold neutron beams have been proposed to look for $n - \bar{n}$ transitions. These experiments have potential to improve current bounds on such by a few orders of magnitude and, as a result, significantly improve bounds on beyond the Standard Model physics.

Bounds on new physics, however, will strongly depend on uncertainties arising from hadron physics. Symmetries of the Standard Model constrain the form of six-quark effective interaction that may turn the neutron into the antineutron[1,2]),

$$\mathcal{O}_{1\,\chi_1\{\chi_2\chi_3\}} = T^s_{ijklmn}\left[u^{iT}_{\chi_1}\mathcal{C}u^j_{\chi_1}\right]\left[d^{kT}_{\chi_2}\mathcal{C}d^l_{\chi_2}\right]\left[d^{mT}_{\chi_3}\mathcal{C}d^n_{\chi_3}\right],$$
$$\mathcal{O}_{2\,\{\chi_1\chi_2\}\chi_3} = T^s_{ijklmn}\left[u^{iT}_{\chi_1}\mathcal{C}d^j_{\chi_1}\right]\left[u^{kT}_{\chi_2}\mathcal{C}d^l_{\chi_2}\right]\left[d^{mT}_{\chi_3}\mathcal{C}d^n_{\chi_3}\right],$$
$$\mathcal{O}_{3\,\{\chi_1\chi_2\}\chi_3} = T^a_{ijklmn}\left[u^{iT}_{\chi_1}\mathcal{C}d^j_{\chi_1}\right]\left[u^{kT}_{\chi_2}\mathcal{C}d^l_{\chi_2}\right]\left[d^{mT}_{\chi_3}\mathcal{C}d^n_{\chi_3}\right],$$

where $\chi_{1,2,3} = L, R$ denote chiral components of the quark fields and $T^{s,a}_{ijklmn}$ are symmetric and antisymmetric color tensors. Symmetry relations reduce the number of independent operators to 14, of which only four are $SU(2)_L$ symmetric. So far, the corresponding $n - \bar{n}$ amplitudes $\langle\bar{n}|\mathcal{O}|n\rangle$ have been computed only using MIT Bag Model[1]).

Advances in lattice QCD, a numerical approach to quantum field theory, only recently made it possible to calculate such amplitudes directly. Preliminary results by our collaboration are shown on Fig. 1, where they are compared to the Bag Model calculation[1]). We perform calculations on an anisotropic QCD lattices with size $\approx (2.5\,\text{fm})^3 \times 9\,\text{fm}$ and lattice spacing $a = 0.123\,\text{fm}$. $N_f = 2 + 1$ "light" and strange quark fields are simulated fully dynamically with $\mathcal{O}(a^2)$-improved Wilson action on anisotropic lattice[3]) such that the mass of the pion is $m_\pi \approx 390\,\text{fm}$. The overall normalization of our lattice QCD results is not known yet; however, the stochastic accuracy of individual amplitudes is surprisingly good. In addition, despite the fact that we use unphysical heavy quarks so that $m_\pi \approx 390$ MeV, the relative magnitude and signs agree very well with the Bag Model.

Currently, our group is working on renormalizing these effective operators on a lattice in order to find their overall factor. The next step is to repeat the calculation using chirally symmetric quarks at the physical point, which are currently possible due to advances in lattice QCD. It is possible that renormalization, operator mixing and light quarks will change the "hierarchy" of operators in Fig. 1 considerably. In addition, the chiral symmetry-violating action we are currently using may lead to additional operator mixing, and chirally-symmetric quark action may be necessary to obtain correct results.

We are excited to report that, as our preliminary results demonstrate, lattice QCD will likely remove hadron physics uncertainties from interpreting future $n - \bar{n}$ oscillation searches.

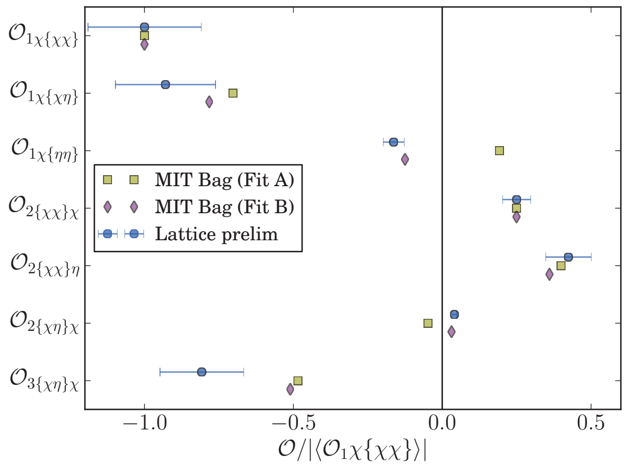

Fig. 1. Comparison of "hierarchy" of matrix elements of 7 different $n - \bar{n}$ operators, ($\{\chi, \eta\} = \{R, L\}$ or $\{L, R\}$), in our calculation to the Bag Model[1]). Since the lattice renormalization factors are not yet known, we normalize results by $|\mathcal{O}_{1\chi\{\chi\chi\}}|$ in each case in order to compare relative size of the matrix elements.

*1 University of Washington, Dept. of Physics and Astronomy, Institute for Nuclear Theory
*2 Lawrence Livermore National Laboratory, Life Sciences Division
*3 RIKEN BNL Research Center, Brookhaven National Laboratory
*4 The City College of New York (CCNY), Department of Physics
*5 Lawrence Livermore National Laboratory, AX Division

References
1) S. Rao and R. Shrock: Phys.Lett. B116, 238 (1982).
2) W. E. Caswell, J. Milutinovic, and G. Senjanovic: Phys.Lett. B122, 373 (1983).
3) R. G. Edwards, B. Joo, and H.-W. Lin.: Phys.Rev. D78:054501 (2008).

Columbia plot and 't Hooft loop at imaginary chemical potential†

K. Kashiwa*1 and R. D. Pisarski*1*2

The investigation of the phase structure in Quantum Chromodynamics (QCD) at finite temperature (T) and real chemical potential (μ_{R}) is an important subject in the particle and nuclear physics. If we obtain the QCD phase diagram from first-principles calculations, the phase structure would be clear, in principle. First-principles calculations such as the lattice QCD (LQCD) simulation, however, has a sign problem at finite μ_{R}, and it is therefore not feasible there. Even if we use several methods and approximations, we cannot reach the $\mu_{\mathrm{R}}/T \geq 1$ region. Therefore, several effective models such as the Nambu–Jona-Lasinio model are widely used to investigate QCD phase diagrams. The effective model approach, however, has large ambiguities. Therefore, at the present, we cannot obtain a reliable phase diagram at finite μ_{R} by using the lattice QCD simulation and effective model approach.

To overcome this problem, we consider the imaginary chemical potential (μ_{I}). At finite μ_{I}, there is no sign problem, and thus we can successfully perform the LQCD simulation. In fact, phase structures have already been investigated by lattice QCD simulations; for example, see References[2,3]. In addition, it is possible to prove that the μ_{I} region has almost all the information of the μ_{R} region[1]. QCD has some characteristic properties at finite μ_{I}. One of the characteristic properties is the Roberge-Weiss (RW) periodicity, which is the special $2\pi/3$ periodicity along the μ_{I}/T axis. This periodicity is a remnant of the Z_3 symmetry in the pure gauge limit. Also, the RW transition and its endpoint which is called the RW endpoint are expected at finite T in the μ_{I} region. This means that we can obtain some important constraints for model design from these special properties of QCD.

In this study, we consider the heavy-quark mass region, which corresponds to the upper part of the Columbia plot. The Colombia plot is the figure drawn as a function of the light-quark and strange-quark masses and shows the phase boundary. In the paper, we reported the following three results:

(1) 't Hooft loop can be well defined at the RW endpoint.
(2) Model ambiguities can appear largely at the RW endpoint.
(3) Thermodynamics with imaginary chemical potential shows unexpected behavior comparing to standard thermodynamics.

The 't Hooft-loop is related with the deconfinement transition at finite T in the pure-gauge limit. It is known that this quantity cannot be well defined in the system with dynamical quarks[4,5]. In the calculation of the 't Hooft loop, we should set different Z_3 images (charges) at the boundary of the box and consider its surface. If the potential energies in both sides of the surface are different, there is a force that modifies the surface, and thus the 't Hooft loop cannot be well defined. However, we showed that the *effective* Z_3 charges are identical at two of the Z_3 images, and thus the 't Hooft loop can be well defined at the RW endpoint for degenerate Z_3 images because there is no force to modify the surface.

The Columbia plot at the heavy-quark mass region was calculated by using the matrix model for deconfinement and the logarithmic-type Polyakov-loop effective potential for describing the deconfinement transition by the Polyakov loop. Those models are low-energy effective models of QCD. In the case of the matrix model, there is a phase boundary that separates the first-order and second-order transition regions. Conversely, the logarithmic-type Polyakov-loop effective potential does not have any phase boundary down to 1 GeV. Therefore, there exists a large model dependence in the upper part of the Columbia plot at the RW endpoint.

Several thermodynamic quantities, such as the pressure, energy density, quark number density, entropy density, and interaction measure, are calculated by using the matrix model for deconfinement. We observed that the energy density and interaction measure show unexpected behavior near the RW transition line, which is induced by the contribution of the quark number density. This behavior can be exploited to remove the model ambiguities when accurate lattice QCD data will be available in the future.

References

1) A. Roberge and N. Weiss: Nucl. Phys. **B275**, 734 (1986).
2) P. de Forcrand and O. Philipsen: Nucl. Phys. **B642**, 290 (2002).
3) M. D'Elia, S. Mukherjee, F. Sanfilippo: Phys. Rev. D **82**, 051501 (2010).
4) C. Korthals-Altes, A. Kovner, M. A. Stephanov: Phys. Lett. B **469**, 205 (1999).
5) C. Korthals-Altes and A. Kovner: Phys. Rev. D **62**, 096008 (2000).

† Condensed from article in Phys. Rev. D **87**, 096009 (2013)
*1 RIKEN Nishina Center
*2 Brookhaven National Laboratory

Progress towards an *ab initio*, Standard Model calculation of direct CP-violation in K-decays

C. Kelly*[1]

Direct CP-violation in $K \to \pi\pi$ decays manifests as a difference in phase between the decay amplitudes in the $I = 2$ and $I = 0$ channels and is parameterized experimentally as ϵ'. This quantity is extremely sensitive to Beyond the Standard Model sources of CP-violation; therefore, an accurate Standard Model calculation is greatly desired. As low-energy strong interactions play an important role, use of lattice QCD is required to study these processes. Although ϵ' has been known experimentally since the late 1990's, it is only recently that the techniques and raw computing power for performing a realistic first-principles calculation have become available. The main technical difficulty is finding a strategy for obtaining an energy conserving decay because only the ground state is easily accessible in lattice calculations. The lowest-energy two-pion state comprises stationary pions, and its energy (assuming physical quark masses) is only 270 MeV, far below the 500 MeV mass of the kaon.

The RBC and UKQCD collaborations have successfully performed calculations of the $I = 2$ channel amplitude[1,2], solving the issue of obtaining physical kinematics by modifying the lattice boundary conditions (BC) of the down quarks from periodic to antiperiodic such that the charged-pion ground state is moving. Unfortunately this manifestly breaks the isospin symmetry. For the $I = 2$ decay, it is possible to relate the amplitude to an unphysical one in which the final state cannot mix with other isospin states, but this cannot be performed for the $I = 0$ decay. Instead, we intend to use G-parity boundary conditions (GPBC).

G-parity is a combination of charge conjugation and an isospin rotation by π radians about the y-axis. Both charged and neutral pions are eigenstates of this operation with eigenvalue -1; hence, its application at a spatial boundary causes the pion states to become antiperiodic in that direction, removing the stationary ground state. However, in this setup, operators involving both strange and light quarks cannot be combined to form G-parity eigenstates e.g., the K^0 state $\bar{s}d$ transforms to the unphysical $\bar{s}\bar{u}$ state at the boundary. We solve this issue by placing the s-quark in an isospin doublet with a fictional degenerate partner, referred to as s', and impose GPBC on this pair. We can then form a state, $\tilde{K} = \frac{1}{\sqrt{2}}(\bar{s}d + \bar{u}s')$, which is an eigenstate of G-parity with eigenvalue $+1$, and thus has a stationary ground state. For the $K \to \pi\pi$ measurement the effects of the fictional state $\bar{u}s'$ are expected to be small as it must propagate across the boundary to interact with the decay operator.

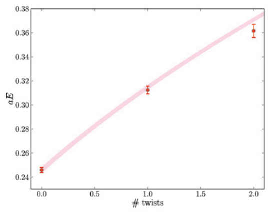

(a) E_π

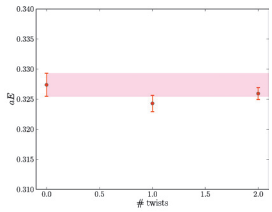

(b) E_K

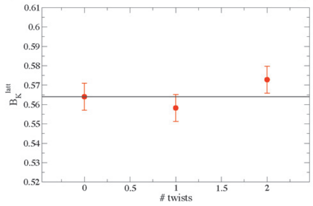

(c) B_K

Fig. 1.: Top: the pion and kaon energies, respectively as a function of the number of G-parity directions (twists), overlaid by the expected continuum dispersion relations. Bottom: B_K as a function of the number of G-parity directions.

To demonstrate that the GPBC have the desired effect, we generated several fully dynamical ensembles with a relatively small volume and a large (420 MeV) pion mass, with GPBC in zero, one, and two directions, each with periodic BC in the remaining directions. In Fig. 1, we plot the measured pion and kaon energies as the number of directions with GPBC is increased. We observe that the pion energies agree well with the continuum dispersion relation and that stationary kaon states can be produced in this framework. Because the quantity B_K, which represents the amplitude of mixing between neutral kaon states via the weak interaction, involves only kaons, we expect it will remain constant as we change the number of directions with GPBC; we observe that this is indeed the case.

We have since began generating a fully dynamical ensemble with a large volume and physical quark masses using the USQCD collaboration's IBM Bluegene/Q machine at BNL, and we expect to soon begin measurements. Once completed, the results can be combined with those for the $I = 2$ channel to finally obtain a first-principles value for ϵ'.

References
1) T. Blum *et al.*, Phys. Rev. Lett. **108** (2012) 141601
2) T. Blum *et al.*, Phys. Rev. D **86** (2012) 074513

*1 RIKEN Nishina Center, Brookhaven National Laboratory

6. Particle Physics

Improved estimate of neutral B meson mixing in static limit of b quark with AMA technique

T. Ishikawa,*[1] Y. Aoki,*[2,*1] T. Izubuchi,*[3,*1] C. Lehner*[3] and A. Soni*[3] (for RBC Collaboration)

The Cabibbo–Kobayashi–Maskawa (CKM) matrix plays a key role in elementary particle physics, and constraints on the elements V_{ts} and V_{td} can be obtained from $B^0-\overline{B^0}$ mixing. Treatments of b quark on the lattice QCD are, however, challenging because of a multi-scale problem where a large hierarchy in mass exists between light quarks (u and d) and b quark. A solution to this problem is using Heavy Quark Effective Theory (HQET), in which the theory is expanded by $1/m_b$, where m_b is b quark mass. The leading order of the HQET is a static approximation of the b quark and is the formulation used in this work. While the static approximation is known to have $O(\Lambda_{\rm QCD}/m_b) \sim 10\%$ uncertainty, it is useful for an interpolation strategy, where the physical b quark mass point (~ 4.2 GeV) is reached by the interpolation between the static limit and simulations in the lower quark mass region (c quark mass region). For this purpose, high precision calculations in the static limit are required.

RBC/UKQCD Collaboration has worked on such calculations for several years [1)2)3)]. While we have successfully improved the estimate, the statistical error remains a major part of the total uncertainty. Recently, an efficient method called All-Mode-Averaging (AMA)[4)] has been proposed for significantly reducing the statistical error. The AMA technique is an operator improvement using symmetries on the action and approximations. The most useful symmetry is translational invariance of space-time. The idea involves locating many source points in the measurement, but using an approximation in obtaining quark propagators to reduce computational cost. As an approximation, we use a sloppy CG, where its stopping condition is relaxed. A crucial point here is the existence of correlation between the original and the approximated operators; thus, we choose the stopping condition so that the good correlation is kept, but the computational cost is reduced significantly. We also note that a low-mode deflation technique helps the cost reduction in addition to enhancement of the correlation in the AMA procedure.

In Fig. 1, we show chiral and continuum extrapolation of the B meson decay constant f_B and the neutral B meson mixing matrix element $\mathcal{M}_B$ without and with AMA. We use gluon ensembles with two lattice spacings, which are depicted as "24c" (coarse) and "32c" (fine). "HYP1" and "HYP2" represent link smearings in the static b action, whose results should coincide

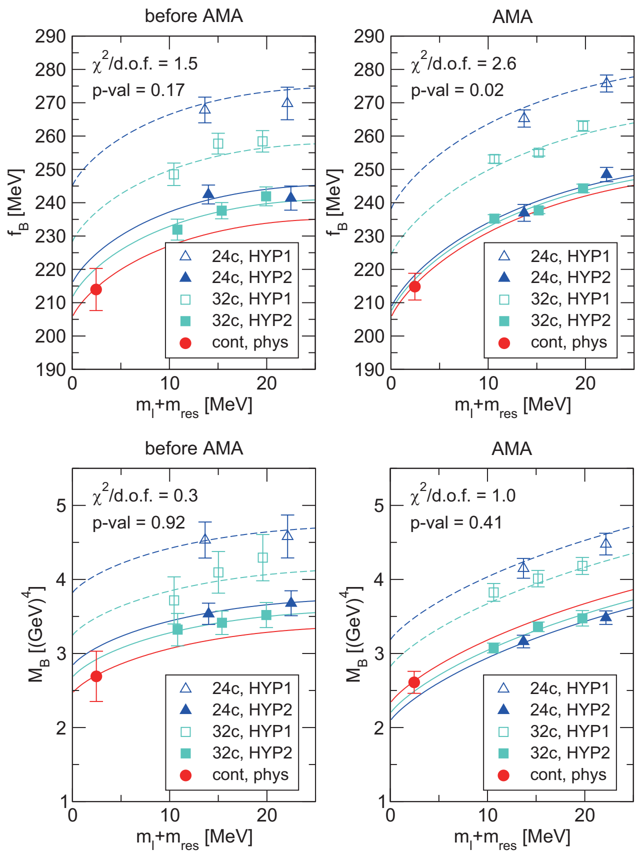

Fig. 1. Chiral and continuum extrapolation of f_B and $\mathcal{M}_B$.

each other in the continuum limit. To obtain the AMA results approximately 30% – 40% cost increase is required from the original one ("before AMA" in the figures). A remarkable improvement in statistics is obtained compared with the small increase in the cost. At the physical point of light quark mass and in the continuum limit, the central values only slightly move by using the AMA; the statistical errors are, however, significantly reduced. In addition, the improvement makes a qualitative fact clear: the results with HYP2 smearing have very small scaling violation. We conclude that the AMA technique has potential to enable us to reach statistically decisive results.

*1 RIKEN Nishina Center
*2 Nagoya University, KMI
*3 Brookhaven National Laboratory

References

1) V. Gadiyak and O. Loktik, Phys. Rev. D **72**, 114504 (2005).
2) C. Albertus *et al.*, Phys. Rev. D **82**, 014505 (2010).
3) T. Ishikawa *et al.*, LATTICE2013:410, 2013.
4) T. Blum *et al.*, Phys. Rev. D **88**, 094503 (2013).

Lorentz invariant CPT violation†

M. Chaichian,*1 K. Fujikawa,*2 and A. Tureanu*1

A Lorentz invariant CPT violation, which may be termed as the long distance CPT violation in contrast to the familiar short distance CPT violation, has been recently proposed[1]. This scheme is based on the non-local interaction vertex and characterized by the infrared divergent form factor. We show that Lorentz covariant $T^\star$-product is consistently defined and the energy-momentum conservation is preserved in perturbation theory if the path integral is suitably defined for this non-local theory, although unitarity is generally lost. It is illustrated that T-violation is realized in the decay and formation processes. It is also argued that the equality of masses and decay widths of the particle and anti-particle is preserved if the non-local CPT violation is incorporated either directly or as perturbation by starting with the conventional CPT-even local Lagrangian. However, we also explicitly show that the present non-local scheme can induce the splitting of particle and anti-particle mass eigenvalues if one considers a more general class of Lagrangians.

We study the specific realization of CPT violation

$$
\begin{aligned}
\mathcal{L} &= \bar{\psi}(x)[i\gamma^\mu\partial_\mu - M]\psi(x) + \frac{1}{2}\partial_\mu\phi(x)\partial^\mu\phi(x) \\
&- \frac{1}{2}m^2\phi(x)^2 + g\bar{\psi}(x)\psi(x)\phi(x) - V(\phi) \\
&+ g_1\bar{\psi}(x)\psi(x)\int d^4y\theta(x^0-y^0)\delta((x-y)^2-l^2)\phi(y)
\end{aligned}
$$

as a main theoretical model. This Lagrangian is formally hermitian and the term with a small real g_1 and the step function $\theta(x^0-y^0)$ stands for the CTP and T violating interaction; l is a real constant parameter. It is interesting that the CPT and T violating term is real in the present case. We define the interaction part

$$
\begin{aligned}
\mathcal{L}_I &= g\bar{\psi}(x)\psi(x)\phi(x) \\
&+ g_1\bar{\psi}(x)\psi(x)\int d^4y\theta(x^0-y^0)\delta((x-y)^2-l^2)\phi(y).
\end{aligned}
$$

We treat this highly non-local Lagrangian in path integral as described in[2].Namely

$$
\begin{aligned}
&\langle 0,+\infty|0,-\infty\rangle_J \\
&= \int \mathcal{D}\bar{\psi}\mathcal{D}\psi\mathcal{D}\phi\exp\{i\int d^4x[\mathcal{L}_0+\mathcal{L}_I+\mathcal{L}_J]\}
\end{aligned}
$$

with the source term $\mathcal{L}_J = \bar{\psi}(x)\eta(x) + \bar{\eta}(x)\psi(x) + \phi(x)J(x)$, and one may generate Green's functions in a power series expansion of perturbation as

$$
(i)^n\langle T^\star\phi(x_1)..\phi(x_N)\int d^4y_1\mathcal{L}_I(y_1)..\int d^4y_n\mathcal{L}_I(y_n)\rangle.
$$

We use the $T^\star$-product which is essential to make the path integral on the basis of Schwinger's action principle consistent[2].

The present way to introduce CPT violation is based on an extra form factor in momentum space as

$$
\int d^4x\bar{\psi}(x)\psi(x)\int d^4y\theta(x^0-y^0)\delta((x-y)^2-l^2)\phi(y)
$$

$$
= \int dp_1dp_2dq(2\pi)^4\delta^4(p_1+p_2+q)\bar{\psi}(p_1)\psi(p_2)f(q)\phi(q)
$$

with

$$
f(q) \equiv \int d^4z\theta(z^0)\delta(z^2-l^2)e^{iqz}
$$

namely, CPT violation is realized by a form factor $f(q)$ which becomes complex for time-like momentum. The ordinary local field theory is characterized by $f(q)=1$. The above form factor is infrared divergent, and it is quadratically divergent in the present example. This infrared divergence arises from the fact that we cannot divide Minkowski space into (time-like) domains with finite *4-dimensional* volumes in a Lorentz invariant manner. The Minkowski space is hyperbolic rather than elliptic. CPT symmetry is related to the fundamental structure of Minkowski space, and thus it is gratifying that its possible breaking is also related to the basic property of Minkowski space.

Based on this setting, we confirmed the followings:
1. The present model produces T-violation in the decay $\phi \to \psi + \bar{\psi}$ and its reversed formation process $\psi + \bar{\psi} \to \phi$.
2. The equality of masses and decay widths of the particle and anti-particle is preserved if the non-local CPT violation is incorporated either directly or as perturbation by starting with the conventional CPT-even local Lagrangian.

Some of the more realistic applications of the present CPT violation scheme to the particle-antiparticle mass splitting, inparticular, the neutrino-antineutrino mass splitting in the standard model have been already dicussed elsewhere[3,4].

References
1) M. Chaichian, A.D. Dolgov, V.A. Novikov and A. Tureanu, Phys. Lett. B**699** (2011) 177.
2) K. Fujikawa, Phys. Rev. D**70** (2004) 085006.
3) M. Chaichian, K. Fujikawa and A. Tureanu, Phys. Lett. B **712**, 115 (2012).
4) M. Chaichian, K. Fujikawa and A. Tureanu, Phys. Lett. B **718**,178 (2012).

† Condensed from the article in Eur. Phys. J. C **73**, 2349 (2013).
*1 Department of Physics, University of Helsinki,
*2 RIKEN Nishina Center

Conditionally valid uncertainty relations†

K. Fujikawa*1

It is shown that the well-defined unbiased measurement or disturbance of a dynamical variable is not maintained for the precise measurement of the conjugate variable, independently of uncertainty relations. The conditionally valid uncertainty relations on the basis of those additional assumptions, which include most of the familiar Heisenberg-type relations, thus become singular for the precise measurement. We clarify some contradicting conclusions in the literature concerning those conditionally valid uncertainty relations: The failure of a naive Heisenberg-type error-disturbance relation and the modified Arthurs-Kelly relation in the recent spin measurement is attributed to this singular behavior. The naive Heisenberg-type error-disturbance relation is formally preserved in quantum estimation theory, which is shown to be based on the strict unbiased measurement and disturbance, but it leads to unbounded disturbance for bounded operators such as spin variables. In contrast, the Heisenberg-type error-error uncertainty relation and the Arthurs-Kelly relation, as conditionally valid uncertainty relations, are expected to be consistently maintained.

A recent experiment[1)], which invalidated a naive Heisenberg-type error-disturbance relation[2)], revived our interest in the subject of uncertainty relations. In contrast to the naive Heisenberg-type error-disturbance relation, the relations which are based on only the positive definite Hilbert space and natural commutator algebra are expected to be valid as long as quantum mechanics is valid, namely, "universally valid"[2)3)]. It was recently shown[4)] that all the known universally valid uncertainty relations are derived from Robertson's relation written for suitable combinations of operators. It is important to distinguish the uncertainty relations which are universally valid from those relations based on additional assumptions and thus only conditionally valid.

In this paper, we analyze the implications of the assumptions of unbiased joint measurements or unbiased measurement and disturbance which are widely used in the formulation of uncertainty relations[5)]. We clarify the origin of quite different conclusions concerning the conditionally valid Heisenberg-type relations in the measurement operator formalism[2)] and in the quantum estimation theory[6)] which is a new approach to uncertainty relations.

We first note that the well-defined unbiased measurement or disturbance of a quantum mechanical operator is not maintained for the precise measurement of the conjugate operator in the framework of the ordinary measurement theory. For example, those assumptions lead to

$$\langle [M^{out}, N^{out}] \rangle = \langle [A, B] \rangle,$$
$$\langle [M^{out}, B^{out}] \rangle = \langle [A, B] \rangle. \quad (1)$$

We work in the Heisenberg picture and the variables without any suffix stand for the initial variables; A, B stand for dynamical variables and M, N stand for the corresponding measurement operators, respectively. The variables $M^{out} = U^\dagger(1 \otimes M)U$ and $N^{out} = U^\dagger(1 \otimes N)U$ stand for the variables after the measurement, and $B^{out} = U^\dagger(B \otimes 1)U$ stands for the variable B after the measurement of A. By assumption, $\langle [M^{out}, N^{out}] \rangle = \langle [M^{out}, B^{out}] \rangle = 0$, and thus relations in (1) are contradictions.

The conditionally valid uncertainty relation such as naive Heisenberg-type error-disturbance relation[1)2)],

$$\sigma(M^{out} - A)\sigma(B^{out} - B) \geq \frac{1}{2}|\langle [A, B] \rangle|, \quad (2)$$

which is based on the assumptions of unbiased measurement and disturbance, thus fails if one formulates the relation in terms of well-defined bounded operators. The naive Heisenberg-type error-disturbance relation is formally preserved in quantum estimation theory, but the disturbance of the bounded operator is forced to be singular and divergent for the precise measurement of the conjugate variable[6)].

In contrast, the Heisenberg-type error-error uncertainty relation

$$\sigma(M^{out} - A)\sigma(N^{out} - B) \geq \frac{1}{2}|\langle [A, B] \rangle|, \quad (3)$$

and the Arthurs-Kelly relation,

$$\sigma(M^{out})\sigma(N^{out}) \geq |\langle [A, B] \rangle|, \quad (4)$$

as conditionally valid uncertainty relations, are expected to be consistently maintained.

References

1) J. Erhart, S. Sponar, G. Sulyok, G. Badurek, M. Ozawa and Y. Hasegawa, Nature Phys. **8**, 185 (2012).
2) M. Ozawa, Phys. Rev. A **67**, 042105 (2003).
3) K. Fujikawa, Phys. Rev. A**85**, 062117 (2012).
4) K. Fujikawa and K. Umetsu, Prog. Theor. Exp. Phys., 013A03 (2013).
5) E. Arthurs and J.L. Kelly Jr, Bell. Syst. Tech. J. **44**, 725 (1965).
6) Y. Watanabe, T. Sagawa and M. Ueda, Phys. Rev. A 84, 042121 (2011).
Y. Watanabe and M. Ueda, arXiv:1106.2526[quant-ph].

† Condensed from the article in Phys. Rev. A**88**, 012126 (2013).
*1 RIKEN Nishina Center

Heisenberg uncertainty relation revisited†

K. Fujikawa*1

Kennard and Robertson formulated the uncertainty relation which appears in any textbook on quantum mechanics

$$\sigma(A)\sigma(B) \geq \frac{1}{2}|\langle[A,B]\rangle|. \tag{1}$$

Another important development in the history of uncertainty relations is the analysis of Arthurs and Kelly[1]. They introduce the measuring apparatus M for A, and N for B, respectively, with $[M,N]=0$. The notion of unbiased measurement is important in their analysis, which is defined by

$$\langle M^{out}\rangle = \langle A\rangle \tag{2}$$

for *any* state of the system ψ in the total Hilbert space of the system and apparatus $|\psi\rangle\otimes|\xi\rangle$ in the Heisenberg picture. Here variables M and N (and also A and B) stand for the variables before the measurement, and the variable $M^{out}=U^{\dagger}MU$ stands for the apparatus M after measurement.

Traditionally, it has been common to take the relation[2]

$$\sigma(M^{out}-A)\sigma(B^{out}-B) \geq \frac{1}{2}|\langle[A,B]\rangle| \tag{3}$$

as the naive Heisenberg error-disturbance relation; we use the adjective "naive" since no reliable derivation of this relation is known. An elegant experiment of spin measurement by J. Erhart et al.[3], invalidated the naive Heisenberg-type error-disturbance relation, which initiated the recent activities on uncertainty relations.

It is shown that all the uncertainty relations are derived from suitably defined Robertson's relation[4]. We start with Robertson's relation

$$\begin{aligned}&\sigma(M^{out}-A)\sigma(B^{out}-B)\\&\geq \frac{1}{2}|\langle[M^{out}-A, B^{out}-B]\rangle|\end{aligned} \tag{4}$$

and use the triangle inequality

$$\begin{aligned}&\sigma(M^{out}-A)\sigma(B^{out}-B)\\ \geq\ &\frac{1}{2}\{|\langle[A,B]\rangle| - |\langle[A,B^{out}-B]\rangle|\\ &-|\langle[M^{out}-A,B]\rangle|\},\end{aligned} \tag{5}$$

where we used $[M^{out},B^{out}]=[M,B]=0$. Using the variations of Robertson's relation, we obtain[2]

$$\begin{aligned}&\sigma(M^{out}-A)\sigma(B^{out}-B)+\sigma(M^{out}-A)\sigma(B)\\&+\sigma(A)\sigma(B^{out}-B) \geq \frac{1}{2}|\langle[A,B]\rangle|,\end{aligned} \tag{6}$$

and[5]

$$\begin{aligned}&\{\sigma(M^{out}-A)+\sigma(A)\}\{\sigma(B^{out}-B)+\sigma(B)\}\\&\geq |\langle[A,B]\rangle|.\end{aligned} \tag{7}$$

We thus conclude that all the known universally valid relations are the secondary consequences of Robertson's relation. Also, the saturation of Robertson's relation is a *necessary condition* of the saturation of universally valid uncertainty relations. If one assumes the unbiased measurement and disturbance, one obtains (3).

By assuming unbiased joint measurements, we conclude[6]

$$\langle[A,B]\rangle = \langle[M^{out},N^{out}]\rangle = 0 \tag{8}$$

which is a contradiction since $\langle[A,B]\rangle \neq 0$ in general. Similarly, one concludes[6]

$$\langle[A,B]\rangle = \langle[M^{out},B^{out}]\rangle = 0 \tag{9}$$

if one assumes the precise measurement of A and the unbiased disturbance of B which implies $\langle B^{out}-B\rangle = 0$ for all ψ. Here $B^{out}=U^{\dagger}(B\otimes 1)U$ stands for the variable B after the *measurement* of A. Note that $[M^{out},B^{out}]=[M,B]=0$.

We interpret the algebraic inconsistency (9) as an indication of the failure of the assumption of unbiased disturbance of B for the precise projective measurement of A, if all the operators involved are *well-defined*. Thus the naive relation (3) fails. On the other hand, the Heisenberg error-error relation

$$\epsilon(M^{out}-A)\epsilon(N^{out}-B) \geq \frac{1}{2}|\langle[A,B]\rangle| \tag{10}$$

and the Arthurs-Kelly relation

$$\sigma(M^{out})\sigma(N^{out}) \geq |\langle[A,B]\rangle| \tag{11}$$

are expected to be valid as conditionally valid uncertainty relations. In this case the apparatus variable N^{out} becomes *singular* for the precise measurement of A, namely, $M^{out}-A\rightarrow 0$ if the unbiasedness condition $\langle N^{out}-B\rangle = 0$ is imposed.

References

1) E. Arthurs and J.L. Kelly Jr, Bell. Syst. Tech. J. **44**, 725 (1965).
2) M. Ozawa, Phys. Rev. A**67**, 042105 (2003).
3) J. Erhart, et al., Nature Phys. **8**, 185 (2012).
4) K. Fujikawa and K. Umetsu, Prog. Theor. Exp. Phys., 013A03 (2013).
5) K. Fujikawa, Phys. Rev. A**85**, 062117 (2012).
6) K. Fujikawa, Phys. Rev. A**88**, 012126 (2013).

† Condensed from the article in Int. J. Mod. Phys. A29 1450016 (2014). Invited talk given at Dyson Festivity, Singapore, August 26-29 (2013).

*1 RIKEN Nishina Center

Note on intersecting branes in topological strings

T. Kimura*1

The intersection of branes is an important object in string theory, in order to study non-perturbative aspects of branes, and also its applicatioins to quantum field theory. In this report we investigate some aspects of the intersecting branes in topological string theory, especially through its matrix model description.

We consider the topological B-model on the Calabi-Yau threefold $uv - H(p,x) = 0$ with $H(p,x) = p^2 - W'(x)^2 - f(x)$. This geometry realizes at the large N limit of the matrix model with the potential function $W(x)$. There are seemingly two kinds of non-compact branes in the topological B-model, which correspond to the characteristic polynomial and the external source in the matrix model.[1] They play a role of the creation operator of branes for x and p coordinates, respectively. By considering both kinds of the branes simultaneously, we can discuss intersection of branes in the B-model. The corresponding matrix model partition function $\Psi_{N,M}(\{a_j\};\{\lambda_\alpha\})$ is given by

$$\int_{N\times N} dX\, e^{-\frac{1}{g_s}\mathrm{Tr}W(X)+\mathrm{Tr}AX} \prod_{\alpha=1}^{M} \det(\lambda_\alpha - X)\,. \quad (1)$$

This is the M-point function of characteristic polynomials in $N\times N$ Hermitian matrix model with external source A. In order to evaluate the partition function (1), we first rewrite it only in terms of eigenvalues by integrating out the angular part of the matrix X. Then, after some calculations, we obtain the determinantal expression of the partition function

$$\frac{1}{\Delta(a)\Delta(\lambda)} \det \begin{pmatrix} Q_{j-1}(a_k) & Q_{N+\alpha-1}(a_k) \\ P_{j-1}(\lambda_\beta) & P_{N+\alpha-1}(\lambda_\beta) \end{pmatrix}, \quad (2)$$

where $\Delta(x) = \prod_{i<j}(x_i - x_j)$ is the Vandermonde determinant, and $P_k(x) = x^k + \cdots$ is arbitrary k-th monic polynomial. The function $Q_k(a)$ is the Fourier (Laplace) transform of $P_k(x)\, e^{-\frac{1}{g_s}W(x)}$. Therefore, from the expression (2), we can see an explicit duality between $\vec{a}$ and $\vec{\lambda}$ through the Fourier transformation. In terms of the topological strings, this duality reflects the symplectic invariance of the canonical pair (p,x) in the B-model, which is also seen as the open/closed string duality. We also note that this kind of symplectic invariance appears quite generally in the topological expansion of the spectral curve.

If we apply the Gaussian potential, two functions $P_k(x)$ and $Q_k(x)$ are essentially equivalent, since it is self-dual against the Fourier transformation. In this case we can rewrite the partition function in terms of $\mathrm{U}(N)\times\mathrm{U}(M)$ bifundamental chiral fermions, which are seen as effective degrees of freedom on the intersecting branes. The corresponding effective action is given by

$$S_{\text{eff}} = \frac{g_s}{2}\psi_i^\alpha \bar{\psi}_j^\alpha \psi_j^\beta \bar{\psi}_i^\beta + \mathrm{Tr}A\psi^\alpha\bar{\psi}^\alpha - \mathrm{Tr}\Lambda\psi_j\bar{\psi}_j\,, \quad (3)$$

In this expression the duality between A and Λ is manifest. In this action the full symmetry of $\mathrm{U}(N)\times\mathrm{U}(M)$ is partially broken due to the source terms.

Let us then comment on the integrability of the brane intersection partition function (2). This kind of determinantal formula generically plays a role as the τ-function,[2] and satisfies the Toda lattice equation by taking the equal parameter limit. To show that, we now consider the equal position limit of (2) as $a_j \to a$ and $\lambda_\alpha \to \lambda$. Then we have

$$\prod_{j=0}^{N-1}\frac{1}{j!}\prod_{\alpha=0}^{M-1}\frac{1}{\alpha!}\det\begin{pmatrix} Q_{j-1}^{(k-1)}(a) & Q_{N+\alpha-1}^{(k-1)}(a) \\ P_{j-1}^{(\beta-1)}(\lambda) & P_{N+\alpha-1}^{(\beta-1)}(\lambda)\end{pmatrix}. \quad (4)$$

This is just a hybritized version of Wronskian. If we apply the simplest choice $P_k(x) = x^k$, $Q_k(a)$ is just given as k-th derivative of the generalized Airy function

$$Q_k(a) = \left(\frac{d}{da}\right)^k \int dx\, e^{-\frac{1}{g_s}W(x)+ax}\,. \quad (5)$$

Applying the Jacobi identity for determinants to the expression (4), we obtain the following 3-term reccurence relations

$$\frac{\tilde{\Psi}_{N+1,M}\cdot\tilde{\Psi}_{N-1,M}}{\left(\tilde{\Psi}_{N,M}\right)^2} = \frac{N}{M}\frac{\partial^2}{\partial a^2}\log\tilde{\Psi}_{N,M}\,, \quad (6)$$

$$\frac{\tilde{\Psi}_{N,M+1}\cdot\tilde{\Psi}_{N,M-1}}{\left(\tilde{\Psi}_{N,M}\right)^2} = \frac{\partial^2}{\partial a\partial\lambda}\log\tilde{\Psi}_{N,M}\,. \quad (7)$$

where we have rescaled the partition function as $\tilde{\Psi}_{N,M}(a,\lambda) = e^{-\lambda}\Psi_{N,M}(a,\lambda)$. The equations (6) and (7) are the Toda lattice equations in one and two dimensions. This means that the brane intersection partition function is the τ-function for the Toda lattice hierarchy in both senses. We can also introduce infinitely many "time" variables for this τ-function in the Miwa coordinate

$$t_n = \frac{1}{n}\mathrm{Tr}\,A^{-n}\,, \quad \tilde{t}_n = \frac{1}{n}\mathrm{Tr}\,\Lambda^{-n}\,. \quad (8)$$

If we take the large N limit of the matrix model, which corresponds to the continuum limit of the Toda lattice equation, we obtain the KdV/KP integrable equations.

*1 RIKEN Nishina Center

References

1) M. Aganagic, R. Dijkgraaf, A. Klemm, M. Mariño, C. Vafa, Commun. Math. Phys. **261** (2006) 451–516.
2) A. Morozov, Phys. Usp. **37** (1994) 1–55.

Non-Lagrangian theories from brane junctions †

L. Bao,*1 V. Mitev,*2 E. Pomoni,*3 M. Taki*4 and F. Yagi*5

In a seminal article[1)], Gaiotto argued that a large class, called class $\mathcal{S}$, of $\mathcal{N}=2$ superconformal field theories (SCFT) in four dimensions (4D) can be obtained by a twisted compactification of a 6D $(2,0)$ SCFT on a Riemann surface of genus g with n punctures. The building blocks of the class $\mathcal{S}$ theories are tubes and pairs of pants that correspond to gauge groups and matter multiplets, respectively. Subsequently, a relation between the partition functions of the $\mathcal{N}=2$ $SU(N)$ gauge theories and the correlation functions of the 2D A_{N-1} Toda CFTs was proposed.[2)] Computation of 2-point and 3-point functions in a CFT would in principle yield a complete understanding of the n-point functions.

It is important to note that there is a fundamental difference between the $SU(2)$ and the $SU(N)$, $N>2$, cases. For the $SU(2)$ quiver gauge theories[2)] that are related to the 2D Liouville CFT, there is only one type of puncture on the Riemann surface and hence the Liouville CFT has only one class of 2D 3-point functions to be calculated. On the other hand, the $SU(N)$ case with $N>2$ has more than one kind of puncture. So far, the case with three special $SU(N)$ punctures T_N has remained elusive, since neither the T_N Nekrasov partition functions nor the Toda three-point correlators are known. The situation is further aggravated by the fact that the corresponding 4D theories do not have a Lagrangian description. Even though there is no known Lagrangian description of the 4D T_N theories, we are able to obtain the partition functions for their 5D uplift[3)] using topological strings on the dual geometry of the 5-brane junctions.

In this paper, we compute the Nekrasov partition functions of the T_N junctions as refined topological string partition functions.[4)] At this point, we make use of the quite recent conjecture of Iqbal and Vafa[5)] that says that the 5D superconformal index, which is the partition function on $S^4\times S^1$, can be obtained from the 5D Nekrasov partition function and thus from the topological string partition function

$$\mathcal{I}^{5D}=\int da\,|Z^{5D}_{\text{Nek}}(a)|^2\propto\int da\,|Z_{\text{top}}(a)|^2. \qquad (1)$$

The E_6 superconformal index is obtained from the T_3 Nekrasov partition function by using the idea presented in Iqbal and Vafa,[5)] and we find that the results coincide with those of Kim et al.,[6)] computed via localization. When parallel external 5-brane legs appear in the toric web diagram, the corresponding partition functions contain extra degrees of freedom. In contrast to the massive spectrum in 5D, which forms a representation of the Wigner little group $SU(2)\times SU(2)$, referred to as the *full spin content representation*, these extra states do not transform as a correct representation under the Poincaré symmetry. Therefore, we call them *non-full spin content* contributions. We interpret this part as the contribution to the extra degrees of freedom appearing from the parallel 5-branes explained above. It should therefore be removed. To obtain the superconformal index from the topological string partition function, we have to eliminate all the non-full spin content from the partition function. Schematically, the partition function can be expressed as a sum of Young diagrams assigned to the product of strip geometries as

$$Z_{T_N}=\frac{1}{Z_{\text{non-full spin}}}\sum_{\boldsymbol{Y}}\prod_{i=1}^{N}Z_i^{\text{strip}}(\boldsymbol{Y})\,. \qquad (2)$$

The factor $Z_{\text{non-full spin}}$ is the BPS spectrum, which does not form a representation of the Poincaré symmetry, and Z^{strip} is the partition function of the strip geometry.

Finally, the 5D version of the AGTW relation, which suggests that the 5D Nekrasov partition functions are equal to the conformal block of q-deformed W_N Toda, implies the following relation between the superconformal index and the correlation functions of the corresponding q-deformed Toda field theory:

$$\mathcal{I}^{5D}(x,y)=\int[da]\left|Z^{\text{5D}}_{\text{Nek}}(a,m,\beta,\epsilon_{1,2})\right|^2$$
$$\propto\langle V_{\boldsymbol{\alpha}_1}(z_1)\cdots V_{\boldsymbol{\alpha}_n}(z_n)\rangle_{q\text{-Toda}}. \qquad (3)$$

This is an important entry in the dictionary of the 5D/2D AGTW correspondence. The partition functions of the T_N brane junctions predict, up to an overall coefficient, the corresponding DOZZ formula for the three-point functions.

References

1) D. Gaiotto: JHEP **1208**, 034 (2012) [arXiv:0904.2715 [hep-th]].
2) L. F. Alday, D. Gaiotto, and Y. Tachikawa, *Lett.Math.Phys.* **91**, 167–197 (2010).
3) F. Benini, S. Benvenuti, and Y. Tachikawa, *JHEP* **0909**, 052 (2009).
4) A. Iqbal, C. Kozcaz, and C. Vafa, *JHEP* **10**, 069 (2009).
5) A. Iqbal and C. Vafa, `arXiv:1210.3605`.
6) H.-C. Kim, S.-S. Kim, and K. Lee, *JHEP* **1210**, 142 (2012).

† arXiv:1301.0721

*1 Chalmers University of Technology
*2 Institut für Mathematik und Institut für Physik, Humboldt-Universität zu Berlin
*3 DESY Theory Group
*4 RIKEN Nishina Center
*5 Korea Institute for Advanced Studyr

Holomorphic blocks for 3D non-Abelian partition functions†

M. Taki*1

The pioneering work by Pestun[1] on the partition function of four-dimensional (4D) $\mathcal{N}=2$ theories has served as a trigger for great progress on localization computation of supersymmetric gauge theories in diverse dimensions and on various manifolds. The localization of three-dimensional (3D) theories is a recent focus of research. Kapustin, Willett, and Yaakov[2] extended Pestun's idea to gauge theories on S^3, and they obtained matrix model representations for the supersymmetric partition functions of these theories. We can solve these matrix-models in the large-N limit; for instance, the ABJM partition function was computed by Drukker, Marino, and Putrov[3]. They found that the free energy of the ABJM theory actually shows the $N^{3/2}$ scaling behavior, which had been suggested in the AdS/CFT argument. This result is a typical example of the power of the localization approach.

The efficiency of localization reaches beyond the large-N approximation. The matrix models for partition functions of $\mathcal{N}=2$ gauge theories on S^3 was derived in Ref.[4,5]. The integrant of this matrix model consists of a complicated combination of double-sine functions, and it appears difficult on first glance to evaluate it exactly. In Ref.[6], however, the authors succeessfully solved these matrix models exactly. In particular, the partition functions of 3D $\mathcal{N}=2$ $U(1)$ theories computed in Ref.[6] show the following factorization property:

$$Z^{U(1)}[S^3]=\sum_{i=1}^{N_f} Z^{(i)}_{\text{vort}}\,\widetilde{Z}^{(i)}_{\text{anti-vort}}. \tag{1}$$

Here, Z_{vort} and $\widetilde{Z}_{\text{anti-vort}}$ are the partition functions of the vortex and antivortex configurations on $S^1\times \mathrm{R}^2$ respectively. The summation is taken over the supersymmetric ground states that specify the vortex sector. This factorization into vortices is the 3D analogue of Pestun's expression,

$$Z^{U(1)}[S^4]=\int da\, Z_{\text{inst}}(a)\,\widetilde{Z}_{\text{anti-inst}}(a). \tag{2}$$

In this 4D case, ground states are labeled by the continuous moduli parameter a; therefore, we take the integral over it after combining the contributions from instantons and anti-instantons. The three-dimensional factorization is therefore expected to originate from the localization after changing the way of carrying out the localization computation.

In this paper, we extend this observation (1) to gauge theories with a more generic gauge group $SU(N)$. To compute the localization partition functions of these non-Abelian gauge theories, we need to evaluate the following complicated matrix integral:

$$Z=\frac{1}{N!}\int d^N x\; e^{-i\pi k\sum x_\alpha^2+2\pi i\xi\sum x_\alpha}\prod_{1\le\alpha<\beta\le N}$$
$$\times 4\sinh\pi b(x_\alpha-x_\beta)\,\sinh\pi b^{-1}(x_\alpha-x_\beta)$$
$$\times\prod_{\alpha=1}^{N}\prod_{i=1}^{N_f}\frac{s_b(x_\alpha+m_i+\mu_i/2+iQ/2)}{s_b(x_\alpha+m_i-\mu_i/2-iQ/2)}. \tag{3}$$

Here, $s_b(x)$ is the double-sine function[7]. Employing the Cauchy formula

$$\prod_{1\le\alpha<\beta\le N} 2\sinh(x_\alpha-x_\beta)2\sinh(\chi_\alpha-\chi_\beta)$$
$$=\sum_{\sigma\in S^N}(-1)^\sigma\prod_{\alpha}\prod_{\beta\neq\sigma(\alpha)}2\cosh(x_\alpha-\chi_\beta), \tag{4}$$

we succeeded to compute the matrix integral, and we found the following factorization:

$$Z^{SU(N)}[S^3]=\sum_{i_1}^{N_f}\cdots\sum_{i_N}^{N_f} Z^{(\vec{i})}_{\text{vort}}\,\widetilde{Z}^{(\vec{i})}_{\text{anti-vort}}, \tag{5}$$

where N_f is the number of flavors. This result suggests that the factorization is universal for the gauge theories in three dimensions, and we can expect a similar relation for gauge theories with other gauge groups on more generic three-dimensional manifolds. It would be also possible to re-derive our result physically without computing the partition functions explicitly.

References

1) V. Pestun, "Localization of gauge theory on a four-sphere and supersymmetric Wilson loops," Commun. Math. Phys. **313**, 71 (2012) [arXiv:0712.2824 [hep-th]].
2) A. Kapustin, B. Willett and I. Yaakov, "Nonperturbative Tests of Three-Dimensional Dualities," JHEP **1010**, 013 (2010) [arXiv:1003.5694 [hep-th]].
3) N. Drukker, M. Marino and P. Putrov, "From weak to strong coupling in ABJM theory," Commun. Math. Phys. **306**, 511 (2011) [arXiv:1007.3837 [hep-th]].
4) D. L. Jafferis, "The Exact Superconformal R-Symmetry Extremizes Z," JHEP **1205**, 159 (2012) [arXiv:1012.3210 [hep-th]].
5) N. Hama, K. Hosomichi and S. Lee, "Notes on SUSY Gauge Theories on Three-Sphere," JHEP **1103**, 127 (2011) [arXiv:1012.3512 [hep-th]].
6) S. Pasquetti, "Factorisation of N = 2 Theories on the Squashed 3-Sphere," JHEP **1204**, 120 (2012) [arXiv:1111.6905 [hep-th]].
7) E. W. Barnes, " Theory of the double gamma function," Phil. Trans. Roy. Soc. A **196** (1901) 265-388

† arXiv:1303.5915

*1 RIKEN Nishina Center

Notes on the enhancement of flavor symmetry and 5d superconformal index[†]

M. Taki[*1]

Perturbative renormalizability has been a criterion for the predictable quantum field theory. Needless to say, this is because renormalization removes ultraviolet (UV) divergences from Feynman diagram, giving a meaningful finite value to a physical quantity. While an effective theory is permitted to include non-renormalizable interactions, this criterion must be satisfied by a fundamental theory without any cut-off scale, and it excludes many models of the quantum field theory. The renormalizable theories, however, do not exhaust all possibilities.

A quantum theory endowed with a UV fixed point is well defined and valid at the whole energy scale. This possibility is known as the Weinberg asymptotic safety scenario[1)], which perhaps preserves the non-renormalizability of the perturbative quantum gravity. This scenario is also very attractive because a renormalizable but asymptotically non-free theory such as pure QED involves the Landau pole, and the convergence radius of the perturbation becomes zero according to popular opinion. By assuming the existence of the UV fixed point, we can avoid such a theoretical inconsistency included in perturbative quantum field theory.

UV fixed point is a very important notion in the quantum field theory, but it is very difficult in general to determine whether a theory has a UV fixed point. 5d minimal supersymmetric gauge theories are typical and attractive exceptions to circumvent this difficulty. Perturbative five-dimensional gauge theories are non-renormalizable, but Seiberg[2)] showed that perturbative description breaks down at high energy but some of these theories flow up to a strongly coupling, non-Gaussian, UV fixed point. $SU(2)$ gauge theory with $N_f = 0, 1, \cdots, 7$ fundamental flavors provides a concrete example[3,4)]. The flavor symmetry of this gauge theory is $SO(2N_f) \times U(1)_I$, where $U(1)_I$ is associated with the instanton current $J = *\mathrm{Tr}F \wedge F$. The UV fixed point is described by a strongly coupled conformal field theory. At this fixed point, the flavor symmetry is expected to enhance to the larger group E_{N_f+1}: $E_1 = SU(2)$, $E_2 = SU(2)\times U(1)$, $E_3 = SU(3)\times SU(2)$, $E_4 = SU(5)$, $E_5 = SO(10)$, and $E_{6,7,8}$ are the usual exceptional Lie groups.

This enhancement of the flavor symmetries was conjectured by employing superstring theory[2)], and so far it has not been easy to show this enhancement based only on field theory arguments. This is because the UV fixed point theories in question are strongly coupled, and it has prevented us from verifying this conjecture directly. Fortunately, with recent progress in the theories of localization and the superconformal index, we can discuss the strongly coupled fixed point theories quantitatively by evaluating the protected indexes of these theories[5)]. The 5d superconformal index is the following extended version of the Witten index:

$$I_{5\mathrm{d}}(u, z_f, \cdots) = \mathrm{Tr}_{\mathcal{H}_{\frac{1}{8}\mathrm{BPS}}} (-1)^F u^k \prod_f z_f^{H_f} \cdots .$$

Here k is the $U(1)$ charge with respect to the instanton current, and H_f is a Cartan generator of the flavor symmetry. u and z_f are the fugacities for these symmetries. In this paper, we study the detailed structure of the superconformal index, and we provide a justification of the enhancement of the flavor symmetry for $N_f = 0, 1, 2$. We find that the superconformal index satisfies

$$I_{5\mathrm{d}}(u, z_f, t, q) = I_{5\mathrm{d}}(u^{-1}, z_f, t, q).$$

This result indicates that the index is actually invariant under the action of the Weyl group of the expected $SU(2)$ flavor symmetry. We then conclude that the $U(1)$ global symmetry of 5d gauge theory is enhanced to $SU(2)$ at the UV fixed point. This $SU(2)$ flavor symmetry is the core of the full E_{N_f+1} symmetry, and therefore we can expect that extending our result should yield a proof of the full enhancement.

References

1) S. Weinberg, “Ultraviolet Divergences In Quantum Theories Of Gravitation,” In General Relativity: An Einstein centenary survey. Eds. S. W. Hawking and W. Israel, Cambridge University Press, 790 (1979)
2) N. Seiberg, “Five-dimensional SUSY field theories, non-trivial fixed points and string dynamics,” Phys. Lett. B **388**, 753 (1996) [hep-th/9608111].
3) D. R. Morrison and N. Seiberg, “Extremal transitions and five-dimensional supersymmetric field theories,” Nucl. Phys. B **483**, 229 (1997) [hep-th/9609070].
4) K. A. Intriligator, D. R. Morrison and N. Seiberg, “Five-dimensional supersymmetric gauge theories and degenerations of Calabi-Yau spaces,” Nucl. Phys. B **497**, 56 (1997) [hep-th/9702198].
5) H. -C. Kim, S. -S. Kim and K. Lee, “5-dim Superconformal Index with Enhanced En Global Symmetry,” JHEP **1210**, 142 (2012) [arXiv:1206.6781 [hep-th]].

† arXiv:1310.7509
*1 RIKEN Nishina Center

From the Berkovits formulation to the Witten formulation in open superstring field theory†

Y. Iimori,*1 T. Noumi,*2 Y. Okawa,*3 and S. Torii*2

Gauge invariance plays a fundamental role in the current formulation of covariant string field theory. In open bosonic string field theory,[1] behind the gauge invariance is the algebraic structure called the A_∞ structure,[2,3] which is closely related to the covering of the moduli space of Riemann surfaces. In open superstring field theory, we therefore expect that the structure underlying its gauge invariance be a supersymmetric extension of the A_∞ structure, which would be closely related to the covering of the supermoduli space of super-Riemann surfaces. However, there is very little understanding of gauge invariance, and some of the problems we are confronted with in open superstring field theory seem to be related to the lack of our understanding in this perspective.

For example, in the Witten formulation of open superstring field theory,[4] the gauge symmetry has proven to be singular because of the collision of picture-changing operators.[5] There are related divergences in tree-level amplitudes, which are also caused by the collision of picture-changing operators. It is possible that the source of these divergences is related to the singular covering of the supermoduli space of super-Riemann surfaces. At the moment, however, such understanding is negligible.

On the other hand, gauge transformation does not suffer from any singularity in the Berkovits formulation of open superstring field theory[6] in the Neveu-Schwarz sector. We do not, however, understand why it works well in the context of the covering of the supermoduli space of super-Riemann surfaces. In the Berkovits formulation, the action contains interaction vertices higher than cubic. We know that the bosonic moduli space of Riemann surfaces is covered by Feynman diagrams with cubic vertices alone, and the higher-order vertices do not contribute to the covering of the bosonic moduli space. Since gauge invariance requires the higher-order vertices, it is expected that these vertices play a role in the covering of the supermoduli space. At the moment, however, such understanding is missing.

In view of recent developments in the understanding of the supermoduli space,[7–10] the exploration of the relation between gauge invariance in open superstring field theory and the covering of the supermoduli space of super-Riemann surfaces can be crucially important for the profound question of whether open superstring field theory can be a consistent quantum theory by itself. In this report, as a first step towards this direction, we address the question of how the divergences in the Witten formulation can be resolved in the Berkovits formulation.

The Hilbert space of the string field in the Berkovits formulation is larger than that in the Witten formulation and, correspondingly, the gauge symmetry in the Berkovits formulation is larger than that in the Witten formulation. We perform partial gauge fixing in the Berkovits formulation to associate it with the Witten formulation. We introduce a one-parameter family of judicious gauge choices labeled by λ, and the cubic interaction in the Berkovits formulation reduces to that in the Witten formulation in the singular limit $\lambda \to 0$. We can think of the Berkovits formulation which is partially gauge fixed with finite λ as a regularization of the Witten formulation. We find that the divergence in the four-point amplitude as $\lambda \to 0$ is canceled by the quartic interaction. We also find that the divergence in the gauge variation of the action to the second order in the coupling constant as $\lambda \to 0$ is resolved by incorporating the quartic interaction. Our approach based on the one-parameter family of gauge choices enables us to discuss the nature of these divergences in a concrete and well-defined setting. Our next step will be to translate the mechanism of canceling the divergences into the language of the covering of the supermoduli space of super-Riemann surfaces, and our ultimate goal is to reveal a supersymmetric extension of the A_∞ structure underlying open superstring field theory.

References

1) E. Witten, Nucl. Phys. **B268**, 253 (1986).
2) J. D. Stasheff, Trans. Amer. Math. Soc. **108**, 275 (1963).
3) J. D. Stasheff, Trans. Amer. Math. Soc. **108**, 293 (1963).
4) E. Witten, Nucl. Phys. **B276**, 291 (1986).
5) C. Wendt, Nucl. Phys. **B314**, 209 (1989).
6) N. Berkovits, Nucl. Phys. B **450**, 90 (1995) [Erratum-ibid. B **459**, 439 (1996)].
7) E. Witten, arXiv:1209.2459.
8) E. Witten, arXiv:1209.5461.
9) E. Witten, arXiv:1304.2832.
10) R. Donagi and E. Witten, arXiv:1304.7798.

† Condensed from the article in arXiv:1312.1677.

*1 Department of Physics, Nagoya University
*2 RIKEN Nishina Center
*3 Institute of Physics, The University of Tokyo

A landscape in boundary string field theory: new class of solutions with massive state condensation†

K. Hashimoto[*1,*2] and M. Murata[*3]

We solve the equation of motion of boundary string field theory allowing generic boundary operators quadratic in X, and explore string theory non-perturbative vacua with massive state condensation. Using numerical analysis, a large number of new solutions are found. Their energies turn out to distribute densely in the range between the D-brane tension and the energy of the tachyon vacuum. We discuss an interpretation of these solutions as perturbative closed string states. From the cosmological point of view, the distribution of the energies can be regarded as the so-called landscape of string theory, as we have a vast number of non-perturbative string theory solutions including one with small vacuum energy.

As a non-perturbative formulation of open bosonic string, boundary string field theory (BSFT)[1)] was proposed as well as cubic string field theory (CSFT). In general, solutions of string field theories are quite important as they would provide non-perturbative vacua of string theory, to look at the true capability of string theory.

Recently, the multiple D-brane solutions, which have greater energies than the trivial vacuum, were proposed in CSFT. It would have a significance equivalent to the proof of the original Sen's conjecture, since the D-brane creation is thought of as a necessary ingredient for a complete non-perturbative formulation of string theory. To climb up the SFT potential hill instead of rolling down the hill to get to the tachyon vacuum, it is indispensable to treat the string massive modes.

After the construction of the analytic solution for tachyon condensation, various analytic solutions in CSFT have been found. In recent times, analytic forms of lump solutions and multiple D-brane solutions were proposed. In BSFT, as well, an analytic solution for tachyon condensation and lump solutions have been found .

To solve the equation of motion of CSFT, we encounter the infinite-dimensional equation, which is hard to solve. In fact, there are some subtleties of proposed solutions. On the other hand, there is a consistent truncation scheme which reduces BSFT to a standard field theory with a finite number of fields. The BSFT action was constructed also for boundary interactions quadratic in the worldsheet field X, corresponding to a subset of massive modes of open string.

† Condensed from the article in PTEP 2013 (2013) 043B01
*1 RIKEN Nishina Center
*2 Department of Physics, Osaka University
*3 Institute of Physics AS CR, Czech Republic

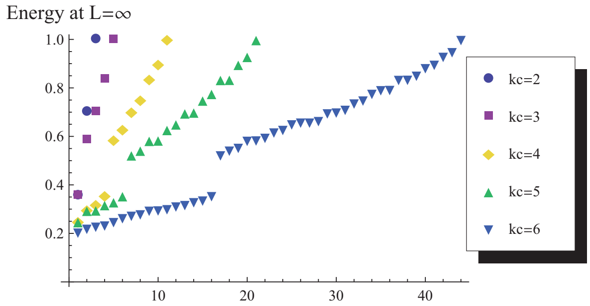

Fig. 1. The plots of the energies for Lorentz invariant solutions of the BSFT. Values are in units of $T_{25}V_{26}$ which is the total energy (tension) of a D25-brane. k_c is a cut-off integer for truncating the excited level considered in the BSFT.

The purpose of this paper is to solve the equation of motion of the BSFT action for the quadratic boundary operators. In contrast to CSFT, only the tachyon field plays a significant role in the BSFT exact solution for tachyon condensation and the lump solutions such that the analysis is rather simple. For this reason, it is natural to expect that one may obtain a new class of solutions by involving some more boundary operators, aiming at new string vacua and a construction of a multiple-D-brane solution.

We adopt the BSFT action for quadratic boundary interactions with arbitrary number of derivatives on the worldsheet, and solve the equation of motion numerically to find homogeneous static solutions. The condensation of the massive fields is taken care of to their all orders. So the solutions are non-perturbative ones at the classical level of SFT, in the same sense as for the non-perturbative tachyon vacuum solutions of the BSFT. We discover a large number of new solutions of BSFT. Interestingly, those energies turn out to be smaller than the D-brane energy, see Fig. 1. Our analysis strongly suggests the existence of an infinite number of solutions. We also find that an approximately uniform distribution of the energies of the solutions, which suggests a relation to closed string excitations at the tachyon vacuum. Furthermore, from a cosmological point of view, the distribution of infinitely many solutions is reminiscent of the so-called string landscape.

References

1) E. Witten, Phys. Rev. D **46** (1992) 5467 [hep-th/9208027]; E. Witten, Phys. Rev. D **47** (1993) 3405 [hep-th/9210065].

Vacuum instability in electric fields via AdS/CFT: Euler-Heisenberg Lagrangian and Planckian thermalization†

K. Hashimoto*1*2 and T. Oka*3

Extreme environments, such as a strong electric field, is one of the frontiers to test physical systems and to reveal new physical phenomena. Particle physics is not an exception. The physics of quantum fields in strong external electric fields, *i.e.*, "strong-field quantum field theory" has a very long history which even dates back to the development era of QED. Nevertheless, the dynamics of quantum fields and their vacuum in strong electromagnetic fields has not been understood well yet, both theoretically and experimentally. One of the present frontiers of strong field QFT is to understand the instability of strongly interacting systems such as the confining vacuum in QCD.

A particular interest is a relation between the confinement in QCD and the strong electric field. Because quarks have electric charges, a strong electric field can induce a vacuum decay at which pairs of a quark and an antiquark are produced from the vacuum to cancel the background electric field. However to estimate the threshold critical electric field, as well as to describe the physical decay process, is a difficult problem, because of several reasons; first, QCD is strongly coupled so the standard perturbative calculation does not work at low energy, and second, strong electromagnetic fields induces effective multi-photon vertices resulting in a complicated nonlinear electromagnetic effective action.

The renowned method for analyzing strongly coupled system, such as QCD, is the AdS/CFT correspondence[1]. This is a well-developed tool in string theory which enables us to analyze strongly coupled QCD analytically. In this paper, we apply the gauge/gravity duality to a certain strongly coupled QCD-like gauge theory, and analyze the instability caused by a strong electric field.

We analyze vacuum instability of strongly coupled gauge theories in a constant electric field using AdS/CFT correspondence. The model is the $\mathcal{N} = 2$ 1-flavor supersymmetric large N_c QCD in the strong 't Hooft coupling limit.[2] We calculate the Euler-Heisenberg effective Lagrangian $\mathcal{L}(E)$, which encodes the nonlinear response and the quantum decay rate of the vacuum in a background electric field E, from the complex D-brane action in AdS/CFT. We find that the decay rate given by $\mathrm{Im}\,\mathcal{L}(E)$ becomes nonzero above a critical electric field set by the confining force between quarks. A large E expansion of $\mathrm{Im}\,\mathcal{L}(E)$ is found to coincide with that of the Schwinger effects in QED, replacing its electron mass by the confining force.

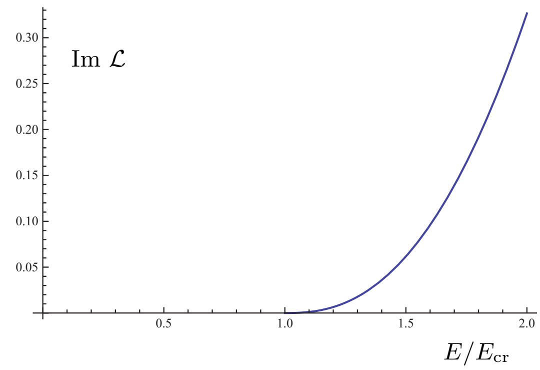

Fig. 1. The imaginary part of the lagrangian of our massive supersymmetric QCD. We find a critical electric field beyond which the instability is detected. The critical electric field means the breaking of the quark confinement.

Then, the time-dependent response of the system in a strong electric field is solved non-perturbatively, and we observe a universal thermalization at a shortest timescale "Planckian thermalization time" $\tau_{\rm th} \sim \frac{\hbar}{k_B T_{\rm eff}^{\infty}} \sim \frac{\hbar}{k_B} E^{-1/2}$. Here, $T_{\rm eff}^{\infty}$ is an effective temperature which quarks feel in the nonequilibrium state with nonzero electric current, calculated in AdS/CFT as a Hawking temperature. Stronger electric fields accelerate the thermalization, and for a realistic value of the electric field in RHIC experiment, we obtain $\tau_{\rm th} \sim 1$ [fm/c], which is consistent with the believed value.

The main result of the present paper is an analytic computation of the full electromagnetic effective Lagrangian for a strongly coupled QCD-like gauge theory. In particular, the imaginary part of the effective Lagrangian shows the decay rate of the vacuum of the gauge theory. The computed imaginary part is shown in Fig. 1.

References
1) J. M. Maldacena, Adv.Theor.Math.Phys. **2** (1998) 231.
2) A. Karch and E. Katz, JHEP **0206** (2002) 043.

† Condensed from the article in JHEP 10 (2013) 116
*1 RIKEN Nishina Center
*2 Department of Physics, Osaka University
*3 Department of Engineering Science, the University of Tokyo

Unitarity bounds from generalised Käbler identities

J. Schmude*1

A textbook result in Kähler geometry relates the de Rham with the Dolbeault Laplacian, $\Delta = 2\Delta_{\bar\partial}$. The topic of this note is a similar identity in the case of Sasaki-Einstein manifolds and its application in to the unitarity bounds in superconformal gauge theories (SCFTs):

$$\begin{aligned}\Delta &= 2\Delta_{\bar\partial_b} - \pounds_\eta^2 - 2\imath(n-d^0)\pounds_\eta + 2L\Lambda \\ &+ 2(n-d^0)L_\eta\Lambda_\eta + 2\imath(L_\eta\bar\partial_b^* - \bar\partial_b\Lambda_\eta).\end{aligned} \tag{1}$$

The right hand side features the tangential Cauchy-Riemann operator, the Lefschetz operator, and the action of the Reeb vector. The equation $\Delta = 2\Delta_{\bar\partial}$ can be derived from the Kähler identities, commutators between the Dolbeault and Lefschetz operators and their adjoints. The proof of equation 1 follows a similar route by obtaining Kähler-like identities that hold on Sasaki-Einstein manifolds. Those identities as well the details of the proof were worked out in[1].

Equation 1 finds application in the AdS/CFT correspondence. Freund-Rubin compactification on Sasaki-Einstein manifolds yields supergravity duals of superconformal field theories. The AdS/CFT dictionary links the conformal energy of SCFT operators to the spectrum of Δ, their R-charge to that of the Lie-derivative along the Reeb vector, $\pounds_\eta$. The conformal energy, R-charge, and spin of any SCFT operator have to satisfy the unitarity bounds[4,5], which should be reflected on the supergravity side in the spectrum of Δ. Indeed, it is possible to re-derive the unitarity bounds from supergravity when using equation 1 in conjunction with the calculations in[2,3].

This leads us to the spectral problem for Δ. Decompose the cotangent bundle as $T^*S = D^* \oplus \eta = \Omega^{1,0} \oplus \Omega^{0,1} \oplus \eta$ and consider a k-form ω with $\pounds_\eta\omega = \imath q$, $q \geq 0$, and $d^0 \leq n$. Clearly all terms on the right hand side of 1 are positive definite except for the mixed term $M = \imath(L_\eta\bar\partial_b^* - \bar\partial_b\Lambda_\eta) = N + N^*$. M is self-adjoint and its spectrum is real. Moreover, $N^2 = 0$ and $N(\bigwedge^* D^*) \subset \bigwedge^* D^* \wedge \eta$ and $N(\bigwedge^* D^* \wedge \eta) = 0$. That is, N maps horizontal to vertical forms and annihilates the latter. N^* behaves accordingly and it follows that $\langle \omega, M\omega\rangle$ vanishes if ω is horizontal or vertical. This is also the case if ω is neither horizontal nor vertical yet holomorphic in the $\bar\partial_b$-sense. As long as we restrict to one of these cases, 1 takes the form of a bound on the spectrum of Δ.

This was conjectured and partially shown in the context of the calculations of the superconformal index in[2,3]. Here, the spectrum was constructed from primitive elements of $\Omega^{p,q}$. For such forms, 1 clearly implies

$$\Delta \geq q^2 + 2q(n-d^0) \tag{2}$$

*1 RIKEN Nishina Center

with equality if and only if $\bar\partial_b\omega = \bar\partial_b^*\omega = 0$. In the Kähler case, the latter of these is implied by transversality — $d^*\omega = 0$. Here however, $d^*\omega = 0$ leads only to the vanishing of the horizontal component of $\bar\partial_b^*\omega$. Indeed,

$$\partial_b^*\omega = \imath L_\eta\Lambda\omega, \quad \bar\partial_b^*\omega = -\imath L_\eta\Lambda\omega, \tag{3}$$

which vanishes since ω was assumed to be primitive. Assuming that every element of $H^{p,q}_{\bar\partial_b}(S)$ has a representative closed under $\bar\partial_b^*$, the bound 2 is saturated on the elements of $H^{p,q}_{\bar\partial_b}(S)$. These are the forms that correspond to the short multiplets in the SCFT, and 2 together with the expressions for the derived eigenmodes of Δ given in[2,3] allows to recover the unitarity bounds from supergravity.

Since we found Sasaki-Einstein equivalents of both $\Delta = 2\Delta_{\bar\partial}$ and the Kähler identities, it is tempting to ask how much more of Kähler geometry can be generalized. For example, since $\Delta_{\bar\partial}$ is self-adjoint and elliptic, one can show that $\Omega^k_{\mathbb{C}} = \mathcal{H}^k \oplus \Delta_{\bar\partial}(\Omega^k_{\mathbb{C}})$ which implies Hodge's theorem. Similarly, the relation between the de Rham and Hodge Laplacians allows for an isomorphism between the respective spaces of harmonic forms. However, $\Delta_{\bar\partial_b}$ is not elliptic. Recall that $\Delta_{\bar\partial_b}$ is elliptic if the symbol $\sigma_{\Delta_{\bar\partial_b}} : Hom(\Omega^k_{\mathbb{C}}, \Omega^k_{\mathbb{C}}) \otimes S^2(T^*S)$ maps any non-zero $\omega \in T^*S$ to an automorphism on $\Omega^k_{\mathbb{C}}$. When calculating the symbol one essentially keeps only those terms of $\Delta_{\bar\partial_b}$ that are of highest order in derivatives. In the context of the tangential Cauchy-Riemann operator, this means that ∂_b and $\bar\partial_b$ can be taken to be anticommuting and that the overall result is essentially the same as for the symbol of the Dolbeault Laplacian on a Kähler manifold. It turns out, that $\sigma_{\Delta_{\bar\partial_b}}(\eta) = 0$ and $\Delta_{\bar\partial_b}$ is not elliptic, yet transversally elliptic.

An obvious problem of interest is the extension of the results presented here beyond the Sasaki-Einstein case. As long as there is a dual SCFT, there is a unitarity bound meaning that there should be some equivalent of 1.

References

1) J. Schmude, arXiv:1308.1027 [hep-th].
2) R. Eager and J. Schmude, arXiv:1305.3547 [hep-th].
3) R. Eager, J. Schmude and Y. Tachikawa, arXiv:1207.0573 [hep-th].
4) J. Kinney, J. M. Maldacena, S. Minwalla and S. Raju, Commun. Math. Phys. **275**, 209 (2007) [hep-th/0510251].
5) J. Bhattacharya, S. Bhattacharyya, S. Minwalla and S. Raju, JHEP **0802**, 064 (2008) [arXiv:0801.1435 [hep-th]].

Superconformal indices for gauge duals of $AdS_4 \times SE_7$

J. Schmude*1

The superconformal index[1,2] of a three-dimensional superconformal field theory can be expressed as the trace over all operators in the theory weighted by their fermion number

$$I(t, z_i) = tr[(-1)^F t^{\epsilon+j_3} z_i^{h_i}]. \quad (1)$$

Here ϵ is the operator dimension, j_3 is the spin of the operator, F is its fermion number, and h_i label the charges of the operator under global symmetries.

In this note we summarise[3] the derivation of the gravity superconformal index for any theory of the form $AdS_4 \times SE_7$. Previously the supergravity index was computed for the homogenous Sasaki-Einstein seven-manifolds using known Kaluza-Klein spectra[4]. However, to match the field theory index and the supergravity index, several of the Kaluza-Klein modes had to be dropped. Since the spectrum has not been well tested, the authors suggested that the Kaluza-Klein spectrum should be revisited. We find that a careful analysis of the Kaluza-Klein modes agrees with known results about field theory index. Our general form of the supergravity index succinctly reproduces previous computations of the gravity index[4]. We find complete agreement with previous large-N computations of the index[4–6].

We construct the Kaluza-Klein multiplets on AdS_4 from various tensors defined on the Sasaki-Einstein manifold following the methodology of[7]. Our analysis focuses on generic Sasaki-Einstein manifolds. Much of our analysis builds upon previous work on Kaluza-Klein spectroscopy for coset manifolds.

Multiplet shortening and the short multiplets contributing to the index can be described using the tangential Cauchy-Riemann operator $\bar{\partial}_b$ and the associated Kohn-Rossi cohomology groups $H^{p,q}_{\bar{\partial}_b}$. In general, the cotangent bundle over a Sasaki-Einstein manifold Y can be decomposed as

$$\Omega_Y = \mathbb{C}\eta \oplus \Omega_Y^{1,0} \oplus \Omega_Y^{0,1}. \quad (2)$$

The operator $\bar{\partial}_b$ is the projection of the exterior derivative on $\Omega_Y^{0,1}$, the cohomology of this complex is $H^{p,q}_{\bar{\partial}_b}$. The Kohn-Rossi cohomology groups are isomorphic to $H^q(X, \wedge^p\Omega'_X)$ defined on the cone, where Ω'_X is the part of the holomorphic cotangent bundle Ω_X perpendicular to the dilatation vector field. Our main result is a formula for the gravity superconformal index as a trace over linear combinations of the groups $H^q(X, \wedge^p\Omega'_X)$.

Table 1 lists the multiplicity of each short multiplet appearing in supergravity solutions of the form $AdS_4 \times SE_7$ and their contribution to the superconformal index. When calculating the index, only states with

$$\{Q, S\} = \epsilon - j_3 - y = 0 \quad (3)$$

contribute, where y is the R-charge. An element f of cohomology has R-charge $\mathcal{L}_D f = 2iDf$. Here $\mathcal{L}_D$ denotes the Lie derivative along the dilation vector field and $2D$ is its corresponding eigenvalue. We normalize each multiplet so that its primary has R-charge y. The R-charge y differs from the R-charge $2D$ of the corresponding cohomology element by a constant shift.

Table 1. Short multiplets and their contribution

Multiplet	(ϵ, j_3, y)	Multiplicity	Index
s. graviton	$(y+2, 1, y)$	$H^0(X, \wedge^3\Omega'_X)$	$-t^{y+4}$
s. gravitino	$(y+\frac{3}{2}, \frac{1}{2}, y)$	$H^0(X, \Omega'_X)$	t^{y+3}
s. vector Z	$(y+1, 0, y)$	$H^1(X, \Omega'_X)$	$-t^{y+2}$
s. vector A	$(y+1, 0, y)$	$H^0(X, \wedge^2\Omega'_X)$	$-t^{y+2}$
hyper	$(y, 0, y)$	$H^1(X, \wedge^2\Omega'_X)$	t^y
hyper	$(y, 0, y)$	$H^2(X, \Omega'_X)$	t^y
hyper	$(y, 0, y)$	$H^0(X, \mathcal{O}_X)$	t^y

Summing the contributions of the short multiplets, we find that the single particle supergravity index is

$$\begin{aligned} 1 + I_{s.t.}(t) = \sum tr[t^{2D} \mid H^0(X, \mathcal{O}_X) \\ \ominus H^0(X, \wedge^2\Omega'_X) \oplus H^1(X, \wedge^2\Omega'_X) \\ \oplus t^2 H^0(X, \Omega'_X) \ominus t^2 H^1(X, \Omega'_X) \oplus t^2 H^2(X, \Omega'_X) \\ \ominus t^2 H^0(X, \wedge^3\Omega'_X)]. \end{aligned} \quad (4)$$

The superconformal index has proven to be a powerful tool in checking proposed dualities. All proposed field theory duals to Saski-Einstein seven manifolds can be tested by computing the field theory index and comparing it with the above gravity index. Currently, there is no general procedure for constructing the field theory dual to a general Sasaki-Einstein seven manifold. One hopes that the superconformal index will help explore new holographic dualities.

References

1) J. Kinney et al.: Commun. Math. Phys. **275**, 209 (2007).
2) J. Bhattacharya et al.: JHEP **0802**, 064 (2008).
3) R. Eager and J. Schmude, arXiv:1305.3547 [hep-th].
4) S. Cheon et al.: JHEP **1105**, 027 (2011).
5) D. Gang et al.: JHEP **1202**, 079 (2012).
6) Y. Imamura et al.: JHEP **1108**, 011 (2011).
7) R. Eager et al.: arXiv:1207.0573 [hep-th].

*1 RIKEN Nishina Center

Sine square deformation and its implications to string theory†

T. Tada*1

It was recently found that certain 1d quantum systems with an open boundary condition can share the same vacuum state with a similar system having a closed boundary condition, if the coupling constants of the system with an open boundary are modulated in a certain way called *sine square deformation*[1–3]. Sine square deformation works similarly in two-dimensional conformal field theories, which describe string theory [4]. We have investigated sine square deformation in the context of string theory, focusing in particular on open/closed duality.

Sine square deformation is the modulation of the coupling of open boundary systems so that

$$J_{i,i+1} \equiv J \sin^2\left(\frac{n}{N}\pi\right) \quad (1)$$

keeping the boundary coupling $J_{0,1} = J_{N,N+1} = 0$ at the both ends (Fig. 1) for the following 1d quantum system:

$$\mathcal{H} = -\sum J_{n,n+1}\left(\sigma_n \cdot \sigma_{n+1}\right). \quad (2)$$

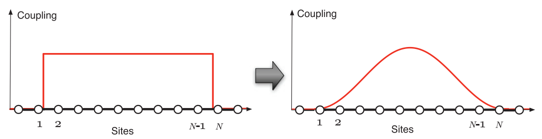

Fig. 1. Sine square deformation of the coupling for a 1d quantum system.

In the case of conformal field theory, the Hamiltonian $\mathcal{H}_{\rm SSD}$ that is sine square deformed is

$$\frac{\pi}{l}\left(L_0 + \bar{L}_0 - \frac{L_1 + L_{-1} + \bar{L}_1 + \bar{L}_{-1}}{2}\right) - \frac{\pi c}{12l}, \quad (3)$$

while the original Hamiltonian is

$$\mathcal{H}_0 = \frac{2\pi}{l}\left(L_0 + \bar{L}_0\right) - \frac{\pi c}{6l}. \quad (4)$$

Then, the vacuum $|0\rangle$ for $\mathcal{H}_0$ is also the vacuum of $\mathcal{H}_{\rm SSD}$ with half the energy.

To interpret the sine square deformation in terms of the dynamics of the world sheet, we need to find the corresponding Lagrangean. We found that the Lagrangean corresponding to $\mathcal{H}_{\rm SSD}$ is obtained by taking α to 1 in the following expression:

$$\mathcal{L}_\alpha = \frac{1}{2}\int dx \left\{\left(\partial_t\varphi\right) f_t \left(\partial_t\varphi\right) - \left(\partial_x\varphi\right) f_x \left(\partial_x\varphi\right)\right\}, \quad (5)$$

where

$$f_x(x) = 1 - \alpha\cos\frac{x}{l}, f_t(x) = N\sum_{k\in Z} r^{|k|}e^{2\pi ikx/l}, \quad (6)$$

and

$$r \equiv \frac{1-\sqrt{1-\alpha^2}}{\alpha}, \ N \equiv \frac{1}{\sqrt{1-\alpha^2}}. \quad (7)$$

One can readily see that the g_{00} component of the world sheet metric in the Lagrangean, f_t, diverges severely as we apply sine square deformation. This is in some sense expected because at the SSD point there occurs an event as singular as the change of the boundary condition.

One can apply sl(2, C) transformation $e^{a\frac{L_1 - L_{-1}}{2}}$ to (the holonomic part of) $\mathcal{H}_0$ to obtain

$$\cosh a L_0 - \sinh a \frac{L_1 + L_{-1}}{2}. \quad (8)$$

The right-hand side of the above would have corresponded to $\mathcal{H}_{\rm SSD}$ if $\cosh a = \sinh a$, which is a direct contradiction with the identity $\cosh^2 a - \sinh^2 a = 1$. One, therefore, needs to take $a \to \infty$ and suitably rescale. Hence, $\mathcal{H}_{\rm SSD}$ is not connected with $\mathcal{H}_0$ through the ordinary sl(2,c) transformation, but through a certain limiting procedure.

We also found that $\mathcal{H}_{\rm SSD}$ has the following different vacua other than $|0\rangle$

$$e^{L_{-1}}|h\rangle, \quad (9)$$

where $|h\rangle$ is the state corresponding to the primary fields of CFT. However, the norm of (9) is divergent. One also needs a certain limiting process to properly define (9).

In summary, we have investigated sine square deformation of string theory to shed light on the relation between open and closed strings. Recent studies of string dualities suggest that one needs to go beyond the realm where open and closed are inseparable to understand the true dynamics of string theory. We hope that we can further uncover the nature of this realm through insights offered by sine square deformation.

References

1) A. Gendiar, R. Krcmar, T. Nishino: Prog. Theor. Phys. **122** 953 (2009) ; *ibid.* **123** 393 (2010).
2) H. Katsura: J. Phys. A: Math. Theor. **44** 252001(2011) .
3) I. Maruyama, H. Katsura, T. Hikihara: Phys. Rev. **B 84** 165132(2011) .
4) H. Katsura: J. Phys. A: Math. Theor. **45** 115003(2012) .

† Condensed from the article in Proceedings of the 12th Asia Pacific Physics Conference (APPC12)

*1 RIKEN Nishina Center

Phase structure of two-dimensional topological insulators by lattice strong-coupling expansion[†]

Y. Araki[*1] and T. Kimura[*2]

Topological insulators have recently attracted a great interest in the field of materials physics, which are characterized by the topologically protected gapless modes localized on the boundary of the system. The effect of electron correlation in such an electronic system has always been an important problem. Even in non-topological Dirac fermion systems, such as graphene, it has been proposed that a sufficiently strong electron-electron interaction can lead to a spontaneous breaking of some symmetries of the system and a dynamical generation of band gap.

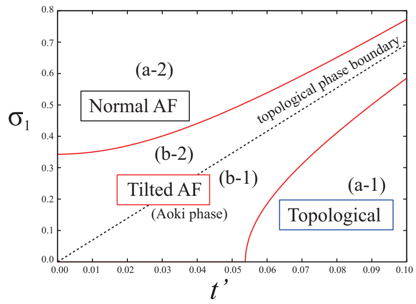

Fig. 1. The phase diagram of the Kane-Mele model in the (t', σ_1)-space. One of the Dirac cones loses its band gap at the phase boundary.

In this report, we study the effect of a sufficiently strong electron-electron interaction on the topological phase structure of 2D quantum spin Hall insulators. By the techniques of strong-coupling expansion of lattice gauge theory, we observe the behavior of the spontaneous antiferromagnetic (AF) order in the strong-coupling limit of the interaction. As a result, we find that the topological phase structure is modified from that of the noninteracting system by the emergence of a new "tilted AF" phase in-between the normal insulator and the topological insulator phases as shown in Fig. 1. Here we use the "modified" mass σ_1, instead of the bare mass (staggered magnetic field) m, and t' is the spin-orbit counpling constant. As a consequence of the interplay between the electron-electron interaction and the spin-orbit interaction, there appears a new "tilted antiferromagnetic (AF)" phase, where the imaginary part of the order parameter becomes nonzero ($\sigma_2 \neq 0$), between the normal AF phase and the topological phase.

The AF order is not parallel to the direction pointed by the spin-orbit interaction and the staggered magnetic field in the spin SU(2) space in the tilted AF phase. σ_1 and σ_2 are antiferromagnetic (AF) orders corresponding to two directions in the remnant U(1) spin space, which we denote M_z and M_x here. If we extend this argument to the full SU(2) spin space, another direction M_y is restored, so that the tilted AF acquires U(1) degree of freedom in choosing its direction, which may result in a massless Nambu-Goldstone mode (Fig. 2).

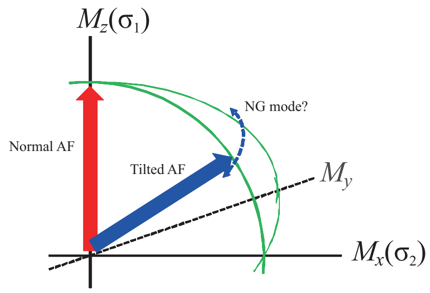

Fig. 2. Schematic picture of the order parameters derived in this study. It is expected that a gapless NG mode appear when the full SU(2) is restored.

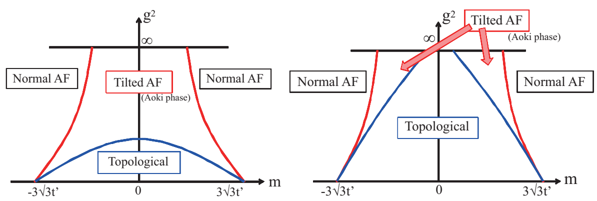

Fig. 3. The schematic phase structure of a graphene-like system with the spin-orbit interaction, conjectured in analogy to that of lattice QCD with the Wilson fermion formalism, for (left) $t' < t'_C$ and (right) $t' > t'_C$.

We also show the analogy between the phase structure of topological insulators and that of the strongly coupled lattice QCD with the Wilson fermion formalism in Fig. 3. In this analogy, σ_1 and σ_2 correspond to $\langle\bar{\psi}\psi\rangle$ and $\langle i\bar{\psi}\gamma_5\psi\rangle$. The tilted AF phase is similar to the so-called "Aoki phase" in lattice QCD in that both of them are characterized by an order parameter orthogonal to the external source term in the continuous symmetry space.[1)] Such an analogy may help us understand the behavior of topological insulators with an electron-electron interaction from the strong-coupling to the weak-coupling regime.

References
1) S. Aoki, Phys. Rev. **D30** (1984) 2653; Nucl. Phys. **B314** (1989) 79.

† Condensed from the article in Phys. Rev. **B87** (2013) 205440
*1 Department of Physics, University of Texas at Austin
*2 RIKEN Nishina Center

Effective gravitational interactions of dark matter axions†

T. Noumi,[*1] K. Saikawa,[*2] R. Sato,[*3] and M. Yamaguchi[*2]

Recent developments of observational studies have constrained the properties of dark matter significantly, yet its origin is unknown. The axion is one of leading candidates of dark matter, which emerges out of the solution to the strong CP problem in QCD. One important property of dark matter axions is that it is produced non-thermally in the early universe and described as a coherently oscillating scalar field. Since this coherent oscillation is interpreted as highly condensed Bose gas, dark matter axions may form Bose-Einstein condensate (BEC) in the universe.

The formation of axion BEC dark matter, if it occurred, leads to some interesting phenomenological implications. It was argued that the angular momentum distribution of infalling dark matter particles affects the structure of inner caustics (the over dense region produced by the fall of dark matter surrounding the galaxy).[1)] If the particles have a net overall rotation, which is predicted by axion BEC dark matter,[2)] the inner caustics become ring-like structure. Since such a structure is not predicted in another leading candidates such as the weakly interacting massive particle (WIMP) dark matter scenario, there is a possibility to distinguish dark matter candidates observationally.

The crucial point for the above scenario is that the thermalization occurs due to gravitational interactions. Gravitational thermalization of dark matter axions was first discussed in detail in[3)]. They claimed that the formation of axion BEC occurs in the condensed regime, where the interaction rate is large compared to the typical energy exchanged in the interaction. The thermalization process in the condensed regime was further studied by two of the present authors.[4)] By representing coherently oscillating axions as coherent states, they evaluated the gravitational self interaction rate Γ of axions within the flat space Newtonian approximation. They showed that the interaction rate Γ exceeds the expansion rate H of the universe when the temperature of the universe is $T \simeq$ keV. This result might imply that the gravitational self interactions affect the evolution of dark matter axions and their occupation number changes rapidly at that time.

In the BEC formation process, however, low energy modes, i.e. superhorizon modes, will play an central role and such a subhorizon mode is sensitive to the cosmic expansion. Therefore, it is not clear whether we can apply the previous result[3,4)] based on the flat space Newtonian approximation. In this report, to clarify this issue, we reanalyze the interaction rate Γ of the axion gravitational self interactions taking into account effects of the cosmic expansion based on general relativity. In the general relativistic framework, the gravitational interaction is mediated by metric perturbations $\delta g_{\mu\nu}$. The kinetic and mass terms of the axion ϕ generically contain cubic interactions schematically in the form $\delta g_{\mu\nu}\phi^2$ and these cubic interactions induce the following effective quartic interactions (Fig. 1):

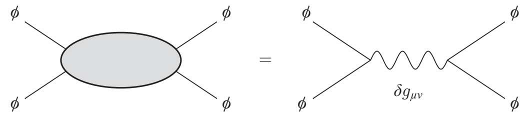

Fig. 1. Effective gravitational interaction of axions.

$$H_{\text{eff}} \simeq -\sum_{\mathbf{k}_i,\,\sum \mathbf{k}_i=0} \frac{2\pi G m^2}{a^3}\frac{f(x)}{(\delta p)^2} a^\dagger_{\mathbf{k}_1} a^\dagger_{\mathbf{k}_2} a_{\mathbf{k}_3} a_{\mathbf{k}_4}\,, \quad (1)$$

with the function $f(x)$ being

$$f(x) = 1-\cos x - x\sin x \simeq \begin{cases} 1 & (x \gg 1)\,, \\ -\dfrac{1}{2}x^2 & (x \ll 1)\,. \end{cases} \quad (2)$$

Here $\delta p = |\mathbf{k}_1 - \mathbf{k}_3|/a$ is the physical exchange momentum and $x = c_s \delta p/H$ represents how it is inside the (sound) horizon. We can see that the gravitational interaction is well approximated by Newton gravity when the exchange momentum is inside the horizon $x \gtrsim 1$, while it is suppressed for $x \lesssim 1$. An important point is that even if some of external momenta are superhorizon, the interaction is not suppressed unless the exchange momentum is superhorizon.

Applying the obtained effective gravitational interaction, we showed that the interaction rate Γ exceeds the expansion rate H of the universe when the temperature of the universe is $T \simeq$ keV, as in the previous studies[3,4)]. However, it should be noted that the thermalization process of axion BEC has been not fully understood yet in the previous studies[3,4)] and it is still nontrivial whether the thermalization occurs at that time (see e.g.[5)] for recent arguments). Further studies in this direction will be required.

References
1) P. Sikivie: Phys. Rev. D **60**, 063501 (1999).
2) P. Sikivie: Phys. Lett. B **695**, 22 (2011).
3) O. Erken, P. Sikivie, H. Tam, and Q. Yang: Phys. Rev. D **85**, 063520 (2012).
4) K. 'i. Saikawa and M. Yamaguchi: Phys. Rev. D **87**, 085010 (2013).
5) S. Davidson and M. Elmer: JCAP **1312**, 034 (2013).

† Condensed from the article in arXiv:1310.0167
*1 RIKEN Nishina Center
*2 Department of Physics, Tokyo Institute of Technology
*3 Theory Center, High Energy Accelerator Research Organization (KEK)

Composite dark matter and lattice simulations†

E. T. Neil[*1,*2] [LSD Collaboration]

The existence of a dark matter sector, which interacts gravitationally with ordinary, baryonic matter, solves several known observational puzzles in astrophysics and cosmology. However, the observed relic abundance of dark matter (DM) in the Universe today differs from the abundance of baryonic matter by a relatively small factor, $\rho_{DM}/\rho_b \approx 5$. This apparent coincidence motivates the existence of some sort of coupling of the dark sector to the Standard Model (SM), to give rise to the DM relic density by way of a primordial asymmetry or by coupling to the early-universe thermal bath of SM particles. Such interactions between DM and SM are strongly constrained by present-day experiments which seek to directly detection the impact of galactic dark matter particles with SM targets.

If the dark sector contains a new, strongly-coupled gauge force, then it may give rise to a composite dark matter candidate as an electroweak-neutral bound state of charged, fundamental constituent particles. This structure generically leads to very strong momentum dependence in interactions of the bound state with the SM, which can resolve the tension since the momentum scales probed in modern direct-detection experiments are much lower than those relevant for early-universe cosmology.

As part of the LSD collaboration, my research focuses on the use of lattice simulation as a tool to study the physics of strongly-coupled gauge theories, of which QCD is only a single example in a broad class. Gauge theories with different choices of the number of colors N_c, number of light fermions N_f, or fermion gauge representation R can exhibit strikingly different properties[1].

In connection with the study of composite dark matter, we have undertaken a calculation from first principles of electromagnetic "nucleon" form factors in SU(3) gauge theories with $N_f = 2$ and $N_f = 6$, in particular the magnetic moment κ and electromagnetic charge radius r_E^2[2]. In a candidate composite dark matter theory, these form factors would govern the interaction of the baryon-like dark matter with ordinary nuclei through single photon exchange. Our calculation results for the magnetic moment (shown in Fig. 1 below) and charge radius indicate no significant trend as the number of fermions N_f is increased. This suggests that regardless of other dynamical considerations, bounds on composite dark matter states may apply quite generally. As studied in the reference[2], these bounds can be quite wrong, with the magnetic moment interaction

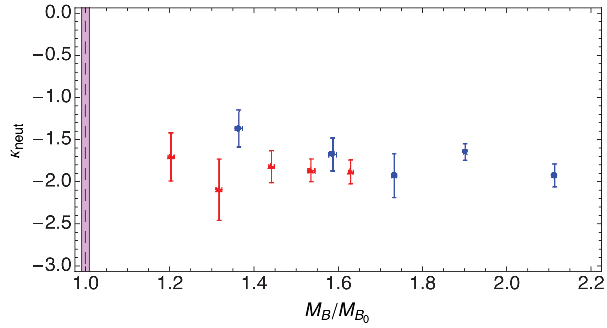

Fig. 1. From[2], magnetic moment κ_{neut} of a neutral baryonic bound state in SU(3) gauge theory with $N_f = 2$ (red) and $N_f = 6$ (blue) light fermions, vs. ratio of simulated "baryon" mass M_B to extrapolated chiral limit mass M_{B_0}.

excluding composite dark matter states in this model below 10 TeV.

Additional studies have focused on the properties of SU(2) gauge theories. The fundamental representation of SU(2) is real, leading to an enhancement of the chiral symmetry group. For a gauge sector in which this chiral symmetry spontaneously breaks, this can lead to the existence of "baryonic" pseudo-Goldstone modes, which can play the role of a dark matter candidate with interesting and unique properties[3]. Recent LSD collaboration results on SU(2)[4] have clarified the range of N_f values for which the spontaneous breaking of chiral symmetry will take place, paving the way for future dynamical studies relevant to SU(2) composite dark matter models.

Finally, extension of our results for composite dark matter form factors to SU(4) gauge theory is planned, with a model construction and a detailed lattice study to be published soon. With an even choice of N_c, the "baryon" states will be bosonic, and can exhibit internal symmetries which cause the leading electromagnetic form factors (magnetic moment and charge radius) to vanish. Our initial studies will therefore focus on the next leading operator, the electromagnetic polarizability, as well as on scalar form factors for Higgs boson exchange.

References

1) E. T. Neil: PoS LATTICE2011 (2011) 009
2) T. Appelquist et al. (LSD Collaboration): Phys.Rev. **D88** (2013), 014502
3) M. R. Buckley and E. T. Neil: Phys.Rev. **D87** (2013) 4, 043510
4) T. Appelquist et al. (LSD Collaboration): submitted to Phys. Rev. Lett.

*1 RIKEN Nishina Center
*2 Department of Physics, University of Colorado, Boulder

7. Astrophysics and Astro-Glaciology

Dynamics of X-ray–emitting ejecta in the oxygen-rich supernova remnant Puppis A revealed by the *XMM-Newton* RGS[†]

S. Katsuda,[*1] Y. Ohira,[*2] K. Mori,[*3] H. Tsunemi,[*4] H. Uchida,[*5] K. Koyama,[*4,*5] and T. Tamagawa[*1]

The Galactic supernova remnant (SNR), Puppis A, is one of the brightest X-ray SNRs with energies below 1 keV. A number of oxygen-rich, fast-moving, optically emitting ejecta knots (OFMKs) are detected in this SNR. Interestingly, all these OFMKs are located in the eastern, mostly northeastern (NE) portion,[1)] whereas a neutron star is running in the opposite direction of the OFMKs[2)]. Given that this ejecta-neutron star recoil phenomenon is consistent with the recent promising supernova (SN) explosion model for explaining core-collapse SN explosions,[3)] Puppis A is an extremely important target for the study of SN explosion mechanisms.

Since significant fractions of SN ejecta are often seen only in X-rays, it is important to reveal ejecta structures in the X-ray domain. In fact, mapping observations with X-ray observatories in orbit, i.e., *XMM-Newton*, *Chandra*, and *Suzaku* have recently recognized signatures of ejecta. These ejecta are found to be localized in three locations. All of them are located in the NE quadrant, further supporting the one-sided ejection of SN debris. Interestingly, one of them showed a hint of blueshifted K-shell line emission[4)]. However, the moderate spectral resolution of these X-ray charge coupled devices (CCDs) used in the previous observations did not allow for conclusive arguments.

To reveal the precise Doppler velocities of two of the X-ray ejecta features (hereafter, the ejecta knot and the ejecta filament), we performed an *XMM-Newton* observation of Puppis A on October 20, 2012. We primarily used the Reflection Grating Spectrometer (RGS[5)]). The RGS is usually considered to be unsuitable for extended sources such as Galactic SNRs, because it is a slitless spectrometer, and hence, the extended sources suffer from energy resolution degradation. However, if the angular size of the target is sufficiently small (less than a few arc minutes) and is brighter than its surroundings, it is possible to obtain high-resolution spectra for such a target. Fortunately, our targets allow for an order-of-magnitude higher resolution spectra ($E/\Delta E \sim 150$) than nondispersive CCDs ($E/\Delta E \sim 20$).

As shown in Fig. 1, we successfully obtained a high-resolution RGS spectrum, which enabled us to reveal unambiguous Doppler velocities of 1500 ± 200 km s^{-1} (blueward) for the knot and 650 ± 130 km s^{-1} (redward) for the filament. In addition, line broadening at 654 eV (corresponding to O Lyα) is obtained to be < 0.9 eV, indicating an oxygen temperature of < 30 keV. This temperature is significantly lower than that expected ($>$100 keV) for a (collisionless) forward shock with a speed of $\sim$2000 km s^{-1} (= 4/3 times 1500 km s^{-1}). We showed that the low oxygen temperature can be reconciled if the ejecta knot was heated by a shock with a velocity of $\sim$600–1200 km s^{-1} and was subsequently equilibrated due to Coulomb interactions. Therefore, the ejecta knot was likely heated by a (slower) reverse shock rather than a (faster) forward shock. This result provides significant support for the idea that a reverse shock reheats the SN ejecta, which has been expected for a long time; however observational evidence is still sparse.

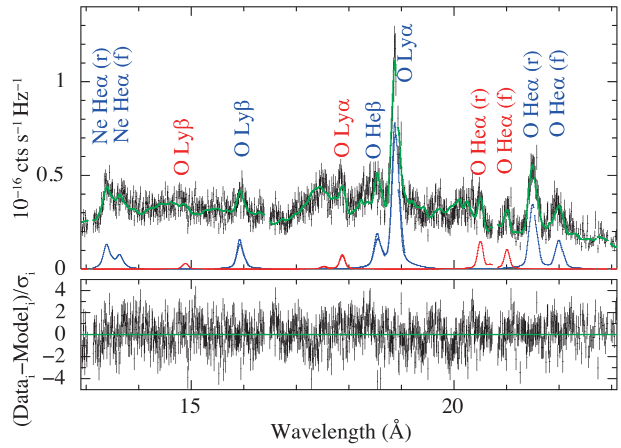

Fig. 1. *XMM-Newton*'s RGS spectrum fitted with a non-ionization equilibrium model (for diffuse background emission: Katsuda et al. 2013 for details) plus Gaussians (for the ejecta knot and ejecta filament). The best-fit models are shown in green, blue, and red for total, knot, and filament emission, respectively. The lower panel shows the residuals.

† Condensed from the article in The Astrophysical Journal **768**, 182 (2013)

*1 RIKEN Nishina Center
*2 Department of Physics and Mathematics, Aoyama Gakuin University
*3 Department of Applied Physics, Faculty of Engineering, University of Miyazaki
*4 Department of Earth and Space Science, Graduate School of Science, Osaka University
*5 Department of Physics, Kyoto University

References
1) P. F. Winkler et al.: IAU Colloq. 101, 65 (1988)
2) P. F. Winkler and R. Petre: ApJ 670, 635 (2007)
3) A. Burrows et al.: ApJ 655, 416 (2007)
4) S. Katsuda et al.: ApJ 678, 297 (2008)
5) J. W. den Herder et al.: A&A 365, L7 (2001)

NuSTAR observation of the fast rotating magnetized white dwarf AE Aquarii†

T. Kitaguchi*1 on behalf of the *NuSTAR* team

AE Aquarii (AE Aqr) is a cataclysmic variable classified as a member of the DQ Herculis or intermediate polar (IP) class, consisting of a white dwarf (WD) and a K4–5 V star. In the IP class, the WD is generally thought to possess a magnetic field ($B \sim 10^{5-7}$ G) sufficiently strong to channel the accretion flow from the secondary star to the WD poles. Accordingly, hard X-rays are produced by the shock-heated gas, which reaches temperatures of a few tens of keV near the WD surface. The X-ray emission exhibits spin modulation caused by the varying aspect of the accreting poles with respect to the rotation of the WD[1)].

The 33.08 s period makes AE Aqr the fastest-spinning magnetic WD with intriguing emission features. In comparison to many IPs, AE Aqr shows a thermal soft X-ray spectrum with a very low luminosity, and therefore the mechanism and location of the X-ray emission are uncertain. In addition, a *Suzaku* observation[2)] showed that AE Aqr may emit non-thermal hard X-rays with a narrow pulse profile at the spin period, suggesting that the source may accelerate charged particles in a manner similar to rotation-powered pulsars[3)]. However, a more recent *Suzaku* observation[2)] did not reproduce the earlier result, leaving the detection of non-thermal X-rays uncertain.

The Nuclear Spectroscopic Telescope Array (*NuSTAR*) satellite[4)], launched in 2012 June, carries the first focusing hard X-ray (3–79 keV) telescope in orbit. Owing to focusing optics, *NuSTAR* achieves the highest sensitivity ever observed in this band, and it has the capability to detect hard X-ray point sources with a flux down to sub μCrab. Therefore, *NuSTAR* can help measure the maximum temperature of the thermal plasma in AE Aqr and test the presence of any beamed non-thermal component. We performed a long observations of this source with *NuSTAR* for an exposure of 125 ks in 2012 September.

Spectral analysis shows that hard X-rays are well fitted by an optically thin thermal plasma model with three temperatures of $0.8^{+0.2}_{-0.5}$, $2.3^{+1.0}_{-0.8}$, and $9.3^{+6.1}_{-2.2}$ keV, the highest of which is higher than that previously observed for this source (3.0 keV)[2)]. In addition, the spectrum is also characterized by an optically thin thermal plasma model with two temperatures of $1.0^{+0.3}_{-0.2}$ and $4.6^{+1.6}_{-0.8}$ keV in combination with a power-law component with index of 2.5 ± 0.2, although the derived index is inconsistent with the *Suzaku* value (1.1 ± 0.6[2)]) and is steeper than those found for rotation-powered pulsars (0.6–2.1)[3)]. Compared with the three-temperature model, the fit with the two-temperature model with the power-law emission is slightly but not significantly preferred. We cannot distinguish whether the hard X-ray component detected with *NuSTAR* is thermal or non-thermal emission.

A timing analysis with Z_1^2-statistic or Rayleigh test[5)] shows that the spin period in the 3–10 keV band is 33.0769 ± 0.0004 s, which is consistent with previously measured values[2)]. The 3–20 keV pulse profile obtained by folding data at the best determined period is broad and approximately sinusoidal with a pulsed fraction of $16.6 \pm 2.3\%$. We do not find any evidence for a sharp feature in the pulse profile.

Two energy sources could, in principle, power the observed X-ray luminosity: liberation of gravitational energy of accreting matter and the rotational energy of the WD. The observed X-ray emission is difficult to explain as a result of rotation-powered emission because synchrotron radiation, which is observed for rotation-powered pulsars, is expected to be strongly beamed along the field lines, which is inconsistent with the observed broad pulse profile. Instead, accretion-powered emission is more probable, although the observed spectrum with the highest temperature of $9.3^{+6.1}_{-2.2}$ keV is softer than a postshock temperature of ~ 30 keV predicted by the standard accretion column model[6)] under the assumption that the WD mass is $\sim 0.7\ M_\odot$ as determined in the optical measurement[7)].

The standard model assumes a high-accretion column heated by the shock close to the WD surface and cooled by thermal bremsstrahlung. However, the accretion rate in AE Aqr is considerably small, which is a consequence of the low X-ray luminosity. We suggest two modifications of the standard model to explain the AE Aqr spectrum: the shock temperature could be low because of a tall accretion column comparable with the WD radius, and cyclotron emission with $B > 10^6$ G could additionally cool down the accretion plasma. Detailed calculations of such models will hopefully reproduce the spectrum and pulse profile of AE Aqr with the optically determined WD mass.

References

1) J. Patterson: PASP **106**, 209 (1994)
2) Y. Terada et al.: PASJ **60**, 387 (2008)
3) V. M. Kaspi et al.: in Compact Stellar X-Ray Sources, edited by W. Lewin & M. van der Klis (Cambridge Univ. Press, Cambridge, 2006), p.279
4) F. A. Harrison et al.: ApJ **770**, 103 (2013)
5) R. Buccheri et al.: A&A **128**, 245 (1983)
6) K. Aizu: PThPh **49**, 1184 (1973)
7) J. Echevarría et al.: MNRAS **387**, 1563 (2008)

† Condensed from the article in ApJ, Vol.782, 3 (2014)
*1 RIKEN Nishina Center

Measurement of nitrogen and oxygen isotope ratios in considerably low nitrate concentration ice core samples

S. Okamoto,[*1] K. Takahashi,[*1] Y. Nakai,[*1] Y. Motizuki,[*1] A. Makabe,[*2] K. Koba,[*2] and H. Motoyama[*3]

Nitrate (NO_3^-) concentration in polar regions is caused by relevant stratospheric sources[1)], related extraterrestrial fluxes of energetic particles, and solar irradiation. In the Talos Dome ice core (Antaractica), NO_3^- data exhibit highly significant agreement with cosmic ray flux reconstructions[2)]. Nitrogen and oxygen isotope ratios (δ^{15}N and δ^{18}O) of NO_3^- in the polar ice core are expected to reflect the difference of isotope fractionations through photochemical reactions in the stratosphere caused by cosmic ray and solar irradiation. Our final object is to clarify the history of solar activity and cosmic events, on the basis of precise analyses of δ^{15}N and δ^{18}O in the ice core. However, it is difficult to measure the isotope ratios of δ^{15}N and δ^{18}O in NO_3^- in the Antarctic ice core, because NO_3^- concentrations are low (typically < 20 μg l^{-1}) and the sample volume is limited.

In this study, we examined the method of measuringδ^{15}N and δ^{18}O with high sensitivity for 11 ice core samples from Dome Fuji drilled in 2010, corresponding to relatively high NO_3^- concentration (average 22.3 μg l^{-1}) using the denitrifier method[4)] and we successfully obtained accurate data. In this method, 10 ml of each sample was used and NO_3^- in sample water was quantitatively converted to N_2O, utilizing denitrifying bacteria (*Pseudomonas aureofaciens*) that lack N_2O-reductase. The isotopic composition of N_2O is then measured using the mass spectrometer (IsoPrime100) in RIKEN. The results of the measurements of δ^{15}N and δ^{18}O are summarized in Fig.1. Each sample is referenced to the internationally recognized standard USGS32, USGS34 and USGS35. In Fig. 2, the blue frame indicates the maximum and minimum values in the measured 11 ice core samples. These standards were diluted

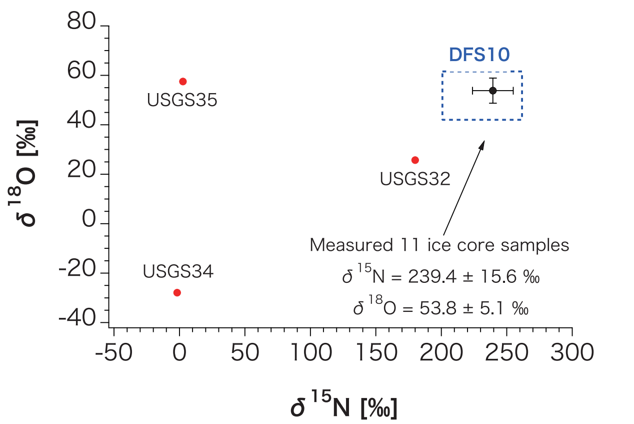

Fig. 1. The δ^{15}N and δ^{18}O of ice core samples and international standards USGS32, USGS34 and USGS35.

*1 RIKEN Nishina Center
*2 Tokyo University of Agriculture and Technology
*3 National Institute of Polar Research

with ice core water in which NO_2^- and NO_3^- were removed using the ion exchange resin for minimizing the effect of the exchange of oxygen atoms between the nitrogen oxide intermediates and water[3)]. We corrected the background N_2O associated with the medium for bacteria, atmosphere and ice core water used for dilution of standard. The error of the δ^{15}N and δ^{18}O in 11 samples were calculated by the propagation of errors including uncertainties in the background and in sample measurement. The maximum errors of the δ^{15}N and δ^{18}O were ± 0.75‰ and ± 0.34‰, respectively.

The δ^{15}N and δ^{18}O range from 201.7‰ to 258.5‰ and from 45.9‰ to 64.1‰, respectively (Fig.2). The variations of δ^{15}N and δ^{18}O show 24% and 34% for 20% NO_3^- change, respectively. δ^{15}N values are inside a certain range except for one sample (201.7‰). High positive δ^{15}N values may be attributed to the nitrate post-depositional effect because of low accumulation rate in Dome Fuji[4)]. NO_3^- and δ^{18}O show significant correlation ($r = -0.69$, $p < 0.05$), while there is no correlation between NO_3^- concentration and δ^{15}N.

We have successfully established the method to measure δ^{15}N and δ^{18}O of NO_3^-. Further detailed measurements are expected to contribute to elucidate the origin of NO_3^- produced by photochemical reactions in the stratosphere.

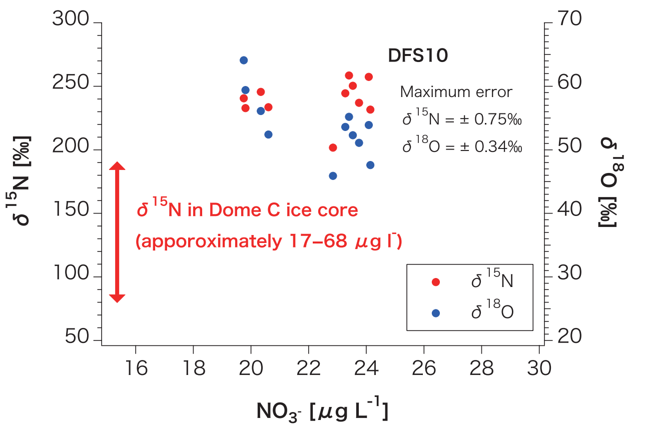

Fig. 2. NO_3^- concentration, δ^{15}N and δ^{18}O of NO_3^- in Dome Fuji ice core. Red arrow indicates the range of δ^{15}N in Dome C ice core, inland Antarctica[5)]. The unit of NO_3^- concentration in Dome C converts assuming ice density 850 kg m^{-3}.

References

1) M. R. Legrand and S. Kirchner: J. Geophys. Res. **95**, p3493-6507 (1990).
2) R. Traversi et al.: Solar Phys. **208**, p237-254 (2012).
3) K. L. Casciotti et al.: Anal Chem. **74**, p4905-4912(2002).
4) J. Erbland et al.: Atmos. Chem. Phys. **13**, p6403-6419 (2005).
5) H. D. Freyer et al., Tellus, **48B**, p93-105 (1996).

8. Accelerator

Conceptual design of SC linac for RIBF-upgrade plan

K. Yamada,*[1] K. Suda,*[1] N. Sakamoto,*[1] and O. Kamigaito*[1]

An upgrade plan for the RIKEN RI-Beam Factory is under discussion, with the objective of significantly increasing the uranium beam intensity. Difficulty in the present acceleration scheme mainly stems from the two-stage charge stripping located at 11 and 50 MeV/u, respectively, which yields a maximum total stripping efficiency of 5%. In the upgrade plan, the fixed-frequency Ring Cyclotron will be replaced by a new cyclotron[1)] that will be designed to accept U^{35+} ions without charge stripping at 11 MeV/u, and the RIKEN ring cyclotron will be replaced by a new linac, mainly consisting of superconducting (SC) cavities, to improve the transmission of the high current beam. To evaluate the feasibility of the new linac, we started a design study of the SC linac in fiscal year 2013[2)].

A layout plan of the new linac is shown in Fig. 1. The present injector, RILAC2, will be used at the low-energy end. We will add a short room-temperature (RT) section to RILAC2, which will boost the beam energy from 0.68 to 1.4 MeV/u. The main part is the succeeding SC section working in the energy range from 1.4 to 11 MeV/u.

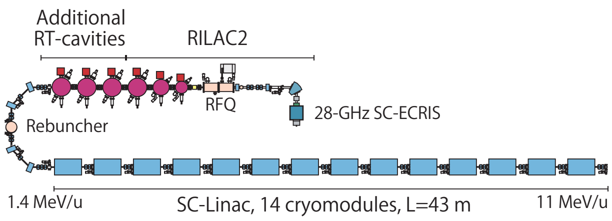

Fig. 1. Layout plan of new linac injector.

The beam energy at the border of the RT and SC sections was chosen so that the SC section could be covered by a single structure of a quater-wavelength resonator (QWR) with two acceleration gaps. Because a broad range of velocity had to be covered, the gap length and cavity diameter of the SC section were optimized to minimize the number of QWRs in the section. The energy gain of each gap was calculated based on hard-edge approximation. The gap voltage was assumed to be 800 kV, and the synchronous phase was chosen to be -25°. After several iterations, we determined a length $d = 160$ mm, which is the length between the gap centers, and a total cavity number of 56. The gap length was decided to be 60 mm.

The modular configuration of the SC section was optimized based on first-order approximation for the transverse and longitudinal motions. Some configurations were checked to determine whether a semi-periodic envelope could be obtained with moderate-strength focusing elements, while keeping the longitudinal acceptance large enough to capture the output beam from the RT section. Finally, we chose a configuration that consists of 14 cryomodules, each of which contains four QWRs operating at 73 MHz, and a RT quadrupole doublet placed in each space between the cryomodules. Quadrupoles with an aperture diameter of 50 mm and a field gradient of less than 20 T/m would be easier for us to make and operate compared to the SC solenoid.

The SC QWRs were designed using CST Microwave Studio 2013. The RF surface resistance is assumed to be 25 nΩ on the safe side, where the BCS resistance is negligibly small. The curently used parameters of the SC section are listed in Table 1. The definition of the effective length for the determination of $E_{\rm acc}$ is selected to be $\beta_{\rm geom}\lambda$.

Table 1. Design parameters of the SC section.

Frequency [MHz]	73
Duty [%]	100
Mass-to-charge ratio (m/q)	∼7
Input energy [MeV/u]	1.4
Output energy [MeV/u]	11.0
Number of cavities	56
Number of cryomodules	14
Number of quadrupole magnets	28
Total length [m]	43
Cavity inner diameter [mm]	ϕ300
Cavity height [mm]	1103
Gap length g [mm]	60
Gap voltage $V_{\rm gap}$ [kV]	800
$\beta_{\rm geom}$ of cavity	0.078
Beam aperture a [mm]	ϕ40
Synchronous phase $\phi_{\rm s}$ for $\beta_{\rm geom}$ [°]	-25
Operating temperature T [K]	4.5
$G = Q_0 \times R_{\rm s}$ [Ω]	22.6
$R_{\rm a}/Q_0$ [Ω]	718
$R_{\rm s} = R_{\rm BCS} + R_{\rm res}$ [nΩ]	25
Q_0	9.0×10^8
Shunt impedance $R_{\rm a}$ [Ω]	6.5×10^{11}
Rf power loss P [W]	4.0
$E_{\rm acc}$ [MV/m]	4.5
$E_{\rm peak}/E_{\rm acc}$	6.0
$B_{\rm peak}/E_{\rm acc}$ [mT/(MV/m)]	9.5

Further study is under way on the SC QWR, including the mechanical considerations, tuner design, and coupler design. We are also going to start thermal and mechanical studies of cryostats based on the initial design shown above.

References
1) J. Ohnishi *et al.*: Proc. of Cyclotrons2013, MOPPT022 (2014).
2) K. Yamada *et al.*: Proc. of SRF2013, MOP021, 137 (2014).

*1 RIKEN Nishina Center

Recent development of RIKEN 28-GHz superconducting electron cyclotron resonance ion source†

Y. Higurashi,[*1] J. Ohnishi,[*1] K. Ozeki,[*1] M. Kidera,[*1] and T. Nakagawa[*1]

Over the past several years, we have endeavored to improve the performance of the RIKEN superconducting electron cyclotron resonance ion source using several methods.[1,2] For the production of U vapor, we employed the sputtering method, although the beam intensity in this method is assumed to be weaker than that in the oven technique. We also used an aluminum (Al) chamber instead of a stainless steel (SS) one. It is possible to observe the so-called "wall-coating effect."[3] Using these methods, we successfully produced ~180 eμA of U^{35+} and ~230 eμA of U^{33+} at the injected radio frequency (RF) power of ~4 kW (28 GHz). Very recently, with the aim of further increasing the beam intensity of U^{35+}, we have the development of high-temperature oven and have successfully produced a highly charged U ion beam.

In this paper, we present a detailed report on the effect of the Al chamber on the beam intensity of highly charged U ion beams. We also report the effects of the two-frequency injection method on the U ion beam intensity.

For this experiment, the maximum mirror magnetic field strength at the RF injection side (B_{inj}), minimum strength of the mirror magnetic field (B_{min})[4], maximum mirror magnetic field strength at the beam extraction side (B_{ext}), and minimum magnetic field strength at the surface of the plasma chamber (B_r) were fixed at 3.2, 0.65, 1.8, and 1.85 T, respectively. The microwave frequency generated by the gyrotron was 28 GHz. The diameters and lengths of both plasma chambers (Al and SS) were 150 and 575 mm, respectively. The typical sputtering voltage was approximately −5.5 kV. We used oxygen as the ionized gas. The gas pressure was (4–5) × 10^{-5} Pa. The extraction voltage was fixed at 22 kV in these experiments. Figure 1 shows the charge state distributions of the highly charged U ion beams. The open and closed circles denoted the results in the cases where SS and Al chambers, respectively were used. The injected RF power was 2 kW for both cases. The ion source was tuned to produce U^{35+}. As shown in Fig. 1, the intensity of the highly charged U ion beam produced with the Al chamber was higher than that produced with the SS chamber. For example, the intensity of the U^{35+} beam produced with the Al chamber was 110 eμA, which was almost twice the value (60 eμA) obtained with the SS chamber.

Ever since enhancement of the beam intensity of the highly charged heavy ions was achieved by injecting power at two frequencies simultaneously,[5] this mechanism has been investigated and used at several laboratories to increase the beam intensity. At RIKEN too, we employed this method to increase the beam intensity. Figure 2 shows the beam intensity of U^{35+} as a function of B_{min}. The opencircles represent the beam intensity of the U ions under a single frequency operation (28 GHz [1.5 kW]). At the lower B_{min}, we added an RF power of 500 W (18 GHz). The closed circles denote the results obtained with 28 GHz (1.5 kW) + 18 GHz (500 W). The beam intensity at a B_{min} of 0.57 T (18 + 28 GHz) was slightly higher than that at a B_{min} of 0.66 T (28 GHz). On comparing results with those at B_{min} of 0.66 T with a 2 kW injection (28 GHz), we did not find any beam enhancement in this experiment. However, as shown in Fig. 2, the X-ray heat load with a B_{min} of 0.57 T is lower than that with a B_{min} of 0.66 T; this is mainly due to the magnetic field gradient effect. As we obtained nearly the same beam intensity with a lower X-ray heat load, this result indicates that the two-frequency injection could be advantageous for our SC-ECRIS.

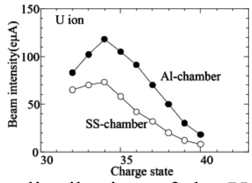

Fig. 1. Charge state distribution of the U ions with the Al chamber (closed circles) and SS chamber (open circles).

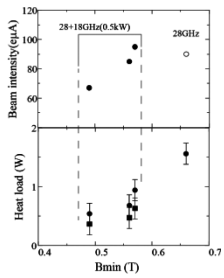

Fig. 2. Beam intensity of U^{35+} with two frequencies (18 + 28 GHz) for several B_{min} values and with a single frequency (28 GHz) for B_{min} = 0.66 T (upper panel). X-ray heat load in the cryostat with two frequencies (18 + 28 GHz) (closed circles) and a single frequency (28 GHz) (closed squares) for several B_{min} values (lower panel).

References
1) Y. Higurashi, et al.:Rev. Sci.Instrum. 83, 02A308 (2012).
2) T. Nakagawa et al.: Rev. Sci. Instrum. 81, 02A320 (2010).
3) T. Nakagawa: Jpn. J. Appl. Phys. 30, L930 (1991).
4) G. D. Alton and D. N. Smithe, Rev. Sci. Instrum. 65 (1994) 775
5) Z. Q. Xie and C. Lyneis: in Proceedings of the 12th International Workshop on ECRIS, Wako, INS-J-182 (University of Tokyo, 1995), p. 24.

† Condensed from the article in Rev. Sci. Instrum **85**, 02A953 (2014)
*1 RIKEN Nishina Center

Development of high-temperature oven for 28-GHz ECR ion source

J. Ohnishi,[*1] Y. Higurashi,[*1] M. Kidera,[*1] K. Ozeki,[*1] A. Uchiyama,[*1] and T. Nakagawa[*1]

U^{35+} ions extracted from the 28-GHz superconducting ECR ion source[1)] are used to supply uranium beams to the RIBF. Although we have thus far used the sputtering method, in which uranium is supplied in the ion source plasma by directly inserting a metal uranium rod, we began developing a high-temperature oven[2)] with the aim of increasing and stabilizing the beams. Because the oven method uses UO_2, a crucible must be heated to a temperature higher than 1900°C to supply an appropriate amount of UO_2 vapor to the inside of the ion source.

Figures 1 and 2 show the dimensions of the crucible and illustrate the oven in its entirety. The crucible is joule-heated with a large DC electric current. The crucible, made by machining a tungsten rod, is supported with upper and lower water-cooled copper blocks. The electric current and cooling water are supplied through brass double pipes. The crucible was designed by performing the electric, thermal, and structural analyses simultaneously using ANSYS.[3)] Figure 3 shows the temperature distribution of the oven, calculated by ANSYS. The boundary conditions are as follows: The temperature of the cooling water is 27°C, the heat transfer coefficient from the water to the copper block is 5000 $W/m^2/K$, and the voltage between the upper and lower copper blocks is 1.25 V. The radiation coefficient of tungsten was assumed to be 0.25. The electric current was calculated to be 439 A. The maximum temperature of the body is 2041°C, and the temperatures of the bottom and the cap are 1960−2000°C.

The oven is placed in a solenoid magnetic field of approximately 3.3 T, which is orthogonal to the axis of the crucible. Therefore, if an electric current of 450 A flows through the crucible, the crucible is subjected to an electromagnetic force of approximately 40 N. According to the ANSYS calculation, a maximum stress of 160 MPa is generated around the tapered parts on the crucible body sides of the upper and lower rods. Since the temperature of these tapered parts increases to higher than 1800°C, it was expected that this stress level could result in the deformation and destruction of the crucible with the decrease in the tungsten's strength. In fact, bends in the upper and lower rods were observed after operation.

We installed the oven loaded with UO_2 in the 28 ECR ion source and tested the generation of uranium beams in April 2013 after a temperature rise test and temperature measurement in a test chamber. In the first test, the oven was operated for 42h and a U^{35+} beam current of 140 μA was successfully obtained at an RF power of approximately 3 kW. After the first test, operation tests of the oven were executed intermittently from July to December. The operation time was a total of 29 days. Although we could maintain a U^{35+} beam current of 50−80 μA at an RF power of 1.5 kW for a maximum of one week, the beam currents often decreased to less than half in 7−8h. This decrease resulted from UO_2 blocking the crucible ejection hole. Since the cause of the ejection hole's blockage was assumed to be that the temperatures of the cap of the crucible and the upper part of the hole are lower than the temperature of the bottom, we reduced the thicknesses of the cap and brim by 0.2 mm. Figure 1 shows the schematic after this reduction. Presently, we have just started to test the crucible of the new design. We are also investigating the use of rhenium instead of tungsten, which has better creep characteristic strength at high temperature for solving the bends and fracture of the rods of the crucible.

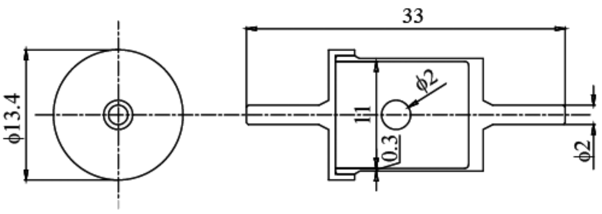

Fig. 1. Schematic of the tungsten crucible. The axis of the crucible is oriented vertically.

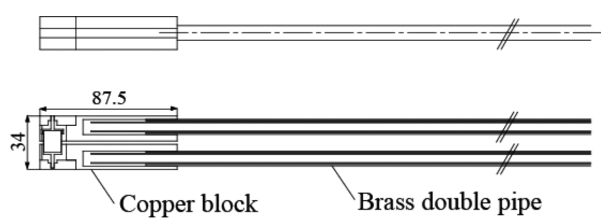

Fig. 2. Schematic of the crucible and support.

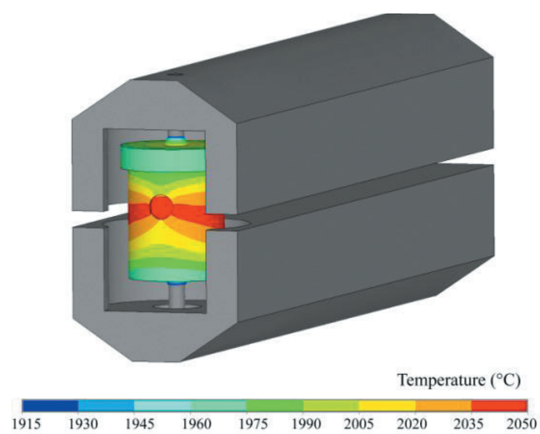

Fig. 3. Temperature distribution of the oven calculated by ANSYS.

References

1) Y. Higurashi, et al., Rev. Sci. Instr. 83, 02A308 (2012).
2) J. Ohnishi, et al., Rev. Sci. Instr. 85, 02A941 (2014).
3) http://www.ansys.com/

*1 RIKEN Nishina Center

Improved beryllium disk stripper for uranium acceleration at RIKEN RIBF

H. Hasebe,[*1] H. Kuboki,[*1] H. Okuno,[*1] H. Imao,[*1] N. Fukunishi,[*1] M. Kase,[*1] and O. Kamigaito[*1]

In 2012, we first attempted to use a rotating beryllium (Be) disk with 0.1 mm thick as the second charge stripper for uranium (U) acceleration[1)]. The Be stripper was successfully provided stable high-intensity U beam (several electric μA on average) during a beam time of 37 days using a single disk with no exchange. The lifetime of the stripper was extended drastically compared to before. The total number of U particles irradiated on one foil/disk increased from 7.12×10^{15} (carbon foil in 2011) to 1.18×10^{18} (Be disk in 2012). A remaining problem was improvement of the thickness uniformity for improving the transmission efficiencies of the subsequent cyclotron IRC and SRC. In addition, the Be disk with a slightly thinner thickness of 0.085 mm was found to be better to match the injection energy of the IRC.

A thinner Be disk, with a thickness of 0.085 mm, was fabricated by Pascal Co., Ltd.[2)], who proposed a special machining method. They reduced the Be disk thickness of 0.15 mm to the desired thickness of 0.085 mm by only diamond-polishing both sides of the disk; diamond polishing was used because in the previous study, we had found that the standard buff finish process made thickness uniformity worse.

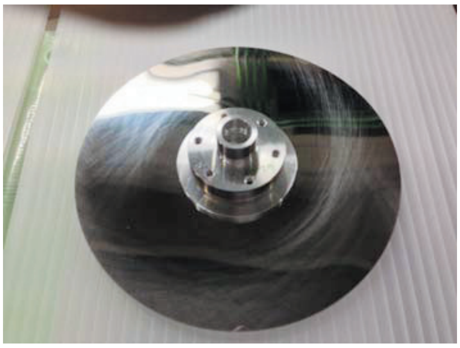

Fig. 1. Polished new Be disk.

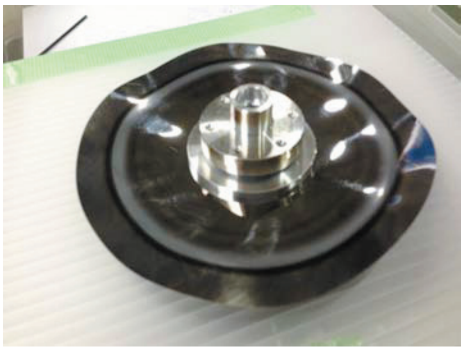

Fig.2. Slightly deformed Be disk after irradiation.

The polished new Be disk was used for a beam time from April to May 2013. The outer diameter of the disk was 120 mm, and the thickness was 0.085 mm, with a tolerance of ± 0.005 mm. The arithmetic average roughness (Ra) was less than 0.01 μm. A U^{64+} beam at 50 MeV/nucleon was irradiated on the Be disk, which rotated at 1000 rpm. Figure 1 shows the polished new Be disk before installation. Figure 2 shows a photograph of the disk after the beam time. As in the previous beam time, the outer circumference of the beam-irradiated part (black band in Fig. 2) was deformed when the irradiated U beam intensity was increased to several electric μA. However, unlike the last beam time, no cracks were observed.

The improvement in the thickness uniformity is shown in figure 3[3)]. The figure shows the beam intensity trends as monitored by Phase Probe (PP)-G01 (G01: downstream of SRC). The vertical and horizontal axes indicate the beam intensity and scan time, respectively. Signals stay at “beam-on level” in the figure if beams are provided from the SRC, whereas signals drop to the bottom “beam-off level” if no beam is available. The upper and lower parts are the trends measured in November 2012 and May 2013, respectively. The red square parts denote a single rotation period of the Be disk (60 ms). Availability of the U beams was improved from 90.7% to 98.8%. A total of 9.29×10^{17} U particles were irradiated on the Be disk over 30 days. It has been shown that the polished new Be disk is now ready for practical use.

Fig. 3. Signals of phase probe monitor (PP-G01). Vertical axis: beam intensity. Horizontal: scan time.

References

1) H. Hasebe et al., RIKEN Accel. Prog. Rep. **46**, 133 (2013).
2) PASCAL CO., LTD.
URL: http://www.pascal-co-ltd.co.jp/home.html
3) R. Koyama et al., Nucl. Instr. and Meth. A 729 (2013) 788-799.

*1 RIKEN Nishina Center

Test of differential pumping system with plasma window using gas cell

H. Kuboki,[*1] H. Okuno,[*1] A. Hershcovitch,[*2] T. Dantsuka,[*1] H. Hasebe,[*1] K. Ikegami,[*1] H. Imao,[*1] O. Kamigaito,[*1] M. Kase,[*1] T. Maie,[*1] T. Nakagawa,[*1] and Y. Yano[*1]

A differential pumping system with a plasma window (PW)[1)] has been developed for application to charge strippers using high-density hydrogen or helium (He) gases, which have a small atomic number. We tested the system with a PW operation using a gas cell where argon (Ar) or He gases were confined up to 100 kPa (1 atm). Figure 1 shows a schematic of the system. The system consists of a gas cell, a PW, and two chambers. The PW has a central bore of 2 mm diameter, which isolates the gas cell from the first chamber. Gas was injected to the gas cell and flowed into the first chamber through the PW. As stated in the previous report,[2)] the two chambers were differentially pumped. The first chamber was mainly evacuated by two mechanical booster pumps with a total pumping rate of approximately 730 $m^3 \cdot h^{-1}$. The second chamber was evacuated by a turbomolecular pump (TMP) with a pumping rate of 792 $m^3 \cdot h^{-1}$. The first and second chambers were connected via a flow constrictor with an inner diameter of 6 mm and length of 15 cm.

At first, the plasma was ignited by Ar gas injection. Next, gas flow rates were increased so that a pressure of 100 kPa was attained at the gas cell (P_0). The typical flow rate for Ar was maintained at 2.3 SLM to keep P_0 at 100 kPa at an arc current of 15 A per cathode. Subsequently, we replaced the injected Ar gas with He gas. We successfully operated the PW with He gas maintaining P_0 at 100 kPa. The flow rate of He for keeping P_0 = 100 kPa was 4.5 SLM at an arc current of 26 A. The differential pumping efficiency was evaluated by the pressures at the first (P_1) and second chambers (P_2). The pressures P_1 and P_2 in the cases of Ar and He are plotted as functions of arc currents in Figs. 2 (a) and (b), respectively. The solid circles and triangles denote Ar and He data, respectively. The plotted data were adequately corrected depending on the gas species. The maximum pressures of P_0 in the absence of the PW operation were 15 and 9 kPa, maintaining P_1 at 20 and 40 Pa in the cases of Ar and He, respectively. The maximum P_0 values were increased by 6.7 times for Ar and 11.5 times for He when the PW operation occurred. We found that the lowest arc currents per cathode for keeping P_0 at 100 kPa were 11 and 26 A for Ar and He, respectively.

The gas flow rates for keeping P_0 at 100 kPa are also dependent on the arc currents, as shown in Fig. 2 (c). It is noteworthy that the flow rate of He can be reduced by more than one order of magnitude as compared to the conventional differential pumping system without a PW, as estimated in advance.[3)] Also, P_0 reached 130 kPa, which is the maximum value of the gauge. The P_1 and P_2 values were 30 and 4.5×10^{-2} Pa for Ar and 36 and 1.4×10^{-1} Pa for He, respectively. Further tests using a PW with an enlarged orifice of 4 mm diameter are planned in the near future.

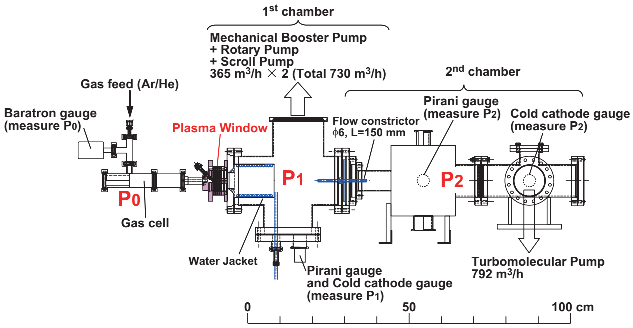

Fig. 1. Differential pumping system with PW.

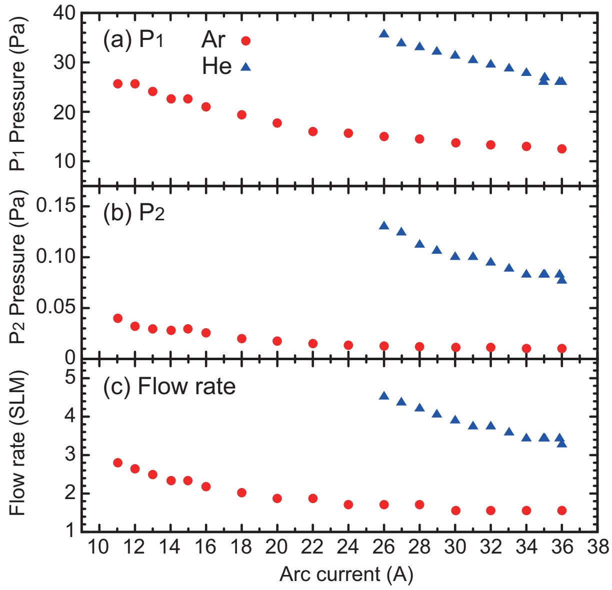

Fig. 2. Pressures (a) P_1 and (b) P_2, and (c) flow rates in cases of Ar and He are plotted as functions of arc current. Please see the text for details.

References
1) A. Hershcovitch: J. Appl. Phys. **78** 5283 (1995).
2) H. Kuboki et al.: J. Rad. Ana. Nucl. Chem. **297** (2013).
3) H. Okuno et al.: Phys. Rev. ST Accel. Beams **14** 033503 (2011).

*1 RIKEN Nishina Center
*2 Brookhaven National Laboratory (BNL)

Charge state distribution measurement of ^{86}Kr in H_2 and He gases at 2.7 MeV/nucleon

H. Kuboki,[*1] H. Okuno,[*1] H. Hasebe,[*1] N. Fukunishi,[*1] E. Ikezawa,[*1] H. Imao,[*1] O. Kamigaito,[*1] and M. Kase[*1]

We can obtain heavy ions with higher charge states in gases with small atomic numbers (low-Z gas) such as hydrogen (H_2) or helium (He) as compared to other standard gases (nitrogen (N_2) or argon).[1)] Recently, a windowless He gas stripper utilizing a strong differential pumping system has been constructed for uranium (U) beams at the RIKEN RI Beam Factory (RIBF).[2)] It has successfully functioned and has provided high intensity U beams stably.

The possibility of application of low-Z gas charge strippers to krypton (Kr) beam acceleration at the RIBF has been studied. The first stripper for ^{86}Kr acceleration is located downstream of the RILAC, where the exit energy becomes 2.7 MeV/nucleon. Carbon foils with thicknesses of 40–80 μg/cm^2 have been used as the first stripper to obtain ^{86}Kr^{26+} for acceleration by the subsequent cyclotron RRC.[3)] A low-Z gas stripper can be one of the candidates for a long-lived stripper if a sufficient fraction of 26+ is obtained.

We have developed a prototype of a gas stripper and measured the charge state distributions of ^{86}Kr in H_2 and He with different thicknesses. The ^{86}Kr^{20+} beams at 2.7 MeV/nucleon were transported to the gas stripper. A schematic of the gas stripper with its differential pumping system is shown in Fig. 1. Gases were injected in the target region (stage 1) located at the center. The length of the target region was 100 cm. The other stages, U2, D2, U3, and D3, are also shown along with the pumping speeds of their respective attached pumps. A 10-cm-long tube with 4-mm inner diameter was installed between each stage. The charge state distributions of ^{86}Kr in H_2 and He are shown in Fig. 2. The fractions calculated for H_2, He, and N_2 are plotted in the figure. In Fig. 2 (a), the data for the H_2 gas with thicknesses of 10, 23, 46, 68, and 107 μg/cm^2 are denoted by asterisks, x-marks, open triangles, open squares, and open diamonds, respectively. In Fig. 2 (b), the data for the He gas with thicknesses of 16, 29, 59, 124, and 247 μg/cm^2 are denoted by asterisks, open triangles, open circles, open squares, and open diamonds, respectively. Finally, in Fig. 2 (c), The data for N_2 gas with thicknesses of 13, 36, 817, and 1221 μg/cm^2 are denoted by asterisks, open triangles, open circles, open squares, and open diamonds, respectively. The mean charge states of ^{86}Kr in H_2 and He gases attained equilibrium at 25.1 and 23.2, respectively. The fraction of ^{86}Kr^{26+} in H_2 is 32% at equilibrium. The mean charge state in N_2 at equilibrium was estimated to be lower than 20+. Since the maximum magnetic rigidity of the dipole magnet for selecting charge states was 0.97 T·m, the data are insufficient to reproduce charge distributions in N_2 gas.

It is found that the H_2 gas stripper can be used for ^{86}Kr acceleration. In addition, the charge states in He are sufficiently high for ^{78}Kr acceleration, since the lowest charge state of ^{78}Kr acceptable for RRC is 23+. Further development of a differential pumping system using orifices with a bore diameter larger than 10 mm is necessary for practical use.

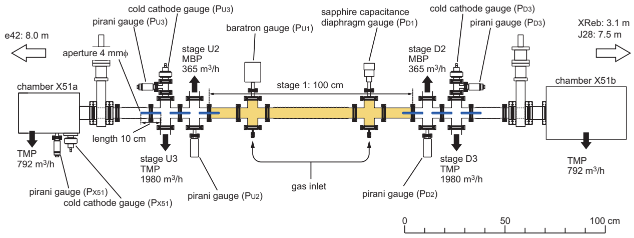

Fig. 1. Schematic of the gas charge stripper. Please see the text for details.

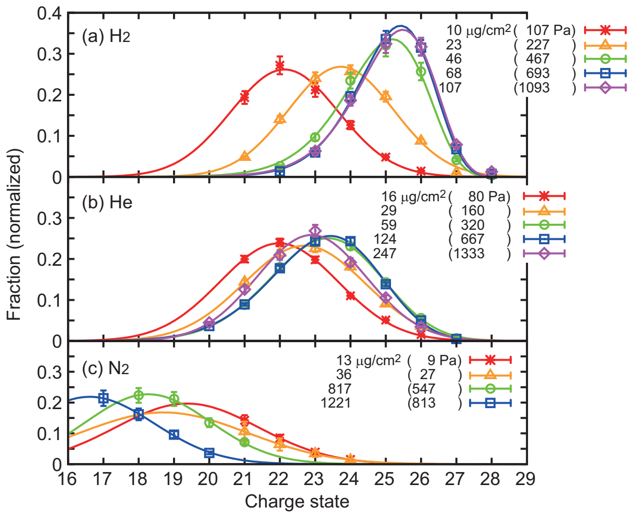

Fig. 2. Charge distributions of ^{86}Kr in (a) H_2, (b) He, and (c) N_2 gases. Please see the text for details.

References
1) H. Okuno et al.: Phys. Rev. ST Accel. Beams **14** 033503 (2011).
2) H. Imao et al.: Proc. of IPAC'13, Shanghai, China (2013), p. 3851.
3) H. Hasebe et al.: Proc. of 17th Int. Conf. on Cyclotrons and Their Applications, Tokyo, Japan (2004), p. 313.

*1 RIKEN Nishina Center

Air stripper for high-intensity xenon beam

H. Imao,[*1] H. Okuno,[*1] H. Kuboki,[*1] O. Kamigaito,[*1] H. Hasebe,[*1] N. Fukunishi,[*1] M. Fujimaki,[*1] M. Kase,[*1] and Y. Yano[*1]

Intensity upgrade of very heavy ions such as U and Xe beams is one of the main concerns at the RIKEN Radioactive Isotope Beam Factory (RIBF). A new injector, RILAC2, which includes a 28-GHz superconducting electron cyclotron resonance ion source[1)], has been successfully developed and became fully operational in the fiscal year 2011. In the acceleration with RILAC2, the possible output intensities have been principally limited by the lifetime problem of the carbon foil strippers. The recently developed recirculating helium gas stripper successfully solved the lifetime problem of the first-stage carbon foil stripper in the use with U beams at 11 MeV/u[2)]. However, the lifetime problem was an issue for the second-stage stripper as well. In the previous runs with Xe beams in 2012, it was necessary to replace the second-stage carbon-foil stripper every 8 h because of the decreasing thickness.

In the present study, we developed a very-thick air stripper as a second-stage stripper applicable for Xe beams at 51 MeV/u. We also tried Xe-beam acceleration only with gas strippers (the first-stage is N_2 gas and the second stage is air) for the first time in the RIBF user runs.

The thickness required to obtain the equilibrium charge state of the beams increases significantly at higher beam injection energies. In the present case, the second-stage stripper also functions as an energy degrader that changes the output energy of a fixed-frequency cyclotron (fRC) which is approximately 51 MeV/u, to the injection energy of the subsequent cyclotron IRC which is approximately 46 MeV/u. The required thickness of the second air stripper is about 30 times higher than the thickness for the first-stage helium stripper. Also, the required pressure at the target region is four times higher than that for the helium stripper.

The new charge stripping system was constructed in the E1 room after the fRC. The same technology of differential pumping for windowless gas confinement as the prototype He gas stripper[2)] was applied to the new system. The stripper consists of two tube-separated five-stage differential pumping systems with 17 pumps (Fig. 1). It is designed to achieve vacuum reduction from the target pressure of 25 kPa to 10^{-5} Pa within a length of 1 m while ensuring a 8.5-mm beam path.

We confined a very thick gas target, up to 20 mg/cm^2 of air, in a 51-cm target chamber. Air in the E1 room was continuously compressed and the inlet pressure of a pressure regulator was kept at 0.7 MPa with a relief valve. The regulator's secondary pressure was set to 0.4 MPa to deliver a steady flow to the target via a mass-flow controller. High-flow air up to 400 STL/min was introduced to the target chamber. Because we used air in the room, which could be inexhaustible, we did not need any recirculation system in the air stripper.

The stripper construction was completed in March 2013 and stably operated as the second-stage stripper in user runs performed in June 2013. We also used nitrogen gas (0.2 mg/cm^2), which is confined in the same system of the recirculating helium gas stripper as the first-stage stripper in the user runs. The availability (actual beam service time/scheduled beam service time) of Xe beams at 345 MeV/u in the user runs reached 91%[3)]. The maximum beam intensity reached 38 pnA, and the average intensity provided to users becomes approximately four times higher than it was in 2012. The new down time-free gas stripper contributed substantially to these improvements.

We note that this is the first observation of successful of the acceleration only with gas strippers at the RIBF, which is an important cornerstone for next-generation high-intensity heavy ion accelerators.

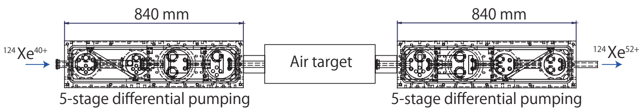

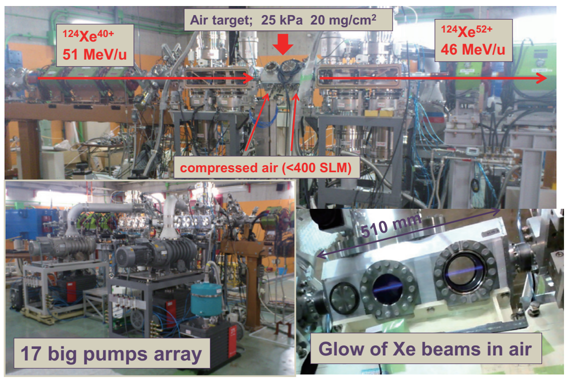

Fig. 1. A schematic view of the air stripper (upper). Pictures of the air stripper and glowing 100-pnA xenon beams (lower).

References
1) Y.Higurashi *et al.*: Rev. Sci Instr. 83, 02A308 (2012).
2) H. Imao *et al.*, Cyclotrons 2013, Vancouver (2013).
3) N. Fukunishi *et al.*, Cyclotrons 2013, Vancouver (2013).

*1 RIKEN Nishina Center

Design and construction of drift tube linac cavities for RIKEN RI Beam Factory[†]

K. Suda,[*1] N. Sakamoto,[*1] K. Yamada,[*1] S. Arai,[*1] Y. Chiba,[*1] M. Kase,[*1] H. Okuno,[*1] Y. Watanabe,[*1] and O. Kamigaito[*1]

A recent intensity upgrade for uranium and xenon beams at the RIKEN RI Beam Factory required the construction of a new injector linac, RILAC2. The acceleration system consists of three drift tube linac cavities (DTL1, DTL2, and DTL3) that operate at $f_0 = 36.5$ MHz in CW mode. The cavity structure is based on a quarter-wavelength resonator, since its size is the smallest in this frequency range among the available cavity structures. The DTL3 was built by modifying the decelerating cavity of the Charge State Multiplier (CSM)[1–3]. Because specifications for the DTL3 were similar to those for the CSM, the design was performed carefully, comparing our simulation with the actual cavity to check the validity of the design procedure. Finally, the DTL3 was built by removing a movable shorting plate and relocating the drift tubes. The other two cavities were newly constructed.

The most significant characteristic of the design is the adoption of the direct coupling method for amplifiers connected to the cavity. The amplifier using a tetrode 4CW50,000E (Eimac) is directly connected to the cavity with a capacitive coupler. Load resistance for the tetrode, or an input impedance, was assumed to be $Z_0 = 700\ \Omega$ in the design. Direct coupling reduces the number of parts, such as the stub and output capacitor, thereby reducing size and construction cost. However, as the resonant frequency of the cavity changes significantly because of the capacitance of the tetrode, the cavity design cannot be independent of the amplifier design.

The design procedure we used comprises the following two steps. We first design the cavity itself without the coupler. We then design the combined cavity and amplifier system, determining the coupling capacitance and size of the cavity. It is helpful to evaluate load impedance of the tetrode using the lumped circuit model, but modeling the coupler as a lumped element neglects some effects; namely, the coupler occupies a certain volume inside the cavity, so capacitance between the outer conductor and the coupler is non-negligible, making it difficult to estimate the resonant frequency shift due to the coupler. Because of this frequency shift, geometric parameters such as cavity height must be carefully determined. we design the The cavity without a coupler was designed first using CST Microwave Studio 2009 (MWS)[4]. We optimized the shape of parts constituting the resonator, such as gaps between the drift tubes, stem geometry, and the inner diameters of the coaxial section, using the eigenmode solver of the MWS to obtain a high parallel shunt impedance considering height and radius limitations. We also calculated RF power loss distributions to determine the flow rate of cooling water for each part. When determining the frequency of the resonator, it is crucial to consider the effect of the coupler; attaching the coupler to the cavity can result in a frequency shift as large as −300 kHz. The target frequency f_0 of the cavity determined by considering the coupler effect can be realized by adjusting the cavity height. The measured frequency shift against a cavity height of DTL3 was approximately 18 kHz/mm. We must determine the cavity height within an accuracy of ±4 mm to realize a frequency within ±73 kHz around f_0.

RF simulations of the cavity including the coupler were performed next. The calculated frequency shift due to the coupler was −290 kHz. Further frequency shifts due to the tetrode were estimated with the aid of the frequency domain solver. The load impedance of the tetrode $Z'(f)$ was roughly estimated by adding a lumped capacitance of tetrode C_p in parallel as $1/Z'(f) = 1/Z(f) + j2\pi f C_p$. $Z'(f)$ takes a real value of 750 Ω, which was close to Z_0. The frequency shift due to the tetrode was estimated to be −19 kHz.

The cavity height of the DTL3 was finally determined by taking these frequency shifts into account. The calculated shift with the tetrode and coupler was −309 kHz, and the measured frequency shift was −288 kHz. The estimation agreed well with the measurement. We also estimated the coupling strength using the frequency domain solver. Input impedance was calculated with various diameters of the coupling disk. Combining the result with the frequency dependence of the impedance $Z'(f)$, we concluded that a plate disk with a diameter of approximately 130 mm would be suited to obtain the desirable load resistance of 700 Ω at f_0. Based on these estimations, the diameter of the coupling disk was adjusted by making iterative measurements with the real structure of the cavity, so that the desirable load resistance was successfully obtained.

References
1) O. Kamigaito et al., Proceedings of LINAC'98, Chicago, TU4085, 603 (1998).
2) O. Kamigaito et al., RIKEN Accel. Prog. Rep. **34**, 322 (2001).
3) O. Kamigaito et al., Rev. Sci. Instrum. **76**, 013306 (2005).
4) http://www.cst.com.

† Condensed from the article in Nucl. Instrum. and Methods in Phys. Res. A 722, 55–64 (2013)

*1 RIKEN Nishina Center

Renewal of automatic tuning systems for RILAC cavities

K. Yamada,*[1] K. Oyamada,*[2] and N. Sakamoto*[1]

The RIKEN Linear Accelerator (RILAC) plays an important role with an injector to the RIBF for heavy-ions up to krypton as well as solo acceleration for super-heavy element synthesis. The resonance frequency of RILAC cavities is conserved by moving a large compensator using a feedback system, which mainly varies according to the capacitive reactance of cavity, because the frequency is fluctuated by disturbances such as heat or pressure. The basic principle of a frequency tuning system is that a relative phase difference between rf signals from a cavity pickup and an amplifier input is detected and the compensator is moved so as to keep the phase difference constant. The previous frequency tuning system caused much interruption of the machine time, because the inert response of feedback led to tripping of amplifier, and the drift of phase reference during a long-term operation had to be adjusted locally by stopping the beam acceleration. Therefore, a new frequency tuning system has been developed to realize long-term operation without interruption.

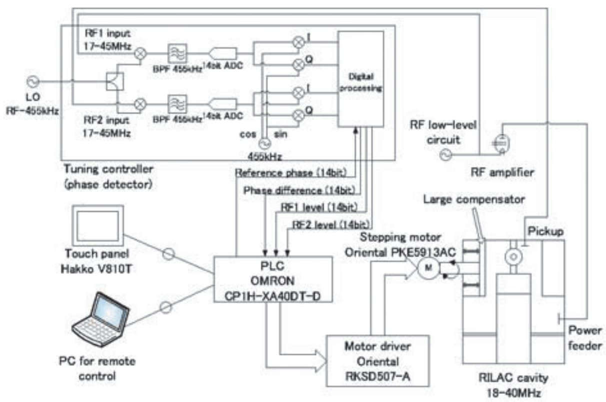

Fig. 1. Block diagram of the new frequency tuning system for RILAC cavities 5 and 6.

We replaced the tuning system for RILAC cavities 5 and 6 at first, because their rated voltage was higher and they experienced frequent trips. Figure 1 shows a block diagram of the new frequency tuning system. Although the basic principle is the same as the old one, much improvement was achieved, as follows.

A tuning controller (phase detector) was newly developed based on the concept of digital signal processing. Since the requied responce speed of the feedback is not very high (it includes a mechanical system), the two input rf signals are reduced to an intermediate frequency (455 kHz) by a double-balanced mixer with a local-oscillator signal, and converted to a 14-bit digital signal. Each digital signal is translated to in-phase (I) and quadrature-phase (Q) signals and the phase difference is determined by digital processing in a field-programmable gate array. The phase difference data is corrected by an applied reference phase to produce the phase deviation from the reference phase and output to a digital interface. The reference phase can be set to an arbitrary value or the present value of the phase output by a local and remote one-push button.

The old tuning system used a geared print motor, which was a DC motor whose rotation speed could not be controllable accurately. By fabricating a mounting plate and driveshaft coupling, the motor was replaced by a new stepping motor. The stepping motor is controlled by a programmable logic controller (PLC) with the principle of proportional speed control feedback based on the phase difference data. The maximum moving speed, feedback gain, and neutral zone can be accurately set locally and remotely.

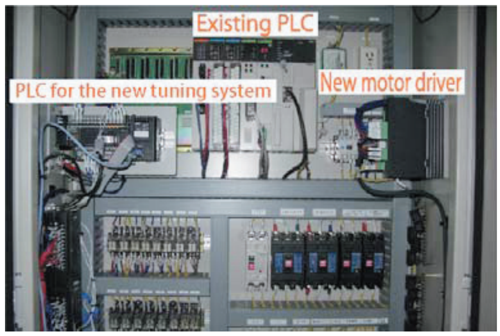

Fig. 2. Control unit of the new tuning system built in the existing RF control system for RILAC cavity 5.

Figure 2 shows the control unit of the new tuning system built in the existing RF control system for RILAC cavity 5. Since the existing PLC was discontinued, we introduced an additional PLC only for the tuning system. A touch panel for the local operation of the tuning system is shared with that for the RF control system. The new tuning system was successfully commissioned in Dec. 2012 on cavity 5, and the replacement for cavity 6 was carried out in Feb. 2013. Owing to the renewal, the stability of feedback was significantly improved and work on its availability during long-term operation is currently in progress.

At the time of the renewal of amplifiers for RILAC cavities 1 and 2 in the winter of fiscal year 2013, the new tuning controller was introduced for these cavities. The residual tuning system for cavities 3 and 4 will be replaced in parallel with the renewal of amplifiers in the future.

*[1] RIKEN Nishina Center
*[2] SHI Accelerator Service Ltd.

Replacement of main coils of RRC-W sector magnet

Y. Watanabe,[*1] M. Kase,[*1] N. Fukunishi,[*1] T. Maie,[*1] K. Kumagai,[*1] M. Nagase,[*1] O. Kamigaito,[*1] S. Fukuzawa,[*2] M. Hamanaka,[*2] S. Ishikawa,[*2] K. Kobayashi,[*2] Y. Kotaka,[*2] R. Koyama,[*2] T. Nakamura,[*2] M. Nishida,[*2] M. Nishimura,[*2] J. Shibata,[*2] N. Tsukiori,[*2] and K. Yadomi[*2]

The RIKEN Ring Cyclotron (RRC) has been in stable operation for over 27 years, and it is expected to work as a first-stage energy booster in any acceleration mode of the Radioactive Isotope Beam Factory (RIBF) in the future. Recently, some problems caused by age-related deterioration have often been occurring in the RRC. In 2011, a layer shorting was found at the upper main coil of the RRC-E sector magnet, and we replaced it with a new one in the summer of 2012.[1)] Furthermore, the lower main coil of RRC-W sector magnet also showed signs of layer shorting in June 2012. This layer shorting of the RRC-W sector magnet was a recurrence of the instance of shorting experienced and repaired in 1999. We again attempted to repair it, as in 1999, but the fluctuations of the coil voltage and magnetic fields were not fully improved. So, we decided to replace the damaged lower main coil and the deteriorated upper main coil of the RRC-W sector magnet with new main coils in FY2013. Fabrication of the new main coils required four months, and the replacement task had been scheduled over a period of eight weeks within the summer maintenance period. This was done because we had no experience in replacing the lower main coil of the RRC in our twenty-six year operation. Table 1 lists the replacement schedule of the main coil of the RRC-W sector magnet in 2013.

In the replacement task, three difficulties were anticipated, as shown in Fig. 1. The first one is how to deposit and store yokes, poles, the main vacuum chamber, and the beam injection line that was removed temporarily in the RRC room. Because of their heavy weight and large size, these removed parts were carried to and stored on the S, N, and E sector magnet, in addition to the south side of resonator No. 2, and in front of the shield door between the RRC room and the D room. The removed main coils were carried out from the RRC room and stored in the IRC room. The second difficulty is that we have to loosen and tighten 13 bolts for fixing the vacuum chambers onto the magnetic pole surfaces. Since these bolts were in the deep and narrow vacuum chamber, we ran a test successfully by using an air drive tool having a long grip in advance in the winter of 2013. The last difficulty is the silver alloy brazing of copper pipes used for cooling water and electrification of trim coils. 116 pipes were cut to remove main vacuum chamber and poles, and parts of the cut pipes were newly fabricated and cleaned for a new silver alloy brazing. Because of the high number of copper pipes, it took a week to braze these pipes with a silver alloy. Furthermore, because several pipe fixing plastic plates were used for the fixation of pipes and maintaining vacuum, we had to frequently investigate the vacuum leak from the sub-vacuum chamber.

The present performance of the RRC-W sector magnet is greatly improved, as shown in Fig. 2. Though the magnetic field of the RRC-W sector magnet before the replacement had been fluctuating over a wide range of ±5ppm, at present, the RRC-W sector magnet has a stable magnetic field without a fluctuation.

Table 1 Replacement schedule of main coils in 2013.

Mar.	Initiation of production of new main coils
11-31 Jul.	Removal of resonators, beam injection line, valley chamber, yokes, main coils, main chamber/poles, certain cables, pipes, decks, etc.
1-10 Aug.	Fabrication/cleaning of copper pipes for trim coils
5-16 Aug.	Carrying in and out of main coils, restoration of main chamber/poles and vacuum test
19 Aug. - 6 Sep.	Restoration of yokes, beam injection line, resonators, valley chamber, certain cables, pipes, decks, etc.
26-31 Aug.	Silver alloy brazing of copper pipes and leak test
6-13 Sep.	Starting up of RRC

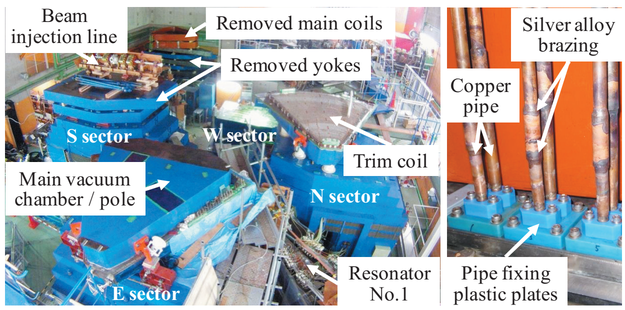

Fig. 1. Deposition and storage of removed parts and copper pipes of trim coil after silver alloy brazing.

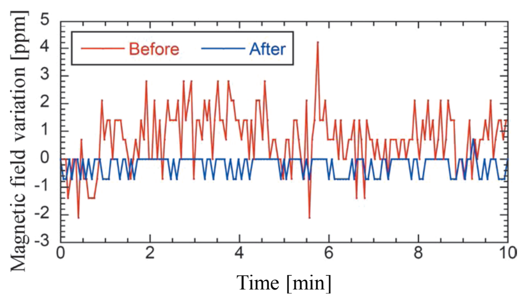

Fig. 2. Fluctuation of magnetic field before and after the replacement of main coils.

*1 RIKEN Nishina Center
*2 SHI Accelerator Service Ltd.

References
1) Y. Watanabe et al.: RIKEN APR 2012, p.130.

Replacement of the RIKEN ring cyclotron (RRC) power supplies

K. Kumagai,[*1] M. Nagase,[*1] and N. Fukunishi[*1]

The RIKEN ring cyclotron (RRC) has been in operation since 1986. The magnet power supplies that have been operating for 28 years were generally aging. For example, their capacitors have exceeded their service life and cooling water has been leaking from pinholes that open on the blocks for thyristor cooling.

This year, we decided to replace the main coil power supply and several trim coil power supplies. The specifications of these power supplies are shown in Table 1.

The replaced six power supplies for the trim coil are being used for the coils 4E, 4S, 5E, 5S, 26E, and 27E. The maximum current of the power supplies has been increased from 500 to 600 A in order to obtain a margin of adjustment for cyclotron's magnetic field. The 4th trim coils were used at the same polarity for various beam operations, the polarity switching systems were not equipped.

The main coil of each sector magnet was composed of two coils. One coil was connected to power supply M1, and the other was connected to power supply M2. M2 also had four bypass circuits (100A-34V), which compensated for the variation in the magnetization of four sector magnets. The new main-coil power supply is connected to two coils that are rewired in series as shown in Fig. 1.

Table 1. Specifications of the new main coil power supply and trim coil power supplies.

	Main coil power supply	Bypass power supplies	Trim coil power supplies
Number	1	4	6
Current (DC) [A]	1080	30	600
Voltage [V]	500	130	20
Output current range [%]	30 - 100	0 - 100	0.8 - 100
Stability, Ripples [*2]	$\pm3\times10^{-6}$	$\pm1\times10^{-5}$	$\pm5\times10^{-6}$
Setting resolution [bits]	20	16	16

*2 The ratio of the maximum current.

It is necessary to slightly adjust the current of the main coil power supply in order to cancel the variation of the magnetic field due to temperature rise of the yoke. The power supply of M1 and M2 had a resolution of 16 bits. However, the change in the current per bit corresponds to 11.1 ppm for M1 and 4.2 ppm for M2, which is insufficient for the fine adjustment of the current. As the new main coil power supply has a digital-to-analog convertor (DAC) with a resolution of 20 bits, the change in the current per bit is 0.95 ppm, which is equivalent to 0.001A/bit. As the NIO-S board used for the remote control of the power supply is capable of setting a current of 16 bits, we used two NIO-S boards for controlling 20 bits. One board is used for coarse current adjustment, and the other is used for fine adjustment of ±33.75A of the preset value.

The main coil power supply is exposed to radiation under the beam operation because it is placed in the same room as the RRC magnets. As a result, there is a risk of malfunction due to the radiation for the precision electronic devices installed in the power supply, such as the programmable logic controller (PLC), NIO-S boards, and the field-programmable gate array (FPGA). These devices are stored in a small chassis and are connected to the main power supply unit by optical cables and serial cables. They can be placed at a maximum distance of 15 m to avoid exposure to radiation.

The current stability over 8 hours was less than ±1 ppm excluding the initial drifts when the environmental temperature change was less than 3 °C, as shown in Fig. 2.

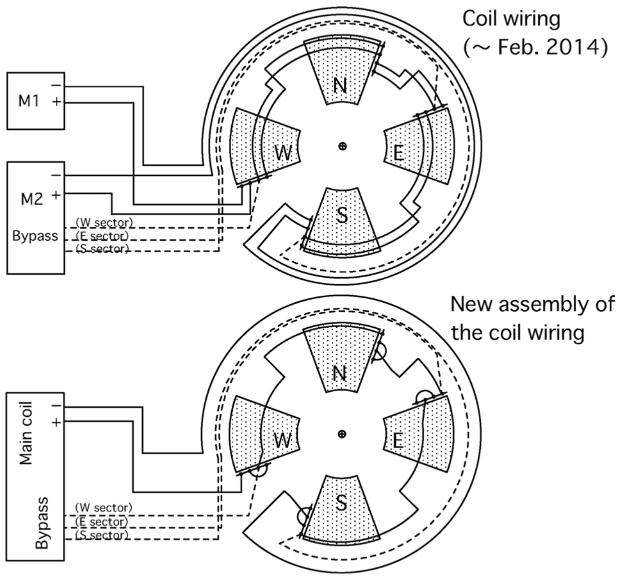

Fig. 1. Wiring of the RRC main coil.

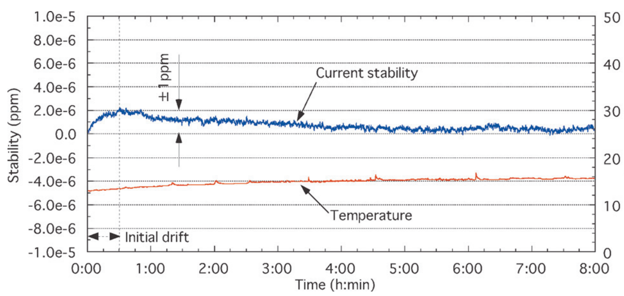

Fig. 2. Current stability of the main coil power supply over 8 hours.

The trim coil power supplies were installed in January 2014 and they began to operate smoothly at the beam service time by the end of January. The installation of the main coil power supply was completed in February 2014. Its usage began in the middle of March.

*1 RIKEN Nishina Center

Vacuum leaks in accelerators

S. Watanabe,*[1] Y. Watanabe,*[1] E. Ikezawa,*[1] M. Kase,*[1] N. Sakamoto,*[1]
K. Oyamada,*[2] M. Nishida,*[2] K. Yadomi,*[2] and J. Shibata*[2]

The vacuum system for accelerators in RIBF has been running without serious problems. However, vacuum leaks have been observed in the following equipments: (1) resonator of CSM-A1, (2) cooling pipe in resonator #2 of RRC, (3) W-resonator of fRC, and (4) a chamber in the dipole magnet DM-G5.

The vacuum chamber that houses the resonator of CSM-A1 has a leakage of vacuum in its bottom plate, which is made of steel with a thickness of 40 mm and copper-plated inside and painted outside. The precise location of the leak in has been searched but has not been specified yet. Because the response of the helium leak detector was very slow. The route of the leak in the bottom plate would be complicated. Then it took time to respond to helium gas. We will continue searching for the leak point. The vacuum pressure of the A1 resonator was around $2x10^{-5}$Pa, which is worse than those of other resonators, by a factor of 2 or 3.

A buildup of pressure was generated in RRC resonator #2 in the spring of 2013.The leak was found in exist somewhere in the cooling pipe of the lower inner conductor of the resonator. The cavity was opened in July, and the inside of the inner conductor was investigated carefully. As a result, water leakage was found in the chamber. However, there is no space around the pipe connection. To solve this problem, a new bypass line was made. The pipe line was cut at two shallow spots, and the spots were connected with a new pipe. The pipe connections were treated with silver braze. This equipment is running without any problems now.

At fRC, a small leak in the W-resonator has been observed for several years. However, with rf power on, the leak was so small that operations had been possible. To investigate the cause of the leak, the upper part of the resonator was removed in June 2013. On doing so, a bad rf-electrical contact was found in a part of the metal C-ring, and the elastomer O-ring seal near to it was damaged. The C-ring was replaced with a new one. To improve the clamping capacity, a long bolt was introduced through an upper flange and the resonator, and the upper flange and the resonator were tightly fastened by a nut. Moreover, the clamping capacity was reinforced by new jigs like a C-clamp.

A vacuum chamber inside a dipole magnet named DM-G5 in the injection beam line into SRC has a leakage of vacuum. The chamber was shaped like a 60-degree arc and had a rectangular cross-sections (58 mm x 86 mm). The main part of the chamber was composed of four aluminum plates with a thickness of 2 mm. The four edges of the chamber were welded. A rough location of the leak could be determined by keeping the chamber inside the magnet pole gap. For precise investigation, we took out the chamber from the magnet yoke. The first anticipated point was confirmed to be the leak point. However, the leak soon became small enough and was not detected. The cause of this phenomenon was considered. The chamber would be pressed by the magnet. Then the leak would be generated by the deformation of the chamber. To confirm this, we pressed onto the chamber using a C-clamp at a place near the leak point; doing so, a leak was detected at the same time, the vacuum pressure changed by a factor of 10. The leak point of the chamber was determined to be on the welding bead. Additional welding on it will result in another deformation on the chamber. Therefore, the leak point was treated with epoxy resin (Torr Seal). The leak was fixed.

*[1] RIKEN Nishina Center
*[2] SHI Accelerator Service Ltd.

Reinforcement of magnetic shield for HTc SQUID beam current monitor at the RIBF†

T. Watanabe,*1 N. Fukunishi,*1 M. Kase,*1 O. Kamigaito,*1 S. Inamori,*2 and K. Kon*2

To measure the DC current of high-energy heavy-ion beams nondestructively at a high resolution, a high-critical-temperature (HTc) superconducting quantum interference device (SQUID) beam current monitor henceforth referred as HTc SQUID monitor has been developed for use in the radioactive isotope beam factory (RIBF) at RIKEN.[1] Beginning this year, the magnetic shielding system has been greatly reinforced. Since the measurement resolution is determined by the signal to noise ratio, this resolution is improved by attenuating the external magnetic noise and RF back ground noise. These noises are mainly produced by the distribution and transmission lines from the high-current power supplies and high-power RF cavities of the cyclotrons.

To reinforce the existing magnetic shield, we developed a hybrid magnetic shielding method based on the properties of perfect diamagnetic materials and ferromagnetic materials; we were able to realize a high shielding effect despite the compact system. This system consists of two shielding parts: one for the HTc current sensor and the other for ferromagnetic shielding materials. The HTc current sensor used to produce a shielding current produced by the beam[1] also works as the superconducting shield via the Meissner effect (perfect diamagnetism). The ferromagnetic shielding materials are composed of high permeability alloys (Permalloy, Mu-metal, etc.). The HTc SQUID is installed inside the frame and onto the HTc current sensor, and the frame is covered by the cap. Consequently, the HTc SQUID is almost completely surrounded by the hybrid magnetic shielding system. A photograph of the completed hybrid magnetic system is shown in Fig. 1.

In the acceleration facility, since there exist AC magnetic noises of 50 Hz and higher order and which are much stronger than terrestrial magnetism, an active magnetic field canceller system (JEOL Ltd.) was designed and introduced to the HTc SQUID monitor. This system is comprised of a magnetic field control unit, combined AC/DC magnetic field sensors, and compensation coils. The compensation coils consist of three pairs of coils that are arranged perpendicular to each other. Each of these pairs forms a so-called "Helmholtz-Coil-Pair," able to produce a homogenous magnetic field in between the pairs; each pair controls one direction (along x-, y-, or z- axis). A photograph of

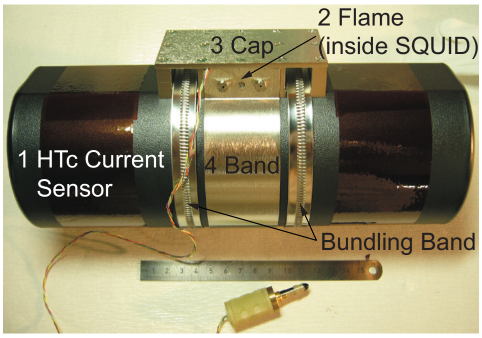

Fig. 1. Photograph of the completed hybrid magnetic system. 1: HTc current sensor with ferromagnetic shielding materials, 2: frame, 3: cap, and 4: band.

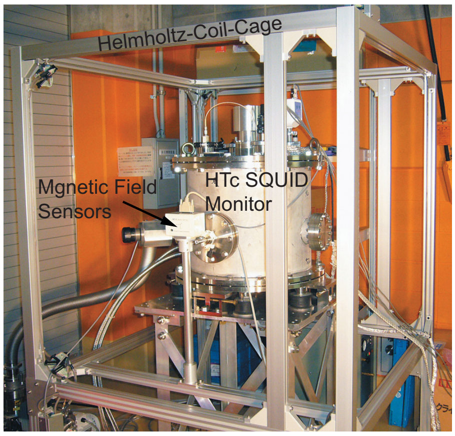

Fig. 2. HTc SQUID monitor with active magnetic field canceller system.

the active magnetic canceller system is shown in Fig. 2.

To evaluate the performance of the hybrid magnetic shielding system and the active magnetic canceller system, the output signals of the HTc SQUID were analyzed in the time and frequency domains. The signal was measured in the room next to where the power supplies for RIBF were located, where the leakage magnetic field of the 50 Hz component was measured by a Gauss meter as 4.5×10^{-4} T. On the other hand, the output signal of the 50 Hz component of the HTc SQUID monitor was 6×10^{-14} T. Based on these findings, we consider that the combination of the hybrid magnetic shielding system and the active magnetic canceller system can attenuate the external magnetic noise to 10^{-10}.

† Condensed from the proceedings in European Conference on Applied Superconductivity (EUCAS 2013)
*1 RIKEN Nishina Center
*2 TEP Corporation

References
1) T. Watanabe et al., Proc. 2010 Beam Instrumentation Workshop (BIW10), Santa Fe, U.S.A (2010) p. 523.

Online monitoring of beam intensity using current transformer at CRIB

R. Koyama,[*1,*2] M. Fujimaki,[*1] N. Fukunishi,[*1] S. Watanabe,[*1,*3] H. Yamaguchi,[*3] and A. Yoshida[*1]

The industrial cooperation team in RNC is developing a method for wear diagnostics of industrial materials using RI beams as tracers in collaboration with SHIEI Ltd. and CNS.[1)] RI nuclei are implanted in the near surface of the machine parts within a depth of 10–100 μm, and its wear-loss is evaluated by the decrease in the measured radioactivity. Continuous γ-ray detection from the exterior of the machine enables real-time diagnostics of the wear in running machines.

In this technique, an intense low-energy RI beam with an intensity of 10^7–10^8 cps are produced at CRIB [2)] and implanted in a sample continuously for a few days in order to obtain the intended activation of a few hundred kBq. The stability of a RI beam irradiation needs to be monitored but it is too intense to monitor using a destructive detector and its energy loss in a detector disturbs the effective activation of a sample. Therefore, we examined the monitoring of the primary beam intensity detected nondestructively by a current transformer (CT) using a monitoring system that incorporates lock-in amplifiers (LIAs). The CT, called the E7 core monitor (E7CM), was developed for precise evaluation of the nuclear-reaction cross section at CRIB.[3)] The monitoring system using LIAs has been developed for stable operation of RIBF.[4)]

The schematic layout of CRIB and the examination setup are shown in Fig. 1. 5.0 MeV/nucleon ^{11}B beam accelerated by the AVF cyclotron was used. The beam-bunch signal detected by E7CM was fed to three LIAs via the three directional couplers in order to measure the three frequency components (1–3f, 1f: acceleration rf of 13.8 MHz) simultaneously, as shown in

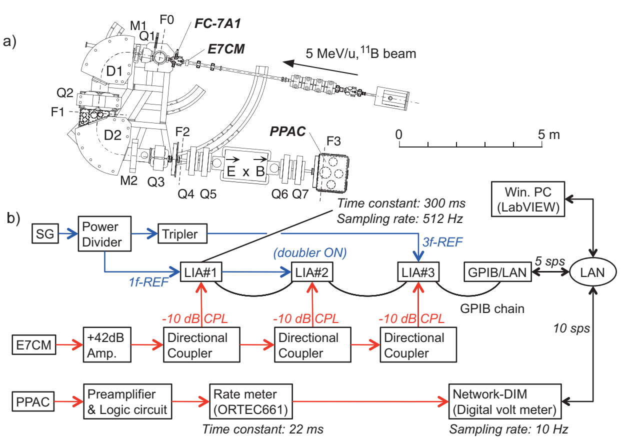

Fig. 1. Schematic layout of CRIB (a) and examination setup (b).

*1 RIKEN Nishina Center
*2 SHI Accelerator Service Ltd.
*3 Center for nuclear study (CNS), University of Tokyo

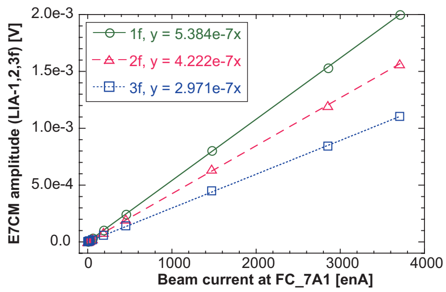

Fig. 2. Linearity between beam current detected by Faraday-cup 7A1 (FC-7A1) and E7CM amplitudes.

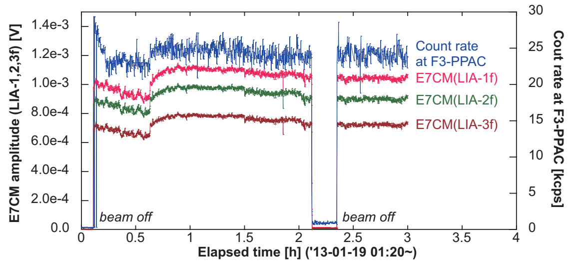

Fig. 3. Correlation between count-rate of secondary beam and E7CM amplitudes. The primary beam current was 1870–2100 enA.

Fig. 1b. A linearity of E7CM amplitudes to the beam current detected by Faraday-cup 7A1 is confirmed, as shown in Fig. 2. In addition, the correlation between E7CM amplitudes and the count-rate of the secondary beam detected by PPAC at F3 was observed, as shown in Fig. 3. For more precise comparison, however, we have to standardize the measurement condition such as time-constant and sampling-rate for the LIA and PPAC systems. At a beam current of 2850 enA, comparable to that of actual experiment, the S/N ratio of 1–3f was 770, 3990 and 1680, respectively. They are all acceptable values but it is favorable to monitor no less than the 2f component, because the origin of background is acceleration-rf and its reference signal, and thus, its 1f component has relatively large amplitude with some fluctuation. From these results, we can conclude that the E7CM and LIA system can fulfill a role for the beam-intensity monitoring.

References

1) A. Yoshida et al.: Nucl. Instr. & Meth. B **317**, (2013) 785–788.
2) Y. Yanagisawa et al.: Nucl. Instr. & Meth. A **539**, (2005) 74–83.
3) S. Watanabe et al.: Nucl. Instr. & Meth. A **633**, (2011) 8–14.
4) R. Koyama et al.: Nucl. Instr. & Meth. A **729**, (2013) 788–799.

Online monitoring of beam phase and intensity using lock-in amplifiers†

R. Koyama,[*1,*2] N. Sakamoto,[*1] M. Fujimaki,[*1] N. Fukunishi,[*1] A. Goto,[*3] M. Hemmi,[*1] M. Kase,[*1] K. Suda,[*1] T. Watanabe,[*1] K. Yamada,[*1] and O. Kamigaito[*1]

We developed a monitoring system dedicated for RIBF that incorporates lock-in amplifiers (LIAs) that can measure the beam phase and intensity of signals from the phase probe (PP) with an amplitude of a few hundred nanovolts. The configuration of the LIA system is schematically shown in Fig. 1. The rf is also monitored using the LIA system. We compared the performance of the LIA system with that of a conventional system that incorporates oscilloscopes (OSCs). It was confirmed that LIA has much higher precision and smaller deviation than the OSC; LIA has a resolution of 0.02° for a 1.0 V standard signal and can measure a signal as small as 200 nV, which corresponds to 10 electric nA of beam current.

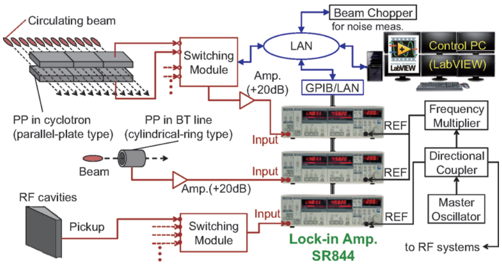

Fig. 1. Configuration of the LIA system.

Since the PPs are placed at relevant positions along the beam lines of the RIBF, we can easily find the instability or decrease of beam intensity caused by the variation of rf or magnetic field by using the LIA system. The correlations between rf, beam phase, beam intensity, and environmental factors such as the ambient temperature and cooling water temperature have also been revealed.[1,2] In addition, we can clearly observe the deterioration of a solid-state charge stripper and the pressure variation of a gas charge stripper.[3]

The isochronism measurement results for the SRC, which has a low velocity gain of 1.5, showed excellent agreement between the three measurement methods (OSC zero-corss, OSC FFT, and LIA) with a discrepancy less than 0.2 ns ($\simeq$2 rf degree), as shown in Fig. 2(a). The isochronism measured for 10 frequency components ($1f$–$10f$) was also in good agreement with an accuracy discrepancy less than 0.5 ns ($\simeq$5 rf degree). However, in the RRC, which has a high velocity gain of 4.0, a phase difference of up to 0.7 ns ($\simeq$7 rf degree) was observed between the three measurement methods. The phase difference was improved to a discrepancy of less than 0.4 ns ($\simeq$4 rf degree) when we corrected for the radial variation of the observed bunch width, as shown in Fig. 2(b).

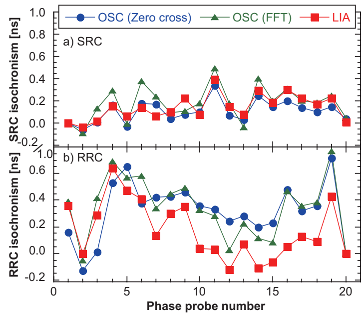

Fig. 2. Comparison of isochronism in a) the SRC and b) the RRC on the basis of three measurement methods.

The remaining phase difference between LIA and OSC is considered to be the effect of the cable dispersion. In fact, it was observed that the cable dispersion via 80 m increases asymmetric distortion of the bunch shape, and it produces a timing advance of 0.14 ns relative to the actual timing, as shown in Fig. 3. Because we measure the single-frequency component of the beam-bunch signal in the LIA system, such cable dispersion does not disturb the beam-phase measurement, and it is concluded that the LIA system gives a more accurate beam phase if the measurement is performed at the control room.

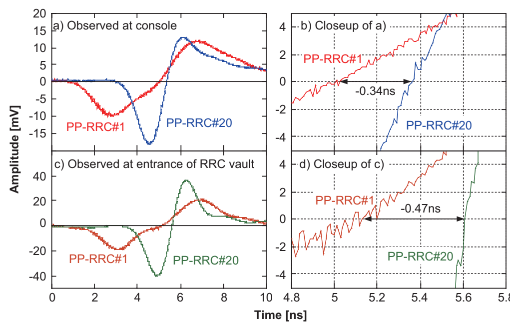

Fig. 3. Bunch shapes observed at the console 90 m downstream of PP-RRC (a) and at the entrance of the RRC vault 10 m downstream of PP-RRC (c).

References

1) R. Koyama et al.: RIKEN Accel. Prog. Rep. **42**, pp. xviii–xix (2009).
2) K. Suda et al.: Proc. of CYCLOTRONS 2010, Lanzhou, China, MOPCP068, pp.186–188.
3) R. Koyama et al.: Proc. of PASJ10, Nagoya, Aichi, August 2013, SAP013, in press.

† Condensed from the article in Nucl. Instr. & Meth. A **729**, (2013) 788–799
*1 RIKEN Nishina Center
*2 SHI Accelerator Service Ltd.
*3 Planning Department, Yamagata University

Modification of beam diagnosis chambers in RILAC2 high-energy beam transport

K. Yamada,*[1] R. Koyama,*[2] T. Nakamura,*[2] M. Hamanaka,*[2] M. Fujimaki,*[1] and N. Fukunishi*[1]

The vacuum chambers in the high-energy beam transport line between the RILAC2 and the RRC have been modified in order to extend the beam diagnosis devices such as a beam profile monitor and movable slits. Figure 1 indicates the schematic view of the beam line. The vacuum level in the section including a rebuncher located at S31 (S3-REB) has also been enhanced by mounting additional vacuum pumps in an arrangement previously presented in report 1. The modifications are listed as follows.

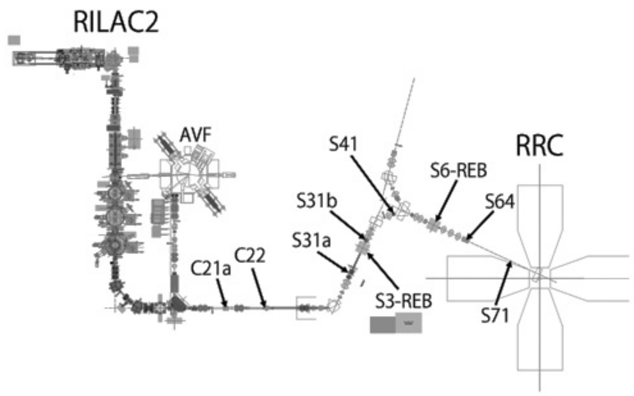

Fig. 1. Schematic view of high-energy beam transport between RILAC2 and RRC.

- location C22 (just upstream of the wall between the AVF and RRC vault):
  The existing vacuum chamber has been replaced by a larger one to increase the number of the port for movable slits that define the beam emittance of RRC injection by combining with the slits at location C21a. A plastic scintillator for time-of-flight measurement, a beam attenuation mesh, a 220 L/s turbo molecular pump, and a beam stopper for radiational safety are also mounted on the C22 chamber. A wire-scanning beam profile monitor will be attached on the chamber to check the beam size on the plastic scintillator.
- location S31a (upstream of the S3-REB):
  The existing chamber has been replaced by a middle-sized chamber used for a standard in RIBF. A 350 L/s turbo molecular pump has newly been attached to the S31a chamber to improve the vacuum level. A beam attenuation mesh, a wire-scanning beam profile monitor, and a Faraday cup are mounted on the chamber as well.
- location S31b (just downstream of the S3-REB):
  A new small chamber has been installed only for mounting a wire-scanning beam profile monitor. This beam profile monitor is used to adjust the beam trajectory in the S3-REB section by combining with the beam profile monitor at S31a.
- location S41 (just downstream of the singlet quadrupole (Q) magnet):
  A beam profile monitor chamber located at S40 (just upstream of the Q-magnet) and a vacuum gate valve located at S41 have been exchanged with the aim of checking the degree of dispersion corrected by the Q-magnet. A 220 L/s turbo molecular pump has been mounted on the S41 chamber.
- S6-REB (rebuncher located at the S61):
  Two gate valves have been installed at each end of the S6-REB. This installation enables maintaining the devices without breaking the vacuum in the long section between S41 and S71.
- location S64:
  A new large vacuum chamber has been installed, as shown in Fig. 2. A plastic scintillator, a beam attenuation mesh, a wire-scanning beam profile monitor, a build up secondary-electron suppressor, a Faraday cup, and a 220 L/min turbo molecular pump have been attached to the chamber. Two other diagnosis devices are expected to be appended onto the chamber. A fast current transformer (C.T.) has newly been installed just upstream of the chamber.

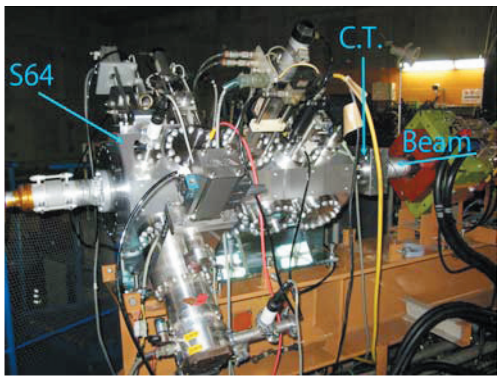

Fig. 2. Photograph of the new chamber installed at S64.

*[1] RIKEN Nishina Center
*[2] SHI Accelerator Service Ltd.

References

1) K. Yamada et al., RIKEN Accel. Prog. Rep. **45**, 99 (2012).

Upgrading the server system using virtualization technology in the RIBF control system

A. Uchiyama,[*1] M. Komiyama,[*1] and N. Fukunishi[*1]

In an RIBF control system, the Experimental Physics and Industrial Control System (EPICS) has been introduced on Linux and vxWorks since 2001[1)]. Owing to a centralized management system, all computers for EPICS programs share common network storage that implements a file transfer protocol (FTP) and a network file system (NFS) as key services. In order to achive service reliability enhancement of the key services, we constructed failover clusters in 2008[2)].

Considering the short life cycle of server hardware, aging servers should be replaced periodically. In term of the reliability, the replaced system should enhance the efficient operation of server hardware resources, for example improvement of CPU utilization. Currently, virtualization technologies, such as KVM, Xen, and VMware are widely used in many scenarios. For the RIBF control system, virtualization software, which realizes a hardware sharing system, was slected for the following reasons:

(1) To reduce operational costs, it is efficient to make virtualized image files from current physical servers without modifications to the system.
(2) Other required services should be constructed by a High-availability (HA) system.
(3) Complex clustering should be avoided in order to minimize maintenance cost.
(4) Virtualization software with reliable support services are commercially available.
(5) Even if physical servers encountered an issue, there should be no downtime for the guest operating system.

Therefore, we adopted VMware vSphere 5 as a virtualization software for the RIBF server system, and Network Attached Storage (NAS) manufactured by NetApp as a shared storage with an HA system has been implemented (See Fig. 1). In this system, the services for the shared EPICS programs and the virtualized image files in VMware environment are provided by the NAS. To improve service reliability, live-migration, which moves the guest hosts to other physical servers without downtime, is provided by VMware vMotion.

For ensuring the scalability and availability of the network, the network between NAS and a network switch uses the Link Aggregation Control Protocol (LACP). LACP bundles several physical Ethernet ports in a single logical channel. In fact, EPICS Input/Output Controllers (IOCs), Domain Name System (DNS), Lightweight Directory Access Protocol (LDAP), PostgreSQL, MySQL, Process Variable gateway[3)], backup systems, and EPICS application servers were constructed on the virtualization environment (See Table 1).

The VMware cluster consists of three physical servers (dual-socket Intel Xeon E5-2630), and 20 virtualized servers have been running on this cluster since Jan 2014. Replacing an aging system with a virtualization system with HA, it can facilitate efficient use of server resources and operational costs.

Table 1. Comparison of the old redundant system and the new server system in the main services.

Service	Old methods	Replaced system
NFS	Failover cluster	Dual NAS controllers
PostgreSQL	Failover cluster	vMotion
FTP	Failover cluster	vMotion
EPICS IOC	None	vMotion
DNS	Primary/Secondary	Primary/Secondary, vMotion
LDAP	None	vMotion
EPICS applications	DNS round robin	DNS round robin, vMotion

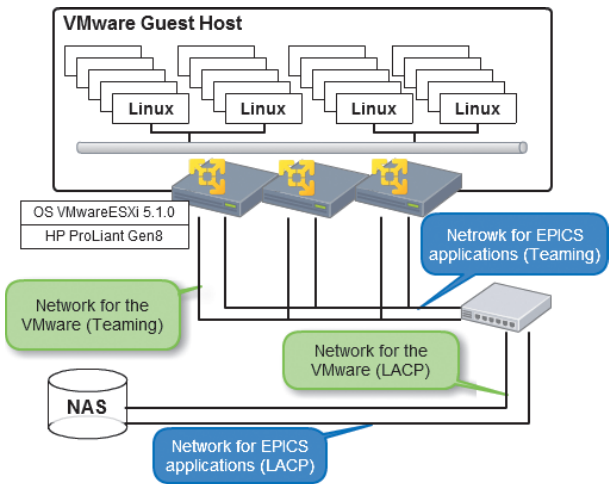

Fig. 1. System chart of the upgraded virtualization server system, NAS, and LACP-based network.

*1 RIKEN Nishina Center

References
1) M. Komiyama et al.: Proc. of ICALEPCS07, P.187.
2) A. Uchiyama et al.: APR. **42**, (2009) P.145.
3) K. Evans, Jr.: Proc. of ICALEPCS 2005, PO1.033-6.

Development of a system for measurement beam service time in RIBF operations

A. Uchiyama,*1 M. Komiyama,*1 and N. Fukunishi*1

To assess the performance of the accelerator facility, it is essential to measure the beam service time provided for the request from experiment users. Previously, beam service time was measured by using the handwritten log notebook records maintained by accelerator operators. In order to measure beam service time more efficiently and accurately, we developed a beam service time measurement system called Beam Status History.

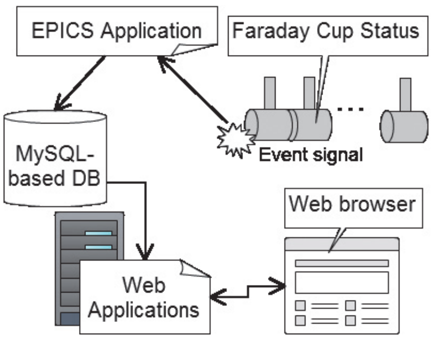

Fig. 1. System chart of developed measurement system for beam service time (Beam Status History).

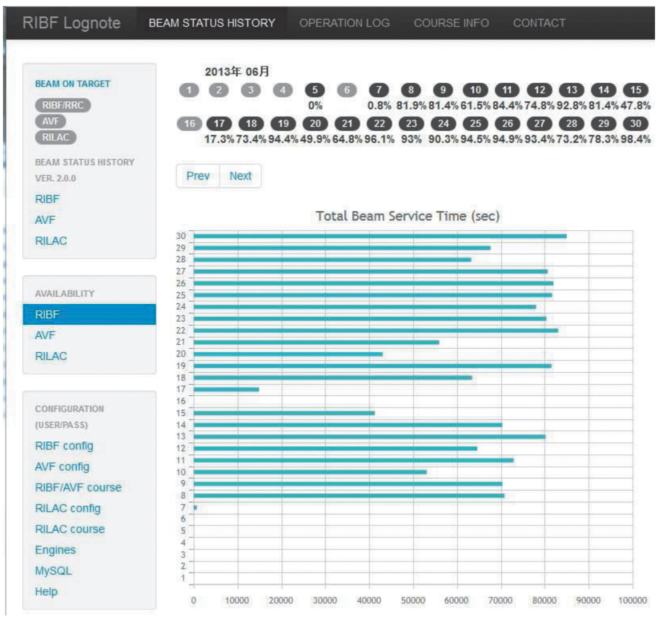

Fig. 2. User interface of Beam Status History. The total beam service time for a day and a month is displayed as a bar chart on the Web browser (Firefox).

*1 RIKEN Nishina Center

The outline of Beam Status History is shown in Fig. 1. The RIBF control system consists of a distributed control system constructed using Experimental Physics and Industrial Control System (EPICS)[1].

On the other hand, Beam Status History consists of EPICS-based client applications, MySQL-based database, and Web applications. Faraday cup statuses set or out, are input as digital signals into EPICS databases, and an event that identifies information about beam service availability status is triggered by the system when all faraday cups reach the out state in the experiment course.

By contrast, when even one of the faraday cups state changes from out to set, the system considers it as the beam-off status. The information of the beam on/off status is stored in the MySQL-based database by the EPICS-based client application that is written in C, and then, beam service time is calculated based on a timestamp of the beam-on/off status by the PHP-based Web applications.

For Beam Status History, servers were constructed by Linux (CentOS 5.9) on a virtualization environment for the RIBF control system[2]. This system consists of the Web server (Apache), MySQL server, and the server for caMonitor, which is an event-driven program that uses the Channel Access protocol, in three virtual hosts. On the other hand, user interfaces are utilized by Web applications using Asynchronous JavaScript and XML (Ajax) technology. From the viewpoint of providing many users with accelerator information, this Web technology is a convenient system. Ajax is a Web development technique used on the client-side to create asynchronous Web applications for implementing a real-time display on the Web browser. In the beam service time measurement system, Ajax is used to display the beam on/off status and the chart of the beam service time (See Fig. 2).

As a system function, all the beam-on and beam-off times, experiment user name, type of beam (ion, charge, energy, and mass) used in the experiment are recorded in the MySQL-based database automatically. Additionally, it is possible to determine the total beam-on time, beam-off time, and current status (beam-on-target or not) in the experiment at first sight.

In the future, we will attempt to improve system usability to entirely satisfy accelerator operators and users requirements.

References

1) M. Komiyama et al.: in progress.
2) A. Uchiyama et al.: in progress.

NISHINA RIBF water-cooling system 2013

T. Maie,[*1] K. Kusaka,[*1] M. Ohtake,[*1] Y. Watanabe,[*1] E. Ikezawa,[*1] M. Kase,[*1] M. Oshima,[*2] K. Kobayashi,[*3] and J. Shibata[*3]

1. Operation condition

In the fiscal year 2013, the Nishina and RIBF water-cooling installation was operated for five and three months, respectively. These operation periods correspond to the scheduled beam service time of RIBF, that is three months. In addition, Nishina's cooling installation was used not only for the full RIBF operation but also for the AVF standalone and AVF + RRC operations. During FY2013, there were no severe problems that caused beam service interruption for the Nishina and RIBF cooling water systems. In addition to the existing system, the new water-cooling system was built only for the rare-RI ring, and its test operations also started in FY2013.

2. Periodic maintenance

Routine maintenance works as listed below are performed during the scheduled summer and winter maintenance periods of the RIBF accelerators.

1) Cleaning the cooling towers

2) Checking and overhauling the cooling-water pumps

3) Checking the control system of the RIBF water-cooling system

4) Replacing some dated UPSs used for the control system of the RIBF water-cooling system

5) Cleaning the plate heat exchangers

6) Checking and overhauling the air compressor

7) Replacing some superannuated hoses, joints, and valves used in the system

8) Cleaning of the strainers and filters used in the deionized water production system

9) Extending the sensing-wires of the water leakage alarm to floors of new areas

3. Extension and improvement of the water-cooling system

A new beam transport line connecting the Intermediate-stage Ring Cyclotron (IRC) to the E5 experimental vault is now under construction , aiming at more efficient production of seaweed mutations induced by heavy-ion beams. Branches of cooling-water supply system were added to the existing system in order to supply cooling water to the magnets and other devices used in this IRC-E5 beam line. The construction of a new experimental apparatus, called SLOWRI, is also ongoing, and a new water-cooling system for SLOWRI has also been constructed. In addition, in order to raise the cooling capability of the RF amplifiers used in IRC and the Superconducting Ring Cyclotron (SRC), we plan to divide the existing supply system commonly used for IRC and SRC into two independent supply systems dedicated to each cyclotron. The present improvement will be effective for achieving high-power operation of the RF amplifiers.

4. Others

Because 30 years have passed since the construction of the Nishina water-cooling system, its deterioration is now remarkable. Performance degradation of the water-cooling system, especially in its temperature stability, is a possible source of the unstable behavior in the RIBF accelerator complex. Hence, the author recommended that the superannuated parts of the Nishina's water-cooling system should be updated as soon as possible.

References

1) T. Maie et al.: RIKEN Accel. Prog. Rep. 46 (2012).
2) M. Wada et al.: In this report.
3) Y. Yamaguchi et al.: In this report.

*1 RIKEN Nishina Center
*2 Nippon Kucho Service Co., Ltd
*3 SHI Accelerator Service Co., Ltd

Magnetic field clamp in direct plasma injection scheme†

M. Okamura,[*1,*2] T. Kanesue,[*1] T. Yamamoto,[*3] Y. Fuwa[*2*4]

A new set of vanes for the radio frequency quadrupole (RFQ) accelerator was commissioned using the highly charged iron beam in Brookhaven National Laboratory (BNL). To supply high intensity heavy ion beams from a laser ion source (LIS) to the RFQ, the direct plasma injection scheme (DPIS)[1,2] with a confinement solenoid was adopted. By in troducing the solenoid field, the plasma expanding angle can be controlled and the capability of LIS drastically enhanced[3]. In an LIS, the peak value of beam current is inversely proportional to the cube of the plasma drift distance. In order to stretch the ion beam pulse length, a longer plasma drift length is required, which simultaneously reduces the current amplitude. The solenoid can compensate this reduction effortlessly. however, the solenoid field causes another difficulty. The fringe field of the solenoid overwraps the ion extraction area where exist a static extraction electric field and focusing RF field. Generally, when we apply a magnetic field on a high-gradient electric field, discharges may be induced. To accelerate Fe^{14+} in the DPIS set up, the nozzle emits ions that have a static voltage gap of 33.3 kV overlaid by the fringe of the RFQ field of ±20.5 kV at 100 MHz. A magnetic field of few hundreds Gauss is present in the same space simultaneously. To investigate the fields, OPERA2D and 3D [4] were used.

Figure 1 shows an example of the electric static field simulation by OPERA2D. The nozzle is filled by the laser plasma, and ions are extracted by the field gradient between the vanes and nozzle. The plasma and the extracted ion beams move along the *z* axis from bottom to top in the figure. The plasma sheath is formed at the top of the nozzle. Another high electric field is induced towards the end wall of the RF cavity. When we apply a solenoid field, magnetic flux of the same direction as the electric field is induced. When discharges occur, electrons emitted from the vane surface are accelerated by the electric field towards the nozzle and guided by the magnetic field. This easily triggers further discharges. To prevent this, the copper-made end wall flange, which is a part of the cavity, was replaced by a plated iron flange. Another iron-made disk called barrier flange was also installed. The magnetic field was reduced to a few gauss, as shown in the simulation in Fig. 2. This modification enabled us to apply sufficient extraction voltage on the nozzle.

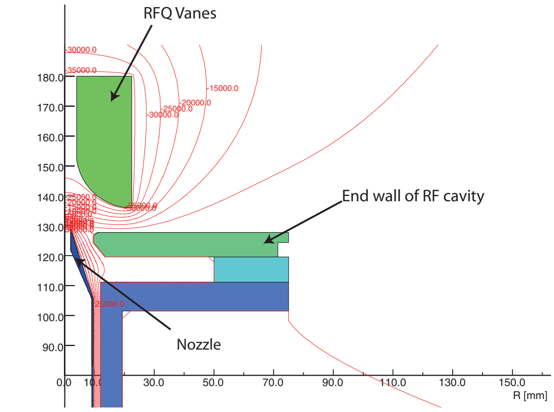

Figure 1 Static electric field simulation at the beam extraction region.

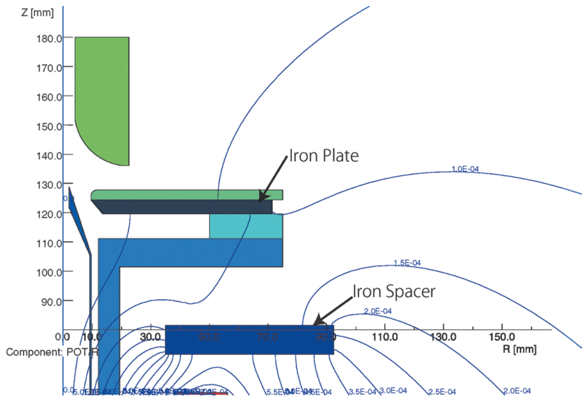

Figure 2 Magnetic field simulation with the field clamps.

Using the modified magnetic structure, we observed the accelerated iron beams at the downstream of the RFQ. The pulse width was about 1.5 μs on using a 1.0 m length solenoid filed at 105 G. The RF power was adjusted to maximize the current, which was about 3 mA. The result was obtained without beam analysis behind the RFQ, and the currents include all accelerated particles. The test was not intended to obtain maximum beam current; however, we could confirm that all the devices are working as intended.

References

1) M. Okamura, T. Takeuchi, R. A. Jameson, S. Kondrashev, H. Kashiwagi, K. Sakakibara, T. Kanesue, J. Tamura, and T. Hattori. Rev. Sci. Instrum. 79, 02B314 (2008)
2) T. Kanesue, J. Tamura, M. Okamura, Rev. Sci. Instrum. 79, 02B311 (2008)
3) M. Okamura, A. Adeyemi, T. Kanesue, J. Tamura, K. Kondo, and R. Dabrowski. Rev. Sci. Instrum. 81, 02A510 (2010)
4) OPERA-TOSCA, www.cobham.com

† Condensed from the article in REVIEW OF SCIENTIFIC INSTRUMENTS **85** 02B907 (2014)

*1 Collider Accelerator Department, BNL
*2 Riken-BNL Research Center
*3 Waseda University
*4 Kyoto University

Creation of cocktail beam from alloy target with laser†

S. Ikeda,[*1,*2] M. Romanelli,[*3] D. Cinquegrani,[*4] M. Sekine,[*1,*2] M. Kumaki,[*1,*5] Y. Fuwa,[*1,*6] N. Munemoto,[*2] T. Kanesue,[*7] Q. Jin,[*8] M. Okamura,[*7] and K. Horioka[*2]

Lasers can create many types of heavy ions from a solid target. Therefore, with the use of a laser and an alloy target, an ion beam composed of several elements can be easily created. The cocktail beam can be used to simulate cosmic rays in a laboratory. A recent paper reported the enhancement of a plasma flux by mixing a few different types of species with an original target.[1] However, the charge state distribution of each ion was not studied. To create a controllable cocktail beam, we investigated the charge state distributions of laser plasma from an alloy composed of Al and Fe.

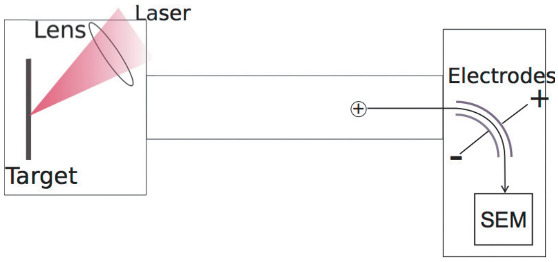

Fig. 1. Schematic of experimental setup.

Figure 1 shows a schematic of the experimental setup. We used a Nd:YAG laser (1064 nm, 6 ns, 615 mJ, and 7.9×10^{-3} cm^2 spot size) for ablation. As the targets, we used pure Al, Fe sheets, and an alloy of Al and Fe (AL-FE-01-F.ALLY) with Al:Fe = 10:19 (number). The chamber was evacuated to 5×10^{-4} Pa. The charge state distribution was measured through a time-of-flight (TOF) method using a cylindrical electrostatic ion energy analyzer. The device was composed of two coaxial electrodes, with a slit in front of the electrodes, and a secondary-electron-multiplier detector (SEM) placed at 3.3 m from the targets. Only the particles with a specific velocity and ratio of charge to mass could pass through the electrode. In addition, we could determine the velocity of particle reaching the SEM from the time of flight. Consequently, we could obtain the ratio of chare to mass and identify the ion.

Figure 2 shows the experimentally obtained results ratios of peak ion flux from the alloy target to the peak ion flux from the pure targets. As shown in the figure, they were Al 1^+: 0.5, Al 2^+: 0.68, Al 3^+: 0.58, Al 4^+: 0.27, Al 5^+: 0.27, Al 6^+: 0.65, Al 7^+: 0.84, Al 8^+: 0.89, Al 9^+: 0.34, Fe 1^+: 0.72, Fe 2^+: 0.60, Fe 3^+: 0.51, Fe 4^+: 0.65, Fe5^+: 3.5, Fe 6^+: 15. Total peaks up to a 4^+ charge state of the Al and Fe ions from the alloy targets were around half those from the pure targets. Hence, the ratios of the peak value were close to the stoichiometric ratio in the target material (Al:Fe =10:19). On the other hand, the ratios of highly charged states were larger than the composition ratio; in particular, Fe 5^+ and Fe 6^+ were much larger than those of the other ions.

The results showed that we can control the ratio of the flux of the Al to Fe ions, except for Fe 5^+ and Fe 6^+, as a function of composition ratio of alloy. A large increase in Fe 5^+ and Fe 6^+ indicates that we can substantially increase the charge state of a specific ion using an alloy.

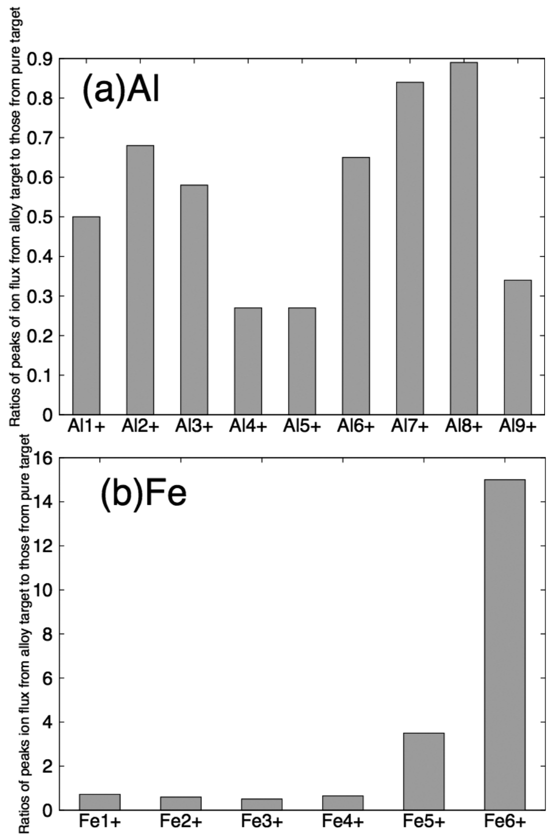

Fig. 2. Ratios of peaks value of Al and Fe ion flux from alloy target to those from pure targets

† Condensed from the article in Rev. Sci. Instrum. **85**, 2 (2014)

*1 RIKEN Nishina Center
*2 Department of Energy Science, Tokyo Institute of Technology
*3 School of Applied and Engineering physics, Cornell University
*4 Nuclear Engineering and Radiological Sciences, University of Michigan
*5 Department of Nuclear Engineering, Waseda University
*6 Department of Physics, Kyoto University
*7 Collider Accelerator Department, Brookhaven National Laboratory
*8 Institution of Modern Physics

References

1) A. Velyhan, J. Krasa, E.Krousky, L. Laska, D. Margarone, M.Pfeifer, K. Rohlena, J. Skala, J. Ulischmied, A. Lorusso, L. Velardi and V. Nassisi : 4th workshop on PPLA2009, Messina, Italy, 165, 6-10 (2010), p488-494

Interaction of plasmas in laser ion source with double laser system†

Y. Fuwa,[*1,*2] S. Ikeda, [*1,*3] M. Kumaki, [*1,*4] M. Sekine, [*1,*5] D. Cinquegrani,[*6] M. Romanelli,[*7] T. Kanesue,[*8] M. Okamura,[*8] and Y. Iwashita[*9]

A laser ion source can provide intense and low-emittance pulsed ion beams. For these advantages, various applications have been studied, such as DPIS (Direct Plasma Injection Scheme) to RFQ (Radio Frequency Quadrupole) Linac[1] and a seed-ion beam provider for the EBIS (Electron Beam Ion Source) at BNL (Brookhaven National Laboratory)[2, 3]. The laser ion source functions on a simple principle. Figure 1 shows the schematic layout of a laser ion source. Laser irradiation with an energy density above the target's ablation threshold generates plasma. This plasma drifts to an extracting electrode and an ion beam is formed. A change in the laser power density on the target can adjust the produced ions' charge states and the expanding velocity of plasma.

In conventional laser ion sources, a nano-second laser has been used. With single nano-second laser irradiation, thermal mechanisms are the dominant processes in plasma production and it results in a Maxwellian ion energy distribution. Since the plasma expands in three dimensions in the drift region from the target to the extracting electrode, an ion beam pulse width is proportional to the drift length L, and the peak ion beam current is inversely proportional to L^{-3}. Therefore, if we need a longer beam pulse width, the total peak current is steeply decreased.

A multi-pulse laser system may be used to elongate the ion beam pulse length or to intensify the beam current. To test the feasibility of these ideas, a double-pulse laser system was used in BNL.

Previous research showed that a multiple laser shot scheme is useful in extending the ion beam pulse length for a low-charge state mode. However, if the interval between the two laser is less than 10 μs, the observed current profile is not just sum of two laser plasmas[4]. In this research, we carried out a more detailed study for the case in which the interval between laser pulses was less than 10 μs, in order to understand this phenomenon.

In our experiment, each laser energy on the target was 560 mJ at maximum and the laser spot was an ellipse of height 3 mm and width 4 mm. The estimated laser power density of each laser shot was between 10^8 and 10^9 W/cm^2, and the induced charge states of ions were mostly single.

Ion current was measured using a Faraday cup. Two lasers were operated with various intervals of trigger timing range from 0.1 μs to 10 μs. In the measured current profile, a prominent peak that does not correspond to any single laser's current profile was observed. Figure 2 shows a typical result. This peak had a maximum peak current for the laser interval from 1 μs to 1.5 μs and the peak height was multiplied five times. This peak appears to have formed owing to the interaction between the second laser and the neutral vapor or particles produced by the first laser.

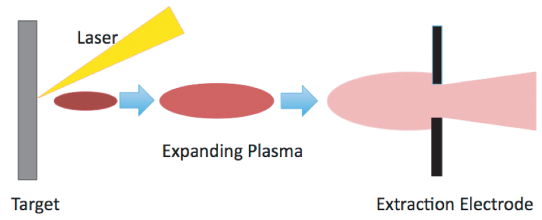

Fig. 1. Schematic layout of a laser ion source

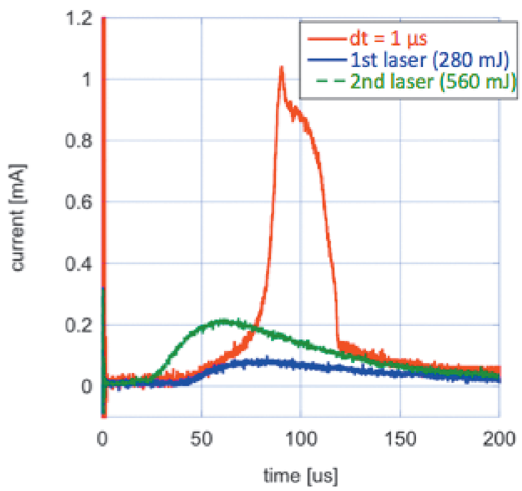

Fig. 2. Comparison of the measured ion current profile between single-laser plasma (blue and green plots) and double-laser (red plots).

† Condensed from the article in Rev. Sci. Instrum. **85**, 02B916 (2014).

*1 RIKEN Nishina Center
*2 Graduate School of Science, Kyoto University
*3 Interdisciplinary Graduate School of Science and Engineering, Tokyo Institute of Technology
*4 Research Institute for Science and Engineering, Waseda University
*5 Department of Nuclear Engineering, Tokyo Institute of Technology
*6 Nuclear Engineering and Radiological Science, University of Michigan
*7 School of Applied and Engineering Physics, Cornell University
*8 Collider-Accelerator Department, Brookhaven National Laboratory
*9 Institute for Chemical Research, Kyoto University

References

1) M. Okamura et al.: Rev. Sci. Instrum. **79**, 02B314 (2008).
2) J. G. Alessi et al.: Rev. Sci. Instrum. **81**, 02A509 (2010).
3) K. Kondo et al.: Rev. Sci. Instrum. **81**, 02B716 (2010).
4) M. Okamura et al.: Rev. Sci. Instrum. **83**, 02B308 (2012).

Control of plasma shape with pulsed solenoid on laser ion source

M. Sekine*1

A laser ion source (LIS) can supply high-current ion beams with solid target. However, the LIS typically forms a sifted-Maxwell-Boltzmann distribution in their current output. This distribution has a peaked output that does not provide constant current over the pulse length. The ability to shape the current output of LIS would increase its versatility as an ion source. In our experiments, we used pulsed magnetic fields to alter the shape of the current output and change the sifted-Maxwell- Boltzmann distribution that is typically produced.

In our experiments, we assembled the test setup shown on the right in Fig. 1. We used a 1064 nm wavelength Nd:YAG laser of Q-switch delay 250 μs and pulse energy 600mJ. Laser pulses were fired into the target chamber at an iron target. The target then ablated into a plasma consisting of +1 iron ions and electrons. The plasma moved past 20 cm of empty space into a 12 cm long solenoid, the pulsed solenoid. The plasma then passed through drift tubes and into a Faraday cup 3.3 m away and of apearture 10 mm. We could control the time for which the pulse was fired relative to the laser's firing time t_p, and the peak of the magnetic field B_{max}. The solenoid had turns 50, its length was 12 cm, and its radius was 44 mm.

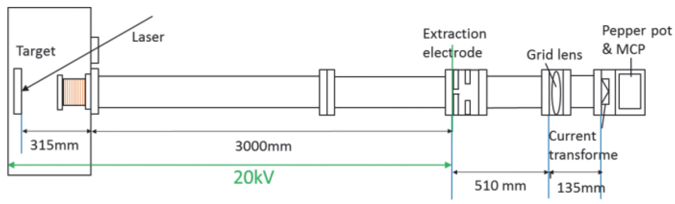

Fig. 1: Experimental setup

The pulsed solenoid was exposed to various magnetic fields ranging from 26 gauss to 510 gauss, as shown in Fig. 2. We altered the time for which the pulsed solenoid was fired from 1μs after the laser was fired to 20 μs after the laser was fired.

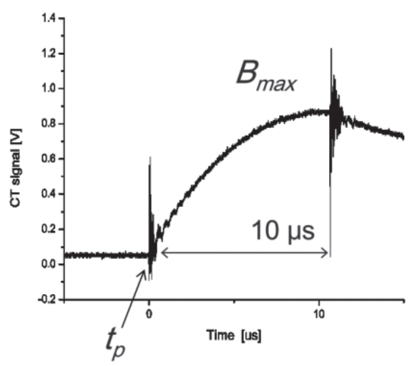

Fig. 2 Supplied magnetic shape by pulsed solenoid

*1 Department of Nuclear Engineering, Tokyo Institute of Technology

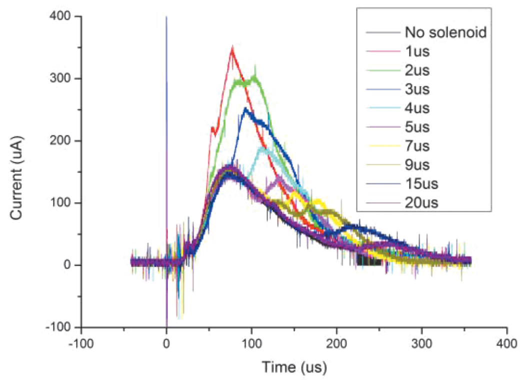

Fig. 3 current shapes for different delays

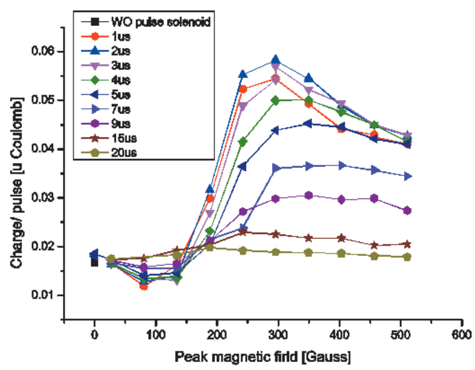

Fig. 4 Maximum current for different delays and magnetic fields

The obtained current shape for different delays is shown in Fig. 3. Magnetic pulses with delays ranging 15 μs and 20 μs range yielded results that appeared nearly identical to the results obtained without a pulsed solenoid. In all cases, the plasma followed the curvature of the pulsed solenoid's magnetic field lines into the pulsed solenoid. Fig. 4 shows the maximum current for different delays and magnetic fields in our experiments. Magnetic pulses with magnitudes lower than 188 gauss also had almost no effect on the shape of the plasma that we recorded. These results show that our technique can be effective in shaping the current of LIS.

We found that the solenoid field could change the beam shape. To control beam flexibility, we may need to control the pulsed field using multiple power supplies or multiple coils. Although the further studies are required, the pulsed solenoid is useful to control the beam current shape, which is a unique.

References

1)Kazumasa Takahashi, etc. AIP Conf. Proc. 1525, 241 (2013).

Analyses of the plasma generated by laser irradiation on sputtered target for determination of the target thickness used for plasma generation†

M. Kumaki,[*1,*2] Y. Fuwa,[*1,*3] S. Ikeda,[*1,*4] M. Sekine,[*1,*4] N.Munemoto,[*1,*4]
D. Cinquegrani,[*5] T. Kanesue,[*6] M. Okamura,[*1,*6] and M. Washio[*2]

A Laser Ion Source (LIS) has been developed at Brookhaven National Laboratory (BNL) [1)]. A focused high-power laser is used to generate plasmas containing highly charged ions from solid targets. For every laser shot, we provide a new surface because the irradiation creates a crater, and the second irradiation on the same spot causes beam instability. However, the depth of the target required to generate the plasma is not yet clear. We assumed that only the surface layers of the material were converted to the plasma, and knowledge of the surface layers to be converted to the plasma is necessary to understand the initial processes of laser-ablation plasma creation. We prepared a carbon-coated aluminum plate as a target. By analyzing the contents of the ablation plasma, the effective depth required to generate the laser plasma was investigated.

The target surface was divided into four segments, and each segment has different carbon coating thickness; the thicknesses were about 25 nm, 125 nm, 250 nm, and 500 nm. To generate ablation plasma, the segmented target with multi thickness coating was irradiated by a Nd:YAG 1064 nm focused laser (Brilliant Quantel, Energy: 728 ± 5 mJ (rms); Pulse Width: 6 ns). We analyzed the generated plasma using an electrostatic ion analyzer (EIA) and a secondary electron multiplier (SEM) to measure the current distribution of ions of each charge state [2)].

Figures 1 and 2 show the charge-state distribution of measured ions of the un-coated aluminum target and 500 nm carbon-sputtered target, respectively. These current distributions were reconstructed from the signals obtained using the SEM with the scanning EIA voltage. The C^{6+} could be clearly separated, but C^{5+} and C^{4+} were contained by the Al^{11+} and Al^{9+} signals.

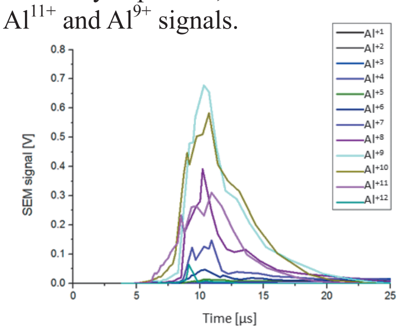

Fig. 1. Current distribution of each charge state (pure Al)

† Condensed from the article in proceedings of ICIS 2013
*1 RIKEN Nishina Center
*2 Cooperative Major in Nuclear Energy, Waseda University
*3 Department of Physics and Astronomy, Kyoto University
*4 Department of Energy Sciences, Tokyo Institute of Technology
*5 American Nuclear Society, University of Michigan
*6 Brookhaven National Laboratory

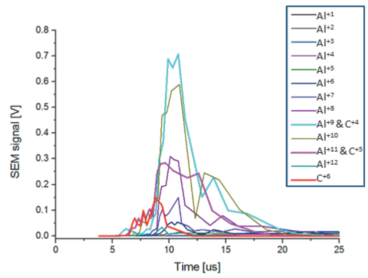

Fig. 2. Current distribution of each charge state (500nm)

Figure 2 indicates that the plasma was generated from the layers deeper than 500 nm because the Al ions still occupy the biggest fraction of the plasma contents. It is also noted that the C^{6+} ions appeared in the earliest part of the observed plasma, and the combination of Al^{+9} and C^{4+} produced the highest yield of ions at the peak position.

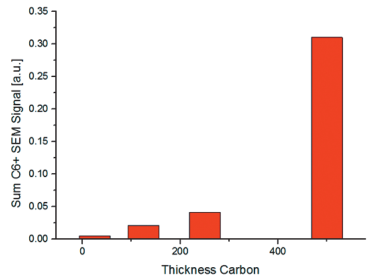

Fig. 3. Total C^{6+} particle number

Figure 3 shows the total yield of C^{6+} ions for each carbon-thickness case. The amount of C^{6+} ions was not linearly increased by the sputtered carbon thickness. The result implies that the surface layer has less contribution to form the ablation plasma. The layers from 250 nm to 500 nm were used more efficiently than the surface layer up to 250 nm depth to generate the plasma.

Using the carbon-coated aluminum target, the charge-state distribution was measured. We confirmed that the required thickness of the target for the plasma generation is more than 500 nm. We also found that the surface layer up to a few hundred nanometers in depth has less contribution than the deeper carbon layers. To investigate further, we need to prepare thicker carbon-sputtered targets thicker than 500 nm.

References

1) M. Okamura, et al., High current carbon beam production with DPIS, Rev. Sci. Inst. 77, 03B303, 2006.
2) S. Kondrashev, T. Kaneue, M. Okamura, K. Sakakibara Journal of applied physics 100,1 (2006)

9. Instrumentation

Ion-optical measurements using uranium primary beam with different charge states

H. Takeda,*1 T. Kubo,*1 N. Fukuda,*1 D. Kameda,*1 H. Suzuki,*1 N. Inabe,*1 and T. Ohnishi*1

Transfer matrix elements are essential for various ion-optical diagnoses, especially for trajectory reconstruction[1)] to improve the particle identification power of the BigRIPS. Thus, it is very important to measure the transfer matrix elements precisely to realize the best possible performance of the BigRIPS.

Primary beams of heavy ions such as uranium could be unique tools for measuring the transfer matrix elements because they are distributed into several charge states after passing through materials such as targets, degraders, and detectors. Such beams with different charge states have the following characteristics:

(1) Small widths at position x and angle a.
(2) Discrete peaks in magnetic rigidity (δ) spectrum. (Each peak is narrow and the peak position is definitely known.)
(3) Same velocity for all the charge states.

Some ion-optical parameters can be measured precisely by utilizing these characteristics. Indeed, we performed such measurements in 2007 during the first BigRIPS commissioning by using uranium beams.

Positions of a ^{238}U beam were measured with parallel plate avalanche counters (PPACs) installed in the BigRIPS foci F3, F5, and F7. The ion-optical system from F3 to F7 is a four-bend achromatic spectrometer with an intermediate dispersive focus F5. Figure 1 shows a spectrum of horizontal position x at F7 versus x at F5 of the ^{238}U beam after it passes through the PPACs at F3. Different charge states generated by the F3 PPACs had different positions at F5 due to the F3-F5 dispersion $(x|\delta)_{35}$, as indicated by red (dashed) lines. The measured result was 31.5 mm/%, which is consistent with the designed value of 31.7 mm/% calculated by COSY INFINITY. Charge state transition because of the PPACs occurred at F5 also. Events connected by each blue (solid) line in Fig. 1 have the same charge state between F5 and F7. They have very different positions at F5 but have the same magnetic rigidity. This situation allows measurement of the F5-F7 magnification $(x|x)_{57}$, which corresponds to the slope of the blue lines. The measured and COSY results were 1.069 and 1.080, respectively. Each green (dash-dot) line in Fig. 1 indicates events of the same charge state transition (ΔQ) at F5. The vertical distances of the green lines indicate the F5-F7 dispersion $(x|\delta)_{57}$. The measured and COSY results were -32.9 mm/% and -34.2 mm/%, respectively. Because the slope of the green lines is $(x|\delta)_{37}/(x|\delta)_{35}$, the green lines become horizontal due to the achromaticity of the F3-F7 optical system. Indeed, the F3-F7 dispersion of -1.1 mm/% deduced from the slope of the green lines was small.

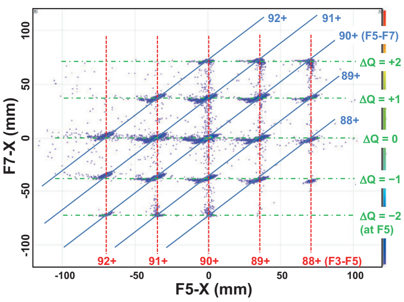

Fig. 1. Spectrum of F7-x vs. F5-x measured with a ^{238}U primary beam after it passes through PPACs at F3. Red and blue lines have information on the F3-F5 dispersion and the F5-F7 magnification, respectively. The F3-F7 dispersion and the F5-F7 dispersion can be deduced from green lines.

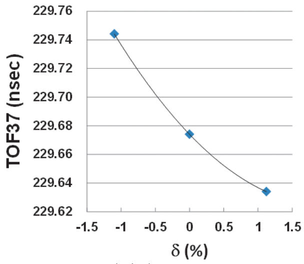

Fig. 2. Measurement of $(\ell|\delta)$ with primary beams. TOF from F3 to F7 was measured for each charge state by selecting the charge state with the F5 slits. The solid curve represents a quadratic fitting, and the slope corresponds to $(\ell|\delta)$.

Charge states are also useful to measure the $(\ell|\delta)$ parameter, where ℓ is a flight-path-length difference with respect to the central orbit. Because all the charge states have the same velocity, ℓ can easily be deduced by the time-of-flight (TOF) measurements. Figure 2 shows the TOFs from F3 to F7 as a function of δ measured by plastic scintillators at F3 and F7 with ^{238}U primary beam. Different charge states were generated by the F3 scintillator. BigRIPS was tuned so that the 90^+ charge state came at the center of F3, F5, and F7. 89^+, 90^+ and 91^+ charge states were selected individually with slits at the dispersive focus F5. The (TOF|δ) value was obtained as -0.0498 ns/% by a quadratic fitting, indicated by a solid curve in Fig. 2. Then, $(\ell|\delta)$ was estimated as -10.2 mm/%, while the COSY result was -6.53 mm/%.

*1 RIKEN Nishina Center

References

1) N. Fukuda et al.: Nucl. Instr. Meth. **B317**, 323 (2013).

Database of radioactive isotopes produced at the BigRIPS separator

Y. Shimizu,*[1] T. Kubo,*[1] N. Fukuda,*[1] N. Inabe,*[1] D. Kameda,*[1] H. Suzuki,*[1] H. Takeda,*[1] and K. Yoshida*[1]

We have been developing a database of radioactive isotopes (RI) produced at the BigRIPS separator[1]. The RI database entries include the following information:

- Production cross section
- Production yield
- Calculated value by LISE++ code[2]
- Experimental conditions
  - Primary beam
  - Target
  - Device settings
  - Magnetic rigidities
  - Measurement date
- Publication list
  - Title
  - Journal
  - First author
  - Journal digital object identifier (DOI)
  - Produced RI beam(s)
- Isomeric nucleus
  - Gamma ray energy
  - Half life

All entries are stored in a relational database that is based on Microsoft Access 2010.

The RI database is synchronized with a web site. The web site is coded using PHP. The top panel of Fig. 1 shows the web interface of the RI database. The RI database consists of nuclides, which includes RIs produced at the BigRIPS separator. RIs differentiated using red color text. The bottom panel of Fig. 1 shows an example, ^{128}Pd isotope. The production cross section and yield together with calculated value by LISE++ code are listed. Two journals about ^{128}Pd are also shown there. The detailed BigRIPS setting for ^{128}Pd can be accessed through the hyperlinked ID value, 80.

This web site also has a retrieval interface. This search allows a Boolean AND search over several categories (mass number A, atomic number Z, neutron number N, and so on). The results of search are listed on the user's browser. Furthermore, the cross section file for LISE++ and figures of production cross sections and production yields can be obtained from the search results.

The RI database and its web site assist on RIBF user to design RI beam experiments using the BigRIPS separator. Work on the system is currently ongoing and it is planned for practical implementation in the near future.

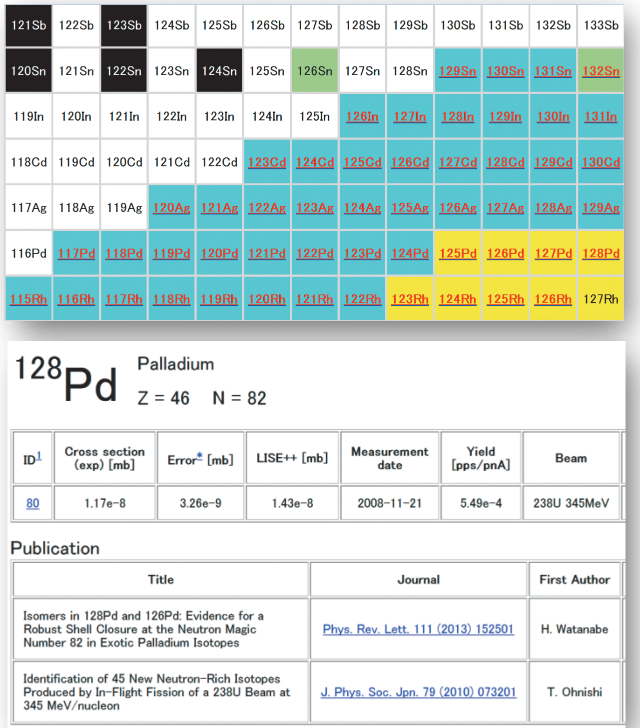

Fig.1. Web interface. The upper panel shows nuclides. Cyan, pale green, and yellow indicate nuclei, isomers, and new isotopes produced at the BigRIPS separator. The production cross section and production yield for the nucleus of interest can be accessed through the hyperlinked site. The lower panel shows an example of ^{128}Pd isotope. The production cross sections and production yields together with the BigRIPS setting are listed. Two journals about ^{128}Pd are also shown.

References

1) T. Kubo et al.: Nucl. Instr. and Meth. **B 204**, 97 (2003).
2) O.B. Tarasov and D. Bazin: LISE++ site, http://lise.nscl.edu, Michigan State University.

*1 RIKEN Nishina Center

Extraction of 3D field maps of magnetic multipoles from 2D surface measurements†

H. Takeda,*1 T. Kubo,*1 K. Kusaka,*1 H. Suzuki,*1 N. Inabe,*1 and J. A. Nolen*2

In large-aperture, short-length magnets with strong magnetic fields, such as superconducting triplet quadrupole (STQ)[1] magnets in the BigRIPS[2], the fringing field region is generally very large, and the shape and effective length of the magnetic field distribution change with the excitation current due to saturation of the iron core. Further, higher-order pseudo terms become relatively large in these magnets compared to those in small-aperture, long-length magnets because they originate from the changes of the magnetic field in the direction along the beam axis. It is indispensable to correctly extract pseudo quadrupole components as well as first-order quadrupole components from measured 3D field maps even for first-order ion-optical simulations.

Pseudo terms have the same azimuthal angle dependence as that for the leading term, such as $\cos 2\theta$ for a quadrupole, but have a higher-order radial dependence, such as r^3 rather than r for a quadrupole. At first glance, it appears that field map data measured at different radii are required to solve the r dependence. However, we present a practical numerical method that eliminates the need for this data. In this method, the measurement data for one radius of one component in the cylindrical coordinates, i.e., 2D field measurements on the surface of a cylinder, are sufficient to determine the full 3D magnetic multipole field in the cylinder. Using this novel method, we can extract the distributions along the beam axis for the coefficient of the first-order $2n$-pole component $b_{n,0}(z)$, which is the leading term of the $2n$-pole components in the multipole expansion of magnetic fields. Higher-order pseudo components $b_{n,m>0}(z)$ can be deduced from the leading term via recursion relations. The full 3D field map of $2n$-pole is completely described by these components. See the original paper† for details about the formalism and procedure of the method. Steps of the process of extraction of full 3D field maps of magnetic multipoles from 2D surface measurements are summarized in Fig. 1.

The proposed method was applied to large-aperture STQ magnets in the BigRIPS fragment separator at the RIKEN Nishina Center RI Beam Factory. Figure 2 shows the leading term $b_{2,0}(z)$ together with the pseudo terms $b_{2,1\cdots4}(z)$, which were obtained from the measurement result of $B_{\theta,2}$ at 100 A. Here $b_{2,1}$ is relatively large, showing that the pseudo terms cannot be ignored.

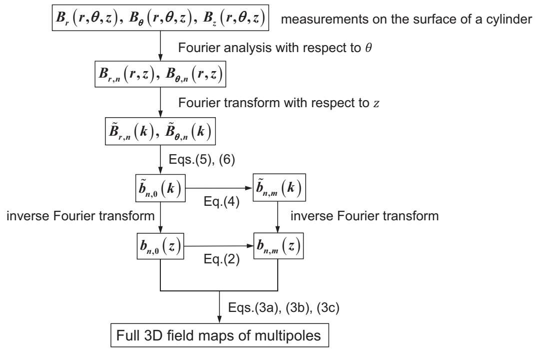

Fig. 1. Diagram of full 3D field map extraction from 2D surface measurements. The process of extracting the leading term $b_{n,0}(z)$ and the pseudo terms $b_{n,m}(z)$ from the 2D measurements of the surface of a cylinder are shown step-by-step. The equation numbers shown by the arrows indicate those used for the corresponding processes described in the original paper†.

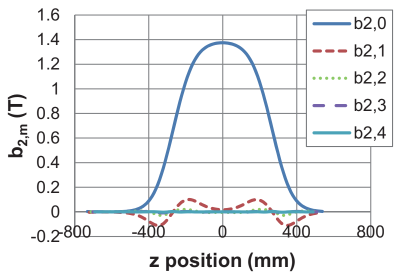

Fig. 2. Examples of $b_{2,0\cdots4}(z)$. $b_{2,0}$ was extracted from $B_{\theta,2}$, which was measured at a radius of 107 mm and at an excitation current of 100 A for a Q500 quadrupole magnet in STQ24. Pseudo terms $b_{2,1\cdots4}$ were calculated from $b_{2,0}$ with the differential recursion relation (2) in the original paper†.

The obtained $b_{2,0}(z)$ distributions were parametrized using the Enge functions to fit the fringe field shapes at all excitation current values, so that unmeasured values are interpolated. We implemented these parameters in the ion-optical calculation code COSY INFINITY[3] and realized a first-order calculation that incorporates the effect of large and varying fringe fields more accurately.

References
1) K. Kusaka et al.: IEEE Trans. Appl. Supercond. **14**, 310 (2004).
2) T. Kubo: Nucl. Instr. Meth. **B204**, 97 (2003).
3) K. Makino, M. Berz: Nucl. Instr. Meth. **A558**, 346 (2006).

† Condensed from the article in Nucl. Instr. Meth. **B317**, 798-809 (2013)
*1 RIKEN Nishina Center
*2 Argonne National Laboratory

Radiation damage of plastic scintillation counter

D. S. Ahn,[*1] N. Fukuda,[*1] T. Kubo,[*1] K. Yoshida,[*1] N. Inabe,[*1] H. Takeda,[*1] D. Kameda,[*1] H. Suzuki,[*1] Y. Shimizu,[*1] D. Murai,[*1,*2] Y. Yanagisawa,[*1] K. Kusaka,[*1] M. Ohtake,[*1] H. Sato,[*1] and Y. Sato[*1]

We studied radiation damage of a plastic scintillation counter in an isospin diffusion experiment (NP0709-RIBF42-01) using the BigRIPS separator[1)] of RIKEN RIBF. Heavy-ion cocktail beams (^{108}Sn,^{107}In,^{106}Cd) with high intensity (0.7∼1 MHz) were produced by projectile fragmentation of a ^{124}Xe beam at an energy of 345MeV/nucleon.

Figure 1 shows the experimental setup of the scintillation counter at F3 of the BigRIPS separator[1)]. To change the position of the scintillation counter after radiation damage, the movable ladder stage was designed to be remotely operated during the experiment. The EJ-212 scintillation counter[2)] was used in an isospin diffusion experiment with a high-intensity beam, and the position of the scintillation counter was changed after 50% damage, which was identified by checking the relative peak position of the light output.

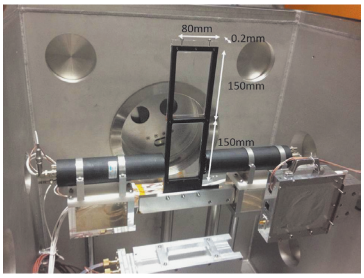

Fig. 1. Experimental setup of the scintillation counter

The radiation damage was reported with respect to the absorbed dose. The radiation absorbed dose was calculated using Eq. 1. A dose of one Gray is equivalent to a unit of energy [J] deposited in a kilogram of a substance.

$$Dose[Gy] = \frac{N_{beam} \cdot \Delta E \cdot R_{beam}}{volume \cdot density}, \tag{1}$$

where N_{beam} denotes beam intensity, ΔE is the energy loss of isotopes at the scintillation counter, and R_{beam} is the ratio of the number of events taking place in an exposed volume to the total number of events taking place at the scintillation counter. The volume is defined as $10{\times}6{\times}0.2\ mm^3$ after checking the beam spot size by the beam profile, and the density of the EJ-212 scintillator[2)] is 1.023 g/cc.

To define the exposed area, the concentrated irradiation region of the scintillation counter was determined using the beam profile shown in Fig. 2. Fig. 2(a) shows a scatter plot of beam profile and (b) and (c) show the x and y distributions of the beam, respectively. The

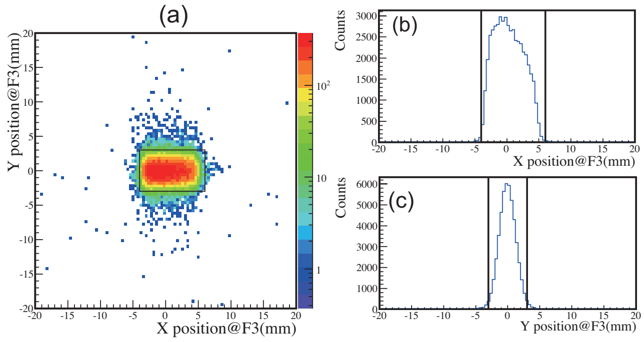

Fig. 2. Beam profile: (a) scatter plot of beam profile and (b), (c) shows x and y distribution of beam, respectively.

black square box in Fig. 2(a) indicates the defined exposed area, which is the concentrated irradiation region with 96.3% isotopes. The energy loss of isotopes at the scintillation counter was calculated with the ratio of the cocktail beams as ^{108}Sn:^{107}In:^{106}Cd = 2.51%: 74.0%: 22.86%. It is noteworthy that the ratio of isotopes rarely influences the energy loss calculation because the difference of energy loss between isotopes is only in the range of 2-3%.

Figure 3 shows the results of a relative light output as a function of the accumulated dose. The relative light output is defined as the relative peak position of the light output before and after irradiation. It is clearly seen that the light output decreases with the increase in the accumulated radiation dose at all the different positions, and a similar decreasing tendency is found at all the positions. The results indicate that about 50% radiation damage of the EJ-212 scintillation counter occurs at an accumulated dose of $12{\times}10^3$ Gy.

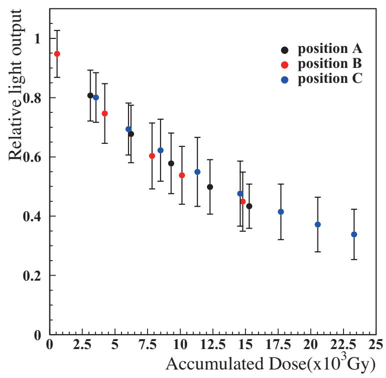

Fig. 3. Relative light output as a function of the accumulated dose: The different colors indicate different positions on the scintillation counter.

References
1) T. Kubo et al.: Prog. Theor. Exp. Phys. **2012**, 03C003
2) http://www.eljentechnology.com/

*1 RIKEN Nishina Center
*2 Department of Physics, Rikkyo University

Development of the fast interlock system at the BigRIPS separator

K. Yoshida,[*1] K. Tanaka, [*1] K. Kusaka, [*1] Y. Yanagisawa, [*1] and T. Kubo[*1]

A beam interlock system is particularly important for protecting beam line devices from the failure of magnets and other devices. The failure of beam line magnets can lead to the miss-steering of the beam and the beam might hit the beam pipe or other devices mounted along the beam line. If the beam power is high, such unexpected beam irradiation can cause serious damage to devices. The ^{238}U beam with an energy of 345 MeV/nucleon and the intensity of 1 particle μA can melt stainless steel even in 1 ms if it is focused at a diameter of 2 mm. In order to prevent damage, the beam should be stopped as soon as possible. The Beam Interlock System (BIS)[1,2] is installed at RIBF for this purpose. The BIS monitors the normal operation of devices and sends a beam-stop signal to the beam chopper installed at the exit of the ion source when a device fails. The beam chopper stops the beam within a few microseconds upon receiving a stop signal. The total response time of the existing BIS is only several milliseconds since the system uses Programmable Logic Unit (PLC) as signal processing. To cope with high-power beams extracted from the Superconducting Ring Cyclotron (SRC) at RIBF, the response time of the existing interlock system is currently inadequate and hence, a new interlock system with a fast response is developed.

A prototype of the fast interlock system with 4 analog inputs and 8 logic inputs has been developed to evaluate the speed of the response. In order to achieve a fast response time, a compact RIO system (cRIO), cRIO-9075 of National Instrument Co. Ltd. is utilized as the processing unit. The cRIO consists of a CPU and a field-programmable gate array (FPGA) that are closely related to each other. The FPGA allows a fast response between the input and output and the CPU provides versatile control of the unit. A fast sampling ADC module, NI-9222 with 500 k sample/sec, is used for analog inputs, and fast digital I/O modules, NI-9401 with 100 ns propagation delay, are used for logical inputs and outputs. Fig. 1 shows the block diagram of the interlock logic. As seen in the figure, an analog input is digitized in the ADC and compared with pre-defined upper and lower limits; the fault output is produced if the digitized value exceeds those limits. The fault output is then masked with an enable/disable flag and latched in a Set-Reset flip-flop in order to hold a fault situation. A logic input is exclusive-or'ed with a polarity flag and latched in the same way. The values in the flip-flops are or'ed together to produce a failure output. These control logics are stored in the FPGA of the cRIO and executed at a fast speed. The CPU of the cRIO is used as the interface to the comprehensive control system of the BigRIPS[3] that utilizes EPICS[4] as the base. Statuses of faults and digitized values of the analog inputs are monitored by the control system of the BigRIPS. The upper and lower limit values of the analog input and input masks are dynamically set from the control system. The programming of cRIO is performed in a LabVIEW developer environment.

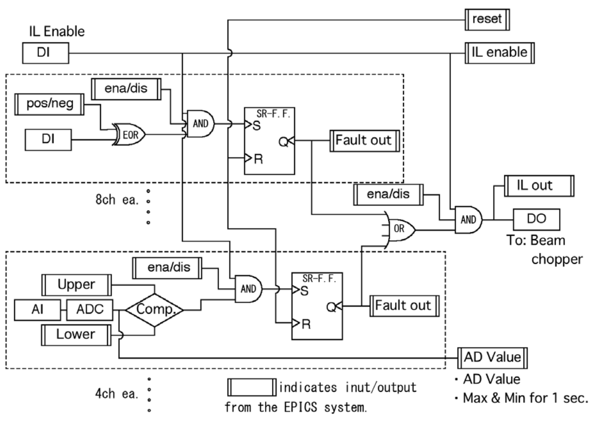

Fig. 1 Logic diagram of the prototype of the fast interlock system.

The response speed of the prototype of the fast interlock system was measured with a test signal. A step signal was inputted to the logical and analog input and the time delay between the input and output signals was measured. The response times are 0.2 μs for logical inputs and 5 μs for analog inputs. These are sufficiently fast for the fast interlock system. The prototype was also examined with the actual current monitor signal of the power supply of the first dipole magnet at BigRIPS. The current monitor signal was connected to one of the analog inputs and the digitized value was monitored. The digitized value was fluctuated within 0.25% due to the noise that appeared in the monitor signal. This is similar to the value compared with the hardware comparator built in the power supply to detect the output current drift.

Based on the successful test results on the prototype, the fast interlock system of the BigRIPS has been designed to monitor the analog and logical signals from power supplies of the 34 magnets placed at the primary beam line and the BigRIPS where a high-power primary beam is transported. The system consists of 4 cRIOs and sends the beam stop signal to the beam chopper as well as BIS. The fabrication of the system will be completed by the end of March 2014 and the system is expected to be operational by the end of July 2014.

References

1) M. Komiyama, M. Fujimaki, and M. Kase, Proc. of 2nd Annu. Meet. of Particle Accelerator Society of Japan and 30th Linear Accelerator Meet. In Japan, Tosu, 2005-7 (2005),p. 615.
2) M. Komiyama, et. al, RIKEN Accel. Prog. Rep., 41 (2008) 242.
3) K. Yoshida, RIKEN Accel. Prog. Rep., 44 (2011) 131 and references there in.
4) http://www.aps.anl.gov/epics/.

*1 RIKEN Nishina Center

Energy resolution of a gas ionization chamber for high-energy heavy ions†

Y. Sato,*1 A. Taketani,*1 N. Fukuda,*1 H. Takeda,*1 D. Kameda,*1 H. Suzuki,*1 Y. Shimizu,*1 D. Nishimura,*1,*2 M. Fukuda,*1,*3 N. Inabe,*1 H. Murakami,*1 K. Yoshida,*1 and T. Kubo*1

Gas ionization chambers are used for the BigRIPS spectrometer to identify the atomic number of the flight particles by using the energy deposition.[1,2] Since the key parameter of the detector in this application is its energy resolution for heavy ions, an understanding of the energy resolution behavior of high-energy heavy ions is essential in discussing the particle identification performance. We report the energy resolution of the gas ionization chamber for heavy ions from the atomic number Z=31 up to Z=52 at low counting rates below 1 kcps, and which have an energy of nearly 340 MeV/nucleon.

The ionization chamber is installed at the F7 focal plane of the BigRIPS[1] spectrometer, which is operated using a counting gas mixture of Ar(90%)+CH_4(10%) at approximately 760 Torr. The effective gas thickness of 48 cm is divided into six segments, and energy spectra can be obtained for every 8 cm of gas thickness.[2] The dependence of energy resolution on the gas thickness is plotted in Fig. 1. As an example, we show the analysis results for ions Z=38 and Z=51. With the horizontal axis scaled as the inverse-square-root of the gas thickness, $L^{-1/2}$, a linear relationship is observed, as shown by the solid linear-fitting result lines; this observation is in good agreement with the experimental data. We conclude that the energy resolution is linearly dependent on $L^{-1/2}$. These results indicate that the energy resolution, $\Omega/\Delta E$, is expressed by statistical fluctuations in the energy loss, i.e., the energy straggling of heavy ions, Ω, and the mean energy deposition within the gas, ΔE, which are explained by the Bohr expression ($\Omega \propto ZL^{1/2}$) and the Bethe-Bloch formula ($\Delta E \propto Z^2L$), respectively.[3,4]

In Fig. 2, we plot the energy resolution as a function of the heavy ion atomic number for the cases of L = 24 cm ≡ L_1 (open circles) and L = 48 cm ≡ L_2 (solid circles). According to the Bohr expression Ω is also proportional to the incident ion atomic number, Z. Therefore, the energy resolution, $\Omega/\Delta E$, should be proportional to Z^{-1} because $\Delta E \propto Z^2$. The solid and dotted lines show the fitting results of CZ^{-1}, where C is the fitting parameter. The best-fit parameters were found to be C_1 = 61.2±1.2 and C_2 = 43.5±1.0 for L_1 and L_2, respectively. The ratio of these values is C_1/C_2 = 1.41±0.04, which shows excellent agreement with the value of $(L_1/L_2)^{-1/2} \approx 1.41$. This result is consistent with the above discussion, $\Omega/\Delta E \propto L^{-1/2}$.

In future works, the experimental energy resolution data for heavier ions up to uranium (Z=92) are required to discuss the performance of the ionization chamber for the identification of these heavy ions. In addition, the performance at high counting rates up to 1 Mcps is still unclear and requires further investigation.

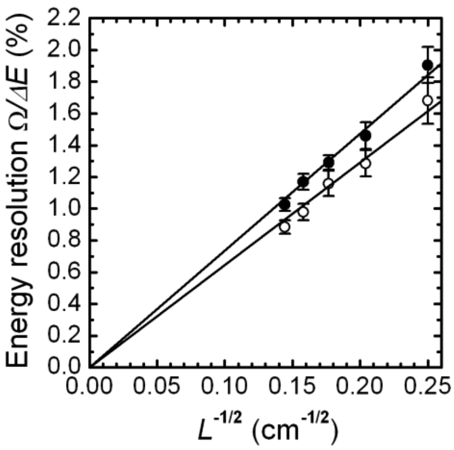

Fig. 1. Dependence of energy resolution on gas thickness obtained for heavy ions Z=38 (solid circles) and Z=51 (open circles). The solid lines are the results of linear fitting, which show the linear dependence on $L^{-1/2}$.

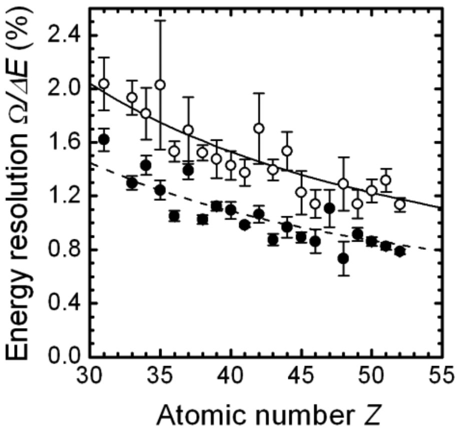

Fig. 2. Energy resolution as a function of the atomic number of fragment heavy ions produced from the in-flight fission of ^{238}U at 345 MeV/nucleon. Open and solid circles represent the cases with L=24 cm and L=48 cm, respectively. The solid and dotted lines are the results of the fitting of Z^{-1}.

References
1) T. Kubo, et al.: Prog. Theor. Exp. Phys. (2012) 03C003.
2) H. Otsu, et al.: RIKEN Accel., Prog. Rep. 42 (2009) 163.
3) N. Bohr: Philos. Mag. 30 (1915) 581.
4) G. F. Knoll: Radiation Detection and Measurement (Wiley, New York, 2000) 3rd ed., Chap. 2.

† Condensed from the article in Jpn. J. Appl. Phys. **53**, 016401 (2014)
*1 RIKEN Nishina Center
*2 Faculty of Science and Technology, Tokyo University of Science
*3 Department of Physics, Osaka University

Development of intense ^{22}Na beam for application to wear diagnostics

A.Yoshida,[*1] T. Kambara,[*1] R. Uemoto,[*2] H. Uno,[*2] H. Yamaguchi,[*3] T. Nakao,[*3] D. Kahl,[*3] and S. Kubono[*3]

The industrial cooperation team in RIKEN and SHIEI Ltd. are developing a method for application to the wear diagnostics of industrial materials using RI beams as tracers. RI nuclei are implanted in the near surface of machine parts within a depth of 100 μm, and the wear-loss of the near surface is evaluated by the decrease in the measured radioactivity. Continuous γ-ray detection from outside the machine enables real-time diagnostics of wear in running machines. For this purpose, we studied intense RI beams of ^{22}Na ($T_{1/2}$ = 2.6y) at the RIPS separator with an energy of 26.6 MeV/u[1)], and ^{7}Be ($T_{1/2}$= 53d) at the CRIB separator with an energy of 4.1 MeV/u [2,3)]. From the point of view of beam cost and beam-time flexibility, the low-energy RI beam production at CRIB using the AVF cyclotron independently is favorable. Then, we studied a low energy ^{22}Na beam production using CRIB.

The ^{22}Na beam was produced via the p(^{22}Ne,^{22}Na)n reaction. A primary beam of $^{22}Ne^{7+}$ with an energy of 6.1 MeV/u and intensity of 0.3 pμA was introduced to the cryogenic gas target[4)]. The H_2 gas at a pressure of 400 Torr was cooled to 90 K and was circulated to the gas cell at a rate of 17 slm. The primary beam was focused on a Havar foil placed at the entrance of the gas cell with a spot size of diameter 1 mm. The target was stable during this experiment. The produced ^{22}Na beam was introduced to the F2 focal plane without a degrader foil at F1. Contaminant nuclei of $^{19}F^{9+}$ (stable) and $^{22}Ne^{10+}$ (primary beam) were then observed (Fig.1). The ^{22}Na beam had two components with different charge states: q=10+ and 11+. Because the $^{22}Na^{10+}$ component had large $^{22}Ne^{10+}$ contamination, we have investigated the optimum magnetic rigidity for the $^{22}Na^{11+}$ beam.

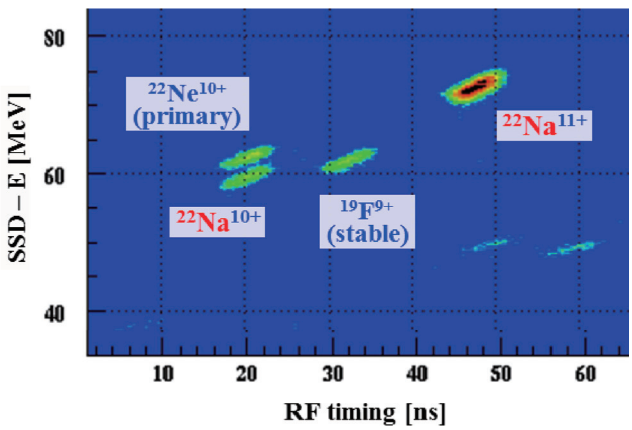

Fig. 1 Contaminant nuclei at optimum magnetic rigidity for the $^{22}Na^{11+}$ beam.

The magnetic rigidity of the CRIB separator was scanned in the range of 0.53 – 0.59 Tm (Fig.2). At the optimum condition of 0.5535 Tm, the energy and radius of the $^{22}Na^{11+}$ beam were 81.2 MeV (3.7 MeV/u) and σ = 1.6 mm, respectively, with a momentum slit of ± 3.1% (± 50 mm) at F1. The ^{22}Na beam was 78 % in purity. The intensity was 3.1×10^{7} pps and was obtained by the following γ-ray measurement. To investigate the implantation-depth profile of ^{22}Na, a stack of 2-μm-thick aluminum foils with 16 mm diameter were irradiated. After irradiation, the stack was disassembled and the intensity of the γ ray (Eγ = 1274 keV) was measured using a Ge detector. From the obtained profile, ^{22}Na was implanted in aluminum at 38 ± 6 μm with a total approximate activity rate of 0.9 kBq/1h irradiation.

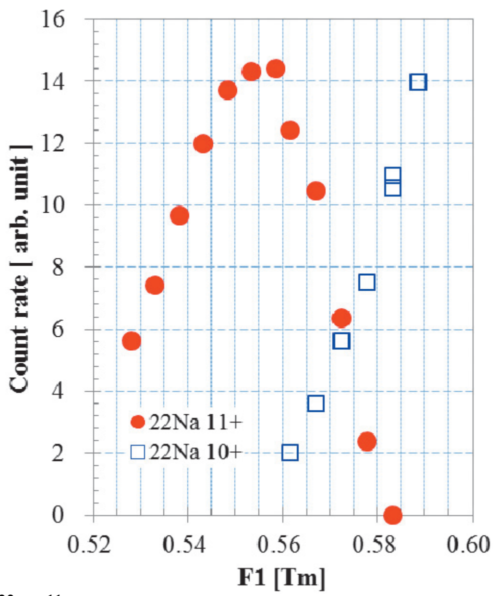

Fig. 2 $^{22}Na^{11+}$ beam intensity dependence on the magnetic rigidity.

The total activation rate of $^{22}Na^{11+}$ beam using RIPS was 5 kBq/1h irradiation[1)], which is five times greater than the intensity of CRIB. However, this difference is nearly compensated with the difference in beam production cost between RIPS+RRC and CRIB+AVF.

References

1) T. Kambara et al.: AIP Conf. Proc. ***1412*** (2011) 423−429.
2) A.Yoshida, T.Kambara, R.Uemoto et.al.: Nucl. Instrum. Methods, Sect. ***B 317***, 785-788(2013).
3) A.Yoshida et. al.: RIKEN Accel. Prog. Rep. ***46***, 252 (2013).
4) H. Yamaguchi et al.: Nucl. Instrum. Methods, Sect. ***A 589***, 150−156 (2008).

[*1] RIKEN Nishina Center
[*2] S.H.I. Examination and Inspection (SHIEI) Ltd., http://www.shiei.co.jp/
[*3] Center for Nuclear Study (CNS), University of Tokyo.

Development of ion-optics mode for the SAMURAI beam line

H. Suzuki,[*1] T. Kubo,[*1] H. Takeda,[*1] H. Sato,[*1] N. Inabe,[*1] N. Fukuda,[*1] D. Kameda,[*1] and Y. Shimizu[*1]

We have developed an ion-optical mode for the SAMURAI beam line, which connects the SAMURAI spectrometer[1)] to the BigRIPS separator[2)]. The schematic view is shown in Fig. 4 of Kobayashi *et al.* (2013)[1)]. There are four standard focal planes: F7, which is the last focal plane of the BigRIPS separator; F8; F12; and F13, which is the reaction target position of the SAMURAI spectrometer. There are two STQ magnets[3)] between F7 and F8, and two between F8 and F12, while only one STQ is located between F12 and F13. The beam shutter between F7 and F8 and the D7 dipole magnet for the ZeroDegree spectrometer restrict the space in the vertical direction in this beam line. To diagnose the beam emittance, we use the PPAC detectors at F7, F8, and F12, and beam drift chambers at F13.

In order to fabricate the beam optics of the SAMURAI beam line, two problems need to be resolved. First, there is only one STQ between F12 and F13; therefore, stronger magnetic fields are required for focusing the beam at both F12 and F13. Second, the beam envelope inside the D7 magnet in the vertical direction needs to be made thin, because the gap in D7 is ±61 mm. To solve these problems, we focus the beam inside the D7 magnet instead of on F8 and F12. At F8 and F12, the beam is set to parallel. This makes it easier to diagnose the beam optics using the PPAC detectors and adjust the magnetic field of each quadrupole magnet. The magnification from F7 to the focal point inside the D7 magnet in the vertical direction is set to be around 2 to reduce the angular magnification and make the beam envelope thinner. The beam trajectories for the SAMURAI beam line are shown in Fig. 1. The position and angular spreads at F7 are set to be ±6 mm and ±10 mrad, respectively, in both the horizontal and vertical directions, which are the typical root-mean-square (r.m.s.) values for the fragments produced from light projectiles such as ^{18}O and ^{48}Ca. Table 1 summarizes the transfer matrices from F7 to F8, F12, and F13. The matrices in the horizontal direction $\begin{pmatrix} (x|x) & (x|a) \\ (a|x) & (a|a) \end{pmatrix}$ and those in the vertical direction $\begin{pmatrix} (y|y) & (y|b) \\ (b|y) & (b|b) \end{pmatrix}$ are shown in the left and right columns, respectively.

From May 2012, we have used this ion-optics mode for transporting the secondary beams to the SAMURAI spectrometer. The typical r.m.s. spot size at F13 was around 10-15 mm, when the r.m.s. spot size of F7 was 6 mm. In such a case, the transmission efficiency from F7 to F13 is around 90%.

*1 RIKEN Nishina Center

Table 1. Transfer matrices from F7 to F8, F12, and F13. The left and right columns show matrices in the horizontal and vertical directions, respectively.

beam line	horizontal	vertical
F7-F8	$\begin{pmatrix} -1.09 & 4.28 \\ -0.23 & 0.00 \end{pmatrix}$	$\begin{pmatrix} -2.80 & 2.20 \\ -0.45 & 0.00 \end{pmatrix}$
F7-F12	$\begin{pmatrix} 0.76 & -2.99 \\ 0.33 & 0.00 \end{pmatrix}$	$\begin{pmatrix} 0.85 & -2.20 \\ 0.45 & 0.00 \end{pmatrix}$
F7-F13	$\begin{pmatrix} 1.86 & 0.00 \\ -0.43 & 0.54 \end{pmatrix}$	$\begin{pmatrix} 2.16 & 0.00 \\ -0.66 & 0.46 \end{pmatrix}$

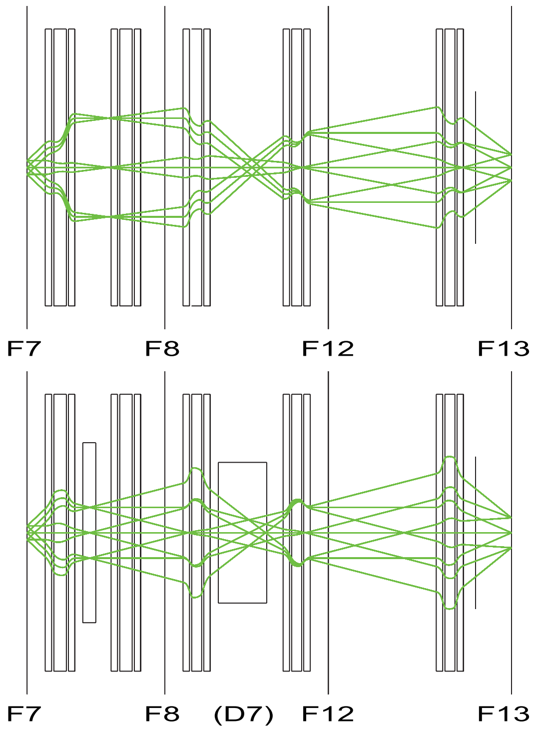

Fig. 1. Beam trajectories from F7 to F13. F13 is the reaction target position of SAMURAI. Top and bottom panels show the trajectories in the horizontal and vertical directions, respectively. The position and angular spreads at F7 are ±6 mm and ±10 mrad, respectively, in both the directions. The box triplet shows each STQ magnet.

References
1) T. Kobayashi et al. : Nucl. Instrum. Meth. Phys. Res., **B 317**, 294 (2013).
2) T. Kubo: Nucl. Instrum. Meth. Phys. Res., **B 204**, 97 (2003).
3) K. Kusaka et al.: IEEE Trans. Appl. Supercond., **14**, 310 (2004).

Operational status of the superconducting SAMURAI magnet

H. Sato,[*1] K. Kusaka,[*1] M. Ohtake,[*1] Y. Shimizu,[*1] K. Yoneda,[*1] and T. Kubo[*1]

Operation of the superconducting SAMURAI magnet was started in June 2011, and experiments using the SAMURAI spectrometer was started in March 2012.[1)] So far, a commissioning and five experiments have been performed.[2–6)] During this period, we had maintained the operation of the cryogenic system of the magnet and overhauled the cryocoolers in October 2012.[7)] However, the operation policy for the magnet was changed from “continuous cooling” to “irregular cooling” in order to save the operation time of the cryocoolers, where “irregular cooling” means that the magnet will be cooled down for every SAMURAI campaign experiments and warmed up after the experiments. Thus, the operation of the magnet was stopped temporarily in September 2013. In this report, the alteration in the temperature of the magnet when it was stopped is shown.

The upper and lower superconducting coils are installed in two separate cryostats and cooled by the liquid helium bath cooling method.[7,8)] Each cryostat is equipped with one 4-K GM/JT cryocooler, which recondenses the evaporating liquid helium. The 20-K as well as 80-K thermal shields are cooled by two GM cryocoolers. Each cryostat is equipped with another GM cryocooler that cools the power leads made by a high-Tc superconductor.

The warming-up procedure was started by stopping these cryocoolers. In order to keep the recovery volume of the liquid helium within the load limit of the recovery compressor at RNC Liquid Helium Plant, the warming-up timing of the lower cryostat was delayed. As a result, the liquid helium was fully recovered, 215 L in 37 h and 227 L in 34 h from the upper and lower cryostats, respectively.

The temperature rise at the major points in the cryostats is shown in Fig. 1. In the figure, the structure is seen when the temperature of the coil vessels exceeded 77 K (Fig. 1(a)). This is because of the heat exchange between the coil vessels and other parts, which happened when the condensed residual atoms such as nitrogen at the outer wall of the coil vessels evaporated into the vacuum layer of the cryostat.

Figure 1(a) shows the temperature of the coil vessel, which corresponds to the cold mass of the cryostat. The cold-mass weight of each cryostat is about 3.5 ton, and it took about 48 and 41 days to reach room temperature for the upper and lower cryostats, respectively. The speed of the temperature rise for the lower cryostat was faster than that for the upper cryostat at all points, as shown in Fig. 1. This is assumed to be due to the difference of the heat load, which results from the difference of the length of the chimney pipe between the liquid helium reservoir vessel and the coil part of the cryostat (see Fig. 1 in Sato et al.[7)]).

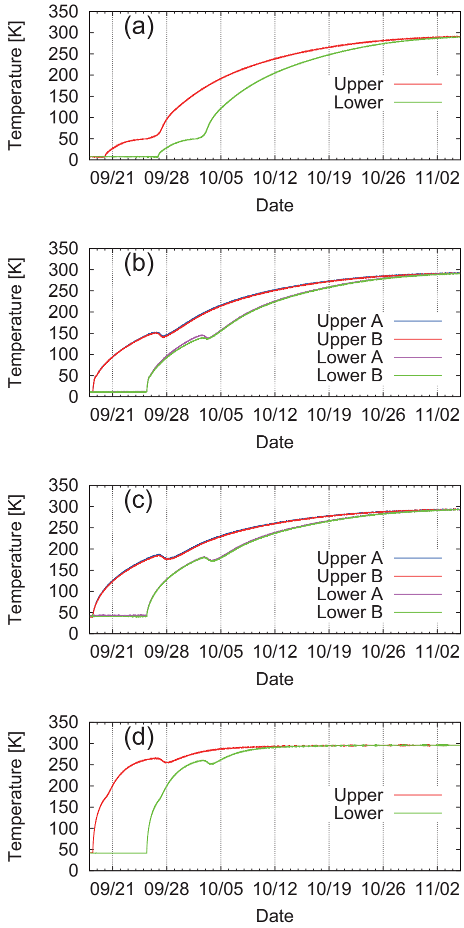

Fig. 1. Temperature rise at each point: (a) coil vessels, (b) 20-K cryocoolers, (c) 80-K cryocoolers, and (d) cryocoolers for power leads. The cryocoolers of the upper and lower cryostats were stopped on 9/18 and 9/25.

References
1) K. Yoneda et al.: RIKEN Accl. Prog. Rep. **45**, i (2012).
2) T. Kobayashi et al.: Nucl. Instrum. Meth. B **317**, 294 (2013).
3) K. Yoneda et al.: RIKEN Accl. Prog. Rep. **46**, 145 (2013).
4) Y. Kondo et al.: RIKEN Accl. Prog. Rep. **46**, 6 (2013).
5) T. Nakamura et al.: RIKEN Accl. Prog. Rep. **46**, 7 (2013).
6) H. Otsu et al.: In this report.
7) H. Sato et al.: RIKEN Accl. Prog. Rep. **46**, 147 (2013).
8) H. Sato et al.: IEEE Trans. Appl. Supercond. **23**, 4500308 (2013).

*1 RIKEN Nishina Center

Vacuum system for the SAMURAI spectrometer†

Y. Shimizu,*1 H. Otsu,*1 T. Kobayashi,*1,*2 T. Kubo,*1 T. Motobayashi,*1 H. Sato,*1 and K. Yoneda*1

The first commissioning experiment of the SAMURAI spectrometer[1] and its beam line was performed in March, 2012. The vacuum system for the SAMURAI spectrometer includes its beam line and the SAMURAI vacuum chamber with the windows for detecting neutrons and charged particles.

The window for neutrons is made of 3 mm-thick stainless steel designed in the shape of a partial cylinder to support itself against atmospheric pressure. The deflection of the window caused by the pressure difference and the induced stress are calculated using the general purpose finite element analysis program code ANSYS[2]. Figure 1 shows the ANSYS calculation result. The calculated displacement by the atmospheric pressure at the central region and the maximum induced stress are 0.17 mm and 44 MPa, respectively. It should be noted that the latter is smaller than 1/10 of the tensile strength. This window is achieved a safety factor of 12.

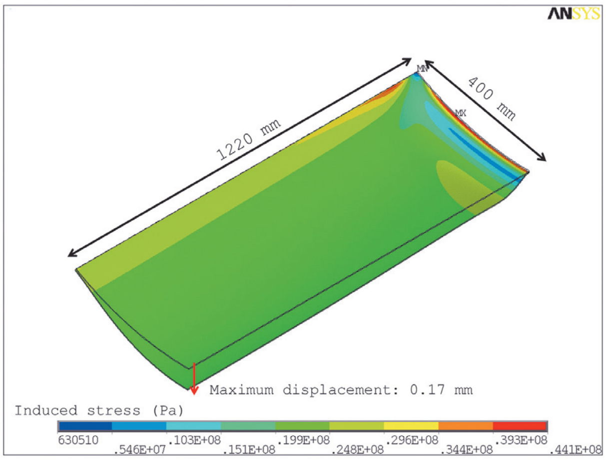

Fig. 1. ANSYS calculation result for the shape of a partial cylinder with a thickness of 3 mm.

The window for charged particles was composed of a combination of Kevlar and Mylar with thicknesses of 280 and 75 μm, respectively. The Kevlar and Mylar were glued with an Araldite® to the top of the window frame, which is made of SUS304. The open geometry of the exit window of the vacuum chamber is 2800 × 800 mm^2, while a 2800 × 400 mm^2 window was used in the commissioning experiment. This was a result of tradeoff between the experimental requirement and the safety and risk management for the breaking of the window. The deflection and stress for the Kevlar textile are calculated by ANSYS. Since the elastic properties of the Kevlar textile are not known, they are determined to reproduce the vacuum test[3]. In order to reduce the displacement and elongation of the Kevlar textile, we performed a calculation considering a flexure of 193 mm in the initial condition. The result is shown in Fig. 2. The displacement and elongation of the Kevlar textile are 73 mm and 6.3%, respectively.

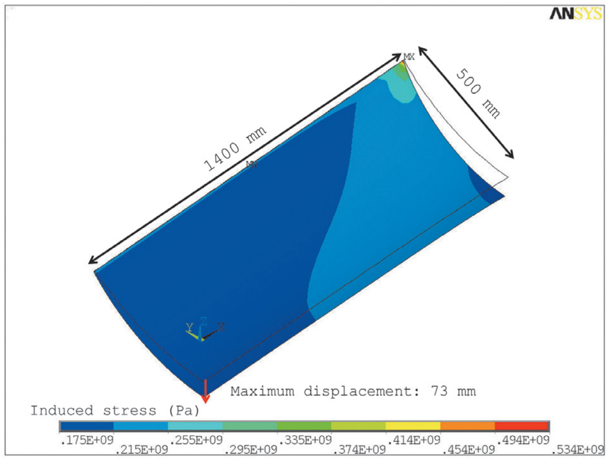

Fig. 2. ANSYS calculation result for Kevlar textile with a flexure of 193 mm in the initial condition.

In order to have a flexure of 40 mm around the center region in the initial condition, both sides of the Kevlar and Mylar were slacked by about 5 mm. The flexure of 40 mm was determined to be the maximum flexure without inducing wrinkles in the Mylar at the corners. The maximum deflection around the center region was estimated to be approximately 60 mm. This indicates that the Mylar elongated about 3.2% due to air pressure, which was 1/3 smaller than that of the tensile elongation at the break. Since this window is achieved a safety factor of only 2.8, the window materials have to be replaced every year for reasons of safety.

The deflections of these windows by visual observation were consistent with the ANSYS calculation results. The pressure in the SAMURAI vacuum chamber was successfully maintained at a few Pa during the commissioning experiment without any problems caused by the windows.

References
1) Y. Shimizu *et al.*, J. Phys.: Conf. Ser. **312**, 052022 (2011).
2) URL: http://www.ansys.com/
3) Y. Shimizu *et al.*, RIKEN Accel. Prog. Rep. **44**, 154 (2011).

† Condensed from the article in Nucl. Instr. Meth. **B 317**, 739 (2013)
*1 RIKEN Nishina Center
*2 Department of Physics, Tohoku University

Full-size partition window for the SAMURAI spectrometer

Y. Shimizu,[*1] H. Otsu,[*1] T. Kobayashi,[*1,*2] T. Kubo,[*1] T. Motobayashi,[*1] H. Sato,[*1] and K. Yoneda[*1]

For future SAMURAI experiments measuring coincident heavy fragments and light charged particles, light charged particles are fully spread on the exit window of the SAMURAI spectrometer. In order to detect light charged particles efficiently, the vacuum partition window should have a maximum vertical size of 800 mm. In this report, the design and development of a full-size partition window for the SAMURAI spectrometer are described.

The window material deflects penetrating particles by multiple scattering and causes their energy fluctuation by energy loss struggling. At the same time, it is necessary to ensure that the material is strong enough to hold the vacuum. The vacuum partition is of the combination of a Kevlar textile for tensile strength support and a Mylar foil for vacuum partitioning. The thicknesses were 280 and 75 μm, respectively. The deflection of the Kevlar textile caused by the pressure difference and the induced stress is calculated by the general purpose finite element analysis program code ANSYS[1]. Since the elastic properties of the Kevlar textile are not known, they are determined to reproduce the vacuum test[2]. Figure 1 shows the results of ANSYS calculation of the displacements for the several flexures in the initial condition. At a larger flexure than 150 mm in the initial condition, the displacement becomes small enough. We determined a flexure of 155 mm in the initial condition.

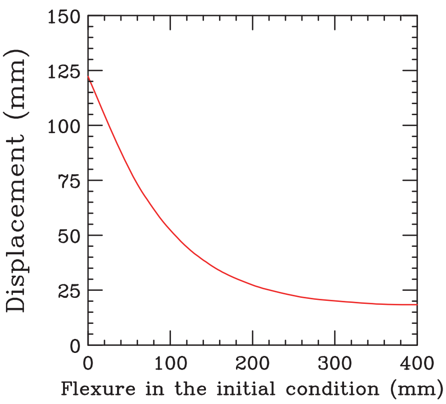

Fig. 1. The flexure dependence of Kevlar textile displacement.

Because of wrinkles of the Mylar at corners, a flat window cannot have larger flexure than 100 mm[2]. In order to have large flexure in every position, a window was designed having the shape of a partial cylinder with a radius of curvature of 715 mm. Figure 2 shows a drawing of the full-size partition window for the SAMURAI spectrometer. A flexure of 155 mm in the initial condition was achieved. The Kevlar and the Mylar were glued with an Araldite to the side pipe of the window frame. Owing to the pipe structure, every adhesion side was perpendicular to the direction in which the Kevlar and Mylar were pulled by the pressure difference

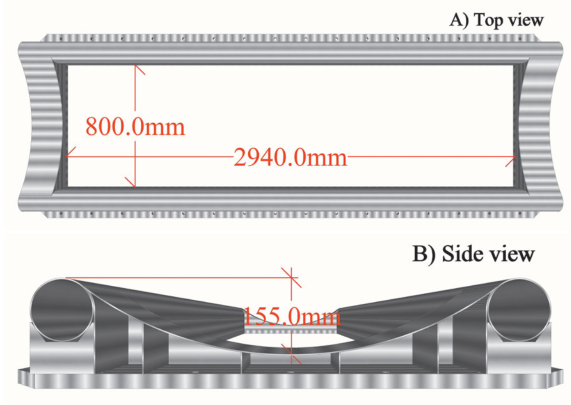

Fig. 2. Drawing of the full-size partition window.

This window was mounted on the test vacuum chamber. The achieved vacuum level was a few kPa. Figure 3 shows a photograph of the full-size partition window on the test vacuum chamber. The deflection was about 10 mm by visual observation. Therefore, since the Mylar foil is hardly extended, there is no fear of it collapsing. However, because this value differs from the ANSYS calculation, it may be necessary to improve the boundary condition in the ANSYS calculation.

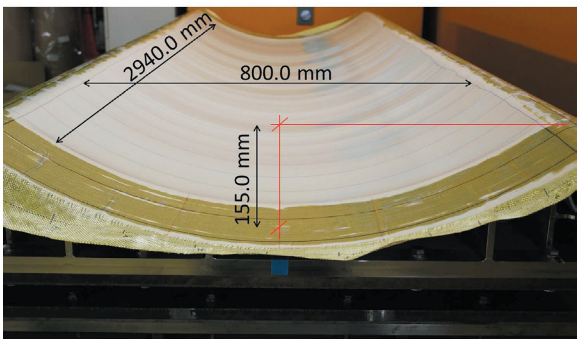

Fig. 3. Photograph of the full-size partition window.

References
1) URL: http://www.ansys.com/
2) Y. Shimizu *et al.*, Nucl. Instrum. Meth. Phys. Res., Sect. **B 317**, 739 (2013).

*1 RIKEN Nishina Center
*2 Department of Physics, Tohoku University

Development Of Multiple-Particle Tracking Algorithm For Forward Drift Chamber In SAMURAI

M. Kurata-Nishimura,[*1] H. Otsu,[*1] and T. Isobe[*1]

The Superconducting Analyzer for MUlti-Particles from RadioIsotope Beam (SAMURAI)[1] has been playing an important role in studying unstable nuclei in RIBF since 2012. In April 2013, $^{16}C(\alpha,\alpha')$ experiment[2] was carried out to investigate a degree of freedom for an exotic cluster which appears above an α emission threshold in high excited states. In the SAMURAI spectrometer, four momenta of α and a residue were measured simultaneously to reconstruct the invariant mass of the excited states. Thus far, no computer code has been developed for multiple charged particle tracking, the primary issue being that track reconstruction takes a long CPU processing time to find a true hits combination from numerous hits combinations. With this background, a new algorithm for multiple charged particle tracking was developed in the anaROOT[3] framework and is described here.

In the SAMURAI spectrometer, two Forward Drift Chambers (FDC1 and FDC2) are installed to reconstruct the tracks of scattered reaction residues in the forward direction. FDC1 and FDC2 are located upstream and downstream of the SAMURAI dipole magnet, respectively. Each FDC consists of three kinds of wire orientation planes referred to as X, U, and V planes, and two planes of the same type are placed next to each other. This pair of two planes is hereafter called a super pair plane. In the X plane, the wires are parallel to the Y axis and, in the U and V planes, the wires are tilted $+30^o$ and -30^o, respectively to resolve the three-dimensional flight path. The planes are assembled in the order of X, X', U, U', V, V', X, X', U, U', V, V', X, and X' in FDC2 and in the opposite order in FDC1.

In the beginning, reliable hits on each plane are selected. When a charged particle passing through ionizing gases around a wire, a δ-ray or X-ray would generate signals on adjacent wires. Since a real hit signal reaches the wire faster than fake ones, it can be chosen as the fastest timing signal delivered from a multiple hit TDC on a common stop mode.

Using these candidates, two hits on the super pair plane are coupled if the difference between the hit wire positions is within the pitch size of the wires. Multiple use of a hit is allowed. Even if a hit is not associated in the super pair plane, it can be used with the same method for coupled hits in the following analysis.

With considerat all combinations of coupled hits among X planes, a track in X-Z plane is evaluated by a linear fitting. If the number of hits included in a track is more than 4 and if χ^2 divided by the number of degree of freedom (NDF) is within 10%, the track information is stored as a candidate. Then, a precise hit position on the plane is calculated from the drift time for the candidate tracks. Two possibilities, i.e., whether the particle passed through in the left side or right side of the wire, are resolved by calculating the minimum χ^2 configuration.

The track reconstructed in the X-Z plane is projected onto the U and V planes, and the wire positions in the Y axis are evaluated. By combining the Y position on these planes, a linear fitting is applied for them with spatial resolution of the wire pitch size. If the χ^2/NDF is less than 1, the ambiguity of the left or right side path is resolved in the same manner as in X-Z plane.

As a result, three-dimensional multiple tracks in FDC1 were reconstructed as shown in Fig.1. In this event, two tracks were found in both FDC1 and FDC2 independently. Tracks reconstructed without bias caused by other detectors enable us to estimate the intrinsic tracking efficiency. This code is applicable for any experiments performed in the SAMURAI spectrometer.

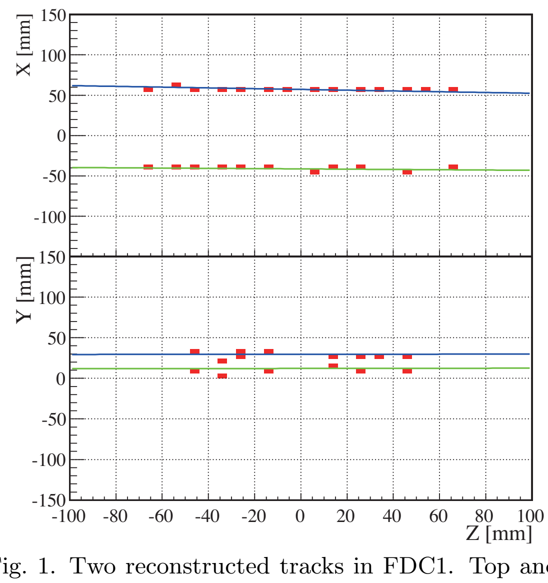

Fig. 1. Two reconstructed tracks in FDC1. Top and bottom figures show the track in the X-Z plane and Y-Z plane, respectively. The color of the linear fitting function indicates correspondences.

References
1) T. Kobayashi, et. al: Nucl. Instr. and Meth. **B**317 294-304 (2013)
2) H. Otsu, et. al.: In this report
3) `https://ribf.riken.jp/RIBFDAQ/index.php?Tools` %2FAnalysis%2FANAROOT

*1 RIKEN Nishina Center

Effect of stray field of the SAMURAI spectrometer on the neutron detector array WINDS

Y. Kubota[*1,*2] and M. Sasano[*2]

The (p, n) reaction has been used as a powerful probe to study nuclear isovector responses such as Gamow–Teller transitions, as extensively done in the region of stable nuclei[1)]. The extension of such studies to unstable nuclei can realized by combining the neutron detector array WINDS[2)] with the SAMURAI spectrometer[3)] for measuring high-intensity radioactive ion beams at the RIKEN RIBF.

From an experimental point of view, however, there is concern that the stray field of the SAMURAI magnet may deteriorate the gain of photomultiplier tubes (PMTs) of the WINDS bars. It is well known that the effect of the stray field is maximized when the direction of the magnetic field is parallel to that of the PMT. In this experiment, we examined this effect with several magnetic settings and also tested the restoration of gain with additional magnetic shielding on PMTs.

One of the WINDS bars was vertically placed near the entrance of the SAMURAI spectrometer. Thus, the PMTs (Hamamatsu H7195) attached at both ends of the bar are also aligned vertically. The direction of the stray field can also be considered more or less vertical, and the strength is large around the PMTs. Therefore, this setup provides the most severe gain-deterioration conditions. In the present work, three settings — (i) without any additional shielding, (ii) with one-fold shielding, and (iii) with two-fold shielding — were tested, as shown in Fig. 1. The magnetic field settings were 1.6, 2.2, 2.9, and 3.0 T. For these settings, the stray field at the location of the PMT was measured to be 0.5, 0.7, 4.5, and 6.0 mT, respectively.

The left panel of Fig. 2 shows the light output spectra of ^{137}Cs for 2.2 T. The relative gain was calibrated with the Compton edge of the 661.7-keV γ-ray emitted from ^{137}Cs. For each spectrum, we assumed the position corresponding to 70% of the maximum height as the Compton edge. The relative gain of the PMT decreased to 28% at 2.2 T when no additional shielding was used. With the addition of one-fold shielding, the relative gain was restored up to 97%. It was also confirmed that a relative gain of 92% or more can be achieved up to 2.9 T by using two-fold shielding, if necessary. However, at 3.0 T, a relative gain of 59% was obtained even with two-fold shielding. This is because of the drastic increase of the stray field due to the saturation effect of the iron yoke of the SAMURAI magnet around 3 T[4)].

The right panel of Fig. 2 shows the light output spectra of ^{241}Am. Gamma rays of 60 keV from ^{241}Am produce almost same light output as 100-keV neutrons. The spectrum was strongly distorted when the magnetic field was changed from 2.9 to 3.0 T because of the same reason as stated above. Below 2.2 T, the effect of the distortion can be made negligibly small with at least one-fold shielding.

In summary, the additional one-fold or, at most, two-fold magnetic shielding is sufficient to restore the gain for the SAMURAI magnet settings up to 2.9 T, but at 3.0 T, shielding of more than three-fold or thicker will be necessary. Thus, the setting of 2.9 T is practically much better than that of 3.0 T for the similar setup with PMTs, if there is no significant difference between 2.9 and 3.0 T in the performance of the SAMURAI spectrometer.

We acknowledge H. Sato for his support with the operation of the SAMURAI magnet.

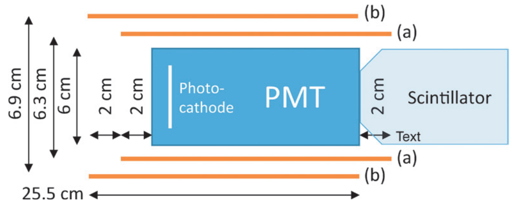

Fig. 1. Schematic view of the additional shielding consisting of 2-mm-thick iron (SUY-1). We use only inner (a) as a one-fold, and both (a) and (b) as a two-fold shielding.

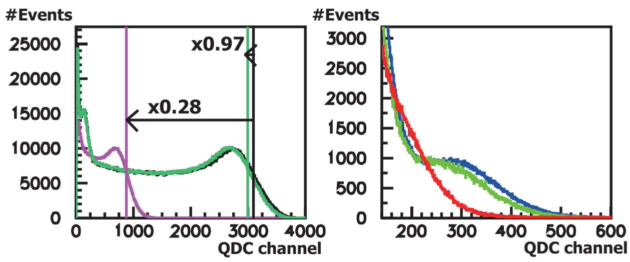

Fig. 2. Left panel shows light output spectra of ^{137}Cs without additional shielding (purple) and with one-fold shielding (green) at 2.2 T. Black line shows that at 0.0 T. Each vertical line shows the position of each Compton edge. Right panel shows light output spectra of ^{241}Am with two-fold shielding at 0.0 T (blue), 2.9 T (green), and 3.0 T (red).

*1 Center for Nuclear Study, University of Tokyo
*2 RIKEN Nishina Center

References

1) M. Sasano *et al.*, Phys. Rev. C **85**, 061301 (2012).
2) K. Yako *et al.*, RIKEN Accel. Prog. Rep. **45**, 137 (2012).
3) T. Kobayashi *et al.*, Nucl. Instr. Meth. B **317**, 294 (2013).
4) H. Sato *et al.*, IEEE Trans. Appl. Supercond. **23**, 4500308 (2013).

Development of a silicon detector array with large dynamic range

M. Kurokawa,[*1] H. Baba,[*1] J. Blackmon,[*2] J. Elson,[*3] M. McCleskey,[*4] T. Motobayashi,[*1] H. Murakami,[*1] T. Murakami,[*5] H. Otsu,[*1] C. Rasco,[*2] A. Saastamoinen,[*4] L. Sobotka,[*3] L. Trache,[*6] R. Tribble,[*4] K. Yoneda,[*1] and J. Zenihiro[*1]

We have developed an array of strip silicon detectors for the Coulomb beakup experiments with proton-rich heavy nuclei at intermediate energies. The breakup reaction, where the final state consists of one or two protons and the residual heavy charged particle, is an inverse reaction of the radiative proton capture and has been considered one of the most promising methods to extract the reaction rate of the capture process. The extracted rate gives us insight into the nucelosynthesis through the *rp* process, consisting of sequential proton captures on nuclei for producing heavier ones. The array measures the four momentum of each particle in the final state for specifying the excitation energy of the state along with the SAMURAI spectrometer. We plan to build an experimental setup capable of measuring the rates involving nuclei with masses up to 100.

The heaviest case is the breakup of a ^{101}Sb nucleus. The energy deposit of the breakup fragment ^{100}Sn is 50^2 times that of a proton. The dynamic range of the array must be larger than the difference in the energy deposit. The design value for the upper and lower detection limits were set to 1 GeV and 200 keV, respectively, after taking into consideration the possibility of the pile-up of events.

The total number of signal channels becomes more than one thousand for sufficient momentum resolution. In order to effectively treat such a large number of signal channels and to suppress the cost per channel, we need to employ the Application Specific Integrated Circuits (ASIC) technology for the array.

In view of the above requirements, we constructed an array consisting of newly developed preamplifier ASIC providing a large dynamic range by implementing high- and low-gain channels,[1)] another ASIC system called HINP for subsequent pulse shaping,[2)] and the silicon detector developed for the GLAST mission.[3)] The items in the following list were examined for the characterization of the array by irradiating the detector directly at the HIMAC facility .

(1) Linearity in the range from 390 keV to 300 MeV
(2) Cross talk between neighboring strips
(3) Yields of δ rays for the irradiation of heavy charged particles

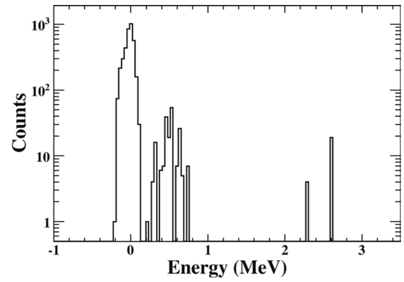

Fig. 1. Energy peak at around 390 keV obtained from the irradiation of a 150-MeV proton beam.

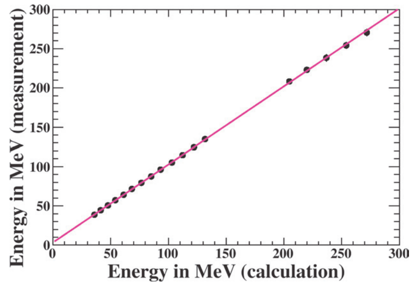

Fig. 2. Measured energy as a function of calculated energy. The slope of the line is 1.

The smallest energy deposit 390 keV was made by a 150-MeV proton beam(Fig. 1). For larger deposits, ^{56}Fe and ^{84}Kr ions were accelerated as primary beams and we selected secondary beams having a mass-to-charge ratio of two. The linear response of the low-gain channel shown in Fig. 2 indicates that the dual gain system of the preamplifier ASIC succeeded in extending the upper limit to higher than 100 MeV, which is the limit of the high-gain channel. The results obtained for the last two items will be used for the estimation of the background rates for the proton detection. The determination of the upper and lower limits is the subject for the next irradiation.

*1 RIKEN Nishina Center
*2 Department of Physics and Astronomy, Louisiana State University
*3 Department of Chemistry, Washington University in St. Louis
*4 Cyclotron Institute, Texas A&M University
*5 Department of Accelerator and Medical Physics, National Institute of Radiological Sciences
*6 IFIN-HH

References
1) M. Kurokawa et al.: RIKEN Acc. Prog. Rep. **44**, 148 (2011).
2) G. L. Engel et al.: Nucl. Instrum. Meth. A **573**, 418 (2007).
3) T. Ohsugi et al.: Nucl. Instrum. Meth. A **541**, 29 (2005).

Development of a γ-ray calorimeter for the measurement of highly excited states

Y. Togano,[*1,*2] M. Shikata,[*1] Y. Kondo,[*1,*2] and T. Nakamura[*1,*2]

The γ-ray calorimeter CATANA (**CA**lorimeter for γ-ray **T**ransitions in **A**tomic **N**uclei at high isospin **A**symmetry) has been developed to measure highly excited states such as the pygmy dipole resonance and/or the giant dipole resonance. CATANA will be used with the SAMURAI facility at RIBF.[1] The excitation energy spectrum will be reconstructed by combining the invariant mass of the reaction products measured by SAMURAI and γ-ray energies from CATANA. CATANA is focused on achieving a high detection efficiency because the probability of multiple γ-ray emissions is high in the decay of the highly excited states. Our goal is to achieve 55% photo peak efficiency for a 1 MeV γ ray from a beam with velocity $\beta = 0.6$.

The cross-sectional view of the CATANA array is shown in Fig.1. The array consists of 200 CsI crystals, whose thickness ranges from 9 cm to 15 cm. The colors indicate the different crystal shapes. The array is composed of six crystal shapes to minimize the empty space between the crystals. The crystals at the forward angle are thicker to cope with the Doppler shift of the γ energy. The array covers angles from 10° to 120° along the beam axis. The angular coverage per one crystal along the beam axis is about 9 degrees, and perpendicular to the beam axis, it is 18 degrees. The space inside the array is of ellipsoidal shape, whose major radius is 25 cm and minor radius is 20 cm. R11265 (Hamamatsu) PMTs will be used for two types of forward detectors, shown as yellow and saffron yellow in Fig. 1, and R580 (Hamamatsu) PMTs will be used for other detector shapes. Signal from a PMT will be processed in the spectroscopic amplifier 4494 from Clear Pulse Corporation. The pulse height information from the amplifier is digitized by a Mesytec MADC32 ADC. The timing information is processed in the 4494 amplifier using a build-in constant fraction discriminator, and digitized by a CAEN V1190A TDC. The logic trigger signal is generated as an "or" signal from the timing information.

The detection efficiency and the energy resolution of the CATANA array was estimated by using a Monte-Carlo simulation based on the code GEANT4. The thickness of the crystal housing and the space between the housing and crystal were assumed to be 1 mm in the simulation. The efficiency was calculated as 56% and 36% for 1 MeV and 10 MeV γ rays, respectively, from a beam with velocity of $\beta = 0.6$.

The prototype CsI crystal was tested at the Tokyo Institute of Technology. Fig. 2 shows the prototype CsI(Tl) crystal. The thickness of the crystal is 9 cm, and the shape of the prototype crystal corresponds to the blue one in Fig.1. The R11265 PMT is attached at the top side of the crystal. The crystal is wrapped by the ESR film (3M) of 65 μm and Teflon tape as reflectors. An energy resolution of 8.5% was achieved for the 662 keV γ ray with the prototype crystal. Based on the measured resolution, the energy resolution (FWHM) of 13% and 9% for 1 MeV and 10 MeV γ rays, respectively, from a beam at $\beta = 0.6$ is expected with the entire CATANA array.

The fabrication of 200 crystals will commence in spring 2014, and the entire system will be completed by spring 2015.

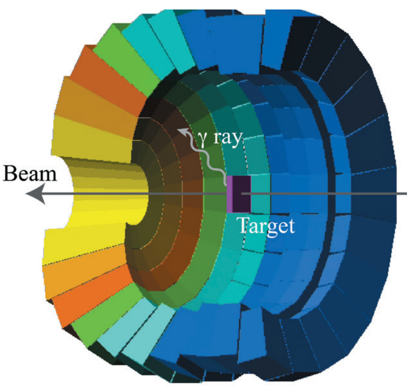

Fig. 1. Cross-sectional view of the CATANA array. Colors of crystals correspond to their shapes.

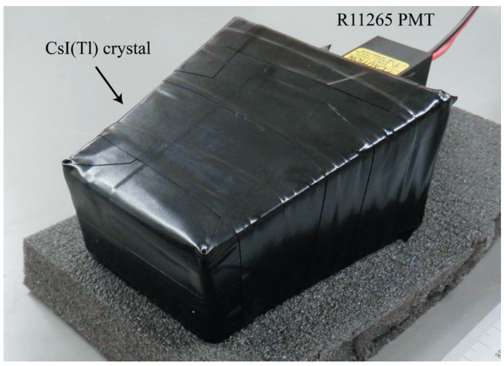

Fig. 2. Photograph of the prototype CsI(Tl) crystal.

*1 Department of Physics, Tokyo Institute of Technology
*2 RIKEN Nishina Center

References
1) T. Kobayashi et al.: Nucl. Instr. Meth. B **317**, 294 (2013).

Development of a next-generation PSD type neutron detector, NiGIRI†

H. Matsuzawa,*1 S. Nishimura,*2 T. Isobe,*2 and K. Ieki*1

The azimuthal angle correlation of neutrons (n) and charged particles (p, d, t, ...) with respect to the reaction planes in heavy-ion collisions is a powerful approach for studying equation of state (EOS) in high density nuclear matter.

A next-generation neutron detector, NiGIRI (Neutron, ion, and Gamma-ray Identification for Radioactive Isotope beam), is designed to achieve (a) particle identification capability with pulse-shape discrimination (PSD), (b) high detection efficiency, and (c) high energy resolution. Feather, it is designed to be applicable for multiple particle detections.

NiGIRI is comprised of arrays of detectors, consisting of plastic scintillators (ELJEN EJ299-33, $35\times35\times60$ mm^3), ultra-high quantum efficiency photomultiplier tubes (Hamamatsu H11265-200), and MPPCs (Multi-Pixel Photon Counter, Hamamatsu S10985-100C). The arrays are capable of particle discrimination and position sensibility. A newly developed plastic scintillator EJ299-33 with PSD capability is employed for identifying neutrons from gamma[1,2]. A novel concept followed by NiGIRI is that it reconstructs the particle interaction points in the scintillator by measuring the pulse height and the timing of the PMT and each MPPC attached on the side of the scintillator (Fig.1).

The performance of the PSD was investigated using a neutron source (^{252}Cf), where two charge-integrated QDCs with different gate widths were measured. One gate covers the whole signal and the other covers only the tail part of the signal. The duration of the two gates (total and tail) were 850 ns and 800 ns. Figure 2 shows the correlation plots between the tail and the total QDC values. The neutrons and gamma rays are separated.

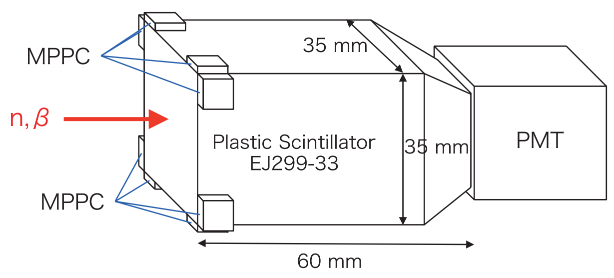

Fig. 1. The overview of the prototype NiGIRI detector.

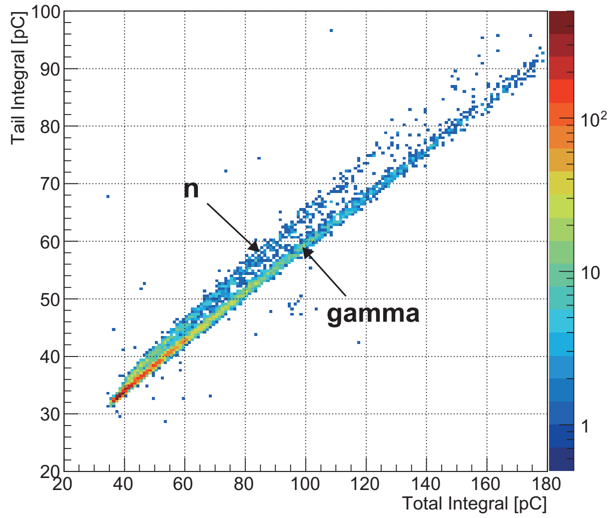

Fig. 2. Pulse shape discrimination between neutrons and gamma rays in EJ299-33.

Position reconstruction of the particles on the surface of the entrance window (35×35 mm^2) was estimated using β rays from ^{90}Sr source, where a 10 mm Al plate with a 1.5 mm diameter hole was used as a collimator. The time difference of signals between PMT and MPPCs was measured. The deviation of the interaction point with regard to depth was ignored in the position calibration owing to its relatively shorter range of β-ray relative to the length of the scintillator. We reconstructed the incident position from the time difference of the averaged two MPPCs between diagonal corners. The position resolution is estimated to be $\sigma_x = 5.8 \pm 0.2$ mm and $\sigma_y = 6.9 \pm 0.4$ mm after the position calibration. Improvement of the position resolution is anticipated by further correction.

Reconstruction of the interaction point in beam direction is under investigation. After the optimization of the prototype NiGIRI detector, mass production of the NiGIRI array will be initialed.

References

1) S.A. Pozzi et al.; Nucl. Instr. Meth. **A 723**, 19-23 (2013)
2) S. Nyibule et al.; Nucl. Instr. Meth. **A 728**, 36-39 (2013)

† Supported by KAKENHI (25247045).
*1 Department of Physics, Rikkyo Univ.
*2 RIKEN Nishina Center

Development of gating grid driver for SPiRIT TPC

T. Usukura,[*1,*2] T. Isobe,[*2] H. Baba,[*2] and K. Ieki[*1]

The symmetry energy part of the nuclear equation of state (EOS) influences various phenomena in nuclear astrophysics, nuclear structure, and nuclear reactions. The behavior of nuclear symmetry energy can be probed through a measurement of the π^-/π^+ ratio in heavy ion collisions. For this purpose, experiments using the Time Projection Chamber (TPC) installed in SAMURAI magnet[1)] have been proposed.[2)] The TPC is necessary to measure charged particles such as pions, protons, and light ions in high multiplicity environment produced by heavy ion collisions. When we perform the experiments at SAMURAI, heavy ions pass through TPC as well as light charged particles, resulting in gain reduction due to the production of a large amount of ions from the avalanche process around anode wires. To avoid such a gain reduction, gating grid wires are located prior to the avalanche region. Techniques to protect the avalanche region have been well established.[3)] In the open gate mode, all the gating grid wires are held at the same potential V_G, admitting electrons from the drift volume to enter the avalanche region. In the closed gate mode, the gating grid is biased with a bipolar field (positive side:$V_G + \Delta V$, negative side:$V_G - \Delta V$), which prevents electrons from the drift volume to reach the avalanche region. The closed gate prevents ions created in the avalanche processes of previous events from drifting back into the drift volume. A gating grid driver (GGD) was developed to realize such protection of the TPC. Figure 1 shows a prototype of the GGD. The design is based on the E907 TPC GGD.[4)]

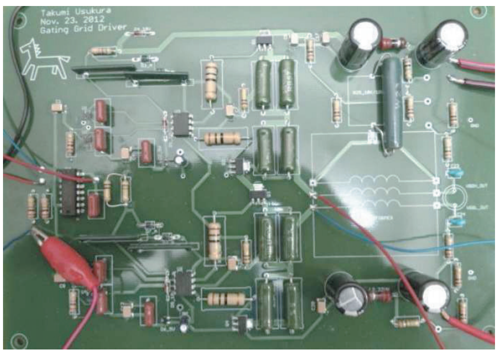

Fig. 1. Prototype of gating grid driver.

The GGD performance was studied by using a Xe beam at HIMAC. Since we could not use the TPC for SAMURAI, we used the BRAHMS TPC[5)] to check the GGD performance. A CsI target was located in front of the TPC so that light charged particles can be measured as well as the Xe beam. T2K-TPC electronics were used to read out 256 (4 ×64) pads. Without switching the gating grid wire using the GGD, we observe a gain attenuation at the beam rate of 10kpps. On the other hand, such a gain attenuation can be suppressed by switching the gating grid wire. The switching potential (V_G) is the same as that for the BRAHMS experiment.[5)] Though we can suppress the gain attenuation, the base line is fluctuated every time by the gate operation, which generates a large noise on the pad readouts with respect to the signal from the MIP particles. One of the main reasons of the noises from the GGD is the different rise times in the positive and negative sides although the sum of the positive and negative side voltages ($2V_G$) should be controlled to be constant. Since the noise shape caused by the GGD is similar among different events, we calibrate the baseline shape with a pedestal run and reconstruct the hit position after the subtraction of the baseline. Figure 2 shows the position resolution along the wire axis of the TPC after the calibrated baseline is subtracted. The position resolution under the bad noise condition created by the GGD is similar to the resolution with GGD. This implies that the noise created by the GGD can be made insignificant by subtracting the baseline as far as the position resolution is the same.

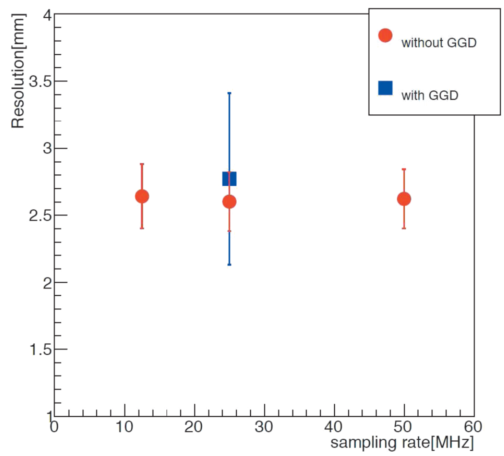

Fig. 2. Position resolution along wire axis as a function of flash ADC sampling frequency for each case, with and without GGD.

*1 Department of Physics, Rikkyo University
*2 RIKEN Nishina Center

References

1) T. Kobayashi et al.: NIM **B317**, 294 (2013).
2) T. Murakami et al.: RIKEN Accel. Prog. Rep. **46**, 150 (2013).
3) P. Nemethy et al.: NIM **212**, 273 (1983).
4) G. Rai et al.: IEEE Trans. Nucl. Sci. **37**, 56 (1990).
5) M. Adamczyk et al.: NIM **A499**, 437 (2003).

SPYBOX: Clock Monitoring at the GET Electronics

A. Perrevoort,[*1] T. Isobe,[*1] H. Baba,[*1] and A. Taketani[*2]

The SPYBOX is a device that measures the time differences between the clock signals of the various AsAd boards (ASIC Support and Analog-Digital conversion) at the GET electronics (General Electronics for TPC)[1)2)] in order to monitor the clock synchronisation. It will be used at SPiRIT - the TPC at the SAMURAI experiment.

At the GET electronics a total number of 120 AsAd boards are available, enabling GET to read out more than 30000 channels of a TPC. At each AsAd board, there are two inspection lines available which can be used to monitor various internal signals such as clock signals. These clock signals are fed into the SPYBOX.

For the SPYBOX two stages of multiplexer are implemented in FPGAs (see figure 1): At the first stage, 64 signals are multiplexed to two. Up to four of these FPGAs exist. The second stage reduces the remaining eight signals to two which are used as start and stop signal for an external TDC. Thus, a total number of 256 clock signals can be monitored, slightly exceeding the 240 inspection lines available in GET.

The time difference between the two signals is read from the TDC by a microcontroller which also serves as communication interface to the user's computer.

So far, two prototypes have been developed.
The first prototype[3)] houses all components on one board. Tests with clock signals show that the principle is feasible and yield a maximum skew of about 0.5 ns (see figure 2).
Nevertheless, this prototype has some drawbacks. For instance, the connectors as implemented on the board are not compatible with the AsAd board, and only about half the total number of clock signals can be processed. Moreover, the large size of this board turns out to be unhandy. By this, the need for a second prototype arose.

The second prototype is compatible with the AsAd board. It has a compact and modular design consisting of an own board for each stage of multiplexer. Thus, it allows the use of a reduced setup – for example at SPiRIT where only about 50 AsAd boards are used.
Additionally, the second prototype leaves space for further developments. One of the inspection lines at AsAd is for example bidirectional. It either outputs internal signals or receives external trigger signals for the AsAd pulse generator. The design of the second board accounts for the bidirectional line.

One additional feature of the second prototype concerns the timing resolution. As this prototype has a significant number of integrated circuit chips, the individual channels are prone to experience different travel times. To improve the timing resolution individual delay can be added to each channel compensating for the different travel times. This is done inside the FPGAs by a chain of LUTs (look-up-tables) which leads to freely selectable wire delay (see figure 3). First tests of the delay adjustment implemented in the FPGA yield additional delays of (0.7 to 0.8) ns per LUT. The time difference between two channels can be measured with a standard deviation of slightly less than 0.05 ns.

Currently, the second prototype is about to be finalized and will be evaluated afterwards.

*1 RIKEN Nishina Center
*2 RIKEN Center for Advanced Photonics

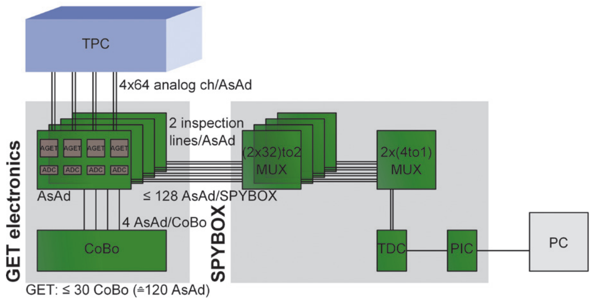

Figure 1. Schematics of GET and SPYBOX

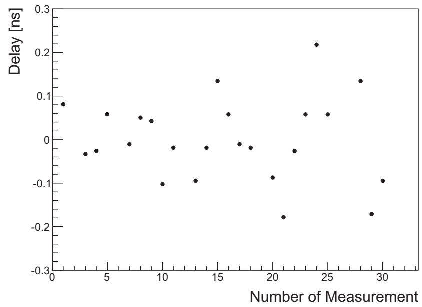

Figure 2. Time difference between two channels fed by the same clock signal corrected by the clock period

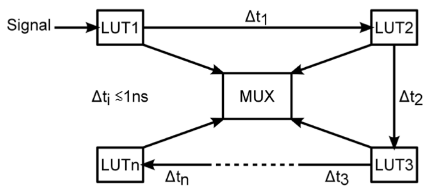

Figure 3. Delaying an individual channel by LUTs

References
1) E. C. Pollacco et al.: LoI for GET - General Electronics for TPC (2008)
2) http://www-actar-get.cea.fr
3) K. Urano et al.: RIKEN Accel. Prog. Rep. **46**, 152 (2013)

Development of TPC readout system for SπRIT project

T. Isobe,*[1] H. Baba,*[1] N. Nakatsuka,*[2] T. Murakami,*[2] W.G. Lynch,*[3] G. Jhang,*[4] W. Powell,*[5] and E. Pollacco,*[6] for the SπRIT Collaboration

For the measurement of multiple charged particle tracks in a heavy-ion collision experiment at RIBF, a time projection chamber (TPC) will be installed in the SAMURAI superconducting dipole magnet. The main aim of the experiment is to study the density dependence of symmetry energy defined in the nuclear equation of state. This project is carried out by an international collaboration, the "Sπ(PI)RIT collaboration"; SπRIT means Samurai PIon Reconstruction and Ion Tracker. As the readout electronics for more than 12k channels of TPC, a novel readout system, GET,[1)] is employed. GET stands for General Electronics for TPC and has been developed mainly by a collaboration between French institutes and American institute. The details of the GET system for the SπRIT project have been reported by Isobe et al.[2)].

For the first experiment at RIBF, we obtained the pre-production AsAd board, which is one of the important boards of the GET system and which was tested with SπRIT TPC at MSU. The pre-production AsAd board is controlled using the Xilinx evaluation board of ML507. ML507 can control only one board. For the massive readout of TPC, a dedicated concentration board, the CoBo board, which can control up to 4 boards, will be produced. Figure 1 shows the cosmic ray signal height of each channel as a function of the time bucket. There are 512 time buckets for one channel, and a sampling rate of up to 100 MHz is available. In the case of SπRIT TPC, a sampling rate of 50 MHz with 256 time buckets is planned to be used to cover the 10 μs drift time, which corresponds to a drift length of 50 cm with a 5 cm/μs drift velocity in P10 gas. Based on the information taken by the GET electronics, we succeeded to reconstruct the track as shown in Fig. 2. Now the analysis of the cosmic ray data is ongoing. It is planned that electron track data will eventually be taken with radioactive source.

As the data acquisition system, we plan to employ NARVAL,[2)] which is used in the French nuclear physics laboratory, such as GANIL. The size of data produced by the SπRIT plus GET system is estimated to be more than 100 MByte per second. NARVAL is selected as it can handle data of such large size.

Finally, 48 electronic boards will be mounted on the TPC and will be tested with cosmic rays in 2014. After that, the TPC will be mounted on the SAMURAI magnet for the first heavy ion collision experiment.

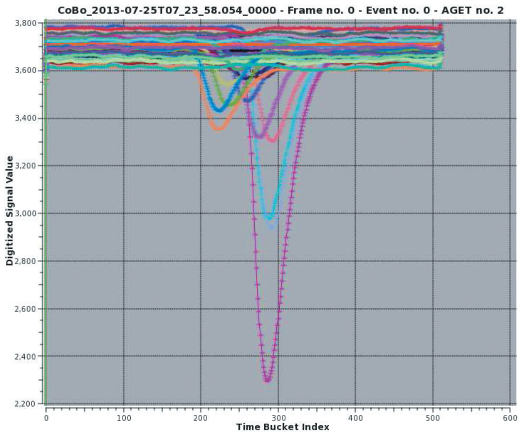

Fig. 1. Cosmic signal detected by SπRIT-TPC with GET electronics. Each line corresponds to one channel. One AsAd board contains four ASIC chips (AGET). One ASIC corresponds to 32 channels. The GET system employs SCA type flash ADC. Up to 512 time buckets can be used for analog data buffering. The pedestal is not suppressed in this figure.

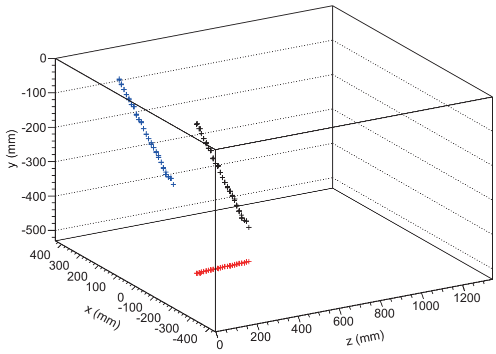

Fig. 2. Cosmic track reconstructed by SπRIT-TPC. The black line denotes the 3D track. The red and blue lines denote the projected track on each plane. A 100-MHz sampling rate is used.

*1 RIKEN Nishina Center
*2 Department of Physics, Kyoto University
*3 National Superconducting Cyclotron Laboratory, Michigan State University
*4 Department of Physics, Korea University
*5 Department of Physics, University of Liverpool
*6 CEA Saclay IRFU/SPhN

References
1) E. Pollacco et al.: Physics Procedia **37**, 1799 (2012).
2) T. Isobe et al.: RIKEN Accel. Prog. Rep. **46**, 151 (2013).
3) X. Grave.: Proc. 14th IEEENPSS Real-Time Conf ,65 (2005).

Simulation study of a trigger scintillator array for the SPiRIT experiment

T. Yoshida,*1 T. Isobe,*2 and K. Ieki*1

The SPiRIT (SAMURAI Pion Reconstruction Ion Tracker) experiment was performed at RIBF using unstable heavy-ion beams with various N/Z ratios. The aim of the experiment was to determine the nuclear equation of state (EOS) by investigating the production ratio of π^- to π^+ in heavy-ion collisions. We designed a scintillator array to trigger central collision events by using a detailed detector simulation, which was performed using the GEANT4 toolkit with the Monte-Carlo transport code PHITS; the PHITS is used as an event generator of heavy-ion collisions.

First, we evaluated charged-particle multiplicity distribution in heavey-ion collisions to confirm the validity of the simulation by comparing the simulated distribution to the measured distribution in the H292 experiment. The H292 experiment was performed with 400 AMeV ^{132}Xe beam on CsI target at HIMAC in March 2013. In H292, a multiplicity counter, which consisted of 60 plastic scintillators, was used to trigger central collision events. By constructing the same setup of H292 in the simulation, we evaluated the charged-particle multiplicity distribution as shown in Fig. 1. The obtained distribution reproduces the experimental result well; in particular, the multiplicities of more than 6 show good agreement.

Then, we examined geometrical configuration of the trigger scintillator array for the SPiRIT experiment to maximize geometrical acceptance for the central collision events. In the experiment we used two sets of trigger arrays located just downstream of the SPiRIT TPC. Here, we assumed scintillator arrays with size 1200 mm (horizontal) × 400 mm (vertical) × 10 mm (thickness) segmented into eight units vertically. Figure 2 shows the obtained acceptance as a function of the centrality in 300 AMeV ^{124}Sn + ^{124}Sn collisions when the trigger scintillator arrays were installed to cover the polar angle ranges of $-40 < \theta < -20$ and $20 < \theta < 40$ degrees. In this configuration, the trigger array can accumulate the central events with more than 30% acceptance in the region of the 0 – 60% centrality, which satisfies the experimental requirement. We also evaluated the charged-particle multiplicity of the trigger array and found that we can precisely investigate the production ratio of π^- to π^+ with track information reconstructed by the SPiRIT TPC.

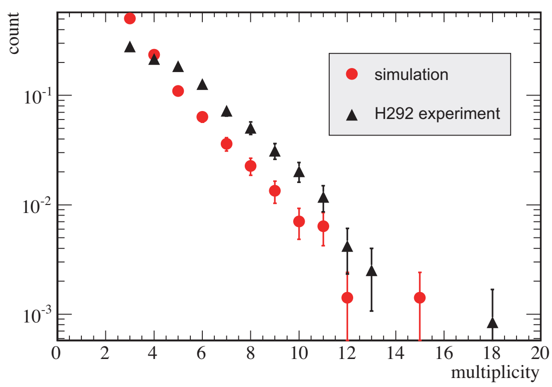

Fig. 1. Comparison of charged-particle multiplicity distribution between the simulation and the H292 experiment, with multiplicities of more than 2. The simulated distribution is normalized to the experimental yield.

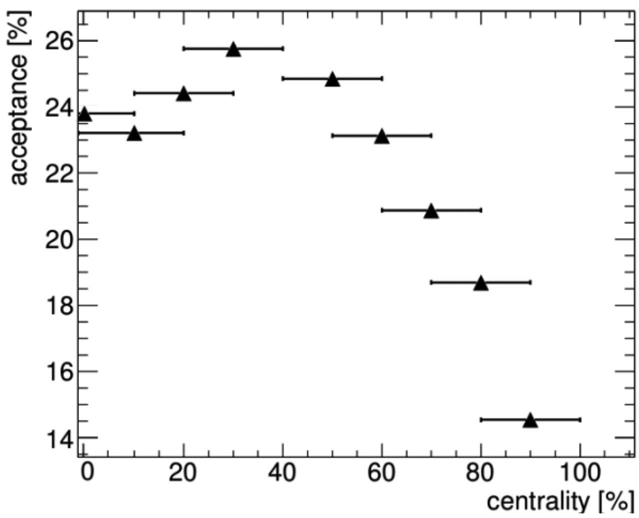

Fig. 2. Acceptance of the trigger scintillator array as a function of the centrality in 300 AMeV ^{124}Sn + ^{124}Sn collisions when the trigger scintillator arrays were installed to cover the polar angles ranges of $-40 < \theta < -20$ and $20 < \theta < 40$ degrees.

References
1) Bao-An Li, Nucl. Phys. A **708**, (2002) 365.
2) M. B. Tsang et al., Phys. Rev. C **86**, 015803 (2012).

*1 Department of Physics, Rikkyo University
*2 RIKEN Nishina Center

SHARAQ spectrometer for high-resolution studies for RI-induced reactions[†]

S. Michimasa,[*1] M. Takaki,[*1] Y. Sasamoto,[*1] M. Dozono,[*2] T. Nishi,[*3] T. Kawabata,[*4] S. Ota,[*1] H. Baba,[*2] T. Baba,[*4] T. Fujii,[*1] S. Go,[*1,*2] S. Kawase,[*1] Y. Kikuchi,[*1] K. Kisamori,[*1,*2] M. Kobayashi,[*1] Y. Kubota,[*1,*2] C.S. Lee,[*1,*2] H. Matsubara,[*2] K. Miki,[*5] H. Miya,[*1,*2] S. Noji,[*6] H. Tokieda,[*1] M. Tsumura,[*4] K. Yako,[*1] R. Yokoyama,[*1] H. Takeda,[*2] Y. Yanagisawa,[*2] T. Kubo,[*2] N. Inabe,[*2] N. Fukuda,[*2] D. Kameda,[*2] H. Suzuki,[*2] Y. Shimizu,[*2] H. Sato,[*2] T. Ichihara,[*2] A. Stolz,[*6] R.G.T. Zegers,[*6] H. Sakai,[*2] T. Uesaka,[*2] and S. Shimoura[*1]

The SHARAQ project[1)], which began in 2004, aims at high-resolution spectroscopy for reactions induced by radioactive ions (RI's) at 100A–350A MeV using the missing-mass method and at exploring new experimental techniques in the field of nuclear physics. In 2009, the construction of the High-Resolution Beamline (HRB)[2)] and SHARAQ spectrometer[1)] was completed at the RI Beam Factory (RIBF). The design specifications of the SHARAQ spectrometer are provided in Ref.[1)]. To date, the SHARAQ and HRB have been used for six experiments involving charge exchange reactions with radioactive isotope beams.

For experiments at SHARAQ, detector developments and ion optics studies are underway to improve the performance for high-resolution nuclear spectroscopy. A CVD diamond detector was developed in collaboration with NSCL/MSU to measure beam timings at achromatic foci with extremely good time resolution. The detector consists of a CVD diamond crystal of active area 28 mm^2 and thickness 0.2 mm, with four strips on one side and one pad on the other side. We performed a test of the diamond detector using a 32-MeV α beam. The time resolution was deduced to be 27 ps (σ). Details of the test and the performance of the CNS diamond detector were reported in Ref.[3)].

Multi-wire drift chambers operating at low gas pressure (LP-MWDC's) were successfully installed at the beamline foci. A tracking detector with high-rate capability and good position resolution enables us to obtain high-statistics data and to correct them through event-by-event momentum tagging. In our previous experiments, because the beam and reaction products were light nuclei with Z = 1–7, operation with low gas pressure was essential for reducing energy straggling and multiple scattering in the tracking detectors. The LP-MWDC achieved a position resolution of better than 300 μm (FWHM) for light ions and successfully operated with RI beams of intensities greater than 1 Mcps during a 1-week experiment. The high-rate performance is described in detail in Ref.[4)].

As in the ion-optics studies for SHARAQ, we also report here the results of the high-resolution achromatic (HA) and dispersion-matching (DM) transport modes. The HA mode is achromatic transport to the secondary target. One advantage of the HA mode is a wider momentum acceptance ($\Delta p/p = 2\%$) compared to the DM mode ($\Delta p/p = 0.6\%$), and thus, higher intensity RI beams can be delivered to the SHARAQ spectrometer. Momentum tagging by LP-MWDC at the intermediate dispersive focus (F6) enables us to improve the spectroscopic resolution of the reaction kinematics with respect to the momentum spread of the radioactive beam. We demonstrate the validity of the correction in Fig. 1.

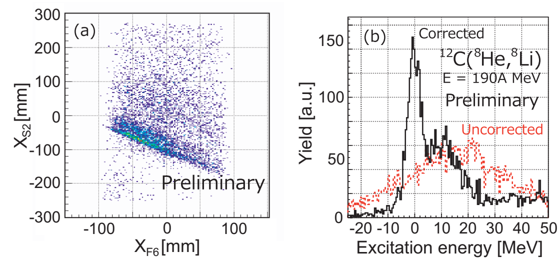

Fig. 1. (a) Correlation plot between F6 and the final dispersive focus of the SHARAQ spectrometer (S2). (b) Energy spectra with and without the event-by-event momentum correction.

The DM mode of SHARAQ spectrometer and HRB was designed to achieve extremely high resolution of reaction kinematics by the lateral and angular dispersion matching conditions in the entire system. Thus far, in the DM mode, we have achieved a momentum resolution of 1/8100 (FWHM) by taking into account the positions and angles of the beam constituents at the third focal plane (F3) of BigRIPS.

References

1) T. Uesaka *et al.*: Prog. Theor. Exp. Phys. **2012**, 03C007 (2012).
2) T. Kawabata *et al.*: Nucl. Instr. Meth. B **266**, 4201 (2008).
3) S. Michimasa *et al.*: Nucl. Instr. Meth. B **317**, 710 (2013).
4) H. Miya *et al.*: Nucl. Instr. Meth. B **317**, 701 (2013).

† Condensed from the article in Nucl. Instr. Meth. B **317**, 305 (2013)

*1 Center for Nuclear Study, the University of Tokyo
*2 RIKEN Nishina Center
*3 Department of Physics, the University of Tokyo
*4 Department of Physics, Kyoto University
*5 RCNP, Osaka University
*6 NSCL, Michigan State University

Development of dual effective gas gain multiplication in CNS Active Target for a high-intensity beam injection

C.S. Lee,[*1,*2] S. Ota,[*2] R. Kojima,[*2] Y.N. Watanabe,[*3] H. Tokieda,[*2] and T. Uesaka[*1]

We are developing a GEM-TPC-based gaseous active target with a pure deuterium gas, called CNS Active Target (CAT),[1)] for performing deuteron inelastic scattering experiments. The CAT is operated with a low-pressure (0.2-0.5 atm) deuterium gas for measuring the scattering to the forward angle closer to 0°. A 400-μm Thick GEM (THGEM) is chosen for the CAT to achieve a gas gain of 10^4 for a low-pressure deuterium gas ; its performance was investigated for the first time in our previous work.[2)]. However, when the gain of THGEM is set to such a high level as 10^4, the amplified charges from the energy loss of the heavy-ion beam, which is impinged with a high-intensity of 10^{5-6}Hz, become too large for the GEM-TPC to operate stably. The effective gas gain along the beam trajectory (BT) area should be reduced by an order of 10-100, keeping the effective gas gain in the region where the recoiled particles (RP) are measured.

A new type of THGEM, called DGGEM (Dual-Gain THGEM), was manufactured via mechanical drilling and it has a thickness of 400 μm, a hole diameter of 450 μm (900 μm-pitch) on the BT region, and a hole diameter of 300 μm (700 μm-pitch) on the RP region ; the DGGEM was used to study the dependence of the gain on the hole diameter. Since the electric field is stronger in a hole with a smaller diameter, a gas gain in the RP region is expected to be lager, by a factor of four, than that in the BT region. Figure 1 shows the obtained gain curves in single, double, and triple DGGEM layer setups as functions of the induction field strength $E_{\text{induction}}$ in kV/cm/atm. The measured difference of gas gain between the BT and RP regions was much smaller than expected. Another solution was suggested, in which a grid mesh covered only the area along the beam path with a triple (normal) THGEM configuration. By changing the electric field in the drift field using the grid along the beam path, a partial gain reduction and a more stable operation of CAT is expected. A test experiment was performed with a high-intensity $^{132}_{54}$Xe (100 MeV/u) beam at the HIMAC facility. A mesh grid with a 2cm width was set along the beam path (4-mm above the THGEMs). The most suitable voltage setup for the grid was identified using a defocused ^{132}Xe beam. Figure 2 shows the relation between the sampled charges after multiplication and the readout pad ID. The widely hatched area, pad ID 60-340, corresponds to the entire beam trajectory region ; and the narrowly hatched area, pad ID 130-270, includes the grid. A significant reduction of gain was achieved only on the grid area. The CAT was stably operated via the optimized grid operation under a high-intensity injection of ^{132}Xe beam up to 10^5 particles per pulse, in combination with tuning of the protection circuit for the high-voltage supply. Further analysis is in progress.

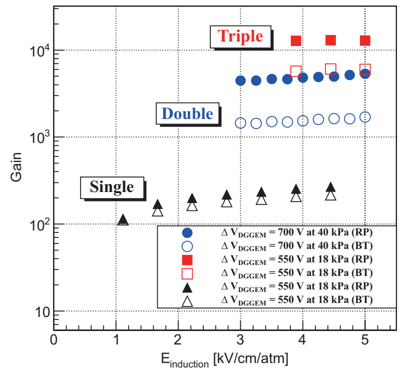

Fig. 1. Results for each layer structure of DGGEM. For each measurement, the drift field strength was 1 kV/cm/atm and the transfer field strength was 2 kV/cm/atm.

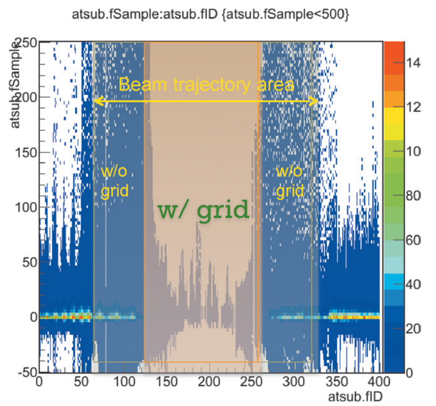

Fig. 2. An example of correlation between sampled charges after the multiplication and readout pad IDs with a defocused beam injection. Reduced multiplication of charges is achieved under the grid area. The color bar indicates the number of events.

References
1) S. Ota et al.: *CNS Annual Report 2011 CNS-REP-90* (2013) 70-71.
2) C.S. Lee et al.: *to be published on CNS Annual Report 2012.*

*1 RIKEN Nishina Center
*2 Center for Nuclear Study (CNS), University of Tokyo
*3 Department of Physics, University of Tokyo

Development of enlarged spin-polarized proton target for RI beam experiments

S. Chebotaryov,[*1,*3] S. Sakaguchi,[*1,*2] T. Kawahara,[*1] E. Milman, [*1,*3] K. Tateishi,[*1] and T. Uesaka[*1]

Spin-dependent interactions play an important role in nuclear structure and reactions. Spin-orbit coupling is one of manifestations of spin-dependent interactions. One of the most straightforward approaches to investigate spin-orbit coupling is the determination of the spin-orbit potential through the nuclear optical model analysis of the vector analyzing power in the $p - A$ scattering (proton elastic scattering from nuclei).

At RIBF in experiments involving short-lived unstable nuclei, a spin-polarized proton target is required, since unstable nuclei are supplied as RI beams. Center for Nuclear Study, Univ. of Tokyo and RIKEN groups have developed a spin-polarized proton target system.[1)] The target material is a crystal of naphthalene doped with a small amount pentacene (0.005%), which serves as a polarization agent. The method of production of spin polarization employed in our target system, is based on the cross-polarization technique,[2)] where polarization of electrons system is transferred to protons by means of dipolar interaction in the presence of microwave irradiation.

Several RI beam experiments have been done with this polarized proton target.[3,4)] For further application the size of the target (14 mm in diameter) is a limiting factor because the typical position spread of RI beams is as large as 20-30 mm. This leads to loss of statistics and also increase in background events from the surrounding materials such as a target holder. Due to the above reasons the crystal size needs to be enlarged.

We performed upgrade of the polarizing system to accommodate an enlarged sample and successfully obtained spin polarization signal from a sample of 24 mm and 3 mm in diameter and thickness, respectively. This is the largest sample that has been polarized with this method. Measurement of a spin polarization was performed by means of the pulsed-NMR method.

To facilitate polarization transfer based on the cross-polarization technique, the energy gaps of electron and proton systems should be made equal, so that these two systems are coupled. This condition: $\hbar\omega_{\text{eff}} = \hbar\omega_I$, is known as the "Hartmann-Hahn condition"[5)]. Here, ω_{eff} is the electron effective Larmor frequency in a coordinate system rotating with frequency ω - the frequency of oscillating microwave magnetic field, and ω_{I} is proton Larmor frequency. ω_{eff} is written as

$$\omega_{\text{eff}} = \sqrt{(\omega_{\text{s}} - \omega)^2 + \omega_{\text{R}}^2}, \tag{1}$$

where ω_{s} is the Larmor frequency of the electron, $\omega_{\text{R}} = \gamma_{\text{s}} H_1$ is the Rabi frequency which depends on the amplitude of the oscillating magnetic field H_1 and electron gyromagnetic ratio γ_{s}. In actual measurements after a resonance condition $\omega_{\text{s}} = \omega$ was met by adjusting a static magnetic field H_{s} as $\omega_{\text{s}} = \gamma_{\text{s}} H_{\text{s}}$, then ω_{eff} was tuned to satisfy "Hartmann-Hahn condition". Tuning of ω_{eff} is done by changing the H_1 field amplitude, which is proportional to the square root of input power $\sqrt{P_{\text{MW}}}$. The ω_{R} is connected to P_{MW} as $\sqrt{P_{\text{MW}}} \propto H_1 = \omega_{\text{R}}/\gamma_{\text{s}}$.

We note here that a maximum proton spin polarization is produced, provided the "Hartmann-Hahn condition" is met. In the proton spin polarization measured as a function of $\sqrt{P_{\text{MW}}}$ shown in Fig. 1, however, no such maximum was identified as a peak. The peak was not obtained even with the highest power that the currently used source can supply. To achieve "Hartmann-Hahn condition", we are redesigning the microwave resonator in order to reduce power loss due to radiation to the outer region.

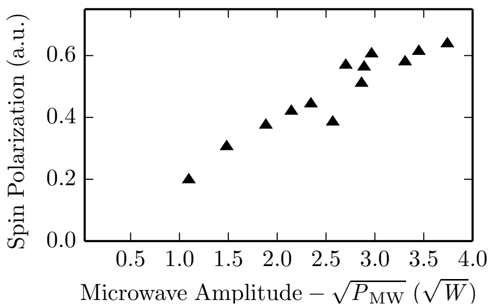

Fig. 1. Dependence of proton spin polarization signal on the square root of applied microwave power.

At the present, we successfully obtained spin polarization signal with very large sample of 24 × 3 mm. Although, magnitude of the polarization can be enhanced by improving the microwave system.

References

1) T. Wakui: in Proceedings of the XI-th International Workshop on Polarized Ion Sources and Polarized Gas Targets 2005 (World Scientific, Singapore, 2007).
2) T. Wakui, T. Uesaka, et al.: Nucl. Instr. Meth. Phys. Res. A **550**, 521 (2005).
3) T. Uesaka, S. Sakaguchi et al.: Phys. Rev. C **82**, 021602(R) (2010).
4) S. Sakaguchi, Y. Iseri et al.: Phys. Rev. C **84**, 024604 (2011).
5) Hartmann S.R., Hahn E.L.: Phys. Rev. **128**, 2042 (1962).

*1 RIKEN Nishina Center
*2 Department of Physics, Kyushu University
*3 Department of Physics, Kyungpook National University

β-NMR measurement of unstable nuclei with cross-polarization technique

T. Kawahara,[*1] K. Tateishi,[*1] R. Kojima,[*2] S. Sakaguchi,[*1,*3] E. Milman,[*1,*4] S. Chebotarov,[*1,*4] T. Wakui[*1,*5] and T. Uesaka[*1]

A polarized solid proton target for RI beam experiments has been developed at RIKEN and the Center for Nuclear Study, University of Tokyo.[1)] By means of electron polarization in photo-excited triplet states of pentacene, proton polarization of approximately 20% has been achieved in a low magnetic field of 0.1 T and at a high temperature of 100 K. The target has been applied to RI beam experiments for several times.[2,3)] One of the next directions in the research is the polarization of unstable nuclei. If the polarization of protons can be transferred to unstable nuclei stopped in the target, measurements of magnetic moments would become possible with the β-NMR method. The polarization condition of high temperature and low magnetic field, which is the distinct advantage of the target, is indispensable in such low-energy beam experiments. In this article, we report on our attempt of transferring proton polarization to ^{13}C nuclei contained in the sample.

As a sample, we used a single crystal of p-terphenyl doped with pentacene molecules. Most of ^{1}H nuclei in p-terphenyl molecules were replaced by deuterium to obtain a higher ^{1}H polarization. The abundance of the ^{1}H was 2%. The weight of the sample was 28 mg. The crystal was irradiated by the pulsed laser light with a wavelength, an average power, pulse width, and repetition rate of 514 nm, 0.3 W, 13 μs, and 7.5 kHz, respectively. The sample temperature was controlled at 293 K by flowing cold nitrogen gas. The optimum power of the microwave was 3 W. Under these conditions, a proton polarization of 6.2±1.2% was obtained.

In the next step, the obtained ^{1}H polarization was transferred to the ^{13}C system by the cross-polarization method. The ^{13}C (or ^{1}H) spin rotates along the static magnetic field at a certain Larmor frequency. In the cross-polarization method, we apply a transverse magnetic field rotating with the Larmor frequency. This rotating field, produced by radio-frequency (RF) waves, effectively changes the level gap between spin up/down states. When the effective level gaps of ^{1}H and ^{13}C are equal, these systems couple to each other and polarization transfer takes place. The level gap is given as $\hbar\omega_R = \gamma\hbar H_{RF}$, where ω_R and γ are the Rabi frequency and gyromagnetic ratio, respectively. The H_{RF} is the strength of the rotating field, which is proportional to the square root of the RF power.

*1 RIKEN Nishina Center
*2 Center for Nuclear Study (CNS),University of Tokyo
*3 Department of Physics,Kyushu University
*4 Department of Physics, Kyungpook National University
*5 Cyclotron and Radioisotope Center, Tohoku University

In the present case, the Larmor frequencies of ^{13}C and ^{1}H are 3.167 and 12.59554 MHz, respectively, in a static field of 0.3 T. By irradiating these two RF waves at the same time and by tuning their powers to satisfy the Hartmann-Hahn condition, $\gamma^{\mathrm{H}}\hbar H^{\mathrm{H}}_{RF} = \gamma^{\mathrm{C}}\hbar H^{\mathrm{C}}_{RF}$, one can realize the polarization transfer between two systems. Here, the superscripts "H" and "C" represent ^{1}H and ^{13}C, respectively. By changing H^{C}_{RF} with fixed H^{H}_{RF} , we searched the point where the Hartmann-Hahn condition is satisfied. The result is shown in Fig. 1 .

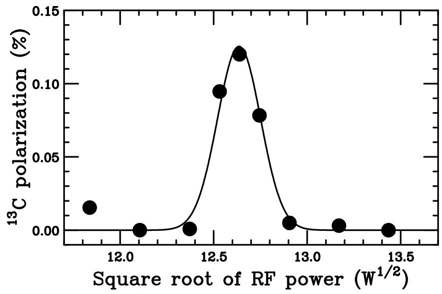

Fig. 1. The RF power dependence of ^{13}C polarization

As seen in the figure, the ^{13}C polarization was successfully obtained for the RF power of ∼160 W. The magnitude of ^{13}C polarization was 0.12 ± 0.05%. The polarization-transfer efficiency, which is the ^{13}C polarization divided by ^{1}H polarization (6.2%), is found to be 1.9%. While this value is not high, it is reasonable becouse the sample is deuterated and the abundance of ^{1}H is 2%. If the sample is not deuterated, the number of ^{1}H nuclei to which ^{13}C couples becomes 50 times larger. In that case, a polarization transfer efficiency of close to 100% would be obtained.

In conclusion, we obtained a high proton polarization of 6.2% bia temperature control and the use of a deuterated p-terphenyl crystal. By transferring the proton polarization, the ^{13}C polarization was successfully obtained with the cross-polarization method. The next step would be the polarization transfer to unstable nuclei stopped in the target. As the gyromagnetic ratio of the unstable nuclei is not precisely known, the parameter search for the Hartmann-Hahn condition will become more difficult. Finding an efficient method of the search is a challenge for the future.

References
1) T. Uesaka *et al.*: Eur. Phys. J. **150** (2007) 71.
2) T. Uesaka *et al.*: Phys. Rev. C. **82** (2010) 021602.
3) S. Sakaguchi *et al.*: Phys. Rev. C. **87** (2013) 021601.

The spin polarization of proton target in SHARAQ04 experiment

T.L. Tang,*[1] S. Kawase,*[1] Y. Kubota,*[1] H. Tokieda,*[1] K. Yako,*[1] T. Fuji,*[1] S. Michimasa,*[1] K. Kisamori,*[1] M. Takaki,*[1] H. Miya,*[1] C.S. Lee,*[1] R. Yokoyama,*[1] M. Kobayashi,*[1] S. Ota,*[1] S. Shimoura,*[1] T. Kawahara,*[2] T. Wakui,*[3] J. Zenihiro,*[4] H. Matsubara,*[4] M. Dozono,*[4] H. Takeda,*[4] K. Kusaka,*[4] N. Fukuda,*[4] D. Kameda,*[4] H. Suzuki,*[4] M. Sasano,*[4] T. Uesaka,*[4] S. Sakaguchi,*[5] T. Wakasa,*[5] J. Yasuda,*[5] T. Fukunaga,*[5] T. Noro,*[5] Y. Maeda,*[6] S.H. Hwang,*[7] W.Y. Kim,*[7] S. Stepanyan,*[7] D. Beaumel,*[8] A. Obertelli,*[9] A. Galindo-Uribarri,*[10] E. Padilla-Rodal*[11]

A (p,2p) knockout reaction was used in the SHARAQ04 experiment to extract the spectroscopic factor of orbital protons, and a spin-polarized proton target was used to extract the analyzing power for distinguishing the spin-up ($J_>$) and spin-down ($J_<$) orbits of the knockout proton. The analyzing power can be determined using the cross section left-right asymmetry and spin polarization. We present the analysis and results of the spin polarization.

The measurement of the spin polarization of the polarized proton target[1,2] was conducted using two methods. The nuclear magnetic resonance (NMR) was used for quick and constant monitoring, and proton-proton elastic scattering was used for measuring the absolute magnitude of the spin polarization.

A 260 MeV pure proton beam was used in proton-proton elastic scattering runs. The spin polarization was reversed during the measurement to eliminate of any systematic asymmetry. A pair of recoil protons was correlated and the opening angle was 180° in the center of mass frame, which is equal to 86.3° to 90° in the laboratory frame. The recoil protons were tracked by two MWDCs[3] located downstream[4]. The MWDCs were arranged 30° to the beam axis and 1022 mm away from the target. The MWDCs covered a forward angle of 20° – 70°, which is equivalent to approximately 40° – 140° in the center of mass frame. The position resolution of the MWDCs is approximately 0.1 mm for X and 0.2 mm for Y.

The NMR method was applied by inserting an NMR coil to surround the target crystal. From the measurement, it was shown that the spin polarization of the spin-down runs was approximately 78% smaller than that of the spin-up runs during proton-proton elastic scattering [2].

The target crystal was made of naphthalene ($C_{10}H_8$). The beam profile was much larger than the size of the target so that significant amount of the beam was incident on the target holder (hydrogen-free plastics) and surrounding structures. These two factors provided us a broad background signal on the opening angle.

*1 Center of Nuclear Study, Tokyo University
*2 Toho University
*3 CYRIC, Tohoku University
*4 RIKEN Nishina Center
*5 Kyushu University
*6 University of Miyazaki
*7 Kyungpook National University
*8 IPN Orsay
*9 CEA Orsay
*10 Oak Ridge National Laboratory
*11 ICN, Nuiversidad Nacional Autonoma de Mexico

By assuming that the reaction point is along the z-axis of the lab frame, we calculated the weighted reaction position (Z-vertex) from the MWDCs' tracking result. The Z-vertex was gated by an opening angle with a central gate (84°-89°) and a side gate (81.5°-84° or 89°-91.5°). The central gate contained the elastic scattering peak and background, while the side gate contained only background because the opening angle is not allowed by kinematics and detector acceptance (Figure 1).

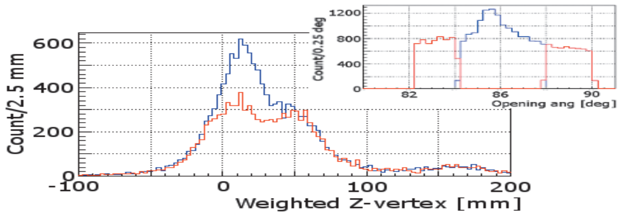

Figure 1. Weighted Z-vertex (reaction vertex on z-axis) with opening angle gate (upper right corner). Elastic scattering runs #7 to #15 were used[2].

We divided the cover angle into five angle sections in the center of mass frame. The yield for each section is

$$Y_x^\beta(\Delta\theta) = fL^\beta\epsilon_x\sigma(\Delta\theta)\Delta\Omega\left(1 + s_x^\beta A_y(\Delta\theta)P^\beta\right)$$

$$L^\beta = N_T\sum N_B^\beta(i)\lambda^\beta(i) \tag{1}$$

$$s_L^\uparrow = s_R^\downarrow = 1 = -s_L^\downarrow = -s_R^\uparrow$$

where x is left or right, β is spin-up or down, f is the fraction of beam on the target, L is the integrated luminosity, N_T is the number of proton in target, $N_B(i)$ is the number of beam protons in the i-th run, λ is the lifetime of the DAQ system, ϵ is the detector efficiency, $\sigma(\Delta\theta)$ is the differential cross section in angle section $\Delta\theta$, $\Delta\Omega$ is the solid angle on the angle section $\Delta\theta$, s is a sign, A_y is the analyzing power and P is the spin polarization of the target. We used the spin-up and spin-down asymmetry to avoid the efficiency non-uniformity of MWDCs. The final spin polarization is a weighted mean from each angle section. The spin-up polarization was 16% ± 14%. The spin polarization is as expected and similar to the results of a previous experiment performed under a similar conditions[5]. An asymmetry of the cross section distribution can be obtained for large statistics.

References

1) T.L. Tang, *et al*., RIKEN Accel. Prog. Rep. **46**, 162 (2012).
2) T.L. Tang, *et al.*, CNS Annual Rep. **59** (2012)
3) H. Okamura *et al.*, Nucl. Instr. and Meth. A, **406**, 78 (1998).
4) S. Kawase, *et al.*, RIKEN Accel. Prog. Rep. **46**, 30 (2012).
5) S. Sakaguchi, *et al.*, Phys Review C, **84**, 024604 (2011)

Proton polarization in photo-excited aromatic molecule at room temperature enhanced by intense optical source and temperature control†

S. Sakaguchi,[*1,*2] T. Uesaka,[*1] T. Kawahara,[*1] T. Ogawa,[*3] L. Tang,[*4] T. Teranishi,[*2] Y. Urata,[*3] S. Wada,[*3] and T. Wakui[*5]

For the study of unstable nuclei with polarization observables, we have constructed a solid polarized proton target[1)] based on the electron polarization in photo-excited aromatic molecules. Proton polarization of about 20 percent has been obtained at a temperature of 100 K, which is much higher than that under conventional conditions. The target has been successfully applied to several RI-beam experiments[2)] carried out at intermediate energies of several tens to a few hundred MeV/nucleon. One of the future directions of this research is conducting experiments at low energies of several to a few tens of MeV/nucleon. This will open up new possibilities such as resonant scattering and polarization transfer to embedded RIs. For such applications, the target should be placed in a vacuum environment and be polarized at room temperature. In our previous measurement at room temperature, a polarization of 4.8±1.2% was achieved by using *p*-terphenyl as the material. The aim of the present work is to investigate the possibility of achieving a high proton polarization of 30 percent for application to scattering experiments.

The magnitude of the polarization is expressed as $P_p = A\overline{P_e}/(A+\Gamma)$. Here, $\overline{P_e}$ is the electron polarization, A is the build-up rate, and Γ is the relaxation rate. In order to achieve a high polarization, we need to increase A and $\overline{P_e}$ or decrease Γ. To enhance the build-up rate A, we should increase the laser power for photo-excitation. However, in Iinuma *et al.*[3)] reported that a high laser power does not necessarily lead to a high polarization. This is considered to be because of the temperature rise of the sample. At temperatures higher than 300 K, the intrinsic relaxation rate Γ_{int} rapidly increases[4)] because of the molecular motion. Thus, it is expected that the polarization can be enhanced by using an intense optical source with the sample temperature controlled at $T \sim$300 K.

The sample used in the present work is a single crystal of *p*-terphenyl doped with pentacene molecules with a concentration of 0.005 mol%. The target temperature was monitored with a platinum resistance thermometer. The temperature of the crystal was controlled by flowing cold N_2 gas. For the light source, we used an Ar ion laser with a wavelength of 514 nm.

The polarization was measured under two different conditions. The first condition (averaged laser power of 80 mW, w/o temperature control) is the same as that used in our previous measurement, where a polarization of 4.8% was achieved. The other condition (1.5 W, w/ temp. control), referred to as "present," was also considered. The time evolution of the polarization is shown in Fig. 1. In the present condition, the polarization is enhanced by a factor of three as compared with the polarization under the first condition. Although the absolute measurement is to be done in the future, the magnitude of achieved polarization corresponds to about 15% if we assume the polarization of 4.8% in the previous condition.

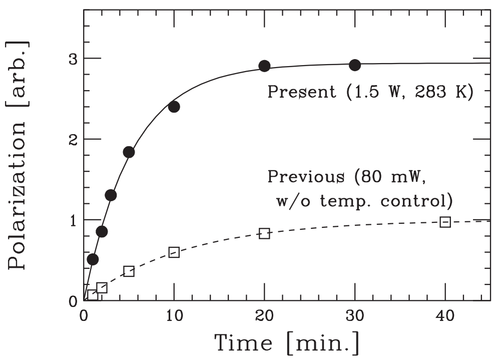

Fig. 1. Time evolution of proton polarization.

Finally, it should be mentioned that optimization of the time structure of the laser pulse would enhance the polarization rate $A\overline{P_e}$ by a factor of ∼5 *without* increasing the relaxation rate Γ (see Ref.[5)]). Thus, such optimization would almost directly improve the magnitude of polarization. Room-temperature polarization of 30 percent would be realized by combining a high power laser with a wavelength of ∼590 nm, through optimization of laser pulse structure, and employing a sophisticated temperature control system.

References

1) T. Wakui: Proc. of PST2005 (World Scientific, 2007).
2) S. Sakaguchi *et al.*: Phys. Rev. C **87**, 021601(R) (2013), and references therein.
3) M. Iinuma *et al.*: Jour. Mag. Res. **175**, 235 (2005).
4) T. Kawahara *et al.*: RIKEN Prog. Rep. **46**, 164 (2013).
5) S. Sakaguchi *et al.*: Nucl. Instr. Meth. B **317** (2013) 679-684

† Condensed from the article in Nucl. Instr. Meth. B **317** (2013) 679-684
*1 RIKEN Nishina Center
*2 Department of Physics, Kyushu University
*3 RIKEN Advanced Science Institute
*4 CNS, University of Tokyo
*5 CYRIC, Tohoku University

Dynamic nuclear polarization with photoexcited triplet electrons in a glassy matrix†

K. Tateishi,[*1] M. Negoro,[*2] A. Kagawa,[*2] and M. Kitagawa[*2]

In this decade, dynamic nuclear polarization (DNP) using equilibrated electron spin has attracted considerable attention in the fields of NMR spectroscopy and MRI as a method to enhance sensitivity.[1)] The intensity of a signal from nuclear spins is proportional to the spin polarization. DNP is a means of transferring spin polarization from electrons to nuclei, and the equilibrated polarization of electron spins is 660 times larger than that of ^{1}H spins. Developing special peripheral equipment, we are able to combine hyperpolarization at cryogenic temperatures around liquid helium temperature with high-resolution NMR spectroscopy or MRI. For such applications, the sample preparation method which materials of interest are codoped into a glassy matrix together with free radicals is one of the most important factors in terms of versatility.

On the other hand, by using single crystal of organic molecules, we have developed a polarized solid-state target with DNP using photoexcited triplet electron spin (triplet-DNP) of pentacene.[2)] The polarization of such non-equilibrated electron spins is more than 70% independent of temperature and magnetic field. Using this method, we can overcome the upper limit (660) of the polarization enhancement factor achieved by conventional DNP. Herein, we report the first demonstration of triplet-DNP in a glassy matrix for application in NMR spectroscopy and MRI.

We applied two types of host molecules that have higher glass transition temperature than conventionally used glasses. One is a non-polar molecule, o-terphenyl (OTP).[3)] The other is a polar molecule, benzophenone (BZP).[4)] Using partially deuterated OTP and BZP as host materials, we obtained 1.5% and 0.7% ^{1}H spin polarization under 0.4 T at 120 K, respectively (Fig. 1). The enhancement factor for OTP and BZP was 4,250 and 1,900, respectively. We have also succeeded in polarizing third molecules, 2, 3, 4-trifluorobenzoic acid and 5-fluorouracil, codoped into a glassy matrix with polarizing agent (Fig. 2). ^{19}F spin in the thrid molecules were polarized using the field cycling method.[5)]

The use of photoexcited triplet electrons is a promising method to extend the limitation of DNP to higher temperatures. If hyperpolarization can be achieved above liquid nitrogen temperature, the peripheral equipment and the experiments for spectroscopy will be simplified, and the application field will be broadened. There are many samples of interest for which a higher temperature is preferable. DNP using photoexcited triplet electrons has the potential to significantly enhance the NMR/MRI sensitivity while the sample is kept at room temperature.

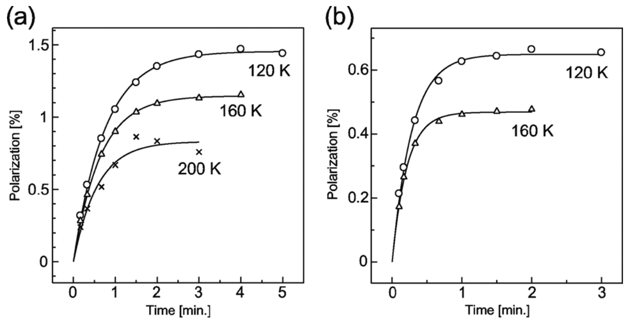

Fig. 1. ^{1}H spin polarization buildup curves for (a) partially deuterated OTP ([D14]OTP/OTP=90:10 wt%) and (b) partially deuterated BZP ([D10]BZP/BZP=90:10 wt%) doped with 0.05 mol% pentacene.

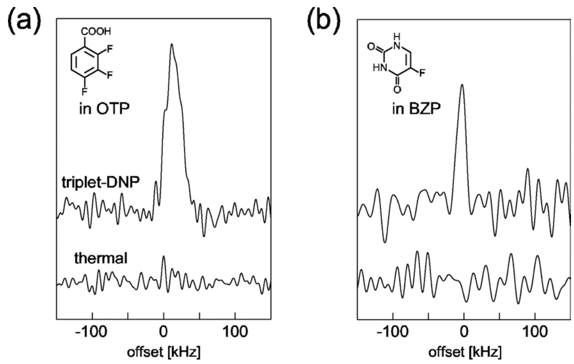

Fig. 2. Polarized ^{19}F NMR spectra of (a) 2,3,4-trifluorobenzoic acid and (b) 5-fluorouracil in glassy matrices. After DNP for 3 min and field cycling, the ^{19}F NMR signals were acquired. The NMR signals of the samples under 0.40 T at 120 K in thermal equilibrium are also shown.

References
1) D. A. Hall et al.: Science **276**, 930 (1997).
2) T. Uesaka et al.: Phys. Rev. C **82**, 021602(R) (2010).
3) S. V. Adichtchev et al.: J. Non-Cryst. Solids **353**, 1491 (2007).
4) L. M. Babkov et al.: J. Mol. Struct. **887**, 87 (2008).
5) M. Negoro et al.: Phys. Rev. Lett. **107**, 050503 (2011).

† Condensed from the article in Angew. Chem. Int. Ed. **52**, 13307-13310 (2013)
*1 RIKEN Nishina Center
*2 Department of Electronics and Materials Physics, Osaka University

Hyperpolarization of thin films with dynamic nuclear polarization using photoexcited triplet electrons†

K. Tateishi,[*1] M. Negoro,[*2] A. Kagawa,[*2] T. Uesaka,[*1] and M. Kitagawa[*2]

With dynamic nuclear polarization using the photoexcited triplet electron spin (triplet-DNP) of pentacene,[1)] nuclear spins can be hyperpolarized more than 10% even in a low magnetic field at room temperature. DNP is a means of transferring spin polarization from electrons to nuclei. In the field of experimental nuclear physics, a nuclear spin polarized target in a low magnetic field (<0.5 T) opens new research possibilities. The polarized target used presently in RI beam experiments is 1-mm thick.[2)] The relatively large target thickness prevents us from applying the target to low-energy experiments. In the experiments, beam and scattered particles have energies as low as several MeV/nucleon and cannot penetrate the 1-mm thick material. In order to perform low-energy scattering experiments, a polarized film with a thickness of less than 100 μm is desirable. However, it is difficult to cut the fragile organic crystals to such a thickness from a large crystal prepared by the conventional method.[1,2)] In this work, we succeeded in polarizing ^{1}H spins in a thin film of *p*-terphenyl and *trans*-stilbene doped with pentacene fabricated with a new method.

In order to achieve the ideal sample thickness and pentacene concentration, we applied the cell method to the sample preparation.[3,4)] The method is as follows: A powder mixture of *p*-terphenyl doped with pentacene was melted and absorbed into a gap between two quartz plates adjusted with copper foils. When this arrangement was cooling at room temperature, a single crystal, shown in Fig. 1(a), was grown in one minute. After removing one of the plates, we measured the thickness of the sample using a surface profiler. The result is shown in Fig. 1(b). From experiments, we determined that the film plane is the cleavage plane. Optimizing the sample thickness and the pentacene concentration, we obtained ^{1}H spin polarization of 12.9% in a 7-μm thick film of *p*-terphenyl doped with 0.05 mol% pentacene in 0.4 T and at room temperature. The slightly lower value of the achieved polarization compared to that for the bulk crystal grown by the conventional method may be due to the degradation of the crystal quality.

The advantage of the cell method is not only in the adjustability of the thickness over a wide range but also in a short crystal growth time. *trans*-Stilbene cannot be grown up to a single crystal doped with pentacene by the conventional method because melted *trans*-stilbene decomposes pentacene immediately. By adopting the cell method, we succeeded in avoiding considerable decomposition, preparing a single crystal of *trans*-stilbene doped with pentacene, and polarizing it with triplet-DNP for the first time. The achieved polarization was improved to 3.9% at 150 K in a 60-μm thick film of *trans*-stilbene doped with 0.05 mol% pentacene.

(a)

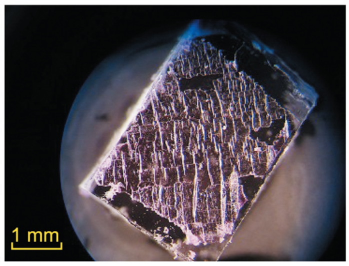

(b)

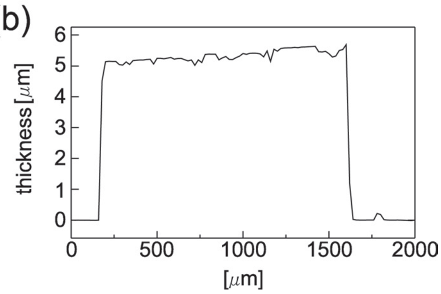

Fig. 1. (a) Photograph of *p*-terphenyl doped with 0.05 mol% pentacene grown by the cell method. (b) Typical sample thickness measured using surface profiler.

The polarized thin films also enable new applications of triplet-DNP in general NMR spectroscopy with the realization of Tycko ' s proposal,[5)] which claims that the use of multi layered structures of hyperpolarizing layers and any material of interest allows polarization transfer through the interfaces. This will open new opportunities in various fields such as chemistry, life science, and medical science.

References

1) K. Takeda: *Triplet State Dynamic Nuclear Polarization* (VDM Verlag, 2009).
2) T. Uesaka et al.: Phys. Rev. C **82**, 021602(R) (2010).
3) S. Hashimoto et al.: Jpn. J. Appl. Phys. **27**, 726 (1988).
4) T. Aoki-Matsumoto et al.: Phys. Status Solidi C **6**, 228 (2009).
5) R. Tycko: Solid State Nucl. Magn. Res. **11**, 1 (1998).

† Condensed from the article in J. Phys. Soc. Jpn. **82**, 084005 (2013)
*1 RIKEN Nishina Center
*2 Department of Electronics and Materials Physics, Osaka University

Room-temperature hyperpolarization of nuclear spins in bulk†

K. Tateishi,*1 M. Negoro,*2 S. Nishida,*3 A. Kagawa,*2 Y. Morita,*3 and M. Kitagawa*2

Dynamic Nuclear Polarization (DNP) is a means of transferring spin polarization from electrons to nuclei. As a method for enhancing bulk nuclear spin polarization, DNP has been successfully applied to areas ranging from fundamental physics to materials science, biology, and medical science. However, as long as electron spins in thermal equilibrium are used as polarizing agents, the upper limit of the polarization enhancement will be 660 for ^{1}H spin and cryogenic temperatures of around 4.2 K will be required for hyperpolarization in the order of 10% even under the strong magnetic fields used for NMR.[1)] One approach for overcoming the upper limit of the enhancement factor is to use non-thermalized electron spins. DNP with electron spins in the photo-excited triplet state (triplet-DNP) can achieve hyperpolarization independent of the magnetic field strength and temperature.[2)] We report 34% ^{1}H spin polarization in 0.40 T at room temperature.

We employed pentacene as a polarizing agent in which the excited electron spins polarize 73%, and *p*-terphenyl as a host material because of its stability at room temperature and large pentacene capacity. The curve obtained using T*h*P*h* in Fig. 1 is the buildup curve of ^{1}H spin polarization by triplet-DNP in a single crystal of *p*-terphenyl-h_{14} doped with pentacene-h_{14} 0.05 mol%. We attained a ^{1}H spin polarization of 14%.

The key breakthrough in the present work for attaining higher polarization at room temperature is the suppression of the spin-lattice relaxation by stable-isotope labeling of the constituent molecules. The ^{1}H spin-lattice relaxation in *p*-terphenyl-h_{14} was mainly due to the pendulum motion of the central benzene ring, which modulates the local dipolar field of the ^{1}H spins in and near the central ring.[3)] To suppress the spin-lattice relaxation, we synthesized *p*-terphenyl-2',3',5',6'-d_4, with which the ^{1}H spin-lattice relaxation time was increased from 11 min to 37 min. The attainable polarization was increased to 16% in the regioselectively-deuterated host doped with pentacene-h_{14} (T*d*P*h* in Fig. 1).

There is another source of ^{1}H spin-lattice relaxation that affects DNP. The triplet electrons play the role of a polarizing agent as well as contribute to ^{1}H spin-lattice relaxation through a perturbation of the local field of the ^{1}H spins in the vicinities. To suppress the spin-lattice relaxation, we used pentacene-d_{14} as the polarizing agent. The attainable polarization was increased to 18% in the *p*-terphenyl-h_{14} doped with pentacene-d_{14} (T*h*P*d* in Fig. 1).

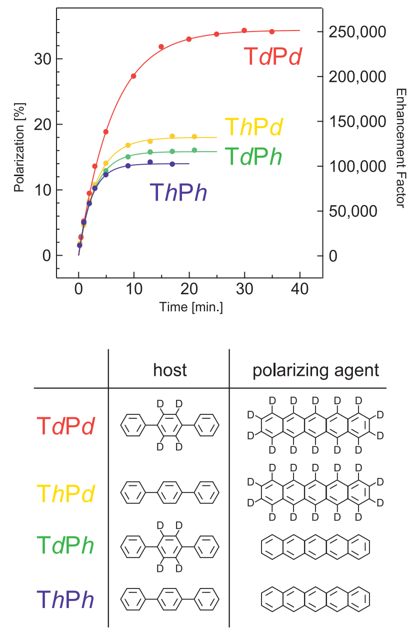

Fig. 1. Polarization buildup curves. The blue, green, yellow, and red curves denote the polarization buildup curves using T*h*P*h*, T*d*P*h*, T*h*P*d*, and T*d*P*d*, respectively. The polarizations and enhancement factors were estimated by comparing the intensities of the hyperpolarized signals and the thermal ones in 0.40 T at room temperature.

Suppressing either of the two relaxation sources was not sufficient. By using *p*-terphenyl-2',3',5',6'-d_4 doped with pentacene-d_{14} (T*d*P*d* in Fig. 1), we achieved a bulk ^{1}H spin polarization of 34% at room temperature in 0.40 T, which results in an enhancement factor of 250,000.

Room-temperature hyperpolarization techniques using photoexcited triplet electrons simplify DNP experiments. The NMR sensitivity of samples that prefer ambient temperatures can be boosted significantly. Bulk nuclear hyperpolarization in such low magnetic fields is also desirable for the polarized target for RI beams[4)] and the polarized filter for neutron beams.[5)]

References

1) T. Maly *et al.*: J. Chem. Phys. **128** 052211 (2008)
2) K. Takeda: *Triplet State Dynamic Nuclear Polarization* (VDM Verlag, 2009).
3) K. Kahda *et al.*: J. Phys. Soc. Jpn. **51** 3936 (1982).
4) T. Uesaka *et al.*: Phys. Rev. C **82** 021602(R) (2010).
5) M. Haag *et al.*: Nucl. Instrum. Methods Phys. Res., Sect. A **678** 91 (2012).

† Condensed from the article in Proc. Natl. Acad. Sci. USA **111**, 7527 (2014)

*1 RIKEN Nishina Center
*2 Department of Electronics and Materials Physics, Osaka University
*3 Department of Chemistry, Osaka University

Development of ^{3}He comagnetometer for ^{129}Xe EDM measurement

Y. Ichikawa,[*1,*2] M. Chikamori,[*2] Y. Ohtomo,[*2] E. Hikota,[*2] Y. Sakamoto,[*2] T. Suzuki,[*2] T. Sato,[*2] S. Kojima,[*2] H. Shirai,[*2] H. Miyatake,[*2] T. Nanao,[*2] K. Suzuki,[*2] T. Inoue,[*3] T. Furukawa,[*1,*4] A. Yoshimi,[*1,*5] C. P. Bidinosti,[*6] T. Ino,[*7] H. Ueno,[*1] Y. Matsuo,[*1,*8] T. Fukuyama,[*9] and K. Asahi[*1,*2]

A permanent electric dipole moment (EDM) that directly violates time reversal symmetry attracts much attention, because an unknown CP-violating phase which is necessary for understanding the present matter-dominated Universe, is expected to be probed by EDM. The present study aimed to measure the EDM in a ^{129}Xe atom to the order of 10^{-28} $e$cm, which is beyond the present upper limit[1]. We employed an active nuclear spin maser[2,3] to sustain the spin precession of ^{129}Xe over a long duration. The active spin maser operates in the following manner. The ^{129}Xe spin is longitudinally polarized through spin exchange with optically pumped Rb atoms. Precession of the ^{129}Xe spin in an applied static field is detected optically by transversely repolarized Rb atoms. By referring to the precession signal thus obtained, a feedback magnetic field is generated such that its direction is kept orthogonal to the transverse component of the spin. The feedback field thus prevents decay of the transverse magnetization.

In an EDM measurement, magnetometry is essential because a large systematic uncertainty in frequency arises from long-term drifts in the external magnetic field. A comagnetometer using ^{3}He was incorporated into the nuclear spin maser system in order to cancel out the drifts[4]. Because a ^{3}He comagnetometer can measure the field exerted on the ^{129}Xe precession, it is an *in situ* magnetometer.

The main difficulty in realizing the ^{3}He comagnetometer stems from the fact that the spin-exchange rate between ^{3}He and Rb is lower than that between ^{129}Xe and Rb by several orders of magnitude. Because there is little source of polarization, spin relaxation at the surface of the cell and impurity in the gas critically degrade the polarization of ^{3}He. Therefore, a GE180 glass with low magnetic impurity and low gas leakage was employed to fabricate the cell. The cell has a spherical shape with a diameter of 20 mm, containing 1 Torr of ^{129}Xe, 470 Torr of ^{3}He, 100 Torr of buffer N_2 gases, and Rb vapor. We typically achieved 3% of the polarization and over 50 hours of the longitudinal spin relaxation time for ^{3}He at 100 °C.

*1 RIKEN Nishina Center
*2 Department of Physics, Tokyo Institute of Technology
*3 Cyclotron and Radioisotope Center, Tohoku University
*4 Department of Physics, Tokyo Metropolitan University
*5 Research Core for Extreme Quantum World, Okayama University
*6 Department of Physics, The University of Winnipeg
*7 Institute of Material Structure Science, KEK
*8 Department of Physics, Hosei University
*9 Research Center for Nuclear Physics, Osaka University

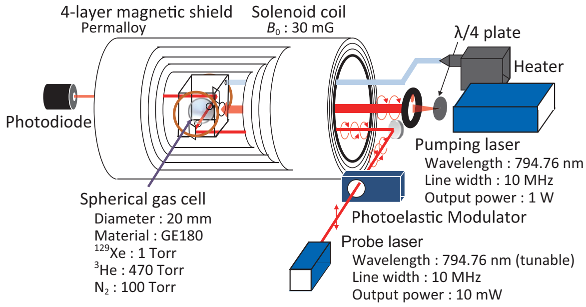

Fig. 1. Experimental setup for active spin maser.

The experimental setup used to test the ^{3}He comagnetometer is shown in Fig. 1. The gas cell is placed in a solenoid coil which generates a static magnetic field B_0 ($\sim$ 30 mG), and is enclosed in a 4-layer magnetic shield. A circularly polarized pumping laser is incident on the cell parallel to B_0. A probe laser passes through the cell in a direction orthogonal to B_0 and is detected by a photodiode. The signal from the photodiode is divided into two, each being lock-in-amplified with ^{129}Xe or ^{3}He precession frequency, and the resulting two beat signals are obtained and processed individually at the same time to generate their feedback magnetic fields through two separate coils.

We succeeded in operating the masers of ^{129}Xe and ^{3}He concurrently[4]. The individual determination precisions of the average frequencies achieved in 10^6 seconds for both ^{129}Xe and ^{3}He are ∼100 nHz. However, the frequency shift due to contact interaction with polarized Rb atoms prevents the ^{3}He comagnetometer from realizing its full potential because the strengths of the Rb-^{129}Xe and Rb-^{3}He contacts are different. Therefore, we decided to employ a double-cell geometry in which the gas volume is divided into a section for optical pumping and another for optical spin detection in order to suppress Rb polarization in the optical detection section and thus reduce the frequency shift[5]. Development of the ^{3}He comagnetometer with the double-cell geometry is in progress.

References

1) M. A. Rosenberry et al.: Phys. Rev. Lett. **86**, 22 (2001).
2) A. Yoshimi et al.: Phys. Lett. A **304**, 13 (2002).
3) A. Yoshimi et al.: Phys. Lett. A **376**, 1924 (2012).
4) Y. Ichikawa et al.: Eur. Phys. J. Web of Conf. **66**, 05007 (2014).
5) E. Hikota et al.: Eur. Phys. J. Web of Conf. **66**, 05005 (2014).

SCRIT electron spectrometer (II)

T. Suda,[*1,*2] A. Enokizono ,[*1,*3] S. Matsuo ,[*1,*3] T. Miyamoto ,[*1,*2] S. Wang,[*1,*4] S. Yoneyama,[*1,*2] T. Tsuru,[*1,*2] and T. Tamae[*1,*2]

The SCRIT electron spectrometer is being constructed at the SCRIT electron scattering facility[1,2]. In this report, the current status of the construction is described. The spectrometer, shown in Fig. 1, will be used to measure the cross section for elastic electron scattering off short-lived nuclei to determine their charge-density distributions[3] . It consists of a dipole magnet, two drift chambers, and a pair of plastic scintillators. The drift chambers sandwich the magnet for trajectory measurements, and the plastic scintillators trigger data acquisition. Knowing the detailed magnetic-field distribution, the momenta, scattering angles, and scattering positions of the electrons are determined. The spectrometer should have large acceptance and a good momentum resolution of the order of 10^{-3} to identify the elastic scattering events.

1 Magnet

The window-frame magnet, the gap region of which is 170 cm (width) × 140 cm (length) × 29 cm (height), is employed. The field cramps were carefully designed to reduce the fringing field down to a few gauss at the electron beam position. Magnetic-field measurements have been performed, and the detailed field distribution was obtained[4] . The magnet is palced on a movable platform, as shown in Fig. 2, such that the magnet can be moved away from the beam line by 1.5 m. The re-positioning accuracy was confirmed to be better than 50 μm. The magnet system will be ready for operation immediately after the power line and cooling water are set up; this is expected to be completed in the first half of 2014.

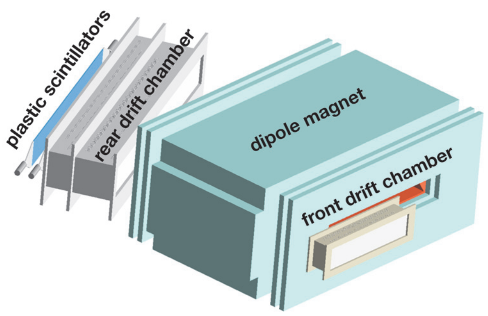

Fig. 1. The SCRIT electron spectrometer.

*1 RIKEN Nishina Center
*2 Research Center for Electron Photon Science, Tohoku University
*3 Department of Physics, Rikkyo University
*4 School of Space Science and Physics, Shandong University, China

2 Detectors

A large drift chamber, which is placed in the rear side of the magnet, was constructed in 2013. The small drift chamber used in the previous SCRIT studies will be used as the front drift chamber. A new readout system, RINEI RP 1212N, which digitizes the drift times on board is currently being tested[5]. A pair of large plastic scintillators of dimensions 220 cm (length) × 30 cm (width) × 2 cm (thickness) are used for detecting the scattered electrons, and their coincidence triggers data acquisition. To reduce non-negligible false triggers due to cosmic rays, veto detectors will be arranged. The drift chambers and the plastic scintillators will be ready for use in the first half of 2014.

3 Spectrometer commissioning

The SCRIT electron spectrometer will be commissioned using the W-wire target installed inside the SCRIT chamber in the second half of 2014. Using the scattered electrons from the W wire target, one can determine the track-reconstruction efficiency, momentum resolution, etc. After commissioning, we will immediately conduct experiments on electron scattering off a short-lived nucleus, which will be ^{132}Sn . The world ' s first observation of electrons scattered off an exotic nucleus is expected to take place in the fiscal year 2014.

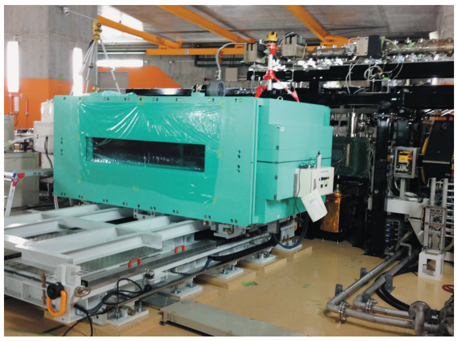

Fig. 2. The magnet with the movable platform.

References
1) T. Adachi *et al.*: Accel. Prog. Rep. **45**, 144 (2012).
2) T. Suda *et al.*: Accel. Prog. Rep. **46**, 144 (2013).
3) T. Suda *et al.*: Prog. Theor. Exp. Phys. **03C**, 008 (2012).
4) T. Tamae *et al.*: In this report.
5) S. Matsuo *et al.*: In this report.

Field measurement of SCRIT electron spectrometer

T. Tamae, [*1,*2] T. Miyamoto, [*1,*2] and T. Suda[*1,*2]

A large-acceptance magnetic spectrometer for electron scattering on unstable nuclei was constructed, and its magnetic field was measured. The analysis of the field distribution and the development of a program of track reconstruction are in progress.

The design[1)] and construction[2), 3)] of the spectrometer have been reported elsewhere. The spectrometer is designed to have a reasonably good resolution of $\Delta p / p$: 10^{-3}, a large solid angle of about 100 msr, and a large scattering coverage of 30-60° .

The spectrometer consists of a single window-frame dipole magnet with an aperture of 29 cm in height (y), 1.4 m in length (z) and 1.71 m in width (x). As the spectrometer has no focal plane, the momentum and vertex position of scattered electrons are fixed through the track reconstruction using the information of drift chambers, as shown in Fig. 1. This implies that the knowledge of the precise distribution of the magnetic field is essential for analysis.

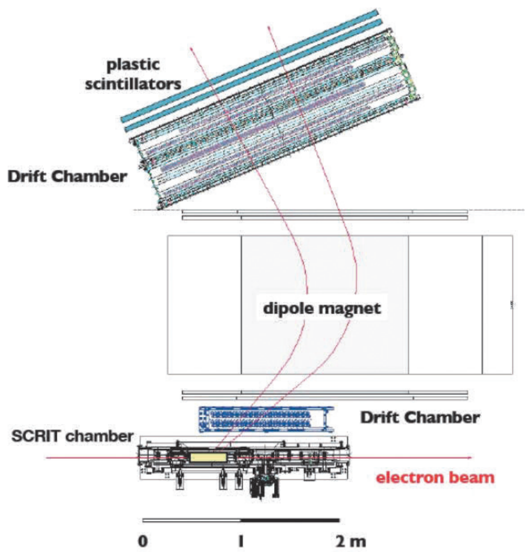

Fig. 1. Layout of the spectrometer, detectors, and SCRIT (Self-Confining Radioactive Isotope ion Target).

The magnetic field distribution was measured using a Hall probe at 37,118 points in 1/8 of the entire volume of the aperture and connecting regions. The absolute magnetic-field values were calibrated using an NMR set at a fixed position in the mid-plane. The field map was obtained at three strengths ((a) 4,096, (b) 7,628, and (c) 8,017 G at the NMR). The measured values were corrected for the drift of a Hall probe and for inaccuracy of the probe orientation. They were normalized to the NMR values.

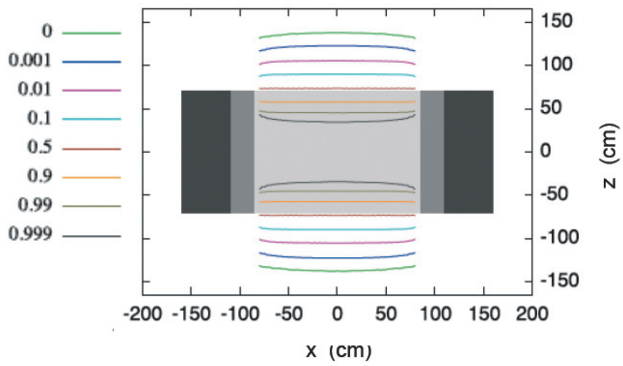

Fig. 2. Contour plot of field strength for a center field of 8,017 gauss. Numbers attached to lines show the ratio of the field strength to the central field strength. The order of lines in the figure is same as the order of lines in the legend. Light-grey region: aperture region of the magnet; dark-grey region: coil; black region: return yoke.

The field strength for case (c) is contoured in Fig. 2; numbers attached to lines show the ratio of the field strength to the central field strength. The figure shows that the field is almost uniform all the way to the coils, which is a unique merit of the window-frame magnet. The measured field along the electron beam at z = -155 cm is about -3 gauss; the leakage field of 3 G gives a closed orbit distortion (COD) of 0.1 mm at the SCRIT (max. 1.5 mm in the ring). These values are within acceptable levels for the ring operation.

The field strengths were also compared to calculations using the program OPERA-3D. The difference between the measured and calculated field strengths is much less than 10^{-3} in the aperture region, but it becomes larger at the fringe field region, especially at positions close to magnetic poles and field clamps. The estimation of errors for the electron momentum and vertex positions due to inaccuracy of the field distribution is in progress.

*1 RIKEN Nishina Center
*2 Research Center for Electron-Photon Science (ELPH), Tohoku University

References
1) T. Adachi *et al.*: Accel. Prog. Rep. **45**, 144 (2012).
2) T. Suda *et al.*: Accel. Prog. Rep. **46** 184 (2013).
3) T. Suda *et al.*: in this progress report.

Design of Recoil-Arm for the SCRIT Experiment

Y. Shimakura,[*1,*2] A. Enokizono,[*1,*2] T. Ohnishi,[*2] K. Kurita,[*1] M. Togasaki,[*1,*2] and M. Wakasugi[*2]

The self-confining RI Ion target (SCRIT) electron scattering facility[1)] is now under construction. Electrons scattered from target ions trapped in the SCRIT device are detected, and their angular distribution is obtained. A recoil ion detector referred to as the "recoil-arm" is being designed. It will be used for the determination of the luminosity distribution in the ion trapping region along the beam axis. We also plan to use the recoil-arm for estimating the contribution of residual gas ions, which are trapped simultaneously with target ions in scattering events[2)].

Figure 1 shows a schematic of the recoil-arm. It consists of returning meshes, multi-stage slits, two quadrupole benders[3)], and a channeltron array consisting of 15 channeltrons. Ions that are recoiled from the trapping region in the SCRIT are accelerated by the electrostatic potential applied to the SCRIT electrodes. Returning meshes are used to reduce the background ions that leak in the trapping region in the SCRIT. Multi-stage slits confine the angular acceptance of recoil ions. Fig.2 shows the first quadrupole bender designed by us. Two quadrupole benders are used to deflect the transported recoiled ions and reduce the background produced by the synchrotron radiation. The channeltrons are arranged in a line so as to minimize dead space. The aperture of every channeltron is rectangular (15mm×30 mm).

Perpendicularly recoiled ions as a result of forward electron scattering are extracted and transported in parallel to the channeltron array. The counting rates of the 15 channneltrons indicate the trapped ion distribution, i.e., luminosity, along the beam axis. We can identify the mass number of the recoil ions in scattering events by measuring the time delay from the instant when forward scattered electrons are detected by the plastic scintillator; accordingly, we can estimate the attributable fraction of residual gas ions in scattering events.

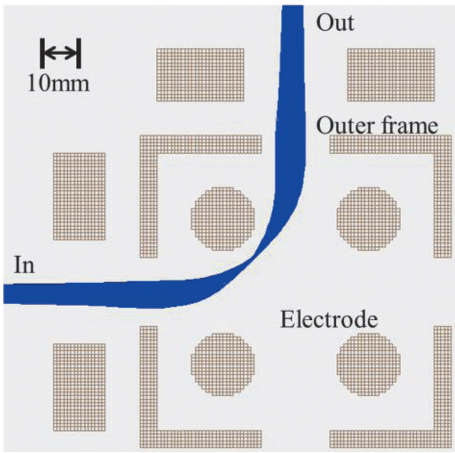

Fig.2. Quadrupole bender

The off-line test bench of the recoil-arm is now under construction. We will be studying the performance of the recoil-arm before its installation in the SCRIT device.

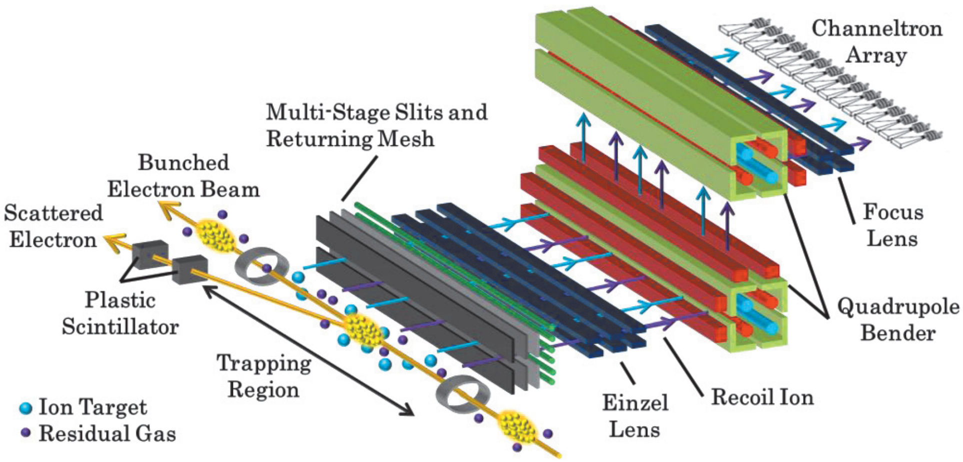

Fig.1. Schematic diagram of the recoil-arm

References
1) M. Wakasugi et al.: Nucl. Instr. and Meth. A [**532**], 216 (2004)
2) R. Ogawara et al.: RIKEN Acc. Prog.Repo. [**45**], 142 (2012)
3) H. D. Zemsn et al.: Rev. Sci. Instrum. [**48**], 8 (1977)

*1 Department of Physics, Rikkyo University
*2 RIKEN Nishina Center

Test of new readout card for the SCRIT drift chamber

S. Matsuo,[*1,*2] A. Enokizono,[*1,*2] K. Kurita,[*1] T. Suda,[*2,*3] T. Tamae,[*2,*3] T. Tsuru,[*2,*3] T. Miyamoto,[*2,*3] S. Yoneyama,[*2,*3] and S. Wang[*4]

The SCRIT electron spectrometer[1)2)] consists of a set of dipole magnets, the front and rear drift chambers (DC), and plastic scintillators for event triggering. The rear DC has a volume of 274 cm x 36 cm x 78 cm, and it has a total of 5 layers of UVX consisting of 1130 channels, which have an intrinsic 150-μm position determination capability with 1-ns timing resolution. It covers a solid angle of 100 mSr for scattered electrons to achieve a good momentum resolution ($\Delta p/p \sim 10^{-3}$) with a wide scattering coverage (30°-60°) . We employed a new TDC card (RINEI RP1212) based on SiTCP technology[3)] for DC data readout. In this article, we report the results of readout tests of RP1212 using the actual experimental setup.

RP1212 has dimensions of 150 mm x 190 mm, and it is capable of processing ADC and TDC data for 64 channels. TDC is implemented in FPGA (Xilinx Kintex7) with 1-ns timing resolution. It is directly attached to the DC, and signals are immediately digitalized by FPGA on the board. The data is transmitted to a PC via Gigabit Ethernet. An advantage of using RP1212 is that the path length of the analog signal can be minimized such that the data is less influenced by analog noise as compared to the earlier readout system using the ASD card and TDC module. Nevertheless, since the DC and RP1212 will be located very close to the RF power source for the electron storage ring[4)], the background effect that originates from the RF noise was investigated.

Figure 1 (A) shows a typical β ray signal (^{90}Sr) using prototype DC and RP1212 under the RF environment. The top panel indicates that the pulse height of the β signal is ~800mV, and the bottom panel in a different time scale clearly illustrates 5-nsec-period oscillation, which is apparently caused by the 191-MHz RF noise. The noise amplitude is less than ~150 mV, which is much smaller than that of the β signal, at the full RF power condition. Fig 1 (B) shows the comparison of noise counts between RF off and on cases as a function of the threshold voltage for the ASD discriminator (Vth). The noise count is zero at Vth ~200 mV, while the noise rate is not negligible below a Vth of 150 mV when RF is on. In fact, the count at Vth = 100 mV is rather dominated by noise from powerline of RP1212. Since a typical height of a β signal with no angle is 600 mV to 800 mV, we found that the appropriate Vth is 400 mV to 500 mV, which is sufficient to trigger a β signal and eliminate RF noise simultaneously.

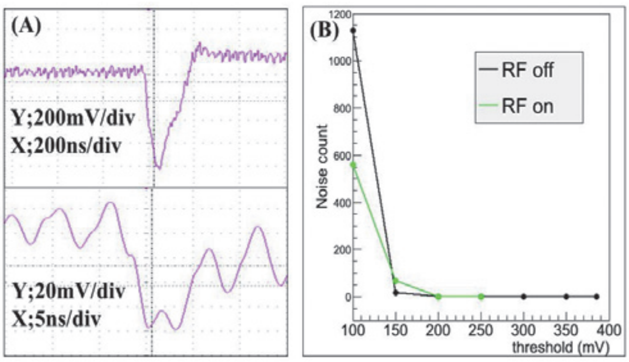

Fig. 1. (A) The top panel shows an analog signal for a beta ray measured with RP1212, and the bottom panel shows the RF noise in expanded scale for both time and pulse height. (B) Noise count rate as a function of threshold value for ASD chip on RP1212.

We measured the timing distribution of β signals using RP1212 and the actual SCRIT-DC for He+CH_4 (50:50) gas mixture. We examined the plateau region of detection efficiencies and then found that the operational voltage range for good efficiency is 2550 V to 2800 V. Therefore, the normal operation voltage is set at 2750 V.

Figure 2 shows the timing distribution of β signals. For better statistics, the histogram adds up TDC data from 64 channels. Since RP1212 has a common stop trigger, which is provided by a trigger scintillator, the right edge of distribution originates from β signals that were received near the anode wire. Since the rising edge is clear, we can use it as a calibration point. We are working on the timing calibration to achieve ~150 μm position resolution.

In 2014, we will proceed to developments of calibrations and tracking framework aiming at the first result of the ^{132}Sn electron scattering experiment.

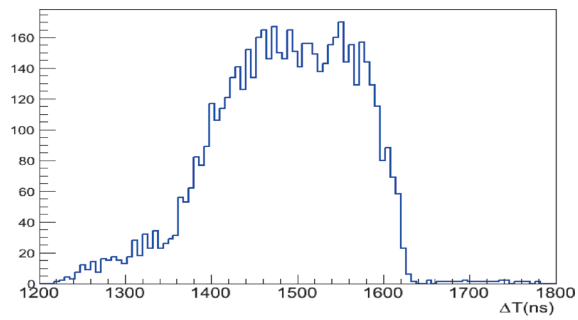

Fig. 2. The timing distribution of the beta signal.

References
1) T. Suda et. al.: In this report.
2) T. Tamae et. al.: In this report.
3) T. Uchida: IEEE VOL.55, NO.3,JUNE 2008
4) T. Suda et. al.: Prog. Theor. Exp. Phys. 03C, 008(2012).

*1 Department of Physics, Rikkyo University
*2 RIKEN Nishina Center
*3 Research Center for Electron Photon Science, Tohoku University
*4 School of Space Science and Physics, Shandong University

Construction status of the Rare-RI Ring (R3)

Y. Yamaguchi,*1 M. Wakasugi,*1 Y. Abe,*1,*2 T. Fujinawa,*1 M. Kase,*1 M. Komiyama,*1 K. Kumagai,*1 T.Maie,*1 D. Nagae,*1,*2 J. Ohnishi,*1 A. Ozawa,*1,*2 F. Suzaki,*1,*3 T. Uesaka,*1 Y. Watanabe,*1 T. Yamaguchi,*1,*3 H. Yamasawa,*1 Y. Yanagisawa,*1 J. Zenihiro,*1 and Y. Yano*1

The Rare-RI Ring (R3) was constructed smoothly[1], and the installation of the magnets and power supplies were completed by the end of March 2013. Subsequently, we tested a cooling water conduction of the magnets and prepared the interlock system for the magnets in order to perform the excitation tests of the magnets. The excitation test was successfully completed at the beginning of July 2013. Subsequently, we performed the precise magnet alignment by using a laser tracker. All the magnets were aligned to the design value by less than 0.1 mm. Figure 1 shows the picture of R3 at the beginning of July 2013.

Fig. 1. Picture of R3 at the beginning of July 2013.

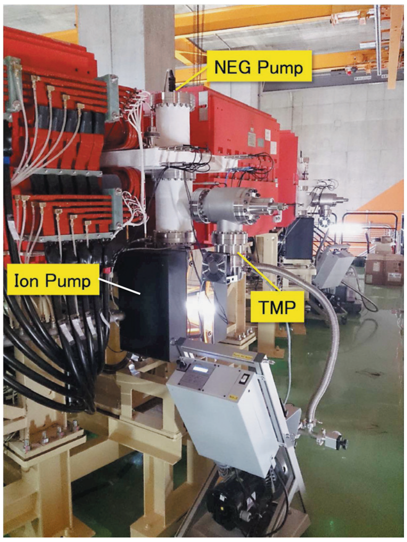

Fig. 2. Vacuum pump combination using TMP, ion pump, and NEG pump.

Next, we installed vacuum pumps and vacuum gauges. Figure 2 shows a vacuum pump combination for the arc section. The turbo moleculer pump (TMP) is movable, and is used as a rough pumping system with a scroll pump. The nominal pumping speed of the TMP is 250 L/s for N_2. Ion and non evaporable getter (NEG) pumps are used for the ultra-high vacuum condition. The nominal pumping speed of the ion pump is 500 L/s for N_2 and that of the NEG pump is 2000 L/s for H_2. The combination of the ion and NEG pumps for R3 is 26 units.

In order to bake the R3 chamber, we installed heater wires on all the chamber surfaces and glued a heat insulator, which is an alumina-silica sheet, onto the heater wires, as shown in Fig. 3. The chamber surface is typically warmed up to about 250 °C. K-type thermocouple is used for thermal control.

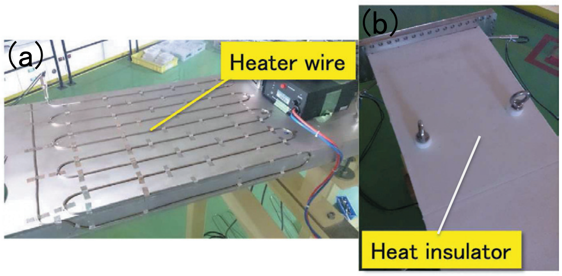

Fig. 3. Straight section of an R3 chamber. (a) heater wire and (b) a heat insulator.

Recently, we succeeded in establishing a control system for power supplies by using EPICS[2]. In addition, we confirmed that a vacuum-integrated control system worked normally. We are now testing beam-monitoring systems[3,4] and a kicker system. We will carry out an off-line performance test for R3 using the α source.

References
1) Y. Yamaguchi et al.: RIKEN Accel. Prog. Rep. **46**, xiv (2013).
2) M. Komiyama et al.: In this report.
3) Y. Abe et al.: In this report.
4) F. Suzaki et al.: In this report.

*1 RIKEN Nishina Center
*2 Institute of Physics, University of Tsukuba
*3 Department of Physics, Saitama University

Developments of time-of-flight detectors for Rare-RI Ring

Y. Abe,[*1,*2] D. Nagae,[*2] S. Okada,[*2] A. Ozawa,[*2] T. Yamaguchi,[*3] Y. Saitoh,[*2] K. Sawahata,[*2] T. Suzuki,[*3] Y. Yamaguchi,[*1] T. Uesaka,[*1] and M. Wakasugi[*1]

Construction of the Rare-RI Ring, which will be used to measure masses of short-lived rare-RI with a relative precision of 10^{-6}, is underway at RIBF.[1,2]

We are developing three types of time-of-flight (TOF) detectors for installation in the Rare-RI Ring; two of the three are placed at the entrance (start detector) of the ring and the third is placed inside the ring as the circulative ion detector (CD). The start detector provides the start signal of the TOF system for the mass measurement. The CD provides a signal corresponding to each circulation. The CD is indispensable for monitoring the motion of the particle inside the ring at the beginning of the storage.

The required specifications for the start detector are i) a good timing resolution less than 100 ps because the total TOF is about 0.7 ms, ii) a large effective area (100 mm × 50 mm) to cover the large beam size, iii) small energy loss and energy straggling so as to not affect the mass resolution of mass measurement in the ring, and iv) no change in the charge state of the nuclei, achieved by passing them through a detector to avoid reduction of the transmission efficiency in the ring. On the other hand, the required specifications for the CD are i) small energy loss to maintain the momentum of the nuclei within the momentum acceptance during 100 circulations, ii) a high detection efficiency, iii) a large effective area (100 mm × 50 mm) to match the large beam size, and iv) a good timing resolution to separate each circulation (the typical time for one revolution is about 350 ns.) Furthermore, the CD should be maintained in ultra high vacuum.

To mount the detector in a limited narrow space, we developed a "T-shaped" TOF detector, as shown in Fig. 1(a). The left part of the detector consists of two 1" photomultipliers (R4998) coupled to the top and bottom parts of a 100 μm-thickness scintillator, while the right part contains one 2" photomultiplier (H2431-50) coupled directly to the right side of the scintillator. It is noted that, in the "T-shaped" TOF detector, we can obtain the horizontal position information, which may be used to improve the timing resolution. In the case of heavy nuclei and changes in the charge state, the 100-μm-thickness of the scintillator is no sufficiently thin. We thus consider introducing a micro channel plate (MCP) detector, as has been used at ESR[3] and CSRe[4], which has a sufficiently thin carbon foil. To cover the larger beam size at the entrance of Rare-RI Ring, we are developing the detector with a lager sensitive area.[5]

As the CD, we developed a similar MCP-type detector, used at the Gas filled Recoil Ion Separator (GARIS). [6] When the beam passes through the thin carbon foil (60 μg/cm^2), secondary electrons are generated in the foil. The generated electrons are transported to the MCP by only the electric field. A schematic view of the detector is shown in Fig. 1(b). A mirror electric field and an acceleration electric field are how they are created using wires. Wires (W+Au) with a 40-μm diameter are set at distance of 8.0 mm from carbon foil with a 1.0-mm pitch, and wires (W+Au) for the triangular part are set with a 3.0-mm pitch.

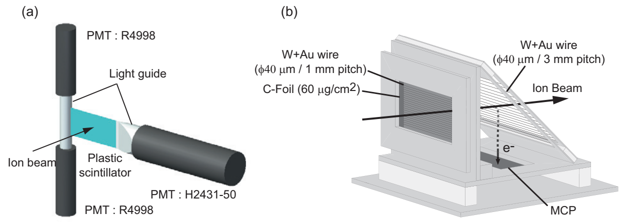

Fig. 1. Schematic view of the (a) "T-shaped" TOF detector and (b) circulative ion detector (CD).

The experiment to check the performance of the TOF detectors was carried out at the secondary beam line, SB2 course,[7] at HIMAC at the National Institute of Radiological Sciences (NIRS). A primary beam of ^{84}Kr was accelerated up to 200 A MeV and delivered to the SB2 course. For the "T-shaped" TOF detector, a timing resolution of $\sigma \approx 60$ ps is obtained. The position resolution in the horizontal axis is around $\sigma \approx$ 2 mm. For the CD, a timing resolution of $\sigma \approx 130$ ps is obtained. The detection efficiency was about 72%. This value is comparable with the efficiency for the isochronous mass measurement at ESR.[8]

We will install these TOF detectors in the Rare-RI Ring in the next fiscal year.

References

1) Y. Yamaguchi, et al.: Nucl. Instr. and Meth. B 317 (2013) 629.
2) A. Ozawa, et al.: Prog. Theor. Exp. Phys. (2012) 03C009.
3) M. Hausmann, et al.: Nucl. Instr. and Meth. A 446 (2000) 569.
4) B. Mei, et al.: Nucl. Instr. and Meth. A 624 (2010) 109.
5) D. Nagae, et al.: Nucl. Instr. and Meth. B 317 (2013) 640.
6) K. Morimoto et al.: RIKEN Accel. Prog. Rep. 46 (2013) 191.
7) M. Kanazawa, et al.: Nucl. Phys. A 746 (2004) 393.
8) N. Kuzminchuk: PhD thesis, Justus-Liebig Universität Gießen, (2011).

*1 RIKEN Nishina Center
*2 Institute of Physics, University of Tsukuba
*3 Department of Physics, Saitama University

Performance of a resonant Schottky pick-up for the Rare-RI Ring project

F. Suzaki,[*1,*2] J. Zenihiro,[*1] A. Ozawa,[*3] T. Suzuki,[*2] T. Uesaka,[*1] M. Wakasugi,[*1] K. Yamada,[*1] T. Yamaguchi,[*2] Y. Abe,[*1,*3] Y. Yamaguchi,[*1] and Rare-RI Ring collaboration

Construction of a new storage ring called "Rare-RI Ring" was started in 2012[1,2] at RIBF. This project aims at precise isochronous mass measurements for extremely neutron-rich exotic nuclei in the r-process nucleosynthesis. To precisely tune the ion-optical condition to be isochronous, the resonant Schottky noise pick-up technique will be employed. We performed an off-line test of the resonant Schottky pick-up.

Figure 1 shows the resonant Schottky pick-up that will be installed in the Rare-RI Ring. It consists of a pillbox-type resonant cavity electrically isolated from the beam pipe by a ceramic tube. A schematic view of the pick-up is shown in Fig. 2(a): a chamber shown in blue is the beam pipe and the shaded cylinder surrounding the beam pipe is the cavity equipped with two ports (yellow). The ports are movable plunger pistons that can adjust the resonance frequency (f_{res}) of the eigenmode. Fig. 2(b) shows the cross-sectional view of the cavity, and the detailed structure of the gap can be seen at the center. The cavity itself is filled with air and has the shape of a pillbox with an outer diameter of 750 mm and length of 200 mm. The inner diameter is 320 mm. The lower flanges (see Fig. 1) are prepared for feedthroughs to take out signals from a loop coil that magnetically couples to the cavity field induced by the beam.

Using a network analyzer, we measured the basic quantities characterizing the resonant cavity: the resonance frequency, the shunt impedance R_{sh}, and the unloaded Q factor Q_0. To measure R_{sh}, the perturbation method was adopted. From the measurements, $f_{\mathrm{res}} = 171.54(\pm0.44)$ MHz, $R_{\mathrm{sh}} = 169$ kΩ, and $Q_0 = 1884$ were obtained.

For tuning the isochronous field settings, the proposed pick-up is required to have an excellent single-ion sensitivity. By using the results of the off-line test, the output signal power corresponding to a single ion with charge q at resonance[3] is estimated to be $P = q^2 \times 2.8 \times 10^{-21}$ W , and the power of thermal noise P_{noise} is 7.1×10^{-19} W. For $q \geq 16$, the signal power exceeds the noise floor, and the signal from the beam can be detected by the present Schottky pick-up. Therefore, the performance is sufficient for precise tuning of isochronus field settings of the Rare-RI Ring.

The resonant Schottky pick-up will be soon installed into the Rare-RI Ring. Detailed results of the off-line test and online beam performance test will be reported in forthcoming publications.

*1 RIKEN Nishina Center
*2 Department of Physics, Saitama University
*3 Institute of Physics, University of Tsukuba

Fig. 1. The resonant Schottky pick-up that will be installed in the Rare-RI Ring. The resonant cavity surrounds the beam pipe with a ceramic gap. The lower flanges for feedthroughs are the output coupler loop, and the upper feedthroughs are the movable plunger pistons, using which the resonance frequency of the eigenmode can be adjusted.

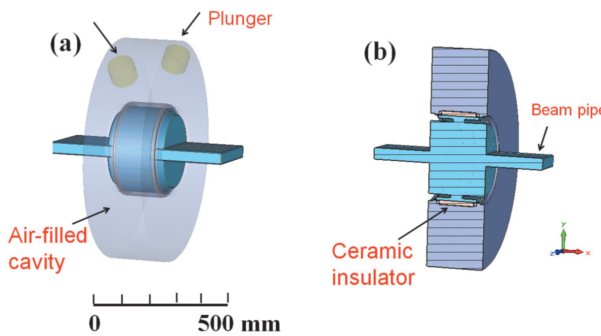

Fig. 2. Schematic view of a resonant cavity for the Rare-RI Ring. (a) The pillbox-type cavity shown translucently surrounds the beam pipe separated by a ceramic tube. (b) A cross-sectional view of the cavity showing the detailed structure of the gap.

References
1) Y. Yamaguchi et al.; Nucl. Instrum. Methods Phys. Res. B 317 (2013) 629.
2) A. Ozawa et al.; Prog. Theor. Exp. Phys. 2012 (2012) 03C009.
3) F. Nolden et al.; Nucl. Instrum. Methods Phys. Res. A 659 (2011) 69.

Control system for the magnet power supplies of the Rare-RI Ring

M. Komiyama,[*1] Y. Abe,[*1,*2] Y. Yamaguchi,[*1] K.Kumagai,[*1] and M. Wakasugi[*1]

We report on the status of the control system of the magnet power supplies of the rare-RI ring. The development of the control system was started at the beginning of 2013, and it has become possible to remotely control the main and trim coils of dipole, septum, and quadrupole magnets since November 2013.

Components to be controlled in the rare-RI ring are classified into two groups: components for operating the rare-RI ring as a storage ring and other components used solely for precise mass measurements. The components belonging to the former group, such as magnets and vacuum systems, are similar to those used in the existing RIBF accelerators. As a first step in implementing the control system for the rare-RI ring, we have started developing the control system for the magnet power supplies that will be first used for magnetic-field measurements of the rare-RI ring. Control systems for vacuum components will be integrated into the control system for the magnet power supplies.

The control system of the rare-RI ring is developed on the basis of Experimental Physics and Industrial Control System (EPICS)[1]. To save construction cost and time, the control system is designed to utilize the software resources developed for the RIBF accelerator control system in the past 10 years. Following recent trends in the control systems of the RIBF accelerators, the programmable logic controllers (PLCs) manufactured by Yokogawa Electric Corporation (hereafter, FA-M3) was chosen as a main controller of the components. The controllers used for the magnet power supplies are summarized in Table 1.

Table 1: Controllers used in the rare-RI ring

Type of Magnet (Number)	Number of magnet power supplies	Type of controller (Number)
Main coil of dipole magnets (24)	1	F3SP66 (1)
Trim coil of dipole magnets (10)	10	Serial-Ethernet Converter (1)
Septum magnet (4)	2	F3SP66 (2)
Kicker magnet (5)	10	Under discussion
Correction coil magnet (24)	6	Under discussion
Quadrupole magnet (10)	10	F3SP66 (5)

Magnet power supplies, except for those exciting the trim coils, were newly developed for the rare-RI ring. F3SP66 is a conventional ladder PLC-CPU for the FA-M3 system, and it is controlled by using netDev, an EPICS device, and driver support for general network devices developed by KEK and RIBF control groups[2]. Old power supplies are reused for the trim coils; these are controlled via serial communication, RS422. We have connected a serial-Ethernet converter to the magnet power supply and controlled it via Ethernet by using StreamDevice, an EPICS device support for devices controlled by sending and receiving strings[3].

For an operator interface (OPI) application, we have selected Control System Studio (CSS).[4] CSS is a user interface framework for control systems based on Eclipse, which has functions of not only a graphical user interface (GUI) but also an alarm system and a data archiving system. It is at the forefront of recent OPIs.

Regarding a network, we have recently installed a local area network (LAN) dedicated to the rare-RI ring (hereafter, rare-RI ring LAN), which will be used in combination with the LAN of the RIKEN Wako campus (hereafter, Wako LAN). Servers and controllers for each component in the rare-RI ring are connected to the rare-RI ring LAN, and client PCs are connected to the Wako LAN. The two networks are connected to each other across a firewall. We can obtain information on the rare-RI ring from every PC on the Wako LAN; however, controlling the components is permitted for only a few dedicated client PCs.

Three types of servers are installed in the rare-RI ring LAN. The first functions as a network file system (NFS) and EPICS-Input/Output Controller (IOC) server and as a firewall and router in the connection of the rare-RI ring LAN and the Wako LAN. As an IOC server, it serves as a soft IOC to control ladder CPUs. The second server is a backup server. The files on the NFS and EPICS-IOC servers' local hard disks are copied to this backup server to avoid loss of files and data. The third server manages a relational database (RDB), in which PostgreSQL is installed to operate the data archiving system and the alarm system of CSS on client PCs. This server also simultaneously executes a data acquisition program to save operation data and a program for operating the GUI of the CSS alarm system.

References

1) http://www.aps.anl.gov/epics/
2) J. Odagiri et al.: Proc. ICALEPCS2003, Gyeongju, Korea, (2003), p. 494.
3) http://epics.web.psi.ch/software/streamdevice/
4) http://cs-studio.sourceforge.net/

*1 RIKEN Nishina Center
*2 Institute of Physics, University of Tsukuba

Installation of SLOWRI-1†

M. Wada,*1 T. Sonoda,*1 I. Katayama,*1 P. Schury,*1 Y. Ito,*1 F. Arai,*1,*2 S. Arai,*1 K. Kusaka,*1 T. Fujinawa,*1 T. Maie,*1 H. Yamasawa*1 and H. Wollnik *1,*3

The installation of SLOWRI[1], a principal facility at RIBF that will provide low-energy, high-purity RI-beams of all elements, started in FY2013. SLOWRI consists of two gas catchers (GasCell-A and -B), mass separators, a 50-m beam transport line, a beam cooler-buncher, and lasers.

The necessary infrastructure was prepared in the summer of 2013. Two 400-mm-diameter holes in the shielding block were drilled for the beam transport line. A 3.5-m long hole was drilled between the laser room and BigRIPS room for creating a laser path. A staircase was closed by a steel roof to extend the SLOWRI experimental room. The cable rack of BigRIPS was modified, and the electronic racks and compressors for the cryogenic cooling system were relocated to install GasCell-A. Large concrete blocks were also relocated to install the mass separator for GasCell-B. A laser hut was built to install pulsed lasers, and utilities for the high-power lasers were prepared.

GasCell-A (RF carpet gas cell)[2] will be installed at the exit of the D5 dipole magnet of BigRIPS. The gas catcher contains a large cryogenic He gas cell with a large traveling wave rf-carpet[3,4]. It will convert the main beams of BigRIPS to low-energy, low-emittance beams without any restrictions on the chemical properties of the elements. GasCell-B (PALIS)[5] will be installed in the vicinity of the second focal plane slit of BigRIPS. It will provide parasitic RI beams from ions lost in the slits during other experiments. In this gas catcher, thermalized RI ions quickly become neutral and will be re-ionized by resonant laser radiations. These gas catchers will be ready for off-line testing by March 2014.

The 50-m beam transport line under installation (Fig. 1) consists of four dipole magnets (SD1 to SD4), two focal plane chambers, 62 electrostatic quadrupole singlets, 11 electrostatic quadrupole quartets (EQQ1 to EQQ11), and 7 beam profile monitors (BPMs). SD1 and SD2, located immediately after the gas catchers will be used for isotope separation. After eliminating contaminant ions at the focal plane chamber, the low-energy beam will be transported by FODO lattice structures with phase space matching using EQQs. The EQQs have multipole elements made of 16 rods on which various potentials can be applied to produce 6-pole and 8-pole fields, simultaneously, to compensate for ion optical aberrations. This multipole element can also produce dipole fields for steering and scanning the beam. The BPMs have a classical cross-wire beam monitor as well as a channel electron multiplier with a pinhole collimator. Combining the scanning capability of the EQQs and the pinhole detector, we can observe a beam profile even for very low-intensity RI-beams.

Fig. 1. Part of SLOWRI beam transport line, under installation.

In the SLOWRI experiment room, a beam cooler-buncher[6] and a multi-reflection time-of-flight mass spectrograph[7] will be installed for conducting various precision experiments.

Off- and on-line commissioning will take place in FY2014, and the low-energy RI-beams will be provided for users in FY2015.

*1 RIKEN Nishina Center
*2 Department of Physics, Tsukuba University
*3 Department of Chemistry and Biochemistry, New Mexico State University

References

1) M. Wada et al., Hyp. Int. 199 (2011) 269.
2) M. Wada et al., Nucl. Instr. Meth. B204 (2003) 570.
3) G. Bollen, Int. J. Mass Spectrom. 299 (2011) 131.
4) F. Arai et al., Int. J. Mass Spectrom., in press.
5) T. Sonoda et al.: In this report.
6) Y. Ito et al.: In this report.
7) P. Schury et al.: In this report.

Performance of an ion surfing rf-carpet in high gas pressure for application in a high energy RI beam gas catcher

F. Arai,[*1,*2] Y. Ito,[*1] I. Katayama,[*1] P. Schury,[*1] M. Wada,[*1] and H. Wollink[*1,*3]

High-energy radioactive isotopes produced in-flight by fragmentation or fission are used in ion trap-based precision experiments after being stopped in a large gas cell. The stopped ions can be extracted from the large gas cell as a low-energy ion beam. In order to transport and extract ions quickly and efficiently, electric fields are required to guide them. In this respect, an rf-carpet (RFC) method utilizing a dc potential gradient is a standard technique[1]. However, such a method is restricted by the transport time to longer half-life isotopes owing to the upper limit on the dc gradient that can be supported before electric discharges occur in the large gas cell. For studying short half-life isotopes, an RFC featuring faster transport is required. Recently, a hybrid technique wherein the dc gradient is replaced by a traveling potential wave was proposed as illustrated in Fig. 1(a), called "ion surfing"[2]. This technique has recently been experimentally verified with a linear RFC[3].

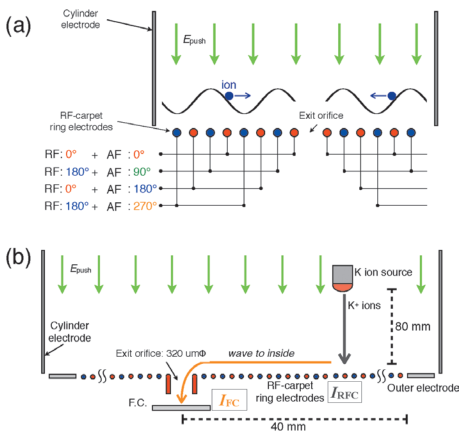

Fig. 1. (a) Concept of ion surfing with schematic of the applied rf and AF signal phases. (b) The efficiency measurement method. An rf frequency of 9.3 MHz and rf amplitude of 104 V_{pp} were used.

As in the standard method, rf signals are applied to the electrodes such that adjacent electrodes are 180° out of phase, creating an effective repelling force for the ions. In the "ion surfing" method, in order to keep the ion just above the RFC surface, the repelling force needs to be balanced by a push force, which is created by a push electric field E_{push}. The confined ions can be transported along the RFC surface by superimposing a weak audio-frequency (AF) signal such that adjacent electrodes are 90° out of phase, forming a traveling potential wave. Under optimal conditions, the ion speed approaches the wave's speed, which is proportional to the AF frequency f_{AF}[2)3)].

Recently, we have demonstrated the transport and extraction of K^+ ions using a circular RFC in 2 kPa of He gas pressure[4]. However, in the practical gas cell, the gas pressure is higher than this value.

In this study, the transport and extraction of K^+ ions were tested in high He gas pressure using a 160 mm cylinder electrode, which created a push electric field E_{push} and circular RFC with 0.32 mm diameter orifice. The RFC consists of 245 ring electrodes, each 0.08 mm with 0.16 mm pitch. Fig. 1 (b) shows the efficiency measurement method. The study required the measurement of two ion currents: the current reaching the RFC electrodes (with rf off) I_{RFC} and the ion current reaching the FC I_{FC}. The FC was biased at −10 V to pull ions out from the extraction orifice. We define the combined transport and extraction efficiency as $\varepsilon_{ext} = I_{FC}/I_{RFC}$.

Fig. 2 shows the ε_{ext} as functions of the gas pressure P_{He}. At E_{push} = 5 V/cm, more than 90% ε_{ext} was obtained. However, at E_{push} = 10 V/cm, ε_{ext} dropped in high pressure. For higher pressure, the effective repelling force becomes small. As a result, E_{push} exceeds the effective repeller field of the RFC and causes ions to hit the RFC electrodes. To allow operation at higher pressures and E_{push}, a larger effective repelling force is needed.

We intend to apply the ion surfing transport method to the SLOWRI gas cell with improved geometry.

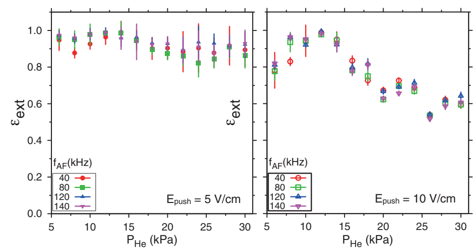

Fig. 2. ε_{ext} as a function of the gas pressure P_{He} for each AF frequency f_{AF} at a push electric field E_{push} of 5 V/cm (left) and 10 V/cm (right).

References
1) M. Wada et al, Nucl. Instr. Meth. B204 (2003) 570.
2) G. Bollen, Int. J Mass Spectrom. 299 (2011) 131
3) M. Brodeur, et al Int. J Mass Spectrom. 336 (2013) 53
4) F. Arai et al, Int. J Mass Spectrom. 362 (2014) 56

*1 RIKEN Nishina Center
*2 Department of Physics, University of Tsukuba
*3 Department of Chemistry and Biochemistry, New Mexico State University

A gas-cell ion cooler and buncher for SLOWRI

Y. Ito,[*1] M. Wada,[*1] P. Schury,[*1] F. Arai,[*1,*2] T. Sonoda,[*1] I. Katayama,[*1] and H. Wollnik[*1,*3]

For future experiments at SLOWRI, ion cooling and bunching will be indispensable for various experiments such as collinear laser spectroscopy, and for all ion trap experiments. The ion beams from SLOWRI gas catchers will be continuous with a beam energy of 30 keV. They must be decelerated and cooled in an ion trap for bunched ions. In general, linear RF quadrupole (RFQ) traps have been used for such a purpose after electrostatic deceleration. Such systems typically use He gas at a pressure of the order of 10^{-2} mbar to cool ions in a ~1 m length RFQ. Due to the limited acceptance of the RFQ, the typical efficiency of such cooler and buncher is a few ten percent[1)2)].

We propose here a new gas-cell cooler and buncher (GCCB) scheme (Fig. 1). It consists of a gas cell (GC) with an RF carpet (RFC) and a flat trap (see Fig. 1). The GCCB will be filled with He gas at up to 2 mbar – much less than the ~100 mbar used in conventional GC – and cryogenically cooled to <77 K. According to calculations with TRIM, a stopping efficiency of ≈100% can be obtained for any 30 keV beams with $Z > 3$ if the GCCB is at least 420 mm long.

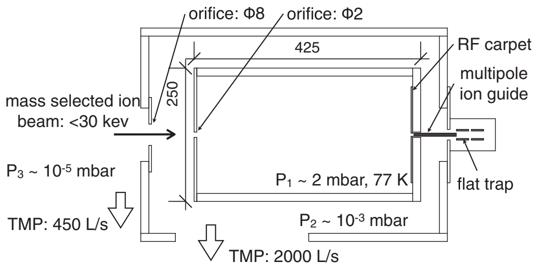

Fig. 1. Schematic diagram of the GCCB. Continuous ion beams will be cooled in the grounded GCCB, transferred to the flat trap, and extracted as a pulsed beam[3)].

The RF carpet is a proven technique for efficient and fast ion transport. Recently, the so-called ion surfing method, in which a traveling potential wave is superimposed on the RF, has been developed for faster transport[4)]. The transport speed was as high as 75 m/s with a linear RFC[4)] and an extraction efficiency of ≈100% was obtained using a circular RF-carpet[5)]. However, it has yet to be used at pressures as low as 2 mbar.

To verify the performance of the RFC at low pressures, the extraction efficiency of the RFC was investigated with a fine-RFC that has an electrode pitch of 0.16 mm and 0.08 mm^2 exit hole. The experimental parameters were optimized to achieve high efficiency using an RF frequency of $f_{\mathrm{RF}} = 5$ MHz. However, when operated at 2 mbar, few ions could be extracted from the GC; at 5 mbar, the efficiency was 22%.

Simulations with SIMION indicated that the low efficiency was the result of unstable ion motion arising from the ions moving between adjacent electrodes in fewer RF periods than required for the validity of the pseudo-potential approximation (see Fig. 2). By increasing the RF frequency to 12 MHz, the simulation indicated that the ion motion would become stable and a high extraction efficiency could be achieved.

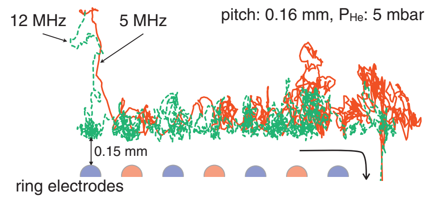

Fig. 2. Comparison of ion motions for $f_{\mathrm{RF}} = 5$ MHz and 12 MHz.

Since the resonance RF frequency is, however, limited by the impedance of the system, such higher frequency is difficult to obtain; however, increasing the electrode pitch should yield a similar effect. In simulation, doubling the electrode pitch and the exit hole diameter yielded near unity extraction efficiency with 2 mbar He for $f_{\mathrm{RF}} = 5$ MHz (see Fig. 3). Taking into account the transport and trapping efficiencies of a multipole ion guide and a flat trap[3)] after the GC, the overall efficiency of the GCCB is expected to be >50%. Such a larger-pitch RF-carpet is being manufactured and will be tested soon. An offline test using 30 keV ion beam counpled to a multi-pole ion guide and the flat trap[3)] will be performed in early FY2014.

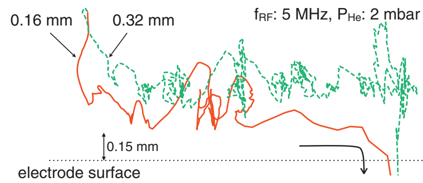

Fig. 3. Comparison of ion motions in 2 mbar He using 0.16 mm and 0.32 mm pitch.

*1 RIKEN Nishina Center
*2 Department of Physics University of Tsukuba
*3 Department of Chemistry and Biochemistry, New Mexico State University

References

1) F. Herfurth et al., Nucl. Instr. Meth. A **469**, 254 (2001)
2) T. Brunner et al., Nucl. Instr. Meth. A **676**, 32 (2012)
3) Y. Ito et al., Nucl. Instrum. Meth. B **317**, 544 (2013)
4) M. Brodeur, et al Int. J Mass Spectrom. **336**, 53 (2013)
5) F. Arai, Y. Ito et al., Int. J. Mass Spectrom. (in press)

Conceptual design of a post accelerator for SLOWRI

S. Arai*1 and M. Wada*1

As an extension plan of the slow radioactive nuclear ion beam facility (SLOWRI)[1], construction of a post accelerator has been proposed. The radioactive ions from SLOWRI are mass-analyzed, charge-bred, and injected into the post accelerator. The post accelerator is a normal conductive linear accelerator complex composed of a radio-frequency quadrupole (RFQ), a medium energy beam transport (MEBT), and a drift-tube linac (DT linac). The RFQ accelerates ions with mass to charge ratio (A/q) of less than 9 from 5 to 500 keV/u. The beam from RFQ is transported to the DT linac through the MEBT. The output beam energy of the DT linac varies between 500 keV/u and 1.5 MeV/u. The layout and main parameters of the post accelerator are shown in Fig. 1 and Table 1, respectively.

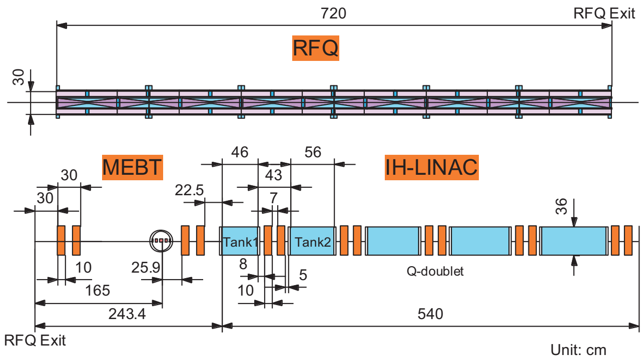

Fig. 1. Layout of the post accelerator.

Table 1. Main parameters of the post accelerator

	RFQ	Drift-tube linac				
Structure	Split coaxial	Interdigital H				
Tank No.		1	2	3	4	5
Frequency (MHz)	79	158				
A/q	9	9				
Duty factor (%)	100	100				
Input energy (kev/u)	5	500	640	810	1000	1230
Output energy (kev/u)	500	640	810	1000	1230	1500
Normalized emittance (π cm·mrad)	0.047	0.047				
Number of cells	290	14	15	16	16	16
Bore radius (cm)	0.54	1.2	1.4	1.6	1.6	1.6
Electrode voltage (kV)	65.1	160	180	200	220	250
Synch. phase (deg)	-30	-25				
Cavity diameter (cm)	30	36				
Total cell length (cm)	719	46.4	56	66.7	74.2	82
Power loss (kW)	186	31	44	62	72	91

RFQ parameters were determined with reference to the RFQ "TALL"[2]. The RFQ has a split coaxial-type structure, which is almost the same as that of the INS-type SCRFQ[3], while the mechanism for supporting the vanes is modified as shown in Fig. 2 in order to reduce the electrode capacitance. The cavity comprises 18 module cavities each of which is 30 cm in inner diameter and 40 cm in length. The cavity dimensions and RF parameters such as resonant frequency, unloaded Q, and power loss were estimated by means of numerical analysis based on an equivalent circuit.

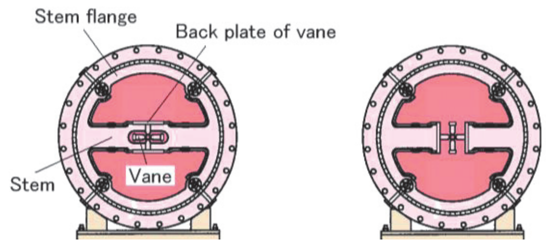

Fig. 2. Cross-sectional views of INS-type SCRFQ (left) and modified RFQ (right).

As the DT linac, an interdigital-H (IH) type comprising five tanks and five quadrupole doublets is adopted to obtain high shunt impedance and variable output energy. Quadrupole doublets are placed in a short space of 37 cm between the tanks to avoid the reduction of longitudinal acceptance of the linac. The IH cavities were designed in the same manner as those of the RFQ were. The longitudinal sectional view of a cavity and the gap-voltage distribution along the beam axis for tank1 are shown in Fig. 3. The goal frequency and uniform distribution are obtained by optimizing the ridge-cut shapes of both the ends. Ridges are made from the flat plate with 4cm thickness. Stems supporting the drift tubes are in the form of a truncated cone with the top and bottom diameters of 1 and 3 cm, respectively.

The beam simulation results are as follows: For the beam with a normalized emittance of 0.047 π cm·mrad, the RFQ transmission is more than 90%. The output beam emittance profile of the RFQ is well matched with the acceptance profile of the IH linac by means of two quadrupole doublets and a 4-gap rebuncher of the quarter-wave resonator in the MEBT. Transmission of the IH linac is 100%.

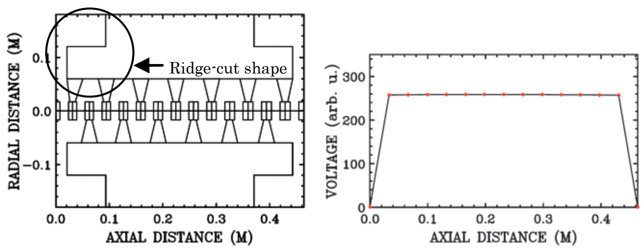

Fig. 3. Longitudinal sectional view (left) and gap-voltage distribution (right) for the 158.1-MHz IH tank1.

References
1) M. Wada et al.: Hyp. Int. 199 (2011) 269-277.
2) N. Ueda et al.: Proc. LINAC'84, 1984, p. 71.
3) S. Arai et al.: Nucl. Instr. and Meth. A 390 (1997) 9-24.

*1 RIKEN Nishina Center

Wide-band mass measurements with a multi-reflection time-of-flight mass spectrograph†

P. Schury,*1 F. Arai,*1 Y. Ito,*1 T. Sonoda,*1 M. Wada,*1 and H. Wollnik*1

The multi-reflection time-of-flight mass spectrograph (MRTOF-MS), first proposed more than 20 years ago[1], uses a pair of electrostatic mirrors to compress a flight path of several hundred meters (or even many kilometers in some cases) within a reflection chamber of ≈1 m length. The MRTOF-MS can achieve mass resolving powers of $R_{\mathrm{m}}>10^5$ while operating at rates of 100 Hz or more[2)3)4)].

Recently, these devices have begun to prove useful for online measurement of nuclear masses[5)6)]. The technique has been demonstrated to accurately provide mass precision of $\delta m/m \sim 5\times10^{-7}$ or better.

However, the multi reflection nature of the measurement has made analysis of rich, wide-band mass spectra difficult or impossible. Much like runners of widely varying skill racing on a circular track, after some time ions with sufficiently differing mass-to-charge ratios make different numbers of laps and create a difficult to interpret spectrum. By developing an analytic method to interpret such spectra, we believe the device could eventually provide wide-band measurements of nuclear masses much in the way of storage rings[7)]. The device could also be useful in analytic chemistry, providing wide-band analysis much like FT-ICR Penning traps, but with greater sensitivity.

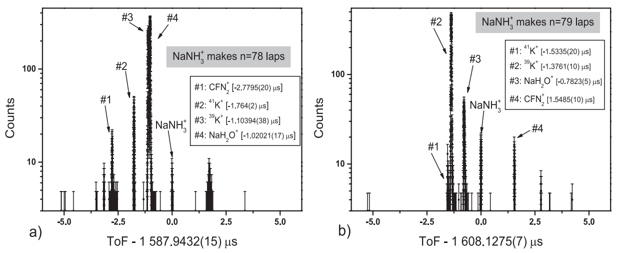

Fig. 1. Example spectra with n_{m1}=78 and 79 laps. Abscissa reflects the time-of-flight of the $NaNH_3^+$ reference.

As reported[8)], using a time-of-flight peak corresponding to a reference ion with known mass-to-charge ratio that makes a known number of laps in the reflection chamber it is possible to determine the mass-to-charge ratio corresponding to any other peak as

$$m_2 = m_1^{(n)} \left(\frac{\zeta + n_{m_1}}{\zeta + n_{m_1} + \Delta n} \right)^2, \tag{1}$$

where reference ions with mass-to-charge ratio $m_1^{(n)}$ make n_{m_1} laps and unknown ions with mass-to-charge ratio m_2 make $n_{m_1}+\Delta n$ laps, while ζ is a system-dependent constant; for our system ζ=0.686 893(20).

† Condensed from Int. J. Mass Spectrom. 359 (2014) 19-25
*1 RIKEN Nishina Center

Determining Δn requires a pair of spectra with different values of n_{m1}. Using this method, it is possible to determine the mass-to-charge ratio of ions over a wide range with a relative mass accuracy of $\sim10^{-6}$, which is typically sufficient to uniquely identify the ions. Such a pair of spectra with ion identity determined is shown in Fig. 1 using $NaNH_3^+$ as a reference.

Once Δn is known, a more precise determination of the ion's mass-to-charge ratio can be determined using the time-of-flight of the reference and unknown with each undergoing the same number of laps, as previously demonstrated online for $^8Li^{+}$[6)]. If there exist isobars, one isobar can be used as a reference while the others are treated as unknown masses and simultaneous accumulation of reference and unknown can be performed, removing possible drift-related errors.

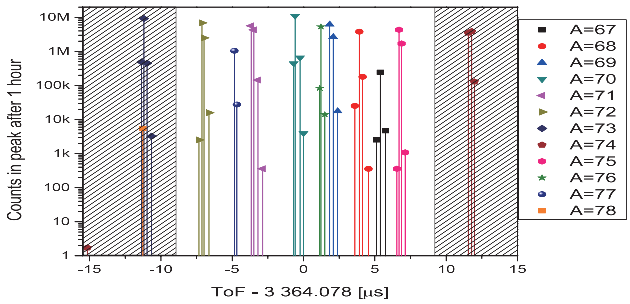

Fig. 2. Calculated spectra at SLOWRI from nuclei produced by in-flight fission of Uranium. In the hashed region, ions will experience time-dependent electric fields from extraction switch and cannot be analyzed.

We foresee the possibility of performing such wide-band mass measurements of r-process nuclei at SLOWRI. As demonstrated in the calculated spectra shown in Fig. 2, it should be possible to measure masses of 20 or more nuclei simultaneously. This would allow the entire region from ^{78}Ni to ^{132}Sn to be investigated with less than 10 tunes of BigRIPS.

References

1) H. Wollnik, M. Przewloka, Int. J. Mass Spectrom. Ion Processes 96 (1990) 267
2) P. Schury et al., Nuclear Instr. and Methods in Physics Research B 317 (2013) 537-543
3) Y. Ito et al., Nuclear Instr. and Methods in Physics Research B 317 (2013) 544-549
4) W. Plaß et al., Int. J. Mass Spectrom. 349 (2013) 134
5) F. Weinholtz et al., Nature 498 (2013) 346-349
6) Y. Ito et al., Physical Review C 88 (2013) 011306(R)
7) F. Bosch and Yu. A. Litvinov, Int. J. Mass Spectrom. 349 (2013) 151
8) P. Schury et al., Int. J. Mass Spectrom. 359 (2014) 19-25

Design work for PALIS system

T. Sonoda,[*1] M. Wada,[*1] I. Katayama,[*1] N. Fukuda,[*1] H. Iimura,[*2] N. Inabe,[*1] T. Kubo,[*1] K. Kusaka,[*1] H. Takeda,[*1] H. Suzuki,[*1] M. Wakasugi,[*1] K. Yoshida[*1] and SLOWRI collaboration

In FY2013, the construction budget for a low-energy RI-beam facility SLOWRI was finally founded. The design drawing for the PArasitic slow RI-beam production by Laser Ion Source (PALIS)[1)] was finalized.

We will restore unused RI-beams for producing slow RI-beam by installing a gas catcher in the vicinity of the second focal plane (F2) of the fragment separator BigRIPS. This will enable the use of parasitic slow RI-beams for various precision experiments whenever BigRIPS experiments are in operation.

In order to realize the reasonable performance under various constrained conditions, there are a lot of novel methods taken into the PALIS design. In particular, the following three worthwhile items were resolved as to avoid any interference to the BigRIPS main beam experiments. The first item is the position of the gas cell, which should be able to move horizontally on the x-axis perpendicular to the BigRIPS beam direction. At F2, RI-beams with slightly different isotones are focused on alongside the x-axis. By applying an overhead beam extraction, the PALIS gas cell collects such the isotone beams neighboring a BigRIPS main beam at both the neutron-rich and neutron-deficient sides, respectively. The extracted RI-beams from the gas cell are transported along the y-axis to the height of 70 cm from the BigRIPS beam, where it bends by 90 degrees in another beam line comprising several bellow combinations. Using a stepping motor, the PALIS gas cell can be moved -60 mm away from the central axis of the BigRIPS beam, and is also pulled by +160 mm toward the evacuation site.

The second item is the differential pumping system for realizing the gas cell pressure for Ar/He up to 10^5 Pa under the totally separated vacuum condition between the PALIS beam line and the BigRIPS F2 chamber. So far, we have developed a novel implementation of differential pumping, in combination with a sextupole ion beam guide (SPIG), which allows a pressure difference from 10^5 to 10^{-3} Pa within a drastically miniaturized geometry compared to conventional systems[2)]. This system can utilize a large exit hole for fast evacuation times, minimizing the decay loss for short-lived nuclei during the extraction from a gas cell, while a sufficient gas cell pressure is maintained for stopping high-energy RI-beams. By following this method, the gas evacuation lines become compact NW-based flanges, resulting in the complete separation of the PALIS vacuum from the BigRIPS beam line.

The third issue is the preparation of the high-voltage platform for ion acceleration, which is necessary for the electrical isolation between the PALIS gas cell, following the beam extraction system including the evacuation lines of differential pumping, and the grounded beam lines. The low-energy RI-beam from PALIS should be transported to the SLOWRI experimental room via 50 m long low-energy beam line. Therefore, ion acceleration is indispensable, while any problem induced from high voltage breakdown should be avoided for the protection of BigRIPS beam profile detectors placed in the F2 chamber. For the first phase, we will adopt the pulsed cavity method[3)] located at the outside of the F2 chamber. The extracted low-energy RI-beam transported via SPIG and QMS first enters a linear ion cooler-buncher, and then, the produced pulsed beam is accelerated toward a cavity at the potential of about 1 kV. When the ion pulse reached the field-free region inside the cavity, the fast switch applies a high voltage potential about 30 kV, the latter is switched again to ground potential for ion acceleration. This pulsed cavity consists of MRTOF[4)] in expectation of future isobar purification. By this way, the electrical isolation is no longer necessary.

The PALIS design work has been almost finalized, as shown in Fig. 1. The off-line and on-line commissioning test for PALIS will be started from June 2014.

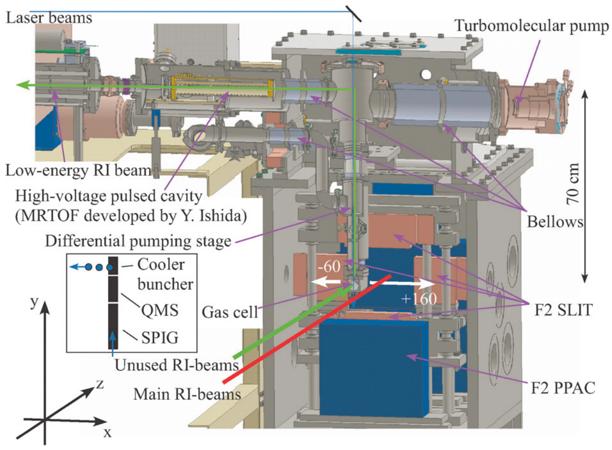

Fig. 1. BigRIPS F2 chamber implemented with PALIS.

References
1) T. Sonoda *et al.*: AIP Conf. Proc. **1104** 132 (2009).
2) T. Sonoda *et al.*.: Nucl. Inst. and Meth. B **295** 1(2013).
3) F. Herfurth *et al.*.: Nucl. Inst. and Meth. B **469** 254(2001).
4) Y. Ishida *et al.*: Nucl. Inst. and Meth. B **241** 983(2005).

*1 RIKEN Nishina Center
*2 Japan Atomic Energy Agency

Transportation of laser beams for PALIS

H. Iimura,[*1,*2] T. Sonoda,[*1] and M. Wada[*1]

PArasitic RI-beam production by Laser Ion-Source (PALIS)[1] is under construction as a part of the slow RI-beam facility, SLOWRI, at RIBF. The PALIS is based on resonant photoionization of reaction products cached in a gas cell. According to the present plan, the gas cell will be installed in the vicinity of the slit at the F2 focal plane in BigRIPS. However, the laser system for PALIS is set up in a room on a different floor located at approximately 50 m in the horizontal and 10 m in the vertical direction from the F2 chamber of BigRIPS. Thus, to transport the laser beams across this long distance we designed an optics system.

The laser system newly installed for the PALIS consists of two dye lasers (Spectra-Physics Credo) pumped by a Nd:YAG laser (EdgeWave IS) at a repetition rate of 10 kHz. We will use a two-step two-color scheme or a three-step two- or three-color scheme for the resonant ionization of atoms. For example, in case of the three-color scheme, the Nd:YAG laser will be used in the third step from an intermediate state to the ionization continuum.

The planned optics system is shown in Fig. 1. Three sets of this system will be installed to transport three different-color laser beams independently. We prepared a few spares of each lens and mirror to exchange them according to the wavelength of laser. Three laser beams overlap each other at the PALIS gas cell. Because mirror M3 is close (~1 m) to the gas cell, it reflects all three laser beams; this is different from other optical components that are used for only one laser beam.

Because the beam size of the laser is small (0.8 mm horizontally and 2 mm vertically) at the exit of the dye laser,

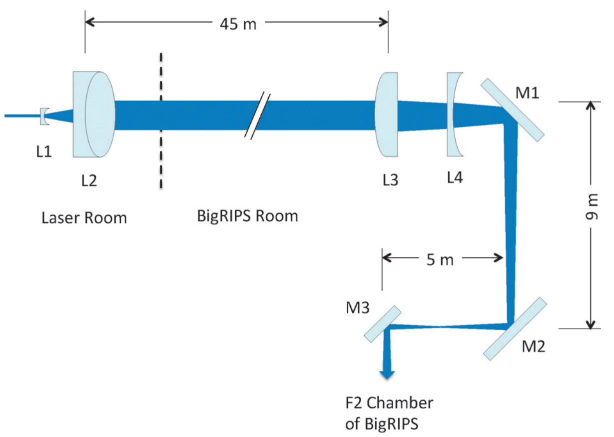

Fig. 1. Planned optics system for transportation of laser beams to PALIS.

it diverges after long distance transportation (with divergence of 1 mrad). Therefore, we expand the laser beam to approximately 7 mm x 17 mm using an expander consisting of a concave lens (L1) and an achromatic lens (L2). The estimated divergence of this beam is 0.1 mrad, and the beam size does not change significantly after a transportation distance of 45 m. Then the laser beam is focused with a long focal length using a combination of convex (L3) and concave (L4) lenses. Finally, the laser beam is injected into the PALIS gas cell in the F2 chamber of BigRIPS. The resonant photoionization occurs inside the SextuPole Ion Guide (SPIG) to which atoms move from the gas cell. We designed the optics system such that the beam size of laser changes to 3 mm x 3 mm along the 25-cm length of SPIG and the laser beam matches the 3-mm inside diameter of SPIG.

Regarding the intensity of the laser beam, outputs of the dye lasers are less than 15 W, or in case of using a second harmonic generator, they are less than 2 W. In many of the ionization schemes, the intensity of ions is not saturated with these laser powers. Therefore, higher transport efficiency of the laser beams is necessary to achieve higher intensity of ions. The designed optics system uses a minimum number of optical components, and the transport efficiency estimated from the transmission and reflectance of the optical components is approximately 50 % at a wavelength of 350 nm. If we use an optical fiber instead, the efficiency lowers to approximately 10 %.

The experimental room where BigRIPS is located cannot be entered when the RI beams are injected, although the laser room can be entered at any time. To handle the laser beams without entering the experimental room, we placed actuators to change the angles of 2-inch mirrors M1 and M2. These actuators can be controlled via Ethernet by a computer. Additionally, several CCD cameras will be installed to monitor the laser beam spots from a distance. We also plan to place a photo detector inside the gas cell to finally confirm that the laser beams pass through apertures of the PALIS.

Transportation of dye laser beam is currently being examined for attenuation of the intensity, spatial fluctuation of the beam spot, and so on. Besides the dye lasers, a narrow band-width injection-locked Ti/Sapphire laser[2] is being developed for the in-source laser spectroscopy. Transportation of this laser beam is also planned.

References

1) T. Sonoda et al: Nucl. Instr. Meth. B **295**, 1 (2013).
2) T. Takatsuka et al: Nucl. Instr. Meth. B **317**, 586 (2013).

*1 RIKEN Nishina Center
*2 Applied Nuclear Physics Laboratory, Japan Atomic Energy Agency

New laser system installation for PALIS

T. Sonoda,*1 H. Iimura,*2 M. Wada,*1 I. Katayama,*1 Y. Adachi,*3 T. Noto,*3 T. Takamatsu,*3 T. Takatsuka,*3 H. Tomita,*3 F. Schneider,*4 K. Wendt*4 F. Arai*5 Y. Itou*5 P. Schury*5 and the SLOWRI collaboration

A new laser system for PArasitic slow RI-beam production by Laser Ion Source (PALIS)[1)] has been installed. This system has higher laser power and repetition rate compared to those previously we used. A gas-jet laser spectroscopy can be applied owing to high repetition rate. A room partition was recently constructed for the laser equipments having laser shield noise barriers. The room is complete with an air conditioning system.

So far, we have developed a resonant ionization laser system and a new laser ion source configuration for future PALIS project. Old laser components consist of two pulsed dye lasers (Lambda Physik) pumped by two excimer XeCl lasers (Lambda Physik). The maximum power and repetition rate for the excimer laser is 150 mJ/pulse, 200 Hz, which corresponds to 30 W. Additionally, Ti:Sapphire laser pumped by YLF laser (10 W, 1 kHz) is available through collaboration with Nagoya university. By using these lasers, off-line resonant laser ionization for stable Co, Cu, Fe, Ni, Ti, Nb, Sn, In, and Pd inside the gas cell, ion extraction and transport to high-vacuum region via SPIG and QMS have been confirmed[2)]. The feasibility study for the gas jet laser spectroscopy was investigated in combination with dye and TiSa lasers[3,4)].

In terms of the efficiency of the gas cell based resonant laser ionization system, the laser power and its duty cycle are important. The ionization efficiency depends on the atomic transition strength determined by the type of the element. High power lasers are widely adopted for a number of elements. Moreover when the moving speed for photo-ionized atoms increases as in the case of ionization inside a gas jet, the duty cycle of the laser pulse should be set suitably high[5)]. Thus, a high power and high duty cycle laser is necessary to realize a higher performance PALIS system.

In FY2013, the construction budget for a low-energy RI-beam facility SLOWRI was finally founded. New high power, high duty cycle lasers were prepared for PALIS experiments. In order to install the new laser assembly, the room size for laser setting and off-line experiment was also extended.

New laser components consist of two pulsed dye lasers pumped by one YAG laser. The maximum repetition rate and power for a YAG laser (Edge wave) is 10 kHz and 90 W for 532 nm with a single mode and 36 W for 355 nm and 40 W for 532 nm with a multimode. Two pulsed dye lasers (Sirah) provide a wide range wavelength from 215 to 900 nm with about 10 W for fundamental frequency and 1 W for a frequency-doubled by a secondary harmonic generator. These dye lasers accept both wavelengths (355/532) from pump laser beam and have an additional option for selecting a line width of 1.5 GHz and 6 GHz, alternately. Additionally, a new YAG laser (Lee) was installed for pumping Ti:Sapphire lasers. The maximum power and repetition rate is 50 W and 10 kHz, respectively. An injection locked Ti:Sapphire laser operated at up to 10 kHz with a line width of 20 MHz will be prepared for high precision laser ionization spectroscopy.

Fig. 1. The photograph of new PALIS lasers: shining two dye lasers pumped by YAG laser.

We confirmed that the new laser system works with a reasonable performance. Fig. 1 shows a photograph taken during tests of the new lasers in October 2013. The off-line and on-line commissioning test for PALIS will begin from April 2014.

References
1) T. Sonoda *et al.*: AIP Conf. Proc. **1104** 132 (2009).
2) T. Sonoda *et al.*.: Nucl. Inst. and Meth. B **295** 1(2013).
3) C. Sakamoto: Master thesis, Nagoya University (2013).
4) T. Takatsuka *et al.*: Nucl. Inst. and Meth. B **295** 1(2013).
5) T. Sonoda *et al.*: Nucl. Inst. Meth. B **267** 2918 (2009).

*1 RIKEN Nishina Center
*2 Japan Atomic Energy Agency
*3 Faculty of Engineering, Nagoya University
*4 Institute of Physics, Johannes Gutenberg University
*5 Institute of Physics, Tsukuba University

PALIS laser interlock system for human and machine protection

T. Sonoda,*1 I. Katayama,*1 M. Wada,*1 H. Iimura,*2 F. Arai,*3 and Y. Itou*3

A laser interlock system has been developed to facilitate safe operation and machine protection in the new laser system for PArasitic slow RI-beam production by Laser Ion Source (PALIS)[1].

Fig. 1 shows the overview of the interlock system for the current PALIS laser setups. There are many items pertaining to laser operation, for example dye circulator, chiller, air compressor, laser beam shutter, power meter, wave meter, and so on. These often depend on each other. If some interruption in dye flow occurs during the irradiation of strong pump laser beam, the dye cell and dye itself are damaged almost immediately. Further, if cooling water stops or leaks, those devices that require refrigeration stop functioning. These accidents are dangerous and can potentially start a fire or cause fatal damage to laser devices. The irradiation of laser beams direct on to the human body, especially on to the eyes must be avoided. Therefore, some safety devices like a beam shutter or door interlock, are necessary. Additionally, a monitoring system is essential to establish a robust system and to reduce the frequency of operator interventions for reading laser beam power, laser beam position, and wavemeter.

In this circumstance, one needs to build an automated system using a programmable logic controller for operating all devices remotely. We adopted a National Instruments (NI) Compact RIO system that are referred from ISOLDE RILIS[2]. NI CompactRIO incorporates a real-time processor and reconfigurable FPGA. The hot-swappable industrial I/O modules can directly connect to sensors and actuators. CompactRIO embedded systems are developed using high-productivity LabVIEW graphical programming tools for rapid development.

The sensor devices for dye circulation are necessary to monitor the dye flow at all times. However, the dye solution is often composed of volatile liquid, and the interconnection of sensor surface on the liquid flow is not adequate. Here, we use two types of sensors on an experimental basis. One is a vibration sensor that can detect a small oscillation of the flow tube synchronized with a circulator's pumping action. The other is an ultrasonic sensor that evaluates the echo of high frequency sound waves received back by the sensor. If any sensor detects an interruption in dye flow, the beam shutter immediately acts to stop the pump laser beam. In addition to these sensors, alcohol sensors monitor a dye leak. Several sensors are used for cooling water to detect a leak and to monitor the dye temperature stability. The laser power meters and beam shutters are coupled with air cylinders. Therefore, the air pressure is also monitored by a pressure sensor. The door interlock system for laser beams was prepared in the BigRIPS room. The laser beams cannot be sent to the BigRIPS room unless any door in the BigRIPS room is closed.

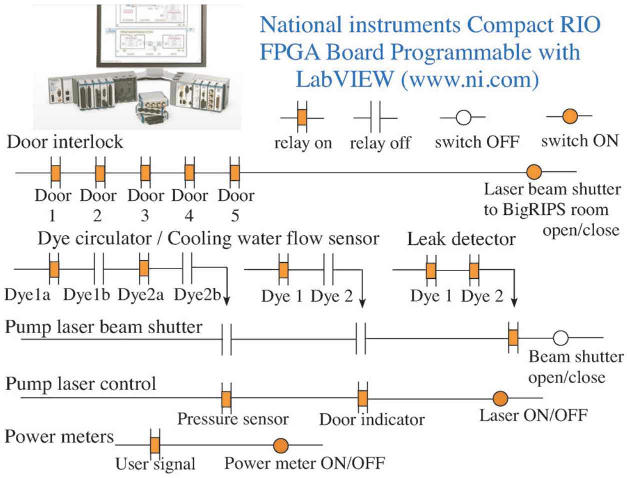

Fig. 1. The overview of the interlock system with interactive equipments for current PALIS laser experiment.

The laser interlock system for PALIS experiment is being developed. This system is motivated not only for human and machine protection but also for facilitating an efficient and robust experimental environment. By effective utilization of these system, the off-line and on-line commissioning test for PALIS will be started from April 2014.

References
1) T. Sonoda *et al.*: AIP Conf. Proc. **1104** 132 (2009).
2) Bruce Marsh, presentation slides in EMIS2012.

*1 RIKEN Nishina Center
*2 Nuclear science and engineering directorate, Japan Atomic Energy Agency
*3 Department of Physics, Tsukuba university

Measurement of the hyperfine structure of ^{197}Au atom in superfluid helium

T. Fujita,[*1] T. Furukawa,[*2] K. Imamura,[*3, *4] X. F. Yang,[*3, *5] Y. Mitsuya,[*4] M. Hayasaka,[*6] T. Sagayama,[*6] S. Kishi,[*6] T. Kobayashi,[*7] H. Ueno,[*3] T. Shimoda,[*1] and Y. Matsuo[*8]

We have developed a new laser spectroscopic technique called Optical Radioisotope atom Observation in Condensed Helium as Ion-catcher (OROCHI) for investigating the structure of exotic nuclei.[1)] In this method, we observe atomic Zeeman splitting (ZMS) and hyperfine splitting (HFS) by using optical pumping and laser-microwave (MW) double resonance spectroscopy in superfluid helium (He II) to derive nuclear spins and electromagnetic moments. The characteristic optical properties of atoms in He II, for example, blue-shifted and considerably broadened absorption spectra, enables us to apply the optical pumping technique to several elements. Recently, we performed a series of on-line experiments by using energetic (up to 66 MeV/u) $^{84\text{-}87}$Rb beams from Riken Projectile-fragment Separator (RIPS), and confirmed the feasibility of the OROCHI method.[2)] Furthermore, we succeeded in producing a large atomic spin polarization (>80 %) of ^{197}Au by means of optical pumping in He II by the laser light of the fourth harmonics of a LD-pumped pulsed Nd:YLF laser (263.5 nm, 3 kHz). Subsequently, we plan to measure the spins and moments of neutron-deficient Au isotopes possessing interesting structures.[3)]

As the first step, we measured the HFS of a stable ^{197}Au atom in an off-line experiment. Fig. 1 shows the experimental apparatus. An open-topped cubic quartz cell in a cryostat is fully filled with He II. The produced Au atoms are introduced into He II by using laser sputtering of the sample material with two pulsed lasers[4)]. We observed the intensity of Laser Induced Fluorescence (LIF) by means of a photomultiplier tube (PMT) through a monochromator for wavelength selection, and performed the laser-MW double resonance spectroscopic measurements (MW power: typically 1 W).

Fig. 2 shows an HFS resonance spectrum of ^{197}Au in He II. In fact, the observed HFS resonance frequencies were shifted because of the Zeeman interaction with the applied magnetic field. Then, we derived the HFS with the zero-magnetic field effect from two HFS resonance frequencies measured by employing opposite polarization directions of the pumping laser, σ^+ and σ^-, respectively, for cancelling the shift due to the Zeeman effect. The deduced HFS in this study was consistent with the literature value of the HFS of ^{197}Au in vacuum (with an accuracy of 0.5 %). The obtained value was slightly different from the literature value as well as the values for ^{133}Cs and ^{85,87}Rb.[1)] The shift is due to the pressure from surrounding helium atoms. However, the slight shift can be neglected in the discussion regarding the structure of nuclei.

The successful HFS measurement indicates the feasibility of future measurements for neutron-deficient nuclei of Au by using the OROCHI method. In the near future, we plan to propose experiments with exotic Au isotopes.

[*1] Department of Physics, Osaka University
[*2] Department of Physics, Tokyo Metropolitan University
[*3] RIKEN Nishina Center
[*4] Department of Physics, Meiji University
[*5] School of Physics, Peking University
[*6] Department of Physics, Tokyo Gakugei University
[*7] Laser Technology Laboratory, RIKEN
[*8] Department of Physics, Hosei University

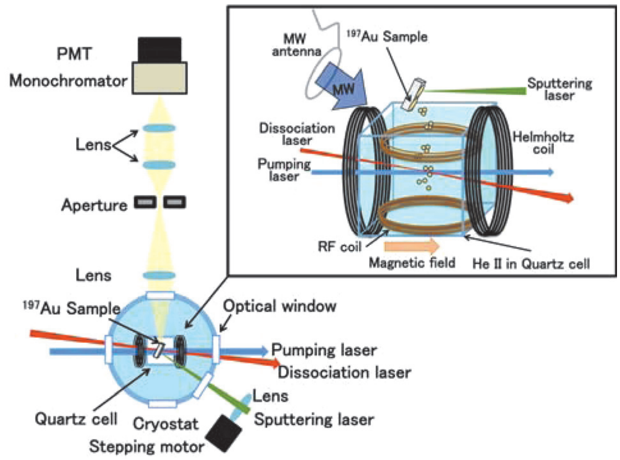

Fig. 1. Experimental apparatus.

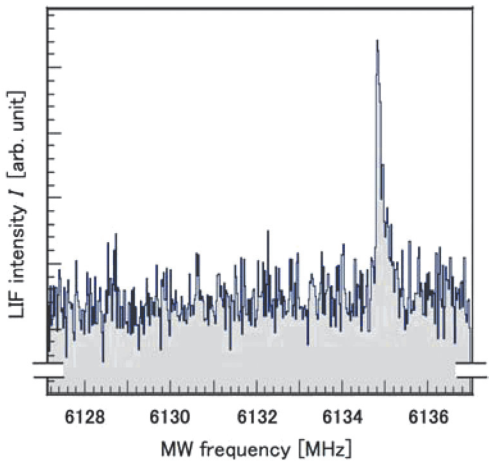

Fig. 2. HFS resonance spectrum of ^{197}Au in He II with σ^+ polarized pumping laser light.

References

1) T. Furukawa et al.: Hyp. Int. **196**, 191(2010).
2) T. Furukawa et al.: Nucl. Instrum. Meth. B **317**, 590 (2013).
3) H.-J. Kluge and W. Nörtershäuser : Spectrochim. Acta Part B **58**, 1031(2003).
4) T. Furukawa et al. : Phys. Rev. Lett. **96,** 095301 (2006).

GARIS-II commissioning #3 and #4

D. Kaji,*1 K. Morimoto,*1 Y. Wakabayashi,*1 M. Takeyama,*1,*2 S. Yamaki,*1,*3 K. Tanaka,*1,*4 H. Haba,*1 M. Huang,*1 J. Kanaya,*1 Y. Ito,*1 H. Kikunaga,*1,*5 F. Tokanai,*1,*2 S. Goto,*6 M. Asai,*1,*7 and K. Morita*1,*8

We developed a new gas-filled recoil ion separator (GARIS-II) to study asymmetric actinide-target based fusion reactions[1)]. As the first step, we measured the solid angle of the separator offline using a standard α-source of ^{241}Am, and it was determined to be 18.2 msr[1)]. As the second step, we performed online testing to evaluate the separation capability of GARIS-II from background particles, and its transmission using ^{40}Ar-induced fusion reactions. These reaction products were collected onto a focal plane detection (FPD) system with high efficiency under extremely low background conditions[2)].

As the third step of commissioning #3, we performed online operating tests on GARIS-II using ^{22}Ne-induced fusion reactions of ^{197}Au, ^{205}Tl, ^{208}Pb, ^{209}Bi, ^{232}Th, and ^{238}U. The reaction products were separated in-flight from projectiles and other by-products using GARIS-II, and then they were guided into the FPD system after passing through the time-of-flight detector[3)]. The separator was filled with He gas at the pressure of 10, 33, 80, and 173 Pa. For further background rejection using GARIS-II, we tested He-H_2 mixture as the filled gas at the same gas pressure. Figure 1(A) shows the intensity distribution of ^{215}Ac, which is produced via the ^{197}Au(^{22}Ne,4n) reaction, at FPD in the case of filling at 33 Pa He gas and 33 Pa He-H_2 mixture (He:H_2=2:1). The optimum $B\rho$ was shifted up to 11% and the transmission was increased from 11.4% to 14.6%. The $B\rho$ shift implies that the average equilibrium charge state of recoil ions moving in a filled gas becomes small. The improvement of transmission is due to a decrease in the multiple scattering between the recoil ion and filled gas atom. Figure 1(B,C) shows a comparison of background (BG) level at each peak of intensity distribution between the He and the He-H_2 mixture. The BG level was significantly changed, and the beam-like particles were strongly suppressed.

As the fourth step of commissioning #4, we performed online tests on GARIS-II using ^{48}Ca-induced fusion reactions of ^{208}Pb . We measured an excitation function of ^{208}Pb(^{48}Ca,2n)^{254}No and the transmission of GARIS-II for ^{254}No. The maximum transmission was 73% assuming σ = 2.05 μb[4)] when the separator was filled with He gas at a pressure of 73 Pa, and the magnetic rigidity $B\rho$ was set to 2.064 Tm. The maximum transmission of GARIS-II is two times higher than that of GARIS, which is 36%. Further, it is better than design value of 61% for GARIS-II. Transmission data are summarized in Fig. 2.

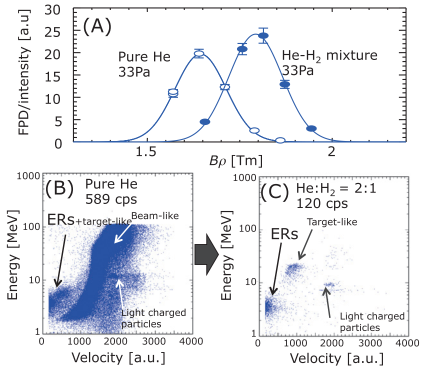

Fig. 1. (A) Intensity distribution of ^{215}Ac at FPD, (B, C) Two-dimensional views of energy measured by Si detector vs. recoil velocity measured using the timing counter.

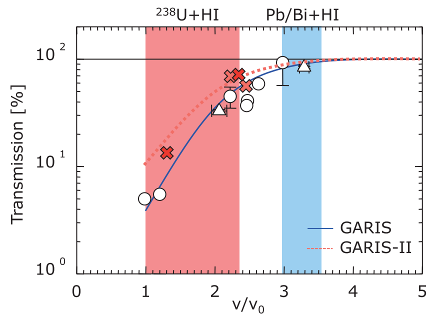

Fig. 2. Transmission curve. Velocity regions of interest for the reactions of both cold fusion and hot fusion are given by the blue and red stripes, respectively. ○, △: GARIS, ×: GARIS-II. Solid and dashed curves are estimated by considering multiple scattering with the filled gas for GARIS and GARIS-II, respectively.

*1 RIKEN Nishina Center
*2 Department of Physics, Yamagata University
*3 Department of Physics, Saitama University
*4 Tokoy University of Science
*5 Research Center for Electron Photon Science, Tohoku University
*6 Department of Chemistry, Niigata University
*7 Advanced Science Research Center, JAEA
*8 Department of Physics, Kyushu University

References

1) D. Kaji et al.: Nucl. Instrum. Methods B 317, p.311 (2013).
2) D. Kaji et al.: RIKEN Accel. Prog. Rep 46, p.189 (2013).
3) D. Kaji et al.: RIKEN Accel. Prog. Rep 46, p.190 (2013).
4) Yu. Ts. Ogganessian et al.: Phys. Rev. C 64, p.054606 (2001).

Study on detector response to spontaneous fission events of heavy nuclides using the $^{206}Pb+^{48}Ca$ reaction

M. Takeyama,[*1,*2] D. Kaji,[*1] K. Morimoto,[*1] Y. Wakabayashi,[*1] and M. Asai[*3]

Detector response to spontaneous fission (SF) of products by the $^{206}Pb+^{48}Ca$ reaction was studied using a new focal plane detector that has a Si-Ge array[1)] installed at a focal plane of the gas-filled recoil ion separator GARIS.

By using GARIS and GARIS-II, we plan to study the production and decay properties of the superheavy element (SHE) produced via actinide-based fusion reaction (hot fusion). It is reported that SHE nuclides produced by the hot fusion are radioactive and decay by α-particles emission or SF, and all decay chains are terminated in SF[2)], which emit γ-rays. Therefore, it is important to measure the γ-rays of the SF of heavy nuclides. In 2013, we newly installed the Si-Ge detector array[3)] for studying the production and decay properties of reaction products by including $^{248}Cm+^{48}Ca$[4)]. Thus far, we have searched for SF using Si detectors, however, the Si-Ge array can carry out a more accurate identification than the Si detector because the Si-Ge array is expected as a probe for the detection of prompt γ-ray coincided with SF. Before the experiment, the Si-Ge array was caliblated using a well-known $^{206}Pb(^{48}Ca,2n)^{252}No$ reaction. The ^{252}No decays by 73.1% α-particle emission and 26.9% SF[5)]. We assigned this reaction based on its branching and half-life.

A $^{48}Ca^{11+}$ beam was extracted from the 18-GHz ECR ion source and accelerated up to 218.5 MeV by the RILAC. The typical beam intensity was 1.0×10^{12} particle/s (0.17 pμA). The metallic ^{206}Pb (enrichment of 99.3%) target was prepared by vacuum evaporation on a backing of 60 μg/cm^2 carbon foil. The target thicknesses had a mean value of 353 μg/cm^2. Sixteen frames of the sector targets were mounted on a ϕ30 cm rotating wheel, which was rotated at 3300 rpm. The reaction products were separated in flight from projectiles and other by-products by GARIS, which was filled with helium gas at a pressure of 73 Pa, and then the products were transported into the focal plane detection system after passing through the time-of-flight (TOF) detectors. The detector system comprised two TOF detectors, a PSD box[1–3)], which is composed of a position-sensitive detector (PSD) and four solid state detectors (SSDs), and a planer typed Ge-detector for counting low-energy photon (CANBERRA, BE6530). The Ge-detector was separated from the other detector vacuum by a 1-mm thick aluminum window. Magnetic rigidity was set to 2.064 T·m for ^{252}No. Gamma rays emitted in coincidence with SF events registered by the PSD box were measured by the Ge-detector.

Figure 1 (A) shows a two-dimensional plot of energy measure between PSD and SSD. SF fragment energy is measured by SSD based on the implantation depth in PSD. When the recoil energy of evaporation residues is low, recoil ions are stopped at the surface of the detector. Then, SF fragments are detected in both PSD and SSD (region a). Conversely, both SF fragments are either stopped in the detector or one of fragment escapes in the backward direction if the recoil energy is high, the implantation depth is deep (region b).

Figure 1 (B) shows a two-dimensional energy plot of SF- and γ-rays observed in prompt coincidence. The probability of coincidence is 52.6% because an SF event emits some γ-rays. From this probability, the Si-Ge array is considered to be useful for the identification of SF fragments.

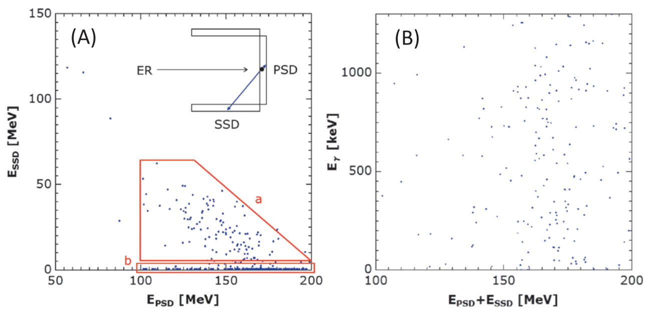

Fig. 1. (A) Two-dimensional plot of energy measure between PSD and SSD. (B) Two-dimensional plot of SF-γ coincidence.

References
1) D. Kaji et al., Contribution in this report.
2) Yu. Ts. Oganessian et al., J. Phys. G: Nucl. Part. Phys. **34**, p.R165 (2007).
3) D. Kaji et al., Contribution in this report.
4) K. Morita et al., Contribution in this report.
5) Table of isotope 8th ed. (John Wiley & Sons, New York, 1998 update).

*1 RIKEN Nishina Center
*2 Department of Physics, Yamagata University
*3 Advanced Science Research Center, JAEA

Identification of every target mounted on a rotating wheel and its application

D. Kaji,*1 K. Morimoto,*1 and K. Tanaka*1,*2

Several pieces of sector-shaped targets mounted on a rotating wheel have been employed for superheavy element (SHE) production experiments with high-intensity beams. Thus far, it had not been possible to determine the thickness difference between each target without which, we adopted the average thickness of all the peaces. To distinguish it, we have developed a new wheel frame with an extra ID-tag placed between the spoke-position-indicator tags on the circumference of the wheel (Fig. 1).

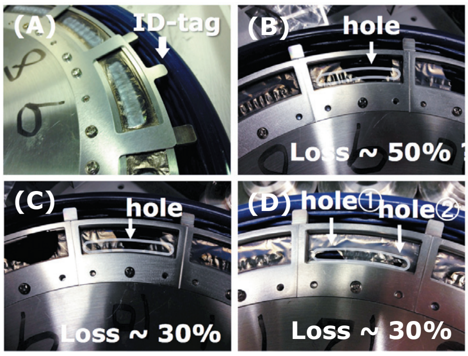

Fig. 1. (A) New wheel frame with an ID-tag. (B,C,D) Observed pin-holes on irradiated targets #11, 12, and 14, respectively.

A circuit block diagram for identifying each target frame is shown in Fig. 2. To avoid unnecessary beam irradiation of the spokes, timing signals of each tag detected by a photo-diode sensor are used. In the case of a rotational speed of 2000 rpm, the timing signals from the spoke tags are periodically generated for every 1.875 ms, whereas an additional signal from the ID-tag is generated for every 30 ms in one rotation. A signal timing chart [A], shown in Fig. 2, indicates that an original signal is generated from the photo sensor. The chart [B] is modified from the signal [A] by changing its delay and width. The chart [C] is obtained by a logical 'AND' operation of the signal [A] with [B], resulting in a useful timing for one rotation of the wheel. This pulse is delivered to a reset scalar and the scaler measure the timing in every rotation. This angle-timing information is recorded together with the reaction-event data measured at the focal-plane detector for each separate event. The chart [E] indicates the timing of the spokes with elimination of the timing of the ID-tag. The [E] is obtained by a logical 'AND' operation of the signal [A] with [D], which is an inverted signal of [B]. This pulse is delivered to the accelerator in order to chop the beam.

As a typical example, a two-dimensional plot (Fig. 3) of the event rate is monitored over a long irradiation period (abscissa) for a rapid rotation timing (ordinate). Event rates for targets #11, 12, and 14 become relatively higher than those for other targets caused by pin-holes on the target foils as shown in Fig 1(B,C,D). Thus, this plot is useful in identifying the condition of every target foil. Moreover, it enables additional beam chopping for masking the broken target, as shown in Fig. 3. The masking signal can be easily obtained with a logical 'OR' operation of the inverted signal [E] with a certain delayed signal of [C].

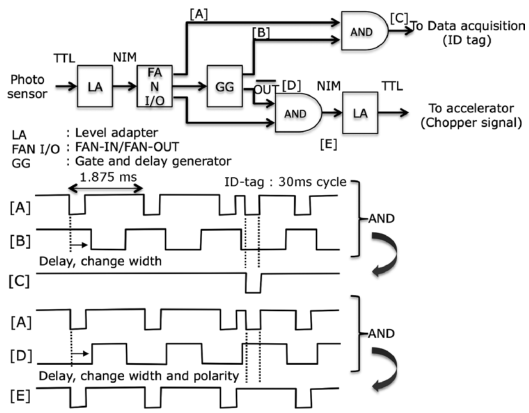

Fig. 2. Block diagram for ID of every target-frames.

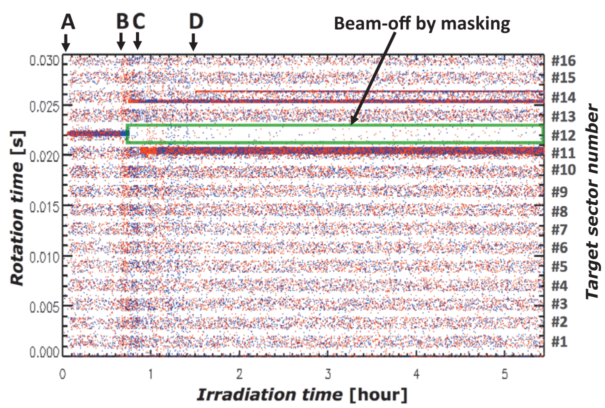

Fig. 3. A target-condition monitoring chart using event timing. Sudden changes in event density at A, B, C, and D indicate the broken parts of the target sector #12, 14,11, and 14, respectively.

*1 RIKEN Nishina Center
*2 Faculty of Science and Technology, Science of Tokyo University

Gamma-ray inspection of rotating object

T. Kambara,*[1] H. Takeichi,*[1] and A. Yoshida*[1]

Radioisotopes (RIs) have long been used as tracers for wear diagnosis of mechanical parts. We proposed a surface activation method that utilizes RI beam implantation[1)] instead of the conventional ion-beam irradiation.

The degree of wear is determined by the decrease of the radioactivity of the object part or the increase of the radioactivity of the lubricant, through external gamma-ray measurements. Therefore, a lubricant circulation system is required for removal of activated surface debris from the machine. If the spatial distribution of the radioactivity in a running machine can be obtained, wear diagnosis can be performed for a closed system without a circulation system.

In many cases, the mechanical parts being subject to wear diagnosis work in continuous and periodical motions such as rotation. We are developing a new method to determine the spatial distribution of positron-emitting RIs on periodically-moving objects in a closed system, which is based on the same principle as medical PET systems but is simpler and less expensive.

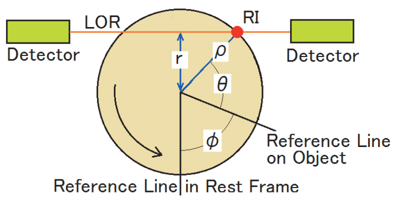

Fig. 1. Geometrical Concept.

Figure 1 shows the geometrical concept. A positron-emitting point source is located at (r, θ) in the polar coordinate fixed to the object. The orientation of the object is denoted by ϕ. A pair of gamma-ray detectors are located at both sides of the object to detect the 511-keV photons from positron annihilations. Since the photons are emitted in the opposite directions, the coincident detection is allowed only when the source is on the straight line between the detectors (line of response: LOR). This condition is followed by an equation $y = r\cos(\theta + \phi)$, where y is the distance between LOR and the rotation center. If the pair of detectors is moved in parallel so that LOR scans the object and the coincidence rate is measured as a function of ϕ and y, the coincidence events from a point source fall on a sinusoidal curve in the ϕ-y plane. If the source is spatially distributed on the object, the coincidence rate on the ϕ-y plane yields a diagram called sinogram, which is a superposition of the sinusoidal curves. Conversely, the spatial distribution of the source can be reconstructed from the sinogram. Therefore, with only two detectors, the RI distribution on a rotating object contained in a vessel can be inspected without stopping the rotation, if y and ϕ at the time of coincidence detection are determined.

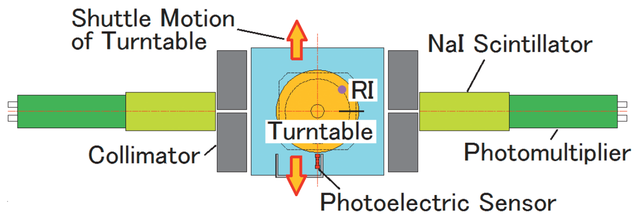

Fig. 2. Prototype setup.

In order to prove the feasibility of the method, we have constructed a prototype (Fig. 2). A pair of NaI scintillator detectors are placed on the opposite sides of a rotating turntable (diameter of 14 cm) that holds RI sources and moves back and forth. Gamma rays from the sources are collimated by a pair of Pb blocks placed in front of each detector. A pin fixed to the turntable generates a pulse signal from a photoelectric sensor at each turn. The orientation of the turntable is determined by a clock-pulse counter that is started by the photoelectric sensor. At each coincidence detection the orientation and the position of the turntable and the pulse heights from the detectors are recorded.

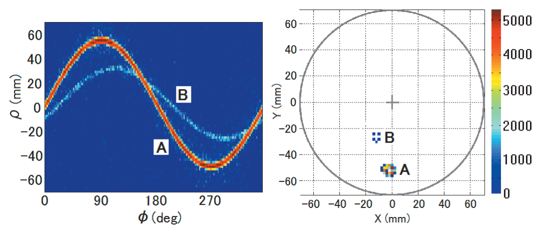

Fig. 3. Sinogram (left) and reproduced image (right) where the circles show the turntable and the RI sources.

Figure 3 shows a sinogram and a reconstructed radioactivity distribution for two ^{22}Na sources, (A) 65 kBq and (B) 1.55 kBq, fixed on the turntable that rotates at 150 rpm and moves back and forth by 2-mm step/minute over a 140-mm range. The aperture width of the collimator is 6 mm. The sinusoidal curves marked A and B in the sinogram correspond to each source. The positions of the sources are reconstructed within 3.5 mm. Details of the reproduction algorithm are described elsewhere.

*1 RIKEN Nishina Center

References

1) A. Yoshida, et al,: Nucl. Instr. Meth. B **317**, 785 (2013).

Image reconstruction algorithm for gamma-ray inspection of rotating objects

H. Takeichi,*[1] T. Kambara,*[1] and A. Yoshida*[1]

We develop a new method to determine the spatial distribution of positron-emitting radioisotopes (RIs) on rotating objects and construct a prototype system. The details of the principle and the prototype system based on this method are described elsewhere[1]. This method is based on the same principle as the medical positron emission tomography (PET) systems in which projection data from all angles are collected. In the PET system, gamma-ray detectors are placed in a circular manner around a stationary object, or the gamma-ray detectors rotate around the object in order to collect projection data. In this method, a pair of gamma-ray detectors are placed in a stationary position and the object being imaged is rotated.

Here, we present the image reconstruction algorithm of the prototype system. The most conventional image reconstruction algorithm in PET is filtered back-projection (FBP) [2]. Projections from all angles are back-projected onto and overlaid in the image plane using the inverse Radon transform to reconstruct the image. Then, an appropriate image filter is applied to deblur the image.

An alternative to the FBP is the maximum likelihood – expectation maximization (ML–EM) algorithm[3, 4]. We assume a two-dimensional distribution $\lambda(x,y)$ of RI (image), and the projection data $p(r,\varphi)$ at an angle φ from the y-axis and at a distance r from the center. ML–EM is an iterative method. The iteration starts with an arbitrary image that is updated gradually as

$$\lambda_j^{n} = (\lambda_j^{n-1} / \sum_i c_{ij})(\sum_i (c_{ij}\, p_i / \sum_k c_{ik}\, \lambda_k^{n-1})), \qquad (1)$$

where λ_j^n is the j-th pixel value in the image λ of the n-th iteration, p_i is the value at the i-th position in the projection p, and c_{ij} is the probability that a gamma-ray emitted from the j-th pixel position is counted at the i-th position in the projection (see Fig. 1).

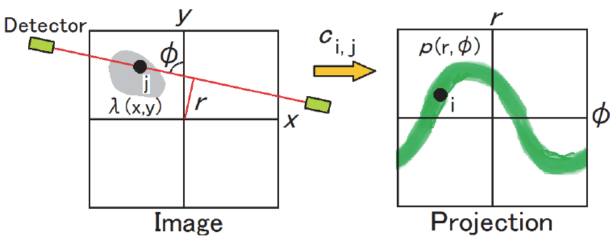

Fig. 1. Schematic illustration of ML–EM

At each iteration, the projection of the current estimate image is calculated and compared with the actual projection. Then, the difference between the estimated and actual projections is back-projected and used to update the current estimate image.

Thus, Equation 1 reads as follows. First, the projection of the current estimate image is calculated ($\Sigma_k\ c_{ik}\ \lambda_k^{n-1}$). Second, the ratio of the actual projection to the estimated projection is calculated (p_i / $\Sigma_k\ c_{ik}\ \lambda_k^{n-1}$). Third, the ratio is back-projected to the image coordinate (1 / $\Sigma_i\, c_{ij}$)($\Sigma_i\,(c_{ij}\, p_i$ / $\Sigma_k\ c_{ik}\ \lambda_k^{n-1}$)). Finally, the back-projected ratio is multiplied by the current estimate image (λ_j^{n-1} / $\Sigma_i\ c_{ij}$)(Σ_i ($c_{ij}\ p_i$ / $\Sigma_k\ c_{ik}\ \lambda_k^{n-1}$)). In the prototype system, the iteration requires 99 steps from the initial uniform image to obtain the current estimate image.

ML–EM is advantageous over FBP for wear diagnosis of mechanical parts in that the image values are all non-negative, the signal to noise ratio is higher, and there are less linear artifacts (see arrows in Fig. 2) around strong RI sources in the image. These advantages are important for the easy detection of weak sources near strong sources. Further, ML–EM is more suitable for quantitative evaluation because the sum of the image values is preserved during the iteration and the gamma-ray attenuation in the machine and collimators can be implemented in c_{ij}.

Figure 2 shows a comparison of the FBP and ML–EM images. The FBP image was obtained using MATLAB *iradon*. The ML-EM image is based on an in-house program.

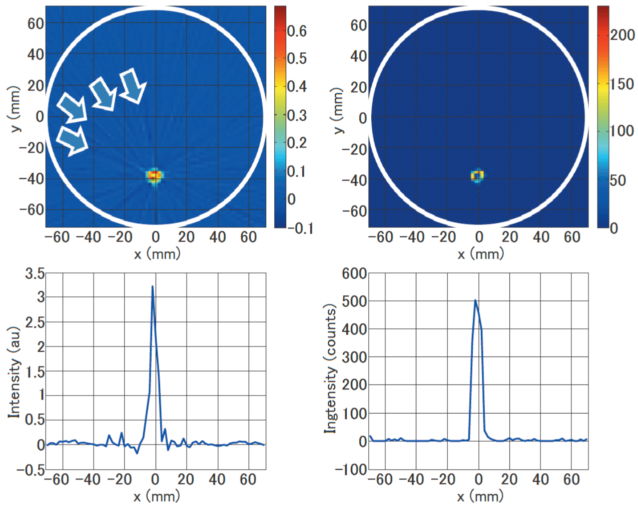

Fig. 2. Comparison of the FBP (left) and ML–EM (right) images (top) and their projections (bottom). The color maps are scaled and optimized for individual images.

References
1) T. Kambara et al.: In this report.
2) J.L. Semmlow: *Biosignal and biomedical image processing* (Marcel Dekker, New York, 2004).
3) L.A. Shepp and Y. Vardi: IEEE Trans. Med. Imag. 1, 113 (1982).
4) K. Lange and R. Carson: J. Comput. Assist. Tomogr. 8, 306 (1984).

*[1] RIKEN Nishina Center

Test of the MINOS liquid H_2 target at RIBF

A. Corsi,[*1,*2] J.-M. Gheller,[*1,*2] L. Audirac,[*1] G. Authelet,[*1,*2] A. Delbart,[*1,*2] P. Doornenbal,[*2] Y. Kubota,[*2] K. Kusaka,[*2] D. Leboeuf,[*1] D. Loiseau,[*1] M. Kurata-Nishimura,[*2] A. Mohamed,[*1] A. Obertelli,[*1,*2] H. Otsu,[*2] C. Péron,[*1,*2] E.C. Pollacco,[*1] J.-Y. Rousse,[*1,*2] C. Santamaria,[*1,*2] M. Sasano,[*1] T. Uesaka,[*2] and Y. Yanagisawa [*2]

MINOS (acronym for MagIc Numbers Off Stability) is a device dedicated to perform the spectroscopy of highly exotic nuclei produced at fragmentation facilities such as the RIBF accelerator of RIKEN. The device[1,2] consists of a thick liquid H_2 target (50–200 mm) surrounded by a time projection chamber (TPC) used to track the vertex position inside the target. The advantage of using such a thick H_2 target is twofold: it increases the luminosity and minimizes the energy loss and straggling of the beam. Furthermore, the use of a structureless probe allows an accurate theoretical description of the reaction mechanism. The vertex information obtained from the TPC helps in preserving the experimental resolution.

The target was developed at the Accelerator, Cryogenics and Magnetism Division - CEA Saclay. The liquid H_2 is contained in a Mylar envelope less than 150 μm thick, composed of two parts glued on an Inox support connected to the H_2 circuit. The target is connected to the cryostat (Fig. 1) equipped with a cryocooler, allowing to reach the liquefaction temperature of 20.3 K. Within the cryostat, the condenser connected to the cold head cools down the H_2 that is transferred by gravity to the target (Fig. 2). This system works in a close loop allowing to minimize the amount of H_2 to be used. A specificity of this system is the possibility to empty the target in less than 30 s. This can be attained by closing a valve on the return circuit, thence producing an overpressure that pushes the liquid to the condenser situated 1 m above. The target can be kept empty for up to 10 h and filled again in 20 s by opening the valve. This functionality allows to easily perform a measurement of the background due to reactions of the beam on the Mylar envelope. Installation and dismounting of the system take 3 and 1 d, respectively.

The system was tested successfully at the RIBF facility in July 2013. A full operation cycle was performed in 72 h: H_2 liquefaction and filling of the target, a demonstration of the “empty target”functionality, H_2 evaporation, and emptying of the target. The liquid H_2 target is expected to be used, coupled with the MINOS detection system, to perform physics experiments at RIBF from Spring 2014.

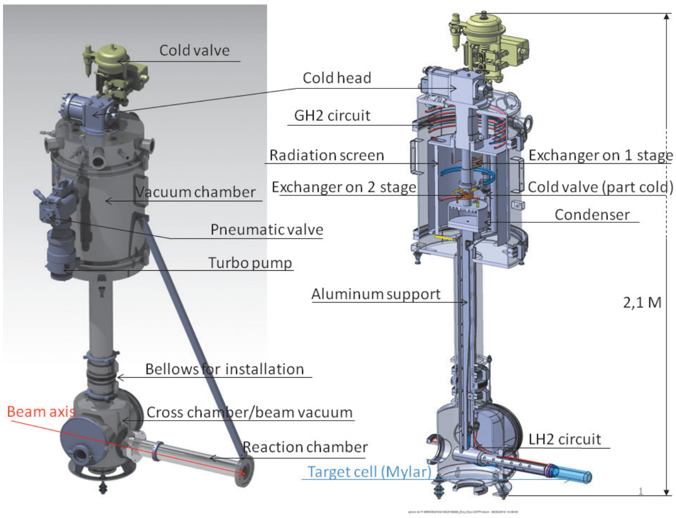

Fig. 1. Schematic view of the cryostat.

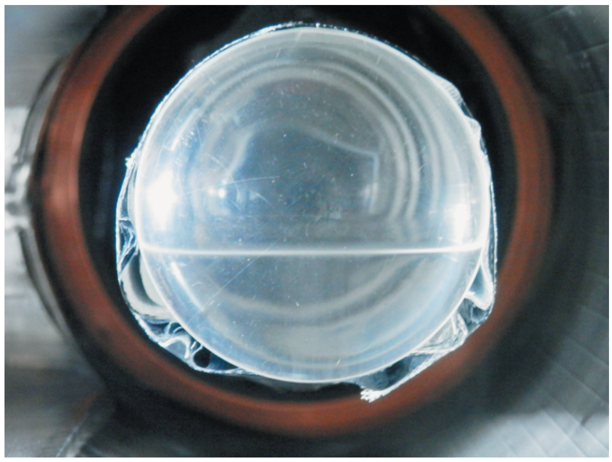

Fig. 2. Front view of the target being filled with liquid H_2.

References

1) A. Obertelli, proceedings in French-Japanese Symposium on Nuclear Structure Problems, Ed. by H. Otsu, T. Motobayashi, P. Roussel-Chomaz and T. Otsuka (2012).
2) A. Obertelli *et al.*, accepted in Eur. Phys. Jour. A (2014).

*1 CEA, Centre de Saclay, IRFU
*2 RIKEN Nishina Center

Development of KEK isotope separation system

Y. Hirayama,*1 N. Imai,*1 H. Ishiyama,*1 S.C. Jeong,*1 H. Miyatake,*1 M. Oyaizu,*1 Y.X. Watanabe,*1 M. Mukai,*2 S. Kimura,*2 Y.H. Kim,*3 M. Wada,*4 T. Sonoda,*4 P. Van Duppen,*5 Yu. Kudryavtsev*5 and M. Huyse*5

We have been constructing the KEK Isotope Separation System (KISS) to study the β-decay properties of the neutron-rich isotopes with neutron numbers around $N = 126$ for astrophysics research[1–3]. In the KISS, a gas cell filled with argon gas at a pressure of 50 kPa, which stops and collects unstable nuclei in it, is an essential equipment for selectively extracting the isotope of interest by using a resonant ionization technique. The absolute extraction efficiency of the gas cell and beam purity of the KISS gas cell can be evaluated only from the measurements of the intensities of beams implanted in and extracted from the gas cell in an on-line test.

We performed on-line tests using the ^{56}Fe beam with the energy of 90 MeV/nucleon and the maximum intensity of 4 pnA. The energy of ^{56}Fe beam was degraded to 1.5 MeV/nucleon in front of the gas cell by using an aluminum energy degrader in order to implant at the center of the argon gas cell. The thermalized and neutralized ^{56}Fe atoms were re-ionized in the gas cell, and the ions were extracted and detected by using a Channeltron detector for ion counting after mass separation.

We successfully extracted laser-ionized ^{56}Fe atoms by cleaning the gas cell system and by using a "bent type" gas cell, which was designed to reduce the plasma effect. Figure 1 shows the measured efficiency and beam purity as a function of the primary beam intensity. The extraction efficiency was defined as S/I. Here, S and I present the numbers of laser-ionized ^{56}Fe atoms and implanted ^{56}Fe atoms in the gas cell, respectively. The measured efficiency was about 0.25% after the correction of the detector efficiency (16%) and the laser repetition rate (20%). The efficiency was independent of the primary beam intensity, as shown in Fig. 1-(a), owing to the bend structure of the gas cell. Beam purity was defined as $S/(S + N)$. Here, N is the number of the extracted ions with $A = 56$, which was measured without irradiation with ionization lasers. Figure 1-(b) shows the obtained beam purity of $> 98\%$, and it depended on the primary beam intensity. The beam purity decreased with increasing primary beam intensity. However, the impurities probably consist of molecular ions of argon, which are stable against radioactive decay and do not affect the β-decay lifetime measurements.

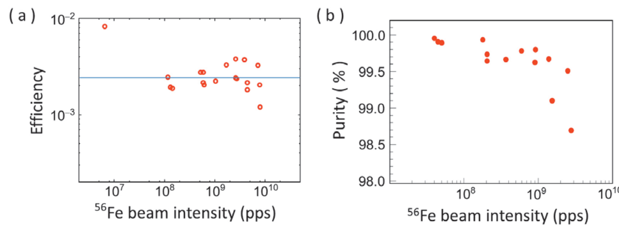

Fig. 1. (a) Extraction efficiency of ^{56}Fe ions and (b) beam purity measured as a function of ^{56}Fe beam intensity.

In the case of the primary beam intensity of 2.5×10^7 pps, we measured mass distributions without and with ionization lasers, as shown in Figs. 2, in order to investigate how many laser-ionized ^{56}Fe atoms formed impurity molecules with H_2O, Ar_2, and hydrocarbons. Figure 2-(a) shows background ions extracted from the gas cell, which are ionized by the primary beam injection. Dimers of argon isotopes and their compounds with hydrogen were dominant. In the case of ionization laser irradiation, we clearly observed laser-ionized ^{56}Fe peak and molecular ion peaks of $^{56}Fe(H_2O)$ and $^{56}FeAr_2$. By reducing the amount of water molecules in the gas cell, the number of laser-ionized ^{56}Fe atoms would increase, and as a result, the extraction efficiency of ^{56}Fe would be doubled.

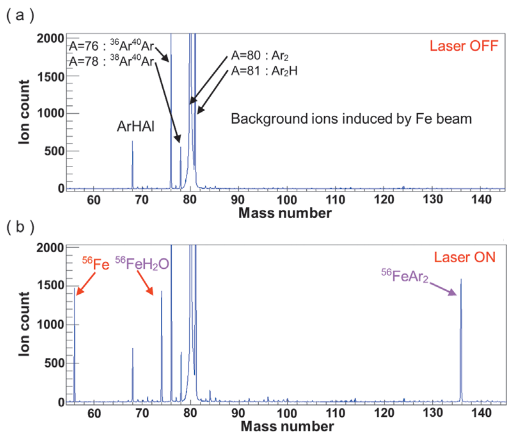

Fig. 2. Measured mass distributions (a) without using ionization lasers and (b) using ionization lasers.

*1 Institute of Particle and Nuclear Studies (IPNS), High Energy Accelerator Research Organization (KEK)
*2 Department of Physics, University of Tsukuba
*3 Department of Physics, Seoul National University
*4 RIKEN Nishina Center
*5 Instituut voor Kern-en Stralingsfysica, KU Leuven

References
1) S.C. Jeong et al.: KEK Report 2010-2.
2) Y. Hirayama et al.: RIKEN Accel. Prog. Rep. **44** (2011) 25; **45** (2012) 152; **46** (2013) 176.
3) H. Ishiyama et al.: RIKEN Accel. Prog. Rep. **45** (2012) 151.

Detection efficiency of segmented neutron detector at 200 MeV

Y. Kubota,[*1,*2] M. Sasano,[*2] T. Uesaka,[*2] M. Dozono,[*2] M. Itoh,[*3] M. Kobayashi,[*1] C.S. Lee,[*1,*2] K. Miki,[*4] S. Ota,[*1] T. Shima,[*4] A. Tamii,[*4] T. Wakasa,[*5] J. Yasuda,[*5] and J. Zenihiro[*2]

Nucleon-knockout (p, pN) reactions at intermediate energies (200–300 MeV) provide a powerful probe of the nature of single particle states (SPSs) in nuclei[1]. The goal of our study is to determine the neutron separation energy with a high resolution of about 500 keV at full-width at half-maximum (FWHM) via the (p, pn) reaction. This is technically challenging because a high position resolution is necessary for neutron detection which cannot be achieved with a conventional design.

At RIKEN RIBF, we are developing a segmented neutron detector consisting of 64 scintillating fibers. Each fiber has dimensions of 3.75 mm (W) × 3.75 mm (D) × 1 m (H) and has two multi-anode photomultiplier tubes (Hamamatsu H7546B) at both ends. Using this setup, we confirmed that the position resolution of 3.75 mm in the total width, corresponding to the fiber size, was actually realized by performing a neutron irradiation experiment at the Cyclotron Radioisotope Center (CYRIC), Tohoku University in November 2012. Furthermore, we determined the neutron detection efficiencies at 50 and 68 MeV to be $1.6 \pm 0.4\%$ and $2.0 \pm 0.5\%$, respectively[2].

For higher neutron energies, we performed another experiment using neutron beams at 200 MeV at the Research Center for Nuclear Physics (RCNP), Osaka University in November 2013. Monoenergetic neutron beams at 199 and 181 MeV were produced from ^{7}Li(p, n) and ^{12}C(p, n) reactions using a proton beam at 200 MeV. The Li and C targets, each with natural isotopic abundance, had thicknesses of 0.94 and 2.1 mm, respectively. Neutrons flew in the neutron time-of-flight (NTOF) tunnel and, were then detected by the segmented neutron detector placed at a distance of 50 m from the target position. The intensity of the proton beam was about 100 nA and the rate of neutrons bombarding on the detector was typically 10^4 particles per second.

A preliminary analysis shows that the detection efficiencies for 181- and 199-MeV neutrons were $2.6 \pm 0.4\%$ and $2.5 \pm 0.4\%$, respectively. The threshold for neutron detection, 4.2 MeV electron equivalent (MeV$_{ee}$) was applied to the light output information obtained from the charge amplitude of the dynode signal.

Figure 1 shows the distribution of the detection position, which is defined as the most upstream fiber hit. When there are several hit fibers at the same depth, the fiber with largest light output is selected. Here, the threshold of each channel was set to 0.5 MeV$_{ee}$. The distribution was found not to be uniform near the surface. Along the beam direction, most events were concentrated on the first plane, and the fibers on the left and right sides had a larger number of events than the inner fibers. This enhancement in the number of events near the surface, which was not observed clearly in the previous experiment because of the lack of the uniformity on the threshold of each channel, is still not understood and is being investigated for details. The inner array of 6 × 6 fibers had a uniform distribution within 10%, possibly reflecting the uniformity of the neutron flux.

The most downstream fibers had a smaller number of events compared to upstream fibers. For these fibers, the light output deposit by recoil protons can be small because the protons go out of the detector volume within a short distance.

In summary, we are developing the segmented neutron detector with a high position resolution for the study of SPSs via the (p, pn) reaction. The detection efficiencies of neutrons at 181 and 199 MeV were determined to be $2.6 \pm 0.4\%$ and $2.5 \pm 0.4\%$, respectively. The distribution of the detection position shows a large enhancement in the number of events at the surface which is being analyzed.

We acknowledge the staff at the RCNP for their efforts and support.

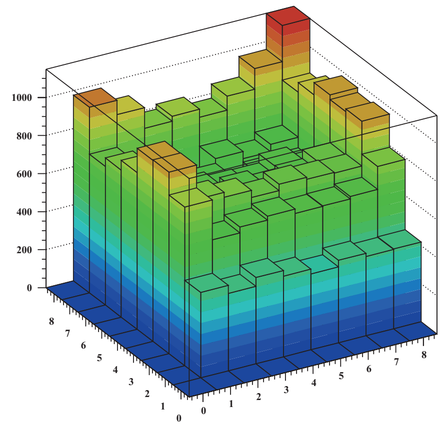

Fig. 1. Distribution of detecting positions indicated by the heights of the 8 × 8 blocks. The neutron beam travelled from top left to right bottom.

References
1) G. Jacob and TH. A. J. Maris, Rev. Mod. Phys. **45**, 6 (1973).
2) M. Sasano *et al.*, RIKEN Accel. Prog. Rep. **46**, 161 (2013).

*1 Center for Nuclear Study, University of Tokyo
*2 RIKEN Nishina Center
*3 Cyclotron and Radioisotope Center, Tohoku University
*4 Research Center for Nuclear Physics, Osaka University
*5 Department of Physics, Kyushu University

Preparation status of the J-PARC E16 experiment : measurement of vector meson mass in nuclei

S. Yokkaichi[*1] for the J-PARC E16 Collaboration

We have proposed the experiment E16[1)] to measure the vector meson decays in nuclei in order to investigate the chiral symmetry restoration in dense nuclear matter. The experiment will be performed at the J-PARC Hadron Experimental Facility. The proposal of the experiment was granted scientific ("stage 1") approval by the PAC in March 2007. For the full approval, we need to establish the experimental feasibility as well as to show the prospects of acquiring sufficient funds and of beam-line construction. Toward the full approval, the technical design report is under preparation for submission to PAC to be held in May 2014.

The mass modification of vector mesons in hot and/or dense matter is predicted on the basis of the QCD because of the restoration of the chiral symmetry in such matter. Mass modifications in matter, however, due to hadronic many-body effects are also predicted. The predictions from these two viewpoints should agree in principle, however, still no clear connections are established between the two thus far.

Many experimental studies, including dilepton invariant mass measurements, have been conducted to approach the problem, and mass modifications in hot and/or dense matter have been observed. However, the origin of the modification has not yet been confirmed; in other words, there is no consensus on the interpretations of the phenomena. Among the experiments, the experiment KEK-PS E325[2)], which was conducted by a collaboration including some of the authors, measured the e^+e^- invariant mass spectra in 12-GeV p+A reactions and reported enhancements on the low mass sides of ω and ϕ mesons. These enhancements are consistent with the decrease in the mass of vector mesons predicted using the QCD sum rule. The mass-shape modification of a narrow resonance, ϕ, can be observed only in E325.

The aim of the J-PARC E16 experiment is to perform a systematic study of the mass modification of vector mesons, particularly the ϕ meson, in nuclei, with statistics that are two orders larger in magnitude than those of the preceding E325 experiment. In other words, the aim is to accumulate 1×10^5 to 2×10^5 events for each nuclear target (H, C, Cu, and Pb), and deduce the dependence of the modification on the matter size and meson momentum, which have never been measured. Furthermore, the e^+e^- decays of the ρ, ω, and J/ψ mesons can be measured at the same time.

For this experiment, we plan to use a 10^{10}-pps, 30-GeV proton beam in the high-momentum beam line, which is being constructed at J-PARC. In order to increase the statistics by a factor of 100, we will construct a large-acceptance spectrometer that can be operated under 10^7 Hz nuclear interactions at the target. In order to cope with such a high-interaction rate, GEM has been adopted for constructing new tracking and PID detectors.

The development of the detectors is underway as reported elsewhere[3–8)], funded by a MEXT Grant-in-Aid[9)]. To summarize, basic studies and beam tests of the two key detectors, the GEM Tracker[3,4)] and HBD[5)], have been performed. For the former, the required performance has almost been achieved. The specification of GEM is fixed and production of GEM has been underway since 2013. For the latter, stability in a high background environment has been confirmed[6)]. The GEM specification is also fixed and we will move to production in 2014. The development of read-out and trigger modules are on going[7)]. In particular, for the GEM readout, a CERN-made system has been tested and adopted[8)].

Construction of the high-momentum beam line has been on-going since 2013 by KEK. The first beam will be delivered by the end of JFY 2015. In spite of the radiation accident at J-PARC in May 2013, the planned schedule of the spectrometer magnet construction has not changed. Therefore, it is expected to be completed in Jan. 2015. After completion of the magnet construction, we can start the installation of the detectors in the magnet. The target day of the construction is the planned first beam, Mar. 2016. Due to the budgetary limitation, our first goal of the staged construction plan is to construct one-third of the spectrometer.

References

1) S. Yokkaichi *et al.*: J-PARC proposal No. 16 (`http://j-parc.jp/researcher/Hadron/en/pac_0606/pdf/p16-Yokkaichi_2.pdf`), Lect. Notes Phys. **781** 161 (2009).
2) M. Naruki *et al.*: *Phys. Rev. Lett.* **96**, 092301 (2006), R. Muto *et al.*: *Phys. Rev. Lett.* **98**, 042501 (2007).
3) Y. Komatsu *et al.*: in this report.
4) W. Nakai *et al.*: in this report.
5) K. Kanno *et al.*: in this report.
6) D. Kawama *et al.*: in this report.
7) T. N. Takahashi *et al.*: in this report.
8) Y. Morino *et al.*: in this report.
9) Grant-in-Aid for Scientific Research on Innovative Areas 2104: "Elucidation of New hadrons with a Variety of Flavors", 2009–2013, `http://www.hepl.phys.nagoya-u.ac.jp/public/new_hadron/index-e.html`

*1 RIKEN Nishina Center

Background estimation and operation test of the GEM detectors for the J-PARC E16 experiment

D. Kawama[*1] for the J-PARC E16 collaboration

In the proposed J-PARC E16[1)] experiment, we will use a 30 GeV primary proton beam at the J-PARC high-momentum beam line. Because the beam intensity will be $\sim 1 \times 10^{10}$ per spill and expected particle counting rate is 5 kHz/mm^2 at most, we will use two types of GEM detector: the GEM tracker[2)] and the Hadron Blind Detector (HBD)[3)]. These detectors need to be operated in high-rate background environment during the experiment. In a test experiment using the 1.0 GeV/c pion beam at the J-PARC K1.1BR beamline, several breakdowns were observed with HBD (30 cm $\times$ 30 cm $\times$ 100 μm^t LCP GEM in CF_4 gas, 3×10^3 gain). The breakdowns are considered to be caused by hadronic background such as neutrons or slow hadrons, because we did not observe such breakdowns with electron beams. In addition, no breakdowns were observed with the GEM trackers (10 cm $\times$ 10 cm $\times$ 50μm^t PI GEM in Ar/CO_2 gas, 1×10^4 gain). Therefore we estimated the background particles and their energies for the E16 experiment and performed an operation test of the GEM detector in the high-rate neutron background.

The background particle counting rate was estimated using the Geant4 simulation. The simulation employed the physics list of "QGSP_BERT_HP",[4)] which includes high-precision treatment of low-energy neutrons ($E_{kin} < 20$ MeV). The validity of this simulation for estimation of background particle counting rate was checked by comparing the background calculation with PHITS[5)] calculation[6)] at the K1.1BR area; both agreed within a factor of 2. For example, the neutron rate was 0.01 Hz/mm^2 at the broken GEM of K1.1BR case.

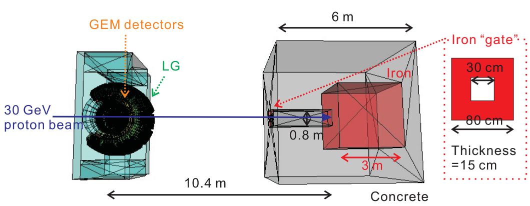

Fig. 1. Schematic model of the E16 experiment used in the simulation. The area is surrounded by concrete blocks, and is filled by air.

The model used in the E16 background simulation is shown in Fig. 1. Using this model, we estimated the particle rate at the detector position, which is located at approximately 120 cm from the target surrounded by the lead-glass calorimeters. Fig. 2 shows the energy spectra from the beam dump and the target, and reveals that the main contribution is by neutrons of several hundred keV. By integrating these spectra, we estimated the neutron counting rate of the E16 detector to be in the order of 0.1 kHz/mm^2 for the beam-dump origin and 0.01 kHz/mm^2 for the target origin.

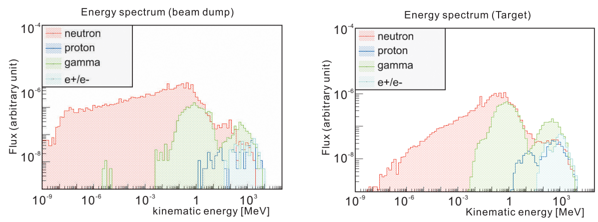

Fig. 2. Energy distribution of the background particles from the beam dump (left panel) and the target (right panel).

We performed an operation test of the GEM detector at AVF cyclotron room in the RIKEN RI beam factory. The detector includes triple-stack 30 cm $\times$ 30 cm $\times$ 50 μm^t PI GEMs in the CF_4 gas. This is the same configuration as that employed in the E16 experiment. During the operation, a 12 MeV deuteron beam with an intensity of 10 pμA was used in the room. The dominant energies of the neutrons were 0.1-10 MeV according to the Geant4 simulation, and the GEM detector was operated in the room background. The neutron radiation level monitored during the operation was 87 mSv/h on average, which is in the order of 1 kHz/mm^2. The counting rate of the GEM itself was approximately 10 Hz/mm^2. The GEM could be stably operated for 15 h without breakdowns with $V_{gem} = 510$ V, which corresponds to a gain of 2×10^4. The total amount of neutrons corresponds to the 2-month operation in the E16 experimental area. From the test operation, we can confirm that PI GEMs can work stably in high neutron background. Further study is necessary to clarify the reason for stable operation.

*1 RIKEN Nishina Center

References
1) S. Yokkaichi *et al.*, in this report
2) Y. Komatsu *et al.*, in this report
3) K. Kanno *et al.*, in this report
4) "Geant4 reference physics list" in the Geant4 homepage, http://geant4.cern.ch/
5) T. Sato *et al.*, J. Nucl. Sci. Technol. 50:9, 913-923 (2013)
6) K. Tanaka, Private communication

Development of the tracking detector with large GEM foils for the J-PARC E16 experiment

Y. Komatsu[*1,*2] for the J-PARC E16 Collaboration

The J-PARC E16[1)] experiment is proposed to measure the mass spectrum of the ϕ meson in nuclear matter. In the spectrometer, the momentum of charged particles is measured using the tracking detectors(called "GEM trackers") in a magnetic field. The details of the GEM tracker are described elsewhere[2)3)]. The development of the tracker with an effective area of 300 mm × 300 mm is reported in this article. A schematic view of the 300 mm×300 mm readout board is shown in Fig. 1. Cartesian strips called "X" and "Y" are made of copper and patterned on the top and the bottom of a polyimide sheet of thickness 25 μm. For charge sharing between X and Y, the base polyimide is etched using the chemical method, except just under the X strips. The glass epoxy of thickness 100 μm is laid under the Y strips as a support.

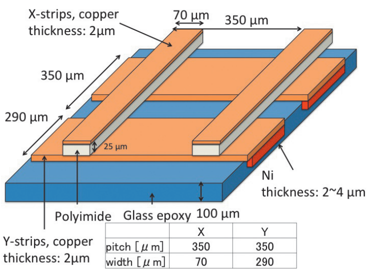

Fig. 1. Schematic view of the 300 mm × 300 mm readout board. Only a part of the readout board is shown in this magnified view.

The positions of the strips were measured using a coordinate measuring machine (Nikon VMR-10080). The coordinates of the cross-points of the left edge of the X strips and the upper edge of the Y strips (x_{ij}, y_{ij})$_{(i,j=0,...,71)}$ were measured for every 12 strips. The subscripts i and j denote the row and column numbers. The deviations of the coordinates of the cross-points from the mean values were calculated for each strip and plotted in Fig. 2. The deviations of the X and Y strips are defined as $x_{i,j} - \sum_{i=0}^{71} x_{i,j}/72$ and $y_{i,j} - \sum_{j=0}^{71} y_{i,j}/72$. The maximum deviation of the X and Y strips were 43 μm and 42 μm, respectively. The deviations were small compared to the spatial resolution of the X and Y strips, which are 100 μm and 400 μm, respectively. The precision of the readout strips was confirmed. GEM foils with an effective area of 300 mm × 300 mm were also fabricated. The average diameters of the holes were 65 μm for copper and 33 μm for polyimide in the top and the middle GEM of the stack,

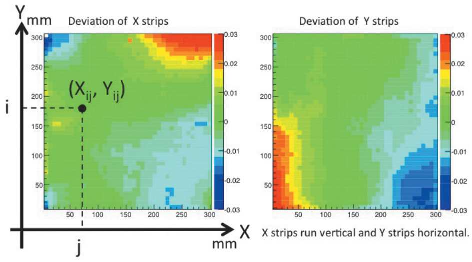

Fig. 2. The measured deviations of the X and Y strips of the 300 mm × 300 mm readout board. The unit of the color bar is mm and the right (up) direction is the positive direction in the left (right) figure.

and 56 μm and 27 μm in the bottom for copper and polyimide, respectively. The spatial resolution of the GEM tracker was evaluated using positron beams at the Research Center for Electron Photon Science, Tohoku University. The setup is shown in the left panel of Fig. 3. The GEM tracker was located between two Silicon Strip Detectors (SSDs). The position resolution was evaluated on the basis of the residual of the hit positions calculated from the hits on SSDs and the GEM tracker. The obtained residual distribution for the 0° beam is shown in the right panel of Fig. 3. The residual distribution was fitted with a Gaussian, and the standard deviation was 73 μm. The requirement of the position resolution is 100 μm, and the 300 mm × 300 mm GEM tracker has sufficient resolution for the experiment.

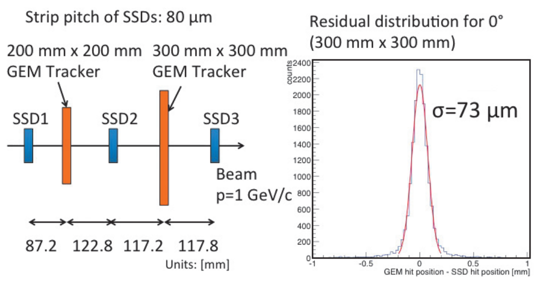

Fig. 3. Setup of the beam test (left) and residual distribution of the 300 mm × 300 mm GEM tracker for 0° beam(right).

References
1) S. Yokkaichi et al.: In this report.
2) Y. Komatsu et al.: RIKEN Accel. Rep. **45** (2011).
3) Y. Komatsu et al.: RIKEN Accel. Rep. **46** (2012).

*1 Department of Physics, University of Tokyo
*2 RIKEN Nishina Center

Development of a prototype module for the lead-glass calorimeter readout and an ASIC for GEM foil trigger for J-PARC E16 experiment

T.N. Takahashi*[1] for the J-PARC E16 Collaboration

Development of detectors for the new spectrometer[1)], GEM tracker (GTR), Hadron Blind Detector (HBD) and lead-glass electromagnetic calorimeter (LG), and electronics is currently in progress.

The number of readout channels of LG is about 1100. Therefore, a dedicated and cost effective readout module has been developed in collaboration with Open-It[2)]. The specification of the prototype module is listed in Table 1 and the picture is shown in Fig. 1, which has benn delivered and is currently undergoing tests. The prototype module is fabricated as the KEK-VME 6U standard. The analog input signals are split into two lines, one is fed into the comparator to generate binary outputs used for trigger primitives, and the other is followed by an analog memory. The analog memory is realized by DRS4[3)] ASIC, which contains 1024 sampling cells per channel and can store the waveform in a gigahertz range. To extend the analog buffer, two channels are cascaded for one analog input on the prototype module. Therefore, 2 μsec analog buffer is available if the sampling speed is set at 1 GHz, which implies that a long delay cable is unnecessary for delaying analog pulses. The waveform stored in the DRS4 is digitized by AD9637 at 33 MHz. Since the DRS4 supports a readout only in the region of interest, the dead time for an analog pulse with the width of ~100 nsec is expected to be less than ~5 μsec. The slow control for setting a discriminator threshold and the data readout are performed by the Xilinx FPGA Spartan6-LX150 via the Ethernet.

The e^+e^- event trigger consists of three-fold coincidence of GTR, HBD, and LG. We will use a cathode plane of a GEM foil of the most outer GTR chamber. The GEM foil is divided into 24 segments. Each segment has detector capacitance of 2 nF and its hit rate is expected to be 1-2 MHz in the forward region of the spectrometer. In order to cope with such a high rate with large input capacitance in the small form factor, we have developed a new Amplifier-Shaper-Discriminator (ASD) IC with low noise and fast shaping time in collaboration with Open-It. The specification is summarized in Table 2 and the photos are shown in Fig. 2. The analog part works nearly as expected. The digital part is currently undergoing tests.

Table 1. Specification of the prototype module for the LG.

parameter	value
number of analog inputs	16
analog input range	0 to -2 V
resolution	12 bit
analog memory	2048 samples / channel
readout time	30 nsec / sample
discriminator out	LVDS
readout/ slow control	TCP (100 Mbps) / UDP
power supply	± 3.3 V (KEK-VME J0 bus)

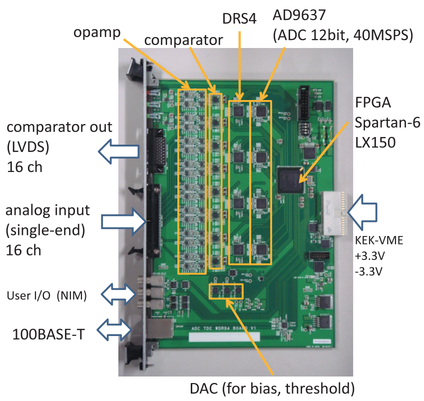

Fig. 1. A picture of the prototype module for the LG.

Table 2. Specification of the GEM trigger ASD.

parameter	value
input range	10 fC – 1 pC
shaper time constant	25 ns
pulse width	< 200 ns
conversion gain	3.0 mV/fC
ENC	20000 (C_d = 2 nF)
number of channel	6
power supply	± 2.5 V

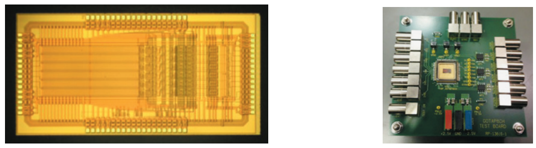

Fig. 2. Pictures of the GEM foil trigger ASIC and its evaluation board.

References
1) S. Yokkaichi *et al.*: in this report.
2) http://openit.kek.jp/
3) http://www.psi.ch/drs/

*1 RIKEN Nishina Center

Testing a GEM tracker in a magnetic field for the J-PARC E16 experiment

W. Nakai[*1,*2] for the J-PARC E16 Collaboration

The J-PARC E16 experiment was conducted to measure the mass modification of ϕ mesons in nuclear matter at J-PARC in order to study the origin of hadron mass. The details of this experiment are presented in another article of this report[1)].

We employed a tracking detector using the Gas Electron Multiplier (GEM)[2)], and have been developing it to be a position-sensitive detector in a magnetic field with a magnitude of 1.8 T at the center of the magnet. To use this detector, a position resolution of 100 μm up to an incident angle of 30° in a high counting rate environment up to 5 kHz/mm^2 is required. Our GEM tracker consists of a drift cathode, a triple GEM, and a readout strip board. We chose a strip pitch of 350 μm to achieve the required position resolution.

Since the directions of the electric and magnetic field in the drift gap are perpendicular, the drift velocity of ionization electrons is inclined to the E field by Lorentz angle α. Therefore we tested the operation of the detector in a large dipole magnet located at the J-PARC Hadron Hall in Apr. 2013. The setup is shown in Fig. 1. A laser with a wavelength of 266 nm was used to make the primary electrons, and the incident angle was fixed at 30°. The E fields of the drift gap, transfer gap, and induction gap were 600 V/cm, 3600 V/cm, and 3600 V/cm, respectively, and the B field was from 0.0 T to about 0.7 T.

As shown in Fig. 2, the expected Lorentz angles were calculated using a Garfield++ toolkit[3)]. Because the Lorentz angle in the drift gap is accidentally almost equal to that of the transfer and induction gap, electrons should drift straight from where they are generated to the readout strip board. The Lorentz angle α can be represented as

$$\tan\alpha = \frac{\Delta_x}{d} \tag{1}$$

where d is the distance between the mesh and the readout, and Δ_x is a shift in the edge position of charge cluster measured in the non-magnetic field to that at readout. The result is plotted in Fig. 3. We found that the result is almost consistent with the calculation but there exists 14% of systematic difference. The reasons behind this systematic error need to be discussed.

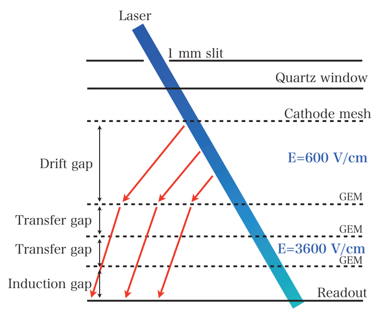

Fig. 1. A schematic view of the setup. Red arrows indicate the drift directions of electrons.

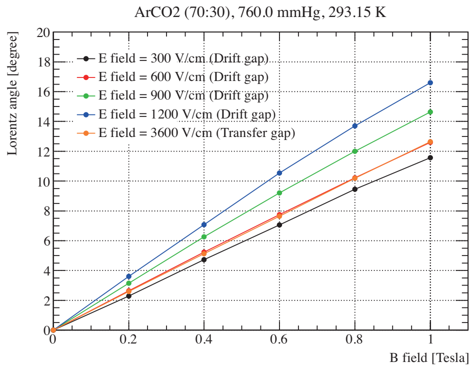

Fig. 2. The results of simulations using Garfield++ codes with various drift electric fields.

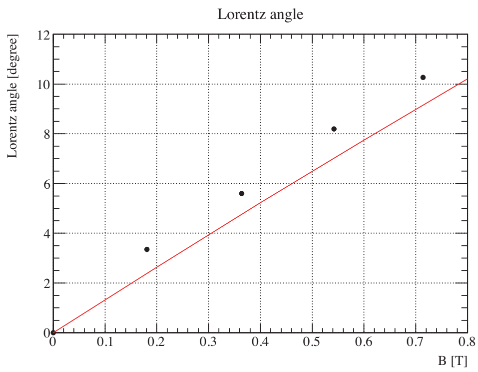

Fig. 3. The measurement of the Lorentz angle as a function of the magnetic field (black points), and the calculation using Garfield++ (red line).

*1 Department of Physics, The University of Tokyo
*2 RIKEN Nishina Center

References
1) S.Yokkaichi, *et al*, in this report
2) F. Sauli, Nucl. Instrum. Meth. A386 (1997) 531
3) http://garfieldpp.web.cern.ch/garfieldpp/

Measurement of photoelectron yield in a hadron blind detector for the J-PARC E16 experiment

K. Kanno[*1,*2] for the J-PARC E16 collaboration

A hadron blind detector (HBD) has been developed for the J-PARC E16 experiment.[1)] The E16 experiment aims to detect the in-medium modification of a ϕ meson in a nucleus via the $\phi \to e^+e^-$ decay. The HBD identifies the positrons and electrons by converting the emitted Čerenkov photons in CF_4 into photoelectrons with a CsI photocathode. The converted photoelectrons are amplified by a triple gas electron multiplier (GEM)[2)] stack to obtain a signal on readout pads. The CsI photocathode is evaporated on the surface of the top GEM of the stack. We perform the measurement in the momentum region (up to 4 GeV/c) where only positrons and electrons can emit Čerenkov photons in the HBD. Although almost all of the ionization electrons emitted from charged particles are removed by applying reversed drift-field before the triple-GEM section, a huge amount of such charged particles would contaminate the HBD signal. Therefore, the detection yield of the photoelectrons is the most significant value required to discriminate the Čerenkov photons at the trigger level.

The detection yield of the photoelectrons depends on the quantum efficiency of the CsI photocathode and photoelectron collection efficiency. The collection efficiency is defined as the ratio of the number of photoelectrons that are collected and subsequently amplified by the GEMs to the number of photoelectrons produced at the CsI photocathode. The collection efficiency is, therefore, supposed to depend on the electric field at the surface of the CsI photocathode, whose strength is determined by the size and pitch of the GEM holes.

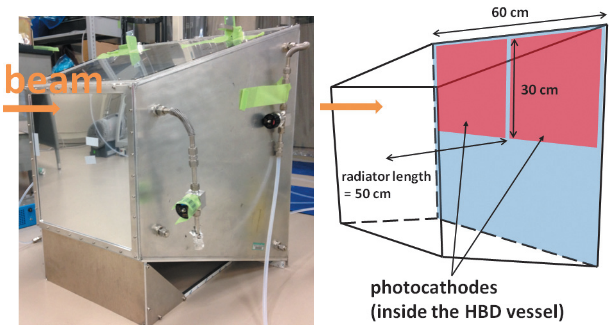

Fig. 1. Photograph (left) and schematic view (right) of the HBD prototype.

To evaluate the pitch dependence of the detection yield of the photoelectrons, we produced a prototype HBD with two types of GEMs: type-A has the hole and pitch sizes of 55 µm and 140 µm, respectively, while type-B has the pitch size of 110 µm with the same hole size. The length of the Čerenkov radiator is 50 cm, and the size of the photocathode is 60 cm × 60 cm, which is divided into four parts with size 30 cm × 30 cm, as shown in Fig. 1. For the prototype, one 30 cm × 30 cm type-A photocathode and one 30 cm × 30 cm type-B photocathode were prepared.

Using the prototype HBD, we performed a beam test with a 1.0 GeV/c positron beam at the Research Center for Electron Photon Science, Tohoku University. Figure 2 shows the obtained charge distribution, where we observed ~7.6 mean photoelectrons with type-A and ~10.7 with type-B.

Because we confirmed that these photocathodes have almost the same quantum efficiency, the difference in the detection yield of the photoelectrons is attributed to the difference in the photoelectron collection efficiency. Based on this result, which fulfills the experimental requirement with type-B GEMs, we have decided to adopt type-B GEMs as the E16 HBD. This is the first result of the HBD made in Japan with large (30 cm × 30 cm) GEMs.

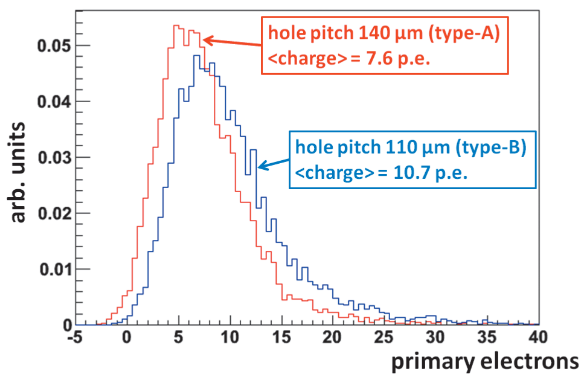

Fig. 2. Charge distribution of two different photocathodes.

References

1) S. Yokkaichi *et al.*: in this report
2) F. Sauli: Nucl. Instr. and Meth. A **386** (1997) 531

*1 RIKEN Nishina Center
*2 Department of Physics, Graduate School of Science, The University of Tokyo

Performance of scalable readout system

Y. Morino *1 for the E16 Collaboration

The aim of the E16 experiment to be conducted at J-PARC is to study the nature of vector mesons in nuclei in order to investigate chiral symmetry restoration in dense nuclear matter[1)]. A readout system is required for measuring the high rate and the large datasets. Our expected trigger rate is approximately 1 kHz, and the expected occupancy reached to be 30% at maximum.

We plan to construct a readout system for the Hadron Blind Detector (HBD) and Gas Electron Multiplier (GEM) trackers using APV Hybrid chips and Scalable Readout System (SRS) module[2)]. An APV chip is an analogue pipeline ASIC[3)]. The chip consists of 128 channels of preamplifiers and shapers driving a 192-column analogue memory. The SRS module is used for the slow control of APV chips, the digitization of analog data from the APV chips, and transfer of digital data to a computer using UDP/IP[4)]. The SRS module has an 8-port HDMI interface to connect APV chips. Therefore, one SRS module can support 8 Master/Slave APV (16 APV chips) hybrid chips. It corresponds to $128 \times 16 = 2048$ detector outputs.

The data size of the SRS output for unit sampling time per event per channel is 2 bytes. If we take data with 27 sampling time units which is sufficient length for the E16 experiment, the entire data size per event per module is $2 \times 2048 \times 27 \sim 110$ kBytes. Since our planned trigger rate is approximately 1 kHz and the expected occupancy is 30% at maximum, the SRS module must read out and transfer data at a rate of $110\ \mathrm{k} \times 1000 \times 0.3 = 33$ MBytes/s. A transfer rate of 33 MBytes/s is the requirement of the E16 experiment for evaluating the performance of the SRS module.

We discovered that the SRS module satisfied the requirement of the E16 experiment. Initially, one SRS module was connected to a computer. Four ADC channels (corresponding to 512 channels) were read out. A trigger was generated by a function generator. We measured the data transfer rate on the computer as function of trigger rate. Figure 1(a) shows the measurement results. In Fig. 1(a), the red line represents the theoretical value at the given trigger rate. Measured values are consistent with the theoretical values until the data transfer rate reaches 110 MBytes/s. The measured value dropped with the rate, 4 kHz, because a part of the trigger was injected within the dead time of the SRS module. This result satisfies the requirement of the E16 experiment. Next, two SRS modules were connected to a computer via a network switch. Then we measured the data transfer rate for this case. Figure 1(b) shows the measurement results. The Y-axis in Fig. 1(b) denotes the sum of the transfer rate. Black squires denote the results when four ADC channels were read out in both SRS modules. Red circles show the results when two ADC channels were read out in one module and six ADC channels in the other. These measured values were consistent with the theoretical values until the transfer rate sum reached 120 MBytes/s. This result supports that the network switch do not affect the data transfer rate. A single computer can handle several SRS modules. In addition, we confirmed in the same manner that the readout performance does not degrade using the zero-suppression process. Since the data transfer was carried out by using UDP, data loss may occur. Since the rate of data loss is less than once per 10 hours of operation, the efficiency of the data taking will not be affected by the rejection of the errors at the event build. Consequently, hardware performance of the SRS module satisfies the requirement of the E16 experiment.

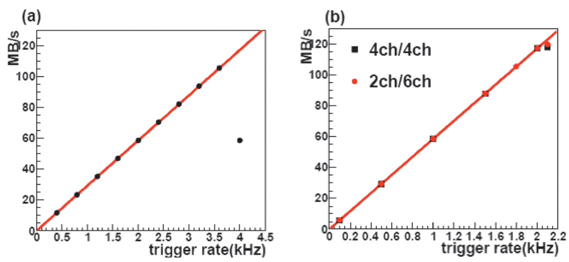

Fig. 1. Data transfer rate.(a)one SRS module. Four ADC channels were read out (b) two SRS module.Black squires show the results when 4/4 ADC channels were read out. Red circles show the results when 2/6 ADC channels were read out.

Approximately 95,000 channels must be read out via the APV chips and the SRS modules. A minimum of 780 APV chips and 49 SRS modules will be necessary. The number of SRS modules handled by one computer will be determined based on the writing speed of the disk. Since the expected occupancy will be about 10% on an average, one computer may handle $8 \sim 10$ SRS modules. Therefore, $5 \sim 6$ computers will be used for DAQ. Further, the performance study with random trigger is also in progress.

References
1) S. Yokkaichi et al. in this report.
2) S. Yokkaichi et al. , J-PARC Proposal No.16 http://j-parc.jp/researcher/Hadron/en/pac_0606/pdf/p16-Yokkaichi_2.pdf
3) https://espace.cern.ch/rd51-wg5/srs/Documentation/APV_User_Guide_2.2.pdf
4) https://espace.cern.ch/rd51-wg5/srs/Documentation/SRS_Slow_Control_Manual.pdf

*1 RIKEN Nishina Center

Status of silicon pixel detector for PHENIX experiment toward RHIC Run-14

M. Kurosawa,[*1] Y. Akiba,[*1] H. Asano,[*2] K. Boyle,[*1] J. Bryshawskyj,[*3] C. Chen,[*1] T. Hachiya,[*1] M. Lentz,[*4] B. Miljko,[*5] T. Moon,[*1] H. Nakagomi,[*6] R. Nouicer,[*4] C. Pancake,[*7] H. Sako,[*8] S. Sato,[*8] P. Stankus,[*5] T. Sumita,[*1] A. Taketani,[*1] H. Torii,[*1] M. Wysocki,[*5] and the PHENIX VTX group

The silicon vertex tracker (VTX) was installed in the PHENIX experiment in 2010, and it successfully collected approximately 5 billion events of Au+Au collisions at $\sqrt{s_{NN}} = 200$ GeV in the 2011 RHIC run (Run-11) at Brookehaven National Laboratory (BNL). The main function of the VTX is the separation of heavy flavor (HF) hadrons, charm and bottom, with the measurement of the distance of closest approach of single electrons from their decays. The nuclear modification factor and azimuthal anisotropy for HF were measured, and analysis results have already been reported[1)].

The VTX is composed of two inner silicon pixel detectors and two outer silicon strip detectors. The silicon pixel ladder is the basic component of a silicon pixel detector. The ladder consists of four silicon sensor modules, two readout buses, and a cooling support. The I/O pads of the silicon sensor module are electrically connected to that of the readout bus via aluminum bonding wires that are encapsulated in epoxy resin. The silicon sensor module is an assembly of a silicon pixel sensor and four readout chips bump-bonded with 25-μm-diameter bumps to the silicon sensor. During Run-11, a small fraction of bump bonds were defected due to thermal stress. In addition, some bonding wires were broken due to a thermal stress caused by the difference in the thermal coefficient between the encapsulation and the readout bus. The active area of a VTX was decreased to 60% because of defected bump bonds and broken bonding wires. The solutions for these issues are to change the operation temperature from 0 degree to the room temperature to avoid thermal stress, and to use a different type of encapsulation. The operation temperature was changed from that used in the physics run in 2012.

After the shutdown of the physics run in 2013, the VTX was dis-assembled at BNL to replace the encapsulation with a different type of encapsulation. All pixel ladders that had broken wires were sent to HAYASHI WATCH-WORKS CO., LTD. where pixel ladders had been mass produced. In total, 15 pixel ladders had been repaired with the yield of almost 100% during 6 months. A small fraction of dead area ($< 1\%$) was remained because of the damage to I/O pads during repair process.

The repaired ladders were electrically tested at RIKEN before being shipped to BNL, and the final electrical test was performed at BNL before the reassembly of the VTX. The following are the test items.

(1) Current consumption of a pixel ladder.
(2) Optimization of a reference voltage for DACs on the readout chip of a pixel module.
(3) Bias voltage dependence of the leakage current for a silicon pixel sensor.
(4) Response of the pixel ladder to a β source (^{90}Sr).

No issue was found in all tests. Figure 1 shows the typical response of a pixel ladder to the β source.

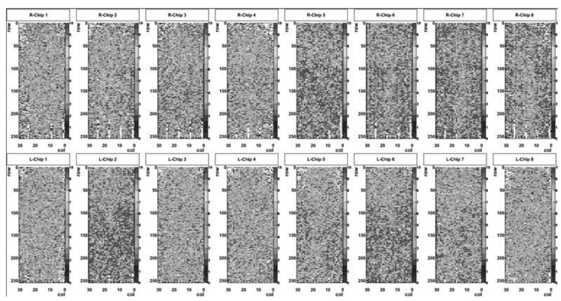

Fig. 1. Response of pixel ladder to a β source. The horizontal and vertical axes represent z and ϕ direction in the PHENIX coordinate, respectively. Low gray-levels represent low number of hits.

Since some pixel ladders had faulty bump bonds, there is a small fraction of unfixable dead area($< 1\%$) in the pixel ladder, and the configuration of pixel ladders in the VTX affects physics data. The optimization of the performance of the pixel detectors had been done by arranging the configuration based on the test results at BNL.

The reassembly of the VTX had been successfully performed at the end of 2013. As a results of the repair work, the active area of the VTX was significantly improved to about 90%. Final optimization of operation parameters for pixel ladders is ongoing. We will collect 200 GeV Au+Au collision data with around 10 times more statistics than that collected in Run-11.

*1 RIKEN Nishina Center
*2 Department of Physics, Kyoto Univ.
*3 Department of Physics, City Univ. of New York
*4 Brookhaven National Laboratory
*5 Oak Ridge National Laboratory
*6 Department of Physics, Tsukuba Univ.
*7 Department of Physics, Stony Brook University
*8 Japan Atomic Energy Agency

References

1) R. Nouicer et al.: Nucl. Phys. A 904-905 (2013) 647c-652c

Construction of PHENIX Silicon Pixel Tracker

H. Torii,[*1] Y. Akiba,[*1] H. Asano,[*1] T. Hachiya,[*1] M. Kurosawa,[*1] T. Moon,[*1] H. Nakagomi,[*1] C. Pankcake,[*2] H. Sako,[*1] S. Sato,[*1] T. Sumita,[*1] A. Taketani,[*1] and the PHENIX VTX group

The PHENIX experiment is upgraded with a central silicon vertex tracker[1)] to enhance its physics capabilities in nearly full azimuthal coverage over $|\eta| < 1.2$. The main goal of the upgrade is to track the production vertex of charged particles with the resolution of $50\mu m$. The central vertex tracker consists of four layers, two layers of silicon pixel type and two layers of silicon strip type. The tracker has been constructed in 2009 and has been producing fruitful physics results. During the operation before 2012, the heat cycle during its operation resulted in about 30% of inactive area on the constructed silicon pixel type. In this paper, we will report the status of repairing such the damaged pixel-type tracker and new construction.

The silicon pixel tracker consists of 10 ladders for inner layer and 20 ladders for outer layer. Each ladder is made of mainly three components; a supporting thermo-plate, four hybrid sensor, and a readout bus. The hybrid sensor is made of a silicon sensor plate and four readout chips, with 32×256 readout pixels whose each size is $50 \times 425\mu m$. All the three components are glued each other by epoxy resin with the thickness of $100\mu m \pm 30\mu m$ while the relative distance between two hybrid sensor is kept within $15\mu m$ accuracy, which is smaller than the estimated electron-drift diffusion of $20\mu m$. They are electrically connected by $25\mu m$ alminum bonding-wire. The wires are encapsulated by soft silicon resin in order to prevent any damage from an accidental contact during construction and from vibration caused by the electrical altenative current of 10MHz through the wire and the PHENIX magnetic field. For the damaged ladder, the electrical connection together with the silicon encapsulation are redone after old bonding-wires and old silicon resin are cleaned.

While entire construction procedure, the readout test by the PHENIX readout system[2)] using electrical pulse and 0.546MeV beta-ray from Sr^{90} are performed three times; before the encapsulation, before the transportation from Wako to RHIC, and before the installation. The main goal of the test is to ensure the electrical connection between the sensor hybrids and the readout bus and to measure the ratio of the active pixels to all pixels. The threshold during the test is set at about 3,000 e^- while the nominal noise of the hybrid sensor is expected to be $200e^-$. When a minimum ionization particle penetrates the silicon sensor with the thickness of $200\mu m$, 14,000 electrons are estimated to be created and collected by pixel pads. The distribution on the pixel pad surface depends on where the electron and hole pairs are created. If we assume the average distance from pixel pads to such the electrons is $100\mu m$ that is in the middle of pixel sensor thickness, the 14,000 electrons distributes on pixel pads like gaussian distribution with $100\mu m$ sigma from a naive estimate. Because one pixel pad has $50 \times 425\mu m$, two pixel pads is expected to be more than the threshold on average.

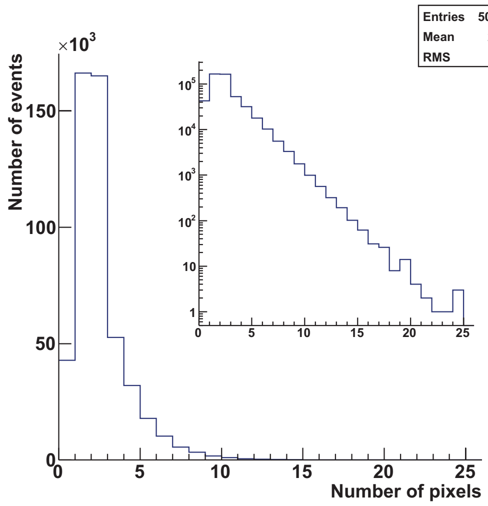

Fig. 1. Number of fired pixels per event in 500k beta-ray events by $Sr - 90$ radio active source.

Figure 1 depicts the number of fired pixels per hit. The average of the number of pixels is 2.1, which is consistent with the above estimate. This fact enables us to measure the accurate rate of the active pixel to all pixel by this beta-ray test. Because some beta-ray enters the silicon sensor with angles due to scattering in materials between the radioactive source and the silicon sensor, some gamma-ray produce wider distribution, that is also observed in the figure.

After reparing procedure of 15 ladders, the selected ones were installed[3)] with <10% inactive pixels, which is caused by due to faulty bump-bonding between the silicon sensor plates and readout chips. For futher improvement, new construction procedure with improved bump-bonding already started. All hybrids sensor[4)] and readout buses are under gluing. At least seven new ladders will be ready for installation before next run of RHIC starting in the beginning of 2015.

References
1) A. Taketani, Nucl. Instrum. Meth. A541(2005)137-143
2) K. Fujiwara, K. Czech. J. Phys. 55(2005)1639-1643
3) M. Kurosawa et al.: In this report.
4) T. Sumita et al.: In this report.

*1 RIKEN Nishina Center
*2 Department of Physics, Stony Brook University

Quality assurance test of hybrid sensors for new silicon pixel detector

T. Sumita,[*1] Y. Akiba,[*1] H. Asano,[*1,*2] T. Hachiya,[*1] M. Kurosawa,[*1] T. Moon,[*1,*3] H. Nakagomi,[*1,*4] C. Pancake,[*5] H. Sako,[*1] S. Sato,[*1] A. Taketani,[*1] H. Torii,[*1] and the PHENIX VTX group

A silicon vertex tracker (VTX) was installed in the PHENIX detector at the Relativistic Heavy Ion Collider. The VTX detector consists of two inner layers of silicon pixel detectors and two outer layers of silicon strip detectors. We are currently fabricating new spare pixel detector ladders. A pixel ladder is composed of a mechanical stave, four hybrid sensors, and two readout buses. A hybrid sensor is an assembly consisting of a silicon pixel sensor and four readout chips (ALICE1LHCb[1)]) bump-bonded to the sensor. One readout chip has 8,192 pixels, with a pixel size of 425 μm $\times$ 50 μm, organized in 32 columns and 256 rows. For production of new pixel ladders, a quality assurance (QA) test is required for the hybrid sensors. The test was conducted by HAYASHI WATCH-WORKS CO., LTD.

Figure 1 shows a schematic of the QA system. The test system consists of a probe station (SUSS MicroTec), a probe card, a DAQ adapter board, VME equipment for a DAQ system, and a Windows PC[2)]. The following tests are performed for each sensor.

(1) Current consumption:
The current consumptions of analog and digital circuits of the chip are measured.

(2) JTAG functionality:
It is confirmed whether the configuration settings in the chip can be controlled by using Joint Test Action Group (JTAG[3)]) protocol.

(3) Minimum threshold:
The minimum threshold in all pixels is determined.

(4) Test with β-ray source (^{90}Sr):
Faulty bump bonds are evaluated by the source test.

The sensor is biased at 50 V during the measurements in items (3) and (4).

The criteria for the hybrid sensor to be used for a ladder are as follows.

- Current consumptions of analog and digital circuits must be lower than 350 mA and 270 mA, respectively.
- The configuration settings in the chip must be controllable using JTAG protocol.
- The number of defect pixels must be less than 163 ($\approx$ 2%) in the source test.

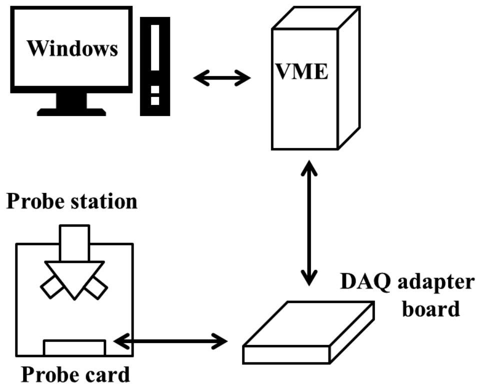

Fig. 1. Schematic of the QA test system.

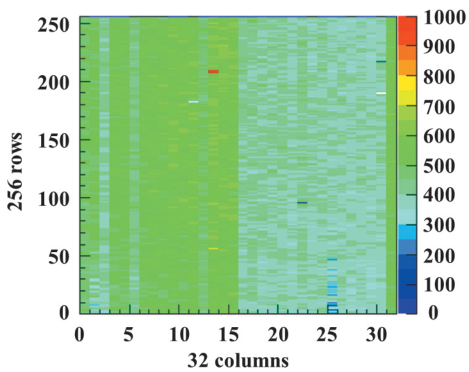

Fig. 2. Typical result of a readout chip in the source test. The color of the pixel indicates the number of hits.

A total of 50 hybrid sensors have been tested, and 33 hybrid sensors met the criteria. The average number of defect pixels is about 21 ($\approx$ 0.3%). A typical result of a readout chip in the source test is shown in Fig. 2. The main reason for failure to meet the criteria was faulty bump bonds. About one or two readout chips out of four readout chips on the sensor may have caused higher current consumption than the upper limit of the criteria.

In summary, we obtained 33 hybrid sensors to be used for new pixel ladders. Currently, the production of new pixel ladders using these sensors is underway.

*1 RIKEN Nishina Center
*2 Department of Physics, Kyoto University
*3 Department of Physics, Yonsei University
*4 Department of Physics, University of Tsukuba
*5 Department of physics, Stony Brook University

References
1) W. Snoeys et al.: Nucl. Instr. Meth. A **466**, 366 (2001).
2) M. Kurosawa et al.: RIKEN Accel. Prog. Rep. **41**, 173 (2008).
3) IEEE Std 1149.1.

Development of SOI pixel sensor for environmental radiation monitor[†]

Y. Sekiguchi,[*1] Y. Arai ,[*2] H. Hamagaki,[*1] and T. Gunji [*1]

We have developed a prototype SOI pixel sensor, called RADPIX, for a radiation monitor. This is based on the silion-on-insulator (SOI) pixel CMOS technology and developed by Y. Arai et al.[1)] The RADPIX is a monolithic pixel detector that consists of a thin CMOS readout array (40 nm, 10 Ω), a buried oxide layer (200 nm), and a thick high-registivity Si-sensor (260 μm, 700 Ω) vertically on a single chip. Figure 1 shows the schematic view of the Nested-Well structure SOI detector (p-in-n type sensor). The buried N-well suppresses the back gate effect from the electric field in the sensor and reduces the cross-talk by isolating the sensor from the circuit.

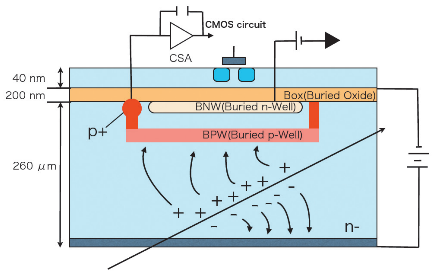

Fig. 1. Schematic diagram of the nested-well SOI structure

RADPIX aims to count the rate of the radiation and to visualize the hit pattern in real time for environmental radiation. From the hit pattern, one can estimate the radiative source such as beta-ray, γ-ray, or α-ray. The sensor is a DC-coupled device and the sensor's capacitance is in a few tens of femtofarads. The typical leakage current for a 40 μm × 40μm pixel is of the order of picoamperes at room temperature, which saturates the baseline within about 10 ms. Therefore, this device needs to reduce the leakage current or compensate the current to be able to measure the environmental radiation, which is of the order of 10^{-2} Hz/cm^2 in 1 μSv/h from ^{137}Cs. The Krummenacher feedback scheme[2)] is used for long exposure, which has an individual leakage current compensation circuit. Figure 2 shows the schematic of RADPIX. We implemented charge-sensitive preamplifers with different gains (1fF and 5fF as feedback capacitors). Two inverter chopper comparators are implemented to generate a trigger signal, and the latched output can be read from each pixel. The analog signal is sampled by the 230 fF store capacitance and is readout from each pixel. This analog information can be used for the pattern recognition and identification of the radiative source.

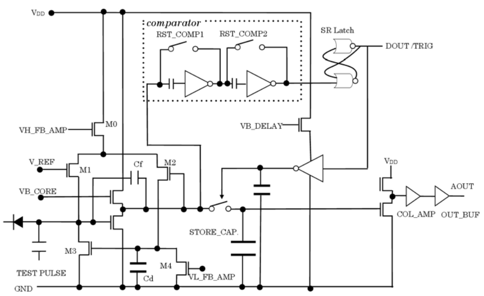

Fig. 2. Schematics of RADPIX

Figure 3 shows the pixel-by-pixel gain variation for two different charge-sensitive preamplifiers. This was studied by using test pulses. The average of the gain is 23 μV/electron (RMS~1.4) and 94 μV/electron (RMS~5.1) for the low gain type and high gain type, respectively. Position dependence is not found. We also evaluated the performance of the comparator. Figure 4 shows the counts of comparator output as a function of comparator threshold. We observe a 5%-10% fake hit rate even at high threshold. This is due to the large noise, which shows up when the digital signal is readout. The reason of the large noise and the strategies for further improvement are under investigation.

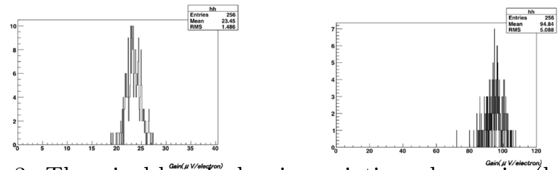

Fig. 3. The pixel-by-pixel gain variation: low gain (left) and high gain (right)

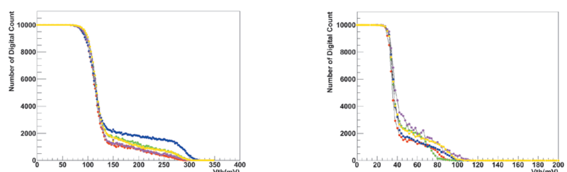

Fig. 4. Counts of comparator output as a function of comparator threshold for four typical pixels : low gain (left) and high gain (right)

[*1] Graduate School of Science, University of Tokyo
[*2] Institute of Particle and Nuclear studies, High Energy Accelerator Research Organization, KEK

References

1) Y. Arai, et al.; Nucl. Instr. and Meth. A636, 31 (2011).
2) F. Krummenacher; Nucl. Instrum. Methods A 305, 527-532 (1991).

High rate capability of gas ionization chamber with flash ADC

M. Sasano,[*1] D. Nishimura,[*2] H. Baba,[*1] T. Isobe,[*1] S. Kinno,[*2] Y. Kanke,[*2] J. Nagumo,[*2] S. Nishimura,[*1] A. Obertelli,[*1] S. Ota,[*3], H. Otsu,[*1] E. Takada,[*4] Y. Taguchi,[*2] D. Watanabe,[*2] Y. Zhu,[*2] T. Yoshinobu,[*2] and H307 and H314 collaborations

At world-leading RI beam facilities such as RIBF, the region of the nuclear chart containing nuclei to be studied simultaneously, or the yield of every nuclear species is often restricted by the high rate capabilities of beam detectors. Herein, we examined the high rate capability of gas ionization chambers (ICs)[1–4]. We recorded the waveforms of preamplifier output signals using a flash analog-to-digital converter (FADC) and corrected for the so-called pile-up effect in the offline analysis, as previously done in a pioneering work[4]. We also shortened the time needed to release amplified charge for recovering the ground level from 10 μs, a commonly used duration, to 1 μs, thereby reducing the probability of pile-up events.

A test has been performed at the Heavy Ion Medical Accelerator in Chiba (HIMAC) during other experimental programs as a parasite setup. Primary beams of Ne and Xe at 180 and 200 AMeV, respectively, were incident on our setup, after passing through other experimental setups. As a result, the beam energy was degraded and well spread at the location of our setup. An IC with an effective length of 440 mm composed of 12 cathode and 11 anode planes, each with an area of 60 mm ϕ and placed at 2-cm intervals, was filled with P10 gas at a pressure of 720 Torr and used in our setup. A positive bias of 400 V was applied to the anode planes to yield a typical drift time of 360-400 ns for 2-cm drift length. Five signals, each from two neighboring planes, plus one signal from the last plane were preamplified with Mesytec MPR-16L, which has a time constant of 1 μs. After the amplified signals were split into two, one part was sent to a CAEN V1740 digitizer with a 62.5-MHz sampling period, and the waveform was recorded. In parallel, using the other part of the split signals, the preamplified charge was digitized with peak-sensing ADCs (Mesytec MADC32) through a shaping amplifier (Mesytec MSCF-16) with a shaping time of 0.5 μs (σ).

The left window of Fig. 1 shows the correlation between the amplitudes of energy loss in the IC obtained using the above two readout methods for the data of Xe beam at 50 kilo particles per spill (kppp) with a duration time of $\sim$1 s for each spill. In addition to well-correlated events, there are events in which the amplitude calculated using the conventional method deviates from the systematics. In such events, the pulse of interest lies on top of the tail of the preceding pulse, producing an unwanted rise of the amplitude of the MADC value, as exemplified in the right figure. Such effects can be removed by decomposing neighboring pulses through the fitting of the waveforms, as shown with the red curve in the figure.

In that example, there are about 10 beam particles in a time window of 188 μs. After time averaging, this can be considered as a beam rate of about 50 kHz in cyclotron facilities such as RIBF but without a RF-periodic time structure. In the Xe beam, the rate defined thus varies from a few tens of kilohertz to about 200 kHz within each spill. The probability of pile up as a function of the beam rate is under analysis. The analysis of the energy resolution requires the correction of the beam energy dependence of the energy loss, which is ongoing.

In summary, we performed an experiment to test a signal-readout method based on FADCs coupled with a preamplifier having a short time constant and showed that the method is feasible for beam rates up to a few hundreds of kilohertz at least, while the method based on the shaping amplifier exhibits a pile-up effect from about several tens of kilohertz. Further analysis is ongoing.

We acknowledge the staff at HIMAC for their efforts and support.

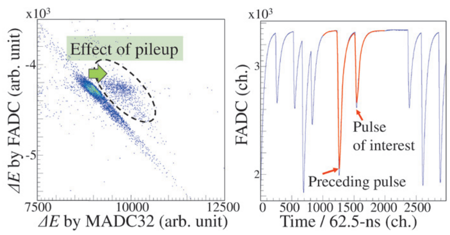

Fig. 1. Two dimensional correlation (left) between the amplitudes of the energy loss obtained from the FADC (vertical axis) and MADC32 (horizontal axis), and a typical waveform for the events enclosed with the dashed curve in the left window (right). See the text for details.

*1 RIKEN Nishina Center
*2 Faculty of Science and Technology Physics, Tokyo University of Science
*3 Center for Nuclear Study, University of Tokyo
*4 Accelerator and Medical Physics Dept., National Institute of Radiological Sciences

References

1) A. Stolz, et al.: GSI Scientific Report, 174 (1998).
2) K. Kimura et al.: Nucl. Instr. Meth. Phys. Res. **A538**, 608-614 (2005).
3) Y. Sato et al.: RIKEN Accel. Prog. Rep. 46, 159 (2013).
4) M. Geoffroy Burgunder, Ph. D. thesis, the University of CAEN (2011).

Development of MWDC readout system for the spectroscopy experiment of η' mesic nuclei at GSI and FAIR

H. Yamakami,[*1,*2] K.-T. Brinkmann,[*3] S. Friedrich,[*3] H. Fujioka,[*1,*2] H. Geissel,[*1,*4] R.S. Hayano,[*5] K. Hosomi,[*6] Y. Igarashi,[*7] K. Itahashi,[*1] M. Iwasaki,[*1] V. Metag,[*3] T. Nagae,[*2] M. Nanova,[*3] T. Nishi,[*1,*5] H. Outa,[*1] K. Suzuki,[*1,*8] T. Suzuki,[*5] Y.K. Tanaka,[*1,*5] Y.N. Watanabe,[*1,*5] and H. Weick[*1,*4]

The $\eta'(958)$ meson has an exceptionally large mass, compared with other pseudoscalar meson such as pions. Theoretically, it has been pointed out that a large mass reduction (∼100 MeV) is expected at the normal nuclear density, which leads to existence of an η' mesic nucleus, a bound state of an η' meson and a nucleus. From an experimental observation of η' mesic nuclei, we may take the first step to understand the η' mass generation mechanism[1]. For this purpose, we perform spectroscopy of η' meson bound states in ^{11}C nuclei by missing-mass measurement of the $^{12}\mathrm{C}(p,d)$ reaction near the η' production threshold at the GSI-SIS facility[2].

In this experiment, a 2.5 GeV proton beam extracted from SIS synchrotron will be injected into a ^{12}C target, and the ejectile deuterons with the momenta of ~ 2.8 GeV/c are momentum-analyzed by the fragment separator(FRS) at a dispersive focal plane with detection of the tracks by two sets of multi-wire drift chamber MWDCs. The first experiment is scheduled in July 2014.

We are working on upgrading the current DAQ system, particularly the readout of MWDCs. We will adopt a 64ch all-in-one readout board equipped with ASD, Flash ADC, and TDC. Almost all the digital processes are designed in the FPGA. This board was originally designed for Belle-II Central Drift Chamber (CDC)[3]. According to Ref. 3), they achieved a dead time of about 0.5% at a trigger rate of 10 kHz in a test experiment. This is approximately a factor 10 improvement compared to the current (our) system.

The digitalized data are transferred through a network with the SiTCP[4] sub-system, which is an implementation of TCP/IP on FPGA. We have been customizing the FPGA program and investigating the potential of the board. In case that the readout board is equipped with performance of reading data at a several kHz trigger, the quality and the quantity of the experimental data will exhibit significant improvement compared to that of the VME based DAQ without the readout board.

The readout board is being updated, so as to operate under a trigger distribution system, which is already adopted in J-PARC hadron experiments. Along with readout boards, we are developing a new "sub trigger module" (STM), for distributing trigger information including the event tag to each readout board. The distribution system with STM is useful to ensure the event matching and to avoid overlooking event slips among different DAQ subsystems.

We will make a performance test of the readout board with respect to the radiation tolerance and the DAQ rate, exploiting the opportunity of beamtime at GSI in July, 2014. By loosening the trigger condition, the performance under a high trigger rate will also be evaluated.

In summary, we will introduce a network-based DAQ with the readout board for MWDCs in the η' experiment at GSI beyond 2014 and FAIR, which is currently under construction. As it will enable us to handle a higher trigger rate, a high-statistics measurement will be possible by using a more intense beam and/or a thicker target.

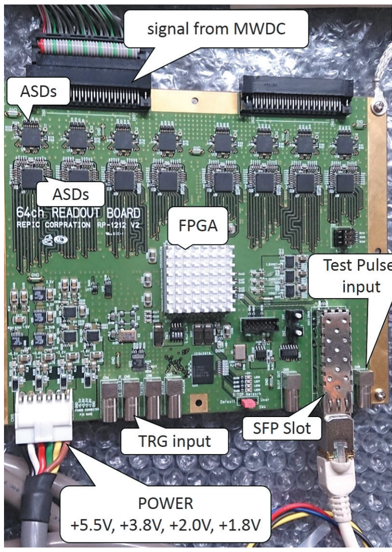

Fig. 1. View of 64ch Readout Board.

*1 RIKEN Nishina Center
*2 Department of Physics, Kyoto University
*3 Universität Gießen
*4 GSI
*5 Department of Physics, University of Tokyo
*6 Japan Atomic Energy Agency
*7 Institute of Particle and Nuclear Studies, KEK
*8 Stefan-Meyer-Institut für subatomare Physik

References
1) H. Nagahiro, D. Jido, H. Fujioka, K. Itahashi, and S. Hirenzaki : Phys. Rev. C **87**, 045201 (2013).
2) K. Itahashi *et al.*: Prog. Theor.Phys. **128**, 601 (2012).
3) N. Taniguchi *et al.*: Nucl. Inst. Meth. **732**, 540 (2013).
4) T. Uchida : IEEE Transaction on Nuclear Science, vol. 55, no. 3, June 2008.

Development of Trigger Circuit for Forward Vertex Detector at PHENIX

T. Nagashima,[*1,*2] W. Saito,[*1,*2] and I. Nakagawa[*2]

The motivation of the PHENIX experiment is to search the origin of proton spin. The proton spin is 1/2, however, it cannot be explained by valence quarks only. The other fraction of the proton spin can be carried by gluons, sea quarks, and their orbital angular momentum. The existing gluon polarization measurements indicate a small contribution. However, the present measurement region is limited in the relatively high-x region, where gluons are less populated. A newly installed detector, Forward Silicon Vertex Detector (FVTX), has the potential to extend the measurements to low-x region where gluons exist with higher probability. Moreover, heavy meson production is advantageous for the measurement of gluon spin as it produces a high gluon purity in its subprocesses. Thus, the detection of heavy mesons at forward rapidity region is an ideal probe to measure gluon polarization. FVTX distinguishes muons decayed from heavy quarks by measuring the distance of the closest approach using its precise position measurement near the vertex.

However, the existing high-momentum muon trigger does not provide sufficient rejection power to detect muons from heavy flavor origin efficiently because one needs to lower the momentum threshold. Thus our motivation is to improve the rejection power by adding the trigger capability to FVTX as an additional matching requirement on the existing high momentum trigger provided by Muon Tracking Chambers. The FVTX trigger can be formed by pattern matching between the observed hits and preprogrammed hit patterns to be a track within the FVTX readout electronics (FPGA).

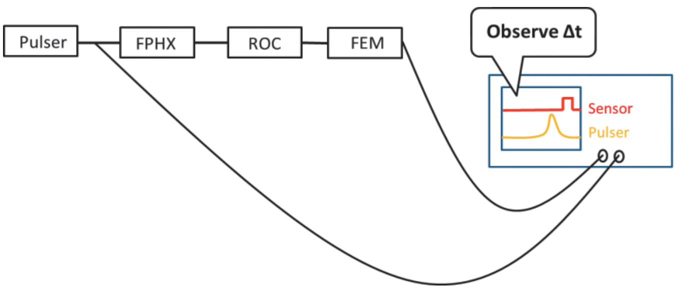

Fig.1 Setup of the timing measurement using a scope and FVTX readout devices[1)]

An FVTX detector and its readout system have been set up at the test bench in RIKEN. It is important to measure the present FVTX readout time to know how much time window allowed (latency) for the new trigger in order to process signals before the trigger decision. The actual latency constraint is known to be 17 Beam Clocks (BCLKs) for all the trigger signals to be received by the Local Level-1 trigger system. As the first step of the trigger development, the signal process time in the readout system was measured using the setup shown in figure 1. As shown in figure 2, the time difference was 2.8μs. Since 13 additional BCLK delay was inserted in the readout system for some purpose, the true time difference is expected to be about 15 BCLKs.

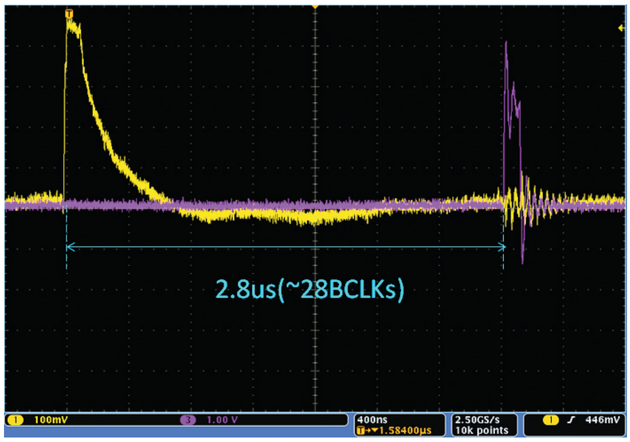

Fig.2 Coincidence between calibration pulse (yellow) and trigger signal (pink)

As the next step, the timing measurement using a radiation source is being conducted to measure the latency, including the FVTX sensor.

References

1) arXiv:1311.3594, to be published from NIM.

*1 Department of Physics, University of Rikkyo
*2 RIKEN Nishina Center

Common trigger firmware for GTO

H. Baba,[*1] T. Ichihara,[*1] T. Ohnishi,[*1] S. Takeuchi,[*1] K. Yoshida,[*1] Y. Watanabe,[*1] S. Ota,[*2] and S. Shimoura[*2]

The data acquisition (DAQ) system at RIKEN RIBF[1)] utilizes the field programmable gate array (FPGA)-based logic modules of LUPO[2)] and GTO[3)]. A common trigger firmware for the GTO has been introduced for experiments in BigRIPS, SHARAQ, EURICA, MINOS, and SAMURAI[4)]. There are two versions of the common trigger firmware: 8-trigger/16-end-of-busy inputs version and 4-trigger/20-end-of-busy inputs version. Both versions provide the same functionality, and the only difference between them is the number of the trigger and busy inputs. Here, we report on the functionality and timing performance of the 8-trigger/16-end-of-busy inputs version of the common trigger firmware.

This firmware was developed to provide acceptable triggers, i.e., the common trigger, for all CAMAC and VME front-end systems. Previously, three logic fan-in/out, three latch and one coincidence NIM modules were used to generate the common trigger. However, the developed firmware can generate the common trigger using only one GTO module. In addition, the remote control capabilities via Ethernet of the GTO allow us to change the trigger configuration without inserting and removing cables. Common trigger firmware consists of trigger multiplexer, multi-channel latch, and trigger veto circuits. Figure 1 shows the functional schematic of the firmware. The trigger multiplexer circuit has 8 inputs, and these input signals are enabled by the remote control function. The multi-channel latch circuit produces the veto signal for the trigger when CAMAC/VME front-end systems are busy. There are 16 end-of-busy inputs; therefore, this firmware can accept up to 16 CAMAC/VME front-end systems. Each latch signal is triggered by the leading edge of the accepted trigger, and it is cleared by the trailing edge of the end-of-busy signal from the front-end system. The trigger veto circuit inhibits trigger signals when either DAQ is not started or at least one of the front-end systems is busy. Using these circuits, the GTO can provide the complete common trigger. The dead time of the DAQ system is determined by the slowest front-end system.

To evaluate the timing performance of the common trigger firmware, the propagation delay and time jitter are measured. The propagation delay is the time between the trigger input and the accepted-trigger output. These parameters are measured by an Agilent Technologies U1060A-002 TDC, which has a timing resolution of 5 ps; the results are shown in Tab. 1.

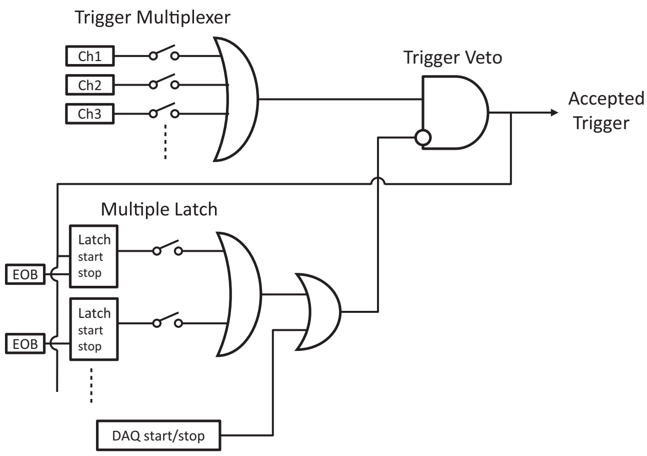

Fig. 1. Circuit schematic of the common trigger firmware. EOB is end-of-busy signal from the front-end system.

Table 1. Propagation delay and time jitter.

Channel	delay (ns)	jitter (ps)
1	15.7	6
2	15.9	6
3	15.5	7
4	15.9	4
5	16.2	7
6	16.1	6
7	16.5	8
8	15.8	5

According to these results, the skew, that is, the maximum difference between the propagation delay of all channels, is 1.0 ns. This 1.0-ns skew is not small but does not present any difficulty to the function of the trigger multiplexer. The maximum time jitter is 8 ps, which is normal for a NIM logic module.

In summary, the common trigger firmware for the GTO has been successfully developed. It allow us to reduce the number of logic NIM modules and change the configuration remotely. Further, the timing performance of the firmware is sufficient for use as a trigger circuit.

References
1) H. Baba et al.: Nucl. Inst. Meth. A **616**, 65 (2010).
2) H. Baba et al.: RIKEN Accel. Prog. Rep. **44**, 213 (2011).
3) H. Baba et al.: RIKEN Accel. Prog. Rep. **46**, 213 (2013).
4) H. Otsu et al.: RIKEN Accel. Prog. Rep. **46**, 146 (2013).

*1 RIKEN Nishina Center
*2 Center for Nuclear Study, University of Tokyo

Computing and network environment at the RIKEN Nishina Center

T. Ichihara,*1 Y. Watanabe,*1 H. Baba,*1 and H. Takeichi*1

We are operating the Linux/Unix NIS/NFS cluster systems[1,2] at the RIKEN Nishina Center (RNC).

Figure 1 shows the current configuration of the Linux/Unix servers at the RNC. We have adopted Scientific Linux as the operation system. The host *RIBF.RIKEN.JP* is used as the mail server, NFS server of the user home directory /rarf/u/, and the NIS master server. Mailing list services are also supported. This is a core server for the RNC Linux/Unix cluster with approximately 600 registered user accounts. The hosts *RIBF00/01* are used as SSH login servers to provide access to external users, and as general-purpose computational servers, printer servers, and gateways to the RIBF intranet.

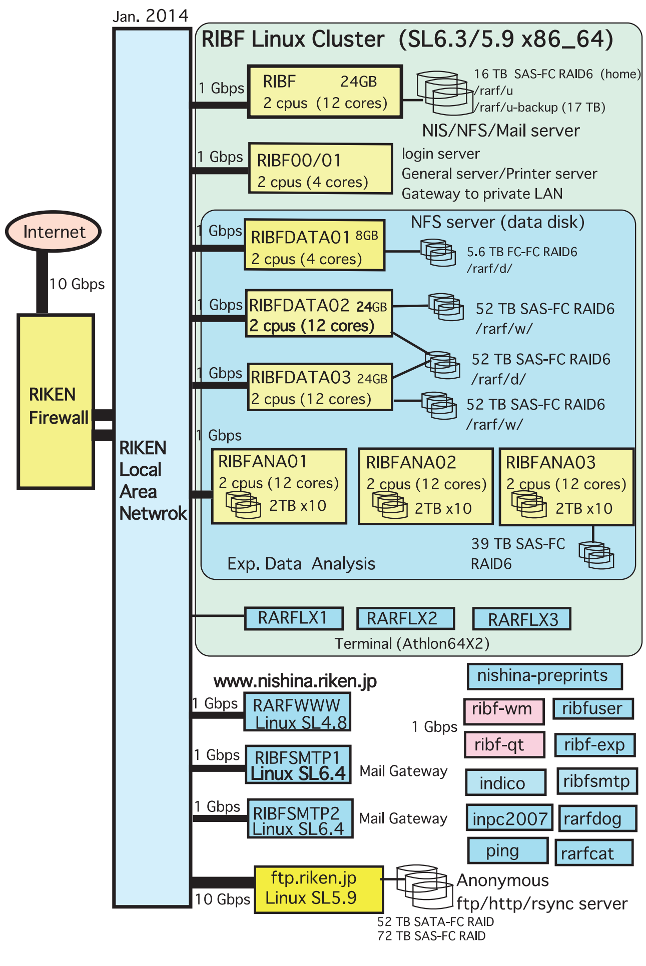

Fig. 1. Configuration of the RIBF Linux cluster.

The file servers *RIBFDATA02/03* and analysis servers *RIBFANA01/02/03* are mostly used to store and analyze experimental data at RIBF. We have a 156 TB RAID system to store the experimental data.

*1 RIKEN Nishina Center

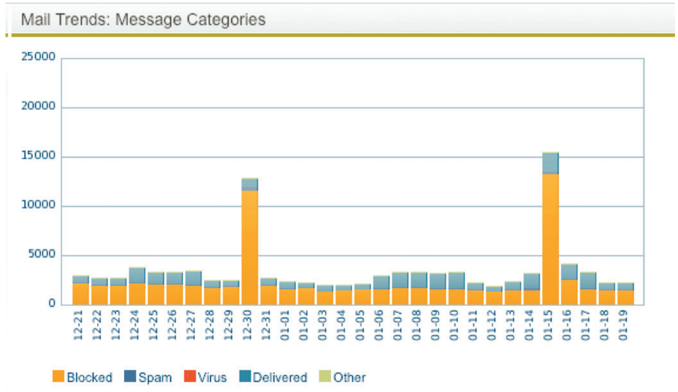

Fig. 2. Mail Trends: Message categories by PMX.

In the April of 2013, a 39 TB RAID was added for data analysis for the EURICA experiment.

The hosts *RIBFSMTP1/2* are the mail front-end servers, and they are used for tagging spam mails and isolating virus-infected mails. Two sets of HP PloLiant DL-145 G3 were installed in 2007, and they were replaced by DL-320e G8 in 2013. The latest version of the Sophos Email Protection-Advanced (PMX 6.0.3) has been installed on these. Figure 2 shows the Mail trends by the PMX for 30 days. Orange indicates the number of spam mails blocked by the IP blocker. Approximately 70 % of the incoming mails are blocked.

The Integrated Digital Conference (INDICO) system[3] has been operated at the host *indico.riken.jp* since 2007. We replaced the hardware and software of this server in February 2013 in order to improve the function and reliability. The indico was updated from indico 0.94 to 0.99.

The host *NISHINA-PREPRINTS* is an electric preprint server. Other servers installed in 2007 such as ribf00/01 and ribf-exp are planned to be replaced by DL-320e G8 in this fiscal year.

An anonymous ftp server, *FTP.RIKEN.JP*, is managed and operated at the RNC. Major Linux distributions, including Scientific Linux, Ubuntu, Debian, etc., are mirrored daily at the ftp server for the convenience of their users and for facilitating high-speed access. A 72 TB RAID system was installed in January 2014 to replace two old RAID systems to ensure the high reliability of the operation.

References
1) http://ribf.riken.jp/comp/
2) T. Ichihara et al.: RIKEN Accel. Prog. Rep. 46, 214 (2013).
3) http://indico-software.org/

CCJ operation in 2013

Y. Ikeda,[*1] H. En'yo,[*1] T. Ichihara,[*1] Y. Watanabe,[*1] and S. Yokkaichi[*1]

1 Overview

The RIKEN Computing Center in Japan (CCJ)[1)] commenced operations in June 2000 as the largest offsite computing center for the PHENIX[2)] experiment being conducted at the RHIC[3)]. Since then, the CCJ has been providing numerous services as a regional computing center in Asia. We have transferred several hundred TBs of raw data files and nano data summary tape (nDST) files, which is a term for a type of summary data files at PHENIX, from the RHIC Computing Facility (RCF)[4)] to the CCJ. The transferred data files are first stored in a High Performance Storage System (HPSS)[5)] before performing the analysis. The CCJ maintains sufficient computing power for simulation and data analysis by operating a PC cluster running a PHENIX-compatible environment.

A joint operation with the RIKEN Integrated Cluster of Clusters (RICC)[6)] was launched in July 2009. Twenty PC nodes have been assigned to us for dedicated use, sharing the PHENIX computing environment.

Many analysis and simulation projects are being carried out at the CCJ, and these projects are listed on the web page `http://ccjsun.riken.go.jp/ccj/proposals/`. As of December 2013, CCJ has been contributed 31 published papers and more than 33 doctoral theses.

2 Configuration

2.1 Calculation nodes

In our machine room 258/260 in the RIKEN main building, we have 28 PC nodes[a)], and these nodes have been used for the analysis of the PHENIX nDST data. Table 1 lists the numbers of job slots, CPU threads, and CPU cores, and the number of nodes (there is no change in 2013). These nodes are operated using a data-oriented analysis scheme that carries out optimization using local disks[7)8)]. The OS on the calculation nodes is Scientific Linux (SL) 5.3[9)], and the same OS works on the 20 nodes at the RICC. As a batch-queuing system, LSF 8.0.0[10)] and Condor 7.4.2[11)] were run on the CCJ and RICC nodes, respectively, as of Dec 2013.

Table 2 lists the numbers of malfunctioned SATA or SAS disks in the HP servers (including NFS/AFS servers described in the next section).

[*1] RIKEN Nishina Center

[a)] HP ProLiant DL180 G5 with dual Xeon E5430 (2.66 GHz, 4 cores), 16 GB memory and 10 TB local SATA data disks for each node, and HP ProLiant DL180 G6 with dual Xeon X5650 (2.66 GHz, 6 cores), 24 GB/20 TB as above, for each node

Table 1. Limitation of number of job slots from LSF queue with cluster node.

	Nodes	Cores	Threads	Jobs
CCJ-hp1	18	144	144	180
CCJ-hp2	10	120	240	200
RICC	19	152	152	144
Total	47	416	536	524

Table 2. Malfunctioned HDDs in 2011, 2012, and 2013

			Malfunctioned		
Yype	Size	Total	2013	2012	2011
SATA	1 TB	192	16	20	9
	2 TB	120	2	5	4
SAS	146 GB	38	0	1	1
	300 GB	24	0	0	1

2.2 Data servers

Two data servers (HP ProLiant DL180 G6 with 20 TB SATA raw disks) are used to manage the RAID framework of the internal hard disks, which contain the user data and nDST files of PHENIX. The disks are not NFS-mounted on the calculation nodes to prevent performance degradation by process and network congestion. These disks can be accessed only using the "rcpx" command, which is the wrapper program of "rcp" developed at CCJ, and it has an adjustable limit for the number of processes on each server.

The Domain Name System, Network Information System, Network Time Protocol, and Network File System servers are operated on the server ccjnfs20[b)] with a 10-TB FC-RAID, where the users' home and work spaces are located. The home and work spaces are formatted with VxFS 5.0[12)]. The backup of home spaces on ccjnfs20 is saved to another disk server once a day and to HPSS once a week. The backups on HPSS are stored for three weeks.

2.3 HPSS

Since Dec 2008, the HPSS servers and the tape robot have been located in our machine room, although they are owned and operated by RICC. The specifications of the hardware used can be found in the literature[13)]. The amount of data and the number of files archived in the HPSS were approximately 1.7 PB and 2.1 million files, respectively, as of Dec 2013. Table 3 lists the files and the current class of service (COS) in the HPSS. No new file has been added in 2013.

[b)] SUN Enterprise M4000 with Solaris 10

Table 3. DST and raw data files in HPSS on Dec 31, 2013

	DST		Raw data	
Run	Size [TB]	COS	Size [TB]	COS
1	4	2,3,100	3	3,205
2	24	2,3,4,100	36	1,3,5,205
3	10	2,3,6	46	100,205
4	14	2,3	11	205
5	287	2,3,6,100	292	5,205
6	92	3,6,100	339	11,100
8	22	3	128	12
9	106	3,7	13	
10	32	3	0	
11	142	3	0	
12	3	3	0	
Total	736		854	

3 Data transfer from BNL and the PHENIX software environment

Data collected during the PHENIX experiment was transferred from the RCF to the CCJ using grid-FTP [16] through the science information nework (SINET) 4 (maintained by NII[17]) with a 10 Gbps bandwidth. The data which transfered from BNL is moved to local disks on the HP calculation nodes and the HPSS. The files are transferred using grid-FTP at a maximum speed of about 300 MB/s. Two PostgreSQL[14] server nodes are operated for the PHENIX database, whose data size was 285 GB as of Dec 2013. The data are copied from the RCF everyday and made accessible to the users. One AFS[15] server node is operated for the PHENIX AFS. The size of the libraries for the PHENIX analysis setup was 1.7 TB as of Dec 2013. The libraries are also copied from the RCF by AFS everyday.

3.1 Uninterruptible power-supply system (UPS)

The power consumption of the CCJ system, excluding the HPSS, is about 25 kW, and the power is supplied through five UPSs (10.5 kVA each) as of Dec 2013. For the HPSS, there is one 7.5-kVA UPS for 100 V and three 10.5-kVA UPSs for 200 V purchased by CCJ. The batteries of the three UPSs expire in 2014 (One have expired in 2013).

3.2 Login server upgrade

CCJ had two login servers, ccjsun (HP Proliant DL145) with SL 5.3 and ccjgw (Supermicro 5011E) with CentOS 3, in 2012. The ccjgw server was upgraded to the HP Proliant DL145 with SL 5.3 in 2013.

References

1) S. Yokkaichi et al.: RIKEN Accel. Prog. Rep. **44**, p228 (2011).
2) `http://www.phenix.bnl.gov/`
3) `http://www.bnl.gov/rhic/`
4) `https://www.racf.bnl.gov/`
5) `http://www.hpss-collaboration.org/`
6) `http://accc.riken.jp/ricc/`
7) T. Nakamura et al.: RIKEN Accel. Prog. Rep. **43**, p167 (2010)
8) J. Phys.: Conf. Ser. **331**, 072025 (2011).
9) `http://www.scientificlinux.org/`
10) `http://www-03.ibm.com/systems/technicalcomputing/platformcomputing/products/lsf/index.html`
11) `http://www.cs.wisc.edu/condor/description.html`
12) Veritas file system (Symantec Corporation).
13) S. Yokkaichi et al.: RIKEN Accel. Prog. Rep. **42**, p223 (2009).
14) `http://www.postgresql.org/`
15) `http://www.openafs.org/`
16) `http://www.globus.org/toolkit/docs/latest-stable/gridftp/`
17) `http://www.nii.ac.jp/`

III. RESEARCH ACTIVITIES II
(Material Science and Biology)

1. Atomic and Solid State Physics (Ion)

Beta-NMR study of ^{58}Cu in Si

M. Mihara,[*1] Y. Ishibashi,[*2] Y. Abe,[*3] Y. Kamisho,[*1] Y. Morita,[*1] J. Ohno,[*1] M. Tanaka,[*1] S. Shinozaki,[*1] R. Kambe,[*1] M. Fukuda,[*1] K. Matsuta,[*1] A. Ozawa,[*2] D. Nagae,[*2] S. Inaba,[*2] S. Okada,[*2] Y. Saito,[*2] H. Ueno,[*3] K. Yamada,[*3] T. Izumikawa,[*4] T. Ohtsubo,[*5] S. Momota,[*6] D. Nishimura,[*7] T. Suzuki,[*8] T. Yamaguchi,[*8] Y. Kobayashi,[*9] K. Imamura,[*10] X. Yan,[*3,*11] T. Nagatomo,[*12] T. Minamisono,[*1] M. Takechi,[*13] M. Ogura,[*1] K. Matsukawa,[*14] K. Shirai,[*15] and T. Fujimura[*15]

Cu impurities in Si devices are considered serious contaminants. The short-lived β emitter ^{58}Cu ($I^\pi = 1^+$, $T_{1/2} = 3.2$ s) is attractive for studying the behavior of Cu impurities in Si using the β-NMR technique, which will provide unique information on the mechanism of fast Cu diffusion[1] or the property of Cu-dopant complex that is related to the gettering technique.[2] The $N = Z$ odd-odd nucleus ^{58}Cu, consisting of ^{56}Ni plus one proton and one neutron, is also interesting in terms of the nuclear moment, from which we can study the proton-neutron interaction in pf-shell nuclei.[3]

We detected an NMR signal of ^{58}Cu in Si in 2010, and the magnetic dipole moment $|\mu[^{58}\mathrm{Cu}]| = (0.46 \pm 0.03)\mu_\mathrm{N}$ was obtained.[4] In 2011, Vingerhoets et al. greatly improved the measurement accuracy using collinear laser spectroscopy, achieving $\mu[^{58}\mathrm{Cu}] = +(0.570 \pm 0.002)\mu_\mathrm{N}$,[5] which is about 20% larger than ours. One possibility for the discrepancy is the existence of an electric field gradient (EFG) which could be generated if some defects are formed at a ^{58}Cu site in Si, though a cubic symmetry site without EFG is expected in terms of the crystal structure of Si. If the EFG exists, the NMR spectrum should split into two lines with frequencies of $\nu_\pm = \nu_0 \pm \nu_\mathrm{Q}/2$ in the case of $I = 1$, where ν_0 and ν_Q are the carrier frequency and the quadrupole splitting frequency, respectively. In this case, our previous NMR line may have originated from ν_-. In the present study, we have applied the multi-radiofrequency (RF) (β-NQR) technique[6] to the β-NMR measurement of ^{58}Cu in Si to search for a quadrupole splitting in order to verify the above picture and to solve the discrepancy problem.

The experimental method is similar to our previous one.[4] Spin-polarized ^{58}Cu nuclei were produced through the charge exchange reaction of ^{58}Ni by impinging a ^{58}Ni primary beam at 63 MeV/u, provided by the RIKEN ring cyclotron with a typical intensity of 100 particle nA, on a 0.5-mm thick Be target. Fully stripped $^{58}\mathrm{Cu}^{29+}$ ions were separated by the RIKEN projectile fragment separator (RIPS) and were implanted into a single crystal sample of B-doped Si at 15 K with the crystal $\langle 001\rangle$ orientation set parallel to the external magnetic field $B_0 = 0.93$ T, the same condition as in the previous experiment. A pair of resonance frequencies $\nu_\pm$ was searched for by changing both ν_0 and ν_Q, using the β-NQR technique in which two frequencies were applied in series as $\nu_- \to \nu_+ \to \nu_-$ during the RF duration to inverse spin polarization of ^{58}Cu.

The resonance was found at ν_0 ~4.1 MHz and ν_Q ~2.6 MHz. The ν_Q spectrum at $\nu_0 = 4.00-4.15$ MHz is shown in Fig. 1, from which $\nu_\mathrm{Q} = 4eqQ/3h(3\cos^2\theta - 1) = (2.6 \pm 0.4)$ MHz was obtained. The EFG q will be obtained using the known Q moment of ^{58}Cu[5] after determining the angle θ between the main axis of the EFG and B_0 from the crystal orientation dependence of ν_Q. $|\mu[^{58}\mathrm{Cu}]| = (0.58 \pm 0.01)\mu_\mathrm{N}$ was obtained from ν_0, which is in agreement with the data reported by Vingerhoets et al.[5] The difference between the present $\mu[^{58}\mathrm{Cu}]$ and the previous one[4] is mostly explained by the quadrupole splitting.

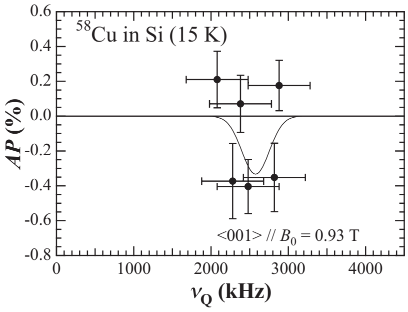

Fig. 1. Beta-NQR spectrum of ^{58}Cu in Si.

*1 Department of Physics, Osaka University
*2 Department of Physics, University of Tsukuba
*3 RIKEN Nishina Center
*4 Radioisotope Center, Niigata University
*5 Department of Physics, Niigata University
*6 Kochi University of Technology
*7 Department of Physics, Tokyo University of Science
*8 Department of Physics, Saitama University
*9 The University of Electro-Communications
*10 Meiji University
*11 Peking University
*12 IMSS, KEK
*13 GSI
*14 SUMCO, Co.
*15 ISIR, Osaka University

References

1) A.A. Istratov and E.R. Weber: J. Electrochemical Soc. **149**, G21 (2002).
2) S.M. Myers et al.: J. Appl. Phys. **88**, 3795 (2000).
3) M. Honma et al.: Phys. Rev. **C 69**, 034335 (2004).
4) M. Mihara, et al.: Hyperfine Interact. **197**, 143 (2010).
5) P. Vingerhoets et al.: Phys. Lett. **B 703**, 34 (2011).
6) M. Mihara et al.: Hyperfine Interact. **136/137**, 339 (2001).

Observation of hyperfine resonance of ^{87}Rb in superfluid helium toward laser spectroscopy of atoms with exotic nuclei

K. Imamura,[*1,*2] T. Furukawa,[*3] T. Wakui,[*4] X. F. Yang,[*5] Y. Mitsuya,[*2] T. Fujita,[*6] M. Hayasaka,[*7] S. Kishi,[*7] T. Sagayama,[*7] Y. Ichikawa,[*1] H. Shirai,[*8] T. Suzuki,[*8] Y. Ebara,[*3] T. Sato,[*8] Y. Otomo,[*8] S. Kojima,[*8] A. Hatakeyama,[*9] T. Kobayashi,[*10] H. Odashima,[*2] K. Asahi,[*8] H. Ueno,[*1] and Y. Matsuo[*11]

We have developed a new nuclear laser spectroscopy technique called OROCHI (Optical RI-atoms Observation in Condensed Helium as Ion-catcher). OROCHI is a laser spectroscopy method based on the combination of the laser-microwave (MW)/radio frequency (RF) double resonance technique and superfluid helium (He II) as a host matrix[1)]. In OROCHI, a highly energetic ion beam is injected into He II. The Injected ion is decelerated, neutralized, and slowly floated in He II. We measure the Zeeman and hyperfine structure (HFS) splitting energy to determine nuclear spins and moments. So far, we have successfully deduced the nuclear spins and moments of stable ^{85,87}Rb, ^{133}Cs, ^{107,109}Ag, and^{197}Au atoms introduced into He II using the laser ablation technique. Furthermore, we successfully observed the Zeeman resonance of ^{85}Rb and radioactive ^{84}Rb produced by the projectile fragmentation[2)]. Since the transition probability of the HFS resonance is small than that of the Zeeman resonance, HFS splitting of the injected Rb atoms is not observed in He II. Recently, we observed for the first time the HFS resonance of an energetic ion beam of ^{87}Rb atoms injected into He II.

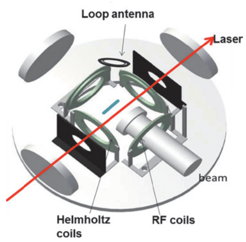

Fig. 1. Schematic layout of the experimental setup.

Figure 1 shows the schematic layout of the experimental setup in the superfluid helium cryostat. The ^{87}Rb beam from the RIPS separator was injected into He II. The stopping position of the genetic ion beam could be adjusted using two Al degraders of various thicknesses located in front of the cryostat[3)]. The stopped ^{87}Rb atoms were subjected to irradiation by circularly polarized CW Ti:S laser light (laser power: 100 mW, laser diameter: 2 mm). The laser wavelength was tuned to the D1 absorption line of Rb atoms in He II (780 nm)[4)]. The laser-induced florescence photons from laser-excited ^{87}Rb atoms were collected, wavelength-separated, and detected using a photodetection system[5)]. To preserve the atomic spin polarization, we applied a static magnetic field of 2.2(1) G using a pair of Helmholtz coils placed along the laser beam axis. In addition, we irradiated MW (power: typically a few watts) generated by an oscillator and an amplifier through an MW loop antenna located above the detection region. By sweeping the MW frequency, we observed HFS resonance as shown in figure 2. The obtained spectra clearly show the effect of the HFS resonance. Since the resonance frequencies of the spectra shift depending on the polarization of the laser light, we observed the case for both σ^+ and σ^- polarization. By taking the average of two frequencies, we could obtain the HFS splitting energy of ^{87}Rb atoms in He II. The asymmetric shape of the spectra is mainly attributed to the inhomogeneity of the applied magnetic field.

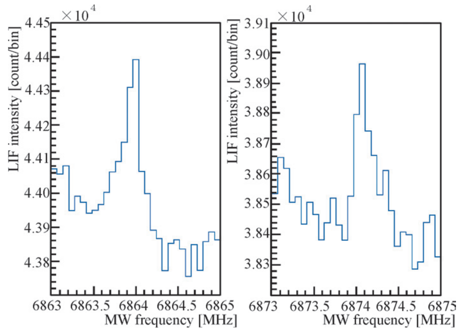

Fig. 2. Observed spectra with an applied static field of 2.2(1)G. The laser polarization is a) σ^+ and b) σ^-.

In conclusion, we have been developing OROCHI that can be applied to investigate the structure of unstable nuclei. We successfully performed double resonance experiments using energetic ion beams. From these results, we confirmed the feasibility of OROCHI, and we are now ready to extend our method to atoms with exotic nuclei.

*1 Nishina Center
*2 Department of Physics, Meiji University
*3 Department of physics, Tokyo Metropolitan University
*4 CYRIC, Tohoku University
*5 School of physics, Peking University
*6 Department of physics, Osaka University
*7 Department of physics, Tokyo Gakugei University
*8 Department of physics, Tokyo Institute of Technology
*9 Department of applied physics, Tokyo University of Agriculture and Technology
*10 Laser Technology Laboratory, RIKEN
*11 Department of advanced science, Hosei University

References

1) T. Furukawa et. al.: Hyp. Int. **196**, 191 (2010).
2) T. Furukawa et al.: RIKEN. APR. **46**, xi (2013).
3) X. F. Yang et al.: NIM B. **317**, 599 (2013).
4) Y. Takahashi et al.: Phys. Rev. Let. **71**, 1035 (1993).
5) A. Sasaki et al.: RIKEN. APR. **44**, 204 (2011).

Search for efficient laser resonance ionization schemes for Ta and W in KISS

M. Mukai,[*1] Y. Hirayama,[*2] N. Imai,[*2] H. Ishiyama,[*2] S.C. Jeong,[*2] H. Miyatake,[*2] M. Oyaizu,[*2] Y.X. Watanabe,[*2] Y.H. Kim,[*3] and S. Kimura[*1]

In KISS (KEK Isotope Separation System) [1], laser resonance ionization is employed for the element-selective ionization of multi-nucleon transfer reaction products. We searched for efficient laser resonance ionization schemes for tantalum (Z = 73) and tungsten (Z = 74), which are the elements that are studied in KISS.

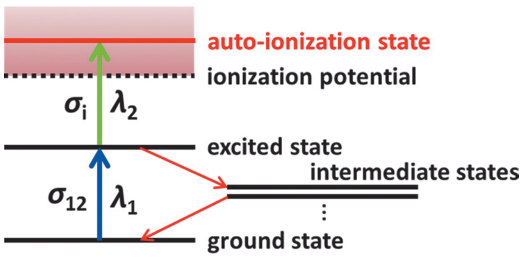

Fig. 1 Two-color laser resonance ionization

Fig. 1 shows a schematic view of two-color laser resonance ionization. An atom is element-selectively excited by the first step laser with a wavelength of λ_1. Through the second step laser with a wavelength of λ_2, the atom then transits from the excited state to an auto-ionization state (AIS), which is located above the ionization potential. The AISs having ionization efficiencies that higher than that by means of the continuum by more than ten times are searched for in general. [2]

We used wavelength-tunable dye lasers pumped by excimer lasers to obtain laser beams of $2\lambda_1$ and λ_2. The wavelength λ_1 in the ultraviolet ray region is generated from the $2\lambda_1$ wavelength by using a second harmonic generator, which consists of a non-linear crystal of BBO. Both lasers are transported into a reference cell that was newly made to search for ionization schemes in off-line experiments. The lasers were focused on a spot of a few mm^2 between ion-acceleration electrodes. Neutral atoms were evaporated from a filament and ionized by laser irradiation between the electrodes. Ions were accelerated by the electrodes and detected by a channeltron at about 30 cm away from the ionization region. The ions were mass-analyzed by measuring the TOF. The mass resolving power was measured to be 12.3%.

We scanned λ_2 to search for AISs; then, we measured laser-ionized atoms by means of the AIS by changing the power of the respective lasers. The λ_1s were selected from the known excited states that had a high Einstein *A* coefficient.[3] We deduced the photon absorption cross section (σ_{12}, σ_i) of each transition by fitting the solution from rate equations[2, 4] to the laser power dependence of ion counts. The rate equations express the time evolution of the number of atoms in the ground state, the excited state, and the AIS. In addition to those states, we considered the intermediate states, where the atoms decay from the excited state, and are located above the ground state. The excitation rate (ionization rate) is proportional to the photon absorption cross section of the transition from the ground state (the excited state) to the excited state (the AIS). These rates are also proportional to the photon densities of the λ_1 laser and λ_2 laser. We deduced the laser powers required for the saturation conditions of ionization probability in the KISS gas cell from the determined photon absorption cross sections.

For tantalum, λ_2 was scanned from 410 to 425 nm with λ_1 = 264.8258 nm, so that four strong peaks were observed. The strongest peak at 421.652 nm yielded σ_{12} = 4.8 ± 0.5 (stat.) ± 1.0 (syst.) $\times 10^{-15}$ cm^2, σ_i = 2.0 ± 0.2 (stat.) ± 0.8 (syst.) $\times 10^{-16}$ cm^2. The laser powers required for the overlap in the gas-cell (φ10 mm) were P_1 ~ 0.5 mJ/pulse, P_2 ~ 29.3 mJ/pulse. On the other hand, for tungsten, λ_2 was scanned from 404 to 414 nm with λ_1 = 245.2737 nm, so that two strong peaks were observed. The stronger peak at 404.393 nm yielded σ_{12} = 4.5 ± 0.6 (stat.) ± 0.6 (syst.) $\times 10^{-16}$ cm^2, σ_i = 7.5 ± 0.7 (stat.) ± 1.6 (syst.) $\times 10^{-17}$ cm^2. The laser powers required for the overlap in the gas-cell (φ10 mm) were P_1 ~ 5.5 mJ/pulse, P_2 ~ 241.9 mJ/pulse. These powers required are too high for our laser system to achieve saturation. In our laser system, the maximum laser power is approximately 200 μJ for the first step laser and about 2 mJ for the second step laser. The ionization probability achieved using our laser system is expected to be as low as 11% for tantalum and 0.33% for tungsten. We will search for other λ_2 values in different wavelength regions with the current λ_1 and also look for AISs with different λ_1 values.

The resonance structure of the AIS might be affected by the isotope shift of the wavelength. We are going to increase the mass resolving power of the reference cell by introducing electric lenses and a longer flight tube, which will provide us with further information on the AIS.

References

1) S.C. Jeong et al.: KEK Report 2010-2.
2) Y. Hirayama et al.: J. Phys. B: At. Mol. Opt. Phys. 47 (2014) 075201.
3) C.H. Corliss and W.R. Bozman: NBS Monograph 53 (1962).
4) V.S. Letokhov: *Laser Photoionization Spectroscopy* (Orlando, FL: Academic, 1987).

*1 Department of Physics, University of Tsukuba
*2 Institute for Particle and Nuclear Studies (IPNS), High Energy Accelerator Res Org. (KEK)
*3 Seoul National University

Reaction-rate measurements of cold ion-polar molecule reactions using a combined Stark-velocity-filter–ion-trap apparatus†

K. Okada,*1,*2 T. Furukawa,*2 T. Takayanagi,*2 H. A. Schuessler,*3 and M. Wada*1

Cold molecules and their ions are attractive subject of research in the fields of fundamental physics and cold chemistry. With regard to cold chemistry, the reaction-rate constants of cold ion-molecule reactions are important information for studying the chemical evolution of interstellar clouds[1]. Recently, we have developed a combined Stark-velocity-filter–ion-trap apparatus for measuring the reaction rate between cold trapped ions and slow polar molecules under ultra-high vacuum conditions[2]. We experimentally measured the reaction rates between sympathetically cooled N_2H^+ ions and velocity-selected polar molecules, namely CH_3CN.

The measurement procedure is as follows. First, we produce a Ca^+ Coulomb crystal in a linear Paul trap. Then a nitrogen gas of about 1×10^{-7} Pa is introduced into the vacuum chamber, and an electron beam is incident to the center of the ion trap in order to produce N_2^+ ions by electron impact ionization. Because the mass of the nitrogen molecular ion is lighter than that of Ca^+, the molecular ions are more tightly bounded by the trapping potential and accumulate near the trap axis. After the preparation of cold N_2^+ ions, a hydrogen gas of about 6×10^{-6} Pa is introduced into the vacuum chamber. All N_2^+ ions change into N_2H^+ ions via the reaction of $N_2^+ + H_2 \rightarrow N_2H^+ + H$ in a reaction time of 240 s[3].

After the preparation of cold N_2H^+ ions, we irradiated the velocity-selected CH_3CN molecules to the two-species Coulomb crystal containing Ca^+ and N_2H^+ ions. Figure 1(a) shows the snapshots of the laser-induced fluorescence (LIF) images of the Coulomb crystal at several reaction times. The dark area containing N_2H^+ progressively decreases with increasing reaction time owing to the progress of $CH_3CN + N_2H^+ \rightarrow CH_3CNH^+ + N_2$ reactions. We also observed an increase in the sparse dark area in the outer peripheral region of the Ca^+ Coulomb crystal because a part of the reaction products (CH_3CNH^+) is trapped. Under the present experimental conditions, the average reaction energy is estimated to be approximately 3 K[2].

In order to obtain the reaction rate, we determine the relative number of molecular ions from the volume of the dark area in the observed fluorescence images under the assumption of a constant number density at 0 K. Figure 1(b) shows the decay curve of the relative number of N_2H^+ ions as a function of the reaction time. In this example, the reaction rate is determined to be $2.4(4)\times10^{-3}$ s^{-1}. We performed 9 measurements and obtained an averaged reaction rate of $2.0(2)\times10^{-3}$ s^{-1}. Using the number density of the velocity-selected CH_3CN, which was separately determined, the reaction-rate constant was also determined to be $1.7(6)\times10^{-8}$ cm^3 s^{-1}. The main reason for the error is considered to be the uncertainty in the number density of CH_3CN[2]. The present reaction-rate constant is consistent with the estimated capture rate, $k_{ts} = 3.6\times10^{-8}$ cm^3 s^{-1}, using the trajectory-scaling formula[4], which is considered to be the maximum value of the reaction-rate constant. In the future, the present velocity filter combined with a cryogenic trap apparatus will enable us to perform systematic measurements of cold ion-polar molecule reactions, which are important problems from a fundamental viewpoint and contribute to astrochemistry.

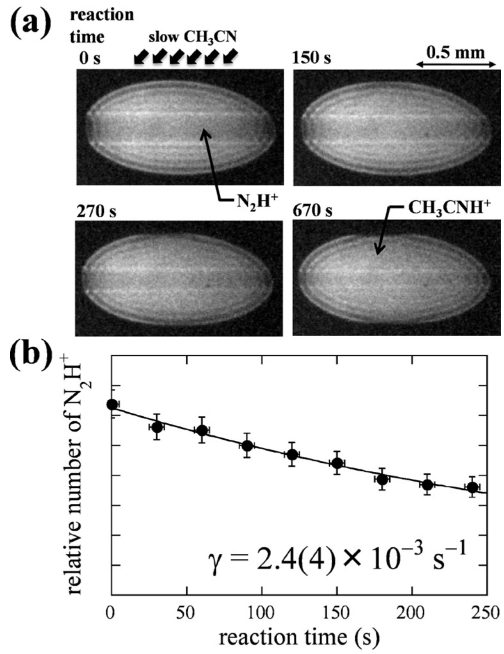

Fig. 1. (a) Sequential LIF images of the two-species Coulomb crystal containing Ca^+ and N_2H^+ during $CH_3CN + N_2H^+ \rightarrow CH_3CNH^+ + N_2$ reactions. (b) Plot of the relative number of N_2H^+ ions as a function of the reaction time.

† Condensed from the article in Phys. Rev. A**87**, 043427(2013)
*1 RIKEN Nishina Center
*2 Department of Physics, Sophia University
*3 Department of Physics, Texas A&M University

References

1) V. Wakelam, *et al.*: Space Sci. Rev. **156** 13 (2010).
2) K. Okada, *et al.*:Phys. Rev. A **87** 043427 (2013).
3) D. Smith, *et al.*: J. Chem. Phys. **69**, 308 (1978).
4) T. Su, *et al.*: J. Chem. Phys. **76** 5183 (1982).

Effects of 2.6-GeV uranium irradiation on (Ba,K)Fe_2As_2 single crystals

T. Tamegai,[*1] T. Taen,[*1] F. Ohtake,[*1] S. Pyon,[*1] T. Kambara,[*2] Y. Kanai,[*3] and A. Yoshida[*2]

Through extensive studies on the recently discovered iron-based superconductors (IBSs), the transition temperature T_c in rare-earth-based iron-oxyarsenides has been increased up to ~55 K within a short period of time. However, the critical current density, J_c, at low temperatures is not large enough. Despite the lower T_c in IBSs compared with that in cuprate superconductors, IBSs have smaller electromagnetic anisotropies and are considered to be attractive for practical applications. J_c can be enhanced by introducing artificial pinning centers. It is well known that the most efficient way to improve the J_c characteristics is to pin vortices with columnar defects (CDs) created by swift particle irradiations. In high-temperature superconductors, the existence of CDs enhances J_c dramatically.[1)]

One of the most extensively studied IBSs, $Ba(Fe_{1-x}Co_x)_2As_2$, with the highest T_c (~24 K) is readily available in a large single crystal. Its J_c reaches 1x10^6 A/cm^2 at T = 2 K, which is potentially attractive for technological applications. We expect that J_c in $Ba(Fe_{1-x}Co_x)_xAs_2$ can be enhanced by introducing CDs that can pin vortices. However, it is well known that morphologies of irradiation-induced defects strongly depend on various parameters such as ion energy, stopping power of incident ions, thermal conductivity, and perfection of the target crystal. Hence, it is still an open question as to what kind of defects can be created in IBSs under a specific condition. Our preliminary study using 200 MeV Au ions has successfully demonstrated that CDs can be introduced and J_c is enhanced by a factor of 5 at low temperatures.[2)] In our previous irradiation in IBS performed at RIKEN, we have used heavier and more energetic 2.6 GeV Uranium (U) ions and found that U also enhances J_c in $Ba(Fe_{1-x}Co_x)_2As_2$[3)]. In this case, however, magnetic hysteresis loop shows an interesting dip structure at low magnetic fields; such a dip has not been observed in the case of Au irradiation. One of the possible origins for this dip is that pinning by CDs is not effective in the remanent state of a thin-plate superconductor, where flux lines have a strong curvature due to the strong demagnetization effect.[4)]

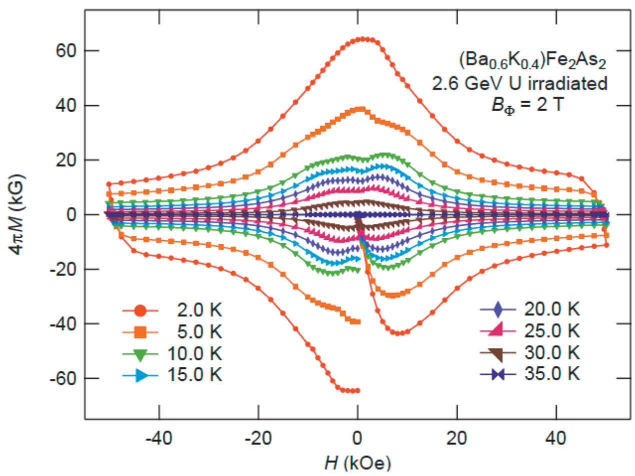

Fig. 1. Magnetic hysteresis loops of 2.6-GeV U-irradiated $(Ba_{0.6}K_{0.4})Fe_2As_2$ (B_Φ = 2 T) at several fixed temperatures.

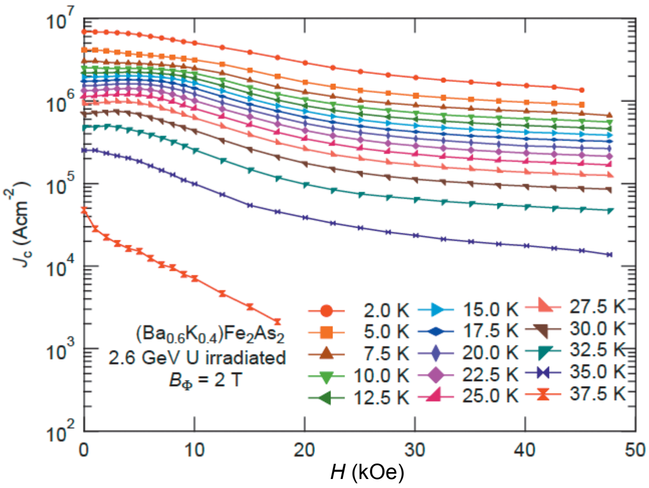

Fig. 2. Magnetic field dependence of J_c in 2.6-GeV U-irradiated $(Ba_{0.6}K_{0.4})Fe_2As_2$ (B_Φ = 2 T).

This year, we have explored similar irradiation effects on another promising IBS, $(Ba_{1-x}K_x)Fe_2As_2$. Figure 1 shows the magnetic hysteresis loops of the 2.6-GeV U-irradiated $(Ba_{0.6}K_{0.4})Fe_2As_2$ at B_Φ = 2 T and at low temperatures. Except for temperatures close to T_c and 2 K, the width of the hysteresis loop is diminished at lower fields, which is similar to the dip structure observed in the case of the U-irradiated $Ba(Fe_{1-x}Co_x)_2As_2$[3)]. In Fig. 2, we convert the width of the hysteresis loop into J_c using the Bean model. After the irradiation, J_c at T = 2 K under a self-field reaches 7x10^6 A/cm^2, which is larger than that in the case of $Ba(Fe_{1-x}Co_x)_2As_2$. It should be noted that J_c at T = 25 K and H = 45 kOe is ~2x10^5 A/cm^2, which is larger than the technologically required value for superconducting wires.

*1 Department of Physics, The University of Tokyo
*2 RIKEN Nishina Center
*3 Atomic Physics Laboratory, RIKEN

References

1) L. Civale *et al.*: Phys. Rev. Lett. **67**, 648 (1991).
2) Y. Nakajima, Y. Tsuchiya, T. Taen, T. Tamegai, S. Okayasu, and M. Sasase: Phys. Rev. B **80**, 012510 (2009).
3) H. Yagyuda, Y. Nakajima, T. Tamegai, Y. Kanai, and T. Kambara: Physica C**471**, 790 (2011).
4) T. Tamegai *et al.*: Supercond. Sci. Technol. **25**, 084008 (2012).

Site occupancies of hydrogen in Nb alloyed with oversized Ta atoms or undersized Mo atoms†

H. Matsuba,[*1,*2] E. Yagi,[*1,*2] C. Sugi,[*2] Y. Okada,[*2] K.Hirabayashi,[*2] T. Iida,[*2] S. Koike,[*3] T. Hayashi,[*2] N. Higami,[*2] Y. Murakami,[*2] A. Takebayashi,[*2] T. Yoshida[*2], T. Sugawara,[*4] T. Shishido,[*4] and K. Ogiwara[*1]

An interaction of hydrogen with solute atoms is one of the fundamental problems on hydrogen in metals, because various hydrogen-related properties are strongly affected by alloying. In order to understand the interaction, the knowledge of the atomistic state of hydrogen in alloys is highly required. However, such information has been extremely limited, because of experimental difficulties. Therefore, the channelling method utilizing a nuclear reaction of $^{1}H(^{11}B,\alpha)\alpha\alpha$ with a $^{11}B^{+}$ beam of about 2 MeV had been developed.[1] This method has been demonstrated to be very useful to locate hydrogen dissolved in metals.[1,2] In previous studies, the lattice location of hydrogen has been investigated systematically in detail in Nb alloyed with undersized Mo atoms up to 60 at. % by the channelling method at room temperature with a tandem accelerator. Their atomic radii are 1.43 Å for Nb and 1.36 Å for Mo atoms. This alloy system forms a solid solution over the entire Mo concentration (C_{Mo}) range, maintaining a bcc crystal structure, although the lattice parameter changes.

It has been demonstrated that the lattice location changes very sensitively with Mo concentration and, with the help of the measurement of width of X-ray reflection lines, that such change can be explained in terms of lattice distortion introduced by alloying with Mo atoms.[3] At low C_{Mo}, lattice is strongly distorted around Mo atoms. Hydrogen is trapped by a Mo atom to be located at a T_{tr} site, which is displaced from an original tetrahedral (T) site by about 0.6 Å towards the Mo atom, so as to reduce the distortion around Mo atom. There exists a strong attractive interaction between hydrogen and Mo atoms.[4] With increasing C_{Mo}, the lattice distortion is reduced owing to interference between strain fields around individual Mo atoms, and most of the H atoms occupy T sites as in Nb. For C_{Mo} higher than 39 at. %, the lattice distortion gradually increases again with increasing C_{Mo} because of the increase in the number of undersized Mo atoms in a unit cell, but not so strongly as that at low C_{Mo}, i.e., up to an intermediate level. In this case, H atoms are distributed over T and d-T sites, which is displaced from T sites to their nearest neighbour octahedral (O) sites by about 0.25 Å. The T-site occupancy is energetically more favourable than the d-T-site occupancy.

In the present study, the site occupancy of hydrogen in Nb alloyed with 2 or 5 at. % of oversized Ta atoms (atomic radius: 1.44 Å), $Nb_{0.98}Ta_{0.02}H_{0.01}$, $Nb_{0.98}Ta_{0.02}H_{0.029}$ and $Nb_{0.95}Ta_{0.05}H_{0.01}$, was investigated by the channelling method at room temperature. The objectives of the present study are to investigate a difference in an interaction of hydrogen with solute atoms between oversized Ta and undersized Mo atoms and to examine the above-described interpretation on the basis of the lattice distortion.

The following results were obtained. Taking account of the previously reported results on $Nb_{0.95}Ta_{0.05}H_{0.018}$ and $Nb_{0.95}Ta_{0.05}H_{0.025}$,[5] in both $Nb_{0.98}Ta_{0.02}$ and $Nb_{0.95}Ta_{0.05}$ alloys, at low hydrogen concentration C_H, most of the H atoms are located at T sites, while at high C_H, most of them are at d-T sites displaced by 0.25 Å from T sites towards their nearest neighbour O sites, and the remains are at T sites. This result is different from that in Nb alloyed with similar concentration of undersized Mo atoms, where hydrogen preferentially occupies T_{tr} sites. It was deduced that, in both $Nb_{0.98}Ta_{0.02}$ and $Nb_{0.95}Ta_{0.05}$ alloys, the T site occupancy is energetically more favourable than the d-T-site occupancy, but the concentration of available T sites is limited. In these alloys, the lattice distortion is small and at an intermediate level, because of the smaller size difference between Nb and Ta atoms than between Nb and Mo atoms. This difference in lattice distortion is reflected in the X-ray line widths. Therefore, hydrogen preferentially occupies T sites in the undistorted or very weakly distorted tetrahedra some distance away from Ta solutes and excess H atoms enter d-T sites in the tetrahedra distorted at an intermediate level near Ta solutes. Therefore, the interaction between hydrogen and an oversized Ta atom is not attractive in Nb, in contrast to the attractive interaction between an undersized Mo atom and hydrogen in Nb.

With the help of measurements of the half-widths of X-ray reflection lines in Nb-Mo and Nb-Ta alloys, the site occupancy of hydrogen in the Nb-Ta alloys is explained in terms of an effect of lattice distortion induced by alloying, as in the case of the site occupancy in Nb-Mo alloys with Mo concentration higher than about 39 at. %. The d-T site is a stable site for hydrogen in a slightly distorted bcc lattice.

References

1) E. Yagi. Kobayashi, S. Nakamura, Y. Fukai, and K. Watanabe: J. Phys. Soc. Jpn. **52**, 84 (1983).
2) E. Yagi, T. Kobayashi, S. Nakamura, Y. Fukai, and K. Watanabe: Phys. Rev. B **31**, 1640 (1985).
3) E. Yagi et al: J. Phys. Soc. Jpn. **79**, 044602 (2010).
4) E. Yagi, S. Nakamura, F. Kano, T. Kobayashi, K. Watanabe, Y. Fukai, and T. Matsumoto: Phys. Rev. B **39**, 57 (1989).
5) E. Yagi et al: J. Phys. Soc. Jpn. **78**, 064601 (2009).

† Condensed from the article in J. Phys. Soc. Jpn. **80,** 104602 (2011).

*1 RIKEN Nishina Center
*2 School of Science and Engineering, Waseda University
*3 Department of Physics II, Tokyo University of Science
*4 Institute for Materials Research, Tohoku University

Evaluation of single-event damages on Silicon Carbide (SiC) power MOSFETs

E. Mizuta,*[1] S. Kuboyama,*[1] T. Kambara,*[2] and T. Tamura*[1]

Silicon carbide (SiC) is the material used in next generation semiconductor devices that is applicable to higher voltage and temperature applications because of the inherent wide energy band-gap of 3.26 eV.[1)] In addition, saturated electron velocity is considerably fast in the SiC material. Therefore, SiC devices can operate in ultra-high frequency applications.[2)] If the SiC material is used in power devices instead of Si, these devices can achieve higher efficiency and lower loss.[3)] In our study, we investigated in detail the fatal destruction mode called Single-Event Burnout (SEBs) on commercial SiC power MOSFETs with the radiation effect during heavy-ion irradiations in space.

A single ion incidence into the device generates some amount of charge according to the Linear Energy Transfer (LET) value of the ion, and the charge can be amplified in the device using mechanisms such as avalanche multiplication. Finally, the charge is collected at the drain terminal and can be measured using a charge sensitive amplifier (CSA). The input charge range and the output voltage of CSA are 0.5 - 50 nC and 0.1 mV - 10 V, respectively. For the cases where the amplification level increases exponentially with the applied voltage to the sample device, the Energetic Particle Induced Charge Spectroscopy (EPICS) is more suitable. EPICS is specially designed for the pulse-height analyzer (PHA) system that is used to analyze the charge collection characteristics in semiconductor devices.[4)] It can measure a wide range of charges using a logarithmic scale. The block diagram of the EPICS system is shown in Fig. 1.

SiC power MOSFETs used in this study were commercial devices. The maximum ratings for the drain-Source breakdown voltage, continuous drain current, and the drain-source on-state resistance are 1200 V, 24 A, and 220 mΩ, respectively.

The test was performed at room temperature by irradiation with a Kr-ion beam of 713 MeV using the RIKEN RILAC+RRC. Fluence was set to 1×10^5 ions/cm^2 at the chip surface. The drain bias voltage, V_{DS}, was increased at an interval of 50 V. The gate voltage, V_{GS}, was set to 0 V to force the devices to enter the OFF state.

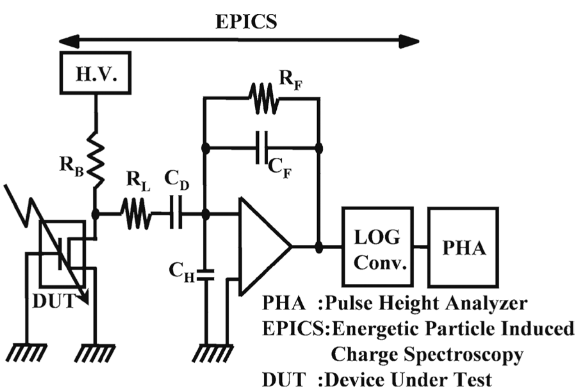

Fig. 1. Block diagram of EPICS system.

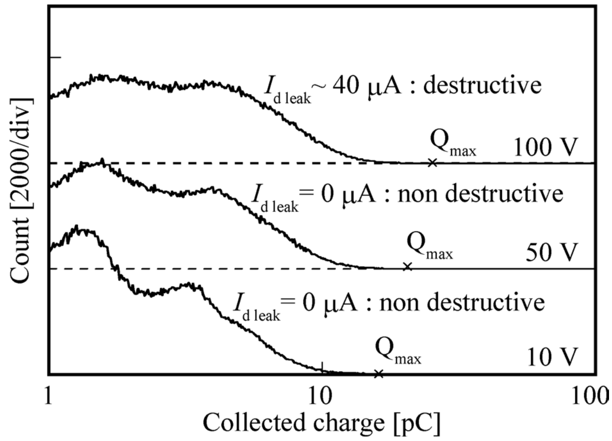

Fig. 2. Collected charge spectra by Kr ion irradiation using the EPICS system.

Figure 2 shows the EPICS spectra on SiC power MOSFETs of Kr-ion irradiation. The cross marks Q_{max} indicate the maximum collected charge for each spectrum. There were two peaks on each spectrum similar to the one of Si power MOSFETs.[4)] At the drain voltage of 100 V, the device was damaged because the leakage current was more than the maximum rated zero gate voltage drain current of 10 μA. In Si power MOSFETs, a high energy collected charge peak Q_{max} of more than 10^5 pC was observed when SEB occurs. However, in SiC power MOSFETs, permanent increase of the leakage current was observed at the drain voltage of 100 V; However, no high SEB peak was observed up to the voltage level, and the maximum collected charge was less than 100 pC. This behavior is the same as our previous study on SiC Schottky barrier diodes.[5)] This fact suggests that the mechanism of SEB was different between SiC power MOSFETs and Si power MOSFETs. Therefore, it is necessary to perform additional experiments to understand the SEB mechanism of SiC power MOSFETs.

*[1] Japan Aerospace Exploration Agency
*[2] RIKEN Nishina Center

References

1) W. E. Nelson et al.: J. Appl. Phys., 37(1), p. 333, (1996).
2) J. A. Cooper et al.: IEEE Trans. Electron Devices, 49 (4), p.658, (2002).
3) S. Yoshida et al.: Appl. Phys. Lett., 46, p. 766, (1985).
4) S. Kuboyama et al.: IEEE Trans. Nucl. Sci., 39 (6), p. 1698, (1992).
5) S. Kuboyama et al.: IEEE Trans. Nucl. Sci., 53 (6), p. 3343, (2006).

2. Atomic and Solid State Physics (Muon)

μSR study of the spin correlation in iron-chalcogenide superconductors $Fe_{1-y}M_ySe_{0.3}Te_{0.7}$ (M = Co, Ni, Zn)

T. Adachi,[*1,*2] T. Inabe,[*2] K. M. Suzuki,[*1,*2] T. Kawamata,[*1,*2] T. Noji,[*2] H. Guo,[*1] I. Watanabe,[*1] and Y. Koike[*1,*2]

In recent years, much attention has been paid to the so-called iron-based superconductors due to their high superconducting (SC) transition temperatures, T_c's, in the research field of superconductivity. Hsu *et al.* have discovered superconductivity with $T_c = 8$ K in the iron-chalcogenide FeSe.[1] It has been found that T_c of FeSe increases through the partial substitution of Te for Se, shows a maximum of 14 K at $x \sim 0.7$ in $FeSe_{1-x}Te_x$ and the superconductivity disappears at $x = 1$, namely, in FeTe.[2] The compound FeTe is not SC but develops an antiferromagnetic (AF) order at low temperatures below ~ 67 K.[2] Therefore, one may guess the mechanism of superconductivity relating to the AF spin fluctuation in the iron-chalcogenide superconductors, which is similar to the case of high-T_c cuprate superconductors.

In order to investigate impurity effects on the SC properties, we have grown impurity-substituted single crystals of $Fe_{1-y}M_ySe_{0.3}Te_{0.7}$ (M = Co, Ni, Zn) with $y = 0 - 0.05$ and have measured the in-plane electrical resistivity.[3] Here, Co and Ni ions are expected to dope one and two electrons, respectively, while Zn is expected to dope no electrons. As a result, it has been found that T_c is reduced through the Co substitution and that the reduction of T_c is more significant in the Ni substitution than in the Co substitution. On the other hand, the decrease in T_c with the Zn substitution has been found to be negligibly small. Moreover, it has been found that both T_c and the residual resistivity depending on the impurity concentration cannot be explained by the Abrikosov-Gor'kov theory, suggesting that a glue to form electron pairs is not the spin fluctuations[4,5] but the orbital fluctuations.[6]

Therefore, in order to investigate the spin fluctuations directly, we have performed μSR measurements of $Fe_{1-y}M_ySe_{0.3}Te_{0.7}$ (M = Co, Ni, Zn) with $y = 0 - 0.05$.[7] Zero-field (ZF) and longitudinal-field μSR measurements were carried out using a Variox cryostat at temperatures down to 1.6 K at RIKEN-RAL.

For the impurity-free crystal of $y = 0$, it has been found that ZF μSR spectra are independent of temperature at low temperatures down to 1.6 K, indicating that the crystal is in a paramagnetic state. Figure 1 shows ZF spectra of the Zn-substituted crystal of $Fe_{1-y}Zn_ySe_{0.3}Te_{0.7}$ with $y = 0.05$. At 29 K, the spectrum shows slow depolarization of muon spins similar to that observed in the impurity-free crystal. On the other hand, the depolarization becomes fast with decreasing temperature and the initial asymmetry is missing at 1.6 K. These results suggest significant development of the spin correlation through the Zn substitution. For the Co and Ni substitution, it has been found that the spin correlation is enhanced at $y = 0.02$ and that further substitution of impurities leads to weakening of the spin correlation at $y = 0.05$. These μSR results depending on the amount and kind of impurities strongly suggest that not the spin fluctuations but the orbital fluctuations may be a glue to form electron pairs in the iron-chalcogenide superconductors.

In summary, we have found impurity-induced development of the spin correlation in $Fe_{1-y}M_ySe_{0.3}Te_{0.7}$ (M = Co, Ni, Zn) from μSR measurements. The present μSR results strongly suggest that the formation of electron pairs is mediated by the orbital fluctuations in iron-chalcogenide superconductors.

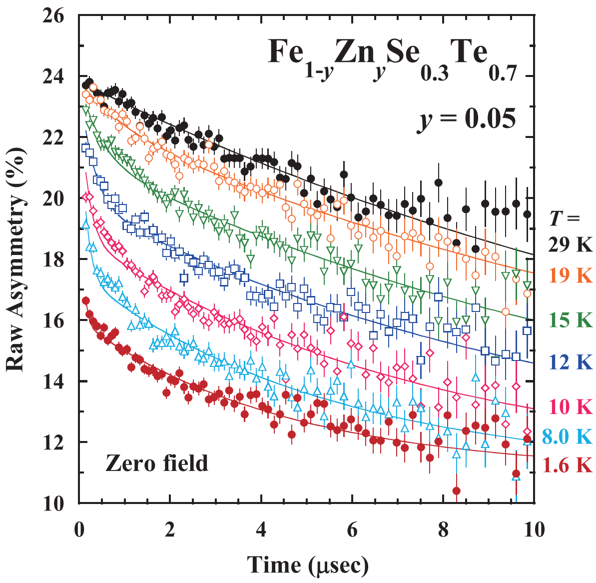

Fig. 1. Zero-field μSR time spectra of $Fe_{1-y}Zn_ySe_{0.3}Te_{0.7}$ with $y = 0.05$.

*1 RIKEN Nishina Center
*2 Department of Applied Physics, Tohoku University

References
1) F.-C. Hsu et al.: Proc. Natl. Acad. Sci. USA **105**, 14262 (2008).
2) T. Noji et al.: J. Phys. Soc. Jpn. **79**, 084711 (2010).
3) T. Inabe et al.: J. Phys. Soc. Jpn. **82**, 044712 (2013).
4) I. I. Mazin et al.: Phys. Rev. Lett. **101**, 057003 (2008).
5) K. Kuroki et al.: Phys. Rev. Lett. **101**, 087004 (2008).
6) H. Kontani et al.: Phys. Rev. Lett. **104**, 157001 (2010).
7) T. Adachi et al.: in preparation.

μSR remeasurement of La_2CuO_4 to reinvestigate muon sites

B. Adiperdana,[*1,*2] T. Kawamata,[*3] T. Adachi,[*4] P. Kumar,[*5] A. Amato, [*5] I. A. Dharmawan,[*2] R. E. Siregar,[*2] S. Sulaiman,[*6] M. I. Mohamed-Ibrahim,[*6] I. Watanabe,[*1,*2,*6] and Y. Koike[*3]

In a previous report,[1)] we have predicted a muon site in La_2CuO_4 (LCO) with the tetragonal structure (the structure above 550 K) by calculating the minimum potential energy for muons, according to the density functional theory (DFT), and the hyperfine field contribution from Cu spins. We predicted two possible muon sites in LCO, although a single muon site with an internal field between 410-430 G was experimentally achieved[2)]. Because of this disagreement, we remeasured the internal field at the muon site using the μSR method with higher statistics. In addition to this experimental effort, we also continued a similar estimation to find all possible minimum potentials in the orthorhombic structure (the structure that occurs below 550 K).

Zero-field (ZF) μSR measurements were performed at the RIKEN-RAL Muon Facility and PSI using a single crystal of LCO in the magnetically ordered state at 10 K and 1.7 K, respectively. The DFT calculation was performed by using the RIKEN integrated cluster of clusters (RICC) system using the Vienna ab-initio simulation package (VASP). A supercell structure that contains 27 unit cells (3×3×3 unit cells) was adopted for calculation taking into account the effect of relaxations of the local lattice and muon positions. The minimum potential in the static case was used to determine the initial positions of lattice points prior to final calculations with relaxation effects. The dipole calculation was performed on the basis of the antiferromagnetic ordered state, which has been experimentally determined by Vaknin et al.[3)] The magnetic moment was traced from 0.10 to 0.70 μ_B/Cu until the dipolar fields fit the internal fields experimentally determined by ZF-μSR.

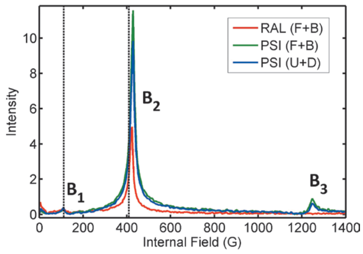

Fig. 1 Fourier spectra of La_2CuO_4 ZF-μSR obtained with high statistics in the RIKEN-RAL and PSI.

Fourier spectra of ZF-μSR are shown in Fig. 1. Three components of internal fields were found. We marked them as B_1, B_2, and B_3 from the lower field component.

B_2 has the largest amplitude while B_1 and B_3 have much smaller amplitudes that are less than 1/30 of that of B_2. The internal field of B_2 corresponds to that experimentally observed.[2)] In terms of DFT calculations, three minimum potentials were found in LCO from our current study, as shown in Fig. 2. This result is qualitatively explained by three muon positions in LCO.

We attempted to explain the observed internal fields on the basis of the dipole-dipole interaction by tuning the magnitude of the magnetic moment of the Cu spin. As a result, we found that the three observed components of the internal field can be explained if the magnetic moment of the Cu spin is reduced to be around 0.23 μ_B, as shown in Fig. 3. Such a local reduction of the Cu spin is currently being argued.[4)]

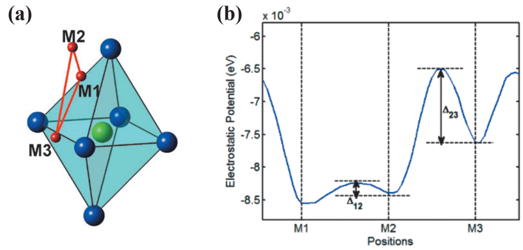

Fig. 2 (a) Minimum potential positions estimated from DFT and (b) shape of the potential energy between minima.

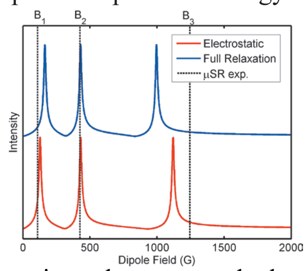

Fig. 3 Comparison between calculated dipolar field spectra and the internal field obtained from μSR experiments.

In conclusion, we found new additional muon sites in LCO from the ZF-μSR experiment with higher statistics. Our DFT calculation supported those three muon sites. Assuming only the dipole-dipole interaction, we suggest the possible local reduction of magnetic moment of the Cu spin to be approximately 50%. The reason for this reduction is currently being discussed.

*1 RIKEN Nishina Center
*2 Department of Physics, Universitas Padjadjaran
*3 Department of Applied Physics, Tohoku University
*4 Department of Engineering and Applied Physics, Sophia University
*5 Lab. For Muon Spin Spectroscopy, Paul Scherrer Institut
*6 Computational Chemistry and Physics Lab., Universiti Sains Malaysia

References

1) B. Adiperdana et al.: RIKEN Accel. Prog. Rep. 46, 224 (2012).
2) B. Hitti et al.: Hyp. Int. 63, 287 (1990).
3) Vaknin et al : Phys. Rev. Lett. 59, 2808 (1987).
4) R. De Renzi et al. : private communications.

Magnetic ordering in Cu_6O_8TbCl probed during the μSR measurement

K. Kawashima,*[1] H. Takeda,*[1] S. Igarashi,*[1] I. Watanabe,*[2] I. Kawasaki,*[2] and J. Akimitsu*[1]

The copper-oxide family of Cu_6O_8MCl (M = cation) has a caged structure (Cu_6O_8 cage) in its crystal structure (crystal system: cubic, space group: *F*m-3m (No. 225)). The form of the surface of the Cu_6O_8 cage is similar to the CuO_2 plane in high-T_c cuprate superconductors. The Cu_6O_8 cage forms a three-dimensional network, sharing their face (left panel of Fig. 1).[1-3] The Cl^- anions are located at the center of the Cu_6O_8 cage, and the M cations, which have a valence of 3+ or 4+, exist in the cuboid space located between Cu_6O_8 cages. The average valence of Cu ions in the Cu_6O_8 cage is 2.33+ for M^{3+}.

For the M = Tb^{3+} compound (Cu_6O_8TbCl), the magnetic susceptibility data indicate a weak magnetic transition at approximately 40 K. Moreover, the electrical resistivity data exhibit a metal-insulator transition at approximately 40 K (right panel of Fig. 1). The effective Bohr magneton P_{eff} is estimated to be ~6.74, which is close to the theoretical value for Tb^{3+}, indicating that a localized magnetic moment exists at the Tb^{3+} site. However, whether the origin of the magnetic ordering state is long range (static) or not and the relationship between the magnetic state and other physical properties is not yet clear. In order to clarify these points, μSR measurement was performed at the RIKEN-RAL Muon Facility in U.K. using a polycrystalline sample of Cu_6O_8TbCl.

Figure 2 (a) shows the time dependence of asymmetry of the zero field (ZF) μSR spectra, $A(t)$, of Cu_6O_8TbCl measured at various temperatures. These spectra were observed using the double-pulse muon beam. The spectra show exponential-like depolarized behaviors, and the muon-spin depolarization becomes faster with decreasing temperature above 40 K. Significant loss of initial asymmetry (at t = 0) is observed below 40 K. In order to observe the change of the spin dynamics in detail, all of the time spectra were analyzed using the following function:

$$A(t) = A_0 \exp(-\lambda t) + A_B, \quad (1)$$

where A_0 is the initial asymmetry, λ is the depolarization rate of the muon spins, and A_B is the background. The parameters obtained from the best fit of Eq. 1 to the data in Fig. 2(a) (solid line) are shown in Fig. 2(b). From Fig. 2(b), A_0 slightly decreases and λ increases above 40 K. Moreover, A_0 and λ values rapidly change at approximately 40 K, indicating that the spin state drastically changes at 40 K. The inset of Fig. 2(a) shows an early time region of the ZF μSR spectra at 5 K (lowest temperature of this measurement) measured using the single-pulse muon beam. Muon-spin precession behavior was observed, indicating the existence of a long-range magnetic-ordered state. Consequently, the weak magnetic transition confirmed in the magnetic susceptibility data of Cu_6O_8TbCl is generated by the development of long-range magnetic order of Tb^{3+}. Moreover, it is suggested that the conducting carrier is trapped and that the ground state changes from metallic to semiconducting with the onset of long-range magnetic order.

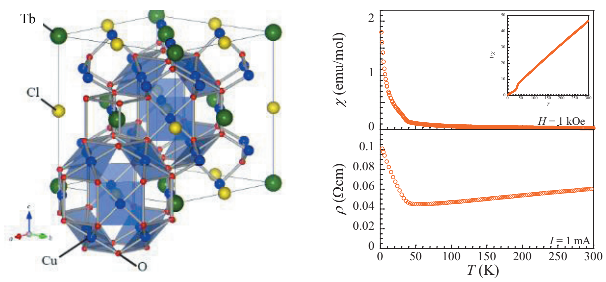

Fig. 1 (Left panel) Crystal structure of Cu_6O_8MCl (program VESTA was used. [4]). Solid line shows the unit cell. (Right panel) Temperature dependence of magnetic susceptibility and electrical resistivity of Cu_6O_8TbCl. Inset shows the inversed magnetic susceptibility as a function of temperature.

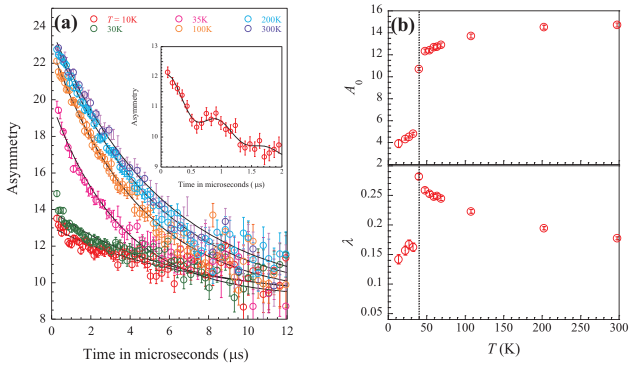

Fig. 2 (a) The time dependence of asymmetry of ZF μSR spectra of Cu_6O_8TbCl measured at various temperatures. Solid lines are fitting results using Eq. (1). (b) The temperature dependence of A_0 and λ obtained by the fitting.

References

1) I. Yazawa *et al.*: Jpn. J. Appl. Phys. **29** (1990) L1693.
2) R. Sugise *et al.*: J. Appl. Phys. **32** (1993) L940.
3) G. Zouganel *et al.*: Sol. St. Comm. **80** (1991) 709.
4) K. Momma *et al.*: Commission Crystallogr. Comput. IUCr Newslett. (2006) No. 7, 106.

*[1] Department of physics and mathematics, Aoyama Gakuin University
*[2] RIKEN Nishina Center

Disappearance of gapped Mott insulating phase neighboring Boseglass phase in $Tl_{1-x}K_xCuCl_3$ detected by longitudinal-field muon spin relaxation[†]

T. Suzuki,[*1,*2] H. Guo,[*2] I. Kawasaki,[*2] I. Watanabe,[*2] T. Goto,[*3] K. Katayama,[*4] and H. Tanaka[*4]

$TlCuCl_3$ and $KCuCl_3$ are isostructural, and are three-dimensionally coupled Cu $3d$ S =1/2 spin dimer systems. The ground states are spin singlets with excitation gaps of Δ = 7.5 K in $TlCuCl_3$ and 31 K in $KCuCl_3$, originating from strong intradimer antiferromagnetic interaction J. Applying magnetic fields to the gapped state, the spin gap is collapsed, and a magnetically ordered state appears, which is qualitatively well described by the magnon Bose-Einstein condensation (BEC) theory[1]. Describing the magnetic states by magnon motions, the spin singlet state corresponds to the gapped Mott Insulating (MI) phase.

By introducing randomness in the intradimer interaction, a new phase, Bose glass (BG) phase was theoretically predicted to appear at T = 0 neighboring the magnon BEC phase[2]. In the mixed system $Tl_{1-x}K_xCuCl_3$, the randomness of the local chemical potential is introduced spatially, because the value of the dominant intradimer interaction J, which corresponds to the local potential of magnons, is different between $TlCuCl_3$ and $KCuCl_3$[3]. Recently, Yamada *et al.* performed electron-spin resonance (ESR) measurements on $Tl_{1-x}K_xCuCl_3$ with x = 0.22 and 0.44 in resonance fields close to the critical field of BEC transition which is confirmed by specific heat measurements, and reported the change of the spectrum shape from Lorentzian shape to the intermediate shape between Gaussian and Lorentzian[4]. This result suggests the localization of magnons at sufficiently low temperature, and suggest the appearance of the BG phase adjacent to the BEC phase. According to the theoretical prediction, the BG phase appears between the gapped MI phase and the BEC phase, and there exist a quantum phase transition point H_B from the BG phase to the gapped MI phase with decreasing the magnetic field. However, magnetization measurements suggest H_B =0. Thus, whether or not the gapped MI phase neighboring the Bose glass phase disappears in the zero-field limit is a controversial problem. The purpose of this study is to microscopically investigate this problem using LF - μSR technique.

Figure 1 shows temperarature dependence of LF - μSR time spectrum of $Tl_{1-x}K_xCuCl_3$ with x = 0.40 down to 25 mK in various longitudinal fields. All time spectra are analyzed using the stretched exponential function $A(t) = A_0 \exp(-\lambda t)^\beta$, and are well fitted as shown with solid lines. A_0 is the initial asymmetry and λ is the muon spin relaxation rate. Fitted results of β are almost constant for all spectra in a range of $\beta = 0.8 \pm 0.06$, which is consistent with the previous data for x = 0.40 in longitudinal fields. LF-μSR time spectra shows an exponential like decay, and the muon spin-relaxation rate does not has a significant temperature dependence down to 25 mK. As a fitted result, λ, which corresponds to a low frequency dynamical susceptibility, is almost constant down to 25 mK although slight changes in λ are observed. The low frequency spectrum seems to be a white spectrum, because λ in each field is finite below 500 gauss. These results mean that internal magnetic fields at the muon sites are fluctuating by low frequencies below $\sim$ 1 MHz down to 25 mK. When the spin system has a tendency toward a magnetic phase transition, λ is expected to increase with decreasing temperature in the zero-field limit below 500 gauss. Thus, in this case, a magnetic ordered state is not experimentally expected, and the ground state is a spin fluctuating state. It is suggested that the theoretically predicted quantum phase transition point from the Bose glass phase to the gapped Mott insulating phase disappears, i.e. H_B =0.

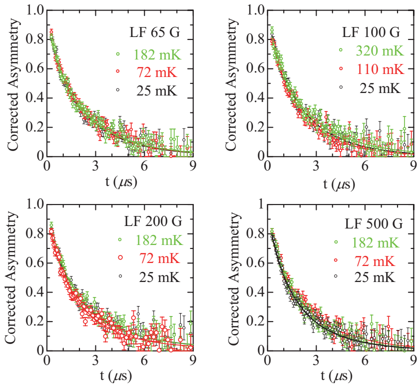

Fig. 1. Temperature dependence of LF-μSR time spectrum of $Tl_{1-x}K_xCuCl_3$ with x = 0.40.

References
1) A. Oosawa, M. Ishii, and H. Tanaka, J. Phys. Condens. Matter **11** (1999) 265.
2) O. Nohadani, S. Wessel, and S. Haas, Phys. Rev. Lett. **95** (2005) 227201.
3) A. Oosawa and H. Tanaka, Phys. Rev. B **65**, (2002) 184437.
4) F. Yamada, H. Tanaka, T. Ono, And H. Nojiri, Phys. Rev. B **83** (2011) 020409(R).

† Condensed from the article submitted to J. Phys. Soc. Jpn.
*1 College of Engineering, Shibaura Institute of Technology
*2 RIKEN Nishina Center
*3 Faculty of Science and Technology, Sophia University
*4 Department of Physics, Tokyo Institute of Technology

Magnetic order in pyrochlore iridate $Nd_2Ir_2O_7$ probed by employing muon spin relaxation†

H. Guo,[*1,*2] K. Matsuhira,[*3] I. Kawasaki,[*2] M. Wakeshima,[*4] Y. Hinatsu,[*4] I. Watanabe,[*2] and Z. Xu[*1]

Pyrochlore iridates are highly suitable to investigate novel topological phases based on the network of corner-sharing tetrahedra structures and the relatively large spin-orbit coupling (SOC) inherent in Ir $5d$ electrons.[1)] The interplay between SOC and electron-electron correlations (U) produces characteristic electronic states. A series of $R_2Ir_2O_7$ (R-227, R = Nd-Ho) compounds exhibit metallic or semi-metallic behavior and undergo metal-insulator transitions (MITs) at a temperature T_{MI}[2)] while Pr-227 shows metallic behavior down to 0.3 K.[3)]

In this study, we focus on Nd-227, which shows metallic behavior at high temperatures and undergoes a MIT at T_{MI} of about 30 K, and the magnetic susceptibility shows the bifurcation below T_{MI} in zero-field-cooling (ZFC) and field-cooling (FC) conditions.[2)] Muon spin precession is observed below T_{MI}, and the spectra were fitted using the following function:

$$A(t) = A_1 e^{-\lambda_1 t} + A_2 \cos(\gamma_\mu H_{\rm int} t + \varphi) e^{-\lambda_2 t} \qquad (1)$$

where $H_{\rm int}$ is the internal field at the muon site, λ_1 is the muon spin-lattice relaxation rate, and λ_2 and φ are the damping rate and initial phase of the muon spin precession, respectively.

The temperature dependence of the extracted parameters is shown in Fig. 1. $H_{\rm int}$ begins to increase below T_{MI}, following the Brillouin-type ordering and tends to saturate below about 20 K to a value of about 350 G. Below about 10 K, $H_{\rm int}$ increases again. λ_2 continues to decrease below T_{MI} and increases again from the same temperature at which $H_{\rm int}$ exhibits an increase. ¿From the inset of Fig. 1(a), it can be seen that λ_1 increases monotonically with decreasing temperature, reflecting the slowing down of the magnetic moments. A small increase is observed around T_{MI}. However, no critical slowing down behavior is observed, as shown in Fig. 1(b). λ_1 continues to increase below T_{MI} and shows a broad peak at around 10 K.

The increase in $H_{\rm int}$ below about 10 K is consistent with the results of the neutron scattering experiment that shows the ordering of Nd^{3+} moments, so it is attributed to the ordering of Nd^{3+} moments from our muon spin relaxation (μSR) experiment. The decrease in λ_1 below about 10 K is then accounted for by the freezing out of the magnetic fluctuations, and the increase in λ_2 suggests that the distribution of the internal field becomes larger at the vicinity of the magnetic ordering. The ordering below T_{MI} is then attributed to the ordering of the Ir^{4+} moments, suggesting its close relationship with the MIT.

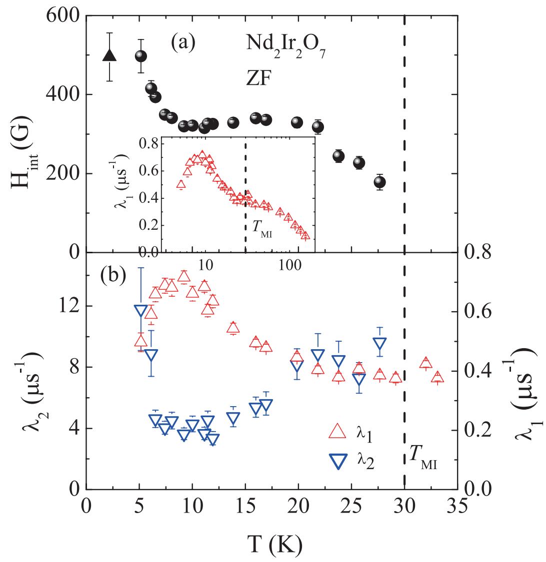

Fig. 1. Temperature dependence of the extracted parameters from our fits to Eq. (1). (a) The internal field at the muon site. (b) The damping rate of muon spin precession and the muon spin-lattice relaxation rate. The inset in (a) shows the whole temperature range of λ_1.

According to a local spin-density approximation calculation including U and SOC, the magnetic structure of the Ir sublattice is the all-in/all-out type, which does not break the lattice periodicity; therefore, the Slater transition is ruled out to account for the relationship between the MIT and the magnetic transition. On the other hand, the Lifshitz-like transition in which the hole band and electron band are moved downward and upward, respectively, due to the specific magnetic structure and the large SOC of Ir $5d$ electrons may explain the mechanism of MIT.

The saturated internal field from the ordered Ir^{4+} moments is found to be much smaller than that in the case of the other pyrochlore iridates with a magnetic insulating ground state. This implies a stronger hybridization between the Ir $5d$ and the O $2p$ electronic orbitals in Nd-227.

† Condensed from the article in Phys. Rev. B 88, 060411 (2013).

*1 Department of Physics, Zhejiang University
*2 RIKEN Nishina Center
*3 Faculty of Engineering, Kyushu Institute of Technology
*4 Division of Chemistry, Hokkaido University

References

1) X. Wan *et al.*, Phys. Rev. B 20, 205101 (2011).
2) K. Matsuhira *et al.*, J. Phys. Soc. Jpn. 80, 094701 (2011).
3) S. Nakatsuji *et al.*, Phys. Rev. Lett. 96, 087204 (2006).

Unconventional spin freezing in a highly two-dimensional spin-1/2 Kagome antiferromagnet $Cd_2Cu_3(OH)_6(SO_4)_2{\cdot}4H_2O$: evidences of partial order and co-existing spin singlet state on distorted Kagome lattice

X.G. Zheng,*1 M. Fujihala,*1 and I. Watanabe*2

The magnetic phases of geometrically frustrated magnets have been rigorously studied both theoretically and experimentally in the last two decades. The Kagome antiferromagnet, a two-dimensional net of corner-sharing triangles, is an excellent choice for investigating spin liquid and other exotic states, because it is expected to be one of the most highly frustrated systems. However, the Kagome system is still not completely understood, leading to many unanswered questions. Even the most essential issue of whether the ground state is a gapped spin liquid or a gapless one remains undetermined. Besides the difficulties of theoretically dealing the quantum spins on the Kagome lattice (which is much more complicate than the simple triangular lattice), the lack of such compounds has been a major obstacle.

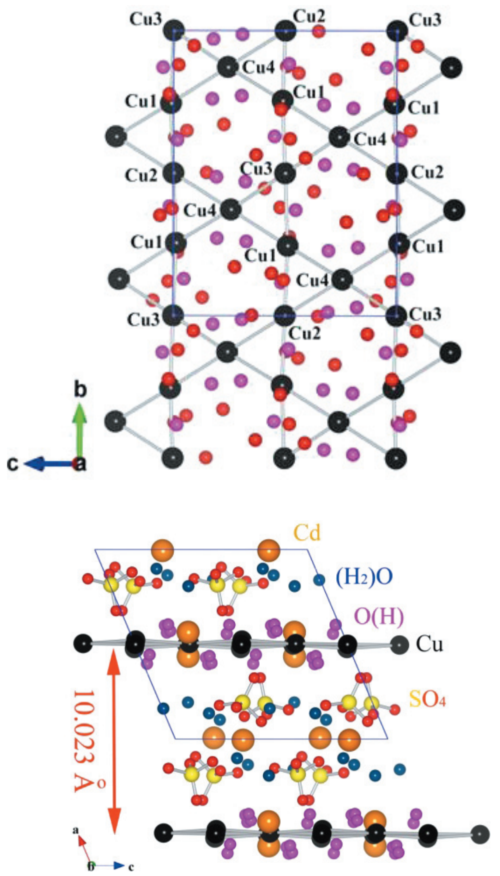

Fig. 1. Structure of $Cd_2Cu_3(OH)_6(SO_4)_2{\cdot}4H_2O$.

*1 Department of Physics, Saga University
*2 RIKEN Nishina Center

We have recently found a new Kagome antiferromagnet, $Cd_2Cu_3(OH)_6(SO_4)_2{\cdot}4H_2O$. It possesses a monoclinic crystal structure identical to that for the previously reported mineral Edwardsite [1]. It crystallizes in the space group P 21/c with lattice parameters of a = 10.8887(2) Å, b = 13.1745(2) Å, c = 11.2258(2) Å, and β = 112.994(1)°. As illustrated in Fig. 1, four Cu^{2+} sites exist, forming a Kagome lattice for the S = 1/2 spins. The structural information show that $Cd_2Cu_3(OH)_6(SO_4)_2{\cdot}4H_2O$ is a slightly distorted Kagome lattice with high two-dimensionality, which is a great advantage in studying the intrinsic spin behaviors on distorted Kagome lattices; it also serves as a reference system for undistorted Kagome lattices.

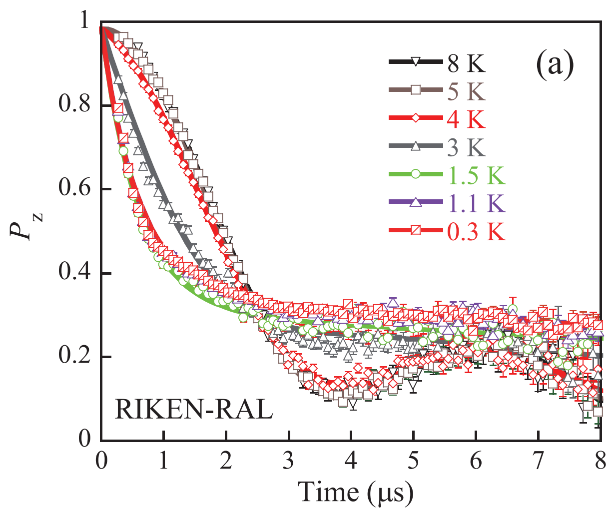

Fig. 2 Zero-field μSR asymmetry spectra at various temperatures.

μSR, having a large gyromagnetic ratio, is a sensitive microscopic probe for magnetic order and spin fluctuations. Figure 2 shows the zero-field (ZF) asymmetry spectra at various temperatures. The asymmetry spectra change obviously from T = 5 K. Detailed analysis showed the formation of static magnetism below 5 K. The magnetic behaviors are distinctly different from the spin liquid sate on an undistorted Kagome lattice, demonstrating the critical role of lattice distortion.

References

1) P. Elliott, J. Brugger, T. Caradoc-Davies, Mineralogical Magazine 74, 39 (2010).

Muon spin relaxation study of spin-glass freezing in the Heusler compound $Ru_{1.9}Fe_{0.1}CrSi$[†]

M. Hiroi,[*1,*2] T. Hisamatsu,[*2] T. Suzuki,[*1,*3] K. Ohishi,[*1,*4] Y. Ishii,[*1,*5] and I. Watanabe[*1]

The magnetic properties of the Heusler compounds $Ru_{2-x}Fe_xCrSi$ have attracted interest. It has been revealed that Fe-rich compounds are ferromagnetic[1] and that the Ru-rich compound Ru_2CrSi shows an antiferromagnetic transition at $T_N = 14$ K.[2] Although the Ru-rich compound $Ru_{1.9}Fe_{0.1}CrSi$ was found to show a peak in magnetic susceptibility at $T_N^* \sim 30$ K, which seemed to indicate an antiferromagnetic transition, no phase transition was found around T_N^* or at any other temperatures in the specific heat.[3,4] Instead, the difference between the magnetic susceptibilities observed in a zero-field-cooling process and a field-cooling process increased significantly below $T_g \sim 15$ K, which was regarded as the onset of strong irreversibility.[3] This observation suggests the formation of a spin-glass (SG) state. In order to reveal the nature of the magnetic transitions, we have performed zero-field (ZF) and longitudinal-field (LF) muon-spin-relaxation (μSR) measurements for $Ru_{1.9}Fe_{0.1}CrSi$. The measurements were carried out at the RIKEN-RAL Muon Facility using a spin-polarized single-pulse positive surface muon beam. In these measurements the time spectra of muon spin depolarization consisted of two components, and the asymmetry, $A_0(t)$, can be expressed as

$$A_0(t) = A_1 \exp(-\lambda_1 t) + A_2 \exp(-\lambda_2 t). \tag{1}$$

The first and second terms represent the fast and slow relaxation components, respectively, and λ_1 and λ_2 are the muon spin relaxation rates for each component. The initial asymmetry A_0 is $A_0(0) = A_1 + A_2$.

The parameters in Eq. (1) were obtained from the fitting of the time spectra, and these temperature dependences in the ZF-μSR measurement are shown in Fig. 1. As shown in the figure, a peak of the relaxation rates was observed at ~16 K, and this suggests the onset of spin freezing at $\sim T_g$. Furthermore, LF-μSR measurement for different values of magnetic field was performed at 0.3 K, which confirmed the presence of a static internal magnetic field. The internal field was estimated to be approximately 0.1308 ± 0.005 T. From these results we conclude that SG freezing occurs at T_g.

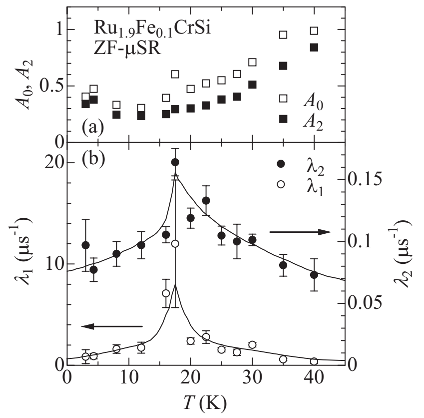

Fig. 1. Temperature dependences of (a) $A_0 = A_1 + A_2$ and A_2, and (b) λ_1 and λ_2, for ZF-μSR. Solid lines are guides to the eye.

On the other hand, an anomaly in the relaxation rate of ZF-μSR, indicating a phase transition, appeared to be absent around T_N^*, whereas with decreasing temperature a large decrease in the initial asymmetry and a gradual increase in the relaxation rates were observed starting at ~40 K, which is slightly higher than T_N^*. The loss of the initial asymmetry may have been caused by a static internal field. To investigate the origin of the large decrease in the initial asymmetry below ~40 K, we performed LF-μSR measurements as a function of magnetic field H_{LF} between T_g and $\sim T_N^*$. The H_{LF} dependence of A_2 was analyzed, and it was found that at temperatures below 30 K, A_2 increases from approximately the same field as at 0.3 K. This analysis suggests that a static field arises at the muon site from temperatures higher than $T_N^* \sim 30$ K and the value of the static field does not change much below ~30 K. These results indicate an inhomogeneous magnetic state. It appears that the formation of independent spin-frozen regions begins at ~40 K. As the temperature decreases, these static regions extend gradually, and this results in the observed decrease in the initial asymmetry. The correlation between static regions becomes larger and eventually SG freezing occurs at T_g.

[†] Condensed from the article in Phys. Rev. B **88** 024409 (2013)

[*1] RIKEN Nishina Center
[*2] Department of Physics and Astronomy, Kagoshima University
[*3] Faculty of Engineering, Shibaura Institute of Technology
[*4] CROSS, JAEA
[*5] Department of Physics, Tokyo Medical University

References

1) M. Hiroi et al.: Phys. Rev. B. **76** 132401 (2007).
2) M. Hiroi et al.: J. Phys.: Conf. Series **400** 032020 (2012).
3) M. Hiroi et al.: Phys. Rev. B. **79** 224423 (2009).
4) M. Ito et al.: Phys. Rev. B **82** 024406 (2010).

μSR study of heavy fermion superconductor URu_2Si_2

I. Kawasaki,[*1] I. Watanabe,[*1] A. D. Hillier,[*2] and D. Aoki[*3,*4]

Despite intensive studies for more than two decades, the order parameter of the mysterious phase transition at $T_0 = 17.5$ K[1)] in URu_2Si_2 has not been identified yet, and thus the ordered phase is referred to as the hidden order (HO) phase.

The symmetry of the HO phase is crucial information for the identification of its order parameter. Recent Shubnikov-de Haas experiments have revealed that the Fermi surfaces in the HO phase are very similar to those of the pressure induced antiferromagnetic phase.[2)] This confirms that translational symmetry is broken in the HO phase, and the ordering vector is $Q_{\rm HO} = (1, 0, 0)$. In addition, in the HO state, NMR and magnetic torque experiments have shown that the four-fold rotational symmetry in the (001) plane is broken.[3,4)] On the other hand, the time-reversal symmetry (TRS) is still a controversial issue, since we can find two types of very recent theoretical models for the HO transition: some of the theoretical models assume that the TRS is conserved in the HO phase,[5)] while the others assume that TRS is broken.[6)] Therefore, although the previous NMR and μSR studies have reported the development of tiny internal magnetic fields below T_0[7,8)] and indicate the breaking of the TRS in the HO phase, further characterization of the internal magnetic field in the HO phase is required. In the present study, we performed zero-field (ZF) and longitudinal-field (LF) μSR experiments on a single crystal of URu_2Si_2 in order to characterize the internal magnetic fields in the HO state.

The inset of Fig. 1 shows ZF-μSR spectra at 11 and 19.5 K, which are below and above T_0. The ZF-spectra were well fitted by a single exponential function $A_0\exp(-\lambda_{\rm ZF}t)$ over the temperature range presently investigated. We observed an enhancement of $\lambda_{\rm ZF}$ in the HO phase, which reflects a development of the TRS breaking magnetic field. Figure 1 exhibits the temperature dependence of $\lambda_{\rm ZF}$, and a sharp increase is clearly observed at T_0. $\lambda_{\rm ZF}$ shows a saturated feature around 10 K, but it exhibits an additional increase with further decreasing temperature and keeps increasing down to the lowest temperature.

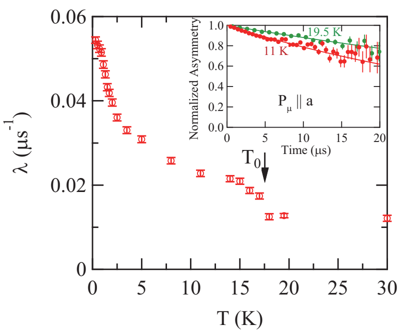

Fig. 1. Temperature dependence of the ZF-relaxation rate. The inset shows the ZF-μSR spectra measured at 11 and 19.5 K.

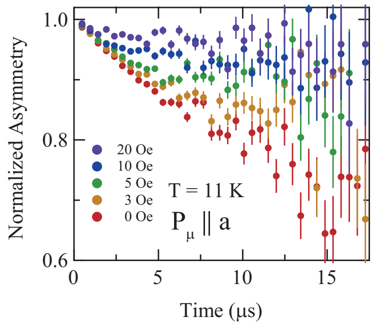

Fig. 2. The LF-μSR spectra at 11 K under several longitudinal fields.

In order to investigate the dynamics of the internal magnetic field in the HO phase, we performed LF-field experiments where LF was applied parallel to the a-axis. Figure 2 shows the LF-μSR spectra measured at 11 K. The long tails of relaxation spectra are strongly affected by applying tiny LFs. This is a characteristic feature in the presence of a static field distribution at muon sites. In this case, the exponential relaxation in the ZF experiments reflects the presence of a Lorentzian field distribution at muon sites. Since the relaxation rate under LFs is a measure of transverse components of field fluctuations at muon sites, the observed decoupling behavior implies the absence of measurable field fluctuations along both the a and c directions. Hence, we conclude that measurable magnetic fluctuations do not exist along any directions at muon sites, and the internal magnetic field developed in the HO phase is static on the time scale of μSR.

*1 RIKEN Nishina Center
*2 ISIS Facility, STFC Rutherford Appleton Laboratory
*3 SPSMS, UMR-E CEA/UJF-Grenoble 1, INAC
*4 Institute for Materials Research, Tohoku University

References

1) T. T. M. Palstra *et al.*, Phys. Rev. Lett. **55**, 2727 (1985).
2) E. Hassinger *et al.*, Phys. Rev. Lett. **105**, 216409 (2010).
3) R. Okazaki *et al.*, Science **331**, 439 (2011).
4) S. Kambe *et al.*, Phys. Rev. Lett. **110**, 246406 (2013).
5) H. Kusunose *et al.*, J. Phys. Soc. Jpn. **80**, 084702 (2011).
6) H. Ikeda *et al.*, Nat. Phys. **8**, 528 (2012).
7) S. Takagi *et al.*, J. Phys. Soc. Jpn. **81**, 114710 (2012).
8) H. Amitsuka *et al.*, Physica B **312-313**, 390 (2002).

Magnetic instability induced by Rh doping in the Kondo semiconductor $CeRu_2Al_{10}$

H. Guo,[*1,*2] H. Tanida,[*1,*3] R. Kobayashi,[*4,*5] I. Kawasaki,[*1] M. Sera,[*3] T. Nishioka,[*6] M. Matsumura,[*6] I. Watanabe, [*1] and Z. Xu[*2]

The ternary compound CeT_2Al_{10} (T = Fe, Ru, and Os) is a unique system that shows Kondo semiconducting behavior at low temperatures, and it exhibits an antiferromagnetically (AFM) ordered state at $T_0 \sim 30$ K for T = Ru and Os, while a nonmagnetic ground state is observed for T = Fe, as is usually the case for Kondo semiconductors (or insulators).[1–3] Since the magnetic susceptibility (χ) systematically decreases on changing the transition metal element in the order from T = Ru to Os to Fe, the $4f$ electron state is located in the vicinity of the boundary between localized and non-localized states, as expected from the Kondo semiconducting behavior. Thus, the c-f hybridization between d- and $4f$-electrons must play a key role for their low-temperature properties involved in the origin of the AFM order.

The AFM order is very unusual. T_0 is quite high for a usual Ce-based intermetallic compound when taking into account, for instance, the long distance of 5.2 Å between neighboring Ce ions.[2] The magnetic anisotropy is also unusual. Although the easy axis is the a axis with the large magnetic anisotropy ($a \gg c \gg b$), the AFM ordered moment (m_{AF}) with a magnitude of 0.3−0.4 μ_B/Ce aligns in the c-axis direction.[4,6] Recently, the Rh-doping effect on $CeRu_2Al_{10}$ has been examined, where Rh ($4d^8$) has one electron more than Ru ($4d^7$).[7,8] On the basis of the results, we infer that χ becomes more Curie−Weiss like and decreases drastically below T_0 for $H \| a$. These results imply that the Rh-doping breaks $m_{AF} \| c$ and $m_{AF} \| a$ is realized instead. In order to clarify the spin alignment and the critical Rh concentration x_c from a microscopic point of view, we performed zero-field μSR on $Ce(Ru_{1-x}Rh_x)_2Al_{10}$ (x = 0, 0.03, 0.05, and 0.1).

Figure 1 shows the temperature dependence of the internal magnetic field (H_{small}, H_{large}) at the muon site for $Ce(Ru_{1-x}Rh_x)_2Al_{10}$. Here, H_{small} (H_{large}) represents the smaller (larger) component of internal magnetic fields. For the undoped sample, H_{small} shows non-mean-field-like behavior, while H_{large} increases below T_0 and saturates to a value of about 180 G below about 15 K. On the other hand, for Rh-doped samples, H_{large} reaches about 800 G at low temperatures. This strongly suggests the spin-flop transition from $m_{AF} \| c$ to $m_{AF} \| a$ on the basis of our dipolar field calculation at the suggested muon site, which is consistent with the bulk properties.[7,8] Since there is no Rh-concentration dependence in H_{large} for $x > 0.03$, the boundary of the different magnetic ground states is identified at around $x \sim 0.03$. The drastic change of the magnetic ground state by such a tiny Rh doping indicates that the magnetic structure in $CeRu_2Al_{10}$ is not robust and can be quite easily tuned using external perturbations such as d-electron doping. On the basis of previous experimental results from thermal electric power,[9] neutron scattering,[4] and NQR measurements,[10] the non-mean-field-like behavior of H_{small} for the $x = 0$ sample is attributed to the Fermi contact field from the polarized electrons at the muon site, while the T dependence of H_{large} for the Rh-doped samples is still an unresolved question; whether it results from the Fermi contact field or from the unusual ordering of Ce^{3+} moments should be clarified by future neutron scattering experiments.

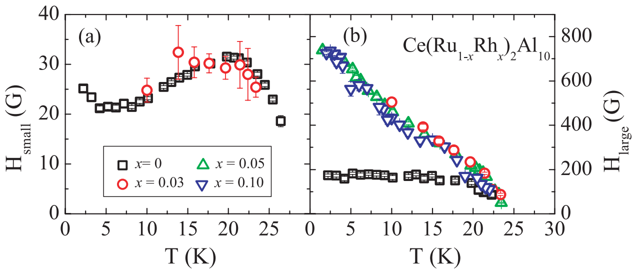

Fig. 1. Temperature dependence of the internal magnetic fields at the muon sites in $Ce(Ru_{1-x}Rh_x)_2Al_{10}$ (x = 0, 0.03, 0.05, and 0.1): (a) H_{small} (b) H_{large}.

† Condensed from the article in Phys. Rev. B **88**, 115206 (2013).

*1 RIKEN Nishina Center
*2 Department of Physics and State Key Laboratory of Silicon Materials, Zhejian University
*3 AdSM, Hiroshima University
*4 Neutron Science Laboratory, ISSP, Tokyo University
*5 Quantum Condensed Matter Division, Oak Ridge National Laboratory
*6 Graduate school of Integrated Arts and Science, Kochi University

References

1) A. M. Strydom: Physica B **404**, 2981 (2009).
2) T. Nishioka *et al.*: J. Phys. Soc. Jpn. **78**, 123705 (2009).
3) Y. Muro *et al.*: J. Phys. Soc. Jpn. **78**, 083707 (2009).
4) D. D. Khalyavin *et al.*: Phys. Rev. B **82**, 100405(R) (2010).
5) K. Kato *et al.*: J. Phys. Soc. Jpn. **80**, 073701 (2011).
6) H. Tanida *et al.*: Phys. Rev. B **84**, 233202 (2011).
7) A. Kondo *et al.*: J. Phys. Soc. Jpn. **82**, 054709 (2013).
8) R. Kobayashi *et al.*: J. Phys. Soc. Jpn. **82**, 093702 (2013).
9) H. Tanida *et al.*: J. Phys. Soc. Jpn. **79**, 063709 (2010).
10) M. Matsumura *et al.*: J. Phys. Soc. Jpn. **78** 123713 (2009).

μSR study on $CeRu_2Al_{10}$ under pressure

H. Guo,[*1,*2] H. Tanida,[*3] I. Kawasaki,[*1] M. Sera,[*3] T. Nishioka,[*4] M. Matsumura[*4] I. Watanabe,[*1] and Z. Xu[*2]

CeT_2Al_{10} (T = Fe, Ru, and Os), which has the orthorhombic $YbFe_2Al_{10}$−type structure, can be categorized as a Kondo semiconductor and is of interest because of numerous anomalous electronic behaviors due to the $c-f$ hybridization effect.[1–3] For instance, the antiferromagnetic (AFM) transition temperature (T_0) is quite high compared to that usually expected for Ce-based intermetallic compounds,[2] and the spin alignment in the AFM ordered state is $m_{AF} \parallel c$, although the easy magnetization axis is the a-axis with the large magnetic anisotropy $a \gg c \gg b$.[4,5] In addition, the magnetic structure is easily changed from $m_{AF} \parallel c$ to $m_{AF} \parallel b$ or $m_{AF} \parallel b$ to $m_{AF} \parallel c$ by application of non-magnetic La doping, magnetic field, or external pressure.[6] Furthermore, tiny d-electron doping, such as Rh($4d^8$)-doping in Ru($4d^7$), easily breaks the $m_{AF} \parallel c$ ordering, and $m_{AF} \parallel a$ ordering is realized instead.[7] These results indicate that the magnetic structure of $CeRu_2Al_{10}$ is not robust and is easily tuned by such perturbations.

Regarding the effect of pressure on $CeRu_2Al_{10}$, T_0 is enhanced up to about P = 2 GPa, beyond which it exhibits a slight decrease; at approximately P_c = 4 GPa, $CeRu_2Al_{10}$ exhibits a first-order-like transition from the AFM Kondo semiconducting state to the nonmagnetic Fermi liquid state.[2] Since T_0 is enhanced at low pressures, the bulk magnetization is expected to also be enhanced by pressure. However, the magnetization is strongly suppressed by pressure.[8] At P = 1 GPa, the magnetization becomes nearly half of that at ambient pressure. That is, the pressure enhances T_0 but suppresses the magnetization. These results seem to contradict each other. In order to verify whether m_{AF} is suppressed on applying pressure, we performed μSR experiments on $CeRu_2Al_{10}$ under pressures up to about P = 0.6 GPa. From the μSR experiment, the pressure dependence of m_{AF} can be clarified through the change in the internal magnetic field at the muon site. To our knowledge, this is the first attempt at investigating the effect of pressure on the m_{AF} in CeT_2Al_{10} (T = Ru, Os).

Figure 1 shows the temperature dependence of the initial asymmetry of $CeRu_2Al_{10}$ at ambient pressure and at P = 0.6 GPa. The initial asymmetry is extracted from the transverse field (TF) measurement. The decrease in the initial asymmetry below T_0 is a good indicator of the appearance of a magnetically ordered state. We clarified that T_0 is enhanced by pressure by observing bulk properties. The temperature dependence of the initial asymmetry at ambient pressure is consistent with our previous μSR experiment.[7] As seen below for T =10 K, the temperature dependence of the asymmetry is different between the data at ambient pressure and at those P = 0.6 GPa, indicating that the evolution of the m_{AF} is different between these two cases. This would be attributed to a change in the hyperfine process through the Fermi contact field caused by pressure.[7] We aimed to clarify a change in the magnitude of m_{AF} under pressure. However, owing to the fraction of stopping muons in the sample being less and the strong restriction of the time resolution of the double-pulsed muon beam, we could not observe the muon spin precession, and thus, from the zero field measurement, no quantitative information on H_{int} could be achieved directly under ambient or high pressure. In order to obtain detailed information on m_{AF}, further studies are needed.

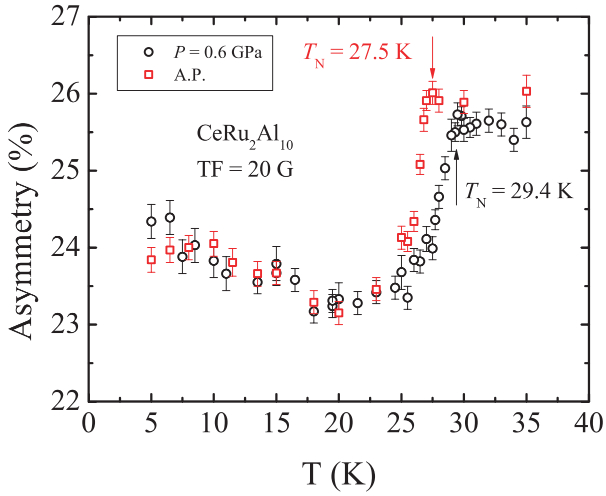

Fig. 1. Temperature dependence of the initial asymmetry of $CeRu_2Al_{10}$ at ambient pressure and at P = 0.6 GPa. The initial asymmetry is extracted from transverse field (TF) measurements.

References
1) A. M. Strydom: Physica B **404**, 2981 (2009).
2) T. Nishioka *et al.*: J. Phys. Soc. Jpn. **78**, 123705 (2009).
3) Y. Muro *et al.*: J. Phys. Soc. Jpn. **78**, 083707 (2009).
4) D. D. Khalyavin *et al.*: Phys. Rev. B **82**, 100405(R) (2010).
5) H. Tanida *et al.*: Phys. Rev. B **84**, 233202 (2011).
6) H. Tanida *et al.*: Phys. Rev. B **88**, 045135 (2013).
7) H. Guo *et al.*: Phys. Rev. B**88**, 115206 (2013).
8) H. Tanida *et al.*: Phys. Rev. B **86**, 085144 (2012).

*1 RIKEN Nishina center
*2 Department of Physics, Zhejiang University
*3 AdSM, Hiroshima University
*4 Graduate school of Integrated Arts and Science, Kochi University

Muon LCR measurements for organic magnets based on [Pd(dmit)$_2$] metal-complex molecules†

M. Abdel Jawad,*1 Y. Ishii,*2 S. Masubuchi,*2 R. Kato,*1 I. Watanabe,*3 and F. L. Pratt*4

Magnetic ground states of quasi two dimensional (Q2D) triangular Heisenberg antiferromagnetic (AF) systems are of great interest. Magnetic frustration arising from the triangular exchange network suppresses the AF order. This kind of quantum-spin states without either long-range magnetic order or lattice symmetry breaking is named quantum spin liquid (QSL) state. Theoretically, this QSL state has been studied extensively and many classes of theoretical models such as Z_2 spin liquid, spinon fermi surface (SFS) and spin-bose metal are proposed. Although experimentalist have sought real model materials with QSL state for quite some time, only a few candidate materials are known to this date.

A series of organic salts, $(Cation)$[Pd(dmit)$_2$]$_2$ (dmit=1,3-dithiole-2- thione-4,5-dithiolate) has triangular exchange network of S = 1/2 unit of molecular dimers[1]. The strength of the spin frustration can be controlled by the choice of cation and most of materials belonging to this family undergo AF states. In such triangular magnets, geometrical frustration is though to play an important role on the magnetic state as the AF transition temperatures is found to increase proportionally to the deviation from the regular triangular exchange networks. It is thought that EtMe$_3$Sb[Pd(dmit)$_2$]$_2$[2] do not show any AF order due to strong spin frustrations. These materials have almost regular triangular exchange networks with exchange interaction J of the order of 200 to 300 K.

Recently, we have performed longitudinal field (LF) μSR measurements on EtMe$_3$Sb[Pd(dmit)$_2$]$_2$ a QSL candidate. Preliminary analysis suggest that field dependence of muon relaxation rate, λ is proportional to $1/\sqrt{B}$ behaviour in a field range of $1 \leq B_{ext} \leq 1000$ Gauss at low-temperatures. Such a behaviour is expected from spins diffusing along a one-dimensional direction. In an ideal 1D spin system model, the field dependence of λ is approximately described as follows:

$$\lambda(\omega) = \frac{A^2}{4}\frac{1}{\sqrt{2D_{\parallel}\omega}} \qquad (1)$$

where $D_{\parallel}$ is the diffusion rate of spinon, $\omega = \gamma_e B$ is the Larmor frequency and A is the scalar hyperfine coupling constant[3]. In order to determine $D_{\parallel}$ and its temperature dependence quantitatively, a Muon level-crossing resonance measurements (LCR) of the Pd(dmit)$_2$ molecule was made. For this purpose, we used (EtMe$_3$Sb)$_2$[Pd(dmit)$_2$], a non-magnetic material, instead of the neutral Pd(dmit)$_2$ molecule due to chemical stability issues.

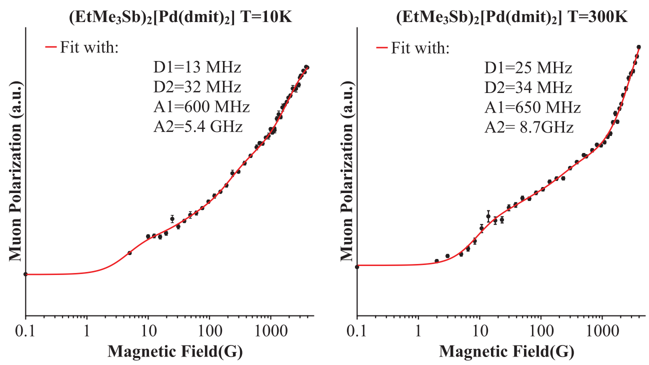

Fig. 1. Longitudinal polarization for the muon radical in (EtMe$_3$Sb)$_2$[Pd(dmit)$_2$] at 10K and 300K together with fitted repolarization curves..

Results of the longitudinal field dependence in (EtMe$_3$Sb)$_2$[Pd(dmit)$_2$] at port-2 of the RIKEN-RAL Muon facility are shown in Fig. 1. The Muon repolarization curve show no resonance in fields up to 0.4 Tesla and show an incredibly broad distribution of hyperfine couplings at 10K. Preliminary DFT calculation with muon radicals at the sulphur ends of the [Pd(dmit)$_2$]$^{-2}$ molecule predicts anisotropic hyperfine parameters (A, D1, D2)=(360, 11, 5) MHz and a resonance around 1T. Fit of the curves require at least a four-term equation with hyperfine values shown within the graph. The deduced values appear to be at least twice those found from the DFT calculation which support the hypothesis of the Muonium formation at the sulphur ends of the [Pd(dmit)$_2$]$^{-2}$ molecule. However another large hyperfine term with GHz values must be added to fit the repolarization curve indicating at least one more predominant Muonium site with a higher field resonance.

Further LCR measurements, in magnetic fields up to 5 Tesla in the Hi-Fi magnet at the ISIS muon facility have recently been awarded and will complete this study to understand the Muonium sites on a Pd(dmit)$_2$ molecule and the hyperfine coupling constant associated with such sites.

References
1) K. Kanoda and R. Kato: Annu. Rev. Condens. Matter Phys. **2**, 167-188 (2011).
2) M. Yamashita et al.: Science, **328**, 1246-1248 (2010).
3) F. L. Pratt et al.: Phys. Rev. Lett. **96**, 247203 (2006).

*1 Condensed Molecular Materials Laboratory, RIKEN
*2 Tokyo Medical University
*3 RIKEN Nishina Center
*4 ISIS Facility

Study on static and dynamic spin-crossover tripyrazolylmethane iron(II) complexes by using μSR spectroscopy

N. Kojima,[*1] H. Kobayashi,[*1] A. Okazawa,[*1] I. Kawasaki,[*2] and I. Watanabe[*2]

Transition-metal complexes have attracted much attention from the viewpoints of magnetic, redox, and optical properties originating from d spins. In particular, complexes with a d^4–d^7 configuration have the possibility of undergoing spin crossover transitions between low-spin (LS) and high-spin (HS) states, showing bistability with color and magnetic susceptibility changes. Spin-crossover phenomena can be classified into two types according to the time window of a measurement, (i) static spin crossover, which is often observed with a thermal hysteresis, and (ii) dynamic spin crossover, which sometimes shows an equilibrium obeying the van't Hoff equation (i.e., spin equilibrium).

A large number of spin-crossover iron(II) complexes have been developed and their spin dynamics has been investigated by means of Mössbauer spectroscopy, nuclear magnetic resonance, neutron scattering, etc. Muon spin relaxation (μSR) spectroscopy, which has the unique time range (10^{-5} ~ 10^{-11} s) to observe magnetic fluctuations, is useful for the investigation of spin-crossover phenomena. However, the μSR spectroscopy has scarcely been applied to the study of dynamic spin-crossover systems. To investigate the rapid spin equilibrium in detail, we selected iron(II) complexes containing tripyrazolylmethane ligands (Fig. 1), $[Fe\{(pz)_3CH\}_2](BF_4)_2$ (**1**; pz = 1-pyrazolyl) and $[Fe\{(pz)_3CH\}\{(3,5\text{-}Me_2pz)_3CH\}](BF_4)_2$ (**2**), which show dynamic and static spin crossover, respectively, on ^{57}Fe Mössbauer spectroscopy.[1,2] Similar molecular structures of **1** and **2** facilitate μSR study. Thus, we can expect that positive muons would be trapped at the same sites in their compounds.

Polycrystalline samples of **1** and **2** were wrapped in silver foil and stuck to a silver plate. We used He-flow cryostats in the temperature range between 50 and 475 K for **1** and between 50 and 300 K for **2**. μSR time spectra were obtained in the zero field (ZF) and longitudinal field (LF) applied along the direction of the initial muon-spin polarization. LF-μSR spectra were analyzed using eq (1):

$$A(t) = a_f\exp(-\lambda_f t) + a_s\exp(-\lambda_s t) + a_{bg}, \qquad (1)$$

where a_f and a_s are initial asymmetries, λ_f and λ_s are the muon-spin relaxation rates for the fast and slow relaxation components, respectively. For ZF-μSR, we analyzed the spectra considering a single relaxation process ($a_s = 0$).

The LF-μSR spectra of both **1** and **2** show a similar tendency. In the spectra at 100 K corresponding to LS states, fast relaxations were observed for **1** and **2**, which were

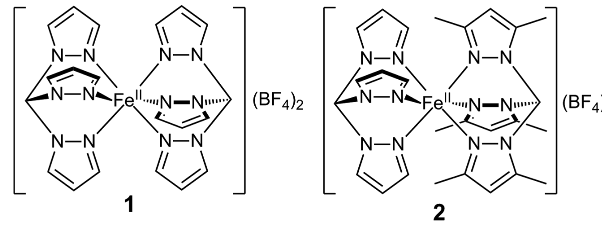

Fig. 1. Structural formula of $[Fe\{(pz)_3CH\}_2](BF_4)_2$ (**1**) and $[Fe\{(pz)_3CH\}\{(3,5\text{-}Me_2pz)_3CH\}](BF_4)_2$ (**2**).

decoupled by a field of 1000 Oe. The behavior indicates the formation of paramagnetic muonium species in pyrazolyl rings. The fluctuation can be completely decoupled at 3000 Oe.

On the other hand, the initial asymmetry in the HS states (**1**: 475 K; **2**: 300 K) is lower, even above 1000 Oe, compared to those in the LS states, suggesting the existence of other strong fluctuations. The time spectra of **1** and **2** in LF = 3000 Oe drastically changed with a change of temperature, and the relaxation rates (λ_f) derived from strong fluctuations increased on heating. We found that the temperature dependences of λ_f strongly correlate with $\chi_{mol}T$ vs T profiles (Fig. 2). Thus, the results clarified that μSR spectroscopy using a high LF can detect spin transitions in both dynamic and static spin-crossover complexes.

In the ZF-μSR spectra, there is an apparent difference between temperature dependences of the initial asymmetries of **1** and **2**. The initial asymmetry of **1** decreased around the spin transition, although that of **2** was constant over the entire temperature range. Such a decay is presumably caused by the spin fluctuation of the equilibrium between the HS and LS. The detailed analysis is now in progress.

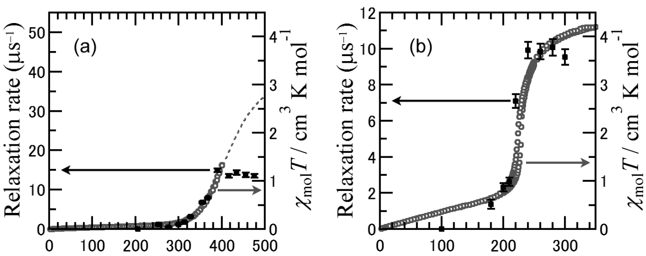

Fig. 2. Temperature dependences of relaxation rates (λ_f) under LF = 3000 Oe for (a) **1** and (b) **2**. The λ_f plots are superimposed on $\chi_{mol}T$ vs T plots.

References
1) D. L. Reger et al.: Inorg. Chem. **40**, 1508 (2001).
2) B. Moubaraki et al.: Dalton Trans. 4413 (2007).

*1 Graduate School of Arts and Sciences, The University of Tokyo
*2 RIKEN Nishina Center

Na dynamics in the quasi-one-dimensional ionic conductor NaM_2O$_4$ (M=Ti and V)

I. Umegaki,[*1] Y. Higuchi,[*1] M. Månsson,[*2] H. Sakurai,[*3] I. Kawasaki,[*4] I. Watanabe,[*4] and J. Sugiyama[*1]

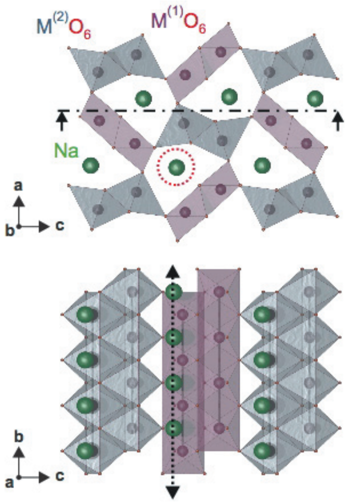

Fig. 1. Crystal structure of NaM_2O$_4$.

In the NaM_2O$_4$ lattice with a CaFe$_2$O$_4$-type orthorhombic structure, the Na^+ ions are located at the center of a one-dimensional (1D) tunnel along the b-axis, which is formed by 1D double chains consisting of edge-sharing MO$_6$ octahedra (M: transition metal) (see Fig. 1). The physical properties of NaM_2O$_4$ are reported to strongly depend on M. In particular, it is very important to clarify their Na^+-ion conductivity (σ_{Na}) and/or Na^+-ion diffusion coefficient (D_{Na}) when using NaM_2O$_4$ as a solid electrolyte in an all-solid-state Na-ion battery.

Following the preliminary report on NaV_2O_4[1)], we explain here in the results of μ^+SR measurements on NaM_2O$_4$ (M=Ti and V). The former is a semiconductor with a small band gap[2)], while the latter is a half metal with anisotropic electric conductivity[3)]. Both ZF- and LF-μ^+SR spectra were measured in the temperature (T) range between 145 and 500 K. The obtained spectra were fitted by a combination of an exponentially relaxing dynamic Kubo-Toyabe signal from a sample and a non-relaxing background signal from a titanium sample holder.

Figure 2 shows the T dependences of field fluctuation rate (ν), field distribution width (Δ), and exponential relaxation rate (λ) for (a) $NaTi_2O_4$ and (b) NaV_2O_4. For $NaTi_2O_4$, as T increases from 150 K, Δ slowly decreases, while ν increases rapidly particularly above 350 K. This indicates that the local nuclear magnetic

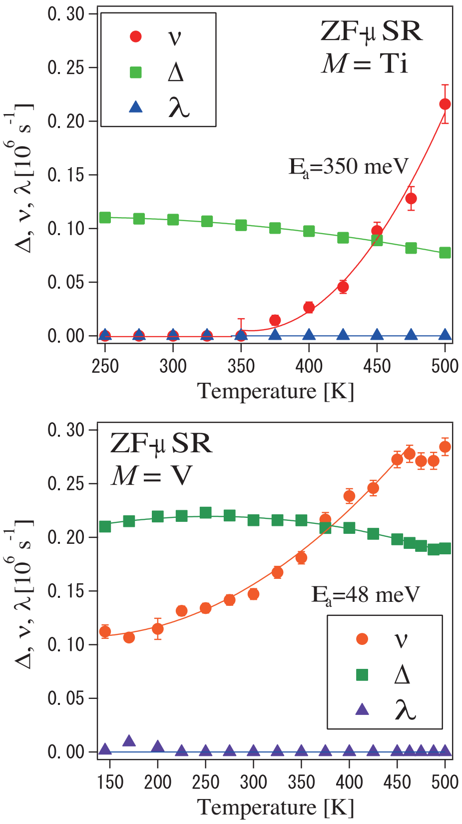

Fig. 2. T-dependences of field fluctuation rate (ν), field distribution width (Δ), and exponential relaxation rate (λ) for (a) $NaTi_2O_4$ and (b) NaV_2O_4.

field experienced by μ^+ starts to fluctuate because of Na^+ diffusion. For NaV_2O_4, on the other hand, even at 150 K ν is comparable to that for $NaTi_2O_4$ at 450 K. This indicates that Na^+ ions diffuse even at 150 K in NaV_2O_4. The anomaly around 450 K in the $\nu(T)$ curve is probably caused by a structural phase transition.

If we assume a thermal activation process for the T dependence of ν, the activation energy (E_a) is estimated to be 350 meV for $NaTi_2O_4$ and 48 meV for NaV_2O_4. Since the simple Nernst-Einstein equation states that $\sigma_{Na} \propto D_{Na}$, where $D \propto \nu$, NaV_2O_4 is expected to be a good candidate for a Na^+-ionic conductor.

References
1) J. Sugiyama et al.: RIKEN Accel. Prog. Rep. 45, 197 (2012).
2) M. J. Geselbracht et al.: J. Solid State Chem. 179, 3489 (2006).
3) K. Yamaura et al.: Phys. Rev. Lett. 99, 196601 (2007).

*1 Toyota Central Research and Development Labs., Inc.
*2 École polytechnique fédérale de Lausanne and Paul Scherrer Institut
*3 National Institute for Materials Science (NIMS)
*4 RIKEN Nishina Center

Lithium-ion diffusion in novel battery materials

J. Sugiyama,[*1] H. Nozaki,[*1] M. Harada,[*1] Y. Higuchi,[*1] I. Umegaki,[*1] K. Mukai,[*1] M. Månsson,[*2] and I. Watanabe[*3]

Diffusion coefficient of Li^+ ions (D_{Li}) in solids is usually evaluated by ^{7}Li-NMR.[1)] However, for materials containing magnetic ions, Li-NMR provides very limited information on D_{Li}, because of the effect of electron spins on the spin-lattice relaxation rate ($1/T_1$).[2,3)] Note that positive electrode materials of Li-ion batteries all include transition metal ions to compensate charge neutrality during the Li^+ intercalation and deintercalation reaction. On the contrary, μ^+ *sees* an internal magnetic field caused by both electrons and nuclei in a zero field (ZF). Thus, μ^+SR extracts the nuclear field even in such positive electrode materials[4)] by combining with weak longitudinal field (LF) measurements.[5)] For the positive electrode materials, since Li ions are known to be more mobile than μ^+ due to a strong μ^+-O bond, the hopping rate (ν) estimated by μ^+SR reflects the dynamics of the Li ions.[4,6)]

A solid solution system between $LiCoO_2$ and $LiNiO_2$, i.e. $Li(Co_{1-x}Ni_x)O_2$ in the rhombohedral symmetry with space group $R\bar{3}m$ is widely used in commercial Li-ion batteries. According to the previous experiment on $Li(Co_{1-x}Ni_x)O_2$ with $x = 0$, 0.33, 0.67, and 1, ν above ambient T drastically increased with increasing x. Since the $\nu(T)$ curve for the $x = 0.67$ sample is clearly different from that for $LiNiO_2$, we have measured ZF- and LF- spectra for the samples with $x = 0.85$, 0.90, and 0.95.

Figure 1 shows the T dependences of the field distribution width (Δ) and ν for the $x = 0.67 - 1$ samples. For all the samples, as T increases from 50 K, Δ decreases linearly up to $\sim$ 250 K, then looks to be T-independent until $\sim$ 400 K, and finally decreases with further increasing T. Here, Δ is mainly determined by the nuclear field of Li, because μ^+ locates at the vicinity of the O^{2-} ion with $d_{\mu-O} = 1$ Å, but not in the $Co_{1-x}Ni_xO_6$ octahedron. As a result, Δ is not sensitive to x. On the other hand, for the present three samples, ν increases with T until 225 K, then decreases with T until 450 K, and then increases again with T.

Note that a stoichiometric $LiNiO_2$ has never been obtained by a solid state reaction technique. A small amount of Ni ions are always located in the Li plane[7)] due to the similarity in ionic radii between Li^+ and Ni^{3+} (see Fig. 2). Thus, the correct formula of $LiNiO_2$ is $(Li^+_{1-y}Ni^{2+}_y)(Ni^{3+}_{1-y}Ni^{2+}_y)O_2$ with $y \leq 0.02$. The Ni ions in the Li plane suppress Li-diffusion.[6)] But, Co substitution for Ni is known to reduce y.[8)] Thus, it is expected that Li-diffusion increases with the Co content, against to the present result. In order to further understand the diffusion nature, it is highly required to investigate the Li-deficient samples, which is prepared by the Li^+ deintercalation reaction, with μ^+SR, because the direct jump of Li^+ from the regular site to the nearest deficient site is predominant for Li-diffusion.

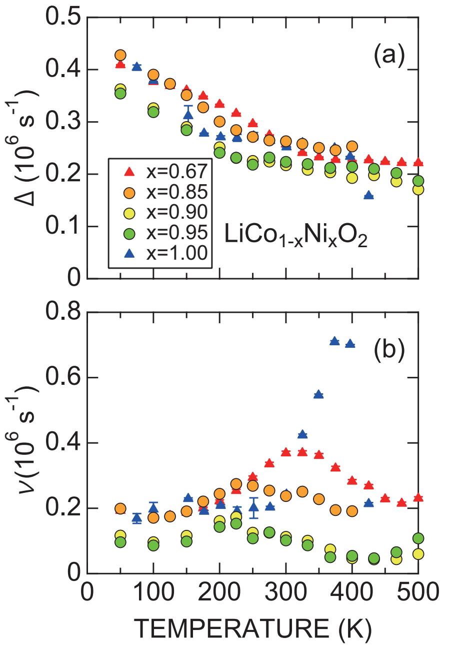

Fig. 1. Temperature dependences of Δ and ν for $LiCo_{1-x}Ni_xO_2$ with $x = 0.67$, 0.85, 0.90, 0.95, and 1.

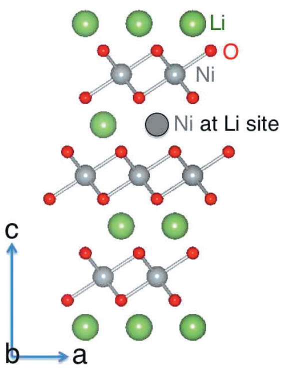

Fig. 2. Crystal structure of $LiNiO_2$.

References
1) P. Heitjans and S. Indris, J. Phys.: Condens. Matter, **15**, R1257 (2003).
2) C. P. Grey and N. Dupré, Chem. Rev. **104**, 4493 (2004).
3) K. Nakamura, Solid State Ionics **121**, 301 (1999).
4) J. Sugiyama *et al.*, Phys. Rev. Lett. **103**, 147601 (2009).
5) R. S. Hayano *et al.*, PRB **20**, 850 (1979).
6) J. Sugiyama *et al.*, Phys. Rev. B **82**, 224412 (2010).
7) J. E. Reimers *et al.*, Solid State Chem. **102**, 542 (1993).
8) T. Ohzuku *et al.*, Electrochim. Acta **38**, 1159 (1993).

[*1] Toyota Central Research and Development Labs., Inc.
[*2] EPFL & PSI, Switzerland
[*3] RIKEN Nishina Center

Muon Detection of Spin-Polarized Conduction Electrons Induced by Circularly-Polarized Direct Band Excitation in n-type Si

H.W.K. Tom,[*1] K. Nagamine,[*1,*2] K. Shimomura,[*2] K. Yokoyama,[*3] J. Muse,[*1] K. Ishida,[*3] F.L. Pratt,[*4] I. Shiraki,[*5] A.D. Pant,[*5] and E. Torikai[*5]

We investigated the possibility that muon spin-relaxation can be used to detect the spin-polarization of conduction electrons in the indirect bandgap semiconductor Silicon. Spin-polarized conduction electrons can be detected optically in direct bandgap semiconductors (i.e., GaAs) through known selection rules at the bandgap. However, Silicon, arguably the most technologically important semiconductor, has no optical analog due to its indirect bandgap. μSR has intrinsic spin-polarization sensitivity and, if able to detect spin polarization in Silicon, may advance Si spintronics. Implanted muons in Si interact with electrons to form bound muonium states. In a mechanism originally proposed by Torikai[1)], anti-parallel conduction electrons may exchange with parallel bound electrons in triplet muonium converting it to singlet muonium which would be detectable by enhanced depolarization of the muon spin.

Earlier we demonstrated that μSR was sensitive to laser-injected spin-polarized electrons in n-GaAs[2)]. Circularly-polarized, 7 ns duration, laser pulses with photon energy tuned below bandgap injected 50% spin-polarized electrons throughout the bulk of a 350 micron thick wafer. Experiments at all B-field and wavelengths are consistent with the laser-excitation enhancing spin-relaxation of muons in only one species, Mu^-. The amplitude reduction is larger for anti-parallel polarized conduction electrons consistent with the proposed exchange mechanism.

We performed similar experiments on n-Si. Although it is generally accepted that optical spin-injection is forbidden by the indirect bandgap of Si, a recent density functional theory calculation by Nastos, et al.[4)] shows that at the direct bandgap, the degeneracy factors for the transitions are as shown in Fig. 1 (left)) and lead to a degree of spin polarization vs photon energy shown in Fig. 1 (right).

Samples were 300 μm thick wafers of n-Si with evaporated Au and ITO (Indium Tin Oxide) electrodes for voltage-biased transport of the injected electrons. Muons were implanted in the 100 μm region closest to the laser-excitation side of the sample. Typical data are as shown in Fig. 2 (Left), for the case of B=1000 G at 20K. The laser pulse arriving at 0.8 μs induces a step-like change in the F-B asymmetry that can reduce as much as 50% of the total F-B asymmetry in <300 ns. Unlike GaAs, however, the laser-induced change effects multiple species. Three species are known in n-Si: Tetrahedral (T) muonium, bond-centered (BC) muonium, and the negative ion (T) Mu^-.

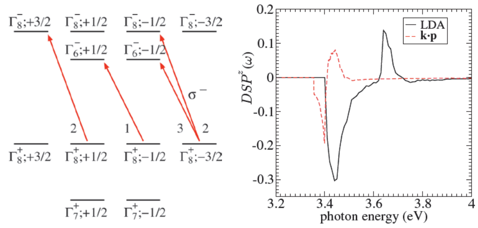

Fig. 1: Ref [4]. (L) Si interband transition degeneracies for σ^- excitation. (R) Degree of Spin Polarization vs photon energy in LDA and k·p approximations.

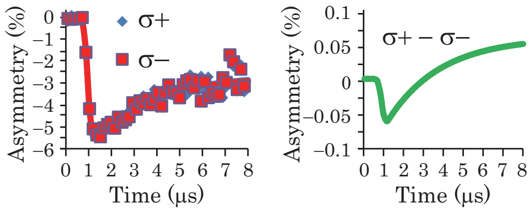

Fig. 2. (Left) n-Si F-B Asymmetry change induced by 372 nm laser excitation. σ^+ and σ^- changes and best fit. (Right) σ^+-σ^- best fit difference.

F-B Asymmetry vs time without laser excitation shows a fixed component and an exponentially decaying component, fitting A+Bexp(-γt). The laser-induced change (σ^+-Laser off) and (σ^--Laser off) can be fit by ΔA+ΔB exp(-γt). Here ΔA and ΔB are both ~ -2.5%. The solid blue and red lines are the best fits to the data for σ^+ and σ^-. The difference between the best fit lines (σ^+- σ^-) is shown in Fig. 2 (right). Spin-dependent ΔA_{+-}=0.073±0.082 and ΔB_{+-}=-0.14±0.13 with 25M events for each laser helicity (100M events total, 50M laser off). We will need significantly higher statistics (15X) to resolve this effect at <0.02% F-B asymmetry. We repeated this measurement at 12 photon energies spanning 3.32 to 3.64 eV, the spectral range in Fig. 1. The signs of ΔA_{+-} and ΔB_{+-} are opposite to each other within experimental uncertainty for all 12 photon energies although the sign of ΔA_{+-} was not always positive. The opposing signs are experimentally significant for the data set as a whole, but we have no explanation presently.

Future followup experiments will require finding ways to restrict the μSR signal to one species such as via ALC resonance, increasing signal to noise and statistics, and/or finding the optical wavelength of maximum spin-injection by some other technique (e.g. spin-polarized fluorescence).

*1 Physics and Astronomy, University of California, Riverside
*2 Muon Science Laboratory, IMSS, KEK
*3 RIKEN Nishina Center
*4 ISIS, Rutherford Appleton Laboratory
*5 Medicine and Engineering, University of Yamanashi

References

1) E. Torikai, et al.: Physica B 289-290, 558 (2000).
2) K. Yokoyama, et al.: Physica B 404, 856 (2009); Physics Procedia 30, 231 (2012).
3) K.H. Chow, et al.: Phys. Rev. Lett. 76, 3790 (1996).
4) F. Nastos, et al.: Phys. Rev. B 76, 205113 (2007).

Response of muonium to oxygen impurities in hemoglobin and other biological aqueous solutions for application to studies on hypoxia

K. Nagamine,[*1, *2, *3] A.D. Pant,[*4] E. Torikai,[*4] K.Shimomura,[*3] F.L. Pratt,[*5] H. Ariga,[*6] K. Ishida,[*7] and J.S. Schultz[*7]

Hypoxia, or low oxygenation, is known as an important factor in tumor biology; in cancer patients, an accurate measurement of O_2 concentration in specific regions may prove important in the management of treatment and outcome of the disease[1]. For this purpose, improved O_2 detection methods are required. Several trials that employ PET, MRI and EPR have been conducted[1].

In this article, we propose the use of μ^+ as a new sensitive method to probe the existence of paramagnetic O_2 in cancerous tumors in the human body. The μ^+ in water is known to take the states of diamagnetic μ^+ such as μ^+OH (60%), paramagnetic muonium (Mu, $\mu^+ + e^-$) (20%), and a missing fraction (20%). In Mu, a half becomes an ortho state with spin 1, providing a spin rotation signal with a precession pattern (1.39 MHz/G) that is 100 times faster than that of diamagnetic μ^+. There have been experimental studies on the oxygen-dissolving effects of the spin relaxation rate (λ_{Mu}) of paramagnetic Mu in pure water due to electron spin exchange interactions with paramagnetic O_2 in water; the rate change of λ_{Mu} against O_2 concentration is $(1.8 \pm 0.1) \times 10^{10}$ (litr/mol) s^{-1}[2]. The sensitivity for $PO_2(\mu)$ in pulsed μSR becomes $0.5 \times 10^{-6} \sim 0.5 \times 10^{-3}$ (mol/litr). The $PO_2(\mu)/PO_2$(s.l.) becomes $0.4 \times 10^{-3} \sim 0.4$, which perfectly corresponds to the condition in hypoxia. The unsolved problem regarding the muon method is the background effect of other magnetic molecules, which provides the motivation for the present study.

The experiment was conducted at Port 2 of RIKEN-RAL using 60 MeV/c decay positive muons. Spin rotation and its relaxation were detected under 2.2 G transverse fields and at room temperature. In pure water, the Mu spin precession was found to achieve faster relaxation against increase in O_2, and this result is consistent with the existing data[2].

The biological samples are as follows. 1) **Albumin:** Bovin serum (plasma) albumin is a single polypeptide chain consisting of about 583 amino acid residues and no carbohydrates. 2) **Serum:** Donor horse serum is sterile filtered serum that has been screened for mycoplasma and adventitous viruses. 3) **Hemoglobin** (Hb): Polymerized hemoglobin of bovine origin in a lactated Ringer's solution at 13 % concentration. It is violet-colored taken and is as deoxy-Hb.

Before measuring the O_2 dependence of $\lambda_{Mu,}$ its dependence on the concentration of each biological molecule was systematically measured. The decreasing rate of λ_{Mu} was obtained as 25 MHz/(g/litr) for albumin, 1 MHz/(vol. %) for serum and 3.1 MHz/(g/litr) for Hb

Then, by determining the relevant concentration for each molecule, the O_2 dependence of λ_{Mu} was measured. The results for these three aqueous solutions are summarized in Fig. 1. The λ_{Mu} in these biological aqueous solutions was found to experience an almost similar change in relaxation against increasing O_2 concentration as that for pure water. For Hb, λ_{Mu} was expected to exhbit a different behavior since the increase in O_2 makes decrease of magnetic Deoxy-Hb and increase of non-magnetic Oxy-Hb causing the decrease in λ_{Mu}. By solving Hill's equation[3], such an effect can be predicted. The obtained result is very encouraging for application to hypoxia; there is one-to-one correspondence between λ_{Mu} and O_2 concentration, which allows the unique determination of PO_2

Before carrying out the clinical application of the proposed method to studies on hypoxia, it is important to conduct systematic studies on the behavior of O_2 impurities in various other biological aqueous systems, especially with high-concentration Hb. On the other hand, by using the concept of the advanced μ^+ beam, which is an accelerated beam of ultra-slow muon, one can expect the stopping region confinement to be 10 μm^3 at cm-region depth of the human body. Thus, we are approaching a realization of the advanced cancer inspection by using muons appears possible.

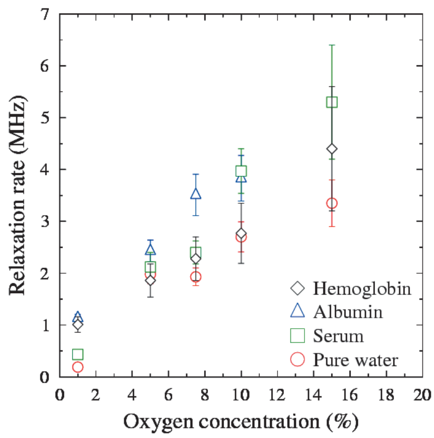

Fig. 1 Summary of dependence on O_2 concentration of muonium relaxation rates in pure water and water solution of 0.04 wt. % albumin, 0.5 vol. % serum and 0.07 wt. % hemoglobin.

[*1]Atomic Physics Laboratory, RIKEN
[*2]Physics & Astronomy, University of California, Riverside
[*3]Muon Science Laboratory, IMSS, KEK
[*4]Medicine and Engineering, University of Yamanashi
[*5]ISIS, Rutherford Appleton Laboratory
[*6]Catalysis Research Center, Hokkaido University
[*7]RIKEN Nishina Center
[*8]Bio-Engineering, University of California, Riverside

References
1) J.L. Tatum et al., *Int. J. Radiat. Biol.* **82**, 699 (2006).
2) E. Roduner et al., *J. Chem. Faraday Trans.* **91**, 1935 (1995).
3) M. Samaja et al., *Clin. Chem.* **20**, 110 (1983).
4) K. Nagamine, *J. Phys. Soc. Japan*, in press (2014).

Development of room-temperature thermal-muonium-emitting material for ultra-slow muon production

S. Okada,[*1] P. Bakule,[*2] G.A. Beer,[*3] Y. Fujiwara,[*1,*4] K. Ishida,[*1] M. Iwasaki,[*1] S. Kanda,[*1,*4] H. Kawai,[*5] N. Kawamura,[*6] R. Kitamura,[*4] W. Lee,[*7] G.M. Marshall,[*8] Y. Matsuda,[*9] T. Mibe,[*10] Y. Miyake,[*6] S. Nishimura,[*4] Y. Oishi,[*1] A. Olin,[*3,*8] N. Saito,[*4,*10] K. Shimomura,[*6] P. Strasser,[*6] M. Tabata,[*5,*11] D. Tomono,[*12] K. Ueno,[*10] E. Won,[*7] and K. Yokoyama[*13]

Ultra-slow muons, which are positive muons having an energy of a few electron volts, are useful tools for producing variable-energy muon beams with extraordinarily small energy spread by accelerating them through an electrostatic field. This technique will extend μSR (muon spin rotation and relaxation) studies to thin films, surfaces and interfaces, and nanostructures, which has not yet been achieved by the conventional μSR technique using surface muons. This technique has also attracted attention for use in measuring the muon anomalous magnetic moment g-2 and electric dipole moment at J-PARC[1)], which requires an intense muon beam having an extremely small transverse momentum.

Ultra-slow muon production has been realized by two-photon resonant laser ionization of thermal muonium atoms (μ^+e^-, Mu) emitted into vacuum, where tungsten foils heated to 2300 K have been employed as a Mu-emitting material[2)].

On the other hand, silica (SiO_2) powder is known as a Mu-emitting material at room temperature[3)]. The room-temperature target resulting in even lower Mu energies than that from a hot tungsten target (2300 K $\rightarrow$ 300 K) has the following significant merits:

- Experimentally easy to handle in terms of the operation temperature (no large radiant heat)
- Smaller emittance of the ionized source due to the lower energies
- Smaller spatial spread and smaller Doppler broadening of the resonant line for Mu excitation (as a result of the lower Mu energy distribution), leading to a more efficient use of the available laser power

Despite the many advantages, silica powder has not yet been employed for ultra-slow muon production. This is simply because powdery materials are not self-standing and are generally unfavorable in terms of handling and vacuum pumping.

In the TRIUMF S1249 experiment, we have investigated the possible use of a silica aerogel that has the same chemical composition as silica powder but is a self-standing solid with extremely low density.

In the earlier measurement of S1249, Mu emission from silica aerogel into vacuum has been successfully observed[4)], and the recent measurement (in Oct 2013) yielded promising results in terms of the Mu emission yields with aerogels having a surface with sub-millimeter structures such as pores (which increase surface area), e.g., laser-drilled aerogel, as shown in the insets of Fig. 1. This result indicates that Mus produced near the surface of the aerogel are essential for vacuum emission. Detailed data analysis is now in progress.

For practical-scale development, we are now preparing an ultra-slow muon beamline dedicated to the research and development of practical ultra-slow muon production with room-temperature targets at RIKEN-RAL port3.

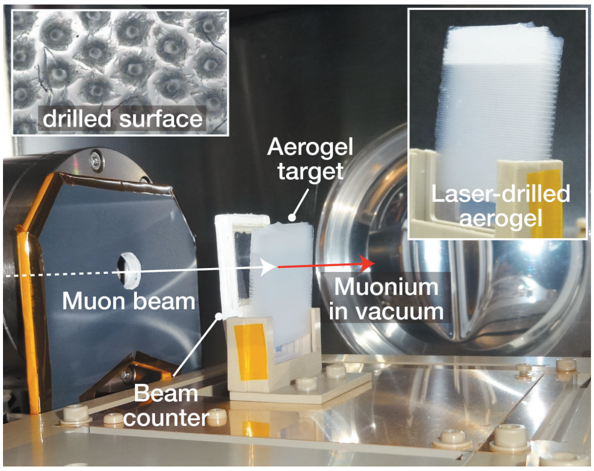

Fig. 1. Photograph of the experimental setup of the recent TRIUMF S1249 experiment. The insets show a laser-drilled aerogel used as a Mu-emitting material (right) and the surface (left).

*1 RIKEN Nishina Center
*2 ELI Beamlines Project Division, FZU
*3 Department of Physics and Astronomy, UVic
*4 Department of Physics, The University of Tokyo
*5 Department of Physics, Chiba University
*6 IMSS, KEK
*7 Department of Physics, Korea University
*8 Science Division, TRIUMF
*9 Department of Basic Science, The University of Tokyo
*10 IPNS, KEK
*11 ISAS, JAXA
*12 Department of Physics, Kyoto University
*13 School of Physics and Astronomy, QMUL

References

1) T. Nagae (ed): Prog. Theor. Exp. Phys., Special issue 2 (2012).
2) K. Nagamine et al.: Phys. Rev. Lett. **74**, 4811 (1995); P. Bakule et al., NIM B **266**, 355 (2008).
3) G. A. Beer et al.: Phys. Rev. Lett. **57**, 671 (1986).
4) P. Bakule et al.: Prog. Theor. Exp. Phys., 103C01 (2013).

Precision measurement of muonium hyperfine splitting at J-PARC; development of high-rate positron detector

S. Kanda,[*1,*2] on behalf of J-PARC MuHFS Collaboration

Muonium is the bound state of a positive muon and an electron. In the standard model of particle physics, muonium is considered as the two-body system of structureless leptons.

At J-PARC, we plan to measure muonium's hyperfine splitting precisely. Our experiment has three major objectives: test of QED with the highest accuracy, precision measurement of the ratio of muon's magnetic moment to proton's magnetic moment, and search for CPT violation via the oscillation with sidereal variations.

The experimental methodology is microwave spectroscopy of muonium. Figure 1 shows the conceptual overview of the experiment. Spectroscopy of the energy states can be performed by measurement of positron decay asymmetry.

The uncertainty of the most recent experimental result[1] was mostly statistical (more than 90% of total uncertainty). Hence, improved statistics is essential for higher precision of the measurement. Our goal is to improve accuracy by an order of magnitude compared to the most recent experiment. For the improvement of precision, we use the J-PARC's highest-intensity pulsed muon beam and highly segmented positron detector with SiPM (Silicon PhotoMultiplier). After the improvement of statistical precision, reduction of systematic uncertainty becomes more important to reduce systematic uncertainty. Thus, we reduce the systematic uncertainty by using a longer cavity, a high-precision superconducting magnet, and an online/offline beam profile monitor.

The detector system consists of several layers of hodoscopes and fast readout circuits with custom ASIC and FPGA-based multi hit TDC. Important requirements of the positron detector are high event rate capability and high detection efficiency. The designed muon beam intensity at J-PARC MUSE H-Line is $1 \times 10^8\ \mu^+/\mathrm{s}$.

To establish the optimal design of the positron detector, we developed GEANT4-based Monte-Carlo simulation tools. Figure 2 shows a simulated muon stopping distribution in the target gas chamber. Under realistic conditions, the highest instantaneous event rate is about 3 MHz/cm^2. The resonance lineshape was calculated numerically, and the systematic uncertainty of the resonance frequency due to the detector specification was evaluated as a function of the detector performance. Based on the results of the simulation study, a new prototype of the detector is under development and a test experiment with high-intensity pulsed muon beam at J-PARC was performed in February of 2014.

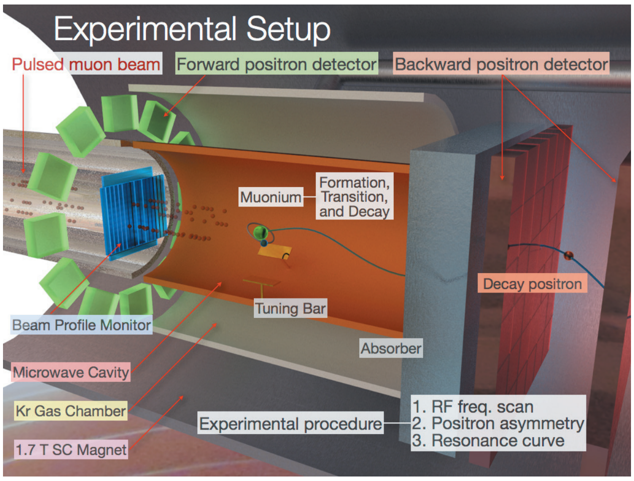

Fig. 1. Experimental overview

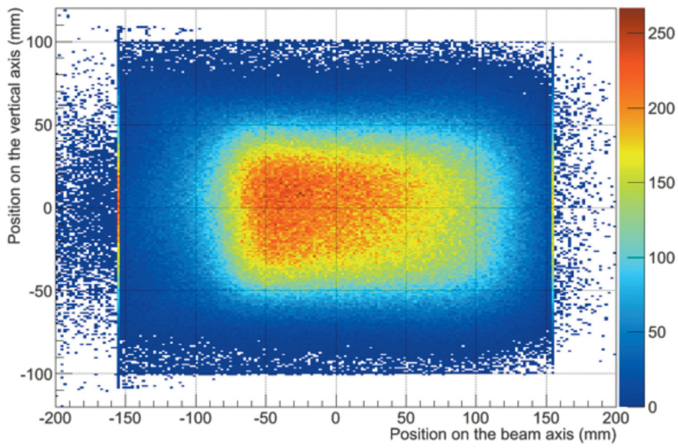

Fig. 2. Simulated muon stopping distribution

References
1) W. Liu et al.: PRL. 82, 711 (1999).
2) S. Kanda et al.: KEK-MSL Progress Report 2012B0117 (2013)
3) S. Kanda et al.: Proceedings of the USM2013 (to be published)

*1 RIKEN Nishina Center
*2 Department of Physics, University of Tokyo

3. Radiochemistry and Nuclear Chemistry

Cross-section measurement of the ^{248}Cm(^{19}F,5n)^{262}Db reaction

M. Murakami,[*1,*2] S. Goto,[*1] K. Ooe,[*1] S. Tsuto,[*1] R. Aono,[*1] H. Haba,[*2] M. Huang,[*2] J. Kanaya,[*2] S. Shibata,[*2] and H. Kudo[*1]

The isotope ^{262}Db ($T_{1/2}$ = 33.8 s[1)]) is used in the chemical studies of element 105, Db. One of the commonly used direct synthetic routes of ^{262}Db is the reaction of ^{19}F with ^{248}Cm. Few cross sections are available for this reaction, but there is a large discrepancy among these data. Dressler et al.[2)] reported a production cross section of $0.26^{+0.15}_{-0.09}$ nb at 106.5 MeV. Nagame et al.[3)] reported a cross section of 1.3 ± 0.4 nb at nearly the same energy, 106 MeV. The same group also reported a maximum cross section of 1.5 ± 0.4 nb at 103 MeV.[4)] Thus, the cross-section data are inadequate, and the optimal beam energy to produce ^{262}Db is not clear. Therefore, we plan to measure the excitation function of the ^{248}Cm(^{19}F,5n)^{262}Db reaction to effectively produce ^{262}Db for the future chemical experiments of Db. First, in this work, we produced ^{262}Db at 102 MeV.

A $^{248}Cm_2O_3$ target of 460-μg/cm^2 thickness and 9-mm diameter was prepared by electrodeposition onto a Be foil of 1.8-mg/cm^2 thickness. $^{nat}Gd_2O_3$ of 23-μg/cm^2 thickness was admixed with the target material to simultaneously produce ^{170}Ta ($T_{1/2}$ = 6.76 min) via the ^{nat}Gd(^{19}F,xn)^{170}Ta reaction. A $^{19}F^{7+}$ beam of 124.9 MeV supplied by the AVF cyclotron was passed through a 3.2-mg/cm^2 Be vacuum window, 0.10 mg/cm^2 of He cooling gas, and the Be backing foil before it entered the target. The primary beam energy was measured using time-of-flight apparatus. The beam energy at the middle of the target was 101.9 MeV, and the energy degradation in the target was estimated to be 1.0 MeV. The average beam intensity was approximately 440 pnA.

The reaction products recoiling out of the target were stopped in 102.0-kPa He gas in the recoil chamber, attached to KCl aerosols generated by sublimation of KCl powder at 640°C, and continuously transported with a flow rate of 2.5 L/min to the rotating wheel detection system MANON (Measurement system for Alpha-particle and spontaneous fissioN ON-line) through a 8.6-m Teflon capillary with 1.59-mm inner diameter. MANON has 7 pairs of Si PIN photodiodes, and the counting efficiency of each photodiode was 38%. In MANON, the aerosols were deposited on Mylar foils of 0.5-μm thickness, 40 of which were set on the periphery of a rotating wheel 420 mm in diameter. The gas-jet transport efficiency was estimated to be 53.5 ± 2.0% by comparing the collected yields of ^{170}Ta on the 10-μm Be catcher foil placed immediately behind the target and on the Al foil set to the position of the Mylar foil in MANON. After the aerosol collection, the wheel was stepped at 20-s nominal interval to move the foils between the detector pair. Because the long-lived activities were accumulated during the irradiation, the wheels containing the Mylar foils were replaced every 6 h. While exchanging the wheels, the aerosols were collected on the glass filters in the collection chamber, and the glass filters were subjected to γ-ray spectrometry to verify whether the yields of ^{170}Ta were stable.

Figure 1 shows the sum of the measured α-spectra in the 2nd–7th top detectors, corresponding to a time interval of 20–140 s. A beam dose of 1.91 × 10^{17} was accumulated. In Fig. 1, α events of ^{262}Db (α branch b_α = 48%, α energies E_α = 8.46 MeV (70%) and 8.68 MeV (30%)[1)]) and its daughter nuclide ^{258}Lr ($T_{1/2}$ = 3.9 s, b_α = 97.4%, E_α = 8.565, 8.595, 8.621, and 8.654 MeV[5)]) are clearly recognized. However, α lines of by-products such as Po isotopes are also observed in the α-energy region of ^{262}Db and ^{258}Lr. Analyses of the time-correlated α-α pairs are needed to extract the decay chains of $^{262}\text{Db} \xrightarrow{\alpha} {}^{258}\text{Lr} \xrightarrow{\alpha}$. Further analyses of the obtained data are in progress.

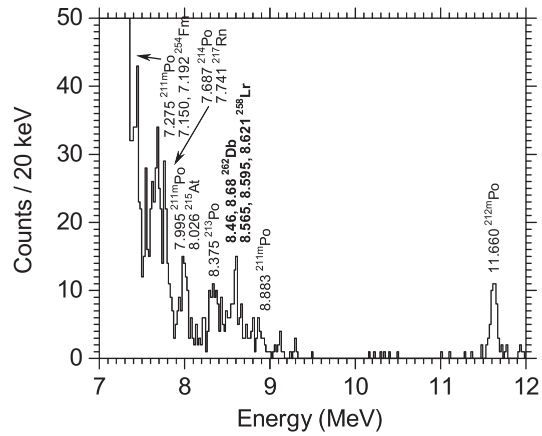

Fig. 1. Sum of α spectra measured in the 2nd–7th top detectors of MANON.

References

1) H. Haba et al.: In this report.
2) R. Dressler et al.: Phys. Rev. C **59**, 3433 (1999).
3) Y. Nagame et al.: J. Nucl. Radiochem. Sci. **3**, 85 (2002).
4) K. Tsukada et al.: Radiochim. Acta **97**, 83 (2009).
5) R. B. Firestone and V. S. Shirley: *Table of Isotopes, 8th ed.* (John Wiley & Sons, 1996).

*1 Department of Chemistry, Niigata University
*2 RIKEN Nishina Center

Excitation functions for production of Nb and Ta isotopes in the (d,x) reactions on ^{nat}Zr and ^{nat}Hf up to 24 MeV

M. Murakami,[*1,*2] H. Haba,[*1] S. Goto,[*2] and H. Kudo[*2]

The isotopes ^{95g}Nb ($T_{1/2}$ = 34.991 d) and ^{179}Ta ($T_{1/2}$ = 1.82 y) are useful radiotracers for the basic studies of the element 105, Db. We have investigated the production of these radiotracers by the activation of ^{nat}Zr and ^{nat}Hf with a 14-MeV proton beam supplied by the RIKEN AVF cyclotron.[1)] From the AVF cyclotron, a deuteron beam is also available.[2,3)] Activation by the deuteron beam is one of the widely used and well-studied methods to produce the radiotracers. However, the production cross sections of ^{95g}Nb by the (d,x) reaction are scanty compared to those of the (p,x) reactions. Furthermore, the cross sections of ^{179}Ta in the (d,x) reaction have not been reported. In this work, we measured the excitation functions for the production of ^{95g}Nb and ^{179}Ta as well as other isotopes in the (d,x) reactions on ^{nat}Zr and ^{nat}Hf.

The excitation functions were measured with a stacked-foil technique. For the measurement of the cross sections of Nb isotopes, thin foils of ^{nat}Zr (20 μm thickness), ^{nat}Ti (20 μm thickness), and ^{nat}Ta (20 μm and 10 μm thickness) were stacked alternately and used as a target. The ^{nat}Ti foils were used to determine the beam energy and intensity by measuring the excitation function of the ^{nat}Ti$(d,x)^{48}$V reaction, and the ^{nat}Ta foils were also used as the energy degrader. For measurement of the cross sections of Ta isotopes, thin foils of ^{nat}Hf (25 μm thickness) and ^{nat}Ti (20 μm thickness) were stacked alternately. The size of all the foils was 15 × 15 mm^2. Both stacks were irradiated by the 24-MeV deuteron beam supplied by the AVF cyclotron for 30 min. The beam was collimated to a diameter of 9 mm, and the average beam currents were 0.48 μA and 046 μA for the Zr/Ti/Ta and Hf/Ti stacks, respectively. After irradiation and proper cooling, γ- and X-rays of each foil were measured by the Ge detectors.

The production cross sections were derived by the well-known activation formula.[4)] The beam energies in the individual target foils were calculated with the SRIM-2008 program.[5)] The experimental data were compared with the cross section data culculated by the TALYS-1.4 code.[6)]

The cross sections of ^{90g,91m,92m,95m,95g,96}Nb, ^{95,97}Zr, and ^{87m,87g,88}Y were measured in the ^{nat}Zr(d,x) reactions, whereas the production cross sections of ^{175,176,178,179,180g}Ta and ^{175,179m2,180m,181}Hf were measured in the ^{nat}Hf(d,x) reactions. Figure 1(a) shows the excitation function of the ^{nat}Zr$(d,x)^{95m+g}$Nb reaction. In Fig. 1(a), the cross sections reported by Gonchar et al.[7)], those reported by Tárkányi et al.,[8)] and those calculated by the TALYS code[6)] are compared. The data reported by Gonchar et al.[7)] and Tárkányi et al.[8)] show a similar shape of the excitation function with a systematically higher magnitude. The TALYS code also indicates a similar shape of the excitation function but lower values than the measured ones. The cross sections of the ^{nat}Hf$(d,x)^{179}$Ta reaction were measured for the first time, as shown in Fig. 1(b). The measured excitation function exhibits the maximum cross section of 489 ± 50 mb at 21.1 ± 0.4 MeV. Again, the calculated cross sections by TALYS indicate lower values, though the shape of the excitation function is similar.

Thick-target yields of ^{95m,g}Nb and ^{179}Ta were deduced from the measured cross sections and the stopping power given by the SRIM-2008 program.[5)] The deduced yields for beam energies up to 24 MeV were 1.3, 0.40, and 0.21 MBq/(μA·h) for ^{95m}Nb, ^{95g}Nb, and ^{179}Ta, respectively.

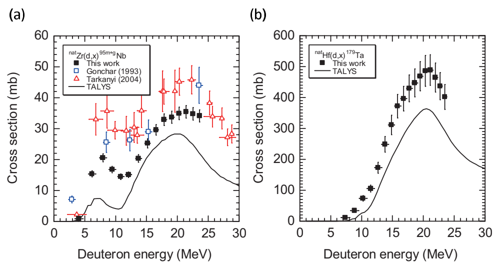

Fig. 1. Excitation functions of (a) ^{nat}Zr$(d,x)^{95m+g}$Nb reaction and (b) ^{nat}Hf$(d,x)^{179}$Ta reaction.

References
1) M. Murakami et al.: RIKEN Accel. Prog. Rep. **46**, 247 (2013).
2) M. U. Khandaker et al.: Nucl. Instrum. Methods Phys. Res. B **296**, 14 (2013).
3) M. U. Khandaker et al.: Nucl. Instrum. Methods Phys. Res. B **316**, 33 (2013).
4) M. S. Uddin et al.: Nucl. Instrum. Methods Phys. Res. B **258**, 313 (2007).
5) J. F. Ziegler et al.: Nucl. Instrum. Methods Phys. Res. B **268**, 1818 (2010).
6) A. J. Koning et al.: in *Proceedings of the International Conference on Nuclear Data for Science and Technology*, edited by O. Bersillon et al. (EDP Sciences, 2008), p. 211.
7) A. V. Gonchar et al.: Atomnaya Énergiya **75**, 205 (1993).
8) F. Tárkányi et al.: Nucl. Instrum. Methods Phys. Res. B **217**, 373 (2004).

*1 RIKEN Nishina Center
*2 Department of Chemistry, Niigata University

Production cross sections of (*d,x*) reactions on natural irons†

M. U. Khandaker,[*1] H. Haba,[*2] J. Kanaya,[*2] and N. Otsuka[*3]

The method for obtaining accurate information of light-charged-particle-induced reaction cross sections has generated significant interest in the nuclear data community because these reactions are being increasingly used in nuclear medicine, accelerator and nuclear technology, and the testing of nuclear reaction theories. Recently, we investigated the production cross sections of deuteron-induced radionuclides from various target elements because measured data of the (*d,x*) processes are limited compared to those of (*p,x*) processes. A survey of existing literature shows that several investigations have been conducted for the ^{nat}Fe(*d,x*) reactions, leading to various applications. The formation of the ^{55}Co radionuclide via the ^{nat}Fe(*d,x*) reaction is useful in PET imaging procedures, especially for diagnosing slower metabolic processes[1]. It also plays an important role as a label for bleomycin in diagnostic nuclear medicine, and more recently, in some cardiac and cerebral studies. Several authors[2] successfully applied ^{55}Co as a PET imaging agent in studies of ischemic stroke for quantifying cerebrospinal fluid kinetics in the brain, and they suggested that its effective clinical use is limited up to 48 h because of the production of the ^{56}Co contaminant. ^{55}Co was also applied as a potential renal imaging agent through the dynamic PET imaging of animal renal functions[3]. Therefore, accurate determination of the production cross sections of the ^{nat}Fe(*d,x*)^{55}Co reaction is required because of its great importance in various practical applications, especially in nuclear medicine.

The objective of the present study was to report the latest cross sections of the ^{nat}Fe(*d,x*)$^{55,56,57,58g+m}$Co, ^{52g,54,56}Mn, ^{51}Cr, ^{59}Fe reactions that were measured with a high precision over the energy range of 2–24 MeV using the AVF cyclotron facility of the RIKEN RI Beam Factory, Wako, Japan. Details on the irradiation technique, radioactivity determination, and data evaluation procedures are available in Ref.[4]. A brief description of the model codes used in this work is also available elsewhere[4]. Owing to the space limitation of this report, we present only the ^{nat}Fe(*d,x*)^{55}Co cross sections and the deduced yield in Figs. 1 and 2, respectively. Measured cross sections with an overall uncertainty of about 12% are listed in Ref.[4]. The cross-sections were normalized by using the ^{nat}Ti(*d,x*)^{48}V monitor cross sections recommended by IAEA. Measured data were critically compared with the available literature data, and an overall good agreement was found. However, only partial agreements were obtained with the data extracted from the TENDL-2012 library based on the TALYS code. The deduced thick-target yields indicate that a low-energy (<13 MeV) cyclotron and a highly enriched ^{54}Fe target could be used to obtain the high purity product ^{55}Co, which is a long-lived positron emitter used in clinical applications.

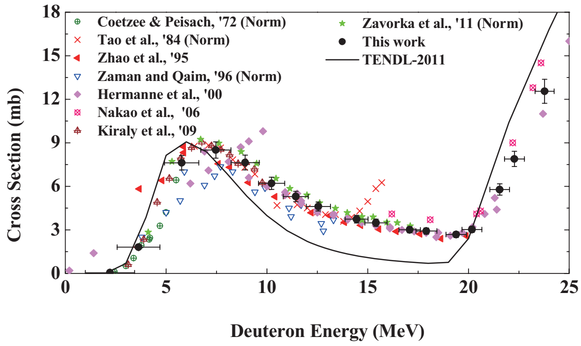

Fig. 1. Excitation function of the ^{nat}Fe(*d,x*)^{55}Co reaction.

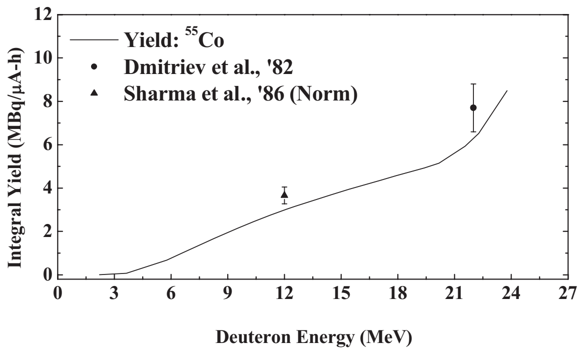

Fig. 2. Physical thick target yields for the ^{55}Co radionuclide.

References
1) H. Sharma, J. Zweit, A. M. Smith, S. Downey et al.: Appl. Radiat. Isot. **37,** 105 (1986).
2) J. De Reuck, K. Vonck, P. Santens, P. Boon, J. De Bleecker, K. Strijckmans, I. Lemahieu: J. Neurol. Sci. **181,** 13 (2000).
3) P. Goethals, A. Volkaert, C. Vandewielle, R. Dierckx, N. Lameire: Nucl. Med. Biol. **27,** 77 (2000).
4) M. U. Khandaker, H. Haba, J. Kanaya, N. Otuka: Nucl. Instrum. Methods Phys. Res. B **316,** 33 (2013).

† Condensed from the article in Nucl. Inst. Meths. B. **316**, 33 (2013).

*1 Department of Physics, University of Malaya, KualaLumpur, Malaysia
*2 RIKEN Nishina Center
*3 Nuclear Data Section, International Atomic Energy Agency, Austria

Deuteron activation cross sections for monitor reactions

N. Otuka,[*1,*2] H. Haba,[*1] M. Murakami,[*1] and M.U. Khandaker[*3]

Structural materials in fusion energy devices like ITER are expected to be exposed to intense neutron flux. Therefore, material tests are important in fusion energy technology. The International Fusion Material Irradiation Facility (IFMIF) is a candidate facility for material tests. Intense neutrons consisting of a peak around 15 MeV are planned to be produced in IFMIF using the ^{7}Li(d,n) reaction with intense (125 mA + 125 mA) deuteron beams that are accelerated to 35 to 40 MeV by two linear accelerators[1]. The prototype is under construction in Rokkasho, Japan within IFMIF Engineering Design Activities (IFMIF/EVEDA). In addition to generating high energy tail (d,n) neutrons up to 55 MeV, the deuteron beams also activate the surrounding materials of the test facility. To perform activation calculations[2] for radiation safety, it is necessary to measure the radioisotope production cross sections for deuteron induced reactions. Accordingly, a deuteron induced reaction sublibrary was added to the latest version of the Fusion Evaluated Nuclear Data Library (FENDL-3.0)[3]. Deuteron-induced reactions could also be useful for efficient radioisotope production. For various applications, we have started the measurements of radioisotope production cross sections for various deuteron-induced reactions by the AVF cyclotron of the RIKEN RIBF.

Radioisotope production cross sections for charged-particle induced reactions are often measured through monitor reactions. Recommended cross sections of various monitor reactions are distributed from the IAEA Nuclear Data Section[4,5], and we have also adopted their recommended ^{27}Al(d,x)^{24}Na and ^{nat}Ti(d,x)^{48}V cross sections in our experimental studies[6,7].

In addition to the best estimate of the cross sections, their uncertainties also become important for modern applications of nuclear reaction cross sections. This point has been stressed on for many decades for low energy neutron-induced reaction applications in relation to critical and radiation safety, and experimentalists are urged to perform error propagation and its documentation properly[8]. This is also a common issue for people who report charged-particle induced reaction cross sections for applications. The recommended cross section for the monitor reaction is a major source of the correlated uncertainty in various experimental works, and its uncertainty must be well-known prior to the error propagation. For the standard neutron-induced reactions like ^{235}U(n,f), IAEA standard cross sections are provided with their uncertainties and covariance matrices[9]. However, we currently assume an uncertainty of 5% in the IAEA recommended cross sections in its error propagation to our measured cross sections because their uncertainties are not provided. This issue is currently being discussed in an IAEA Coordinated Research Project[10]. However, we decided to determine the uncertainties in the monitor reaction cross sections by ourselves for more appropriate error propagation in our future deuteron-induced isotope production cross section experiments. The purpose of this work is to determine the cross sections and their uncertainties for three monitor reactions ^{27}Al(d,x)^{24}Na, ^{nat}Ti(d,x)^{48}V, and ^{nat}Cu(d,x)^{65}Zn by using the stacked target activation technique.

A target stack consisting of Al foils (25 μm and 50 μm thick), Ti foils (20 μm thick), and Cu foils (12.5 μm and 25 μm thick) was prepared and irradiated by a deuteron beam (about 200 nA) extracted from the AVF cyclotron of the RIKEN RIBF for two hours. In order to determine the cross sections without reference cross sections for the monitor reactions, we provided an electric current of exactly 200 nA to the target holder and measured the electric current by a current integrator. We have confirmed that the current integrator may be calibrated by a very small correction factor (about 0.995). After the irradiation, the target stack was dissembled, and the gamma activity measurement was started 4.25 hours after the end of irradiation by using a germanium detector calibrated by a multiple gamma ray emitting point source covering the gamma energy range between 60 and 1836 keV. The off-line measurement is ongoing, and we plan to report the cross sections with well-determined uncertainties for the three monitor reactions (^{27}Al(d,x)^{24}Na, ^{nat}Ti(d,x)^{48}V, ^{nat}Cu(d,x)^{65}Zn) as well as other useful reactions like ^{nat}Cu(d,x)^{64}Cu for positron-emitter production application.

References
1) E. Daum et al.: FZKA-5868, FZ Karlsruhe (1997).
2) R. A. Forrest et al.: Fus. Eng. Design **82**, 2478 (2007).
3) R. A. Forrest et al.: INDC(NDS)-0628, IAEA (2012).
4) S. Takács et al.: Nucl. Instrum. Meth. B **174**, 235 (2001).
5) S. Takács et al.: Nucl. Instrum. Meth. B **262**, 7 (2007).
6) M. U. Khandaker et al.: Nucl. Instrum. Meth. B **296**, 14 (2013).
7) M. U. Khandaker et al.: Nucl. Instrum. Meth. B **316**, 33 (2013).
8) D. L. Smith et al.: Nucl. Data Sheets **113**, 3006 (2012).
9) A. D. Carlson et al.: Nucl. Data Sheets **110**, 3215 (2009).
10) A. Nicols and R. Capote (ed.): INDC(NDS)-0630, IAEA (2013).

*1 RIKEN Nishina Center
*2 Nuclear Data Section, International Atomic Energy Agency
*3 Department of Physics, University of Malaya

Solvent extraction of tungsten from oxalic acid solution with Aliquat 336 toward chemical studies of seaborgium

N. Goto,[*1] K. Ooe,[*1] M. Murakami,[*1,2] H. Haba,[*2] S. Goto,[*1] and H. Kudo[*3]

The aqueous chemical experiments of element 106, seaborgium (Sg), have been reported by Schädel et al. in 1997[1)] and 1998[2)]. In these experiments, the cation exchange chromatography of Sg was conducted in HF/HNO_3[1)] and HNO_3[2)] solutions. However, no chemical experiments for Sg have been reported since these experiments. Therefore, further experimental results are required for detailed discussion of chemical properties of Sg in aqueous solutions. We are planning to investigate solvent extraction behavior of Sg. Oxalic acid is a typical organic acid used as ligand for transition metals. It is reported that molybdenum (Mo) and tungsten (W), which are lighter homologs of Sg, form anionic oxalate complexes and are extracted into an organic phase with ion-pair extractant. In this work, we investigated the extraction behavior and extracted species of W from oxalic acid solution into toluene with Aliquat 336 toward the chemical studies of Sg. The experiments were performed using ^{181}W in tracer scale to prevent the formation of polyoxometalate complexes of W.

The radiotracer ^{181}W ($T_{1/2}$ = 121.2 d) was produced in the bombardments of 24-MeV deuteron beam supplied by the RIKEN AVF cyclotron on ^{nat}Ta target foils. The ^{181}W tracer was chemically separated from the target material by an anion exchange method and stored in 1 M HCl solution.

The solvent extraction of ^{181}W was carried out as following procedure. One μL of the tracer solution was pipetted to a 1.5 mL polypropylene tube. Then, 700 μL of the oxalic acid solution containing 0.1 M HCl/0.9 M LiCl for keeping ionic strength constant was added. The same volume of Aliquat 336/toluene solution was mixed to the aqueous solution, and the mixture was shaken by a mechanical shaker for 5 min. After centrifuging for 30 s, 500 μL aliquot of each phase was separately taken into vials, and radioactivities of both phases were measured with a Ge detector. The distribution ratio (D) of ^{181}W was calculated using the following equation:

$$D = (A_{org} / V_{org}) / (A_{aq} / V_{aq}),$$

where A_{org} and A_{aq} are the radioactivities of organic and aqueous phases, respectively, and V_{org} and V_{aq} are the volumes of organic and aqueous phases, respectively. The extraction kinetics was also investigated from 1.0×10^{-2} M oxalic acid with 0.1 M HCl/0.9 M LiCl into 2.0×10^{-3} M Aliquat 336/toluene solution by changing the shaking time from 3 to 3600 s.

In the experiment of the investigation of extraction kinetics, the D value of ^{181}W became constant in shaking time longer than 30 s. This result shows that the extraction of W from oxalic acid solution with Aliquat 336 is fast. The dependence of the D values of ^{181}W on the Aliquat 336 concentration from 1.0×10^{-2} M oxalic acid with 0.1 M HCl/0.9 M LiCl is shown in Fig. 1. The D value of W increases with increasing [Aliquat 336]. The slope of the D value of W vs. [Aliquat 336] plot in logarithmic scale is estimated to be 0.95 ± 0.08 with a weighted least-squares fitting. This indicates that extracted anionic oxalate complex of W is associated with one molecule of Aliquat 336. However, in macro scale, it was reported that W is extracted as $(R_3NH)_2WO_2(C_2O_4)_2$, where R_3N shows a trioctylamine (TOA) molecule, when the mole ratio (Oxalate / WO_4^{2-}) in the aqueous phase was higher than 4.5[4)]. This discrepancy might be caused by the protonation to the W complex in the present experimental condition. Further experiments such as an investigation of dependence of D value on H^+ concentration would be performed for the speciation of the extracted species.

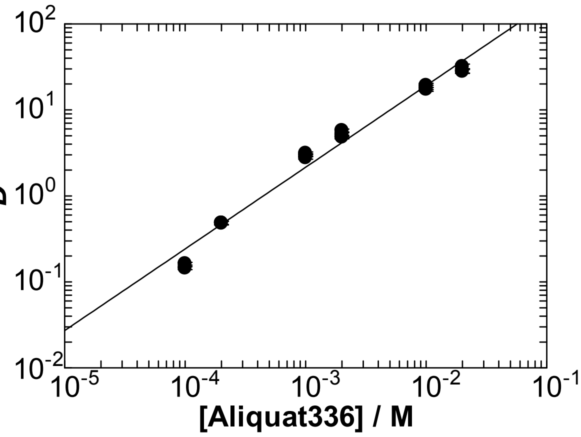

Fig. 1. Variation of the distribution ratio of ^{181}W from 1.0×10^{-2} M oxalic acid with 0.1 M HCl/0.9 M LiCl as a function of the concentration of Aliquat 336.

References

1) M. Schädel et al.: Radiochim. Acta **77**, 149 (1997).
2) M. Schädel et al.: Radiochim. Acta **83**, 163 (1998).
3) K. Yakabe and S. Minami: Nippon Kagaku Kaishi **1983**, 1045 (1983).
4) K. Yakabe, K. Iwamoto and S. Minami: Nippon Kagaku Kaishi **1985**, 714 (1985).

*1 Graduate School of Science and Technology, Niigata University
*2 RIKEN Nishina Center
*3 Department of Chemistry, Faculty of Science, Niigata University

Solvent extraction behavior of ^{95g}Nb and ^{179}Ta in HF medium with tributyl phosphate

S. Tsuto,[*1] M. Murakami,[*1,*2] K. Ooe,[*1] H. Haba,[*2] J. Kanaya,[*2] M. Huang,[*2] S. Goto,[*1] and H. Kudo[*3]

In a previous study,[1)] a long-lived isotope with a half-life of 27 h, ^{268}Db, was assigned as the descendant nucleus of ^{288}115 because of its similar chemical behavior to group-5 elements. It was also reported that the chemical behavior of Db was similar to that of Ta rather than of Nb.[1)] Recently, a chemical experiment on ^{262}Db ($T_{1/2}$ = 34 s) has been carried out in a mixed HF/HNO_3 solution.[2)] In contrast, this experiment showed a contrary result that the chemical behavior of Db is similar to that of Nb. Therefore, more detailed studies on the chemical properties of Db are required for the clear identification of element 115. In this study, extraction behaviors of the lighter homologs of Db, Nb and Ta, and the extraction kinetics is investigated toward the chemical identification of Db. To carry out chemical experiments of Db on a atom-at-a-time scale, the chemical studies of Nb and Ta should be conducted on a tracer scale. Moreover, in the experiment on Db, rapid kinetics for the extraction equilibrium is required because only short-lived radioisotopes of Db can be produced directly by heavy-ion induced nuclear reactions. We tried solvent extraction with ^{95g}Nb ($T_{1/2}$ = 34.991 d) and ^{179}Ta ($T_{1/2}$ = 1.82 y) with tributyl phosphate (TBP), which is widely used in the industrial separation of Ta from Nb.[3, 4)]

The radiotracers of ^{95g}Nb and ^{179}Ta were produced via ^{nat}Zr(p,xn) and ^{nat}Hf(p,xn) reactions, respectively, using a 14-MeV proton beam supplied by the RIKEN AVF cyclotron.[5)] These tracers were chemically separated from the target materials by means of anion exchange chromatography and stored in a 1 M HF solution. After evaporation of this solution, HF solution with a desired concentration was added to the tracers. One milliliter of the aqueous solution with the desired HF concentration containing ^{95g}Nb and ^{179}Ta tracers was mixed with the same volume of 1.8 M TBP in 1, 2-dichloroethane. The mixture was shaken mechanically for 180 min at 25°C. After centrifugation, 700 μL aliquots of each phase were taken separately. Gamma- and X-rays emitted from the ^{95g}Nb and ^{179}Ta tracers were measured using a Ge detector. From these results, we calculated the distribution ratio (D) :

$$D = (A_{\mathrm{org}} / V_{\mathrm{org}}) / (A_{\mathrm{aq}} / V_{\mathrm{aq}}),$$

where A is the radioactivity of the metals, and V is the volume of each phase. The subscripts aq and org denote the aqueous and organic phases, respectively.

We also studied the extraction kinetics of this system by changing the shaking time t (t = 0.2, 0.5, 1, 5, 10, 90, and 180 min). In the experiment for investigating extraction kinetics with 1.8 M TBP in 1, 2-dichloroethane and 5.4 M HF solutions, the D values of ^{95g}Nb and ^{179}Ta were almost constant in the studied range of shaking time studied, suggesting that the extraction equilibrium is very fast.

Figure 1 shows HF concentration dependences of the distribution ratios of ^{95g}Nb and ^{179}Ta in 1.8 M TBP in 1, 2-dichloroethane. When $[HF]_{ini}$ = 0.27 M, the D value of ^{179}Ta has a maximum of 346 ± 58, while the value of ^{95g}Nb is approximately 10^{-2}. This indicates that Ta can be clearly separated from Nb in the 0.27 M HF solution and the predominant complex of Ta in HF solution varies near this concentration. Therefore, this experimental condition would be suitable to investigate whether Db behaves like Nb or Ta.

For chemical experiments on short-lived Db, an on-line rapid extraction apparatus is required. The development of an apparatus utilizing a flow injection analysis system is in progress.[6)] The on-line extraction of Nb and Ta from HF solution into TBP will be performed using the apparatus.

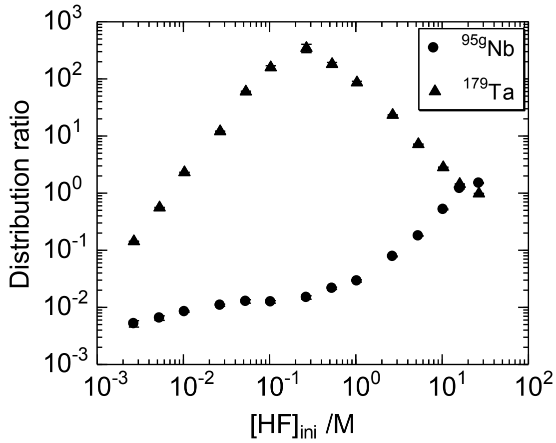

Fig. 1. HF concentration dependences of distribution ratios of ^{95g}Nb and ^{179}Ta into 1.8 M TBP in 1, 2-dichloroethane.

References

1) N. J. Stoyer et al.: Nucl. Phys. **A787**, 388c (2007)
2) Y. Kasamatsu et al.: Chem. Lett. **38**, 1084 (2009).
3) Z. Zhu and C. Y. Cheng: Hydrometallurgy **107**, 1 (2011).
4) S. Nishimura et al.: Trans. JIM **5**, 79 (1964).
5) M. Murakami et al.: Appl. Radiat. Isot. in press.
6) T. Koyama et al.: In this report.

*1 Graduate School of Science and Technology, Niigata University
*2 RIKEN Nishina Center
*3 Faculty of Science, Niigata University

Extraction behavior of Nb and Ta with Aliquat 336 in HF solutions

D. Sato,[*1] M. Murakami,[*1,*2] K. Ooe,[*1] H. Haba,[*2] S. Goto,[*1] and H. Kudo[*3]

Studies on the chemical properties of transactinide elements with atomic numbers Z ≥ 104 are extremely interesting. It is suggested that the chemical properties of these elements are different from those of their lighter homologs because of the strong relativistic effects on the valence electrons[1]. Therefore, comparative studies on the chemical behaviors of transactinide elements and their lighter homologs are very important.

We are planning to investigate the chemical properties of Db, which is the 105th element in the periodic table. Because a fluoride ion is known as a strong complexing reagent for group 5 elements[2], ion-pair extractions of Nb and Ta, which are the lighter homologs of Db, with quaternary ammonium (Aliquat 336) in HF solutions were carried out to study complex formations of these elements with fluoride ions.

Long-lived radiotracers, ^{95g}Nb ($T_{1/2}$ = 34.97 d) and ^{179}Ta ($T_{1/2}$ = 665 d), were produced during proton bombardments of Zr and Hf metallic foil targets with natural isotopic abundances, respectively, using the RIKEN AVF Cyclotron. These radiotracers in the targets were chemically isolated by ion-exchange separation. The tracers were dissolved in 600 μL of 1 M HF and then mixed with the same volume of 10^{-8}-10^{-3} M Aliquat 336-1,2-dichloroethane solutions in a polypropylene tube. After shaking the solutions for 5 min, followed by centrifugation, the two phases were separately pipetted into sample tubes. The radioactivities of the two samples were assessed with a Ge detector. Distribution ratios (*D*) of Nb and Ta were obtained from the ratio of the radioactivities of the two phases.

The dependence of the distribution ratios of ^{95g}Nb and ^{179}Ta in 1 M HF on the concentrations of Aliquat 336 are shown in Fig. 1. The results show a linear relation with a slope of ≈1 for both Nb and Ta, which indicates that univalent anionic fluoride complexes are extracted by Aliquat 336.

The dependences of *D* values of ^{95g}Nb and ^{179}Ta on the HF concentration were also investigated for varying HF concentrations (10^{-2}-10 M) with 10^{-4} M Aliquat 336-1,2-dichloroethane solution (Fig. 2). The maximum *D* value of Ta is obtained in 0.27 M HF. On the other hand, the *D* value of Nb decreases gradually with HF concentration from 10^{-2} M to 10 M, thus, there was a clear differences in the extraction behaviors of Nb and Ta. The large differencein the *D* values of Nb and Ta is probably due to the fact that Ta forms fluoro-complexes TaF_n^{5-n}, while Nb is predominantly present as oxo-fluoro complexes $NbOF_n^{3-n}$ [3].

As mentioned above, the results obtained from Fig.1 show that the extracted species of Nb and Ta are both univalent anionic complexes. Therefore, Nb and Ta exist as TaF_6^- and $NbOF_4^-$ under these experimental conditions.

The fluoro-complex formation of Db needs to be investigated from the experimental result to dtermine whether the extraction behavior of Db from HF solutions into Aliquat 336-1,2-dichloroethane solution is closer to that of Nb or Ta.

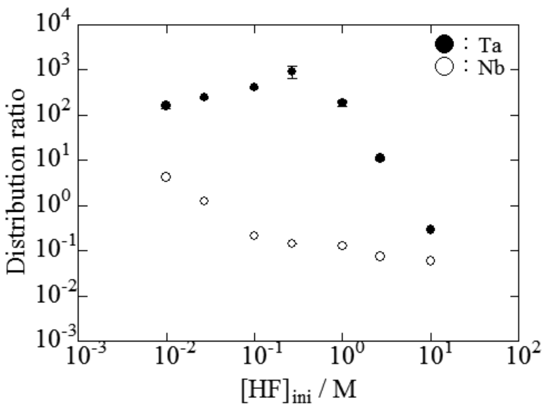

Fig. 1: Variation of the distribution ratio *D* of ^{95g}Nb and ^{179}Ta vs. concentration of Aliquat 336 in 1 M HF

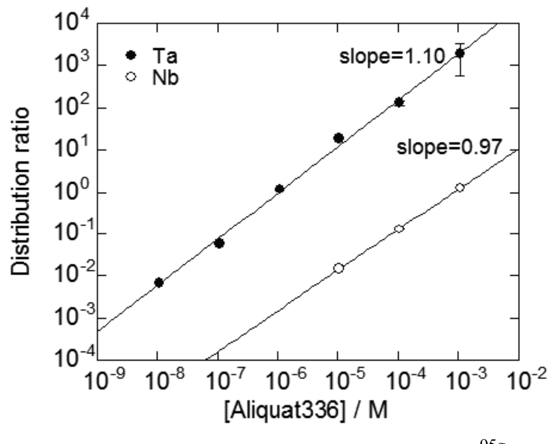

Fig. 2: Variation of the distribution ratio *D* of ^{95g}Nb and ^{179}Ta vs. initial concentration of HF

References
1) P. Pyykko: Chem. Rev. 88, 563 (1988)
2) Y. Kasamatsu, A. Toyoshima, H. Toume, K. Tsukada, H. Haba, Y. Nagame: J. Nucl. Radiochem. Sci., Vol. 8, No. 2, 69-72 (2007)
3) F. Monroy Guzman, D. Trubert, L. Brillard, J. B. Kim, M. Hussonnois, and O. Constantinescu: J. Radioanal. Nucl. Chem. 208, 461-466 (1996).

*1 Graduate School of Science and Technology, Niigata University
*2 RIKEN, Nishina Center
*3 Department of Chemistry, Faculty of Science, Niigata University

Online coprecipitation experiment of ^{85}Zr and ^{169}Hf with Sm hydroxide for chemical study of Rf

Y. Kasamatsu,[*1] K. Toyomura,[*1,*2] T. Yokokita,[*1,*2] Y. Komori,[*1] Y. Shigekawa,[*1,*2] H. Haba,[*2] J. Kanaya,[*2] M. Huang,[*2] M. Murakami,[*2,*3] K. Morita,[*2] H. Kikunaga,[*2,*4] and A. Shinohara[*1,*2]

Elucidating chemical properties of transactinide elements with atomic numbers $Z \geq 104$ is an intriguing and important topic. Transactinide elements are produced at accelerators using heavy-ion-induced nuclear reactions. The production rates of these elements are low and their half-lives are short ($T_{1/2} \leq \sim 1$ min). Thus, chemical studies on these elements are conducted on a one-atom-at-a-time basis using rapid chemical separation techniques, and products transported online by a gas-jet system from a nuclear reaction chamber are used. For unambiguous identification of a single atom, detection of α or spontaneous fission decay is required. Owing to these difficulties, so far, simple partition methods such as gas-phase and aqueous-phase chromatographic experiments have been applied to the studies of transactinide elements.

Recently, the anion- and cation-exchange behaviors of rutherfordium (Rf, $Z = 104$) in HF and HF/HNO_3 solutions were successfully investigated at the Japan Atomic Energy Agency Tandem Facility, the behaviors of Rf was reported to be different from those of its homologues Zr and Hf.[1)] Detailed studies on Rf in various chemical systems are needed for a further understanding of its chemical properties. To establish a new chemical experiment for superheavy elements, thus far, we have developed a method to rapidly prepare a coprecipitated sample, which has good energy resolution in alpha spectrometry. For the coprecipitation study of Rf, we have studied coprecipitation properties of group-4 elements, Zr, Hf, and Th with $Sm(OH)_3$,[2)] and also developed an apparatus for rapid preparation of precipitate samples. In this study, we performed online coprecipitation experiments of ^{85}Zr and ^{169}Hf using the developed apparatus, and determined the experimental conditions for Rf.

We produced carrier-free radiotracers ^{85}Zr ($T_{1/2}$ = 7.9 min) and ^{169}Hf ($T_{1/2}$ = 3.25 min) in the ^{nat}Ge/^{nat}Gd(^{18}O, xn) reactions using the RIKEN K70 AVF cyclotron. The reaction products were transported online by a He/KCl gas-jet system to the chemistry laboratory. They were deposited on the collection site of a dissolution apparatus, and then dissolved in 120 μL of a 0.46 M HNO_3 solution containing Sm ions (460 mg/L). Various compositions of basic solutions (dilute and concentrated aqueous NH_3, 0.15, 1, 6, and 12 M NaOH) were added into the sample solution. The resultant concentrations were 0.28 and 13 M NH_3, and 0.08, 0.84, 5.3, and 11 M NaOH, respectively. After stirring the sample for 10 s, the coprecipitate sample was prepared by suction filtration on a polypropylene membrane filter (0.1 μm, ϕ20, Eichrom) using a semiautomatic filtration apparatus for repetitive experiments. The sample was dried using a heater at 100 °C and was subjected to γ-ray measurement using a Ge detector. On the other hand, radioactivities of the products dissolved using the dissolution apparatus were also determined. From the ratio of the measured radioactivities of the precipitate to those of the dissolved solution, precipitation yields of Zr and Hf were determined.

The dependence of the yield on the composition of the added basic solution is depicted in Fig. 1. It was found that almost the entire amounts of Zr and Hf were coprecipitated with Sm hydroxide when aqueous NH_3 and 0.1 M NaOH were used. This suggests that Zr and Hf form a neutral hydroxide complex and coprecipitate with $Sm(OH)_3$ precipitate in these basic solutions. For more concentrated NaOH solutions, the yields decreased as the concentration of the hydroxide ion increased, indicating that the Zr and Hf form anionic hydroxide complexes. These results are consistent with those obtained in the offline coprecipitation experiment using ^{88}Zr and ^{175}Hf.[2)] It was found that the coprecipitation yields of Zr and Hf with Sm hydroxide in the rapid and online precipitation experiment can be obtained using the developed apparatus connected to the accelerator at RIKEN; the present experimental systems are applicable to Rf experiments.

Very recently, we indeed produced ^{261}Rf in a ^{248}Cm(^{18}O, 5n)^{261}Rf reaction and performed the first trial of coprecipitating Rf with $Sm(OH)_3$. Approximately 43 alpha events were detected in the energy region of ^{261}Rf.

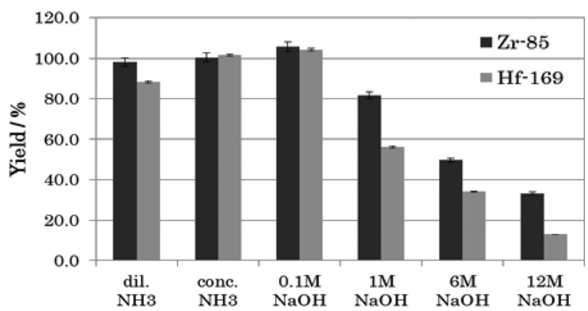

Fig. 1. Coprecipitation yields of ^{85}Zr and ^{175}Hf.

*1 Graduate School of Science, Osaka University
*2 RIKEN Nishina Center
*3 Department of Chemistry, Niigata University
*4 Research Center for Electron Photon Science, Tohoku University

References

1) Y. Ishii et al.: Bull. Chem. Soc. Jpn. **84**, 903 (2011).
2) Y. Kasamatsu et al.: RIKEN Accel. Prog. Rep. **43**, 270 (2010).

Adsorption behavior of Zr and Hf to TTA-resin in microcolumn for determining the forming ability of Rf monofluoride complex

A. Yokoyama,[*1,*2] Y. Kitayama,[*2,*3] Y. Fukuda,[*2,*4] A. Toyoshima,[*5] K. Tsukada,[*5] E. Maeda,[*2,*3] H. Kimura,[*2,*3] T. Taniguchi,[*2,*4] S. Ueno,[*2,*3] K. Hayashi,[*2,*4] H. Kikunaga,[*2,*6] M. Murakami,[*2,*7] J. Kanaya,[*2] M. Huang,[*2] and H. Haba[*2]

The present study aims to elucidate the relevant chemical species of Rf by reversed-phase extraction chromatography with 2-thenoyltrifluoroacetone (TTA) as a stationary phase. Because TTA has been suggested to extract quadrivalent metallic ions, the distribution ratios of the system may make it possible to determine the specific complex-formation constant of Rf. We have so far performed several experiments for the chemical systems with Zr and Hf ions, but failed to find an experimental condition appropriate for measuring the adsorption of Rf.[1,2]

In order to optimize an appropriate experimental condition for Rf, in the present study, the equilibration time and distribution ratios for extraction have been measured by batch method experiments with carrier-free radiotracers of Zr and Hf on TTA-resin in the $1.0\times10^{-4}-1.0\times10^{-3}$ M HF/1.0×10^{-2} M HNO_3 solutions. An online experiment has been also performed for investigating the reversed-phase chromatographic behaviors of Zr and Hf on the TTA resin with Automated Rapid Chemistry Apparatus (ARCA)[3] to simulate the Rf experiments.

The radioisotopes of ^{88}Zr ($t_{1/2}$ = 83.4 d) and ^{175}Hf ($t_{1/2}$ = 70.0 d) used in the batch experiments were produced by the ^{89}Y(p, 2n) and ^{175}Lu(p, n) reactions, respectively, at the RIKEN K70 AVF Cyclotron. The short-lived ^{85}Zr and ^{169}Hf isotopes were also produced by the ^{18}O-induced reaction with the ^{nat}Ge and ^{nat}Gd targets, respectively, for the on-line experiments. The TTA-resin was simultaneously produced by mixing the CHP20/P20 resin with a TTA-octanol solution of 50 or 30 wt.%, which includes 50 or 20 wt.% of TTA in n-octanol, respectively. The prepared TTA-resin was used for the batch experiments, as well as for the on-line reversed-phase extraction chromatography. The details of the procedures can be found elsewhere.[2]

In the batch experiments, the D value of 50 wt.% resin was found to be higher than that of the other resin, while the time for chemical equilibration of the former is almost the same as that of the other. The elution curves of Zr and Hf at a flow rate of 0.15 mL/min in the range $1.0\times10^{-4}-1.0\times10^{-3}$ M of HF concentration on the former resin are shown in Fig. 1; the peaks of the curves are clearly visible in the figure for all the conditions of HF concentration.

The D values for the on-line experiments are evaluated from the elution curves by using the following equation, $D = V_p/m$ [mL/g], where V_p is the peak volume of an elution curve, and m is the resin weight in a microcolumn. The D values of Zr tend to be higher than those of Hf in the on-line experiments, although, based on the batch experiments, the D value of Hf should be higher than that of Zr at the chemical equilibrium. For instance, in Fig.1(a) the D value of Zr was found to be higher than that of Hf by a factor of 1.2, although in the batch experiments the D value of Zr was found lower than that of Hf by a factor of 2.8. These results in the on-line experiments show that the chemical equilibrium time of Zr is shorter than that of Hf, which agrees with the results of the present batch experiments measured as a function of shaking time. The kinetic behavior observed here should be clarified in order to perform the Rf experiment in the expected project.

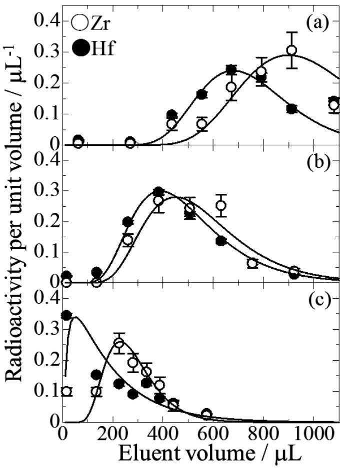

Fig. 1. Elution curves of Zr and Hf against the HF concentration, (a) 1.0×10^{-4} M, (b) 6.0×10^{-4} M, (c) 1.0×10^{-3} M, in the HF/0.010-M HNO_3 solution, at a flow rate of 0.15 mL/min. The radioactivity values in the figure represent the values relative to the total eluted radioactivity. Solid lines are curves fitted to a theoretical equation derived by Glückauf model[4].

*1 Institute of Science and Engineering, Kanazawa University
*2 RIKEN Nishina Center
*3 Graduate School of Natural Science and Technology, Kanazawa University
*4 College of Science and Engineering, Kanazawa University
*5 Advanced Science Research Center, Japan Atomic Energy Agency
*6 Research Center for Electron Photon Science, Tohoku University
*7 Faculty of Science, Niigata University

References

1) M. Araki,*et al.*: RIKEN Accel. Prog. Rep. **43**, 271 (2010).
2) A. Yokoyama,*et al.*: RIKEN Accel. Prog. Rep. **46**, 242 (2012).
3) Y. Nagame *et al.*: Radiochim. Acta, **93**, 519 (2005).
4) E. Glückauf: Trans Faraday Soc. **51**, 34 (1955).

Coprecipitation experiment of various elements with Sm hydroxide using multitracer

Y. Kasamatsu,[*1] K. Toyomura,[*1,*2] T. Yokokita,[*1,*2] H. Haba,[*2] J. Kanaya,[*2] Y. Kudou,[*2] and A. Shinohara[*1,*2]

Chemical studies on transactinide elements with atomic numbers $Z \geq 104$ are currently at the frontier in nuclear chemistry. The transactinide elements are produced at accelerators using heavy-ion-induced nuclear reactions. Rapid chemistry on a one-atom-at-a-time basis is applied to these elements because of their low production rates and short half-lives. In addition, for unambiguous identification of these elements, it is necessary to detect α or spontaneous fission decays. Therefore, chemical experiments of transactinides are not abundant. In the ion-exchange chromatography, the fluoride complex formation of Rf (Z = 104) was successfully investigated, and the behavior of Rf was reported to be clearly different from those of the homologues Zr and Hf. Chemical studies on transactinides in various chemical systems should be conducted to understand their characteristic chemical properties.

The purpose of the present study is to establish a coprecipitation method as a new method for the chemistry of transactinide elements. Because these elements can be treated as only one atom at a time, we must study their coprecipitation behaviors with a carrier element. For this, a preparation method of coprecipitated samples with Sm hydroxide, which facilitated the α spectrometry with a high energy resolution, was established.[1)] We are planning to apply this method to transactinide chemistry and to investigate the coprecipitation behaviors of transactinides. In the chemistry of transactinides, model experiments with their homologues are usually performed to establish the experimental method and to determine the conditions. In this work, we investigated the coprecipitation behaviors of various elements with Sm hydroxide using a multitracer produced by nuclear spallation reactions in RIKEN.

A multitracer was produced by irradiating the ^{nat}Ta foil targets by 135-MeV/nucleon ^{14}N ions accelerated by RIKEN Ring Cyclotron[2)]. Various nuclides, namely various elements, with Z < 73 (Ta) were produced by nuclear spallation reactions. Only the nuclear reaction products recoiling out of the target foils were transported from the reaction chamber to the chemical laboratory by the He/KCl gas-jet system.[2)] The products collected on a glass filter paper for about 40 h were dissolved in 1 mL of 0.01 M HCl solution, and the solution sample was filtrated with a filter paper to remove the glass chips from the solution.

The Sm standard solution (20 μL) containing 20 μg of Sm was added into 220 μL of the multitracer solution. The solution was stirred, and then 2 mL of the basic solution (dilute and concentrated aqueous NH_3, and 0.1, 1, 6, and 12 M NaOH solutions) was added. The solution was stirred for 10 s or 10 min. Then, the solution containing the precipitate was filtrated by suction with a polypropylene membrane filter (0.1 μm, ϕ20, Eichrom). The filtrate was collected in a vial. Both the precipitate and filtrate were dried using a heater at 100°C and then subjected to γ-ray spectrometry with a Ge detector. The precipitation yields (Y_1) were determined from these radioactivities. The reference radioactivities of the radiotracers were also determined. The precipitation yield (Y_2) as a relative value to the reference was also determined to check the accuracy of the obtained precipitation yields.

The product nuclides were identified from the energies and half-lives of the observed γ-ray peaks. We found the following nuclides: ^{24}Na, ^{42}K, ^{82m}Rb, ^{127,129}Cs (alkali metals), ^{28}Mg, ^{47}Ca, ^{128}Ba (group 2), ^{44,47,48}Sc, ^{87}Y (group 3), ^{132,135}Ce, ^{145,146}Eu, ^{146,147,149}Gd, $^{149\text{-}153,155}$Tb, ^{155,157}Dy, ^{160m}Ho, ^{161}Er, ^{165,167}Tm, ^{166,169}Yb, ^{169,171,172}Lu (lanthanides), ^{89}Zr, ^{170,173}Hf (group 4), ^{90}Nb, ^{176}Ta (group 5), ^{93m}Mo (group 6), ^{96}Tc (group 7), ^{99m,100}Rh (group 9), ^{65}Zn, (group 12), ^{67}Ga, ^{110,111}In (group 13), ^{71,72}As, ^{118m,120m}Sb (group 15), ^{73}Se, and ^{119m}Te (group 16).

For these elements, the precipitation yields and their dependences on the composition of the basic solution were obtained. Overall, the yields reflecting the properties of each element in the hydroxide precipitation were observed. For example, the yields of alkali metal elements were almost 0% under all the conditions. The yields of lanthanides were almost 100%, and decreased in the case using 6 and 12 M NaOH. In addition, the precipitation yield of Zn was decreased to almost 0% in adding concentrated aqueous NH_3, indicating the well-known properties that Zn forms a cationic ammine complex in such a solution. The yields of Zr and Hf, the homologues of Rf, were close to 100% and decreased with an increase in the hydroxide-ion concentration, while those of Nb and Ta, the homologues of Db, were always high. In contrast, the yields of Mo, the homologue of Sg, were 0% under all the conditions. It would be interesting to study the precipitation behaviors of these transactinides. The Y_1 values were consistent with the Y_2 values. In comparison between the results with 10-s and 10-min stirring, both the yields agreed with each other for many elements, suggesting rapid chemical reactions; only exception was the result using 12 M NaOH. We believe that the coprecipitation properties of transactinides with Sm hydroxide could be investigated by the present method.

*1 Graduate School of Science, Osaka University
*2 RIKEN Nishina Center

References

1) H. Kikunaga et al., *Appl. Radiat. Isot.* **2008**, *67*, 539.
2) H. Haba et al., *Radiochim. Acta* **2005**, *93*, 539.

Development of rapid solvent extraction technique with flow injection analysis for superheavy element chemistry

T. Koyama,*1 N. Goto,*1 M. Murakami,*1,*2 K. Ooe,*1 H. Haba,*2 S. Goto,*1 and H. Kudo*3

For the chemical investigation of superheavy elements with atomic numbers ≥ 104, rapid chemical separation is needed because they have relatively short half-lives. We developed a solvent extraction system applying flow injection analysis (FIA). This FIA system consists of solvent extraction and phase separation parts (Fig. 1). In the solvent extraction part, aqueous and organic phases are mixed in a tube with a very small inner diameter of 100–200 μm. Because of the large specific interfacial area and short diffusion length in the tube, extraction equilibrium is rapidly attained. In the phase separation part, on-line liquid-liquid phase separation is achieved with a hydrophobic poly(tetrafluoroethylene) (PTFE) membrane. In this work, solvent extraction of ^{95g}Nb ($T_{1/2}$ = 35 d) using this system was investigated as a model experiment for element 105, Db.

The ^{95g}Nb tracer was produced through the bombardment of a ^{nat}Zr metal target foil with a 14-MeV proton beam supplied by the RIKEN AVF cyclotron. The carrier-free ^{95g}Nb tracer was prepared by the chemical separation from the target using an anion-exchange technique.[1)]

In the solvent extraction experiment using the FIA system, 5 M HCl solution containing ^{95g}Nb tracer and 0.1 M Aliquat 336 in 1,2-dichloroethane solution were used as aqueous and organic solutions, respectively. The aqueous and organic solutions were pumped using double-plunger pumps and mixed in a T-connector. The mixture was fed into the extraction coil of the PTFE tube of inner diameter 0.17 mm, and on-line liquid-liquid phase separation was performed using the membrane phase separator of thickness 75 μm and a 0.8-μm pore size PTFE filter.

In order to evaluate the time needed for attaining extraction equilibrium, the flow rate and extraction coil length were varied. After extraction, both solutions eluting from the phase separator were collected in polypropylene tubes. Experiments without the phase separator were also performed. Batch extraction experiments of ^{95g}Nb using 0.6 mL of each phase were also performed for comparison with the results obtained using the FIA system. The two separated phases were then subjected to γ-ray spectrometry using a Ge detector in all experiments. The distribution ratio (D) was calculated as the radioactivity ratio of each phase by using the same flow rate (Eq.1).

$$D = A_{\text{org}} / A_{\text{aq}} \qquad (1)$$

*1 Graduate School of Science and Technology, Niigata University
*2 RIKEN Nishina Center
*3 Department of Chemistry, Faculty of Science, Niigata University

The results of using the FIA system and the shaking time in the batch experiments are shown in Figs. 2 (a) and (b), respectively. In the experiment using the FIA system, the extraction equilibrium was attained within a contact time of approximately 2 s. On the other hand, a shaking time of 40 min was needed to attain extraction equilibrium in the batch experiment. This result shows that extraction equilibrium can be rapidly attained using the FIA system. On-line liquid-liquid phase separation was successfully performed using the membrane phase separator in the FIA system.

Thus, the developed FIA system is applicable for the solvent extraction experiments of superheavy elements with half-lives of several tens of seconds considering other time-consuming steps such as dissolution and sample preparation for α-particle measurement.

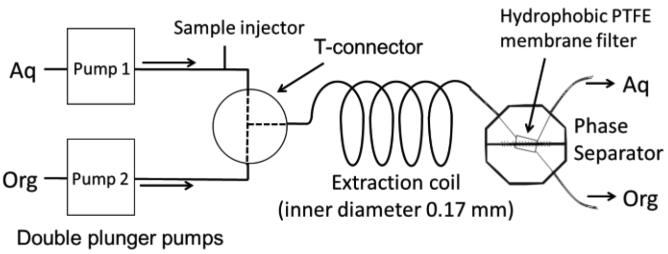

Fig. 1. Schematic view of the FIA system.

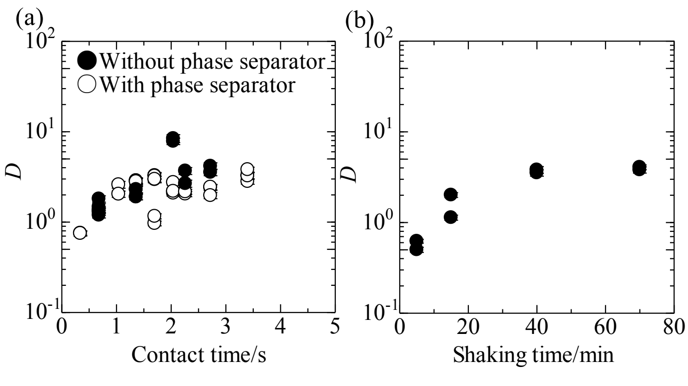

Fig. 2. The dependence of D value of ^{95g}Nb on the contact time in the FIA system (a) and the shaking time in the batch experiment (b).

References

1) Y. Kasamatsu et al : J. Nucl. Radiochem. Sci. **8**, 69 (2007).

Production of ^{179m}W in the form of a carbonyl complex

M. Huang,[*1] J. Kanaya,[*1] M. Murakami,[*1] H. Haba,[*1] and S. Shibata[*1]

We are developing a CO gas-jet technique and plan to apply it to the separation of neutron-rich isotopes of Sg produced in the transfer reaction ^{248}Cm + ^{48}Ca. In this preliminary investigation, we successfully separated ^{179m}W, the lighter homologue element of Sg, from other heavy ions (^{89m}Zr, ^{28}Al et al.) in the form of a volatile carbonyl complex.

A 24-MeV d beam was extracted from the AVF cyclotron of the RIKEN RI Beam Factory. Five ^{nat}Ta targets were stacked with one ^{nat}Nb target in the sequence Ta/Nb/Ta/Ta/Ta/Ta. All targets were fixed in an Al holder with 5-mm distance between each other. The thicknesses of ^{nat}Ta and ^{nat}Nb target were 7.62 and 0.917 mg/cm^2, respectively. Reaction products emitted from the targets were thermalized and stopped in the He/CO mixed gas. Elements that could form volatile complexes with the CO reagent, e.g. $W(CO)_6$, were flushed out from the target chamber and extracted along capillaries of inner diameter (i.d.) 1.59 or 2.0 mm. After the volatiles were passed through a PTFE filter (SMC SFB 300-02) mounted at the outlet of the target chamber and a 2.1-m quartz column (2.0-mm i.d.) immersed in a chiller, they were collected using a charcoal filter (ADVANTEC CP20) and subjected to γ-ray spectrometry with a Ge detector. Because of the beam irradiation, CO molecules would be decomposed into carbon and oxygen. Most products adhered to the carbon particles and were removed by the PTFE filter. The length from the PTFE filter to the collection site was about 17 m. Flow rates of He and CO were controlled independently to adjust their concentrations in the target chamber. The lowest flow rate controlled by the mass-flow meter was 0.2 L/min.

As explained above, reaction products could be transported out in the form of volatile molecules or by using aerosols. First, to check all the products, a high-intensity beam with 2.9 particle μA (pμA) as well as 1.2(He)+0.2(CO) L/min mixed gas was used to generate many carbon aerosols. All nuclear products were efficiently carried to the charcoal filter by carbon particles without selectivity when the PTFE filter was removed. The 6.4-min ^{179m}W and 4.16-min ^{89m}Zr were identified by their γ-energies and decay curves. The production yields after 1-min collection were deduced to be 9.86±0.84 and 0.40±0.04 kBq/pμA for ^{179m}W and ^{89m}Zr, respectively. By changing the i.d. of the capillary and increasing the He/CO flow rate, the yield could not be improved further.

After the PTFE filter was installed, the 221.5-keV γ-line of ^{179m}W was observed subsequent to 7-min beam irradiation under 0.03 pμA (See Fig.1). Other nuclides, which could not form volatiles in a CO atmosphere, were removed, such as ^{89m}Zr. The transport efficiency for ^{179m}W in the carbonyl form was decreased with the beam intensity and CO flow rate, but it could be improved by increasing the He gas flow rate. By changing the i.d. of capillary from 1.59 to 2.0 mm, the maximum flow rate of He gas was increased from 1.2 to 4.0 L/min, corresponding to about 1 atm in the target chamber. Under 4.0 L/min He flow rate, the count of 221.5-keV γ-line was improved by a factor of 4 (see Fig. 1). The optimal relative transport efficiency for ^{179m}W was 13.1±2.2%, which was obtained by normalizing to the production yield of using carbon aerosols as the transmission medium under 2.9-pμA beam intensity. The yield of ^{179m}W that passed through an isothermal column at different temperatures was measured, and the results are displayed in Fig. 2. By fitting the breakthrough curve with a Monte-Carlo simulation[1)], the adsorption enthalpy of the carbonyl complex was determined to be -47±1 kJ/mol, which agrees well with the 46.5±2.5 kJ/mol reported for $W(CO)_6$ in Reference[2)].

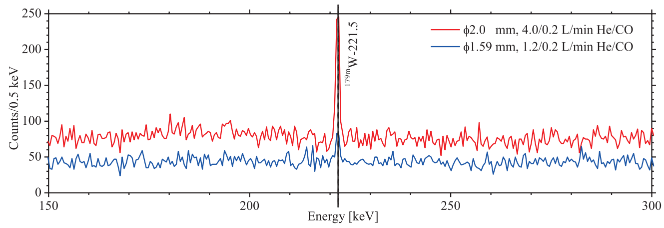

Fig. 1. γ-ray spectra obtained for ^{179}W in the form of a volatile carbonyl complex.

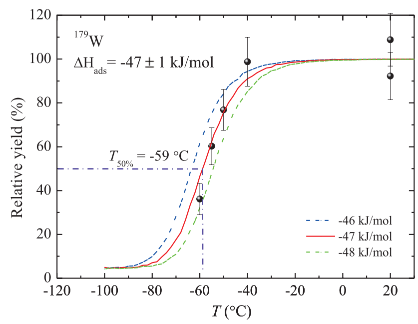

Fig. 2. Yields of ^{179m}W passing through the quartz column.

References
1) I. Zvara: Radiochim. Acta **38**, 95-102 (1985)
2) J. Even et al.: Inorg. Chem. **51**, 6431-5433 (2012).

*1 RIKEN Nishina Center

Recovery of ^{248}Cm material from mixed Cm/Gd target

M. Murakami[*1,*2] and H. Haba[*1]

In the chemical experiments on superheavy elements (SHEs), the lighter homologue elements in the periodic table are simultaneously produced, and their chemical behaviors are compared to those of SHEs under identical experimental conditions. For this purpose, a mixed ^{248}Cm/Gd target deposited on a thin metallic backing foil has been often used.[1,2] The target as well as the backing material are gradually damaged by the irradiation with the intense heavy-ion beams. Since the available amount of ^{248}Cm is limited, its recovery, which involves purification from the used target, is essential to produce a new target.

Bis(2-ethylhexyl)phosphoric acid (HDEHP) is one of the widely used extractants for separating lanthanide ions.[3] Separation of lanthanide and actinide through extraction chromatography using an HDEHP-laden resin has been studied.[4,5] Using the HDEHP resin, one can perform stepwise separation of lanthanide and actinide elements by simply changing the concentration of the HNO_3 eluents. The distribution coefficients (K_d) of these elements strongly depend on the HNO_3 concentration: The K_d values for +3 ions are inverse third power dependent on the mean activity of the hydrogen ion.[4] Therefore, in this work, we investigated several schemes to effectively separate Cm and Gd with the HDEHP resin using a multitracer of lanthanide elements. Further, we separated the ^{248}Cm material from ^{nat}Gd with the optimized scheme.

The commercially available Ln Resin (Eichrom), the HDEHP-laden hydrophobic resin with the particle size of 100–150 μm, was packed into a polyethylene column (5 mm i.d. × 50 mm height; column volume: ≈1 mL). The multitracer was produced by bombarding a ^{nat}Hf target with a 135-MeV/nucleon ^{14}N beam from the RIKEN Ring Cyclotron. After the irradiation, the rare earth elements were separated from the target material by an establised procedure, detailed in Ref. 6. The multitracer including ^{133}Ba, ^{139}Ce, ^{143}Pm, ^{145}Sm, and ^{153}Gd in 0.1 M HNO_3 was stocked in a polypropylene (PP) tube. The K_d values are reported to be in the order Ba ≪ Ce < Cm < Pm < Sm < Gd in the Ln Resin–HNO_3 system.[5] After the conditioning of the column with 3.0 mL of 0.1 M HNO_3 solution, 1 mL of the stock solution was loaded onto the column. 4 mL of 0.1 M HNO_3 was then fed onto the column as a first eluent. According to the reported K_d values, [5] most of the +1 and +2 metal ions such as ^{133}Ba elute in this fraction. As a second eluent, 0.2–0.5 M HNO_3 solutions were fed until ^{143}Pm was completely eluted from the column. Finally, 6 mL of 1.0 M HNO_3 was fed to elute ^{153}Gd completely. The flow rate was 230–240 μL/min at room temperature. Each 1 mL of the effluent was collected in a separate PP tube and subjected to γ-ray spectrometry at fixed geometry.

Figures 1(a)–(d) show the elution curves of the multitracer with 0.2, 0.3, 0.4, and 0.5 M HNO_3 as the second eluent. ^{133}Ba was eluted with 5 mL of 0.1 M HNO_3 with a recovery of 100.3 ± 2.5%. 30 mL of 0.2 M HNO_3 (Fig. 1(a)) was used to elute ^{139}Ce and then ^{143}Pm, as expected from the difference in the K_d values.[5] ^{145}Sm and ^{153}Gd were not eluted in these fractions. Owing to the increase in the concentration of the second eluent, the peaks of the elution curves of ^{139}Ce and ^{143}Pm get shifted to lower volumes and approach to each other. In the case of 0.5 M HNO_3, 6.2 ± 0.6% of ^{153}Gd was eluted until ^{139}Ce was completely eluted. Since Cm is expected to be found between Ce and Pm from the order of the K_d values,[5] Cm and Gd can be separated with the schemes shown in Fig. 1(a)–(c). However, the scheme shown in Fig. 1(a) takes a large amount of eluent, and in the case of 0.4 M HNO_3, the condition for separation is stricter than that in the case of 0.2 M and 0.3 M HNO_3, owing to the close peaks of the elution curves. Therefore, we selected the scheme in Fig. 1(b) for the separation of ^{248}Cm and ^{nat}Gd.

By applying the scheme of Fig. 1(b) to the purification of 830-μg ^{248}Cm target material containing ^{nat}Gd (about 10 wt%), 99.3 ± 4.1% of ^{248}Cm was collected in the fraction of the 12-mL 0.3 M HNO_3 solution.

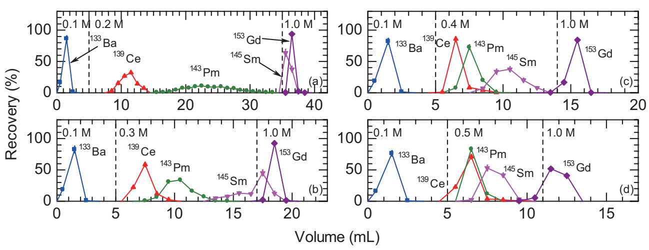

Fig. 1. Elution curves of ^{133}Ba, ^{139}Ce, ^{143}Pm, ^{145}Sm, and ^{153}Gd. The concentrations of the second eluents are (a) 0.2 M, (b) 0.3 M, (c) 0.4 M, and (d) 0.5 M.

*1 RIKEN Nishina Center
*2 Department of Chemistry, Niigata University

References

1) K. Tsukada et al.: Radiochim. Acta **97**, 83 (2009).
2) Z. J. Li et al.: Radiochim. Acta **100**, 157 (2012).
3) S. Cotton: *Lanthanide and Actinide Chemistry* (John Wiley & Sons, 2006).
4) E. P. Horwitz et al.: J. Inorg. Nucl. Chem. **31**, 3255 (1969).
5) E. P. Horwitz and C. A. A. Bloomquist: J. Inorg. Nucl. Chem. **37**, 425 (1975).
6) Y. Ezaki et al.: J. Nucl. Radiochem. Sci. **10** Suppl., 123 (2009) (In Japanese).

Method for preparing ultra-thin sources for low-energy particle spectrometry

H. Kikunaga,[*1,*2] H. Haba,[*1] and J. Kanaya[*1]

Generally, internal conversion electrons originate from the K shell. If the decay energy of a nuclear isomer is less than the binding energy of an inner-shell electron, the emission of an electron from the shell is forbidden, in which case the isomer interacts with outer-shell electrons. As a result, the probability of internal conversion is affected by the outer-shell electron state, namely the chemical state. Examples of this type of nuclides are $^{99}Tc^{m}$ (2.17 keV) and $^{229}Th^{m}$ (7.6 eV). The goal of our research is to measure such low-energy internal conversion electrons of various chemical states. For high-resolution energy spectrometry, it is necessary to prepare radionuclides as a thin source. In this report, we attempt to prepare an ultra-thin source using the Self-assembled Molecular (SAM) technique. The performance of the SAM substrate was investigated through radio-tracer experiments.

RIKEN Ag-based multi-isotope tracers and single-isotope tracers were used for the experiments. The multi-tracers were produced by irradiation of a Ag metal plate with a ^{14}N ion beam accelerated by the RIKEN Ring Cyclotron. Ag target material was removed by a precipitation method with the use of hydrochloric acid. Single-isotope tracers were prepared using the AVF cyclotron at CYRIC, Tohoku University.

The procedure for the preparation of SAM substrates was similar to that described in Ref[1]. An Al plate 25 mm in diameter was polished and rinsed with distilled water. After drying, the Al plate was treated with 1 vol.% 3-aminopropyltriethoxysilane (APTES) in absolute toluene through chemical vapor deposition in a self-made PTFE cell at 100 °C for 2 h; subsequently, it was rinsed with methanol and absolute toluene. Phosphonation of the terminal amino groups of APTES was performed with phosphoryl chloride and γ-collidine in absolute acetonitrile, and the sample was then rinsed with absolute acetonitrile and distilled water. The coupling of the SAM substrate and radionuclides was carried out in an aqueous solution or an isopropyl alcohol solution.

The bound radionuclides were assayed by γ-ray spectrometry with an HPGe semiconductor detector. A γ-ray spectrum of a multitracer-SAM sample is shown in Fig. 1. The γ-peaks of ^{46}Sc, ^{54}Mn, ^{65}Zn, ^{75}Se, ^{83}Rb, ^{85}Sr, ^{88}Zr, ^{88}Y, ^{101}Rh, and $^{102}Rh^{m}$ are observed in the spectrum. By comparison of γ-peak counts of each nuclide, we found that the yield of nuclides with oxidation states +3 and +4 is relatively high. On the other hand, ^{22}Na and ^{57}Co were not detected, although these nuclides were included in the multi-tracer solution. This tendency was found regardless of the reaction solvent to be combined with radionuclides.

To confirm the uniformity of the SAM source, the α source was prepared with ^{241}Am tracer and subjected to autoradiography. A photograph taken using an imaging plate is shown in Fig. 2. The deviation of α activity is observed at the upper-left part of the image. This deviation probably originates from fine scratches on the Al plate. With the exception of this part, the α activity is spread uniformly over the entire SAM substrate. Although there are still some problems, the present method will provide us with a reliable ultra-thin source after some improvements.

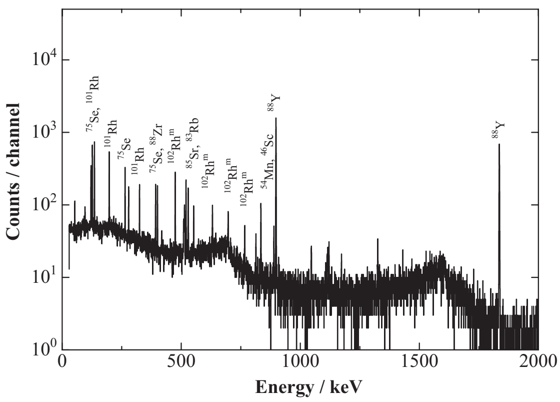

Fig. 1. An example of a γ-ray spectrum of a multitracer-SAM sample.

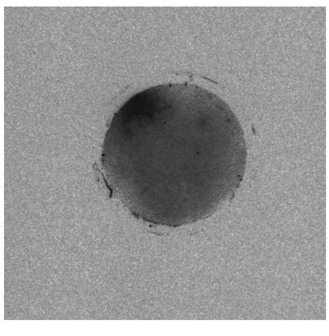

Fig. 2. Photographic image of a ^{241}Am-SAM sample taken using an imaging plate.

*1 RIKEN Nishina Center
*2 Research Center for Electron Photon Science, Tohoku University

References
1) A. Shida et al.: Surf. Coat. Technol. **169-170**, 686 (2003).

Production of purified ^{85}Sr solution

S. Yano,[*1,*2] Y. Wakitani,[*1,*2] T. Yamada,[*1,*2] J. Kanaya,[*2] S. Shibata,[*2] and H. Haba[*2]

Since 2007, we have distributed purified radioisotopes such as ^{65}Zn, ^{88}Y, and ^{109}Cd to the general public.[1)] After the Fukushima Dai-ichi Nuclear Power Plant accident in 2011, the demand for ^{85}Sr solutions having a high specific radioactivity has been growing. In this work, we investigated the production of ^{85}Sr in the ^{85}Rb(d,2n)^{85}Sr reaction using a 24-MeV deuteron beam from the RIKEN AVF cyclotron. We also studied a chemical procedure to obtain a purified ^{85}Sr solution.

^{85}Sr ($T_{1/2}$ = 64.853 d) was produced by irradiating an RbCl disk (Sigma-Aldrich; chemical purity: > 99.99%; thickness: 500 mg cm^{-2}) of natural isotopic abundance with 24-MeV deuterons. The average beam intensity was 159 nA. The irradiation time was 17 min. ^{85}Sr was chemically separated in accordance with the scheme shown in Fig. 1. The irradiated RbCl target was dissolved in 2 mL of H_2O and 2 mL of 8 M HNO_3. After evaporating the solution almost to dryness, the residue was again dissolved in 2 mL of 8 M HNO_3. The resulting solution was evaporated to dryness to remove chloride ions, and the residue was dissolved in 4 mL of 8 M HNO_3 and loaded onto a reversed-phase extraction chromatography column (ϕ5 mm×50 mm height) packed with Sr Resin (Eichrom; 100–150 mesh). The column was then washed with 12 mL of 8 M HNO_3. In this process, ^{85}Sr was absorbed on the Sr Resin, and the target material of Rb was completely eluted, as traced with byproducts of ^{84}Rb and ^{86}Rb. ^{85}Sr was then eluted with 8 mL of 0.05 M HNO_3. The eluent was evaporated to dryness, and the residue was dissolved in 1 mL of concentrated HCl (c. HCl). After evaporating the solution almost to dryness, the residue was dissolved in 2 mL of 0.1 M HCl and loaded onto a column (ϕ5 mm×40 mm height) packed with a cation-exchange resin (Dowex 50W×8; 200–400 mesh). The column was then washed with 3 M HCl. ^{85}Sr was eluted with 6 M HCl. The activity of ^{85}Sr was determined through γ-ray spectrometry using a calibrated Ge detector.

The γ-ray spectra of the produced ^{85}Sr are shown in Fig. 2. The produced activity of ^{85}Sr was 145 kBq, and the radionuclidic purity was > 99.9%. The production yield of ^{85}Sr under the present experimental condition was about 3 MBq μA^{-1} h^{-1}. The chemical yield was 89%.

The chemical impurity in the purified solution will be evaluated by using ICP MS for a control sample, which was treated using the same procedure as that used for the irradiated sample, in further studies.

[*1] Japan Radioisotope Association
[*2] RIKEN Nishina Center

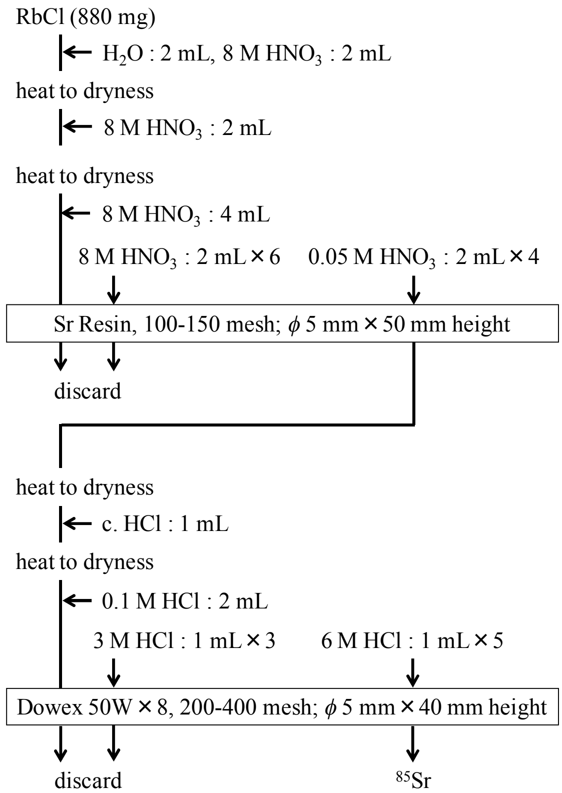

Fig. 1. The chemical separation procedure of ^{85}Sr from the irradiated RbCl target employed in the present study.

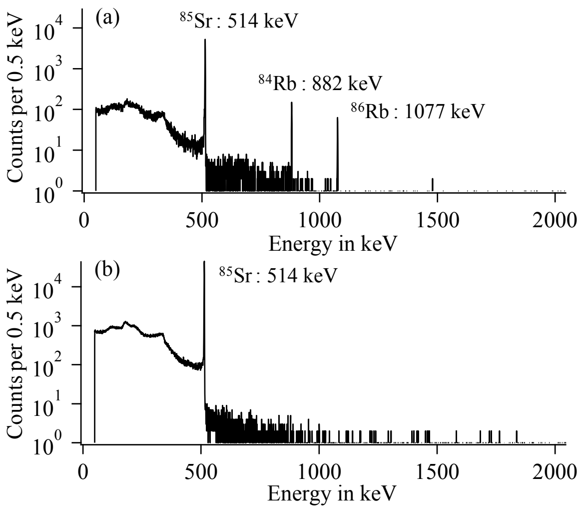

Fig. 2. The measured γ-ray spectra of the produced ^{85}Sr. (a) and (b) were obtained before and after the chemical separation, respectively.

References

1) T. Kambara et al.: a separate paper in this issue.

4. Radiation Chemistry and Biology

Linear-energy-transfer dependence of polymer gel dosimeters under carbon beam irradiation

T. Maeyama,[*1] N. Fukunishi,[*1] K. L. Ishikawa,[*2] T. Furuta,[*2] K. Fukasaku,[*2,*3] S. Takagi,[*2] S. Noda,[*2] R. Himeno,[*2] and S. Fukuda[*4]

Polymer gel dosimeters are widely used for quality assurance in the treatment planning of cancer therapy using low linear-energy-transfer (LET) radiations such as X-rays, and γ-rays. They consist of gel-fixed radiation-sensitive compounds, and the amount of the reaction products after irradiation depends on the dose accumulated at each position in the gel. The proton NMR is sensitive to the reaction products, and its three-dimensional map can be read out by using the magnetic resonance imaging (MRI) technique [1]. With regard to the application of gel dosimeters to heavy-ion beams that have higher biological effectiveness than low-LET radiations, it has been reported that the dose response of all the gel dosimeters except for the nanocomposite Fricke gel developed recently [2] changes with radiation quality, which depends on the charge and velocity of the ion in the case of heavy-ion beams. The dose distribution hence cannot be evaluated directly from the measured MRI signal strength in these gel dosimeters.

In this study, we investigated the dose response of the VIP polymer gel dosimeters [3] for carbon beams having a wide LET range, by comparing the relaxation rate (R_2 [s^{-1}]) obtained by MRI with the dose estimated by the Particle and Heavy Ion Transport code System (PHITS) [4]. The LET is a representative index of radiation quality, and a reliable estimation of the LET and the dose is now available by PHITS. VIP polymer gel dosimeters were prepared following the prescription [3] and sealed into containers, the length of which is sufficient to stop the ions injected into the gel dosimeters. They were irradiated with 135-AMeV and 290-AMeV $^{12}C^{6+}$ ions accelerated by the RIKEN Ring Cyclotron and the Heavy Ion Medical Accelerator in Chiba, respectively. The dose response of irradiated samples was obtained from 1.5-T MRI (Philips).

Results of the dose response [$s^{-1}Gy^{-1}$] are plotted as functions of the dose-weighted average of the LET (hereafter, dose-averaged LET) where the projectile ions and all the secondary particles produced by the nuclear reaction are included. The dose response decreases with increasing LET, as reported in the literature. In addition, the dose response is approximately 10% higher for the 290-AMeV beam than for the 135-AMeV beam at the same dose-averaged LET (Fig 1, symbols). This sizable difference can be explained by the different contributions from secondary particles. Ions with higher injection energy pass the thicker gel before reaching the given dose-averaged LET, and yield mode of secondary particles, mainly light fragments of the projectile. Furthermore, low-LET fragments contribute more effectively to R_2 than high-LET particles. Hence, the 290-AMeV beam has higher dose response than 135-AMeV beam. For the above effects, we are investigating the contribution of minor ions such as target fragments.

To confirm the present explanation quantitatively, we investigated whether the observed 10% difference can be reproduced by assuming that the dose response of the gel dosimeter depends only on the LET value for all the relevant ions. As a result, we found a universal dose response function of the LET (R(LET), blue-dashed line in Fig. 1) that reproduced well the measured dose response for both the 135-AMeV and 290-AMeV carbon beams. The dose-averaged responses R_{ave} defined in Eq. 1 are shown in Fig. 1.

$$R_{ave} = \frac{\int R(LET)Dose(LET)dLET}{\int Dose(LET)dLET} \qquad (1)$$

The dose response obtained here was used for predicting a geometrically more complicated R_2 map measured by the VIP gel under a heterogeneous irradiation condition. The calculated R_2 distributions reproduced the measured ones with the accuracy of ±5% except for the end of the ion range, the position of which was also reproduced within 1-2 mm.

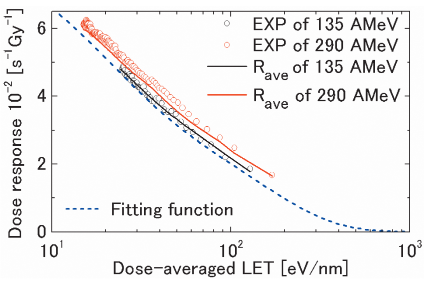

Fig. 1. Comparison of dose response of VIP gel obtained at different incident energies. Symbols represent experimental results, continuous lines represent dose-averaged response calculated by PHITS, and the dashed line represents the assumed fitting function.

References
1) Baldock, C., et al.: Phys. Med. Biol. **2010**, 55
2) Maeyama, T., et al.: Radiat. Phys. Chem. **2014**, 96
3) Kipouros, P., et al.: Phys. Med. Biol. **2001**, 46.
4) Sato, T., et al.: J. Nucl. Sci. Technol. **2013**, 50.

*1 RIKEN Nishina Center
*2 RIKEN Advanced Center for Computing and Communication
*3 Dept. of neurosurgery, Himon'ya Hospital
*4 NIRS Research Center for Charged Particle Therapy

Observation of unrepairable lesions in DNA by using 3-MeV proton microbeams produced by glass capillaries

T. Ikeda,*1 M. Izumi,*1 V. Mäckel,*2 T. Kobayashi,*2 K. Ogiwara,*2 T. Hirano,*3 Y. Yamazaki,*2 and T. Abe*1,*3

Microbeams allow extremely efficient alteration of or damage to a small region in the target with minimum beam intensity. To date, X-ray, UV, and visible light laser have been used as microbeams. However, to create double strand breaks (DSBs) in DNA, which are difficult to repair, multiple photons are required and have to be focused on the DNA. Because of the finite size of the focal spot, the beam intensity needs to be high. This intense beam creates multiple DSBs. In contrast, when ion beams are used, a single ion can create a DSB via ballistic electrons and radicals generated along the ion's trajectory. This is an advantage of ion-beam irradiation. We developed a method involving ion-microbeam irradiation to single cells in culture using tapered glass capillaries with outlet diameters of ~1 μm.[1,2] The capillary is known as glass pipet for microinjection or a glass electrode for real time measurements of the voltage potential within the neurons. The number of ions irradiated to single cells is controlled by a pulsed beam. However, some DSBs can be repaired quickly even if ions hit the DNA. Here, we measured the fluorescence brightness corresponding to unrepaired DSBs after irradiation for different numbers of ions input per cell to confirm that a small number of protons can cause unrepairable damage.

The beam used for irradiation was composed of 3-MeV protons that were generated by a RIKEN Pelletron accelerator and transported to the cell irradiation port, which uses an inverted microscope (OLYMPUS IX-71). A glass capillary optics system with a thin plastic end-window (diameter, 2 μm) was mounted at the beam port at 45° so that a petri dish filled with solution can be used. The capillary tip can go close to the cells which is advantageous for suppressing multiple scattering of ions before they reach the target. To adjust the number of protons, which is proportional to the dose, the time window of the beam pulse, which included a maximum of 10 ions, was set at 1 - 5 μs, wherein the number of ions in a pulse follows Poisson distribution. We irradiated 50-1,000 ions per cell to reduce statistical error.

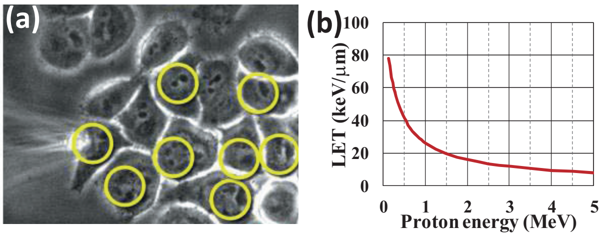

Fig. 1. (a) HeLa cells (yellow circles) and the tip of the glass capillary, (b) LET in water vs. proton energy.

Figure 1(a) is a microscopic view of HeLa cells during irradiation. Cell nuclei marked by yellow circles were selected. The capillary tip, which was above the cells, is at the lower left in Fig. 1(a). It took ~20 min to irradiate 60 cells in one dish. After the irradiation, cells grown in glass-bottom dishes were washed three times with ice-cold phosphate-buffered saline (PBS) and fixed with 4% formaldehyde in PBS at 4°C for 20 min. Then, the cells were permeabilized with 0.5% Nonidet P-40 in PBS at 4°C for 5 min, and phosphorylated histone H2AX was detected by using rabbit antibody (Millipore) and an Alexa488-conjugated donkey anti-rabbit IgG (Jackson ImmunoResearch Laboratories).

We obtained clear fluorescence distributions only in the irradiated nuclei. The brightness of the foci (determined in terms of Alexa488 fluorescence) in each irradiated nucleus was proportional to the number of *unrepaired* lesions in DNA at the time cell fixation was initiated. The brightness data were displayed in a histogram by using the software, *Image-J*.[3] After subtracting the low background level of foci seen for the non-irradiated cells, histogram integration was compared according to the microbeam intensities [Table 1]. The brightness increased with but was not proportional to microbeam intensity, perhaps because of saturated damage due to the large number of ions.

The linear energy transfer (LET) of 3-MeV proton was ~10 keV/μm [Fig. 1(b)]. When heavier ion pieces are selected, higher LETs will be obtained. Moreover, the ion stopping positions can be localized at a certain depth inside a cell because of their short ranges. In this case, extremely high energy deposition corresponding to the Bragg peak is available for destroying a single cell or a small region of tissue.

Table 1. Integrated brightness of the foci.

Microbeam intensity (ions/cell)	Brightness of Alexa488 (arbitrary unit)
50	733
200	875
1,000	940

*1 RIKEN Nishina Center
*2 Atomic Physics Laboratory, RIKEN
*3 RIKEN Innovation Center

References
1) Y. Iwai, T. Ikeda, T. M. Kojima, Y. Yamazaki, K. Maeshima, N. Imamoto, T. Kobayashi, T. Nebiki, T. Narusawa, and G. P. Pokhil: Appl. Phys. Lett. **92**, 023509 (2008).
2) V. Mäckel, W. Meissl, T. Ikeda, M. Clever, E. Meissl, T. Kobayashi, T. M. Kojima, N. Imamoto, K. Ogiwara, and Y. Yamazaki: Rev. Sci. Instrum. **85**, 014302 (2014).
3) *Image-J* 1.47v, downloaded from http://rsbweb.nih.gov/ij/

Effects of trichostatin A on radiosensitivity to high-linear energy transger (LET) radiation in mammalian cells with defects in DNA repair proteins

M. Izumi[*1] and T. Abe[*1]

In eukaryotes, DNA is associated with histones and packaged into nucleosomes, which are arranged into higher order structures to form chromatin. The chromatin structure contributes to various aspects of DNA metabolism including replication, recombination, and transcription. However, it is still unclear how repair reactions and checkpoint responses caused by heavy-ion irradiation are regulated by chromatin structures. To investigate the roles of chromatin structures in DNA repair after heavy-ion irradiation, we have been focusing on the damage response observed after cells are treated with a potent histone deacetylase inhibitor, trichostatin A (TSA).

To analyze the effects of TSA on repair pathways, we investigated the X-ray sensitivity of wild-type CHO-AA8 cells and CHO mutant lines deficient in homologous recombination (irs1SF cells) [1], non-homologous end-joining (V3 cells) [2], and base excision repair (EM9 cells) [3] in the absence or presence of TSA in a previous study[4]. All three mutant cell lines showed increased X-ray sensitivity (Fig. 1a). TSA treatment enhanced the X-ray sensitivity of wild-type CHO cells. In contrast, TSA enhanced the X-ray radioresistance of irs1SF cells, suggesting that the homologous recombination pathway is involved in radiosensitivity enhancement by TSA. However, TSA did not affect V3 and EM9 survival. These results suggest that non-homologous end-joining and/or base excision repair are stimulated by TSA.

In this study, we investigated argon-ion (LET = 300 keV/μm) sensitivity using the same cell lines. We compared the radiosensitivity of the four cell lines without TSA treatment (Fig. 1a). We found that CHO and V3 cells showed nearly identical dose-response profiles after argon-ion irradiation. We obtained the same results after carbon-ion (LET = 80 keV/μm) irradiation (data not shown), suggesting that non-homologous end-joining is not involved in the repair pathway induced by high-LET ionizing radiation. EM9 and irs1SF cells showed increased sensitivity to argon ions. These results are compatible with those of several recent studies[5,6].

We investigated the effect of TSA on cell line survival (Fig. 1b). TSA treatment enhanced CHO cell sensitivity to argon ions. However, TSA did not affect irs1SF cell sensitivity, which is compatible with the conclusion that non-homologous end-joining is not involved in the repair pathway induced by high-LET irradiation. In contrast, TSA slightly enhanced V3 and EM9 cell radiosensitivity, which seems to be due to the inhibitory effect of TSA on homologous recombination.

Although our survival assay suggests that the non-homologous pathway is not involved in repair after heavy-ion irradiation, we observed that DNA-PK was recruited to the DNA damage sites (data not shown). Currently, we are investigating the localization of repair proteins by indirect immunofluorescence and studying the mechanism underlying the suppression of non-homologous end-joining after heavy-ion irradiation.

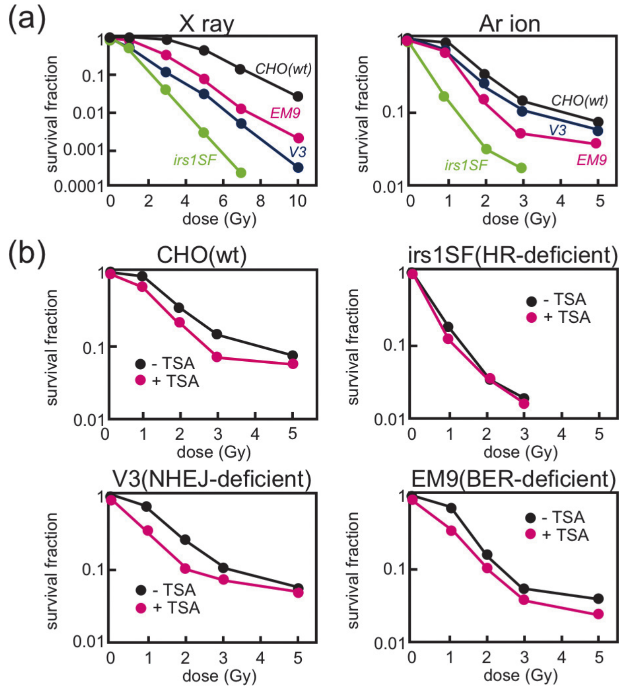

Fig. 1 (a) X-ray and argon-ion sensitivity of CHO, irs1SF, V3, and EM9 cells. Cells were irradiated with X-rays or argon ions (LET = 300 keV/μm), and radiosensitivity was estimated by the clonogenic survival assay. (b) Effects of trichostatin A (TSA) on the radiosensitivity of CHO, irs1SF, V3, and EM9 cells. Cells were pretreated with TSA (0.1 μM) for 10 h and irradiated with argon ions. Subsequently, the cells were cultured for an additional 14 h in the presence of TSA, and radiosensitivity was estimated by the clonogenic survival assay. Abbreviations: wt, wild type; HR, homologous recombination; NHEJ, non-homologous end-joining; BER, base excision repair.

References

1) R.S. Tebbs, et al.: Proc. Natl. Acad. Sci. USA **92,** 6354 (1995)
2) S.R. Peterson, et al.: Proc. Natl. Acad. Sci. USA **92,** 3171 (1995)
3) L.H. Thompson, et al.: Mol. Cell. Biol. **10,** 6160 (1990)
4) M. Izumi, et al.: RIKEN Accel. Prog. Rep. **46,** 254 (2013)
5) H. Wang, et al: Nucl. Acids Res. **38,** 3245 (2010)
6) S.C. Genet, et al.: Oncology Rep. **28,** 1591 (2012)

*1 RIKEN Nishina Center

Cell-killing effect of low doses of high-LET heavy ions (VI)

M. Tomita,[*1,*2] T. Tsukada,[*1] and M. Izumi[*1]

Non-DNA-targeted effects are not a direct consequence of radiation-induced initial lesions produced in cellular DNA, but are an indirect consequence of intra- and intercellular communications involving both irradiated and nonirradiated cells. These effects include low-dose hyper-radiosensitivity (HRS) and radiation-induced bystander response (RIBR).[1,2] RIBR is a cellular response induced in nonirradiated cells that receive bystander signals from directly irradiated cells within an irradiated cell population.[1,2] RIBR induced by low doses of high-LET radiations is an important issue concerning the health of astronauts and in heavy-ion radiation cancer therapy. Here, we investigated the molecular mechanisms underlying and biological implications of RIBR induced by such low doses of high-LET radiations. We previously found that HRS was induced in normal human fibroblast WI-38 cells that were irradiated with low doses of high-LET argon (Ar) and iron (Fe) ions, suggesting that RIBR was induced.[3–5] Nitric oxide (NO) was found to be involved in this process.[3–5] Furthermore, we found that reactive oxygen species (ROS), gap-junction intercellular communication (GJIC), and cyclooxygenase-2 (COX-2) protein as well as NO may be involved in Ar-ion-induced bystander signal transfer.[4] Here, we examined the effects of a scavenger of ROS (DMSO) and an inhibitor of GJIS (lindane) or COX-2 (NS-398) on Fe-ion-induced RIBR.

Here, we have shown the revised clonogenic survival curve of WI-38 cells irradiated with Fe ions; the curve was obtained by adding new data to previous results[3)] [Fig.1]. HRS could be clearly observed in cells irradiated with Fe ions at doses lower than 0.2 Gy and was partly suppressed by pretreatment with carboxy-PTIO (c-PTIO), an NO scavenger.

Next, we examined HRS suppression at 0.1 Gy by DMSO, lindane, c-PTIO or NS-398 pretreatment [Fig. 2]. Lindane and NS-398 were dissolved in DMSO. DMSO did not significantly suppress the HRS, although the standard errors of the mean (SEM) were large. In contrast, lindane, NS-393, and c-PTIO significantly suppressed HRS to similar levels. These results suggested that the GJIC and COX-2 mediated pathway as well as NO was also involved in Fe-ion-induced bystander signal transfer. Currently, we are examining the role of the NF-κB/Cox-2/prostaglandin E2 and NF-κB/iNOS/NO pathways,[2)] which may be activated in bystander cells that have been subjected to ROS and NO, in HRS induced by high-LET radiations.

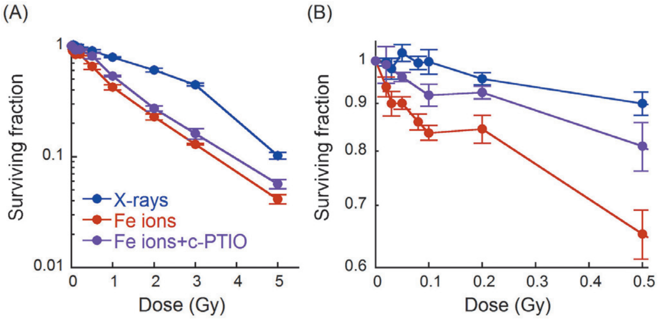

Fig. 1. Cell-survival curves of WI-38 cells. Confluent monolayers of WI-38 cells were irradiated with 90 MeV/u Fe ions (1000 keV/μm) and some of the cells were pretreated with c-PTIO (20 μM). The surviving fraction was determined by a colony forming assay. The error bars represent the standard error of the mean (SEM) (n=3-5).

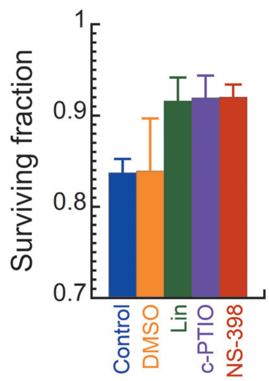

Fig. 2. Effect of inhibitors or scavengers. DMSO (0.1%), lindane (Lin, 50 μM), c-PTIO (20 μM) or NS-398 (50 μM) was added to the medium 2 h before irradiation.[6)] WI-38 cells were irradiated with 0.1 Gy Fe ions. The error bars represent the standard error of the mean (SEM) (n=3-4).

*1 RIKEN Nishina Center
*2 Radiation Safety Research Center, Central Research Institute of Electric Power Industry

References

1) K. M. Prise et al.: Radiat. Prot. Dosimetry **99**, 223 (2002).
2) T. K. Hei et al.: Curr. Mol. Pharmacol **4**, 96 (2011).
3) M. Tomita et al.: RIKEN Accel. Prog. Rep. **43**, 276 (2010).
4) M. Tomita et al.: RIKEN Accel. Prog. Rep. **45**, 207 (2012).
5) M. Tomita et al.: RIKEN Accel. Prog. Rep. **46**, 253 (2013).
6) M. Tomita et al.: Radiat. Res. **173**, 380 (2010).

Development of the mutant isolation system in fruit flies

K. Tsuneizumi,[*1] and T. Abe,[*1]

Heavy-ion beam mutagenesis is an effective mutation breeding method [1, 2]. Although this method has been highly successful with plants, its use for animals has been limited. To extend its application to animals, we plan to acquire more basic data to determine optimal conditions for heavy-ion-beam irradiation using *Drosophila melanogaster* (fruit fly) as a useful model system.

Over the past century, several unique genetics tools have been developed using the fruit fly. A balancer chromosome is one such popular tool and is known to prevent homologous recombination during meiosis. A single balancer line was previously found to be more suitable for stabilizing the mutant isolation system than a double balancer line[3]. Therefore, we focused only on third-chromosome events and re-established a third chromosome balancer line before starting the irradiation experiment.

To overcome the instability problem of a graphic record at previous data[3], we decided to use commercial cuvettes with a plane surface [Fig. 1a]. Because most of the vials commonly used for fly maintenance have a curved surface, heavy-ion-beam irradiation condition is uneven in the vials depending on the thickness of curved plastic. To decrease the opportunity of the energy loss in heavy-ion beam by flies overlapping, only two flies were put into each cuvette. Then, six cuvettes were arranged in a commercial container in order to use a uniform irradiation range with an automatic sample changer [Fig. 1b]. To evaluate the stability of the improved mutant isolation system, we subjected the fruit flies to a carbon-ion beam with linear energy transfer (LET) values of [80keV/μm] at several dose levels (1.0, 3.0, 10.0, 30.0, and 60.0 Gy).

To estimate the effect of heavy-ion-beam irradiation, we measured the number of F1 progeny as a biological effect. In this study, males and females were immediately separated after eclosion and were bred for 3 days. Then every two males were put into each cuvette for irradiation [Fig. 1b]. It was performed in the females equally. After irradiation with different heavy-ion-beam doses, the males were provided fresh harems of virgin females every 2–3 days. The females were provided with males and the medium was replaced every 2–3 days. The oviposited eggs were bred, and the number of progeny that survived to the adult stage was determined.

Decrease in the reproductive ability of males was found to be caused by aging and not irradiation. In contrast, the reproductive ability of females did not change during the observation period [Fig.2]. The results for the males showed a linear correlation between the number of progeny and irradiation dose. In contrast, a non-linear curve was observed for the females [Fig. 2]. These data suggest that a radiosensitivity is different between males and females.

We have developed a stable mutant isolation system using fruit flies by using heavy-ion-beam irradiation. Currently, we are establishing various mutants and will be analyzing DNA damage in homozygotes. These data will be helpful for optimizing the irradiation system in the future.

*1 RIKEN Nishina Center

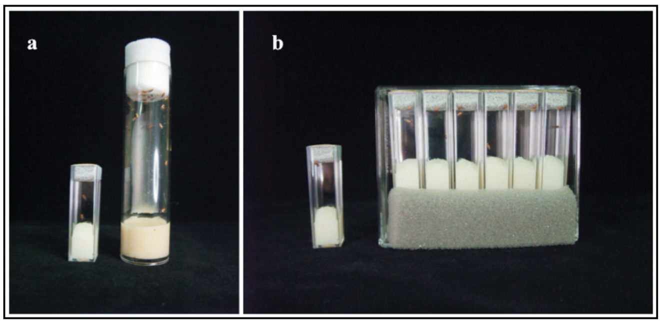

Fig. 1. a) A photograph of a cuvette and a breeding vial. b) A photograph of sample cuvettes for irradiation using an automatic sample changer.

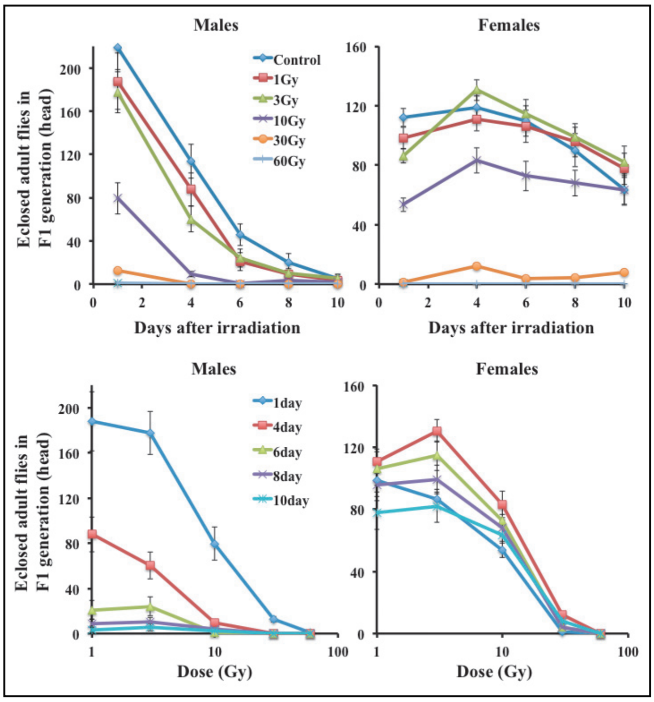

Fig. 2. Upper panels show the correlation between the number of F1 progeny and the days after heavy-ion-beam irradiation. Lower panels show the correlation between the number of F1 progeny and the irradiation dose. F: filial generation.

References
1) T. Abe et al.: Gamma Field Symp. **39**, 45 (2000).
2) A. Tanaka et al.: J. Radiat. Res. **51**, 223 (2010).
3) K. Tsuneizumi et al.: RIKEN Accel. Prog. Rep. **46**, 255 (2013).

Detection of deletions induced by Fe-ion irradiation in *Arabidopsis thaliana* using array comparative genomic hybridization†

Y. Kazama,*[1] T. Hirano,*[1] K. Nishihara,*[2] S. Ohbu,*[2] Y. Shirakawa,*[2] and T. Abe*[1,*2]

Heavy-ion irradiation mainly induces deletions. The size of deletions increases with increasing linear energy transfers (LETs)[1]. Because large deletions are useful for producing null mutations as well as disrupting multiple genes arrayed in tandem, high-LET ion beams are considered powerful mutagens in the field of genome science. However, the determination of deleted chromosomal region(s) in a mutant by using classical PCR-based methods is difficult because designing primers at both sides of a large unidentified deletion is quite difficult. Thus, a method for rapidly detecting deletions at the whole-genome level is desired.

Array comparative genomic hybridization (array CGH) is a powerful tool for detecting deletions at the whole-genome level[2]. In the present study, we herein optimized the array CGH experiment to develop a method for investigating large heavy-ion induced deletions at the whole-genome level. For the array CGH, we used an *Arabidopsis* mutant having downward-pointing flowers (Fe-148-pg1) as an example of a mutant harboring large deletions, which was induced by Fe-ion beam irradiation (90 MeV/nucleon, 640 keV/μm) at a dose of 50 Gy. Through the phenotypic characterization and PCR confirmation, Fe-148-pg1 was found to have a large deletion around the *BREVIPEDICELLUS* (*BP*) gene.

Arabidopsis thaliana ecotype Columbia (Col-0) was used as a wild-type plant. The whole-genome sequence of Col-0 was tiled with oligonucleotides that started every 50 bp. Probe lengths were constrained to a minimum of 50 and a maximum of 75 bp. Considering this design, our array was expected to detect deletions of more than 200 bp at the whole-genome level.

The DNA of the wild-type and the mutant plant (Fe-148-pg1) were labelled with Cy5 and Cy3, respectively. Hybridization, washing, and scanning were conducted by Roche NimbleGen Inc (Madison, WI, USA). Raw fluorescence intensity data were obtained from scanned images of the oligonucleotide tiling arrays by using NimbleScan 2.4 extraction software (Roche NimbleGen Inc.). For each spot on the array, log2 ratios of the Cy3-labelled sample to the Cy5 reference sample were calculated.

Candidate deletions were identified as follows. First, regions supported by more than 4 consecutive probes with log2 ratios of over 1.0 were listed as candidate deletions. Then, the candidate deletions were confirmed by performing PCR. For the PCR test, 7 individual M_3 plants were tested; when some of the plants showed amplification in the candidate deletion region, the candidate deletion was determined as being heterozygous in the M_2 generation. Finally, we detected 7 deletions (Table 1). Candidate deletions supported by the higher log2 ratio tended to be homozygous. However, candidate deletions supported by log2 ratios lower than 1.209 were false positives. As expected, the Fe-148-pg1 had a large deletion covering the *BP* gene; the size of deletion was found to be 90,307 bp by conducting PCR-based confirmation and sequencing. The results suggest that our array platform can detect both homozygous and heterozygous deletions at the whole genome level, although the estimated deletion size is not completely consistent with the actual one.

Table 1 List of deletion peaks estimated by array CGH in Fe-148-pg1.

Start site of Peak area		Estimated		Detected	Genetic
Chr.	Position	deletion size	Signal*	deletion	homogeneity in M_3
4	5,129,711	88069	1.500–6.097	○	homogeneous
4	7,875,508	81108	3.375–6.047	○	homogeneous
1	17,030,769	467	2.289	-	-
3	17,831,368	450	2.076	○	homogeneous
4	8,550,408	264	1.992	○	homogeneous
5	8,060,900	84816	1.744–1.930	○	heterogeneous
4	2,179,908	850	1.777	-	-
4	2,177,558	814	1.767	-	-
4	2,185,508	723	1.743	○	heterogeneous
4	2,181,208	469	1.209	○	heterogeneous

*When several peaks were detected in a naborhood, the peaks were combined and the range of signal values were considered.

† Condensed from the article in Genes Genet. Syst. **88**, 189-197 (2013)

*1 RIKEN Innovation Center
*2 RIKEN Nishina Center

References

1) T. Hirano et al.: Mutat. Res. **735**, 19 (2012).
2) A. J. Nagano et al.: Plant J. **56**, 1058 (2008).

Exome resequencing reveals mutations in rice induced by heavy-ion beam with LETmax

R. Morita,[*1] K. Ishii,[*1] H. Takehisa,[*2] Y. Hayashi,[*1] S. Kogure,[*1]
K. Ichinose,[*1] H. Tokairin,[*1] T. Sato[*3,*4] and T. Abe[*1,*4]

Heavy-ion beam irradiation induces mutations at a high rate without severely inhibiting growth at a relatively low dose. Heavy-ion beam with high linear energy transfer (LET) cause greater biological effects than low-LET radiation such as gamma rays and X-rays. LET can be controlled by adjusting the speed of the ions or choosing appropiate ion species. We found that the highest mutation rate is obtained at an LET of 30 keV/μm in Arabidopsis thaliana[1)]. This high-efficiency LET (termed LETmax) mostly induced small deletions[2)]. In rice, the LETmax value was determined as 50-70 keV/μm. However, the mutations induced in rice when we irradiated heavy-ion beams with LETmax were unclear. We performed exome-resequencing analysis to reveal the nature of the mutations in rice induced by heavy-ion beams with LETmax in rice.

We selected seven rice (*Oryza sativa* L. cv. Nipponbare) mutants induced by LETmax irradiation to perform exome-resequencing analysis. Paired-end libraries were constructed using SeqCap EZ developer library (Roche). Sequencing was performed using Hiseq 2000 (Illumina). Mutations were detected by using SAMtools and BEDTools software. We detected 16 deletions and 14 base substitutions among seven mutants (Table 1). Of the 16 deletions, 14 were small deletions (1-18 bp) and two were large deletions (739 bp and 102158 bp). Of the 16 deletions, 14 were located in coding regions. Two were located in the 5' untranslated region and intron. Of the 14 base substitutions, 9 induced alteration of the amino-acid sequence of each gene, such as missence mutation, nonsense mutation, and START gain mutation. Four base substitutions were located in 3' untranslated region. The one remain was a silent mutation. Of the 14 deletions located in coding regions, 1-18 bp deletions constituted 85.7% (12/14) of the total deletions. These findings indicate that heavy-ion beams with LETmax induce small deletions suitable for single-gene disruption in rice.

Table 1. Homozygous deletion and base substitution detected by Exome resequencing

Line	Ion / Dose / LET (Gy) (keV/μm)	Deletion		Base substitution	
		size (bp)	Remarks	change base	Remarks
3-14	C / 15 / 50	1*		A→G*	Missense mutation (K/R)
		1*			
5-12	C / 15 / 50	1*		A→G*	Missense mutation (Q/R)
		10	intron		
		18*			
4-13	C / 15 / 60	1*		A→T	3'UTR
		9*			
7-3B	Ne / 10 / 63	2+1*	Filler DNA	G→T*	START gain mutation
		3	5' UTR	T→G	Silent mutation
		739*	disruption of 2 genes	G→T*	Nonsense mutation
				C→T*	Missense mutation (G/S)
6-62	Ne / 15 / 63	1*		G→T*	Missense mutation (Q/K)
		1*		C→A*	Missense mutation (P/T)
		13*		A→T	3'UTR
		102158*	disruption of 7 genes		
Ne-1779	Ne / 15 / 63	14*		T→A*	Missense mutation (L/H)
				T→A*	Nonsense mutation
7-30	Ne / 15 / 70	12+1*	Filler DNA	C→T	3'UTR
				C→T	3'UTR

* Mutations that change the aino-acid sequences

*1 RIKEN Nishina Center
*2 National Institute of Agrobiological Sciences
*3 Graduate School of Life Science, University of Tohoku
*4 Innovation Center, RIKEN

References

1) Y. Kazama et al.: Plant Biotech. **25**, 113 (2008).
2) Y. Kazama et al.: BMC Plant Biol. **11**, 161 (2011).
3) Y. Hayashi et al.: Cyclotrons 2007, 237 (2008).

*mPing*SCAR marker, a powerful tool for genetic analysis of agricultural traits in rice mutants induced using ion-beam irradiation

H. Saito,[*1] R. Morita,[*2] Y. Okumoto,[*1] K. Ishii,[*2] Y. Hayashi,[*2] S. Kogure,[*2] K. Ichinose,[*2] and T. Abe[*2,*3]

Rice is a major cereal crop that is the dietary staple for more than half of the world's population. For sustainable production and increased yield, it is important to perform molecular regulation of various agricultural traits. Mutagenesis study is an effective approach to identify novel genes that impart desired agricultural traits and to investigate their functions. Many of the agricultural traits, however, are quantitative traits and controlled by complex multiple genetic networks. Therefore, it is difficult to identify the mutant gene(s) when the F_2 population derived from the crosses between distantly related varieties is used to develop several available DNA markers. On the other hand, it is difficult to develop available DNA markers for genetic linkage analysis when using the F_2 population derived from the crosses between closely related varieties, to make it easy to identify the mutant gene(s) without multiple genetic segregations.

mPing is reported as the first active miniature inverted-repeat transposable element as well as the first active DNA transposon in rice[1]. Our previous study revealed that the *japonica* rice variety Gimbozu harbored over 1000 copies of *mPing*, whereas most of the closely related *japonica* varieties harbored less than 50 copies[2]. Therefore, polymorphic insertions of *mPing* are available for genetic analysis by using the F_2 population crossed between the closely related *japonica* varieties and Gimbozu[3]. Here, we evaluate the availability *mPing*SCAR (sequence characterized amplified region) marker based on the polymorphic insertions of *mPing* in Gimbozu and mutants derived from closely related varieties.

The imbibition seeds of *japonica* rice variety (cv. Nipponbare) were exposed to C, Ar, and Ne ions accelerated to 135, 95, and 135 MeV/nucleon, respectively. M_1 plants were grown in a paddy field, and M_2 seeds were harvested separately from each M_1 plant. In our paddy field research of the M_2 lines, we isolated a total of 11 mutants in which we observed mutations in the agricultural traits (Table 1). These mutants were crossed with Gimbozu and then the F_2 populations were applied to the genetic analysis for mapping the candidate region of the mutant genes by using the *mPing*SCAR markers.

All the F_2 populations, comprising 24–96 plants, showed bimodal distribution within the parental ranges. The mutant type to wild type ratio fit the 1:3 ratio expected for one-locus segregation. These results indicate that each mutant phenotype is conferred by a single recessive mutant gene. The linkage analyses by using 50 selective *mPing*SCAR markers, which are evenly distributed in all chromosome, identified markers that are closely linked with the mutant phenotypes. Further analyses by using additional *mPing*SCAR markers around the closely linked marker showed that the mutant genes were located in the region at physical distances of 1.13–13.82 Mb on chromosome 1, 3, 4, 5, 8 and 9 (Table 1). The rice annotation project database (RAP-DB: http://rapdb.dna.affrc.go.jp) showed that 195–973 genes were located in each region. Further, we extracted and isolated the DNA segments, including the exon regions of over 30,000 genes from the five mutant lines, and performed exome analysis by using the next-generation sequencing analyzer, Hiseq2000 (Illumina, San Diego, CA, USA). The experimental results showed that a single genomic mutation responsible for the mutant phenotype was identified in the candidate gene (or region) of the four mutant lines.

Although the current progress of next-generation sequencing techniques is remarkable, obtaining the sequence information of the whole genome alone is not enough to identify the candidate gene responsible for the mutant phenotype. Delimiting the candidate genes by using *mPing*SCAR markers in combination with the sequencing techniques and well developed database information would ensure further efficiency in detecting the mutant gene. Thus, we are confident that *mPing*SCAR marker is a powerful tool for the genetic analysis of the agricultural quantitative traits.

Table 1 The mapping summary of mutants in this study.

Number of analyzed mutants	11
Chromosomes for locating the mutant genes	1, 3, 4, 5, 8, 9
The size range of the candidate region	1.13–13.82 Mb
Number of genes located in the candidate region	195–973

References
1) T. Nakazaki et al.: Nature, 421, 170 (2003).
2) K. Naito et al.: PNAS, 103(47), 17620 (2006).
3) Y. Monden et al.: DNA Res., 16(2), 131 (2009).

*1 Graduate School of Agriculture, Kyoto University
*2 RIKEN Nishina Center
*3 Innovation Center, RIKEN

Identification of mutated sites induced by Ar-ion-beam irradiation in rice

S. Kogure,[*1] R. Morita,[*1] Y. Hayashi,[*1] K. Ichinose,[*1] M. Yamada,[*1] T. Wakana,[*1] H. Tokairin,[*1] K. Ishii,[*1] T. Sato,[*2,*3] and T. Abe[*1,*2]

Our team has studied the mutation induction in rice as an effect of heavy-ion-beam irradiation. Rice is a model plant of monocots, and it is useful for identifying mutation sites because its entire genome sequences are available. In previous studies, we showed that C-ion beams (15 Gy, LET 50 keV/μm) and Ne-ion beams (15 Gy, LET 63 keV/μm) cause small size deletion (6 mutant lines include 2 to 12 bp, 1 mutant line include 72348 bp) in rice genome.[1)-4)] In this study, we report the screening and identification of mutated genes and sites induced by Ar-ion beams.

Last year, we grew 1370 lines of M_2 generation obtained by irradiation of imbibed rice seeds with Ar-ion beams (2.5 or 5 Gy, LET 290 keV/μm) in both a greenhouse and a field. Over 100 mutant lines were isolated by screening, and some were suitable for PCR and sequence analysis.

Two mutant lines were selected in a greenhouse 2–3 weeks after germination and identified as mutated sites. Ar5-587 showed the phenotype of plastochron (PLA) mutants, which cause the rapid initiation of vegetative leaves without affecting phyllotaxy[5)] (Fig. 1a). A sequence analysis revealed that it contained 176-bp deletion and 7-bp insertion in the 1st exon of *PLA1*. Ar5-672 showed the phenotype of rice gibberellin (GA)-related mutants, which cause severe dwarfness with wide leaf blades and dark green leaves[6)] (Fig. 1b). It contained 2,627-bp deletion in the GA positive regulator, *GIBBERELLIN-INSENSITIVE DWARF 2* (*GID2*).[6)]

Three mutant lines were selected in a field, and identified as mutated sites. Ar5-62 exhibited heading 20 days earlier than wild type (Nipponbare). It contained 65,534-bp deletion and 2-bp (TG) insertion in chromosome 7, and lacked whole *GRAIN NUMBER, PLANT HEIGHT AND HEADING DATE 7* (*Ghd7*),[7)] which is an important regulator of heading date and yield potential in rice. Ar5-154 exhibited tall phenotype at the heading stage. It contained 47,930-bp deletion in chromosome 5, and lacked whole *ELONGATED UPPERMOST INTERNODE 1* (*EUI1*).[8)] Ar5-90 showed short grains (Fig. 1c) and semi-dwarfness. TAIL-PCR and several sequence analyses revealed that it contained 22,148-bp deletion in chromosome 1, and lacked whole *DAIKOKU DWARF1* (*D1*).[9)]

The data from these five mutant lines show that Ar-ion beams (5 Gy, LET 290 keV/μm) cause large deletions (>100 bp) in the rice genome.

It is necessary to identify more mutated regions of rice mutants for characterizing the mutations induced by heavy-ion-beam irradiation. We have isolated various rice mutants, and the research is in progress.

Table 1. Isolated mutants by Ar-ion-beam irradiation

Line	Phenotype	Gene	Mutation size
Ar5-62	Early heading	*Ghd7*(Os07g0261200)	65534-bp + 2-bp in
Ar5-90	Short grain	*DAIKOKU DWARF1*(Os05g0333200)	22148-bp del
Ar5-154	Elongation at heading stage	*EUI1*(Os05g0482400)	47930-bp del
Ar5-587	Plastochron	*PLA1*(Os10g0403000)	176-bp del + 7-bp in
Ar5-672	Severe dwarf	*GID2*(Os02g0580300)	2627-bp del

del: deletion, in: insertion

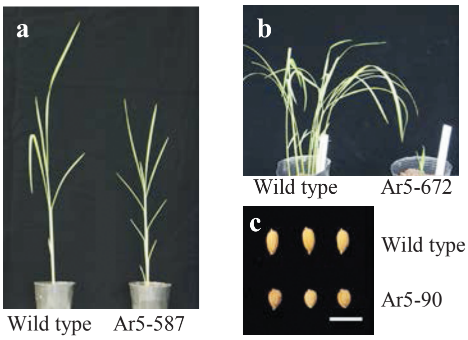

Fig. 1. Photograph of 4-weeks-old seedlings of Ar5-587 (a), 2-weeks-old seedlings of Ar5-672 (b), and seeds of Ar5-90 (c). Bar = 1 cm.

[*1] RIKEN Nishina Center
[*2] RIKEN Innovation Center
[*3] Graduate School of Life Sciences, Tohoku University

References
1) Y. Hayashi et al.: RIKEN Accel. Prog. Rep. **43**, 282 (2010).
2) R. Morita et al.: RIKEN Accel. Prog. Rep. **45**, 212 (2012).
3) S. Kogure et al.: RIKEN Accel. Prog. Rep. **45**, 213 (2012).
4) S. Kogure et al.: RIKEN Accel. Prog. Rep. **46**, 260 (2013).
5) K. Miyoshi et al.: Proc. Natl. Acad. Sci. USA **101**, 875 (2004).
6) A. Sasaki et al.: Science **299**, 1896 (2003).
7) W. Xue et al.: Nat. Genet. **40**, 761 (2008).
8) Y. Zhu et al.: Plant Cell **18**, 442 (2006).
9) Y. Fujisawa et al.: Plant Cell Physiol. **42**, 789 (2001).

Relationship between gene expression level and LET immediately after heavy-ion beam irradiation in rice

K. Ishii,[*1] R. Morita,[*1] T. Hirano,[*2] Y. Kazama,[*2] T. Ikeda,[*1] Y. Nagamura,[*3] and T. Abe[*1,*2]

In plant mutagenesis by heavy-ion beam irradiation, linear energy transfer (LET) is one of the most important factors that determines the mutation rate. The most effective linear energy transfer (LETmax) has been defined and reported for *Arabidopsis thaliana*[1] and rice.[2] In wet seeds of rice, the mutation rate was low at low LET (22.5 keV/μm) and high at LETmax (50−70 keV/μm).[2] The relationship between the mutation rate and LET curved sigmoidally, however, the reason is still unknown. In this study, we tried to reveal the relationship between the gene expression level and LET after heavy-ion beam irradiation and to show whether the change of gene expression corresponds to that of the mutation rate.

Wet seeds of rice (*Oryza sativa* L. cv. Nipponbare) were imbibed for three days and used as samples. Heavy-ion beam irradiation (C-ions for LETs of 22.5 and 50 keV/μm and Ne-ions for LETs of 63 and 80 keV/μm), RNA extraction, and gene expression analysis were conducted as previously described.[3] All the analyses in this study were conducted on the samples sampled two hours after irradiation.

Out of 45,221 probe sets, 81 probe sets showed significantly ($p < 0.01$) higher expression levels when irradiated at all LETs (22.5, 50, 63, and 80 keV/μm) than when not irradiated (control). These probe sets contained the homologs of *Rad51*, *Rad21/Rec8*, and *Artemis*, which are the genes involved in DNA double-strand break repair. It was shown that the gene expression analysis successfully reflected the immediate response to the heavy-ion beam irradiation.

It was found that 1575 probe sets showed significantly ($p < 0.05$) higher expression levels when irradiated at 63 or 80 keV/μm of LET than when not irradiated. On each probe set, the relationship between the expression level and LET was fitted to both the linear and sigmoid functions (Fig. 1). Moreover, 826 probe sets were significantly ($R^2 \geq 0.8$) fitted to either function. Among these 826 probe sets, the relationships between the expression level and LET of 594 probe sets (72%) were fitted better to linear function, whereas those of the remaining 232 probe sets (28%) were fitted better to sigmoid function [Table 1]. In these 232 probe sets, the relationships between the expression level and LET of only three probe sets (0.4%) were coincident with the relationship between the mutation rate and LET.

This is the first observation of the relationship between the gene expression level and LET immediately after heavy-ion beam irradiation. On almost all the researched genes, the relationship between the gene expression level and LET was not coincident with that between the mutation rate and LET. The three exceptional genes can be used as the indicators of LETmax.

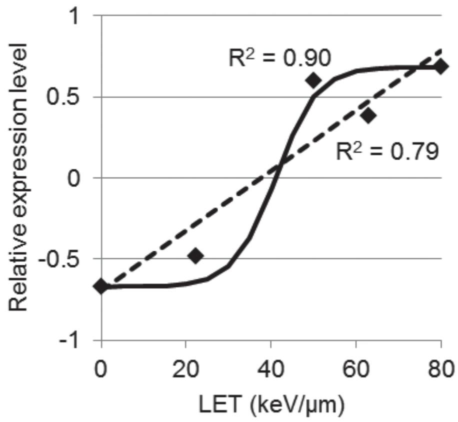

Fig. 1. Example of curve fitting of the relationship between expression level and LET. Squares indicate the measured values of a typical probe set. Line and dashed line indicate sigmoidal and linear regression curves, respectively.

Table 1. Classification of probe sets based on the nature of relationship between their expression level and LET.

	Probe set (number)			
Classification	80 keV/μm > ctrl.*	63 keV/μm > ctrl.**	Subtotal	(%)
Fitted to linear function	559	35	594	72
Fitted to sigmoid function	197	35	232	28
LETmax > 22.5 keV/μm†	(2)	(1)	(3)	
Sum total	756	70	826	

*Expression level when irradiated at 80 keV/μm was significantly higher than that of control.
**Expression level was not significantly higher than control when irradiated at 80 keV/μm but significantly higher when irradiated at 63 keV/μm.
†Expression levels when irradiated at 50 and 63 keV/μm were significantly higher than that when irradiated at 22.5 keV/μm.

*1 RIKEN Nishina Center
*2 RIKEN Innovation Center
*3 Agrogenomics Research Center, National Institute of Agrobiological Science

References

1) Y. Kazama et al.: Plant biotechnology **25**, 113-117 (2008).
2) Y. Hayashi et al.: RIKEN Accel. Prog. Rep. **42**, 285 (2009).
3) K. Ishii et al.: RIKEN Accel. Prog. Rep. **46**, 258 (2013).

Isolation of early-heading mutants induced by heavy-ion radiation in an Indonesian native rice cultivar

E. Hanzawa,[*1] Y. Kazama,[*1] Y. Hayashi,[*2] T. Abe,[*2,*3] A. Higashitani[*1] and T. Sato[*1,*2]

Rice is cultivated as far as 50º N in China and 40° S in Argentina. [1)] The period from seeding to heading is important for cultivation over a wide latitude. The heading time can be determined by the period of vegetative growth phase, from seedling to panicle primordium initiation, and reproductive phase, from panicle initiation to heading.[2)] The vegetative growth phase consists of the basic vegetative phase (BVP) and photoperiod sensitive phase (PSP). Cultivated rice is classified as a short-day plant, and it exhibits a wide genetic diversity with respect to sensitivity to photoperiod [3)]. Tanisaka et al. isolated a longer BVP mutant line induced by γ-irradiation of seeds of the Japanese lowland rice cultivar 'Ginbozu' with a longer PSP and shorter BVP.[3)] Indonesian rice cultivars belonging to the ecotype bulu have a shorter PSP and longer BVP.[4)] The aim for this study was to isolate a shorter BVP mutant line induced by heavy-ion radiation.

Dry seeds of an Indonesian native rice cultivar (*Oryza sativa* L. 'Gemdjah Beton' belonging to the ecotype bulu) were irradiated with C-ions accelerated to 135 MeV/nucleon by (RRC) at a dose of 125 Gy in April 2011. LET values of the C-ions corresponded to 22.5 keV/μm.

In 2011, the M_1 seeds were sown in seedling trays at the end of April and grown in a greenhouse for 4 weeks. Field experiments were conducted in the paddy fields of the Experimental Farm Station, Graduate School of Life Sciences, Tohoku University, in Kashimadai, Osaki, Miyagi, Japan (37º28', 141º06'). A fertilizer was applied to the paddy fields at rates of 30 kg of N, P, and K/ha. We transplanted 3,000 seedlings (age, four weeks) into a single lot at the end of May. Plants were grown at a density of a plant per hill, with 30-cm spacing between hills. In the middle of September, more than 15 M_1 plants flowered one week earlier than the other M_1 plants and the wild-type 'Gemdjah Beton'. We sampled the M_2 seeds of these M_1 plants in the beginning of November.

In 2012, we planted the M_2 seeds of these selected lines at the end of April and then transplanted 50 seedlings per each line in a paddy field at the end of May. One mutant line flowered over about ten days earlier than the other M_2 lines and the wild-type in the middle of September. At the end of October, M_3 seeds of 26 plants were sampled in the M_2 line.

In 2013, we randomly selected 10 M_3 lines from 26 M_3 lines and grew 50 plants of each M_3 line. The period from transplanting to the heading of wild-type was 17 weeks. Six M_3 lines exhibited the segregation from 15 to 17 weeks. The heading day of two M_3 lines was the same as that of the wild-type. All plants of another two M_3 lines showed heading two weeks earlier than the wild-type. Therefore, we succeeded in isolating early-heading mutant lines induced by heavy-ion radiation.

Seven loci that control the period of BVP were detected in cultivated rice.[5)] We are currently attempting to determine the locus of the mutant gene that shortens the period of BVP in the mutant lines isolated in this study.

Fig. Early-heading M_3 mutant line (left) and wild-type (right) grown in a paddy field on October 18, 2013

References
1) D. A. Vaughan: *Wild relatives of rice. A Genetic resources handbook.* (IRRI, Philippines 1986).
2) B. S. Vergara and T. T. Chang: *The flowering response of the rice plant to photoperiod . A review of the literature. 4th Edition* (IRRI, Philippines 1985).
3) T. Tanisaka et al.: Japan J. Breed. 42, 657 (1992).
4) N. Takahashi: in Biology of Rice, edited by S. Tsunoda and N. Takahashi (Japan Scientific Societies Press, Tokyo, 1984), P 31.
5) Q. Yuan et al.: Theor. Appl. Genet. 119, 675 (2009)

[*1] Graduate School of Life Sciences, Tohoku University
[*2] RIKEN Nisina Center
[*3] RIKEN Innovation Center

The wheat plastochron mutant, *fushi-darake*, produced by heavy-ion beam mutagenesis†

C. Tahira,*1 N. Shitsukawa,*1 Y. Kazama,*2 T. Abe,*3 and K. Murai*1

Grasses such as wheat (*Triticum aestivum*) are the major source of carbohydrates for humans, and the yield of grain from these crops is largely dependent on inflorescence architecture. A detailed understanding of development in wheat plants is of value not only to wheat breeding but also for basic scientific research. From the large scale mutant panel of diploid einkorn wheat (*Triticum monococcum*) developed by heavy-ion beam irradiation[1], we identified a mutation that had an abnormally large number of nodes; we termed this mutation *fushi-darake* (*fdk*), which means too many nodes in Japanese.

The *fdk* showed drastic changes to their structural organization compared to wild type (WT) plants in the field (Fig. 1). Contrary to WT, *fdk* plants had 1/2 alternate phyllotaxy with rapid leaf emergence. Consequently, the *fdk* plants had a larger number of nodes and leaves compared to the WT plants. In the *fdk* plants, vegetative shoot branches emerged from the nodes in the upper part of the culm of most tillers (Fig. 1). In these ectopic shoots, normal leaves were produced with 1/2 alternate phyllotaxy. The culms of *fdk* plants were unable to support the heavy upper vegetative shoots, with the result that the plants collapsed onto the ground (Fig. 1).

We examined the timing of leaf unfolding in WT and *fdk* seedlings grown in a growth chamber. The rate of leaf emergence was more rapid in *fdk* compared to WT after the 3-leaf stage. This indicates that rapid leaf emergence in *fdk* resulted from a rapid rate of leaf initiation: the plastochron of *fdk* plants was estimated to be half of that in WT.


fdk WT

Fig. 1. *fushi-darake* (*fdk*) mutant plant grown in the field and green house. WT: wild-type wheat strain KU104-1

To investigate further the morphological differences between WT and *fdk* plants, we carried out an SEM (scanning electron microscope) analysis of shoot apical meristem (SAM) development. SAM development in *fdk* plants was very different to that of WT plants. The SAM elongated but its branch meristems (BMs) resembled leaf primordia rather than spikelet meristems (SMs). Ectopic flat dome-like BMs that were similar to leaf primordia were initiated with a1/2 alternate pattern. These observations, together with those on the morphology of the *fdk*, suggest that the flat dome-like BMs develop into vegetative shoots.

The inflorescence of grass species is composed of a unique unit called the spikelet. When the wheat plant transits from the vegetative to reproductive growth phase (flowering), the SAMs are elongated and spikelet meristems (SMs) initiate as lateral branches. Our SEM analysis of the *fdk* mutant indicated that differentiation of SMs was delayed and the leaf primordia were initiated from branch meristems (BMs) with 1/2 alternate phyllotaxy. These observations suggest that 1/2 alternate phyllotaxy with rapid leaf emergence produced the shortened plastochron in the *fdk* mutant. The SAMs further elongated and produced flat dome-like BMs at the position of the original SMs. We also found that *fdk* plants had vegetative shoot branches emerging from the nodes of upper part of culm of almost all tillers. Thus, our results suggest that these vegetative shoots are likely to be developed from the BMs of elongated SAMs. In conclusion, our findings indicate that the abnormal phenotype of the *fdk* mutant resulted from transformation of SMs into vegetative shoots.

Three plastochron mutants, *plastochron 1* (*pla1*)[2], *pla2*[3] and *pla3*[4], have been identified in rice (*Oryza sativa*). Among them, we found that wheat *fdk* and rice *pla1* mutants show similar phenotypes. These facts indicate that some common genetic cascades are involved in the phenotype of wheat *fdk* and rice *pla1*. The WT gene, *PLASTOCHRON 1* (*PLA1*), encodes a member of a plant-specific subfamily of cytochrome P450, CYP78A11, which potentially catalyzes substances controlling plant development[5]. The similar phenotypes of the *fdk* with *pla1*, suggest that *PLA1* or related genes may be candidates for the *fdk* mutation in wheat.

References

1) K. Murai et al.: Nuclear Instruments and Methods in Physics Research B 314. **2013**, 59.
2) J.-I. Itoh et al.: The Plant Cell 10. **1998**, 1511.
3) T. Kawakatsu et al.: The Plant Cell 18. **2006**, 612.
4) T. Kawakatsu et al.: The Plant Journal 58. **2009**, 1028.
5) K. Miyoshi et al.: PNAS 101, **2004**, 875.

† Condensed from the article in American J. Plant. Sci. **4**, 28 (2013)
*1 Department of Bioscience, Fukui Prefectural University
*2 RIKEN Innovation Center
*3 RIKEN Nishina Center

Constructing *S*-locus deletion mutant in common buckwheat by using heavy-ion-beam irradiation

M. Ueno,*[1] T. Abe,*[2] Y. Hayashi,*[2] and Y. Yasui*[1]

In *Fagopyrum esculentum* (common buckwheat), the plants exhibit short-styled or long-styled flowers, showing distyly. The floral morphology and intra-morph incompatibility are both determined by a single genetic complex named *S*-locus. Plants with short-styled flowers are heterozygous (*S/s*) and plants with long-styled flowers are homozygous recessive (*s/s*) at *S*-locus. Previously we discovered a new gene, *S-LOCUS EARLY FLOWERING 3* (*S-ELF3*), which is a candidate gene for short-styled phenotypes of distyly, and its flanking region of about 500 kbp has already been sequenced[1]. Recombination around the *S*-locus is supposed to be restricted, because no recombination between floral morphology and intra-morph incompatibility was observed. Thus, genetic mapping is not possible to determine the genomic region containing the *S*-locus. The purpose of this study is to construct mutants that lack the genomic region around the *S*-locus by heavy-ion-beam irradiation, in order to use the mutants for narrowing down the *S*-locus in the future.

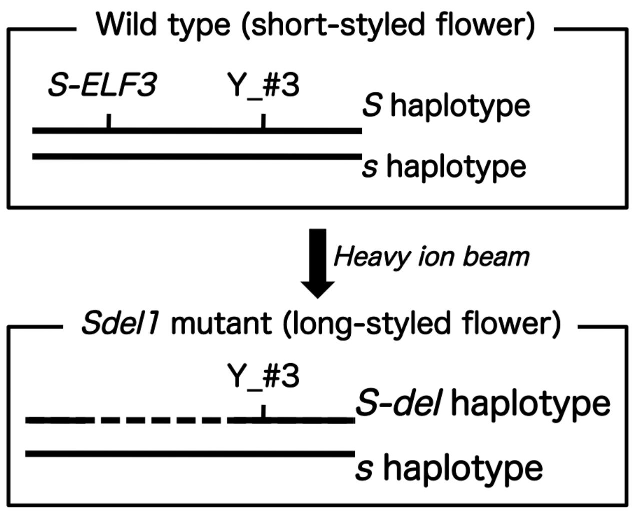

Fig. 1. Schematic diagram of the screening of *S-del* haplotypes. New mutant *S-del1* possessed only Y_#3 marker, which is tightly linked to *S*-locus, i.e., no *S-ELF3* was found. The flower phenotypes of *S-del1* were long styled. Dashed line indicates the genomic region deleted by heavy-ion-beam irradiation.

For obtaining an *S*-locus-deletion plant, buckwheat seeds were irradiated with accelerated $^{12}C^{6+}$ ions in doses ranging from 100 Gy to 125 Gy. The linear energy transfer (LET) range of $^{12}C^{6+}$ was from 22.5 keV/μm to 30 keV/μm. The total DNA was extracted from 1,152 plants of M_2 growing in the experimental room, and their flower types were investigated. For screening of the *S*-locus-deletion plant, PCR was performed using an *S*-haplotype specific primer set (Y_#3) obtained using cDNA-Amplified Fragment Length Polymorphism (AFLP) analysis (Yasui et al., in preparation). The Y_#3 PCR marker showed perfect linkage with the *S*-locus in 1,400 mapping population and was amplified only with short-styled buckwheat plants collected from all over the world. *S-ELF3* and Y_#3 marker were located physically distant to each other, because the DNA sequence of Y_#3 marker could not be found on the 500 kbp BAC contig flanking of *S-ELF3* (Yasui et al., in preparation). Further, if short-styled plants lack genomic region only around the *S*-locus, the flower type of the plant is expected to become long-styled, but must possess the Y_#3 marker (Fig. 1).

In 1,152 plants investigated, one showed both positive Y_#3 PCR amplification and long-styled flowers and was named *S-del1*. Furthermore, *S-ELF3* and six dominant PCR markers covering the 500 kbp sequence flanking *S-ELF3*[1] produced no PCR products with *S-del1* DNA. It is considered that the large genomic region (>500 kbp) harboring the *S*-locus was deleted in the *S-del1* mutant and that the flower type of *S-del1* changed from short-styled to long-styled (Fig. 1). These results imply that *S-ELF3* or its flanking gene controlled short-styled phenotypes.

It is expected that combining PCR amplification with *S*-linked maker (Y_#3) and phenotyping of flower type on M_2 plants is effective in the screening of *S*-locus-deletion plants. We are planning to screen other sets of M_2 population. In the near future, we will be able to construct a fine deletion map such as that of the Y chromosome of *Silene latifolia*[2].

In this study, we observed a phenotypic change from short-styled to long-styled flowers in the mutant progeny. This makes the creating of *S-del* homozygous (*S-del*/*S-del*) plant possible, and the resulting plants will enable us to estimate the role of *s*-haplotype genes and to narrow down the genomic region harboring these genes.

References
1) Yasui et al.: PLoS ONE **7**, e31264 (2012).
2) Fujita et al.: G3 (Bethesda) **2**, 271 (2012).

*1 Graduate School of Agriculture, Kyoto University
*2 RIKEN Nishina Center

DNA marker analysis revealed that the deletion is relatively small in loss-of-apomixis mutants

M. Takahara,[*1] M. Ebina,[*1] R. Morita,[*2] Y. Kazama,[*3] T. Abe,[*2,*3] T. Takamizo,[*1] and H. Nakagawa[*4]

Apomixis produces seed progeny that are genetically identical to the mother plant. This process is widely observed among wild plant species but is almost completely absent in major crop species. Apomixis will have a great impact on agriculture through clonal seed production. As the first step of the agricultural use of apomixis, we aimed to isolate the gene(s) controlling apomixis for application in major crops. Guinea grass (*Panicum maximum* Jacq.), a major tropical forage grass, has some characteristics suitable for the study of apomixis. However, recent studies have suggested that recombination is suppressed at the apomixis-controlling locus in guinea grass. To narrow down the apomixis-controlling genomic region, we developed deletion mutants for this region by using irradiation with heavy-ion beams.[1), 2), 3)] In a previous study, we found that two mutant lines (SM-1 and SM-2) showed different AFLP patterns between M_2 progenies within each line.[3)] This result suggested that they lost the apomicitic pathway of reproduction and propagated using the sexual mode of reproduction. In the present study, we analyzed the deletion size of these loss-of-apomixis mutants with apomixis-specific sequence-tagged site (STS) markers.

The M_1 plants of SM-1 and SM-2 were generated from dry seeds (an apomictic cultivar ‘Natsukaze’) irradiated with $^{20}Ne^{10+}$ (63 keV/μm) ions at 200 Gy and $^{56}Fe^{24+}$ (624 keV/μm) ions at 20 Gy, respectively.[2)] Approximately ten M_2 plants of each line were grown in a field. DNA from five M_2 plants of each line were extracted from leaves and analyzed using polymerase chain reaction (PCR) with 83 apomixis-specific STS markers. The SM-1-1, SM-1-4, and SM-1-6 plants were blighted before analysis.

Fig. 1 shows that SM-1 lost four markers (CA-A14-252, CI-A1-296, CI-T1-217, and CK-T2-374) among the 83 analyzed markers (4.8%). In case of the SM-2 line, two markers (CA-A3-354 and CA-A11-355) among the 83 analyzed markers (2.4%) were lost in only three M_2 plants (SM-2-3–5). Fig. 1 also shows that SM-2-1 possessed all markers, suggesting that it had an intact apomixis chromosome. In contrast, SM-2-2 lost all markers, suggesting that it lost the entire apomixis chromosome. These results can be explained by the exchange of chromosomes during the process of sexual reproduction in SM-2. SM-2-3–5 were suggested to have a partially deleted apomixis chromosome.

These results suggested that the size of the deletion in SM-1 and SM-2 was relatively small, probably several percent of the apomixis-controlling genomic region. Previously, we obtained 22 other mutants in which the apomixis-controlling genomic region was partially deleted, and these mutants lost 2–12 STS markers out of a total of 48 markers (4.2–25%).[3)] Compared to these mutants, the size of the deletion in SM-1 and SM-2 were suggested to be relatively small. However, we could not estimate the exact physical size of these deletions because the whole DNA sequence of this region has not been obtained. Sequencing and scaffolding of BAC clones of this region is currently in progress. This result will be useful in estimating the exact size of the deletions and in searching for the genes within these deletion regions.

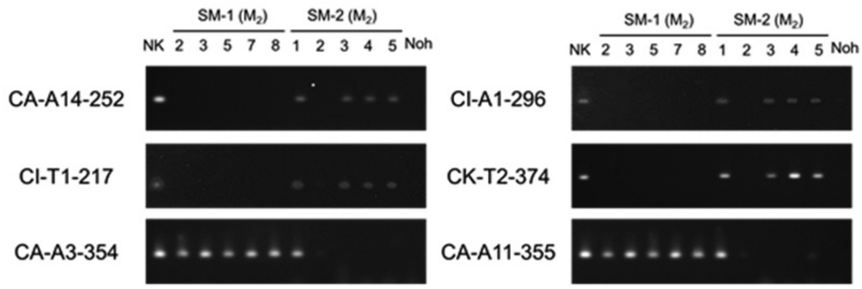

Fig. 1 PCR analysis using STS markers lost in SM-1 or SM-2 mutant line. Five M2 individuals were analyzed in each mutant line. An apomictic cultivar ‘Natsukaze’ (NK) and a sexual line ‘Noh PL1’ (Noh) were used as the positive and negative controls, respectively.

*1 National Agriculture and Food Research Organization (NARO) Institute of Livestock and Grassland Science
*2 RIKEN Nishina Center
*3 RIKEN Innovation Center
*4 Japan International Research Center for Agricultural Sciences (JIRCAS)

References
1) M. Takahara et al.: RIKEN Accel. Prog. Rep. **44,** 273 (2011).
2) M. Takahara et al.: RIKEN Accel. Prog. Rep. **45,** 215 (2012).
3) M. Takahara et al.: RIKEN Accel. Prog. Rep. **46,** 263 (2013).

Effect of C-ion beam irradiation on survival rates and flower color mutations in statice (*Limonium sinuatum* Mill.)

D. Ogawa,[*1] T. Fujioka,[*1] T. Hirano,[*2] and T. Abe[*2,*3]

Statice (*Limonium sinuatum* Mill.) is one of the popular cut flowers for flower arrangement or flower tribute because of the long-term keeping quality of the flower and wide variety of flower color. Generally, flower color of statice, which is defined by the color of the calyx, can be classified into five groups: purple, pink, blue, yellow, and white. Wakayama Prefecture, which is the major statice-producing region of Japan, has developed 7 cultivars by cross-breeding. However, a superior pink cultivar has not been developed. Therefore, we aimed to obtain statice mutants with pink calyx by heavy-ion beam irradiation. In this study, we investigated the suitable doses of heavy-ion beam irradiation for statice and flower color mutations.

Multiple-shoot cultures of statice Kishu Fine Grape were irradiated using C-ion beam (LET 23 keV/μm) at doses of 5–30 Gy. After irradiation, the samples were cut into single shoot segments and transferred to a medium supplemented with 0.2 mg/l α-naphthaleneacetic acid for root induction. Eight weeks after irradiation, the surviving shoots and rooted shoots were counted (Fig. 1). The survival frequency of the shoots was found to be 95.5% when the irradiation dose was 5 Gy. On the contrary, at doses of over 10 Gy, the survival frequency apparently decreased. The rooting frequency of the shoots decreased from 87.7% at 0 Gy to 29.9%. No root formation was observed at 5 and 10 Gy. These results suggest that the suitable dose of C-ion irradiation for statice is less than 5 Gy.

Thus, for the improvement of flower color, we irradiated one purple cultivar (Kishu Fine Grape) and two light purple cultivars (Kishu Fine Lavender and Kishu Star) with C-ion beams at doses of 2 and 5 Gy in our further experimentation. Four weeks after the irradiation, the rooting rates of Kishu Star were 87.5%, 87.3%, and 67.7% at 0, 2, and 5 Gy, respectively. Similar results were obtained for the other cultivars Kishu Fine Grape and Kishu Fine Lavender (data not shown). The rooted plants were acclimated to outside conditions and subsequently transplanted to pots containing soil.

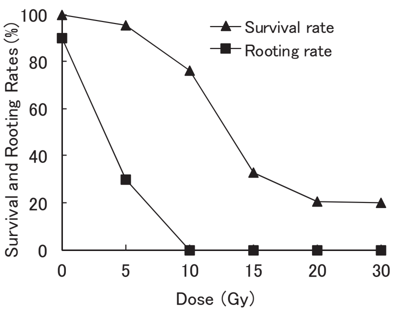

Fig. 1. Effect of C-ion beam irradiation on the survival and rooting rates in statice Kishu Fine Grape. Data were recorded 8 weeks after the irradiation.

Table 1 shows the flower-color mutants obtained in this study. Among the 3 cultivars, Kishu Fine Lavender and Kishu Star showed flower color mutations. However, we failed to obtain the mutants from Kishu Fine Grape. Six mutants were induced from Kishu Fine Lavender. All six mutants exhibited paler flower color (e.g., Royal Horticulture Society [RHS] Color Chart value N91D) than that of the original cultivar (RHS Color Chart value N87D). Ten mutants were induced from Kishu Star. Among them, 5 and 2 were pale and deep color mutants, respectively (Fig. 2). The other 2 mutants changed to reddish color (e.g., RHS Color Chart value N81C).

Although a pink-colored mutant was not obtained in this study, we confirmed that flower color mutants of statice could be obtained by heavy-ion beam irradiation. Furthermore, other interesting mutations were found, such as small flower, variations in the calyx shape, and no hair on the peduncle (data not shown). These results suggest that heavy-ion beam irradiation is effective for developing various useful mutants in statice. Mutant screening for the above-mentioned aim are currently in progress.

Table 1. Type and number of flower color mutants by C-ion beam irradiation.

Cultivars	Dose (Gy)	No. of plants investigated	No. of mutants		
			Pale color	Deep color	Reddish color
Kishu Fine Grape	0	16	0	0	0
	2	60	0	0	0
	5	14	0	0	0
Kishu Fine Lavender	0	20	0	0	0
	2	166	4	0	0
	5	51	2	0	0
Kishu Star	0	10	0	0	0
	2	52	3	2	1
	5	20	2	0	2

Pale color mutant (N84D) | Original cultivar (N82B) | Deep color mutant (N87A)

Fig. 2. Flower color mutants of statice Kishu Star. Royal Horticulture Society Color Chart values are indicated in parentheses.

*1 Horticultural Experiment Center, Wakayama Agricultural Experiment Station
*2 RIKEN Innovation Center
*3 RIKEN Nishina Center

Flower color mutants of chrysanthemum obtained using C-ion beam irradiation

K. Tamaki,[*1] M. Yamanaka,[*1] Y. Mizutani,[*1] Y. Hayashi,[*2] T. Hirano,[*3] and T. Abe[*2,*3]

Chrysanthemum is a major agricultural product in Hyogo Prefecture. We tried to use ion beams to induce flower color variation in chrysanthemum. We irradiated 53 cultivars of chrysanthemum with carbon beams. We have previously reported their mutant frequency and flower color mutants.[1] We tried to increase variation in flower color by using a single origin. We irradiated flower color mutants from 'Benitsubaki' with C-ion beams and obtained more mutants.

'Benitsubaki' is a purplish red small mum that blooms at the end of November (Fig. 1). In 2009, we irradiated cuttings with C-ion beams (energy, 135MeV/nucleon; LET, 23 keV/μm) at doses of 4 and 6 Gy. After irradiation, herbaceous cutting was performed, and four weeks later, fix planting was carried out in a glass house. Cultivation conditions were no pinching and no picking the bud. Other conditions for cultivation were standard. At the time of full bloom, we observed the mutation rate with respect to flower shapes. Stability of the mutation was confirmed in 2010. We irradiated the cuttings of VT4Pi and VT6RB mutants with C-ion beams at doses of 4 and 6 Gy in 2011. Other conditions were the same in 2009. Relative DNA contents of somatic nuclei in 'Benitsubaki' and mutants derived after re-irradiation were compared using flow cytometry.

The mutation frequencies of 'Benitsubaki' were 6.3% at 4 Gy and 4.3% at 6 Gy. We obtained two flower color mutants, deep pink (VT4Pi) and red (VT6RB), that bloomed at the end of November. These mutations were stable in 2010. Since the flower color of VT4Pi was not different from that of the original 'Benitsubaki', we tried re-irradiation to obtain more varied mutants.

The mutation frequencies of VT4Pi were 7.8% at 4 Gy and 3.9% at 6 Gy. We obtained 4 flower color mutants from VT4Pi (Fig. 1). One of them was double-colored, purplish red outside and white inside (VT4Pi6WT-Wh), that bloomed at the middle of December. Two mutants were also double-colored flowers that bloomed at the end of December and were deep pink outside and white inside (VT4Pi6Pi-Wh) and light pink outside and white inside (VT4PiLtPi-Wh). The fourth mutant was also double-colored, orange outside and yellow inside (VT4Pi6Or-Yr) and bloomed at the middle of December. The difference among three mutants, VT4Pi6WT-Wh, VT4Pi6Pi-Wh and VT4PiLtPi-Wh, was the strength of the color. The mutation frequencies of VT6RB were 7.3% at 4 Gy and 14.3% at 6 Gy. The yellow mutant (VT6RB6Yr・RB) bloomed in the middle of December (Fig. 1).

Although this mutant had a reddish bud, the flowers were bright yellow with green core.

Flower color changes under the influence of cultivation temperature. We are currently carrying out cultivation experiments to reveal the effect of temperature on the blooming period and flower color of these mutants. In terms blooming period, all the obtained mutants bloomed late. The mutation frequency by re-irradiation was higher than that after a single irradiation. The relative DNA contents in the mutants obtained after re-irradiation did not decrease to that in 'Benitsubaki'. These results indicate that ion-beam re-irradiation of mutants is effective in increasing the variety of mutants.

Fig. 1 'Benitsubaki' and its flower color mutants

*1 The part of Agricultural Horticulture, Hyogo Prefectural Institute for Agriculture, Forestry and Fisheries
*2 RIKEN Nishina Center
*3 RIKEN Innovation Center

References

1) K. Tamaki et al.: RIKEN Accel. Prog. Rep. **44** p.276-277 (2010).

Effects of heavy-ion-beam irradiation on flower-color mutation in chrysanthemum

Y. Tanokashira,*[1] S. Nagayoshi,*[1] T. Hirano,*[2] and T. Abe*[2],*[3]

Kagoshima Prefecture is a leading spray-mum production region in Japan. Until date, we have developed more than 50 spray-mum cultivars by cross breeding; in addition, we also performed mutation breeding by using heavy-ion-beam irradiation. In this study, we investigated the effects of heavy-ion-beam irradiation on flower-color mutation of spray-mum.

We irradiated cuttings of the spray-mum cultivar ‘Southern Chelsea’, which was developed in Kagoshima Prefecture, with C-ion (LET 23 keV/μm) at doses of 2–5 Gy, Ne-ion (LET 62 keV/μm) at doses of 2 and 5 Gy, Ar-ion (LET 280 keV/μm) at doses of 2 and 5 Gy, and X-ray at doses of 5–20 Gy. After the irradiation, we planted the cultivars in a greenhouse and investigated the variations in flower-color mutation.

Among 4,741 irradiated branches, we obtained 468 branches with flower-color mutations (Table 1). The mutants from ‘Southern Chelsea’ with pink flower showed flower colors of white, light pink, deep pink, yellow, light reddish yellow, and deep reddish yellow (Fig. 1).

On the basis of the analysis of flower pigments in the mutants, the relationship between the variations in the amount of the pigments and colors was considered, as shown in Figure 2. The mutants with deep pink flowers had higher anthocyanin content in their flowers than that in ‘Southern Chelsea’, and the mutants with white, yellow, and light pink flowers had low anthocyanin content. The light reddish yellow, deep reddish yellow, and yellow flowers were because of increased carotenoid content. The flower-color mutation was high in the order of deep reddish yellow, white, and light reddish yellow.

Table 1. Flower-color mutation induced by heavy-ion-beam and X-ray irradiations.

Variation source			Flower-color mutation									
Line class	Dose (Gy)	Number of irradiated plants	Deep reddish yellow	White	Light reddish yellow	Yellow	Deep pink	Light pink	The tip of the petal (The origin of the petal): White (pink)	The tip of the petal (The origin of the petal): Yellow (Reddish yellow)	Number of mutants	Mutation rate(%)
C	2	84	2		2						4	4.8
	3	540	25	11	9			1			46	8.5
	5	354	25	20	7						52	14.7
Ne	2	348	16	11	7	1					35	10.1
	5	84	9	7	5						21	25.0
Ar	2	434	30	27	12	4	3	1	2	1	80	18.4
	5	21	2								2	9.5
X-ray	5	552	23	9	9		1				42	7.6
	10	1955	73	40	31	3		1			148	7.6
	15	180	6	6	5						17	9.4
	20	189	8	9	4		1				22	11.6
Total		4741	219 (37)	140 (59)	91 (16)	8 (0)	5 (2)	3 (3)	2 (0)	1 (0)	469	9.9

( ): Mutated sector in the flower was defined as the area of the petals with changed color that accounted for more than 50% of the whole petal area in a flower. The total number of irradiated and mutated plants with the number of plants having mutated sectors shown with in parenthesis.

In the irradiations at 5 Gy, the flower-color mutation rate was high in the order of Ne-ion, C-ion, Ar-ion, and X-ray (Table 1), indicating that the heavy-ion-beam irradiations were more effective for the induction of flower-color mutation than that by X-ray irradiation. Since the majority of the shoot tips died after Ar-ion irradiation at 5 Gy, mutant screening should be performed at low-dose irradiations such as 2Gy.

The mutation rate for yellow flowers was 0–0.2% after C-ion, Ne-ion, and X-ray irradiations. On the other hand, the mutation rate after Ar-ion irradiation was 0.9% and was higher than that after the other irradiations (Table 1). In addition, some mutants showed flower-shape and color variations at the tips of the petals, such as to yellow or white (Fig. 1-B). These variations were only observed in the Ar-ion irradiation, suggesting that the Ar-ion beam at a LET of 280 keV/μm might have more different effects on mutation induction than that by the lower LET Ar-ion-beam irradiation.

The results in this study indicated that heavy-ion-beam can induce a broad spectrum of mutant phenotypes in chrysanthemum. Currently, we are screening the mutants derived from Ar-ion irradiation.

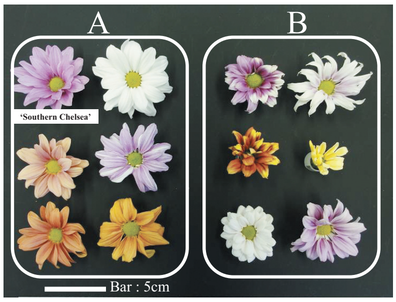

Fig. 1 Spectrum of mutant phenotypes. (A) Flower-color mutations. (B) Color variations at the tips of the petals and variations in the flower shape.

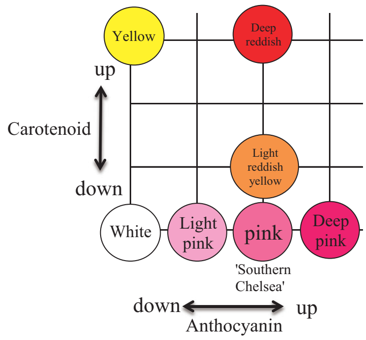

Fig. 2 Relationship between the amount of pigments and color variations in the mutants.

*[1] Kagoshima Prefectural Institute for Agricultural Development
*[2] RIKEN Innovation Center
*[3] RIKEN Nishina Center

Effect of heavy-ion beam irradiation on seeds reduction of 'Konta' kumquat fruit

K. Tomura,[*1] T. Teraoka,[*2] T.Nakajima, [*1] Y. Kobayashi,[*1] I. Sawano,[*3]
Y. Hayashi,[*4] N. Fukunishi,[*4] T. Abe[*4]

'Konta' kumquat was found as a bud mutant in the field by a farmer in Shizuoka Prefecture. 'Konta' has some unique characteristics compared with 'Neiha' kumquat. It has higher sugar content and lesser citric acid content than 'Neiha' kumquat, which tastes extremely good. On the other hand 'Konta' has more seeds (6-7) than 'Neiha' (5-6). [1)] If we can develop seedless 'Konta', it will be a valuable cultivar. Recently, heavy-ion beam irradiation has been reported as an effective mutation breeding technique. Especially since 'Konta' has multi-embryonic seeds, it is difficult to breed this cultivar.

In this study, we investigated the effect of heavy-ion beam irradiation on seed reduction and attempted to obtain a mutant of 'Konta' kumquat fruit with reduced number of seeds.

In 2007 and 2008, dormant scions from the hard branches of 'Konta' kumquat were irradiated with $^{12}C^{6+}$ and $^{20}Ne^{10+}$ at a dose of 10Gy(135 MeV/u, 61.1 keV/μm). After irradiation, the scions were grafted on *Poncirus trifoliata* to create the vegetative mutant 1(vM_1) generation. After sprouting, the treetops were subjected to cutting back at least 3 times. As the control, original 'Konta' was grafted on P. trifoliata. These plants are pollinated naturally, and superfluous fruits were not removed for securing the number of fruits.

We counted the number of perfect seeds on the equatorial cut surface of all the fruits obtained from Ne-ion irradiated vM_1 and C-ion irradiated vM_1 in 2011 and 2012. We considered fruits with 0-2 perfect seeds as "seeds reduced fruit" (Fig. 1) and calculated the ratio of seeds reduced fruits (i.e., number of fruits with two or less seeds/number of examined fruits).

For Ne-ion beam irradiation, the appearance ratio of seeds reduced fruit in vM_1 plants was 6%, while that in the control was 1% (Table 1). One of thirty-six vM_1 plants bore more than 80% seeds reduced fruits by Ne-ion beam irradiation. For C-ion beam irradiation, the appearance ratio of seeds reduced fruit in vM_1 plants was 13%, while that in the control was 8% (Table 2). In four plants, the ratio of seeds reduced fruit per vM_1 plant exceeded 70% by C-ion beam irradiation. The ratios of seeds reduced fruit per control plant were less than 10% in both the irradiation studies. These results indicate that heavy-ion beam irradiation is effective for seed reductions in 'Konta' fruit.

We selected the vM1 plants with high seeds reduced fruits rate (Fig. 2). Furthermore, we isolated the branches bearing more seeds reduced fruits from these selected vM_1 plants. The fixation of seeds reduction is currently under investigation.

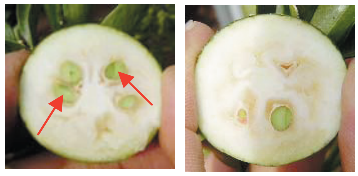

Fig.1 fruit surfaces after equatorial cuts.
Perfect seeds (left) and reduced seed (right)

Table 1. Appearance of seeds reduced fruits of 'Konta' by Ne-ion beam irradiation

Irradiation	Number of vM_1	Number of total fruits	Number of perfect seeds (%) 0-2 seeds	>3 seeds
Ne	36	2125	128(6%)	1997(94%)
Control	29	1651	21(1%)	1630(99%)

Table 2. Appearance of seeds reduced fruits of 'Konta' by C-ion beam irradiation

Irradiation	Number of vM_1	Number of total fruits	Number of perfect seeds (%) 0-2 seeds	>3 seeds
C	128	7307	962(13%)	6345(87%)
Control	5	208	17(8%)	191(92%)

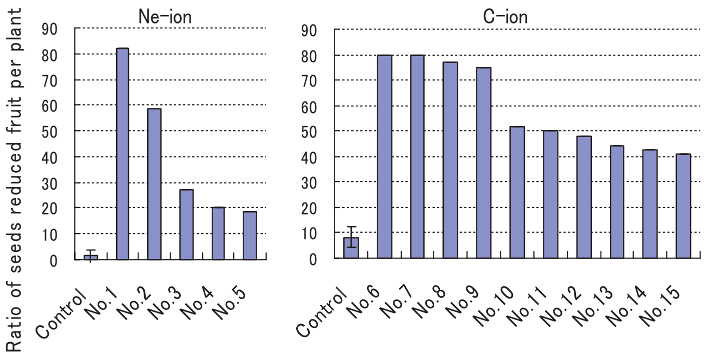

Fig. 2 Examples of vM_1 plant with high seeds reduced fruits rate. Vertical bars represent ± SD(Ne: n = 29, C: n = 5).

References

1) Y. Araki : Izu Agric. Res. Center, Shizuoka Res. Inst. of Agric. and For. Rep. (2003) p.158-159

[*1] Fruit Tree Res. Center, Shizuoka Res. Inst. of Agric. and For.
[*2] present : Shizuoka Agric. Promotion div.
[*3] present : Shizuoka Toubu Agric. and For. Office
[*4] RIKEN Nishina Center

Rapid evaluation of mutational effects resulting from heavy-ion irradiation of *Undaria pinnatifida*

T. Hirano,[*1] Y. Sato,[*1,*2] K. Ichinose,[*3] Y. Hayashi,[*3] N. Fukunishi,[*3] and T. Abe[*1,*3]

Undaria pinnatifida, called wakame in Japan, is a major commercial seaweed. Recently, there has been a demand for new cultivars with enhanced properties, such as high yield, high environmental adaptability, or high concentration of available contents for human health, to expand the market for wakame. Therefore, we performed the mutation breeding of *U. pinnatifida* through heavy-ion-beam irradiation.[1)] Optimization of the dose and linear energy fransfer (LET) in heavy-ion mutagenesis is essential for efficient mutant induction.[2)] However, a method for evaluating mutation frequency has never established in *U. pinnatifida*, and the optimization is still difficult. Moreover, in macroalgae, the analysis of mutation frequency in M_2 generation consumes much time and requires large space. In the present study, we irradiated zoospores with heavy-ion beams. Because the female and male gametophytes developed from the zoospores are in the haploid stage of its life cycle, mutant screening can be performed in M_1 generation. Through the mutant screening and investigation of the mutant phenotypes, we tried to develop a method for the effectiveness of heavy-ion mutagenesis.

Samples (3 cm × 3 cm) of sporophylls of *U. pinnatifida* were irradiated with C ions (LET: 30.0 keV/μm) at a dose of 0–25 Gy or Ar ions (LET: 280 keV/μm) at a dose of 0–10 Gy. The irradiated pieces were placed in beakers filled with sterilized seawater, and zoospores were induced. The zoospore suspension were diluted with Provasoli's enriched seawater with Iodine[3)] and poured into plastic dishes. The dishes were incubated at 20 ºC with 12 h photoperiods and a light intensity of 5 μmol m^{-2} s^{-1}. The gametophyte size was measured after 3 weeks of culture. The gametophyte over 100 μm in size of the longest cell filament was defined as a developed gametophyte, and the formation rate of developed gametophyte was calculated. Mutant screening was performed after 5 weeks of culture.

When we investigated the growth of the gametophytes developed from the irradiated zoospores, the number of developed gametophytes decreased with increasing irradiated dose (Fig. 1). A comparison between C-ion and A-ion irradiation revealed that the Ar-ion irradiation has high biological effect to the cell division or cell growth. After 5 weeks of culture, some mutants in cell shape, cell size, and intracellular structure were observed. One of the mutants showed a reduction in cell elongation (Fig. 2C, D). In the untreated control, the female gametophyte cells were larger than the male gametophyte cells (Fig. 2A, B). There were at least two types of cell elongation mutants: small-cell type (Fig. 2C) and large-cell type (Fig. 2D). One possible interpretation is that the small-cell type and the large-cell type cells were induced in male and female gametophytes, respectively. The mutation frequency for the cell elongation mutant tended to increase in a dose-dependent manner (data not shown). Therefore, the mutants can be used as an indicator for investigating the effectiveness of heavy-ion mutagenesis. We will evaluate LET-dependent effects for mutation induction in *U. pinnatifida* using this method.

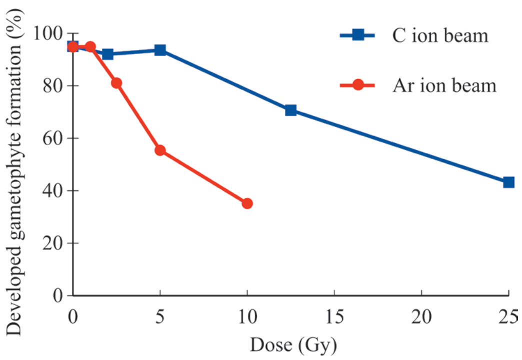

Fig. 1 Effect of heavy-ion irradiation on gametophyte development. The formation rates after 3 weeks of culture are expressed as the mean of two individual experiments.

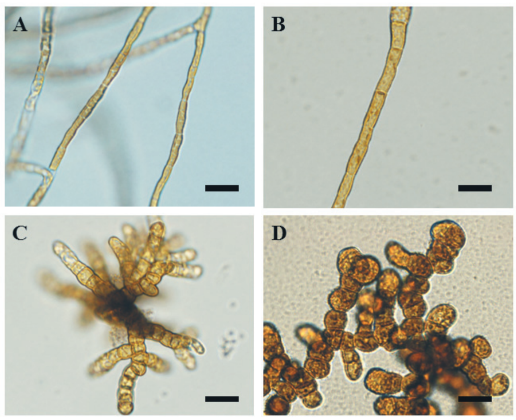

Fig. 2 Morphological mutants induced by C-ion irradiation. The male (A) and female gametophytes (B) from unirradiated zoospores were cultured for 5 weeks. The cell elongation mutants after 5 weeks of culture derived from the C-ion irradiation at 5 Gy (C) and 12.5 Gy (D). Bars indicate 20 μm.

*1 RIKEN Innovation Center
*2 Riken Food Co., Ltd.
*3 RIKEN Nishina Center

References
1) Y. Sato et al.: RIKEN Accel. Prog. Rep. **46**, 267 (2012).
2) Y. Kazama et al.: Plant Biotechnol. **25**, 113 (2008).
3) M. Tatewaki: Phycologia **6**, 62 (1966).

Effects of heavy-ion beam irradiation on sporophyte survival and growth in *Undaria pinnatifida*

Y. Sato,[*1,*2] T. Hirano,[*3] Y. Hayashi,[*4] M. Kasahara,[*1] N. Fukunishi,[*4] T. Abe[*3,*4] and S. Kawano[*2]

Undaria pinnatifida, called wakame in Japanese, is one of the most popular seaweed in Japan, Korea, and China. It is the most important cultivated seaweed in Iwate and Miyagi Prefectures in Japan. In recent years, the wakame yield has been decreasing because of changing environment, unimproved productivity, and damage due to Tsunami. For the purpose of yield restoration and sustainable growth market of *U. pinnatifida*, the development of new cultivars with properties such as high yield or high environmental adaptability is necessary. We used heavy-ion-beam irradiation to induce mutagenesis in *U. pinnatifida* for the production of new cultivars.[1)] However, since not enough studies have been conducted in the mutagenesis of marine algae, it is important to produce efficient mutation breeding in *U. pinnatifida* to assess the relationship between survival rate after irradiation and mutation frequency. In this study, we irradiated *U. pinnatifida* sporophytes with C-ion and Ar-ion beam and analyzed the effects on sporophyte survival and growth in the M_1 generation toward successful mutant screening in M_2 generation.

Sporophytes of *U. pinnatifida* were obtained after fertilizing the male and female gametes. The sporophytes of 1-mm length were transferred into 15-ml plastic tubes for C-ion irradiation and hybribags for Ar-ion irradiation, both containing sterilized seawater, and were irradiated at dose ranges of 0–25 Gy (C ions) or 0–10 Gy (Ar ions). Each tube or hybribag contained 50 sporophytes. After the irradiation, the sporophytes were cultivated in 500-ml Erlenmeyer flasks containing 1/4 PESI medium, [2)] with aeration, at 15°C, photoperiod of 12 h/12 h (light/dark), and a light intensity of 90 μmol photons m^{-2} s^{-1}. The survival rate was measured after 3 weeks of culture. The plants surviving and reaching 20-mm with in the culture period were further cultivated in the Rotating and Flowing Land Tank System (PAT.P) at 10°C, photoperiod of 12 h/12 h (light / dark), and a light intensity of 180 μmol photons m^{-2} s^{-1} for 8 weeks. The total length and fresh weights of all the sporophytes were measured after blotting them dry.

In the flask cultivation after irradiation, dead sporophytes were observed. Almost all the dead sporophytes had formed within 1 week of cultivation and had wrinkled leaves (data not shown). The survival rates after 3 weeks of cultivation were decreased with increasing irradiation dose (Fig. 1). The survival rates in sporophytes irradiated using C-ion beam in sporophytes irradiated using C-ion beam were almost similar to those in female gametophytes derived from sporophylls irradiated using C-ion beam.[1)]

[*1] Riken Food Co.,Ltd
[*2] Graduate School of Frontier Sciences, University of Tokyo
[*3] RIKEN Innovation Center
[*4] RIKEN Nishina Center

The surviving sporophytes of 20-mm length were transferred to the land tanks. The total length and individual weight differed between the doses and ion species. The sporophytes irradiated with 2 Gy of C-ion beam were the largest: the maximum length and weight were 75 cm and 45.6 g, respectively. These values were approximately two times higher than those for the largest sporophytes in the control. The sporophytes irradiated with 25 Gy of C-ion and 2.5–10 Gy of Ar-ion remained withered for up to 2 weeks after culturing in the tanks.

The sporophytes irradiated with 2-12.5 Gy of C-ion and 1 Gy of Ar-ion formed sporophylls after cultivation for 2 months. Currently, we have cultured and performed mutant screening of the sporophytes in the M_2 generation. We will analyze the next generation of the large sporophytes obtained after C-ion irradiation at 2 Gy to confirm whether the phenotype is inheritable.

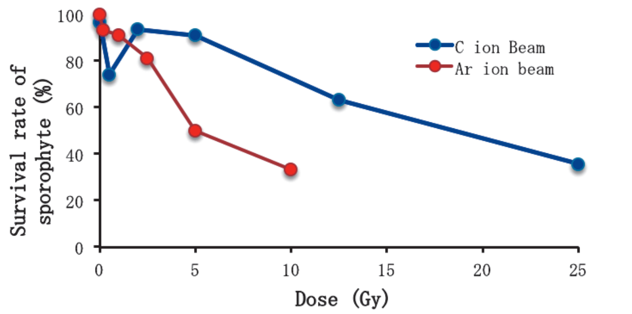

Fig. 1 Survival rates of young sporophytes irradiated with C-ion and Ar-ion beams.

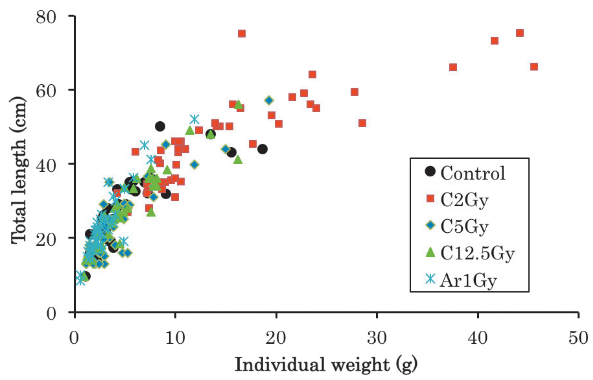

Fig. 2 Total length and individual weight of *Undaria pinnatifida* sporophytes measured 8 weeks after the irradiation with C-ion and Ar-ion beams.

References

1) Y. Sato et al.: RIKEN Accel. Prog. Rep. 46, 267 (2012)
2) M. Tatewaki: Phycologia 6, 62 (1966)

Mutation rates of *Parachlorella kessleri* by heavy-ion-beam irradiation and classification of their genomic deletion types

T. Yamazaki,[*1,*2] S. Ota,[*1,*2] K. Oshima,[*1] M. Hattori,[*1] Y. Kazama,[*3] T. Abe,[*3,*4] S. Kawano,[*1,*2]

Consumption of fossil fuels such as petroleum oil not only depletes a finite resource but also increases carbon dioxide levels, which causes global warming. Because of carbon fixation, plants can contribute to the reduction of carbon dioxide levels. Moreover, biofuels from plant have been considered as substitutes for fossil fuels. Microalgae, which perform photosynthesis like terrestrial plants, have been attracting attention as a feedstock of biodiesel production in recent years. To increase the production of biomass and improve the amount of biofuel from microalgae, the common process used is the isolation of strains with high biomass productivity and/or high oil content from the natural environment and optimization of culture conditions for the isolated strains. However, this strategy does not necessarily obtain the best strains. Therefore, we artificially modified the genome of microalgae by using the heavy-ion-beam irradiation. The heavy-ion beam is considered a mutagen that causes the partial deletion of genomic DNA very effectively, and it can also be used to breed a variety of organisms, including flowering plants. Because little is known about breeding of unicellular microalgae by using heave-ion-beam irradiation, evaluation of its effectiveness is necessary.

In this study, we used a green microalga, *Parachlorella kessleri*, the draft genome of which has been determined by our group. A search for the draft genome sequence revealed that *NR*, *NRT* and *NIR* are single-copy genes, and *NAR* is duplicated into two genes (*NAR1-1*, *NAR1-2*). The transcript of *NAR1-1* was not detected in transcriptome data, suggesting that nitrate is metabolized to ammonia through a single pathway (NRT-NR-NAR-NiR pathway) in *P. kessleri* (Fig. 1A). Therefore, a *P. kesseleri* mutant that can grow in an ammonia-containing medium but not in a nitrate-containing medium is considered to have a defective in the nitrate assimilation pathway.

P. kessleri cells were irradiated by heavy-ion beams of different doses and nuclear species, and then screening was performed using following steps: (1) a single clone derived from irradiated *P. kessleri* cells was inoculated in a TAP medium containing ammonia[1)]; (2) After the *P. kessleri* cells were grown, they were inoculated in both TAP medium and a modified TAP medium containing only nitrate as a nitrogen source; (3) a putative mutant grow in the TAP medium, but not in the modified TAP medium. Doses and nuclear species used for the screening are carbon ions the

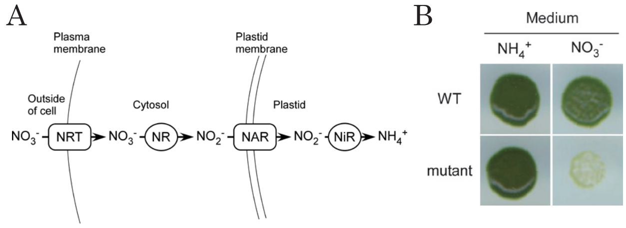

Figure 1. (A) Nitrate assimilation pathway. NRT, nitrate transporter; NR, nitrate reductase; NAR, nitrite transporter; NiR, nitrite reductase. (B) Phenotype of the mutant requiring annmonium. Wild type and mutant *P. kessleri* cells of wild type and mutant were grown on a medium containing ammonium or nitrate. After one week, their colonies were photographed.

(50 Gy, 25 Gy) and argon ions (25 Gy, 50 Gy). Fig. 1B shows a representative phenotype of the mutant isolated from the heavy-ion-beam irradiated mutant that requires ammonia as a nitrogen source.

A large-scale of screening was performed, and the mutants were isolated from about 4000 clones for 25 Gy and 50 Gy of argon-ion beams, and 25 Gy and 50 Gy carbon-ion beams, respectively. As a result, the mutants requiring ammonia from the individual doses and nuclear species were obtained each 0, 4, 3 and 4, respectively. The incidence in each experiment was 0.00, 0.10, 0.07, and 0.10% (Table 1). In the future, we plan to calculate the mutation rate of the irradiation by iron-ion beams.

Table 1. Mutation frequency by heavy-ion-beam irradiation

Nuclear species	Dose (Gy)	Isolated clone number	Positive clone number	Frequency (%)	Survival rate (%)*
C	25	4005	0	0.00	n.d.
	50	4007	4	0.10	59
Ar	25	4007	3	0.07	50
	50	4012	4	0.10	28

*Ota et al. (2013)

Next, the PCR fragment analysis and restriction fragment length polymorphism-PCR analysis were performed for the *NR* gene. However, there was no difference between the wild-type and all mutants, suggesting that the deletions of genomic DNA by heavy-ion-beam irradiation are very small in microalgae. Currently, we are performing re-sequence analysis using the next generation sequencer IonProton for the 11 mutants, expecting a detailed comparison of the deletion pattern of a set of genes involved in nitrate metabolism, including the *NR* gene.

This study was supported by JST, CREST (to SK).

References

1) Ota et al. : Bioresour Technol. 149:432-438. (2013)

[*1] Department of Integrated Biosciences, Graduate School of Frontier Sciences, University of Tokyo
[*2] JST, CREST
[*3] RIKEN Innovation Center
[*4] RIKEN Nishina Center

IV. OPERATION RECORDS

Program Advisory Committee meetings for nuclear physics and for material and life science

K. Yoneda, K. Ishida, H. Ueno, and H. Sakai

The Program Advisory Committees (PAC) is in charge of reviewing scientific proposals submitted for use of the accelerator facility of RIKEN Nishina Center (RNC). In Fiscal Year 2013, three PAC meetings were held; two for proposals of nuclear physics (NP-PAC), and one for proposals of material and life science (ML-PAC). The NP-PAC meetings were co-organized by RNC and the Center for Nuclear Study (CNS), the University of Tokyo. The NP-PAC reviewed experimental proposals at RIBF, whereas the ML-PAC reviewed proposals at RAL and RIBF.

NP-PAC

The 12th and 13th NP-PAC meetings were held on June 28 and 29, 2013, and December 13 and 14, 2013, respectively[1]. The outcome of these NP-PAC meetings is summarized in Table 1.

After the 12th NP-PAC meeting, eight NP-PAC members were renewed. The PAC members of the 12th and 13th NP-PAC meetings are as follows:

12th NP-PAC meeting: R. Tribble (Texas A&M, the chair), R.F. Casten (Yale Univ.), H. Emling (GSI), T. Glasmacher (MSU), M.N. Harakeh (KVI), M. Huyse (KU Leuven), T. Kishimoto (Osaka Univ.), M. Lewitowicz (GANIL), C.J. (Kim) Lister (UMass Lowell), T. Nakamura (Tokyo Tech.), T. Nakatsukasa (RNC), A. Ono (Tohoku Univ.), C. Scheidenberger (GSI), T. Shimoda (Osaka Univ.), F.-K. Thielemann (Univ. of Basel), M. Yahiro (Kyushu Univ.), and Y. Ye (Peking Univ.).

13th NP-PAC meeting: M.N. Harakeh (KVI, the chair), R.F. Casten (Yale Univ.), H. Emling (GSI), H. Iwasaki (Michigan State Univ.), C.J. (Kim) Lister (UMass Lowell), W. Loveland (Oregon State Univ.), S. Nakamura (Tohoku Univ.), T. Nakatsukasa (RNC), T. Nilsson (Chalmers Univ. of Technology), C. Scheidenberger (GSI), B. Sherrill (FRIB Lab.), O. Sorlin (GANIL), A. Tamii (RCNP, Osaka Univ.), F.-K. Thielemann (Univ. of Basel), Y. Utsuno (JAEA), M. Yahiro (Kyushu Univ.), and Y. Ye (Peking Univ.)

Table 1. Summary of the outcome of the 12th and 13th NP-PAC meetings. Proposals ranked with S and A are treated as “approved” proposals.

12th NP-PAC (June 28 – 29, 2013)	requested proposals (days)	approved proposals (days)
GARIS (RILAC)	2 (33)	1 (15)
RIPS (RRC)	1 (6)	0 (0)
BigRIPS/ZDS	17 (137.5)	7 (26)
SHARAQ	0 (0)	0 (0)
SAMURAI	8 (101.5)	4 (21.5)
Construction	0 (-)	0 (-)
Total	28 (278)	12 (62.5)

13th NP-PAC (December 13 – 14, 2013)	requested proposals (days)	approved proposals (days)
GARIS (RILAC)	2 (51)	2 (51)
RIPS (RRC)	4 (51.5)	3 (34)
BigRIPS/ZDS	13 (134.5)	5 (49.5)
SHARAQ	1 (8.5)	1 (8.5)
SAMURAI	4 (51.5)	4 (31.5)
Construction	1 (-)	1 (-)
Total	25 (297)	16 (174.5)

ML-PAC

The 10th ML-PAC meeting was held on July 2 and 3, 2013[2]. Before the meeting, one of the PAC members from RAL was renewed. In this meeting, twenty-four RAL proposals and seven RIBF proposals were reviewed. The summary of the outcome of the meeting is given in Table 2.

Table 2. Summary of the outcome of the 10th ML-PAC meeting.

10th ML-PAC (July 2 – 3, 2013)	requested proposals (days)	approved proposals (days)
RAL	24 (131)	23 (75)
RIBF	7 (75.5)	6 (60.12)
Total	31 (208.5)	29 (135.12)

The 10th ML-PAC members are J.-M. Poutissou (TRIUMF, the chair), A. Amato (PSI), T. Azuma (RIKEN), A. Hiller (ISIS, RAL), R. Kadono (KEK), A. Kawamoto (Hokkaido Univ.), N. Kojima (Univ. of Tokyo), K. Kubo (ICU), D.E. MacLaughlin (UC Riverside), S. Maekawa (JAEA), P. Mendels (Univ. Paris, Orsay), H. Yamase (NIMS), S. Yoshida (Yokohama City Univ.), and X.G. Zheng (Saga Univ.).

References
1) http://www.nishina.riken.jp/RIBF/NP-PAC/index.html
2) http://www.nishina.riken.jp/RIBF/ML-PAC/index.html

Beam-time statistics of RIBF experiments

K. Yoneda, H. Ueno, and H. Sakai

This report describes the statistics of the beam times (BTs) at the RIBF facility in Fiscal Year (FY) 2013. In the following, the BTs are categorized into two groups: high-energy-mode and low-energy-mode BTs. In the former, beams were delivered in the acceleration scheme of AVF, RILAC, or RILAC2 → RRC → (fRC → IRC →) SRC, where the accelerators in parentheses can be skipped in the cascade acceleration, depending on the beam species used. In the latter, the acceleration scheme is AVF or RILAC (→ RRC).

BTs in the high-energy mode were scheduled in April – July 2013 and in the latter half of March 2014, considering the restriction of utility-power use, budgetary constraints, maintenance schedule of the accelerator system and co-generation system as well as other constraints. In particular, we skipped the October – December period in FY2013, where we regularly assigned high-energy-mode BTs so far. This is mainly due to the rise in electricity costs and lack of operation budget. Big demand of large-scale maintenances, including replacement of the RRC main colis, is also the reason. In the high-energy-mode BTs in FY2013, the primary beams of ^{18}O, ^{124}Xe, and ^{238}U were delivered to users, for $T_{\mathrm{BT}} = 60.5$ days to conduct 13 experimental programs approved by the RIBF Program Advisory Committees[1]. Including $T_{\mathrm{BT}} = 14.3$ days used by RIKEN for facility development programs, defined as machine study (MS) experiments, $T_{\mathrm{BT}} = 74.8$ days was used in total for the experiments in the high-energy mode. The data summary of the high-energy-mode BTs in FY2013 is shown in Fig. 1 as a bar chart, where the total BTs provided for the users' experiments and those provided for the MS experiments are indicated by blue and orange bars, respectively.

The data summary of FY2013 BTs conducted in the low-energy mode is shown in Fig. 2. The BTs are classified by the accelerator operation modes AVF, RILAC, and RRC. Experiments in which the AVF or RILAC was operated in the stand-alone mode were able to be conducted in parallel with the high-energy-mode BTs. As seen in Fig. 2, the total low-energy-mode BT in FY2013 was reduced by 50 days compared with that in FY2012. This reduction is simply due to the long-term maintenances of RILAC and RRC scheduled in FY2013. $T_{BT} = 140.7$ days was used for 75 experiments in FY2013, which is more than 68 experiments conducted in FY2012.

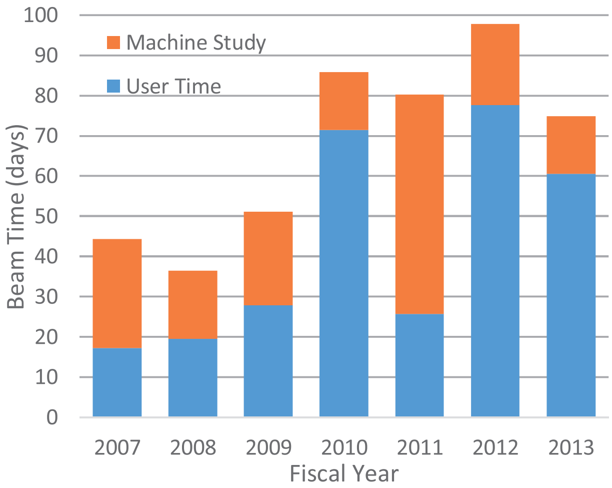

Fig. 1. Bar chart showing the BT statistics for high-energy-mode experiments from FY2007 to FY2013. The statistics of accelerator tuning time are not included.

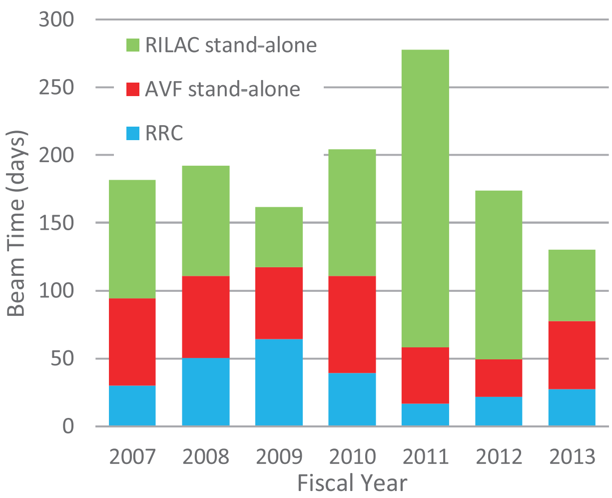

Fig. 2. Bar chart showing the BT statistics for low-energy-mode experiments from FY2007 to FY2013.

References

1) K. Yoneda, K. Ishida, H. Ueno, and H. Sakai: In this report.

Fee-based distribution of radioisotopes

T. Kambara,*[1] A. Yoshida,*[1] H. Haba,*[1] J. Kanaya,*[1] S. Shibata,*[1] Y. Wakitani,*[1,*2] and S. Yanou*[1,*2]

RIKEN distributes radioisotopes (RIs) produced at RIBF to users in Japan for a fee. This project was started in October 2007 in collaboration with the Japan Radioisotope Association[1)] (JRIA), an organization established to support the utilization of RIs in Japan. According to a material transfer agreement (MTA) drawn between JRIA and RIKEN, JRIA mediates the transaction of the RIs and distributes them to users for a fixed fee. The distributed RIs are ^{65}Zn ($T_{1/2}$ = 244 days), ^{109}Cd ($T_{1/2}$ = 463 days), and ^{88}Y ($T_{1/2}$ = 107 days).
The RIs are produced by the RI Applications Team at the AVF cyclotron. ^{65}Zn and ^{88}Y are produced through (p,n) reactions with natural Cu and SrO targets, respectively. ^{109}Cd is produced through the ^{109}Ag(d,2n)^{109}Cd reaction with a 24-MeV deuteron beam since the (d,2n) reaction is more efficient than the conventional (p,n) reaction and the produced RI has almost the same specific activity.[2)]

The prices of the distributed RIs listed in the MTA were determined on the basis of the production costs and efficiencies before the start of the distributions and have been unchanged for more than five years. The production costs and efficiencies were reviewed in 2012, and new prices were set effective in 2013. The price of ^{65}Zn has been increased except for quantities smaller than 1 MBq. The prices for ^{109}Cd and ^{88}Y have been reduced, reflecting an improvement in the production yields. In particular, the use of the (d,2n) reaction for the ^{109}Cd production has contributed to the price reduction.

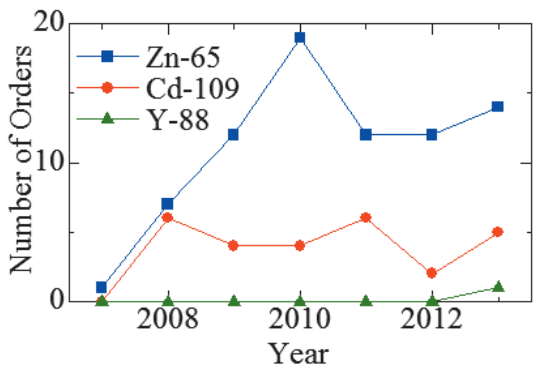

Fig. 1. Number of orders of ^{65}Zn, ^{109}Cd, and ^{88}Y distributed yearly from 2007 to 2013.

In 2013, we delivered five shipments of ^{109}Cd with a total activity of 14.15 MBq, 14 shipments of ^{65}Zn with a total activity of 72.7 MBq, and one shipment of ^{88}Y with an activity of 0.03 MBq. The shipment of ^{88}Y was the first one since February 2010 when the distribution of this radioisotope was formalized. The final recipients of the RIs were eight universities, two research institutes, and one private company. Compared with 2012, the amount of ^{109}Cd distributed in 2013 was lower by about 30 % (20 MBq in 2012) and the amount of ^{65}Zn was higher by about 24 % (58.4 MBq in 2012). Figure 1 shows the yearly trends in the number of orders, and Fig. 2 shows the amounts of the distributed RIs. Data for ^{88}Y are not included in Fig. 2 because the amount of 0.03 MBq is too small to be displayed.

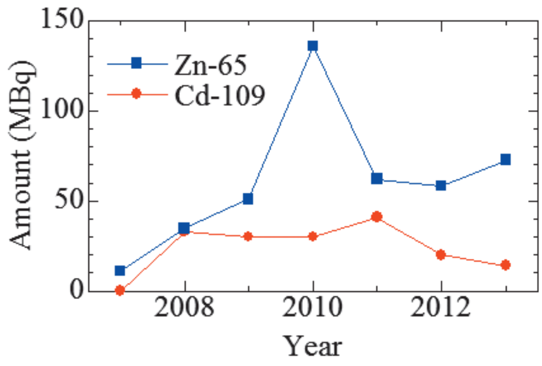

Fig. 2. Amounts of ^{65}Zn and ^{109}Cd distributed yearly from 2007 to 2013.

Information on the RIs can be obtained from JRIA through their dedicated website (https://www.j-ram.net/jram/DispatchTopPage.do; in Japanese), FAX (03-5395-8055), or E-mail (gyomu1@jrias.or.jp).

References

1) http://www.jrias.or.jp/ (Japanese), http://www.jrias.or.jp/e/ (English).
2) J. Kanaya et al.: RIKEN Accel. Prog. Rep. **46**, 250 (2013).

*1 RIKEN Nishina Center
*2 Japan Radioisotope Association

Electric power condition of Wako campus in 2013

E. Ikezawa, *[1] T. Fujinawa, *[1] M. Kato, *[1] H. Yamazawa, *[1] and M. Kase*[1]

The monthly electrical power consumption data for RIKEN Wako campus (Wako) and RIKEN Nishina Center (RNC) and the energy supply by the cogeneration system (CGS) are shown in Fig.1. The hourly electrical power consumption of RNC in 2013 is shown in Fig.2. The annual data of energy supply and consumption in 2013 is listed in Table 1. The total electrical power consumption of Wako in 2013 was 143,508 MWh, which was 14% lower than that in 2012. On the other hand, the total electrical power consumption of RNC in 2013 was 55,820 MWh, which was 32% lower than that in 2012. When the RI Beam Factory (RIBF) experiments using the uranium (^{238}U) beam were conducted, the maximum electrical power supply to Wako from Tokyo electric power corporation (TEPCO) reached 21.00 MW with a CGS output of 4.00 MW on May 24, 2013, and the maximum electrical power consumption of RNC reached 16.8 MW on April 26, 2013.

A complete overhaul of the gas turbine of the CGS #1 after 24,000 h of operation was carried out between February and March 2013. After that, an inspection of the gas turbine of the CGS #1 after 4,000 h of operation was carried out in August 2013.

We experienced the following problems during the reporting period. The absorption chillers of the CGS #1 had problems, such as corrosion of the surface of the heat transfer tube. Therefore, work for replacing two markedly impaired absorption chillers is currently in progress by the manufacturer since December 2013, and the work is to be completed by the middle of February 2014. We had a short interruption in power twice, in July and August 2013, due to thunderbolts. Earth leakages also occurred 21 times. However, the origin of most of those leakages was unexplained.

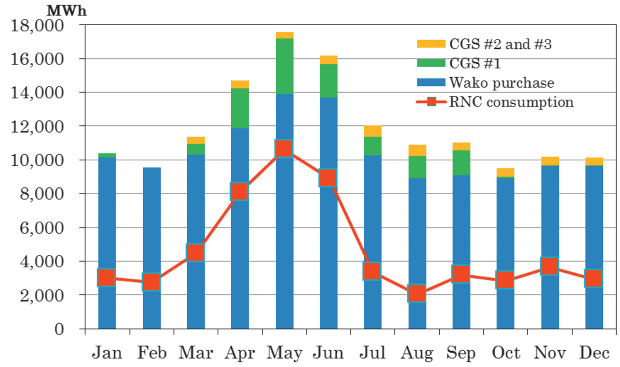

Fig.1 Monthly electrical power consumption and energy supply by CGSs in 2013.

Fig.2 Hourly electrical power consumption of RNC in 2013.

Table 1 Annual data of energy supply and consumption in 2013.

	Total	Unit	Note	% of 2012
Wako purchase	125,923	MWh	Total electrical power supply to Wako from TEPCO	91%
Wako consumption	143,508	MWh	Wako electrical power consumption (CGSs + TEPCO)	86%
RNC purchase	43,278	MWh	Total electrical power supply to RNC from TEPCO	76%
CGS #1	12,542	MWh	CGS #1 total electrical power output	49%
RNC consumption	55,820	MWh	RNC total electrical power consumption	68%
CGS #1 thermal	32,696	tons	RNC total thermal power	74%

*1 RIKEN Nishina Center

Radiation safety management at RIBF

K. Tanaka,*1 Y. Uwamino,*1 H. Sakamoto,*1 R. Hirunuma-Higurashi,*1 H. Mukai,*2 A. Akashio,*1 T. Okayasu,*1 H. Fukuda,*1 S. Hashiguchi,*3 M. Takekoshi,*3 Y. Yamauchi,*3 S. Fujita,*1 K. Nakano,*1 H. Aiso,*1 K. Igarashi*1 and S. Iizuka*1

Since 1986, residual radioactivity at the deflectors of cyclotrons has been measured regularly just before maintenance work. The variations in the dose rates are shown in Fig. 1. New measurements in 2013 were conducted only at AVF and RRC owing to their maintenance work. The beam intensity of AVF has been increased since 2006 for the radioisotope production, and the dose rate has also increased. Because the high intense beam was not provided to RRC in 2013, there was a reduction in the dose rates as shown in Fig. 1. The change in the dose rate at RRC from 1990 to 2006 is not large, and the value is typically around 20 mSv/h. After 2006, large variations in the dose rate are observed. It depends on the beam intensity of RIBF and the cooling time. The dose rate of SRC increased in 2011, and the value became similar to those of AVF and RRC. The dose rates of IRC and fRC were measured in 2012 only.

The residual radioactivity was measured along the beam lines after almost every experiment. Points 1–26, marked with solid circles in Fig. 2, are the locations where high-residual dose rates were usually observed. Table 1 lists these dose rates and the measurement dates, beam conditions, and the decay periods after the end of operation. The maximum dose rate was found to be 7 mSv/h at point 25, which is below the beam dump chamber of BigRIPS. The dose rates on the site boundary in 2013 have been monitored to prevent it be over legal limit of 1 mSv/y.

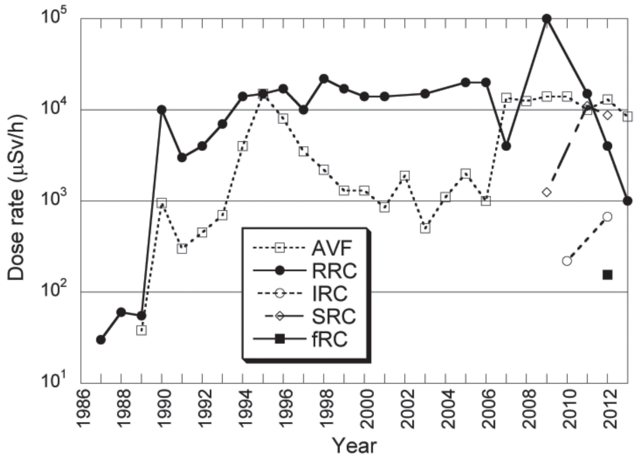

Fig. 1. Dose rates of residual radioactivity at the deflectors of 5 cyclotrons.

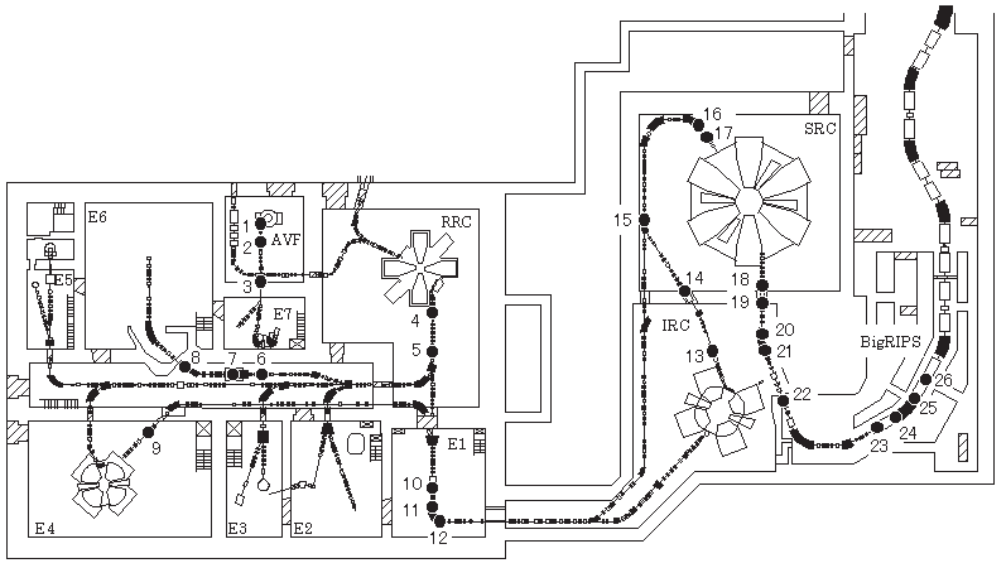

Fig. 2. Layout of beam lines at RIBF. Locations where high dose rates were observed are indicated by solid circles 1–26.

*1 RIKEN Nishina center
*2 Japan Environment Research Corporation
*3 Daiwa Atomic Engineering Corporation

Table 1. Dose rates measured at beam lines in 2013. Points 1−26 indicate the measured locations shown in Fig. 2.

Point	Dose rate (μSv/h)	Date (M/D)	Particle	Energy (MeV/u)	Intensity (pnA)	Decay period (h)
1	630	8/22	d	12	10000	414
2	300	8/22	d	12	10000	414
3	500	7/24	O-18	6.28	1000	50
4	110	12/24	Xe-124	10.75	1210	424
5	300	7/1	Xe-124	10.75	1300	1300
6	180	12/26	Xe-124	10.75	200	466
7	920	12/26	Xe-124	10.75	200	466
8	300	7/17	Rb-87	66	0.07	31
9	200	7/4	Xe-124	50	143	74
10	1300	7/4	Xe-124	50	143	74
11	1000	7/4	Xe-124	50	143	74
12	1300	7/4	Xe-124	50	143	74
13	80	7/4	Xe-124	114	51	74
14	80	7/4	Xe-124	345	36	75
15	160	7/4	Xe-124	345	36	75
16	143	4/19	O-18	250	200	2
17	260	7/4	Xe-124	345	36	75
18	230	4/19	O-18	250	200	2
19	6000	7/4	Xe-124	345	36	75
20	110	7/4	Xe-124	345	51	74
21	250	7/4	Xe-124	345	51	74
22	3000	7/4	Xe-124	345	36	75
23	400	7/4	Xe-124	345	36	75
24	1400	7/4	Xe-124	345	36	75
25	7000	7/4	Xe-124	345	36	75
26	250	7/4	Xe-124	345	36	75

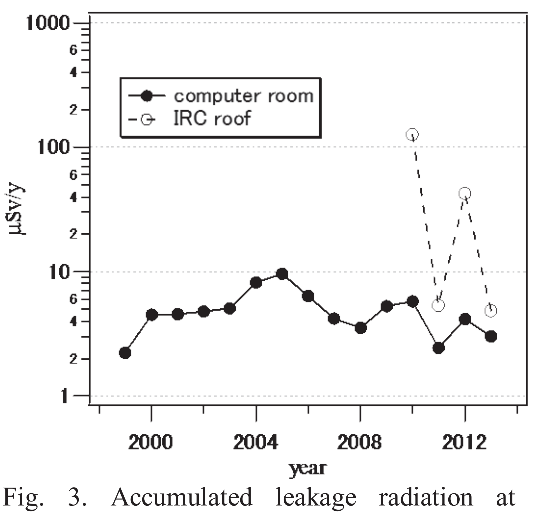

Fig. 3. Accumulated leakage radiation at the boundary of the radiation-controlled area.

We continuously monitor the radiation in and around the RIBF facility using neutron and gamma area monitors. The background dose rates were evaluated and the measured values were corrected. The background data have been acquired over a period of a month in August 2013 when all the accelerators were not in operation. The background of gamma-ray dose is currently about 2 times higher than the natural dose rate because of the fallout due to the accident at the Fukushima Dai-ichi power station. Before the accident, the natural background of the gamma-ray dose at the site boundary near the BSI East Bldg. was 0.039 μSv/h in January 2011. The background of gamma-ray dose in 2013 was 0.062 μSv/h. Just like before, all of the corrected dose rates monitored at 2013 were below the detection limit, corresponding to 2 μSv/y for neutrons and 8 μSv/y for gamma-rays. The total dose rate was less than 10 μSv/y and was considerably lower than the legal limit.

The radiation dose on the boundary of the radiation-controlled area have also been monitored. The monitors of gamma-rays and neutrons are placed at the three points on the boundary. One is in the computer room of the Nishina building, and the two other are on the roofs of the IRC and BigRIPS in the RIBF accelerator building. The highest value was observed on the IRC roof as a result of the beam loss at the transport line between SRC and BigRIPS. The annual neutron doses at these locations since 1999, which are sufficiently lower than the legal limit, are shown in Fig. 3. The value of the BigRIPS roof was similar to the background level and is not shown in Fig. 3. The legal limit of a boundary of a radiation-controlled area is 1.3 mSv/3month, and all the measured doses were low enough.

RILAC operation

E. Ikezawa,*[1] T. Ohki,*[2] M. Kase,*[1] T. Nakagawa,*[1] N. Sakamoto,*[1] H. Okuno,*[1] N. Fukunishi,*[1] M. Komiyama,*[1] A. Uchiyama,*[1] T. Maie,*[1] M. Nagase,*[1] M. Fujimaki,*[1] T. Watanabe,*[1] H. Hasebe,*[1] H. Imao,*[1] H. Kuboki,*[1] K. Ozeki,*[1] K. Suda,*[1] Y. Higurashi,*[1] K. Yamada,*[1] Y. Watanabe,*[1] T. Aihara,*[2] H. Yamauchi,*[2] K. Oyamada,*[2] M. Tamura,*[2] A. Yusa,*[2] K. Kaneko,*[2] and O. Kamigaito*[1]

The RIKEN heavy-ion linac (RILAC) has been operating steadily throughout the reporting period and has been supplying various ion beams for different experiments. Some statistics regarding the RILAC operation from January 1 to December 31, 2013, are given in Table 1. The total beam-service time of the RILAC accounted for 75.4% of its operation time. The two operation modes of the RILAC, namely, the stand-alone mode and the injection mode, in which the beam is injected into the RIKEN Ring Cyclotron (RRC), accounted for 62.2% and 37.8% of the total beam-service time of the RILAC, respectively. For the beam experiment and the machine study of the RI Beam Factory (RIBF), a 2.648-MeV/nucleon ^{18}O-ion beam and a 2.932-MeV/nucleon ^{40}Ar-ion beam accelerated by the RILAC was injected into the RRC between April and June 2013. Table 2 lists the beam-service times in the stand-alone mode of the RILAC allotted to each beam course in the RILAC target rooms in 2013. The e2 beam course in target room no. 1 was used in the machine study of a new gas-filled recoil ion separator (GARIS-Ⅱ). The e3 beam course in target room no. 1 was used in experiments involving the heaviest elements and the study of the physical and chemical properties of these elements using the GARIS. The e6 beam course in target room no. 2 was used in the analysis of trace elements. Table 3 lists the operation time of the 18-GHz ECR ion source (18G-ECRIS) in 2013.

We carried out the following improvements and overhauls during the reporting period.

1) In the RF systems, the DC high-voltage power supplies were subjected to annual inspection. In addition, the major components of mechanical parts were subjected to simple inspection.
2) Two water pumps of the cooling tower circuits were overhauled. The other water pumps were subjected to simple inspection. All cooling towers were subjected to monthly inspection and annual cleaning.
3) All the turbomolecular pumps were subjected to annual inspection. Eight cryogenic pumps used for the RILAC and CSM cavities were overhauled.

We experienced the following mechanical problems during the reporting period.

1) Water was found to have splashed in the 18G-ECRIS because of leakage from a cooling water jacket; it took approximately twelve days to repair it.
2) A section of the cooling pipe of stem-2 in the FC-RFQ cavity had a vacuum leak; it took approximately four days to repair it.
3) Water was found to have splashed in the RF power amplifier no. 3 because of leakage from a water joint outside the plate stub; it took approximately two days to repair it.
4) Water was found to have splashed in the CSM-A3 cavity because of leakage from a cooling pipe on the outside wall of the cavity; it took approximately two days to repair it.

Table 1. Statistics on RILAC operation from January 1 to December 31, 2013.

Operation time of RILAC	2779.4	h
Mechanical trouble	42.9	h
Stand-alone RILAC	1304.0	h
Injection into RRC	791.3	h
Total beam service time of RILAC	2095.3	h

Table 2. Beam service time of the stand-alone RILAC allotted to each beam course in target rooms no. 1 and no. 2 in 2013.

Beam course	Total time (h)	%
e2	110.8	8.5
e3	1151.3	88.3
e6	33.2	2.5
RRC injection course	8.6	0.7
Total	1304.0	100.0

Table 3. Operation time of the 18G-ECRIS in 2013.

Ion	Mass	Charge state	Total time (h)
N	15	3	72.0
O	18	6	252.1
F	19	6	105.0
Ne	22	6	599.9
Mg	24	7	338.7
Al	27	6	300.8
Ar	40	11	238.2
Ca	40	11	61.7
Ca	48	11	599.0
Ni	58	13	215.4
Kr	82	18	144.0
Kr	86	18, 20	162.3
Xe	136	20	12.5
U	238	35	128.0
	Total		3229.6

*1 RIKEN Nishina Center
*2 SHI Accelerator Service Ltd.

Radiation monitoring in the RIBF using ionization chambers

M. Nakamura,*[1] K. Yamada,*[1] A. Uchiyama,*[1] H. Okuno,*[1] and M. Kase*[1]

In recent years, we attempted to monitor radiation due to beam loss at several important components in the RIBF by using self-made ionization chambers (ICs)[1)-5)]. Furthermore, we input an alarm signal from the IC to the RIBF beam interlock system (BIS)[5)]. The next focus of this study is the detection of the most suitable alarm level for acceleration operations. Firstly, we attempted to calibrate the alarm level by using an IC near the electrostatic deflection channel (EDC) of SRC[3)-5)]. In SRC operations, many ions, such as N, O, Ar, Ca, Zn, Xe, and U, were used. In the present study, we investigated beam-loss calibration for the N, O, Ca, and U beams. In this report, we summarize the results and consider the suitable alarm levels for the BIS.

The experimental conditions of IC measurements have been described in the previous papers[2),-4)]. When we attempted the calibrations, $^{18}O^{8+}$, $^{48}Ca^{20+}$, and $^{238}U^{86+}$ were accelerated at 345 MeV/nucleon, and only $^{14}N^{7+}$ was accelerated at 245 MeV/nucleon. The beam currents of these ions were less than about 300 enA. In the calibration tests, firstly, each ion beam current was attenuated to about 1/40 to 1/2 times the current under usual experimental conditions by using an attenuator. Subsequently, the EDC was irradiated by these attenuated ion beams for a fairly short time such that the EDC was never damaged. We measured the IC signal at this time. As a result, we could estimate the signal intensity when the beam loss was about 2.5% to 50%, and we could calibrate the IC signal for determining alarm levels.

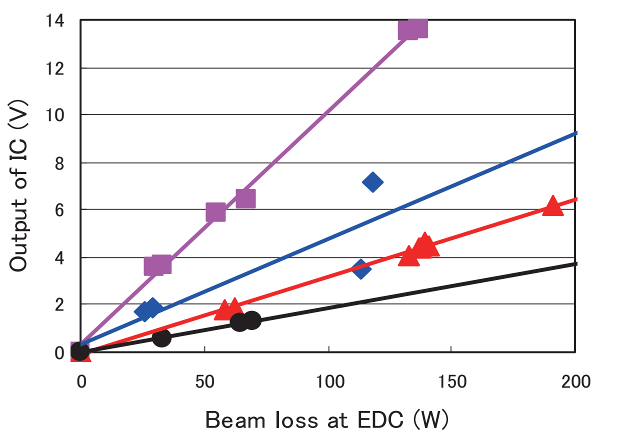

Fig. 1. The correlation between beam power loss and IC intensity.
blue rhombus: $^{14}N^{7+}$
pink square: $^{18}O^{8+}$
red triangle: $^{48}Ca^{20+}$
black circle: $^{238}U^{86+}$

The results are shown in Fig. 1. The horizontal axis shows the beam power lost at the EDC. The vertical axis shows the output voltage of the IC. The calibration curves of $^{14}N^{7+}$, $^{18}O^{8+}$, $^{48}Ca^{20+}$, and $^{238}U^{86+}$ beams are drawn and compared with each other in the same figure.

The data of $^{18}O^{8+}$ and $^{48}Ca^{20+}$ beams showed little dispersion, and most of the data existed near the calibration curves. In the case of the $^{238}U^{86+}$ beam, we could collect only three data. However, the dispersion of the data was low, and a favorable calibration curve could be drawn. In the case of the $^{14}N^{7+}$ beam, we collected only four data at this stage, and the dispersion of the data was significant. Hence, the $^{14}N^{7+}$ beam should be studied further in the near future. Furthermore, among the calibration curves of $^{14}N^{7+}$, $^{18}O^{8+}$, $^{48}Ca^{20+}$, and $^{238}U^{86+}$ beams, the sharpest slope was observed for the calibration curve of the $^{18}O^{8+}$ beam. This result showed that the intensity of radiation caused by the $^{18}O^{7+}$ beam loss is the largest, at least in the present calibrations. Conversely, the calibration curve of the $^{238}U^{86+}$ beam showed the lowest slope, indicating that the intensity of radiation caused by the $^{238}U^{86+}$ beam loss is the smallest among these ion beams.

We investigated the alarm signal for the BIS using these data. In a previous paper[4)], we reported that problems with $^{48}Ca^{20+}$ ion beam in the EDC of SRC frequently occurred when the IC output had risen to about 4 V. On comparing the values in the previous paper with the values in Fig. 1, problems occurred in the EDC when the $^{48}Ca^{20+}$ beam loss at the EDC increased beyond about 130 W. The exact value of this threshold is still under investigation. Furthermore, the thresholds of the beam loss at which problems begin to occur in the EDC have to be studied for each ion. However, from these estimations, suitable alarm levels can be determined and input to the BIS.

At present, in addition to the elements estimated in this paper, Zn, Ar, and Xe ion beams were accelerated in the experiments using SRC. We plan to investigate the beam loss and alarm levels for these elements in the near future.

References

1) M. Nakamura et al.: RIKEN Accel. Prog. Rep. 42, 141 (2009)
2) M. Nakamura et al.: RIKEN Accel. Prog. Rep. 43, 138 (2010)
3) M. Nakamura et al.: Proc 7th Annual Meeting of Particle Accelerator Society of Japan, WEPS135, Himeji, Japan.
4) M. Nakamura et al.: RIKEN Accel. Prog. Rep. 44, 293 (2011)
5) M. Nakamura et al.: RIKEN Accel. Prog. Rep. 45, 228 (2012)

*1 RIKEN Nishina Center

Operations of RIBF ring cyclotrons (RRC, fRC, IRC, and SRC)

R. Koyama,[*2] T. Dantsuka,[*1] M. Fujimaki,[*1] T. Fujinawa,[*1] N. Fukunishi,[*1] S. Fukuzawa,[*2] M. Hamanaka,[*2] H. Hasebe,[*1] Y. Higurashi,[*1] E. Ikezawa,[*1] H. Imao,[*1] S. Ishikawa,[*2] T. Kageyama,[*1] O. Kamigaito,[*1] M. Kase,[*1] M. Kidera,[*1] K. Kobayashi,[*2] M. Komiyama,[*1] Y. Kotaka,[*2] H. Kuboki,[*1] K. Kumagai,[*1] T. Maie,[*1] M. Nagase,[*1] T. Nakagawa,[*1] M. Nakamura,[*1] T. Nakamura,[*2] M. Nishida,[*2] M. Nishimura,[*2] J. Ohnishi,[*1] H. Okuno,[*1] K. Ozeki,[*1] N. Sakamoto,[*1] J. Shibata,[*2] K. Suda,[*1] N. Tsukiori,[*2] A. Uchiyama,[*1] S. Watanabe,[*1] T. Watanabe,[*1] Y. Watanabe,[*1] K. Yadomi,[*2] K. Yamada,[*1] and H. Yamazawa[*1]

The yearly report on the operation of the four RIBF ring cyclotrons RRC, fRC, IRC, and SRC, including statistics of beam service time as well as developments and troubles in the January–December 2013 period, is presented.

The yearly operation status of the RIBF ring cyclotrons is summarized in Table 1. The medium-energy beams accelerated by the RRC in the last stage were used for the experiments and machine studies (MS) for 1166 h in total. Similarly, the high-energy beams accelerated by the SRC in the last stage were used for 1646 h in total. The total operation time of RIBF ring cyclotrons was 2812 h, of which only 304 h involved temporary suspension due to the accelerator troubles. We achieved a high beam availability of 94%. The beam availability is defined as the ratio of the actual beam time after deduction of temporary suspension time to the scheduled beam time.

The notable events in those operations are as follows (itemized figures correspond to those in Table 1):

a) The highest-energy beam ever of 400 MeV/nucleon was successfully extracted from the SRC in the MS using an ^{40}Ar beam in May.

b) Two gas strippers using He and air were used in the double charge-exchanging process downstream of the RRC and fRC, respectively, in June for the first time. Owing to the gas strippers and other continuous efforts, a 345 MeV/nucleon-^{124}Xe beam of 38 particle nA was provided to the beam users with an availability as high as 91%.

c) Layer short of the RRC main-coil of the west-sector magnet was fixed by replacing it with a new one in August. Its soundness was confirmed in the MS of 50.5 MeV/nucleon-^{40}Ca acceleration in September.

d) The improvement of efficiency of injection to the RRC from RILAC2 was confirmed when a saw-tooth wave was used for the prebuncher instead of a usual sine wave in the MS of 11 MeV/nucleon-^{124}Xe acceleration in December. The acceleration at harmonic numbers $h = 12$ and $h = 18$ instead of the usual $h = 9$ was also tested for the future upgrade of the RRC in the same MS. The obtained data is now under analysis.

For more details of those operations and others, refer to Ref. 1.

References

1) R. Koyama et al.: Proc. of PASJ10, Nagoya, Aichi, August 2013, SAP013, in press.

Table 1. Yearly operation results of the RIBF ring cyclotrons. For notable events a)–d), see text.

Last stage cyclotron	Preaccelerators	Particle	Energy [MeV/nucleon]	Experimental course	Intensity [particle nA]		Beam time [h]		Temporary suspension [h]	Availability [%]*	Notable events
					Requested	Actual	Scheduled	Actual			
RRC 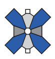	RILAC	^{40}Ca	50.5	RRC	MS	143	84.0	84.0	0.0	100	c)
		^{48}Ca	63	E6	200	294	156.0	156.6	28.5	82	
		^{58}Ni			> 200	87	144.0	157.5	10.4	102	
		^{86}Kr	36	E3A	1	38	12.0	12.7	0.0	106	
	RILAC2	^{238}U	10.75	E5A	2	29	24.0	24.0	0.0	100	
		^{124}Xe		E2B	10	772	48.0	47.2	0.0	98	
				D-room	MS	1211	24.0	24.0	0.0	100	d)
	AVF	^{12}C	70	E6	400	383	312.0	305.8	9.3	95	
			135	E5B	10	367	52.0	52.0	0.0	100	
		^{40}Ar	95		1	26	34.5	34.5	0.0	100	
		^{56}Fe	90	E2B/E5B	1	4	199.0	199.0	0.0	100	
		^{87}Rb	66	E6	1	0.1	48.0	68.9	0.7	142	
	Subtotal of medium-energy experiment at old facility:						**1137.5**	**1166.1**	**49.0**	**98**	
SRC 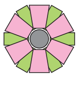	AVF-RRC	^{18}O	250	SAMURAI	200	231	108.0	123.0	6.2	108	
	RILAC-RRC -IRC		345	BigRIPS	100	313	120.0	132.0	33.7	82	
		^{40}Ar	400		MS	16@beam duty2%	137.5	137.5	0.0	100	a)
	RILAC2-RRC -fRC-IRC	^{238}U	345	BigRIPS/ZDS /EURICA	> 5	13	660.0	700.3	109.9	89	
		^{124}Xe			> 20	38	492.0	553.3	105.3	91	b)
	Subtotal of high-energy experiment at new facility:						**1517.5**	**1646.1**	**255.2**	**92**	
Total:							**2655.0**	**2812.2**	**304.1**	**94**	

*Availability = (Actual beam time - Suspension)/(Scheduled beam time)x100

*1 RIKEN Nishina Center
*2 SHI Accelerator Service Ltd.

Operation of the superconducting ring cyclotron cryogenic system

H. Okuno,[*1] T. Dantsuka,[*1] Y. Mori,[*2] M. Ohshima,[*2] H. Hazama,[*2] A. Mikami,[*2] H. Miura,[*2] H. Shiba,[*2] H. Shiraki,[*2] Y. Tezuka,[*2] S. Watanabe,[*2] and K. Yamamoto[*2]

The SRC (Superconducting Ring Cyclotron) cryogenic system, which consists of three compressors, a He refrigerator, and four He buffer tanks for cooling the 240-MJ superconducting magnets used for the SRC, has a cooling capacity of approximately 1 kW at 4.5 K and an inventory of 5000 L of liquid He. The cooling system was operated for approximately six months in 2013, with a five-month maintenance shutdown in summer (July–December) and a shutdown to conserve electrical power in January, as shown in Fig. 1. The trend observed for the main coil current of the SRC sector magnet is also shown in this figure. During system operation, there was no major hindrance to stop the He refrigerator and compressor. Because of the extensive He leak during operation in 2012, approximately 200 m^3 of He gas had to be refiled once in two months.[1)] The leak was found to occur in the flange connection between the power lead and He gas pipes used for their cooling. The connection mainly consists of an insulation flange and O-ring as shown in Fig. 2. The main parts were replaced with new ones. The replacement was successfully accomplished in the August. Furthermore, the heater system for the power lead was also upgraded to moderate the heat cycle on parts of the flange connection.

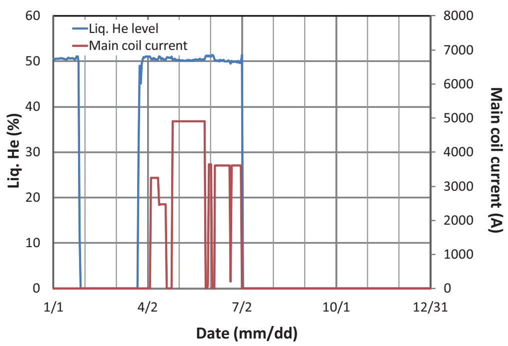

Fig. 1. Trend observed in liquid He level in the dewar and main coil current for the SRC superconducting sector magnet.

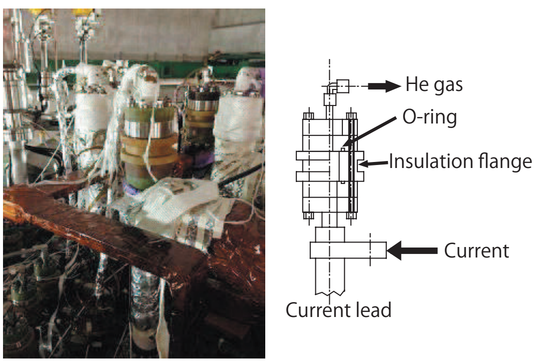

Fig. 2. Photograph and structural schematic of the current leads at which the leak occurred.

References
1) H. Okuno, et al.,: RIKEN Accel. Prog. Rep. **46**, 278(2013).

*1 RIKEN Nishina Center
*2 Nippon Kucho Service Co., Ltd

Present status of the BigRIPS cryogenic plant

K. Kusaka,[*1] M. Ohtake,[*1] T. Kubo,[*1] K. Yoshida,[*1] Y. Mori,[*2] M. Ohshima,[*2] K. Yamamoto,[*2] S. Watanabe,[*2] Y. Tezuka,[*2] A. Mikami,[*2] H. Shiba,[*2] H. Hazama,[*2] H. Miura,[*2] M. Noguchi,[*3] and N. Suzuki[*3]

Periodic maintenance of the BigRIPS cryogenic plant is essential to ensure long-term continuous operations of BigRIPS. In addition to periodically calibrating the pressure and temperature sensors installed in the system, maintaining the oil-removal module in the helium compressor unit is crucial[1]. The oil-removal module comprises an oil vessel with a demister, which is used as a bulk oil separator (1SP), three coalescer vessels (2SP, 3SP, and, 3.5SP), and two adsorbent vessels (4SP and 5SP) that contain activated charcoal and molecular sieves. The periodic replacement of coalescer filters and adsorbents ensure the small oil contamination in helium gas. The contamination ranges between 0.008 - 0.02 weight ppm (wt. ppm), depending on the quality of the coalescers used.

We replaced all the coalescer filters in three coalescer vessels during the summer maintenance in 2008, 2010, and 2012. Each coalescer vessel contains four coalescer filters, manufactured by Domnick Hunter[3], and the drain oil separated from the helium gas is sent to the compressor via a drain line with solenoid valves, depending on the oil level in the vessel. The expected oil contamination levels at the exit of the coalescer vessels are 15-50 and 0.75-1.25 wt. ppm for 3SP and 3.5SP, respectively. The oil contamination level can be easily measured with an oil check kit[2].

Figure 1 shows the contamination measured at the entrance of 3SP as a function of the coalescer filter operation time. The oil check kit values are shown as open symbols in Fig. 1. The open triangles, squares, and circles represent results for the 2008-2009, 2010-2011, and 2012 operations, respectively. An estimate from the oil drain from the 3SP is also shown in Fig. 1. We estimate the oil contamination level by measuring the operation interval of the solenoid valve installed in 3SP. The navy blue, green, and, yellow diamonds represent the estimates for the 2008-2009, 2010-2011, and 2012 operations, respectively. The estimates of oil drain increase to 50~75 wt. ppm up to an operation time of 2000 h for the period of 2008-2009 and 2010-2011 and then stays constant. Corresponding oil check kit results show a similar increasing tendency. On the other hand, the estimate from the oil drain for the period of 2012 shows monotonous increasing tendency and does not stay constant for any long period. We shall continue observations in the next operation. This difference indicates the performance efficiency of different coalescer filters.

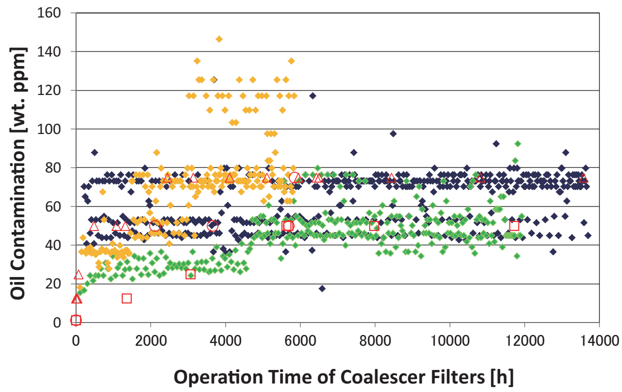

Fig. 1. Oil contamination at the entrance of the second coalescer vessel (3SP).

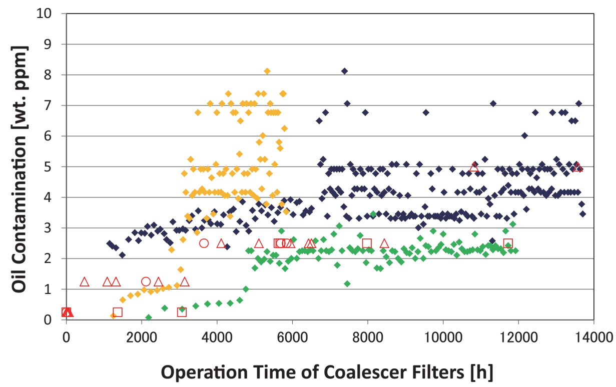

Fig. 2. Oil contamination at the entrance of the third coalescer vessel (3.5SP).

In Fig. 2, we show a similar analysis of the oil contamination at the entrance of 3.5SP. Symbols and colors used in Fig. 2 are same as those in Fig. 1. A gradual increasing tendency of the oil contamination is seen in all operation periods. Following the less oil contamination at the entrance of the 3SP, the results for the period of 2010-2011 are approximately half of that of the other period. However, the oil contamination estimated from the oil drain for the period of 2012 unexpectedly increased faster than other periods. We shall continue observations in the next operation and investigate the coalescer filters in the maintenance planned in the summer of 2014.

References

1) K. Kusaka et al.: RIKEN Accel. Prog. Rep. **41**, 244 (2008).
2) K. Kusaka et al.: RIKEN Accel. Prog. Rep. **43**, 309 (2010).
3) http://www.parker.com/

*1 RIKEN Nishina Center
*2 Nippon Kucho Service Co., Ltd.
*3 Mayekawa Mfg. Co., Ltd.

Present status of liquid-helium supply and recovery system

T. Dantsuka,[*1] H. Okuno,[*1] M. Nakamura,[*1] K. Ikegami,[*1] M. Kase,[*1] S. Tsuruma,[*1]
M. Ohshima,[*2] H. Miura,[*2] Y. Tezuka,[*2] H. Hazama[*2] and H. Shiba[*2]

The liquid-helium supply and recovery system[1)], which can produce liquid helium from pure helium gas at a rate of 200 L/h from pure helium gas, has been stably operated since the beginning of April 2001. The volumes of liquid helium supplied each year from 2001 to 2012 are shown in Fig. 1. The volume gradually increased from 2001 to 2008 but sharply increased in 2010, before decreasing sharply in 2011, and again sharply increasing in 2012.

We extended the recovery line at one place. A new recovery line was connected to the existing line at the RIBF Building at B3F.

The purity of helium gas recovered from laboratories gradually improved once the construction of the system was completed. Currently, the impurity concentration in the recovered gas is rarely more than 200 ppm. The volume of helium gas recovered from each building in the Wako campus and the volume transported to the liquid-helium supply and recovery system were measured. The recovery efficiency, which is defined as the ratio of the amount of recovered helium gas to the amount of supplied liquid helium, was calculated. The recovery efficiency for the buildings on the south side of the Wako campus, such as the Cooperation Center building of the Advanced Device Laboratory, the Chemistry and Material Physics building, and the Nanoscience Joint Laboratory building, increased to more than 90%. The average recovery efficiency from January 2008 to July 2013 is shown in Fig. 2. This value also increased to over 90%.

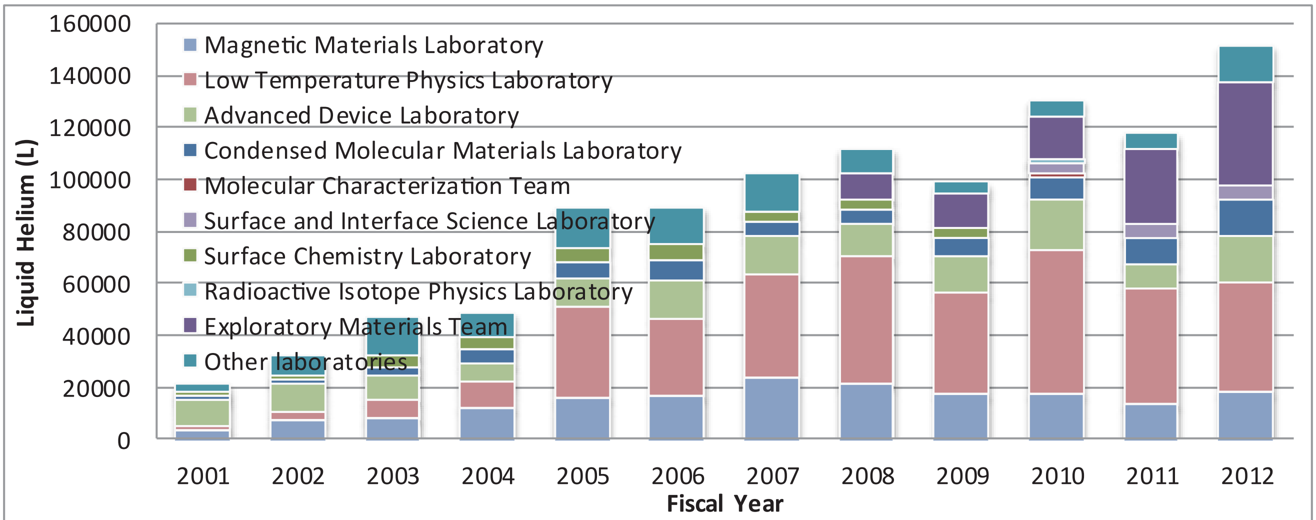

Fig.1. Volumes of liquid helium supplied to laboratories for each fiscal year from 2001 to 2012

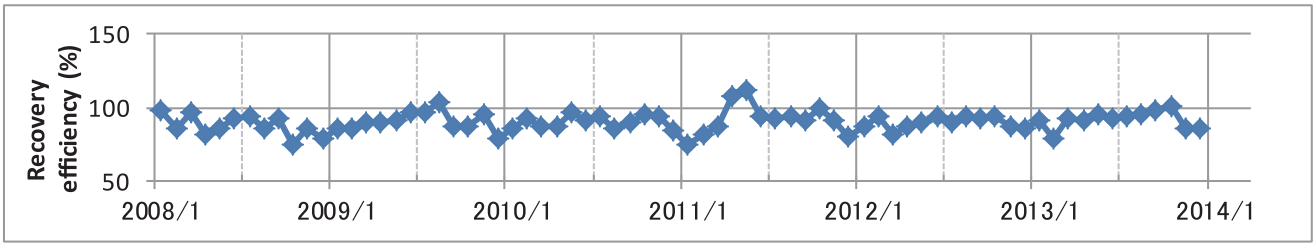

Fig.2. Average recovery efficiency measured from January 2008 to July 2013

† Condensed from the article in Phys. Rev. Lett. **85**, 1827 (2000)
*1 RIKEN Nishina Center
*2 Nippon Air Conditioning Service K.K

References
1) K. Ikegami et al.: RIKEN Accel. Prog. Rep. 34, 349 (2001).

V. EVENTS

The 7th Nishina School

T. Kishida*[1]

The Nishina School was held from Aug. 6 to 16. The School was for the students of Peking University (11 M0 students), Seoul National University (8 undergraduate students) and the University of Tokyo (4 graduate students). Although the School was held every year for each university, this was the first one which was held together for these three universities.

The first week program consisted of lectures and basic trainings. The second week program consisted of several experiments. On the last day of the School, the presentation session by the students was held.

As well as the Nishina School, the Summer School for Phillips Exeter Academy (a high school in the United States) was held from Jul. 30 to Aug. 16. Two high school students attended the school. They also joined the first program and the presentation session of the Nishina School.

Thus, the Nishina School became a real international school where international cultural exchange was made among China, Korea, U.S. and Japan. All the students enjoyed the School fully. Figure 1 shows a photograph taken at the opening ceremony on Aug. 6.

Fig. 1. Opening Ceremony of the Nishina School.

*[1] RIKEN Nishina Center, the Principal of the Nishina School

VI. ORGANIZATION AND ACTIVITIES OF RIKEN NISHINA CENTER
(Activities and Members)

1. Organization

1.1 Organization Chart as of April 1, 2013

1.2 Topic in FY2013

Apr. 1, 2013	Start of **Nuclear Spectroscopy Laboratory**
	Start of **Research Group for Superheavy Element**, taking over Superheavy Element Laboratory, associated with following two teams **Superheavy Element Production Team** **Superheavy Element Device Development Team**
	Personnel Change Deputy Director of RNC: Hiroyosi SAKURAI Director of RBRC: Samuel H. ARONSON Team Leader of User Support Office: Ken-ichiroYONEDA Team Leader of SAMURAI Team: Hiromi SATO New Appointment Deputy Group Director of Accelerator Group (Energy Efficient Management): Masayuki KASE Senior Adviser: Walter F. HENNING
Nov. 1, 2013	New Appointment Deputy Director of RBRC: Robert PISARSKI

2. Finances

Breakdown expenses of the RNS FY2013 budget and transition for past five years are shown in following figures.

Due to the budgetary limitation caused by the aftermath of Tohoku earthquake and Fukushima nuclear disaster, beam time for the RIBF users as recommended in NCAC2011 is not able to be provided sufficiently at present. For FY2013, RNC managed to realize 3.5 month operation by receiving additional President’s Discretionary Fund and cancelling accelerator operation in autumn which was replaced by a consecutive operation from the year-end to the next fiscal year.

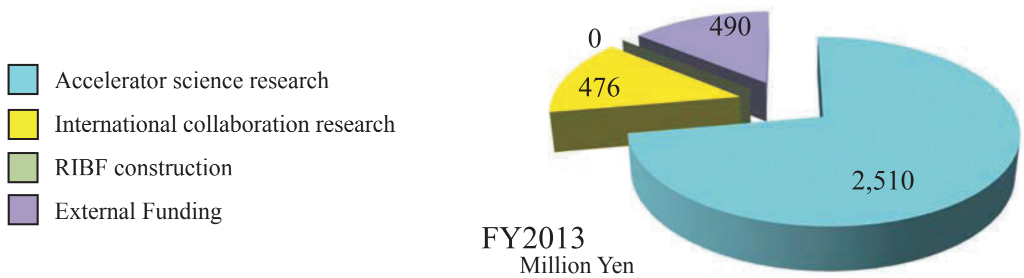

3. Staffing

Having reached a consensus within RIKEN on the issue of supplementing additional permanent staff to the Accelerator Group, RNC now have a better outlook for solving personnel shortage problem. RNC eagerly anticipate additional permanent staff to join the Accelerator Group in the near future, with one new arrival in FY2013, another one to be selected for FY2014. On the other hand, while there is several permanent staffs that underwent career shift from research to research support, the number is still not enough. To further promote an increase in permanent research support staff, RNC are recruiting from entire RIKEN for qualified candidates.

Breakdown to six personnel categories in FY2013 and transition for past five years are shown in following figures.

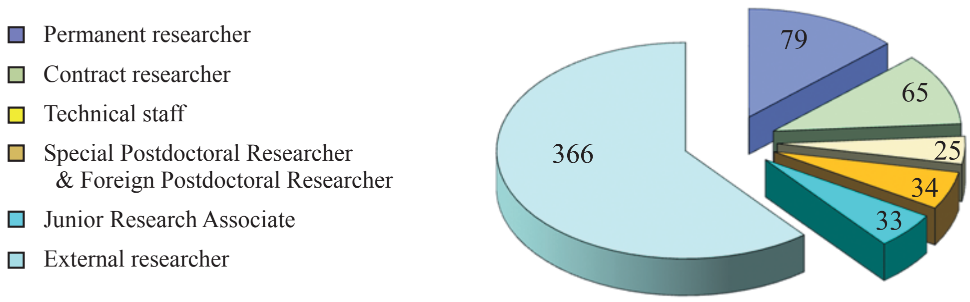

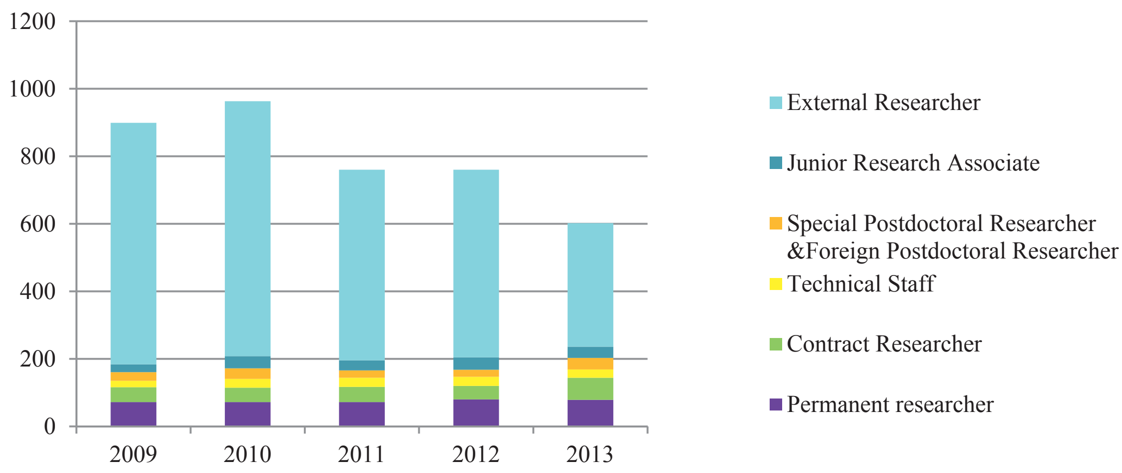

4. Management

RIKEN Nishina Center for Accelerator-Based Science (**RNC**) is now composed of, under RNC Director Hideto En'yo,

10 Laboratories,
1 Research unit,
7 Groups with 20 Teams,
2 overseas research center with 3 Groups.

There are also three 'Partner Institutes' which conduct research in the laboratories arranged in RNC.

RNC is managed by its Director through the majority decision in the RNC Coordination Committee. Accelerator Research Promotion Section which carries out administrative function of RNC under the President of RIKEN is set close to RNC.

In order to support the management of RNC, there are

Scientific Policy Committee,
Program Advisory Committee,
Safety Review Committee,
RIBF Machine Time Committee, and
Public Relations Committee.

There are also committees to support the President of RIKEN or the Director of RNC.

RBRC Management Steering Committee (MSC) and Nishina Center Advisory Council, which has two subcommittees.

RBRC Scientific Review Committee (SRC) and
Advisory Committee for the RIKEN-RAL Muon Facility.

Nishina Center for Accelerator-based Science

Executive Members (as of March 31, 2014)

Hideto EN'YO	Director, RNC; Chief Scientist, Director of Radiation Laboratory
Tetsuo HATSUDA	Deputy Director (Theoretical Research), RNC; Chief Scientist, Director of Quantum Hadron Physics Laboratory
Hiroyoshi SAKURAI	Deputy Director (RIBF Research), RNC; Chief Scientist, Director of Radioactive Isotope Physics Laboratory
Tohru MOTOBAYASHI	RIBF Synergetic-Use Coordinator
Walter F. HENNING	Senior Advisor
Yasushige YANO	Senior Advisor
Minami IMANISHI	Assistant

RNC Coordination Committee

Following subjects relating to RNC management are deliberated under the chairmanship of RNC Director.

Establishment of the new organization or reorganization in RNC,
Personnel management of RNC researchers,
Research themes and research budget
Approval of the Partner Institutes,
Evaluation as to the management of RNC and the response to recommendations by external evaluation.

RNC Coordination Committee is held monthly.

Members (as of March 31, 2014)

Hideto EN'YO	Director, RNC; Chief Scientist, Director of Radiation Laboratory
Hiroyoshi SAKURAI	Deputy Director, RNC; Chief Scientist, Director of Radioactive Isotope Physics Laboratory
Tetsuo HATSUDA	Deputy Director, RNC; Chief Scientist, Director of Quantum Hadron Physics Laboratory
Walter F. HENNING	Senior Advisor
Tohru MOTOBAYASHI	RIBF synergetic-use coordinator
Yasushige YANO	Senior Advisor
Masahiko IWASAKI	Chief Scientist, Director of Advanced Meson Science Laboratory
Tomohiro UESAKA	Chief Scientist, Director of Spin isospin Laboratory
Hideki UENO	Chief Scientist, Director of Nuclear Spectroscopy Laboratory; Deputy Group Director, User Liaison and Industrial Cooperation Group
Toru TAMAGAWA	Associate Chief Scientist, Director of High Energy Astrophysics Laboratory
Takashi NAKATSUKASA	Associate Chief Scientist, Director of Theoretical Nuclear Physics Laboratory
Emiko HIYAMA	Associate Chief Scientist, Director of Strangeness Nuclear Physics Laboratory
Koji HASHIMOTO	Associate Chief Scientist, Director of Mathematical Physics Laboratory
Kosuke MORITA	Group Director, Research Group for Superheavy Element; Team Leader, Superheavy Element Production Team
Osamu KAMIGAITO	Group Director, Accelerator Group
Hideyuki SAKAI	Group Director, User Liaison and Industrial Cooperation Group
Hiroki OKUNO	Deputy Group Director, Accelerator Group; Team Leader, Accelerator R&D Team; Team Leader, Cryogenic Technology Team
Nobuhisa FUKUNISHI	Deputy Group Director, Accelerator Group; Team Leader, Beam Dynamics & Diagnostics Team
Masayuki KASE	Deputy Group Director, Accelerator Group; Team Leader, Infrastructure Management Team
Tomoko ABE	Group Director, Accelerator Applications Research Group; Team Leader, Radiation Biology Team
Yoshitomo UWAMINO	Group Director, Safety Management Group
Toshiyuki KUBO	Group Director, Research Instruments Group; Team Leader, Detector Team
Masanori WAKASUGI	Group Director, Instrumentation Development Group; Team Leader, Rare RI-ring Team; Team Leader, SCRIT Team
Eiji IKEZAWA	Team Leader, RILAC Team
Takashi ICHIHARA	Team Leader, Computing and Network Team
Naruhiko SAKAMOTO	Team Leader, Cyclotron Team
Hiromi SATO	Team Leader, SAMURAI Team (-Mar. 2014), Team Leader, Detector Team (Apr. 2014-)
Takahide NAKAGAWA	Team Leader, Ion Source Team
Hiromitsu HABA	Team Leader, RI Applications Team
Koji MORIMOTO	Team Leader, Superheavy Element Device Development Team
Atsushi YOSHIDA	Team Leader, Industrial Cooperation Team
Koichi YOSHIDA	Team Leader, BigRIPS Team
Ken-ichiro YONEDA	Team Leader, User Support Office
Michiharu WADA	Team Leader, SLOWRI Team
Yasuyuki Akiba	Vice Chief Scientist, Radiation Laboratory; Group Leader, Experimental Group, RIKEN BNL Research Center
Katsuhiko ISHIDA	Vice Chief Scientist, Advanced Meson Science Laboratory
Tsukasa TADA	Vice Chief Scientist, Quantum Hadron Physics Laboratory
Yuko MOTIZUKI	Research Unit Leader, Astro-Glaciology Research Unit
Akihiko UEDA	Senior Manager; Director, Head of Accelerator Research Promotion Section

Accelerator Research Promotion Section

The scope of business of Accelerator Research Promotion Section is Planning and coordination as to research program and research system of RNC, Planning and management of budget use of RNC, Public relations activity.

Members (as of March 31, 2014)

Akihiko UEDA	Senior Manager; Director, Head of Accelerator Research Promotion Section
Mitsuru KISHIMOTO	Manager, Accelerator Research Promotion Section
Hayato NISHIMURA	Deputy Manager (-May 2014)
Kazunori MABUCHI	Deputy Manager
Yukari ONISHI	Chief
Kumiko SUGITA	Special Administrative Employee
Yuko OKADA	Task-Specific Employee
Yukiko SATO	Task-Specific Employee
Kyoji YAMADA	Special Temporary Employee
Yoshio OKUIZUMI	Temporary Employee
Masatoshi MORIYAMA	Consultant for Advisory Committee, Research Review, etc.
Rie KUWANA	Temporary Staff

Scientific Policy Committee

Scientific Policy Committee deliberates on Research measures and policies of RNC, Administration of research facilities under RNC's control. Committee members are selected among professionals within and without RNC. The Committee is held annually.

Members (as of March 31, 2014)

Hirokazu Tamura	Chair Prof., Graduate School of Science, Tohoku University
Yujiro IKEDA	Director, J-PARC Center
Akira UKAWA	Prof., Faculty of Pure and Applied Sciences, University of Tsukuba
Takaharu OTSUKA	Director, Center for Nuclear Study (CNS), University of Tokyo
Hideo OHNO	Research Advisor, Japan Synchrotron Radiation Research Institute (JASRI)
Ryosuke KADONO	PI, Muon Science Laboratory, Institute of Materials Structure Science, High Energy Accelerator Research Organization (KEK)
Takashi NAKANO	Director of Research Center for Nuclear Physics (RCNP), Osaka University
Hirohiko TSUJII	Fellow, National Institute of Radiological Sciences (NIRS)
Tomofumi NAGAE	Prof. Graduate School of Science, Kyoto University
Hitoshi NAKAGAWA	Auditor, Japan International Research Center for Agricultural Sciences
Yoshiyuki FUJII	Project Prof., Arctic Environment Research Center, National Institute of Polar Research
Yasuhiko FUJII	Director, Research Center for Neutron and Technology, Comprehensive Research Organization for Science and Society (CROSS-TOKAI)
Shoji FUTATSUGAWA	Executive Director, Japan Radioisotope Association
Masanori YAMAUCHI	Director, Institute of Particle and Nuclear Studies, High Energy Accelerator Research Organization (KEK)
Kazuyoshi YAMADA	Director, Institute of materials Structure Science, High Energy Accelerator Research Organization (KEK)
Kazuo SHINOZAKI	Director, Center for Sustainable Resource Science, RIKEN
Ryutaro HIMENO	Director, Advanced Center for Computing and Communication, RIKEN

The meeting of FY2013 was held on July 11, 2013 at Tokyo Liaison Office of RIKEN.

Program Advisory Committee

Program Advisory Committee reviews experimental proposals submitted by researchers and reports the acceptance or the denial of the adaptation of proposals to RNC Director. The Committee also reports to RNC Director the available period (days) of RIBF or Muon Facility at RAL allotted to researchers.

The name and scope of the Committees are follows;

(1) Nuclear Physics Experiments at RIBF (NP-PAC): academic research for nuclear physics,
(2) Materials and Life Science Researches at RNC (ML-PAC): academic research for material science and life science,
(3) Industrial Program Advisory Committee (In-PAC): non-academic research

Program Advisory Committee for Nuclear Physics Experiments at RI Beam Factory (NP-PAC)

Members

Muhsin N. HARAKEH	Chair Prof. KVI (Kernfysisch Versneller Instituut), University of Groningen, Netherlands
Yanlin YE	Prof. State Key Lab. of Nucl. Phys. and Tech., School of Physics, Peking University, Chaina

Christoph SCHEIDENBERGER	Head, NuSTAR/ENNA Department, GSI, Germany
Friedrich-K. THIELEMANN	Prof. Department of Physics, University of Basel, Switzerland
Rick F. CASTEN	Physics Department, Yale University, USA
Christopher J. (KIM) LISTER	Prof. Department of Physics and Applied Physics, University of Massachusetts, Lowell, USA
Hans EMLING	GSI, Germany
Hironori IWASAKI	Assistant Professor of Physics, National Superconducting Cyclotron Laboratory, Michigan State University, USA
Walter D. LOVELAND	Full Prof. Department of Chemistry, Oregon State University, USA
Thomas NILSSON	Prof. Department of Fundamental Physics, Chalmers Univ. of Technology, Sweden Chair of BFC (Board of FAIR Collaborations)
Bradley. M.SHERRILL	FRIB Chief Scientist, Michigan State University, USA
Olivier SORLIN	Grand Accélérateur National d'Ions Lourds (GANIL), France
Satoshi N. NAKAMURA	Associate Prof. Nuclear Experiment Group, Faculty of Science, Tohoku University
Atsushi TAMII	Associate Prof. Experimental Nuclear Physics Division, Research Center for Nuclear Physics, Osaka University
Yutaka UTSUNO	Frontier Research on Heavy Element System, Advanced Science Research Center, JAEA
Masanobu YAHIRO	Prof. Fundamental particle physics, Department of Physics, Faculty of Sciences, Kyushu University
Takashi NAKATSUKASA	Associate Chief Scientist, Director of Theoretical Nuclear Physics Laboratory, RNC, RIKEN

Program Advisory Committee for Materials and Life Science Researches at RIKEN Nishina Center (ML-PAC)

Members

Jean-Michel POUTISSOU	Chair Senior research scientist Emeritus, TRIUMF, Canada
Alex AMATO	Muon Spin Spectroscopy, Paul Scherrer Institute, Switzerland
Douglas E. MACLAUGHLIN	(University of California, Riverside, USA)
Sadamichi MAEKAWA	(JAEA, JAPAN)
Kenya KUBO	Prof. The College of Liberal Arts, International Christian University
Adrian HILLIER	ISIS, RAL, UK
Philippe MENDELS	Laboratorie de Physique des Solides, Universite Paris-SUD, France
Xu-Guang ZHENG	Saga University
Hiroyuki YAMASE	(NIMS, JAPAN)
Ryosuke KADONO	PI, Muon Science Laboratory, Institute of Materials Structure Science, High Energy Accelerator Research Organization (KEK)
Norimichi KOJIMA	University of Tokyo, JAPAN)
Toshiyuki AZUMA	Chief Scientist, Atomic, Molecular & Optical Physics Laboratory, RIKEN
Atsushi KAWAMOTO	(Hokkaido University, JAPAN)
Shigeo YOSHIDA	(Yokohama City University, JAPAN)

Industrial Program Advisory Committee (In-PAC) Members (July 1, 2012--March 31, 2014)

Members

Akihiro IWASE	Chair Prof. Graduate School of Engineering, Osaka Prefecture University
Kenya KUBO	Prof. The College of Liberal Arts, International Christian University
Hitoshi NAKAGAWA	Auditor, Japan International Research Center for Agricultural Sciences
Nobuhiko NISHIDA	Full time research fellow, Toyota Physical and Chemical Research Institute
Toshinori MITSUMOTO	Chief Engineer, Quantum Equipment Division, Sumitomo Heavy Industries, Ltd
Toshiyuki AZUMA	Chief Scientist, Atomic, Molecular & Optical Physics Laboratory, RIKEN

Safety Review Committee

Safety Review Committee is composed of two sub committees, Safety Review Committee for Accelerator Experiments and Hot-Labo Safety Review Committee. These Committees review the safety of the usage scenario about radiation generating equipment submitted to RNC Director from the spokesperson of the approved experiment.

Safety Review Committee for Accelerator Experiments

Members

Takashi KISHIDA	Chair, Sakurai Radioactive Isotope Physics Laboratory
Kouji MORIMOTO	Superheavy Element Research Device Development Team
Eiji IKEZAWA	RILAC Team
Hiromitsu HABA	RI Applications Team
Shinichiro MICHIMASA	Assistant Prof., Center for Nuclear Study, University of Tokyo
Hidetoshi YAMAGUCHI	Lecturer, Center for Nuclear Study, University of Tokyo
Hiroshi WATANABE	Lecturer, KEK
Hiromi SATO	Detector Team

Atsushi YOSHIDA	Industrial Cooperation Team
Koichi YOSHIDA	BigRIPS Team
Naoki FUKUDA	BigRIPS Team
Naruhiko SAKAMOTO	Cyclotron Team
Hisao SAKAMOTO	Safety Management Group
Yoshitomo UWAMINO	Safety Management Group
Kanenobu TANAKA	Safety Management Group

Hot-Labo Safety Review Committee

Members

Masako IZUMI	Chair, Radiation Biology Team
Yoshitomo UWAMINO	Safety Management Group
Hisao SAKAMOTO	Safety Management Group
Hiroki MUKAI	Safety Management Group
Kanenobu TANAKA	Safety Management Group
Hiromitsu HABA	RI Applications Team

RIBF Machine Time Committee

Upon request of RNC Director, RIBF Machine Time Committee deliberates the operating program of RIBF and returns the results to him.

Members

Hideyuki SAKAI	Chair, User Liaison and Industrial Cooperation Group
Tomoko ABE	Group Director, Accelerator Applications Research Group
Nobuhisa FUKUNISHI	Deputy Group Director, Accelerator Group
Osamu KAMIGAITO	Group Director, Accelerator Group
Masayuki KASE	Deputy Group Director, Accelerator Group
Toshiyuki KUBO	Group Director, Research Instruments Group
Kouji MORIMOTO	Team Leader, Superheavy Element Research Device Development Team
Hiroki OKUNO	Deputy Group Director, Accelerator Group
Hiroyoshi SAKURAI	Chief Scientist, Sakurai Radioactive Isotope Physics Laboratory
Hideki UENO	Chief Scientist, Nuclear Spectroscopy Laboratory
Tomohiro UESAKA	Chief Scientist, Spin isospin Laboratory
Yoshitomo UWAMINO	Group Director, Safety Management Group
Masanori WAKASUGI	Group Director, Instrumentation Development Group
Ken-ichiro YONEDA	Team Leader, User Support Office
Susumu SHIMOURA	Professor, Center for Nuclear Study, University of Tokyo
Hidetoshi YAMAGUCHI	Lecturer, Center for Nuclear Study, University of Tokyo
Hiroari MIYATAKE	Professor, KEK

Public Relations Committee

Upon request of RNC Director, Public Relations Committee deliberates and coordinates following matters.
(1) Construction of the public relation system of the overall RNC,
(2) Prioritization of the public relation activities of the overall RNC,
(3) Other basic matters and important matters concerning the public relations of the overall RNC.

Members

Akihiko UEDA	Chair, Senior Manager; Director, Head of Accelerator Research Promotion Section (-Mar. 2014)
Hiroyoshi SAKURAI	Deputy Director, RNC; Chief Scientist, Director of Radioactive Isotope Physics Laboratory
Tetsuo HATSUDA	Deputy Director, RNC; Chief Scientist, Director of Quantum Hadron Physics Laboratory
Tohru MOTOBAYASHI	RIBF synergetic-use coordinator
Walter F. HENNING	Senior Advisor
Yasushige YANO	Senior Advisor
Masahiko IWASAKI	Chief Scientist, Director of Advanced Meson Science Laboratory
Tomohiro UESAKA	Chief Scientist, Director of Spin isospin Laboratory
Hideki UENO	Chief Scientist, Director of Nuclear Spectroscopy Laboratory; Deputy Group Direcotr, User Liaison and Industrial Cooperation Group
Toru TAMAGAWA	Associate Chief Scientist, Director of High Energy Astrophysics Laboratory
Takashi NAKATSUKASA	Associate Chief Scientist, Director of Theoretical Nuclear Physics Laboratory
Emiko HIYAMA	Associate Chief Scientist, Director of Strangeness Nuclear Physics Laboratory
Koji HASHIMOTO	Associate Chief Scientist, Director of Mathematical Physics Laboratory
Kosuke MORITA	Group Director, Research Group for Superheavy Element; Team Leader, Superheavy Element Production Team

Osamu KAMIGAITO	Group Director, Accelerator Group
Hideyuki SAKAI	Group Director, User Liaison and Industrial Cooperation Group

RBRC Management Steering Committee (MSC)

RBRC MSC is set up according to Memorandum of Understanding Between RIKEN and BNL concerning the collaboration on the Spin Physics Program at the Relativistic Heavy Ion Collider (RHIC).

Members

Maki KAWAI	Executive Director, RIKEN
Shoji NAGAMIYA	Science Advisor, RIKEN
Hideto EN'YO	Director, RNC
Peter BOND	Senior Advisor, BNL
David LISSAUER	Deputy Chair, Physics Department, BNL
Satoshi OZAKI	Senior Advisor, BNL

Nishina Center Advisory Council

The charge to NCAC is set by the Terms of Reference presented by the Director of the RIKEN and the RNC Director on the fundamental issues about research activities and research administration. NCAC submits its report to the President of RIKEN, and to the Director of Nishina Center if necessary. The members of NCAC are recommended by the Director of Nishina Center to the President of RIKEN from among highly knowledgeable individuals and experts worldwide. NCAC has two sub-councils for the RBRC and the RAL Muon Facility respectively.

Members

Robert TRIBBLE	Chair Deputy Director for Science and Technology, BNL, USA
Juha ÄYSTÖ	Director of Helsinki Institute of Physics, Finland
Angela BRACCO	Prof., Department of Physics, the University of Milan, Italy
Ken'ichi IMAI	Prof., Emeritus (Kyoto Univ.), Group Leader, Research Group for Hadron Physics, Advanced Science Research Center, JAEA
Marek LEWITOWICZ	Deputy Director, Grand Accélérateur National d'Ions Lourds, France
Lia MERMINGA	Head, Accelerator Division, TRIUMF, Canada
Witold NAZAREWICZ	Prof., Department of Physics and Astronomy, the University of Tennessee, USA
Susumu SHIMOURA	Prof., Center for Nuclear Study (CNS), University of Tokyo
Matthias SCHÄDEL	Group Leader, Research Group for Superheavy Elements, Advanced Science Research Center, JAEA. (Visiting Scientist, GSI, Germany)
GuoQing XIAO	Director, Institute of Modern Physics, Chinese Academy of Sciences, Chaina
Akira YAMAMOTO	Head, Linear Collider Project Office, Department of Advanced Accelerator Technologies, KEK
Wolfram WEISE	Director, European Center for Theoretical studies in Nuclear Physic and Related Areas, Italy
Masaki FUKUSHIMA	Prof., Institute for Cosmic Ray Research, University of Tokyo
Jun SUGIYAMA	Principal Research Scientist, Toyota Central R&D Labs., INC
Richard MILNER	Prof., Director, Laboratory for Nuclear Science, MIT, USA
Hirokazu TAMURA	Prof., Department of Physics, Graduate School of Science, Tohoku University
Muhsin N. HARAKEH	Prof., Emeritus, KVI (Kernfysisch Versneller Instituut), University of Groningen, Netherlands
Jean-Michel POUTISSOU	Senior research scientist Emeritus, TRIUMF, Canada
Andrew TAYLOR	Executive Director, STFC National Laboratories, UK

RBRC Scientific Review Committee (SRC)

Members

Richard MILNER	Chair Prof., Director, Laboratory for Nuclear Science, MIT, USA
Shinya AOKI	Prof. Yukawa Institute for Theoretical Physics, Kyoto University
Ken'ich IMAI	Group Leader, Research Group for Hadron Physics, Advanced Science Research Center, JAEA Prof. emeritus, Kyoto University
Tetsuo MATSUI	Prof. Department of Basic Science, Graduate School of Arts and Sciences, Komaba, University of Tokyo
Alfred MUELLER	Prof. Department of Physics, Columbia University, USA
Peter Braun-MUNZINGER	Prof. Dr. GSI Helmholtzzentrum für Schwerionenforschung, Germany
Charles PRESCOTT	Prof. Stanford Linear Accelerator Center, USA
Akira UKAWA	Prof. Graduate School of Pure and Applied Science, University of Tsukuba

Advisory Committee for the RIKEN-RAL Muon Facility

Members

Andrew TAYLOR	Chair Executive Director, STFC National Laboratories, UK
Jean-Michel POUTISSOU	Senior research scientist Emeritus, TRIUMF, Canada
Klaus P. JUNGMANN	Prof. University of Groningen, Netherlands
Roberto De RENZI	Prof. Department of Physics and Earth Sciences, University of Parma, Italy
Yasuyuki MATSUDA	Asso. Prof. Graduate School of Arts and Sciences, the University of Tokyo
Jun SUGIYAMA	Principal Research Scientist, Toyota Central R&D Labs., INC

5. International Collaboration

Country	Partner Institute	Objects	RNC contact person
Belgium	Katholieke Universiteit te Leuven	Framework	Michiharu Wada, Team Leader, SLOWRI Team
Bulgaria	the Institute for Nuclear Research and Nuclear Energy (INRNE)	Framework	Hedeki Ueno, Chief Scientist, Nuclear Spectroscopy Laboratory
Canada	TRIUMF	Accelerator-based Science	Hiroyoshi Sakurai, Deputy Director, Chief Scientist, Radioactive Isotope Physics Laboratory
China	China Nuclear Physics Society	The creation of the council for China -Japan research collabortion on nuclear physics	Hiroyoshi Sakurai, Deputy Director, Chief Scientist, Radioactive Isotope Physics Laboratory
	Peking University	Nuclear Science	Hiroyoshi Sakurai, Deputy Director, Chief Scientist, Radioactive Isotope Physics Laboratory
	Peking University	Strategic cooperation (Nishina School)	Hiroyoshi Sakurai, Deputy Director, Chief Scientist, Radioactive Isotope Physics Laboratory
	Shanghai Jiao Tong University	International Joint Graduate School Program	Takashi Nakatsukasa, Associate chief scientist, Theoretical Nuclear Physics Laboratory
	ZHEJIANG University	International Joint Graduate School Program	Isao Watanabe, Advanced Meson Science Laboratoy
	Institute of Modern Physics	Physics of heavy ions	Hiroyoshi Sakurai, Deputy Director, Chief Scientist, Radioactive Isotope Physics Laboratory
	School of Nuclear Science and Technology, Lanzhou University	Framework	Yue MA, Advanced Meson Science Laboratory
	School of Physics, Nanjing University	Framework	Emiko Hiyama, Associate chief scientist, Strangeness Nuclear Physics Laboratory
EU	European Gamma-Ray Spectroscopy Pool Owners Committee	The use of Euroball ditector at RIKEN	Shunji Nishimura, Radioactive Isotope Physics Laboratory
	European Center for Theoretical Studies in Nuclear Physics and Related Areas (ECT*)	Theoretical physics	Tetsuo Hatsuda, Deputy Director, Chief Scientist, Quantum Hadron Physics Laboratory
	CERN	RD-51:R&D programme for micro-pattern gas detectors (MPGD)	Satoshi Yokkaichi, Senior Research Scientist, Radiation Laboratory
Finland	University of Jyvaskyla	Basic nuclear physics and related instrumentation	Michiharu Wada, Team Leader, SLOWRI Team
France	GANIL	The creation of an associated international laboratory (LIA)	Tohru Motobayashi, RIBF synergetic-use coordinator
	DSM/IRFU, GANIL, IN2P3/IPNO	The preparation and realization for the MUST2 campaign of experiments at RIKEN	Hiroyoshi Sakurai, Deputy Director, Chief Scientist, Radioactive Isotope Physics Laboratory

Country	Partner Institute	Objects	RNC contact person
France	Natioanl Institute of Nuclear Physics and Particle Physics (IN2P3)	Physics of heavy ions	Tohru Motobayashi, RIBF synergetic-use coordinator
	SIMEM Graduate School, Department of Physics,Caen University	Framework	Tomohiro Uesaka, Chief Scientist, Spin Isospin Laboratory
	CEA-DSM	The use of MINOS device at RIKEN	Tomohiro Uesaka, Chief Scientist, Spin Isospin Laboratory
Germany	Technische Universität München	Nuclear physucs, hadron physics, nuclear astrophysics	Emiko Hiyama, Associate chief scientist, Strangeness Nuclear Physics Laboratory
	Max-Planck Gesellschaft	Comprehensive agreement	Hiroyoshi Sakurai, Deputy Director, Chief Scientist, Radioactive Isotope Physics Laboratory
	GSI	Physics of heavey ions and accelerator	Hiroyoshi Sakurai, Deputy Director, Chief Scientist, Radioactive Isotope Physics Laboratory
Hungary	the Institute of Nuclear Reseach of the Hungarian Academy of Sciences (ATOMKI)	Nuclear physics, Atomic Physics	Tomohiro Uesaka, Chief Scientist, Spin Isospin Laboratory
Italy	Natinal Institute of Nuclear Physics (INFN)	Physics of heavy ions	Tohru Motobayashi, RIBF synergetic-use coordinator
	Applied Physics Division, National Institute for New Technologies, Energy and Environment (ENEA)	Research program with the Radiation Laboratory	Tohru Motobayashi, RIBF synergetic-use coordinator
Indonesia	ITB, UNPAD, ITS, UGM	Material science using muons at the RIKEN-RAL muon facility	Isao Watanabe, Advanced Meson Science Laboratoy
	UNPAD	International Joint Graduate School Program	Isao Watanabe, Advanced Meson Science Laboratoy
	ITB	International Joint Graduate School Program	Isao Watanabe, Advanced Meson Science Laboratoy
Korea	Seoul National University	Nishina School	Hiroyoshi Sakurai, Deputy Director, Chief Scientist, Radioactive Isotope Physics Laboratory
	Seoul National University	International Joint Graduate School Program	Itaru Nakagawa, Radiation Laboratory
	Institute of Basic Science, Rare Isotope Science Project	Rare ion accelerator and related fields	Hiroyoshi Sakurai, Shunji Nishimura
	College of Natural Sciences of Kyungpook National University	International Joint Graduate School Program	Tomohiro Uesaka, Chief Scientist, Spin Isospin Laboratory
	Department of Physics, Kyungpook National University	Framework	Tomohiro Uesaka, Chief Scientist, Spin Isospin Laboratory
	College of Science, Yonsei University	Spin physics and High energy heavy ion physics	Yasuyuki Akiba, Radiation Laboratory
	Department of Physics, Yonsei University	International Joint Graduate School Program	Yasuyuki Akiba, Radiation Laboratory
	Department of Physics, Korea University	High energy physics, heavy ion physics	Yuji Goto, Radiation Laboratory
Malaysia	Universiti Sains Malaysia	Muon Science	Isao Watanabe, Advanced Meson Science Laboratoy
Poland	the Henryk Niewodniczanski Institute of Nuclear Physics, Polish Academy of Sciences(IFJ PAN)	Nuclear physics and related subjects	Hiroyoshi Sakurai, Deputy Director, Chief Scientist, Radioactive Isotope Physics Laboratory
Romania	"Horia Hulubei" National Institute of Physics and Nuclear Engineering Bucharest-Magurele, Romania	Nuclear physics and related subjects	Tomohiro Uesaka, Chief Scientist, Spin Isospin Laboratory
Russia	Joint Institute for Nuclear Research (JINR)	Framework of scientific and technical cooperarion	Tomohiro Uesaka, Chief Scientist, Spin Isospin Laboratory
	Russion Research Center "Kurchatov Institute"	Nuclear physics, Atomic Physics	Hiroyoshi Sakurai, Tomohiro Uesaka, Osamu Kamigaito, Masanori Wakasugi

Country	Partner Institute	Objects	RNC contact person
Switzerland	Paul Scherrer Institute	Improve the performance and reliability of accelerator systems	Osamu Kamigaito, Group Director, Chief Scientist, Accelerator Group
UK	The Science and Technology Facilities Council	Muon science using the ISIS Facility at the Rutherford Appleton Laboratory	Director of RIKEN-RAL muon facility
	University of Liverpool	International Joint Graduate School Program	Hiroyoshi Sakurai, Deputy Director, Chief Scientist, Radioactive Isotope Physics Laboratory
USA	BNL	The Spin Physics Program at the Relativistic Heavy Ion Collider(RHIC)	Director of RNC
	Columbia University	The development of QCDCQ	Taku Izubuchi, Group Leader, Computing Group, RBRC
	Michigan State University	Comprehensive	Tomohiro Uesaka, Chief Scientist, Spin Isospin Laboratory
		TPC(Time Projection Chamber)	Hiroyoshi Sakurai Deputy Director, Chief Scientist, Radioactive Isotope Physics Laboratory & Tadaaki ISOBE, Radioactive Isotope Physics Laboratory
Vietnam	Vietnam Atomic Evergy Commission	Nuclear Science	Tohru Motobayashi, RIBF synergetic-use coordinator
	Institute for Nuclear Sciences and Technique	Nuclear Physics	Hiroyoshi Sakurai, Deputy Director, Chief Scientist, Radioactive Isotope Physics Laboratory
	Hanoi University of Science	International Joint Graduate School Program	Hiroyoshi Sakurai, Deputy Director, Chief Scientist, Radioactive Isotope Physics Laboratory
	Institute of Physics, Vietnam Academy of Science and Technology	Academic exhange	Hiroyoshi Sakurai, Deputy Director, Chief Scientist, Radioactive Isotope Physics Laboratory

Theoretical Research Division
Quantum Hadron Physics Laboratory

1. Abstract

Atomic nuclei are made of protons and neutrons bound by the exchange of Yukawa's pion and other mesons. Also, protons and neutrons are made of quarks bound by the exchange of gluons. These strong interactions are governed by the non-Abelian gauge theory called the quantum chromodynamics (QCD). On the basis of theoretical and numerical analyses of QCD, we study the interactions between the nucleons, properties of the dense quark matter realized at the center of neutron stars, and properties of the hot quark-gluon plasma realized in the early Universe. Strong correlations common in QCD and cold atoms are also studied theoretically to unravel the universal features of the strongly interacting many-body systems. Developing perturbative and non-perturbative techniques in quantum field theory and string theory are of great importance not only to solve gauge theories such as QED and QCD, but also to find the theories beyond the standard model of elementary particles. Various theoretical approaches along this line have been attempted.

2. Major Research Subjects

(1) Nucleon structure and nuclear force from QCD
(2) Theory of spontaneous symmetry breaking
(3) QCD under extreme conditions
(4) Non-perturbative study of supersymmetric quantum field theories and string theories
(5) QED calculation of the lepton anomalous magnetic moments
(6) Physics of particles with resonant interactions

3. Summary of Research Activity

(1) Nucleon structure and nuclear force from QCD

(1-1) Nucleon structure from lattice QCD

The structure of nucleon is a crucial quantity to understand the low energy behaviors of QCD, and to detect the possible sign of physics beyond the standard model. In particular, the precise values of scalar matrix elements are required for the dark matter search experiments, and we performed the lattice QCD calculation for strangeness and charmness scalar matrix elements using chiral fermions. The so-called "spin crisis" is one of the most challenging issues in nucleon structure. Its lattice QCD study is also challenging since the computation of the disconnected insertions and glue matrix elements are required. We developed a novel method to calculate these components and performed the first complete lattice calculation for the nucleon spin.

(1-2) Lattice nuclear force

While the nuclear force serves as the cornerstone in nuclear physics, theoretical understanding of them from the underlying theory, QCD, has not been established yet. Our HAL QCD Collaboration has been developing the lattice QCD method to determine the nuclear forces. The method has been successfully applied to various hadron-hadron interactions including the hyperon forces. The physical origin of the repulsive core was revealed as the quark Pauli blocking effect. The equation of state based on lattice nuclear forces was studied and the saturation of nuclear matter was observed for the first time. Of particular interest is the determination of the three-nucleon forces from lattice QCD. Facing the challenge of the enormous computational cost for this study, we developed a novel algorithm which reduces the cost by a factor of 192. The lattice QCD results indicate that repulsive three-nucleon forces exist at short distance.

(2) Theory of spontaneous symmetry breaking

The general counting rule for Nambu-Goldstone (NG) modes is derived using Mori's projection operator method in non-Lorentz invariant systems at zero and finite temperatures. We classified NG modes into two types: One is the same type (Type-I or A) as that in relativistic systems. The other is type-II or B NG mode that is characterized by the expectation value of $[Q_a, Q_b]$, where Q_a and Q_b are broken charges. The motion of the type-II NG mode is precessional, while that of type-I NG mode is harmonic. The total number of Nambu-Goldstone modes is equal to the number of broken charges minus half the rank of the expectation value of $[Q_a, Q_b]$.

(3) QCD under extreme conditions

(3-1) QCD under strong magnetic field

We discussed the fate of chiral symmetry in an extremely strong magnetic field B, taking into account not only quark fluctuations but also neutral meson effects. The former would enhance the chiral-symmetry breaking at finite B according to the Magnetic Catalysis, while the latter would suppress the chiral condensate once B exceeds the scale of the hadron structure. Using a chiral model we demonstrate how neutral mesons are subject to the dimensional reduction and the low dimensionality favors the chiral-symmetric phase. We pointed out that this effect, the Magnetic Inhibition, can be a feasible explanation for recent lattice QCD data indicating the decreasing behavior of the chiral-restoration temperature with increasing B. We also discussed the behavior of vector-meson mass and the possibility of its condensation in a strong magnetic field. Several hadronic models show that the mass of the charged vector meson degreases as the magnetic field increases, and at some critical magnetic field, the charged vector meson condenses. We, however, showed, by using the Vafa-Witten theorem, that the vector meson condensation does not happen in QCD. We also performed the numerical analysis for the meson mass and condensation in lattice QCD. The lattice QCD data confirmed no charged vector meson condensation in a magnetic field.

(3-2) Relativistic hydrodynamics

We studied relativistic hydrodynamics in the linear regime, based on Mori's projection operator method. In relativistic hydrodynamics, it is considered that an ambiguity about the fluid velocity occurs from a choice of a local rest frame: the Landau and Eckart frames. We derived hydrodynamic equations in the both frames by the projection operator method. We found that the difference of the frames was not the choice of the local rest frame, but rather that of dynamic variables in the linear regime.

(4) Non-perturbative study of supersymmetric quantum field theories and string theories

(4-1) Lattice formulation of the N=2 supersymmetric Landau-Ginzburg model and numerical simulation

Noting the fact that a simple momentum cutoff applied to an off-shell supersymmetric multiplet does not break supersymmetry (SUSY), we constructed a lattice formulation of the two-dimensional N=2 supersymmetric Wess-Zumino (WZ) model that preserves manifest SUSY. Although the locality is broken with this lattice formulation, one can argue that the locality is restored in the continuum limit because of the preserved SUSY. Using this formulation, we further carried out a numerical simulation of a massless WZ model with a cubic superpotential, which is believed to become an N=2 superconformal field theory in the infrared limit. We measured a scaling dimension and the central charge in the infrared limit and obtained values consistent with the theoretical conjecture.

(4-2) Theoretical basis for a lattice formulation of the four-dimensional N=1 supersymmetric Yang-Mills (SYM) theory

Since there is no lattice formulation of the four-dimensional N=1 SYM theory that can preserve manifest SUSY, it is important to understand how SUSY is restored in the continuum limit. In a precise theoretical treatment, this issue should be addressed in terms of the Ward-Takahashi (WT) relation associated with SUSY. We pointed out there was a flaw in past treatments of the WT relation and provided a proper analysis of the WT relation by using a generalized BRS transformation that treats the chiral symmetry, SUSY and the translational invariance in a unified way. Since the lattice regularization breaks the infinitesimal translation, it is not straightforward to construct the EMT, a Noether correct associated with the translational invariance. We pointed out that in lattice formulations of the four-dimensional N=1 SYM theory, there is a natural method to define an EMT in view of the Ferrara-Zumino supermultiplet, a supermultiplet that contains the supercurrent and the EMT. In the continuum limit, because of the restored SUSY, the EMT also restores the conservation law.

(4-3) Lattice EMT using the Yang Mills gradient flow

Although the EMT is a fundamentally important object in quantum field theory, its construction in lattice field theory is not straightforward because there the translational invariance is explicitly broken. The difficultly of the problem comes from the fact that a composite operator generally contains the ultraviolet (UV) divergence and its definition inevitably depends on the UV regularization adopted. Here, noticing the UV finiteness of composite operators defined through the so-called Yang-Mills gradient flow, we construct a formula for the EMT in the lattice formulation of the pure Yang-Mills theory. The formula reproduces a correctly-normalized conserved EMT in the continuum limit.

(4-4) Matrix model for a type-IIA superstring and the non-perturbative SUSY breaking

We studied analytically and numerically a matrix model that is supposed to provide a non-perturbative definition of a type IIA superstring in a two-dimensional spacetime. We found that the spacetime SUSY in the system, although it does not contain the translations, is spontaneously broken as a result of a non-perturbative dynamics. This is the first example in which one can concretely address a non-perturbative spontaneous breaking of the spacetime SUSY in superstring theory.

(4-5) Novel quantum effects on non-perturbative dynamics of string theory

While perturbative aspects of string theories are well understood by the worldsheet calculations applying powerful techniques of conformal field theories, non-perturbative dynamics are difficult to comprehend. An exception would be the non-critical string in less-than one-dimension, which can be formulated non-perturbatively with matrix models. Therefore, studies of matrix models are potentially important to the understanding non-perturbative dynamics of string theory, in this regard. To represent the dynamics of non-critical string, the potential of the corresponding matrix model is tuned so that it exhibits the second-order critical point. Thus, the matrix model which composes discretized strings becomes continuous smooth string theory. It is found, however, with a certain type of the potential, a matrix model can manifest the first order transition. This phenomenon is due to the quantum effect known as the resonant tunneling. This effect has not been considered in the studies of matrix models so far. Incorporating these kinds of quantum effects into the study of matrix models may reveal novel dynamics of string theory.

(4-6) Investigations of string duality through worldsheet dynamics

String duality is a powerful concept that has been leading us to better understandings of the non-perturbative aspects of string theory. One type of duality is particularly of interest, namely open-closed duality. Open string corresponds to gauge theories while closed one shows gravity. Thus, open-closed duality suggests relation between gauge theories and the theory of gravity. This relation could be behind another duality, AdS/CFT correspondence. The difference between open string and closed string is, from the view point of the world sheet of string theory, nothing but the difference of the boundary condition of the worldsheet field theory. Since the difference is predetermined by the boundary condition, investigating directly the relation between open and closed string is a difficult task. Recently, it is found that certain quantum systems exhibit the change from the closed-boundary vacuums to open-boundary ones through the spatial modulation of the couplings. This procedure is called Sine-Square Deformation (SSD). Since open string may become closed one through SSD, it is interesting to investigate SSD in the context of string theory. We found a divergence in the worldsheet metric and also degenerated vacua other than the ordinary sl(2,C) invariant vacuum.

(5) QED higher-order calculation of lepton anomalous magnetic moments

The electron and muon anomalous magnetic moments (g-2) were precisely measured at Harvard and at Brookheaven, respectively. Comparing the measurements to the theoretical predictions of g-2, we are able to test the standard model of elementary particles in rigorous ways and find a possible window to new physics. To carry out such tests the tenth-order contribution of the perturbation theory of Quantum Electrodynamics (QED), which consists of 12,671 Feynman diagrams, must be known. About ten years ago we started the project calculating all QED contributions of the tenth order by numerical means. With help of the code-generator developed by ourselves, we made all computer programs necessary to determine the tenth-order g-2. In 2012 we have finally obtained the preliminary values of the tenth-order g-2 for both electron and muon and announced them publicly. Improvement of numerical evaluation has also been attempted to meet the precision proposed by the on-going new experiments of both electron and muon g-2's.

(6) Physics of particles with resonant interactions

(6-1) Universal physics of particles with resonant interactions

We investigated the universal physics that arises in presence of resonant interactions, in particular the Efimov effect for three particles which can bind them into a trimer. Efimov trimers are characterised by a parameter called the three-body parameter. Performing calculations using realistic helium-4 atomic interactions, we have shown that helium-4 atoms follows the van der Waals universality of the Efimov three-body parameter previously observed in ultracold atom experiments. This universality has then been explained by the universality of the atomic pair correlation, using pair models and separable potentials. It has been generalized to other short-range interactions, such as interactions in nuclear physics and condensed matter, making predictions for the trimer energies in these systems. It was also investigated the case of mass-imbalanced three-body systems where one particle is significantly lighter than the other two. Depending on the mass ratio and scattering length, the three-body system can form universal trimers determined solely by the scattering length, or Efimov trimers determined by the three-body parameter. Using numerical calculations, we have mapped out the crossover between these two limits.

(6-2) Coherent photoassociation of a Bose-Einstein condensate

Photoassociation is the process of binding a pair of atoms by shining light onto it. It usually results in incoherent losses, but some years ago we predicted the conditions for the observation of coherent oscillations when a Bose-Einstein condensate of atoms is photoassociated. This prediction has been successfully observed by experimentalists at Rice University with whom we have collaborated to analyze the experimental data.

Head

Tetsuo HATSUDA (Chief Scientist)

Members

Tsukasa TADA (Vice Chief Scientist) (Apr. 1, 2013 -)
Hiroshi SUZUKI (Senior Research Scientist) (- Aug. 31, 2013)
Takumi DOI (Research Scientist)
Yoshimasa HIDAKA (Research Scientist)
Pascal Raphaël Gabriel NAIDON (Research Scientist)

Nishina Center Research Scientist

Makiko NIO

Special Postdoctoral Researchers

Daisuke KADOH (- Mar. 31, 2013)
Arata YAMAMOTO (- Mar. 31, 2014)
Kanabu NAWA
Yuji SAKAI
Akihiko MONNAI (Apr. 1, 2013 – Jul., 2013)
Kazuhiko KAMIKADO (Apr. 1, 2013 -)
Takashi SANO (Apr. 1, 2013 -)

Foreign Postdoctoral Researchers

Michael Gordon ENDRES (- Sep. 14, 2013)
Gergely Peter FEJOES

Postdoctoral Researchers

Yoichi IKEDA
Taichi KAWANAI (Apr. 1, 2013 -)
Shinsuke YOSHIDA (Apr. 1, 2013 -)
Daisuke SATO (Apr. 1, 2013 -)
Koich HATTORI (Feb. 1, 2014 -)

Visiting Scientists

Motoi TACHINBANA (Faculty of Science and Engineering, Saga University)
Toichiro KINOSHITA (Physics Department, Cornell University)
Sinya AOKI (Yukawa Institute for Theoretical Physics, Kyoto University)
Taichi KAWANAI (Graduate School of Science, University of Tokyo) - Mar. 31, 2013
Masahito UEDA (Graduate School of Science, University of Tokyo)
Tatsuyuki TAKATSUKA (Faculty of Humanities and Social Science, Iwate University)
Hong MAO (Hangzhou Normal University, China)
Sho OZAKI (Yonsei University, Korea)
Takashi OKA (Graduate School of Science, University of Tokyo)
Shoichi SASAKI (Graduate School of Science, Tohoku University)
Keitaro NAGATA (IPNS, KEK)
Takashi INOUE (College of Bioresource Science, Nihon University)
Yoshitaka HATTA (Yukawa Institute for Theoretical Physics, Kyoto University)
Teiji KUNIHIRO (Graduate School of Science, Kyoto University)
Kenji MORITA (Yukawa Institute for Theoretical Physics, Kyoto University)
Kazuyuki KANAYA (Graduate School of Pure and Applied Science University of Tsukuba)

Makoto TAKIZAWA (Showa Pharmaceutical University)
Sachiko TAKEUCHI (Faculty of Social Welfare, Japan College of Social Work)
Yuji HIRONO (Graduate School of Science, University of Tokyo)
Hiroshi TOKI (RCNP, Osaka University) Apr. 1, 2013 -
Masashi HAYAKAWA (Graduate School of Science, Nagoya University)
Kenji SASAKI (Center for Computational Sciences, University of Tsukuba)
Takayuki MATSUKI (Department of Environmental Science and Education, Tokyo Kasei University)
Daisuke KADOH (IPNS, KEK) - Apr. 30, 2013
Hiroshi SUZUKI (Faculty of Sciences, Kyushu University) Sep. 1, 2013 -

Visiting Researcher
Takashi SANO (Japan Society for the Promotion of Science) - Mar. 31, 2013

Research Consultant
Hiroshi TOKI (RCNP, Osaka University) - Mar. 31, 2013

Junior Research Associate
Masaru HONGO (Graduate School of Science, University of Tokyo) Apr. 1, 2013 -

Short-term Program for International Program Associate
Robert Friedrich LANG (Department of Physics, Technical University of Munich) Oct. 7, 2013 – Feb. 12, 2014

Student Trainees
Bruno CHARRON (Graduate School of Science, University of Tokyo)
Akihiko MONNAI (Graduate School of Science, University of Tokyo) - Mar. 31, 2013
Yasufumi ARAKI (Graduate School of Science, University of Tokyo)
Yusuke HAMA (Graduate School of Science, University of Tokyo)
Tomoya HAYATA (Graduate School of Science, University of Tokyo)
Yasuki TACHIBANA (Graduate School of Science, University of Tokyo)
Koichi MURASE (Graduate School of Science, University of Tokyo)
Kota MASUDA (Graduate School of Science, University of Tokyo)
Masaru HONGO (Graduate School of Science, University of Tokyo) - Mar. 31, 2013
Yuya TANIZAKI (Graduate School of Science, University of Tokyo)
Ryuichi KURITA (Graduate School of Science, University of Tokyo)
Sho KAMATA (Graduate School of Science, Rikkyo University)
Masanori YAMADA (Graduate School of Pure and Applied Science, University of Tsukuba)
Koichiro HIRANUMA (Graduate School of Science & Engineering, Tokyo Institute of Technology)
Simpei ENDO (Graduate School of Science, University of Tokyo)

Assistants
Yoko FUJITA
Yuri TSUBURAI

Theoretical Research Division
Theoretical Nuclear Physics Laboratory

1. Abstract

Nuclei are finite many-particle systems composed of protons and neutrons. They are self-bound in femto-scale (10^{-15}m) by the strong interaction (nuclear force) whose study was pioneered by Hideki Yukawa. Uncommon properties of the nuclear force (repulsive core, spin-isospin dependence, tensor force, etc.) prevent complete microscopic studies of nuclear structure. There exist number of unsolved problems even at present. In addition, radioactive beam facilities reveal novel aspects of unstable nuclei. We are tackling these old problems and new issues in theoretical nuclear physics, developing new models and pursuing large-scale calculations of quantum many-body systems. We are also strongly involved in research on other quantum many-body systems, to resolve mysteries in the quantum physics.

2. Major Research Subjects

(1) Nuclear structure and quantum reaction theories
(2) First-principle calculations with the density functional theory for many Fermion systems
(3) Computational nuclear physics

3. Summary of Research Activity

(1) Energy-density-functional calculation including proton-neutron mixing

We have performed mean-field calculation based on the Skryme energy density functional (EDF) including arbitrary mixing between protons and neutrons. Isobaric analogue states (IASs) were calculated using the isocraking method. Through the calculations for IASs in A=14 and 40-56 isobars, we demonstrated that our model is capable of qualitative description of the excited IASs. The T=1 IAS in the A=14 exhibits asymmetry between the relative energy of the T_z=1 state and that of the T_z=-1 states measured from the T_z=0 state, which may be related to charge asymmetry and independence of the NN interaction. To investigate this point, we also started a systematic calculation of the T = 1 triplets in the A=10-58 region. We also performed a benchmark calculation by comparing the results obtained with our 3D EDF solver and those obtained with an axial EDF solver.

(2) Finite amplitude method in covariant density functional theory

The ^{22}C nucleus is currently of significant interest, since its halo structure with extremely weak binding was suggested by experiments. We have performed the Glauber analysis on this nucleus based on the density distribution calculated with the Skyrme energy density functional. To reproduce the large experimental cross section, we need to readjust the t_0 parameter of the Skyrme functional. It is desirable to have new experimental data on the reaction cross section with higher bombarding energy which should be available in current RIBF. In addition, we calculated the electric dipole modes of excitation with the RPA using the finite amplitude method (FAM). The computer code was previously developed, however, we need a very large space to treat such a weakly bound nucleus. The calculation with the 3D coordinate space of radius of 100 fm has been carried out, thanks to available high performance computing systems. It suggests that a very strong low-energy peak does not consist only of weakly bound s-wave neutrons, but also of sizable amount of d-wave components.

(3) Reaction cross section and electric dipole excitations in ^{22}C

The ^{22}C nucleus is currently of significant interest, since its halo structure with extremely weak binding was suggested by experiments. We have performed the Glauber analysis on this nucleus based on the density distribution calculated with the Skyrme energy density functional. To reproduce the large experimental cross section, we need to readjust the t_0 parameter of the Skyrme functional. It is desirable to have new experimental data on the reaction cross section with higher bombarding energy which should be available in current RIBF. In addition, we calculated the electric dipole modes of excitation with the RPA using the finite amplitude method (FAM). The computer code was previously developed, however, we need a very large space to treat such a weakly bound nucleus. The calculation with the 3D coordinate space of radius of 100 fm has been carried out, thanks to available high performance computing systems. It suggests that a very strong low-energy peak does not consist only of weakly bound s-wave neutrons, but also of sizable amount of d-wave components.

(4) Systematic study on pygmy dipole strength in heavy isotopes

We have systematically studied the low-lying electric dipole mode, so-called the pygmy dipole resonances (PDR) in neutron-rich isotopes in a region of nuclei with N<90, using the linear response calculation with the Skyrme energy density functional. The strong neutron shell effects have been found, which suggest several magic numbers for the enhancement of the PDR strength. We also investigate the deformation effect on the PDR. The K=0 component of E1 strength become dominant in Sr and Zr isotopes with prolate deformation. However, it is not associated with the orientation dependence of the neutron skin thickness. In fact, it is opposite, namely, the neutron skin thickness along the symmetry axis si smaller than that in the perpendicular directions. The close examination of the PDR strength in nuclei beyond N=82 indicates different characters for the peaks at E > 5 MeV and those at E < 5 MeV. The low-energy dipole states appearing at very low energies (E < 5 MeV) indicates no hindrance of the E1 strength from the pure single-particle strength. This suggests that these PDR peaks are completely decoupled from the giant dipole resonance (GDR).

(5) Deformed nuclei in the black-sphere approximation

In order to study the value of the density derivative L of the symmetry energy of nearly symmetric nuclear matter, the total reaction cross section, σ_R, of neutron-rich nuclei is one of the most important observables. We focus on the reactions involving the isotopes of Ne and Mg using the black-sphere approximation of nuclei. In this region of nuclei, we have to face the nuclear deformation. We change the black sphere into a spheroid of the same volume in order to take into account nuclear deformation before the discussion of L dependence. The values of the deformation parameter, β, are taken from microscopic nuclear structure models. Before drawing conclusion, we have to check the interaction dependence by adopting SkM*, SLy4, KTUY etc. The study is now in progress.

(6) Giant dipole resonance in ^{88}Mo at finite temperature and angular momentum

The line shapes of giant dipole resonance (GDR) in the decay of the compound nucleus 88Mo, which is formed after the fusion-evaporation reaction 48Ti + 40Ca at various excitation energies E* from 58 to 308 MeV, are generated by averaging the GDR strength functions predicted within the phonon damping model (PDM) using the empirical probabilities for temperature and angular momentum. The average strength functions are compared with the PDM strength functions calculated at the mean temperature and mean angular momentum, which are obtained by averaging the values of temperature and angular momentum using the same temperature and angular-momentum probability distributions, respectively. It is seen that these two ways of generating the GDR linear line shape yield very similar results. It is also shown that the GDR width approaches a saturation at angular momentum $J \geq 50\hbar$ at T= 4 MeV and at $J \geq 70\hbar$ at any T.

The evolution of the GDR width and shape at finite temperature T and angular momentum J is described within the the PDM. The PDM description is compared with the established experimental systematics obtained from heavy-ion fusion and inelastic scattering of light particles on heavy target nuclei, as well as with predictions by other theoretical approaches. Extended to include the effect of angular momentum J, its strength functions have been averaged over the probability distributions of T and J for the heavy-ion fusion-evaporation reaction, which forms the compound nucleus ^{88}Mo at high T and J. The results of theoretical predictions are found in excellent agreement with the experimental data. The predictions by PDM and the heavy-ion fusion data are also employed to predict the viscosity of hot medium and heavy nuclei.

(7) Study of pygmy dipole resonance with the exact treatment of the pairing

The strength functions of giant dipole resonance (GDR) in oxygen $^{18-24}$O, calcium $^{50-60}$Ca, and tin $^{120-130}$Sn isotopes are calculated within the phonon damping model under three approximations: without superfluid pairing, including BCS pairing, and exact pairing gaps. The analysis of the numerical results shows that exact pairing decreases the two-neutron separation energy in light nuclei, but increases it in heavy nuclei as compared to that obtained within the BCS theory. In neutron-rich medium and heavy nuclei, exact pairing significantly enhances the strength located at the low-energy tail of the GDR, which is usually associated with the pygmy dipole resonance (PDR). The line shape of the GDR changes significantly with increasing the neutron number within an isotopic chain if the model parameter is kept fixed at the value determined for the stable isotope.

(8) Microscopic analysis of fusion hindrance in heavy systems

We study the reaction mechanism of fusion reactions and analyze origins of fusion hindrance in heavy systems with microscopic time-dependent Hartree-Fock (TDHF) theory. We have developed a method to directly extract nucleus-nucleus potential and energy dissipation from the relative motion of colliding nuclei to nuclear intrinsic excitations in fusion reactions from TDHF trajectories. We show that the Coulomb barrier disappears in potentials obtained in heavy systems and they monotonically increase as relative distance decreases, which are different from those of light, medium-mass systems. Further analysis shows that main origin of fusion hindrance is a dynamical change of extracted potential at short relative distance.

(9) Nuclear β-decay half-lives and r-process matter flow

Nucleosynthesis via rapid neutron capture, i.e., the r-process, is a major mechanism for producing the elements heavier than Fe in Universe. Understanding this process requires knowledge of properties such as masses, β-decay half-lives, and neutron-capture cross sections for a large number of extremely neutron-rich nuclei far from the stability line. In order to reliably predict the β-decay half-lives of thousands of unknown nuclei relevant to the r-process, the full self-consistency of the quasi-particle RPA (QRPA) approach is essential. Meanwhile, the proton-neutron pairing correlations in both isovector (T = 1) and isoscalar (T = 0) channels must be taken into account properly. In a very recent work, we established a fully self-consistent charge-exchange QRPA with both T = 1 and T = 0 proton-neutron pairing, based on the relativistic Hartree-Fock-Bogoliubov (RHFB) framework. Then, we systematically investigated the β-decay half-lives of neutron-rich even-even nuclei with $20 \leq Z \leq 50$. It is shown that the available data are well reproduced, where the isospin-dependent T = 0 proton-neutron pairing is one of the most important ingredients. With the calculated β-decay half-lives, a classical r-process calculation has been performed with neutron density n_n = 1022-1024 cm^{-3} and temperature T = 1.5×109 K, and a remarkable speeding up of r-matter flow is predicted. This leads to enhanced r-process abundances of elements with $A \geq 140$, an important result for understanding the origin of heavy elements in Universe.

(10) Pseudospin symmetry in nuclear single-particle spectra

In nuclear single-particle spectra, pairs of single-particle states with quantum numbers (n-1, l+2, j=l+3/2) and (n, l, j=l+1/2) are always found to be quasi-degenerate. Arima et al. and Hecht et al. introduced in 1969 the so-called pseudospin symmetry (PSS) to explain this phenomenon. Although it has been already more than 40 years since the suggestion of PSS in atomic nuclei and comprehensive efforts have been made, the origin of PSS is still a puzzle. Recently, we suggested that it is promising to understand PSS and its breaking mechanism in a fully quantitative way by combining the similarity renormalization group technique, supersymmetric (SUSY) quantum mechanics, and perturbation theory. We took the Schrödinger equation as an example, which corresponds to the lowest-order approximation in transforming a Dirac equation into a diagonal form by using the similarity renormalization group. It is shown that while the spin symmetry-conserving term appears in nuclear single-particle Hamiltonian, the PSS-conserving term appears naturally in its SUSY partner Hamiltonian. The eigenstates of these two Hamiltonians are exactly identical except for the so-called intruder states, which have no pseudospin partners. In such a way, the origin of PSS deeply hidden in the original Hamiltonian can be traced in its SUSY partner.

Head

Takashi NAKATSUKASA (Associate Chief Scientist)

Member

Akihisa KOHAMA (Senior Research Scientist)

Nishina Center Research Scientist

Nguyen Dinh DANG

Special Postdoctoral Researchers

Koichi SATO
Kohei WASHIYAMA

Foreign Postdoctoral Researcher

Haozhao LIANG (Jan. 1, 2014 -)

Research Consultants

Akitsu IKEDA (- Mar. 31, 2014)
Kenichi MATSUYANAGI (- Mar. 31, 2014)

Visiting Researcher

Haozhao LIANG (JSPS) (- Dec. 31, 2013)

Visiting Scientists

Takashi ABE (Univ. of Tokyo)
Wataru HORIUCHI (Hokkaido Univ.) - Mar. 31, 2013
Kei IIDA (Kochi Univ.)
Kiyomi IKEDA (Niigata Univ.)
Naoyuki ITAGAKI (Kyoto Univ.)
Kaori KAKI (Shizuoka Univ.)
Lu GUO (Univ. of Chinese Academy) - Mar. 31, 2013
Nguyen Quang HUNG (Tan Tao Univ.) Aug., 2013 – Sep., 2013, Feb. 1, 2014 -
Kazuyuki OGATA (Osaka Univ.)
Kazuhiro OYAMATSU (Aichi Shukutoku Univ.)
Yasuyuki SUZUKI (Niigata Univ.)
Kazuko TANABE (Otsuma Women's Univ.)
Yasutaka TANIGUCHI (Univ. of TSUKUBA) - Mar. 31, 2013

Assistants

Keiko SUZUKI
Noriko KIYAMA (- Aug. 31, 2013)
Mitsue YAMAMOTO (Sep. 1, 2013 -)

Theoretical Research Division
Strangeness nuclear physics Laboratory

1. Abstract

We proposed accurate calculation method called 'Gaussian Expansion Method using infinitesimally shifted Gaussian lobe basis function'. When one proceeds to four-body systems, calculation of the Hamiltonian matrix elements becomes much laborious. In order to make the four-body calculation tractable even for complicated interactions, the infinitesimally-shifted Gaussian lobe basis function has been proposed. The GEM with the technique of infinitesimally-shifted Gaussians has been applied to various three-, four- and five-body calculations in hypernuclei, the four-nucleon systems, and cold-atom systems. As results, we succeeded in extracting new understandings in various fields.

2. Major Research Subjects

(1) Hypernuclear structure from the view point of few-body problem
(2) Structure of exotic hadron system
(3) Baryon-baryon interaction based on lattice QCD
(4) Structure of three- and four-body ^{4}He atom systems

3. Summary of Research Activity

(1) By a addition of Λ particle to neutron-rich Λ hypernuclei, we found that states of the $^{7}_{\Lambda}$He and $^{6}_{\Lambda}$H became more stable. Especially, in $^{7}_{\Lambda}$He, our prediction for the ground state is not inconsistent with the observed data within the error bar. The calculated result in $^{6}_{\Lambda}$H did not find any bound state, which is inconsistent with the observed data. To understand the observed data for $^{6}_{\Lambda}$H, theoretically it is requested to calculate reaction cross section of ^{6}Li(π^+,K^+) $^{6}_{\Lambda}$H.

(2) As one of nuclear response by addition of Λ particle, we found that Λ-separation energy was dependent on the degree of deformation of core nuclei. Especially, energy gain by the Λ-particle addition in super-deformed state is much smaller than that in normal-deformed state in $^{10}_{\Lambda}$Be and $^{41}_{\Lambda}$Ca.

(3) By solving ^{4}He trimer and tetramer systems accurately, we succeeded in exploring their level structure and a universality between those atomic systems and few-nucleon systems. Furthermore, we succeeded in explaining some fundamental results of the cold atom experiments using alikali atoms (Li, K, Rb, Cs) on account of the universality between ^{4}He atoms and the alkali atoms.

Head
Emiko HIYAMA (Associate Chief Scientist)

Researcher (appointment across AICS)
Hiroya SUNO

Contract Researcher
Yasuro FUNAKI

Foreign Postdoctoral Researcher
Philipp Gubler

Special Postdoctoral Researcher
Masahiro ISAKA (Apr. 1, 2013 -)

Postdoctoral Researchers
Kenji FUKUKAWA (- 2013/10)
Naoyuki SAKUMICHI (JSPS) (Apr. 1, 2013 -)

Visiting Scientists
Takayuki MYO (Osaka Institute of Technology)
Taiichi YAMADA (Kanto Gakuin University)
Tetsuo HYODO (YITP, Kyoto University)
Makoto OKA (Tokyo Institute of Technology)
Tomokazu FUKUDA (Osaka Electro-Communication University)
Daisuke JIDO (Tokyo Metropolitan University)
Hidekatsu NEMURA (University of Tsukuba)
Soichi ISHIKAWA (Hosei University)
Takenori FURUMOTO (Ichinoseki National College of Technology) -Mar. 31,2014
Atsushi HOSAKA (RCNP, Osaka University)
Shoji SHINMURA (Gifu University)
Akinobu DOTE (High Energy Accelerator Research Organization, KEK)
Thomas RIJKEN (Radboud University Nijmegen)
Kazuma NAKAZAWA (Gifu University)

Atsushi UMEYA (Nihon Institute of technology)
Toru SATO (Osaka University)
Satoru HIRENZAKI (Nara Women's University)
Masayuki ASAKAWA (Osaka University)
Masakiyo KITAZAWA (Osaka Univeristy)
Wolfram WEISE (Technical University of Munich)
Keiko MURANO (YITP, Kyoto University)
Jinjiu HU (Peking University)
Yoshikazu FUJIWARA (Kyoto University) -Mar. 31,2014
Shuichi GOJUKI (SGI Japan Ltd.)

Research Consultants
Yasuo YAMAMOTO
Toshio MOTOBA

Short-term Program for International Program Associate
Bo ZHOU (Nanjng University) (Jan. 11, 2013 – May 31, 2013)

Junior Research Associate
Shota Ohnishi (Grad. Sch. Sci. & Eng., Tokyo Institute of Technology)

Student Trainees
Akira YOKOTA (Grad. Sch. Sci. & Eng., Tokyo Institute of Technology)
Saori MAEDA (Grad. Sch. Sci. & Eng., Tokyo Institute of Technology)
Tetsuya YOSHIDA (Grad. Sch. Sci. & Eng., Tokyo Institute of Technology)
Yongwoo CHOI (Kyungpook National University)
Hana GIL (Kyungpook National University)

Assistants
Yoko FUJITA
Yuri TSUBURAI

Theoretical Research Division
Mathematical Physics Laboratory

1. Abstract

The aim of mathematical physics laboratory is to apply mathematical scheme to resolve long-standing issues in various subjects of physics. Mathematics, in particular that originates in superstring theory, has universal feature which is common to wide range of physics. This covers elementary particle physics, hadron physics, nuclear physics, cosmology, general relativity and condensed matter physics. We apply mathematical scheme such as superstring theory, D-branes, AdS/CFT correspondence, solitons, statistical mechanics and integrable systems. Topics which the laboratory covers currently include non-perturbative analysis of quantum chromo-dynamics, superstrings, and models beyond the standard model of particle physics, and soliton physics.

2. Major Research Subjects

(1) Application of Superstring Theory
(2) Non-perturbative analyses of strongly-coupled gauge theories
(3) Physics of Black Holes and Cosmology
(4) Solitons physics
(5) Mathematical physics
(6) Lattice gauge theory

3. Summary of Research Activity

Interplay between mathematics and physics is indispensable, as any physics law is described in terms of mathematics. However, the present status of various theoretical physics does not fully appreciate the usefulness of mathematics, as each topics goes into details and has less interaction with other subjects even nearby. We integrate various subjects of physics, by applying recent development of mathematics and mathematical physics, to solve long-standing issues in physics. In particular, mathematical methods in superstring theory has been developed and is mature enough to be applied to other physics. We put efforts on the application as described below, in addition to some other mathematical techniques such as numerical simulations, solitons and integrable systems.

(1) Application of superstring theory

1) AdS/CFT correspondence and nuclear physics

The renowned AdS/CFT correspondence, which was initiated in superstring theory, is a useful and powerful tool for analyzing strongly-coupled gauge theories. This has been applied to QCD, the dynamics of quarks. We studied how this powerful tool can have an impact on nuclear physics. We computed an effective action of multi-baryon systems, which should serve as a basic quantum action for nuclear physics. This turned out to reproduce nicely nuclear forces and baryon spectrum. In addition, three-body nuclear force was computed.

2) Vacuum Instability in Electric Fields via AdS/CFT: Euler-Heisenberg Lagrangian and Planckian Thermalization

We analyze vacuum instability of strongly coupled gauge theories in a constant electric field using AdS/CFT correspondence. The model is the N=2 1-flavor supersymmetric large N_c QCD in the strong 't Hooft coupling limit. We calculate the Euler-Heisenberg effective Lagrangian L(E), which encodes the nonlinear response and the quantum decay rate of the vacuum in a background electric field E, from the complex D-brane action in AdS/CFT. We find that the decay rate given by Im L(E) becomes nonzero above a critical electric field set by the confining force between quarks. A large-E expansion of Im L(E) is found to coincide with that of the Schwinger effects in QED, replacing its electron mass by the confining force. Then, the time-dependent response of the system in a strong electric field is solved non-perturbatively, and we observe a universal thermalization at a shortest timescale "Planckian thermalization time" t ~ 1/T ~ E^{-1/2}. Here, T is an effective temperature which quarks feel in the nonequilibrium state with nonzero electric current, calculated in AdS/CFT as a Hawking temperature. Stronger electric fields accelerate the thermalization, and for a realistic value of the electric field in RHIC experiment, we obtain t ~ 1 [fm/c], which is consistent with the believed value.

(2) Cosmology

1) Primordial spectra from sudden turning trajectory

Effects of heavy fields on primordial spectra of curvature perturbations are discussed in inflationary models with a sudden turning trajectory. When heavy fields are excited after the sudden turn and oscillate around the bottom of the potential, the following two effects are generically induced: deformation of the inflationary background spacetime and conversion interactions between adiabatic and isocurvature perturbations, both of which can affect the primordial density perturbations. In this paper, we calculate primordial spectra in inflationary models with sudden turning potentials taking into account both of the two effects appropriately. We find that there are some non-trivial correlations between the two effects in the power spectrum and, as a consequence, the primordial scalar power spectrum has a peak around the scale exiting the horizon at the turn. Though both effects can induce parametric resonance amplifications, they are shown to be canceled out for the case with the canonical kinetic terms. The peak feature and the scale dependence of bispectra are also discussed.

2) A Parallel World in the Dark

The baryon-dark matter coincidence is a long-standing issue. Interestingly, the recent observations suggest the presence of dark radiation, which, if confirmed, would pose another coincidence problem of why the density of dark radiation is comparable to that of photons. These striking coincidences may be traced back to the dark sector with particle contents and interactions that are quite similar, if not identical, to the standard model: a dark parallel world. It naturally solves the coincidence problems of dark matter and dark radiation, and predicts a sterile neutrino(s) with mass of (0.1−1)eV, as well as self-interacting dark matter made of the counterpart of ordinary baryons. We find a robust prediction for the relation between the abundance of dark radiation and the sterile neutrino, which can serve as the smoking-gun evidence of the dark parallel world.

(3) Lattice gauge theory

1) Phase structure of 2-dimensional topological insulators by lattice strong coupling expansion

The phase structure of 2-dimensional topological insulators under a sufficiently strong electron-electron interaction is investigated. The effective theory is constructed by extending the idea of the Kane-Mele model on the graphenelike honeycomb lattice, in terms of U(1) lattice gauge theory (quantum electrodynamics, QED). We analyze the phase structure by the techniques of strong coupling expansion of lattice gauge theory. As a result, we find that the topological phase structure of the system is modified by the electron-electron interaction. There evolves a new phase with the antiferromagnetism not parallel to the direction pointed by the spin-orbit coupling, in between the conventional and the topological insulator phases. We also discuss the physical implication of the new phase structure found here, in analogy to the parity-broken phase in lattice quantum chromodynamics (QCD), known as "Aoki phase".

(4) Mathematical physics

1) Non-Lagrangian Theories from Brane Junctions

In this article we use 5-brane junctions to study the 5D T_N SCFTs corresponding to the 5D N=1 uplift of the 4D N=2 strongly coupled gauge theories, which are obtained by compactifying N M5 branes on a sphere with three full punctures. Even though these theories have no Lagrangian description, by using the 5-brane junctions proposed by Benini, Benvenuti and Tachikawa, we are able to derive their Seiberg-Witten curves and Nekrasov partition functions. We cross-check our results with the 5D superconformal index proposed by Kim, Kim and Lee. Through the AGTW correspondence, we discuss the relations between 5D superconformal indices and n-point functions of the q-deformed W_N Toda theories.

2) SUSY breaking by nonperturbative dynamics in a matrix model for 2D type IIA superstrings

We explicitly compute nonperturbative effects in a supersymmetric double-well matrix model corresponding to two-dimensional type IIA superstring theory on a nontrivial Ramond-Ramond background. We analytically determine the full one-instanton contribution to the free energy and one-point function, including all perturbative fluctuations around the one-instanton background. The leading order two-instanton contribution is determined as well. We see that supersymmetry is spontaneously broken by instantons, and that the breaking persists after taking a double scaling limit which realizes the type IIA theory from the matrix model. The result implies that spontaneous supersymmetry breaking occurs by nonperturbative dynamics in the target space of the IIA theory. Furthermore, we numerically determine the full nonperturbative effects by recursive evaluation of orthogonal polynomials. The free energy of the matrix model appears well-defined and finite even in the strongly coupled limit of the corresponding type IIA theory. The result might suggest a weakly coupled theory appearing as an S-dual to the two-dimensional type IIA superstring theory.

3) Conditionally valid uncertainty relations

It is shown that the well-defined unbiased measurement or disturbance of a dynamical variable is not maintained for the precise measurement of the conjugate variable, independently of uncertainty relations. The conditionally valid uncertainty relations on the basis of those additional assumptions, which include most of the familiar Heisenberg-type relations, thus become singular for the precise measurement. We clarify some contradicting conclusions in the literature concerning those conditionally valid uncertainty relations: The failure of a naive Heisenberg-type error-disturbance relation and the modified Arthurs-Kelly relation in the recent spin measurement is attributed to this singular behavior. The naive Heisenberg-type error-disturbance relation is formally preserved in quantum estimation theory, which is shown to be based on the strict unbiased measurement and disturbance, but it leads to unbounded disturbance for bounded operators such as spin variables. In contrast, the Heisenberg-type error-error uncertainty relation and the Arthurs-Kelly relation, as conditionally valid uncertainty relations, are consistently maintained.

4) W_3 irregular states and isolated N=2 superconformal field theories

We explore the proposal that the six-dimensional (2,0) theory on the Riemann surface with irregular punctures leads to a four-dimensional gauge theory coupled to the isolated N=2 superconformal theories of Argyres-Douglas type, and to two-dimensional conformal field theory with irregular states. Following the approach of Gaiotto-Teschner for the Virasoro case, we construct W_3 irregular states by colliding a single SU(3) puncture with several regular punctures of simple type. If n simple punctures are colliding with the SU(3) puncture, the resulting irregular state is a simultaneous eigenvector of the positive modes L_n, ..., L_{2n} and W_{2n}, ..., W_{3n} of the W_3 algebra. We find the corresponding isolated SCFT with an SU(3) flavor symmetry as a nontrivial IR fixed point on the Coulomb branch of the SU(3) linear quiver gauge theories, by confirming that its Seiberg-Witten curve correctly predicts the conditions for the W_3 irregular states. We also compare these SCFT's with the ones obtained from the BPS quiver method.

5) A Landscape in Boundary String Field Theory: New Class of Solutions with Massive State Condensation

We solve the equation of motion of boundary string field theory allowing generic boundary operators quadratic in X, and explore string theory non-perturbative vacua with massive state condensation. Using numerical analysis, a large number of new solutions are found. Their energies turn out to distribute densely in the range between the D-brane tension and the energy of the tachyon vacuum. We discuss an interpretation of these solutions as perturbative closed string states. From the cosmological point of view, the distribution of the energies can be regarded as the so-called landscape of string theory, as we have a vast number of non-perturbative string theory solutions including one with small vacuum energy.

Head
Koji HASHIMOTO (Associate Chief Scientist)

Special Postdoctoral Researchers
Toshifumi NOUMI
Masato TAKI
Shingo TORII

Postdoctoral Researchers
Johannes SCHMUDE (-Sep. 30,2013)
Taro KIMURA (JSPS)
Yuki MINAMI

Senior Visiting Scientist
Koichi YAZAKI

Visiting Scientists
Tatsumi AOYAMA (Nagoya Univ.)
Minoru ETO (Yamagata Univ.) Aug. 1,2013 -
Kazuo FUJIKAWA (Univ. of Tokyo)
Masanori HANADA(KEK)
Masashi HAYAKAWA (Nagoya Univ.) - Mar. 31, 2013
Tetsutaro HIGAKI(KEK) Jan. 1, 2014 -
Keiji IGI(Univ. of Tokyo)
Hideaki IIDA (Kyoto Univ.) - Mar. 31, 2013
Norihiro IIZUKA (CERN) - Mar. 31, 2013
Nobuyuki ISHIBASHI (Univ. of Tsukuba)
Hiroshi ITOYAMA (Osaka City Univ.)
Yu MAEZAWA(Universiät Bielefeld)
Shoichi MIDORIKAWA (Aomori Univ.)
Muneto NITTA (Keio Univ.) - Mar. 31, 2013
Noriaki OGAWA(KIAS) - Mar. 31, 2013
Kazutoshi OHTA (Meiji Gakuin Univ.)
Makoto SAKAGUCHI (Keio Univ.)
Norisuke SAKAI (Tokyo Women's Christian Univ.)
Yuuichirou SHIBUSA (Nagasaki Inst. of Applied Science)
Asato TSUCHIYA (Shizuoka Univ.)
Yoshio YAMAGUCHI (Univ. of Tokyo)
Tamiaki YONEYA (The Open Univ. of Japan) - Mar. 31, 2013

Assistants
Keiko SUZUKI
Noriko KIYAMA (- Aug. 31, 2013)
Mitsue YAMAMOTO (Sep. 1, 2013 -)

Sub Nuclear System Research Division
Radiation Laboratory

1. Abstract

Nucleons, such as protons and neutrons, are a bound state of constituent quarks glued together with gluons. The detail structure of nucleons, however, is not well understood yet. Especially the mechanism to build up the spin of proton, which is 1/2, is a major problem in physics of the strong force. The research goal of Radiation Laboratory is to solve this fundamental question using the world first polarized-proton collider, realized at RHIC in Brookhaven National Laboratory (BNL) in USA. RHIC stands for Relativistic Heavy Ion Collider, aiming also to create Quark Gluon Plasma, the state of Universe just after the Big Bang. RIKEN-BNL Research Center (RBRC) directed by N. Samios, and recently by S. Aronson carries our core team at BNL for those exciting researches using the PHENIX detector. We have found that the proton spin carried by gluons is indeed small, which is a very striking finding beyond our expectations. Recently we successfully identified W boson in the electron/positron decay channel, with which we established the method to determine how much anti-quarks carry the proton spin. Other than the activities at RHIC we are preparing new experiments at SPring-8, J-PARC and Fermilab to study the nature of hadron. We are also performing technical developments such as novel ion sources, fine-pitch silicon pixel detectors and high-performance trigger electronics. We also have developed neutron optical devices, whose know-how has been transferred to the other new research center where Neutron Beam Technology Team was newly established.

2. Major Research Subjects

(1) Spin physics with relativistic polarized-proton collisions at RHIC
(2) Study of nuclear matter at high temperature and/or at high density
(3) Technical developments on radiation detectors and accelerators

3. Summary of Research Activity

(1) Experimental study of spin structure of proton using RHIC polarized proton collider

[See also RIKEN-BNL Research Center Experimental Group for the activities at BNL]

After the establishment of small gluon polarization inside the proton, we are investigating the antiquark spin and partonic orbital motion inside the proton with polarized proton collisions at RHIC using the PHENIX detector in order to understand the last piece of the proton-spin puzzle. We have collected W-boson production data to extract flavor-separated antiquark polarizations. The data analysis is ongoing to obtain the final results of the antiquark polarization. The Drell-Yan process (quark-antiquark annihilation) with polarized proton collisions is one of the key measurements to investigate the orbital motion in the proton. We are proposing to perform such measurement by upgrading the PHENIX detector. As a pilot measurement, some of us are participating in the Fermilab SeaQuest experiment which has been collecting $\mu^+\mu^-$ pairs using a 120-GeV unpolarized proton at Fermilab. By measuring unpolarized Drell-Yan process, we can study quark spin-orbit effects which supplement what can be learned in the polarized Drell-Yan process.

(2) Experimental study of quark-gluon plasma using RHIC heavy ion collider

[See also RIKEN-BNL Research Center Experimental Group for the activities at BNL]

We have completed several key measurements in the study of quark-gluon plasma at RHIC. As the top of them, we lead the analysis of the first thermal photon measurement in heavy ion collisions. The measurement indicates that the initial temperature reached in the central Au+Au collision at 200 GeV is about 350MeV, far above the expected transition temperature Tc~170MeV, from hadronic phase to quark-gluon plasma. This work was rewarded by Nishina Memorial Prize in 2011. Using the same "virtual photon" method used in the thermal photon measurement, we measured direct photons in d+Au collisions. The results show that there is little cold nuclear effects in direct photons. This supports that the large enhancement of direct photons observed in Au+Au is indeed due to hot quark-gluon plasma formed in Au+Au collisions.

We also measured the elliptic flow strength, v2, of direct photons in Au+Au collisions. The results show surprisingly large v2, which means the source of those photons expands elliptically. This is one of the most interesting results from RHIC in the last three years. One of the JRA students of Radiation Laboratory led this important analysis. Also, the most recent measurements of high p_T π^0 suppression in Au+Au collisions show that the suppression reduces at very high pT (pT~20GeV). Analysis of heavy quark using the silicon vertex detector is ongoing. The first preliminary results from the 2011 Au+Au run and 2012 p+p run was reported in the Quark Matter 2012 conference. We are now finalizing the results for publication.

In Wako we are operating a cluster computer system specialized to analyze huge data sets taken with the PHENIX detector. It consists of 28 nodes (18 old nodes and 10 new nodes) each of which has two CPUs and 10 sets of local disk for data repository (old node: quad-core CPU, 1TB disk, new node: six-core CPU, 2TB disk). There are 264 CPU cores and 380 TB disks in total. This configuration ensures the fastest disk I/O when the jobs are assigned to the nodes where the required data sets are stored. It is also important that this scheme doesn't require an expensive RAID system and network. Through this development we have established a fast and cost-effective solution in analyzing massive data.

(3) Study of properties of mesons and exotic hadrons with domestic accelerators

Preparation of the experiment E16 at J-PARC 50-GeV PS is underway with the Grant-in-Aid for Scientific Research on Innovative Areas (MEXT). This experiment aims to perform a systematic study of the mass modification of low-mass vector mesons in nuclei to explore the chiral symmetry breaking in dense nuclear matter, namely, the mechanism proposed by Nambu to generate the major part of hadron mass.

Gas Electron Multiplier (GEM) technology is adopted for the two key detectors, GEM Tracker (GTR) and Hadron-blind Cherenkov detector (HBD). With cooperation with Japanese industries, GEM foils with a world-largest size (30cm x 30cm) are newly developed.

Through the beam tests at ELPH, J-PARC, LEPS, and RIKEN RIBF, the followings are achieved and proven; 1) required position resolution of 0.1 mm, and 2) stable operation under the hadron-background environment, typically 30 times higher rate than that expected in the J-PARC experimental area. The design parameters of the GTR and HBD were finalized and the mass-production of GTR GEM started. HBD GEM is under the final tuning to achieve the required stability, efficiency and pion-rejection power.

For the readout electronics of GEM, a preamp using the APV25 ASIC chip is developed and tested. For the digitization and the data transfer, the SRS system developed by CERN is also tested and adopted. Another preamp-ASIC for the trigger signal from GEM foils is also developed and tested. Trigger logic boards, which are developed by Belle II, are tested with the firmware customized for this experiment.

The development phase of the detector components is just finished and we are moving to the production phase. For the electronics, mass production will start in a year after some remained tests. The construction of the beam line is finally funded in KEK and started at J-PARC in 2013. It will be completed by March 2016. The spectrometer construction at the beam line is planned to start in March 2015 and the commissioning with a primary beam will be performed in early 2016.

(4) Detector development for PHENIX experiment

After 7 years of hard work, we finally completed and installed the silicon vertex tracker (VTX) into the PHENIX detector at RHIC in December 2010. VTX is a 4-layer silicon tracker to measure heavy quark (charm and bottom) production in p+p and heavy ion collisions at RHIC. The detector was funded by RIKEN and the US DOE. We and RIKEN BNL Research Center are responsible for construction and operation of the inner two pixel detectors. The VTX was successfully commissioned during the 500 GeV p+p run in the 2011 of RHIC. Subsequently, we collected 5 billion Au+Au events in the 2011 run, 11/pb of p+p data at 510 GeV, 3/pb of p+p data at 200 GeV, 110/μb of U+U data at 193 GeV, and 2.9/nb of Cu+Au at 200 GeV. We are now analyzing those datasets to study the interaction between heavy quarks and the quark-gluon plasma.

During the 2011 run, part of the pixel detector was damaged due to thermal stress on the detector. We improved the operation procedure and there is no additional damage on the detector since 2012. We repaired the damaged pixel detectors in 2012 to 2013, and this repair work has been completed. The detector was re-installed in PHENIX before the 2014 run and has been successfully re-commissioned. We will have a long (~15 weeks) of Au+Au run at 200 GeV and we expect that we have high quality data with much higher statistics than the 2011 Au+Au run.

Sea quark polarization measurement via W-boson production is one of the highlight of PHENIX spin program. In order to detect high momentum muons from W-decay, we developed the momentum-sensitive trigger system for the PHENIX forward muon arms with collaborators from KEK, Kyoto and Rikkyo University. Together with new hadron absorber, W-boson measurement was successfully carried out using the new high momentum trigger. We accumulated high-integrated luminosity of about 250pb^{-1} in Run13 and almost achieved our goal. The intensive analysis is underway towards the publication.

(5) Neutron optics

Cold or thermal neutron beam is a high-sensitivity probe to study not only the structure of condensed matter, but also fundamental physics. Recently interests arise to apply those neutrons for the internal imaging of industrial material, sometimes at the fabrication stage or sometimes after aging. RANS (RIKEN Accelerator-driven compact neutron source) has been developed at the K1 space of RIBF building, and became operational in January 2013. By bombarding protons accelerated to 7MeV onto the beryllium target, neutrons are produced in low-energy nuclear reactions, Be(p,n)B. Fast and slow neutrons are detected at the end of the beam line, 5m away from the target. The large-area neutron imaging detectors, the combination of plastic scintillators and MPPCs, have been developed for the non-destructive inspections of the large scale structures such as bridges. Initial imaging experiments were successful with thermal and cold neutrons, and also in neutron-induced prompt gamma-ray analysis. Instrumentations for the polarized-neutron imaging and pulsed-neutron imaging are under construction.

The technology for a neutron interferometer using multilayer mirrors is adopted for differential phase imaging, to see an internal structure of a bulk. We have demonstrated that an internal crack in an acrylic plate is observable.

These activities were transferred to Neutron Beam Technology Team in RIKEN Center for Advanced Photonics.

(6) Development of beam source

Under the collaboration with BNL, we are developing various techniques for a laser ion source (LIS) to provide high quality heavy-ion beams to the accelerators at present or in the future. We have demonstrated the instantaneous beam intensity of more than 70 mA with highly-charged carbon and aluminum. This is the highest-current heavy-ion beam produced by any methods. The technical developments are well accumulated and now being applied to the DIGITAL accelerator in KEK. The beam commissioning of this new system is expected in 2014 with fully-stripped carbon beam. We have also established stable operation of low charge state heavy ion beams with an extremely low emittance.

We just installed another new LIS at the most upstream of the RHIC accelerator complex in BNL. The new LIS allows rapid switching among a wide variety of beam species so that the complex can be operated with large flexibility.

At Wako, the development of a next-generation electron beam source was performed using the novel photocathode based on a super-lattice semiconductor with negative electron affinity (NEA) surface. This activity was transferred to Nagoya University.

Head
Hideto EN'YO (Chief Scientist; Director, RNC)

Members
Yasuyuki AKIBA (Vice Chief Scientist)
Yuji GOTO (Senior Research Scientist)
Itaru NAKAGAWA (Senior Research Scientist)
Yoshie OTAKE (Senior Research Scientist) (- Mar. 31, 2013)
Yasushi WATANABE (Senior Research Scientist)
Satoshi YOKKAICHI (Senior Research Scientist)
Ralf SEIDL (Senior Research Scientist)
Hiroaki ONISHI (concurrent; Senior Research Scientist)

Special Postdoctoral Researcher
Yoshichika SEKI

Contract Researchers
Takashi HACHIYA
Hisayuki TORII (May 1, 2013 – Mar. 31, 2014)

Postdoctoral Researchers
Yoki ARAMAKI (- Mar. 31, 2014)
Yoshimasa IKEDA (- Mar. 31, 2014)
Yoshimitsu IMAZU (- Jun. 30, 2013)
Daisuke KAWAMA (JSPS)
Takayuki SUMITA (May 1, 2013 -)
Tomonori TAKAHASHI (- Mar. 31, 2014)
Yuhei MORINO (May 1, 2013 -)

Senior Visiting Scientists
Toshiaki SHIBATA (Grad. Sch. of Sci. and Eng., Tokyo Inst. of Tech.)
Takashi NAKANO (RCNP, Osaka University)

Visiting Scientists
Kazuya AOKI (Inst. of Particle and Nuclear Studies, KEK) Jun. 1, 2013 -
Alexander BAZILEVSKY (BNL, USA) Jul. 15, 2013 -
Wolfgang BENTZ (Tokai Univ.)
Akitomo ENOKIZONO (Grad. Sch. of Sci., Rikkyo Univ.)
Hirotsugu FUJII (Grad. Sch./College of Arts and Sciences, Univ. of Tokyo) - Mar. 31, 2013
Yoshinori FUKAO (Inst. of Particle and Nuclear Studies, KEK)
Kenji FUKUSHIMA (Keio Univ.)
Haruhiko FUNAHASHI (Grad. Sch. of Sci., Kyoto Univ.) - Mar. 31, 2013
Taku GUNJI (CNS, Univ. of Tokyo) Jul. 1, 2013 -
Noriyosu HAYASHIZAKI (Tokyo Inst. Tech.)
Masanori HIRAI (Tokyo Univ. of Science)
Kensuke HOMMA (Grad. Sch. of Sci., Hiroshima Univ.) - Mar. 31, 2013
Ryo ICHIMIYA (KEK) Jun. 1, 2013 -
Noriyoshi ISHII (Grad. Sch. of Pure and Applied Sci., Univ. of Tsukuba)
Robert JAMESON (Goethe Universitat Frankfurt, Germany) - Mar. 31, 2013
Masashi KANETA (Tohoku Univ.) Oct. 1, 2013 -
Hirotsugu KASHIWAGI (Takasaki Advanced Radiation Res. Inst., JAEA)
Shunzo KUMANO (Inst. of Particle and Nuclear Studies, KEK)
Teiji KUNIHIRO (Grad. Sch. of Sci., Kyoto Univ.) - Mar. 31, 2013
Makoto KUWAHARA (Nagoya Univ.)
Youngil KWON (Yonsei Univ., Korea) Jul. 22, 2013 -
Yoshikazu MAEDA (RCNP, Osaka Univ.) - Mar. 31, 2013
Yajun MAO (Peking Univ., China) - Mar. 31, 2013
Tsutomu MIBE (KEK)
Yoshiyuki MIYACHI (Tokyo Inst. Tech.) - Mar. 31, 2013
Norihito MURAMATSU (RCNP, Osaka Univ.) - Mar. 31, 2013
Ryotaro MUTO (KEK)
Tomofumi NAGAE (Grad. Sch. of Sci., Kyoto Univ.) - Mar. 31, 2013
Atsushi NAKAMURA (Information Media Center, Hiroshima Univ.) May 1, 2013 -
Tomoaki NAKAMURA (ICEPP, Univ. of Tokyo) - Mar. 31, 2013
Kenichi NAKANO (Tokyo Inst. Tech.)
Megumi NARUKI (KEK) Jul. 1, 2013 -
Masayuki NIIYAMA (Grad. Sch. of Sci., Kyoto Univ.) - Mar. 31, 2013
Tomohiro NISHITANI (Nagoya University)

Munehisa OHTANI (Kyorin Univ.)
Masahiro OKAMURA (BNL, USA)
Kyoichiro OZAWA (KEK)
Petra RIEDLER (CERN, Switzerland) - Mar. 31, 2013
Naohito SAITO (J-PARC, KEK) - Mar. 31, 2013
Hiroyuki SAKO (JAEA) - Mar. 31, 2013
Murad SARSOUR (Georgia State University) - Mar. 31, 2013
Susumu SATO (JAEA)
Shin-ya SAWADA (Inst. of Particle and Nuclear Studies, KEK)
Michiko SEKIMOTO (Inst. of Particle and Nuclear Studies, KEK)
Maya SHIMOMURA (Iowa State University)
Kazutaka SUDO (Inst. of Particle and Nuclear Studies, KEK) - Mar. 31, 2013
Mizuki SUMIHAMA (RCNP, Osaka Univ.) - Mar. 31, 2013
Taneja SWADHIN (SUNY at Stony Brook) - Mar. 31, 2013
Masao TABUCHI (Nagoya Univ.) - Mar. 31, 2013
Junpei TAKANO (KEK)
Kiyoshi TANIDA (Seoul National Univ., Korea)
Feng WEI (New Mexico State Univ., USA) Jul.1, 2013 – Jul. 24, 2013
Yorito YAMAGUCHI (CNS, Univ. of Tokyo)
Satoru YAMASHITA (ICEPP, Univ. of Tokyo) - Mar. 31, 2013
Imuran YOUNUS (Univ. of New Mexico, USA) - Mar. 31, 2013

Student

Junior Research Associates

Yasuhiro FUWA (Grad. Sch. of Sci., Kyoto Univ.) Apr. 1, 2013 -
Shinichi HAYASHI (CNS, Univ. of Tokyo)
Tomoya HOSHINO (Grad. Sch. of Sci., Hiroshima Univ.) Apr. 1, 2013 -
Shunsuke Ikeda (Tokyo Inst. Tech.) Apr. 1, 2013 -
Kouki KANNO (Fac. Sci., Univ. of Tokyo) Apr. 1, 2013 -
Yuya KOMATSU (Fac. Sci. , Univ. of Tokyo)
Masafumi KUMAKI (Fac. Sci. and Eng., Waseda Univ.) Apr. 1, 2013 -
Sanshiro MIZUNO (Grad. Sch. of Pure and Applied Sci., Univ. of Tsukuba)
Hiroshi NAKAGOMI (Grad. Sch. of Pure and Applied Sci., Univ. of Tsukuba) Apr. 1, 2013 -
Wataru NAKAI (Fac. Sci., Univ. of Tokyo) Apr. 1, 2013 -
Masaya NIHASHI (Grad. Sch. of Sci., Hiroshima Univ.) - Mar. 31, 2013
Yuko SEKIGUCHI (CNS, Univ. of Tokyo) Apr. 1, 2013 -
Megumi SEKINE (Tokyo Inst. Tech.)
Takahito TODOROKI (Grad. Sch. of Pure and Applied Sci., Univ. of Tsukuba) - Mar. 31, 2013
Tomoya TSUJI (CNS, Univ. of Tokyo)
Daisuke WATANABE (Univ. of Tsukuba) Apr. 1, 2013 -
Satoshi YANO (Grad. Sch. of Sci., Hiroshima Univ.) Apr. 1, 2013 –

International Program Associates

Chong KIM (Korea Univ., Korea) Dec. 10, 2013 -
Taebong MOON (Yonsei Univ., Korea) Jul. 1, 2013 -
Sanghwa PARK (Seoul National Univ., Korea)
Inseok YOON (Seoul National Univ., Korea)

Student Trainees

Nobuaki AMANO (Grad. Sch. of Sci., Kyoto Univ.) - Mar. 31, 2013
Nerangika Sadeera BANDARA (Univ. of Massachusetts, Amherst, USA) Jul. 1, 2013 – Jul. 23, 2013
Michael BEAUMIER (Univ. of California, Riverside, USA) Jul. 8, 2013 – Aug. 4, 2013
Jeongsu BOK (New Mexico State Univ., USA) Jun. 30, 2013 – Jul. 11, 2013
Kazuya HAYASE (Tokyo Univ. of Science) - Mar. 31, 2013
Daniel JUMPER (Univ. of Illinois at Urbana Champaign, USA) Jul. 8, 2013 – Jul. 26, 2013
Sotaro KANDA (Fac. Sci., Univ. of Tokyo) - Mar. 31, 2013
Aaron KEY (Univ. of New Mexico, USA) Jul. 1, 2013 – Jul. 21, 2013
Paul KLINE (Dept. of Physics, SUNY at Stony Brook, USA) - Mar. 31, 2013
Yukiyoshi KON (RCNP, Osaka Univ.) - Mar. 31, 2013
Andrew MANION (Dept. of Physics, SUNY at Stony Brook, USA) - Mar. 31, 2013
Shinichi MASUMOTO (Fac. Sci., Univ. of Tokyo) - Mar. 31, 2013
Abraham MELES (New Mexico State Univ., USA) Jul. 1, 2013 – Jul. 20, 2013
Shou MIYASAKA (Tokyo Inst. Tech.) - Mar. 31, 2013
Pedro MONTUENGA (Univ. of Illinois at Urbana Champaign, USA) Jul. 8, 2013 – Jul. 29, 2013
Hikari MURAKAMI (Fac. Sci., Univ. of Tokyo) Nov. 1, 2013 -
Kazuya NAGASHIMA (Grad. Sch. of Sci., Hiroshima Univ.)
Shoichiro NISHIMURA (Fac. Sci., Univ. of Tokyo) - Mar. 31, 2013
Yuki OBARA (Fac. Sci., Univ. of Tokyo)

Hideyuki OIDE (Fac. Eng., Univ. of Tokyo) - Mar. 31, 2013
Yusuke OYA (Grad. Sch. of Sci., Hiroshima Univ.)
Gonaduwage PERERA (New Mexico State Univ., USA) Jul. 1, 2013 – Jul. 20, 2013
Joshua PERRY (Iowa State Univ., USA) Jul. 2, 2013 – Jul. 31, 2013
Dai SAKURAI (Grad. Sch. of Eng., Tokyo Univ. of Science) - Mar. 31, 2013
Takahiro SAWADA (RCNP, Osaka Univ.) - Mar. 31, 2013
Takuya SHIBUKAWA (Fac. Sci., Univ. of Tokyo) Apr. 1, 2013 -
Akihisa TAKAHARA (CNS, Univ. of Tokyo) - Mar. 31, 2013
Yosuke WATANABE (Fac. Sci., Univ. of Tokyo) - Mar. 31, 2013
Yuki WATANABE (Tokyo Univ. of Science) - Mar. 31, 2013
Haiwang YU (Peking Univ., China) Jul. 7, 2013 – Aug. 4, 2013

Interns
Hidemitsu ASANO (Fac. of Sci., Kyoto Univ.) - Mar. 31, 2014
Ciprian GAL (Dept. of Physics , SUNY at Stony Brook) Jun. 28, 2013 – Aug. 4, 2013
Minjung KIM (Seoul National Univ., Korea) Jul. 1, 2013 – Aug. 31, 2013
Katsuro NAKAMURA (Grad. Sch. of Sci., Kyoto Univ.) - Mar. 31, 2013
Masako YAMADA (Grad. Sch. of Sci., Kyoto Univ.) - Mar. 31, 2013
Takayuki YAMAMOTO (Waseda Univ.) - Mar. 31, 2013

Part-time Staff (Research Assistance)
Ryoji AKIMOTO (CNS, Univ. of Tokyo)
Kimiaki HASHIMOTO (Fac. of Sci., Rikkyo Univ.)
Takeru IGURI (Rikkyo Univ.)
Toru NAGASHIMA (Rikkyo Univ.)
Wataru SAITO (Rikkyo Univ.)

Assistants
Keiko SUZUKI
Noriko KIYAMA (- Aug. 31, 2013)
Mitsue YAMAMOTO (Sep. 1, 2013 -)

Sub Nuclear System Research Division
Advanced Meson Science Laboratory

1. Abstract

Particles like muons, pions, and kaons have finite life times, so they do not exist in natural nuclei or matters. By implanting these particles into nuclei/matters, exotic phenomena in various objects can be studied from new point of view.

Kaon is the second lightest meson which has strange-quark as a constituent quark. It is expected that if one embed mesons into nuclei, the sizes of the nuclei become smaller and one can form a high density object beyond the normal nuclear density. Study of this object could lead to better understanding of the origin of the mass of the matter, and may reveal the quark degree of freedom beyond the quark-confinement. The other example is the weak interaction in nuclear matter. It can only be studied by the weak decay of hypernuclei, which have Lambda particle in the nuclei.

Muon provides even wider scope of studies, covering condensed matter physics as well as nuclear and atomic physics, and we are trying to extend the application field further into chemical and biological studies. For instance, stopping positively charged muon in a material, we obtain information on the magnetic properties or the local field at the muon trapped site (μSR). Injecting negatively charged muon to hydrogen gas, muonic hydrogen atom (μp) is formed. We are planning to measure μp hyperfine splitting energy to measure proton magnetic radius, which is complementary quantity to the proton charge radius and its puzzle lately attracts strong interest. We are also interested in precision measurement of muon property itself, such as muon anomalous magnetic moment (g-2).

In our research, we introduce different kind of impurities into nuclei / matters, and study new states of matter, new phenomena, or the object properties.

2. Major Research Subjects

(1) Study of meson property and interaction in nuclei
(2) Origin of matter mass / quark degree of freedom in nuclei
(3) Condensed matter and material studies with muon
(4) Nuclear and particle physics studies via muonic hydrogen
(5) Development of ultra cold muon beam, and its application from material science to particle physics

3. Summary of Research Activity

(1) Hadron physics at J-PARC, RIKEN-RIBF, GSI and SPring-8

Kaon and pion will shed a new insight to the nuclear physics. The recent discovery of deeply bound pionic atom enables us to investigate the properties of mesons in nuclear matter. At RIKEN-RIBF, we are preparing precise experimental study of the pionic atom. We have also started next generation kaon experiments (E15 and E31) at J-PARC. In these experiments, we are aiming at precise determination of the $K^{bar}N$ interaction, and clarify the nature of kaon in nuclei and the nature of Λ(1405), which could be K^-p bound state. At Spring-8 and at GSI, we are also aiming to study ω and η' nuclei. By these experiments, we aim to be a world-leading scientific research group using these light meta-stable particles.

(1-A) Deeply bound kaonic nuclei

We have performed experimental exploration of theoretically predicted deeply bound kaonic nuclear states, such as the $\langle K^-pp \rangle$ bound state. One of the most interesting features of the kaonic nucleus is the strong attraction of the $K^{bar}N$ interaction. Because of this strong attraction, the kaon in nucleus will attract surrounding nucleons resulting in extremely high-density object, which is several times larger than normal nuclear density. Measurement of the kaon properties at such high energy density will provide precious information on the origin of hadron masses and the chiral symmetry breaking and its partial restoration.

The experiment J-PARC E15 aims to identify the nature of the $\langle K^-pp \rangle$ bound state by the in-flight $^3He(K^-, n)$ reaction, which allows us to investigate such state both in the formation via the missing-mass spectroscopy using the emitted neutron, and in its decay via the invariant-mass spectroscopy by detecting decay particles from $\langle K^-pp \rangle$. For the experiment, we constructed a dedicated spectrometer system at the secondary beam-line, K1.8BR, in the hadron hall of J-PARC.

The first physics data-taking was carried out in March and May, 2013 with 6×10^9 kaons on ^3He target, corresponding to a ~1% of the approved proposal. We successfully obtained semi-inclusive $^3He(K^-, n)$ X missing-mass spectrum, and found a tail structure just below the mass threshold of $(K^- + p + p)$ which cannot be explained by well-known processes and backgrounds. We also demonstrated an exclusive analysis by reconstructing $^3He(K^-, \Lambda p)$ n events. To derive more information on the $K^{bar}N$ interaction by the exclusive measurement, we are planning to perform the second physics-run, in which 10 times more data will be accumulated.

(1-B) Precision X-ray measurement of kaonic atom

Simultaneously with the above experiment (1), we have performed an X-ray spectroscopy of atomic $3d \rightarrow 2p$ transition of negatively charged K mesons captured by helium atoms. Many Kaonic atom x-rays are measured and most of them can be explained by theoretical calculation, however, very large deviation exist on kaonic helium (and the oxygen) which can never been explained in the present theoretical scheme. Therefore, a new and high precision data have been long awaited for. This large deviation could be due to the existence of deeply bound kaonic states in nuclei, well below the atomic levels of kaons in energy. Very recently, we performed a kaonic helium X-ray measurement. We have achieved much more precise X-ray measurement, resulting in the shift to be 2 ± 2 (stat.) ± 2 (syst.) eV, which is in good agreement with the theoretical calculation. Therefore, previous data should be replaced by the present value, and the so called "kaonic helium puzzle" has been dissolved.

Another important X-ray measurement of kaonic atom would be $2p \rightarrow 1s$ transition of kaonic deuteron. We have measured same transition of kaonic hydrogen, but the width and shift from electro-magnetic (EM) value reflect only isospin average of the $K^{bar}N$

interaction. We can resolve isospin dependence of the strong interaction by the measurement. We are presently preparing a proposal to J-PARC PAC to measure kaonic deuteron X-ray.

(1-C) Deeply bound pionic atoms and η' mesic nuclei

We have been working on precision spectroscopy of pionic atoms systematically, that leads to understanding of the origin of hadron mass. The precision data set stringent constraints on the chiral condensate at nuclear medium. We are presently conducting the precision measurement at RIBF. The first measurement is aiming at pionic tin 121 as the first step for the systematic spectroscopy. A pilot experiment was performed in 2010, and the first main experiment was performed in 2014 showing a very good performance of the system. We have been analyzing the data to improve experimental setup of the pionic atom spectroscopy at the RIBF in RIKEN. We expect to achieve better experimental resolution with much reduced systematic errors.

We are also working on spectroscopy of η' mesic nuclei in GSI/FAIR. Theoretically, peculiarly large mass of η' is attributed to UA(1) symmetry and chiral symmetry breaking. As a result, large binding energy is expected for η' meson bound states in nuclei (η'-mesic nuclei). From this measurement, we can access information about partial restoration of chiral symmetry in nuclear media via the binding energy and decay width of η'-nuclear bound state.

(1-D) Hadron physics at SPring-8/LEPS2

Photo production of meson in nuclei is known to be a powerful tool to investigate property of the hadron in nuclear media. For this study, we started a new experimental project named LEPS2 (Laser Electron Photon at SPring-8 II) in this RIKEN Mid-term. The experimental hutch for LEPS2 at SPring-8 was constructed in March 2011, lead by RIKEN. The Large solenoid spectrometer magnet (2.96 m inner diameter x 2.22 m length) was successfully transported from BNL (US) to SPring-8 and installed into LEPS2 hutch in 2011.

One of the first physics programs is photo-production of η' in nuclei. Especially (γ, p) is most important reaction channel, where we can perform missing mass spectroscopy by detecting forward going proton. One of the big advantages of photo-production reaction is that the initial reaction is expected to be much cleaner than the hadron channel.

Detector construction for the first physics program is in progress. The 4π Electro-Magnetic calorimeter has been constructed and proton counter to detect forward going proton produced via (γ,p) reaction was partially installed in November 2013. Engineering run for the first experiment was performed in December 2013 to confirm performance of our detector system. Full set of the detector will be installed by mid April 2014 and we are planning to perform first physics data taking run starting from mid April 2014 to end of July 2014.

(2) Muon science at RIKEN-RAL branch

The research area ranges over particle physics, condensed matter studies, chemistry and life science. Our core activities are based on the RIKEN-RAL Muon Facility located at the Rutherford Appleton Laboratory (UK), which provides intense pulsed-muon beam. We have variety of important research activities such as particle / nuclear physics studies with muon's spin and condensed matter physics by muon spin rotation / relaxation / resonance (μSR).

(2-A) Condensed matter/materials studies with μSR

We are going to serve new μSR spectrometer named CHRONUS to collaborative experiments from the May-June cycle in 2014. To have higher affinity on μSR studies with ISIS muon facility, common data acquisition (DAQ) system with ISIS standard DAQ (DAEIII) and front-end control system (SEKI) have been installed and optimized along with other equipment in Port-4. Installations of an experimental platform over Port-4 and a pillar crane have been completed. Thus, we can perform two independent μSR experiments in Port-2 and 4 at the same time, switching double-pulse to share beam between the two.

Among our scientific activities on μSR studies from year 2011 to 2013, following six subjects of material sciences are most important achievements at the RIKEN-RAL muon facility:

1) One-dimensional diffusive motion of spin-excited states in the spin liquid of molecular magnet, $EtMe_3Sb[Pd(dmit)_2]_2$, has been found. The data shows that this material could be the first example that realized one-dimensional resonating valence bond state.
2) A static ordering of small Ir moments in the pyrochlore iridate, $Nd_2Ir_2O_7$, was examined. We found that this system is located close to the quantum critical point.
3) A static ordering of Yb moment in pyrochlore structure of $Yb_2Ti_2O_7$ crystal has been confirmed. This ordering can be explained by the Higgs mechanism.
4) Spontaneous small static internal fields in the superconducting state of URu_2Si_2 have been measured. From the data and its crystal structure, we obtained a scenario to explain superconducting mechanism of this system.
5) The universality class of the Mott transition in $EtMe_3P[Pd(dmit)_2]_2$ has been confirmed by pressure dependences of transportation properties.
6) Muon sites in La_2CuO_4 crystal have been evaluated based on ab-initio calculation on spatial distribution of the potential energy, taking into account the Cu spin spatial distribution effect.

(2-B) Nuclear and particle physics studies via ultra cold muon beam and muonic atoms

If we can improve muon beam-emittance, beam-timing and energy dispersion (*so-called* "ultra-slow muon"), then the capability of μSR study will be drastically improved. The ultra-slow muon beam can be stopped in thin foils, multi-layered materials and artificial lattices and we can apply the μSR techniques to surface and interface science. The development of ultra-slow muon beam is also very important as the source of ultra-cold (pencil-like small emittance) muon beam for muon g-2 measurement. Therefore, we have been working on R&D study.

We had been working on the "ultra-slow muon" generation based on the following technique, namely, positive muon beam with thermal energy has been produced by laser ionization of muoniums in vacuum (bound system of μ^+ and electron) emitted from the hot tungsten surface by stopping "surface muon beam" at Port-3. However, the muon yield and obtained emittance was far from satisfactory, and remained to be far from any kind of realistic application.

Therefore, in this mid-term, we decided to start developing two key components first, namely high efficiency muonium generator at room temperature and high intensity ionization laser. The study of muonium generator has been done in collaboration with TRIUMF. Very recently, we demonstrated tremendous increase of the muonium emission efficiency by fabricating fine laser drill-holes on the surface of silica aerogel. We also developed a high power Lyman-α laser in collaboration with laser group at RIKEN. In this laser development, we succeeded to synthesize novel laser crystal Nd:YGAG, which has an ideal wave-length property for laser amplification to generate Lyman-α by four wave mixing in Kr gas cell. The developed new laser will ionize muoniums 100 times more efficiently for slow muon beam generation. In order to fully apply these new developments to slow muon generation, we are designing a new beam line based on microscope optics.

(3) Theoretical Researches

(3-A) Physics of Quantum Hall system

We have investigated the interlayer phase coherence and the Josephson currents in the bi-layer quantum Hall system based on the non-commutative geometrical approach. We have demonstrated that the Josephson in-plane current provokes anomalous behaviors in the Hall resistance in counter flow and drag experiments. Furthermore, we investigate the condition on the input current for the tunneling current to be coherent and dissipation less. Our results explain quite well the experimental report on the input current due to the von Klitzing group [Phys. Rev. Lett. 104 (2010) 116802]. We have predicted also how the condition changes when the sample is tilted in the magnetic field.

Head

Masahiko IWASAKI (Chief Scientist)

Members

Katsuhiko ISHIDA (Vice Chief Scientist)
Kenta ITAHASHI (Senior Research Scientist)
Yue MA (Research Scientist)
Hiroaki OHNISHI
Haruhiko OUTA (Senior Research Scientist)
Fuminori SAKUMA (Senior Research Scientist)
Tsukasa TADA (Vice Chief Scientist - Mar. 31, 2013)
Isao WATANABE (Senior Research Scientist)

Special Postdoctoral Researcher

Ikuto KAWASAKI

Contract Researchers

Yu OISHI
Shinji OKADA
Masaharu SATO (Apr. 1, 2013 -)

Special Temporary Employee

Teiichiro MATSUZAKI

Senior Visiting Scientist

Kazuhiro TANAKA (IPNS, KEK)

Visiting Scientists

Tadashi ADACHI (Grad. Grad. Sch. Eng., Tohoku Univ.)
Jun AKIMITSU (Coll. Sci. Eng., Aoyama Gakuin Univ.)
Kunio AWAGA (Grad. Sch. Sci., Nagoya Univ.)
Pavel BAKULE (IPS AS CR, Czech)
Ayi BAHTIAR (UNPAD, Indonesia)
George BEER (Univ. of Victoria, Canada)
HyoungChan BHANG (Seoul Natl Univ., Korea)
Graeme BLAKE (Univ. of Groningen, Netherlands)
N. Ludmila BOGDANOVA (ITEP, Russia)
Kwang Yong CHOI (Chung-Ang Univ., Korea)
Lee CHOW (UCF, USA)
Catalina CURCEANU (INFN, Italy)
Prasad Tara DAS (SUNY, USA)
Irwan DHARMAWAN (UNPAD, Indonesia)
Yasuaki EINAGA (Fac. Sci & Tech., Keio. Univ.)
Masaya ENOMOTO (Fac. Sci., Tokyo Univ. of Sci.)
Zyun Francis EZAWA (Grad. Sch. Sci., Tohoku Univ.)
Mark FAYFMAN (Kurchatov Inst., Russia)
Donald FLEMING (Univ. of British Columbia/TRIUMF)
Yutaka FUJII (Fac. Eng., Fukui Univ.)
Hiroyuki FUJIOKA (Grad. Sch. Sci., Kyoto Univ.)
Masaki FUJITA (IMR, Tohoku Univ.)

Hideto FUKAZAWA (Grad. Sch. Sci., Chiba Univ.)
Takayuki GOTO (Fac. Sci. & Tech., Sophia Univ.)
Kazuo HAYAKAWA (Fac of Sci. & Tech., Shizuoka Inst. Sci. & Tech.)
Ryugo S. HAYANO (Grad. Sch. Sci., Univ. of Tokyo)
Wataru HIGEMOTO (ASRC, JAEA)
Yuki HIGUCHI (Toyota Central R&D Labs.)
Satoru HIRENZAKI (Fac. Sci., Nara Women's Univ.)
Masahiko HIROI (Fac. Sci., Kagoshima Univ.)
Koichi ICHIMURA (Fac. of Eng., Hokkaido Univ.)
Youichi IGARASHI (IPNS, KEK)
Hiromi IINUMA (IPNS, KEK)
Masami IIO (CSC, KEK)
Susumu IKEDA (IMSS, KEK)
Yutaka IKEDO (IMSS, KEK)
Rintaro INOUE (ICR, Kyoto Univ.)
Takayuki ISHIDA (Grad. Sch. Infor. & Eng., Univ. Elect. Commu.)
Yasuyuki ISHII (Dept. Phys., Tokyo Medical Univ.) - Mar. 31. 2014
Shigeru ISHIMOTO (IPNS, KEK)
Tomoichi ISHIWATARI (SMI, Austria)
Ryosuke KADONO (IMSS, KEK)
Kazuya KAMAZAWA (Toyota Central R&D Labs.)
Toshiji KANAYA (ICR, Kyoto Univ.)
Roland KAWAKAMI (UC Riverside, USA)
Takayuki KAWAMATA (Grad. Sch. Eng., Tohoku Univ.)
Naritoshi KAWAMURA (IMSS, KEK)
Seiko KAWAMURA (J-PARC, JAEA)
Kenji KAWASHIMA (Coll. Sci. Eng., Aoyama Gakuin Univ.) - Mar. 31. 2014
Hikomitsu KIKUCHI (Grad. Sch. Eng., Univ. of Fukui)
Yasushi KINO (Fac. Sci., Tohoku Univ.)
Wataru KOBAYASHI (Grad. Sch. Pure & Applied Sci., Univ. of Tsukuba)
Yoshio KOBAYASHI (Grad. Sch. of Info. & Eng., Univ. of Elec.-Com.)
Akihiro KODA (IMSS, KEK)
Yoh KOHORI (Fac. Sci., Chiba Univ.)
Yoji KOIKE (Grad. Sch. Eng., Tohoku Univ.)
Kenji KOJIMA (IMSS, KEK)
Norimichi KOJIMA (Grad. Sch. Arts & Sci., Univ. of Tokyo)
Kenya KUBO (Grad. Sch. Sci., ICU)
Shoko KUME (Grad. Sch. Sci., Univ. of Tokyo)
Yoshitaka KUNO (Grad. Sch. Sci., Osaka Univ.)
Takuya KURAHASHI (IMS, NINS)
Haruhiko KUROE (Fac. Sci. & Tech., Sophia Univ.)
Guido LANGOUCHE (NVAO, Netherlands)
Shunsuke MAKIMURA (IMSS, KEK)
Hirotaka MANAKA (Grad. Sch. Sci. & Eng., Kagoshima Univ.)
Kenji MATSUDA (Grad. Sch. Sci. &Eng. for Edu., Univ. of Toyama)
Yasuyuki MATSUDA (Grad. Sch. Arts & Sci., Univ. of Tokyo)
Tsutomu MIBE (IPNS, KEK)
Mototsugu MIHARA (Grad. Sch. Sci., Osaka Univ.)
Yasuhiro MIYAKE (IMSS, KEK)
Jun MIYAZAKI (Fac. Sci. Div., Nihon Univ.) - Mar. 31. 2014
Soichiro MIZUSAKI (Coll. Sci. & Eng., Aoyama Gakuin Univ.)
Mohamed Ismail MOHAMED IBRAHIM (USM, Malaysia)
Kazuhiko MUKAI (Toyota Central R&D Labs.) - Mar. 31. 2014
Yujiro NAGATA (Coll. Sci. Eng., Aoyama Gakuin Univ.)
Takashi NAGATOMO (IMSS, KEK) - Dec. 31, 2013
Hiroyuki NAKAMURA (Grad. Sch. Eng., Kyoto Univ.)
Jin NAKAMURA (Grad. Sch. Infor. & Eng., Univ. Elect. Commu.)
Satoshi NAKAMURA (Grad. Sch. Sci., Tohoku Univ.)
Takashi NAKAMURA (Grad. Sch. Sci. & Eng., Tokyo Tech.)
Takayoshi NAKAMURA (RIES, Hokkaido Univ.)
Takehito NAKANO (Grad. Sch. Sci., Osaka Univ.)
Saburou NASU (Grad, Sch. Eng. & Sci., Osaka Univ.)
Kazuhiko NINOMIYA (Grad. Sch. Sci., Osaka Univ.)
Nobuhiko NISHIDA (Fac. Sci., Tokyo Tech.)
Katsuhiko NISHIMURA (Grad. Sch. Sci.&Eng. for Edu., Univ. of Toyama)
Kusuo NISHIYAMA (IMSS, KEK)
Hiroyuki NOUMI (RCNP, Osaka Univ.)
Hiroshi NOZAKI (Toyota Central R&D Labs.) - Mar. 31. 2014

Yasuo NOZUE (Grad. Sch. Sci., Osaka Univ.)
Agung NUGROHO (ITB, Indonesia)
Kazuki OHISHI (CROSS Tokai)
Yoshitaka OHKUBO (KURRI, Kyoto Univ.)
Atsushi OKAZAWA (Grad. Sch. Arts & Sci., Univ. of Tokyo)
Leonid PONOMAREV (Kurchatov Institute, Russia)
Francis PRATT (RAL, UK)
Risdiana (UNPAD, Indonesia)
Lusy SAFRIANI (UNPAD, Indonesia)
Naohito SAITO (IPNS, KEK)
Shin-ichi SAKAMOTO (J-PARC, JAEA)
Tobat SARAGI (Univ. of Kassel, Germany)
Kazuhiko SATO (Grad. Sch. Sci. & Eng., Saitama Univ.)
Masaharu SATO (Grad. Sch. Sci., Univ. of Tokyo)
Ralph SCHEICHER (Michigan Tech. Univ., USA)
Ryoichi SEKI (California State Univ., Northridge, USA)
Hexi SHI (Grad. Sch. Sci., Univ. of Tokyo) - Mar. 31. 2014
Kouichirou SHIMOMURA (IMSS, KEK)
Ichiro SHIRAKI (Grad. Sch. Medi. & Eng. Sci., Univ. of Yamanashi)
Patrick STRASSER (IMSS, KEK)
Hiroyuki SUGAI (ASRC, JAEA)
Jun SUGIYAMA (Toyota Central R&D Labs.) - Mar. 31. 2014
Shukri SULAIMAN (USM,, Malaysia)
Hiroyuki SUZUKI (AKTD, NIMS)
Ken SUZUKI (SMI, Austria)
Soh SUZUKI (CRC, KEK)
Takao SUZUKI (Shibaura Inst. of Tech.)
Takatoshi SUZUKI (Grad. Sch. Sci., Univ. of Tokyo)
Yoshikazu TABATA (Grad, Sch. Eng. & Sci., Kyoto Univ.)
Shigeru TAKAGI (Grad, Sch. Sci., Tohoku Univ.)
Kazuyuki TAKAI (Grad. Sch. Sci. & Eng., Tokyo Tech.)
Nao TAKESHITA (NeRI, AIST)
Yoichi TANABE (WPI, Tohoku Univ.)
Manobu TANAKA (IPNS, KEK)
Hiroshi TANIDA (Grad. Sch. Adv. Sci. Matter, Hiroshima Univ.)
Harry TOM (UC Riverside, USA)
Dai TOMONO (Grad. Sch. of Sci., Kyoto Univ.)
Eiko TORIKAI (Grad. Sch. Medi. & Eng. Sci., Univ. of Yamanashi)
Akihisa TOYODA (IPNS, KEK)
Kyo TSUKADA (Grad. Sch. Sci., Tohoku Univ.)
Satoshi TSUTSUI (JASRI) - Mar. 31. 2014
Masatomo UEHARA (Grad. Sch. Eng., Yokohama Natl.Univ.)
Kazuki UENO (IPNS, KEK)
Izumi UMEGAKI (Toyota Central R&D Labs.)
Helmut WEICK (GSI, Germany)
Eberhard WIDMANN (SMI, Vienna)
Zhuan XU (Zhejiang Univ. China)
Eiichi YAGI (Fac. Sci. & Eng., Waseda Univ.)
Yasuhiro YAMADA (Fac. Sci., Tokyo Univ. of Sci.)
Ichihiro YAMAUCHI (IMSS, KEK) - Mar. 31. 2014
Toshimitsu YAMAZAKI (Grad. Sch. Sci., Univ. of Tokyo)
Koji YOKOYAMA (Queen Marry Univ., UK)
Makoto YOKOYAMA (Coll. Sci., Ibaraki Univ.)
Yutaka YOSHIDA (Fac of Sci. & Tech., Shizuoka Inst. Sci. & Tech.)
Masaru YOSOI (RCNP, Osaka Univ.)
Arkady YUKHINCHUK (VNIIEF, Russia)
Johann ZMESKAL (SMI, Austria)

Visting Technicians
Yuya FUJIWARA (Grad. Sch. Sci., Univ. of Tokyo)
Shinji KAI (Tanaka Kikinzoku Kogyo K.K.)
Kazuo OOYAMA (JOHO com.)
Kunihiro SHIMA (Tanaka Kikinzoku Kogyo K.K.)

Research Consultants
Yoshinori AKAISHI
Atsuko ITO
Masayasu KAMIMURA

Hironari MIYAZAWA

Junior Research Associates

Hirotomo HAMANO (Grad. Sch. Sci., Osaka Univ.) Apr. 1, 2013 -
Sohtaro KANDA (Grad. Sch. Sci., Univ. of Tokyo) Apr. 1, 2013 – Mar. 31, 2014
Yuki NOZAWA (Grad. Sch. Sci., Kyoto Univ.)
Yuta SADA (Grad. Sch. Sci., Kyoto Univ.) - Mar. 31, 2013
Makoto TOKUDA (Grad. Sch. Sci. & Eng., Tokyo Tech.) - Mar. 31, 2013

International Program Associates

Noraina Binti ADAM (USM, Malaysia) Feb. 15, 2014 -
Budi ADIPERDANA (UNPAD, Indonesia) - Nov. 29, 2013
Hanjie GUO (Zhejiang Univ., China) - Dec. 20, 2013
Edi SUPRAYOGA (Bandung Inst. Tech., Indonesia) Apr. 1, 2013 -
Zhang QI (Lanzhou Univ., China) Feb. 3,2013 -

Student Trainees

Malik Anjelh BAQIYA (Sch. Eng., Tohoku Univ.)
Shun ENOMOTO (Grad, Sch. Sci., Osaka Univ.)
Kenji FUJIMURA (Grad. Sch. Sci. & Eng., Ibaraki Univ.)
Daisuke FURUSAWA (Grad. Sch. Eng., Kyoto Univ.)
Yoshiyuki FURUYA (Fac. Sci., Tokyo Univ. Sci.)
Hanjie GUO (Zhejiang Univ., China)
Tadashi HASHIMOTO (Grad. Sch. Sci., Univ. of Tokyo)
Fuminao HOSOMI (Fac. Sci., Univ. of Tokyo)
Suguru IGARASHI (Grad. Sch. Sci. & Eng., Aoyama Gakuin Univ.)
Takuya INABE (Grad. Sch. Eng., Tohoku Univ.)
Kentaro INOUE (Grad. Sch. Sci., Osaka Univ.)
Wataru ITO (Grad. Sch. Sci. & Eng., Aoyama Gakuin Univ.)
Richika KATO (Grad. Sch. Sci., ICU)
Shingo KAWASAKI (Grad. Sch. Sci., Osaka Univ.)
Taehyung KIM (Fac. Sci., Univ. of Toyama)
Ryo KITAMURA (Grad. Sch. Sci., Univ. of Tokyo)
Hiroaki KOBAYASHI (Grad. Sch. Arts & Sci., Univ. of Tokyo)
Sajjad MARI (IUT, Iran)
Kazuki MATSUI (Fac. Sci.& Tech., Sophia Univ.)
Go MISHIMA (Grad. Sch. Sci., Univ. of Tokyo)
Ryo MIYATANI (Fac. Sci., Tokyo Univ. o f Sci.)
Saidah Sakinah bt MOHD JAJUDIN (Univ. Saints Malaysia, Malaysia)
Yohei MURAKAMI (Grad. Sch. Sci., Univ. of Tokyo)
Daiki NATORI (Fac. Info & Eng., Univ. of Elec.-Com.)
Takahiro NISHI (Grad. Sch. Sci., Univ. of Tokyo)
Ayumi OCHIAI (Fac. Sci., Tokyo Univ. o f Sci.)
Shinji OGAWA (Fac. Sci., Univ. of Tokyo)
Kaori OTAKE (Coll. of Liberal Arts, ICU)
Anba Datt PANT (Grad. Sch. Sci. & Eng., Yamanashi Univ.)
Ainul Fauzeeha Binti ROZLAN (Univ. Saints Malaysia, Malaysia)
Yuta SADA (Grad. Sch. Sci., Kyoto Univ.)
Daisuke SAKATE (Grad. Sch. Sci. & Eng. Saitama Univ.)
Yukiko SATO (Fac. Info. & Eng., Univ. of Elec.-Com.)
He Xi SHI (Grad. Sch. Sci., Univ. of Tokyo)
Kazuma SHIGA (Fac. Sci., Tokyo Univ. of Sci.)
Ryo SHIMIZU (Fac. Sci., Tokyo Univ. of Sci.)
SUNARYONO (ITS, Indonesia)
Edi SUPRAYOGA (ITB, Indonesia)
Miho SATOU (Fac. Sci., Tokyo Univ. Sci.)
Kensuke SUZUKI (Grad. Grad. Sch. Eng., Tohoku Univ.)
Masato SUZUKI (Fac. Info. & Eng., Univ. of Elec.-Com.)
Kenichi TANABE (Fac. Sci., Tokyo Univ. Sci.)
Yoshiki TANAKA (Grad. Sch. Sci., Univ. of Tokyo)
Hiroki TAKEDA (Grad. Sch. Sci. & Eng., Aoyama Gakuin Univ.)
Ahmad TANFIQ (ITS, Indonesia)
Makoto TOKUDA (Grad. Sch. Sci. & Eng., Tokyo Inst. of Tech.)
Shotaro TANIGAWA (Fac. Info. & Eng., Univ. of Elec.-Com.)
Natsuki TOMIDA (Grad. Sch. Sci., Kyoto Univ.)
Yuni WATANABE (Grad. Sch. Sci., Univ. of Tokyo)
Takumi YAMAGA (Grad. Sch. Sci., Osaka Univ.)
Hiroyuki YAMADA (Grad. Sch. Sci., Univ. of Tokyo)

Hiroki YAMAKAMI (Grad. Sch. Sci., Kyoto Univ.)
Shingo YAMADA (Grad. Sch. Sci. & Eng., Aoyama Gakuin Univ.)
Sungwon YOON (Catholic Univ., Korea)
Xingliang XU (Grad. Sch. Sci. & Eng., Saga Univ.)
Ruidong ZHU (Fac. Sci., Univ. of Tokyo)

Part-time Workers

Toshihiko HIRAIWA (Grad. Sch. Sci., Kyoto Univ.) - Mar. 31, 2013
Yuko KATO (Grad. Sch., Tokyo Gakugei Univ.) Mar. 21, 2013 – Sep. 30, 2013
Yuta SADA (Grad. Sch. Sci., Kyoto Univ.) Apr. 1, 2013 – Mar. 31, 2014
Makoto TOKUDA (Grad. Sch. Sci. & Eng., Tokyo Inst. of Tech.) Apr. 1, 2013 -

Assistants

Yoko FUJITA
Yuri TSUBURAI

Sub Nuclear System Research Division
RIKEN-BNL Research Center

1. Abstract

The RIKEN BNL Research Center was established in April 1997 at Brookhaven National Laboratory with Professor T. D. Lee of Columbia University as its initial Director. It is funded by the Rikagaku Kenkyusho (RIKEN, The Institute of Physical and Chemical Research) of Japan. The Center is dedicated to the study of strong interactions, including spin physics, lattice QCD and RHIC physics through the nurturing of a new generation of young physicists. Professor Lee was succeed by BNL Distinguished Scientist, N. P. Samios, who served until 2013. The current director is Dr. S. H. Aronson. Support for RBRC was initially for five years and has been renewed three times, and presently extends to 2018. The Center is located in the Physics Department. The RBRC Theory Group activities are closely and intimately related to those of the Nuclear Theory, High Energy Theory, and Lattice Gauge Theory Groups at BNL. The RBRC Experimental Group works closely with the DOE RHIC Spin Group, the RIKEN Spin Group at BNL, and the PHENIX heavy ion groups. BNL provides office space, management, and administrative support. In addition, the Computer Science Center (CS) and Information Technology Division (ITD) at BNL provides support for computing, particularly the operation and technical support for the RBRC 400 Teraflop QCDCQ (QCD Chiral Quark) lattice gauge theory computer. The Deputy Director of RBRC is R. Pisarski (BNL). L. McLerran (BNL) is leader of the Theory Group. Y. Akiba (RIKEN) is Experimental Group leader with A. Deshpande (Stony Brook) deputy. T. Izubuchi (BNL) is Computing Group leader.

2. Major Research Subjects

Major research subjects of the theory group are

(1) Heavy Ion Collision
(2) Perturbative QCD
(3) Phenomenological QCD

Major research subjects of the computing group are

(1) Search for new law of physics through tests for Standard Model of particle and nuclear physics
(2) Dynamics of QCD and related theories
(3) Theoretical and algorithmic development for lattice field theories, QCD machine design

Major research subject of the experimental group are

(1) Experimental Studies of the Spin Structure of the Nucleon
(2) Study of Quark-Gluon Plasma at RHIC
(3) PHENIX detector upgrades

3. Summary of Research Activity

Summary of Research Activities of the three groups of the Center are given in the sections of each group.

Director

Samuel H. ARONSON (Ph. D)

Deputy Director

Robert PISARSKI (Ph. D)

Administrative Staff

Mituru KISHIMOTO (Administration Manager, Accelerator-based Research Promotion Section)
Kazunori MABUCHI (Deputy Administration Manager, RBRC)
Colleen MICHAEL (Secretary)
Taeko ITO (Assistant to Account Manager for Administration)

Sub Nuclear System Research Division
RIKEN-BNL Research Center
Theory Group

1. Abstract

The efforts of the RBRC theory group are concentrated on the major topics of interest in High Energy Nuclear Physics. This includes: understanding of the Quark-Gluon Plasma; the nature of dense quark matter; the initial state in high energy collisions, the Color Glass Condensate; its evolution through a Glasma; spin physics, as is relevant for polarized hadronic collisions; physics relevant to electron-hadron collisions.

Theory Group hosted many joint tenure track positions with universities in U.S. and Japan.

2. Major Research Subjects

(1) Heavy Ion Collision
(2) Perturbative QCD
(3) Phenomenological QCD

3. Summary of Research Activity

(1) Spin Physics

The experimental program at RBRC is strongly focused on determining the origin of spin in the proton and neutron. To extract the spin content of nucleon requires both precise data and precise computation. Dr. Jianwei Qiu of the Nuclear Theory group is one of the world's leading theorists in perturbative QCD, and leading the effort at BNL in spin physics. Their effort will continue to concentrate on computing perturbative QCD effects to sufficient precision that one can reliably extract information from the evolving experimental program. In addition they are developing ideas which might be tested in an electron-hadron collider, such as the one proposed to be built by adding an electron ring to RHIC.

(2) Matter at High Energy Density

The RHIC experimental heavy ion program is designed to study the properties of matter at energy densities much greater than that of atomic nuclei. This includes the initial state of nucleus-nucleus collisions, the Color Glass Condensate, the intermediate state to which it evolves, the Glasma, and lastly the thermal state to which it evolves, the Quark-Gluon Plasma. Theorists at the RBRC have made important contributions to all of these subjects.

Matter at high temperature has been studied by a variety of techniques involving both numerical and analytic methods. Much of the high precision work on numerical simulations of lattice QCD at nonzero temperature and density such matter have been done by members of the Lattice Gauge Theory Group at BNL, including Frithjof Karsch, Peter Petreczsky, Swagato Mukherjee, and postdoctoral assistants. These groups, along with collaborators at Columbia University, the University of Bielefeld, and other groups, have computed numerous properties of QCD in thermodynamic equilibrium. This includes the equation of state for physical quark masses, susceptibilies with respect to quark chemical potentials, and transport coefficients.

Phenomenological theories of the Quark-Gluon Plasma, based upon results from lattice simulations, have been developed by R. Pisarski of the Nuclear Theory Group, in collaboration with Dr. Y. Hidaka (previously of RBRC/BNL, and now a permanent member at RIKEN in Waco), Shu Lin, Daisuke Sato, and other postdoctoral research assistants at RBRC/BNL.

The theory of the Color Glass Condensate and Glasma was largely developed by RBRC scientists. This theory has been successfully applied to a wide variety of experimental results involving high energy collisions of hadrons, electrons and nuclei. There is recent data on heavy ion collisions that are naturally explained by such matter, including data on proton (or deuteron) nucleus collisions. Much of the effort here will be aimed towards excluding or verifying the Color Glass Condensate and Glasma hypothesis in RHIC and LHC experiments.

Thermal matter at high temperature and baryon density has been traditionally conjectured to be of two phases: confined and deconfined, with a direct correlation between deconfinement and the restoration of chiral symmetry. RBRC scientists have recently conjectured a third phase, of quarkyonic matter. This is baryonic matter at energy densities very high compared to the QCD scale. It has a pressure and energy density typical of quarks, yet it is confined. The name arises because it shares properties of confined baryonic matter with unconfined quark matter. This hypothesis is new and predicts new classes of phenomena that might be observed in collisions of nuclei of relatively low energy at RHIC. There are a number of first principle theoretical issues also to be understood.

Efforts on RHIC phenomenology proceed on a broad front. Recent efforts include improving hydrodynamic computations using state of the art equations of state derived from lattice gauge theory. Understanding the nature of matter at high baryon number density has generated the idea of Quarkyonic Matter, that may have implications for an upcoming low energy run at RHIC and eventual experiments in the future at FAIR and NICA. An issue being studied is the nature of mass generation and the breaking of translational invariance. A central focus of work at RBRC, the Color Glass Condensate and the Glasma, matter that controls the high energy limit of QCD, is being realized in experiments at RHIC. Much activity focuses on the relation between observations at LHC and the implications made at RHIC.

Group Leader
Larry McLERRAN

Deputy Group Leader
Robert PISARSKI (concurrent)

Members
RHIC Physics Fellows
Adrian DUMITRU (- Mar. 31, 2014)
Cecilia LUNARDINI (-Mar. 31, 2013)
Anna STASTO (-Mar. 31, 2013)
Jinfeng LIAO
Fedor BEZRUKOV
HoUng YEE

Research Associates
Adam BZDAK
Daniel PITONYAK (Sep. 3, 2013 -)
Shu LIN (RIKEN FPR)
Sergey SYRITSYN (RIKEN FPR) (Oct. 1, 2013-)

Special Postdoctoral Researchers
Koji KASHIWA (- Mar. 31, 2014)
Akihiko MONNAI (Apr. 1, 2013-)

Visiting Scientists
Taku IZUBUCHI (RBRC Computing Group)
Miklos GYULASSY
Robert L. JAFFE
Edward SHURYAK
Testufumi HIRANO
Feng YUAN

Secretarial Staff
Pamela ESPOSITO (Theory Group Secretary)

Sub Nuclear System Research Division
RIKEN-BNL Research Center
Computing Group

1. Abstract

The computing group founded in 2011 as a part of the RIKEN BNL Research Center established at Brookhaven National Laboratory in New York, USA, and dedicated to conduct researches and developments for large scale physics computations important for particle and nuclear physics. The group was forked from the RBRC Theory Group.

The main mission of the group is to provide important numerical information that is indispensable for theoretical interpretation of experimental data using the theories of particle and nuclear physics. Their primary area of research is lattice quantum chromodynamics (QCD), which describes the sub-atomic structures of hadrons, which allow us the ab-initio investigation for strongly interacting quantum field theories beyond pertrubative analysis.

The RBRC group and its collaborators have emphasized the necessity and importance of precision calculations, which will precisely check the current understandings of nature, and will have a potential to find a physics beyond the current standard model of fundamental physics. We have therefore adopted techniques that aim to control and reduce any systematic errors. This approach has yielded many reliable results.

The areas of the major activities are R&D for high performance computers, developments for computing algorithms, and researches of particle, nuclear, and lattice theories. Since the inception of RBRC, many breakthroughs and pioneering works has carried out in computational forefronts. These are the use of the domain-wall fermions, which preserve chiral symmetry, a key symmetry for understanding nature of particle nuclear physics, the three generations of QCD devoted supercomputers, pioneering works for QCD calculation for Cabibbo-Kobayashi-Maskawa theory, QCD+QED simulation for isospin breaking, novel algorithm for error reduction in general lattice calculation. Now the chiral quark simulation is performed at the physical up, down quark mass, the precision for many basic quantities reached to accuracy of sub-percent, and the group is aiming for further important and challenging calculations, such as the full and complete calaution for $K\to\pi\pi$ decay, ε'/ε, or hadronic contributions go muon's anomalous magnetic moment, or Nucleon's shape and structures.

2. Major Research Subjects

(1) Search for new law of physics through tests for Standard Model of particle and nuclear physics, especially in the framework of the Cabibbo–Kobayashi–Maskawa (CKM), hadronic contributions to the muon's anomalous magnetic moment (g-2).
(2) Dynamics of QCD and related theories, including study for the structures of nucleons
(3) Theoretical and algorithmic development for lattice field theories, QCD machine design

3. Summary of Research Activity

In 2011, QCD with Chiral Quarks (QCDCQ), a third-generation lattice QCD computer that is a pre-commercial version of IBM's Blue Gene/Q, was installed as an in-house computing resource at the RBRC. The computer was developed by collaboration among RBRC, Columbia University, the University of Edinburgh, and IBM. Two racks of QCDCQ having a peak computing power of 2 × 200 TFLOPS are in operation at the RBRC. In addition to the RBRC machine, one rack of QCDCQ is owned by BNL for wider use for scientific computing. In 2013, 1/2 rack of Blue Gene/Q is also installed by US-wide lattice QCD collaboration, USQCD. The group has also used the IBM Blue Gene supercomputers located at Argonne National Laboratory and BNL (NY Blue), and RICC, the cluster computers at RIKEN (Japan), Fermi National Accelerator Laboratory, the Jefferson Lab, and others.

Such computing power enables the group to perform precise calculations using up, down, and strange quark flavors with proper handling of the important symmetry, called chiral symmetry, that quarks have. Several projects are ongoing: flavor physics in the framework of the CKM theory for kaons and B mesons; the electromagnetic properties of hadrons; hadronic contributions to the muon's anomalous magnetic moment; the proton's and neutron's electric dipole moments; proton decay; nucleon form factors, which are related to the proton spin problem; and QCD thermodynamics in finite temperature/density systems such as those produced in heavy-ion collisions at the Relativistic Heavy Ion Collider. Major breakthroughs on important problems such as the direct CP violation process ($K \to \pi\pi$, ε'/ε) will be attempted using this computer.

The RBRC group and its collaborators have emphasized the necessity and importance of precision calculations, which will precisely check the current understandings of nature, and will have a potential to find physics beyond the current standard model of fundamental physics. We have therefore adopted techniques that aim to control and reduce any systematic errors. This approach has yielded many reliable results.

The group also delivers an algorithmic breakthrough, which speed up generic lattice gauge theory computation typically by a factor of 20 or more. In this novel technique called All Mode Averaging (AMA), the whole calculation is divided into frequent approximated calculations, and infrequent expensive and accurate calculation using lattice symmetries.

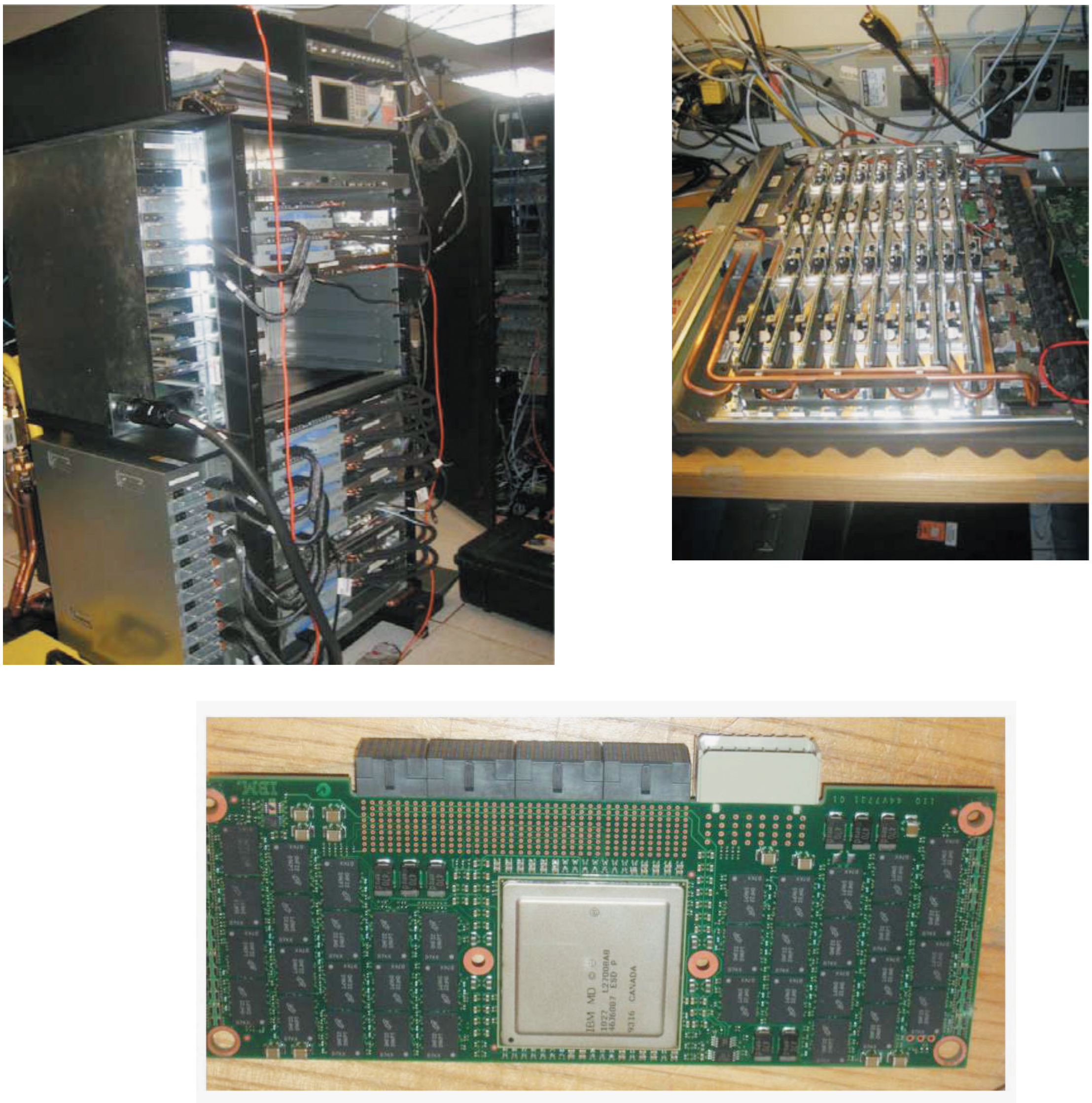

Fig. The rack, motherboard, and chips of QCDCQ

Group Leader
Taku IZUBUCHI

Members
RIKEN BNL Fellow
Tomomi ISHIKAWA (Apr. 1,2013 -)

RHIC Physics Fellow
Brian TIBURZI
Ethan NEIL (Sep. 1, 2013 -)

Research Associates
Eigo SHINTANI (- Sep. 30, 2013)
Christoph LEHNER (RIKEN FPR)
Christopher KELLY (RIKEN FPR)(Sep. 1,2013-)

Visiting Scientists
Robert MAWHINNEY (Columbia Univ., USA)
Shigemi OHTA (KEK)
Yasumichi AOKI (Nagoya Univ.) Apr. 1, 2013-
Meifeng LIN (Yale Univ.) Apr. 1,2013-
Hyung-Jin KIM (BNL)
Chulwoo JUNG (BNL)
Takeshi YAMAZAKI (Nagoya Univ.)
Thomas Blum (University of Connecticut)

Sub Nuclear System Research Division
RIKEN-BNL Research Center
Experimental Group

1. Abstract

RIKEN BNL Research Center (RBRC) Experimental Group studies the strong interactions (QCD) using RHIC accelerator at Brookhaven National Laboratory, the world first heavy ion collider and polarized p+p collider. We have three major activities: Spin Physics at RHIC, Heavy ion physics at RHIC, and detector upgrades of PHENIX experiment at RHIC. We study the spin structure of the proton using the polarized proton-proton collisions at RHIC. This program has been promoted by RIKEN's leadership. The first focus of the research is to measure the gluon spin contribution to the proton spin. Our recent data analysis has shown that the proton spin carried by the gluons is small, which is a very striking finding beyond our expectations. The aim of Heavy ion physics at RHIC is to re-create Quark Gluon Plasma (QGP), the state of Universe just after the Big Bang. Two important discoveries, jet quenching effect and strong elliptic flows, have established that new state of dense matter is indeed produced in heavy ion collisions at RHIC. We are now studying the property of the matter. Recently, we have measured direct photons in Au+Au collisions for $1<p_T<3$ GeV/c, where thermal radiation from hot QGP is expected to dominate. The comparison between the data and theory calculations indicates that the initial temperature of 300 MeV to 600 MeV is achieved. These values are well above the transition temperature to QGP, which is calculated to be approximately 170 MeV by lattice QCD calculations.

We have major roles in detector upgrades of PHENIX experiment, namely, the silicon vertex tracker (VTX) and muon trigger upgrades. Both of the upgrade is now complete. VTX detector was installed in PHENIX in 2011 and we are taking data since then. Muon trigger was complete and it was essential for $W\rightarrow\mu$ measurement in 2013.

2. Major Research Subjects

(1) Experimental Studies of the Spin Structure of the Nucleon
(2) Study of Quark-Gluon Plasma at RHIC
(3) PHENIX detector upgrades

3. Summary of Research Activity

We study the strong interactions (QCD) using the RHIC accelerator at Brookhaven National Laboratory, the world first heavy ion collider and polarized p+p collider. We have three major activities: Spin Physics at RHIC, Heavy ion physics at RHIC, and detector upgrades of PHENIX experiment.

(1) Experimental study of spin structure of proton using RHIC polarized proton collider

How is the spin of proton formed with 3 quarks and gluons? This is a very fundamental question in Quantum Chromodynamics (QCD), the theory of the strong nuclear forces. The RHIC Spin Project has been established as an international collaboration between RIKEN and Brookhaven National Laboratory (BNL) to solve this problem by colliding two polarized protons for the first time in history. This project also has extended the physics capabilities of RHIC.

The first goal of the Spin Physics program at RHIC is to determine the gluon contribution to proton spin. It is known that the spin of quark accounts for only 25% of proton spin. The remaining 75% should be carried either by the spin of gluons or the orbital angular momentum of quarks and gluons. One of the main goals of the RHIC spin program has been to determine the gluon spin contribution. Before the start of RHIC, there was little experimental constraint on the gluon polarization, ΔG.

PHENIX measures the double helicity asymmetry (A_{LL}) of π^0 production to determine the gluon polarization. Our publication from 2006 run has shown that the gluon polarization in the proton is small and only about half of proton spin can be accounted by gluon spin in the measured region of gluon momentum in proton. Figure 1 shows our most recent results of π^0 ALL measurement, which has just submitted to Physical Review D. The figure shows the combined results of RUN5, RUN6, and RUN9. The new data give even stronger constraint on the gluon spin. RBRC exp. G led the gluon spin analysis in PHENIX. K. Bolye, a fellow of RBRC experimental group has a major role in this paper.

RHIC achieved polarized p+p collisions at 500 GeV in 2009. The collision energy increased to 510 GeV in 2012 and 2013. We have recorded The main goal of these high energy p+p run is to measure anti-quark polarization via single spin asymmetry AL of the W boson production. We have published the first results on $W\rightarrow e$ measurement at mid-rapidty from 2009 dataset in 2011. We upgraded the muon trigger system to measure $W\rightarrow m$ decays in the forward direction. With the measurement of $W\rightarrow e$ and $W\rightarrow\mu$, we can cover a wide kinematic range in anti-quark polarization measurement. The 2013 run is the main spin run at 510 GeV. PHENIX has recorded more than 150/pb of data in the run. Combined with the datasets in 2009 (8.6/pb), 2011(18/pb), and 2012(~30/pb), we will have a definite measurement of anti-quark spin.

Figure 2 show the results of the AL measurement from the 510 GeV polarized proton run in 2012. This is approximately 1/5 of the data that was recorded in the 2013 run. Much improved results are expected in the combined data set. The analysis of the data is in progress.

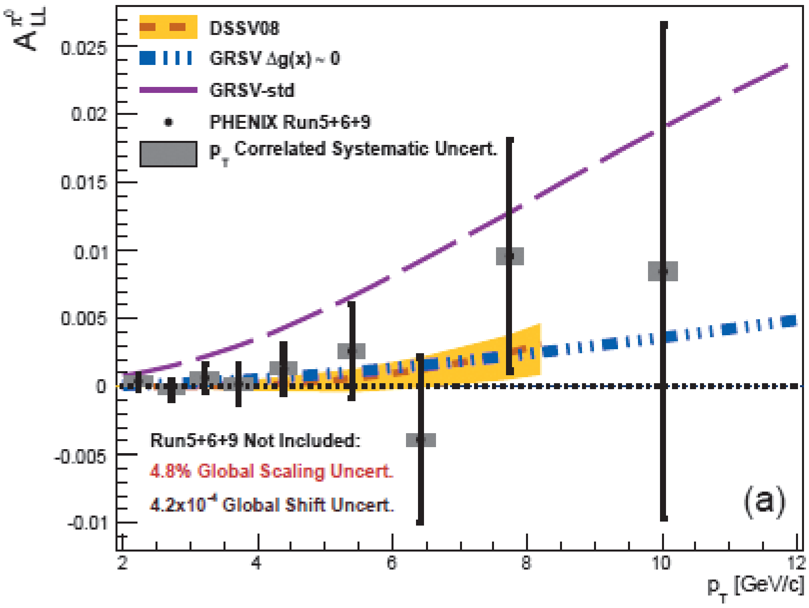

Figure 1 Double spin asymmetry ALL in π^0 production as function of transverse momentum pT compared with expectations for different gluon polarization ΔG(x). Submitted to Physical Review D (arXiv:1402.6296 (2014)).

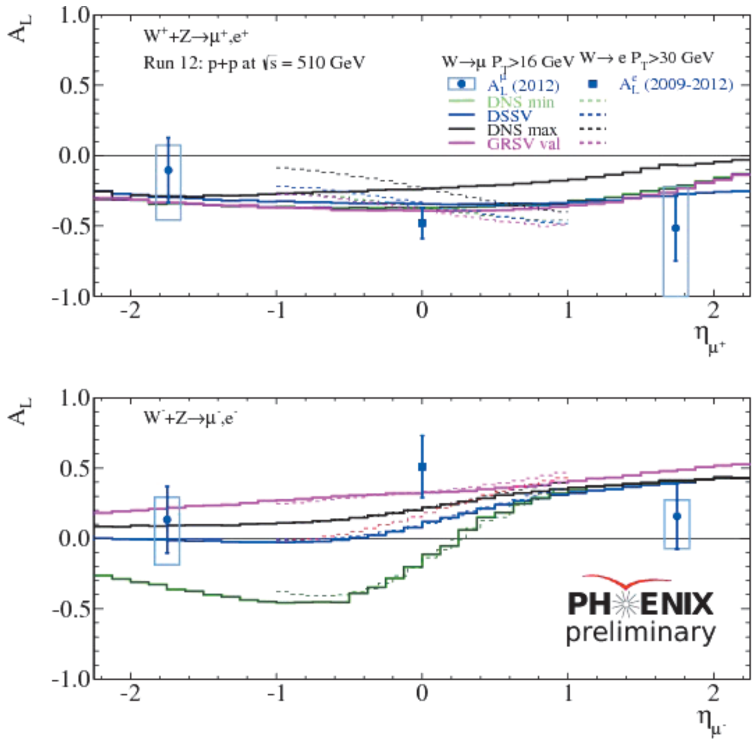

Figure 2 Single spin asymmetry AL of W→e and W→μ measured by PHENIX in the 2012 polarized proton run

(2) Experimental study of Quark-Gluon Plasma using RHIC heavy-ion collider

The goal of high energy heavy ion physics at RHIC is study of QCD in extreme conditions i.e. at very high temperature and at very high energy density. Experimental results from RHIC have established that dense partonic matter is formed in Au+Au collisions at RHIC. The matter is very dense and opaque, and it has almost no viscosity and behaves like a perfect fluid. These conclusions are primarily based on the following two discoveries:

- Strong suppression of high transverse momentum hadrons in central Au+Au collisions (jet quenching)
- Strong elliptic flow

These results are summarized in PHENIX White paper, which has over 1700 citations to date.

The focus of the research in heavy ion physics at RHIC is now to investigate the properties of the matter. RBRC have played the leading roles in some of the most important results from PHENIX in the study of the matter properties. These include (1) measurements of heavy quark production from the single electrons from heavy flavor decay (2) measurements of J/Psi production (3) measurements of di-electron continuum and (4) measurements of direct photons.

The most important recent result is the measurement of direct photons for $1<p_T<5$ GeV/c in p+p and Au+Au through their internal conversion to e+e- pairs. If the dense partonic matter formed at RHIC is thermalized, it should emit thermal photons. Observation of thermal photon is direct evidence of early thermalization, and we can determine the initial temperature of the matter. It is predicted that thermal photons from QGP phase is the dominant source of direct photons for $1<p_T<3$ GeV/c at the RHIC energy. We measured the direct photon in this p_T region from measurements of quasi-real virtual photons that decays into low-mass e+e- pairs. Strong enhancement of direct photon yield in Au+Au over the scaled p+p data has been observed. Several hydrodynamical models can reproduce the central Au+A data within a factor of two. These models assume formation of a hot system with initial temperature of Tinit = 300 MeV to 600 MeV. This is the first measurement of initial temperature of quark gluon plasma formed at RHIC. These results are recently published in Physical Review Letters. Y. Akiba is the leading person of the analysis and the main author of the paper. He received 2011 Nishina memorial Prize mainly based on this work.

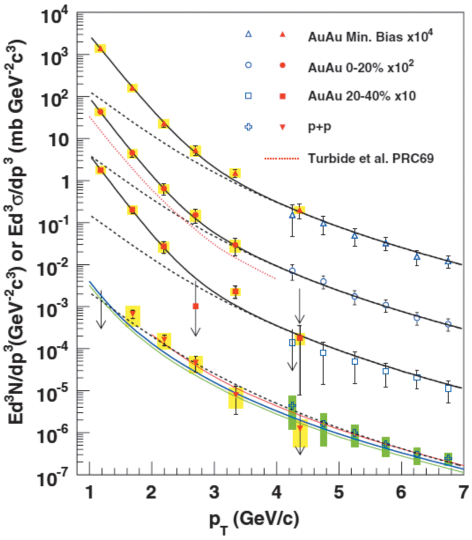

Figure 3 Invariant cross section (p+p) and invariant yield (Au+Au) of direct photons as function of pT. Published in Phys. Rev. Lett. 104, 132301 (2010).

(3) PHENIX detector upgrade

The group has major roles in several PHENIX detector upgrades, namely, the silicon vertex tracker (VTX) and muon trigger upgrades.

VTX is a high precision charged particle tracker made of 4 layers of silicon detectors. It is jointly funded by RIKEN and the US DOE. The inner two layers are silicon pixel detectors and the outer two layers are silicon strip detectors. Y. Akiba is the project manager and A. Deshpande is the strip system manager. The VTX detector was completed in November 2010 and subsequently installed in PHENIX. The detector started taking data in the 2011 run. With the new detector, we are measuring heavy quark (charm and bottom) production in p+p, A+A collisions to study the properties of quark-gluon plasma.

Muon trigger upgrades are needed for $W\rightarrow\mu$ measurement at 500 GeV. New trigger electronics (Muon Trigger FEE) and new Muon trigger detectors using RPC technology were installed in PHENIX muon arms. Additional hadron absorbers were installed in front of the muon arms to reduce the background. These upgrades were essential for the high statistic $W\rightarrow\mu$ measurement in 2013 run. Over 150/pb of data was recorded in the run. I. Nakagawa is the leading person of the installation of the Muon Trigger FEE, and R. Seidl have major role in the RPC project. He is also leading the $W\rightarrow\mu$ analysis.

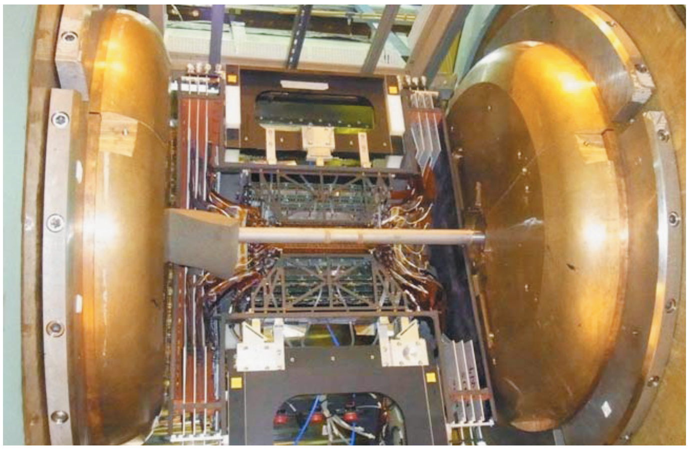
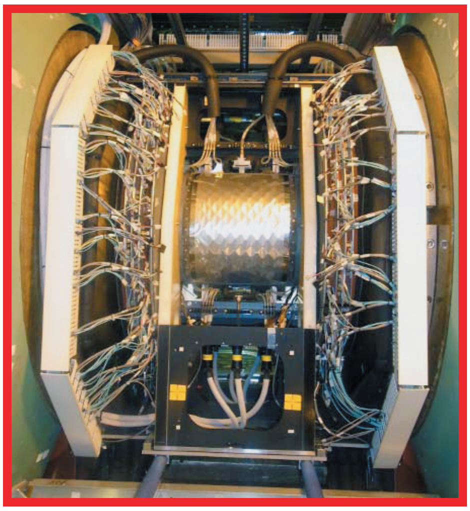

Figure 4 Left: a picture of West half of VTX detector installed in PHENIX experiment. The interior of the detector can be seen. Right: The VTX detector completed with all cables, cooling tubes and dry gas connections.

Group Leader
Yasuyuki AKIBA

Deputy Group Leader
Abhay DESHPANDE

Members
Yuji GOTO (concurrent)
Itaru NAKAGAWA (concurrent)
Takashi ICHIHARA (concurrent)
Atsushi TAKETANI (concurrent)
Yasushi WATANABE (concurrent)
Satoshi YOKKAICHI (concurrent)

RIKEN BNL Fellows
Kieran BOYLE
Josef SEELE (- Feb. 7, 2014)

RHIC Physics Fellows
Stefan BATHE
Xiaorong WANG

Research Associates
John KOSTER (RIKEN FPR) (- May 23, 2013)
Chin-Hao CHEN

Special Postdoctoral Researcher
Maki KUROSAWA (- Mar. 31, 2014)

Visiting Members
Zheng LEE (BNL)
Kiyoshi TANIDA (Seoul Univ.)
Akio OGAWA (BNL)
Masahiro OKAMURA (BNL)
Rachid NOUICER (BNL)
Ady HERSHCOVITCH (BNL)

Intern
Minjung KIM (- Jun. 10, 2013)

Sub Nuclear System Research Division
RIKEN Facility Office at RAL

1. Abstract

Our core activities are based on the RIKEN-RAL Muon Facility located at the Rutherford Appleton Laboratory (UK), which provides intense pulsed-muon beam. Muons have their own spins with 100% polarization, and can detect very precisely local magnetic fields and their fluctuations at muon stopping sites. The method to study characteristic of materials by observing time dependent changes of muon spin polarization is called "Muon Spin Rotation, Relaxation and Resonance (μSR method), and is applied to studies of electro-magnetic proerties of insulating, metallic, magnetic, superconducting systems. Muons reveal static and dynamic properties of electronic state of materials in the zero-field condition which is the ideal magnetic condition for reasearches on the magnetism. We have carried out μSR investigations on frustrated organic system which has a triangular spin network. We found the one dimensional properties of the spin-spin correlations in the system. This proves the first example which has the one-dimensional resonating spin state in real materials.

Positive muon beam with thermal energy has been produced by laser ionization of muoniums (bound system of mu+ and electron) emitted from hot tungsten surface with stopping surface muon beam at Port-3. The ultra-slow muon beam can be stopped in thin foils, multi-layered materials and artificial lattices and we can apply the μSR techniques to surface and interface science. The development of ultra-slow muon beam is also very important as the source of ultra-cold (pencil-like small emittance) muon beam for muon g-2 measurement. We have been developing muonium generators to create more muoniums in vacuum even at room temperature. Very recently, we demonstrated tremendous increase of the muonium emission efficiency by fabricating fine laser drill-holes on the surface of silica aerogel. We also developed a high power Lyman-alpha laser in collaboration with laser group at RIKEN. The new laser will ionize muoniums 100 times more efficiently for slow muon beam generation.

2. Major Research Subjects

(1) Materials science by muon-spin-relaxation method
(2) Hyperfine interactions at muon sites studied by the computation science
(3) Nuclear and particle physics studies via muonic atoms and ultra cold muon beam

3. Summary of Research Activity

(1) Material Science at the RIKEN-RAL Muon Facility

Muons have their own spins with 100% polarization, and can detect very precisely local magnetic fields and their fluctuations at muon stopping sites. The method to study characteristic of materials by observing time dependent changes of muon spin polarization is called "Muon Spin Rotation, Relaxation and Resonance (μSR method), and is applied to studies of newly fabricated materials. Muons with their own spin polarization enable us to conduct (1) material studies under external zero field condition, (2) magnetism studies with samples without nuclear spins, and (3) measurements of muon spin relaxation changes at wide temperature range with same detection sensitivity. The detection time range of local field fluctuations by μSR is 10^{-6} to 10^{-11} second, which is medium region between neutron scattering method (10^{-10}-10^{-12} second) and Nuclear Magnetic Resonance (NMR) (longer than 10^{-6} second). At port-2 of the RIKEN-RAL Muon Facility, we have been performing μSR researches on newly fabricated strong correlated-electron systems, organic molecules and biological samples to study electron structures, superconductivity, magnetism, molecular structures and crystal structures.

In the period from 2011 to 2013, we have obtained excellent results, and the highlights are listed in the following,

1) One-dimensional diffusive motion of spin-excited states in the spin liquid state of molecular magnet, $EtMe_3Sb[Pd(dmit)_2]_2$
2) Static ordering of small Ir moments in the pyrochlore iridate, $Nd_2Ir_2O_7$
3) Static ordering of Yb moment on the corner of the pyrochlore structure of $Yb_2Ti_2O_7$ which can be explained by the Higgs mechanism.
4) Spontaneous small static internal fields in the superconducting state of URu_2Si_2.
5) Universality class of the Mott transition in $EtMe_3P[Pd(dmit)_2]_2$.
6) Finding new muon sites in La_2CuO_4 and success to explain those sites from the potential view point on the basis of a newly developed calculation method taking into account an effect of the special distribution of Cu spin.
7) International collaborations to organize new μSR experiments and to develop a group to work on muon-site calculations by using computational technique.

Soft matters with small spins like organic molecules are now good target for the pulsed muon beam to be applied. The one-dimensional diffusive motion in the two-dimensional crystal structure has been observed. This indicates a strong possibility to observe the one-dimensional RVB state appears in the frustrated spin liquid state in organic molecules (result-1). Solid observations of a static magnetically ordered state of corner-shared magnetic moments on pyrochlore systems gave us new interpretations to understand exotic phenomena (result-2 and 3). We measured an increase of static internal fields at the muon site in the zero-field condition just below the superconducting transition temperature of URu_2Si_2. This could give a light on the mechanism of the superconductivity which has been a long-standing problem of this system (result-4). We have been developing gas-pressurized high-pressure apparatus which can be not only be used for μSR but also other purposes. We have applied this pressure system to $EtMe_3P[Pd(dmit)_2]_2$ and have found that pressure dependent resistivity and thermoelectric effect measurements have shown that the Mott transition belongs to the Ising universality class even in two-dimensional states (result-5). Well known and deeply investigate La_2CuO_4 did open a new scheme of the Cu spin. Taking into account the effect of the distribution of Cu spin, we succeeded to explain newly found muon sites and hyperfine fields at those sites (result-6). We have been very keen to develop muon activities in Asian countries. We have formed MOU with Universiti Sains Malaysia (USM) in order to develop activities on the muon-site calculation. We have newly started to collaborate in μSR experiments on strongly correlated systems with researchers from Taiwan and Korea including the student acceptance (result-7).

A new μSR spectrometer "Chronus" which has finely multi-segmented forward and backward μ-e counter arrays (303 counters each) is now being used for real muon experiments. Software systems which control the data acquisition and experimental conditions are well working in Port-4. The same data acquisition system with that being used in the ISIS muon facility (DAE-III) was adopted. Muon signals more than 70 million events per hour have been recorded even in the single-pulse mode by using DAE-III system in Port-4.

(2) Ultra Slow (low energy) Muon Beam Generation and Applications

Positive muon beam with thermal energy has been produced by laser ionization of muoniums (bound system of μ^+ and electron) emitted from hot tungsten surface with stopping surface muon beam at Port-3. The method generates positive muon beam with acceleration energy from several 100 eV to several 10 keV, small beam size (a few mm) and good time resolution (less than 8 nsec). By stopping the ultra-slow muon beam in thin foils, multi-layered materials and artificial lattices, we can precisely measure local magnetic field in the materials, and apply the μSR techniques to surface and interface science. Since there has been no appropriate probe to study magnetism at surface and interface, the ultra-slow muon beam will open a new area of these research fields. In addition, the development of ultra-slow muon beam is very important as the source of ultra-cold (pencil-like small emittance) muon beam for muon g-2 measurement.

It is essential to increase the slow muon beam production efficiency by 100 times for these applications. There are three key techniques in ultra-slow muon generation: production of thermal muonium, high intensity Lyman-alpha laser and the ultra-slow muon beam line.

In the period from 2011 to 2013, we developed a high power Lyman-alpha laser in collaboration with laser group at RIKEN. The new laser will ionize muoniums 100 times more efficiently for slow muon beam generation. This development was funded mostly by the Grant-in-Aid for Scientific Research on Innovative Areas "Frontier in Materials, Life and Particle Science Explored by Ultra Slow Muon Microscope". This Grant-in-Aid research group is a complex of research institutions from universities together with J-PARC muon group and RIKEN. Therefore, the new laser system should be installed to J-PARC slow muon beam line. On the other hand, we succeeded to synthesize novel ceramic-based Nd:YGAG crystal in this development, and this crystal can also be applicable to the flash-lamp based Lyman-alpha laser system of RIKEN-RAL to realize substantial improvement of the laser power at a much reduced cost based on the experiences.

Another plan in 2011-2013 was to achieve drastic improvements in the ultra-slow muon source with much reduced emittance. We have been developing muonium generators to create more muoniums in vacuum even at room temperature. Very recently, we demonstrated tremendous increase of the muonium emission efficiency by fabricating fine laser drill-holes on the surface of silica aerogel. The measurement was carried out at TRIUMF in collaboration with J-PARC muon g-2 group. Analysis is in progress and the result will be published soon. We believe that the better efficiency and beam quality can be achieved in ultra-slow muon generation by using this new muonium source.

Based on these two new key components, we are planning to feed these new techniques to RIKEN-RAL ultra-slow muon beam line to realize further development of ultra-slow muon technology. The present muonium production target section, which had been designed with hot tungsten, will be rebuilt to use advantage of the new room temperature target, such as no need of thermal shielding etc. Also, we adopt an all-cylindrical beam-transport design, because of its simpler optics and better manufacture precision, which will contribute to the ultimate cold muon source required for muon g-2. We plan the construction and testing be finished in time for the RIKEN-RAL muon beam recovery in Feb 2015 after ISIS shutdown.

(3) Other topics

Muon catalyzed fusion has been one of the main subject of studies since the start of the RIKEN-RAL Muon Facility. It has produced many new results by using the advantage of the high-intensity pulsed muon beam and the advanced tritium handling facility as was reported in previous RIKEN-RAL IACs. Even though, huge increase of the catalysis rate that is enough for energy production is yet difficult to achieve. Considering the limited funds and human resources maintaining the tritium facility, we plan the safe closure of the tritium facility well before 2018. We have started discussion of safe removal of the tritium handling facility. The decommissioning is planned in early 2015.

New demand is emerging utilizing the muon beam for electronics chips radiation effect studies. Recent progress of semiconductor devices has produced electronics chips with very fine structure. It is concerned that the single memory upset by the ionization effect of single muon may result in malfunction or errors of advanced electronics. Muon is the main component of the cosmic ray in our ordinal life and difficult to be removed. Measurements are being performed at RIKEN-RAL to measure such an error rate. There is also measurement to test the electronics chips in a condition equivalent to the high radiation environment in accelerator experiment.

A new proposal was submitted recently to measure the proton radius by using the hyperfine splitting of the 1S states of muonic hydrogen. This is in contrast to the recent measurement at PSI using 2S-2P energy splitting. The hyperfine transition measurement needs a high intensity laser so it needs to be matched with pulsed muon beam. Design of the hydrogen target, the laser, and the detector is in progress.

Director
Philip KING

Member
Isao WATANABE (concurrent)

Administration Manager
Mitsuru KISHIMOTO

RIBF Research Division
Radioactive Isotope Physics Laboratory

1. Abstract
This laboratory explores exotic nuclear structures and dynamics in exotic nuclei that have never been investigated before, such as those with largely imbalanced proton and neutron numbers. Our aim is to develop new experimental techniques utilizing fast RI beams to discover new phenomena and properties in exotic nuclei. Another important subject is the equation-of-state in asymmetric nuclear matter, and its association with the origin of elements and with neutron stars. For instance, we are making attempts to the better understand underlying mechanism for exotic stability-enhancements of very neutron-rich fluorine isotopes, the large deformation of the nucleus Mg-34 with N=22 in spite of its vicinity to the N=20 magic neutron number and anomalous collectivity in C-16. We are further extending these studies to medium- and heavy-mass regions by developing facilities, detectors and unique methods at RIBF, thereby leading on the challenging task to find new exotic phenomena. We also perform numerical simulations of nucleosynthesis under the environment of core-collapse supernovae, and moreover quest for footprints of supernovae and solar activities in the past, embedded in Antarctic ice core.

2. Major Research Subjects
(1) Study of structure and dynamics of exotic nuclei through developments of new tools in terms of reaction- and technique-based methodology
(2) Research on EOS in asymmetric nuclear matter via heavy-ion induced reactions
(3) Detector developments for spectroscopy and reaction studies

3. Summary of Research Activity
(1) In-beam gamma spectroscopy

In the medium and heavy mass region explored at RIBF, collective natures of nuclei are one of important subjects, which are obtained through production and observation of high excited and high spin states. To populate such states, heavy-ion induced reactions such as fragmentation, fission are useful. So far, we have developed two-step fragmentation method as an efficient method to identify and populate excited states, and lifetime measurements to deduce transition strength.

Devices utilized for the in-beam gamma spectroscopy are ZeroDegree Spectrometer (ZDS) and a NaI array DALI2. Since the end of 2008, the first spectroscopy on nuclei island-of-inversion region was performed, we have explored step-by-step new and unknown regions in the nuclear chart. The second campaign in 2009 was organized to study background components originating from atomic processes in a heavy target. Neutron-rich nuclei at N=20 to 28 were studied in 2010. In 2011-2013, we conducted experiment programs for Ca-54, Ni-78, neutron-rich nuclei at N=82 and neutron-deficient nuclei at Z=50.

A multitude of data obtained with inelastic, nucleon knock-out, fragmentation channels have been analyzed and published. In 2011-2013, collective natures of Mg-36, 38 and Si-42 were both published in PRL. Excited states firstly observed in Ca-54 were reported in Nature to demonstrate a new nuclear magic number of 34. Fragmentation reaction has been found efficient for nuclei with A>100 and low-lying excited state in Pd-126 has been successfully observed and reported in PRC.

To further strengthen the in-beam gamma spectroscopy at RIBF, we have proposed a new setup of MINOS + DALI2 to search for the 1st excited states in even-even neutron-rich nuclei with Z~20 to 40. The program was submitted to the PAC 2013 as a new category "proposal for scientific program" and was S-ranked. A dedicated collaboration "SEASTAR" has been established as a subset of in-beam gamma collaboration "SUNFLOWER". The first campaign will be organized in April 2014 to study neutron-rich Cr, Fe and Ni isotopes.

Concerning a next generation detector, a construction proposal of a LaBr3 array "SHOGUN", was submitted to the PAC 2009, and an international workshop was organized in Feb. 2011 to form the SHOGUN collaboration. A technical development with small sized crystals is now in progress.

(2) Decay spectroscopy

Beta- and isomer-spectroscopy is an efficient method for studying nuclear structure, especially for non-yrast levels. We had accumulated experimental techniques at the RIPS facility to investigate nuclear structure in light mass region via beta-gamma and beta-p coincidence. Concerning the medium and heavy mass region available at RIBF, we have developed two position-sensitive active-stoppers, strip-silicon detectors and a cylindrical active stopper called CAITEN, to achieve a low-background measurement by taking correlation between heavy ion stop position and beta-ray emission position. A site of decay-spectroscopy at the new facility of RIBF is the final focal plane of ZDS, where high precision of TOF in particle identification is obtained due to a long flight path from BigRIPS to ZDS.

At the end of 2009, the first decay spectroscopy was organized with a minimum setup of four clover gamma detectors and silicon strip detectors, to study neutron-rich nuclei with A~110. The first campaign was found successful and efficient to publish four letter articles in 2011, two PRL's and two PLB's. One of the PRL papers is associated to the r-process path where half-lives for 18 neutron-rich nuclei were determined for the first time. The other PRL paper reported a finding of deformed magic number 64 in the Zr isotopes.

The success of the first decay-spectroscopy campaign stimulated to form a new large-scale collaboration "EURICA", where a twelve Euroball cluster array is coupled with the silicon-strip detectors to enhance gamma efficiency by a factor of 10. A construction proposal of "EURICA" was approved in the PAC 2011, and the commissioning was successfully organized in spring 2012. Since then, physics runs have been conducted for programs approved to survey nuclei of interest as many as possible, such as Ni-78, Pd-128, Sn-100. So far, three papers, two PRL's and one PRC, were published. One of the highlights is discovery of a seniority isomer in Pd-128, of which cascade gamma decay gives the energy of 1st excited state and robustness of N=82 magic number.

Beta-delayed neutron emission probability of medium and heavy neutron-rich nuclei is important to understand nuclear structure and the r-process path. In 2013, a new collaboration "BRIKEN" has been established to form a He-3 detector array. A present design of the array has neutron efficiency as high as 70% up to 3 MeV. The array will be coupled with the AIDA silicon strip system. A construction proposal was approved at the PAC 2013 and physics proposals will be discussed at the PAC 2014.

The CAITEN detector was successfully tested with fragments produced with a Ca-48 beam in 2010.

(3) Equation-of-state via heavy-ion central collisions

Equation-of-state in asymmetric nuclear matter is one of major subjects in physics of exotic nuclei. Pi-plus and pi-minus yields in central heavy ion collisions at the RIBF energy are considered as one of EOS sensitive observables at the RIBF energy. To observe charged pions, a TPC for the SAMURAI spectrometer is being constructed under an international collaboration "SPiRIT". Construction proposal was submitted at the PAC 2012, and physics proposals were approved at the PAC 2012 and 2013. Physics runs are scheduled in 2015.

An international symposium "NuSYM" on nuclear symmetry energy was organized at RIKEN July 2010 to invite researchers in three sub-fields, nuclear structure, nuclear reaction and nuclear astrophysics, and to discuss nuclear symmetry energy together. Since then, the symposium series have been held every year and been useful to encourage theoretical works and to strengthen the collaboration.

(4) Nucleon correlation and cluster in nuclei

Nucleon correlation and cluster in nuclei are matters of central focus in a "beyond mean-field" picture. The relevant programs with in-beam gamma and missing-mass techniques are to depict nucleon condensations and correlations in nuclear media as a function of density as well as temperature. Neutron-halo and –skin nuclei are objects to study dilute neutron matter at the surface. By changing excitation energies in neutron-rich nuclei, clustering phenomena and role of neutrons are to be investigated.

In 2013, two programs were conducted at the SAMURAI spectrometer. One is related to proton-neutron correlation in the C-12 nucleus via p-n knockout reaction with a carbon target. The other is to search for a cluster state in C-16, which was populated via inelastic alpha scattering. The data is being analyzed.

(5) Nuclear data for nuclear waste of long-lived fission products

The nuclear waste problem is an inevitable subject in nuclear physics and nuclear engineering communities. Since the Chicago Pile was established in 1942, nuclear energy has become one of major sources of energy. However, nowadays the nuclear waste produced at nuclear power plants has caused social problems. Minor actinide components of the waste have been studied well as a fuel in fast breeder reactors or ADS. Long-lived fission products in waste, on the other hand, have not been studied extensively. A deep geological disposal has been a policy of several governments, but it is difficult to find out location of the disposal station in terms of security, sociology and politics. To solve the social problem, a scientific effort is necessary for nuclear physics community to find out efficient methods for reduction of nuclear waste radioactivity.

In 2013, we have started up a new project to take nuclear data for transmutation of long-lived fission products to obtain cross section data needed for designing a nuclear waste treatment system. In 2014, we will make the first attempt to measure fragmentation reaction data with Cs-137 and Sr-90 beams at 200A MeV.

(6) Missing mass method

Missing mass technique is one of fundamental spectroscopy methods at RIBF. Detection of recoil particles from target is essential in excitation energy determination of particle unbound states without any assumption of particle- and gamma-decay processes, and also giving transfer angular momentum from the angular distribution measurement. We have developed a solid hydrogen target as well as a detector system called ESPRI for proton-(in)elastic scattering. In 2010, the ESPRI system was placed at GSI to measure proton elastic scattering with Ni isotope beams. In addition, the first missing mass spectroscopy was performed at RIBF, where the start-of-art detector MUST2 was invited from France to investigate O-24 and its neighboring nuclei. The (p,2p) reaction study for the light neutron-rich nuclei was carried out with the Kappa spectrometer installed at the new facility of RIBF.

The missing mass activity based on direct reactions has been moved to Spin-Isospin Laboratory in RNC since Uesaka was appointed as a chief scientist in April 2011.

(7) Interdisciplinary study for nuclear astrophysics

To understand the origin of elements beyond ion, interdisciplinary works are important in linking data from nuclear physics programs. In this respect, we did promote the ice core analysis activity to find out historical supernovae and to estimate event rates of supernovae.

This activity has been moved to Astro-Glaciology Research Unit in RNC since Motizuki was appointed as a unit leader in July 2011.

(8) Laser spectroscopy of radioactive isotope atoms

Electromagnetic moment is one of the most important quantities for studying nuclear structures because they are directly correlated with the quantum states and configurations of valence nucleons. Precision laser spectroscopy of radioisotope atoms (RI atoms) reveals these nuclear properties through the measurement of atomic level structures affected by hyperfine interactions. We have been developing a novel laser spectroscopic method for RI atoms named "*OROCHI* (Optical RI-atom Observation in Condensed Helium as Ion-catcher)." It is a combination of superfluid helium (He II) as a stopper of energetic RI beam with several tens MeV/u and in situ laser-microwave/-RF double resonance spectroscopy of stopped RI atoms. We expect that this method is applicable to a wide variety of atomic species whose yields are as low as 10 pps.

The laser spectroscopy activity has been moved to Nuclear Spectroscopy Laboratory in RNC since Ueno was appointed as a chief scientist in April 2013.

Head
Hiroyoshi SAKURAI (Chief Scientist; Deputy Director, RNC)

Members
Takashi ICHIHARA (Vice Chief Scientist)
Yoichi NAKAI (Senior Research Scientist)
Hideaki OTSU (Senior Research Scientist)
Takashi KISHIDA (Senior Research Scientist)
Shunji NISHIMURA (Senior Research Scientist)
Hiu Ching LEE (Research Scientist)
Tadaaki ISOBE (Research Scientist)
Pieter DOORNENBAL (Research Scientist)

Contract Researcher
Satoshi TAKEUCHI (Apr. 1, 2013 -)

Foreign Postdoctoral Researchers
Giuseppe LORUSSO
Paer-Anders SOEDERSTROEM (Feb. 1, 2014 -)

Postdoctoral Researchers
Paer-Anders SOEDERSTROEM (Oct. 18, 2013 – Jan. 31, 2014)
Paer-Anders SOEDERSTROEM (JSPS) (- Oct. 17, 2013)
Ann-Kathrin PERREVOORT (JSPS) (Apr. 1, 2013 – Feb. 3, 2014)

Senior Visiting Scientists
Shigeru KUBONO (University of Tokyo)
Kengo OGAWA (Chiba Univ.)

Visiting Scientists
Nori AOI (RCNP, Osaka University)
Dam Nguyen BINH (Institue of Physicks, Vietnam Academy of Science and Technology) - Mar. 31, 2013
Silivio CHERUBINI (University of Catania, Italy)
Alessia DI (INFN Laboratori Nazionali del Sud,Catania,Itary) Jun. 1, 2013 – Mar. 31, 2014
Pierpaolo FIGUERA (INFN Laboratori Nazionali del Catania,Italy) Jun. 1, 2013 – Mar. 31, 2014
Daiki NISHIMURA (Tokyo University of Science)
Mitsunori FUKUDA (Osaka University)
Adrian GELBERG (Universitat zu Köln, Germany) - Aug. 12, 2013
Mikhail GOLOVKOV (Flerov Lab. of Nuclear Reaction, JINR) - Mar. 31, 2014
Andrey FOMICHEV (Flerov Lab. of Nuclear Reaction, JINR) - Mar. 31, 2014
Atsushi HATAKEYAMA (Tokyo University of Agriculture and Technology) - Mar. 31, 2014
Chuangye HE (China Institute of Atomic Energy) - Mar. 31, 2013
Byungsik HONG (Korea University) Feb. 24, 2014 -
Kazuo IEKI (Rikkyo University)
Hyo Soon JUNG (University of Notre Dame)
Le Hong KHIEM (Institue of Physicks, Vietnam Academy of Science and Technology)
Nobuyuki KOBAYASHI (School of Science, the University of Tokyo)
Yosuke KONDO (Tokyo Institute of Technology) -Mar. 31, 2013
Nikolaus Ludwig KURZ (GSI) -Mar. 31, 2013
Yukari MATSUO (Hosei University)
Indranil MAZUMDAR (GSI)
Takamasa MOMOSE (The University of British Columbia, Canada)
Tetsuya MURAKAMI (Graduate School of Science, Kyoto University)
Takashi NAKAMURA(Tokyo Institute of Technology) -Mar. 31, 2013
Megmi NIIKURA (the University of Tokyo)
Evgueni NIKOLSKI (RRC Kurchatov Institute, Institute of General and Nuclear Physics, Russia)
Alexey OGLOBLIN (RRC Kurchatov Institute, Institute of General and Nuclear Physics, Russia)
Hooi Jing ONG (RCNP)
Naohiko OTSUKA (International Atomic Energy Agency, Austria)
Paul PAPKA (Department Fisika, Universiteit Stellenbosch) Aug. 1,2013 – Mar. 31, 2014
Toshiyuki SUMIKAMA (Tohoku University)
Maya TAKECHI (GSI) - Mar. 31, 2013
Xiaolong WANG (Kyoto Univ.) - Mar. 31, 2014
Hiroshi WATANABE (Beihang University)

Visiting Technician
Andrey BEZBAKH (Flerov Lab. of Nuclear Reaction, JINR) Sep. 1, 2013 - Mar. 31, 2014
Alexander KNYAZEV (Flerov Lab. of Nuclear Reaction, JINR) Sep. 1, 2013 - Mar. 31, 2014

Ivan KOJOUHAROV (GSI Helmholtzzentrum fuer Schwerionenforschung GMBH)
Sergey KRUPKO (Flerov Lab. of Nuclear Reaction, JINR) Sep. 1, 2013 - Mar. 31, 2014
Sergey SIDORCHUK (Flerov Lab. of Nuclear Reaction, JINR) Sep. 1, 2013 - Mar. 31, 2014
Roman SLEPNEV (Flerov Lab. of Nuclear Reaction, JINR) Sep. 1, 2013 - Mar. 31, 2014

Research Associates
Mizuki NISHIMURA (- Mar. 31, 2014)
Satoshi TAKEUCHI (- Mar. 31, 2013)

Junior Research Associates
Shintaro GO - Mar. 31, 2014
Yoshiaki SHIGA

International Program Associates
Xiaofei YANG (Peking Univ., China) -Feb. 16, 2014
Hongna LIU (Peking Univ., China)
Jin WU
Frank BROWNE - Sep. 30, 2013
Zena PATEL Mar. 21, 2013 - Sep. 30, 2013
Simon RICE Mar. 31, 2013 – Jul. 7, 2014
William POWELL
Laura SINCLAIR Apr. 19, 2013 – Oct. 19, 2013
Daniel LUBOS May 22, 2013 – Dec. 14, 2013

Research Consultant
Masayasu ISHIHARA

Consultant
Tateaki TORII

Part-time worker
Zhengyu XU (- Mar. 31, 2014)

Intern
Takatoshi MATSUKURA (Tokyo Metropolitan College of Industrical Technology) Aug. 22, 2013 – Sep. 13, 2013

Student Trainees
Jin-hee CHANG (Korea University)
Rie DAIDO (Osaka University)
Justin ESTEE (Michigan State University)
Yifan FANG (Osaka University)
Tomomi FUJITA (Osaka University)
Lauren HEILBORN (Texas A&M University)
Hisaya HOTAKA (Tohoku Univ.)
Tomoki ISHIGAKI (Osaka University)
Rachel HODGES (Michigan State University)
Akira HOMMA (Niigata University)
Jongwon HWANG (Seoul National Univ.)
Kei IMAMURA (Meiji University)
Yasuto KAMISHOU (Osaka Univ.)
Masanori KANEKO (Kyoto University)
Sunji KIM (Soul Univ., Korea)
Shumpei KINNO (The Tokyo University of Science)
Kazuma KOBAYASHI (Rikkyo University)
Akihiro KOJIMA (Tohoku Univ.)
JungWoo LEE (Korean University)
Keishi MATSUI (The University of Tokyo)
Hideyuki MATSUZAWA (Rikkyo University)
Takuya MIYAZAKI (The University of Tokyo)
Yosuke MITSUYA (Meiji Univ.)
Satoru MOMIYAMA (The University of Tokyo)
Shouta MORIMOTO (Osaka University)
Yosuke MORITA (Osaka University)
Motoki MURATA (Kyoto University)
Daiki MUROOKA (Niigata University)
Kotomi MUTO (Tohoku Unversity)
Masayuki NAGASHIMA (Nigata University)
Junichi OHNO (Osaka University)

Noritsugu NAKATSUKA (Kyoto University)
Hiroki NISHIBATA (Osaka University)
Ippei NISHIZUKA (Tohoku University)
Masami SAKO (Kyoto University)
Philipp SCHROCK (Technical University Darmstadt)
Hirotaka SUZUKI (Osaka University)
Tadashi TAKO (Tohoku University)
Kohei TAKENAKA (Kyoto University)
Mana TANAKA (Osaka University)
Suwat TANGWANCHAROEN (Michigan State University)
Ryo TANIUCHI (The University of Tokyo)
Keisuke TASHIRO (Nigata University)
Takumi USUKURA (Rikkyo University)
He WANG (Peking University)
Daisuke WATANABE (The Tokyo University of Science)
Kouta WATANABE (Osaka University)
Jack WINKELBAUER (Michigan State University)
Zhengyu XU (The University of Tokyo)
Ayumi YAGI (Osaka University)
Tetsuya YAMAMOTO (Osaka University)
Shintoro YAMAOKA (Osaka University)
Takamasa YOSHIDA (Rikkyo University)
Kenta YOSHINAGA (The Tokyo University of Science)
Andrew ZARRELLA (Texas A&M University)
Yifan ZHU (The Tokyo University of Science)

Assistant

Yu NAYA
Tomoko FUJII (- Mar. 31, 2013)

RIBF Research Division
Spin isospin Laboratory

1. Abstract

The Spin Isospin Laboratory pursues research activities putting primary focus on interplay of spin and isospin in exotic nuclei. Investigations on isospin dependences of nuclear equation of state, spin-isospin responses of exotic nuclei, occurrence of various correlations at low-densities, evolution of spin-orbit coupling are main subjects along the line. One of our goals is to elucidate a variety of nuclear phenomena in terms of interplay of spin and isospin.

Establishment of storage-ring science in Japan is another big goal of our laboratory. We are leading, in collaboration with the Wakasugi group, the Rare RI Ring project to achieve precision mass measurement of r-process nuclei.

2. Major Research Subjects

(1) Direct reaction studies of neutron-matter equation of state
(2) Study of spin-isospin responses with RI-beams
(3) Production of spin polarized protons and its application to RI-beam experiments
(4) R-process nucleosynthesis study with heavy-ion storage ring
(5) Development of special targets for RI-beam experiments

3. Summary of Research Activity

(1) Direct reaction studies of neutron matter equation of state

Direct reactions induced by light-ions serve as powerful tools to investigate various aspects of nuclei. We are advancing experimental programs to explore equation of state of neutron matter, via light-ion induced reactions with RI-beams.

(1-a) Determination of a neutron skin thickness by proton elastic scattering

A neutron skin thickness is known to have strong relevance to asymmetry terms of nuclear equation of state, especially to a term proportional to density. The ESPRI project aims at determining density distributions in exotic nuclei precisely by proton elastic scattering at 200−300 MeV/nucleon. An experiment for ^{132}Sn that is a flagship in this project is planned to be performed in 2015. Prior to the ^{132}Sn experiment, we have applied the ESPRI setup that consists of a solid hydrogen target and recoil proton detectors to ^{16}C in 2012.

(1-b) Asymmetry terms in nuclear incompressibility

Nuclear incompressibility represents stiffness of nuclear matter. Incompressibility of symmetric nuclear matter is determined to be 230±20 MeV, but its isospin dependence still has a large uncertainty at present. A direct approach to the incompressibility of asymmetric nuclear matter is an experimental determination of energies of isoscalar giant monopole resonances (GMR) in heavy nuclei. We have developed, in close collaboration with Center for Nuclear Study (CNS) of University of Tokyo, an active gas target for deuteron inelastic scattering experiments to determine GMR energies. The active gas target has been already tested with oxygen and xenon beams at HIMAC and will be applied to a ^{132}Sn experiment in 2015.

(1-c) Multi-neutron andα-cluster correlations at low densities

Occurrences of multi-neutron andα-cluster correlations are other interesting aspects of nuclear matter and define its low-density behavior. The multi-neutron andα-cluster correlations can be investigated with the large-acceptance SAMURAI spectrometer. The SAMURAI has been already applied to experiments to explore light neutron-rich nuclei close to the dripline. We plan to reinforce experimental capabilities of the SAMURAI by introducing advanced devices such as MINOS (Saclay) and NeuLAND (GSI).

(1-d) Fission barrier heights in neutron-rich heavy nuclei

The symmetry energy has a strong influence on fission barrier heights in neutron-rich nuclei. Knowledge on the fission barrier heights, which is quite poor at present, is quite important for our proper understanding on termination of the r-process. We are planning to perform, in collaboration with the TU Munich group, (p,2p)-delayed fission experiments at the SAMURAI to determine the fission barrier heights in neutron-rich nuclei in Pb region.

(2) Study of spin-isospin responses with RI-beams

The study of spin-isospin responses in nuclei forms one of the important cores of nuclear physics. A variety of collective states, for example isovector giant dipole resonances, isobaric analogue states, Gamow-Teller resonances, have been extensively studied by use of electromagnetic and hadronic reactions from stable targets.

The research opportunities can be largely enhanced with light of availabilities of radioactive isotope (RI) beams and of physics of unstable nuclei. There are three possible directions to proceed. The first direction is studies of spin-isospin responses of unstable nuclei via inverse-kinematics charge exchange reactions. A neutron-detector array WINDS has been constructed, under a collaboration of CNS, Tokyo and RIKEN, for inverse kinematics (*p*,*n*) experiments at the RI Beam Factory. We have already applied WINDS to the (*p*,*n*) experiments for ^{12}Be, ^{132}Sn and plan to extend this kind of study to other exotic nuclei.

The second direction is studies with RI-beam induced charge exchange reaction. RI-beam induced reactions have unique properties which are missing in stable-beam induced reactions and can be used to reach the yet-to-be-discovered states. We have constructed the SHARAQ spectrometer and the high-resolution beam-line at the RI Beam Factory to pursue the capabilities of RI-beam induced reactions as new probes to nuclei. One of the highlights is an observation of β^+ type isovector spin monopole resonances (IVSMR) in ^{208}Pb and ^{90}Zr via the (t, ^{3}He) reaction at 300 MeV/nucleon.

The third direction is studies of neutron- and proton-rich nuclei via stable-beam induced charge exchange reactions, which is conducted under collaboration with Research Center for Nuclear Physics (RCNP), Osaka University. We have performed the double charge exchange ^{12}C(^{18}O, ^{18}Ne)^{12}Be reaction at 80 MeV/nucleon to investigate structure of a neutron-rich ^{12}Be nucleus. Peaks corresponding to ground and excited levels in ^{12}Be have been clearly observed.

(3) Production of spin-polarized protons and its application to RI-beam experiments

Recent experimental and theoretical studies have revealed that spin degrees of freedom play a vital role in exotic nuclei. Tensor force effects on the evolution of shell and possible occurrence of p-n pairing in the proton-rich region are good examples of manifestations of spin degrees of freedom.

In exploring the spin effects in exotic nuclei, scattering with polarized protons should be a powerful tool. We have constructed a novel polarized proton solid target aiming to shed light of polarization on the physics of exotic nuclei. A distinguished feature of the target system is that it works under a low magnetic field of 0.1 T and temperature higher than 100 K, which exhibits a striking contrast to standard DNP targets working in extreme conditions of several Tesla and sub-Kelvin. It should be noted that we have recently achieved a proton polarization of 40% at room temperature in a pentacene-d_{14} doped p-terphenyl crystal.

The polarized proton target was applied, for the first time, to measurement of vector analyzing power in the proton elastic scattering of neutron-rich $^{6,8}He$ nuclei at 71 MeV/nucleon at RIPS, RIKEN. At RI Beam Factory, a hole-state spectroscopy via the (p, 2p) knockout reaction from unstable oxygen isotopes was performed with the polarized target.

(4) R-process nucleosynthesis study with heavy-ion storage ring

Most of the r-process nuclei become within reach of experimental studies for the first time at RI Beam Factory at RIKEN. The Rare RI Ring at RIBF is the unique facility with which we can perform mass measurements of r-process nuclei. Construction of the Rare RI Ring started in FY2012 in collaboration with Tsukuba and Saitama Universities. A major part of the ring has been completed and the commissioning run is planned in FY2014.

We are planning to start precise mass measurements of r-process nuclei in 2015. A series of experiments will start with nuclei in the A=80 region and will be extended to heavier region.

(5) Development of special targets for RI-beam experiments

For the research activities shown above, we are developing and hosting special targets for RI-beam experiments listed below:

a) Polarized proton target
b) Thin solid hydrogen target
c) MINOS (developed at Saclay and hosted by the Spin Isospin Laboratory)

Head

Tomohiro UESAKA (Chief Scientist)

Members

Masaki SASANO (Research Scientist)
Juzo ZENIHIRO (Research Scientist)

Postdoctoral Researchers

Masanori DOZONO - Mar. 31, 2014
Valerii PANIN Dec. 1, 2013-

Senior Visiting Scientists

Hiroyuki SAGAWA (Aizu University) - Mar. 31, 2014
Didier BEAUMEL (IPN) Apr. 1, 2013 -

Visiting Researcher

Alexandre OBERTELLI (JSPS) Sep. 2, 2013 -

Research Associate

Kenichiro TATEISHI Apr. 1, 2013 -

Junior Research Associates

Keiichi KISAMORI
Yuki KUBOTA Apr. 1, 2013 -
CheongSoo LEE Apr. 1, 2013 -
Fumi SUZAKI Apr. 1, 2013 -

International Program Associates

Sergey S. CHEBOTARYOV Jun 1, 2013 -
Sylvain R. LEBLOND Mar. 6, 2013 – Sep. 3, 2013
Evgeniy V. MILMAN Apr. 1, 2013 -
Clementine A. SANTAMARIA Sep. 3, 2013 – Sep. 22, 2013
Chao WEN Oct. 25, 2013 -

Visiting Scientists

Anna CORSI (CEA Saclay) Jun. 24, 2013 -
Alain GILLIBERT (CEA Saclay) Feb. 24, 2014 -
Yosuke KONDO (Graduate School, Tokyo Institute of Technology)

Attila KRASZNAHORKAY (ATOMKI) Mar. 15, 2014 -
Yohei MATSUDA (RCNP) May 1, 2013 -
Kenjiro MIKI (RCNP) Apr. 1, 2013 -
Dennis MUECHER (TU Munchen) Dec. 15, 2013 -
Takashi NAKAMURA (Graduate School, Tokyo Institute of Technology)
Kimiko SAKAGUCHI (Graduate School, Tohoku University)
Satoshi SAKAGUCHI (Kyusyu University)
Yasuhiro TOGANO (Graduate School, Tokyo Institute of Technology)
Takashi WAKUI (Tohoku University)
Takayuki YAMAGUCHI (Saitama University)

Visiting Technicians

Gilles AUTHELET (CEA Saclay) Jun. 25, 2013 -
Denis CALVET (CEA Saclay) Oct. 14, 2013 -
Frederic CHATEAU (CEA Saclay) Oct. 14, 2013 -
Alain DELBART (CEA Saclay) Oct. 14, 2013 -
Arnaud GIGANON (CEA Saclay) Oct. 14, 2013 -
Caroline LAHONDE-HAMDOUN (CEA Saclay) Oct. 14, 2013 -
Jean-Marc GHELLER (CEA Saclay) Jun. 25, 2013 -
Cedric PERON (CEA Saclay) Jun. 25, 2013 -
Alan PEYAUD (CEA Saclay) Oct. 14, 2013 -
Jean-Yves ROUSSE (CEA Saclay) Jun. 25, 2013 -

Research Consultant

Harutaka SAKAGUCHI

Interns

SungHan BAE Aug. 6, 2013 - Aug. 16, 2013
Sungha BAEK Aug. 6, 2013 - Aug. 16, 2013
JiHwan BHYUN Aug. 6, 2013 - Aug. 16, 2013
ZhenXing CHEN Aug. 6, 2013 - Aug. 16, 2013
Seungbum CHUNG Aug. 6, 2013 - Aug. 16, 2013
BaoShan HU Aug. 6, 2013 - Aug. 16, 2013
ZhiMeng HU Aug. 6, 2013 - Aug. 16, 2013
Wei JIANG Aug. 6, 2013 - Aug. 16, 2013
WeiGuang JIANG Aug. 6, 2013 - Aug. 16, 2013
JaeSung KIM Aug. 6, 2013 - Aug. 16, 2013
JinHa KIM Aug. 6, 2013 - Aug. 16, 2013
YoungHoon LIM Aug. 6, 2013 - Aug. 16, 2013
LanDiao LIU Aug. 6, 2013 - Aug. 16, 2013
FaFu NIU Aug. 6, 2013 - Aug. 16, 2013
Seongho SHIN Aug. 6, 2013 - Aug. 16, 2013
YiWen WEN Aug. 6, 2013 - Aug. 16, 2013
ZhaoRu ZHANG Aug. 6, 2013 - Aug. 16, 2013
TongKe ZHAO Aug. 6, 2013 - Aug. 16, 2013
WenJie ZHU Aug. 6, 2013 - Aug. 16, 2013

Student Trainees

Sergey Chebotaryov (Kyung pook National University) Jun. 30, 2013 – Jul. 15, 2014
Naruki INABA (University of Tsukuba) Apr. 1, 2013 -
Yuki ISHII (Kyoto University) Apr. 25, 2013 -
Tomomi KAWAHARA (Toho University) - Mar. 31, 2013
Tatsuo BABA (Kyoto University) Apr. 1, 2013 - Mar. 31, 2014
Taku FUKUNAGA (Kyusyu University) Apr. 1, 2013 - Mar. 31, 2014
Shota FUKUOKA (University of Tsukuba) Apr. 1, 2013 -
Tatsuya FURUNO (Kyoto University) Apr. 1, 2013 - Mar. 31, 2014
Shuhei GOTANDA (University of Miyazaki) Apr. 1, 2013 -
Tomosuke KADOYA (Tohoku University) - Mar. 31, 2013
Yoshihisa KANAYA (University of Miyazaki) Apr. 1, 2013 -
Junpei KOUNO (Saitama University) Apr. 1, 2013 - Mar. 31, 2014
Satoshi MATSUNAGA (Saitama University) Apr. 1, 2013 -
Ryogo MINAKATA (Tokyo Institute of Technology) Apr. 1, 2013 - Mar. 31, 2014
Hiroshi MIURA (Saitama University) May 27, 2013 -
Takuma NISHIMURA (Saitama University) May 27, 2013 -
Shun OGOSHI (Tokyo Institute of Technology) Apr. 1, 2013 - Mar. 31, 2014
Syunichirou OHMIKA (Saitama University) May 27, 2013 -
Muduki ONO (Saitama University) May 27, 2013 - Mar. 31, 2014
Kazuki SAWAHATA (Tokyo Institute of Technology) May 1, 2013 -

Mizuki SHIKATA (Tokyo Institute of Technology) May 1, 2013 -
Chihiro SHIMURA (Saitama University) May 27, 2013 - Mar. 31, 2014
Yuuta SHIOKAWA (Tohoku University) Apr. 1, 2013 - Mar. 31, 2014
Takahiro TAGUCHI (Tohoku University) - Mar. 31, 2014
Megumi TAKAHASHI (Tohoku University) - Mar. 31, 2013
Yuuki TAKEUCHI (Saitama University) May 27, 2013 -
Zhengyang TIAN (Peking University) - Mar. 31, 2014
Junichi TSUBOTA (Tokyo Institute of Technology) May 1, 2013 -
Miho TSUMURA (Kyoto University) Apr. 1, 2013 - Mar. 31, 2014
Yasunori WADA (Tohoku University) Apr. 1, 2013 - Mar. 31, 2014
Hidetomo WATANABE (Tohoku University) - Mar. 31, 2013
Junpei YASUDA (Kyusyu University) Apr. 1, 2013 -

Part-time workers

Tomomi KAWAHARA Apr. 1, 2013 -
Reiko KOJIMA - May 31. 2013

Assistant

Emiko ISOGAI
Yu Naya
Tomoko FUJII (- Mar. 31, 2013)

RIBF Research Division
Nuclear Spectroscopy Laboratory

1. Abstract

The group has conducted nuclear-physics studies utilizing stopped/slowed-down radioactive-isotope (RI) beams at the RIKEN RIBF facility based on the technique of nuclear spectroscopy that takes advantage of intrinsic nuclear properties such as nuclear spins, electromagnetic moments, and decay modes. In particular, by combining the techniques and devices for the production of spin-controlled RI beams to spectroscopic studies, high-sensitivity measurements to spin precessions/resonances have been conducted through a change in the angular distribution of radiations. The nuclear structures and properties of far-unstable nuclei are discussed based on thus determined spin-related observables. The methods are also applied to condensed matter studies, such as semiconductors, ferromagnets, fullerenes, and systems with dilute magnetic impurities, by exploiting RIs as microscopic probes.

2. Major Research Subjects

(1) Nuclear spectroscopy with stopped/slowed-down RI beams
(2) R&D studies on the production of spin-oriented RI beam
(3) Application of RI probes
(4) Fundamental physics: Study of symmetry

3. Summary of Research Activity

(1) Nuclear spectroscopy with stopped/slowed-down RI beams

Measurements of static electromagnetic nuclear moments over a substantial region of the nuclear chart have been conducted for structure studies on the nuclei far from the β-decay stability. Utilizing nuclear spin orientation phenomena of RIs created in the projectile-fragmentation reaction, ground- and excited-state nuclear moments of nuclei far from the stability have been determined by means of the β-ray-detected nuclear magnetic resonance (β-NMR) and γ-ray time differential perturbed angular distribution (γ-TDPAD) methods. To extend these observations to extremely rare RIs, a new method has been developed based on the laser spectroscopy which makes use of characteristic atomic properties of RIs surrounded by liquid helium.

(2) R&D studies on the production of spin-oriented RI beams

A new method has been developed for controlling spin in a system of rare RIs, taking advantage of the mechanism of the two-step projectile fragmentation reaction combined with the momentum-dispersion matching technique. This success allows us to utilize spin-controlled world's highest intensity rare RIBs delivered from BigRIPS for researches on the nuclear structure of species situated outside the traditional region of the nuclear chart. In parallel with this work, the development of a new apparatus to produce highly spin-polarized RI beams will be conducted by extending the atomic beam resonance method to fragmentation-based RI beams.

(3) Application of RI probes

The application of RI and heavy ion beams as a probe for condensed matter studies is also conducted by the group. The microscopic material dynamics and properties have been investigated through the deduced internal local fields and the spin relaxation of RI probes based on various spectroscopies utilizing RI probes such as the β-NMR/nuclear quadrupole resonance (NQR) methods, in-beam Mössbauer spectroscopy and the γ-TDPAC spectroscopy.

(4) Fundamental physics: Study of symmetry

The nuclear spins of stable and unstable isotopes sometimes play important roles in fundamental physics research. New experimental methods and devices have been developed for studies of the violation of time reversal symmetry (T-violation) using spin-polarized nuclei. These experiments aim to detect the small frequency shift in the spin precession arising from new mechanisms beyond the Standard Model.

Head

Hideki UENO (Chief Scientist)

Members

Yuichi ICHIKAWA (Oct. 1, 2013-) (Research Scientist)
Aiko NAKAO (May 1, 2013-) (Senior Research Scientist)

Research Consultant

Takuya OKADA

Visiting Scientists

Hisazumi AKAI (Osaka Univ.)
Koichiro ASAHI (Tokyo Tech)
Dimiter BALABANSKI (Bulgarian Academy of Sciences)
Takeshi FURUKAWA (Tokyo Metropolitan Univ.)
Atsushi HATAKEYAMA (Tokyo Univ. of Agriculture and Technology)
Yuichi ICHIKAWA (Tokyo Institute of Technology) - Sep. 30, 2013
Radomira LOZEVA (CNRS/IN2P3)
Yukari MATSUO (Hosei Univ.)

Kensaku MATSUTA (Osaka Univ.)
Takamasa MOMOSE (Kyoto Univ.)
Jiro MURATA (Rikkyo Univ.)
Wataru SATO (Kanazawa Univ.)
Makoto UCHIDA (Tokyo Tech)
Xiaolong WANG (Kyoto Univ.) -Mar. 31, 2014
Akihiro YOSHIMI (Okayama Univ.)

Junior Research Associates

Yoko ISHIBASHI (Univ. of Tsukuba) - Mar. 31, 2014
Kei IMAMURA (Meiji Univ.)

Student Trainees

Aleksey GLADKOV (Kyungpook National University) -Mar. 31, 2014
Miki HAYASAKA (Tokyo Gakugei Univ.)
Ryosuke KANBE (Osaka Univ.) -Mar. 31, 2014
Yuki KANNO (Tokyo Tech)
Shota KISHI (Tokyo Gakugei Univ.) -Mar. 31, 2014
Shuichiro KOJIMA (Tokyo Tech) -Mar. 31, 2014
Yuichi OHTOMO (Tokyo Tech) -Mar. 31, 2014
Tsubasa SAGAYAMA (Tokyo Gakugei Univ.) -Mar. 31, 2014
Yu SAKAMOTO (Tokyo Tech)
Tomoya SATO (Tokyo Tech)
Yonggeun SEON (Kyungpook National University)
Hazuki SHIRAI (Tokyo Tech) -Mar. 31, 2014
Takahiro SUZUKI (Tokyo Tech)
Masaomi TANAKA (Osaka Univ.)
Masato TSUCHIYA (Tokyo Tech)

Assistant

Emiko ISOGAI

RIBF Research Division
High Energy Astrophysics Laboratory

1. Abstract

In the immediate aftermath of the Big Bang, the beginning of our universe, only hydrogen and helium existed. However, nuclear fusion in the interior of stars and the explosion of supernovae in the universe over the course of 13.8 billion years led to the evolution of a world brimming with the many different elements we have today. By using man-made satellites to observe X-rays and gamma-rays emitted from celestial objects, we are observing the synthesis of the elements at their actual source. Our goal is to comprehensively elucidate the scenarios for the formation of the elements in the universe, together with our research on sub-atomic physics through the use of an accelerator.

2. Major Research Subjects

(1) Nucleosynthesis in Stars and Supernovae
(2) Particle Acceleration Mechanism in Astronomical Objects
(3) Physics in Extremely Strong Magnetism and Gravity
(4) Research and Development of Innovative X-ray and Gamma-ray detectors

3. Summary of Research Activity

High Energy Astrophysics Laboratory started on April 2010. The goal of our research is to reveal the mechanism of nucleosynthesis in the universe, and to observe exotic physical phenomena in extremely strong magnetic and/or gravitational field. We have observed supernova remnants, strongly magnetized neutron stars, pulsars, black holes and galaxies with X-ray astronomical satellites.

We showed that the expansion of ejecta in Tycho's supernova remnant was consistent with a spherically symmetric shell, based on Suzaku (Japanese X-ray observatory) measurements of the Doppler broadened X-ray emission lines. This is the first direct measurement of the expansion velocity of the elements produced in the thermonuclear expansion supernova. This information tells us the stratified structure of the elements, implying that the heavier elements such as Fe are produced deeper interior of the explosion.

We discovered the emission line of aluminum in supernova remnant G344.7-0.1 for the first time. Aluminum is produced in the neutron rich environment of supernova explosions. We also found manganese, which is enriched in the environment of neutron excess, in some supernova remnants. A systematic study of those lines emitted from the neutron rich elements will be a good tool to explore the nucleosynthesis in the interior of star explosions.

High-energy X-rays from radioactive Ti-44, which is a direct tracer of the supernova blast, was first imaged with the focusing telescope, NuSTAR. The map of Ti-44 in Cassiopeia A does not show spherical or axial symmetry, but asymmetry, supporting a mildly asymmetric explosion model with low-mode convection. This is the first astronomical image with nuclear gamma-rays and new observational evidence to understand the mechanism of supernova explosion and nucleosynthesis.

Gamma-ray emission up to 10 MeV was detected from thundercloud, suggesting that the detected gamma-rays were produced by relativistic electrons via bremsstrahlung. Those relativistic electrons are probably accelerated through an electrical potential difference in the thundercloud. This observation gives us a hint of the particle acceleration probably occurred near the neutron stars.

We continue to construct the Gravity and Extreme Magnetism Small Explorer (GEMS) under the collaboration with NASA Goddard Space Flight Center (USA). GEMS is the first dedicated satellite for the X-ray polarimetry, which is opening a new field in Astrophysics and Astronomy. The construction of an engineering model and basic performance studies of an X-ray polarimeter were carried out in FY2010, and the semiflight model of the detector was built in FY2012 and tested in FY2013. Unfortunately, NASA stops the GEMS project due to an expected cost overrun in 2012, but we will repropose the mission in 2014 with some modification. RIKEN will become a co-principal investigator institute and takes more responsibility on the X-ray polarimeter system and science.

Head
Toru TAMAGAWA (Associate Chief Scientist)

Contract Researcher
Goro SATO

Special Postdoctoral Researchers
Satoru KATSUDA
Shin'ya YAMADA
Asami HAYATO
Kumi ISHIKAWA

Postdoctoral Researcher
Takao KITAGUCHI

Visiting Scientists
Aya BAMBA (ISAS/JAXA)
Naohisa INADA (Univ. of Tokyo)

Madoka KAWAHARADA (ISAS/JAXA)
Atsushi SENDA (JST)
Poshak GANDHI (ISAS/JAXA)
Ken OHSUGA (NAOJ)
Toru MISAWA (Shinshu Univ.)
Yujin NAKAGAWA (Waseda Univ.)
Rohta TAKAHASHI (Tomakomai Nat'l College of Tech.)
Yukikatsu TERADA (Saitama Univ.)
Harufumi TSUCHIYA (JAEA)
Masaki WAKABAYASHI (Jakulin commercial company LC)
Hiroya YAMAGUCHI (CfA/Harvard Univ.)

Visiting Researchers (JSPS)
Teruaki ENOTO (Stanford Univ.)
Wataru IWAKIRI (Saitama Univ.)

Part-time Workers
Shigeru ENDO
Megu KUBOTA
Rie YOSHII

Student Trainees
Takanori IWAHASHI (Tokyo Univ. of Science)
Saori KONAMI (Tokyo Univ. of Science)
Wataru IWAKIRI (Saitama Univ.)
Fumi ASAMI (Tokyo Univ. of Science)
Kenta KANEKO (Kogakuin Univ.)
Kenichi IWATA (Shibaura Institute of Technology)
Megu KUBOTA
Yoko TAKEUCHI (Tokyo Univ. of Science)
Rie YOSHII (Tokyo Univ. of Science)
Akifumi YOSHIKAWA (Tokyo Univ. of Science)

Assistant
Yu NAYA

RIBF Research Division
Astro-Glaciology Research Unit

Our Astro-Glaciology Research Unit, organized in July 2011, promotes both theoretical and experimental studies to open up a new interdisciplinary research field between astrophysics and glaciology. On the theoretical side, we numerically simulate:

(1) Changes in the chemical composition of the stratosphere induced by high-energy photons and/or particles emitted from explosive astronomical phenomena, such as solar proton events and galactic supernovae, and

(2) The explosive nucleosynthesis, including the rapid neutron capture process (the r-process) for the creation of the elements heavier than iron, arising in the environment of core-collapse supernova explosions.

Subjects (1) and (2) themselves are very important in solar–terrestrial research and nuclear astrophysics, respectively; furthermore, the items (1) and (2) are intended to be coupled with experimental studies described below.

On the experimental side, we analyze the ice cores drilled at the Dome Fuji station in Antarctica in collaboration with the National Institute of Polar Research, Tokyo. These ice cores correspond to time capsules of the past. In particular, the ice cores obtained at Dome Fuji are known to be unique because they contain much more information on conditions in the stratosphere than any other ice cores recovered from other locations in either hemisphere. This means that the Dome Fuji ice cores may have an original advantage to study astronomical phenomena of the past, since γ-rays and high-energy protons emitted from astronomical events affect the chemical and isotopic compositions in the stratosphere and not those in the troposphere. Accordingly, we measure:

(3) Variations in the nitrate ion (NO_3^-) concentrations in the ice cores, in order to seek the proxy of past solar activity and the footprints of supernovae in our galaxy,

(4) Variations in the water isotopes (^{18}O and ^{2}H) in the ice cores, in order to reconstruct past temperature changes on the earth, and

(5) Variations in the nitrate isotope (^{15}N) in the ice cores, in order to investigate the possibility of this isotope becoming a new and a more stable proxy for solar activity and/or galactic supernovae.

Items (3), (4), and (5) have been analyzed with Dome Fuji ice cores with a temporal resolution of about 1 year. By comparing the results for items (3) and (4), we aim to understand the correlation between solar activity and climate changes in the past on the millennium scale. The basis for item (4) is already established in glaciology. Item (5) will be the one of very first measurements taken in ice cores. The theoretical studies related to items (1) and (2) will provide a background for distinguishing the characteristics of the astronomical events from meteorological noise that usually appears in the ice core data. Finally, we note that the supernova rate in our galaxy is crucial to understand the r-process nucleosynthesis but yet remains unknown. Our item (3) is also intended to diagnose the galactic supernova rate ultimately.

Head

Yuko MOTIZUKI (Research Unit Leader)

Members

Kazuya TAKAHASHI (Concurrent: Senior Research Scientist)
Yoichi NAKAI (Concurrent: Senior Research Scientist)

Contract Researcher

Kentaro SEKIGUCHI (- Mar. 31, 2013)

Postdoctoral Researcher

Sachiko OKAMOTO (- Mar. 31, 2014)

Visiting Scientists

Hideharu AKIYOSHI (National Institute for Environmental Studies)
Bradley MEYER (Clemson Univ., USA) - Mar. 31, 2013
Sachiko AMARI (Washington Univ.,USA) - Mar. 31, 2013
Akira HORI (Kitami Institute of Technology)
Hiroyuki KOURA (Japan Atomic Energy Agency) - Mar. 31, 2013
Hideki MADOKORO (Mitsubishi Heavy Industries, Ltd.)
Takahiro TACHIBANA (Waseda High Sch., Waseda Univ.) - Mar. 31, 2013
Kohji TAKAHASHI (Universite Libre de Bruxelles) - Mar. 31, 2013

Junior Research Associate

Satomi KIKUCHI (Saimata University) - Mar. 31, 2013

Student Trainees

Daiti SUZUKI - Mar. 31, 2013

Part-time Workers

Keiko FUKUSHIMA
Manami MARUYAMA
Yuri OBI

Ai TANEICHI

Assistants

Yoko FUJITA

Yuri TSUBURAI

RIBF Research Division
Research Group for Superheavy Element

1. Abstract

The elements with their atomic number Z>103 are called as trans-actinide or superheavy elements. The chemical properties of those elements have not yet been studied in detail. Those elements do not exist in nature. Therefore, they must be produced by artificially for the scientific study of those elements. In our laboratory, we have been studying the physical and chemical properties of the superheavy elements utilizing the accelerators in RIKEN and various methods of efficient production of the superheavy elements.

2. Major Research Subjects

(1) Search for new superheavy elements
(2) Decay spectroscopy of the heaviest nuclei
(3) Study of the chemical properties of the heaviest elements
(4) Study of the reaction mechanism of the fusion process (theory)

3. Summary of Research Activity

(1) Searching for new elements

To expand the periodic table of elements and the nuclear chart, we will search for new elements.

(2) Spectroscopic study of the nucleus of heavy elements

Using the high sensitivity system for detecting the heaviest element, we plan to perform a spectroscopic study of nuclei of the heavy elements.

(3) Chemistry of superheavy elements

Study of chemistry of the trans-actinide (superheavy element) has just started world-wide, making it a new frontier in the field of chemistry. Relativistic effects in chemical property are predicted by many theoretical studies. We will try to develop this new field.

(4) Study of a reaction mechanism for fusion process

Superheavy elements have been produced by complete fusion reaction of two heavy nuclei. However, the reaction mechanism of the fusion process is still not well understood theoretically. When we design an experiment to synthesize nuclei of the superheavy elements, we need to determine a beam-target combination and the most appropriate reaction energy. This is when the theory becomes important. We will try to develop a reaction theory useful in designing an experiment by collaborating with the theorists.

(5) Research Highlight

The discovery of a new element is one of the exciting topics both for nuclear physicists and nuclear chemists. The elements with their atomic number Z>103 are called as trans-actinides or superheavy elements. The chemical properties of those elements have not yet been studied in detail. Since those elements do not exist in nature, they must be produced by artificially, by using nuclear reactions for the study of those elements. Because the production rate of atoms of those elements is extremely small, an efficient production and collection are key issues of the superheavy research. In our laboratory, we have been trying to produce new elements, studying the physical and chemical properties of the superheavy elements utilizing the accelerators in RIKEN.

Although the Research Group for Superheavy element has started at April 2013, the Group is a renewal of the Superheay Element Laboratory started at April 2006, based on a research group which belonged to the RIKEN accelerator research facility (RARF), and had studied the productions of the heaviest elements. The main experimental apparatus is a gas-filled recoil ion separator GARIS. The heaviest elements with their atomic numbers, 107 (Bohrium), 108 (Hassium), 109 (Meitnerium), 110 (Darmstadtium), 111 (Roentogenium), and 112 (not yet named) were discovered as new elements at Helmholtzzentrum für Schwerionenforschung GmbH (GSI), Germany by using ^{208}Pb or ^{209}Bi based complete fusion reactions, so called “cold fusion” reactions. We have made independent confirmations of the productions of isotopes of 108th, 110th, 111th, and 112th elements by using the same reactions performed at GSI. After these work, we observed an isotope of the 113th element, ^{278}113, in July 2004, in April, 2005, and in August 2012. The isotope, ^{278}113, has both the largest atomic number, (Z = 113) and atomic mass number (A = 278) which have determined experimentally among the isotopes which have been produced by cold fusion reactions. We could show the world highest sensitivity for production and detection of the superheavy elements by these observations.

We decided to make one more recoil separator GARIS-II, which has an acceptance twice as large as existing GARIS, in order to realize higher sensitivity. The design of GARIS-II has finished in 2008. All fabrication of the separator will be finished at the end of fiscal year 2008. It will be ready for operation in fiscal year 2009 after some commissioning works.

Preparatory work for the study of the chemical properties of the superheavy elements has started by using the gas-jet transport system coupled to GARIS. The experiment was quite successful. The background radioactivity of unwanted reaction products has been highly suppressed. Without using the recoil separator upstream the gas-jet transport system, large amount of unwanted radioactivity strongly prevents the unique identification of the event of our interest. This new technique makes clean and clear studies of chemistry of the heaviest elements promising.

The spectroscopic study of the heaviest elements has started by using alpha spectrometry. New isotope, ^{263}Hs (Z=108), which has the smallest atomic mass number ever observed among the Hassium isotopes, had discovered in the study. New spectroscopic information for ^{264}Hs and its daughters have obtained also. The spectroscopic study of Rutherfordium isotope ^{261}Rf (Z=104) has done and 1.9-s isomeric state has directly produced for the first time.

Preparatory works for the study of the new superheavy elements with atomic number 119 and 120 have started in 2013. We measured the reaction products of the ^{248}Cm(^{48}Ca, xn)$^{296\text{-}x}$Lv(Z=116) previously studied by Frelov Laboratory of Nuclear Reaction, Russia, and GSI.

We observed 5 isotopes in total which tentatively assigned to ^{293}Lv, and ^{292}Lv.

Head
Kosuke MORITA (Group Director)

Visiting Scientist
Kunihiro FUJITA (Kyushu University) Nov. 1, 2013-

Student Trainees
Yoshihiro NARIKIYO
Taiki TANAKA - Mar 31, 2014
Shoya YAMAMOTO - Mar 31, 2014

Assistant
Yu NAYA

RIBF Research Division
Research Group for Superheavy Element
Superheavy Element Production Team

For this year, see the section of Research Group for Superheavy Element.

Head
Kosuke MORITA (Group Director)

Member
Kouji MORIMOTO (concurrent)

Nishina Center Research Scientist
Daiya KAJI (concurrent)

Nishina Center Technical Scientist
Akira YONEDA

Special Postdoctoral Researcher
Yasuo WAKABAYASHI

Visiting Scientist
Hiroyuki KOURA (JAEA)

Research Consultant
Kenji KATORI (- Mar. 31, 2014)

Part-time Worker
Kengo TANAKA

Students
Junior Research Associate
Mirei TAKEYAMA

Student Trainees
Yukiko KOMORI (Osaka Univ.) - Mar 31 ,2014
Takuya YOKOKITA (Osaka Univ.) - Mar 31 ,2014
Kengo TANAKA (concurrent)

RIBF Research Division
Research Group for Superheavy Element
Superheavy Element Device Development Team

1. Abstract

A gas-filled recoil ion separator has been used as a main experimental device for the study of superheavy elements. This team is in charge of maintain, improve, develop and operate the separators and rerated devices. There are two gas-filled recoil ion separators installed at RILAC experimental hall. One is GARIS that is designed for symmetric reaction such as cold-fusion reaction, and the other is newly developed GARIS-II that is designed for asymmetric reaction such as hot-fusion reaction. New element $^{278}113$ were produced by ^{70}Zn + ^{209}Bi reaction using GARIS. Further the new element search Z > 118 are preparing by using GARIS-II.

2. Major Research Subjects

(1) Maintenance of GARIS and development of new gas-filled recoil ion separator GARIS-II.
(2) Maintenance and development of detector and DAQ system for GARIS and GARIS-II.
(3) Maintenance and development of target system for GARIS and GARIS-II.

3. Summary of Research Activity

The GARIS-II is newly developed which has an acceptance twice as large as existing GARIS, in order to realize higher sensitivity. It will be ready for operation in fiscal year 2014 after some commissioning works. We will also offer user-support if a researcher wishes to use the devices for his/her own research program.

Head
Kouji MORIMOTO (Team Leader)

Nishina Center Research Scientist
Daiya KAJI

Nishina Center Technical Scientist
Akira YONEDA (concurrent)

Visiting Scientist
Fuyuki TOKANAI (Yamagata University)

Part-time Worker
Sayaka YAMAKI (- Mar. 31, 2014)

Student Trainee
Sayaka YAMAKI (concurrent)

RIBF Research Division
Accelerator Group

1. Abstract

The accelerator group, consisting of seven teams, pursues various upgrade programs of the world-leading heavy-ion accelerator facility, RI-Beam Factory (RIBF), to enhance the accelerator performance and operation efficiency. The programs include the R&D of superconducting ECR ion source, charge stripping systems, beam diagnostic devices, radiofrequency systems, control systems, and beam simulation studies. We are also maintaining the large infrastructure to realize effective operation of the RIBF, and are actively promoting the applications of the facility to a variety of research fields.

Our primary mission is to supply intense, stable heavy-ion beams for the users through effective operation, maintenance, and upgrade of the RIBF accelerators and related infrastructure. The director members shown below govern the development programs that are not dealt with by a single group, such as intensity upgrade and effective operation. We also promote the future plans of the RIBF accelerators along with other laboratories belonging to the RIBF research division.

2. Major Research Subjects

(1) Intensity upgrade of RIBF accelerators (Okuno)
(2) Effective and stable operation of RIBF accelerators (Fukunishi)
(3) Operation and maintenance of infrastructures for RIBF (Kase)
(4) Promotion of the future projects (Kamigaito, Fukunishi, Okuno)

3. Summary of Activity

(1) The stripping schemes for Xe and U beams have been renewed.
(2) The intensity of the xenon beam reached 38 pnA.
(3) The beam availability exceeded 90 %.
(4) The large infrastructure was properly maintained based on a well-organized cooperation among the related sections.
(5) A new upgrade plan was proposed for further enhancement of the beam intensity. Basic study is in progress.

Group Director
Osamu KAMIGAITO (Chief Scientist)

Deputy Group Directors
Hiroki OKUNO (Intensity upgrade)
Nobuhisa FUKUNISHI (Stable and efficient operation)
Masayuki KASE (Energy-efficiency management)

International Program Associate
Vasileios TZOGANIS (University of Liverpool)

Visiting Scientists
Akira GOTO (Yamagata University)
Toshiyuki HATTORI (Tokyo Institute of Technology)

Assistant
Karen SAKUMA

RIBF Research Division
Accelerator Group
Accelerator R&D Team

1. Abstract

We are developing the key hardware in upgrading the RIBF accelerator complex. Our primary focus and research is charge stripper which plays an essential role in the RIBF accelerator complex. Charge strippers remove many electrons in ions and realize efficient acceleration of heavy ions by greatly enhancing charge state. The intensity of uranium beams is limited by the lifetime of the carbon foil stripper conventionally installed in the acceleration chain. The improvement of stripper lifetimes is essential to increase beam power towards the final goal of RIBF in the future. We are developing the low-Z gas stripper. In general gas stripper is free from the lifetime related problems but gives low equilibrium charge state because of the lack of density effect. Low-Z gas stripper, however, can give as high equilibrium charge state as that in carbon foil because of the suppression of the electron capture process. Another our focus is the upgrade of the world's first superconducting ring cyclotron.

2. Major Research Subjects

(1) Development of charge strippers for high power beams (foil, low-Z gas)
(2) Upgrade of the superconducting ring cyclotron
(3) Maintenance and R&D of the electrostatic deflection/inflection channels for the beam extraction/injection

3. Summary of Research Activity

(1) Development of charge strippers for high power beams (foil, low-Z gas)

(Hasebe, H., Imao, H. Okuno., H.)

We are developing the charge strippers for high intensity heavy ion beams. We are focusing on the developments on carbon or berrilium foils and gas strippers including He gas stripper.

(2) Upgrade of the superconducting ring cyclotron

(Ohnishi, J., Okuno, H.)

We are focusing on the upgrade of the superconducting ring cyclotron.

(3) Maintenance and R&D of the electrostatic deflection/inflection channels for the beam extraction/injection

(Ohnishi, J., Okuno, H.)

We are developing high-performance electrostatic channels for high power beam injection and extraction.

Team Leader

Hiroki OKUNO (Deputy Group Director)

Members

Jun-ichi OHNISHI (Senior Technical Scientist)
Hiroshi IMAO (Research Scientist)

Nishina center Technical Scientist

Hiroo HASEBE

Special Postdoctoral Researcher

Hironori KUBOKI (- Mar. 31, 2014)

Visiting Scientists

Noriyosu HAYASHIZAKI (Tokyo Institute of Technology)
Mitsuhiro FUKUDA (RCNP, Osaka Univ.) - Mar. 31, 2013
Andreas ADELMANN (PSI, Switzerland)

Research Consultants

Yoshiaki CHIBA - Mar. 31, 2013
Isao YAMANE - Mar. 31, 2013

RIBF Research Division
Accelerator Group
Ion Source Team

1. Abstract

Our aim is to operate and develop the ECR ion sources for the accelerator-complex system of the RI Beam Factory. We focus on further upgrading the performance of the RI Beam Factory through the design and fabrication of a superconducting ECR heavy-ion source for production of high-intensity uranium ions.

2. Major Research Subjects

(1) Operation and development of the ECR ion sources
(2) Development of a superconducting ECR heavy-ion source for production of high-intensity uranium ions

3. Summary of Research Activity

(1) Operation and development of ECR ion sources

(T. Nakagawa, M. Kidera, Y. Higurashi, K. Ozeki, T. Nagatomo, H. Haba, and T. Kageyama)

We routinely produce and supply various kinds of heavy ions such as zinc and calcium ions for the super-heavy element search experiment as well as uranium ions for RIBF experiments. We also perform R&D's to meet the requirements for stable supply of high-intensity heavy ion beams.

(2) Development of a superconducting ECR ion source for use in production of a high-intensity uranium beam

(T. Nakagawa, J. Ohnishi, M. Kidera, Y. Higurashi, K. Ozeki and T. Nagatomo)

The RIBF is required to supply uranium beams with very high intensity so as to produce RI's. We have designed and are fabricating an ECR ion source with high magnetic field and high microwave- frequency, since the existing ECR ion sources have their limits in beam intensity. The coils of this ion source are designed to be superconducting for the production of high magnetic field. We are also designing the low-energy beam transport line of the superconducting ECR ion source.

Team Leader
Takahide NAKAGAWA

Member
Takeshi NAGATOMO (Technical Scientist)

Nishina Center Research Scientists
Masanori KIDERA
Yoshihide HIGURASHI

Contract Researcher
Kazutaka OHZEKI

Postdoctral Researcher
Tatsuya URABE (- Mar. 31, 2014)

Temporary Employee
Tadashi KAGEYAMA (- Mar. 31, 2014)

Part-time Worker
Yumi KURAMITSU

RIBF Research Division
Accelerator Group
RILAC Team

1. Abstract

The operation and maintenance of the RIKEN Heavy-ion Linac (RILAC) have been carried out. There are two operation modes: one is the stand-alone mode operation and the other is the injection mode operation. The RILAC has been used especially as an injector for the RIKEN RI- Beam Factory accelerator complex. The RILAC is composed of the ECR ion source, the frequency-variable RFQ linac, six frequency-variable main linac cavities, and six energy booster cavities (CSM).

2. Major Research Subjects

(1) The long term high stability of the RILAC operation.
(2) Improvement of high efficiency of the RILAC operation.

3. Summary of Research Activity

The RILAC was started to supply ion beams for experiments in 1981. Thousands hours are spent in a year for delivering many kinds of heavy-ion beams to various experiments.

The RILAC has two operation modes: one is the stand-alone mode operation delivering low-energy beams directly to experiments and the other is the injection mode operation injecting beams into the RRC. In the first mode, the RILAC supplies a very important beam to the nuclear physics experiment of "the research of super heavy elements". In the second mode, the RILAC plays a very important role as upstream end of the RIBF accelerator complex.

The maintenance of these devices is extremely important in order to keep the log-term high stability and high efficiency of the RILAC beams. Therefore, improvements are always carried out for the purpose of more stable and more efficient operation.

Team Leader
Eiji IKEZAWA

Member
Yutaka WATANABE (Senior Technical Scientist)

Research Consultants
Toshiya CHIBA (- Mar. 31, 2014)
Masatake HEMMI (- Mar. 31, 2014)

RIBF Research Division
Accelerator Group
Cyclotron Team

1. Abstract

Together with other teams of Nishina Center accelerator division, maintaining and improving the RIBF cyclotron complex. The accelerator provides high intensity heavy ions. Our mission is to have stable operation of cyclotrons for high power beam operation. Recently, stabilization of the rf system is a key issue to provide 10 kW heavy ion beam.

2. Major Research Subjects

(1) RF technology for Cyclotrons
(2) Operation of RIBF cyclotron complex
(3) Maintenance and improvement of RIBF cyclotrons
(4) Single turn operation for polarized deuteron beams
(5) Development of superconducting cavity for the rebuncher system

3. Summary of Research Activity

Development of the rf system for a reliable operation
Development of highly stabilized low level rf system
Development of superconducting rebuncher cavity
Development of the intermediate-energy polarized deuteron beams.

Team Leader
Naruhiko SAKAMOTO

Nishina Center Research Scientist
Kenji SUDA

Foreign Postdoctoral Researcher
Liang LU (-July 31, 2013)

Research Consultant
Yoshiaki CHIBA (-Mar.31, 2014)

RIBF Research Division
Accelerator Group
Beam Dynamics and Diagnostics Team

1. Abstract

The cascaded cyclotrons used in RIKEN RI Beam Factory (RIBF) requires not only severe matching of the beam but also high stability of all the accelerator components in order to establish stable operation of the world's most intense heavy-ion beams. Beam Dynamics and Diagnostics Team is responsible for power supplies, beam instrumentation, computer control and beam dynamic studies of the RIBF accelerator complex and strongly contributes to the performance upgrade of the RIBF.

2. Major Research Subjects

(1) Seeking the best operation method of the RIBF accelerator complex based on the beam dynamics study.
(2) Maintenance and development of the beam instrumentation, especially non-destructive monitors.
(3) Upgrade of the computer control system of the RIBF accelerator complex.
(4) Maintenance and improvements of the magnets and power supplies.

3. Summary of Research Activity

(1) The world-first beam current monitor with a high-Tc current sensor and SQUID has been developed.
(2) The bending power of the fixed-frequency Ring Cyclotron has been upgraded to 700 MeV. It enables us to accelerate $^{238}U^{64+}$ ions obtained by the helium gas stripper and contributes to stable and high-intensity operation of RIBF.
(3) An EPICS-based control system and a homemade beam interlock system have been stably working. Replacement of the existing legacy control system used in the old half of our facility is ongoing. Construction of the new control system for the new injector RILAC2 was successfully completed, where the embedded EPICS system running on F3RP61-2L CPU module, developed by KEK and RIKEN control group, was used.
(4) We replaced some dated power supplies of RIKEN Ring Cyclotron by new ones, which have better long-term stability than the old ones. The other existing power supplies (~900) are stably operated owing to elaborate maintenance work.
(5) We have contributed to RILAC2 construction, especially in its beam diagnosis, control system, magnet power supplies, vacuum system, high-energy beam transport system etc.

Team Leader

Nobuhisa FUKUNISHI (Deputy Group Director)

Members

Masaki FUJIMAKI (Senior Technical Scientist)
Keiko KUMAGAI (Senior Technical Scientist)
Tamaki WATANABE (Senior Technical Scientist)
Kazunari YAMADA (Senior Technical Scientist)

Nishina Center Technical Scientists

Misaki KOBAYASHI-KOMIYAMA
Akito UCHIYAMA

Postdoctral Researcher

Takuya MAEYAMA

Temporary Employee

Makoto NAGASE (- Mar. 31, 2014)

Visiting Scientists

Hiromichi RYUTO (Photonics and Electronics Science and Engineering Center, Kyoto University)
Jun-ichi ODAGIRI (Accelerator Laboratory, High Energy Accelerator Research Organization (KEK))
Shin-ichiro HAYASHI (Faculty of Health Science, Hiroshima International University) - Mar. 31, 2014

RIBF Research Division
Accelerator Group
Cryogenic Technology Team

1. Abstract

We are operating the cryogenic system for the superconducting ring cyclotron in RIBF. We are operating the helium cryogenic system in the south area of RIKEN Wako campus and delivering the liquid helium to users in RIKEN. We are trying to collect efficiently gas helium after usage of liquid helium.

2. Major Research Subjects

(1) Operation of the cryogenic system for the superconducting ring cyclotron in RIBF

(2) Operation of the helium cryogenic plant in the south area of Wako campus and delivering the liquid helium to users in Wako campus.

3. Summary of Research Activity

(1) Operation of the cryogenic system for the superconducting ring cyclotron in RIBF
(Okuno, H., Dantsuka, T., Nakamura, M., Maie, T.,)

(2) Operation of the helium cryogenic plant in the south area of Wako campus and delivering the liquid helium to users in Wako campus.
(Dantsuka, T., Tsuruma, S., Okuno, H.).

Team Leader
Hiroki OKUNO (Deputy Group Director)

Member
Masato NAKAMURA (Senior Technical Scientist)

Nishina Center Technical Scientist
Takeshi MAIE

Technical Staff-I
Tomoyuki DANTSUKA

Temporary Employee
Kumio IKEGAMI (- Mar. 31, 2014)

Part time Worker
Shizuho TSURUMA

RIBF Research Division
Accelerator Group
Infrastructure Management Team

1. Abstract

The RIBF facility is consisting of many accelerators and its infrastructure is very important in order to make an efficient operation of RIBF project. We are maintaining the infrastructure of the whole system and to support the accelerator operation with high performance. We are also concerning the contracts of gas- and electricity-supply companies according to the annual operation plan. The contracts should be reasonable and also flexible against a possible change of operations. And we are searching the sources of inefficiency in the operation and trying to solve them for the high-stable machine operation.

2. Major Research Subjects

(1) Operation and maintenance of infrastructure for RIBF accelerators.
(2) Renewal of the old equipment for the efficient operation.
(3) Support of accelerator operations.

Team Leader
Masayuki KASE (Deputy Group Director)

Members
Shu WATANABE (Senior Technical Scientist)
Hiromi YAMASAWA (Manager)

Research Consultant
Shin-ichi WATANABE (- Mar. 31, 2014)

Temporary Employee
Tadashi FUJINAWA (-Mar. 31, 2014)

Visiting Scientist
Hideshi MUTO (Tokyo Univ. of Sci. Suwa)

RIBF Research Division
Instrumentations Development Group

1. Abstract

This group develops core experimental installations at the RI Beam factory. Experimental installations currently under construction include designs containing common elements enabling multiple use (SLOWRI), as well as others that are highly program specific (SCRIT and Rare-RI Ring). All are designed to maximize the research potential of the world's most intense RI beams, made possible by the exclusive equipment available at the RI Beam Factory. Beam manipulation techniques, such as a beam accumulation and a beam cooling etc., will be able to provide opportunities of new experimental challenges and the foundation for future developments of RIBF.

2. Major Research Subjects

(1) SCRIT Project
(2) SLOWRI Project
(3) Rear RI Ring Project

3. Summary of Research Activity

We are developing beam manipulation technology in carrying out above listed project. They are the high-quality slow RI beam production (SCRIT and SLOWRI), the beam cooling and stopping (SCRIT and SLOWRI), and the beam accumulation technology (Rare RI Ring). The technological knowhow accumulated in our projects will play a significant role in the next generation RIBF. Future Plan for each project is described in subsections. SCRIT is now partially under construction and the system has been already tested using stable isotopes. ISOL system for SCRIT experiment (ERIS) is now under development. Rare RI Ring construction has been started in 2012 and we succeeded in the first beam circulation using alpha particle in this year. There are many things we have to do to make it ready for starting mass measurement, but it is now ready for operation. SLOWRI is now under construction.

Group Director
Masanori WAKASUGI

Senior Visiting Scientist
Akira OZAWA

Student Trainees
Saki MATSUO
Yohei SUMI
Mamoru TOGASAKI

Assistants
Yoshiko SAKATA
Noriko KIYAMA

RIBF Research Division
Instrumentations Development Group
SLOWRI Team

1. Abstract

Construction of a next-generation stopped and low-energy radioactive ion beam facility (SLOWRI) which will provide low-energy, high-purity and small emittance ion beams of all elements has been started in FY2013 as one of the principal facilities at the RIKEN RI-beam factory (RIBF). High-energy radioactive ion beams from the projectile fragment separator BigRIPS are thermalized in a large He gas catcher cell (RFC cell) or in a small Ar gas catcher cell (PALIS cell). In the RFC cell, thermalized ions in buffer gas are guided and extracted to a vacuum environment by a combination of dc electric fields and inhomogeneous rf fields (rf carpet ion guide). The PALIS cell will be placed in the vicinity of the second focal plane slits of BigRIPS and can be used continuously during other experiments. From these gas cells, the low-energy ion beams will be delivered via mass separators and switchyards to various devices: such as an ion trap, a collinear fast beam apparatus, and a multi-reflection time of flight mass spectrograph. In the R&D works at the present ring cyclotron facility, an extraction efficiency of 33% for a 100A MeV ^{8}Li ion beam from the projectile fragment separator RIPS was achieved and the dependence of the efficiency on the ion beam intensity was investigated.

First spectroscopy experiment at the prototype SLOWI was performed on Be isotopes. Energetic ions of ^{7,10,11}Be from the RIPS were trapped and laser cooled in a linear rf trap and precision spectroscopy was performed. The evaluated ion temperature of <10 mK demonstrates that a reduction of more than 15 orders of magnitude for the kinetic energy of radioactive Be was achieved online. The ground state hyperfine constants of all Be isotopes have been measured precisely by laser and microwave. These precision measurements will be used to confirm the anomalous mean radius of the valence neutron of the so called neutron halo nucleus. Other laser spectroscopy experiments using the slow RI-beams are also under progress in off-line setups. A collinear fast beam apparatus for nuclear charge-radii measurements was build and tested with stable Ar^{+} ion beams.

A multi-reflection time-of-flight mass spectrograph (MRTOF) has been developed and tested online for radioactive lithium isotope, ^{8}Li. A high mass resolving power of 170,000 has been obtained for an isobaric doublet of ^{40}K and ^{40}Ca with a very short flight time of 2 ms. This performance allowed accurate mass determination of $<10^{-7}$ accuracy by a single isobaric reference. Two mass measurement projects using MRTOF mass spectrographs have been started: one is for trans uranium elements at the GARIS facility and the other is for r-process nuclides at SLOWRI facility.

Resonance ionization spectroscopy has been tested during the offline development of PALIS gas cell. Stable isotopes of Co, Cu, Fe, Ni, Ti, Nb, Sn, In, and Pd were resonantly ionized by excimer pumped dye lasers or Nd:YAG laser pumped Ti:Sapphire lasers with the prototype gas cell setup. The resonance spectra are in many cases sufficient to resolve the hyperfine structures. Nuclear spins and magnetic moments will be determined for various isotopes obtained during other experiments.

2. Major Research Subjects

(1) Construction of stopped and low-energy RI-beam facility, SLOWRI.
(2) Laser spectroscopy of trapped radioactive Beryllium isotopes.
(3) Development of a multi-reflection time-of-flight mass spectrograph for precision mass measurements of short-lived nuclei.
(4) Development of parasitic slow RI-beam production method using resonance laser ionization.
(5) Development of ion-surfing gas cell.

3. Summary of Research Activity

(1) Construction of stopped and low-energy RI-beam facility (SLOWRI)

(WADA, Michiharu, SONODA, Tetsu, KATAYAMA, Ichiro, SCHURY, Peter, ITO, Yuta, ARAI, Fumiya, ARAI, Shigeaki, KUBO, Toshiyuki, KUSAKA, Kensuke, FUJINAWA Tadashi, MAIE Takeshi, YAMASAWA Hideyuki, WOLLNIK, Hermann,)

Installation of SLOWRI has been started in FY2013. It consists of two gas catchers (RF Carpet gas cell and PALIS gas cell), mass separators a 50-m beam transport line, a beam cooler-buncher, an isobar separator, and a laser system. The RFCarpet gas cell will be installed at the exit of the D5 dipole magnet of BigRIPS. The gas catcher contains a large cryogenic He gas cell with a large traveling wave rf-carpet. It will convert main beams of BigRIPS to low-energy, low-emittance beams without any restrictions on the chemical properties of the elements. The PALIS gas cell will be installed in the vicinity of the second focal plane slit of BigRIPS. It will provide parasitic RI-beams from those ions lost in the slits during other experiments. In this gas catcher, thermalized RI ions quickly become neutral and will be re-ionized by resonant laser radiations. These gas catchers will be tested off-line in FY2014. The 50 m beam transport line consists of four dipole magnets (SD1 to SD4), two focal plane chambers, 62 electrostatic quadrupole singlets, 11 electrostatic quadrupole quartets (EQQ1 to EQQ11) and 7 beam profile monitors (BPM). SD1 and SD2, located right after the gas catchers will be used for isotope separation. After eliminating contaminant ions at the focal plane chamber, the low energy beam will be transported by FODO lattice structure with phase space matching using EQQs. The EQQs have multipole elements made of 16 rods on which various potentials can be applied to produce 6-pole and 8 pole fields, simultaneously, for compensation of ion optical aberrations. This multipole element can also produce dipole fields for steering and scanning the beam. The BPM have a classical cross-wire beam monitor as well as a channel electron multiplier with a pinhole collimator. Combining the scanning capability of the EQQs and the pinhole detector, we can observe a beam profile even for a very low-intensity RI-beams. Off- and on-line commissioning will take place in FY2014 and the low-energy RI-beams will be provided for users in FY2015.

(2) Laser spectroscopy of trapped radioactive beryllium isotope ions

(WADA, Michiharu, TAKAMINE, Aiko, SCHURY Peter, SONODA Tetsu, OKADA, Kunihiro, KANAI, Yasuyuki, YOSHIDA, Atsushi, KUBO, Toshiyuki, WOLLNIK, Hermann, SCHUESSLER, Hans, Shunsuke, KATAYAMA Ichiro)

As a first application of the prototype SLOWRI setup, we applied hyperfine structure spectroscopy to the beryllium isotopes to determine in particular the anomalous radius of the valence neutron of the neutron halo nucleus ^{11}Be, and to determine the charge radii of these beryllium isotopes through laser-laser double resonance spectroscopy of laser-cooled ions. Laser cooling is an essential prerequisite for these planned experiments. The first laser spectroscopy experiments for beryllium isotopes were performed to measure the resonance frequencies of 2s $^2S_{1/2}$ - 2p $^2P_{3/2}$ transition of ^{7}Be+, ^{9}Be+, ^{10}Be$^+$ and ^{10}Be+ ions and the nuclear charge radii of these isotopes were determined. The hyperfine structures of ^{11}Be$^+$ and ^{7}Be$^+$ ions using the laser-microwave double resonance spectroscopy were also performed and the magnetic hyperfine constants of ^{7}Be$^+$ and ^{11}Be$^+$ ions were determined with accuracies of better than10^{-7}.

(3) Development of a multi-reflection TOF mass spectrograph for short-lived nuclei

(WADA, Michiharu, SCHURY Peter, ITO, Yuta, ARAI Fumiya, SONODA Tetsu, WOLLNIK, Hermann, MORIMOTO, Koji, KAJI, Daiya, HABA, Hiromitsu, KOURA, Hiroyuki)

The atomic mass is one of the most important quantities of a nucleus and has been studied in various methods since the early days of physics. Among many methods we chose a multi-reflection time-of-flight (MR-TOF) mass spectrometer. Slow RI beams extracted from the RF ion-guide are bunch injected into the spectrometer with a repetition rate of ~100 Hz. The spectrometer consists of two electrostatic mirrors between which the ions travel back and forth repeatedly. These mirrors are designed such that energy-isochrononicity in the flight time is guaranteed during the multiple reflections while the flight time varies with the masses of ions. A mass-resolving power of 170,000 has been obtained with a 2 ms flight time for 40K and 40Ca isobaric doublet. This mass-resolving power should allow us to determine ion masses with an accuracy of 10^{-7}. An online mass measurement for radioactive lithium isotope has been carried out at the prototype SLOWRI setup.

The MR-TOF mass spectrograph has been placed under the GARIS-II separator aiming at direct mass measurements of trans-uranium elements. A small cryogenic gas catcher cell will be placed at the focal plane box of GARIS-II and a bunched low-energy heavy ion beam can be transported to the trap of MR-TOF. An online commissioning experiment is planned in FY2014.

(4) Development of collinear fast beam apparatus for nuclear charge radii measurements

(WADA, Michiharu, SCHUESSLER, Hans, IIMURA, Hideki, SONODA, Tetsu, SCHURY, Peter, TAKAMINE, Aiko, OKADA, Kunihiro, WOLLNIK, Hermann)

The root-mean-square charge radii of unstable nuclei have been determined exclusively by isotope shift measurements of the optical transitions of singly-charged ions or neutral atoms by laser spectroscopy. Many isotopes of alkaline, alkaline-earth, noble-gases and several other elements have been measured by collinear laser spectroscopy since these ions have all good optical transitions and are available at conventional ISOL facilities. However, isotopes of other elements especially refractory and short-lived ones have not been investigated so far.

In SLOWRI, isotopes of all atomic elements will be provided as well collimated mono-energetic beams. This should expand the range of applicable nuclides of laser spectroscopy. In the first years of the RIBF project, Ni and its vicinities, such as Ni, Co, Fe, Cr, Cu, Ga, Ge are planned to be investigated. They all have possible optical transitions in the ground states of neutral atoms with presently available laser systems. Some of them have so called recycle transitions which enhance the detection probabilities noticeably. Also the multistep resonance ionization (RIS) method can be applied to the isotopes of Ni as well as those of some other elements. The required minimum intensity for this method can be as low as 10 atoms per second.

We have built an off-line mass separator and a collinear fast beam apparatus with a large solid-angle fluorescence detector. A 617 nm transition of the metastable Ar+ ion at 20 keV was measured with both collinear and anti-collinear geometry that allowed us to determine the absolute resonant frequency of the transition at rest with more than 10^{-8} accuracy. Such high accuracy measurements for Ti and Ni isotopes are in progress.

(5) Development of parasitic slow RI-beam production scheme using resonance laser ionization

(SONODA Tetsu, IIMURA Hideki, WADA Michiharu, KATAYAMA Ichiou, ADACHI Yoshitaka, NOTO Takuma, TAKATSUKA Takaaki, TOMITA Hideki, WENDT Klaus, ARAI Fumiya, ITOU Yuta, SCHURY Peter, FUKUDA Naoki, INABE Naohito, KUBO Toshiyuki, KUSAKA Kensuke, TAKEDA Hiroyuki, SUZUKI H., WAKASUGI Masanori, YOSHIDA Koichi)

More than 99.9% of RI ions produced in projectile fission or fragmentation are simply dumped in the first dipole magnet and the slits. A new scheme, named PALIS, to rescue such dumped precious RI using a compact gas catcher cell and resonance laser ionization was proposed as a part of SLOWRI. The thermalized RI ions in a cell filled with Ar gas can be quickly neutralized and transported to the exit of the cell by gas flow. Irradiation of resonance lasers at the exit ionizes neutral RI atoms efficiently and selectively. The ionized RI ions can be further selected by a magnetic mass separator and transported to SLOWRI experimental area for various experiment. The resonance ionization scheme itself can also be a useful method to perform hyperfine structure spectroscopy of RI of many elements.

A prototype setup has been tested for resonance ionization scheme of several elements, extraction from the cell, and transport to a high vacuum chamber. An online setup, which will be placed at the second focal plane (F2) of BigRIPS, has been fabricated in FY2013 and commissioning is scheduled in FY2014.

Team Leader
Michiharu WADA

Member
Hideyuki YAMAZAWA (concurrent)

Nishina Center Research Scientists
Tetsu SONODA
Kensuke KUSAKA (concurrent)

Nishina Center Technical Scientist
Takeshi MAIE (concurrent)

Contract Researcher
Peter SCHURY

Research Associate
Yuta ITO (- Mar. 31, 2014)

Research Consultant
Hirokane KAWAKAMI (- Mar. 31, 2014)

Visiting Scientists
Hideki IIMURA (Japan Atomic Energy Agency)
Kunihiro OKADA (Sophia University)
Hans SCHUESSLER (Texas A&M University)
Aiko TAKAMINE (Aoyama Gakuin University) - Mar. 31, 2014
Hideki TOMITA (Graduate School of Engineering, Nagoya University)
Klaus WENDT -Mar. 31, 2014
Hermann WOLLNIK (University of Giessen) - Mar. 31, 2014

Part-time Workers
Shigeaki ARAI
Ichirou KATAYAMA
Tadashi FUJINAWA (-Mar. 31, 2014)

Student Trainees
Takuma NOTO
Takaaki TAKATSUKA - Mar. 31, 2014
Fumiya ARAI
Yoshitaka ADACHI - Mar. 31, 2014
Takahide TAKAMATSU - Mar. 31, 2014

RIBF Research Division
Instrumentations Development Group
Rare RI-ring Team

1. Abstract
Mass measurement is one of the most important contributions to a nuclear property research especially for short-lived unstable nuclei far from the beta-stability line. In particular, a high-precision mass measurement for nuclei located around the r-process pass (rare-RI) is required in nucleosynthesis point of view. We chose a method of isochronous mass spectrometry (IMS) to make a measurement time shorter than 1 ms. Heavy-ion storage ring named “Rare-RI RIng (R3)” is now under construction at RIKEN RI Beam Factory. Our target performance in the mass determination is to achieve an accuracy of the order of 10^{-6} (~100 keV) even if we get only one event. Since an isochronism in R3 is established over a wide range of the momentum, rare-RIs with a large momentum spread, $\Delta p/p=0.5$ %, are acceptable. Another significant feature of the R3 system is an individual injection scheme in which a produced rare-RI itself triggers the injection kicker. Design study for R3 has been continued from more than ten years ago, and the construction has been started in 2012. Construction of the infrastructures and fabrication of major parts of hardware relating to R3 have already been roughly completed. We are now setting up and testing all equipment including the power supplies, the control system, the vacuum system, and so on, toward the first commissioning planed in 2014.

2. Major Research Subjects
Developments of isochronous storage ring to measure mass of rare RI.

3. Summary of Research Activity
Since the lattice design of R3 is based on the cyclotron motion, it can provide an isochronism in a wide range of the momentum. We expect a great improvement in mass resolution in IMS as long as the isochronous field is precisely formed in R3. Therefore, IMS using R3 is capable of both a high-precision measurement and a fast measurement. All the devices in R3 was designed under the assumption that an incoming beam has an energy of 200 MeV/u and a charge to mass ratio, m/q, of less than 3. The ring structure was designed with a similar concept of a separate-sector ring cyclotron. It consists of six sectors and 4.02-m straight sections, and each sector consists of four rectangular bending magnets. They are reused magnets used in TARN-II, which was constructed at INS Tokyo University more than 20 years ago. A radially homogeneous magnetic field is produced in the magnet, and a magnetic rigidity is 6.5 Tm at maximum. Main coils of all the bending magnets are connected in series, and the current of 3000 A is required for rare-RIs, for instance, ^{78}Ni with the magnetic rigidity of 5.96 Tm. Two magnets at both ends of each sector are additionally equipped with ten trim coils to form a precise isochronous magnetic field. For $\Delta p=0$ particle, the circumference is 60.35 m and the betatron tunes are $\nu x=1.21$ and $\nu y=0.84$ in horizontal and vertical directions, respectively. The momentum acceptance is $\Delta p/p=0.5$ % and the transverse acceptances are 20π mmmrad and 10π mmmrad in horizontal and vertical directions, respectively. Although the transverse acceptances of the R3 itself are actually larger than these values, they are limited by that of the injection beam line. Of special note is that the isochronism is precisely fulfilled in a wide range of momentum (full width 1 %) due to a cyclotron-motion based lattice design.

Another performance required for R3 is to efficiently seize hold of an opportunity of the measurement for rare-RIs produced unpredictably. We adopted an individual injection scheme in which the produced rare-RI itself triggers the injection kicker magnets. Full activation of the kicker magnetic field has to be completed within the flight time of the rare-RI from an originating point of the trigger signal to the kicker position in R3. Development of an ultra-fast response kicker system is a key issue for establishing the individual injection scheme. Performances required for the kicker system are an ultra-fast response, a fast charging, and a full-time charging. Output current of our kicker power supply rises at 250 ns and the center of the flat top of the magnetic field is at smaller than 500 ns from the trigger input.

We provided ordinary beam diagnostic devices such as a screen monitor and a beam position monitor based on triangle pickup electrodes. Although five sets of these monitors distributed along the orbit in R3 are useful in a machine tuning process using a high-intensity primary beam. They, however, are incapable for rare-RIs because of the poor sensitivity. Therefore, we inserted high-sensitive monitors, which are applicable even for a single particle circulation. One of them is a cavity type of Schottky pick-up. A resonance frequency is designed to be 172 MHz, which corresponds to the harmonic number of 56, and a measured quality factor is over 7000 and shunt impedance is 400 kΩ. We can detect single ion circulation of $^{78}Ni^{28+}$ with only a few ms measurement. Another is a timing monitor, which detects secondary electrons emitted from thin carbon foil placed on the accumulation orbit. The thickness of the foil will be 50 μg/cm^2. The rare-RI with the energy of 200 MeV/u survives only for first 1000 turns because of an energy loss at the foil.

Major components of R3 have already been fabricated and the ring components were precisely arraigned. We are now setting up and testing every device individually, and we advance all preparations towards the commissioning scheduled in 2014.

Team Leader
Masanori WAKASUGI (Group Director)

Members
Tamaki WATANABE (concurrent)
Yutaka WATANABE (concurrent)
Naohito INABE (concurrent)
Yoshiyuki YANAGISAWA (concurrent)
Hideyuki YAMAZAWA (concurrent)

Nishina Center Research Scientist
Yoshitaka YAMAGUCHI

Nishina Center Technical Scientists
Takeshi MAIE (concurrent)
Misaki KOMIYAMA (concurrent)

Junior Research Associate
Yasushi ABE (University of Tsukuba)

Visiting Scientists
Daisuke NAGAE (Inst. Phys., Univ.of Tsukuba)
Tetsuro KOMATSUBARA (University of Tsukuba) - Mar. 31, 2014

Research Consultant
Akira NODA (- Mar. 31, 2014)

Student Trainees
Ayano ENOMOTO
Shunsuke OKADA - Mar. 31, 2014
Yuta SAITO - Mar. 31, 2014

RIBF Research Division
Instrumentations Development Group
SCRIT Team

1. Abstract

The SCRIT Electron Scattering Facility is now under construction at RIKEN RIBF. This aims at investigation of internal nuclear structure for short-lived unstable nuclei by means of electron scattering. SCRIT (Self-Confining RI Ion Target) is a novel method to form internal targets in an electron storage ring. This technique has made electron scattering experiments for unstable nuclei possible. Construction of the facility has been started in 2009. This facility consists of an electron accelerator (RTM), a SCRIT-equipped electron storage ring (SR2), an electron-beam-driven RI separator (ERIS), and a detector system for scattered electrons. Operation of accelerators, RTM and SR2, was started in 2010, performance test of the SCRIT system using stable isotopes, ^{133}Cs and ^{132}Xe, was successfully done in 2011 and 2012. Construction of ERIS was started in 2011 and it was commissioned in 2012. The first RI beams from ERIS were supplied in 2013, and the ion source is now under improvement. The detector system consisting of a high-resolution magnetic spectrometer, drift chambers, trigger scintillators, and luminosity monitors is now under construction. We are going to perform the first experiment of electron scattering from unstable nuclei within a fiscal year 2014.

2. Major Research Subjects

Development of SCRIT electron scattering technique and construction of the SCRIT electron scattering facility.

3. Summary of Research Activity

Development of an electron scattering experimental system for short-lived unstable nuclei using a novel internal target of unstable nuclei (SCRIT).

(Wakasugi, Ohnishi, Kurita, Suda, Tamae, Hori, Hara, Ichikawa)

SCRIT is novel technique to form internal target in an electron storage ring. Positive ions are confined in the electron beam axis by transverse focusing force given by the circulating electron beam. This is well known "ion trapping" phenomenon. The created ion cloud in which RI ions injected from outside are confined works as a target of electron scattering.

In 2010, we successfully commissioned electron accelerators RTM and SR2. Current of electron beams stored in SR2 and its storage lifetime have been reached to 300 mA and 2 hours, respectively, in the energy range of 150-300 MeV that is required in electron scattering experiments. In test experiments of the SCRIT system performed in 2011 and 2012, we used stable isotopes, ^{133}Cs and ^{132}Xe, and revealed many details of the SCRIT performance. The luminosity of 10^{27} /(cm^{2}s) was obtained in case of the number of injected ions of 10^8. The lifetime of the ion confinement was obtained to be over 1 s. They are performances satisfactory to the electron scattering experiment. In fact, we succeeded in measurements of angular distributions of scattered electrons from the target ions trapped in the SCRIT device.

Development of ERIS is one of the most important issues in the facility construction. RIs are generated by photo-fission process of ^{238}U, which is driven by the 150-MeVelectron beams from RTM. ERIS consists of a target ion source including UCx targets and a mass separation system. ERIS was constructed in 2011 and performances such as the extraction efficiency of 21 % and the mass resolving power of 1660 were obtained in the commissioning in 2011. We developed production method of UCx targets by ourselves. The first RI production was succeeded in last year, and $^{126\text{-}132}$Sn and $^{138\text{-}141}$Xe isotopes were extracted. Since the yield of extracted RIs is still below our expectation and there is some problem in durability of the ion source, the target ion source is now under improvement. A cooler buncher system connected to the ERIS beam line is indispensable, because the continuous beam from ERIS has to be converted to pulsed beam for ion injection to the SCRIT device. We are now developing the cooler buncher based on a RFQ linear trap. This was constructed in 2013 and is now under testing offline. This will be installed within this year.

In last year, we constructed a new detector for scattered electrons. This consists of a high-resolution magnetic spectrometer, a beam tracking system using drift chambers, trigger scintillators, and a luminosity monitor. This has a solid angle of 100 msr, energy resolution of 10^{-3}, and the scattering angle coverage of 30-60 degrees. A wide range of momentum transfer, 80-300 MeV/c, is covered by changing the electron beam energy from 150 to 300 MeV. This detector system is now under setting up offline and they are expected to be available soon.

Team Leader

Masanori WAKASUGI (Group Director)

Member

Tetsuya OHNISHI (Senior Technical Scientist)

Senior Visiting Scientist

Toshitada HORI (Hiroshima University)

Visiting Scientists

Toshimi SUDA (Research Center of Electron Photon Science, Tohoku Univ.)

Shuo WANG (Research Center of Electron Photon Science, Tohoku Univ.) - Jun. 30, 2013

Research Consultants

Takeshi EMOTO (-Mar. 31, 2014)
Shin-ichi ICHIKAWA (-Mar. 31, 2014)
Masahiro HARA (-Mar. 31, 2014)
Tadaaki TAMAE (-Mar. 31, 2014)

Student Trainees

Takaya MIYAMOTO - Mar. 31, 2014
Yuto SHIMAKURA - Mar. 31, 2014
Yuji HARAGUCHI
Shunpei YONEYAMA
Teruaki TSURU

RIBF Research Division
Research Instruments Group

1. Abstract

The research instruments group is the driving force at RI Beam Factory (RIBF) for continuous enhancement of activities and competitiveness of experimental research. Consisting of five teams, we are in charge of the design, construction, operation and improvement of the core research instruments at RIBF, such as BigRIPS separator, ZeroDegree spectrometer, GARIS spectrometer and SAMURAI spectrometer, and the related infrastructure and equipment. The group also conducts related experimental research as well as R&D studies on the research instruments.

2. Major Research Subjects

Design, construction, operation and improvement of the core research instruments at RIBF and related R&D studies. Experimental studies on exotic nuclei

3. Summary of Research Activity

The current research subjects are summarized as follows:

(1) Design, construction, operation, and improvement of the core research instruments at RIBF and their related infrastructure and equipment for continuous enhancement of activities and competitiveness of experimental research
(2) R&D studies on technical issues of the core research instruments and related equipment at RIBF
(3) Experimental research on exotic nuclei using the core research instruments at RIBF

Group Director
Toshiyuki KUBO

Senior Visiting Scientist
Toshio KOBAYASHI (Tohoku University)

Junior Research Associate
Daichi MURAI

Student Trainee
Katrina KOEHLER

Research Supporting Staff (part time Worker)
Meiko UESAKA

Assistant
Emiko ISOGAI

RIBF Research Division
Research Instruments Group
BigRIPS Team

1. Abstract

This team is in charge of design, construction, development and operation of BigRIPS in-flight separator and its related research instruments at RI beam factory (RIBF). They are employed not only for the production of RI beams but also the experimental studies using RI beams.

2. Major Research Subjects

Design, construction, development and operation of BigRIPS in-flight separator, RI-beam transport lines, and their related research instruments.

3. Summary of Research Activity

This team is in charge of design, construction, development and operation of BigRIPS in-flight separator, RI-beam transport lines, and their related research instruments such as ZeroDegree spectrometer at RI beam factory (RIBF). They are employed not only for the production of RI beams but also various kinds of experimental studies using RI beams.

The research subjects may be summarized as follows:

(1) General studies on RI-beam production using in-flight scheme.
(2) Studies on ion-optics of in-flight separators, including particle identification of RI beams
(3) Simulation and optimization of RI-beam production.
(4) Development of beam-line detectors and their data acquisition system.
(5) Experimental studies on production reactions and unstable nuclei.
(6) Experimental studies of the limits of nuclear binding.
(7) Development of superconducting magnets and their helium cryogenic systems.
(8) Development of a high-power production target system.
(9) Development of a high-power beam dump system.
(10) Development of a remote maintenance and remote handling systems.
(11) Operation, maintenance and improvement of BigRIPS separator system, RI-beam transport lines and their related research instruments such as ZeroDegree spectrometer and so on.
(12) Experimental research using RI beams.

Team Leader
Koichi YOSHIDA

Members
Naohito INABE (Senior Technical Scientist)
Masao OHTAKE (Senior Technical Scientist)
Yoshiyuki YANAGISAWA (Senior Research Scientist)
Kanenobu TANAKA (concurrent)

Nishina Center Research Scientists
Kensuke KUSAKA
Naoki FUKUDA
Hiroyuki TAKEDA

Contract Researcher
Daisuke KAMEDA

Postdoctoral Researchers
Deuk Soon AHN
Hiroshi SUZUKI

Part-time Worker
Hidekazu KUMAGAI (- Mar. 31, 2014)

Senior Visiting Scientist
Jerry NOLEN (ANL)

Visiting Scientists
Bradley SHERRILL (NSCL, Michigan State Univ., USA)

Daniel BAZIN (NSCL, Michigan State Univ., USA)
Oleg TARASOV (NSCL, Michigan State Univ., USA)
David MORRISSEY (NSCL, Michigan State Univ., USA)
Mauricio PORTILLO (NSCL, Michigan State Univ., USA)
Hans GEISSEL (GSI, Germany)
Martin WINKLER (GSI, Germany)
Michael FAMIANO (Western Michigan Univ., USA)
Yutaka MIZOI (Osaka Electro-Commnication Univ.)
Naohito IWASA (Tohoku Univ.)
Sadao MOMOTA (Kochi University of Technology)
Kazuo IEKI (concurrent) (Rikkyo Univ.) - Mar. 31, 2013

Student Trainee

Yohei OHKODA (Tohoku Univ.) - Mar. 31, 2014

RIBF Research Division
Research Instruments Group
SAMURAI Team

1. Abstract

In collaboration with research groups in and outside RIKEN, the team designs, develops and constructs the SAMURAI spectrometer and relevant equipment that are and will be used for reaction experiments using RI beams at RI Beam Factory. The SAMURAI spectrometer consists of a large superconducting dipole magnet and a variety of detectors to measure charged particles and neutrons. After the commissioning experiment in March 2012, the team prepared and conducted, in collaboration with researchers in individual experimental groups, the first series of experiments with SAMURAI in May 2012. The team also provides basis for research activities by, for example, organizing collaboration workshops by researchers who are interested in studies or plan to perform experiments with the SAMURAI spectrometer.

2. Major Research Subjects

Design, operation, maintenance and improvement of the SAMURAI spectrometer and its related research instruments.
Help and management for SAMURAI-based research programs.

3. Summary of Research Activity

The current research subjects are summarized as follows:

(1) Operation, maintenance and improvement of a large superconducting dipole magnet that is the main component of the SAMURAI spectrometer
(2) Design, development and construction of various detectors that are used for nuclear reaction experiments using the SAMURAI spectrometer.
(3) Preparation for planning experiments using SAMURAI spectrometer.
(4) Maintenance and improvement of the SAMURAI beam line.
(5) Formation of a collaboration platform called "SAMURAI collaboration"

Team Leader
Hiromi SATO

Member
Ken-ichiro YONEDA (concurrent: Deputy Team Leader)

Research Associate
Yohei SHIMIZU

Visiting Scientists (JST)
Bertis Charles RASCO (Louisiana State University, USA)
Julien Didier GIBELIN (JSPS: LPC-Caen, France) -Aug. 8, 2013

Visiting Technician
Nobuyuki CHIGA (Tohoku University) -Mar. 31, 2014

RIBF Research Division
Research Instruments Group
Computing and Network Team

1. Abstract

This team is in charge of development, management and operation of the computing and network environment, mail and information servers and data acquisition system and management of the information security of the RIKEN Nishina Center.

2. Major Research Subjects

(1) Development, management and operation of the general computing servers
(2) Development, management and operation of the mail and information servers
(3) Development, management and operation of the data acquisition system
(4) Development, management and operation of the network environment
(5) Management of the information security

3. Summary of Research Activity

This team is in charge of development, management and operation of the computing and network environment, mail and information servers and data acquisition system and management of the information security. The details are described elsewhere in this progress report.

(1) Development, management and operation of the general computing servers

We are operating Linux/Unix NIS/NFS cluster system for the data analysis of the experiments and general computing. This cluster system consists of eight computing servers with 28 CPU cores and totally 200 TB RAID of highly-reliable Fibre-channel HDD. We have replaced the data analyses servers and RAID file systems for the experimental data in the spring of 2012. Approximately 600 user accounts are registered on this cluster system. We are adopting the latest version of the Scientific Linux (X86_64) as the primary operating system, which is widely used in the accelerator research facilities, nuclear physics and high-energy physics communities in the world.

(2) Development, management and operation of the mail and information servers

We are operating RIBF.RIKEN.JP server as a mail/NFS/NIS server. This server is a core server of RIBF Linux/Unix cluster system. This server was replaced in the summer of 2011 since it passed more than five years from the installation. Postfix has been used for mail transport software and dovecot has been used for imap and pop services. These software packages enable secure and reliable mail delivery. Sophos Email Security and Control (PMX) installed on the mail front-end servers tags spam mails and isolates virus-infected mails. The probability to identify the spam is approximately 95-99%. We are operating several information servers such as WWW servers, Integrated Digital Conference (INDICO) server, Wiki servers, Groupware servers, Windows Media and Quick Time streaming servers, and an anonymous FTP server (FTP.RIKEN.JP).

(3) Development, management and operation of the data acquisition system

We have developed the standard data-acquisition system named as RIBFDAQ. This system can process up to 40 MB/s data. By using parallel readout from front-end systems, the dead time could be small. To synchronize the independent DAQ systems, the time stamping system has been developed. The resolution and depth of the time stamp are 10 ns and 48 bit, respectively. This time stamping system is very useful for beta decay experiments such as EURICA and BRIKEN projects. The current main task is the DAQ coupling, because detector systems with dedicated DAQ systems are transported to RIBF from foreign facilities. In case of SAMURAI Silicon (NSCL/TUM/WUSTL), the readout system is integrated into RIBFDAQ. The projects of MUST2 (GANIL), MINOS (CEA Saclay), and NeuLAND (GSI) cases, data taken by their DAQ systems are transferred to RIBFDAQ. For SPIRIT (RIKEN/GANIL/CEA Saclay/NSCL), RIBFDAQ data are sent to GET system that is a large-scale signal processing system for the time projection chamber. These cases, data are merged in online. On the other hand, EURICA (GSI) and BRIKEN (GSI/Univ. Liverpool/IFIC) projects, we adopt the time stamping system to use individual trigger for each detector system. In this case, data are merged in offline. In addition to the development DAQ system, we are developing intelligent circuits based on FPGA. Mountable Controller (MOCO) is a very fast readout controller for VME modules. General Trigger Operator (GTO) is an intelligent triggering NIM module. These new circuits are successfully working.

(4) Development, management and operation of the network environment

We have been managing the network environment collaborating with Advanced Center for Computing and Communications (ACCC). All the Ethernet ports of the information wall sockets are capable of the Gigabit Ethernet connection (10/100/1000BT). Approximately 60 units of wireless LAN access points have been installed to cover the almost entire area of Nishina Center.

(5) Management of the information security

It is essential to take proper information security measures for information assets.

We are managing the information security of Nishina Center collaborating with ACCC.

Team Leader
Takashi ICHIHARA (concurrent)

Member
Yasushi WATANABE (concurrent)

Nishina Center Research Scientist
Hidetada BABA

Student Trainee
Ryousuke TANUMA - Mar. 31, 2014

RIBF Research Division
Research Instruments Group
Detector Team

1. Abstract

This team is in charge of development, fabrication, and operation of various detectors used for nuclear physics experiments at RIBF. Our current main mission is maintenance and improvement of beam-line detectors which are used at BigRIPS separator and its succeeding beam lines for beam diagnosis and particle identification of RI beams. We are also engaged in research and development of new detectors that can be used for higher-intensity RI beams.

2. Major Research Subjects

Development, fabrication, and operation of various detectors for nuclear physics experiments, including beam-line detectors which are used for the production and delivery of RI beams (beam diagnosis and particle identification).

3. Summary of Research Activity

The current research subjects are summarized as follows:

(1) Maintenance and improvement of the beam-line detectors which are used at BigRIPS separator and its succeeding beam lines.
(2) Development of new beam-line detectors with radiation hardness and tolerance for higher counting rates
(3) Development of a high dynamic range preamplifier for silicon strip detectors

Team Leader
Toshiyuki KUBO (Group Director)

Special Postdoctoral Researcher
Yuki SATO

Visiting Scientist
Kohei FUJIWARA (Tokyo Metropolitan Industrial Technology Research Institute)

Research Consultant
Hiroyuki MURAKAMI (- Mar. 31, 2014)

Students
Junior Research Associate
Hiroyuki MIYA - Mar. 31, 2014

RIBF Research Division
Accelerator Applications Research Group

1. Abstract

This group promotes various applications of ion beams from RI Beam Factory. Radiation Biology Team studies various biological effects of fast heavy ions and develops new technology to breed plants and microbials by heavy-ion irradiations. RI Applications Team studies production and application of radioisotopes for various research fields, development of trace element analysis and its application, and development of chemical materials for ECR ion sources.

2. Major Research Subjects

Research and development in biology, chemistry and materials science utilizing heavy-ion beams from RI Beam Factory.

3. Summary of Research Activity

(1) Biological effects of fast heavy ions.
(2) Development of heavy-ion breeding.
(3) Production and application of radioisotopes.
(4) Developments of trace elements analyses

Group Director
Tomoko ABE

Assistants
Yoshiko SAKATA
Noriko KIYAMA

RIBF Research Division
Accelerator Applications Research Group
Radiation Biology Team

1. Abstract
Radiation biology team studies various biological effects of fast heavy ions. It also develops new technique to breed plants by heavy-ion irradiations. Fast heavy ions can produce dense and localized ionizations in matters along their tracks, in contrast to photons (X rays and gamma rays) which produce randomly distributed isolated ionizations. This localized and dense ionization can cause double-strand breaks of DNA which are not easily repaired and result in mutation more effectively than single-strand breaks. A unique feature of our experimental facility at the RIKEN Ring Cyclotron (RRC) is that we can irradiate living tissues in atmosphere since the delivered heavy-ion beams have energies high enough to penetrate deep in matter. This team utilizes a dedicated beam line (E5B) of the RRC to irradiate microbes, plants and animals with beams ranging from carbon to iron. Its research subjects cover physiological study of DNA repair, genome analyses of mutation, and development of mutation breeding of plants by heavy-ion irradiation. Some new cultivars have already been brought to the market.

2. Major Research Subjects
(1) Study on the biological effects by heavy-ion irradiation
(2) Studies on ion-beam breeding and genome analysis
(3) Innovative application of heavy-ion beams

3. Summary of Research Activity
We study biological effects of fast heavy ions from the RIKEN Ring Cyclotron using 135A MeV C, N, Ne ions, 95A MeV Ar ions and 90A MeV Fe ions. We also develop breeding technology of microbes and plants. Main subjects are:

(1) Study on the biological effects by heavy-ion irradiation

Heavy-ion beam deposits a concentrated amount of dose at just before stop with severely changing the LET. The peak of LET is achieved at the stopping point and known at the Bragg peak (BP). It is well known to be good for cancer therapy to adjust the BP to target malignant cells. On the other hand, a uniform dose distribution is a key to the systematic study, and thus to the improvement of the mutation efficiency. Therefore plants and microbes are treated using ions with stable LET. We investigated the effect of LET ranging from 22.5 to 640 keV/μm, on mutation induction using the model plant *Arabidopsis thaliana*. The most effective LET (LETmax) was 30.0 keV/μm. In the case of microbe (*Mesorhizobium lothi*), the results showed a higher incidence of deletion mutations for Fe ions at 640 KeV/μm than for C ions at 23-40 keV/μm. Thus, the LET of ion beams seems to be an important factor affecting mutagenesis.

(2) Study on ion-beam breeding and genome analysis

In contrast to X rays and gamma rays, fast heavy ions are found to be useful for plant breeding since they only cause localized damage on DNA and can induce mutations more effectively with lower dosage. Our team utilizes beams of fast heavy ions from the RRC to develop heavy-ion breeding techniques. LETmax is effective for breeding because of its very high mutation frequency. Since most mutations are small deletions, these are sufficient to disrupt a single gene. Thus, irradiation can efficiently generate knockout mutants of a target gene, and can be applied to reverse genetics. Higher LET (> 290 keV/μm) was shown to efficiently generate large deletions ranging from several to several tens of kbp. Many genes in the *Arabidopsis* genome (> 10%) are composed of tandem duplicated genes that share functions. Previous studies demonstrated that large deletions were required to knockout tandem arrayed genes, and the appropriate deletion size was estimated to be approximately 5–10 kbp, based on gene density in *Arabidopsis*. No method is currently available to efficiently generate deletion mutants of this size. As such, higher LET irradiation is promising as a new mutagen suitable for the functional analysis of tandem duplicated genes.

(3) Innovative application of heavy-ion beams

We have formed a consortium for ion-beam breeding. It consisted of 24 groups in 1999. In 2013 it consisted of 164 groups from Japan and 18 from overseas. Breeding was performed previously using mainly flowers and ornamental plants. We have recently put a new Japanese barnyard millet cultivar with low amylose content and short culm, ‘Nebarikko No. 2’ on the market. Beneficial variants have been grown for various plant species, such as high yield rice, semi-dwarf early rice, semi-dwarf buckwheat, hypoallergenic peanut, spineless oranges, non-flowering Eucalyptus and lipids-hyperaccumulating unicellular alga. We also successfully isolated 4 salt-resistant lines of rice from 325 progeny lines. We collaborate with Miyagi prefecture and Tohoku University to breed salt-resistant lines in the more delicious commercial rice varieties, ‘Hitomebore’ and ‘Manamusume’, that will grow normally and retain their good taste in saline paddy fields affected by the recent tsunami. The target of heavy-ion breeding is extended from flowers to crops like grains so that it will contribute to solve the global problems of food and environment.

Team Leader
Tomoko ABE (Group Director)

Members
Katsunori ICHINOSE (Senior Technical Scientist)
Masako IZUMI (Senior Research Scientist)
Tokihiro IKEDA (Senior Research Scientist)
Kazuhide TSUNEIZUMI (Senior Research Scientist)
Teruyo TSUKADA (Senior Research Scientist)
Ryouhei MORITA (Technical Scientist)

Postdoctoral Researcher
Kotaro ISHII

Technical Staff I
Yoriko HAYASHI
Sachiko KOGURE (-Mar. 31, 2014)

Technical Staff II
Sumie OHBU

Visiting Scientists
Ryutaro AIDA (Natl. Inst. Floricult. Sci.) -Mar. 31, 2013
Mari AMINO (Tokai University Hospital) -Mar. 31, 2013
Chang-Hyu BAE (Sunchon Natl. Univ., Korea) -Mar. 31, 2013
Hiroyuki DAIMON (Osaka Pref. Univ.) -Mar. 31, 2013
Ali FERJANI (Tokyo Gakugei Univ.)
Makoto FUJIWARA (Grad. Sch., Col. Arts Sci., Univ. of Tokyo)
Eitaro FUKATSU (Forest tree beeding Cet.)
Yoshiya FURUSAWA (Natl. Inst. Radiol. Sci.) -Mar. 31, 2013
Toshinari GODO (Botanic Gardens Toyama)
Misako HAMATANI (Hiroshima City Agric. Forest. Promot. Cen.) -Mar. 31, 2013
Yasuhide HARA (Kanagawa Inst. Agric. Sci.) -Mar. 31, 2013
Masanori HATASHITA (Wakasa Wan Energy Res. Cen.) -Mar. 31, 2013
Atsushi HIGASHITANI (Grad. Sch. Life Sci., Tohoku Univ.) -Mar. 31, 2013
Ryoichi HIRAYAMA (Natl. Inst. Radiol. Sci.) -Mar. 31, 2013
Akiko HOKURA (Tokyo Denki Univ.)
Ichiro HONDA (Natl. Agric. Res. Cen.) -Mar. 31, 2013
Mitsugu HORITA (Hokuren Agri. Res. Inst.) -Mar. 31, 2013
Hiroyuki ICHIDA (Meiji Univ.)
Yuji ITO (Natl. Agric. Res. Cen., Hokkaido Region)
Akihiro IWASE (Grad. Sch. Engin., Osaka Pref. Univ.)
Hiroshi KAGAMI (Shizuoka Citrus Exp. Station) -Mar. 31, 2013
Tetsuya KAKO (Suntory Flowers, Ltd.) -Mar. 31, 2013
Tsutomu KUBOYAMA (Ibaraki Univ.) -Mar. 31, 2013
Norihiko MISHIMA (Fukuda Denshi Co., Ltd.) -Mar. 31, 2013
Yutaka MIYAZAWA (Grad. Sch. Life Sci., Tohoku Univ.)
Kazumitsu MIYOSHI (Fac. Bioresour. Sci., Akita Pref. Univ.)
Toshikazu MORISHITA (Inst. Rad. Breeding, Natl. Inst. Agric. Res.)
Koji MURAI (Fukui Pref. Univ.)
Francesco MUSUMECI (Catania Univ.) -Mar. 31, 2013
Koichiro NISHIKAWA (FLORSAIKA CIA. LTDA.) -Mar. 31, 2013
Norihiro OHTSUBO (Natl. Inst. Floricult. Sci.)
Tomo OOMIYA (Hokkaido Ornamental Plants Veg. Res. Cen.) -Mar. 31, 2013
Masaya SAKAI (Fukuda Denshi Co., Ltd.) -Mar. 31, 2013
Kouichi SAKAMOTO (YUKIGUNI AGURI Co., Ltd.) -Mar. 31, 2013
Katsutomo SASAKI (National Agriculture and Food Research Organization)
Mikio SHIMADA (Kyoto Univ.) -Mar. 31, 2013
In-Ja SONG (Jeju National University)
Fumio SUGAWARA (Tokyo Univ. of Sci.) -Mar. 31, 201
Masao SUGIYAMA (Hokko Chem. Ind. Co., Ltd.) -Mar. 31, 2013
Keita SUGIYAMA (Nat. Inst. Veg.Tea Sci.) -Mar. 31, 2013
Ryuji SUGIYAMA (Ajinomoto, Co., INC.) -Mar. 31, 2013
Kazunori SUZUKI (Plant Biotech. Inst. Ibaraki Agric. Cen.) -Mar. 31, 2013
Masao SUZUKI (Natl. Inst. Radiol. Sci.) -Mar. 31, 2013
Kenichi SUZUKI (Suntory Flowers, Ltd.) -Mar. 31, 2013
Kunio SUZUKI (Technoflora, Co., Ltd.)
Hinako TAKEHISA (Natl. Inst. Agric. Sci.)

Sachie TANAKA (Tokai Univ.) -Mar. 31, 2013
Teruhiko TERAKAWA (Hokko Chem. Ind. Co., Ltd.) -Mar. 31, 2013
Ken TOKUHARA (Dogashima Orchid Cen.) -Mar. 31, 2013
Masanori TOMITA (CRIEPI)
Tomojiro KOIDE (RIKEN VITAMIN Co., Ltd.)
Hisashi TSUJIMOTO (Fac. Agri., Tottori Univ.)
Kozo TSUKADA (Nippon Veterinary and Life-sci. Univ.) -Mar. 31, 2013
Makoto UBUKATA (Hokkaido Univ.)
Masao WATANABE (Fac. Agri., Tohoku Univ.)
Yasuko YOSHIHARA(Japan Atomic Energy Agency) -Mar. 31, 2013
Koichiro YOSHIOKA (Tokai University Hospital) -Mar. 31, 2013

Visting Technicians
Tomojirou KOIDE (Riken Vitamin Co., Ltd.)
Takuji YOSHIDA (Takii Seed Co., Ltd.)

Research Fellows
Hideki ASAUMI (Ehime Agricultural Experiment Station) -Mar. 31, 2013
Masataka CHAYA (Nagasaki Agr. Forest. Exp. Station) -Mar. 31, 2013
Fumiko HIDAKA (Kagoshima Pref. Inst. for Agric. Dev.) -Mar. 31, 2013
Takeya ICHIKI - Mar. 31, 2014
Shunsuke IMANISHI (Natl. Inst.Veg. and Tea Sci.) - Mar. 31, 2014
Hiroaki KISAKA (Ajinomoto, Co., INC.) -Mar. 31, 2013
Yuri KURUMATANI (Chiba Pref. Agr. Res. Cent.) -Mar. 31, 2013
Chikara KUWATA (Chiba Pref. Agr. Res. Cent.) -Mar. 31, 2013
Tadanori MINO (Wadomari Cho Agr. Exp. Station) -Mar. 31, 2013
Miyuki NISHI (Saga Agricultural Experiment Station) -Mar. 31, 2014
Kyousuke NIWA (Hyogo Pref. Res. Inst.) -Mar. 31, 2014
Tadahito OOTUBO (Wadomari Cho Agr. Exp. Station) -Mar. 31, 2013
Yoshihide SAKITA (Wadomari Cho Agr. Exp. Station) -Mar. 31, 2013
Tsukasa SHIRAO (Kagoshima Biotechnology Inst.) -Mar. 31, 2013
Keiichi TAKAGI (Wakasa-wan Energy Research Center) -Mar. 31, 2013
Tomihiro TAKESHITA -Mar. 31, 2014
Kei-ichiro UENO (Kagoshima Biotechnology Inst.) -Mar. 31, 2013
Naoji WAKITA (Wadomari Cho Agr. Exp. Station) -Mar. 31, 2013

Consultant
Hiroyuki SAITO (-Mar. 31, 2013)

Part-time Workers
Yuki SHIRAKAWA
Hideo TOKAIRIN
Taeko WAKANA
Satoko YASUDA
Mieko YAMADA
Anju MATSUNAGA (- Apr. 5, 2013)
Honami OOHASHI (Aug.22, 2013-Sep. 6, 2013)

Students
Junior Research Associate
Liqiu MA (Grad. Sch. Sci. & Engin., Saitama Univ.) -Mar. 31, 2013

Student Trainees
Kentaro FUJITA
Hiroki KAWAMOTO -Mar. 31, 2014
Kana MIYOSHI
Takuto TAKAHASHI -Mar. 31, 2014
Fumitaka TAMEZAWA
Megumi UTSUGI
Fumitaka YAMAGISHI

RIBF Research Division
Accelerator Applications Research Group
RI Applications Team

1. Abstract

The RI Applications Team develops production technologies of radioisotopes (RIs) at RIKEN RI Beam Factory (RIBF) for application studies in the fields of physics, chemistry, biology, medicine, and pharmaceutical and environmental sciences. We use the RIs mainly for nuclear and radiochemical studies such as development of RI production technologies and chemistry of superheavy elements. The purified RIs such as ^{65}Zn and ^{109}Cd are delivered to universities and institutes through Japan Radioisotope Association. We also develop new technologies of mass spectrometry for the trace-element analyses using accelerator technology and apply them to the research fields such as cosmochemistry, environmental science, archaeology and so on. We also develop chemical materials for ECR ion sources of the RIBF accelerators.

2. Major Research Subjects

(1) Research and development of RI production technology at RIBF
(2) RI application researches
(3) Development of trace element analysis using accelerator techniques and its applications to geoscience and environmental science
(4) Development of chemical materials for ECR ion sources of RIBF accelerators

3. Summary of Research Activity

RI Applications Team utilizes RIBF heavy-ion accelerators for following research subjects:

(1) Research and development of RI production technology at RIBF and RI application studies

Due to its high sensitivity, the radioactive tracer technique has been successfully applied for investigations of the behavior of elements in the fields of chemistry, biology, medicine, engineering, and environmental sciences. We have been developing production technologies of useful radiotracers at RIBF and conducted their application studies in collaboration with many researchers in various fields. With 14-MeV proton, 24-MeV deuteron, and 50-MeV alpha beams from the AVF cyclotron, we presently produce about 30 long-lived radiotracers from ^{7}Be to ^{206}Bi. Among them, ^{65}Zn, ^{109}Cd, and ^{88}Y are delivered to Japan Radioisotope Association for fee-based distribution to the general public in Japan. On the other hand, radionuclides of a large number of elements are simultaneously produced from metallic targets such as ^{nat}Ti, ^{nat}Ag, ^{nat}Hf, and ^{197}Au irradiated with a 135-MeV nucl.$^{-1}$ ^{14}N beam from the RIKEN Ring Cyclotron. These multitracers are also supplied to universities and institutes as collaborative researches.

In 2013, we installed a new RI production system having an effective shield on the beam line of AVF to increase production yields of RIs by intense beam irradiations. We produced ^{65}Zn, ^{109}Cd, and ^{88}Y for our scientific researches on a regular schedule and supplied the surpluses through Japan Radioisotope Association to the general public. In 2013, we have accepted 14 orders of ^{65}Zn with a total activity of 72.7 MBq, 5 orders of ^{109}Cd with 14.15 MBq, and 1 order of ^{88}Y with 30 kBq. We also developed production technologies for new radioisotopes such as ^{28}Mg, ^{75}Se, ^{85}Sr, ^{99}Mo, and ^{124}I which were strongly demanded but lack supply sources in Japan. We also investigated the excitation functions for the ^{nat}Ni(d,x), ^{nat}Zn(d,x), ^{nat}Zr(d,x), ^{nat}Zr(α,x), ^{nat}Hf(d,x), and ^{nat}Pt(d,x) reactions to effectively produce useful RIs.

(2) Superheavy element chemistry

Chemical characterization of newly-discovered superheavy elements (SHEs, atomic numbers $Z \geq 104$) is an extremely interesting and challenging subject in modern nuclear and radiochemistry. We are developing SHE production systems as well as rapid single-atom chemistry apparatuses at RIBF. Using heavy-ion beams from RILAC and AVF, long-lived SHEs such as ^{261}Rf, ^{262}Db, and ^{265}Sg are produced, and their chemical properties are investigated.

We have been developing a gas-jet transport system at the focal plane of the gas-filled recoil ion separator GARIS at RILAC. This system is a promising approach for exploring new frontiers in SHE chemistry: (i) the background radioactivity of unwanted reaction products are strongly suppressed, (ii) the intense beam is absent in the gas-jet chamber and hence high gas-jet efficiency is achieved, and (iii) the beam-free condition also allows for investigations of new chemical systems. In 2013, the isotope of ^{262}Db was produced in the reaction of ^{248}Cm(^{19}F,5n)^{262}Db, and the decay properties of ^{262}Db and its α-decay daughter ^{258}Lr were investigated in detail using the rotating wheel apparatus MANON for α/SF spectrometry. Toward the SHE chemistry behind GARIS, we also developed a gas-chromatograph apparatus directly coupled to GARIS, which enabled in-situ complexation and gas-chromatographic separation of a large variety of volatile compounds of SHEs. In 2013, a cryogenic gas-chromatograph apparatus developed by the GSI-Mainz Univ. group was shipped to RIKEN, and the gas-phase chemistry with the organo-metallic compound of $Sg(CO)_6$ was successfully conducted in collaboration with Helmholtz-Institut Mainz, GSI, Mainz Univ., JAEA, Bern Univ., PSI, IMP, Hirosima Univ., Kyushu Univ., Niigata Univ., UC Berkeley, LBNL, and Saitama Univ.

At the AVF cyclotron, an automated hydroxide precipitation apparatus was developed in collaboration with Osaka Univ. Using the apparatus, the hydroxide complexation of ^{261}Rf was investigated with its homologues ^{85}Zr and ^{169}Hf. A batch-type solid-liquid extraction apparatus for a repetitive extraction experiment of SHEs was also developed in the HCl-TIOA system with Osaka Univ. using ^{85}Zr and ^{169}Hf. In 2013, a reversed-phase TTA extraction of ^{261}Rf and its homologues ^{85}Zr and ^{169}Hf was conducted in HF/HNO_3 solutions using Automated Rapid Chemistry Apparatus (ARCA) developed at GSI-Mainz Univ.-JAEA. In collaboration with Niigata Univ. and JAEA, a reversed-phase TBP extraction experiment of ^{90}Nb and ^{170}Ta were conducted using ARCA for the future ^{262}Db chemistry.

(3) Applications of RIKEN RI technologies for the Fukushima accident in 2011

Since the Fukushima Dai-ichi power plant accident in 2011, we have contributed radioactivity measurements of various samples such as soils and foods, and developed a low-cost radiation detector for foods.

(4) Development of trace element analysis using accelerator techniques and its application to geoscience and environmental science

We developed new mass spectrometry technologies for trace element analyses as an application of accelerator technology to various fields such as cosmochemistry, environmental science, and archaeology. ECRIS-AMS is a new type of accelerator mass spectrometry at RILAC equipped with an ECR ion source. This system is available for measuring trace elements (10^{-14}–10^{-15} level) and is expected to be especially effective for measurements of low-electron-affinity elements such as ^{26}Al, ^{41}Ca, and ^{53}Mn. In 2013, we have renovated the detection system and examined the sensitivity and mass resolution power. We also attempted to develop another technology by customizing a mass spectrometer equipped with a stand-alone ECR ion source for analyses of elemental and isotopic abundances. Furthermore, we analyzed sulfur and lead isotope ratios for cinnabar samples from ancient tombs in Japan to elucidate the origin of cinnabar.

(5) Development of chemical materials for ECR ion sources of RIBF

In 2013, we investigated a production method of $^{238}U(C_8H_8)_2$ for the ECR ion source of RIBF. We also prepared metallic ^{238}U and $^{238}UO_2$ on a regular schedule.

Team Leader
Hiromitsu HABA

Member
Kazuya TAKAHASHI (Senior Research Scientist)

Postdoctoral Researcher
Minghui HUANG (- Mar. 31, 2014)

Technical Staff I
Jumpei KANAYA (- Mar. 31, 2014)

Research Consultant
Seiichi SHIBATA (- Mar. 31, 2014)

Junior Research Associate
Masashi MURAKAMI (Niigata Univ.)

Part-time Worker
Michiko KITAGAWA

Visiting Scientists
Mayeen Uddin KHANDAKER (Univ. Malaya)
Hidetoshi KIKUNAGA (Tohoku Univ.)
Kazuhiro OOE (Niigata Univ.)
Hiroshi SHIMIZU (Rissho University)
Miho TAKAHASHI (Tokyo Univ. Marine Sci. and Tech.)
Masayoshi TODA (Tokyo Univ. Marine Sci. and Tech.)
Takahiro YAMADA (Japan Radiation Association)
Akihiko YOKOYAMA (Kanazawa Univ.)

Visting Technicians
Yuichiro WAKITANI (Japan Radiation Association)
Shinya YANOU (Japan Radiation Association)

Student Trainees
Ryuji AONO (Niigata Univ.) -Mar. 31, 2014
Yoshiki FUKUDA (Kanazawa Univ.) -Mar. 31, 2014
Naoya GOTO (Niigata Univ.) -Mar. 31, 2014
Kazunori HAYASHI (Kanazawa Univ.) -Mar. 31, 2014
Junichi HIRATA (Tokyo Univ. Marine Sci. and Tech.)
Hajime KIMURA (Kanazawa Univ.) -Mar. 31, 2014
Yuuta KITAYAMA (Kanazawa Univ.) -Mar. 31, 2014
Takumi KOYAMA (Niigata Univ.) -Mar. 31, 2014
Eita MAEDA (Kanazawa Univ.) -Mar. 31, 2014
Kouhei NAKAMURA (Osaka Univ.) -Mar. 31, 2014
Yuri OBI (Tokyo Univ. Marine Sci. and Tech.) -Mar. 31, 2014
Daisuke SATO (Niigata Univ.) -Mar. 31, 2014
Yudai SHIGEKAWA (Osaka Univ.) -Mar. 31, 2014
Yuuki SHIGEYOSHI (Kanazawa Univ.) -Mar. 31, 2014
Takumi TANIGUCHI (Kanazawa Univ.) -Mar. 31, 2014
Keigo TOYOMURA (Osaka Univ.) -Mar. 31, 2014

Shohei TSUTO (Niigata Univ.) -Mar. 31, 2014
Shingo UENO (Kanazawa Univ.) -Mar. 31, 2014

RIBF Research Division
User Liaison and Industrial Cooperation Group

1. Abstract

The essential mission of the “User Liaison and Industrial Cooperation (ULIC) Group” is to maximize the research activities of RIBF by attracting users in various fields with a wide scope.

The ULIC Group consists of two teams.

The User Support Team provides various supports to visiting RIBF users through the User’s Office. The Industrial Cooperation Team supports potential users in industries who use the beams for application purposes or for accelerator related technologies other than basic research. Production of various radioisotopes by the AVF cyclotron is also one of the important missions. The produced radioisotopes are distributed to researchers in Japan for a charge through the Japan Radioisotope Association.

In addition the ULIC Group takes care of laboratory tours for RIBF visitors from public. The numbers of visitors amounts to 2,300 per year.

Group Director
Hideyuki SAKAI

Deputy Group Director
Hideki UENO (concurrent: User Support)

Members
Mieko KOGURE (Technical Assistant) (-Mar. 31, 2014)
Aiko NAKAO (Senior Research Scientist) (Feb. 1, 2013-Apr. 30, 2013)

Special Temporary Employee
Tadashi KAMBARA

Senior Visiting Scientists
Ikuko HAMAMOTO (The Lund University)
Munetake ICHIMURA (The University of Tokyo)

Assistants
Yoshiko SAKATA (- Oct. 31, 2013)
Noriko KIYAMA
Tomoko IWANAMI
Katsura IWAI
Emiko ISOGAI (- Mar. 31,2013)

RIBF Research Division
User Liaison and Industrial Cooperation Group
User Support Office

1. Abstract

To enhance synergetic common use of the world-class accelerator facility, the Radioisotope Beam Factory (RIBF), it is necessary to promote a broad range of applications and to maximize the facility's importance. The facilitation and promotion of the RIBF are important missions charged to the team. Important operational activities of the team include: i) the organization of international Program Advisory Committee (PAC) meetings to review experimental proposals submitted by RIBF users, ii) RIBF beam-time operation management, and iii) promotion of facility use by hosting outside users through the RIBF Independent Users program, which is a new-user registration program begun in FY2010 at the RIKEN Nishina Center (RNC) to enhance the synergetic common use of the RIBF. The team opened the RIBF Users Office in the RIBF building in 2010, which is the main point of contact for Independent Users and provides a wide range of services and information.

2. Major Research Subjects

(1) Facilitation of the use of the RIBF
(2) Promotion of the RIBF to interested researchers

3. Summary of Research Activity

(1) Facilitation of the use of the RIBF

The RIBF Users Office, formed by the team in 2010, is a point of contact for user registration through the RIBF Independent User program. This activity includes:

- registration of users as RIBF Independent Users,
- registration of radiation workers at the RIKEN Wako Institute,
- provision of an RIBF User Card (a regular entry permit) and an optically stimulated luminescence dosimeter for each RIBF Independent User, and
- provision of safety training for new registrants regarding working around radiation, accelerator use at the RIBF facility, and information security, which must be completed before they begin RIBF research.

The RIBF Users Office is also a point of contact for users regarding RIBF beam-time-related paperwork, which includes:

- contact for beam-time scheduling and safety review of experiments by the In-House Safety Committee,
- preparation of annual Accelerator Progress Reports, and
- maintaining the above information in a beam-time record database.

In addition, the RIBF Users Office assists RIBF Independent Users with matters related to their visit, such as invitation procedures, visa applications, and the reservation of on-campus accommodation.

(2) Promotion of the RIBF to interested researchers

- The team has organized an international PAC for RIBF experiments; it consists of leading scientists worldwide and reviews proposals in the field of nuclear physics (NP) purely on the basis of their scientific merit and feasibility. The team also assists another PAC meeting for material and life sciences (ML) organized by the RNC Advanced Meson Laboratory. The NP and ML PAC meetings are organized twice a year.
- The team coordinates beam times for PAC-approved experiments and other development activities. It manages the operating schedule of the RIBF accelerator complex according to the decisions arrived at by the RIBF Machine Time Committee.
- To promote research activities at RIBF, proposals for User Liaison and Industrial Cooperation Group symposia/mini-workshops are solicited broadly both inside and outside of the RNC. The RIBF Users Office assists in the related paperwork.
- The team is the point of contact for the RIBF users' association. It arranges meetings at RNC headquarters for the RIBF User Executive Committee of the users' association.
- The Team conducts publicity activities, such as arranging for RIBF tours, development and improvement of the RNC official web site, and delivery of RNC news via email and the web.

Team Leader
Ken-ichiro YONEDA

Deputy Team Leader
Yasushi WATANABE (concurrent)

Technical Staff I
Narumasa MIYAUCHI

Visiting Scientists
Yoshiteru SATO (Seoul National University) - Aug. 31, 2013
Masayuki YAMAGAMI (University of Aizu) - Aug. 31, 2013

RIBF Research Division
User Liaison and Industrial Cooperation Group
Industrial Cooperation Office

1. Abstract

Industrial cooperation team handles non-academic activities at RIBF corresponding to industries and to general public.

2. Major Research Subjects

(1) Fee-based distribution of radioisotopes produced at RIKEN AVF Cyclotron
(2) Support of industrial application using the RIBF accelerator beam and its related technologies including novel industrial applications.
(3) Development of real-time wear diagnostics of industrial material using RI beams

3. Summary of Research Activity

(1) Fee-based distribution of radioisotopes

This team handles fee-based distribution of radioisotopes Zn-65, Y-88 and Cd-109 from 2007, which are produced by the RI application team at the AVF cyclotron, to nonaffiliated users under a Material Transfer Agreement between Japan Radioisotope Association and RIKEN. In 2013, we delivered five shipments of Cd-109 with a total activity of 14.15 MBq and 14 shipments of Zn-65 with a total activity of 72.7 MBq. In addition, we delivered the first shipment of Y-88 with an activity of 0.03 MBq. The final recipients of the RIs were eight universities, two research institutes and one private company.

(2) Support of Industrial application using RIBF

In November 2009, RNC started a new project “Promotion of applications of high-energy heavy ions and RI beams” as a grant-in-aid program of MEXT “Sharing Advanced Facilities for Common Use Program”. In this project, RNC opens the old part of the RIBF facility, which includes the AVF cyclotron, RILAC, RIKEN Ring Cyclotron and experimental instruments like RIPS, to non-academic proposals from users including private companies. This MEXT program was terminated in September 2010, but RNC succeed and promote this facility sharing program after that. The proposals are reviewed by a program advisory committee, industrial PAC. The proposals which have been approved by the industrial PAC are allocated with beam times and the users pay RIKEN the beam time fee. The intellectual properties obtained by the use of RIBF belong to the users. In order to encourage the use of RIBF by those who are not familiar with utilization of ion beams, the first two beam times of each proposal can be assigned to trial uses which are free of beam time fee.

The industrial PAC met for the first time in January 2010, and reviewed and approved two proposals as trial uses. The beam times of both proposals were executed successfully in 2010 at the RIKEN Ring Cyclotron and RILAC. The second meeting held in June 2010 reviewed four proposals and approved three of them as trial uses. Beam times of two of the proposals were successfully executed in 2010 and 2011 at the RIKEN Ring Cyclotron. The third meeting held in July 2012 reviewed one proposal and approved it.

(3) Development of real-time wear diagnostics using RI beams

We are promoting a method for real-time wear diagnostics of industrial material using RI beams as tracers. This new method was developed by a close collaboration with Sumitomo Heavy Industry, which led to an application of a patent. For that purpose, very intense RI beams of 7Be (T1/2=52 days) at 4.1 MeV/u and 22Na (T1/2=2.6 years) at 3.7 MeV/u were produced via the (p,n) reaction at the CRIB separator using beams from the AVF cyclotron. In the past, those RIs were produced at the RIPS separator using beams from the RRC, which are constantly used for the academic research. The RI beam production by the AVF cyclotron alone increases flexibility in the beam-time scheduling and more importantly leads to reduce the production cost for industrial users.

As we can provide RI beams of different nuclides and control the implantation depth, we have developed a novel method of wear diagnostics in collaboration with Sumitomo Heavy Industry (SHI) Examination & Inspection Ltd., SHI Technology Research Center and CNS and jointly applied for a patent. Implantation of different RI for both machine parts contacting each other, one can distinguish the wear-loss rate of both interacting parts simultaneously. Implantation of one or a few RIs with controlling its depth profile, it can be applicable for processing a wear-loss gauge on a machine part. We are also developing a new method to determine the spatial distribution of positron-emitting RIs on periodically-moving objects in a closed system, which can be used for real-time evaluation of wear loss in a running machine. This is based on the same principle as the medical PET systems but is simpler and less expensive.

Team Leader
Atsushi YOSHIDA

Members
Hiroshige TAKEICHI (Senior Research Scientist)
Aiko NAKAO (-Jan. 31, 2013)

Visiting Scientists
Shuhei TATEMICHI (Fuji Electric Systems)
Masanori INOUE (Fuji Electric Systems)

RIBF Research Division
Safety Management Group

1. Abstract

The RIKEN Nishina Center for Accelerator-Based Science possesses one of the largest accelerator facilities in the world, which consists of two heavy-ion linear accelerators and five cyclotrons. This is the only site in Japan where uranium ions are accelerated. The center also has electron accelerators of microtron and synchrotron storage ring. Our function is to keep the radiation level in and around the facility below the allowable limit and to keep the exposure of workers as low as reasonably achievable. We are also involved in the safety management of the Radioisotope Center, where many types of experiments are performed with sealed and unsealed radioisotopes.

2. Major Research Subjects

(1) Safety management at radiation facilities of Nishina Center for Accelerator-Based Science
(2) Safety management at Radioisotope Center
(3) Radiation shielding design and development of accelerator safety systems

3. Summary of Research Activity

Our most important task is to keep the personnel exposure as low as reasonably achievable, and to prevent an accident. Therefore, we daily patrol the facility, measure the ambient dose rates, maintain the survey meters, shield doors and facilities of exhaust air and wastewater, replenish the protective supplies, and manage the radioactive waste. Advice, supervision and assistance at major accelerator maintenance works are also our task.

We revised the safety interlock system of RIBF building to meet the requirement due to the installations of SLOWRI and R3 detectors. Four neutron monitors were additionally placed around the rooms, and connected with the interlock system to stop the ion beam when radiation level rose. The local shields in the experiment vaults were partly modified.

A new experiment room for measurement of short-half-life radionuclide was made in the pump room of the linac building, and an exhaust system with a high-efficiency particulate air (HEPA) filter was installed there. Contamination test apparatuses were installed.

For the above modifications we applied for the government license 5 times, and underwent the government inspections 4 times.

We developed ionization chambers which were fairly resistant to radiation, and installed them in the SRC vault. The real-time dose rate values are shown at the entrance of the vault.

Group Director
Yoshitomo UWAMINO

Deputy Group Director
Kanenobu TANAKA (Technical Scientist)

Nishina Center Technical Scientists
Hisao SAKAMOTO
Rieko HIGURASHI HIRUNUMA
Takeshi MAIE (concurrent)

Technical Staff I
Atsuko AKASHIO
Tomoyuki DANTSUKA (concurrent)

Assistant
Tomomi OKAYASU

Assigned Employee
Hiroki MUKAI

Temporary Staffing
Hiroyuki FUKUDA (- Mar. 31, 2014)
Satoshi HASHIGUCHI (- Mar. 31, 2013)
Mamoru TAKEKOSHI (Apr. 1, 2013 -)
Yoshiyuki YAMAUCHI (Apr. 1, 2013 -)

Research Consultant
Masaharu OKANO

Visiting Scientists
Takashi NAKAMURA (Shimizu Corporation)
Koji OHISHI (Shimizu Corporation)
Noriaki NAKAO (Shimizu Corporation)

Part-time Workers

Hiroko AISO
Shin FUJITA
Kimie IGARASHI
Satomi IIZUKA
Hiroshi KATO
Kazushiro NAKANO (- Mar. 31, 2014)
Tsutomu YAMAKI (- Mar. 31, 2013)

Partner Institution

The Nishina Center established the research partnership system in 2008. This system permits an external institute to develop its own projects at the RIKEN Wako campus in equal partnership with the Nishina Center. At present, three institutes, Center for Nuclear Study of the University of Tokyo (CNS), Institute of Particle and Nuclear Studies of KEK (KEK), and Department of Physics, Niigata University (Niigata) are conducting research activities under the research partnership system.

CNS and the Nishina Center signed the partnership agreement in 2008. Until then, CNS had collaborated in joint programs with RIKEN under the “Research Collaboration Agreement on Heavy Ion Physics” (collaboration agreement) signed in 1998. The partnership agreement redefines procedures related to the joint programs while keeping the spirit of the collaboration agreement. The joint programs include experimental nuclear physics activities using CRIB, SHARAQ, GRAPE at RIBF, theoretical nuclear physics activities with ALPHLEET, accelerator development, and activities at RHIC PHENIX.

The partnership agreement with the Niigata University was signed in 2010. The activity includes theoretical and experimental nuclear physics, and nuclear chemistry.

KEK started low-energy nuclear physics activity at RIBF in 2011 under the research partnership system. The newly constructed isotope separator KISS will be available for the users in near future.

The activities of CNS, Niigata, and KEK are reported in the following pages.

Partner Institution
Center for Nuclear Study, Graduate School of Science
The University of Tokyo

1. Abstract

The Center for Nuclear Study (CNS) aims to elucidate the nature of nuclear system by producing the characteristic states where the Isospin, Spin and Quark degrees of freedom play central roles. These researches in CNS lead to the understanding of the matter based on common natures of many-body systems in various phases. We also aim at elucidating the explosion phenomena and the evolution of the universe by the direct measurements simulating nuclear reactions in the universe. In order to advance the nuclear science with heavy-ion reactions, we develop AVF upgrade, CRIB and SHARAQ facilities in the large-scale accelerators laboratories RIBF. We started a new project OEDO for a new energy-degrading scheme is proposed, where a RF deflector system is introduced to obtain a good quality of low-energy beam. We promote collaboration programs at RIBF as well as RHIC-PHENIX and ALICE-LHC with scientists in the world, and host international meetings and conferences. We also provide educational opportunities to young scientists in the heavy-ion science through the graduate course as a member of the department of physics in the University of Tokyo and through hosting the international summer school.

2. Major Research Subjects

(1) Accelerator Physics
(2) Nuclear Astrophysics
(3) Nuclear spectroscopy of exotic nuclei
(4) Quark physics
(5) Nuclear Theory
(6) SHARAQ project
(7) Active Target Development

3. Summary of Research Activity

(1) Accelerator Physics

One of the Major tasks of the accelerator group is the AVF upgrade project that includes development of ion sources, upgrading the AVF cyclotron of RIKEN and the beam line to CRIB. Development of ECR heavy ion sources is to provide a new HI beams, higher and stable beams of metallic ions, and to improve the control system. The Hyper ECR and the Super ECR sources provide all the beams for the AVF cyclotron and support not only CRIB experiments but also a large number of RIBF experiments. Injection beam monitoring and control are being developed and studied. Detailed study of the optics from the ion sources are expected to improve transmission and qualities of beams for the RIBF facility.

(2) Nuclear Astrophysics

The nuclear astrophysics group in CNS is working for experiments using the low-energy RI beam separator CRIB.

In September, 2013, beta-delayed alpha decay of 16N, which is relevant for the astrophysical 12C(a,g) reaction rate,was measured at CRIB using an active target system (GEM-MSTPC).
Many decay events were detected from 16N beam particles stopped in the active target. 15O and 10Be beams were produced for the first time at CRIB, and both beams will be used for resonant scattering experiments.
Based on recent collaboration on nuclear astrophysics at CRIB, two memorunda of understanding on the collaborated research have been made between CNS and IBS (Korea), and CNS, INFN-LNS (Italy) and CNS-SKKU (Korea).

(3) Nuclear structure of exotic nuclei

The NUSPEQ (NUclear SPectroscopy for Extreme Quantum system) group studies exotic structures in high-isospin and/or high-spin states in nuclei. The CNS GRAPE (Gamma-Ray detector Array with Position and Energy sensitivity) is a major apparatus for high-resolution in-beam gamma-ray spectroscopy. Missing mass spectroscopy using the SHARAQ is going to start as another approach on exotic nuclei. In 2013, the following progress has been made.

Experimental programs under the EURICA collaboration were performed for studying evolution of deformation in neutron-rich Z~60 nuclei, which are being analyzed now. High-spin states in A~40 nuclei were measured at Tandem ALTO facility at IPN Orsay by using fusion reaction, where a new candidate of superdeformed states were found in ^{35}S.

Gamow-Teller transitions of ^{8}He were studied by the (p,n) reaction in inverse kinematics, where a prominent sharp peak at Ex~8 MeV was found to be the Gamow-Teller resonance. Exothemic charge exchange reactions (^{8}He,^{8}Li*(1+)) on ^{12}C and ^{4}He are being analyzed now. Experiment on the tetra-neutron system via the ^{4}He(^{8}He,^{8}Be)4n reaction is being analyzed, where several tens of events were identified to be candidates of the 4n system just above the threshold.

The readout system of 14 detectors of the CNS GRAPE was upgraded, where digital pulse data taken by sampling ADCs are analyzed by FPGAs on boards.

Experimental setup of studying tetra neutron system using the double-charge exchange reaction ^{4}He(^{8}He,^{8}Be)4n at 200 A MeV was prepared for the measurement in April 2012.

(4) Quark Physics

Main goal of the quark physics group is to understand the properties of hot and dense nuclear matter created by colliding heavy nuclei at relativistic energies. The group has been involved in the PHENIX experiment at Relativistic Heavy Ion Collider (RHIC) at Brookhaven National Laboratory, and the ALICE experiment at Large Hadron Collider (LHC) at CERN.

As for PHENIX, the group has been concentrating on the physics analysis involving leptons and photons; dark photon searches in low mass Dalitz decays, J/ψ production in ultra-peripheral Au+Au collisions, and electron measurement from semi-leptonic decay of heavy flavor mesons which uses the Si VTX detector subsystem.

As for ALICE, the group has involved in the data analyses, which include production of multi-particle correlation in Pb+Pb collisions, nuclear modification of energetic neutral pions in Pb+Pb collisions, and measurement of low-mass lepton pairs in Pb+Pb and p+Pb collisions. The group started to involve in the ALICE-TPC upgrade using a Gas Electron Multiplier (GEM) in 2012. Systematic studies of gain stability, ion back flow, and energy resolutions with various field configurations are underway at CNS and at CERN. Performance evaluation of the COBRA-GEM for the ALICE-TPC upgrade is underway.

R&D of GEM and related techniques has been continuing. Development of resistive GEM with resistive anodes and GEM with glass insulator have been progressing in collaboration with the Tamagawa group of RIKEN.

(5) Nuclear Theory

The nuclear theory group has been promiting the RIKEN-CNS Collaboration project on large-scale nuclear structure calculations since 2001 and maintain its PC cluster. Based on this experience and its achievements, we participated in activities of HPCI Strategic Programs for Innovative Research (SPIRE) Field 5 “The origin of matter and universe” since 2011. The SPIRE project aims at an integral understanding of the origin and structure of matter and the universe utilizing the K computer.

In the SPIRE project, we are in charge of the elucidation of nuclear prop-erties using ultra large-scale simulations of quantum many-body systems and its applications. In order to perform large-scale shell-model calcu- lations, we developed an efficient computer program of the Monte Carlo Shell Model (MCSM) method for massive parallel computation, and per- formed benchmark calculations at K computer. We have studied both the medium-heavy and light nuclei with large model space on K computer in 2013. In medium-heavy nuclei, we successfully describe the shape coexis- tence for 68Ni. In light nuclei, systematic calculations have been performed with increasing the number of the major shells. The α cluster structure in Be isotopes has been also studied.

(6) SHARAQ project

A main subject of the SHARAQ program is charge-exchange reactions induced by heavy-ion beams, with which a variety of selectivities in transferred quantum numbers, ΔS, ΔT, ΔTz, ΔL etc, are available.

This year SHARAQ group made preparations for the coming two experiments.
One was for the develpment of parity-transfer probe (^{16}O, ^{16}F(g.s.)) reaction.
A MWDC was installed at the exit of the first dipole magnet of SHARAQ to track the proton produced from the instant decay of ^{16}F(g.s.) → ^{15}F + p.
The other was for the mass measurement around A~50 isotopes including ^{54}Ca by the Bρ-TOF method.
For this purpose, a set of CVD diamond detectors was developed and we attained a time resolution of 27~ps.
Also a detector system for tagging the isomers at the final focal plane of the SHARAQ was developed.

As a project of near future, a letter of intent was submitted to NP-PAC aiming at studying spin-isospin response of isomers by (p,n) reaction.

(7) Active Target Development

In a project of active target development launched as an intergroup collaboration in 2009, two types of active target have been developed. Technical development such as a capability of gating operation of GEM has been done for one active target and the alpha emission following the beta decay of ^{16}N was measured with the same active target. The development for the high intensity beam injection is being performed for the other active target. The test experiment with a high intensity ^{132}Xe beam was performed.

Director

Takaharu OTSUKA

Scientific Staff

Susumu SHIMOURA (Professor)
Hideki HAMAGAKI (Professor)
Kentaro YAKO (Associate Professor)
Noritaka SHIMIZU (Project Associate Professor)
Hidetoshi YAMAGUCHI (Lecturer)
Shin'ichiro MICHIMASA (Assistant Professor)
Taku GUNJI (Assistant Professor)
Shinsuke OTA (Assistant Professor)

Guest Scientists

Hiroaki UTSUNOMIYA (Guest Professor)
Yutaka UTSUNO (Guest Associate Professor)

Technical Staff

Norio YAMAZAKI
Yukimitsu OHSHIRO

Techinical Assistants

Shin-ichi WATANABE (~3.2013)
Hiroshi KUREI
Takehiko SENOO
Akira YOSHINO
Shoichi YAMAKA
Kazuyuki YOSHIMURA
Masahiko TANAKA

Project Research Associates

Hisayuki TORII (~3.2013)
Tooru YOSHIDA
Yoritaka IWATA (1.2013~)

Post Doctoral Associates

Shuichiro EBATA (~3.2013)
Yorito YAMAGUCHI
Taro NANAO
David, STEPPENBECK
Tomoaki TOGASHI (3.2013~)

Graduate Students

David. M KAHL
Masashi, MATSUSHITA
Akihisa TAKAHARA
Hiroyuki MIYA
Ryoji AKIMOTO (~3.2013)
Hiroshi TOKIEDA
Tomoya TSUJI
Shintaro GO (~3.2013)
Shoichiro KAWASE
ShinIchi HAYASHI
KeiIchi KISAMORI
Motonobu TAKAKI
Tang T. LEUNG (~3.2013)
Yuko SEKIGUCHI
Rin YOKOYAMA
Yuki KUBOTA
CheongSoo LEE
Kohei TERASAKI
Motoki KOBAYASHI
Kentaro YUKAWA (4.2013~)

Administration Staff

Hiroshi YOSHIMURA
Ikuko YAMAMOTO
Takako ENDO
Yukino KISHI
Toshiko ITAGAKI
Yuko SOMA

Partner Institution
Center for Radioactive Ion Beam Sciences, Institute of Natural Science and Technology Niigata University

1. Abstract

The Center for Radioactive Ion Beam Sciences, Niigata University, aims at uncovering the properties of atomic nuclei and heavy elements and their roles in the synthesis of elements, with use of the advanced techniques of heavy ion and radioactive ion beam experiments as well as the theoretical methods. Main research subjects include the measurements of various reaction cross sections and moments of neutron- or proton-rich nuclei, synthesis of super-heavy elements and radio-chemical studies of heavy nuclei, and theoretical studies of exotic nuclei based on quantum many-body methods and various nuclear models. In addition, we promote interdisciplinary researches related to the radioactive ion beam sciences, such as applications of radioactive isotopes and radiation techniques to material sciences, nuclear engineering and medicine. Many of them are performed in collaboration with RIKEN Nishina Center and with use of the RIBF facilities. The center emphasizes also its function of graduate education in corporation with the Graduate School of Science and Technology, Niigata University, which invites three researchers in RIKEN Nishina Center as visiting professors.

2. Major Research Subjects

(1) Reaction cross section and radii of neutron-rich nuclei
(2) Production of superheavy nuclei and radiochemistry of heavy elements
(3) Nuclear theory

3. Summary of Research Activity

(1) Reaction cross section and radii of neutron-rich nuclei

The experimental nuclear physics group has studied nuclear structure with the RI beam. One of our main interests is the interaction/reaction cross section measurements. They are good probes to investigate nuclear matter radii and nuclear matter distributions including halo or skin structure. Recently we have measured the interaction sections of Ne, Na, Mg and Al isotopes from stable region to neutron drip line with BigRIPS in RIBF. We found a large enhancement of cross section at ^{31}Ne. It suggests that ^{31}Ne nucleus has a neutron halo. It is consistent with the soft E1 excitation measurement. We also found an enhancement at ^{37}Mg. For odd-Z nuclei, Na and Al, we did not find such a large enhancement from neighbor isotopes. The systematics of observed interaction/reaction cross sections shows the changing of nuclear structure from stable region to neutron drip line via island of inversion.

(2) Production of superheavy nuclei and radiochemistry of heavy elements

The nuclear chemistry group has been investigating decay properties of super-heavy nuclei, measured the excitation functions of rutherfordium isotopes, and clarified the ambiguity of the assignment of a few-second spontaneously fissioning isotope of 261Rf. The new equipment designed for measurement of short-lived alpha emitters is under development.

For the chemistry research of super-heavy elements, preparatory experiments, such as solvent extraction for the group 4, 5, and 6th elements and gaseous phase chemistry for group-4 elements, have been performed using radioisotopes of corresponding homolog elements.

(3) Nuclear theory

One of the main activities of the nuclear theory group concerns with developments of the nuclear density functional theory and exploration of novel correlations and excitations in exotic nuclei. A fully selfconsistent scheme of the quasiparticle random phase approximation (QRPA) on top of the Skyrme-Hartree-Fock-Bogoliubov mean-field for deformed nuclei has been developed in the group. The versatility of this method to describe the deformation splitting of the giant resonances associated with the onset of deformation has been demonstrated for the first time by the intensive numerical calculation performed for Nd and Sm isotopes. The same method is further extended to describe the spin-isospin modes of excitation in deformed neutron-rich nuclei. A successful description of the Gamov-Teller beta-decay transition rate in the neutron-rich Zr isotopes is achieved with this method. Another correlation of interest in neutron-rich nuclei is the pair correlation, for which the spatial di-neutron correlation has been a key topic. Applying the continuum QRPA to the pairing modes of excitation in neutron-rich Sn isotopes, we predict the emergence of an anomalous pair vibration for isotopes with A>132. Furthermore the new mode is predicted to exhibits the di-neutron character. In addition to these studies, activities related to the proton-neutron pairing, the di-neutron correlation in the asymptotic tail in drip-line nuclei, the quasiparticle resonances in unbound odd-N nuclei are under way. Cluster structure and the ab initio studies of light nuclei are also important research subjects of the theory group.

Director

Masayuki MATSUO (Professor)

Scientific Staff

Hisaaki KUDO (Professor)
Takashi OHTSUBO (Associate Professor)
Shin-ichi GOTO (Associate Professor)
Shigeyoshi AOYAMA (Associate Professor)
Takuji IZUMIKAWA (Associate Professor)
Kenichi YOSHIDA (Assistant Professor)
Kazuhiro OOE (Assistant Professor)

Jun GOTO (Assistant Professor)

Post Doctoral Associate

Hirotaka SHIMOYAMA

Graduate Students

Kazuya HIROKAWA
Yoshihiko KOBAYASHI
Junpei ANZAI
Sho KANESAWA

Partner Institution
Radioactive Nuclear Beam Group, IPNS (Institute for Particle and Nuclear Studies) KEK (High Energy Accelerator Research Organization)

1. Abstract

The on-line tests of the KISS (KEK Isotope Separation System) were performed by using ^{56}Fe and ^{124}Xe beam from RIKEN Ring Cyclotron. The performance (overall extraction efficiency and selectivity) with increasing those beam intensities was investigated. Especially in the test using the ^{124}Xe beam, the target (^{198}Pt)-recoils were successfully extracted as singly charged ions. Although the overall efficiency achieved so far was smaller by about one order of magnitude than expected, measurements of lifetime of beta-decaying Pt-like recoils are to be performed, while further developing the performance by using ^{136}Xe beam. Some other activities related to the research subjects itemized below are also included.

2. Major Research Subjects

(1) Radioactive isotope beam production and manipulation for nuclear experiments.
(2) Explosive nucleosyhnthesis (rp- and r-process).
(3) Heavy ion reaction mechanism for producing heavy neutron-rich nuclei.
(4) Single particle states of neutron-rich nuclei by isobaric analog resonances.
(5) Development of RNB probes for materials science applications.

3. Summary of Research Activity

The KISS is an element-selective isotope separator using a magnetic mass separator combined with in-gas-cell resonant laser ionization. The gas cell filled with argon gas of 50 kPa is a central component of the KISS for extracting only the element of interest as ion beam for subsequent mass separation. In the cell, the element primarily produced by low-energy heavy ion reactions is stopped (thermalization and neutralization), transported by buffer gas (argon gas-flow of ~50 kPa in the present case), and then re-ionized by laser irradiation just before the exit. Therefore, it is desirable that the gas cell would keep high performance of extraction efficiency and selectivity (ratio of the number of ions extracted with laser operation to that without laser operation) throughout these processes. The absolute extraction efficiency and selectivity of the gas cell was investigated in the on-line test experiments where stable beams of ^{56}Fe and ^{124}Xe were directly injected for providing the gas cell with controlled number of atoms (^{56}Fe case) and energetic target (a thin foil of ^{198}Pt irradiated by ^{124}Xe)-like recoils, respectively. Also investigated were the so-called plasma effects which are thought to degrade the performance due to the plasma formed in the cell by the primary beam injection.

Injecting into the cell the ^{56}Fe beam of 90 MeV/nucleon from the RRC after being properly energy-degraded to 1.5 MeV/nucleon for complete stop around the center of the cell, we extracted laser-ionized ^{56}Fe atoms. Here, we have used a modified gas-cell, which was originally designed to reduce the plasma effect, but more deeply bent for better shadowing the beam irradiation region (plasma formation region) than previously used. The extraction efficiency for ^{56}Fe was measured to be about 0.25% and almost constant with increasing primary beam intensity (increasing number of injected iron atoms). The selectivity of about 50 was achieved, though showing a moderate deterioration by beam intensity of up to 4 pnA. Although the gas cell was well baked (outgassed) for the test, additional contamination was observed due to the beam irradiation, by which the laser-ionized ^{56}Fe atoms were fragmented into ^{56}Fe (A=56), ^{56}Fe (H_2O) (A=74) and ^{56}Fe Ar_2 (A=136) at the same intensity. Once the contamination could be removed, the extraction efficiency for ^{56}Fe would be restored accordingly.

After successfully demonstrating the performance of the KISS with iron, a series of online tests are planned to check the universality of the performance (if the performance demonstrated is element-independent). In a first test along the line, we used the ^{198}Pt atoms introduced into the gas cell as recoils out of the ^{198}Pt target by elastic scattering of ^{124}Xe of 10.75 MeV/nucleon from the RRC. The transformation of those laser-ionized ^{198}Pt atoms to sidebands was different from what was observed for ^{56}Fe; the laser-ionized-^{198}Pt - related ions were mostly observed as ions of ^{198}Pt, ^{198}Pt (H_2O), and ^{198}Pt Ar_2 in the intensity ratio of 1:4:10. The extraction efficiency for ^{198}Pt in the form of ^{198}Pt Ar_2 was estimated to be about 0.15% from the cross section of elastic scattering between ^{198}Pt and ^{124}Xe. Even with the present efficiency of 0.15%, the beta-decay half-lives of more than 20 unknown nuclei around N = 126 and Z<82 would be measured. While addressing the current development issues, we are going to measure the lifetime of beta-decaying Pt-like recoils in the year of 2014.

For the beta-decay lifetime measurements of the nuclei, mostly having $Q\beta$ values as small as 2 MeV, two double-layered plastic scintillators holding the implantation spot on a tape transport station in-between will be used. Two 0.5-mm and 1.0-mm thick scintillators with a size of 20-cm wide and 14-cm height were fabricated and tested. Almost full solid angle can be covered with the size (geometrical acceptance of 80%). When we measured the detection efficiency of the thinner scintillator wrapped with the aluminized Mylar, we found a rather large position dependency of the detection efficiency. While using instead a reflection sheet which is often used for the liquid crystal display, the position dependence as well as the detection efficiency was improved. Due to the thinness of the tested, multi-reflection of the scintillation lights in the scintillator seemed to make the efficiency worse. Using the ^{90}Sr/^{90}Y source, the coincidence efficiency of the two layers was observed to be 60% which is consistent with the GEANT simulation. The remaining 20% were almost stopped in the first layer, indicating the absolute efficiency of close to 100%. The tape transport station equipped with the plastic scintillators will be installed in the beginning of the 2014.

As a continuing effort for search for effective laser ionization scheme of elements of our interest (Z<82), a reference cell was fabricated, and is currently being used to search for auto ionizing states in Ta, W, and etc…

In order to investigate the feasibility of the multi-nucleon transfer (MNT) in the reaction system of ^{136}Xe on ^{198}Pt for producing heavy neutron-rich isotopes around the mass number of 200 with the neutron magic number of 126, the analysis of the data taken at GANIL in March 2012 is under progress. Using the elastic scattering data for ^{136}Xe, special efforts are currently being paid for extracting the absolute cross sections of projectile-like MNT channels, as well as of target-like fragments (TLFs) identified by their de-excitation gamma-rays. Some of the results, especially the cross sections of TLFs, would be directly compared to those estimated from the ongoing test experiments of the KISS as mentioned above.

The systematics of the single particle structure of even-odd nuclei along isotopic and/or isotonic chains give insights into the evolution of the relevant nuclear shell structure. We have investigated the first three bound states of ^{31}Mg by measuring their isobaric analog resonances through the proton resonance elastic scattering off ^{30}Mg in order to pin down the underlying mechanism of the island of inversion. The experiment was performed by using the post-accelerator REX-ISOLDE at CERN. A thick polyethylene target of 5.6 mg/cm^2 was impinged on by the ^{30}Mg ion beam accelerated up to 2.92 MeV/nucleon. The excitation function of the protons scattered around 0 degree in the laboratory frame was measured. The angular momenta (l) and spectroscopic factors (S^{pp}) of the first three bound states in ^{31}Mg were deduced. The l values are consistent with those previously assigned by the beta decay. Comparing the S^{pp} with the spectroscopic factors for the N=19 nuclei ^{37}Ar and ^{35}S measured by the (d, p) reaction shows that the S^{pp} for the positive parity states in ^{31}Mg were largely quenched. This means that the overlap between the wave function of the positive parity state and that of the neutron coupled to the ground state of ^{30}Mg is small, demonstrating that the border of the island of inversion is placed between ^{30}Mg and ^{31}Mg.

We have developed a nanoscale diffusion measurement method using alpha-emitting radioactive ^{8}Li tracer. In the method, while implanting a pulsed ^{8}Li beam of 8 keV, the alpha particles emitted at a small angle (θ = 10±1◦) relative to a sample surface were detected as a function of time. The method has been successfully applied to measure the lithium diffusion coefficients for an amorphous Li4SiO4 - Li3VO4 (LVSO) of several hundreds nm in thickness, well demonstrating that the present method has a sensitivity to the diffusion coefficients down to a value of 10^{-12} cm^2/s, more sensitive by about two orders magnitude than previously achieved. It should be noted that in the previous method sensitive to microscale diffusion the angles subtended by the α-particle detectors were within 63 ±14◦ and the incident energy of ^{8}Li was about 4 MeV. The present method is therefore supposed to be sensitive to nanoscale Li diffusion as compared to the previous method where tracer atoms were deeply implanted (several micrometers).

Group Leader
Hiroari MIYATAKE

Members
Yoshikazu HIRAYAMA
Nobuaki IMAI
Yutaka WATANABE
Hironobu ISHIYAMA
Sunchan JEONG
Michihiro OYAIZU
Yung-Hee KIM (PhD. Student, Seoul National University)
Momo MUKAI (D. Student, Tsukuba University)
Sota KIMURA (D. Student, Tsukuba University)

Events (April 2013 - March 2014)

RNC

2013	Apr. 1	Start of Nuclear Spectroscopy Laboratory, taking over Polarized RI Beam Team Start of Research Group for Superheavy Element
	Apr. 20	Wako Open campus
	May 7	RBRC Managing and Steering Committee held in Wako Campus
	May 28	New-Comers Seminar
	May 30	Effect of MOU between College of Science, Yonsei Univ. (Korea) and RNC
	Jun. 5	Effect of MOU between RNC and Department of Physics, Kyungpook National University (Korea)
	Jun. 26 - 27	RIBF Users Meeting 2013
	Jun. 28 - 29	RNC NP-PAC
	Jul. 2-3	RNC ML-PAC
	Jul. 11	Scientific Policy Committee (FY2013)
	Aug. 6 - 16	Nishina School
	Aug. 19 - 23	HPCI,京大基研、計算基礎科学連携拠点共催サマースクール「クォークから超新星爆発までー基礎物理の理想への挑戦ー」
	Aug. 28	Effect of MOU between Department of Physics, Korea Univ. and RNC
	Sep. 12	Effect of MOU For the use of MINOS device at RIKEN between CEA-DSM and RNC
	Oct. 2	President of Vietnam National University of Hanoi-Hanoi University of Science visits RNC
	Oct. 16	Effect of MOU between Institute of Basic Science, Rare Isotope Science Project, Korea and RNC for research collaboration in the area of rare ion accelerator and related fields
	Oct. 23	Effect of Agreement for International Joint Graduate School Program between RIKEN and Department of Physics, Yonsei University (Korea)
	Oct. 31 - Nov. 1	RBRC Scientific Review Committee
	Nov. 9 - 10	Participation in Science Agora 2013 held in Odaiba
	Dec. 13 - 14	RNC NP-PAC
	Dec. 27	Effect of Addendum No.26 to the Memorandum of Understanding for the RD51 Collaboration Participation of the Nishina Center for Accelerator-Based Science, RIKEN
2014	Jan. 30	Effect of Extension of MoU between RNC and Michigan State University
	Feb. 4	Effect of Memorandum of Understanding for Research Collaboration between RNC and the "Horia Hulubei" National Institute of Physics and Nuclear Engineering Bucharest-Magurele, Romania
	Feb. 20	Associate Chief Scientist Interim Review Program (Dr. Emiko HIYAMA)
	Feb. 26	Effect of Statement of Work for MOU between RNC and MSU

CNS

2013	Aug. 28 - Sep. 03	The 12th CNS international Summer School (CNSS13) http://indico.cns.s.u-tokyo.ac.jp/conferenceDisplay.py?confId=81

Awards (April 2013 - March 2014)

Awardee	Laboratory	Award	Organization	Date
Hiroshi Imao	Accelerator R&D Team	ACFA-IPAC13 Accelerator Prize	The Asian Committee for Future Accelerators	May 16
Emiko Hiyama	Strangeness Nuclear Physics Laboratory	The 33rd annual Saruhashi Award	The Association for the Bright Future of Women Scientists	May 25
Kimiko Sekiguchi	Visiting Scientist Spin Isospin Laboratory	15th Morita Fellowship Award	Japanese Association of University Women	May 25
Hiroshi Imao, Hiroki Okuno & Hironori Kuboki	Accelerator R&D Team / Accelerator Group / Special Postdoctoral Researcher, Accelerator Group	PASJ Award for Technical Contributions	Particle Accelerator Society of Japan	Aug. 4
Tomoko Abe & 7 others	Accelerator Applications Research Group	Excellent Presentation Award: 123rd Meeting of The Japanese Society of Breeding	Japanese Society of Breeding	Aug. 4
Tomoko Abe	Accelerator Applications Research Group	The BSJ Special Prize for Botanical Research	The Botanical Society of Japan	Sep. 14
Tomoko Abe & 3 others	Accelerator Applications Research Group	Excellent Presentation Award: 124th Meeting of The Japanese Society of Breeding	Japanese Society of Breeding	Nov. 19
Nobuyuki Chiga	Visiting Technician Research Instruments Group	FY2013 Technical Division Award: Graduate School of Science	Technical Division Graduate School of Science Tohoku University	Nov. 28
Yasushi Watanabe, et al.	RIKEN Nishina Center for Accelerator-Based Science	Science Agora Award	Japan Science and Technology Agency	Dec. 26

Press Releases (April 2013 - March 2014)

RNC

Apr. 4	Unvail the last 1/100 seconds of mass falling into a black hole – the first discovery of the high energy X-rays from a gas just falling into a black hole	Shin'ya Yamada, et al. (High-Energy Astrophysics Lab.)
Jul. 17	Development of high precision mass spectrometry for short-lived nuclei, MRTOF --- sub ppm precision with a few millisecond flight times ---	Michiharu Wada, et al. (SLOWRI Team)
Sep. 14	From quarks to the structure of neutron stars – intimate relation between the quark mass and the neutron-star mass is revealed –	Takumi Doi, et al. (Quantum Hadron Physics Lab.)
Oct. 9	Discovery of exotic isomers with a magic number	Hiroshi Watanabe, Shunji Nishimura & Hiroyoshi Sakurai (Radioactive Isotope Physics Lab.)
Oct. 10	Evidence for a new nuclear 'magic number' of 34 --- a key to access a dream region of 'island-of-stability'	David Steppenbeck & Satoshi Takeuchi (Radioactive Isotope Physics Lab.)
Oct. 11	Harvest of salt-tolerance rice in saline paddy field	Tomoko Abe (Radiation Biology Team)
Nov. 20	'Magic numbers' disappear and expand area of nuclear deformation	Pieter Doornenbal ＆ Hiroyoshi Sakurai (Radioactive Isotope Physics Lab.)
Feb. 20	Asymmetric explosion of core-collapse supernovae – the first mapping of radioactive 44Ti nuclei in Cassiopeia A	Takao Kitaguchi (High-Energy Astrophysics Lab.)

VII. LIST OF PUBLICATIONS
& PRESENTATIONS

RIKEN Nishina Center for Accelerator-Based Science

Publications

[Book · Proceedings]

（Others）

Enyo H.: “Prospect of RIKEN RI Beam Factory for Coming 5 Years”, Proceedings of International Symposium on Exotic Nuclei (EXON2012), (Far Eastern Federal University), Vladivostok, Russia, pp. 441–448 (2012).

Motobayashi T.: “World new facilities for radioactive isotope beams”, Proceedings of INPC2013 - International Nuclear Physics Conference, EPJ Web of Conferences 66, 01013 (2014).

Oral Presentations

(International Conference etc.)

Enyo H.: “Prospect of RIKEN RI Beam Factory for Coming 5 Years”, The VI International Symposium on Exotic Nuclei (EXON2012), (Far Eastern Federal University), Vladivostok, Russia, Oct. (2012).

Enyo H.: “Nuclear Physics in Japan-Prospects being engaged in RIBF, J-PARC and other facilities”, The 2012 Fall meeting of the Division of Nuclear Physics (DNP2012), CA, USA, Oct. (2012).

Motobayashi T.: “Experimental challenges for heavy element synthesis at new-generation RIB facilities”, International Workshop on Open progblems and futher directions in heavy element nucleo-systhesis, (ATOMKI), Debrecen, Hungary, Apr. (2013).

Enyo H.: “Future Nuclear Physics Facilities around the world”, IUPAP WG.9 Nuclear Science Symposium, (Frascati National Laboratory), Italy, May. (2013).

Motobayashi T.: “World new facilities for radioactive ion beams”, International Nuclear Physics Conference (INPC2013), (Istituto Nazionale di Fisica Nucleare), Firenze, Italy, June. (2013).

Motobayashi T.: “Coulomb dissociation experiments”, 7th European Summer School on Experimental Nuclear Astrophysics, (INFN Catania), Santa Tecla, Italy, Sep. (2013).

Motobayashi T.: “In-beam γ-ray spectroscopy at RIBF”, French-Japanese Symposium on Nuclear Structure Problems, (CNRS, CEA), Paris, France, Sep. (2013).

Enyo H.: “RIKEN Radio Isotope Beam Factory, Japanese Flag Ship for Nuclear Science”, The first International African Symposium on Exotic Nuclei (IASEN2013), Cape Town, South Africa, Dec. (2013).

Motobayashi T.: “Nuclear structure studies of very neutron-rich nuclei at RIKEN RIBF”, International Symposium on Nuclear Physics (ISNP2013), (Bhaba Atomic Research Center), Mumbai, India, Dec. (2013).

Motobayashi T.: “Nuclear physics and nuclear astrophysics at light- and heavy-ion accelerators in Japan”, 6th Asian Nuclear Physics Association Symposium, (Variable Energy Cyclotron Center), Kolkata, India, Feb. (2014).

Motobayashi T.: “Nuclear astrophysics studies at the RIKEN RIBF”, 11th Russbach School on Nuclear Astrophysics, (GANIL, EPS), Russbach, Austria, Mar. (2014).

(Domestic Conference)

延與秀人: “理研における中性子利用研究 -事始め -　”, H23 年度理研シンポジウム「理研から発信する中性子利用の新たな展開-ものづくり産業利用に向けた小型中性子源の開発-」, 埼玉県　和光市, 11 月 (2011).

延與秀人: “Nishina Center Overview”, 理研-IMP ワークショップ, 埼玉県　和光市, 4 月 (2013).

延與 秀人: “Introduction to RIKEN Nishina Center for Accelerator-Based Science”, Workshop on the INFN-RIKEN collaboration on nuclear physics activities, (イタリア文化会館), 東京, 5 月 (2013).

Quantum Hadron Physics Laboratory

Publications

[Journal]

(Original Papers) *Subject to Peer Review

Hidaka Y. and Yamamoto A. :"Charged vector mesons in a strong magnetic field ",Phys. Rev. D**87**, 094502 (2013)*.

Miura K., Hidaka Y., Satow D., and Kunihiro T. :"Neutrino spectral density at electroweak scale temperature ",Phys. Rev. D**88**, 065024 (2013)*.

Kouno H., Makiyama T., Sasaki T., Sakai Y., and Yahiro M. :"Confinement and Z3 symmetry in three-flavor QCD ",J. Phys.**G40**,095003 (2013)*.

Aoki S., Balog J., Doi T., Inoue T., and Weisz P. :"Short Distance Repulsion Among Baryons ",Int. J. Mod. Phys.**E22**,1330012 (2013)*.

Endres M. G., :"Numerical study of unitary fermions in one spatial dimension ",Phys. Rev. A**87**, 063617 (2013)*.

Masuda K., Hatsuda T., and Takatsuka T. :"Hadron-Quark Crossover and Massive Hybrid Stars ",Astrophys. J.**764**,12 (2013)*.

Hyodo T., Hatsuda T., and Nishida Y. :"Universal physics of three bosons with isospin ",Phys. Rev. C**89**, 032201 (2014)*.

Gong M., Alexandru A., Chen Y., Doi T., Dong S. J., Draper T., Freeman F., Glatzmaier M., Li A., Liu K. F., and Liu Z. (chiQCD Collaboration) :"Strangeness and charmness content of nucleon from overlap fermions on 2+1-flavor domain-wall fermion configurations ",Phys. Rev. D**88**, 014503 (2013)*.

Araki Y. and Kimura T. :"Phase structure of 2-dimensional topological insulators by lattice strong coupling expansion ",Phys. Rev. B**87**, 205440 (2013)*.

Aoki S., Ishii N., Doi T., Ikeda Y., T.Ionoue T. :"Asymptotic behavior of Nambu-Bethe-Salpeter wave functions for multi-particles in quantum field theories ",Phys. Rev. D**88**, 014036 (2013)*.

Yamamoto A., and Hirono Y. :"Lattice QCD in rotating frames ",Phys. Rev. Lett.**111**,081601(2013)*.

Hama Y., Tsitsishvili G., and Ezawa Z. F. :"Nambu-Goldstone modes and the Josephson supercurrent in the bilayer quantum Hall system ",Prog. Theor. Exp. Phys,053I01 (2013)*.

Suzuki H. :"Energy-momentum tensor from the Yang-Mills gradient flow ",Prog. Theor. Exp. Phys, 083B03 (2013)*.

Tanizaki Y. :"Flow equation of functional renormalization group for three-body scattering problems ",Prog. Theor. Exp. Phys., 113A01(2013)*.

Kurth T., Ishii N., Doi T. , Aoki S. , and Hatsuda T. :"Phase shifts in I=2 $\pi\pi$-scattering from two lattice approaches ",JHEP**1312**015 (2013)*.

Sekine A, Nakano T. Z., Araki Y., and Nomura K. :"Strong Coupling Expansion in a Correlated Three-Dimensional Topological Insulator ",Phys. Rev. B**87**, 165142 (2013)*.

Hayata T. :"Dynamical Mass Generation of Light-vector Mesons from QCD Trace Anomaly ",Phys. Rev. D**88**,036007(2013)*.

Inoue T., Aoki S., Doi T., Hatsuda T. , Ikeda T. , Ishii N., Murano K. , Nemura H., Sasaki K. (HAL QCD Collaboration) :"Equation of State for Nucleonic Matter and its Quark Mass Dependence from the Nuclear Force in Lattice QCD ",Phys. Rev. Lett.**111**,112503(2013)*.

Endres M., Kuroki T. , Suguno F., and Suzuki H. :"SUSY breaking by nonperturbative dynamics in a matrix model for 2D type IIA superstrings ",Nucl. Phys.**B876**,758-793 (2013)*.

Hirono Y., Nitta M., and Yasui S. :"Vortices and Other Topological Solitons in Dense Quark Matter ",Prog. Theor. Exp. Phys.,012D01(2013)*.

Tanizaki Y. , Fejos G., and Hatsuda T. :"Fermionic Functional Renormalization Group Approach to Superfluid Phase Transition ",Prog. Theor. Exp. Phys.,043I01(2014)*.

Fukda R. , Fukushima K. , Hayata T., and Hidaka Y. :"Sign problem and the chiral spiral on the finite-density lattice ",Phys. Rev. D**89**,014508 (2014)*.

Eto M., Hirono Y. , and Nitta M. :"Domain Walls and Vortices in Chiral Symmetry Breaking "Prog. Theor. Exp. Phys.,033B01(2014)*.

Mao H., Wei T., and Jin J. :"Chiral soliton model at finite temperature and density ",Phys. Rev. C**88**,035201 (2013)*.

Mao H. :"On the symmetry improved CJT formalism in the $O(4)$ linear sigma model ",Nucl. Phys.**A925**,185-198 (2014)*.

Tanizaki Y. :"Fermionic Functional Renormalization Group Approach to Bose-Einstein Condensation of Dimers ",Prog. Theor. Exp. Phys.,023A04(2014)*.

Ikeda Y., Charron B., Aoki S., Doi T., Hatsuda T., Inoue T., Ishii N., Murano K., Nemura H., and Sasaki K. (HAL QCD Collaboration) :"Charmed Tetraquarks Tcc and Tcs from Dynamical Lattice QCD Simulations ",Phys. Lett.**B729**,85-90 (2014)*.

Satow D. :"Ultrasoft fermion mode and off-diagonal Boltzmann equation in quark-gluon plasma at high temperature ",Phys. Rev. D**87**,096011 (2013)*.

Kamikado K. and Kanazawa T. :"Chiral dynamics in a magnetic field from the functional renormalization group ",JHEP**03**,009 (2014)*.

Ndaidon P., Endo S., and Ueda M. :"Microscopic Origin and Universality Classes of the Efimov Three-Body Parameter ",Phys. Rev. Lett**112**, 105301(2013)*.

Yan M., DeSalvo B. J., Huang Y., Ndaidon P., and Killian T. C. :"Rabi Oscillations between Atomic and Molecular Condensates Driven with Coherent One-Color Photoassociation ",Phys. Rev. Lett**111**, 150402(2013)*.

Nawa K., Ozaki S., Nagahiro H., Jido D., and Hosaka A. :"Complex 2D Matrix Model and Geometrical Map on Complex-Nc Plane ",Prog. Theor. Exp. Phys.,083D01(2013)*.

Hatta Y., Kanazawa K., and Yoshida S. :"Double-spin asymmetry A_{LT} in open charm production ",Phys. Rev. D**88**,014037(2013)*.

Beppu H. , Kanazawa K., Koike Y., and Yoshida S. :"Three-gluon contribution to the single spin asymmetry for light hadron production in pp collision ",Phys. Rev. D**89**,034029(2014)*.

Ohnishi S., Ikeda Y. *et al.* " Signature of strange dibaryons in kaon- and photon-induced reactions ",Phys. Rev. C**88**,025204 (2013)*.

Ozaki S. :"QCD effective potential with strong $U(1)_{\mathrm{em}}$ magnetic fields ",Phys. Rev. D**89**,054022(2014)*.

Fujii H., Honda D., Kato M., Kikukawa Y., Komatsu S., and Sano T. :"Hybrid Monte Carlo on Lefschetz thimbles - A study of the residual sign problem ",JHEP**1310**,147 (2013)*.

[Book・Proceedings]

(Original Papers)

Charron B. (HAL QCD Collaboration) :"A comparative study of two lattice approaches to two-body systems ",PoS LAT2013,223 (2013).

Doi T. (HAL QCD Collaboration) :"Cutoff effects on lattice nuclear forces ",PoS LAT2013,226(2013).

Ikeda Y. (HAL QCD Coll.) :"Search for possible bound Tcc and Tcs on the lattice ",PoS LAT2013,261(2013).

Yamamoto A. and Hirono Y. :"Rotating lattice ",PoS LAT2013,351(2013).

Hidaka Y. , Tsitsishvili G. , and Ezawa Z. F. :"Goldstone Modes in Bilayer Quantum Hall Systems at $\nu = 2$ ",Journal of Physics: Conference Series**456**,0120 (2013).

Tada T., :"Sine Square Deformation and String Theory ",Proceedings of the 12th Asia Pacific Physics Conference (APPC12) ,013003(2014).

Tachibana Y. and Hirano T. :"Emission of Low Momentum Particles at Large Angles from Jet ",Nucl. Phys.**A904-905**,1023c-1026c(2013).

Hatsuda T. :"Heavy quarkonium in hot medium ",Nucl. Phys.**A904-905**,210c-216c (2013).

Hatsuda T. :"Strangeness nuclear physics from lattice QCD ",Nucl. Phys.**A914**,211-219 (2013).

Doi T. (HAL QCD Collaboration) :"Few-baryon interactions from lattice QCD ",Few-Body Syst. **54**,827-833 (2013).

Oral Presentations

(International Conference etc.)

Hattori K.: "Vacuum birefringence and real-photon decay in strong magnetic fields", International School on Neutron Star Matter, YITP, Japan, Mar. (2014).

Hattori K.: "Photon propagation in strong magnetic fields – vacuum birefringence and real-photon decay", Frontiers of Hadronic Physics: Brains Recirculate Two, BNL, USA, Mar. (2014).

Kanazawa T.: "Chiral model analysis of QCD in magnetic fields", German-Japanese Seminar 2013 "Lattice Field Theory on multi-PFLOPS computers" Regensburg, Germany, Nov. (2013).

Kamikado K: "Effects of baryon number density fluctuation around QCD critical point '' , Extreme QCD 2013 Bern, Switzerland, Aug. (2013).

Naidon P: "Microscopic origin of the Efimov three-body parameter ", HPCI Workshop on Few-body systems and multi-particle resonances RIKEN, Wako, Japan, October (2013).

Naidon P: "Universality of the three-body parameter in atomic Efimov physics", 2013 joint meeting of the APS Division of Atomic, Molecular, & Optical Physics and the CAP Division of Atomic, Molecular & Optical Physics (DAMOP 2013) Quebec city, Canada, June (2013).

Naidon P: "Universality of the Efimov three-body parameter", First international conference on Few-body Physics in Cold Atomic Gases Beijing, China, April (2013).

Doi T.: "Cutoff effects on Lattice Nuclear Forces", The 31st International Symposium on Lattice Field Theory (Lattice 2013) Mainz, Germany, Jul.-Aug. (2013).

Doi T.: "Lattice in Nuclear Physics", 10th European Research Conference on Electromagnetic Interactions with Nucleons and Nuclei (EINN2013) Paphos, Cyprus, Nov. (2013).

Doi T.: "Hadron interactions from Lattice QCD", The workshop on strangeness nuclear physics (SNP2013) Xiamen, China, Dec. (2013).

Doi T.: "Baryon interactions from lattice QCD", KEK theory center workshop on J-PARC hadron physics in 2014 Tokai, Japan, Feb. (2014).

Doi T.: "Nucleon spin from lattice QCD", Workshop on High-energy QCD and nucleon structure Tokai, Japan, Mar. (2014).

Fejos G.: "Chiral symmetry breaking patterns in the U(n)xU(n) meson model", Workshop on Future Prospects of Hadron Physics at J-PARC and Large Scale Computational Physics in 2013 Tokai, Japan, February(2013).

Fejos G.: "Strongly coupled fermionic superfluidity and the functional renormalization group method" Eotvos University Particle Physics Meeting Budapest, Hungary, September(2013).

Fejos G.: "Chiral symmetry breaking patterns in the U(n)xU(n) meson model" New Frontiers in QCD 2013 Kyoto,Japan December(2013).

Satow D.: "(Quasi-) Nambu-Goldstone Fermion in Hot QCD Plasma and Bose-Fermi Cold Atom System", NFQCD 2013 Kyoto, Japan, Nov. (2013).

Satow D.: "Ultrasoft Fermion Mode at Finite Temperature and Density", Frontiers of Hadronic Physics: Brain

Circulation Kick off Workshop BNL, USA, Mar. (2013).

Tada T: "Sine Square Deformation and string theory", The 12th Asia Pacific Physics Conference Chiba, Japan, July (2013).

Tada T: "Sine Square Deformation and string theory", Todai/Riken joint workshop on Super Yang-Mills, solvable systems and related subjects Tokyo, Japan, Oct. (2013).

Tada T: "Sine Square Deformation and string theory", 3rd Bangkok workshop on high energy theory Bangkok, Thailand, Jan. (2014).

Hidaka Y, "Vector mesons in a strong magnetic field", New Frontiers in QCD 2013 Kyoto, Japan, Nov. (2013).

Hidaka Y. "Symmetry breaking of QCD in a strong magnetic field", Frontiers of Hadronic Physics New York, USA, Mar. (2013).

Hidaka Y. "QCD in a strong magnetic field", Recent progress in hadron physics -From hadrons to quark and gluon Soul, Korea, Feb. (2013).

Yamamoto A.: "Strong external electric fields in lattice QCD", Extreme QCD 2013Bern,Swiss,August(2013).

Yamamoto A. and Hirono Y. : "Rotating lattice", The XXXI International Symposium on Lattice Field TheoryMeintz,Germany,August(2013).

Hayata T., Nawa K., Hatsuda T. : "Heavy quakonium spectral functions with complex potenrial from Gauge/Gravity duality", Heavy quarks and quakonia in thermal QCDTrent,Italy,April(2013).

Nawa K., Ozaki S., Nagahiro H., Jido D. and Hosaka J. : "Complex 2D matrix model and its application to no-deoendence hadron structures", XV International conference on hadron spectroscopy (Hadron2013)Nara,Japan,Nov.(2013).

Matsuki K. and Seo K. : "Chiral partilce/photon emission from heavy-light mesons", Hadron nuclear physics in 2013Zhangiiajie,China,July(2013).

(Domestic Conference)

金澤拓也, TiloWettig, 山本直希: "高密度 QCD の Banks-Casher 関係式とランダム行列理論", 日本物理学会 2013 年秋季大会高知大学朝倉キャンパス, 9 月 (2013).

上門和彦: "Real Time Correlation Function in the O(N) model from the Functional-RG'', RCNP/九大研究会「ハドロン物理と原子核物理のクロスオーバー」九州大学, 福岡, 9 月 (2013).

上門和彦, 国広悌二, 大西明, 森田健司 : "Effects of baryon number density fluctuation on QCD critical point'', 日本物理学会秋季大会高知大学, 高知県, 9 月 (2013).

Naidon P: "Origin and Universality of the Efimov three-body parameter", Physical Society of Japan (JPS) meeting Tokai University, Hiratsuka, Japan, March (2014).

R. Kurita and T. Hirano: "重イオン衝突反応における核生成ダイナミクス", 日本物理学会秋季大会高知, 日本, Sep. (2013).

谷崎佑弥: "非相対論的な少数系に対する汎関数繰り込み群の構造" 日本物理学会高知, 日本, 9 月 (2013).

土井琢身: "格子 QCD による原子核物理・核力計算の現状と展望", 新学術領域「素核宇宙融合による計算科学に基づいた重層的物質構造の解明」のまとめと今後を語る研究会鳴子, 日本, 12 月 (2013).

土井琢身: "格子 QCD による原子核物理", 「京」、ポスト「京」と基礎物理和光, 日本, 1 月 (2014).

土井 琢身: "Quark mass dependence of Three-nucleon forces in Lattice QCD", 日本物理学会平塚, 日本, 3 月 (2014).

日高義将, 早田智也, 広野雄二: "非一様相における南部ゴールドストンの定理", 日本物理学会 2013 年秋季大会高知, 日本, 9 月 (2013).

日高義将: "時空対称性を含む南部・ゴールドストンの定理の一般化", 基研研究会「熱場の量子論とその応用」京都, 日本, 8 月 (2013).

日高義将, 山本新: "強磁場中でのベクトル中間子", 日本物理学会第 68 回年次大会広島, 日本, 3 月 (2013).

日高義将: "南部・ゴールドストンの定理の非相対論的な系への一般化", 日本物理学会第 68 回年次大会広島, 日本, 3 月 (2013).

山本新, 広野雄士: "Lattice QCD in rotating frames", 日本物理学会第 68 回年次大会 高知, 日本, 9 月 (2013).

名和要, 尾崎翔, 永廣秀子, 慈道大介, 保坂淳: "Complex 2D matrix model and internal structure of resonances", ハドロン物理と原子核物理のクロスオーバー九州大学, 日本 ,9 月 (2013).

Theoretical Nuclear Physics Laboratory

Publications

[Journal]

(Original Papers) *Subject to Peer Review

Avogadro P., and Nakatsukasa T.: "Efficient calculation for the quasiparticle random-phase approximation matrix", Phys. Rev. C **87**, 014331-1–014331-7 (2013). *

Fukuoka Y., Shinohara S., Nakatsukasa T., and Yabana K.: "Deformation and cluster structures in 12C studied with configuration mixing using Skyrme interactions", Phys. Rev. C **88**, 014321-1–014321-14 (2013). *

Yoshida K. and Nakatsukasa T.: "Shape evolution of giant resonances in Nd and Sm isotopes", Phys. Rev. C **88**, 034309-1–034309-15 (2013). *

Inakura T., Nakatsukasa T., and Yabana K.: "Low-energy E1 strength in select nuclei: Possible constraints on neutron skin and symmetry energy", Phys. Rev. C **88**, 051305(R)-1–051305(R)-5 (2013). *

Gu H. Q., Liang H. Z., Long W. H., Van Giai N., and Meng J.: "Slater approximation for Coulomb exchange effects in nuclear covariant density functional theory", Phys. Rev. C **87**, 041301(R) (2013). *

Liang H. Z., Nakatsukasa T., Niu Z. M., and Meng J.: "Feasibility of the finite-amplitude method in covariant density functional theory", Phys. Rev. C **87**, 054310 (2013). *

Niu Z. M., Niu Y. F., Liang H. Z., Long W. H., Niksic T., Vretenar D., and Meng J.: "β-decay half-lives of neutron-rich nuclei and matter flow in the r-process", Phys. Lett. B **723**, 172-176 (2013). *

Niu Z. M., Niu Y. F., Liu Q., Liang H. Z., and Guo J. Y.: "Nuclear β^+/EC decays in covariant density functional theory and the impact of isoscalar proton-neutron pairing", Phys. Rev. C **87**, 051303(R) (2013). *

Shen S. H., Liang H. Z., Zhao P. W., Zhang S. Q., and Meng J.: "Pseudospin symmetry in supersymmetric quantum mechanics. II. Spin-orbit effects", Phys. Rev. C **88**, 024311 (2013). *

Sato K., Dobaczewski J., Nakatsukasa T., and Satuła W.: "Energy-density-functional calculations including proton-neutron mixing", Phys. Rev. C **88**, p. 061301(R) (2013). *

Sheikh J. A., Hinohara N., Dobaczewski J., Nakatsukasa T., Nazarewicz W., Sato K.: "Isospin-invariant Skyrme energy-density-functional approach with axial symmetry", Phys. Rev. C **89**, p. 054317 (2014). *

Iida K., and Oyamatsu K.: "Symmetry energy, unstable nuclei and neutron star crusts", The European Physical Journal A **50**, 42 (2014). *

Dinh Dang N.,: "Giant dipole resonance in highly excited nuclei", EPJ Web of Conferences **66**, 02024-p.1– 02024-p.4 (2014). *

Dey B., Mondal D., Pandit D., Mukhopadhyay S., Pal S., Bhattacharya A., De A., Banerjee K., Dinh Dang N., Quang Hung N., Banerjee S.R.,: "Probing the critical behavior in the evolution of GDR width at very low temperatures in $A \sim 100$ mass region", Phys. Lett. B **731**, 92–96 (2014). *

Dinh Dang N., Quang Hung N.: "On the importance of using exact pairing in the study of pygmy dipole resonance", J. Phys. G **40**, 105103-1–105103-19 (2013). *

Dinh Dang N., Ciemala N., Kmiecik M., Maj A.: "Giant dipole resonance in ^{88}Mo from phonon damping model's strength functions averaged over temperature and angular momentum distributions", Phys. Rev. C **87**, 054313-1– 054313-8 (2013). *

Dinh Dang N.: "Damping of giant dipole resonance in highly excited nuclei", Acta Physica Polonica B **44**, 595 – 604 (2013).

(Review)

中務孝: "$N = Z$ 原子核の謎と新しい対凝縮", パリティ**28**, No. 1, pp. 41–42 (2013).

[Book・Proceedings]

(Original Papers) *Subject to Peer Review

Ebata S., Inakura T., and Nakatsukasa T.: "Time-dependent density-functional studies on strength functions in neutron-rich nuclei", Proceedings of 5th International Conference on Fission and properties of neutron-rich nuclei (ICFN5) (World Scientific), Sanibel Island, USA, 2012–7, World Scientific, Singapore, p. 635–642 (2013).

Liang H. Z., Meng J., Nakatsukasa T., Niu Z. M., Ring P., Roca-Maza X., Van Giai N., and Zhao P. W.: "Nuclear charge-exchange excitations in localized covariant density functional theory", EPJ Web of Conferences Vol. 66, The 25th International Nuclear Physics Conference, Florence, Italy, 2013–6, EDP Sciences, Les Ulis, p. 02064 (2014). *

Matsuo M., Hinohara N., Sato K., Matsuyanagi K., Nakatsukasa T., and Yoshida K.: "Quadrupole shape dynamics from the viewpoint of a theory of large-amplitude collective motion", Proceedings of 20th Nuclear Physics Workshop "Marie and Pierre Curie", Kazimierz, Poland, Sep., 2013, IOP Publishing, Bristol, p. 054020 (2013). *

鷲山広平: "微視的反応模型による低エネルギー重イオン反応", 原子核研究 Vol.58 Supplement 2 2013 年夏の学校特集号, 蒲郡, 2013–8, 原子核研究, pp. 27–32 (2014).

Oral Presentations

(International Conference etc.)

Nakatsukasa T.: "Stochastic generation of low-energy configurations and configuration mixing calculation", INT workshop on Computational and Theoretical Advances for Exotic Isotopes in the Medium Mass Region, (INT, University of Washington), Seattle, USA, March–April (2013).

Nakatsukasa T.: "Time-dependent density-functional theory with the continuum", ECT* workshop THEXO on Nuclear structure and astrophysical applications, (ECT*), Trento, Italy, July (2013).

Nakatsukasa T.: "Rotational effects on nuclear structure properties", 8pi Spectrometer Symposium: a Celebration of Discovery, (TRIUMF), Vancouver, Canada, July (2013).

Nakatsukasa T.: "Finite amplitude method in linear response TDDFT calculations", International School on Nuclear Physics, Neutron Physics and Applications, (Bulgarian Academy of Sciences), Varna, Bulgaria, September (2013).

Nakatsukasa T.: "Basic issues in theories of large amplitude collective motion", INT workshop on Quantitative Large Amplitude Shape Dynamics: fission and heavy ion fusion, (INT, University of Washington), Seattle, USA, September–November (2013).

Liang H. Z.: "Localized form of Fock terms in nuclear covariant density functional theory", THEXO Workshop on Nuclear Structure and Astrophysical Applications, (ECT*), Trento, Italy, Jul. (2013).

Liang H. Z., Meng J., Nakatsukasa T., Niu Z. M., Ring P., Roca-Maza X., Van Giai N., and Zhao P. W.: "Nuclear charge-exchange excitations in localized covariant density functional theory", The 25th International Nuclear Physics Conference, (INFN), Florence, Italy, Jun. (2013).

Liang H. Z.: "Pseudospin symmetry in supersymmetric quantum mechanics", iTHES workshop on "Exploration of hidden symmetries in atomic nuclei", (RIKEN), Wako, Jul. (2013).

Liang H. Z., Meng J. Shen S. H., Van Giai N., Zhang S. Q., Zhang Y., and Zhao P. W.: "Pseudospin symmetry in nuclear single-particle spectra and its perturbative interpretation", The XX International School on Nuclear Physics, Neutron Physics and Applications, (Institute for Nuclear Research and Nuclear Energy), Varna, Bulgaria, Sep. (2013).

Liang H. Z., Nakatsukasa T., Niu Z. M., and Meng J.: "Finite amplitude method in covariant density functional theory", The 20th Nuclear Physics Workshop "Marie & Pierre Curie", (Maria Curie-Sklodowska University), Kazimierz, Poland, Sep. (2013).

Liang H. Z.: "Nuclear charge-exchange excitation and its microscopic mechanism", Seminar of Institute of Theoretical Physics, Chinese Academy of Sciences, (Institute of Theoretical Physics, Chinese Academy of Sciences), Beijing, China, Nov. (2013).

Liang H. Z.: "Nuclear collective excitations in covariant density functional theory", The 4th Lectures on Covariant Density Functional Theory in Nuclear Physics, (Guangxi Normal University), Guilin, China, Nov. (2013).

Liang H. Z.: "Finite amplitude method in covariant density functional theory", JUSTIPEN-JUSEIPEN Workshop, (RIKEN / U.S. DOE), Wako, Dec. (2013).

Liang H. Z.: "Relativistic studies of spin-isospin resonances", IInd Topical Workshop on Modern Aspects in Nuclear Structure, (Universita degli Studi di Milano), Bormio, Italy, Feb. (2014).

Liang H. Z.: "Nuclear beta-decay half-lives and the impact of isoscalar proton-neutron pairing", International Molecule-type Workshop on New correlations in exotic nuclei and advances of theoretical models, (YITP), Kyoto, Mar. (2014).

Sato K., Nakatsukasa T., Satula W., and Dobaczewski J.: "Energy-density-functional calculations including the proton-neutron mixing", JUSTIPEN-JUSEIPEN Workshop, Wako, Dec. (2013).

Sato K., Nakatsukasa T., Satula W., and Dobaczewski J.: "Energy-density-functional calculations including the proton-neutron mixing", 2nd Topical Workshop on Modern Aspects in Nuclear Structure, Bormio, Italy, Feb. (2014).

Sato K., Nakatsukasa T., Satula W., and Dobaczewski J.: "Mean-field calculations based on the proton-neutron mixed energy density functional", International Molecule-type Workshop on New correlations in exotic nuclei and advances of theoretical models, 京都, Mar. (2014).

Washiyama K.: "Internuclear potential and energy dissipation in fusion reactions from a time-dependent energy density functional model", Advances in time-dependent methods for quantum many-body systems, (ECT*), Trento, Italy, Oct. (2013).

Washiyama K.: "Macroscopic properties in low-energy nuclear reactions by microscopic TDDFT", Quantitative Large Amplitude Shape Dynamics: fission and heavy ion fusion, (Institute for Nuclear Theory, University of Washington), Seattle, USA, Oct. (2013).

Washiyama K.: "Regularized multi-reference energy density functional calculations with new Skyrme parametrizations", Symposium in honour of Paul-Henri Heenen, (Université Libre de Bruxelles), Brussels, Belgium, Oct. (2013).

Washiyama K.: "Microscopic TDDFT for low-energy fusion reactions", JUSTIPEN-JUSEIPEN Workshop, (RIKEN Nishina Center and Center for Nuclear Study, University of Tokyo) Wako, Japan, Dec. (2013).

Washiyama K.: "Fusion and quasi-fission in heavy systems with the microscopic time-dependent energy density functional theory", VI International Conference FUSION14, (Inter Univerisity Accelerator Centre), New Delhi, India, Feb. (2014).

Dinh Dang N.: "Giant dipole resonance from phonon-damping model's strength functions averaged over temperature and angular momentum", Invited seminar, (Saha Institute of Nuclear Physics), Kolkata, December (2013).

Dinh Dang N.: "Viscosity: From air to hot nuclei", International Symposium on Nuclear Physics, (Bhabha

Atomic Research Center), Mumbai, December (2013).

Dinh Dang N.: “Giant dipole resonance in highly excited nuclei”, International Nuclear Physics Conference INPC 2013, June 2 - 7, 2013, (IUPAP), Florence, June (2013).

(Domestic Conference)

中務孝: “TDDFT 計算による原子核の集団励起と反応”, 第3回 HPCI 戦略プログラム分野 2 ×分野 5 異分野交流研究会「量子多体系のダイナミクス計算 ー原子核から物質科学までー」, (分子科学研究所), 岡崎, 11 月 (2013).

中務孝: “原子核物理入門”, KEK サマーチャレンジ, (KEK), つくば, 8 月 (2013).

中務孝: “原子核密度汎関数理論”, サマースクール「クォークから超新星爆発まで」, (京都大学基礎物理学研究所), 京都, 8 月 (2013).

中務孝: “計算核物理学のフロンティア”, 日本物理学会第6８会年次大会, (日本物理学会), 東広島, 3 月 (2013).

中務孝: “核子多体系の基本的性質と原子核集団運動”, 中性子星核物質ウィンタースクール, (日本学術振興会), 和光, 12 月 (2013).

中務孝: “原子核の量子的集団ダイナミクス”, 卓越した大学院拠点形成シンポジウム, (早稲田大学), 東京, 12 月 (2013).

中務孝: “密度汎関数法による核構造・核反応計算”, 新学術領域「素核宇宙融合による計算科学に基づいた重層的物質構造の解明」のまとめと今後を語る研究会, (日本学術振興会), 大崎, 12 月 (2013).

Liang H. Z.: “Nuclear charge-exchange excitations in covariant density functional theory”, RCNP Seminar, (Osaka University), Ibaraki, 9 月 (2013).

Liang H. Z.: “Nuclear charge-exchange excitations in covariant density functional theory”, HPCI-CNS seminar, (University of Tokyo), Tokyo, 10 月 (2013).

Liang H. Z.: “Pseudospin symmetry in single-particle spectra and its perturbative interpretation”, The 163rd RIKEN RIBF Nuclear Physics Seminar, (RIKEN), Wako, 4 月 (2013).

佐藤弘一, 中務孝, Satula W., Dobaczewski J.: “陽子-中性子混合密度汎関数による T = 1 アイソバリックアナログ状態の系統的計算”, 日本物理学会 第 69 回年次大会, (日本物理学会), 東海大学, 3 月 (2014).

佐藤弘一, 中務孝, Satula W., Dobaczewski J.: “中重核における陽子ー中性子混合を含んだ拘束 Hartree-Fock 計算”, 日本物理学会 2013 年秋季大会, (日本物理学会), 高知, 9 月 (2013).

鷲山広平： ” 微視的反応模型による低エネルギー重イオン反応”，原子核三者若手夏の学校原子核パート研究会，(原子核三者若手), 蒲郡，8 月 (2013).

鷲山広平： “重い原子核同士の融合反応における原子核間ポテンシャルと散逸エネルギーの微視的導出”，日本物理学会秋季大会，(日本物理学会), 高知，9 月 (2013).

鷲山広平： “TDDFT 計算による低エネルギー重イオン核融合反応”，HPCI 戦略プログラム分野 2 ×分野 5 異分野交流研究会「量子多体系のダイナミクス計算ー原子核から物質科学までー」，(分子科学研究所), 岡崎，11 月 (2013).

鷲山広平： “TDHF による重い原子核同士の核融合反応と準核分裂反応”，日本物理学会年次大会，(日本物理学会), 平塚，3 月 (2014).

小濱洋央, 飯田圭, 親松和浩: “中間エネルギーでの不安定核全反応断面積と変形度”, 日本物理学会 2013 年第 68 回年次大会, (日本物理学会), 東広島, 3 月 (2013).

小濱洋央, “RIKEN-JCPRG 活動の全体報告”, The 1st JCPRG-RNC Joint Workshop on nuclear data, 和光, 8–8 月 (2013).

Strangeness Nuclear Physics Laboratory

Publications

[Journal]

(Original Papers)

Fukukawa K., Fujiwara Y.,
"Coulomb effect in Nucleon-Deuteron Elastic Scattering", Few-Body Systems, Vol. 54, Nos. 7-10, pp.1331-1334, (2013). *

Fujiwara Y., Fukukawa K.,
"Deuteron Breakup Differential Cross Sections and Analyzing Powers of Scattering at Ed = 16 and 130 MeV", Few-body Systems, Vol 54, Nos. 7-10, pp. 1307-1310, (2013). *

Fujiwara Y., Fukukawa K.,
"Few-nucleon systems interacting via non-local quark-model baryon-baryon interaction", Journal of conference series, Vol 436, 012081, (2013). *

Hiyama E.,
"Few-Body Aspects of Hypernuclear Physics", Few-Body Systems. Vol. 53, Issue 3-4, pp. 189-236, (2012). *

Yokota A., Hiyama E., Oka M.,
"Possible existence of charmonium–nucleus bound states", PTEP, 113D01 (18pages), (2013). *

Nakamura S., Matsumura A., Okayasu Y., Seva T., Rodriguez V. M., Baturin P., Yuan L., Acha A., Ahmidouch A., Androic D., Asaturyan A., Asaturyan R., Baker O. K., Benmokhtar F., Bosted P., Carlini R., Chen C., Christy M., Cole L., Danagoulian S., Daniel A., Dharmawardane V., Egiyan K., Elaasar M., Ent R., Fenker H., Fujii Y., Furic M., Gan, L., Gaskell D., Gasparian A., Gibson E. F., Gogami T., Gueye P., Han Y., Hashimoto O., Hiyama E., Honda D., Horn T, Hu B., Hungerford Ed V., Jayalath C., Jones M., Johnston K., Kalantarians N., Kanda H., Kaneta M., Kato F., Kato S., Kawama D., Keppel C., Lan K. J., Luo W., Mack D., Maeda K., Malace S., Margaryan A., Marikyan G., Markowitz P., Maruta T., Maruyama N., Miyoshi T., Mkrtchyan A., Mkrtchyan H., Nagao S., Navasardyan T., Niculescu G., Niculescu, Nomura H., Nonaka K., Ohtani A., Oyamada M., Perez N., Petkovic T., Randeniya S., Reinhold J., Roche J., Sato Y., Segbefia E. K., Simicevic N., Smith G., Song Y., Sumihama M., Tadevosyan V., Takahashi T., Tang L., Tsukada K., Tvaskis V., Vulcan W., Wells S., Wood S. A., Yan C., and Zhamkochyan S,
"Observation of the $^7_{¥Lambda}$He Hypernucleus by the (e, e′K+) Reaction", Physical Review Letters, Vol.110, Issue1, 012502, (2013). *

Hiyama E., Ohnishi S., Kamimura M., Yamamoto Y.,
"Four-body structure of neutron-rich hypernucleus $^6_[¥Lambda]$H", Nuclear Physics A, Vol. 908, pp. 29-39, (2013). *

Ohtsubo S., Fukusima Y., Kamimura M., Hiyama E.,
"Complex-scaling calculation of three-body resonances using complex-range Gaussian basis functions: Application to 3α resonances in ^{12}C", PTEP, 073D02 (16pages), (2013). *

Suzuki K., Gubler P., Morita K., Oka M.,
"Thermal modification of bottomonium spectra from QCD sum rules with the maximum entropy method", Nuclear Physics A, Vol. 897, pp. 28-41, (2013). *

Ohtani K., Gubler P., Oka M.,
"Parity projection of QCD sum rules for the nucleon", Physical Review D, Vol. 87, No. 3 P. 034027-1 - 034027-17 ,(2013). *

Gubler P., Suzuki K., Morita K., Oka M.,
"Modification of hadronic spectral functions under extreme conditions: An approach based on QCD sum rules and the maximum entropy method", Nuclear Physics A, Vol. 914, P. 512-516, (2013). *

Gubler P., Suzuki K., Morita, K., Oka M.,
"Quarkonia at Finite T: An Approach Based On QCD Sum Rules and the Maximum Entropy Method", Few-Body Systems, Vol. 54, pp. 1059-1062, (2013). *

Ohtani K., Gubler P., Oka M.,
"Parity Projected QCD Sum Rule of the Nucleon with MEM", Few-Body Systems, Vol. 54, pp. 1063-1066, (2013). *

Ohtani K., Gubler P., Oka M.,
"MEM Analysis of the QCD Sum Rule and its Application to nucleon spectrum", Proceedings of Science, CD12, Vol. 079, pp. 1-6, (2013).

Oka M., Suzuki K., Morita K., Gubler P.,
"Thermal Modification of bottomonium spectral functions from QCD sum rules", Proceedings of Science, CD12, Vol. 080, P. 1-6, (2013).

Suno H., Hiyama E., Kamimura M.,
"Theoretical Study of Triatomic Systems Involving Helium Atoms", Few-Body Systems, Vol. 54, pp. 1557-1560, (2013). *

Sakumichi N., Nishida Y, Ueda M.,
"Lee-Yang cluster expansion approach to the BCS-BEC crossover: BCS and BEC limits", arXiv:1310.4665, (2013).

Ohnishi S., Ikeda Y., Kamano H., Sato T.,
"Signature of strange dibaryons in kaon- and photon-induced reactions", Physical Review, C88, 025204, (2013). *

Ohnishi S., Ikeda Y., Kamano H., Sato T.,
"Production Reaction of $KNN−¥piYN$ Resonance from Faddeev Equations", Few-Body Systems, Volume 54, Issue 7-10, pp. 1119-1122, (2013). *

Ikeda Y., Hyodo T., Jido D., Kamano H., Sato T., Yazaki K.,
"Structure of Lambda(1405) and Threshold Behavior of pi Sigma Scattering", Prog. Theor. Phys., 125, 1205-1224, (2011). *

Inoue T., Ishii N., Aoki S., Doi T., Hatsuda T., Ikeda Y., Murano K., Nemura H., Sasaki K.,
"Bound H Dibaryon in Flavor SU(3) Limit of Lattice QCD", Phys. Rev. Lett. 106, 162002 (4pages), (2011). *

Jido D., Sekihara T., Ikeda Y., Hyodo T., Kanada-En'yo Y., Oset E.,
"The nature of the $¥Lambda(1405)$ hyperon resonance in chiral dynamics", Nucl. Phys. A, 835,

59—66, (2010). ∗

Fukuoka Y., Funaki Y., Nakatsukasa T., Yabana K., "Large scale calculations for cluster structure of light nuclei with Skyrme interaction", Journal of Physics, Conference Series, 436, 012012, (2013). ∗

Funaki Y., Yamada T., Horiuchi H., Roepke G., Schuck P., Tohsaki A., "Resonance States and Alpha Condensation in ^{12}C and ^{16}O", Few-Body Systems, 54, 521-525, (2013). ∗

Funaki Y., Yamada T., Horiuchi H., Roepke G., Schuck P., Tohsaki A., "Gas-like cluster states in finite nuclei" Few-Body Systems, 54, 1453-1456, (2013). ∗

Funaki Y., Yamada T., Hiyama E., Ikeda K., "Alpha-particle condensation in light hypernuclei", Nuclear Physics A, 914, 194-198, (2013) ∗

Funaki Y., Horiuchi H., Ren Z.Z., Roepke G., Schuck P., Tohsaki A., Xu C., Yamada T., Zhou B., "New concept in clusterings and alpha-particle condensates", AIP Conference Proceedings, 1533, 33-40, (2013). ∗

Funaki Y., Yamada T., Horiuchi H., Roepke G., Schuck P., Tohsaki A., "Gas-like alpha-cluster states and condensates in nuclei", Journal of Physics, Conference Series, 436, 012004, (2013). ∗

Fukuoka Y., Shinohara S., Funaki Y., Nakatsukasa T., Yabana K., "Deformation and cluster structures in ^{12}C studied with configuration mixing using Skyrme interactions", Phys. Rev. C, 88, 014321, (2013). ∗

Zhou. B., Funaki Y., Horiuchi H., Ren Z.Z., Roepke G., Schuck P., Tohsaki A., Xu C., Yamada T., "Nonlocalized Clustering: A New Concept in Nuclear Cluster Structure Physics", Phy. Rev. Lett., 110, 262501, (2013). ∗

Isaka M., Honma H., Kimura M., Dote A., Ohnishi A., "Excited states with $¥Lambda$ hyperon in p-orbit in $^{25}_¥Lambda$Mg", Nuclear Physics A, Vol. 914, pp 189-193, (2013). ∗

Isaka M., Honma H., Kimura M., Dote A., Ohnishi A., "Structure of Be Hyper Isotopes", Few-Body Systems, Vol.54, pp.1219-1222, (2013). ∗

Isaka M., Honma H., Kimura M., "Structure of Be hyper isotopes", Journal of Physics: Conference Series, Vol. 436, p. 012082, (2013).

Isaka M., Hukukawa K., Kimura M., Hiyama E., Sagawa H., Yamamoto Y., "Superdeformed $¥Lambda$ hypernuclei with antisymmetrized molecular dynamics", Phys. Rev. C, Vol. 89, 024310, (2014). ∗

Sakumichi N., Nishida Y., Ueda M., "Lee-Yang cluster expansion approach to the BCS-BEC crossover: BCS and BEC limits", Phys. Rev. A 89, 033622, Vol. 89, Pages. 033622, (2014). ∗

Suno H., "A Theoretical Study of Pure and Mixed Spin-Polarized Tritium and Helium Triatomic Systems Using Hyperspherical Coordinates", Few-Body Systems, Vol.54, pp. 229-239, (2014). ∗

Suhara T., Funaki Y., Zhou B., Horiuchi H.,. Tohsaki A, "One-Dimensional α Condensation of α-Linear-Chain States in ^{12}C and ^{16}O", Phys. Rev. Lett., 112, 062501, (2014). ∗

Zhou B., Funaki Y., Horiuchi H., Ren Z.Z., Roepke G., Schuck P., Tohsaki A., Xu C., Yamada T., "Nonlocalized cluster dynamics and nuclear molecular structure", Physical Review C, 89, 034319, (2014). ∗

Hiyama E., Funaki Y., Kaiser N.and Weise W., "Alpha-clustered hypernuclei and chiral SU(3) dynamics", PTEP (Progress of Theoretical and Experimental Physics), 013D01, (2013). ∗

[Book · Proceedings]

(Others)

Gubler P., "A Bayesian Analysis of QCD Sum Rules", Springer Thesis, P. 1-190 (全体), (2013).

Ikeda Y., Aoki S., Doi T., Hatsuda T., Inoue T., Ishii N., Murano K., Nemura H., Sasaki K., "Kaon-Nucleon potential from lattice QCD", EPJ Web of Conferences, 3, 03007 (5pages), (2010).

Oral Presentations

(International Conference etc.)

Fukukawa K., "Hyperon-Hyperon Interaction Based on Quark-Model Baryon-Baryon Interaction", 第１２回アジア太平洋国際会議，千葉，7 月(2013).

Fukukawa K., "Hyperon-Hyperon Interaction Based on Quark-Model Baryon-Baryon Interaction", Hadron Nuclear Physics 2013, Zhangjiajie, China, Jul.(2013).

Hiyama E., "Three-and four-body structure of hypernuclei using cluster model", Clustering Aspects in Nuclei, Beijing, China, Apr.(2013).

Hiyama E., "Four- and five-body calculation of double Lambda hypernuclei", "The 11th International Conference on Low Energy Antiproton Physics" (LEAP 2013), Uppsala, Sweden, Jun.(2013).

Hiyama E., "$¥Lambda N$-$¥Sigma N$ coupling in A = 4 Λ hypernuclei", the Importance of Tensor Interactions in Nuclear and Hadron Structures, Osaka, Jul.(2013).

Hiyama E., "Theoretical situation about $^6_{¥Lambda}$H", The informal workshop on "Present status on subject of H5 and H6Lambda", Osaka、Aug.(2013).

Hiyama E., "Few-body structure of light hypernuclei", The 22nd European Conference on Few-Body Problems in Physics, Kraków, Poland, Sep.(2013).

Hiyama E.,
"Recent progress in hypernuclear physics", Radioactive isotopes and Nuclear Astrophysics with related topics (RIaNA), Pohang, Korea, Sep.(2013).

Hiyama E.,
"Structure of light Lambda hypernuclei", NUFRA2013 International Conference on Nuclear Fragmentation 2013, Kemer (Antalya), Turkey, Oct.(2013).

Hiyama E.,
"Three- and Four-Body Structure of Neutron-Rich $¥Lambda$ Hypernuclei", Inelastic Reaction in Light Nuclei, Jerusalem, Israel, Oct.(2013).

Hiyama E.,
"Few-body structure of light hypernuclei", The Seventh International Symposium on Chiral Symmetry in Hadrons and Nuclei, Beijing, China, Oct.(2013).

Hiyama E.,
"Precise calculation of light hypernuclei", The 10th JSPS Core-to-Core Symposium, Prague, Czech, Dec.(2013).

Yokota A., Hiyama E., Oka M.,
"Possible existence of charmonium-nucleus bound states", The 22nd European Conference on Few-Body Problems in Physics, Kraków, Poland, Sep.(2013).

Gubler P., Yamamoto N., Nishida Y., Hatsuda T.,
"OPE + sum rule approach to single-particle spectral functions of the unitary fermi gas", Seminar, Seoul, Korea, May(2013).

Gubler P.,
"Exploring the QCD Phase Diagram from Hadronic Obsevables", Seminar, Xiamen, China, Oct.(2013).

Gubler P.,
"Applications of sum rules in QCD and cold atoms", Workshop on theoretical study of superheavy nuclei, asymmetric nuclear matter and exotic nuclei, Beijing, China, Oct.(2013).

Gubler P., Suzuki K., Ohtani K., Morita K., Oka M.,
"Recent results from QCD sum rule analyses based on the maximum entropy method", International Symposium on Chiral Symmetry in Hadrons and Nuclei, Beijing, China, Oct.(2013).

Gubler P., Ohtani K.,
"The phi meson at finite density from a QCD sum rules + MEM approach", YITP workshop on "Hadrons in Nucleus", Kyoto, Nov. (2013).

Gubler P., Ohtani K.,
"Vector mesons at finite density from QCD sum rules and the maximum entropy method", XV International Conference on Hadron Spectroscopy (Hadron 2013), Nara, Nov. (2013).

Ohnishi S., Ikeda Y., Hyodo T., Hiyama E., Weise W.,
"Energy spectrum of 1S kaonic deuterium", Workshop on "Strangeness in the Universe? Theoretical and experimental progress and challenges", Trento, Italy, Oct.(2013).

Funaki Y.,
"Gas-like alpha cluster states in nuclei", The international workshop on ``Clustering Aspects in Nuclei", Beijing, China, Apr.(2013)

Funaki Y.,
"Alpha-cluster structures in light hypernuclei", The international workshop on ``Strangeness Nuclear Physics'', Xiamen, China, Dec.(2013).

Funaki Y.,
"Cluster states in light nuclei studied with ``new" THSR wave function", The international workshop on ``Clustering Aspects in Nuclei and Nuclear Matter'', Rostock, Germany, Sep.(2013).

Funaki Y.,
"Gas-like alpha-cluster states in light nuclei", The international workshop on ``Alpha decay as a probe of nuclear structure'', Stockholm, Sweden, Sep. (2013).

Funaki Y.,
"Alpha-cluster states in light hypernuclei", The 22nd European Conference on ``Few-Body Problems in Physics (EFB22)", Cracow, Poland, Sep. (2013).

Isaka M.,
"Structure of p-sd shell Lambda hypernuclei modified and probed by $¥Lambda$ hyperon"", セミナー, Institute of Theoretical Physics, Chinese Academy of Sciences, Beijing, China, May.(2013).

Isaka M., Honma H., Kimura M.,
"Structure of Be hyper isotopes", The 22nd European Conference on Few-Body Problems in Physics, Auditorium Maximum of the Jagiellonian University, Cracow, Poland, Sep. (2013).

Isaka M.,
"Studies of hypernuclei with the AMD method", The Seventh International Symposium on Chiral Symmetry in Hadrons and Nuclei, Beijing, China, Oct.(2013).

Isaka M.,
"Deformation of hypernuclei", JSPS core-to-core seminar (Study of Lambda Hypernuclei with Electron Beams), Vila Lanna, Prague, Czech, Dec.(2013).

Isaka M.,
"Deformations of $sd-pf$ shell hypernuclei", International Workshop on Strangeness Nuclear Physics, Xiamen, China, Dec. (2013).

Suno H., Nakamura Y., Ishikawa K., Kuramashi Y.,
"Block BiCGSTAB for lattice QCD on the K computer", The 4th AICS International Symposium, Kobe, Dec.(2013).

Hiyama E.,
"Gaussian Expansion Method and its application to atomic and nuclear physics", Seminar at Institut Non Lineaire de Nice, Nice, France, Jan.(2014).

Hiyama E.,
"Gaussian Expansion Method and its application to atomic and nuclear physics", Seminar at Universita degli studi di MILANO, Milano, Italy, Feb.(2014).

Hiyama E.,
"Recent advances in studies of neutron-rich hypernuclei's structure", Seminar at Universita degli studi di TORINO, Torino, Italy, Feb.(2014)

Sakumichi N., Nishida Y., Ueda M.,
"Lee-Yang cluster expansion approach to BCS-BEC

crossover", 2013 Joint Meeting of the APS Division of Atomic, Molecular and Optical Physics and the CAP Division of Atomic, Molecular and Optical Physics, Quebec City, Canada, Jun.(2013).

Sakumichi N.,
"Cluster expansion approach to the BCS-BEC crossover", 東京理科大学 二国研究室セミナー, 新宿（神楽坂キャンパス）, Dec.(2013).

Sakumichi N.,
"Cluster expansion approach to BCS-BEC crossover", 新学術領域研究「中性子星の核物質」第二回研究会, 和光, 12月(2013).

Sakumichi N.,
"Cluster expansion approach to BCS-BEC crossover in cold-atom systems", 東京工業大学 岡研究室セミナー, 東京工業大学, 5月(2013).

Sakumichi N.,
"Cluster expansion approach to BCS-BEC crossover in cold-atom systems", 理化学研究所 橋本研究室セミナー, 和光, 6月(2013).

Sakumichi N., Kawakami N., Ueda M.,
"Perron-Frobenius theorem on the superfluid transition of an ultracold Fermi gas", RIKEN-APW joint workshop "Highlights in condensed matter physics", Wako-shi, Jan.(2014).

Sakumichi N.,
"Lee-Yang Cluster Expansion Study of BCS-BEC crossover", Bose-Einstein Condensation 2013 "Frontiers in Quantum Gases", Sant Feliu de Guixols、Spain, Sep.(2013).

Sakumichi N.,
"Lee-Yang cluster expansion for BCS-BEC crossover: BCS and BEC limits", The 11th US-Japan Joint Seminar, Nara, Apr.(2013).

Isaka M., Fukukawa K., Kimura M., Hiyama E., Sagawa H., Yamamoto Y.,
"Deformations of $sd-pf $ shell $¥Lambda$ hypernuclei", KEK theory center workshop on J-PARC hadron physics in 2014, Tokai, Feb.(2014).

Isaka M., Fukukawa K., Kimura M., Hiyama E., Sagawa H., Yamamoto Y.,
"Superdeformed states in hypernuclei", International School for Strangeness Nuclear Physics (SNP School 2014), Tokai, Feb.(2014).

Isaka M., Fukukawa K., Kimura M., Hiyama E., Sagawa H., Yamamoto Y.,
"Deformations of sd and pf shell $¥Lambda$ hypernuclei", Japan-Korea Joint Workshop for Hyperons in Nuclear and Astrophysics with related topics (Hyperon*), Seoul, Korea, Mar.(2014).

Isaka M., Fukukawa K., Kimura M., Hiyama E., Sagawa H., Yamamoto Y.,
"Deformations of sd and pf shell $¥Lambda$ hypernuclei with AMD", The 3rd Korea-Japan Workshop on Nuclear and Hadron Physics at J-PARC, Incheon, Korea, Mar.(2014).

Ohnishi S., Ikeda Y., Hyodo T., Hiyama E., Weise W.,
"$d(K^-,n)$ reaction and structure of $¥Lambda(1405)$", The 3rd Korea-Japan Workshop on Nuclear and Hadron Physics at J-PARC, Incheon, Korea, Mar.(2014).

Hiyama E.,
"Structure of few-body hypernuclei", Japan-Korea Joint Workshop for Hyperons in Nuclear and Astrophysics with related topics (Hyperon*), Seoul, Korea, Mar.(2014)

Hiyama E.,
"^{4}He trimer and tetramer systems using realistic ^{4}He potential", International Molecule-type Workshop on New correlations in exotic nuclei and advances of theoretical models, Kyoto, Mar.(2014).

Hiyama E.,
"Structure of $S=-1$ system", Third Korea-Japan workshop on nuclear and hadron physics at J-PARC, Incheon, Korea, Mar.(2014).

Hiyama E.,
"Recent Progress in Nuclear Physics", A celebration of the Science of Female Researchers in JAPAN, Wako-shi, Mar.(2014).

Gubler P., Yamamoto N., Nishida Y., Hatsuda T.,
"OPE + sum rule approach to single-particle spectral functions of the unitary fermi gas", Seminar, Seoul, Korea, May.(2013).

Gubler P., Oka M., Morita K., Ohtani k., Suzuki K.,
"Quarkonia at finite T from QCD sum rules and MEM", NFQCD2013, Kyoto, Dec.(2013).

Gubler P., Ohtani K.,
"The $¥phi$ meson at finite density, revisited", Workshop on J-PARC hadron physics in 2014, Tokai, Feb.(2014).

(Domestic Conference)

肥山詠美子: "「$Ｓ＝－２$原子核の構造」", 「ハイパー核物理の発展と今後の展望」, 志摩, 7月(2013).

吉田哲也, 岡真, 肥山詠美子: "チャームバリオンのスペクトルと構造の研究", 日本物理学会 2013 年秋季大会, 高知, 9月(2013).

横田朗, 肥山詠美子, 岡真: "チャーモニウム-原子核束縛状態における$J/¥Psi$と$¥eta_c$の混合", 日本物理学会 2013年秋季大会, 高知, 9月(2013).

前田沙織, 横田朗, 肥山詠美子, 岡真, Yan-Rui Liu: "短距離斥力を含むY_cN 相互作用とチャーム原子核", 日本物理学会 2013年秋季大会, 高知, 9月(2013).

Philipp Gubler: "QCD 和則と MEM を用いた有限密度中の vector meson の研究の現状と最近の発展", ワークショップ「原子核媒質中のハドロン研究＝魅力と課題＝」, 東海, 8月(2013).

Philipp Gubler, 山本直希, 西田祐介, 初田哲男: "ユニタリー・フェルミ気体の一粒子スペクトル関数に対する和則の構築", 基研研究会「熱場の量子論とその応用」, 京都, 8月(2013).

Philipp Gubler, 山本直希, 西田祐介, 初田哲男: "演算子積展開法を用いたユニタリー・フェルミ気体の一粒子スペクトル関数の解析", 日本物理学会 ２０１３年秋季大会, 高知, 9月(2013).

Philipp Gubler, 山本直希, 西田祐介, 初田哲男: “ユニタリー・フェルミ気体の一粒子スペクトル関数に対する和則の構築とその最大エントロピー法による解析”, 日本物理学会 ２０１３年秋季大会, 松山, 9 月(2013).

大西祥太，池田陽一，兵藤哲雄，肥山詠美子，Wolfram Weise: “$K-d$原子の理論計算の現状と今後の課題”, KEK（東海）研究会「原子核媒質中のハドロン研究＝魅力と課題＝」, 東海, 8 月(2013).

大西祥太，池田陽一，兵藤哲雄，肥山詠美子，Wolfram Weise: “反 K 中間子-重陽子原子における 1S 状態のエネルギー・スペクトルの研究”, 日本物理学会 2013 年秋季大会, 高知, 9 月(2013).

船木靖郎: “^{12}C における一次元ガス的 3α クラスター構造の研究”, 日本物理学会 2013 年秋季大会, 高知, 9 月(2013).

船木靖郎，山田泰一，肥山詠美子，池田清美: “軽い$¥Lambda$ハイパー核における$¥alpha$クラスター構造”, 日本物理学会 2013 年秋季大会, 高知, 9 月(2013).

井坂政裕: “"Structure of $p-sd$ shell $¥Lambda$ hypernuclei modified and probed by $¥Lambda$ hyperon "”, ＫＥＫ理論セミナー, つくば, 5 月(2013).

井坂政裕，本間裕明，木村真明:“Be 同位体における $¥Lambda$ 粒子による核構造の変化”, ＲＣＮＰ研究会「核子・ハイペロン多体系におけるクラスター現象」, 横浜, 7 月(2013).

井坂政裕: “"Structure of $p-sd$ shell $¥Lambda$ hypernuclei modified and probed by $¥Lambda$ hyperon"”, ＫＥＫ東海セミナー, つくば, 9 月(2013).

井坂政裕, 木村真明, 肥山詠美子, 佐川弘幸, 山本安夫: “AMD による $^{46}_¥Lambda$Sc 及び $^{48}_¥Lambda$Sc の構造研究”, 日本物理学会 ２０１３年秋季大会, 高知, 9 月(2013).

作道直幸: “孤立量子系におけるエントロピー増大則”, 第 6 回基礎物理セミナー合宿, 箱根, 12 月(2013).

作道直幸: “Lee-Yang のクラスター展開法による BCS 理論の導出”, 基研研究会「熱場の量子論とその応用」, 京都, 8 月(2013).

井坂政裕: “$sd-pf$ 殻ハイパー核の超変形状態”, 阪大 RCNP セミナー, 大阪, 2 月(2014).

肥山詠美子:“Structure of light $¥Lambda$ hypernuclei”, 「バリオン多体系構造の新たな局面を考える」研究会, 長野県青木村, 3 月 (2014).

井坂政裕, 福川賢, 木村真明, 肥山詠美子, 佐川弘幸, 山本安夫, “Deformations of sd and pf shell $¥Lambda$ hypernuclei with AMD”,「バリオン多体系構造の新たな局面を考える」研究会, 長野県青木村, 3 月 (2014).

井坂政裕，木村真明，肥山詠美子，佐川弘幸，山本安夫:“AMD によるハイパー核の超変形状態の研究”, 日本物理学会 第 69 回年次大会, 平塚, 3 月(2014).

作道直幸: “孤立量子系の熱力学エントロピー“, 基研研究会「量子情報の新展開」, 京都, 3 月(2014).

数納広哉: “弱結合 3 原子系の理論研究”, 日本物理学会 第 69 回年次大会, 平塚, 3 月(2014).

大西祥太，池田陽一，兵藤哲雄，肥山詠美子，Wolfram Weise: “Faddeev 方程式による$K-d→¥pi¥Sigma n$反応の研究”, 日本物理学会 第 69 回年次大会, 平塚, 3 月(2014).

前田沙織, 横田朗, 肥山詠美子, 岡眞, Yan-Rui Liu, 福川賢治 :“Y_cN 相互作用のパラメーター決定と $¥Lambda_cNN$ 原子核”, 日本物理学会 第 69 回年次大会, 平塚, (2014).

吉田哲也, 岡眞, 肥山詠美子: “ヘビーバリオンのスペクトルとその構造の研究”, 日本物理学会 第69回年次大会, 平塚, 3 月(2014).

Philipp Gubler, 大谷圭介: “核子のストレンジネスが原子核中の$¥Phi$ メソンの測定からどのように制限されるか？”, 日本物理学会 ２０１４ 年年次大会, 平塚, 3 月(2014).

船木靖郎: “拡張されたアルファ凝縮模型を用いた軽い核の構造研究”, 日本物理学会第 69 回年次大会, 平塚, 3 月(2014).

Mathematical Physics Laboratory

Publications

[Journal]

(Original Papers) *Subject to Peer Review

Araki Y. and Kimura T. "Phase structure of two-dimensional topological insulators by lattice strong-coupling expansion", Phys. Rev. **B 87**, 205440 (2013). *

Noumi T., Yamaguchi M. and Yokoyama D., "Effective field theory approach to quasi-single field inflation and effects of heavy fields", Journal of High Energy Physics **Vol.1306**, No.52, P.1-47 (2013). *

Kimura T., Koyama S. and Kurokawa S., "Euler Products Beyond the Boundary", Letters in Mathematical Physics **104**, Issue 1, pp 1-19 (2013). *

Fujikawa K., "Conditionally valid uncertainty relations", Physical Review **A 88**, 012126 (2013). *

Fujikawa K., "Heisenberg uncertainty relation re-visited" International Journal of Modern Physics **A 29**, No. 1 1450016 (2014). *

Chaichian M., Fujikawa K. and Tureanu A., "Lorentz invariant CPT violation", The European Physical Journal **C73**, 2349 (2013). *

Noumi T. and Yamaguchi M., "Primordial spectra from sudden turning trajectory" Journal of Cosmology and Astroparticle Physics **1312**, No.38, P.1-49 (2013). *

Hashimoto K. and Masaki M., "A Landscape in Boundary String Field Theory: New Class of Solutions with Massive State Condensation", Progress of Theoretical and Experimental Physics **2013**, 043B01 (2013). *

Hashimoto K. and Oka T., "Vacuum Instability in Electric Fields via AdS/CFT: Euler-Heisenberg Lagrangian and Planckian Thermalization", Journal of High Energy Physics **1310**, 116 (2013). *

Shumude J., "Laplace operators on Sasaki-Einstein manifolds", Journal of High Energy Physics **1404** 008 (2014). *

Noumi T., Saikawa K., Sato R. and Yamaguchi M., "Effective gravitational interactions of dark matter axions", Phys. Rev. **D89** 065012 (2014). *

Bao L., Mitev V., Pomoni E. and Taki M., "Non-Lagrangian Theories from Brane Junctions", Journal of High Energy Phys. **1401** 175 (2014). *

Iimori Y., Noumi T., Okawa Y. and Torii S., "From the Berkovits formulation to the Witten formulation in open superstring field theory", Journal of High Energy Phys. **1403** 044 (2014). *

Oral Presentations

(International Conference etc.)

Taki M.: "5d SCFTs, TN junctions and Seiberg duality", KIKEN, International Conference: Integrability, Symmetry and Quantum Space-Time, Kyoto university, Jan.(2014).

Torii S.: "Discussion on the Weak Value", RIKEN-OIST mathphys workshop, Okinawa institute for science and technology, Feb. (2014).

Hashimoto K.: "Vacuum instability in holography", APCTP workshop on holography, Pohang APCTP, Korea, June (2013).

Hashimoto K.: "Superstrings and condensed matter physics", Colloquium, National Taiwan university, Taipei, Sep. (2013).

Hashimoto K.: "Vacuum instability in holography", IPMU workshop on holography and QCD, University of Tokyo, Kashiwa, Sep. (2013).

Hashimoto K.: "Vacuum structure of superstring and CPT violation", International conference on antimatter and gravity, Bern university, Switzerland, Nov. (2013).

Hashimoto K.: "Vacuum instability in holography", PASCOS 2013, Taipei, Taiwan, Nov. (2013).

Kimura T.: "FQH/CFT and q-CFT", Kavli IPMU MS Seminar, University of Tokyo, Kashiwa, March (2014).

Kimura T., Hashimoto K. and Iizuka N.: "Spin transport via gauge/gravity duality", Emergent Quantum Phases in Condensed Matter, University of Tokyo, Kashiwa, June (2013).

Noumi T.: "Effects of heavy fields on primordial spectra", New Horizons for Observational Cosmology, Villa Monastero, Jul. (2013).

Noumi T.: "Primordial spectra from sudden turning trajectory during inflation", Theoretical Physics Seminar, Institute for Theoretical Physics, Goettingen University, Germany, Jul. (2013).

Kimura T., Koyama S. and Kurokawa S.: "Scaling behavior of Euler products and random matrix theory", XXV IUPAP International Conference on Statistical Physics (STATPHYS25), Seoul, Korea, Jul. (2013).

Fujikawa K.: "Heisenberg uncertainty relation revisited", International Conference in honor of 90th birthday of Freeman Dyson, Singapore, Aug. (2013)

Fujikawa K.: "Conditionally valid uncertainty relations", Asia-Pacific Conference and Workshop on Quantum Information Science 2013, Seoul, Korea, Dec. (2013).

Fujikawa K.: "Hidden-variables models and entanglement", Quantum Science Symposium-Asia 2013, Sanjoh-Kaikan, Univeristy of Tokyo, Nov. (2013).

Noumi T.: "Primordial spectra from sudden turning trajectory", JGRG23 The 23rd Workshop on General Relativity and Gravitation in Japan, Hirosaki university, Nov. (2013).

Noumi T.: "Primordial spectra from sudden turning trajectory", New Perspectives on Cosmology, Asian Pacific Center for Theoretical Physics, Korea, Nov. (2013).

Noumi T.: "Primordial tensor correlations from effective field theory approach", Particle Theory and Cosmology Seminar, Institute for Advanced Study, the Hong Kong University of Science and Technology, Dec. (2013).

Noumi T.: “Primordial spectra from sudden turning trajectory”, KEK Theory Center Seminar, KEK, Dec. (2013)

(Domestic Conference)

木村太郎: “ゲージ・重力対応によるスピン輸送現象 (Spin transport analysis via gauge/gravity duality)”, 京都大学基礎物理学研究所素粒子論セミナー, 京都大学, 基礎物理学研究所, 5月 (2013).

野海俊文: “Effective field theory approach to quasi-single field inflation”, 早稲田大学理論宇宙物理学研究室セミナー, 早稲田大学理論宇宙物理学研究室, 5月 (2013).

鳥居真吾, 飯森悠樹, 野海俊文, 大川祐司: “From the Berkovits formulation to the Witten formulation in open superstring field theory”, 京都大学基礎物理学研究所研究会「場の理論と弦理論」, 京都大学, 8月 (2013).

木村太郎: “Topological vertex for Type IIA string on C2/Zk × CY3”, 場の理論と弦理論, 京都大学, 8月 (2013).

木村太郎, 橋本幸士, 飯塚則裕: “ゲージ重力対応によるスピン輸送現象”, 日本物理学会　2013 年秋季大会, 高知, 9月 (2013).

木村太郎, 小山信也, 黒川信重: “ゼータ関数・L 関数における深リーマン予想とオイラー積のスケーリング則”, 日本物理学会　2013 年秋季大会, 徳島, 9月 (2013).

南佑樹, 日高義将, 中村真: “Phenomenology of the novel nonequilibrium critical phenomena”, 熱場の量子論とその応用, 基礎物理学研究所, 京都大学, 8月 (2013).

南佑樹, 日高義将: “射影演算子法の視点からみた相対論的流体力学 (Relativistic hydrodynamics from projection oparetor method)”, New frontier in QCD 2013, 京都大学基礎物理学研究所, １２月 (2013).

野海俊文: “Effective field theory approach to quasi-single field inflation and effects of heavy fields”, 基研研究会「場の理論と弦理論」, 京都大学基礎物理学研究所, 8月 (2013).

野海俊文, 山口昌英: “Primordial spectra from sudden turning trajectory”, 日本物理学会２０１３年秋期大会, 高知大学, 9月 (2013).

野海俊文: “Effects of heavy fields during inflation”, 東京大学素粒子論研究室セミナー, 東京大学素粒子論研究室, １０月 (2013).

瀧雅人: “5 次元共形場理論、5 ブレイン、AGT 関係のジャンクション (Junction of 5d CFT, 5-branes and AGT relation)”, Todai/Riken joint workshop on Super Yang-Mills, solvable systems and related subjects, 東京, １０月, (2013).

橋本幸士: “超弦理論とその応用”, 素粒子物理学の進展２０１３, 京都大学基礎物理学研究所, 8月 (2013).

橋本幸士: “Solving condensed matter by superstring”, 富山大学物理学科コロキウム、日本物理学会北陸支部講演会, 富山, １２月 (2013).

橋本幸士: “Domain walls and magnetars”, 名古屋大学ソリトン研究会, 名古屋, 1月 (2014).

橋本幸士: “AdS/CFT による真空不安定性”, 九後汰一郎教授退官記念研究会 , 京都大学基礎物理学研究所, 5月 (2013).

木村太郎: “ランダム行列模型における特性多項式と外場の双対性”, 日本物理学会　第 69 回年次大会, 東海大学　湘南キャンパス, 3月 (2014).

Radiation Laboratory

Publications

[Journal]

(Original Papers) *Subject to Peer Review

Adare A, *et al.* (the PHENIX Collaboration): "Event Structure and Double Helicity Asymmetry in in Jet Production from Polarized p+p Collisions at $\sqrt{s}$ = 200 GeV", Phys. Rev. D 84, 012006, 2011-07-28 *

Adare A, *et al.* (the PHENIX Collaboration): "Suppression of away-side jet fragments with respect to the reaction plane in Au+Au collisions at $\sqrt{s_{NN}}$ = 200 GeV", Phys. Rev. C 84, 024904, 2011-08-09 *

Adare A, *et al.* (the PHENIX Collaboration): "Cold Nuclear Matter Effects on J/psi Yields as a Function of Rapidity and Nuclear Geometry in Deuteron-Gold Collisions at $\sqrt{s_{NN}}$ = 200 GeV", Phys. Rev. Lett. 107, 142301, 2011-09-27 *

Adare A, *et al.* (the PHENIX Collaboration): "Production of omega mesons in p+p, d+Au, Cu+Cu and Au+Au collisions at $\sqrt{s_{NN}}$ = 200 GeV", Phys. Rev. C 84, 044902, 2011-10-08 *

Adare A, *et al.* (the PHENIX Collaboration): "Heavy Quark Production in p+p and Energy Loss and Flow of Heavy Quarks in Au+Au Collisions at $\sqrt{s_{NN}}$=200 GeV", Phys. Rev. C 84, 044905, 2011-10-10 *

Adare A, *et al.* (the PHENIX Collaboration): "Suppression of back-to-back hadron pairs at forward rapidity in d+Au Collisions at $\sqrt{s_{NN}}$=200 GeV", Phys. Rev. Lett. 107, 172301, 2011-10-18 *

Adare A, *et al.* (the PHENIX Collaboration): "J/psi suppression at forward rapidity in Au+Au collisions at $\sqrt{s_{NN}}$=200 GeV", Phys. Rev. C 84, 054912, 2011-11-21 *

Adare A, *et al.* (the PHENIX Collaboration): "Measurements of Higher-Order Flow Harmonics in Au+Au Collisions at $\sqrt{s_{NN}}$ = 200 GeV", Phys. Rev. Lett. 107, 252301, 2011-12-15 *

Adare A, *et al.* (the PHENIX Collaboration): "Identified charged hadron spectra in p+p collisions at $\sqrt{s}$ = 200 and 62.4 GeV", Phys. Rev. C 83, 064903, 2011/06/23 *

Adare A, *et al.* (the PHENIX Collaboration): "Ground and excited charmonium state production in p+p collisions at $\sqrt{s}$=200 GeV", Phys. Rev. D 85, 092004, 2012-05-09 *

Adare A, *et al.* (the PHENIX Collaboration): "Deviation from quark-number scaling of the anisotropy parameter v_2 of pions, kaons, and protons in Au+Au collisions at $\sqrt{s_{NN}}$ = 200 GeV", Phys. Rev. C 85, 064914, 2012-06-27 *

Adare A, *et al.* (the PHENIX Collaboration): "Nuclear-Modification Factor for Open-Heavy-Flavor Production at Forward Rapidity in Cu+Cu Collisions at $\sqrt{s_{NN}}$=200 GeV", Phys. Rev. C 86, 024909, 2012-08-20 *

Adare A, *et al.* (the PHENIX Collaboration): "Observation of direct-photon collective flow in Au+Au collisions at $\sqrt{s_{NN}}$=200GeV", Phys. Rev. Lett. 109, 122302, 2012-09-19 *

Adare A, *et al.* (the PHENIX Collaboration): "Evolution of pi 0 suppression in Au+Au collisions from $\sqrt{s_{NN}}$ = 39 to 200 GeV", Phys. Rev. Lett. 109, 152301, 2012-10-12 *

Afanasiev S, *et al.* (the PHENIX Collaboration): "Measurement of Direct Photons in Au+Au Collisions at $\sqrt{s_{NN}}$ = 200 GeV", Phys. Rev. Lett. 109, 152302, 2012-10-12 *

Adare A, *et al.* (the PHENIX Collaboration): "Direct Photon Production in p+p Collisions at $\sqrt{s}$=200 GeV in Mid-rapidity", Phys. Rev. D 86, 072008, 2012-10-23 *

Adare A, *et al.* (the PHENIX Collaboration): "Cross Sections and Double Helicity Asymmetries of Mid-Rapidity Inclusive Charged Hadrons in p+p at $\sqrt{s}$ = 62.4 GeV", Phys. Rev. D 86, 092006, 2012-11-08 *

Adare A, *et al.* (the PHENIX Collaboration): "J/psi suppression at forward rapidity in Au+Au collisions at $\sqrt{s_{NN}}$=39 and 62.4 GeV", Phys. Rev. C 86, 064901, 2012-12-06 *

Adare A, *et al.* (the PHENIX Collaboration): "Cold-nuclear-matter effcts on heavy-quark production in d+Au collisions at $\sqrt{s_{NN}}$=200 GeV", Phys. Rev. Lett. 109, 242301, 2012-12-12 *

Adare A, *et al.* (the PHENIX Collaboration): "Double Spin Asymmetry of Electrons from Heavy Flavor Decays in p+p Collisions at $\sqrt{s}$=200 GeV", Phys. Rev. D 87, 012011, 2013-01-29 *

Adare A, *et al.* (the PHENIX Collaboration): "Transverse-Momentum Dependence of the J/psi Nuclear Modification in d+Au Collisions at $\sqrt{s_{NN}}$=200 GeV", Phys. Rev. C 87, 034904, 2013-03-14 *

Adare A, *et al.* (the PHENIX Collaboration): "Neutral pion production with respect to centrality and reaction plane in Au+Au collisions at $\sqrt{s_{NN}}$ = 200 GeV", Phys. Rev. C 87, 034911, 2013-03-28 *

Adare A, *et al.* (the PHENIX Collaboration): "Upsilon (1S+2S+3S) production in d+Au and p+p collisions at $\sqrt{s_{NN}}$=200 GeV and cold-nuclear matter effects", Phys. Rev. C 87, 044909, 2013-04-25 *

Adare A, *et al.* (the PHENIX Collaboration): "Direct photon production in d+Au collisions at $\sqrt{s_{NN}}$=200 GeV", Phys. Rev. C 87, 054907, 2013-05-17 *

Adare A, *et al.* (the PHENIX Collaboration): "Medium modification of jet fragmentation in Au+Aucollisions at $\sqrt{s_{NN}}$ = 200 GeV measured in direct photon-hadron correlations", Phys. Rev. Lett. 111, 32301, 2013-07-16 *

Adare A, *et al.* (the PHENIX Collaboration): "Inclusive cross section and single transverse spin asymmetry for very forward neutron production in polarized p+p collision at sqrts = 200 GeV", Phys. Rev. D 88, 032006, 2013-08-08 *

Adare A, *et al.* (the PHENIX Collaboration): "Spectra and ratios of identified particles in Au+Au and d+Au collisions at $\sqrt{s_{NN}}$=200 GeV", Phys. Rev. C 88, 024906, 2013-08-22 *

Adare A, *et al.* (the PHENIX Collaboration): "Nuclear modification of ψ', χ_c' and J/psi production in d+Au collisions at $\sqrt{s_{NN}} = 200$ GeV", Phys. Rev. Lett. 111, 202301, 2013-11-12 *

Adare A, *et al.* (the PHENIX Collaboration): "Quadrupole Anisotropy in Dihadron Azimuthal Correlations in Central d+Au Collisions at $\sqrt{s_{NN}} = 200$ GeV", Phys. Rev. Lett. 111, 212301, 2013-11-20 *

Adare A, *et al.* (the PHENIX Collaboration): "Azimuthal anisotropy of π^0 and eta mesons in Au+Au collisions at $\sqrt{s_{NN}}$=200 GeV", Phys. Rev. C 88, 064910, 2013-12-20 *

Adare A, *et al.* (the PHENIX Collaboration): "Heavy-flavor electron-muon correlations in p+p and d+Au collisions at $\sqrt{s} = 200$ GeV", Phys. Rev. C 89, C034915, 2014/03/31 *

Sanghwa P, for the PHENIX collaboration: "W Physics Result of PHENIX", Proceedings of Science PoS (DIS 2013) 209, 2013

Goto Y, PHENIX Collaboration: "PHENIX detector upgrades for enhanced physics programs", Proceedings of Science PoS (DIS 2013) 249, 2013

Goto Y, PHENIX Collaboration: "Inclusive Cross Section and Single Transverse-Spin Asymmetry of Very Forward Neutron Production at PHENIX", Physics of Particles and Nuclei Volume 45, Issue 1, pp 79-81, 2014/01

Leitgab M, Ralf Seidl and the Belle collaboration: "Precision measurement of charged pion and kaon multiplicities in electron-positron annihilation at Q = 10.52 GeV", Phys.Rev.Lett. 111 (2013) 062002, 2013/08/06 *

Kawama D, and the J-PARC E16 Collaboration "Experimental Investigation for Mass Modification of Vector Mesons at J-PARC", JPS Conference Proceedings 1, 013074, 2014/03/26 *

Ikeda S, Romanelli Mark, Cingquegrani David, Sekine Megumi, Kumaki Masafumi, Fuwa Yasuhiro, Munemoto Naoya, Kanesue Takeshi, Jin Qianyu, Okamura Masahiro, Horioka Kazuhiko: "Creation of cocktail beam from alloy target with Laser", Review of Scientific Instruments Vol. 85, p 02B913, 2013/11/12 *

Fuwa Y, S.Ikeda, M.Okamura, *et al.*: "Interaction of plasmas in laser ion source with double laser system", Review of Scientific Instruments 85, 02B916, 2013/12/31 *

Fuwa Y, S.Ikeda, M.Okamura, *et al.*: "Comparison of graphite materials for targets of laser ion source", Review of Scientific Instruments 85, 02B924, 2014/01/24 *

Ikeda S, Romanelli Mark, Cingquegrani David, Sekine Megumi, Kumaki Masafumi, Fuwa Yasuhiro, Kanesue Takeshi, Okamura Masahiro, Horioka Kazuhiko: "Investigation of effect of solenoid magnet on emittances of ion beam from laser ablation plasma", Review of Scientific Instruments 85, 02B919, 2014/01/24 *

Sekine M, S.Ikeda, M.Okamura, *et al.*: "Multiple Species Beam Production on Laser Ion Source for electron beam ion source in Brookhaven National Laboratory", review of scientific instruments 85, 02B920, 2014/02 *

Kumaki M, Y. Fuwa, M. Okamura, *et al.*: "Analyses of the plasma generated by laser irradiation on sputtered target for determination of the thickness used for plasma generation", Review of Scientific Instruments 85, 02B925, 2014/02/24 *

Oral Presentations

(International Conference etc.)

Itaru Nakagawa, "Recent Results on PHENIX Longitudinal Asymmetry Measurements", 3rd Workshop on the QCD Structure of the Nucleon (University of the Basque Country) Bilbao、Spain, 2012/10/22

Hideto En'yo, "Nuclear Physics in Japan Prospects being engaged in RIBF, J-PARC and other facilities", The 2012 Fall meeting of the Division of Nuclear Physics (DNP2012) (University of California), Hyatt Regency Newport Beach, CA, USA, 2012/10/24

Hideto En'yo, "Prospect of RIKEN RI Beam Factory for Coming 5 Years", The traditional VI International Symposium on EXOtic Nuclei (EXON2012) (JINR), Far EasternFederal University, Vladivostok, Russia, 2012/10/3

Park Sanghwa, "W Physics Result of PHENIX", XXI International Workshop on Deep-Inelastic Scattering and Related Subjects (Center for Particle Physics of Marseilles (CPPM)), Marseilles, France, 2013/04/23

Yuji Goto, "PHENIX detector upgrades for enhanced physics programs", XXI. International Workshop on Deep-Inelastic Scattering and Related Subjects (Center for Particle Physics of Marseilles), Marseilles, France, 2013/04/24

Hideto En'yo, "Nishina Center Overview", 理研-IMP ワークショップ (理研), 理研 RIBF 棟大会議室, 2013/04/17

Hideto En'yo, "Introduction to RIKEN Nishina Center for Accelerator-Based Science", Workshop on the INFN-RIKEN collaboration on nuclear physics activities (INFN), イタリア文化会館, 2013/05/17

Hideto En'yo, "Future Nuclear Physics Facilities around the world", IUPAP WG.9 Nuclear Science Symposium (Frascati National Laboratory (LNF)), Frascati National Laboratory (LNF), Italy, 2013/05/29

Ralf Seidl, "Results from W-Production at RHIC", ECT* workshop: Flavor Structure of the Nucleon Sea (ECT*), Trento, Italy, 2013/07/01

Kim Chong, "Status of W Physics at PHENIX", The 12th Asia Pacific Physics Conference (AAPPS, JPS, JSAP), Makuhari, Chiba, Japan, 2013/07/15

Yoshimasa Ikeda, "Measurement of Azimuthal Anisotropy of hadron in Au+Au collision at $\sqrt{s_{NN}}$ = 39, 62 and 200 GeV in PHENIX experiment at RHIC", The 12th Asia Pacific Physics Conference (AAPPS, JPS, JSAP), Makuhari, Chiba, Japan, 2013/07/17

Kawama, Daisuke, "Experimental investigation for mass modification of vector mesons (J-PARC E16 experiment)", The 12th Asia Pacific Physics Conference (AAPPS, JPS, JSAP), Makuhari, Chiba, Japan, 2013/07/18

Yoshimasa Ikeda, "Measurement of azimuthal anisotropy of hadrons in Au+Au collisions from the beam energy scan program by the PHENIX experiment at RHIC.", SQM 2013 (Univ. of Birmingham), Birmingham、UK, 2013/07/17

Yasuyuki Akiba, "Workshop Summary", PHENIX workshop on Physics Prospects with Detector and Accelerator Upgrades (RIKEN Radiation Lab.), Wako, Japan, 2013/08/02

Yasuyuki Akiba, "Photons and Dilepton Physics at RHIC", Future Trends in High Energy Nuclear Collisions (清華大学), 北京, China, 2013/08/19

Megumi Sekine, "Multiple Species Beam Production on Laser Ion Source for electron beam ion source in Brookhaven National Laboratory", The 15th International Conference on Ion Sources (NIRS), Makuhari, Chiba, Japan 2013/09/12

Yasuhiro Fuwa, "Interaction of plasmas in laser ion source with double laser system", The 15th International Conference on Ion Sources (NIRS), Makuhari, Chiba, Japan 2013/09/12

Yasuhiro Fuwa, "Comparison of graphite materials for targets of laser ion source", The 15th International Conference on Ion Sources (NIRS), Makuhari, Chiba, Japan 2013/09/12

Ikeda Shunsuke, "Investigation of effect of solenoid magnet on emittances of ion beam from laser ablation plasma", The 15th International Conference on Ion Sources (NIRS), Makuhari, Chiba, Japan 2013/09/12

Ikeda Shunsuke, "Creation of cocktail beam from alloy target with Laser", The 15th International Conference on Ion Sources (NIRS), Makuhari, Chiba, Japan 2013/09/12

Masashi Kumaki, "Determination the Thickness Used for Plasma Generation by Laser Irradiation on Sputtering Target", The 15th International Conference on Ion Sources (NIRS), Makuhari, Chiba, Japan 2013/9/12

Shunsuke Ikeda, "Control of plasma shape with pulsed solenoid on laser ion source", Young research symposium 2013 (Brookhaven national laboratory), Brookhaven national laboratory, NY, USA, 2013/10/14

Yuji Goto, "Drell-Yan experiments at Fermilab/RHIC/J-PARC", QCD Frontier 2013 (Thomas Jefferson National Accelerator Facility), Newport News, VA, USA, 2013/10/21

Wataru Nakai, "Development of the GEM Tracker for the J-PARC E16 experiment", IEEE NUCLEAR SCIENCE SYMPOSIUM 2013 (IEEE Nuclear and Plasma Sciences Society), Seoul, Korea, 2013/10/27-11/02

Kanno Koki, "Development of a Hadron Blind Detector for the J-PARC E16 Experiment", IEEE NUCLEAR SCIENCE SYMPOSIUM 2013 (IEEE Nuclear and Plasma Sciences Society), Seoul, Korea, 2013/10/28

Yoki Aramaki, "Experimental approach to the mass modification in nucleus by the J-PARC E16 experiment", YITP workshop on Hadron in Nucleus (YITP), Kyoto, Japan, 2013/11/02

Ralf Seidl, "Fragmentation function measurements", XV International Conference on Hadron Spectroscopy (Hadron 2013) (科研費 新学術領域研究 「新ハドロン」総括班), Nara, Japan, 2013/11/07

Yuji Goto, "Polarized nucleon-structure physics at RHIC-PHENIX", XV International Conference on Hadron Spectroscopy (Hadron 2013) (科研費 新学術領域研究 「新ハドロン」総括班), Nara, Japan, 2013/11/07

Kawama, Daisuke, "Experimental investigation for mass modification effect in nuclei (J-PARC E16 experiment)", XV International Conference on Hadron Spectroscopy (Hadron 2013) (科研費 新学術領域研究 「新ハドロン」総括班), Nara, Japan, 2013/11/07

Hideto En'yo, "RIKEN Radio Isotope Beam Factory, Japanese Flag Ship for Nuclear Science", IASEN 2013 (Joint Institute for Nuclear Research), Lord Charles Hotel, Cape Town, Shouth Africa, 2013/12/03

Ralf Seidl, "Polarized fragmentation function measurements at Belle", Indiana-Illinois Workshop on Fragmentation Functions (Indiana University, University of Illinois), Bloomington, IN, USA, 2013/12/12

Itaru Nakagawa, "Latest Results of Nucleon Spin Structure Measurement from PHENIX", High Energy Physics in LHC Era (Universidad Tecnica Federico Santa Maria) Valparaiso, Chile, 2013/12/17

(Domestic Conference etc.)

延與秀人, " 理研における中性子利用研究 – 事始め –", 理研シンポジウム「理研から発信する中性子利用の新たな展開 ～ものづくり産業利用に向けた小型中性子源の開発～」(理化学研究所), 理研和光事業所　鈴木梅太郎ホール , 2011/11/17

Kim Chong, "Recent status of PHENIX spin program", 「高エネルギー QCD・核子構造」研究会 (KEK), Tokai, Japan, 2014/03/08

不破康裕, "マルチパルスレーザーを用いたレーザーイオン源", 第 10 回日本加速器学会年会 (日本加速器学会), 名古屋、日本, 2013/08/03

四日市 悟, "vector meson の媒質中での崩壊の測定とその解釈", 研究会　原子核媒質中のハドロン研究=魅力と課題= (高エネルギー物理学研究機構), 高エネルギー物理学研究機構 東海一号館, 2013/08/06

小松雄哉, "J-PARC E16 実験における大型 GEM フォイル

を用いた飛跡検出器の開発", 日本物理学会 2013 年秋季大会 (日本物理学会), 高知大学朝倉キャンパス、日本, 2013/09/20

秋葉康之, "RHIC での衝突エネルギー走査実験や多種原子核衝突を通じたクォーク物質物性の研究", 日本物理学会 2013 年秋季大会 (日本物理学会), 高知大学朝倉キャンパス、日本, 2013/09/21

林真一, "Dielectron measurement in $\sqrt{s}$ = 5.02 TeV p+Pb collisions at LHC-ALICE", 日本物理学会 2013 年秋季大会 (日本物理学会), 高知大学、日本, 2013/09/21

水野三四郎, "RHIC-PHENIX 実験における高次方位角異方性の直接光子依存性測定", 日本物理学会 2013 年秋季大会 (日本物理学会), 高知大学、日本, 2013/09/21

蜂谷崇, "PHENIX-VTX を用いた 電子対の 2 次崩壊点及び DCA 測定の現状", 日本物理学会 2013 年秋季大会 (日本物理学会), 高知大学、日本, 2013/09/21

星野知也, "RHIC-PHENIX 実験 $\sqrt{s_{NN}}$= 200 GeV 原子核衝突における強磁場探索", 日本物理学会 2013 年秋季大会 (日本物理学会), 高知大学、日本, 2013/09/21

後藤雄二, "RHIC-PHENIX 実験の検出器高度化計画", 日本物理学会 2013 年秋季大会 (日本物理学会), 高知大学、日本, 2013/09/22

Ralf Seidl, "Accessing the sea quark polarization via W to mu measurements in PHENIX", 2013 Fall Meeting of the Japanese Physical Society (Japanese Physical Society), Kochi, Japan, 2013/09/22

川間大介, "J-PARC E16 実験に用いる GEM 検出器の中性子耐性テストについて", 第 10 回 Micro-Pattern Gas Detector 研究会 (京都大学、KEK 測定器開発室), 京都, 2013/12/14

蜂谷崇, "高エネルギー原子核衝突における重いクォークの測定", Heavy Ion Pub (名古屋大学・大阪大学・広島大学), 京都, 2013/12/20

熊木雅史, "Present Status of Laser Ion Source with ps Laser System at BNL", ビーム物理学会２０１３ (沖縄科学技術大学院大学), 沖縄、日本, 2013/09/12

荒巻陽紀, "金+金衝突における方位角ごとの中性パイ中間子測定", 日本物理学会　第 69 回年次大会 (日本物理学会), 東海大学湘南キャンパス、平塚、日本, 2014/03/27

中井恒, "J-PARC E16 実験のための GEM 飛跡検出器の磁場中での性能評価", 日本物理学会　第 69 回 年次大会 (日本物理学会), 東海大学湘南キャンパス、平塚、日本, 2014/03/27

池田峻輔, "Magnetic control of plasma flux for laser ion source", 日本物理学会　第 69 回 年次大会 (日本物理学会), 東海大学湘南キャンパス、平塚、日本, 2014/03/28

池田義雅, "RHIC-PHENIX 実験における核子当たり 39GeV 金原子核衝突のハドロン方位角異方性の測定", 日本物理学会　第 69 回 年次大会 (日本物理学会), 広島大学, 2014/03/29

辻智也, "Event plane dependence of neutral pion production in Pb+Pb collisions at $\sqrt{}$ sNN = 2.76 TeV with ALICE", 日本物理学会　第 69 回 年次大会 (日本物理学会), 東海大学湘南キャンパス、平塚、日本, 2014/03/30

水野三四郎, "RHIC-PHENIX 実験における AuAu 衝突を用いた直接光子の方位角異方性の研究", 日本物理学会　第 69 回 年次大会 (日本物理学会), 東海大学湘南キャンパス、平塚、日本, 2014/03/30

八野哲, "Neutral pion anslysis in pp collisions at 8TeV with ALICE", 日本物理学会　第 69 回 年次大会 (日本物理学会), 東海大学湘南キャンパス、平塚、日本, 2014/03/30

星野知也, "PHENIX 実験 $\sqrt{s_{NN}}$=200GeV 金原子核衝突における電子対測定を用いた強磁場探索", 日本物理学会　第 69 回 年次大会 (日本物理学会), 東海大学湘南キャンパス、平塚、日本, 2014/03/30

Kim Chong, "Introduction and Status of W physics in PHENIX Muon Arms", Korean Physical Society 2013 Fall meeting (Korean Physical Society), Changwon, Korea, 2013/10/30

Moon Taebong, "The Measurement of D^0 Meson in P+P Collisions at $\sqrt{s}$=200 GeV using the VTX in the PHENIX Experiment at RHIC", Korean Physical Society 2013 Fall meeting (Korean Physical Society), Changwon, Korea, 2013/10/30

Yoon Inseok, "Report of Anaylsys Progress : A_{LL} of π^0 production at $\sqrt{s}$ = 510 GeV at PHENIX", Korean Physical Society 2013 Fall meeting (Korean Physical Society), Changwon, Korea, 2013/10/30

Park Sanghwa, "Sea Quark Polarization Measurement via W-boson to Muon Decays at RHIC-PHENIX", Korean Physical Society 2013 Fall Meeting (Korean Physical Society), Changwon, Korea, 2013/10/30

Advanced Meson Science Laboratory

Publications

[Journal]

(Original Papers) ＊Subject to Peer Review

Adiperdana B., Dharmawan I.A., Siregar R.E., Sulaiman S., Ibrahim M.I.M., and Watanabe I., "Muon Site Estimation on La_2CuO_4 Using Dipole Field and Density Functional Theory Calculation", AIP Conf. Proc. **1554**, 214-217 (2013)

Agnello H., Outa H., FINUDA collaboration, "Search for the neutron-rich hypernucleus 9ΛHe", Phys.Rev. C86 (2012) 057301 ＊

Agnello H., Outa H., FINUDA collaboration, "Results on Λp emission from K− absorption at rest on light nuclei", Nucl.Phys. A914 (2013) 310-314

Agnello H., Outa H., FINUDA collaboration, "First determination of the one-proton induced Non-Mesonic Weak Decay width of p-shell Λ-Hypernuclei", Phys.Lett. B738 (2014) 499-504 ＊

Ajimura S., Hashimoto T., Itahashi K., Iwasaki M., Ma. Y., Okada S., Ohnishi H., Outa H., Sakuma. F., Sato M., Tokuda M., Yamazaki T. (J-PARC E15 collaboration), "A search for deeply-bound kaonic nuclear state at the J-PARC E15 experiment", Proceedings of XI International Conference on Hypernuclear and Strange Particle Physics (HYP2012) Nucl. Phys. A 914, 315 (2013) ＊

Ajimura S., Hashimoto T., Itahashi K., Iwasaki M., Ma. Y., Okada S., Ohnishi H., Outa H., Sakuma. F., Sato M., Tokuda M., Yamazaki T. (J-PARC E15 collaboration), "A Search for Deeply Bound Kaonic Nuclear States at J-PARC", Proceedings of the 20th International IUPAP Conference on Few-Body Problems in Physics (FB20) Few-Body Syst. 54, 1195 (2013) ＊

Ariga H., Shimomura K., Ishida K., Pratt F., Yoshizawa, Wataru K., Higemoto W., Torikai E., Asakura K. "Detection of Oxygen Vacancy in Rutile TiO_2 Single Crystal by μSR Measurement" ＊ JPS Conference Proceedings 2 (2014) 010307

Bakule P., Beer G.A., Contreras D., Esashi M., Fujiwara Y., Fukao Y., Hirota S., Iinuma H., Ishida K., Iwasaki M., Kakurai T., Kanda S., Kawai H., Kawamura N., Marshall G.M., Masuda H., Matsuda Y., Mibe T., Miyake Y., Okada S., Olchanski K., Olin A., Onishi H., Saito N., Shimomura K., Strasser P.E., Tabata M., Tomono D., Ueno K., Yokoyama K., Yoshida S., "Measurement of muonium emission from silica aerogel", Prog. Theor. Exp. Phys. (2013), 103C0. ＊

Bazzi M., Iwasaki M., SIDDHARTA collaboration, "L-series X-ray yields of kaonic 3He and 4He atoms in gaseous targets", Eur.Phys.J. A50 (2014) 91

Bazzi M,, Iwasaki M., Okada S., SIDDHARTA collaboration, "X-ray transition yields of low-Z kaonic atoms produced in Kapton", Nucl.Phys. A916 (2013) 30-47 ＊

Bazzi M., Iwasaki M., Okada S., SIDDHARTA collaboration, "Preliminary study of kaonic deuterium X-rays by the SIDDHARTA experiment at DAFNE", Nucl.Phys. A907 (2013) 69-77 ＊

Bhang H., Ajimura S., Aoki K., Banu A., Fukuda T., Hashimoto O.,Hwang J.I., Kameoka S., Kang B.H., Kim E., Kim J.H., Kim M., Maruta T., Miura Y., Miyake Y., Nagae T., Nakamura M., Nakamura S.N., Noumi H., Okada S., Okayasu Y., Outa H., Park K.,Saha P.K., Sato Y., Sekimoto M., Takahashi T., Tamura H., Tanida K.,Toyoda A., Tshoo K., Tsukada K., Watanabe T., Yim H.J., "The Strong Three-body Weak Interaction Contribution in the Nonmesonic Weak Decay of p-shell Λ Hypernuclei", Few Body Syst. 54 (2013) 1239-1243 ＊

Bhang H., Ajimura S., Aoki K., Banu A., Fukuda T., Hashimoto O.,Hwang J.I., Kameoka S., Kang B.H., Kim E., Kim J.H., Kim M., Maruta T., Miura Y., Miyake Y., Nagae T., Nakamura M., Nakamura S.N., Noumi H., Okada S., Okayasu Y., Outa H., Park K.,Saha P.K., Sato Y., Sekimoto M., Takahashi T., Tamura H., Tanida K.,Toyoda A., Tshoo K., Tsukada K., Watanabe T., Yim H.J., "Three-body ΛNN ---> nNN nonmesonic weak decay process of Lambda hypernuclei", Few Body Syst. 54 (2013) 103-110 ＊

Cargnello M., Iwasaki M., SIDDHARTA collaboration, "X-ray spectroscopy of kaonic atoms at SIDDHARTA", EPJ Web Conf. 73 (2014) 05008 ＊

Chang L. –J., Lees M.R., Watanabe I., Hillier A.D., Yasui Y., and Onoda S., "Static Magnetic Moments Revealed by Muon Spin Relaxation and Thermodynamic Measurements in Quantum Spin Ice $Yb_2Ti_2O_7$", Phys. Rev. B **89**, 184416-1-5 (2014) ＊

Enomoto S., Hashimoto T., Itahashi K., Iwasaki M., Ma. Y., Okada S., Ohnishi H., Outa H., Sakuma. F., Sato M., Tokuda M., Yamazaki T. (J-PARC E15 collaboration), "Search for deeply-bound Kbar-nuclear states via the 3He(inflight-K-,n) reaction at J-PARC", Proceedings of XV International Conference on Hadron Spectroscopy (Hadron 2013), Proceedings of Science (Hadron 2013) 182 (2014)

Fujihala M., Xu-Guang Zheng, Norodomi H., Kawae T., and Watanabe I., "Magnetic Transition in $K_4Cu_4OCl_{10}$: A Model System of Three-Dimensional Spin-1/2 Tetrahedra", Phys. Rev. B **87**, 144425-1-6 (2013) ＊

Fujihala M., Xu-Guang Zheng, Norodomi H., Kawae T., Matsuo A., Kindo K., and Watanabe I., "Unconventional Spin Freezing in the Highly Two-Dimensional Spin-1/2 Kagome Antiferromagnet $Cd_2Cu_3(OH)_6(SO_4)_2 \cdot 4H_2O$: Evidence of Partial Order and Coexisting Spin Singlet State on a Distorted Kagome Lattice", Phys. Rev. B **89**, 100401(R)-1-5 (2014) ＊

Fujioka H., Brinkmann K.T., Friedrich S., Geissel H.,Hayano R.S., Hirenzaki S., Itahashi K., Itoh S., Jido D., Metag V., Nagahiro H., Nanova M., Nishi T., Okochi K., Outa H., Suzuki K., Suzuki T.,Tanaka Y.K., Watanabe Y.N., Weick H., "Spectroscopy of eta-prime

Mesic Nuclei via Semi-Exclusive Measurement at FAIR" EPJ Web Conf. 66 (2014) 09006

Goto T., Suzuki T., Watanabe I., Manaka H., Luetkens H., and Amato A., "Ground State of Bond-Disordered Quasi-One-Dimensional Spin System $(CH_3)_2CHNH_3Cu(Cl_xBr_{1-x})_3$ with x=0, 0.025 and 0.3" J. Phys. Soc. Conf. Proc. **2**, 010207-1-5 (2014). ＊

Guo H., Matsuhira K., Kawasaki I., Wakeshima M., Hinatsu Y., Watanabe I., and Xu Z., "Magnetic Order in Pyrochlore Iridate $Nd_2Ir_2O_7$ Probed by Muon Spin Relaxation", Phys. Rev. B **88**, 060441(R)-1-5(2013) ＊

Guo H., Tanida H., Kobayashi R., Kawasaki I., Sera M., Nishioka T., Matsumura M., Watanabe I., and Xu Z., "Magnetic Instability Induced by Rh-Doping in Kondo Semiconductor $CeRu_2Al_{10}$", Phys. Rev. B **88**, 115206-1-8 (2013) ＊

Hashimoto T. *et al.* (J-PARC E15 collaboration), "A search for the K-pp bound state in the 3He(K- in-flight, n) reaction at J-PARC", Proceedings of the 25th International Nuclear Physics Conference (INPC 2013), EPJ Web of Conferences 66, 09008 (2014)

Hiroi M., Hisamatsu T., Suzuki T., Ohishi K., Ishii Y., and Watanabe I., "Muon Spin Relaxation Study of Spin-Glass Transition in the Heusler Compound $Ru_{1.9}Fe_{0.1}CrSi$", Phys. Rev. B. **87**, 024409-1-5 (2013) ＊

Ikedo Y., Miyake Y., Shimomura K., Strasser P., Kawamura N., Nishiyama K., Makimura S., Fujimori H., Koda A., Nakamura J., Nagatomo T., Kobayashi Y., Adachi T., Pant A.D., Ogitsu T., Nakamoto T,, Sasaki K., Ohhata H., Okada R., Yamamoto A., Makida Y., Yoshida M., Okamura T., Ohkubo R., Higemoto W., Ito T.U., Nakahara K., Ishida K., "U-Line at MLF/J-PARC for Ultra Slow Muon Microscopy", JPS Conference Proceedings 2 (2014) 010103

Iliescu M., Iwasaki M., Okada S., SIDDHARTA collaboration, "Kaon-Nucleon Strong Interaction in Kaonic Atoms: The SIDDHARTA Program", Few Body Syst. 54 (2013) 1123-1126 ＊

Itahashi K., "Meson Bound States Spectroscopy in Nuclei: Pionic Atoms at RIBF and η' -Mesic Nuclei at GSI/FAIR", Acta Phys.Polon. B45 (2014) 773 ＊

Itahasshi K., Berg G.P.A., Dozono M., Fujioka H., Fukuda M., Furuno T., Geissel H., Hayano R.S., Inabe N., Itahashi K., Itoh S., Kameda D., Kubo T., Matsubara H., Michimasa S., Miki K., Miya H., Murakami Y., Nakamura M., Nakatsuka M.,Nishi T., Noji S., Okochi K., Ota S., Suzuki H., Suzuki K., Takaki M., Takeda H., Tanaka Y.K., Todoroki K.,Tsukada K., Uesaka T., Watanabe Y.N., Weick H., Yamada H., Yoshida K.,"First Precision Spectroscopy of Pionic Atoms at RI Beam Factory ", Few Body Syst. 54 (2013) 1569-1572 ＊

Itahashi K., "Pionic atom factory project at RIBF — Present status and future perspectives — ", PoS Hadron2013 (2013) 015

Ishiwatari T., Iwasaki M., Okada S., SIDDHARTA collaboration, "Strong-interaction shifts and widths of kaonic helium isotopes", Nucl. Phys. A914 (2013) 305-309 ＊

Kanda S., Fujimori H., Fukao Y., Ikedo Y., Ishida K., Iwasaki M., Kawamura N., Kojima K.M., Lee M., Makimura S., Mibe T., Miyake Y., Nakamura J., Nagashima Y., Nagatomo T., Nagumo K., Nishimura S., Okada S., Saito N., Shimomura K., T. Suzuki, Strasser P., Ueno K., Won E., "Development of High-Rate Positron Tracker for the Muonium Production Experiment at J-PARC", JPS Conference Proceedings 2 (2014) 010404 ＊

Kawasaki I., Watanabe I., Hillier A.D., and Aoki D., "Evidence for Time-Reversal Symmetry Breaking in Both the Hidden Order and Superconducting States of URu_2Si_2", J. Phys. Soc. Jpn. **83**, 094720-1-5 (2014) ＊

Kawasaki I., Watanabe I., Amitsuka H., Tanida H., and Ohnuki Y., "Superconducting Properties of Noncentrosymmetric Superconductor $LaPt_3Si$ Studied by Muon Spin Spectroscopy", J. Phys. Soc. Jpn. **82**, 084713-1-6 (2013) ＊

Konieczny P., Pelka R., Zielinski P.M., Pratt F.L., Pinkowicz D., Sieklucka B. and Wasiutynski T. "Scaling analysis of $[Fe(pyrazole)_4]_2[Nb(CN)_8]$ molecular magnet", J. Magn. Magn. Mat. **344**, 105 (2013) ＊

Kuroe H., Aoki K., Sato T., Kino R., Kuwahara H., Sekine T., Hase M., Kawasaki I., Kawamata T., Suzuki T., Watanabe I., Oka K., Ito T., and Eisaki H., "Muon spin Spectroscopy in Multiferroic $(Cu,Zn)_3Mo_2O_9$" , J. Phys. Soc. Conf. Proc. **2**, 010206-1-8 (2014). ＊

Liu Z., Waki T., Tabata Y., Yuge K., Nakamura H., and Watanabe I., "Magnetic Ground State of the $M_{n+1}AX_n$ Phase Nitride Cr_2GaN", Phys. Rev. B **88**, 1334401-1-7 (2013) ＊

Miyazaki K., Saito N., Okamura K., Oishi Y., Louchev O.A., Iwasaki M. and Wada S., "Tunable 820.65 nm Light Source by Injection-Seeded Optical Parametric Oscillator and Amplifier for Muonium Lyman-Alpha Generation", JPS Conference Proceedings 2 (2014) 010107 ＊

Moller J.S., Bonfa P., Ceresoli D., Bernardini F., Blundell S.J., Lancaster T., De Renzi R., Marzari N., Watanabe I., Sulaiman S., and Mohamed-Ibrahim M.I., "Playing Quantum Hide-and-Seek with The Muon: Localizing Muon Stopping Sites", Phys. Scr. **88**, 068510-1-7 (2013) ＊

Moritsu M., Itahashi K., J-PARC E19 collaboration, "High-resolution search for the Θ+ pentaquark via a pion-induced reaction at J-PARC ", Phys.Rev. C90 (2014) 035205 ＊

Moritsu M., Itahashi K., J-PARC E19 collaboration, "Search for the Θ+ pentaquark at J-PARC", Nucl.Phys. A914 (2013) 91-96 ＊

Mukai K., Aoki Y., Andreica D., Amato A., Watanabe I., Giblin S.R., and Sugiyama J., "Thermally Activated Spin Fluctuations in

Stoichiometric LiCoO2 Clarified by Electron Paramagnetic Resonance and Muon-Spin Rotation and Relaxation Measurements", Phys. Rev. B **89**, 094406-1-11 (2014) ＊

Nagahiro H., Jido D., Fujioka H., Itahashi K., Hirenzaki S., "Formation of eta-prime(958)-mesic nuclei by (p,d) reaction", Phys.Rev. C87 (2013) 045201 ＊

Nakamura J., Nagatomo T., Oishi Y., Ikedo Y., Strasser P., Saito N., Miyazaki K., Yokoyama K., Okamura K., Miyake Y., Makimura S., Nishiyama K., Shimomura K., Kawamura N., Koda A., Higemoto W., Wada S., Iwasaki M., Torikai E., "Ultra Slow Muon Microscope at MUSE / J-PARC", J.Phys.Conf.Ser. 502 (2014) 012042 ＊

Nakamura J., Oishi Y., Saito N., Miyazaki K., Yokoyama K., Okamura K,, Makimura S., Miyake Y., Nagatomo T., Strasser P., Ikedo Y., Tomono D., Shimomura K., Wada S., Kawamura N., Koda A. and Nishiyama K., "Transport of Coherent VUV Radiation to Muon U-Line for Ultra Slow Muon Microscope", JPS Conference Proceedings 2 (2014) 010108 ＊

Naruki M., Itahashi K., J-PARC E19 collaboraton, "Search for Pentaquark Θ+ in Hadronic Reaction at J-PARC ", Few Body Syst. 54 (2013) 955-960 ＊

Nishi T., Berg G.P.A., Dozono M., Fujioka H., Fukuda M., Furuno T., Geissel H., Hayano R.S., Inabe N., Itahashi K., Itoh S., Kameda D., Kubo T., Matsubara H., Michimasa S., Miki K., Miya H., Murakami Y., Nakamura M., Nakatsuka M., Noji S., Okochi K., Ota S., Suzuki H., Suzuki K., Takaki M., Takeda H., Tanaka Y.K., Todoroki K.,Tsukada K., Uesaka T., Watanabe Y.N., Weick H., Yamada H., Yoshida K., "The first precision measurement of deeply bound pionic states in 121Sn" , EPJ Web Conf. 66 (2014) 09014

Nishi T., Berg G.P.A., Dozono M., Fujioka H., Fukuda M., Furuno T., Geissel H., Hayano R.S., Inabe N., Itahashi K., Itoh S., Kameda D., Kubo T., Matsubara H., Michimasa S., Miki K., Miya H., Murakami Y., Nakamura M., Nakatsuka M., Noji S., Okochi K., Ota S., Suzuki H., Suzuki K., Takaki M., Takeda H., Tanaka Y.K., Todoroki K.,Tsukada K., Uesaka T., Watanabe Y.N., Weick H., Yamada H., Yoshida K., "BigRIPS as a high resolution spectrometer for pionic atoms", Nucl. Instrum.Meth. B317 (2013) 290-293 ＊

Ohnishi H., Iwasaki M., Sakuma F., Yokkaichi S., Bühler P., Hartmann O., Ishiwatari T., Marton J., Suzuki K., Widmann E., Zmeskal J. Curceanu C., Guaraldo C., Okada S., Vidal A.R., Sirghi D., Sirghi F., Vazquez Doce O., Hicks K., Muto R., Naruki M., Sawada S., Niiyama M., Noumi H., Sakaguchi A., Tsukada K., "A Search for φ Meson Nucleus Bound State Using Antiproton Annihilation on Nucleus", Acta Phys.Polon. B45 (2014) 819-826 ＊

Oishi Y., Okamura K., Miyazaki K., Saito N., Iwasaki M., Wada S., "All-solid-state laser amplifiers for intense Lyman-α generation" Proceedings of the International Symposium on Science Explored by Ultra Slow Muon. Vol.2, 010105-1～5 (2014) ＊

Okamura K., Saito N., Miyazaki K., Oishi Y., Louchev O,, Iwasaki M. and Wada S., "Temporally Resolved Spectral Structure of 821 nm Broad-Area Laser Diode Seeder for Muonium Lyman-Alpha Generation", JPS Conference Proceedings 2 (2014) 010106 ＊

Risdiana, Safriani L., Somantri W.A., Saragi T., Adachi T., Kawasaki I., Watanabe I., and Koike Y., "Impurity-Induced Magnetic Order in Electron-Doped Superconducting Cuprates $Eu_{1.85}Ce_{0.15}Cu_{1-y}Ni_yO_{4+\alpha-\delta}$ Studied by Muon-Spin-Relaxation", Advanced Materials Research **896**, 354-357 (2014) ＊

Safriani L., Risdiana, Bahtiar A., Aprilia A., Siregar R.E., Hidayat R., Saragi T.P.I, Kawasaki I., and Watanabe I., "Charge Carrier Dynamics of Active Material Solar Cell P3HT: ZnO Nanoparticles Studied by Muon Spin Relaxation（μSR)", Advanced Materials Research **896**, 477-480 (2014) ＊

Sakuma F., Hashimoto T., Itahashi K., Iwasaki M., Ma. Y., Okada S., Ohnishi H., Outa H., Sato M., Tokuda M., Yamazaki T. (J-PARC E15 collaboration), "A Search for Deeply-bound Kaonic Nuclear States by In-flight 3He(K-,n) Reaction at J-PARC", Proceedings of the Second International Symposium on Mesic Nuclei, Acta Phys. Pol. B45, 767 (2014) ＊

Saragi T.P.I, Risdiana, Safriani L., Kawasaki I., Salbeck J. and Watanabe I. "Muon-Spin-Relaxation Study of Organic Semiconductor Spiro-Linked Compound" Organic Electronics **14**, 62–66 (2013) ＊

Suzuki K., Brinkmann K.T., Friedrich S., Fujioka H., Geissel H.,Hayano R.S., Hirenzaki S., Itahashi K., Itoh S., Jido D., Metag V., Nagahiro H., Nanova M., Nishi T., Okochi K., Outa H., Suzuki T.,Tanaka Y.K., Watanabe Y.N., Weick H., "Spectroscopy of η′ mesic nuclei using (p,d) reaction", PoS Hadron2013 (2013) 166

Suzuki T., Watanabe I., Yamada F., Ishii Y., Ohishi K., Goto T., and Tanaka H., "Gradual Evolution in Spin Dynamics of $TlCu_{1-x}Mg_xCl_3$ Probed by Mon-Spin-Relaxation（μSR) Technique" Journal of Physics: Conference Series **502**, 012041-1-14 (2014). ＊

Tanabe Y., Adachi T., Suzuki K. , Akoshima M., Kawamata T., Ishii Y., Suzuki T., Watanabe I., and Koike Y., "Development of Spatial Inhomogeneity of Internal Magnetic Field above T_C in$Bi_2Sr_2Ca_{1-x}Y_xCu_2O_{8+}$ Observed by Longitudinal-Field Muon-Spin-Relaxation" J. Phys. Soc. Jpn. **83**, 074707-1-5 (2014) ＊

Tanaka K.S., Aoki M., Iinuma H., Ikedo Y., Ishida K., Iwasaki M., Ueno Y., Ohkubo R., Ogitsu T., Kadono R., Kamigaito O., Kawamura N., Kawall D., Kanda S., Kubo K., Kume T., Koda A., Kojima K., Saito N., Sakamoto N., Sasaki K., Shimomura K., Sugano M., Tomono D., Toyoda A., Torii H.A., Torikai E., Nagamine K., Nishiyama K., Strasser P., Fukao Y., Fujiwara Y., Matsuda Y., Mibe T., Miyake Y., Yoshida M., "Measurement of Muonium Hyperfine Splitting at J-PARC", JPS Conference Proceedings 2 (2014) 010405 ＊

Tanaka Y.K., Brinkmann K.T., Friedrich S., Fujioka H., Geissel H.,Hayano R.S., Hirenzaki S., Itahashi K., Itoh S., Jido D., Metag V., Nagahiro H., Nanova M., Nishi T., Okochi K., Outa H., Suzuki K., Suzuki T., Watanabe Y.N., Weick H., "Missing Mass Spectroscopy of η' Mesic Nuclei with the (p,d) Reaction at GSI", EPJ Web Conf. 66 (2014) 09019

Tanaka Y.K., Brinkmann K.T., Friedrich S., Fujioka H., Geissel H.,Hayano R.S., Hirenzaki S., Itahashi K., Itoh S., Jido D., Metag V., Nagahiro H., Nanova M., Nishi T., Okochi K., Outa H., Suzuki K., Suzuki T., Watanabe Y.N., Weick H., "Spectroscopy of η' mesic nuclei with (p,d) reaction", Few Body Syst. 54 (2013) 1263-1266 ＊

Tomida N., Niiyama M., Ohnishi H., Tran M., Hsieh C.-Y., Chu M.-L., Chang W.-C., Chen J.-Y., "Large strip RPCs for the LEPS2 TOF system", Nucl. Instrum. Meth. A766 (2014) 283-287 ＊

Watanabe Y.N., Berg G.P.A, Dozono M., Fujioka H., Fukuda N., Furuno T., Geissel H., Hayano R.S., Inabe N., Itahashi K., Itoh S., Kameda D., Kubo T., Matsubara H., Michimasa S., Miki K., Miya H., Murakami Y., Nakamura M., Nakatsuka N., Nishi T., Noji S., Okochi K., Ota S., Suzuki H., Suzuki K., Takaki M., Takeda H., Tanaka Y.K., Todoroki K., Tsukada K., Uesaka T., Weick H., Yamada H., Yamakami H., Yoshida K., "Status and future plan of the spectroscopy of pionic atoms", J. Phys. Conf. Ser. 503 (2014) 012037

Wenner S., Nishimura K., Matsuda K., Matsuzaki T., Tomono D., Pratt F.L., Marioara C.D. and Holmestad R. "Muon kinetics in heat treated Al(-Mg)(-Si) alloys" Acta. Mat. **61**, 6082 (2013) ＊

Oral Presentations

(International Conference etc.)

Adiperdana B., Dharmawan I.A., Siregar R.E., Sulaiman S., Ismail M.I.M., WatanabeO.,"Muon Site Estimation on La_2CuO_4 Using Dipole Field and Density Functional Theory", Padjadjaran International Physics Symposium 2013 (PIPS2013), Contribution of Physics on Environmental and Energy Conservations, Padjadjaran Univerisity, Jatinagor, Indonesia, May(2013)

Enomoto S., Hashimoto T., Itahashi K., Iwasaki M., Ma. Y., Okada S., Ohnishi H., Outa H., Sakuma. F., Sato M., Yamazaki T. (J-PARC E15 collaboration),"Search for deeply-bound Kbar-nuclear states via the 3He(inflight-K-,n) reaction at J-PARC", XV International Conference on Hadron Spectroscopy (Hadron 2013), Nov.(2013)

Hashimoto T., Hashimoto T., Itahashi K., Iwasaki M., Ma. Y., Okada S., Ohnishi H., Outa H., Sakuma. F., Sato M., Yamazaki T.
(J-PARC E15 collaboration), "A search for the K-pp bound state in the 3He(inflight-K-,n) reaction at J-PARC", The 25th International Nuclear Physics Conference (INPC 2013), Firenze, Jun(2013)

Hashimoto T., Itahashi K., Iwasaki M., Ma. Y., Okada S., Ohnishi H., Outa H., Sakuma. F., Sato M., Yamazaki T. (J-PARC E15 collaboration), "Search for the K-pp bound state via the 3He(K-,n) reaction at 1 GeV/c", 3rd International Workshop on "State of the Art in Nuclear Cluster Physics" (SOTANCP3), KGU Kannai Media Center, Kanto Gakuin University, Yokohama, Japan., May(2014)

Hashimoto T., Itahashi K., Iwasaki M., Ma. Y., Okada S., Ohnishi H., Outa H., Sakuma. F., Sato M., Yamazaki T. (J-PARC E15 collaboration), "Search for the K-pp bound state via the infight-kaon reaction on helium-3", 20th Particles and Nuclei International Conference 2014 (PANIC2014), Hamburg, Germany, Aug.(2014)

Inoue K., Hashimoto T., Itahashi K., Iwasaki M., Ma. Y., Okada S., Ohnishi H., Outa H., Sakuma. F., Sato M., Yamazaki T. (J-PARC E15 collaboration), "A Search forDeeply-bound Kaonic nuclear states", The 3rd Korea-Japan Workshop on Nuclear and Hadron Physics at J-PARC, Inha University, Korea, Mar.(2014)

Ishida K. for muon g-2/EDM collaboration,
"Status and prospect of g-2 experiment at J-PARC", PHIPSI13, Rome, September (2013)

Itahashi K., "Meson bound states spectroscopy in nuclei: pionic atoms at RIBF and eta-prime mesic nuclei at GSI/FAIR", II International Symposium on Mesic Nuclei, Cracow, Poland, Sep.(2013)

Itahashi K., "Systematic study of deeply bound pionic atom and future perspectives", YITP workshop on Hadron in Nucleus, Kyoto, Oct. (2013)

Itahashi K., "Pionic atom factory project at RIKEN, HADRON 2013, Nara, Nov. (2013)

Iwasaki M., "RIKEN's activity at J-PARC Hadron Hall", 25th International Nuclear Physics Conference (INPC 2013), Firenze, Italy, Jun. (2013).

Iwasaki M., "From kaonic atom to kaonic nuclear system", Workshop on Strangeness in the Universe? Theoretical and experimental progress and challenges, Trento, Italy, Oct. (2013).

Iwasaki M., "Search for deeply-bound Kbar-nuclear states via the ^{3}He (inglight-K^-,n) reaction at J-PARC", International workshop on strangeness nuclear physics (SNP2013), Xiamen, China, Dec.(2013).

Kawasaki S.,Hashimoto T., Itahashi K., Iwasaki M., Ma. Y., Okada S., Ohnishi H., Outa H., Sakuma. F., Sato M., Yamazaki T. (J-PARC E15 collaboration), "Experimental search for K-pp deeply bound statevia in-flight 3He(K-,n) reaction at J-PARC K1.8BR", The 2nd International Symposium on Science at J-PARC 2014, Tsukuba, Japan, Jul.(2014)

Ma Y., Hashimoto T., Itahashi K., Iwasaki M., Okada S., Ohnishi H., Outa H., Sakuma. F., Sato M., Yamazaki T. (J-PARC E15 collaboration), "Search for deeply-bound Kbar-nuclear states via the 3He(inflght K-, N) reaction at J-PARC", The Seventh International Symposium on Chiral Symmetry in Hadrons and Nuclei (Chiral13), Beijing, China, Oct.(2013)

Miyazaki K., Saito N., Okamura K., Oishi Y., Louchev O., Iwasaki M., and Wada S., “Development of Lyman-α light source for muonium excitation: Tunable 820.65 nm light source by injection-seeded optical parametric oscillator and amplifier”, Nonlinear Optics 2013, Hawaii, July (2013)

Oishi Y., Okamura K., Miyazaki K., Saito N., Iwasaki M., and Wada S., “Intense Lyman-α light source for generation of ultra-slow Muon”, Conference on Laser and Electro-Optics/Europe - IQEC 2013, Munich, May (2013)

Oishi Y., Okamura K., Miyazaki K., Saito N., Iwasaki M., and Wada S.,“Amplifying high energy pulses at 1062.78 nm with diode pumped Nd:YGAG ceramic”, Advanced-Solid-State Lasers 2013, Paris, France, October (2013)

Okada S., Beer G., Fujiwara Y., Ishida K., Iwasaki M., Kawai H., Marshall G., Mibe T., Oishi Y., Olin A., Saito N., Tabata M., Tomono D., Ueno K. and Yokoyama K., “Development of room-temperature thermal-muonium-emitting material for ultra-slow muon production and afure plan of ultra-slow-muon beamline at RIKEN-RAL”, International Symposium on Science Explored by Ultra Slow Muon (USMM2013), Matsue, August (2013)

Okada S.,”High-precision spectroscopy of kaonic-atom X-rays with TES microcalorimeters” Workshop on Strangeness in the Universe? Theoretical and experimental progress and challenges, Trento, Italy, Oct. (2013).

Okada S., Bennett D. A., Doriese. W. B., Fowler. J. W., Irwin. K. D., Ishimoto S., Sato M., Schmidt. D. R., Swetz. D. S., Tatsuno H., Ullom. J. N., Yamada S., “Study of strong interaction between anti-kaon and nucleus via high-resolution kaonic-atom x-ray spectroscopy with superconducting transition-edge-sensor microcalorimeters”, Suzaku-MAXI 2014 (Expanding the Frontiers of the X-ray Universe), Matsuyama, Feb. (2014).

Okada S., Bennett D. A., Doriese W. B., Fowler J. W., Irwin K. D., Ishimoto S., Sato M., Schmidt D. R., Swetz D. S., Tatsuno H., Ullom. J. N., Yamada S., “High-resolution Kaonic-atom X-ray Spectroscopy with Transition-edge-sensor Microcalorimeters” Pasadena, USA, Jun. (2013).

Okada S., Beer. G., Fujiwara Y., Ishida K., Iwasaki M., Kawai H., Marshall G., Mibe T., Oishi Y., Olin A., Saito N., Tabata M., Tomono D., Ueno K., Yokoyama K., “Development of room-temperature thermal-muonium -emitting material for ultra-slow muon production and a future plan of ultra-slow muon beamline at RIKEN-RAL”, International Symposium on Science Explored by Ultra Slow Muon (USM2013), Matsue, Aug.(2013).

Okada S., “High-resolution hadronic-atom x-ray spectroscopy with transition-edge-sensor microcalorimeters”, YITP international workshop on Hadron in Nucleus, Kyoto, Nov. (2013).

Risdiana, W.A. Somantri, L.Safriani, T.Saragi, Adachi T., Kawasaki Y., Watanabe I.,Koike Y., ”Effects of Ni-Impurities on the Cu-Spin Dynamics of Electron-Doped Superconducting Cuprates”, Padjadjaran International Physics Symposium 2013 (PIPS2013) Contribution of Physics on Environmental and Energy Conservations, Padjadjaran Univerisity, Jatinagor, Indonesia, May (2013)

Risdiana, L.Safriani, W.A. Somantri, T.Saragi, Adachi T., Kawasaki Y., Watanabe O., Koike I.,“Possible Existence of the Stripe Correlations in Electron-Doped Superconducting Cuprates $Eu_{1.85}Ce_{0.15}Cu_{1-y}Ni_{y}O_{4+\alpha-\beta}$ Studied by Muon-Spin-Relaxation”, The 2013 International Conference on Advanced Material Science and Technology (ICAMST2013), University Gadjah Mada, Yogyakarra, Indonesia, Sep.(2013)

Sada Y., Hashimoto T., Itahashi K., Iwasaki M., Ma. Y., Okada S., Ohnishi H., Outa H., Sakuma. F., Sato M., Yamazaki T. (J-PARC E15 collaboration), "Analysis status of the J-PARC E15 experiment (a search for deeply-bound Kaonic nuclear state)", YITP workshop on Hadron in Nucleus, Kyoto-Univ., Kyoto, Nov. (2013)

Sada Y., Hashimoto T., Itahashi K., Iwasaki M., Ma. Y., Okada S., Ohnishi H., Outa H., Sakuma. F., Sato M., Yamazaki T. (J-PARC E15 collaboration), "Search for the K-pp bound state via the in-flight 3He(K-,n) reaction", 13th International Workshop on Meson Production, Properties and Interaction (MESON2014), Krakow, Poland, Jun.(2014)

Sato M.,Hashimoto T., Itahashi K., Iwasaki M., Ma. Y., Okada S., Ohnishi H., Outa H., Sakuma. F., Yamazaki T. (J-PARC E15 collaboration), "Search for kaonic nuclei by in-flight K- reaction on 3He at J-PARC", ECT* workshop "Strangeness in the Universe", ECT*, Italy, Oct.(2013)

Safriani L., Risdiana, Bahtiar A., Aprilia A., Siregar R.E., Hidayat R., Saragi T.P.I., Kawasaki I, Watanabe I., “Charge Carrier Dynamics of Active Material Solar Cell P3HT: ZnO Nanoparticles Studied by Muon Spin Relaxation (μSR)”, The 2013 International Conference on Advanced Material Science and Technology (ICAMST2013), University Gadjah Mada, Yogyakarra, Indonesia, Sep.(2013)

Sakuma F., Itahashi K., Iwasaki M., Ma Y., Okada S, Ohnishi H, Outa H., Sato M., Yamazaki T., E15 collaborator., “A search for deeply-bound kaonic nuclear states by in-flight $^{3}He(K^{-}, n)$ reaction at J-PARC” II International Symposium on Mesic Nuclei, Cracow, Poland, Sep.(2013).

Sakuma F., “Search for double strangeness dibaryons at J-PARC” Workshop on Strangeness in the Universe Theoretical and experimental progress and challenges, Trento, Italy, Oct. (2013).

Sakuma F., Hashimoto T., Itahashi K., Iwasaki M., Ma. Y., Okada S., Ohnishi H., Outa H., Sato M., Yamazaki T. (J-PARC E15 collaboration), "Recent results and future prospects of the KbarNN search via the (K-,N) reaction at J-PARC", Achievements and Perspectives in Low-Energy QCD with Strangeness, ECT*, Italy, Oct.(2014)

Sato F., Itahashi K., Iwasaki M., Ma Y., Okada S., Ohnishi H., Outa H., Sakuma F., Yamazaki T., E15 collaborator., "Search for kaonic nuclei by in-flight K- reaction on ^{3}He at J-PARC" Workshop on Strangeness in the Universe? Theoretical and experimental progress and challenges, Trento, Italy, Oct. (2013).

Tokuda M., Hashimoto T., Itahashi K., Iwasaki M., Ma. Y., Okada S., Ohnishi H., Outa H., Sakuma. F., Sato M., Yamazaki T. (J-PARC E15 collaboration), "A Search for Deeply Bound Kaonic Nuclear States at J-PARC", The 12th Asia Pacific Physics Conference of AAPPS (APPC12), Chiba, Japan, Jul.(2013)

Tokuda M. Hashimoto T., Itahashi K., Iwasaki M., Ma. Y., Okada S., Ohnishi H., Outa H., Sakuma. F., Sato M., Yamazaki T. (J-PARC E15 collaboration), "A Search for Deeply Bound Kaonic Nuclear States at J-PARC", The 13th International Conference on Meson-Nucleon Physics and the Structure of the Nucleon (MENU 2013), Rome, Italy, Oct.(2013)

Watanabe I., "Applications and Simulations of Muons for Material Sciences", RIKEN-USM Sypsium, Universiti Sains Malaysia (USM), Penang,Malaysia, Feb. (2013)

(Domestic Conference)

足立匡, 今泉真人, 稲辺拓也, 鈴木謙介, 川股隆行、野地尚, 大石一城, Hanjie Guo, 渡邊功雄, 小池洋二： "鉄カルコゲナイド超伝導体における磁性と超伝導のμSR による研究", KEK-IMSS Science Festa, KEK、茨城県つくば市, 3 月(2013)

足立匡, 高橋晶, 稲辺拓也, 鈴木謙介, M.A. Baqiya, 川股隆行, 野地, Hanjie Guo, 渡邊功雄, 幸田章宏, 宮崎正範, 小池洋二： "μSR Study of the Spin Fluctuation in Electron-Doped High-Tc Cuprates and Impurity-Substituted Iron Chalcogenides", ICC-IMR Workshop "Superconductivity Research Advanced by New Materials and Spectroscopies", 東北大金研、宮城県仙台市, 7 月(2013)

足立匡, 稲辺拓也, 鈴木謙介, 川股隆行, 野地尚, Hanjie Guo, 渡邊功雄, 小池洋二： "Impurity-Induced Development of the Spin Correlation in Iron-Chalcogenide Superconductors", International Symposium on Science Explored by Ultra Slow Muon (USM2013), 松江コンベンションビューロー, 島根県松江市, 8 月(2013)

足立匡, 稲辺拓也, 鈴木謙介, 川股隆行, 野地, Hanjie Guo, 渡邊功雄, 小池洋二: "μSR から見た鉄カルコゲナイド超伝導体 $Fe_{1-y}M_ySe_{0.3}Te_{0.7}$（M = Co, Ni, Zn）単結晶におけるスピン相関の不純物置換効果", 日本物理学会 2013 年秋季大会, 徳島大学, 徳島県徳島市, 9 月(2013)

足立匡, 高橋晶, 稲辺拓也, 鈴木謙介, A.M.A. Baqiya, 川股隆行, 野地尚, H. Guo, 渡邊功雄, 幸田章宏, 宮崎正範, 門野良典, 小池洋二： " T' 型銅酸化物と鉄カルコゲナイド超伝導体におけるスピン揺らぎのμSR による研究", 第 7 回物性科学領域横断研究会（領域合同研究会）,東京大学たけだ先端知ビル, 12 月(2013)

足立匡, 高橋晶, 鈴木謙介, M.A. Baqiya, 渡邊功雄, 幸田章宏, 宮崎正範, 門野良典, 小池洋二： "μSR からみた電子型T'-214 高温超伝導体における Cu スピン相関とノンドープ超伝導", 第2回物構研サイエンスフェスタ, KEK, 茨城県つくば市, 1 月(2014)

井上謙太郎, 板橋健太, 岩崎雅彦, 應田治彦, 岡田信二, 大西宏明, 佐藤将春, 佐久間史典, 徳田真, 橋本直, 山崎敏光, Ma Yue (J-PARC E15 実験): "J-PARC K1.8BR ビームラインにおける液体 3He 標的への K-ビーム照射実験(5)", 日本物理学会 2013 年秋季大会, 高知大学, 高知, 9 月(2013)

榎本瞬, 板橋健太, 岩崎雅彦, 應田治彦, 岡田信二, 大西宏明, 佐藤将春, 佐久間史典, 徳田真, 橋本直, 山崎敏光, Ma Yue (J-PARC E15 実験): "J-PARC K1.8BR ビームラインにおける液体3He 標的への K-ビーム照射実験(4)", 日本物理学会 2013 年秋季大会, 高知大学, 高知, 9 月(2013)

應田治彦, 板橋健太, 岩崎雅彦, Ma Y, 岡田信二,大西宏明, 佐久間史典, 佐藤将春, 山崎敏光, E15 collaborator： " E15 experiment on K-pp ", KEK theory center workshop on J-PARC hadron physics in 2014, つくば市, 2 月(2014).

岡田信二: "超伝導遷移端マイクロカロリメータを用いたハドロニック原子 X 線精密分光", 第 2 回中性子星核物質研究会, 和光市, 12 月(2013).

岡田信二, 石田勝彦, 岩崎雅彦, 上野一樹, Eunil Won, 大石裕, Art Olin, 河合秀幸, 河村成肇, 神田聡太郎, 北村遼, 齊藤直人, 下村浩一郎, Patrick Strasser, 田端誠, 友野大, 西村昇一郎, Pavel Bakule, George Beer, 藤原裕也, Glen Marshall, 松田恭幸, 三部勉, 三宅康博, 横山幸司, Woodo Lee: "超低速ミュオン生成のための室温ミュオニウム真空放出源の開発" 日本物理学会第 69 回年次大会, 平塚市, 3 月(2014).

小林弘明, 岡澤厚, 小島憲道, 川崎郁斗, 渡邊功雄: "スピン平衡を示すスピンクロスオーバー鉄 (II) 錯体におけるメスバウアー分光とミュオン分光からみた動的挙動", 2013 年度メスバウアー分光研究会, 東大本郷キャンパス, 3 月(2014)

佐田優太, 板橋健太, 岩崎雅彦, 應田治彦, 岡田信二, 大西宏明, 佐藤将春, 佐久間史典, 徳田真, 橋本直, 山崎敏光, Ma Yue (J-PARC E15 実験): "J-PARC E15 実験における in-flight 3He(K-,n)反応での K 中間子原子核の探索", 日本物理学会第 68 回年次大会,広島大学, 東広島, 3 月(2013)

佐田優太, 板橋健太, 岩崎雅彦, 應田治彦, 岡田信二, 大西宏明, 佐藤将春, 佐久間史典, 徳田真, 橋本直, 山崎敏光, Ma Yue (J-PARC E15 実験): "J-PARC K1.8BR ビームラインにおける液体3He 標的への K-ビーム照射実験(3)", 日本物理学会 2013 年秋季大会, 高知大学, 高知, 9 月(2013)

佐田優太, 板橋健太, 岩崎雅彦, 應田治彦, 岡田信二, 大西宏明, 佐藤将春, 佐久間史典, 徳田真, 橋本直, 山崎敏光, Ma Yue (J-PARC E15 実験): "J-PARC K1.8BR における 3He(K-, Λpn)反応を用いての K-多核子吸収の研究",日本物理学会第 69 回年次大会, 東海大学, 神奈川, 3 月(2014)

鈴木謙介, 足立匡, 佐藤秀孝, 渡邊功雄, 小池洋二：

"Magnetic Ground State of Fe-Substitued La-214 High-T_C Superconductors " Excellent Graduate Schools 2012 Annual Meeting and Japan-Russia Workshop on Advanced Materials Synthesis Process and Nanostructure, 秋保温泉、宮城県仙台市, 3 月 (2013)

鈴木謙介, 足立匡, 佐藤秀孝, 渡邊功雄, 小池洋二: "Fe を置換した $La_{2-x}Sr_xCu_{1-y}Fe_yO_4$ における遍歴磁性と局在磁性", 日本物理学会 2013 年秋季大会, 徳島大学, 徳島県徳島市, 9 月(2013)

鈴木謙介, 足立匡, Hanjie Guo, 川崎郁斗, 渡邊功雄, 小池洋二："$La_{2-x}Sr_xCu_{1-y}Al_yO_4$ のオーバードープ領域における Al 誘起磁気秩序",日本物理学会大 69 回年次大会, 東海大学湘南キャンパス, 神奈川県, 3 月(2014)

鈴木栄男, Hanjie Guo, 川崎郁斗, 渡邊功雄, 片山和哉, 後藤貴行, 田中秀数: "ミュオンスピン緩和でみたボースグラス相 Tl$_{1-x}$K$_x$CuCl$_3$ のゼロ磁場極限における磁気的基底状態", 日本物理学会大 69 回年次大会, 東海大学湘南キャンパス, 神奈川県, 3 月(2014)

高橋晶, 足立匡, 鈴木謙介, M.A. Baqiya, 渡邊功雄, 幸田章宏, 宮崎正範, 門野良典, 小池洋二:
"μSR から見た電子型超伝導体 $Pr_{1.3-x}La_{0.7}Ce_xCuO_{4+\delta}$ (x = 0.10)におけるスピンダイナミクの還元効果", 日本物理学会 2013 年秋季大会, 徳島大学、徳島県徳島市、9 月 (2013)

高橋晶, 足立匡, 鈴木謙介, M.A.Baquya, 渡邊功雄, 幸田章宏, 宮崎正範, 門野良典, 小池洋二: "ミュオンスピン緩和から見た電子型超伝導体 T'-$Pr_{1.3-x}La_{0.7}Ce_xCuO_{4+\delta}$ (x=0.10) における電子・スピン状態", 平成 25 年度応用物理学会東北支部学術講演会, 山形大学, 山形市, 12 月 (2013)

徳田真, 板橋健太, 岩崎雅彦, 應田治彦, 岡田信二, 大西宏明, 佐藤将春, 佐久間史典, 橋本直, 山崎敏光, Ma Yue (J-PARC E15 実験): "J-PARC K1.8BR ビームラインにおける液体 3He 標的への K-ビーム照射実験(1)", 日本物理学会 2013 年秋季大会, 高知大学, 高知, 9 月(2013)

中野岳仁, 花澤宏文, 松浦直人, 廣田和馬, 末廣龍一, 渡邊功雄, Alex Amato, Francis L. Pratt,福田直起, 瀬戸誠, 小林康浩, 依田芳卓, 野末泰夫:
"Antiferromagnetic ordering of s-electrons confined in regular nanospace of sodalite studied by neutron diffraction, μSR and synchrotron-radiation-based Mossbauer spectroscopy", JAEA Synchrotron Radiation Research Symposium "Magnetism in Quantum Beam Science", SPring-8 Harima Science Garden Sity、兵庫県, 3 月(2013 年)

中野岳仁, Gayan Prasad Hettiarachchi, 石井康之, 渡邊功雄, 野末泰夫: "ゼオライト LSX 中の Na-K 合金クラスターが示すフェリ磁性の He による圧力効果" , 日本物理学会大 69 回年次大会, 東海大学湘南キャンパス, 神奈川県, 3 月(2014)

野崎洋, 原田雅史, 太田慎吾, 渡邊功雄, 三宅康博, 池戸豊, Niina H Jalarvo, Eugene Mamontov,杉山純: "ミュオンと中性子による固体電解質中の Li イオン拡散", 日本物理学会 2013 年秋季大会, 徳島大学, 徳島県徳島市, 9 月 (2013)

橋本直, 板橋健太, 岩崎雅彦, 應田治彦, 岡田信二, 大西宏明, 佐藤将春, 佐久間史典, 徳田真, 山崎敏光, Ma Yue (J-PARC E15 実験): "J-PARC K1.8BR ビームラインにおける液体 3He 標的への K-ビーム照射実験(2)", 日本物理学会 2013 年秋季大会, 高知大学, 高知, 9 月(2013)

廣井政彦, 渡邊功雄, 川崎郁斗, 鈴木栄男, 伊藤昌和, 重田出: "ホイスラー化合物 $Ru_{2-x}Fe_xCrSi$ の磁気転移", 日本物理学会第６８回年次大会, 広島大学, 広島県東広島市, 3 月(2013 年)

真中浩貴, 川崎郁斗, 渡邊功雄: "歪んだ三角スピンチューブ α-$KCrF_4$ のμSR 測定",日本物理学会第６８回年次大会, 広島大学, 広島県東広島市, 3 月(2013)

向和彦, 青木良文, Daniel Andreica, Alex Amato, 渡邊功雄, Sean R.Giblin, 杉山純: "化学量論組成 $LiCoO_2$ におけるスピン揺らぎ", 東工大, 東京都目黒区大岡山, 9 月(2013)

渡邊功雄:
"理研 RAL ミュオン施設における高圧物性実験条件の開発および最近のμSR" 第５回 Muon 科学と加速器研究, KEK、茨城県つくば市, １月 (2013)

渡邊功雄, 石井康之, F.L. Pratt, 加藤礼三："Introduction of the RIKEN-RAL Muon Facility and Applications of Muons to Organic Molecules", 2014 Collaborative Conference 3D and Materials Researchs (CC3DMR2013), 韓国済州島, 6 月(2013)

渡邊功雄 "Applications of a DC Muon Source to the Muon to Material Science", RISP scientific Seminar, RISP, 太田市, 韓国 1 月(2014)

渡邊功雄: "Applications of Pulsed Muon Beam to Material Science at the RIKEN-RAL Muon Facility", NTNU Science Seminar, NTNU, Trondheim, ノルウェー, 1 月(2014)

渡邊功雄: "μSR から見たパイロクロア酸化物 $Yb_2Ti_2O_7$ のスピンダイナミクス", 三機関連携による量子複雑現象研究会, 理研、埼玉県和光市, 1 月(2014)

渡邉功雄："Applications of the Pulsed Muon Beam at the RIKEN-RAL Muon Facility", 3rd Workshop for Light/Quantum Beam Science Promotion, Tohoku University New insight into materials and life sciences using light/quantum beams (III) ---Introduction of overseas facilities and cooperation with Tohoku University--- 宮城県仙台市, 東北大学金研, 3 月(2014)

Aina Adam, Budi Adiperdana, Edi Suprayoga, Saidah Sakinah Mohd-Tajudin, Ainul Fauzeeha Rozlan, Shukri Slaiman, Mohamad Ismail Mohamed-Ibraham, Hanjie Guo, 谷田博司, 世良正文, 西岡孝, 松村政博, 渡邊功雄: "$Ce(Ru,Rh)_2Al_{10}$ におけるミュオン位置計算と磁気モーメント構造および超微細場に関する考察", 日本物理学会大 69 回年次大会, 東海大学湘南キャンパス, 神奈川県, 3 月 (2014)

Budi Adiperdana, Irwan Ary Dharmawa, Shukri Sulaiman, M.I. Mohamad Ismail, Hanjie Guo,松平和之, 分島 亮, 日夏幸雄, 川崎郁斗, 渡邊功雄: "Muon Site Determination on $Nd_2Ir_2O_7$ Using Dipole Field and *ab-initio* Calculation", 日本物理学会第６８回年次大会, 広島大学、広島県東広島市, 3 月(2013 年)

Budi Adiperdana, Edi Suprayoga, Aina Adam, Irwan A. Dharmawan, Rustam Siregr, Saidah Sakinah Mohd-Tajudin, Ainul Fauzeeha Rozlan, Shukri Slaiman, Mohamad Ismail Mohamed-Ibraham, 川股隆行, 足立匡, 小池洋二，Pabitra Kumar, Alex Amato, 渡邊功雄: “La_2CuO_4 におけるミュオン位置計算およびミュオンから見た Cu モーメントの状態”, 日本物理学会大 69 回年次大会, 東海大学湘南キャンパス, 神奈川県, 3 月(2014)

Hanjie Guo, 松平和之, 川崎郁斗, 分島 亮, 日夏幸雄, 渡邊功雄: “Muon Spin Relaxation Study on Pyrochlore Iridate $Nd_2Ir_2O_7$”, 日本物理学会第６８回年次大会, 広島大学, 広島県東広島市, 3 月(2013 年)

Edi Suprayoga, Budi Adiperdana, Aina Adam, Saidah Sakinah Mohd-Tajudin, Ainul Fauzeeha Rozlan, Shukri Slaiman, Mohamad Ismail Mohamed-Ibraham, Hanjie Guo, 谷田博司, 世良正文, 西岡孝, 松村政博, Agung A. Nugroho, 渡邊功雄: “Study on the Hyperfine Fields and Muon Site Calculation in $CeRu_2Al_{10}$ Kondo-Semiconductor”, 日本物理学会大 69 回年次大会, 東海大学湘南キャンパス, 神奈川県, 3 月(2014)

劉鐘昇, 和氣剛, 田畑吉計, 弓削是貴, 渡邊功雄, 中村裕之: “層状化合物 Cr_2GaN の SDW 転移”, 日本物理学会第６８回年次大会, 広島大学、広島県東広島市, 3 月(2013 年)

RBRC Theory group

Publications

[Journal]

(Original Papers) *Subject to Peer Review

Albacete JL, Dumitru A , Marquet C: "THE INITIAL STATE OF HEAVY ION COLLISIONS", International Journal of Modern Physics A Volume 28 Issue 11 Article 1340010, 2013/04/30 *

Berger J, Stasto, AM: "Exclusive vector meson production and small-x evolution", Journal of High Energy Physics Issues 1, Article 001, 2013/01 *

Bezrukov F, Karananas GK, Rubio J, Shaposhnikov M: "Higgs-dilaton cosmology: An effective field theory approach", Physical Review D, Volume 87 Issue 9 Article 096001 2013/05/01 *

Bezrukov F, Gorbunov, D: "Light inflaton after LHC8 and WMAP9 results", Journal of High enerrgy Physics Issue 7 Article 140, 2013/07 *

Bezrukov F, Kartavtsev, A; Lindner, M: "Leptogenesis in models with keV sterile neutrino dark matter", Journal of Physics G Nuclear and Particle Physics Volume 40 Issue 9 Article 095202, 2013/09/01 *

Bicudo P, Pisarski, R; Seel, E: "Matrix model for deconfinement in a SU(2) gauge theory in 2+1 dimensions", Physical Review D Volume 88, Issues 3, Article 034007, 2013/08/06 *

Bzdak A, Teaney D: "Longitudinal fluctuations of the fireball density in heavy-ion collisions", Physical Review C Volume 87 Issue 2, 2013/02/15 *

Bzdak A, Skokov, V: "Anisotropy of Photon Production: Initial Eccentricity or Magnetic Field" , Physical Review Letters, Volume110 Issue 19 2013/05/08 *

Bzdak A, Schenke, B; Tribedy, P; Venugopalan, R: "Initial-state geometry and the role of hydrodynamics in proton-proton, proton-nucleus, and deuteron-nucleus collisions", Physical Review C Volume 87 Issue 6 Article 064906, 2013/06/20 *

Bzdak A, Skokov. V: "Average transverse momentum of hadrons in proton-nucleus collisions in the wounded nucleon model", Physics Letters B Volume 726, Pages 408-411, 2013/10/07 *

Bzdak A, Skokov, V: "Decisive Test of Color Coherence in Proton-Nucleus Collisions at the LHC", Physical Review Letters Volume 111 Issue 18 Article 182301 Pages 1-5, 2013/10/28 *

Chiu M, Hemmick TK, Khachatryan V, Leonidov A, Liao JF , McLerran L: "Production of photons and dileptons in the Glasma", Nuclear Physics A Volume 900 Page 16-37, 2013/02/05 *

Dominguez F, Marquet, C, Stasto, AM ,Xiao, BM: "Universality of multiparticle production in QCD at high energies", Physical Review D Volume 87 Issue 3 Article 034007, 2013/02/04 *

Dumitru A, : "Review of Recent Developments in the CGC", Nuclear Physics A Volume 904 Page 51C-58C, 2013/05/02 *

Dumitru A, Nara Y,Petreska E: "Magnetic flux loop in high-energy heavy-ion collisions", Physical Review D Volume 88 Issue 5 Article 054016, 2013/09/17 *

Dumitru A, Hirotsugu, F, Nara Y: "Magnetic screening in high-energy heavy-ion collisions", Physical Review D Volume 88 Issue 3 Article 031503, 2013/08/21 *

Dumitru A, Yun Guo, Chris P. Korthals Altes: "Two-loop perturbative corrections to the thermal effective potential", Physical Review D 89, 016009, 2014/01/08 *

Fukushima K, Kouji Kashiwa: "Polyakov loop and QCD thermodynamics from the gluon and ghost propagators", Physics Letter B Volume 723, Issue 4-5, pp 360, 2013/06/25 *

Gursoy U, Lin, S; Shuryak, E: "Instabilities near the QCD phase transition in the holographic models", Physical Review D Volume 88 Issue 10 Article 105021 Page 1-11, 2013/11/19 *

Hell T, Kouji Kashiwa, Wolfram Weise: "Impact of Vector-Current Interactions on the QCD Phase Diagram", Journal of Modern Physics Volume 4, pp 644-650, 2013/05 *

Huang XG, Liao, JF: "Axial Current Generation from Electric Field: Chiral Electric Separation Effect" , Physical Review Letters, Volume 110 Issue 23 Article 232302 2013/06/06 *

Kashiwa K, Misumi T: "Phase structure and Hosotani mechanism in gauge theories with compact dimensions revisited", Journal of High Energy Physics Issue 5 Article 042, 2013/05/01 *

Kashiwa K, Robert D. Pisarski: "Roberge-Weiss transition and 't Hooft loops", Physical Review D 87, 096009, 2013/05/14 *

Kashiwa K, Akihiko Monnai: "Quark contribution for center domain in heavy ion collisions", Phys. Rev. D Vol. 89, 011501(R), 2014/01/07 *

Kiminad A Mamo, Ho-Ung Yee: "Spin polarized photons and dileptons from axially charged plasma", Physical Review D 88, 114029 (2013), 2013/12/26 *

Kouno H, Misumi, T; Kashiwa, K; Makiyama T; Sasaki T; Yahiro, M: "Differences and similarities between fundamental and adjoint matters in SU(N) gauge theories", Physical Review D Volume 88 Issue 1 Article 016002, 2013/07/01 *

Lin S, Erdmenger, J; Hoyos, C: "Evolution of singularities in unequal time correlator in thermalization of quark gluon plasma", Nuclear Physics A Volume 904 Pages 977C-980C, 2013/05/02 *

Lin S, Yee Ho Ung: "Out-of-equilibrium chiral magnetic effect at strong coupling", Physical Review D "Volume 88 Issue 2 Article 025030" 2013/07/18 *

Lin S, Pisarski, R; Skokov, V: "Zero interface tensions at the deconfining phase transition for a matrix model of a SU(infinity) gauge theory", Physical Review D Volume

87 Issue 10 Pages 105002, 2013/05/15 *

McLerran L, Praszalowicz, Michael, Schenke, Bjorn: "Transverse momentum of protons, pions and kaons in high multiplicity pp and pA collisions:Evidence for the color glass condensate?", Nuclear Physics A, 916, 210-218 2013/10/23 *

Pisarski R, Kashiwa K, Skokov V: "Quasi-particle and matrix models of the semi Quark Gluon Plasma", Nuclear Physics A "Volume 904 Page 973C-976C", 2013/05/02 *

Shi SZ, Liao, JF: "Conserved charge fluctuations and susceptibilities in strongly interacting matter", JOURNAL OF HIGH ENERGY PHYSICS Issue 6 Article 104, 2013/07/18 *

Smith D, Dumitru, A; Pisarski, R; von Smekal, L: "Effective potential for SU(2) Polyakov loops and Wilson loop eigenvalues", Physical Review D No. 88 Issue 8 Article 054020 page1 to14, 2013/09/20 *

Stasto A, Xiao, BW; Zaslavsky, D: "Drell-Yan Lepton-Pair-Jet Correlation in pA Collisions", Nuclear Physics A Volume 904 Pages 837C-840C, 2013/05/02 *

Stasto A, David Zaslavsky, Bo-Wen Xiao: "Towards the Test of Saturation Physics Beyond Leading Logarithm", Physical Review Letters 112, 012302 (2014), 2014/01/08 *

Stasto A.M., Cruz-Santiago, C.A.: "Recursion in rlations and scattering amplitudes in the light-front formalism", Nuclear Physics B No 875, P368-387, 2013/10/13 *

Stephanov M, Yee, HU: "Charged elliptic flow at zero charge asymmetry", Physical Review C Volume 88 Issue 1 014908 Pages 1-5, 2013/07/29 *

Yee H, : "Flows and polarization of early photons with magnetic field at strong coupling", Physical Review D Volume 88 Issue 2 Article 026001, 2013/07/01 *

Yee Ho Ung, : "Recent Theoretical Developments in Strongly Coupled QCD", Nuclear Physics A Volume 904 Pages 310C-317C, 2013/05/02 *

Zhang XL, Liao. JF: "Event-by-event azimuthal anisotropy of jet quenching in relativistic heavy ion collisions", Physical Review C Volume 87 Issue 4 Article 044910, 2013/04/26 *

[Book · Proceedings]

(Original Papers) *Subject to Peer Review

McLerran, L, "The Color Glass Condensate, Glasma and the Quark Gluon Plasma in the Context of Recent pPb Results from LHC", Journal of Physics Conference Series Volume 458 Article Number 012024, 2013

McLerran, L, "High energy nuclear physics: from bear mountain to the LHC", 100 Years of Subatomic Physics Page 171-197, 2013

Liao, JF, "Hard Probe of Soft Matter Geometry and Fluctuations from RHIC to LHC", AIP Conference Series 11th Conference on the Intersections of Particle and Nuclear Physics Volume 1560 Pages 669-671, 2013

Oral Presentations

(International Conference etc.)

Koji Kashiwa, "Phase structure and Hosotani mechanism in QCD-like gauge theory with compact dimensions", 31th International Symposium on Lattice Field Theory (Lattice 2013) (Johannes Gutenberg University Mainz), Mainz, 2013/08/02

Koji Kashiwa, "Phase diagram and Hosotani mechanism in QCD-like theory with compact dimensions", Workshop on QCD under extreme condition (AEC, Univ. Bern), Bern, 2013/08/07

Akihiko Monnai, "Pre-equilibrium dynamics of QCD matter by gluon splitting", New Frontiers in QCD 2013 (YITP), YITP, Kyoto, Japan, 2013/12/13

RBRC Computing group

Publications

[Journal]

(Original Papers) *Subject to Peer Review

N. H. Christ, T. Izubuchi, C. T. Sachrajda, A. Soni, J. Yu, "Long distance contribution to the KL-KS mass difference" arXiv:1212.5931 [hep-lat], Phys.Rev. D88 (2013) 1, 014508*.

RBC and UKQCD Collaborations (R. Arthur et al.), "Domain Wall QCD with Near-Physical Pions", arXiv:1208.4412 [hep-lat], Phys.Rev. D87 (2013) 094514*.

Thomas Blum, Taku Izubuchi, Eigo Shintani, "New class of variance-reduction techniques using lattice symmetries", arXiv:1208.4349 [hep-lat], Phys.Rev. D88 (2013) 9, 094503*.

Aoki S, Ting-Wai Chiu, Guido Cossu, Xu Feng, Hidenori Fukaya, Shoji Hashimoto, Tung-Han Hsieh, Takashi Kaneko, Hideo Matsufuru, Jun-Ichi Noaki, Tetsuya Onogi, Eigo Shintani, Kouhei Takeda: "Simulation of quantum chromodynamics on the lattice with exactly chiral lattice fermions", Prog Theor Exp Phys 01A106 3 pages*

Lin M, Ohta, S: "Nucleon structure from 2+1-flavor dynamical DWF lattice QCD at nearly physical pion mass", Progess in Particle and Nuclear Physics Volume 67 Issue 2 Pages 218-222, 2012/04/01 *

Tiburzi B, : "Chiral symmetry restoration from a boundary", Physical Review D Volume 88 Issue 3 Article 034027 Page 1-8, 2013/08/23 *

Tiburzi B, Vayl, SO: "Method to extract charged hadron properties from lattice QCD in magnetic fields", Physical Review D Volume 87, Issues 5, Article 054507, 2013/03/25 *

T. Appelquist et al. (LSD Collaboration): "Lattice calculation of composite dark matter form factors", arXiv:1301.1693, Phys. Rev. D 88:014502, 2013 *.

Joachim Kopp, Ethan T. Neil, Reinard Primulando, and Jure Zupan: "From gamma ray line signals of dark matter to the LHC" arXiv:1301.1683, Phys. Dark. Univ. 2:22- 34, 2013 *.

A. Bazavov et al. (Fermilab Lattice/MILC Collaborations): "Kaon semileptonic vector form factor and determination of $|V_u s|$ using staggered fermions", arXiv:1212.4993, Phys. Rev. D 87:073012, 2013, *.

Matthew R. Buckley and Ethan T. Neil: "Thermal Dark Matter from a Confining Sector", arXiv:1209.6054, Phys. Rev. D 87:043510, 2013 *.

T. Appelquist et al. (LSD Collaboration): "Two-Color Theory with Novel Infrared Behavior", arXiv:1311.4889, Phys. Rev. Lett. 112 (2014), 111601 *.

A. Bazavov et al. (Fermilab Lattice/MILC Collaborations): "Determination of —Vus— from a lattice-QCD calculation of the $K \to \pi l \nu$ semileptonic form factor with physical quark masses", arXiv:1312.1228, Phys. Rev. Lett.112 (2014), 112001 *.

Michael I. Buchoff, Michael Cheng, Norman H. Christ, H. -T. Ding, Chulwoo Jung, F. Karsch, Zhongjie Lin, R.D. Mawhinney et al..: "QCD chiral transition, U(1)A symmetry and the dirac spectrum using domain wall fermions", arXiv:1309.4149 [hep-lat], Phys.Rev. D89 (2014) 5, 054514*.

RBC and UKQCD Collaborations (P.A. Boyle et al.): "Emerging understanding of the $\Delta I = 1/2$ Rule from Lattice QCD" arXiv:1212.1474 [hep-lat], Phys.Rev.Lett. 110 (2013) 15, 152001*.

Qi Liu, Norman H. Christ, Chulwoo Jung: "Light Quark Mass Reweighting", arXiv:1206.0080 [hep-lat], Phys.Rev. D87 (2013) 5, 054503*.

Oral Presentations

(International Conference etc.)

Izubuchi, T: *"Nucleon Structure by Lattice QCD"*, PHENIX Workshop on Physics Prospects with Detector and Accelerator Upgrades RIKEN, Wako, Japan, 2013/07/29.

Izubuchi, T: *"Lattice QCD and the HEP Intensity Frontier"*, Lattice QCD Computational Science Workshop, Oak Ridge National Laboratory, TN, 2013/04/29.

Izubuchi, T: *"Nucleon electric dipole moment studies using statistical error reduction techniques on lattice"*, Seminar at MIT Lattice Club, MIT, MA, 2013/04/03.

Izubuchi, T: *"Nucleon electric dipole moment studies using statistical error reduction techniques on lattice"*, Seminar at Theoretical Elementary Particle Physics group, Syracuse University, NY, 2013/03.

Izubuchi, T: *"Lattice-QCD Calculations for EDMs"*, Winter Workshop on Electric Dipole Moments (EDMs13), Fermi National Accelerator Laboratory, IL, 2013/02.

Izubuchi, T: *"Muon $g-2$ on Lattice"*, HET/RIKEN lunch Seminar, Brookhaven National Laboratory, Upton, NY, 2013/9.

Ishikawa, Tomomi: "Neutral B meson mixing with static heavy and domain-wall light quarks", 31st International Symposium on Lattice Field Theory (LATTICE 2013) Mainz, Germany, 2013/7/29-2013/8/3.

Tiburzi, B: "Towards exploring fundamental symmetries with lattice QCD", Institute for Nuclear Theory Program 13-2b "Nuclei and Fundamental Symmetries", Seattle Washington, 2013/08/14.

Tiburzi, B: "Chiral symmetry restoration from a boundary", Nuclear Theory seminar, Lawrence Berkeley National Laboratory, California, 2013/03/07.

Tiburzi, B: "Anatomy of hadronic parity violation on the lattice", Theory seminar, Thomas Jefferson National Laboratory, Newport News Virginia, 2013/02/01.

Tiburzi, B: "Looking under the femtoscope: a focus on strong interactions", Physics Department Colloquium, The College of William and Mary, Williamsburg Virginia, 2013/01/31.

Neil Ethan: "Composite Bosonic Dark Matter", RIKEN Lunch Seminar, Brookhaven National Laboratory, Brookhaven, NY, 2013/12.

Neil Ethan: "Two Tales of Composite Dark Matter", RIKEN Nuclear Theory Seminar, Brookhaven National Laboratory, Brookhaven, NY, 2013/4.

Neil Ethan: "Two Tales of Composite Dark Matter", Nuclear and Particle Theory Seminar, MIT, Cambridge, MA, 2013/2.

Neil Ethan: "Lattice field theory: QCD and beyond", Invited presentation, APS Four Corners Section 2013 Meeting, University of Denver, 2013/10.

Neil Ethan: "Splitting the Higgs boson: Composite models at the high-energy frontier" Physics Colloquium, University of Colorado, Boulder, CO, 2013/3.

Meifeng Lin: "Nucleon Form Factors with 2+1 Flavors of Domain Wall Fermions and All-Mode-Averaging", 31th International Symposium on Lattice Field Theory (Lattice 2013) (Johannes Gutenberg University Mainz), Mainz, 2013/08/01.

Kelly, C: "Standard Model Direct CP-violation in K-¿pi pi Decays from First Principles using Lattice QCD", RBRC Scientific Review Committee Meeting, Brookhaven National Laboratory, 2013/11/01.

Syritsyn Sergey: " Neutron-Antineutron Oscillation Matrix Elements on a Lattice", "Lattice Meets Experiment : Beyond the Standard Model", Brookhaven National Laboratory, Upton, NY, USA, 2013/12/5-6.

Syritsyn Sergey: 2. Nucleon Structure and Quark Angular Momentum from Lattice QCD at the Physical Point, theory seminar in ITEP, Moscow, Russia, Sep 5, 2013.

Syritsyn Sergey: "Review of Hadron Structure Calculations on a Lattice", plenary presentation at LATTICE 2013, Mainz Germany, 2013/7/29-8/3.

Syritsyn Sergey: "Generalized form factors and decomposition of nucleon spin from lattice QCD", APS Topical Group on Hadronic Physics meeting, Denver,Colorado, USA, 2013/04/11.

Syritsyn Sergey: "Nucleon Structure from Lattice QCD at the Physical Point", APS April meeting, Denver, Colorado, 2013/4/13-16.

Conference Proceedings

Eigo Shintani, Hyung-Jin Kim, Thomas Blum, Taku Izubuch: "Vacuum polarization function in $N_f = 2 + 1$ domain-wall fermion", PoS LATTICE2013 (2014) 487 .

T. Blum, M. Hayakawa, T. Izubuch: "Update on the hadronic light-by-light contribution to the muon $g - 2$ and inclusion of dynamically charged sea quarks", PoS LATTICE2013 (2014) 439 .

RBC and UKQCD Collaborations (T. Blum et al.), : "Weak Decay Measurements from 2+1 flavor DWF Ensembles", PoS LATTICE2013 (2014) 404 .

Eigo Shintani, Thomas Blum, Amarjit Soni, Taku Izubuch: "Neutron and proton EDM with $N_f = 2 + 1$ domain-wall fermion", PoS LATTICE2013 (2014) 298 .

Hyung-Jin Kim, T. Izubuch: "Möbius domain wall fermion method on QUDA", PoS LATTICE2013 (2014) 033 .

RBC and UKQCD Collaborations (Norman Christ et al.), : "Calculating the $K_L - K_S$ mass difference and ϵ_K to sub-percent accuracy", arXiv:1402.2577 [hep-lat] , PoS LATTICE2013 (2014) 397 .

Tomomi Ishikawa, Yasumichi Aoki, Taku Izubuchi, Christoph Lehner, Amarjit Son: "Neutral B meson mixing with static heavy and domain-wall light quarks", arXiv:1312.1010 [hep-lat] , PoS LATTICE2013 (2014) 410 .

Shane Drury, Thomas Blum, Masashi Hayakawa, Taku Izubuchi, Chris Sachrajda, Ran Zho: "Non-degenerate light quark masses from 2+1f lattice QCD+QED", arXiv:1312.0477 [hep-lat] , PoS LATTICE2013 (2014) 268 .

T. Blum, M. Hayakawa, T. Izubuch: "Hadronic corrections to the muon anomalous magnetic moment from lattice QCD", arXiv:1301.2607 [hep-lat] , PoS LATTICE2012 (2012) 022 .

Tiburzi, B: "Boundary restoration of chiral symmetry", Proceedings of Science (Lattice 2013), Article 113, 2013.

Y. Liu et al. (Fermilab Lattice/MILC Collaborations): "Heavy-meson semilep- tonic decays for the Standard Model and beyond", Proceedings of Science (LATTICE 2013).

A. Bazavov et al. (Fermilab Lattice/MILC Collaborations): "Charmed and strange pseudoscalar meson decay constants from HISQ simulations", Proceedings of Science (LATTICE 2013).

E. Gamiz et al. (Fermilab Lattice/MILC Collaborations): "K semileptonic form factor with HISQ fermions at the physical point", Proceedings of Science (LATTICE 2013).

T. Blum, R. S. Van de Water, D. Holmgren, R. Brower, S. Catterall, N. Christ, A. Kronfeld, J. Kuti, P. Mackenzie, E. T. Neil, S. R. Sharpe, R. Sugar, "Report of the Snowmass 2013 Computing Frontier working group on Lattice Field Theory – Lattice field theory for the energy and intensity frontiers: Scientific goals and computing needs", Proceedings of the Community Summer Study "Snowmass 2013".

T. Appelquist, R. Brower, S. Catterall, G. Fleming, J. Giedt, A. Hasenfratz, J. Kuti, E. Neil, D. Schaich, "Lattice Gauge Theories at the Energy Frontier", Proceedings of the Community Summer Study "Snowmass 2013".

Meifeng Lin:, "Nucleon Form Factors with 2+1 Flavors of Domain Wall Fermions and All-Mode-Averaging", Proceedings of Science (LATTICE2013) 275 (2013).

J.M. Flynn, P. Fritzsch,T. Kawanai, C. Lehner, C.T. Sachrajda, B. Samways, R.S. Van de Water, O. Witzel:

"The $B^*B\pi$ coupling with relativistic heavy quarks", PoS LATTICE2013 (2014) 408.

Kelly, C: "Progress Towards an ab Initio, Standard Model Calculation of Direct CP-Violation in K decay", PoS(LATTICE 2013)401.

Kelly, C: "Weak Decay Measurements from 2+1 flavor DWF Ensembles", PoS(LATTICE 2013)404.

Kelly, C: "Progress Towards an ab initio, Standard Model Calculation of Direct CP-Violation in K-decays", arXiv:1310.0434 [hep-lat] (Note, this is a different article with the same name, as the above; these are for the DPF2013 conference).

RBC-UKQCD Collaboration (Julien Frison et al.): "The Kaon Bag Parameter at Physical Mass" arXiv:1312.2374 [hep-lat], PoS LATTICE2013 (2014) 460.

T. Janowski, C.T. Sachrajda, P.A. Boyle, N.H. Christ, R.D. Mawhinney, H. Yin, D. Zhang, N. Garron et al..:, "Determination of the A_2 amplitude of $K \to \pi\pi$ decays", arXiv:1311.3844 [hep-lat], PoS LATTICE2013 (2014) 402.

RBRC Experimental group

Publications

[Journal]

(Original Papers) *Subject to Peer Review

Adare A, *et al.* (the PHENIX Collaboration): "Event Structure and Double Helicity Asymmetry in in Jet Production from Polarized p+p Collisions at $\sqrt{s} = 200$ GeV", Phys. Rev. D 84, 012006, 2011-07-28 *

Adare A, *et al.* (the PHENIX Collaboration): "Suppression of away-side jet fragments with respect to the reaction plane in Au+Au collisions at $\sqrt{s_{NN}} = 200$ GeV", Phys. Rev. C 84, 024904, 2011-08-09 *

Adare A, *et al.* (the PHENIX Collaboration): "Cold Nuclear Matter Effects on J/psi Yields as a Function of Rapidity and Nuclear Geometry in Deuteron-Gold Collisions at $\sqrt{s_{NN}} = 200$ GeV", Phys. Rev. Lett. 107, 142301, 2011-09-27 *

Adare A, *et al.* (the PHENIX Collaboration): "Production of omega mesons in p+p, d+Au, Cu+Cu and Au+Au collisions at $\sqrt{s_{NN}} = 200$ GeV", Phys. Rev. C 84, 044902, 2011-10-08 *

Adare A, *et al.* (the PHENIX Collaboration): "Heavy Quark Production in p+p and Energy Loss and Flow of Heavy Quarks in Au+Au Collisions at $\sqrt{s_{NN}}$=200 GeV", Phys. Rev. C 84, 044905, 2011-10-10 *

Adare A, *et al.* (the PHENIX Collaboration): "Suppression of back-to-back hadron pairs at forward rapidity in d+Au Collisions at $\sqrt{s_{NN}}$=200 GeV", Phys. Rev. Lett. 107, 172301, 2011-10-18 *

Adare A, *et al.* (the PHENIX Collaboration): "J/psi suppression at forward rapidity in Au+Au collisions at $\sqrt{s_{NN}}$=200 GeV", Phys. Rev. C 84, 054912, 2011-11-21 *

Adare A, *et al.* (the PHENIX Collaboration): "Measurements of Higher-Order Flow Harmonics in Au+Au Collisions at $\sqrt{s_{NN}} = 200$ GeV", Phys. Rev. Lett. 107, 252301, 2011-12-15 *

Adare A, *et al.* (the PHENIX Collaboration): "Identified charged hadron spectra in p+p collisions at $\sqrt{s} = 200$ and 62.4 GeV", Phys. Rev. C 83, 064903, 2011/06/23 *

Adare A, *et al.* (the PHENIX Collaboration): "Ground and excited charmonium state production in p+p collisions at $\sqrt{s}$=200 GeV", Phys. Rev. D 85, 092004, 2012-05-09 *

Adare A, *et al.* (the PHENIX Collaboration): "Deviation from quark-number scaling of the anisotropy parameter v_2 of pions, kaons, and protons in Au+Au collisions at $\sqrt{s_{NN}} = 200$ GeV", Phys. Rev. C 85, 064914, 2012-06-27 *

Adare A, *et al.* (the PHENIX Collaboration): "Nuclear-Modification Factor for Open-Heavy-Flavor Production at Forward Rapidity in Cu+Cu Collisions at $\sqrt{s_{NN}}$=200 GeV", Phys. Rev. C 86, 024909, 2012-08-20 *

Adare A, *et al.* (the PHENIX Collaboration): "Observation of direct-photon collective flow in Au+Au collisions at $\sqrt{s_{NN}}$=200GeV", Phys. Rev. Lett. 109, 122302, 2012-09-19 *

Adare A, *et al.* (the PHENIX Collaboration): "Evolution of pi 0 suppression in Au+Au collisions from $\sqrt{s_{NN}}$ = 39 to 200 GeV", Phys. Rev. Lett. 109, 152301, 2012-10-12 *

Afanasiev S, *et al.* (the PHENIX Collaboration): "Measurement of Direct Photons in Au+Au Collisions at $\sqrt{s_{NN}} = 200$ GeV", Phys. Rev. Lett. 109, 152302, 2012-10-12 *

Adare A, *et al.* (the PHENIX Collaboration): "Direct Photon Production in p+p Collisions at $\sqrt{s}$=200 GeV in Mid-rapidity", Phys. Rev. D 86, 072008, 2012-10-23 *

Adare A, *et al.* (the PHENIX Collaboration): "Cross Sections and Double Helicity Asymmetries of Mid-Rapidity Inclusive Charged Hadrons in p+p at $\sqrt{s} = 62.4$ GeV", Phys. Rev. D 86, 092006, 2012-11-08 *

Adare A, *et al.* (the PHENIX Collaboration): "J/psi suppression at forward rapidity in Au+Au collisions at $\sqrt{s_{NN}}$=39 and 62.4 GeV", Phys. Rev. C 86, 064901, 2012-12-06 *

Adare A, *et al.* (the PHENIX Collaboration): "Cold-nuclear-matter effcts on heavy-quark production in d+Au collisions at $\sqrt{s_{NN}}$=200 GeV", Phys. Rev. Lett. 109, 242301, 2012-12-12 *

Adare A, *et al.* (the PHENIX Collaboration): "Double Spin Asymmetry of Electrons from Heavy Flavor Decays in p+p Collisions at $\sqrt{s}$=200 GeV", Phys. Rev. D 87, 012011, 2013-01-29 *

Adare A, *et al.* (the PHENIX Collaboration): "Transverse-Momentum Dependence of the J/psi Nuclear Modification in d+Au Collisions at $\sqrt{s_{NN}}$=200 GeV", Phys. Rev. C 87, 034904, 2013-03-14 *

Adare A, *et al.* (the PHENIX Collaboration): "Neutral pion production with respect to centrality and reaction plane in Au+Au collisions at $\sqrt{s_{NN}} = 200$ GeV", Phys. Rev. C 87, 034911, 2013-03-28 *

Adare A, *et al.* (the PHENIX Collaboration): "Upsilon (1S+2S+3S) production in d+Au and p+p collisions at $\sqrt{s_{NN}}$=200 GeV and cold-nuclear matter effects", Phys. Rev. C 87, 044909, 2013-04-25 *

Adare A, *et al.* (the PHENIX Collaboration): "Direct photon production in d+Au collisions at $\sqrt{s_{NN}}$=200 GeV", Phys. Rev. C 87, 054907, 2013-05-17 *

Adare A, *et al.* (the PHENIX Collaboration): "Medium modification of jet fragmentation in Au+Aucollisions at $\sqrt{s_{NN}} = 200$ GeV measured in direct photon-hadron correlations", Phys. Rev. Lett. 111, 32301, 2013-07-16 *

Adare A, *et al.* (the PHENIX Collaboration): "Inclusive cross section and single transverse spin asymmetry for very forward neutron production in polarized p+p collision at sqrts = 200 GeV", Phys. Rev. D 88, 032006, 2013-08-08 *

Adare A, *et al.* (the PHENIX Collaboration): "Spectra and ratios of identified particles in Au+Au and d+Au collisions at $\sqrt{s_{NN}}$=200 GeV", Phys. Rev. C 88, 024906, 2013-08-22 *

Adare A, *et al.* (the PHENIX Collaboration): "Nuclear modification of ψ', χ_c' and J/psi production in d+Au collisions at $\sqrt{s_{NN}} = 200$ GeV", Phys. Rev. Lett. 111, 202301, 2013-11-12 *

Adare A, *et al.* (the PHENIX Collaboration): "Quadrupole Anisotropy in Dihadron Azimuthal Correlations in Central d+Au Collisions at $\sqrt{s_{NN}} =$ 200 GeV", Phys. Rev. Lett. 111, 212301, 2013-11-20 *

Adare A, *et al.* (the PHENIX Collaboration): "Azimuthal anisotropy of π^0 and eta mesons in Au+Au collisions at $\sqrt{s_{NN}}$=200 GeV", Phys. Rev. C 88, 064910, 2013-12-20 *

Adare A, *et al.* (the PHENIX Collaboration): "Heavy-flavor electron-muon correlations in p+p and d+Au collisions at $\sqrt{s} = 200$ GeV", Phys. Rev. C 89, C034915, 2014/03/31 *

Sanghwa P, for the PHENIX collaboration: "W Physics Result of PHENIX", Proceedings of Science PoS (DIS 2013) 209, 2013

Goto Y, PHENIX Collaboration: "PHENIX detector upgrades for enhanced physics programs", Proceedings of Science PoS (DIS 2013) 249, 2013

Goto Y, PHENIX Collaboration: "Inclusive Cross Section and Single Transverse-Spin Asymmetry of Very Forward Neutron Production at PHENIX", Physics of Particles and Nuclei Volume 45, Issue 1, pp 79-81, 2014/01

Ikeda S, Romanelli Mark, Cingquegrani David, Sekine Megumi, Kumaki Masafumi, Fuwa Yasuhiro, Munemoto Naoya, Kanesue Takeshi, Jin Qianyu, Okamura Masahiro, Horioka Kazuhiko: "Creation of cocktail beam from alloy target with Laser", Review of Scientific Instruments Vol. 85, p 02B913, 2013/11/12 *

Fuwa Y, S.Ikeda, M.Okamura, *et al.*: "Interaction of plasmas in laser ion source with double laser system", Review of Scientific Instruments 85, 02B916, 2013/12/31 *

Fuwa Y, S.Ikeda, M.Okamura, *et al.*: "Comparison of graphite materials for targets of laser ion source", Review of Scientific Instruments 85, 02B924, 2014/01/24 *

Ikeda S, Romanelli Mark, Cingquegrani David, Sekine Megumi, Kumaki Masafumi, Fuwa Yasuhiro, Kanesue Takeshi, Okamura Masahiro, Horioka Kazuhiko: "Investigation of effect of solenoid magnet on emittances of ion beam from laser ablation plasma", Review of Scientific Instruments 85, 02B919, 2014/01/24 *

Sekine M, S.Ikeda, M.Okamura, *et al.*: "Multiple Species Beam Production on Laser Ion Source for electron beam ion source in Brookhaven National Laboratory", review of scientific instruments 85, 02B920, 2014/02 *

Kumaki M, Y. Fuwa, M. Okamura, *et al.*: "Analyses of the plasma generated by laser irradiation on sputtered target for determination of the thickness used for plasma generation", Review of Scientific Instruments 85, 02B925, 2014/02/24 *

Radioactive Isotope Physics Laboratory

Publications

[Journal]

(Original Papers) *Subject to Peer Review

Steppenbeck D., Takeuchi S., Aoi N., Doornenbal P., Matsushita M., Wang H., Baba H., Fukuda N., Go S., Honma M., Lee J., Matsui K., Michimasa S., Motobayashi T., Nishimura D., Otsuka T., Sakurai H., Shiga Y., Söderström P.-A., Sumikama T., Suzuki H., Taniuchi R., Utsuno Y., Valiente-Dobon J. J., Yoneda K.: "Evidence for a new nuclear 'magic number' from the level structure of ^{54}Ca", Nature. **502**, 207-210 (2013).

Doornenbal P., Scheit H., Takeuchi S., Aoi N., Li K., Matsushita M., Steppenbeck D., Wang H., Baba H., Crawford H., Hoffman C. R., Hughes R., Ideguchi E., Kobayashi N., Kondo Y., Lee J., Michimasa S., Motobayashi T., Sakurai H., Takechi M., Togano Y., Winkler R., Yoneda K.: "In-Beam γ-Ray Spectroscopy of ^{34,36,38}Mg: Merging the N=20 and N=28 Shell Quenching", Phys. Rev. Lett. **111**, 212502 (2013).

Watanabe H., Lorusso G., Nishimura S., Xu Z. Y., Sumikama T., Söderström P.-A., Doornenbal P., Browne F., Gey G., Jung H. S., Taprogge J., Vajta Zs., Wu J., Yagi A., Baba H., Benzoni G., Chae K. Y., Crespi F. C. L., Fukuda N., Gernhaeuser R., Inabe N., Isobe T., Jungclaus A., Kameda D., Kim G. D., Kim Y. K., Kojouharov I., Kondev F. G., Kubo T., Kurz N., Kwon Y. K., Lane G. J., Li Z., Moon C. -B., Montaner-Piza A., Moschner K., Naqvi F., Niikura M., Nishibata H., Nishimura D., Odahara A., Orlandi R., Patel Z., Podolyak Zs., Sakurai H., Schaffner H., Simpson G. S., Steiger K., Suzuki H., Takeda H., Wendt A., Yoshinaga K.: "Isomers in ^{128}Pd and ^{126}Pd: Evidence for a Robust Shell Closure at the Neutron Magic Number 82 in Exotic Palladium Isotopes", Phys. Rev. Lett. **111**, 152501 (2013).

Söderström P.-A., Nishimura S., Doornenbal P., Lorusso G., Sumikama T., Watanabe H., Xu Z. Y., Baba H., Browne F., Go S., Gey G., Isobe T., Jung H.: "Installation and commissioning of EURICA – Euroball-RIKEN Cluster Array", Nucl. Instrum. and Meth. Res. Set. B **317**, 649 – 652 (2013).

Steiger K., Nishimura S., Li Z., Chen R., Faestermann T., Gernhäuser R., Hinke C., Krücken R., Kurata-Nishimura M., Lorusso G., Miyashita Y., Sugimoto K., Sumikama T., Watanabe H., Yoshinaga K.: "Half-lives of neutron-rich nuclei around ^{35,36}Mg", Proceedings of Science Bormio **32** (2013).

Kobayashi T., Chiga N., Isobe T., Kondo Y., Kubo T., Kusaka K., Motobayashi T., Nakamura T., Ohnishi J., Okuno H., Otsu H., Sako T., Sato H., Shimizu Y., Sekiguchi K., Takahashi K., Tanaka R., Yoneda K.:"SAMURAI spectrometer for RI beam experiments", Nucl. Instr. Meth. B **317** (2013) 294-304.

Suzuki H., Aoi N., Takeshita E., Takeuchi S., Ota S., Baba H., Bishop S., Fukui T., Hashimoto Y., Ideguchi E., Ieki K., Imai N., Ishihara M., Iwasaki H., Kanno S., Kondo Y., Kubo T., Kurita K., Kusaka K., Minemura T., Motobayashi T., Nakabayashi T., Nakamura T., Nakao T., Niikura M., Okumura T., Ohnishi T. K., Ong H. J., Sakurai H., Shimoura S., Sugo R., Suzuki D., Suzuki M. K., Tamaki M., Tanaka K., Togano Y., Yamada K.: "Collectivity of neutron-rich Ti isotopes", Phys. Rev. C**88**, 024326 (2013).

Söderström P.-A., Lorusso G., Watanabe H., Nishimura S., Doornenbal P., Thiamova G., Browne F., Gey G., Jung H. S., Sumikama T., Taprogge J., Vajta Zs., Wu J., Xu Z. Y., Baba H., Benzoni G., Chae K. Y., Crespi F. C. L., Fukuda N., Gernhaeuser R., Inabe N., Isobe T., Jungclaus A., Kameda D., Kim G. D., Kim Y. -K., Kojouharov I., Kondev F. G., Kubo T., Kurz N., Kwon Y. K., Lane G. J., Li Z., Montaner-Piza A., Moschner K., Naqvi F., Niikura M., Nishibata H., Odahara A., Orlandi R., Patel Z., Podolyak Zs., Sakurai H., Schaffner H., Simpson G. S., Steiger K., Suzuki H., Takeda H., Wendt A., Yagi A., Yoshinaga K.: "Shape evolution in ^{116,118}Ru: Triaxiality and transition between the O(6) and U(5) dynamical symmetries", Phys. Rev. C **88**, 024301 (2013).

Leguillon R., Nishibata H., Ito Y., Petrache C. M., Odahara A., Shimoda T., Hamatani N., Tajiri K., Takatsu J., Yokoyama R., Ideguchi E., Watanabe H., Wakabayashi Y., Yoshinaga K., Suzuki T., Nishimura S., Beaumel D., Lehaut G., Guinet D., Desesquelles P., Curien D., Astier A., Konstantinopoulos T., and Zerrouki T., "Spectroscopy of ^{135}La", Phys. Rev. C **88**, 044309 (2013).

Ueno H., Miyatake H., Yamamoto Y., Tanimoto S., Shimoda T., Aoi N., Asahi K., Ideguchi E., Ishihara M., Izumi H., Kishida T., Kubo T., Mitsuoka S., Mizoi Y., Notani M., Ogawa H., Ozawa A., Sasaki M., Shirakura T., Takahashi N., Yoneda K.: "β-delayed neutron and γ-ray spectroscopy of ^{17}C utilizing spin-polarized ^{18}B", Phys. Rev. C **87**, 034316 (2013).

Sato H., Kubo T., Yano Y., Kusaka K., Ohnishi J., Yoneda K., Shimizu Y., Motobayashi T., Otsu H., Isobe T., Kobayashi T., Sekiguchi K., Nakamura T.: "Superconducting Dipole Magnet for SAMURAI Spectrometer", IEEE Trans. Appl. Supercond, **23** (2013) 4500308.

Furukawa T., Wakui T., Yang X., Fujita T., Imamura K., Yamaguchi Y., Tetsuka H., Tsutsui Y., Mitsuya Y., Ichikawa Y., Ishibashi Y., Yoshida N., Shirai H., Ebara Y., Hayasaka M., Arai S., Muramoto S., Hatakeyama A., Wada M., Sonoda T., Ito Y., Kobayashi T., Nishimura S., Nishimura M., Kondo Y., Yoneda K., Kubono S., Ohshiro Y., Ueno H., Shinozuka T., Shimoda T., Asahi K., Matsuo Y.: "Novel nuclear laser spectroscopy method using superfluid helium for measurement of spins and moments of exotic nuclei", Nucl. Instrum. Methods Phys. Res., Sect. B 590-594 (2013).

Wang H., Aoi N., Takeuchi S., Matsushita M., Doornenbal P., Motobayashi T., Steppenbeck D., Yoneda K., Baba H., Caceres L., Dombradi Zs., Kobayashi K., Kondo Y., Lee J., Li K., Liu H., Minakata R., Nishimura D., Otsu H., Sakaguchi S., Sakurai H., Scheit H., Sohler D., Sun Y., Tian Z., Tanaka R., Togano Y., Vajta Zs., Yang Z., Yamamoto T., Ye Y., Yokoyama R.: "Collectivity evolution in the neutron-rich Pd isotopes toward the N=82 shell closure", Phys. Rev. C **88**, 054318 (2013).

Audirac L., Obertelli A., Doornenbal P., Mancusi D., Takeuchi S., Aoi N., Baba H., Boissinot S., Boudard A., Corsi A., Gillibert A., Isobe T., Jungclaus A., Lapoux V., Lee J., Leray S., Matsui K., Matsushita M., Motobayashi T., Nishimura D., Ota S., Pollacco E. C., Potel G., Sakurai H., Santamaria C., Shiga Y., Sohler D., Steppenbeck D., Taniuchi R., Wang H.: "Evaporation-cost dependence in heavy-ion fragmentation", Phys. Rev. C**88**, 041602 (2013).

Jin S. J., Wang Y. B., Su J., Yan S. Q., Li Y. J., Guo B., Li Z. H., Zeng S., Lian G., Bai X. X., Liu W. P., Yamaguchi H., Kubono S., Hu J., Kahl D., Jung, H.: "Resonant scattering of ^{22}Na $+p$ studied by the thick-target inverse-kinematic method", Phys. Rev. C **88**, 035801 (2013).

Lu F., Lee J., Tsang M. B., Bazin D., Coupland D., Henzl V., Henzlova D., Kilburn M., Lynch W. G., Rogers A. M., Sanetullaev A., Sun Z. Y., Youngs M., Charity R. J., Sobotka L. G., Famiano M., Hudan S., Horoi M., Ye Y. L.: "Neutron-hole states in ^{45}Ar from ^{1}H(^{46}Ar, d) ^{45}Ar reactions", Phys. Rev. C **88**, 017604 (2013).

Muto H., Ohshiro Y., Yamaka S., Watanabe S., Oyaizu M., Kubono S., Yamaguchi H., Kase M., Hattori T., Shimoura S.: "Grating monochromator for electron cyclotron resonance ion source operation", Rev. Sci. Instrum. **84**, 073304 (2013).

Wang He, Aoi N., Takeuchi S., Matsushita M., Doornenbal P., Motobayashi T., Steppenbeck D., Yoneda K., Kobayashi K., Lee J., Liu H., Kondo Y., Yokoyama R., Sakurai H., Ye Y.,: "Observation of New Isotope ^{131}Ag via the Two-Step Fragmentation Technique", Chin. Phys. Lett.**30-4**, 042501 (2013)

Matsuda Y., Sakaguchi H., Takeda H., Terashima S., Zenihiro J., Kobayashi T., Murakami T., Iwao Y., Ichihara T., Suda T., Ohnishi T., Watanabe Y., Otsu H., Yoneda K., Satou Y., Ozeki K., Kanazawa M.: "Elastic scattering of protons from ^{9}C with a 290 MeV/nucleon ^{9}C beam", Phys. Rev. C **87**, 034614 (2013).

Adare A., Afanasiev S., Aidala C., Ajitanand N. N., Akiba Y., Akimoto R., Al-Ta'ani H., Alexander J., Andrews K. R., Angerami A., Aoki K., Apadula N., Appelt E., Aramaki Y., Armendariz R., Aschenauer E. C., Awes T. C., Azmoun B., Babintsev V., Bai M., Bannier B., Barish K. N., Bassalleck B., Basye A. T., Bathe S., Baublis V., Baumann C., Bazilevsky A., Belmont R., Ben-Benjamin J., Bennett R., Berdnikov A., Berdnikov Y., Blau D. S., Bok J. S., Boyle K., Brooks M. L., Broxmeyer D., Buesching H., Bumazhnov V., Bunce G., Butsyk S., Campbell S., Castera P., Chen C-H, Chi C. Y., Chiu M., Choi I. J., Choi J. B., Choudhury R. K., Christiansen P., Chujo T., Chvala O., Cianciolo V., Citron Z., Cole B. A., del Valle Z. Conesa, Connors M., Csanad M., Csoergo T., Dairaku S., Datta A., David G., Dayananda M. K., Denisov A., Deshpande A., Desmond E. J., Dharmawardane K. V., Dietzsch O., Dion A., Donadelli M., Drapier O., Drees A., Drees K. A., Durham J. M., Durum A., D'Orazio L., Efremenko Y. V., Engelmore,T., Enokizono A., En'yo H., Esumi S., Fadem B., Fields D. E., Finger M., Finger M. Jr., Fleuret F., Fokin S. L., Frantz J. E., Franz A., Frawley A. D., Fukao Y., Fusayasu T., Garishvili I., Glenn A., Gong X., Gonin M., Goto Y., de Cassagnac R. Granier, GrauN., Greene S. V., Perdekamp M. G., Gunji T., Guo L., Gustafsson H-A, Haggerty J. S., Hahn K. I., Hamagaki H., Hamblen J., Han R., Hanks J., Harper C., Hashimoto K., Haslum E., Hayano R., He X., Hemmick T. K., Hester T., Hill J. C., Hollis R. S., Holzmann W., Homma K., Hong B., Horaguchi T., Hori Y., Hornback D., Huang S., Ichihara T., Ichimiya R., Iinuma H., Ikeda Y., Imai K., Inaba M., Iordanova A., Isenhower D., Ishihara M., Issah M., Isupov A., Ivanischev D., Iwanaga Y., Jacak B. V., Jia J., Jiang X., John D., Johnson B. M., Jones T., Joo K. S., Jouan D., Kamin J., Kaneti S., Kang B. H., Kang J. H., Kang J. S., Kapustinsky J., Karatsu K., Kasai M., Kawall D., Kazantsev A. V., Kempel T., Khanzadeev A., Kijima K. M., Kim B. I., Kim D. J., Kim E-J, Kim Y-J, Kim Y. K., Kinney E., Kiss A., Kistenev E., Kleinjan D., Kline P., Kochenda L., Komkov B., Konno M., Koster J., Kotov D., Kral A., Kunde G. J., Kurita K., Kurosawa M., Kwon Y., Kyle G. S., Lacey R., Lai Y. S., Lajoie J. G., Lebedev A., Lee D. M., Lee J., Lee K. B., Lee K. S., Lee S. H., Lee S. R., Leitch M. J., Leite M. A. L., Li X., Lim S. H., Levy L. A. Linden, Litvinenko A., Liu H., Liu M. X., Love B., Lynch D., Maguire C. F., Makdisi Y. I., Malakhov A., Manion A., Manko V. I., Mannel E., Mao Y., Masui H., McCumber M., McGaughey P. L., McGlinchey D., McKinney C., Means N., Mendoza M., Meredith B., Miake Y., Mibe T., Mignerey A. C., Miki K., Milov A., Mitchell J. T., Miyachi Y., Mohanty A. K., Moon H. J., Morino Y., Morreale A., Morrison D. P., Motschwiller S., Moukhanova T. V., Murakami T., Murata J., Nagamiya S., Nagle J. L., Naglis M., Nagy M. I., Nakagawa I., Nakamiya Y., Nakamura K. R., Nakamura T., Nakano K., Newby J., Nguyen M., Nihashi M., Nouicer R., Nyanin A. S., Oakley C., O'Brien E., Ogilvie C. A., Oka M., Okada K., Oskarsson A., Ouchida M., Ozawa K., Pak R., Pantuev V., Papavassiliou V., Park B. H., Park I. H., Park S. K., Pate S. F., Pei H., Peng J-C, Pereira H., Peresedov V., Peressounko D. Yu, Petti R., Pinkenburg C., Pisani R. P., Proissl M., Purschke M. L., Qu H., Rak J., Ravinovich I., Read K. F., Reygers K., Riabov V., Riabov Y., Richardson E., Roach D., Roche G., Rolnick S. D., Rosati M., Rosendahl S. S. E., Rukoyatkin P., Sahlmueller B., Saito N., Sakaguchi T., Samsonov V., Sano S., Sarsour M., Sato T., Savastio M., Sawada S., Sedgwick K., Seidl R., Seto R., Sharma D., Shein I., Shibata T-A, Shigaki K., Shim H. H., Shimomura M., Shoji K., Shukla P., Sickles A., Silva C. L., Silvermyr D., Silvestre C., Sim K. S., Singh B. K., Singh C. P., Singh V., Slunecka M., Sodre T., Soltz R. A., Sondheim W. E., Sorensen S. P., Sourikova I. V., Stankus P. W., Stenlund E., Stoll S. P., Sugitate T., Sukhanov A., Sun J., Sziklai J., Takagui E. M., Takahara, A., Taketani A., Tanabe R., Tanaka Y., Taneja S., Tanida K., Tannenbaum M. J., Tarafdar S., Taranenko A., Tennant E., Themann H., Thomas D., Togawa M., Tomasek L., Tomasek M., Torii H., Towell R. S., Tserruya I., Tsuchimoto Y., Utsunomiya K., Vale C., van Hecke H. W., Vazquez-Zambrano E., Veicht A., Velkovska J., Vertesi R., Virius M., Vossen A., Vrba V., Vznuzdaev E., Wang X. R., Watanabe D., Watanabe K., Watanabe Y., Watanabe Y. S., Wei F., Wei R., Wessels J., White S. N., Winter D., Woody C. L., Wright R. M., Wysocki M., Yamaguchi Y. L., Yang R., Yanovich A., Ying J., Yokkaichi S., Yoo J. S., You Z., Young G. R., Younus I., Yushmanov I. E., Zajc W. A., Zelenski A., Zhou S., Zolin L.: "Double-spin asymmetry of electrons from heavy-flavor decays in p plus p collisions at root s=200 GeV", Phys. Rev. D **87**, 012011 (2013).

Michimasa S., Takaki M., Sasamoto Y., Dozono M., Nishi T., Kawabata T., Ota S., Baba H., Baba T., Fujii T., Go S., Kawase S., Kikuchi Y., Kisamori K., Kobayashi M., Kubota Y., Lee C. S., Matsubara H., Miki K., Miya H., Noji S., Tokieda H., Tsumura M., Yako K., Yokoyama R., Takeda H., Yanagisawa Y., Kubo T., Inabe N., Fukuda N., Kameda D., Suzuki H., Shimizu Y., Sato H., Ichihara T., Stolz A., Zegers R. G. T., Sakai H., Uesaka T., Shimoura S.: "SHARAQ spectrometer for high-resolution studies for RI-induced reactions", Nucl. Instrum. Methods Phys. Res., Sect. B **317** 305-310 (2013).

Yang X. F., Furukawa T., Wakui T., Imamura K., Tetsuka H., Fujita T., Yamaguchi Y., Tsutsui Y., Mitsuya Y., Ichikawa Y., Ishibashi Y., Yoshida N., Shirai H., Ebara Y., Hayasaka M., Arai S., Muramoto S., Hatakeyama A., Wada M., Sonoda T., Ito Y., Kobayashi T., Nishimura S., Nishimura M., Kondo Y., Yoneda K., Ueno H., Shinozuka T., Shimoda T., Asahi K., Matsuo Y.: "Control of stopping position of radioactive ion beam in superfluid helium for laser spectroscopy experiments", Nucl. Instrum. Methods Phys. Res., Sect. B **317** 599-602 (2013).

Yamaguchi H., Kahl D., Nakao T., Wakabayashi Y., Kubono S., Hashimoto T., Hayakawa S., Kawabata T., Iwasa N., Teranishi T., Kwon Y. K., Binh D. N., Khiem L. H., Duy N. N.: "Recent developments and research projects at the low-energy RI beam facility CRIB", Nucl. Instrum. Methods Phys. Res., Sect. B **317** 664-667(2013).

Shimizu Y., Otsu H., Kobayashi T., Kubo T., Motobayashi T., Sato H., Yoneda K.: "Vacuum system for the SAMURAI spectrometer", Nucl. Instr. Meth. B 317 (2013) 739-742.

Nakai Y., Nakano Y., Ikeda T., Kanai Y., Kambara T., Fukunishi N., Kondo C., Azuma T., Komaki K., Yamazaki Y.: "Stark effect in resonant coherent excitation of 2s electron of Li-like Fe^{23+} ions channeling in a Si crystal", Nuclear. Instr. and Meth. B **315**, 94 (2013).

Shane R., McIntosh A. B., Barney J., Chajecki Z., Estee J., Famiano M., Isobe T., Jhang G., Lu F., Lynch W. G., Murakami T., Nakatsuka N., Powell W., Sakurai H., Taketani A., Tangwancharoen S., Tsang M.B., Yennello S. J., : "Constraining the nuclear symmetry energy at high density", Abs.Pap.Acs. **246** (2013).

Nakano Y., Hatakeyama A., Nakai Y., Komaki K., Takada E., Murakami T., Azuma T., "Effects of fine structure depolarization studied by resonant coherent excitation of H-like Ar^{17+}", Phys. Scr. **T156** 014061 (2013).

Chen R. J., Otsu H., Lapoux V., Boissinot S., Baba H., Matta A., Kurata-Nishimura M., Pollacco E., Blumenfeld Y., Flavigny F., Franchoo S., Fukuda N., Gangnant P., Hammache F., Houarner C., Inabe N., Kameda D., Libin J. F., Louchart C., Matsushita M., Motobayashi T., Nalpas L., Nikolskii E. Y., Obertelli A., Onishi T., Rindel E., Rosier P., Sakurai H., Saillant F., Takechi M., Takeuchi S., Togano Y., Yoneda K., Yoshida A., Yoshida K.: "Proton Elastic Scattering of $^{23,25}F$", Few-Body Syst.**54** 1405-1407 (2013).

Kobayashi N., Nakamura T., Kondo Y., Aoi N., Baba H., Deguchi S., Fukuda N., Lee G. S., Lee H. S., Inabe N., Ishihara M., Kawada Y., Kanungo R., Kubo T., Famiano M. A., Matsushita M., Motobayashi T., Ohnishi T., Orr N. A., Otsu H., Barthelemy R., Sakurai H., Kim S., Sako T., Sumikama T., Satou Y., Takahashi K., Takeda H., Takechi M., Takeuchi S., Tanaka K. N., Tanaka N., Tanaka R., Togano Y., Yoneda K.: "Breakup Reactions of Drip-Line Nuclei Near N=20, 28", Few-Body Syst.**54** 1441-1444 (2013).

Ito M., Otsu H.: "Studies of Light Neutron-Excess Systems from Bounds to Continuum", Few-Body Syst.**54** 1461-1464 (2013).

Tshoo K., Satou Y., Bhang H., Choi S., Nakamura T., Deguchi S., Kawada Y., Kondo Y., Kobayashi N., Nakayama Y., Tanaka K. N., Tanaka N., Aoi N., Ishihara M., Motobayashi T., Otsu Sakurai H.: H., Takeuchi S., Togano Y., Yoneda K., Li Z. H., Delaunay F., Gibelin J., Marques F. M., Orr N. A., Honda T., Matsushita M., Kobayashi T., Miyashita Y., Sumikama T., Yoshinaga K., Shimoura S., Sohler D., Zheng T., Cao Z. X.: "The N=16 Spherical Shell Closure in ^{24}O", Few-Body Syst.**54** 459-463 (2013).

Satou Y., Tshoo K., Bhang H., Choi S., Hwang J. W., Nakamura T., Kondo Y., Nakayama Y., Kobayashi N., Tanaka K. N., Deguchi S., Kawada Y., Tanaka N., Motobayashi T., Sakurai H., Otsu H., Aoi N., Takeuchi

S., Yoneda K., Togano Y., Ishihara M., Shimoura S., Kobayashi T., Matsushita M., Honda T., Sumikama T., Miyashita Y., Yoshinaga K., Orr N. A., Marques F. M., Gibelin J., Delaunay F., Sohler D., Zheng T., Li Z. H., Cao Z. X.: "Invariant Mass Spectroscopy of ^{23}O via the (p, p') Reaction in Inverse Kinematics", Few-Body Syst. **54** 287-290 (2013).

Yamaguchi H., Kahl D., Wakabayashi Y. , Kubono S., Hashimoto T., Hayakawa S., Kawabata T., Iwasa N., Teranishi T., Kwon Y. K., Binh D.N.,, Khiem L.H., Duy N.N.: "α-resonance structure in ^{11}C studied via resonant scattering of ^{7}Be+α and with the ^{7}Be(α,p) reaction", Phys. Rev. C **87** 034303-12 (2013).

Duy N.N., Kubono S., Yamaguchi H., Kahl D., Wakabayashi Y., Teranishi T., Iwasa N.,Kwon Y.K., Khiem L.H., Kim Y.H., Song J.S., Hu J., Ayyad Y.: "Low-energy radioactive ion beam production of ^{22}Mg", Nucl. Instr. Meth. **A723** 99 (2013)

Guo B., Su J., Li Z. H., Wang Y. B., Yan S. Q., Li Y. J., Shu N.C., Han Y.L., Bai X.X., Chen Y.S., Liu W. P., Yamaguchi H., Binh D.N., Hashimoto T., Hayakawa S., Kahl D., Kubono S., He J.J., Hu J., Xu S. W., Iwasa N., Kume N., Li Z.H.: "Determination of the astrophysical ^{12}N(p,γ)^{13}O reaction rate from the ^{2}H(^{12}N,^{13}O)n reaction and its astrophysical implications", Phys. Rev. C**87** 015803-7 (2013)

Muto H., Ohshiro Y., Yamaka S., Watanabe S., Oyaizu M., Kubono S., Yamaguchi H., Kase M., Hattori T., Shimoura S.: "Grating monochromator for electron cyclotron resonance ion source operation", Rev. Sci. Instrum. **84** (2013) 073304

He J. J., Zhang L. Y., Parikh A., Xu S. W., Yamaguchi H., Kahl D., Kubono S., Hu J., Ma P. , Chen S. Z. , Wakabayashi Y. , Sun B. H. , Wang H. W., Tian W. D., Chen R. F., Guo B., Hashimoto T., Togano Y., Hayakawa S., Taranishi T., Iwasa N., Yamada T., Komatsubara T.: "The ^{18}Ne(α,p)^{21}Na breakout reaction in x-ray bursts: Experimental determination of spin-parities for α resonances in ^{22}Mg via resonant elastic scattering of ^{21}Na+p", Phys. Rev. C 88, 012801(R) (2013)

Jin S. J., Wang Y. B., Su J., Yan S. Q., Li Y. J., Guo B., Li Z. H., Zeng S., Lian G., Bai X. X., Liu W. P. , Yamaguchi H., Kubono S., Hu J., Kahl D., Jung H. S., Moon J. Y., Lee C. S., Teranishi T., Wang H. W., Ishiyama H., Iwasa N., Komatsubara T., Brown B. A.: "Resonant scattering of ^{22}Na +p studied by the thick-target inverse-kinematic method", Phys. Rev. C 88, 035801 (2013)

Furukawa T., Wakui T. , Yang X., Fujita T., Imamura K., Yamaguchi Y., Tetsuka H., Tsutsui Y., Mitsuya Y., Ichikawa Y., Ishibashi Y., Yoshida N., Shirai H., Ebara Y. , Hayasaka M., Arai S., Muramoto S., Hatakeyama A., Wada M., Sonoda T. , Ito Y., Kobayashi T., Nishimura S., Nishimura M., Kondo Y., Yoneda K., Kubono S., Ohshiro Y., Ueno H., Shinozuka T. , Shimoda T. , Asahi K., Matsuo Y.: "Novel Nuclear Laser Spectroscopy Method using Superfluid Helium for Measurement of Spin and Moments of Exotic Nuclei", Nucl. Instr. Meth. B 317 (2013) 590 – 594.

Zhang L. Y., He J. J., Parikh A., Xu S. W., Yamaguchi H., Kahl D., Kubono S., Mohr P., Hu J., Ma P., Chen S. Z., Wakabayashi Y., Wang H. W., Tian W. D., Chen R. F., Guo B., Hashimoto T., Togano Y., Hayakawa S., Teranishi T., Iwasa N., Yamada T., Komatsubara T., Zhang Y. H., Zhou X. H.: "Investigation of the thermonuclear ^{18}Ne(α, p)^{21}Na reaction rate via resonant elastic scattering of ^{21}Na + p ", Phys. Rev. C 89 (2014) 015804 (13).

Xu Z. Y., Nishimura S., Lorusso G., Browne F., Doornenbal P., Gey G., Jung H.-S., Li Z., Niikura M., Söderström P.-A., Sumikama T., Taprogge J., Vajta Zs., Watanabe H., Wu J., Yagi A., Yoshinaga K., Baba H., Franchoo S., Isobe T., John P. R., Kojouharov I., Kubono S., Kurz N., Matea I., Matsui K., Mengoni D., Morfouace P., Napoli D. R., Naqvi F., Nishibata H., Odahara A., Şahin E., Sakurai H., Schaffner H., Stefan I. G., Suzuki D., Taniuchi R., Werner V.: "β-Decay Half-Lives of ^{76,77}Co, ^{79,80}Ni, and ^{81}Cu: Experimental Indication of a Doubly Magic ^{78}Ni", Phys. Rev. Lett. **113** (2014) 032505-5

Muto H., Ohshiro Y., Yamaka S., Watanabe S., Oyaizu M., Kubono S., Yamaguchi H., Kase M., Hattori T., Shimoura S.: "Plasma spectroscopy of metal ions for hyper-electron cyclotron resonance ion source", Rev. Sci. Instrum. **85** (2014) 02A905

Komatsubara T., Kubono S., Hayakawa T., Shizuma T., Ozawa A., Ito Y., Ishibashi Y., Moriguchi T., Yamaguchi H., Kahl D., Hayakawa S., Binh D. N., Chen A. A., Chen J., Setoodehnia K., and Kajino T.: "Excited states above the proton threshold in ^{26}Si", Eur. Phys. J. A **50** (2014) 136

Hu J., He J. J., Parikh A., Xu S. W., Yamaguchi H., Kahl D., Ma P., Su J., Wang H. W., Nakao T., Wakabayashi Y., Teranishi T., Hahn K. I., Moon J. Y., Jung H. S., Hashimoto T., Chen A. A., Irvine D., Lee C. S., Kubono S.: "Examination of the role of the ^{14}O(α, p)^{17}F reaction rate in type-I x-ray bursts", Pys. Rev. C **90** (2014) 025803 – 7

Mcneice E., Setoodehnia K., Singh B., Abe Y., Binh D.N., Chen A.A., Chen J., Cherubini S., Fukuoka S., Hashimoto T., Hayakawa T., Ishibashi Y., Ito Y., Kahl D., Komatsubara T., Kubono S., Moriguchi T., Nagae D., Nishikiori R., Niwa T., Ozawa A., Shizuma T., Suzuki H., Yamaguchi H., Yuasa T.: "In-beam γ-ray Spectroscopy of ^{30}P via the ^{28}Si(^{3}He,pγ)^{30}P Reaction", Nucl. Data Sheets, **120** (2014) 88 -90.

Jung H. S., Lee C. S., Kwon Y. K., Moon J. Y., Lee J. H., Yun C. C., Kim M. J., Hashimoto T., Yamaguchi H., Kahl D., Kubono S., Wakabayashi Y., Togano Y., Choi Seonho, Kim Y. H., Kim Y. K., Park J. S., Kim E. J., Moon C.-B., Teranishi T., Iwasa N., Yamada T., Kato S., Cherubini S., Hayakawa S., Rapisarda G. G.: "Elastic scattering of ^{25}Al + p to explore the resonance structure in ^{26}Si ", Phys. Rev. C **90** (2014) 035805 – 8

Yang Xiaofei, Furukawa T., Wakui T., Fujita T., Imamura

K., Mitsuya Y., Hayasaka M., Ichikawa Y., Ishibashi Y., Shirai H., Suzuki T., Ebara Y., Hatakeyama A., Wada M., Sonoda T., Ito Y., Kobayashi T., Nishimura S., Kurata-Nishimura M., Kondo Y., Yoneda K.-I., Kubono S., Ohshiro Y., Ueno H., Shinozuka T., Shimoda T., Asahi K., Matsuo Y.: "Laser-RF Double Resonance Spectroscopy of $^{84-87}$Rb Isotopes Trapped in Superfluid Helium ", Phys. Rev. A (2014) 052516-

Kurata-Nishimura M., Yokoyama R., Kisamori K., Otsu H., and Kondo Y.: "Technical knowledge about cooling of CRYPTA for liquid helium", RIKEN Accel. Prog. Rep. **46** 165 (2013).

[Book · Proceedings]

(Original Papers) *Subject to Peer Review

Nakano Y., Hatakeyama A., Nakai Y., Komaki K., Takada E., Murakami T., Azuma T.: "X-ray and Auger electron study of highly charged ions using resonant coherent excitation", NIFS Proceedings, **91**, 87 (2013)

Russotto P., Isobe T. et al., "The ASY-EOS experiment at GSI: investigating the symmetry energy at supra-saturation densities", J. Phys. Conf. Ser. **420**, 012092 (2013)

Lorusso G., et al.: "β-decay spectroscopy at RIBF: The EURICA project",
Proceedings of the Origin of Matter and Evolution of Galaxies International Symposium (OMEG12)

Lorusso G., et al.: "β-decay spectroscopy of neutron rich nuclei at RIBF", Proceedings of the International African Symposium on Exotic Nuclei (IASEN-2013)

Watanabe H., et al.: "Recent results of decay spectroscopy at RIBF", Proceedings EPJ Web Conf. **63**, 01001 (2013)

櫻井 博儀：
"元素はどうしてできたのか−誕生・合成から「魔法数」まで−"
PHP Science World074 株式会社 PHP 研究所
（2013 年 12 月 2 日第一版第一刷発行）

Oral Presentations

(International Conference etc.)

Nishimura S.: "Decay spectroscopy of very neutron-rich nuclei at RIBF", 10th ASRC International Workshop "Nuclear Fission and Decay of Exotic Nuclei", JAEA, Japan March 21-22 (2013).

Nishimura S.: "Decay spectroscopy of very neutron-rich nuclei at RIBF", 25th International Nuclear Physics Conference (INPC2013), Firenze, Italy, June 2-7 (2013).

Nishimura S.: "Decay spectroscopy of exotic nuclei at RIBF", Symposium Nuclear Structure Physics with Advanced Gamma-Detector Arrays (NSP13), Padva, Italy, June 10-12 (2013).

Nishimura S.: "Neutron-rich nuclei lifetimes for *r*-process", Seventh European Summer School on Experimental Astrophysics, Santa Tela, Italy, Sep. 15-27 (2013).

Nishimura S.: "Decay Spectroscopy", The 1st RIBF-RISP Workshop, Seoul, Republic of Korea, Nov. 06-07 (2013).

Akiyoshi H., Yamashita Y., Kadowaki M., Sekiguchi K., Nakai Y., Imamura Y., Motizuki Y.:
"A CCM experiment on the effects of solar proton events on HNO3 and O3 in the polar middle and lower atmosphere" Japan Geoscience Union Meeting 2013, Chiba, May 19-24 (2013).

Motizuki Y., Sekiguchi K., Nakai Y., Akiyoshi H., Imamura T.: "Influence of a giant solar energetic particle event on atmospheric chemistry", Japan Geoscience Union Meeting 2013, Chiba, May 19-24 (2013).

Fujita S., Hori A., Motizuki Y., Takahashi K., Nakai Y., Kawamura K., Motoyama H.: "Densification of layered firm of the ice sheet in the vicinity of Dome Fuji, Antarctica", The Fourth Symposium on Polar Science, Tokyo, Japan, Nov 12-15 (2013).

Sakurai H.: "Recent results at RIBF" Invited talk at XLI International Workshop on Gross Properties of Nuclei and Nuclear Excitations, Hirschegg (Austria), Jan. 26 - Feb. 1, 2013.

Sakurai H.: "Emergence of Exotic Nuclei" Invited talk at GSI Kolloquium, Darmstadt (Germany), Feb. 5, 2013.

Sakurai H.: "Nuclear data produced at the RIBF", Invited talk at New Energy Forum 2013, Xi'an, China, Sept., 2013.

Sakurai H.: "Overview of RIBF" Invited talk at 1st RIBF-RISP Joint Workshop, Daejeon, Korea, Nov., 2013.

Sakurai H.: "The RIKEN RI Beam Factory –Its Scientific Programs–", Invited talk at 17th International Conference on Accelerators and Beam Utilization (ICABU 2013), Daejeon, Korea, Nov. (2013).

Sakurai H.: "Present Status of RIBF", Invited talk at JUSTIPEN-JUSEIPEN Joint Workshop, Wako, Japan, Dec., 2013.

Kubono S.:"Low-Energy RI Beams and Nuclear Clusters in Explosive Burning - RI beam methods and pp-chain breakout -", Invited talk at VI European Summer School on Experimental Nuclear Astrophysics, September 15-27, 2013, Santa Tecla, Italy, (To be published).

Kubono S. : "Low-Energy Reactions in Astrophysics" Invited talk at An inauguration symposium for Center for Nuclear Astrophysics (CNA), Shanghai Jiao Tong University in Shanghai, China. May 29-31, 2013.

Kubono S. : "Experimental Approach to Astrophysical Nuclear Reactions", Invited talk at International workshop on Nuclear Sciences with High-intensity Lasers, Osaka University. February 3, 2014.

Isobe T.: "ANAROOT: new online/offline framework for RIBF data analysis based on ROOT", RIBF Users meeting, RIKEN, Wako, June (2013)

Isobe T.: "H(R)IC experiment at RIBF", RIBF-ULIC-mini Workshop: Nuclear symmetry-energy and nucleus-nucleus collision simulation, RIKEN, Wako, July (2013)

Isobe T.: "Nuclear Physics at RIBF", 3rd RIKEN-Liverpool Symposium, Univ. of Liverpool, Liverpool UK, July

(2013)

Isobe T.: “SAMURAI: large acceptance spectrometer for experimental RI physics at RIKEN-RIBF”, Nuclear Physics seminar, Univ. of Liverpool, Liverpool UK, July (2013)

Isobe T.: “Status of SPiRIT for heavy ion collision experiment”, SAMURAI international workshop, Tokyo institute of Technology, Tokyo, September (2013)

Isobe T.: “SAMURAI-TPC with GET system for next generation HIC experiments”, French – Japanese LIA Symposium, Paris, September (2013)

Doornenbal P.: “In-Beam Gamma-Ray Spectroscopy at the RIBF” Invited talk at the 1st RISP-RIBF Workshop, Daejon, Korea, November 7-8, 2013

Otsu H.: “SAMURAI Spectometer”, The 1st RISP-RIBF Workshop, Daejon, Korea, November 7-8, 2013.

Doornenbal P.: “Status of the EURICA Project”, Invited talk at the 3rd EGAN Workshop, Liverpool, UK, June 24-26, 2013

Doornenbal P.: “In-Beam Gamma-Ray Spectroscopy at the RIBF”, Invited talk at Nuclear Structure Physics with Advanced Gamma-Detector Arrays (NSP13), Padova, Italy, June 10-12, 2013

Doornenbal P.: “In-beam gamma-ray spectroscopy at the RIBF - Present limitations and future perspectives (SHOGUN)”, Invited talk at the IFJ PAN - RIKEN JSPS Collaboration Workshop, Zakopane, Poland, Mar 20- 21, 2013

Lorusso G.: “Spectroscopy of N = 82 nuclei and the physical conditions of the *r*-process”, The first International African Symposium on Exotic Nuclei IASEN 2013, Cape Town, South Africa, December 2-6, 2013

Lorusso G.: “Decay Spectroscopy of exotic nuclei at RIBF—The EURICA project”, The 12th International Symposium on Origin of Matter and Evolution of Galaxies, Tsukuba, Japan, November 18-21,2013

Lorusso G.: “Spectroscopy of N = 82 nuclei and the physical conditions of the r-process”, XXXIII Mazurian Lakes Conference on Physics Frontiers in Nuclear Physics, Piaski, Poland, September 1-7, 2013

Watanabe H.:“Shape-phase transitions in very neutron-rich nuclei from 40Zr to 46Pd”, The 7th International Symposium on Chiral Symmetry in Hadrons and Nuclei, October 27-30, 2013, Beihang University, Beijing, China

Watanabe H.: “Recent results of decay spectroscopy at RIBF”, Heavy Ion Accelerator Symposium on Fundamental and Applied Science (HIAS2013), April 8-12, 2013, Australian National University, Canberra, Australia

Wu J.: “Beta-decay of neutron-rich Z~60 nuclei and the origin of Rare-Earth Elements”, Nuclei in the Cosmos (NIC)-XIII, July 7-11, 2014, Debrecen, Hungary

(Domestic Conference)

櫻井博儀: “非対称核物質 EOS への挑戦” (招待講演), 日本物理学会第 68 回年次大会（日本物理学会）, 広島, 3 月(2013)

岸田隆：“リスクの時代と科学” 鳥居薬品外部講師講演会、東京 （ 2013、2 月）

岸田隆：“エネルギー問題 の考え方” 鳥居薬品外部講師講演会、東京（ 2013、9 月）

八木彩祐未、磯部忠昭 et al.: “Report on the recent EURICA Campaign aiming at β-decay study around ^{78}Ni”, 日本物理学会第 68 回年次大会, 広島, 3 月(2013).

田中隆己、磯部忠昭 et al.: “SAMURAI を用いた ^{14}Be の分解反応実験”, 日本物理学会第 68 回年次大会,広島, 3 月 (2013).

生越駿、磯部忠昭 et al.: “^{19}B の分解反応”, 日本物理学会第 68 回年次大会, 広島, 3 月(2013).

南方亮吾、磯部忠昭 et al.: “^{22}C の分解反応”, 日本物理学会第 68 回年次大会, 広島, 3 月(2013).

徐正宇、磯部忠昭 et al.: “Report on the recent EURICA campaign with ^{238}U beam at RIBF, RIKEN”, 日本物理学会第 68 回年次大会, 広島, 3 月(2013).

中塚徳継、磯部忠昭 et al.: “SAMURAI-TPC 用読み出しエレクトロニクスの開発”, 日本物理学会第 68 回年次大会, (日本物理学会), 広島, 3 月(2013).

磯部忠昭: “原子核状態方程式の解明を目指した重イオン衝突実験への PHITS の利用”, PHITS 研究会, JAEA, 茨城県東海村, 8 月

Ann-Kathrin Perrevoort et al.: “SPYBOX: External hardware for GET electronics at SAMURAI-TPC”, 日本物理学会平成 25 年秋季大会, 高知, 9 月(2013).

中塚徳継、磯部忠昭 et al.: “Performance eveluation of a TPC for heavy-ion collision experiment at RIBF”, 日本物理学会平成 25 年秋季大会, 高知, 9 月(2013).

大道理恵、磯部忠昭 et al.: “$LaBr_3$ 検出器を用いた中性子過剰核の励起状態の寿命測定”, 日本物理学会平成 25 年秋季大会,高知, 9 月(2013).

井手口栄治、磯部忠昭 et al.: “中性子過剰領域 Z～60 原子核における K アイソマーの探索”, 日本物理学会平成 25 年秋季大会, 高知, 9 月(2013).

田中まな、磯部忠昭 et al.: “中性子過剰 Nd 同位体におけるアイソマー分光”, 日本物理学会平成 25 年秋季大会, 高知, 9 月(2013).

方一帆、磯部忠昭 et al.: “Study of beta decay of neutron-rich I isotopes at RIKEN RIBF using a stack of Si-strip detectors WASA3Bi combined with a cluster-Ge array EURICA”, 日本物理学会平成 25 年秋季大会, 高知, 9 月(2013).

八木彩祐未、磯部忠昭 et al.: “理研 RIBF の EURICA を用いた中性子過剰な Cs 同位体(A≲150)のアイソマーの研究”, 日本物理学会平成 25 年秋季大会, 高知, 9 月(2013).

横山輪、磯部忠昭 et al.: “過剰変形領域の Pm 同位体における新アイソマーの発見”, 日本物理学会平成 25 年秋季大会, 高知, 9 月(2013).

南方亮吾、磯部忠昭 et al.: “^{22}C の分解反応 II”, 日本物理学会平成 25 年秋季大会, 高知, 9 月(2013).

磯部忠昭: “RIBF-SPiRITプロジェクトにおけるGET読み出し回路の利用”, 新学術領域中性子星の核物質・検出器交流会, JAXA, 東京, 10月(2013).

磯部忠昭: “原子核衝突中における核子拡散の観測による、対称エネルギー密度依存性の測定”, 新学術領域中性子星の核物質研究会, 理研, 和光, 12月(2013).

中井陽一,日高宏, 渡部直樹, 小島隆夫: “イオン打ち込み移動管を用いた水和クラスターイオンの生成実験の現状3”, 日本物理学会 2013 年秋季大会,徳島, 9月(2013).

大津秀暁: “RIBF における長寿命 FP をビームとした破砕反応実験”, 第一回長寿命核分裂核廃棄物の核変換データとその戦略ワークショップ, 埼玉, 3月(2014).

Spin Isospin Laboratory

Publications

[Journal]

(Original Papers) *Subject to Peer Review

C. L. Bai, H. Sagawa, M. Sasano, T. Uesaka, K. Hagino, H. Q. Zhang, X. Z. Zhang, F. R. Xu "Role of T=0 pairing in Gamow-Teller states in N = Z nuclei", Physics Letters B **719**, 116 (2013).

E. Khan, N. Paar, D. Vretenar, L. G. Cao, H. Sagawa, G. Colo, "Incompressibility of finite fermionic systems: Stable and exotic atomic nuclei", Physical Review C **87**, 064311 (2013).

A. Li, E. Hiyama, X. R. Zhou, and H. Sagawa, "Tensor correlation, pairing interaction, and deformation in Ne isotopes and Ne hypernuclei", Physical Review C **87**, 014333 (2013).

A. Li, X. R. Zhou, and H. Sagawa, "Tensor force and shape evolution of Si isotopes in the Skyrme-Hartree-Fock model", Progress of Theoretical and Experimental Physics **2013**, 063D03 (2013).

Y. A. Litvinov, S. Bishop, K. Blaum, F. Bosch, C. Brandau, L. X. Chen, I. Dillmann, P. Egelhof, H. Geissel, R. E. Grisenti, S. Hagmann, M. Heil, A. Heinz, N. Kalantar-Nayestanaki, R. Knobel, C. Kozhuharov, M. Lestinsky, X. W. Ma, T. Nilsson, F. Nolden, A. Ozawa, R. Raabe, M. W. Reed, R. Reifarth, M. S. Sanjari, D. Schneider, H. Simon, M. Steck, T. Stohlker, B. H. Sun, X. L. Tu, T. Uesaka, P. M. Walker, M. Wakasugi, H. Weick, N. Winckler, P. J. Woods, H. S. Xu, T. Yamaguchi, Y. Yamaguchi, and Y. H. Zhang "Nuclear physics experiments with ion storage rings", Nuclear Instruments and Methods in Physics Research Section B-Beam Interactions with Materials and Atoms **317**, 603 (2013).

Y. Maeda, T. Saito, H. Miyasako, T. Uesaka, S. Ota, S. Kawase, T. Kikuchi, H. Tokieda, T. Kawabata, K. Yako, T. Wakasa, S. Sakaguchi, R. Chen, H. Sakaguchi, T. Shima, T. Suzuki, and A. Tamii "Study of the Three-Nucleon Force Effects in the H-2(p, n) Breakup Reaction at 170 MeV", Few-Body Systems **54**, 1311 (2013).

H. Matsubara, M. Takaki, T. Uesaka, S. Shimoura, N. Aoi, M. Dozono, T. Fujii, K. Hatanaka, T. Hashimoto, T. Kawabata, S. Kawase, K. Kisamori, Y. Kikuch, Y. Kubota, C. S. Lee, H. C. Lee, Y. Maeda, S. Michimasa, K. Miki, H. Miya, S. Noji, S. Ota, S. Sakaguchi, Y. Sasamoto, T. Suzuki, L. T. Tang, K. Takahisa, H. Tokieda, A. Tamii, K. Yako, Y. Yasuda, N. Yokota, R. Yokoyama, and J. Zenihiro, "Spectroscopic Measurement in He-9 and Be-12", Few-Body Systems **54**, 1433 (2013).

Y. Matsuda, H. Sakaguchi, H. Takeda, S. Terashima, J. Zenihiro, T. Kobayashi, T. Murakami, Y. Iwao, T. Ichihara, T. Suda, T. Ohnishi, Y. Watanabe, H. Otsu, K. Yoneda, Y. Satou, K. Ozeki, and M. Kanazawa "Elastic scattering of protons from ^{9}C with a 290 MeV/nucleon ^{9}C beam", Physical Review C **87**, 034614 (2013).

S. Michimasa, M. Takaki, M. Dozono, S. Go, H. Baba, E. Ideguchi, K. Kisamori, H. Matsubara, H. Miya, S. Ota, H. Sakai, S. Shimoura, A. Stolz, T. L. Tang, H. Tokieda, T. Uesaka, and R. G. T. Zegers "Development of CVD diamond detector for time-of-flight measurements", Nuclear Instruments and Methods in Physics Research Section B-Beam Interactions with Materials and Atoms **317**, 710 (2013).

S. Michimasa, M. Takaki, Y. Sasamoto, M. Dozono, T. Nishi, T. Kawabata, S. Ota, H. Baba, T. Baba, T. Fujii, S. Go, S. Kawase, Y. Kikuchi, K. Kisamori, M. Kobayashi, Y. Kubota, C. S. Lee, H. Matsubara, K. Miki, H. Miya, S. Noji, H. Tokieda, M. Tsumura, K. Yako, R. Yokoyama, H. Takeda, Y. Yanagisawa, T. Kubo, N. Inabe, N. Fukuda, D. Kameda, H. Suzuki, Y. Shimizu, H. Sato, T. Ichihara, A. Stolz, R. G. T. Zegers, H. Sakai, T. Uesaka, and S. Shimoura "SHARAQ spectrometer for high-resolution studies for RI-induced reactions ", Nuclear Instruments and Methods in Physics Research Section B-Beam Interactions with Materials and Atoms **317**, 305 (2013).

H. Miya, S. Ota, T. Fujii, S. Kawase, Y. Kubota, C. S. Lee, H. Matsubara, K. Miki, A. Saito, S. Michimasa, T. Uesaka, H. Sakai, and S. Shimoura "Development of low-pressure multi-wire drift chambers for high-resolution spectroscopy with radioactive isotope beams", Nuclear Instruments and Methods in Physics Research Section B-Beam Interactions with Materials and Atoms **317**, 701 (2013).

D. Nagae, Y. Abe, S. Okada, A. Ozawa, T. Yamaguchi, H. Suzuki, T. Moriguchi, Y. Ishibashi, S. Fukuoka, R. Nishikiori, T. Niwa, T. Suzuki, F. Suzaki, K. Sato, H. Furuki, N. Ichihashi, S. Miyazawa, Y. Yamaguchi, T. Uesaka, and M. Wakasugi "Time-of-flight detector applied to mass measurements in Rare-RI Ring", Nuclear Instruments and Methods in Physics Research Section B-Beam Interactions with Materials and Atoms **317**, 640 (2013).

T. Nishi, G. P. A. Berg, M. Dozono, H. Fujioka, N. Fukuda, T. Furuno, H. Geissel, R. S. Hayano, N. Inabe, K. Itahashi, S. Itoh, D. Kameda, T. Kubo, H. Matsubara, S. Michimasa, K. Miki, H. Miya, Y. Murakami, M. Nakamura, N. Nakatsuka, S. Noji, K. Okochi, S. Ota, H. Suzuki, K. Suzuki, M. Takaki, H. Takeda, Y. K. Tanaka, K. Todoroki, K. Tsukada, T. Uesaka, Y. N. Watanabe, H. Weick, H. Yamada, and K. Yoshida "BigRIPS as a high resolution spectrometer for pionic atoms", Nuclear Instruments and Methods in Physics Research Section B-Beam Interactions with Materials and Atoms **317**, 290 (2013).

H. J. Ong, I. Tanihata, A. Tamii, T. Myo, K. Ogata, M. Fukuda, K. Hirota, K. Ikeda, D. Ishikawa, T. Kawabata, H. Matsubara, K. Matsuta, M. Mihara, T. Naito, D. Nishimura, Y. Ogawa, H. Okamura, A. Ozawa,

D. Y. Pang, H. Sakaguchi, K. Sekiguchi, T. Suzuki, M. Taniguchi, M. Takashina, H. Toki, Y. Yasuda, M. Yosoi, and J. Zenihiro "Probing effect of tensor interactions in ^{16}O via (p, d) reaction", Physics Letters B **725**, 277 (2013).

X. Roca-Maza, G. Colo, and H. Sagawa "New Skyrme energy density functional for a better description of the Gamow-Teller resonance", Physica Scripta **T154**, 014011 (2013).

H. Sagawa, Y. Tanimura, and K. Hagino "Competition between T=1 and T=0 pairing in pf - shell nuclei with N = Z", Physical Review C **87**, 034310 (2013).

S. Sakaguchi, Y. Iseri, T. Uesaka, M. Tanifuji, N. Aoi, E. Hiyama, Y. Ichikawa, S. Ishikawa, K. Itoh, M. Itoh, H. Iwasaki, T. Kawabata, T. Kawahara, H. Kuboki, Y. Maeda, T. Nakao, H. Okamura, H. Sakai, Y. Sasamoto, M. Sasano, Y. Satou, K. Sekiguchi, K. Suda, D. Suzuki, A. Tamii, T. Wakui, K. Yako, M. Yamaguchi, and Y. Yamamoto "Analyzing Power in Elastic Scattering of Polarized Protons from Neutron-rich Helium Isotopes", Few-Body Systems **54**, 1393 (2013).

S. Sakaguchi, T. Uesaka, T. Kawahara, T. Ogawa, L. Tang, T. Teranishi, Y. Urata, S. Wada, and T. Wakui "Proton polarization in photo-excited aromatic molecule at room temperature enhanced by intense optical source and temperature control", Nuclear Instruments and Methods in Physics Research Section B-Beam Interactions with Materials and Atoms **317**, 679 (2013).

A. P. Severyukhin and H. Sagawa "Tensor correlation effects on Gamow-Teller resonances in Sn-120 and N=80, 82 isotones", Progress of Theoretical and Experimental Physics **2013**, 103D03 (2013).

F. Suzaki, J. Zenihiro, T. Yamaguchi, A. Ozawa, T. Uesaka, M. Wakasugi, K. Yamada, and R. R. C. Yamaguchi, Y. for the Rare RI Ring Collaboration "Design study of a resonant Schottky pick-up for the Rare-RI Ring project", Nuclear Instruments and Methods in Physics Research Section B-Beam Interactions with Materials and Atoms **317**, 636 (2013).

K. Tateishi, M. Negoro, A. Kagawa, and M. Kitagawa "Dynamic Nuclear Polarization with Photoexcited Triplet Electrons in a Glassy Matrix", Angewandte Chemie-International Edition **52**, 13307 (2013).

K. Tateishi, M. Negoro, A. Kagawa, T. Uesaka, and M. Kitagawa "Hyperpolarization of Thin Films with Dynamic Nuclear Polarization Using Photoexcited Triplet Electrons", Journal of the Physical Society of Japan **82**, 084005 (2013).

Y. Yamaguchi, M. Wakasugi, T. Uesaka, A. Ozawa, Y. Abe, T. Fujinawa, M. Kase, M. Komiyama, T. Kubo, K. Kumagai, T. Maie, D. Nagae, J. Ohnishi, F. Suzaki, A. Tokuchi, Y. Watanabe, K. Yoshida, K. Yamada, T. Yamaguchi, H. Yamasawa, Y. Yanagisawa, J. Zenihiro, and Y. Yano "Construction of rare-RI ring at RIKEN RI Beam Factory", Nuclear Instruments and Methods in Physics Research Section B-Beam Interactions with Materials and Atoms **317**, 629 (2013)

J. Yasuda, T. Wakasa, M. Okamoto, M. Dozono, K. Hatanaka, M. Ichimura, S. Kuroita, Y. Maeda, T. Noro, Y. Sakemi, M. Sasano, and K. Yako "", Progress of Theoretical and Experimental Physics **2013**, 063D02 (2013).

Oral Presentations

(International Conference etc.)

T. Uesaka: "Proposal of Joint Research on Mass measurements with storage rings", RIKEN-CAS IMPJoint workshop, (RIKEN Nishina Center and Institute of Modern Physics, Chinese Academy of Science), Wako, Japan, Apr. (2013).

T. Uesaka: "Giant Resonance Studies at RIBF", Workshop on the INFN-RIKEN collaboration on nuclear physics activities, (RIKEN and INFN), Tokyo, Japan, May (2013).

M. Sasano: "Gamow-Teller transitions from ^{56}Ni and future studies of the (p,n) reaction on unstable nuclei", Gordon research conference, (Gordon research conference), Colby-Sawyer College, New London, NH, USA, Jun. (2013).

T. Uesaka: "Spin-orbit splitting and Tensor Force", RCNP Workshop on the Importance of Tensor Interactions in Nuclear and Hadron structure, (RCNP, Osaka University), Osaka, Japan, July (2013).

J. Zenihiro: "Proton elastic scattering with RI beams", 3rd International Symposium on Nuclear Symmetry Energy (NuSYM13), (NSCL/FRIB), Michigan, USA, July (2013).

T. Uesaka: "Quasi-Free Scattering Experiments at RIBF", 1st JCPRG-RNC Joint Workshop on Nuclear Data, (RIKEN and Hokkaido University), Saitama, Japan, Aug. (2013).

T. Uesaka: "$(p, 2p)$ Experiments with a Polarized Target at RIBF", 2nd International Workshop on Quasi-Free Scattering with Radioactive Ion Beams (QFS-RB13), (TU Darmstadt and Lisbon University), Terceira, Portugal, Sep. (2013).

T. Uesaka: "RIBF Overview", 3rd LIA French-Japanese Nuclear Structure Problems Symposium, (CNRS, CEA, and RIKEN), Paris, France, Sep. (2013).

J. Zenihiro: "Study of simultaneous extractions of proton and neutron density distributions from proton elastic scattering of 90, 92, 94Zr at 200 and 300 MeV", 3rd LIA French-Japanese Nuclear Structure Problems Symposium, (CNRS, CEA, and RIKEN), Paris, France, Sep. (2013).

Y. Matsuda: "Proton elastic scattering on proton-rich carbon isotopes: 9,10,11C", 3rd LIA French-Japanese Nuclear Structure Problems Symposium, (CNRS, CEA, and RIKEN), Paris, France, Sep. (2013).

T. Uesaka: "Polarized Targets in RI-Beam Experiments", 1st RIBF-RISP Worshop, (IBS and RIKEN), Daejeon, Nov. (2013).

T. Uesaka: "Interplay between Spin and Isospin in Exotic Nuclei", Winger111 Scientific Symposium, (Hungarian Academy of Science), Budapest, Nov. (2013).

J. Zenihiro: "ESPRI experiment", JUSTIPEN-JUSEIPEN Workshop, (RIKEN), Saitama, Japan, Dec. (2013).

T. Uesaka: "Knockout reaction studies of Borromean nuclei with MINOS at RIBF", Halo workshop, (GSI), Darmstadt, Germany, Feb. (2014).

T. Uesaka: "Quasi-Free Scattering Experiments with Radioactive Beams at RIBF", TU-Darmstadt CRC Workshop, (TU Darmstadt), Black Forest, Germany, Feb. (2014).

(Domestic Conference)

笹野匡紀: "^{56}Ni のガモフ・テラー遷移強度"(若手奨励賞受賞記念講演), 日本物理学会第 68 回年次大会, (日本物理学会), 東広島市, 3 月 (2013).

笹野　匡紀、矢向　謙太郎: "Double-beta decay matrix elements and charge exchange reactions", 極低バックグラウンド素粒子原子核研究懇談会, (極低バックグラウンド素粒子原子核研究懇談会), 富山市, 4 月 (2013).

久保田悠樹、笹野匡紀、上坂友洋、李清秀、伊藤正俊、大田晋輔、川瀬頌一郎、小林幹、田口貴大、Leung Tsz Tang、堂園昌伯、時枝紘史、松原礼明、宮裕之、涌井崇志: "不安定核研究のための高粒度中性子検出器の開発", 日本物理学会第 68 回年次大会, (日本物理学会), 東広島市, 3 月 (2013).

李清秀、大田晋輔、時枝紘史、上坂友洋: "低圧重水素中における厚い GEM の基礎特性", 日本物理学会第 68 回年次大会, (日本物理学会), 東広島市, 3 月 (2013).

木佐森慶一、下浦享、宮裕之、馬場秀忠、馬場辰彦、堂園昌伯、福田直樹、藤井俊彦、郷慎太郎、井手口栄治、稲辺尚人、伊藤正俊、亀田大輔、川畑貴裕、川瀬頌一郎、久保敏幸、久保田悠樹、小林幹、近藤洋介、李清秀、前田幸重、松原礼明、三木謙二郎、道正新一郎、西隆博、西村美月、大田晋輔、坂口聡志、酒井英行、笹野匡紀、佐藤広海、清水陽平、鈴木宏、高木基伸、民井淳、竹田浩之、武内聡、時枝紘史、津村美保、上坂友洋、柳沢善行、矢向謙太郎、横山輪、吉田光一、Marlene Assie, Didier Beaumel, Fariouz Hammache, Andreas Stolz: "二重荷電交換反応をもちいた 4 中性子系質量欠損核分光実験", 日本物理学会秋季大会, (日本物理学会), 高知市, 9 月 (2013).

銭廣十三 "陽子弾性散乱で見る核子密度分布", 九大分野横断型研究会 -クォーク・原子核・中性子星を俯瞰する-, (九州大学), 福岡市, 3 月 (2014).

Nuclear Spectroscopy Laboratory

Publications

[Journal]

(Original Papers) *Subject to Peer Review

Ichikawa Y. and Ueno H.: "Production of spin-controlled rare isotope beams" (in Japanese), *Butsuri* **62**, 823–827 (2013).*

Ueno H., Miyatake H., Yamamoto Y., Tanimoto S., Shimoda T., Aoi N., Asahi K., Ideguchi E., Ishihara M., Izumi H., Kishida T., Kubo T., Mitsuoka S., Mizoi Y., Notani M., Ogawa H., Ozawa A., Sasaki M., Shirakura T., Takahashi N., and Yoneda K.: "Beta-delayed neutron and gamma-ray spectroscopy of ^{17}C utilizing spin-polarized ^{17}B", Phys. Rev. C **87**, 034316, 15 pages (2013).*

Ichikawa Y., Ueno H., Ishii Y., Furukawa T., Yoshimi A., Kameda D., Watanabe H., Aoi N., Asahi K., Balabanski D.L., Chevrier R., Daugas J.M., Fukuda N., Georgiev G., Hayashi H., Iijima H., Inabe N., Inoue T., Ishihara M., Kubo T., Nanao T., Ohnishi T., Suzuki K., Tsuchiya M., Takeda H., Rajabali M.M.: "Novel method for the production of spin-aligned RI beams in projectile fragmentation reaction with the dispersion matching technique", Hyperfine Interact. **220**, 47–51 (2013).*

Momota S., Mihara M., Nishimura D., Fukuda M., Kamisho Y., Wakabayashi M., Matsuta K., Suzuki S., Nagashima M., Zhu S., Yuan D., Zheng Y., Yi Z., Fan P., Izumikawa T., Kitagawa A., Sato S., Kanazawa M., Torikoshi M., Minamisono T., Nakamura Y., Tashiro K., Honma A., Yoshida N., Shirai H., Ohtsubo T., Nagatomo T., Uenishi H., Iwamoto K., Yaguchi M., Ogura T., Ito T., Yamamura K., Ichikawa Y., Nojiri Y., Alonso J.R., Symons T.J.M.: "Momentum dependence of spin polarization for beta emitting nuclei produced through charge exchange reaction at intermediate energy", Hyperfine Interact. **220**, 53–58 (2013).*

Inoue T., Furukawa T., Yoshimi A., .Ichikawa Y, Chikamori M., Ohtomo Y., Tsuchiya M., Yoshida N., Shirai H., Uchida M., Suzuki K., Nanao T., Miyatake H., Ueno H., Matsuo Y., Fukuyama T., Asahi K.: "Nuclear spin maser and experimental search for ^{129}Xe atomic EDM", Hyperfine Interact. **220**, 59-63 (2013).*

Ishibashi Y., Nagae D., Abe Y., Nagatomo T., Ozawa A., Suzuki H., Fukuoka S., Nishikiori R., Niwa T., Matsuta K., Tagishi Y.: "Production of nuclear polarization of unstable nuclei via polarization transfer reactions", Hyperfine Interact. **220**, 71-77 (2013).*

Furukawa T., Wakui T., Yang X.F., Fujita T., Imamura K., Yamaguchi Y., Tetsuka H., Tsutsui Y., Mitsuya Y., Ichikawa Y., Ishibashi Y., Yoshida N., Shirai H., Ebara Y., Hayasaka M., Arai S., Muramoto S., Hatakeyama A., Wada M., Sonoda T., Ito Y., Kobayashi T., Nishimura S., Nishimura M., Kondo Y., Yoneda K., Ueno H., Shinozuka T., Shimoda T., Asahi K., Matsuo Y.: "Novel nuclear laser spectroscopy method using superfluid helium for measurement of spins and moments of exotic nuclei", Nucl. Instr. Meth. Phys. Res. **B 317**, 590-594 (2013).*

Imamura K., Furukawa T., Wakui T., Yang X.F., Yamaguchi Y., Tetsuka H., Mitsuya Y., Tsutsui Y., Fujita T., Ebara Y., Hayasaka M., Arai S., Muramoto S., Ichikawa Y., Ishibashi Y., Yoshida N., Shirai H., Hatakeyama A., Wada M., Sonoda T., Ito Y., Odashima H., Kobayashi T., Ueno H., Shimoda T., Asahi K., Matsuo Y.: "Development of a helium cryostat for laser spectroscopy of atoms with unstable nuclei in superfluid helium", Nucl. Instr. Meth. Phys. Res. **B 317**, 595–598 (2013).*

Yang X.F., Furukawa T., Wakui T., Imamura K., Tetsuka H., Fujita T., Yamaguchi Y., Tsutsui Y., Mitsuya Y., Ichikawa Y., Ishibashi Y., Yoshida N., Shirai H., Ebara Y., Hayasaka M., Arai S., Muramoto S., Hatakeyama A., Wada M., Sonoda T., Ito Y., Kobayashi T., Nishimura S., Nishimura M., Kondo Y., Yoneda K., Ueno H., Shinozuka T., Shimoda T., Asahi K., Matsuo Y.: "Control of stopping position of radioactive ion beam in superfluid helium for laser spectroscopy experiments", Nucl. Instr. Meth. Phys. Res. **B 317**, 599–602 (2013).*

Yoshida N., Ueno H., Yoshimi A., Ishibashi Y., Ichikawa Y., Abe Y., Asahi K., Chikamori M., Fujita T., Furukawa T., Hikota E., Nagae D., Ohtomo Y., Saito Y., Shirai H., Suzuki T., Yang X.F., "Development of a new device control system for β-NMR experiments", Nucl. Instr. Meth. Phys. Res. **B 317**, 705–709 (2013).*

Ishibashi Y., Yoshida N., Ueno H., Yoshimi A., Ichikawa Y., Abe Y., Asahi K., Chikamori M., Fujita T., Furukawa T., Hikota E., Nagae D., Ohtomo Y., Saito Y., Shirai H., Suzuki T., Yang X.F., Sakamoto N.: "Development of an adiabatic field rotation system to measure spin polarization of unstable nuclei", Nucl. Instr. Meth. Phys. Res. **B 317**, 714–716 (2013).*

Ichikawa Y., Ueno H., Ishii Y., Furukawa T., Yoshimi A., Kameda D., Watanabe H., Aoi N., Asahi K., Balabanski D.L., Chevrier R., Daugas J.M., Fukuda N., Georgiev G., Hayashi H., Iijima H., Inabe N., Inoue T., Ishihara M., Kubo T., Nanao T., Ohnishi T., Suzuki K., Tsuchiya M., Takeda H., Rajabali M.M.: "Spin-aligned RI beams via two-step fragmentation reactions", Nucl. Instr. Meth. Phys. Res. **B 317**, 769–773 (2013).*

Ishiyama H., Jeong S.C., Watanabe Y.X., Hirayama Y., Imai N., Miyatake H., Oyaizu M., Katayama I., Sataka M., Osa A., Otokawa Y., Matsuda M., Makii H., Nishio K., Sato T.K., Nakao A.: "In situ diffusion measurements in solids using short-lived radioactive tracers of ^{8}Li and ^{20}Na", Nucl. Instr. Meth. Phys. Res. **B 317**, 789–792 (2013).*

Akamatsu K., Okuyama M., Mitsumori K., Yoshino A., Nakao A., Nakao S.: "Effect of the composition of the copolymer of carboxybetaine and n-butylmethacrylate

on low-fouling property of dynamically formed membrane", Sep. Purif. Technol. **118**, 463–469 (2013).*

Yamada Y., Kobayashi Y., Kubo M.K., Mihara M., Nagatomo T., Sato W., Miyazaki J., Sato S., Kitagawa A.: "In-beam Mssbauer spectra of ^{57}Mn implanted into low-temperature solid Ar", Chem. Phys. Lett. **567**, 14–17 (2013).*

Yamada Y., Kobayashi Y., Kubo M.K., Mihara M., Nagatomo T., Sato W., Miyazaki J., Sato S., Kitagawa A.: "In-beam Mssbauer study of ^{57}Mn implanted into a low-temperature xenon", Hyperfine Interact. **226**, 35–40 (2013).*

Kobayashi Y., Mihara M., Nagatomo T., Yamada Y., Kubo M.K., Miyazaki J., Sato W., Sato S., Kitagawa A., "Time-resolved Mössbauer spectra obtained after ^{57}Mn implantation in Si", Hyperfine Interact. **226**, 679–685 (2013).*

Kobayashi Y., "In-beam Mössbauer Spectroscopy Using a Radioisotope Beam and a Nuclear Capture Reaction", Mössbauer Spectroscopy – Applications in Chemistry, Biology, Nanotechnology, ed. by V.K. Sharma, G. Klingelhfer, and T. Nishida (John Wiley Sons, New Jersey, USA) pp. 58–70, (2013).

Yang X.F., Furukawa T., Wakui T., Imamura K., Fujita H., Mitsuya Y., Hayasaka M., Ichikawa Y., Ishibashi Y., Shirai H., Ebata Y., Hatakeyama A., Wada M., Sonoda T., Ito Y., T. Kobayashi , Nishimura S., Kondo Y., Yoneda K., Ueno H., Shinozuka T., Shimoda T., Asahi K., Matsuo Y.: "An effective method for trapping ion beams in superfluid helium for laser spectroscopy experiments", EPJ Web of Conf. **66**, 11041, 4 pages (2014).*

Ichikawa Y., Chikamori M., Ohtomo Y., Hikota E., Sakamoto Y., Suzuki T., Bidinosti C.P., Inoue T., Furukawa T., Yoshimi A., Suzuki K., Nanao T., Miyatake H., Tsuchiya M., Yoshida N., Shirai H., Ino T., Ueno H., Matsuo Y., Fukuyama T., and Asahi K.: "Search for electric dipole moment in ^{129}Xe atom using active nuclear spin maser", EPJ Web of Conf. **66**, 05007, 4 pages (2014).*

Hikota E., Chikamori M., Ichikawa Y., Ohtomo Y., Sakamoto Y., Suzuki T., Bidinosti C.P., Inoue T., Furukawa T., Yoshimi A., Suzuki K., Nanao T., Miyatake H., Tsuchiya M., Yoshida N., Shirai H., Ino T., Ueno H., Matsuo Y., Fukuyama T., and Asahi K.: "Hyperfine structure constant of the neutron halo nucleus 11Be", EPJ Web of Conf. **66**, 05005, 4 pages (2014).*

Oral Presentations

(International Conference etc.)

Yang X.F., Furukawa T., Fujita T., Matsuo Y.: "Precision measurement of laser RF double resonance spectra with an effective compensation of residual magnetic field", The 9th International Workshop on Application of Laser and Storage Device in Atomic Nuclei Research (LASER 2013), Poznan, Poland, May (2013).

Ueno H.: "RIBF research activities with slowed-down/stopped RI beams", Workshop on the INFN-RIKEN collaboration on nuclear physics activities, Tokyo Japan, May (2013).

Furukawa T., Fujita T., Wakui T., Yang X.F., Imamura K., Yamaguchi Y., Tetsuka H., Tsutsui Y., Mitsuya Y., Ichikawa Y., Ishibashi Y., Yoshida N., Shirai H., Ebara Y., Hayasaka M., Arai S., Muramoto S., Hatakeyama A., Wada M., Sonoda T., Ito Y., Kobayashi T., Nishimura S., Nishimura M., Kondo Y., Yoneda K., Ueno H., Shinozuka T., Shimoda T., Asahi K., Matsuo Y.: "Laser spectroscopy of RI atoms stopped in superfluid helium", The 25th International Nuclear Physics Conference (INPC 2013), Firenze, Italy, June (2013).

Ueno H.: "Spin-oriented RI beams at RIBF and their applications", RIBF Nuclear Physics Seminar (RIKEN Nishina Center) , Wako, Japan, June (2013).

Ueno H.: "Research programs with stopped/slowed-down RI beams at RIBF", RIBF User Meeting 2013, Wako, Japan, June (2013).

Ichikawa Y., Ohtomo Y., Sakamoto Y., Suzuki T., Hikota E., Miyatake H., Nanao T., Suzuki K., Tsuchiya M., Inoue T., Furukawa T., Yoshimi A., Bidinosti C.P., Ino T., Ueno H., Matsuo Y., Fukuyama T., and Asahi K.: "Experimental search for atomic EDM in ^{129}Xe using active nuclear spin maser", 3rd International Workshop on the Physics of fundamental Symmetries and Interactions at low energies and the precision frontier (PSI2013), Villigen, Switzerland, September (2013).

Ueno H.: "Spin-oriented RI beams at RIBF", Keynote speech at Institute of Modern Physics, Chinese Academy of Sciences, Lanzhou, China, September (2013).

Ueno H.: "Researches with stopped radioisotopes at the RIKEN RIBF facility", The 5th Asia-Pacific Symposium on Radiochemistry '13 (APSORC13), Kanazawa, Japan, September (2013).

Ueno H.: "Present status of nuclear moment measurements at RIBF", French-Japanese Symposium on Nuclear Structure Problems, Paris, France, September (2013).

Ueno H., "Spin-polarized RI beams", The First RIBF-RISP Joint Workshop, Daejeon, Korea, November (2013).

Asahi K.: "Spin masing, and looking for an atomic EDM of nuclear origin", Physical Research Laboratory Colloquium, (Physical Research Laboratory), Ahmedabad, India, December (2013).

Ichikawa Y., Ohtomo Y., Sakamoto Y., Kojima S., Suzuki T., Chikamori M., Hikota E., Miyatake H., Nanao T., Suzuki K., Tsuchiya M., Inoue T., Furukawa T., Yoshimi A., Bidinosti C.P., Ino T., Ueno H., Matsuo Y., Fukuyama T., and Asahi K.: "Search for electric dipole moment of ^{129}Xe using active spin maser", 7th International Workshop on Fundamental Physics Using Atoms, Tokyo, Japan, March (2014).

(Domestic Conference)

小林義男: "加速器インビーム・メスバウアー分光の現状と新展開", 第 50 回アイソトープ・放射線 研究発表会　パネル討論シンポジウム, 東京, 7 月 (2013).

小林義男, 三原基嗣, 山田康洋, 久保謙哉, 長友傑, 宮崎淳, 佐藤渉, 佐藤眞二, 北川敦志: "シリコンにおける時間分解 ^{57}Fe(←^{57}Mn) インビーム・メスバウアースペクトル", 第 50 回アイソトープ・放射線 研究発表会, 東京, 7 月 (2013).

石山博恒, 鄭淳讃, 渡辺裕, 平山賀一, 今井伸明, 宮武宇也, 西尾勝久, 牧井宏之, 長明彦, 乙川義憲, 松田誠, 佐藤哲也, 桑田直明, 河村純一, 中尾愛子, 上野秀樹: "放射性トレーサー ^{8}Li によるリチウム電池固体材料中のリチウム拡散係数測定法開拓", 第 16 回超イオン導電体物性研究会・第 63 回固体イオニクス研究会, 茨城, 7 月 (2013).

上野秀樹: "RI ビームファクトリー施設と利用研究", 第 74 回応用物理学会秋季学術講演会 分科企画シンポジウム「イオン加速器に関する先端技術の現状」, 京都, 9 月 (2013).

市川雄一, 佐藤智哉, 大友祐一, 坂本雄, 鈴木貴大, 近森正敏, 彦田絵里, 宮武裕和, 七尾翼, 鈴木都文, 土屋真人, 井上壮志, 古川武, 吉見彰洋, BIDINOSTI ,Christopher P., 猪野隆, 上野秀樹, 松尾由賀利, 福山武志, 旭耕一郎: "^{3}He 共存磁力計の導入による ^{129}Xe 原子 EDM 測定実験 II", 日本物理学会 2013 年秋季大会, 高知, 9 月 (2013).

佐藤智哉, 市川雄一, 大友祐一, 坂本雄, 鈴木貴大, 近森正敏, 彦田絵里, 宮武裕和, 七尾翼, 鈴木都文, 土屋真人, 井上壮志, 古川武, 吉見彰洋, BIDINOSTI, Christopher P., 猪野隆, 上野秀樹, 松尾由賀利, 福山武志, 旭耕一郎: "^{3}He 共存磁力計のダブルセルへの適用", 日本物理学会 2013 年秋季大会, 高知, 9 月 (2013).

大友祐一, 市川雄一, 佐藤智哉, 坂本雄, 鈴木貴大, 近森正敏, 彦田絵里, 宮武裕和, 七尾翼, 鈴木都文, 土屋真人, 井上壮志, 古川武, 吉見彰洋, BIDINOSTI, Christopher P., 猪野隆, 上野秀樹, 松尾由賀利, 福山武志, 旭耕一郎: "^{129}Xe/^{3}He の偏極生成及び緩和機構", 日本物理学会 2013 年秋季大会, 高知, 9 月 (2013).

上庄康斗, 三原基嗣, 松多健策, 福田光順, 森田祐介, 大野淳一, 田中正聖, 篠崎真一, 神戸峻輔, 南園忠則, 小倉昌子, 小沢顕, 長江大輔, 石橋陽子, 阿部康志, 稲葉成紀, 岡田俊祐, 齋藤佑多, 上野秀樹, 山田一成, 大坪隆, 泉川卓司, 百田佐多生, 西村太樹, 今村慧, YANG, Xiaofei, 鈴木健, 山口貴之, 白井光雲, 藤村卓功, 松川和人: "^{58}Cu の β-NMR 測定", 日本物理学会 2013 年秋季大会, 高知, 9 月 (2013).

旭耕一郎: "Nuclear EDM", 日本物理学会 2013 年秋季大会, 高知, 9 月 (2013).

上野秀樹: "核スピン偏極・整列 RI ビームの生成と応用", 日本放射化学会原子核プローブ分科会, 金沢, 9 月 (2013).

上野秀樹: "理研 RIBF における RI ビーム利用研究", 大学共同利用機関法人自然科学研究機構 分子科学研究所 機能分子システム創成研究部門オープンセミナー, 岡崎, 10 月 (2013).

佐藤智哉: "能動帰還型核スピンメーザーを用いた ^{129}Xe 原子永久電気双極子能率の探索", 精密周波数委員会, 東京, 12 月 (2013).

小林義男, 三原基嗣, 山田康洋, 久保謙哉, 長友傑, 宮崎淳, 佐藤渉, 谷川祥太郎, 佐藤祐貴子, 名取大樹, 鈴木聖人, 佐藤眞二, 北川敦志, "β-γ 同時計数法を用いた時間分解インビーム・メスバウアー分光法", 京大原子炉実験所専門研究会「不安定原子核の理工学と物性応用研究 III」, 大阪, 12 月 (2013).

石山博恒 , 鄭淳讃 , 渡辺裕 , 平山賀一 , 今井伸明 , 宮武宇也 , 西尾勝久 , 牧井宏之 , 木村創大 , 向井もも , 長明彦 , 乙川義憲 , 松田誠 , 佐藤哲也 , 桑田直明 , 河村純一 , 中尾愛子 , 上野秀樹 , KIM, Yung Hee: " 短寿命核トレーサー ^{8}Li による電池材料中のリチウム拡散係数測定 ", 京大原子炉実験所専門研究会「不安定原子核の理工学と物性応用研究 III」, 大阪 , 12 月 (2013).

三原基嗣, 石橋陽子, 阿部康志, 上庄康斗, 森田祐介, 大野淳一, 田中聖臣, 篠崎真一, 神戸峻輔, 福田光順, 松多健策, 小沢顕, 長江大輔, 稲葉成紀, 岡田俊祐, 斉藤佑多, 上野秀樹, 山田一成, 泉川卓司, 大坪隆, 百田佐多生, 西村太樹, 鈴木健, 山口貴之, 小林義男, 今村慧, YANG, Xiaofei, 長友傑, 南園忠則, 武智麻耶, 小倉昌子, 松川和人, 白井光雲, 藤村卓功: "シリコン中 ^{58}Cu の β-NMR 測定", 京大原子炉実験所専門研究会「不安定原子核の理工学と物性応用研究 III」, 大阪, 12 月 (2013).

上野秀樹: "理研 RIBF 施設と最近の研究成果", 首都大学東京物理学教室談話会, 八王子, 2 月 (2014).

上野秀樹: "低速偏極 RI ビーム", 第 7 回　停止・低速不安定核ビームを用いた核分光研究会（SSRI-7）, 和光, 3 月 (2014).

今村慧, 古川武, 涌井崇志, YANG, Xiaofei, 三津谷洋助, 早坂美希, 嵯峨山翼, 岸翔太, 市川雄一, 白井葉月, 鈴木貴大, 佐藤智哉, 大友祐一, 小島修一郎, 畠山温, 小林徹, 小田島仁司, 旭耕一郎, 上野秀樹, 松尾由賀利: "超流動ヘリウム中へ打ち込まれた原子のゼーマン準位構造及び超微細構造測定", 第 7 回　停止・低速不安定核ビームを用いた核分光研究会（SSRI-7）, 和光, 3 月 (2014).

市川雄一: "スピン操作した RI ビームの生成", 日本物理学会第 69 回年次大会, 平塚, 3 月 (2014).

白井葉月, 市川雄一, 上野秀樹, 石橋陽子, 鈴木貴大, 古川武, 吉見彰洋, 阿部康志, 旭耕一郎, DAUGAS, Jean-Michel, 藤田朋美, 早坂美希, 今村慧, 岸翔太, 小島修一郎, 長江大輔, 中尾愛子, 大友祐一, 嵯峨山翼, 坂本雄, 佐藤智哉: " 中性子過剰核 S 同位体の核磁気モーメント", 日本物理学会第 69 回年次大会, 平塚, 3 月 (2014).

小島修一郎, 佐藤智哉, 市川雄一, 大友祐一, 坂本雄, 鈴木貴大, 白井葉月, 近森正敏, 彦田絵里, 宮武裕和, 七尾翼, 鈴木都文, 土屋真人, 井上壮志, 古川武, 吉見彰洋, BIDINOSTI, Christopher P., 猪野隆, 上野秀樹, 松尾由賀利, 福山武志, 旭耕一郎: "EDM 測定のためのスピンメーザーデジタルフィードバックシステム", 日本物理学会第 69 回年次大会, 平塚, 3 月 (2014).

坂本雄, BIDINOSTI, Christopher P., 市川雄一, 佐藤智哉, 大友祐一, 小島修一郎, 鈴木貴大, 白井葉月, 近森正敏, 彦田絵里, 宮武裕和, 七尾翼, 鈴木都文, 土屋真人, 井上壮志, 古川武, 吉見彰洋, 猪野隆, 上野秀樹, 松尾由賀利, 福山武志, 旭耕一郎: "EDM 測定に向けた改良型磁場安定化システムの構築と性能評価 2", 日本物理学会第 69 回年次大会, 平塚, 3 月 (2014).

大友祐一, 市川雄一, 佐藤智哉, 坂本雄, 小島修一郎, 鈴木

貴大, 白井 葉月, 近森 正敏, 彦田 絵里, 宮武 裕和, 七尾翼, 鈴木 都文, 土屋 真人, 井上 壮志, 古川 武, 吉見 彰洋, BIDINOSTI, Christopher P., 猪野 隆, 上野 秀樹, 松尾由賀利, 福山 武志, 旭 耕一郎: "Performance evaluation of cell with coexisting ^{129}Xe/^{3}He", 日本物理学会第 69 回年次大会, 平塚, 3 月 (2014).

佐藤 智哉, 市川 雄一, 大友 祐一, 坂本 雄, 小島 修一郎, 鈴木貴大, 白井 葉月, 近森 正敏, 彦田 絵里, 宮武 裕和, 七尾翼, 鈴木 都文, 土屋 真人, 井上 壮志, 古川 武, 吉見 彰洋, BIDINOSTI, Christopher P., 猪野 隆, 上野 秀樹, 松尾由賀利, 福山 武志, 旭 耕一郎: "^{3}He 共存磁力計の導入による ^{129}Xe 原子 EDM 測定実験", 日本物理学会第 69 回年次大会, 平塚, 3 月 (2014).

藤田朋美, 古川武, 今村慧, YANG, Xiaofei, 三津谷洋助, 早坂美希, 嵯峨山翼, 岸翔太, 小林徹, 上野秀樹, 下田正, 松尾由賀利: "超流動ヘリウム中 Au 原子の超微細構造測定", 日本物理学会第 69 回年次大会, 平塚, 3 月 (2014).

High Energy Astrophysics Laboratory

Publications

[Journal]

(Original Papers) *Subject to Peer Review

Yamada, S., Torii, S., Mineshige, S., Ueda, Y., Kubota, A., Gandhi, P., Done, C., Noda, H., Yoshikawa, A., Makishima, K.: "Highly Ionized Fe-K Absorption Line from Cygnus X-1 in the High/Soft State Observed with Suzaku" Astrophysical Journal Letter 767, L35 (2013).

Yamada, S., Negoro, H., Torii, S., Noda, H., Mineshige, S., Makishima, K.: "Rapid Spectral Changes of Cygnus X-1 in the Low/Hard State with Suzaku" Astrophysical Journal Letter 767, L34 (2013).

Yamada, S., Makishima, K., Done, C., Torii, S., Noda, H., Sakurai, S.: "Evidence for a Cool Disk and Inhomogeneous Coronae from Wide-Band Temporal Spectroscopy of Cygnus X-1 with Suzaku" Publications of the Astronomical Society of Japan 65, 80 (2013).

Sakurai, S., Torii, S., Noda, H., Zhang, Z., Ono, K., Nakazawa, K., Makishima, K., Takahashi, H., Yamada, S., Matsuoka, M.: "Suzaku studies of luminosity-dependent changes in the low-mass X-ray binary Aquila X-1" Publications of the Astronomical Society of Japan 66, 10 (2014).

Kouzu, T., Tashiro, M. S., Terada, Y., Yamada, S., Bamba, A., Enoto, T., Mori, K., Fukazawa, Y., Makishima, K.: "Spectral Variation of Hard X-Ray Emission from the Crab Nebula with the Suzaku Hard X-Ray Detector" Publications of the Astronomical Society of Japan 65, 74 (2013).

Asami, F., Enoto, T., Iwakiri, W., Yamada, S., Tamagawa, T., Mihara, T., Nagase, F.: "Broad-band spectroscopy of Hercules X-1 with Suzaku" Publications of the Astronomical Society of Japan 66, 44 (2014)

Enoto, T., Sasano, M., Yamada, S., Tamagawa, T., Makishima, K., Pottschmidt, K., Marcu, D., Corbet, R. H. D., Fuerst, F., Wilms, J.: "Spectral and Timing Nature of the Symbiotic X-Ray Binary 4U 1954+319: The Slowest Rotating Neutron Star in an X-Ray Binary System" Astrophysical Journal 786, 127 (2014).

Winkler, P. F., Williams, B. J., Reynolds, S. P., Petre, R., Long, K. S., Katsuda, S., Hwang, U.: "A High-resolution X-Ray and Optical Study of SN 1006: Asymmetric Expansion and Small-scale Structure in a Type Ia Supernova Remnant" Astrophysical Journal 781, 65 (2013).

Katsuda, S., Maeda, K., Nozawa, T., Pooley, D., Immler, S.: "SN 2005ip: A Luminous Type IIn Supernova Emerging from a Dense Circumstellar Medium as Revealed by X-Ray Observations" Astrophysical Journal 780, 184 (2013).

Katsuda, S., Ohira, Y., Mori, K., Tsunemi, H., Uchida, H., Koyama, K., Tamagawa, T.: "Dynamics of X-Ray-emitting Ejecta in the Oxygen-rich Supernova Remnant Puppis A Revealed by the XMM-Newton Reflection Grating Spectrometer" Astrophysical Journal 768, 182 (2013).

Iwahashi, T., Enoto, T., Yamada, S., Nishioka, H., Nakazawa, K., Tamagawa, T., Makishima, K.: "Suzaku Follow-Up Observation of the Activated Magnetar 1E 1547.0-5408" Publications of the Astronomical Society of Japan 65, 52 (2013).

An, H., Hascoet, R., Kaspi, V. M., Beloborodov, A. M., Dufour, F., Gotthelf, E. V., Archibald, R., Bachetti, M., Boggs, S. E., Christensen, F. E., Craig, W. W., Greffenstette, B. W., Hailey, C. J., Harrison, F. A., Kitaguchi, T., Kouveliotou, C., Madsen, K. K., Markwardt, C. B., Stern, D., Vogel, J. K., Zhang, W. W.: "NuSTAR Observations of Magnetar 1E 1841-045" Astrophysical Journal 779, 163 (2013).

Tsuchiya, H., Enoto, T., Iwata, K., Yamada, S., Yuasa, T., Kitaguchi, T., Kawaharada, M., Nakazawa, K., Kokubun, M., Kato, H., Okano, M., Tamagawa, T., Makishima, K.: "Hardening and Termination of Long-Duration γ Rays Detected Prior to Lightning" Physical Review Letters 111, 015001 (2013).

Konami, S., Matsushita, K., Nagino, R., Tamagawa, T.: "Abundance Patterns in the Interstellar Medium of Early-type Galaxies Observed with Suzaku" Astrophysical Journal 783, 8 (2014).

Grefenstette, B. W., Harrison, F. A., Boggs, S. E., Reynolds, S. P., Fryer, C. L., Madsen, K. K., Wik, D. R., Zoglauer, A., Ellinger, C. I., Alexander, D. M., An, H., Barret, D., Christensen, F. E, Craig, W. W., Forster, K., Giommi, P., Hailey, C. J., Hornstrup, A., Kaspi, V. M., Kitaguchi, T., Koglin, J. E., Mao, P. H., Miyasaka, H., Mori, K., Perri, M., Pivovaroff, M. J., Puccetti, S., Rana, V., Stern, D., Westergaard, N. J., Zhang, W. W.: "Asymmetries in core-collapse supernovae from maps of radioactive ^{44}Ti in Cassiopeia A" Nature 506, 339-342 (2014).

Kitaguchi, T., An, H., Beloborodov, A. M., Gotthelf, E. V., Hayashi, T., Kaspi, V. M., Rana, V. R., Boggs, S. E., Christensen, F. E., Craig, W. W., Hailey, C. J., Harrison, F. A., Stern, D., Zhang, W. W.: "NuSTAR and Swift Observations of the Fast Rotating Magnetized White Dwarf AE Aquarii" Astrophysical Journal 782, 3 (2014).

[Book · Proceedings]

(Original Papers) *Subject to Peer Review

Uchida, H., Tanaka, T., Katsuda, S., Mori, K., Koyama, K., Tsunemi, H.: "Enhancement of the Forbidden Line in the Southwestern Knot of the Cygnus Loop" 40th COSPAR Scientific Assembly, COSPAR Meeting Proceedings 40, 3429 (2013)

Katsuda, S., "Revisiting the Southwestern Limb of RCW˜86 with the Chandra X-Ray Observatory" 40th COSPAR Scientific Assembly, COSPAR Meeting Proceedings 40, 1426 (2013)

Reynolds, S., Katsuda, S., Petre, R., Long, K. S., Winkler,

P. F., Ressler, S., Williams, B.: “Constraints on shock acceleration physics from the Chandra Large Project observations of SN 1006” 40th COSPAR Scientific Assembly, COSPAR Meeting Proceedings 40, 2738 (2013)

Wakabayashi, M., Komiya, K., Tamagawa, T., Takeuchi, Y., Aoki, K., Taketani, A., Hamagaki, H.: “Development of a Diehard GEM using PTFE insulator substrate” Journal of Instrumentation 9, C3043 (2014).

(Review)

佐藤悟朗, 渡辺 伸: “テルル化カドミウム半導体を用いたガンマ線イメージャの開発とこれを支えるアナログ ASIC 技術” 日本真空学会誌 57, 57-65 (2014)

(Others)

榎戸輝揚: “ふり返れば『坂の上ではダメである』” 東京大学大学院理学系研究科・理学部ニュース, 世界に羽ばたく理学博士第 13 回, 2014 年 1 月

Oral Presentations

(International Conference etc.)

Enoto, T.: “X-ray View of Magnetars, the strongest magnet in the Universe?” Montana State University Invited Colloquium, Montana State University, USA, April (2013)

Enoto, T.: “Diversity and Evolution of Neutron Stars and Magnetars” Supernovae and Gamma-Ray Burst 2013, Yukawa Institute for Theoretical Physics (YITP), Kyoto University, Kyoto, Japan, October (2013)

Enoto, T.: “Observational Indication with Suzaku on the Toroidal Magnetic Field inside a Magnetar” International Symposium on Neutron Star Matter, Yukawa Institute for Theoretical Physics (YITP), Kyoto University, Kyoto, Japan, October (2013)

Yamada, S.: “Suzaku Wide-band and Temporal Analysis of Cygnus X-1: inhomogeneous coronae and cool disk” Prague Synergy 2013, Prague, Chech, Nobember (2013).

Sato, G.: “Development of a High Counting Rate ASIC for Heavy-ion Beam Monitoring” International Hiroshima Symposium on the Development and Application of Semiconductor Tracking Detectors, Hiroshima, Japan, September (2013)

Sato, G: “CdTe Imagers for X-ray Astronomy” The 12th Symposium on X-ray Imaging Optics, Osaka, Japan, November (2013)

(Domestic Conference)

佐藤悟朗: “ASTRO-H 衛星搭載硬 X 線イメージャ (HXI) の開発” 宇宙科学技術連合講演会, 米子, 10 月 (2013).

榎戸輝揚: “中性子星の物理と観測” 新学術領域「実験と観測で解き明かす中性子星の核物質」第二回中性子星ウィンタースクール・中性子星の核物質, 理化学研究所, 和光, 12 月 (2013)

榎戸輝揚: “Persistent X-ray Emission rom the Expanding Magnetar Class” マグネター研究交流会理化学研究所, 和光, 12 月 (2013)

榎戸輝揚: “すざく、Swift 衛星によるマグネター観測の現状と将来展望” 宇宙線研究所小研究会「強磁場中性子星の構造と粒子加速・電磁波放出過程」, 宇宙線研究所、東京大学柏キャンパス 10 月 (2013)

吉川瑛文, 山田真也, 杉崎睦, 松岡勝, 三原建弘, 玉川徹, 中平聡志, 根來 均: “ブラックホール連星 Swift J1753.5–0127 の短時間ソフト化の詳細解析” 日本天文学会 2013 年秋季年会, (日本天文学会), 東北大学, 9 月 (2013).

玉川徹, 早藤麻美, 北口貴雄, 榎戸輝揚, 山田真也, 岩切 渉, 阿佐美ふみ, 吉川瑛文, 武内陽子, 金子健太, 幸村孝由, 田原譲, 高橋忠幸, 牧島一夫, Keith Jahoda, Joanne Hill, ほか GEMS collaboration, 林田清, 郡司修一, 米徳大輔, ほか PolariScollaboration: “X 線偏光観測衛星 GEMS の現状と PolariS との協力” 日本天文学会 2013 年秋季年会, (日本天文学会), 東北大学, 9 月 (2013).

勝田 哲, 大平 豊, 森 浩二, 常深博, 内田裕之, 小山勝二, 玉川徹 “X 線精密分光で明らかにする Puppis A SNR 爆発噴出物の運動学” 日本天文学会 2013 年秋季年会, (日本天文学会), 東北大学, 9 月 (2013).

榎戸輝揚: “マグネター 磁場エネルギーで輝く宇宙最強の磁石星 ” 学融合プロジェクト「自然界の様々なスケールに現れる高エネルギージェットの解明」全体会合, KEK, つくば市, 10 月 (2013)

榎戸輝揚: “見直しが必要か？X 線連星の分類と中性子星の磁場” 連星天文学研究会, 基礎物理学研究所, 京都大学, 2 月 (2014)

榎戸輝揚: “超新星が残す不思議な星々” フロンティア物理講演会, 山形大学, 2 月 (2014)

武内陽子, 玉川徹, 北口貴雄, 岩切渉, 阿佐美ふみ, 吉川瑛文, 早藤麻美, 榎戸輝揚, 山田真也, 金子健太, 幸村孝由, ほか X 線偏光計チーム: “低圧の純ジメチルエーテル下での GEM 動作特性” 日本物理学会 2013 年秋季大会, (日本物理学会), 高知大, 9 月 (2013).

楳本大悟, 土屋晴文, 榎戸輝揚, 山田真也, 湯浅孝行, 川原田円, 北口貴雄, 中澤知洋, 国分紀秀, 岩田憲一, 加藤博, 岡野眞治, 玉川徹, 牧島一夫: “2012 年中における日本海沿岸の冬季雷雲からのガンマ線観測” 日本物理学会 2013 年秋季大会, (日本物理学会), 高知大, 9 月 (2013).

Takao Kitaguchi, Kevin Black, Teruaki Enoto, Scott Griffiths, Asami Hayato, Joanne Hill, Keith Jahoda, Philip Kaaret, Hannah Marlowe, Toru Tamagawa “Performance Evaluation of Micro-pattern Gas Polarimeter with Synchrotron X-ray Beamline” 日本物理学会 2013 年秋季大会, (日本物理学会), 高知大, 9 月 (2013).

佐藤悟朗, 国分紀秀, 中澤知洋, 内山秀樹, 内山泰伸, 榎戸輝揚, 太田方之, 大野雅功, 小高裕和, 片岡淳, 川原田円, 佐藤理江, 高橋忠幸, 高橋弘充, 武田伸一郎, 田島宏康, 田中孝明, 寺田幸功, 深沢泰司, 牧島一夫, 水野恒史, 谷津陽一, 山岡和貴, 湯浅孝行, 渡辺伸, Olivier Limousin, Philippe Laurent, Francois Lebrun, ほか HXI チーム: “ASTRO-H 衛星搭載硬 X 線撮像検出器 (HXI) の開発の現状” 日本物理学会 2013 年秋季大会, (日本物理学会), 高知大, 9 月 (2013).

玉川徹, 早藤麻美, 北口貴雄, 榎戸輝揚, 山田真也, 岩切 渉, 阿佐美ふみ, 吉川瑛文, 武内陽子, 金子健太, 幸村孝由, 田原譲, 高橋忠幸, 牧島一夫, Keith Jahoda, Joanne Hill, ほか GEMS collaboration, 林田清, 郡司修一, 水野恒史, 米徳大輔, ほか PolariS collaboration: “X 線偏光観測衛星

GEMS の現状（II）” 日本天文学会 2014 年春季年会, (日本天文学会), 国際基督教大学, 3 月 (2014).

窪田恵, 金子健太, 武内陽子, 吉川瑛文, 阿佐美ふみ, 北口貴雄, 玉川徹, 岩切渉, 山田真也, 榎戸輝揚, “X 線ビームラインの高偏光化と較正用コンプトン散乱型偏光計の性能評価” 日本天文学会 2014 年春季年会, (日本天文学会), 国際基督教大学, 3 月 (2014).

竹井洋, 満田和久, 山崎典子, 辻本匡弘, 小川美奈, 杉田寛之, 佐藤洋一, 篠崎慶亮, 岡本篤, 藤本龍一, 大橋隆哉, 石崎欣尚, 江副祐一郎, 三石郁之, 小波さおり, 田代信, 寺田幸功, 北本俊二, 星野晶夫, 瀬田裕美, 玉川徹, 山田真也, 石川久美, 佐藤浩介, 太田直美, 澤田真理, 村上正秀, 村上弘志, 伊豫本直子, R.L. Kelley, C.A. Kilbourne, 他 ASTRO-H SXS チーム: “ASTRO-H 搭載 精密軟 X 線分光装置 SXS の開発の現状 XI” 日本天文学会 2014 年春季年会, (日本天文学会), 国際基督教大学, 3 月 (2014).

佐藤悟朗, 国分紀秀, 中澤知洋, 高橋忠幸, 渡辺 伸, 川原田円, 太田方之, 佐藤理江, 武田伸一郎, 小高裕和, 湯浅孝行, 林 克洋, 原山 淳, 牧島一夫, 野田博文, 片岡 淳, 谷津陽一, 中森健之, 内山秀樹, 田島宏康, 山岡和貴, 深沢泰司, 水野恒史, 高橋弘充, 大野雅功, 寺田幸功, 榎戸輝揚, 田中孝明, 内山泰伸, Olivier Limousin, Philippe Laurent, Francois Lebrun, ほか ASTRO-H HXI チーム: “ASTRO-H 衛星搭載硬 X 線撮像検出器（HXI）開発の現状” 日本天文学会 2014 年春季年会, (日本天文学会), 国際基督教大学, 3 月 (2014).

山田真也, D.A. Bennett, W.B. Doriese, J.W. Fowler, K.D. Irwin, 石元茂, 岡田信二, G.C. O’Neil, 佐藤将春, D.R.Schmidt, D.S. Swetz, 竜野秀行, J.N. Ullom: “超伝導 TES カロリメータを用いた K 中間子原子 X 線の精密分光プロジェクト” 日本天文学会 2014 年春季年会, (日本天文学会), 国際基督教大学, 3 月 (2014).

満田和久, 山崎典子, 竹井洋, 辻本匡弘, 小川美奈, 杉田寛之, 佐藤洋一, 篠崎慶亮, 岡本篤, 藤本龍一, 大橋隆哉, 石崎欣尚, 江副祐一郎, 三石郁之, 小波さおり, 田代信, 寺田幸功, 北本俊二, 星野晶夫, 瀬田裕美, 玉川徹, 山田真也, 石川久美, 佐藤浩介, 太田直美, 澤田真理, 村上正秀, 村上弘志, R.L. Kelley, C.A. Kilbourne, 他 ASTRO-H SXS チーム: “ASTRO-H 搭載 精密軟 X 線分光装置 SXS の開発の現状 (VI)” 日本物理学会第 69 回年次大会, (日本物理学会), 東海大, 3 月 (2014).

楪本大悟, 土屋晴文, 榎戸輝揚, 山田真也, 湯浅孝行, 川原田円, 北口貴雄, 中澤知洋, 国分紀秀, 加藤博, 岡野眞治, 玉川徹, 牧島一夫: “2012 年以降の日本海沿岸の冬季雷雲からの粒子線観測” 日本物理学会第 69 回年次大会, (日本物理学会), 東海大, 3 月 (2014).

玉川徹, 早藤麻美, 北口貴雄, 榎戸輝揚, 山田真也, 岩切渉, 阿佐美ふみ, 吉川瑛文, 武内陽子, 金子健太, 幸村孝由, 田原譲, 高橋忠幸, 牧島一夫, Keith Jahoda, Joanne Hill, ほか GEMS チーム: “X 線偏光観測衛星 GEMS 開発の現状（III）” 日本物理学会第 69 回年次大会, (日本物理学会), 東海大, 3 月 (2014).

玉川 徹, 早藤麻美, 北口貴雄, 榎戸輝揚, 山田真也, 岩切 渉, 阿佐美ふみ, 吉川瑛文, 武内陽子, 金子健太, 幸村孝由, 田原譲, 高橋忠幸, 牧島一夫, Keith Jahoda, Joanne Hill, ほか GEMS チーム, 林田清, ほか PolariS チーム: “X 線偏光観測衛星 GEMS の現状と今後” 宇宙科学シンポジウム, (宇宙航空研究開発機構 宇宙科学研究所), 相模原, 1 月 (2014).

Astro-Glaciology Research Unit

Publications

[Journal]

(Original Papers) ＊Subject to Peer Review

Motizuki Y., Nakai Y., Takahashi K., Igarashi M., Motoyama H., Suzuki K.: "Dating of a Dome Fuji (Antarctica) shallow ice core by volcanic signal synchronization with B32 and EDML1 chronologies", The Cryosphere Discussions, vol. 8, No. 1, pp. 769-804, (2014). ＊

Motizuki Y., Nakai Y., Takahashi K., Igarashi M., Motoyama H., Suzuki K.: "Dating of a Dome Fuji (Antarctica) shallow ice core by volcanic signal synchronization with B32 and EDML1/EDC3 chronologies", RIKEN Accel. Prog. Rep. vol. 46, p. 126, (2013) ＊

Kikuchi S., Okamoto S., Takahashi K., Nakai Y., Motizuki Y.: "Annually-resolved water isotope measurements in a shallow ice core drilled in a vicinity of Dome Fuji station, East Antarctica", RIKEN Accel. Prog. Rep., vol. 46, p.125, (2013). ＊

Sekiguchi K., Nakai Y., Imamura T., Akiyoshi H., Motizuki Y.: "Modeling Chemical Reactions in the Middle Atmosphere Induced by Solar Energetic Particle Events", RIKEN Accel. Prog. Rep., vol. 46, p.124, (2013). ＊

Okamoto S., Takahashi K., Motoyama H., Makabe A., Koba K., Motizuki Y.: "Measurement of nitrogen and oxygen isotope ratios of nitrate in a shallow ice core drilled in a vicinity of Dome Fuji station, East Antarctica", RIKEN Accel. Prog. Rep., vol. 46, p.123, (2013). ＊

[Book ・Proceedings]

(Proceedings)

Famiano M., Boyd N. R., Kajino T., Meyer B., Motizuki Y. , Roederer I.: "Implementing the r-process in metal-poor stars via black hole collapse and relevance to the light element enhancement", Journal of Physics Conference Series, 445, pp. 2025-2029. (2013). ＊

Oral Presentations

(International Conference etc.)

Motizuki Y.: "Diagnose oscillation properties observed in an Antarctic ice core oxygen isotope record", AGU 2013 Fall Meeting, San Francisco, USA, Dec. (2013).

Sigl M., McConnell J.R., Toohey M., Maselli O., Pasteris D., Layman L., Isaksson E., Kawamura K., Motizuki Y., Edwards R., Curran M., Das S., Krueger K.: "Volcanic forcing during the Common Era reevaluated based on new ice core evidence", AGU 2013 Fall Meeting, San Francisco, USA, Dec.(2013).

Motizuki Y.: "Diagnosis of Yearly-Resolved Nitrate Content Obtained from Dome Fuji, East Antarctica, as an Indicator of Solar Variability", Int. CAWSES-II Symposium, Nagaya, Nov. (2013).

Miyake F., Suzuki A., Masuda K., Horiuchi K., Motoyama, H., Matsuzaki H., Motizuki Y., Okamoto S., Takahashi K., Nakai Y.: "The AD 775 cosmic ray event shown in 10Be yearly data from the Antarctic Dome Fuji ice core"(a poster paper), Int. CAWSES-II Symposium, Nagoya, Nov.(2013).

Motizuki Y., Sekiguchi K., Nakai Y., Akiyoshi H., Imamura T.: "Influence of a giant solar energetic particle event on atmospheric chemistry", Int. session on Space Weather, Japan Geoscience Union Meeting 2013, Chiba, May (2013).

(Domestic Conference)

望月優子: "DFS10 コア過去 2000 年・１年時間分解能の水同位体およびイオン分析とその考察", 2013 年度第一回 ICC（ドームふじアイスコアコンソーシアム）運営委員会, 立川, 3 月(2014).

望月優子: "DFS10 アイスコアの酸素同位体比 10 年周期と太陽活動との関連", 第 13 回 NEXT ディスカッション・ミーティング「アイスコア中の水同位体比と太陽活動」, 立川, 3 月(2014)

望月優子: "過度なストレスから心と身体の健康を守ってよい研究を～知らないと損する１０の知恵～ ", 日本天文学会 2014 年春季年会「女性天文研究者の会」, 三鷹, 3 月(2014)

望月優子: "氷床コア中の超新星爆発の痕跡と放射線によるオゾン層破壊", 葉山, 12 月(2013).

藤田秀二, 堀彰, 望月優子, 高橋和也, 中井陽一, 川村賢二, 本山秀明:「南極ドームふじ近傍の氷床における、フィルン層の圧密」, "Densification of layered firn of hte ice sheet in the vicinity of Dome Fuji, Antarctica", 極域科学シンポジウム, 立川, 11 月(2013)

望月優子: "DFS10（JARE51）表面積雪＋浅層コアのイオン濃度と水同位体比、過去 2000 年の新結果", 平成 25 年度低温科学研究所共同研究「南極表面雪中に含まれる不純物解析と物質起源・輸送過程の復元に関する研究集会」, 札幌, 9 月(2013).

田代信, 遠藤輝, 坂本明弘, 山岡和貴, 大野雅功, 寺田幸功, 望月優子、ほか HXD-WAM チーム: "すざく衛星搭載 WAM による太陽フレア硬 X 線放射観測", 平成 25 年度第 1 回 STE 現象報告会, 小金井, 8 月(2013).

望月優子: "太陽活動と気候変動～昔、今、そして未来予測。私たちと宇宙とはつながっている～", 「国民との科学・技術対話」第 5 回目 平成２５年度 女子中高生夏の学校２０１３～科学・技術者のたまごたちへ～, 嵐山(埼玉), 8 月(2013).

望月優子, 中井陽一, 高橋和也, 岡本祥子, 秋吉英治, 今村隆史, 本山秀明: "太陽活動と気候変動に関する研究と動向～過去、現在、未来～", 第 2 回 NEXT ワークショップ「気候変動の理論研究にフォーカスして」, 和光, 6 月(2013).

岡本祥子, 高橋和也, 本山秀明, 眞壁明子, 木庭啓介, 望月優子: "南極ドームふじ南 10 km 地点掘削 (2010 年) 浅層コアにおける硝酸塩同位体比の測定", 日本地球惑星科学連合 2013 年連合大会, 千葉, 5 月(2013).

秋吉英治, 山下陽一, 門脇正尚, 関口健太郎, 中井陽一, 今村隆史, 望月優子: "太陽プロトンイベントが極域大気の硝酸およびオゾン濃度に及ぼす影響に関する数値実験", 日本地球惑星科学連合 2013 年連合大会, 千葉, 5 月(2013).

Superheavy Element Production Team

Publications

[Journal]

(Original Papers) *Subject to Peer Review

Sumita T., Morimoto K., Kaji D., and Morita K.: "New Result on the Production of ^{277}Cn by the ^{208}Pb + ^{70}Zn Reaction", J. Phys. Soc. Jpn. **82**, 024202 (2013).

Murakami M., Kaji D., Morimoto K., and Morita K.: "Excitation function of Rf isotopes in the ^{248}Cm + ^{18}O reaction", Phys. Rev. C **88**, 024618 (2013).

Haba H., Kaji D., Morimoto K., and Morita K.: "Production of ^{262}Db in the ^{248}Cm(^{19}F, 5n)^{262}Db reaction and decay properties of ^{262}Db and ^{258}Lr", Phys. Rev. C **89**, 024618 (2014).

Kaji D., Morimoto K., and Tokanai F.: "Beam intensity monitor based on gas scintillation emitted from helium gas molecules in a gas-filled recoil ion separator", Nucl. Instr. and Meth. B317, p.311 (2014).

Even J., Yakushev A., Düllmann Ch. E., Haba H., Asai M., Sato T. K., Brand H., Di Nitto A., Eichler R., Fan F. L., Hartmann W., Huang M.,x Jäger M., Kaji D., Kanaya J., Kaneya Y., Khuyagbaatar J., Kindler B., Kratz J. V., Krier J., Kudou Y., Kurz N., Lommel B., Miyashita S., Morimoto K., Morita K., Murakami M., Nagame Y., Nitsche H., Ooe K., Qin Z., Schädel M., Steiner J., Sumita T., Takeyama M., Tanaka K., Toyoshima A., Tsukada K., Türler A., Usoltsev I., Wakabayashi Y., Wang Y., Wiehl N., Yamaki S.: "Synthesis and detection of a seaborgium carbonyl complex", *Science* **345**, 1491 (2014).

[Book · Proceedings]

(Original Papers) *Subject to Peer Review

Kaji D., Morimoto K., Haba H., Wakabayashi Y., Kudou Y., Huang M., Goto S., Murakami M., Goto N., Koyama T., Tamura N., Tsuto S., Sumita T., Tanaka K., Takeyama M., Yamaki S., and Morita K.: "Startup of a new gas-filled recoil separator GARIS-II ", J. Radioanal. Nucl. Chem. (2015). [DOI:10.1007/s10967-014-3706-9]

Kaji D., Morimoto K., Haba H., Wakabayashi Y., Kudou Y., Huang M., Goto S., Murakami M., Goto N., Koyama T., Tamura N., Tsuto S., Sumita T., Tanaka K., Takeyama M., Yamaki S., and Morita K.: "Research and development of a new gas-filled recoil separator GARIS-II ", JPS Conf. Proc. 1, p.013051 (2014).

Kaji D., Morimoto K., Sato N., Yoneda A., and Morita K.: "Gas-filled recoil ion separator GARIS-II ", Nucl. Instr. and Meth. B317, p.311 (2013).

Even J., Ackermann D., Asai M., Block M., Brand H., Di Nitto A., Düllmann C. E., Eichler R., Fan F., Haba H., Hartmann W., Hübner A., Heßberger F. P., Huang M., Ja¨ger E., Kaji D., Kanaya J., Kaneya Y., Khuyagbaatar J., Kindler B., Kratz J. V., Krier J., Kudou Y., Kurz N., Laatiaoui M., Lommel B., Maurer J., Miyashita S., Morimoto K., Morita K., Murakami M., Nagame Y., Nitsche H., Ooe K., Qin Z., Sato T. K., Scha¨del M., Steiner J., Sumita T., Takeyama M., Tanaka K., Toyoshima A., Tsukada K., Türler A., Usoltsev I., Wakabayashi Y., Wang Y., Wiehl N., Yakushev A., and Yamaki S.: "In situ synthesis of volatile carbonyl complexes with short-lived nuclides" J Radioanal Nucl Chem, DOI 10.1007/s10967-014-3793-7

Morimoto K.: " 新元素探索の最前線", 放射線 Vol. 40, No.2, 2014, 93

Oral Presentations

(International Conference etc.)

Morimoto K.: "Discovery of superheavy nucleus ^{278}113 -New Result in the Production and Decay of ^{278}113-"XXXIII Mazurian Lakes Conference on Physics (MAZURIAN2013), Piaski, Poland, September (2013).

Morimoto K.: "New result in the production and decay of ^{278}113", French-Japanese Symposium on Nuclear Structure Problems, Paris, France, October (2013).

Morimoto K.: "Status of GARIS and GARIS-II", 9th ASRC International Workshop "Chemistry of the superheavy elements", RIKEN, Japan, March (2013).

Kaji D.: "Present status of superheavy element production target for gas-filled recoil separators GARIS and GARIS-II", INTDS 2014, Japan, September (2014).

Kaji D.: "Performance of New Gas-filled Recoil Ion Separator GARIS-II for Asymmetric Fusion Reaction" "The first α -γ spectroscopic study by using a Si-Ge detector array installed at the focal plane of GARIS", ARIS 2014, Japan, June (2014).

Kaji D.: "SHE experiments with GARIS-I/-II at RIKEN", NUSTAR meeting 2014, Germany, March (2014).

Kaji D.: "Research and development of a new gas-filled recoil separator GARIS-II", APPC12, Japan, July (2013).

Kaji D.: "Startup of a new gas-filled recoil separator GARIS-II", APSORC13, Japan, September (2013).

Kaji D.: "Status of a new gas-filled recoil separator GARIS-II developed for SHE chemistry", CHE8, Japan, September (2013).

Yamaki S., Morimoto K., Kaji D., and Wakabayashi Y.: "Pulse Shape Analysis Using Flash-ADC for Short-lived Decay of Super Heavy Elements", ARIS2014, Tokyo, June (2014).

Morita K., "Recent Results on Superheavy Element Research at RIKEN" Fusion14 International Conference, New Delhi India, Feb. 24-28, 2014.

Morita K., "Research of Superheavy Elements at RIKEN - Present Status and Perspective -", The 2nd Conference on "Advances in Radioactive Isotope Science" (ARIS2014), Tokyo, Japan, June 1 - 6, 2014.

M. Takeyama, D. Kaji, K. Morimoto, Y. Wakabayashi, M. Asai "Detector response to spontaneous fission events of heavy nuclide produced by using 206Pb+48Ca reaction" ARIS2014, Tokyo, Japan, June (2014)

Morita K., "Research of Superheavy Elements at RIKEN - Present Status and Perspective – Zakopane Conference on Nuclear Physics, "Extremes of Nuclear Landscape", Zakopane, Poland, Aug. 31 - Sep. 7 2014.

(Domestic Conference)

若林泰生、西尾勝久、光岡真一、森本幸司、加治大哉、羽場宏光、西中一朗、牧井宏之、住田貴之、米田晃、森田浩介："中性子魔法数 126 領域の中性子欠損したアクチノイド原子核の新同位体合成", 日本物理学会 2013 年秋季大会, 高知, 9 月(2013).

山木さやか: "Flash-ADC により取得したプリアンプ波形のための解析アルゴリズムの開発", 日本物理学会第 68 回年次大会, (日本物理学会), 湘南, 3 月(2014).

田中謙伍: "超重元素生成のための標的開発とそのモニターシステム", 2014 日本放射化学会年会・第 58 回放射化学討論会, 名古屋, 9 月(2014).

加 治 大 哉： "GARIS を用いたホットフュージョン反 応 $^{248}Cm+^{48}Ca\rightarrow^{296}Lv^*$ に関する研究", 第 58 回放射化学討論会, 愛知, 9 月 (2014).

加治大哉: "気体充填型反跳分離装置 GARIS-II の非対称系反応に対する性能試験", 第 58 回放射化学討論会, 愛知, 9 月 (2014).

加治大哉: "GARIS を用いた 113 番元素研究の総括", 第 58 回放射化学討論会, 愛知, 9 月 (2014).

加治大哉: "超重核研究のための焦点面検出器の開発", 第 58 回放射化学討論会, 愛知, 9 月 (2014).

加治大哉: "GARIS-II commissioning #3", 第 69 回 日本物理学会, 神奈川, 3 月 (2014).

加治大哉: "理研における 113 番元素探索(まとめ)", 京都大学原子炉研究所 有用放射性トレーサーの開発と利用に関する専門研究会, 大阪, 1 月 (2014).

加治大哉: "GARIS-II commissioning #2", 第 68 回 日本物理学会, 広島, 3 月 (2013).

森本幸司: "加速器を用いた新元素探索-113 番線元素の発見-第 26 回タンデム加速器及びその周辺技術の研究会 山形, 7 月, (2013).

森本幸司: "新元素探索の最前線", 第 74 回応用物理学会秋季学術講演会 京都, 9 月, (2013).

Superheavy Element Device Development Team

Publications

[Journal]

(Original Papers) *Subject to Peer Review

Sumita T., Morimoto K., Kaji D., and Morita K.: "New Result on the Production of ^{277}Cn by the ^{208}Pb + ^{70}Zn Reaction", J. Phys. Soc. Jpn. **82**, 024202 (2013).

Murakami M., Kaji D., Morimoto K., and Morita K.: "Excitation function of Rf isotopes in the ^{248}Cm + ^{18}O reaction", Phys. Rev. C **88**, 024618 (2013).

Haba H., Kaji D., Morimoto K., and Morita K.: "Production of ^{262}Db in the ^{248}Cm(^{19}F, 5n)^{262}Db reaction and decay properties of ^{262}Db and ^{258}Lr", Phys. Rev. C **89**, 024618 (2014).

Kaji D., Morimoto K., and Tokanai F.: "Beam intensity monitor based on gas scintillation emitted from helium gas molecules in a gas-filled recoil ion separator", Nucl. Instr. and Meth. B317, p.311 (2014).

Even J., Yakushev A., Düllmann Ch. E., Haba H., Asai M., Sato T. K., Brand H., Di Nitto A., Eichler R., Fan F. L., Hartmann W., Huang M.,x Jäger M., Kaji D., Kanaya J., Kaneya Y., Khuyagbaatar J., Kindler B., Kratz J. V., Krier J., Kudou Y., Kurz N., Lommel B., Miyashita S., Morimoto K., Morita K., Murakami M., Nagame Y., Nitsche H., Ooe K., Qin Z., Schädel M., Steiner J., Sumita T., Takeyama M., Tanaka K., Toyoshima A., Tsukada K., Türler A., Usoltsev I., Wakabayashi Y., Wang Y., Wiehl N., Yamaki S.: "Synthesis and detection of a seaborgium carbonyl complex", *Science* **345**, 1491 (2014).

[Book · Proceedings]

(Original Papers) *Subject to Peer Review

Kaji D., Morimoto K., Haba H., Wakabayashi Y., Kudou Y., Huang M., Goto S., Murakami M., Goto N., Koyama T., Tamura N., Tsuto S., Sumita T., Tanaka K., Takeyama M., Yamaki S., and Morita K.: "Startup of a new gas-filled recoil separator GARIS-II ", J. Radioanal. Nucl. Chem. (2015). [DOI:10.1007/s10967-014-3706-9]

Kaji D., Morimoto K., Haba H., Wakabayashi Y., Kudou Y., Huang M., Goto S., Murakami M., Goto N., Koyama T., Tamura N., Tsuto S., Sumita T., Tanaka K., Takeyama M., Yamaki S., and Morita K.: "Research and development of a new gas-filled recoil separator GARIS-II ", JPS Conf. Proc. 1, p.013051 (2014).

Kaji D., Morimoto K., Sato N., Yoneda A., and Morita K.: "Gas-filled recoil ion separator GARIS-II ", Nucl. Instr. and Meth. B317, p.311 (2013).

Even J., Ackermann D., Asai M., Block M., Brand H., Di Nitto A., Düllmann C. E., Eichler R., Fan F., Haba H., Hartmann W., Hübner A., Heßberger F. P., Huang M., Ja¨ger E., Kaji D., Kanaya J., Kaneya Y., Khuyagbaatar J., Kindler B., Kratz J. V., Krier J., Kudou Y., Kurz N., Laatiaoui M., Lommel B., Maurer J., Miyashita S., Morimoto K., Morita K., Murakami M., Nagame Y., Nitsche H., Ooe K., Qin Z., Sato T. K., Scha¨del M., Steiner J., Sumita T., Takeyama M., Tanaka K., Toyoshima A., Tsukada K., Türler A., Usoltsev I., Wakabayashi Y., Wang Y., Wiehl N., Yakushev A., and Yamaki S.: "In situ synthesis of volatile carbonyl complexes with short-lived nuclides" J Radioanal Nucl Chem, DOI 10.1007/s10967-014-3793-7

Morimoto K.: " 新元素探索の最前線", 放射線 Vol. 40, No.2, 2014, 93

Oral Presentations

(International Conference etc.)

Morimoto K.: "Discovery of superheavy nucleus ^{278}113 -New Result in the Production and Decay of ^{278}113-"XXXIII Mazurian Lakes Conference on Physics (MAZURIAN2013), Piaski, Poland, September (2013).

Morimoto K.: "New result in the production and decay of ^{278}113", French-Japanese Symposium on Nuclear Structure Problems, Paris, France, October (2013).

Morimoto K.: "Status of GARIS and GARIS-II", 9th ASRC International Workshop "Chemistry of the superheavy elements", RIKEN, Japan, March (2013).

Kaji D.: "Present status of superheavy element production target for gas-filled recoil separators GARIS and GARIS-II", INTDS 2014, Japan, September (2014).

Kaji D.: "Performance of New Gas-filled Recoil Ion Separator GARIS-II for Asymmetric Fusion Reaction" "The first α -γ spectroscopic study by using a Si-Ge detector array installed at the focal plane of GARIS", ARIS 2014, Japan, June (2014).

Kaji D.: "SHE experiments with GARIS-I/-II at RIKEN", NUSTAR meeting 2014, Germany, March (2014).

Kaji D.: "Research and development of a new gas-filled recoil separator GARIS-II", APPC12, Japan, July (2013).

Kaji D.: "Startup of a new gas-filled recoil separator GARIS-II", APSORC13, Japan, September (2013).

Kaji D.: "Status of a new gas-filled recoil separator GARIS-II developed for SHE chemistry", CHE8, Japan, September (2013).

Yamaki S., Morimoto K., Kaji D., and Wakabayashi Y.: "Pulse Shape Analysis Using Flash-ADC for Short-lived Decay of Super Heavy Elements", ARIS2014, Tokyo, June (2014).

M. Takeyama, D. Kaji, K. Morimoto, Y. Wakabayashi, M. Asai "Detector response to spontaneous fission events of heavy nuclide produced by using 206Pb+48Ca reaction" ARIS2014, Tokyo, Japan, June (2014)

(Domestic Conference)

若林泰生、西尾勝久、光岡真一、森本幸司、加治大哉、羽場宏光、西中一朗、牧井宏之、住田貴之、米田晃、森田浩介："中性子魔法数 126 領域の中性子欠損したアクチノイド原子核の新同位体合成", 日本物理学会 2013 年秋季大会, 高知, 9 月(2013).

山木さやか: "Flash-ADC により取得したプリアンプ波形のための解析アルゴリズムの開発", 日本物理学会第 68 回年次大会, (日本物理学会), 湘南, 3 月(2014).

田中謙伍: "超重元素生成のための標的開発とそのモニターシステム", 2014 日本放射化学会年会・第 58 回放射化学討

論会, 名古屋, 9 月(2014).
加 治 大 哉： ”GARIS を用いたホットフュージョン反 応 $^{248}Cm+^{48}Ca \rightarrow ^{296}Lv^*$ に関する研究”, 第 58 回放射化学討論会, 愛知, 9 月 (2014).
加治大哉: ”気体充填型反跳分離装置 GARIS-II の非対称系反応に対する性能試験”, 第 58 回放射化学討論会, 愛知, 9 月 (2014).
加治大哉: ”GARIS を用いた 113 番元素研究の総括”, 第 58 回放射化学討論会, 愛知, 9 月 (2014).
加治大哉: ”超重核研究のための焦点面検出器の開発”, 第 58 回放射化学討論会, 愛知, 9 月 (2014).
加治大哉: “GARIS-II commissioning #3”, 第 69 回 日本物理学会, 神奈川, 3 月 (2014).
加治大哉: “理研における 113 番元素探索(まとめ)”, 京都大学原子炉研究所 有用放射性トレーサーの開発と利用に関する専門研究会, 大阪, 1 月 (2014).
加治大哉: “GARIS-II commissioning #2”, 第 68 回 日本物理学会, 広島, 3 月 (2013).
森本幸司: “加速器を用いた新元素探索-113 番線元素の発見-第 26 回タンデム加速器及びその周辺技術の研究会 山形, 7 月, (2013).
森本幸司: “新元素探索の最前線”, 第 74 回応用物理学会秋季学術講演会 京都, 9 月, (2013).

Accelerator Group

Publications

[Journal]

(Original Papers) *Subject to Peer Review

Okuno H., Fukunishi N., and Kamigaito O.: "Progress of RIBF Accelerators", Progress of Theoretical and Experimental Physics **2012**, No. 1, 03C002 (2012). *

Fujinawa T.: "RIKEN Nishina Center's Response to the Fukushima Daiichi Nuclear Disaster: Radiation Screening", Journal of Physical Science and Application **3**, No. 1, p. 39–46 (2013). *

Ozeki K., Higurashi Y., Ohnishi J., and Nakagawa T.: "Effect of Biased Disc on Brightness of Highly Charged Uranium Ions from RIKEN 28 GHz", Japanese Journal of Applied Physics **52**, No. 6, 068001 (2013). *

Fujinawa T.: "Development of Cranes Used at Super-Sized Accelerator Facility RIKEN RI Beam Factory", Journal of Material Science and Engineering **A3**, No. 9, p. 640–645 (2013). *

Suda K., Sakamoto N., Yamada K., Arai S., Chiba Y., Kase M., Okuno H., Watanabe Y., and Kamigaito O.: "Design and construction of drift tube linac cavities for RIKEN RI Beam Factory", Nuclear. Instr. and Meth. A **722**, p. 55–64 (2013). *

Urabe T., Takahashi K., Kitagawa M., Kondo T., Enomoto S., Kidera M., and Seto Y.: "Development of portable mass spectrometer with electron cyclotron resonance ion source for detection of chemical warfare agents in air", Spectrochimica Acta Part A: Molecular and Biomolecular Spectroscopy **120**, p. 437–444 (2013). *

Fujinawa T.: "Development of Superconducting Maglev Ground Coils", Journal of Physical Science and Application, **4**, No. 1, p. 36–42 (2014). *

Haba H., Muang M., Kaji D., Kanaya J., Kudou Y., Morimoto K., Morita K., Murakami M., Ozeki K., Sakai R., Sumita T., Wakabayashi Y., Yoneda A., Kasamatsu Y., Kikutani Y., Komori Y., Nakamura K., Shinohara A., Kikunaga H., Kudo H., Nishio K., Toyoshima A., and Tsukada K.: "Production of ^{262}Db in the ^{248}Cm(^{19}F,5n)^{262}Db reaction and decay properties of ^{262}Db and ^{258}Lr", Physical Review C **89**, 024618-1-11 (2014). *

Maeyama T., Fukunishi N., Ishikawa K.L., Furuta T., Fukasaku K., Takagi S., Noda S., Himeno R., and Fukuda S.: "A diffusion-free and linear-energy-transfer-independent nanocomposite Fricke gel dosimeter", Radiation Physics and Chemistry **96**, p. 92–96 (2014). *

(Others)

長谷部裕雄: "Report of the Medical Treatment Screening in Fukushima", 加速器 **8**, No. 3, p. 02A320 (2010).

[Book・Proceedings]

(Original Papers) *Subject to Peer Review

Kamigaito O.: "Rare-Isotope Beam Facilities in Asia", Proceedings of the 12th International Conference on Heavy Ion Accelerator Technology (HIAT2012) p. 28–32 (2012).

Maeyama T., Fukunishi N., Ishikawa K.L., Furuta T., Fukasaku K., Takagi S., Noda S., Himeno R., and Fukuda S.: "Response of aqueous dichromate and nanoclay dichromate gel dosimeters to carbon ion irradiation", Journal of Physics: Conference Series **444**, 012033 (2013). *

Maeyama T., Fukunishi N., Ishikawa K.L., Furuta T., Fukasaku K., Takagi S., Noda S., Himeno R., and Fukuda S.: "Diffusion suppression in gel dosimetry by addition of nanoclay", World Congress on Medical Physics and Biomedical Engineering May 26-31, 2012, Beijing, China **39**, p. 1183–1186 (2013). *

Taylor M.L., Maeyama T., Fukunishi N., Ishikawa K.L., Furuta T., Fukasaku K., Takagi S., Noda S., Himeno R., and Fukuda S.: "Radiological characteristics of charged particle interactions in the first clay-nanoparticle dichromate gel dosimeter", Journal of Physics: Conference Series **444**, 012110 (2013). *

Taylor M.L., Maeyama T., Fukunishi N., Ishikawa K.L., Fukasaku K., Furuta T., Takagi S., Noda S., Himeno R., and Fukuda S.: "A novel clay-nanoparticle dichromate gel: radiological properties for electron and hadron interactions", Australasian Physical & Engineering Sciences in Medicine: 2012 Engineering and Physical Sciences in Medicine Conference **36**, p. 136–137 (2013). *

Suda K., Arai S., Chiba Y., Kamigaito O., Kase M., Okuno H., Watanabe Y., Sakamoto N., Yamada K.: "Design of Coupler for Direct Coupled Amplifier to Drift Tube Linac Cavities of the Injector RILAC2 for RIKEN RI Beam Factory", Proceedings of the 26th International Linear Accelerator Conference (LINAC12) p. 684–686 (2013).

Kamigaito O., Dantsuka T., Fujimaki M., Fujinawa T., Fukunishi N., Hasebe H., Higurashi Y., Ikegami K., Ikezawa E., Imao H., Kageyama T., Kase M., Kidera M., Komiyama M., Kuboki H., Kumagai K., Maie T., Nagase M., Nakagawa T., Nakamura M., Ohnishi J., Okuno H., Ozeki K., Sakamoto N., Suda K., Watanabe H., Watanabe T., Watanabe Y., Yamada K., and Yamasawa H.: "Progress towards High-intensity Heavy-ion beams at RIKEN RIBF", Proceedings of the 4th International Particle Accelerator Conference (IPAC2013) p. 333–335 (2013).

Kamigaito O.: "Overview of the World-wide RIB Facilities - Status and Challenges", Proceedings of the 4th International Particle Accelerator Conference (IPAC2013) p. 4000–4004 (2013).

Nakai Y., Nakano Y., Ikeda T., Kanai Y., Kambara T., Fukunishi N., Kondo C., Azuma T., Komaki K., and Yamazaki Y.: "Stark effect in resonant coherent excitation of 2s electron of Li-like Fe23+ ions channeling in a Si crystal", Nuclear Instruments and Methods in Physics Research Section B: Beam Interactions with Materials and Atoms **299**, p. 1029–1034 (2013). ∗

Kuboki H., Okuno H., Hershcovitch A., Ikegami K., Imao H., Kase M., Kamigaito O., Dantsuka T., Nakagawa T., Hasebe H., Maie T., and Yano Y.: "Development of differential pumping system using plasma window", Journal of Radioanalytical Nuclear Chemistry **299**, p. 1029–1034 (2013). ∗

Okuno H., Fukunishi N., Kuboki H., Hasebe H., Imao H., Kase M., and Kamigaito O.: "Charge strippers for Radioisotope Beam Factory at RIKEN", Journal of radioanalytical and nuclear chemistry **299**, p. 945–949 (2013). ∗

Yamaguchi Y., Wakasugi M., Uesaka T., Ozawa A., Abe Y., Fujinawa T., Kase M., Komiyama M., Kubo T., Kumagai K., Maie T., Nagae D., Ohnishi J., Suzaki F., Tokuchi A., Watanabe Y., Yoshida K., Yamada K., Yamaguchi T., Yamasawa H., Yanagisawa Y., Zenihiro J., and Yano Y.: "Construction of rare-RI ring at RIKEN RI Beam Factory", Nuclear Instruments and Methods in Physics Research **B317**, p. 629–635 (2013). ∗

Hasebe H., Kuboki H., Okuno H., Imao H., Yamane I., Fukunishi N., Kase M., and Kamigaito O.: "Development of a new foil compounded from carbon nanotubes and sputterdeposition carbon", Journal of radioanalytical and nuclear chemistry **299**, p. 1013–1018 (2014). ∗

Imao H., Okuno H., Kuboki H., Kamigaito O., Hasebe H., Fukunishi N., Watanabe Y., Fujimaki M., Maie T., Dantsuka T., Kumagai K., Yamada K., Watanabe T., Kase M., and Yano Y.: "Charge-stripping system for 238U ion beam with recirculating He gas", Journal of radioanalytical and nuclear chemistry **299**, p. 941–944 (2014). ∗

Ohnishi J., Higurashi Y., Kidera M., Ozeki K., and Nakagawa T.: "Development of a high-temperature oven for the 28 GHz electron cyclotron resonance ion source", Review of Scientific Instruments **85**, No. 2, 02A924 (2014). ∗

Ozeki K., Kageyama T., Kidera M., Higurashi Y., and Nakagawa T.: "Operational test of micro-oven for 48Ca beam", Review of Scientific Instruments **85**, No. 2, p. 941–944 (2014). ∗

大関和貴, 日暮祥英, 大西純一, 中川孝秀, "理研 28 GHz 超伝導 ECR イオン源のエミッタンス測定", Proc. of the 9th Annual Meeting of Particle Accelerator Society of Japan p. 252 (2013).

Oral Presentations

(International Conference etc.)

Kamigaito O.: "International Symposium on Vacuum Science & Technology and Its Application for Accelerators", ernational Symposium on Vacuum Science & Technology and Its Application for Accelerators, (Variable Energy Cyclotron Center), Kolkata, India, February (2012).

Maeyama T., Fukunishi N., Ishikawa K.L., Fukasaku K., Furuta T., Takagi S., Noda S., and Himeno R.: "Diffusion suppression in gel dosimetry by addition of nanoclay", World Congress on Medical Physics and Biomedical Engineering (WC2012), Beijing, China, May (2012).

Kamigaito O.: "Rare-Isotope Beam Facilities in Asia", The 12th International Conference on Heavy Ion Accelerator Technology (HIAT2012), (International Organization Committee of HIAT2012), Chicago, USA, June (2012).

Kamigaito O.: 'Status of RIBF Accelerators at RIKEN", Workshop on Science with Rare Ion Beams SCRIBE-2012, (International Organization Committee of SCRIBE2012), Kolkata, India, November (2012).

Maeyama T., Fukunishi N., Ishikawa K.L., Fukasaku K., Furuta T., Takagi S., Noda S., and Himeno R.: "Diffusion suppression in gel dosimetry by addition of nanoclay", World Congress on Medical Physics and Biomedical Engineering (WC2012), Sydney, Australia, November (2012).

Suda K., Sakamoto N., Yamada K., Okuno H., Higurashi Y., Kamigaito O., and Kase M.: "Operation of the RF system for heavy ion accelerators in RIKEN RI Beam Factory", Accelerator Reliability Workshop 2013 (ARW 2013), (Australian Synchrotron), Melbourne, Australia, April (2013).

Fujinawa T.: "Cogeneration system for RIKEN RI Beam Factory", Accelarator Reliability Workshop 2013, (Australian Synchrotron), Melbourne, Australia, April (2013).

Kamigaito O., Dantsuka T., Fujimaki M., Fujinawa T., Fukunishi N., Hasebe H., Higurashi Y., Ikegami K., Ikezawa E., Imao H., Kageyama T., Kase M., Kidera M., Komiyama M., Kuboki H., Kumagai K., Maie T., Nagase M., Nakagawa T., Nakamura M., Ohnishi J., Okuno H., Ozeki K., Sakamoto N., Suda K., Watanabe H., Watanabe T., Watanabe Y., Yamada K., and Yamasawa H.: " Progress towards High-intensity Heavy-ion beams at RIKEN RIBF", The 4th International Particle Accelerator Conference (IPAC2013), (International Organization Committee of IPAC13), Shanghai, China, May (2013).

Imao H.: " Realization of New Charge-state Stripper for High-power Uranium Ion Beams", The 4th International Particle Accelerator Conference (IPAC2013), (International Organization Committee of IPAC13), Shanghai, China, May (2013).

Kamigaito O.: " Overview of the World-wide RIB Facilities - Status and Challenges", The 4th International Particle Accelerator Conference (IPAC2013), (International Organization Committee of IPAC13), Shanghai, China, May (2013).

Okuno H.: "Status Reports on the RIBF accelerators", RIBF users meeting, (RBF users group), Wako, Japan, June (2013).

Okuno H., Dantsuka T., Ohnishi J., Nakamura M.: "Operational experience of the Superconducting Ring cyclotron at RI Beam Factory (RIBF) and upgrade plans for RIBF accelerators", The 23rd International conference on magnet technology, (International Organization Committee of MT23), Boston, USA, July (2013).

Fujinawa T.: "The Major Fukushima Daiichi Nuclear Disaster", The 11th International Workshop of the IEIEJ, (IEIEJ), Osaka, Japan, September (2013).

Fukunishi N., Dantsuka T., Fujimaki M., Fujinawa T., Hasebe H., Higurashi Y., Ikegami K., Ikezawa E., Imao H., Kageyama T., Kamigaito O., Kase M., Kidera M., Komiyama M., Kuboki H., Kumagai K., Maie T., Nagase M., Nakagawa T., Nakamura M., Ohnishi J., Okuno H., Ozeki K., Sakamoto N., Suda K., Uchiyama A., Watanabe T., Watanabe Y., Yamada K., and Yamasawa H.: "Accleration of intense heavy ion beams in RIBF cascaded-cyclotrons", 20th International Conference on Cyclotrons and their Applications, (International Organizaing Committee of 20th International Conference on Cyclotrons and their Applications), Vancouver, Canada, September (2013).

Imao H., Okuno H., Kuboki H., Kamigaito O., Hasebe H., Fukunishi N., Watanabe Y., Fujimaki M., Maie T., Dantsuka T., Kumagai K., Yamada K., Watanabe T., Kase M., and Yano Y.: "R&D of Helium Gas Stripper for Intense Uranium Beams", 20th International Conference on Cyclotrons and their Applications, (International Organizaing Committee of 20th International Conference on Cyclotrons and their Applications), Vancouver, Canada, September (2013).

Watanabe T., Fukunishi N., Kase M., Kamigaito O., Inamori S., and Kon K.: "Development of a beam current monitor that uses a high-Tc SQUID at RIBF", Forschungszentrum Jülich GmbH PGI-5 Colloquium, (Forschungszentrum Jülich GmbH), Jülich , Germany, September (2013).

Okuno H.: " RIKEN Radioactive Isotope Beam Factory (Accelerators and Scientific Results) ", 日中粒子線加速器科技シンポジウム, (日中科学技術交流協会), 上海、蘭州、北京, China, November. (2013).

(Domestic Conference)

前山拓哉, 福西暢尚, 石川顕一, 古田琢哉, 深作和明, 高木周, 野田茂穂, 姫野龍太郎: "フリッケゲル線量計による炭素線の線量分布測定", 第 54 回放射線化学討論会, (日本放射線化学会), 大阪, 9 月 (2011).

前山拓哉, 福西暢尚, 石川顕一, 古田琢哉, 深作和明, 高木周, 野田茂穂, 姫野龍太郎: "ナノクレイ添加による拡散のないゲル線量計の開発", 第 103 回日本医学物理学会学術大会, (日本医学物理学会), 横浜, 4 月 (2012).

前山拓哉, 福西暢尚, 石川顕一, 古田琢哉, 深作和明, 高木周, 野田茂穂, 姫野龍太郎: "炭素線治療における VIPAR ポリマーゲル線量計を用いた線量分布測定・検証の検討", 第 104 回日本医学物理学会学術大会, (日本医学物理学会), つくば, 9 月 (2012).

奥野広樹: "理研 RI ビームファクトリーにおける重イオン加速器技術", 先端加速器科学技術推進協議会 第２７回技術部会, (先端加速器科学技術推進協議会), 東京, 10 月 (2012).

前山拓哉, 福西暢尚, 石川顕一, 古田琢哉, 深作和明, 高木周, 野田茂穂, 姫野龍太郎: "ゲル線量計による重粒子線線量分布測定", 第 1 回 3D ゲル線量計研究会, (林慎一郎（広島国際大学 診療放射線学科）・村上祐司（広島大学病院 放射線治療科）), 広島, 12 月 (2012).

前山拓哉, 福西暢尚, 石川顕一, 古田琢哉, 深作和明, 高木周, 野田茂穂, 姫野龍太郎: "炭素線治療におけるゲル線量計を用いた線量分布測定とシミュレーションとの比較", 第 16 回弥生研究会～放射線効果の解明と応用～, (東京大学、勝村・工藤研究室), 東京, 3 月 (2013).

前山拓哉, 福西暢尚, 石川顕一, 古田琢哉, 深作和明, 高木周, 野田茂穂, 姫野龍太郎: "重粒子線線量分布測定のための VIPAR ポリマーゲル線量計の特性評価", 第 60 回応用物理学会春季学術講演会, (応用物理学会), 神奈川, 3 月 (2013).

前山拓哉, 福西暢尚, 石川顕一, 古田琢哉, 深作和明, 高木周, 野田茂穂, 姫野龍太郎: "炭素線治療における VIPAR ポリマーゲル線量計を用いた線量分布測定・検証の検討 (2)", 第 105 回日本医学物理学会学術大会, (日本医学物理学会), 横浜, 4 月 (2013).

前山拓哉, 福西暢尚, 石川顕一, 古田琢哉, 深作和明, 高木周, 野田茂穂, 姫野龍太郎, 福田茂一: "LET 依存性のないゲル線量計の開発", 平成 24 年度 HIMAC　共同利用研究成果発表会, (放射線医学総合研究所), 千葉, 4 月 (2013).

前山拓哉, 福西暢尚, 石川顕一, 古田琢哉, 深作和明, 高木周, 野田茂穂, 姫野龍太郎, 福田茂一: "PHITS コードを用いた炭素線照射時の VIPAR ゲル線量計の特性評価と線量分布評価", 第 9 回 PHITS 定期講習会/研究会, (日本原子力研究開発機構), 茨城, 8 月 (2013).

藤縄雅, 山口由高, 山澤秀行, 眞家武士, 熊谷桂子, 若杉昌徳: "理研 RIBF 稀少 RI リングの付帯設備", 第 10 回日本加速器学会年会, (日本加速器学会), 名古屋, 8 月 (2013).

今尾浩士, 奥野広樹, 久保木浩功: 第 10 回日本加速器学会年会, (日本加速器学会), 名古屋, 8 月 (2013).

長谷部裕雄, 久保木浩功, 奥野広樹, 今尾浩士, 山根功, 福西暢尚, 加瀬昌之, 上垣外修一: "カーボンナノチューブとカーボン蒸着複合膜の開発", 第 45 回 フラーレン・ナノチューブ・グラフェン　総合シンポジウム, (フラーレン・ナノチューブ・グラフェン学会), 大阪, 8 月 (2013).

前山拓哉, 福西暢尚, 石川顕一, 古田琢哉, 深作和明, 高木周, 野田茂穂, 姫野龍太郎, 福田茂一: "炭素線照射におけるゲル線量計の LET 依存性", 第 56 回放射線化学討論会, (日本放射線化学会、日本化学会), 広島, 9 月 (2013).

久保木浩功, 奥野広樹, HershcovitchAdy, 池上九三男, 今尾浩士, 加瀬昌之, 上垣外修一, 段塚知志, 中川孝秀, 長谷部裕雄, 眞家武士, 矢野安重: "プラズマウィンドウを用いた差動排気システムの開発", プラズマ研究会, (日本電気学会), 長崎, 9 月 (2013).

前山拓哉, 福西暢尚, 石川顕一, 古田琢哉, 深作和明, 高木周, 野田茂穂, 姫野龍太郎, 福田茂一: "ナノクレイを添加したゲル線量計の開発", 第 56 回放射線化学討論会, (電気学会、

ナノメディシンに向けた光・量子ビーム応用技術調査専門委員会，ナノ学会　ナノ機能・応用部会　研究会，日本生体医工学会専門別委員会　次世代治療技術開発の為の細胞組織・分子機能計測・制御研究会), 埼玉, 11 月 (2013).

前山拓哉: “フリッケゲル線量計入門”, 第 2 回 3D ゲル線量計研究会, (林慎一郎（広島国際大学 診療放射線学科）・小西良幸（東京女子医科大学 先端生命医科学研究所）), 東京, 12 月 (2013).

前山拓哉, 福西暢尚, 石川顕一, 古田琢哉, 深作和明, 高木周, 野田茂穂, 姫野龍太郎, 福田茂一: “フリッケゲル線量計の拡散抑制と線質効果の抑制”, 第 2 回 3D ゲル線量計研究会, (林慎一郎（広島国際大学 診療放射線学科）・小西良幸（東京女子医科大学 先端生命医科学研究所）), 東京, 12 月 (2013).

前山拓哉, 福西暢尚, 石川顕一, 古田琢哉, 深作和明, 高木周, 野田茂穂, 姫野龍太郎, 福田茂一: “有機無機複合ゲルをフリッケ水溶液線量計に浸した三次元線量計の開発”, 第 17 回弥生研究会〜放射線効果の解明と応用〜, (東京大学、勝村・工藤研究室), 東京, 12 月 (2013).

藤縄雅: “理研 RI ビームファクトリー 稀少 RI リングの建設”, 日本大学生産工学部第 46 回学術講演会, (日本大学生産工学部), 日本大学生産工学部津田沼校舎, 12 月 (2013).

前山拓哉, 福西暢尚, 石川顕一, 古田琢哉, 深作和明, 高木周, 野田茂穂, 姫野龍太郎, 福田茂一: “粒子線三次元線量分布評価のためのフリッケ・ナノコンポジッドゲル線量計”, 第七回原子力発電所事故に関連する放射線・放射能計測技術調査専門委員会, (電気学会), 東京, 1 月 (2014).

奥野広樹: “大強度重イオンビーム照射時の He ガスの発光機構”, 「プラズマ分光と素過程研究の深化と展開」研究会, (核融合科学研究所), 岐阜, 1 月 (2014).

前山拓哉, 福西暢尚, 石川顕一, 古田琢哉, 深作和明, 高木周, 野田茂穂, 姫野龍太郎, 福田茂一: “ゲル線量計における LET 効果”, 先端放射線化学シンポジウム, (日本放射線化学会、応用物理学会放射線分科会（放射線物理学研究会）), 東京, 3 月 (2014).

Accelerator R&D Team

Publications

[Journal]

(Original Papers)　*Subject to Peer Review

Okuno H., Fukunishi N., and Kamigaito O.: "Progress of RIBF Accelerators", Progress of Theoretical and Experimental Physics **2012**, No. 1, 03C002 (2012). *

Ozeki K., Higurashi Y., Ohnishi J., and Nakagawa T.: "Effect of Biased Disc on Brightness of Highly Charged Uranium Ions from RIKEN 28 GHz", Japanese Journal of Applied Physics **52**, No. 6, 068001 (2013). *

Suda K., Sakamoto N., Yamada K., Arai S., Chiba Y., Kase M., Okuno H., Watanabe Y., and Kamigaito O.: "Design and construction of drift tube linac cavities for RIKEN RI Beam Factory", Nuclear. Instr. and Meth. A **722**, p. 55–64 (2013). *

(Others)

長谷部裕雄: "Report of the Medical Treatment Screening in Fukushima", 加速器 **8**, No. 3, p. 02A320 (2010).

[Book・Proceedings]

(Original Papers)　*Subject to Peer Review

Suda K., Arai S., Chiba Y., Kamigaito O., Kase M., Okuno H., Watanabe Y., Sakamoto N., Yamada K.: "Design of Coupler for Direct Coupled Amplifier to Drift Tube Linac Cavities of the Injector RILAC2 for RIKEN RI Beam Factory", Proceedings of the 26th International Linear Accelerator Conference (LINAC12) p. 684–686 (2013).

Kamigaito O., Dantsuka T., Fujimaki M., Fujinawa T., Fukunishi N., Hasebe H., Higurashi Y., Ikegami K., Ikezawa E., Imao H., Kageyama T., Kase M., Kidera M., Komiyama M., Kuboki H., Kumagai K., Maie T., Nagase M., Nakagawa T., Nakamura M., Ohnishi J., Okuno H., Ozeki K., Sakamoto N., Suda K., Watanabe H., Watanabe T., Watanabe Y., Yamada K., and Yamasawa H.: "Progress towards High-intensity Heavy-ion beams at RIKEN RIBF", Proceedings of the 4th International Particle Accelerator Conference (IPAC2013) p. 333–335 (2013).

Kuboki H., Okuno H., Hershcovitch A., Ikegami K., Imao H., Kase M., Kamigaito O., Dantsuka T., Nakagawa T., Hasebe H., Maie T., and Yano Y.: "Development of differential pumping system using plasma window", Journal of Radioanalytical Nuclear Chemistry **299**, p. 1029–1034 (2013). *

Okuno H., Fukunishi N., Kuboki H., Hasebe H., Imao H., Kase M., and Kamigaito O.: "Charge strippers for Radioisotope Beam Factory at RIKEN", Journal of radioanalytical and nuclear chemistry **299**, p. 945–949 (2013). *

Yamaguchi Y., Wakasugi M., Uesaka T., Ozawa A., Abe Y., Fujinawa T., Kase M., Komiyama M., Kubo T., Kumagai K., Maie T., Nagae D., Ohnishi J., Suzaki F., Tokuchi A., Watanabe Y., Yoshida K., Yamada K., Yamaguchi T., Yamasawa H., Yanagisawa Y., Zenihiro J., and Yano Y.: "Construction of rare-RI ring at RIKEN RI Beam Factory", Nuclear Instruments and Methods in Physics Research **B317**, p. 629–635 (2013). *

Hasebe H., Kuboki H., Okuno H., Imao H., Yamane I., Fukunishi N., Kase M., and Kamigaito O.: "Development of a new foil compounded from carbon nanotubes and sputterdeposition carbon", Journal of radioanalytical and nuclear chemistry **299**, p. 1013–1018 (2014). *

Imao H., Okuno H., Kuboki H., Kamigaito O., Hasebe H., Fukunishi N., Watanabe Y., Fujimaki M., Maie T., Dantsuka T., Kumagai K., Yamada K., Watanabe T., Kase M., and Yano Y.: "Charge-stripping system for 238U ion beam with recirculating He gas", Journal of radioanalytical and nuclear chemistry **299**, p. 941–944 (2014). *

Ohnishi J., Higurashi Y., Kidera M., Ozeki K., and Nakagawa T.: "Development of a high-temperature oven for the 28 GHz electron cyclotron resonance ion source", Review of Scientific Instruments **85**, No. 2, 02A924 (2014). *

大関和貴, 日暮祥英, 大西純一, 中川孝秀,
"理研 28 GHz 超伝導 ECR イオン源のエミッタンス測定", Proc. of the 9th Annual Meeting of Particle Accelerator Society of Japan p. 252 (2013).

Oral Presentations

(International Conference etc.)

Suda K., Sakamoto N., Yamada K., Okuno H., Higurashi Y., Kamigaito O., and Kase M.: "Operation of the RF system for heavy ion accelerators in RIKEN RI Beam Factory", Accelerator Reliability Workshop 2013 (ARW 2013), (Australian Synchrotron), Melbourne, Australia, April (2013).

Kamigaito O., Dantsuka T., Fujimaki M., Fujinawa T., Fukunishi N., Hasebe H., Higurashi Y., Ikegami K., Ikezawa E., Imao H., Kageyama T., Kase M., Kidera M., Komiyama M., Kuboki H., Kumagai K., Maie T., Nagase M., Nakagawa T., Nakamura M., Ohnishi J., Okuno H., Ozeki K., Sakamoto N., Suda K., Watanabe H., Watanabe T., Watanabe Y., Yamada K., and Yamasawa H.: " Progress towards High-intensity Heavy-ion beams at RIKEN RIBF", The 4th International Particle Accelerator Conference (IPAC2013), (International Organization Committee of IPAC13), Shanghai, China, May (2013).

Imao H.: " Realization of New Charge-state Stripper for High-power Uranium Ion Beams", The 4th International Particle Accelerator Conference (IPAC2013), (International Organization Committee of IPAC13), Shanghai, China, May (2013).

Okuno H.: "Status Reports on the RIBF accelerators", RIBF users meeting, (RBF users group), Wako, Japan, June (2013).

Okuno H., Dantsuka T., Ohnishi J., Nakamura M.: “Operational experience of the Superconducting Ring cyclotron at RI Beam Factory (RIBF) and upgrade plans for RIBF accelerators”, The 23rd International conference on magnet technology, (International Organization Committee of MT23), Boston, USA, July (2013).

Fukunishi N., Dantsuka T., Fujimaki M., Fujinawa T., Hasebe H., Higurashi Y., Ikegami K., Ikezawa E., Imao H., Kageyama T., Kamigaito O., Kase M., Kidera M., Komiyama M., Kuboki H., Kumagai K., Maie T., Nagase M., Nakagawa T., Nakamura M., Ohnishi J., Okuno H., Ozeki K., Sakamoto N., Suda K., Uchiyama A., Watanabe T., Watanabe Y., Yamada K., and Yamasawa H.: “Accleration of intense heavy ion beams in RIBF cascaded-cyclotrons”, 20th International Conference on Cyclotrons and their Applications, (International Organizaing Committee of 20th International Conference on Cyclotrons and their Applications), Vancouver, Canada, September (2013).

Imao H., Okuno H., Kuboki H., Kamigaito O., Hasebe H., Fukunishi N., Watanabe Y., Fujimaki M., Maie T., Dantsuka T., Kumagai K., Yamada K., Watanabe T., Kase M., and Yano Y.: “R&D of Helium Gas Stripper for Intense Uranium Beams”, 20th International Conference on Cyclotrons and their Applications, (International Organizaing Committee of 20th International Conference on Cyclotrons and their Applications), Vancouver, Canada, September (2013).

Watanabe T., Fukunishi N., Kase M., Kamigaito O., Inamori S., and Kon K.: “Development of a beam current monitor that uses a high-Tc SQUID at RIBF”, Forschungszentrum Jülich GmbH PGI-5 Colloquium, (Forschungszentrum Jülich GmbH), Jülich , Germany, September (2013).

Okuno H.: “ RIKEN Radioactive Isotope Beam Factory (Accelerators and Scientific Results) ”, 日中粒子線加速器科技シンポジウム, (日中科学技術交流協会), 上海、蘭州、北京, China, November. (2013).

(Domestic Conference)

奥野広樹: “理研 RI ビームファクトリーにおける重イオン加速器技術”, 先端加速器科学技術推進協議会 第２７回技術部会, (先端加速器科学技術推進協議会), 東京, 10 月 (2012).

今尾浩士, 奥野広樹, 久保木浩功: 第 10 回日本加速器学会年会, (日本加速器学会), 名古屋, 8 月 (2013).

長谷部裕雄, 久保木浩功, 奥野広樹, 今尾浩士, 山根功, 福西暢尚, 加瀬昌之, 上垣外修一: “カーボンナノチューブとカーボン蒸着複合膜の開発”, 第 45 回 フラーレン・ナノチューブ・グラフェン　総合シンポジウム, (フラーレン・ナノチューブ・グラフェン学会), 大阪, 8 月 (2013).

久保木浩功, 奥野広樹, HershcovitchAdy, 池上九三男, 今尾浩士, 加瀬昌之, 上垣外修一, 段塚知志, 中川孝秀, 長谷部裕雄, 眞家武士, 矢野安重: “プラズマウィンドウを用いた差動排気システムの開発”, プラズマ研究会, (日本電気学会), 長崎, 9 月 (2013).

奥野広樹: “大強度重イオンビーム照射時の He ガスの発光機構”, 「プラズマ分光と素過程研究の深化と展開」研究会, (核融合科学研究所), 岐阜, 1 月 (2014).

Ion Source Team

Publications

[Journal]

(Original Papers)　*Subject to Peer Review

Ozeki K., Higurashi Y., Ohnishi J., and Nakagawa T.: "Effect of Biased Disc on Brightness of Highly Charged Uranium Ions from RIKEN 28 GHz", Japanese Journal of Applied Physics **52**, No. 6, 068001 (2013). *

Urabe T., Takahashi K., Kitagawa M., Kondo T., Enomoto S., Kidera M., and Seto Y.: "Development of portable mass spectrometer with electron cyclotron resonance ion source for detection of chemical warfare agents in air", Spectrochimica Acta Part A: Molecular and Biomolecular Spectroscopy **120**, p. 437–444 (2013). *

Haba H., Muang M., Kaji D., Kanaya J., Kudou Y., Morimoto K., Morita K., Murakami M., Ozeki K., Sakai R., Sumita T., Wakabayashi Y., Yoneda A., Kasamatsu Y., Kikutani Y., Komori Y., Nakamura K., Shinohara A., Kikunaga H., Kudo H., Nishio K., Toyoshima A., and Tsukada K.: "Production of ^{262}Db in the ^{248}Cm(^{19}F,5n)^{262}Db reaction and decay properties of ^{262}Db and ^{258}Lr", Physical Review C **89**, 024618-1-11 (2014). *

[Book・Proceedings]

(Original Papers)　*Subject to Peer Review

Kamigaito O., Dantsuka T., Fujimaki M., Fujinawa T., Fukunishi N., Hasebe H., Higurashi Y., Ikegami K., Ikezawa E., Imao H., Kageyama T., Kase M., Kidera M., Komiyama M., Kuboki H., Kumagai K., Maie T., Nagase M., Nakagawa T., Nakamura M., Ohnishi J., Okuno H., Ozeki K., Sakamoto N., Suda K., Watanabe H., Watanabe T., Watanabe Y., Yamada K., and Yamasawa H.: "Progress towards High-intensity Heavy-ion beams at RIKEN RIBF", Proceedings of the 4th International Particle Accelerator Conference (IPAC2013) p. 333–335 (2013).

Kuboki H., Okuno H., Hershcovitch A., Ikegami K., Imao H., Kase M., Kamigaito O., Dantsuka T., Nakagawa T., Hasebe H., Maie T., and Yano Y.: "Development of differential pumping system using plasma window", Journal of Radioanalytical Nuclear Chemistry **299**, p. 1029–1034 (2013). *

Ohnishi J., Higurashi Y., Kidera M., Ozeki K., and Nakagawa T.: "Development of a high-temperature oven for the 28 GHz electron cyclotron resonance ion source", Review of Scientific Instruments **85**, No. 2, 02A924 (2014). *

Ozeki K., Kageyama T., Kidera M., Higurashi Y., and Nakagawa T.: "Operational test of micro-oven for 48Ca beam", Review of Scientific Instruments **85**, No. 2, p. 941–944 (2014). *

大関和貴, 日暮祥英, 大西純一, 中川孝秀, "理研 28 GHz 超伝導 ECR イオン源のエミッタンス測定", Proc. of the 9th Annual Meeting of Particle Accelerator Society of Japan p. 252 (2013).

Oral Presentations

(International Conference etc.)

Suda K., Sakamoto N., Yamada K., Okuno H., Higurashi Y., Kamigaito O., and Kase M.: "Operation of the RF system for heavy ion accelerators in RIKEN RI Beam Factory", Accelerator Reliability Workshop 2013 (ARW 2013), (Australian Synchrotron), Melbourne, Australia, April (2013).

Kamigaito O., Dantsuka T., Fujimaki M., Fujinawa T., Fukunishi N., Hasebe H., Higurashi Y., Ikegami K., Ikezawa E., Imao H., Kageyama T., Kase M., Kidera M., Komiyama M., Kuboki H., Kumagai K., Maie T., Nagase M., Nakagawa T., Nakamura M., Ohnishi J., Okuno H., Ozeki K., Sakamoto N., Suda K., Watanabe H., Watanabe T., Watanabe Y., Yamada K., and Yamasawa H.: " Progress towards High-intensity Heavy-ion beams at RIKEN RIBF", The 4th International Particle Accelerator Conference (IPAC2013), (International Organization Committee of IPAC13), Shanghai, China, May (2013).

Fukunishi N., Dantsuka T., Fujimaki M., Fujinawa T., Hasebe H., Higurashi Y., Ikegami K., Ikezawa E., Imao H., Kageyama T., Kamigaito O., Kase M., Kidera M., Komiyama M., Kuboki H., Kumagai K., Maie T., Nagase M., Nakagawa T., Nakamura M., Ohnishi J., Okuno H., Ozeki K., Sakamoto N., Suda K., Uchiyama A., Watanabe T., Watanabe Y., Yamada K., and Yamasawa H.: "Accleration of intense heavy ion beams in RIBF cascaded-cyclotrons", 20th International Conference on Cyclotrons and their Applications, (International Organizaing Committee of 20th International Conference on Cyclotrons and their Applications), Vancouver, Canada, September (2013).

(Domestic Conference)

久保木浩功, 奥野広樹, HershcovitchAdy, 池上九三男, 今尾浩士, 加瀬昌之, 上垣外修一, 段塚知志, 中川孝秀, 長谷部裕雄, 眞家武士, 矢野安重: "プラズマウィンドウを用いた差動排気システムの開発", プラズマ研究会, (日本電気学会), 長崎, 9 月 (2013).

RILAC Team

Publications

[Journal]

(Original Papers) *Subject to Peer Review

Suda K., Sakamoto N., Yamada K., Arai S., Chiba Y., Kase M., Okuno H., Watanabe Y., and Kamigaito O.: "Design and construction of drift tube linac cavities for RIKEN RI Beam Factory", Nuclear. Instr. and Meth. A **722**, p. 55–64 (2013). *

[Book · Proceedings]

(Original Papers) *Subject to Peer Review

Suda K., Arai S., Chiba Y., Kamigaito O., Kase M., Okuno H., Watanabe Y., Sakamoto N., Yamada K.: "Design of Coupler for Direct Coupled Amplifier to Drift Tube Linac Cavities of the Injector RILAC2 for RIKEN RI Beam Factory", Proceedings of the 26th International Linear Accelerator Conference (LINAC12) p. 684–686 (2013).

Kamigaito O., Dantsuka T., Fujimaki M., Fujinawa T., Fukunishi N., Hasebe H., Higurashi Y., Ikegami K., Ikezawa E., Imao H., Kageyama T., Kase M., Kidera M., Komiyama M., Kuboki H., Kumagai K., Maie T., Nagase M., Nakagawa T., Nakamura M., Ohnishi J., Okuno H., Ozeki K., Sakamoto N., Suda K., Watanabe H., Watanabe T., Watanabe Y., Yamada K., and Yamasawa H.: "Progress towards High-intensity Heavy-ion beams at RIKEN RIBF", Proceedings of the 4th International Particle Accelerator Conference (IPAC2013) p. 333–335 (2013).

Yamaguchi Y., Wakasugi M., Uesaka T., Ozawa A., Abe Y., Fujinawa T., Kase M., Komiyama M., Kubo T., Kumagai K., Maie T., Nagae D., Ohnishi J., Suzaki F., Tokuchi A., Watanabe Y., Yoshida K., Yamada K., Yamaguchi T., Yamasawa H., Yanagisawa Y., Zenihiro J., and Yano Y.: "Construction of rare-RI ring at RIKEN RI Beam Factory", Nuclear Instruments and Methods in Physics Research **B317**, p. 629–635 (2013). *

Imao H., Okuno H., Kuboki H., Kamigaito O., Hasebe H., Fukunishi N., Watanabe Y., Fujimaki M., Maie T., Dantsuka T., Kumagai K., Yamada K., Watanabe T., Kase M., and Yano Y.: "Charge-stripping system for 238U ion beam with recirculating He gas", Journal of radioanalytical and nuclear chemistry **299**, p. 941–944 (2014). *

Oral Presentations

(International Conference etc.)

Kamigaito O., Dantsuka T., Fujimaki M., Fujinawa T., Fukunishi N., Hasebe H., Higurashi Y., Ikegami K., Ikezawa E., Imao H., Kageyama T., Kase M., Kidera M., Komiyama M., Kuboki H., Kumagai K., Maie T., Nagase M., Nakagawa T., Nakamura M., Ohnishi J., Okuno H., Ozeki K., Sakamoto N., Suda K., Watanabe H., Watanabe T., Watanabe Y., Yamada K., and Yamasawa H.: " Progress towards High-intensity Heavy-ion beams at RIKEN RIBF", The 4th International Particle Accelerator Conference (IPAC2013), (International Organization Committee of IPAC13), Shanghai, China, May (2013).

Fukunishi N., Dantsuka T., Fujimaki M., Fujinawa T., Hasebe H., Higurashi Y., Ikegami K., Ikezawa E., Imao H., Kageyama T., Kamigaito O., Kase M., Kidera M., Komiyama M., Kuboki H., Kumagai K., Maie T., Nagase M., Nakagawa T., Nakamura M., Ohnishi J., Okuno H., Ozeki K., Sakamoto N., Suda K., Uchiyama A., Watanabe T., Watanabe Y., Yamada K., and Yamasawa H.: "Accleration of intense heavy ion beams in RIBF cascaded-cyclotrons", 20th International Conference on Cyclotrons and their Applications, (International Organizaing Committee of 20th International Conference on Cyclotrons and their Applications), Vancouver, Canada, September (2013).

Imao H., Okuno H., Kuboki H., Kamigaito O., Hasebe H., Fukunishi N., Watanabe Y., Fujimaki M., Maie T., Dantsuka T., Kumagai K., Yamada K., Watanabe T., Kase M., and Yano Y.: "R&D of Helium Gas Stripper for Intense Uranium Beams", 20th International Conference on Cyclotrons and their Applications, (International Organizaing Committee of 20th International Conference on Cyclotrons and their Applications), Vancouver, Canada, September (2013).

Cyclotron Team

Publications

[Journal]

(Original Papers) *Subject to Peer Review

Suda K., Sakamoto N., Yamada K., Arai S., Chiba Y., Kase M., Okuno H., Watanabe Y., and Kamigaito O.: "Design and construction of drift tube linac cavities for RIKEN RI Beam Factory", Nuclear. Instr. and Meth. A **722**, p. 55–64 (2013). *

(Others)

長谷部裕雄: "Report of the Medical Treatment Screening in Fukushima", 加速器 **8**, No. 3, p. 02A320 (2010).

[Book · Proceedings]

(Original Papers) *Subject to Peer Review

Suda K., Arai S., Chiba Y., Kamigaito O., Kase M., Okuno H., Watanabe Y., Sakamoto N., Yamada K.: "Design of Coupler for Direct Coupled Amplifier to Drift Tube Linac Cavities of the Injector RILAC2 for RIKEN RI Beam Factory", Proceedings of the 26th International Linear Accelerator Conference (LINAC12) p. 684–686 (2013).

Kamigaito O., Dantsuka T., Fujimaki M., Fujinawa T., Fukunishi N., Hasebe H., Higurashi Y., Ikegami K., Ikezawa E., Imao H., Kageyama T., Kase M., Kidera M., Komiyama M., Kuboki H., Kumagai K., Maie T., Nagase M., Nakagawa T., Nakamura M., Ohnishi J., Okuno H., Ozeki K., Sakamoto N., Suda K., Watanabe H., Watanabe T., Watanabe Y., Yamada K., and Yamasawa H.: "Progress towards High-intensity Heavy-ion beams at RIKEN RIBF", Proceedings of the 4th International Particle Accelerator Conference (IPAC2013) p. 333–335 (2013).

Oral Presentations

(International Conference etc.)

Suda K., Sakamoto N., Yamada K., Okuno H., Higurashi Y., Kamigaito O., and Kase M.: "Operation of the RF system for heavy ion accelerators in RIKEN RI Beam Factory", Accelerator Reliability Workshop 2013 (ARW 2013), (Australian Synchrotron), Melbourne, Australia, April (2013).

Kamigaito O., Dantsuka T., Fujimaki M., Fujinawa T., Fukunishi N., Hasebe H., Higurashi Y., Ikegami K., Ikezawa E., Imao H., Kageyama T., Kase M., Kidera M., Komiyama M., Kuboki H., Kumagai K., Maie T., Nagase M., Nakagawa T., Nakamura M., Ohnishi J., Okuno H., Ozeki K., Sakamoto N., Suda K., Watanabe H., Watanabe T., Watanabe Y., Yamada K., and Yamasawa H.: " Progress towards High-intensity Heavy-ion beams at RIKEN RIBF", The 4th International Particle Accelerator Conference (IPAC2013), (International Organization Committee of IPAC13), Shanghai, China, May (2013).

Fukunishi N., Dantsuka T., Fujimaki M., Fujinawa T., Hasebe H., Higurashi Y., Ikegami K., Ikezawa E., Imao H., Kageyama T., Kamigaito O., Kase M., Kidera M., Komiyama M., Kuboki H., Kumagai K., Maie T., Nagase M., Nakagawa T., Nakamura M., Ohnishi J., Okuno H., Ozeki K., Sakamoto N., Suda K., Uchiyama A., Watanabe T., Watanabe Y., Yamada K., and Yamasawa H.: "Accleration of intense heavy ion beams in RIBF cascaded-cyclotrons", 20th International Conference on Cyclotrons and their Applications, (International Organizaing Committee of 20th International Conference on Cyclotrons and their Applications), Vancouver, Canada, September (2013).

Beam Dynamics & Diagnostics Team

Publications

[Journal]

(Original Papers) *Subject to Peer Review

Okuno H., Fukunishi N., and Kamigaito O.: "Progress of RIBF Accelerators", Progress of Theoretical and Experimental Physics **2012**, No. 1, 03C002 (2012). *

Suda K., Sakamoto N., Yamada K., Arai S., Chiba Y., Kase M., Okuno H., Watanabe Y., and Kamigaito O.: "Design and construction of drift tube linac cavities for RIKEN RI Beam Factory", Nuclear. Instr. and Meth. A **722**, p. 55–64 (2013). *

Maeyama T., Fukunishi N., Ishikawa K.L., Furuta T., Fukasaku K., Takagi S., Noda S., Himeno R., and Fukuda S.: "A diffusion-free and linear-energy-transfer-independent nanocomposite Fricke gel dosimeter", Radiation Physics and Chemistry **96**, p. 92–96 (2014). *

[Book · Proceedings]

(Original Papers) *Subject to Peer Review

Maeyama T., Fukunishi N., Ishikawa K.L., Furuta T., Fukasaku K., Takagi S., Noda S., Himeno R., and Fukuda S.: "Response of aqueous dichromate and nanoclay dichromate gel dosimeters to carbon ion irradiation", Journal of Physics: Conference Series **444**, 012033 (2013). *

Maeyama T., Fukunishi N., Ishikawa K.L., Furuta T., Fukasaku K., Takagi S., Noda S., Himeno R., and Fukuda S.: "Diffusion suppression in gel dosimetry by addition of nanoclay", World Congress on Medical Physics and Biomedical Engineering May 26-31, 2012, Beijing, China **39**, p. 1183–1186 (2013). *

Taylor M.L., Maeyama T., Fukunishi N., Ishikawa K.L., Furuta T., Fukasaku K., Takagi S., Noda S., Himeno R., and Fukuda S.: "Radiological characteristics of charged particle interactions in the first clay-nanoparticle dichromate gel dosimeter", Journal of Physics: Conference Series **444**, 012110 (2013). *

Taylor M.L., Maeyama T., Fukunishi N., Ishikawa K.L., Fukasaku K., Furuta T., Takagi S., Noda S., Himeno R., and Fukuda S.: "A novel clay-nanoparticle dichromate gel: radiological properties for electron and hadron interactions", Australasian Physical & Engineering Sciences in Medicine: 2012 Engineering and Physical Sciences in Medicine Conference **36**, p. 136–137 (2013). *

Suda K., Arai S., Chiba Y., Kamigaito O., Kase M., Okuno H., Watanabe Y., Sakamoto N., Yamada K.: "Design of Coupler for Direct Coupled Amplifier to Drift Tube Linac Cavities of the Injector RILAC2 for RIKEN RI Beam Factory", Proceedings of the 26th International Linear Accelerator Conference (LINAC12) p. 684–686 (2013).

Kamigaito O., Dantsuka T., Fujimaki M., Fujinawa T., Fukunishi N., Hasebe H., Higurashi Y., Ikegami K., Ikezawa E., Imao H., Kageyama T., Kase M., Kidera M., Komiyama M., Kuboki H., Kumagai K., Maie T., Nagase M., Nakagawa T., Nakamura M., Ohnishi J., Okuno H., Ozeki K., Sakamoto N., Suda K., Watanabe H., Watanabe T., Watanabe Y., Yamada K., and Yamasawa H.: "Progress towards High-intensity Heavy-ion beams at RIKEN RIBF", Proceedings of the 4th International Particle Accelerator Conference (IPAC2013) p. 333–335 (2013).

Nakai Y., Nakano Y., Ikeda T., Kanai Y., Kambara T., Fukunishi N., Kondo C., Azuma T., Komaki K., and Yamazaki Y.: "Stark effect in resonant coherent excitation of 2s electron of Li-like Fe23+ ions channeling in a Si crystal", Nuclear Instruments and Methods in Physics Research Section B: Beam Interactions with Materials and Atoms **299**, p. 1029–1034 (2013). *

Okuno H., Fukunishi N., Kuboki H., Hasebe H., Imao H., Kase M., and Kamigaito O.: "Charge strippers for Radioisotope Beam Factory at RIKEN", Journal of radioanalytical and nuclear chemistry **299**, p. 945–949 (2013). *

Yamaguchi Y., Wakasugi M., Uesaka T., Ozawa A., Abe Y., Fujinawa T., Kase M., Komiyama M., Kubo T., Kumagai K., Maie T., Nagae D., Ohnishi J., Suzaki F., Tokuchi A., Watanabe Y., Yoshida K., Yamada K., Yamaguchi T., Yamasawa H., Yanagisawa Y., Zenihiro J., and Yano Y.: "Construction of rare-RI ring at RIKEN RI Beam Factory", Nuclear Instruments and Methods in Physics Research **B317**, p. 629–635 (2013). *

Hasebe H., Kuboki H., Okuno H., Imao H., Yamane I., Fukunishi N., Kase M., and Kamigaito O.: "Development of a new foil compounded from carbon nanotubes and sputterdeposition carbon", Journal of radioanalytical and nuclear chemistry **299**, p. 1013–1018 (2014). *

Imao H., Okuno H., Kuboki H., Kamigaito O., Hasebe H., Fukunishi N., Watanabe Y., Fujimaki M., Maie T., Dantsuka T., Kumagai K., Yamada K., Watanabe T., Kase M., and Yano Y.: "Charge-stripping system for 238U ion beam with recirculating He gas", Journal of radioanalytical and nuclear chemistry **299**, p. 941–944 (2014). *

Oral Presentations

(International Conference etc.)

Maeyama T., Fukunishi N., Ishikawa K.L., Fukasaku K., Furuta T., Takagi S., Noda S., and Himeno R.: "Diffusion suppression in gel dosimetry by addition of nanoclay", World Congress on Medical Physics and Biomedical Engineering (WC2012), Beijing, China, May (2012).

Maeyama T., Fukunishi N., Ishikawa K.L., Fukasaku K., Furuta T., Takagi S., Noda S., and Himeno R.: "Diffusion suppression in gel dosimetry by addition of nanoclay", World Congress on Medical Physics and Biomedical Engineering (WC2012), Sydney, Australia, November (2012).

Suda K., Sakamoto N., Yamada K., Okuno H., Higurashi Y., Kamigaito O., and Kase M.: “Operation of the RF system for heavy ion accelerators in RIKEN RI Beam Factory”, Accelerator Reliability Workshop 2013 (ARW 2013), (Australian Synchrotron), Melbourne, Australia, April (2013).

Kamigaito O., Dantsuka T., Fujimaki M., Fujinawa T., Fukunishi N., Hasebe H., Higurashi Y., Ikegami K., Ikezawa E., Imao H., Kageyama T., Kase M., Kidera M., Komiyama M., Kuboki H., Kumagai K., Maie T., Nagase M., Nakagawa T., Nakamura M., Ohnishi J., Okuno H., Ozeki K., Sakamoto N., Suda K., Watanabe H., Watanabe T., Watanabe Y., Yamada K., and Yamasawa H.: “ Progress towards High-intensity Heavy-ion beams at RIKEN RIBF”, The 4th International Particle Accelerator Conference (IPAC2013), (International Organization Committee of IPAC13), Shanghai, China, May (2013).

Fukunishi N., Dantsuka T., Fujimaki M., Fujinawa T., Hasebe H., Higurashi Y., Ikegami K., Ikezawa E., Imao H., Kageyama T., Kamigaito O., Kase M., Kidera M., Komiyama M., Kuboki H., Kumagai K., Maie T., Nagase M., Nakagawa T., Nakamura M., Ohnishi J., Okuno H., Ozeki K., Sakamoto N., Suda K., Uchiyama A., Watanabe T., Watanabe Y., Yamada K., and Yamasawa H.: “Accleration of intense heavy ion beams in RIBF cascaded-cyclotrons”, 20th International Conference on Cyclotrons and their Applications, (International Organizaing Committee of 20th International Conference on Cyclotrons and their Applications), Vancouver, Canada, September (2013).

Imao H., Okuno H., Kuboki H., Kamigaito O., Hasebe H., Fukunishi N., Watanabe Y., Fujimaki M., Maie T., Dantsuka T., Kumagai K., Yamada K., Watanabe T., Kase M., and Yano Y.: “R&D of Helium Gas Stripper for Intense Uranium Beams”, 20th International Conference on Cyclotrons and their Applications, (International Organizaing Committee of 20th International Conference on Cyclotrons and their Applications), Vancouver, Canada, September (2013).

Watanabe T., Fukunishi N., Kase M., Kamigaito O., Inamori S., and Kon K.: “Development of a beam current monitor that uses a high-Tc SQUID at RIBF”, Forschungszentrum Jülich GmbH PGI-5 Colloquium, (Forschungszentrum Jülich GmbH), Jülich , Germany, September (2013).

(Domestic Conference)

前山拓哉, 福西暢尚, 石川顕一, 古田琢哉, 深作和明, 高木周, 野田茂穂, 姫野龍太郎: “フリッケゲル線量計による炭素線の線量分布測定”, 第 54 回放射線化学討論会, (日本放射線化学会), 大阪, 9 月 (2011).

前山拓哉, 福西暢尚, 石川顕一, 古田琢哉, 深作和明, 高木周, 野田茂穂, 姫野龍太郎: “ナノクレイ添加による拡散のないゲル線量計の開発”, 第 103 回日本医学物理学会学術大会, (日本医学物理学会), 横浜, 4 月 (2012).

前山拓哉, 福西暢尚, 石川顕一, 古田琢哉, 深作和明, 高木周, 野田茂穂, 姫野龍太郎: “炭素線治療における VIPAR ポリマーゲル線量計を用いた線量分布測定・検証の検討”, 第 104 回日本医学物理学会学術大会, (日本医学物理学会), つくば, 9 月 (2012).

前山拓哉, 福西暢尚, 石川顕一, 古田琢哉, 深作和明, 高木周, 野田茂穂, 姫野龍太郎: “ゲル線量計による重粒子線線量分布測定”, 第 1 回 3D ゲル線量計研究会, (林慎一郎（広島国際大学 診療放射線学科）・村上祐司（広島大学病院 放射線治療科）), 広島, 12 月 (2012).

前山拓哉, 福西暢尚, 石川顕一, 古田琢哉, 深作和明, 高木周, 野田茂穂, 姫野龍太郎: “炭素線治療におけるゲル線量計を用いた線量分布測定とシミュレーションとの比較”, 第 16 回弥生研究会〜放射線効果の解明と応用〜, (東京大学、勝村・工藤研究室), 東京, 3 月 (2013).

前山拓哉, 福西暢尚, 石川顕一, 古田琢哉, 深作和明, 高木周, 野田茂穂, 姫野龍太郎: “重粒子線線量分布測定のための VIPAR ポリマーゲル線量計の特性評価”, 第 60 回応用物理学会春季学術講演会, (応用物理学会), 神奈川, 3 月 (2013).

前山拓哉, 福西暢尚, 石川顕一, 古田琢哉, 深作和明, 高木周, 野田茂穂, 姫野龍太郎: “炭素線治療における VIPAR ポリマーゲル線量計を用いた線量分布測定・検証の検討 (2)”, 第 105 回日本医学物理学会学術大会, (日本医学物理学会), 横浜, 4 月 (2013).

前山拓哉, 福西暢尚, 石川顕一, 古田琢哉, 深作和明, 高木周, 野田茂穂, 姫野龍太郎, 福田茂一: “LET 依存性のないゲル線量計の開発”, 平成 24 年度 HIMAC　共同利用研究成果発表会, (放射線医学総合研究所), 千葉, 4 月 (2013).

前山拓哉, 福西暢尚, 石川顕一, 古田琢哉, 深作和明, 高木周, 野田茂穂, 姫野龍太郎, 福田茂一: “PHITS コードを用いた炭素線照射時の VIPAR ゲル線量計の特性評価と線量分布評価”, 第 9 回 PHITS 定期講習会/研究会, (日本原子力研究開発機構), 茨城, 8 月 (2013).

藤縄雅, 山口由高, 山澤秀行, 眞家武士, 熊谷桂子, 若杉昌徳: “理研 RIBF 稀少 RI リングの付帯設備”, 第 10 回日本加速器学会年会, (日本加速器学会), 名古屋, 8 月 (2013).

長谷部裕雄, 久保木浩功, 奥野広樹, 今尾浩士, 山根功, 福西暢尚, 加瀬昌之, 上垣外修一: “カーボンナノチューブとカーボン蒸着複合膜の開発”, 第 45 回 フラーレン・ナノチューブ・グラフェン　総合シンポジウム, (フラーレン・ナノチューブ・グラフェン学会), 大阪, 8 月 (2013).

前山拓哉, 福西暢尚, 石川顕一, 古田琢哉, 深作和明, 高木周, 野田茂穂, 姫野龍太郎, 福田茂一: “炭素線照射におけるゲル線量計の LET 依存性”, 第 56 回放射線化学討論会, (日本放射線化学会、日本化学会), 広島, 9 月 (2013).

前山拓哉, 福西暢尚, 石川顕一, 古田琢哉, 深作和明, 高木周, 野田茂穂, 姫野龍太郎, 福田茂一: “ナノクレイを添加したゲル線量計の開発”, 第 56 回放射線化学討論会, (電気学会、ナノメディシンに向けた光・量子ビーム応用技術調査専門委員会，ナノ学会　ナノ機能・応用部会　研究会，日本生体医工学会専門別委員会　次世代治療技術開発の為の細胞組織・分子機能計測・制御研究会), 埼玉, 11 月 (2013).

前山拓哉: “フリッケゲル線量計入門”, 第 2 回 3D ゲル線量計研究会, (林慎一郎（広島国際大学 診療放射線学科）・小

西良幸（東京女子医科大学 先端生命医科学研究所）), 東京, 12 月 (2013).

前山拓哉, 福西暢尚, 石川顕一, 古田琢哉, 深作和明, 高木周, 野田茂穂, 姫野龍太郎, 福田茂一: “フリッケゲル線量計の拡散抑制と線質効果の抑制”, 第 2 回 3D ゲル線量計研究会, (林慎一郎（広島国際大学 診療放射線学科）・小西良幸（東京女子医科大学 先端生命医科学研究所）), 東京, 12 月 (2013).

前山拓哉, 福西暢尚, 石川顕一, 古田琢哉, 深作和明, 高木周, 野田茂穂, 姫野龍太郎, 福田茂一: “有機無機複合ゲルをフリッケ水溶液線量計に浸した三次元線量計の開発”, 第 17 回弥生研究会〜放射線効果の解明と応用〜, (東京大学、勝村・工藤研究室), 東京, 12 月 (2013).

前山拓哉, 福西暢尚, 石川顕一, 古田琢哉, 深作和明, 高木周, 野田茂穂, 姫野龍太郎, 福田茂一: “粒子線三次元線量分布評価のためのフリッケ・ナノコンポジッドゲル線量計”, 第七回原子力発電所事故に関連する放射線・放射能計測技術調査専門委員会, (電気学会), 東京, 1 月 (2014).

奥野広樹: “大強度重イオンビーム照射時の He ガスの発光機構”, 「プラズマ分光と素過程研究の深化と展開」研究会, (核融合科学研究所), 岐阜, 1 月 (2014).

前山拓哉, 福西暢尚, 石川顕一, 古田琢哉, 深作和明, 高木周, 野田茂穂, 姫野龍太郎, 福田茂一: “ゲル線量計における LET 効果”, 先端放射線化学シンポジウム, (日本放射線化学会、応用物理学会放射線分科会（放射線物理学研究会）), 東京, 3 月 (2014).

Cryogenic Technology Team

Publications

[Journal]

(Original Papers) *Subject to Peer Review

Okuno H., Fukunishi N., and Kamigaito O.: "Progress of RIBF Accelerators", Progress of Theoretical and Experimental Physics **2012**, No. 1, 03C002 (2012). *

Suda K., Sakamoto N., Yamada K., Arai S., Chiba Y., Kase M., Okuno H., Watanabe Y., and Kamigaito O.: "Design and construction of drift tube linac cavities for RIKEN RI Beam Factory", Nuclear. Instr. and Meth. A **722**, p. 55–64 (2013). *

[Book · Proceedings]

(Original Papers) *Subject to Peer Review

Suda K., Arai S., Chiba Y., Kamigaito O., Kase M., Okuno H., Watanabe Y., Sakamoto N., Yamada K.: "Design of Coupler for Direct Coupled Amplifier to Drift Tube Linac Cavities of the Injector RILAC2 for RIKEN RI Beam Factory", Proceedings of the 26th International Linear Accelerator Conference (LINAC12) p. 684–686 (2013).

Kamigaito O., Dantsuka T., Fujimaki M., Fujinawa T., Fukunishi N., Hasebe H., Higurashi Y., Ikegami K., Ikezawa E., Imao H., Kageyama T., Kase M., Kidera M., Komiyama M., Kuboki H., Kumagai K., Maie T., Nagase M., Nakagawa T., Nakamura M., Ohnishi J., Okuno H., Ozeki K., Sakamoto N., Suda K., Watanabe H., Watanabe T., Watanabe Y., Yamada K., and Yamasawa H.: "Progress towards High-intensity Heavy-ion beams at RIKEN RIBF", Proceedings of the 4th International Particle Accelerator Conference (IPAC2013) p. 333–335 (2013).

Kuboki H., Okuno H., Hershcovitch A., Ikegami K., Imao H., Kase M., Kamigaito O., Dantsuka T., Nakagawa T., Hasebe H., Maie T., and Yano Y.: "Development of differential pumping system using plasma window", Journal of Radioanalytical Nuclear Chemistry **299**, p. 1029–1034 (2013). *

Okuno H., Fukunishi N., Kuboki H., Hasebe H., Imao H., Kase M., and Kamigaito O.: "Charge strippers for Radioisotope Beam Factory at RIKEN", Journal of radioanalytical and nuclear chemistry **299**, p. 945–949 (2013). *

Yamaguchi Y., Wakasugi M., Uesaka T., Ozawa A., Abe Y., Fujinawa T., Kase M., Komiyama M., Kubo T., Kumagai K., Maie T., Nagae D., Ohnishi J., Suzaki F., Tokuchi A., Watanabe Y., Yoshida K., Yamada K., Yamaguchi T., Yamasawa H., Yanagisawa Y., Zenihiro J., and Yano Y.: "Construction of rare-RI ring at RIKEN RI Beam Factory", Nuclear Instruments and Methods in Physics Research **B317**, p. 629–635 (2013). *

Hasebe H., Kuboki H., Okuno H., Imao H., Yamane I., Fukunishi N., Kase M., and Kamigaito O.: "Development of a new foil compounded from carbon nanotubes and sputterdeposition carbon", Journal of radioanalytical and nuclear chemistry **299**, p. 1013–1018 (2014). *

Imao H., Okuno H., Kuboki H., Kamigaito O., Hasebe H., Fukunishi N., Watanabe Y., Fujimaki M., Maie T., Dantsuka T., Kumagai K., Yamada K., Watanabe T., Kase M., and Yano Y.: "Charge-stripping system for 238U ion beam with recirculating He gas", Journal of radioanalytical and nuclear chemistry **299**, p. 941–944 (2014). *

Oral Presentations

(International Conference etc.)

Kamigaito O., Dantsuka T., Fujimaki M., Fujinawa T., Fukunishi N., Hasebe H., Higurashi Y., Ikegami K., Ikezawa E., Imao H., Kageyama T., Kase M., Kidera M., Komiyama M., Kuboki H., Kumagai K., Maie T., Nagase M., Nakagawa T., Nakamura M., Ohnishi J., Okuno H., Ozeki K., Sakamoto N., Suda K., Watanabe H., Watanabe T., Watanabe Y., Yamada K., and Yamasawa H.: " Progress towards High-intensity Heavy-ion beams at RIKEN RIBF", The 4th International Particle Accelerator Conference (IPAC2013), (International Organization Committee of IPAC13), Shanghai, China, May (2013).

Okuno H.: "Status Reports on the RIBF accelerators", RIBF users meeting, (RBF users group), Wako, Japan, June (2013).

Okuno H., Dantsuka T., Ohnishi J., Nakamura M.: "Operational experience of the Superconducting Ring cyclotron at RI Beam Factory (RIBF) and upgrade plans for RIBF accelerators", The 23rd International conference on magnet technology, (International Organization Committee of MT23), Boston, USA, July (2013).

Fukunishi N., Dantsuka T., Fujimaki M., Fujinawa T., Hasebe H., Higurashi Y., Ikegami K., Ikezawa E., Imao H., Kageyama T., Kamigaito O., Kase M., Kidera M., Komiyama M., Kuboki H., Kumagai K., Maie T., Nagase M., Nakagawa T., Nakamura M., Ohnishi J., Okuno H., Ozeki K., Sakamoto N., Suda K., Uchiyama A., Watanabe T., Watanabe Y., Yamada K., and Yamasawa H.: "Accleration of intense heavy ion beams in RIBF cascaded-cyclotrons", 20th International Conference on Cyclotrons and their Applications, (International Organizaing Committee of 20th International Conference on Cyclotrons and their Applications), Vancouver, Canada, September (2013).

Imao H., Okuno H., Kuboki H., Kamigaito O., Hasebe H., Fukunishi N., Watanabe Y., Fujimaki M., Maie T., Dantsuka T., Kumagai K., Yamada K., Watanabe T., Kase M., and Yano Y.: "R&D of Helium Gas Stripper for Intense Uranium Beams", 20th International Conference on Cyclotrons and their Applications, (International Organizaing Committee of 20th International Conference on Cyclotrons and their Applications), Vancouver, Canada, September (2013).

Okuno H.: " RIKEN Radioactive Isotope Beam Factory (Accelerators and Scientific Results) ", 日中粒子線加速器科技シンポジウム, (日中科学技術交流協会), 上海、蘭州、北京, China, November. (2013).

(Domestic Conference)

奥野広樹: "理研 RI ビームファクトリーにおける重イオン加速器技術", 先端加速器科学技術推進協議会 第２７回技術部会, (先端加速器科学技術推進協議会), 東京, 10 月 (2012).

藤縄雅, 山口由高, 山澤秀行, 眞家武士, 熊谷桂子, 若杉昌徳: "理研 RIBF 稀少 RI リングの付帯設備", 第 10 回日本加速器学会年会, (日本加速器学会), 名古屋, 8 月 (2013).

今尾浩士, 奥野広樹, 久保木浩功: 第 10 回日本加速器学会年会, (日本加速器学会), 名古屋, 8 月 (2013).

長谷部裕雄, 久保木浩功, 奥野広樹, 今尾浩士, 山根功, 福西暢尚, 加瀬昌之, 上垣外修一: "カーボンナノチューブとカーボン蒸着複合膜の開発", 第 45 回 フラーレン・ナノチューブ・グラフェン　総合シンポジウム, (フラーレン・ナノチューブ・グラフェン学会), 大阪, 8 月 (2013).

久保木浩功, 奥野広樹, HershcovitchAdy, 池上九三男, 今尾浩士, 加瀬昌之, 上垣外修一, 段塚知志, 中川孝秀, 長谷部裕雄, 眞家武士, 矢野安重: "プラズマウィンドウを用いた差動排気システムの開発", プラズマ研究会, (日本電気学会), 長崎, 9 月 (2013).

奥野広樹: "大強度重イオンビーム照射時の He ガスの発光機構", 「プラズマ分光と素過程研究の深化と展開」研究会, (核融合科学研究所), 岐阜, 1 月 (2014).

Infrastructure Management Team

Publications

[Journal]

(Original Papers) *Subject to Peer Review

Fujinawa T.: "RIKEN Nishina Center's Response to the Fukushima Daiichi Nuclear Disaster: Radiation Screening", Journal of Physical Science and Application **3**, No. 1, p. 39–46 (2013). *

Fujinawa T.: "Development of Cranes Used at Super-Sized Accelerator Facility RIKEN RI Beam Factory", Journal of Material Science and Engineering **A3**, No. 9, p. 640–645 (2013). *

Suda K., Sakamoto N., Yamada K., Arai S., Chiba Y., Kase M., Okuno H., Watanabe Y., and Kamigaito O.: "Design and construction of drift tube linac cavities for RIKEN RI Beam Factory", Nuclear. Instr. and Meth. A **722**, p. 55–64 (2013). *

Fujinawa T.: "Development of Superconducting Maglev Ground Coils", Journal of Physical Science and Application, **4**, No. 1, p. 36–42 (2014). *

[Book · Proceedings]

(Original Papers) *Subject to Peer Review

Suda K., Arai S., Chiba Y., Kamigaito O., Kase M., Okuno H., Watanabe Y., Sakamoto N., Yamada K.: "Design of Coupler for Direct Coupled Amplifier to Drift Tube Linac Cavities of the Injector RILAC2 for RIKEN RI Beam Factory", Proceedings of the 26th International Linear Accelerator Conference (LINAC12) p. 684–686 (2013).

Kamigaito O., Dantsuka T., Fujimaki M., Fujinawa T., Fukunishi N., Hasebe H., Higurashi Y., Ikegami K., Ikezawa E., Imao H., Kageyama T., Kase M., Kidera M., Komiyama M., Kuboki H., Kumagai K., Maie T., Nagase M., Nakagawa T., Nakamura M., Ohnishi J., Okuno H., Ozeki K., Sakamoto N., Suda K., Watanabe H., Watanabe T., Watanabe Y., Yamada K., and Yamasawa H.: "Progress towards High-intensity Heavy-ion beams at RIKEN RIBF", Proceedings of the 4th International Particle Accelerator Conference (IPAC2013) p. 333–335 (2013).

Kuboki H., Okuno H., Hershcovitch A., Ikegami K., Imao H., Kase M., Kamigaito O., Dantsuka T., Nakagawa T., Hasebe H., Maie T., and Yano Y.: "Development of differential pumping system using plasma window", Journal of Radioanalytical Nuclear Chemistry **299**, p. 1029–1034 (2013). *

Okuno H., Fukunishi N., Kuboki H., Hasebe H., Imao H., Kase M., and Kamigaito O.: "Charge strippers for Radioisotope Beam Factory at RIKEN", Journal of radioanalytical and nuclear chemistry **299**, p. 945–949 (2013). *

Yamaguchi Y., Wakasugi M., Uesaka T., Ozawa A., Abe Y., Fujinawa T., Kase M., Komiyama M., Kubo T., Kumagai K., Maie T., Nagae D., Ohnishi J., Suzaki F., Tokuchi A., Watanabe Y., Yoshida K., Yamada K., Yamaguchi T., Yamasawa H., Yanagisawa Y., Zenihiro J., and Yano Y.: "Construction of rare-RI ring at RIKEN RI Beam Factory", Nuclear Instruments and Methods in Physics Research **B317**, p. 629–635 (2013). *

Hasebe H., Kuboki H., Okuno H., Imao H., Yamane I., Fukunishi N., Kase M., and Kamigaito O.: "Development of a new foil compounded from carbon nanotubes and sputterdeposition carbon", Journal of radioanalytical and nuclear chemistry **299**, p. 1013–1018 (2014). *

Imao H., Okuno H., Kuboki H., Kamigaito O., Hasebe H., Fukunishi N., Watanabe Y., Fujimaki M., Maie T., Dantsuka T., Kumagai K., Yamada K., Watanabe T., Kase M., and Yano Y.: "Charge-stripping system for 238U ion beam with recirculating He gas", Journal of radioanalytical and nuclear chemistry **299**, p. 941–944 (2014). *

Oral Presentations

(International Conference etc.)

Suda K., Sakamoto N., Yamada K., Okuno H., Higurashi Y., Kamigaito O., and Kase M.: "Operation of the RF system for heavy ion accelerators in RIKEN RI Beam Factory", Accelerator Reliability Workshop 2013 (ARW 2013), (Australian Synchrotron), Melbourne, Australia, April (2013).

Fujinawa T.: "Cogeneration system for RIKEN RI Beam Factory", Accelarator Reliability Workshop 2013, (Australian Synchrotron), Melbourne, Australia, April (2013).

Kamigaito O., Dantsuka T., Fujimaki M., Fujinawa T., Fukunishi N., Hasebe H., Higurashi Y., Ikegami K., Ikezawa E., Imao H., Kageyama T., Kase M., Kidera M., Komiyama M., Kuboki H., Kumagai K., Maie T., Nagase M., Nakagawa T., Nakamura M., Ohnishi J., Okuno H., Ozeki K., Sakamoto N., Suda K., Watanabe H., Watanabe T., Watanabe Y., Yamada K., and Yamasawa H.: " Progress towards High-intensity Heavy-ion beams at RIKEN RIBF", The 4th International Particle Accelerator Conference (IPAC2013), (International Organization Committee of IPAC13), Shanghai, China, May (2013).

Fujinawa T.: "The Major Fukushima Daiichi Nuclear Disaster", The 11th International Workshop of the IEIEJ, (IEIEJ), Osaka, Japan, September (2013).

Fukunishi N., Dantsuka T., Fujimaki M., Fujinawa T., Hasebe H., Higurashi Y., Ikegami K., Ikezawa E., Imao H., Kageyama T., Kamigaito O., Kase M., Kidera M., Komiyama M., Kuboki H., Kumagai K., Maie T., Nagase M., Nakagawa T., Nakamura M., Ohnishi J., Okuno H., Ozeki K., Sakamoto N., Suda K., Uchiyama A., Watanabe T., Watanabe Y., Yamada K., and Yamasawa H.: "Accleration of intense heavy ion beams in RIBF cascaded-cyclotrons", 20th International

Conference on Cyclotrons and their Applications, (International Organizaing Committee of 20th International Conference on Cyclotrons and their Applications), Vancouver, Canada, September (2013).

Imao H., Okuno H., Kuboki H., Kamigaito O., Hasebe H., Fukunishi N., Watanabe Y., Fujimaki M., Maie T., Dantsuka T., Kumagai K., Yamada K., Watanabe T., Kase M., and Yano Y.: "R&D of Helium Gas Stripper for Intense Uranium Beams", 20th International Conference on Cyclotrons and their Applications, (International Organizaing Committee of 20th International Conference on Cyclotrons and their Applications), Vancouver, Canada, September (2013).

Watanabe T., Fukunishi N., Kase M., Kamigaito O., Inamori S., and Kon K.: "Development of a beam current monitor that uses a high-Tc SQUID at RIBF", Forschungszentrum Jülich GmbH PGI-5 Colloquium, (Forschungszentrum Jülich GmbH), Jülich , Germany, September (2013).

(Domestic Conference)

藤縄雅, 山口由高, 山澤秀行, 眞家武士, 熊谷桂子, 若杉昌徳: "理研 RIBF 稀少 RI リングの付帯設備", 第 10 回日本加速器学会年会, (日本加速器学会), 名古屋, 8 月 (2013).

長谷部裕雄, 久保木浩功, 奥野広樹, 今尾浩士, 山根功, 福西暢尚, 加瀬昌之, 上垣外修一: "カーボンナノチューブとカーボン蒸着複合膜の開発", 第 45 回 フラーレン・ナノチューブ・グラフェン　総合シンポジウム, (フラーレン・ナノチューブ・グラフェン学会), 大阪, 8 月 (2013).

久保木浩功, 奥野広樹, HershcovitchAdy, 池上九三男, 今尾浩士, 加瀬昌之, 上垣外修一, 段塚知志, 中川孝秀, 長谷部裕雄, 眞家武士, 矢野安重: "プラズマウィンドウを用いた差動排気システムの開発", プラズマ研究会, (日本電気学会), 長崎, 9 月 (2013).

藤縄雅: "理研 RI ビームファクトリー 稀少 RI リングの建設", 日本大学生産工学部第 46 回学術講演会, (日本大学生産工学部), 日本大学生産工学部津田沼校舎, 12 月 (2013).

SLOWRI Team

Publications

[Journal]

(Original Papers) *Subject to Peer Review

Arai F., Ito Y., Wada M., Schury P., Sonoda T., Mita H.: "Investigation of the ion surfing transport method with a circular rf carpet", Int. J. Mass Spectrom. **362**, 56 (2014). *

Schury P., Wada M., Ito Y., Arai F., Naimi S., Sonoda T., Wollnik H., Shchepunov V. A., Smorra C., Yuan C.: "A high-resolution multi-reflection time-of-flight mass spectrograph for precision mass measurements at RIKEN/SLOWRI", Nucl. Instr. and Meth. in Phys. Res. B **335**, 39 (2014). *

Schury P., Ito Y., Wada M., Wollnik M.: "Wide-band mass measurements with a multi-reflection time-of-flight mass spectrograph", Int. J. Mass Spectrom. **359**, 19 (2014). *

Ito Y., Schury P., Wada M., Naimi S., Sonoda T., Mita H., Arai F., Takamine A., Okada K., Ozawa A., Wollnik H.: "Single-reference high-precision mass measurement with a multi-reflection time-of-flight mass spectrograph", Phys. Rev. C **88**, 011306 (2013). *

Ito Y., Schury P., Wada M., Naimi S., Smorra C., Sonoda T., Mita H., Arai F., Takamine A., Okada K., Ozawa A., Wollnik H.: "A novel ion cooling trap for multi-reflection time-of-flight mass spectrograph", Nucl. Instrum. Methods Phys. Res. B **317**, 544 (2013). *

Jordan D.,Algora A.,Taĺn J. L.,Rubio B.,Agramunt J.,Perez-Cerdan A. B.,Molina ,F.Caballero L.,Nácher E., Krasznahorkay A.,Hunyadi M. D.,Gulyás J.,Vitéz A.,Csatlós M.,Csige L.,Äysto J.,Penttilä H.,Moore I. D.,Eronen T.,Jokinen A.,Nieminen A.,Hakala J.,Karvonen P.,Kankainen A.,Saastamoinen A.,Rissanen J.,Kessler T.,Weber C.,Ronkainen J.,Rahaman S.,Elomaa V.,Hager U.,Rinta-Antila S.,Sonoda T.,Burkard K.,Hüller W.,Batist L.,Gelletly W.,Nichols A. L.,Yoshida T.,Sonzogni A. A.,Peräjärvi K.,Petrovici A.,Schmid K. W., Faessler A.: "Total absorption study of theβ decay of102,104,105Tc", Phys. Rev. C **87**, 044318 (2013). *

[Book・Proceedings]

(Others)

Schury P., Wada M., Ito Y., Naimi S., Sonoda T., Mita H., Takamine A., Okada K., Wollnik H., Chon S., Haba H., Kaji D., Koura H., Miyatake H., Morimoto K., Morita K., Ozawa A.: "A multi-reflection time-of-flight mass spectrograph for short-lived and super-heavy nuclei", Nucl. Instr. and Meth in Phys. Res. B, 317, 537-543 (2013). *

Wada M.: "Genealogy of gas cells for low-energy RI-beam production", Nucl. Instr. and Meth in Phys. Res. B, 317, 450-456 (2013). *

Takatsuka T., Tomita H., Sonnenschein V., Sonoda T., Adachi Y., Sakamoto C., Mita H., Noto T., Ito C., Maeda S., Iguchi T., Wada M., Wendt K., Moore I.: "Development of resonance ionization in a supersonic gas-jet for studies of short-lived and long-lived radioactive nuclei", Nucl. Instr. and Meth in Phys. Res. B, 317, 586-589 (2013). *

Hirayama Y., Watanabe Y., Imai N., Ishiyama H., Jeong S., Miyatake H., Oyaizu M., Kim Y., Mukai M., Matsuo Y., Sonoda T., Wada M., Huyse M., Kudryavtsev Y., Duppen P.: "Off-line test of the KISS gas cell", Nucl. Instr. and Meth in Phys. Res. B, 317, 480-483 (2013). *

Yang X.F., Furukawa T., Wakui T., Imamura K., Tetsuka H., Fujita T., Yamaguchi Y., Tsutsui Y., Mitsuya Y., Ichikawa Y., Ishibashi Y., Yoshida N., Shirai H., Ebara Y., Hayasaka M., Arai S., Muramoto S., Hatakeyama A., Wada M., Sonoda T., Ito Y., Kobayashi T., Nishimura S., Nishimura M., Kondo Y., Yoneda K., Ueno H., Shinozuka T., Shimoda T., Asahi K., Matsuo Y.: "Control of stopping position of radioactive ion beam in superfluid helium for laser spectroscopy experiments", Nucl. Instr. and Meth in Phys. Res. B, 317, 599-602 (2013). *

Imamura K., Furukawa T., Wakui T., Yang X.F., Yamaguchi Y., Tetsuka H., Mitsuya Y., Tsutsui Y., Fujita T., Ebara Y., Hayasaka Ichikawa Y., Ishibashi Y., Yoshida N., Shirai H., M., Arai S., Muramoto S., Hatakeyama A., Wada M., Sonoda T., Ito Y., Kobayashi T., Nishimura S., Nishimura M., Kondo Y., Yoneda K., Ueno H., Shinozuka T., Shimoda T., Asahi K., Matsuo Y.: "Development of a helium cryostat for laser spectroscopy of atoms with unstable nuclei in superfluid helium", Nucl. Instr. and Meth in Phys. Res. B, 317, 595-598 (2013). *

Furukawa T., Wakui T., Yang X.F., Fujita T., Imamura K., Tetsuka H., Yamaguchi Y., Tsutsui Y., Mitsuya Y., Ichikawa Y., Ishibashi Y., Yoshida N., Shirai H., Ebara Y., Hayasaka M., Arai S., Muramoto S., Hatakeyama A., Wada M., Sonoda T., Ito Y., Kobayashi T., Nishimura S., Nishimura M., Kondo Y., Yoneda K., Ueno H., Shinozuka T., Shimoda T., Asahi K., Matsuo Y.: "Novel nuclear laser spectroscopy method using superfluid helium for measurement of spins and moments of exotic nuclei", Nucl. Instr. and Meth in Phys. Res. B, 317, 590-594 (2013). *

Takatsuka T., Tomita H., Sonoda T., Sonnenschein V., Sakamoto C., Mita H., Noto T., Ito C., Maeda S., Iguchi T., Wada M., Wendt K., Moore I.: "Development of high resolution resonance ionization mass spectrometry for trace analysis of ^{93m}Nb", Hyperfine Interactions, 216, 41 (2013). *

Sonoda T., Wada M., Tomita H., Sakamoto C., Takatsuka T., Noto T., Iimura H., Matsuo Y., Kubo T., Shinozuka T., Wakui T., Mita H., Naimi S., Furukawa T., Ito Y., Schury P., Miyatake H., Jeong S., Ishiyama H., Watanabe Y.: “Development of a gas cell-based laser ion source for RIKEN PALIS”, Hyperfine Interactions, 216, 103 (2013). *

Oral Presentations

(International Conference etc.)

Schury P.: “Status and Future of Multi-Reflection Time-of-Flight Mass Measurements at RIKEN: r-process and Super Heavy Elements”, JUSTIPEN-JUSEIPEN Workshop, (RIKEN), Saitama, Dec. (2013).

Schury P.: “Multi-reflection time-of-flight mass spectrograph for extremely fast, high-precision mass measurements”, 25th International Nuclear Physics Conference, (Palazzo dei Congressi), Firenze, Italy, June (2013).

Sonoda T.: “Parasitic production of slow RI-beam from BigRIPS by laser ionization gas catcher”, International Expert Meeting on In-Flight Separators and Related Issues Challenges and Solutions of the Present & Future Facilities, (RIKEN), Saitama, Japan, Dec. (2013).

(Domestic Conference)

新井郁也, 和田道治, Schury Peter, 伊藤由太, 園田哲, Wollnik Hermann: “高エネルギー RI 用ガスキャッチャーのための高圧下における ion surfing 型 RF カーペットの性能評価”, 日本物理学会, (東海大学), 神奈川, 3 月 (2014).

Schury Peter, 伊藤 由太, 和田 道治, Wollnik Hermann,: “Wide-band operation of a multi-reflection time-of-flight mass spectrograph”, 日本物理学会, (東海大学), 神奈川, 3 月 (2014).

伊藤由太, Schury Peter, 和田道治, 新井郁也, 加治大哉, 森本幸司, 園田哲, Wollnik Hermann: “MRTOF-MS を用いた超ウラン元素の精密直接質量測定”, 日本物理学会, (高知大学), 高知, 9 月 (2013).

伊藤由太, 和田道治, Schury Peter, 新井郁也, 園田哲, Wollnik Hermann: “SLOWRI クーラーバンチャーのための低圧下における ion surfing 型 RF カーペットの性能評価”, 日本物理学会, (東海大学), 神奈川, 3 月 (2014).

篠塚勉，涌井崇志，松尾由賀利，古川武，宮武宇也，石山博恒，今井伸明，平山賀一，渡辺裕，鄭淳讃，岡田邦宏，伊藤由太，中尾愛子園田哲, 和田道治, 飯村秀紀, 上野秀樹, 富田英生, 足立義貴, 高塚卓旦, Wendt Klaus, 久保敏幸, 若杉昌徳, 日下健祐, 眞家武士, 山澤秀行, 藤縄雅, 片山一郎, 新井郁也, Schury Peter, 篠塚勉, 涌井崇志, 松尾由賀利, 古川武, 宮武宇也, 石山博恒, 今井伸明, 平山賀一, 渡辺裕, 鄭淳讃, 岡田邦宏, 伊藤由太, 中尾愛子: “RIBF-SLOWRI 共鳴イオン化レーザーイオン源 (PALIS) の開発とレーザー核分光への応用”, 日本物理学会, (高知大学), 高知, 9 月 (2013).

和田道治: “SLOWRI の現状と計画”, 第 7 回停止・低速不安定核ビームを用いた核分光研究会, (理研), 埼玉, 3 月 (2014).

園田哲: “パラサイト低速 RI ビーム生産とレーザー核分光への応用”, 第 7 回停止・低速不安定核ビームを用いた核分光研究会, (理研), 埼玉, 3 月 (2014).

伊藤 由太: “Future MRTOF-based experiments at SLOWRI”, 第 7 回停止・低速不安定核ビームを用いた核分光研究会, (理研), 埼玉, 3 月 (2014).

Rare RI-ring Team

Publications

[**Book・Proceedings**]

(Original Papers)

Yamaguchi Y., Wakasugi M., Uesaka T., Ozawa A., Abe Y., Fujinawa T., Kase M., Komiyama M., Kubo T., Kumagai K., Maie T., Nagae D., Ohnishi J., Suzaki F., Tokuchi A., Watanabe Y., Yoshida K., Yamada K., Yamaguchi T., Yamasawa H., Yanagisawa Y., Zenihiro J., and Yano Y.:

"Construction of rare-RI ring at RIKEN RI Beam Factory", Nucl. Instrum. Methods **B317**, p. 629–635 (2013).

Suzaki F., Zenihiro J., Yamaguchi T., Ozawa A., Uesaka T., Wakasugi M., Yamada K., Yamaguchi Y., and rare-RI ring collaboration:

"Design study of a resonant Schottky pick-up for the Rare-RI Ring project", Nucl. Instrum. Methods **B317**, p. 636–639 (2013).

Nagae D., Okada S., Ozawa A., Yamaguchi T., Suzuki H., Moriguchi T., Ishibashi Y., Fukuoka S., Nishikiori R., Niwa T., Suzuki T., Sato K., Furuki H., Ichihashi N., Miyazawa S., Yamaguchi Y., Uesaka T., and Wakasugi M.:

"Time-of-flight detector applied to mass measurements in Rare-RI Ring", Nucl. Instrum. Methods **B317**, p. 640–643 (2013).

Yamaguchi T., Yamaguchi Y., Ozawa A.:

"The challenge of precision mass measurements of short-lived exotic nuclei: Development of a new storage-ring mass spectrometry", International Journal of Mass Spectrometr **349–350**, p. 240–246 (2013).

Yamaguchi T., Izumikawa T., Miyazawa S., Suzuki T., Tokanai F., Furuki H., Ichihashi N., Ichikawa C., Kitagawa A., Kuboki T., Momota S., Nagae D., Nagashima M., Nakamura Y., Nishikiori R., Ohtsubo T., Ozawa A., Sato K., Sato S., and Suzuki S.:

"Performance of high-resolution position-sensitive detectors developed for storage-ring decay experiments", Nucl. Instrum. Methods **B317**, p. 697–700 (2013).

Abe Y., Nagae D., and rare-RI ring collaboration:

"Developments of time-of-flight detectors for Rare-RI Ring", Proceedings of the 12th Asia Pacific Physics Conference **1**, p. 013059 (2013).

Suzaki F., Yamaguchi T., and rare-RI ring collaboration:

"Time-of-flight detector applied to mass measurements in Rare-RI Ring", Proceedings of the 12th Asia Pacific Physics Conference **1**, p. 013058 (2013).

Oral Presentations

(International Conference etc.)

Wakasugi M., and rare-RI ring collaboration: "Construction of the Rare RI Ring (R3) at the RIKEN RI Beam Factory", The 20th International Conference on Cyclotrons and Their Applications, Vancouver, CANADA, September (2013).

Yamaguchi T.: "Rare-RI Ring project in RIKEN", Sino-German Symposium on (High precision experiments with stored exotic and stable nuclei), Lanzhou, CHINA, CHINA, November (2013).

Yamaguchi Y., and rare-RI ring collaboration: "Construction status of the Rare-RI Ring", RIBF Users Meeting 2013, Wako, JAPAN, June (2013).

Ozawa A., and rare-RI ring collaboration: "Rare-RI Ring for Mass measurements at RIBF", The 12th International Symposium on Origin of Matter and Evolution of Galaxies (OMEG12), Tsukuba, JAPAN, November (2013).

(Domestic Conference)

阿部康志, 長江大輔, 岡田俊祐, 小沢顕, 山口貴之, 石橋陽子, 斉藤祐多, 沢畑克樹, 鈴木健, 河野準平, 山木さやか, 山口由高, 上坂友洋, 若杉昌徳: "稀少 RI リングのビームモニターの開発", 日本物理学会　2013 年秋季大会, (日本物理学会), 高知市, 9 月 (2013).

洲嵜ふみ, 銭廣十三, 小沢顕, 鈴木健, 上坂友洋, 若杉昌徳, 山田一成, 山口貴之, 山口由高: "稀少 RI リングの共鳴ショットキーピックアップ設計のための電磁場シミュレーション", 日本物理学会　2013 年秋季大会, (日本物理学会), 高知市, 9 月 (2013).

洲嵜ふみ, 銭廣十三, 小沢顕, 鈴木健, 上坂友洋, 若杉昌徳, 山田一成, 山口貴之, 山口由高: "稀少 RI リングの共鳴ショットキーピックアップの性能試験", 日本物理学会　第 69 回年次大会, (日本物理学会), 平塚市, 3 月 (2014).

SCRIT Team

Publications

[Journal]

(Original Papers) *Subject to Peer Review

Wakasugi M., Ohnishi T., Wang S., Miyashita Y., Adachi T., Amagai T., Enokizono A., Enomoto A., Haraguchi Y., Hara M., Hori T., Ichikawa S., Kikuchi T., Kitazawa R., Koizumi K., Kurita K., Miyamoto T., Ogawara R., Shimakura Y., Takehara H., Tamae T., Tamaki S., Togasaki M., Yamaguchi T., Yanagi K., Suda T.: "Construction of the SCRIT electron scattering facility at the RIKEN RI Beam Factory", Nucl. Instr. Meth. B, **317**, 668–673, (2013).*

Ogawara R., Ohnishi T., Togasaki M., Tamaki S., Miyashita Y., Takehara H., Koizumi K., Kurita K., Wakasugi M., Yamaguchi T., Yanagi K., Suda T.: "Ion-trapping properties of SCRIT", Nucl. Instr. Meth. B, **317**, 674–678, (2013).*

Ohnishi T., Ichikawa S., Koizumi K., Kurita K., Miyashita Y., Ogawara R., Tamaki S., Togasaki M., Wakasugi M.: "Electron-beam-driven RI separator for SCRIT (ERIS) at RIKEN RI beam factory", Nucl. Instr. Meth. B, **317**, 357–360, (2013).*

Wakasugi M., Ohnishi T., Suda T., Kurita K.: "Development of a Femto Scope for Short-Lived Unstable Nuclei", BUTSURI, **68**, 810–817, (2013).*

Oral Presentations

(International Conference etc.)

Enokizono A., "SCRIT Electron Scattering Facility at RIKEN ", Asia Pacific Physics Conference 12, (The Association of Asia Pacific Physical Societies), Makuhari, Chiba, July (2013).

Suda T., "Electron Scattering for Exotic Nuclei", International Symposium on Nuclear Physics, (Bhabha Atomic Research Center), Mumbai, India, December (2013).

Suda T., "Electron Scattering for Exotic Nuclei", Strangeness Nuclear Physics Winter Schhol, (Tohoku University), Sendai, Japan, Feburary (2013).

(Domestic Conference)

宮本嵩也: "SCRIT 実験のための Spectrometer の磁場測定及び解析", 原子核素粒子三者若手夏の学校, (原子核素粒子三者若手), 蒲郡市, 愛知, 8 月 (2013).

須田利美: "電子散乱による不安定核構造の研究"
集中講義, (大阪大学), 大阪, 6 月 (2013).

島倉優人, 市川進一, 榎園昭智, 大西哲哉, 栗田和好, 鷲見洋平, 戸ヶ崎衛, 原雅弘, 原口祐司, 松尾咲希, 若杉昌徳: "SCRIT 電子散乱実験における反跳核検出器の開発"
日本物理学会第６９回年次大会, (日本物理学会), 神奈川, 3 月 (2014).

Research Instruments Group

Publications

[Journal]

(Original Papers) *Subject to Peer Review

Suzuki H., Kubo T., Fukuda N., Inabe N., Kameda D., Takeda H., Yoshida K., Kusaka K., Yanagisawa Y., Ohtake M., Sato H., Shimizu Y., Baba H., Kurokawa M., Ohnishi T., Tanaka K., Tarasov O.B., Bazin D., Morrissey D.J., Sherrill B.M., Ieki K., Murai D., Iwasa N., Chiba A., Ohkoda Y., Ideguchi E., Go S., Yokoyama R., Fujii T., Nishimura D., Nishibata H., Momota S., Lewitowicz M., DeFrance G., Celikovic I., Steiger K.: "Production cross section measurement of radioactive isotopes by BigRIPS separator at RIKEN RI Beam Factory", Nucl. Instr. Meth. B **317**, 756–768 (2013). *

Fukuda N., Kubo T., Ohnishi T., Inabe N., Takeda H., Kameda D., Suzuki H.: "Identification and separation of radioactive isotope beams by the BigRIPS separator at the RIKEN RI Beam Factory", Nucl. Instr. Meth. B **317**, 323–332 (2013). *

Yoshida K., Fukuda N., Yanagisawa Y., Inabe N, Mizoi Y., Kubo T.: "High-power beam dump system for the BigRIPS fragment separator at RIKEN RI Beam Factory", Nucl. Instr. Meth. B **317**, 373–380 (2013). *

Kumagai H., Ohnishi T., Fukuda N., Takeda H., Kameda D., Inabe N., Yoshida K., Kubo T.: "Development of Parallel Plate Avalanche Counter (PPAC) for BigRIPS fragment separator", Nucl. Instr. Meth. B **317**, 717–727 (2013). *

Takeda H,, Kubo T., Kusaka K., Suzuki H., Inabe N., Nolen J.A.: "Extraction of 3D field maps of magnetic multipoles from 2D surface measurements with applications to the optics calculations of the large-acceptance superconducting fragment separator BigRIPS" Nucl. Instr. Meth. B **317**, 798–809 (2013). *

Tanaka K., Inabe N., Yoshida K, Kusaka K., Kubo T.: "Pillow seal system at the BigRIPS separator", Nucl. Instr. Meth. B **317**, 734–738 (2013). *

Nishi T., Berg G.P.A., Dozono M., Fujioka H., Fukuda N., Furuno T., Geissel H., Hayano R.S., Inabe N., Itahashi K., Itoh S., Kameda D., Kubo T., Matsubara H., Michimasa S., Miki K., Miya H., Murakami Y., Nakamura M., Nakatsuka N., Noji S., Okochi K., Ota S., Suzuki H., Suzuki K., Takaki M., Takeda H., Tanaka Y.K., Todoroki K., Tsukada K., Uesaka T., Watanabe Y.N., Weick H., Yamada H., Yoshida K.: "BigRIPS as a high resolution spectrometer for pionic atoms", Nucl. Instr. Meth. B **317**, 290–293 (2013). *

Ichikawa Y., Ueno H., Ishii Y., Furukawa T., Yoshimi A., Kameda D., Watanabe H., Aoi N., Asahi K., Balabanski D.L., Chevrier R., Daugas J.M., Fukuda N., Georgiev G., Hayashi H., Iijima H., Inabe N., Inoue T., Ishihara M., Kubo T., Nanao T., Ohnishi T., Suzuki K., Tsuchiya M., Takeda H., Rajabali M.M.: "Spin-aligned RI beams via two-step fragmentation reactions", Nucl. Instr. Meth. B **317**, 769–773 (2013). *

Shimizu Y., Otsu H., Kobayashi T., Kubo T., Motobayashi T., Sato H., Yoneda K.: "Vacuum system for the SAMURAI spectrometer", Nucl. Instr. Meth. B **317**, 739–742 (2013). *

Kobayashi T., Chiga N., Isobe T., Kondo Y., Kubo T., Kusaka K., Motobayashi T., Nakamura T., Ohnishi J., Okuno H., Otsu H., Sako T., Sato H., Shimizu Y., Sekiguchi K., Takahashi K., Tanaka R., Yoneda K.: "SAMURAI spectrometer for RI beam experiments", Nucl. Instr. Meth. B **317**, 294–304 (2013). *

Michimasa S., Takaki M., Sasamoto Y., Dozono M., Nishi T., Kawabata T., Ota S., Baba H., Fujii T., Go S., Kawase S., Kikuchi Y., Kisamori K., Kobayashi M., Kubota Y., Lee C.S., Matsubara H., Miki K., Miya H., Noji S., Tokieda H., Tsumura M., Yako K., Yokoyama R., Takeda H., Yanagisawa Y., Kubo T., Inabe N., Fukuda N., Kameda D., Suzuki H., Shimizu Y., Sato H., Ichihara T., Stolz A., Zegers R.G.T., Sakai H., Uesaka T., Shimoura S.: "SHARAQ spectrometer for high-resolution studies for RI-induced reactions", Nucl. Instr. Meth. B **317**, 305–310 (2013). *

Yamaguchi Y., Wakasugi M., Uesaka T., Ozawa A., Abe Y., Fujinawa T., Kase M., Komiyama M., Kubo T., Kumagai K., Maie T., Nagae D., Ohnishi J., Suzuki F., Tokuchi A., Watanabe Y., Yoshida K., Yamada K., Yamaguchi T., Yamasawa H., Yanagisawa Y., Zenihiro J., Yano Y.: "Construction of rare-RI ring at RIKEN RI Beam Factory", Nucl. Instr. Meth. B **317**, 629–635 (2013). *

Yoshida A., Kambara T., Nakao A., Uemoto R., Uno H., Nagano A., Yamaguchi H., Nakao T., Kahl D., Yanagisawa T., Kameda D., Ohnishi T., Fukuda N., Kubo T.: "Wear diagnostics of industrial material using RI beams of ^{7}Be and ^{22}Na", Nucl. Instr. Meth. B **317**, 785–788 (2013). *

Kusaka K., Ohtake M., Ohnishi T., Yoshida K., Kubo T., Ito H., Tsuchihashi T.: "Long-Term Operation of the Superconducting Triplet Quadrupoles With Small Cryocoolers for BigRIPS In-Flight Separator and RI-Beam Delivery Line at RIKEN" IEEE Trans. Appl. Supercond. **vol. 23, No.3**, 4101305 (2013). *

Watanabe H., Lorusso G., Nishimura S., Xu Z.Y., Sumikama T., Söderström P.-A., Doornenbal P., Browne F., Gey G., Jung H.S., Taprogge J., Vajta Zs., Wu J., Yagi A., Baba H., Benzoni G., Chae K.Y., Crespi F.C.L., Fukuda N., Gernhäuser R., Inabe N., Isobe T., Jungclaus A., Kameda D., Kim G.D., Kim Y.K., Kojouharov I., Kondev F.G., Kubo T., Kurz N., Kwon Y.K., Lane G.J., Li Z., Moon C.-B., Montaner-Pizá A., Moschner K., Naqvi F., Niikura M., Nishibata H., Nishimura D., Odahara A., Orlandi R., Patel Z., Podolyák Zs., Sakurai H., Schaffner H., Simpson G.S., Steiger K., Suzuki H., Takeda H., Wendt A., Yoshinaga

K.: "Isomers in ^{128}Pd and ^{126}Pd: Evidence for a Robust Shell Closure at the Neutron Magic Number 82 in Exotic Palladium Isotopes", Phys. Rev. Lett. **111**, 152501 (2013). ∗

Söderström P.A., Lorusso G., Watanabe H., Nishimura S., Doornenbal P., Thiamova G., Browne F., Gey G., Jung H.S., Sumikama T., Taprogge J., Vajta Zs., Wu J., Xu Z.Y., Baba H., Benzoni G., Chae K.Y., Crespi F.C.L., Fukuda N., Gernhäuser R., Inabe N., Isobe T., Jungclaus A., Kameda D., Kim G.D., Kim Y.K., Kojouharov I., Kondev F.G., Kubo T., Kurz N., Kwon Y.K., Lane G.J., Li Z., Montaner-Pizá A., Moschner K., Naqvi F., Niikura M., Nishibata H., Odahara A., Orlandi R., Patel Z., Podolyák Zs., Sakurai H., Schaffner H., Simpson G.S., Steiger K., Suzuki H., Takeda H., Wendt A., Yagi A., Yoshinaga K.: "Shape evolution in ^{116,118}Ru: Triaxiality and transition between the O(6) and U(5) dynamical symmetries", Phys. Rev. C **88**, 024301 (2013). ∗

Steppenbeck D., Takeuchi S., Aoi N., Doornenbal P., Matsushita M., Wang H., Baba H., Fukuda N., Go S., Honma M., Lee J., Matsui K., Michimasa S., Motobayashi T., Nishimura D., Otsuka T., Sakurai H., Shiga Y., Sumikama T., Suzuki H., Taniuchi T., Utsuno Y., Valiente-Dobon J.J., Yoneda K.: "Evidence for a new nuclear 'magic number' from the level structure of ^{54}Ca" Nature **502**, 207 (2013). ∗

Ichikawa Y., Ueno H., Ishii Y., Furukawa T., Yoshimi A., Kameda D., Watanabe H., Aoi N., Asahi K., Balabanski D.L., Chevrier R., Daugas J.M., Fukuda N., Georgiev G., Hayashi H., Iijima H., Inabe N., Inoue T., Ishihara M., Kubo T., Nanao T., Ohnishi T., Suzuki K., Tsuchiya M., Takeda H., Rajabali M.M.: "Novel method for the production of spin-aligned RI beams in projectile fragmentation reaction with the dispersion matching technique", Hyperfine Interact **220**, 47–51 (2013). ∗

(Review)

吉田光一, 久保敏幸, 日下健祐, 福田直樹, 柳澤善行, 竹田浩之, 稲辺尚人, 大竹政雄, 亀田大輔, 田中鐘信, 鈴木宏.: "理研の超伝導 RI ビーム生成装置 BigRIPS について", 加速器 **Vol. 10**, 93–100 (2013).

Oral Presentations

(International Conference etc.)

Kubo T.: "Overview of the Search for New Isotopes and New Isomers at RIKEN RI Beam Factory", International Nuclear Physics Conference INPC2013, Firenze, Italy, June–June (2013).

Kameda D., Kubo T.: "Search for new isotopes and new isomers using in-flight fission of a 345 MeV/u ^{238}U beam", RIBF Users Meeting, (RIKEN), Wako, Japan, June–June (2013).

Kubo T.: "Overview of the Experimental Facilities at RIKEN RI Beam Factory (RIBF)", Gordon Research Conference on Nuclear Chemistry, (Colby-Sawyer College), New London, USA, June–June (2013).

Kubo T.: "Observation of New Isotopes and New Isomers at RIKEN RI Beam Factory", 33rd Mazurian Lakes Conference on Physics "Frontiers in Nuclear Physics", Piaski, Poland, September–September, (2013).

Kameda D., Kubo T.: "New isomers in the neutron-rich rare earth region by in-flight fission of 345 MeV/nucleon ^{238}U" RCNP international workshop on Physics Opportunities using Compton Suppressed Ge Clover Array (CAGRA13), (RCNP), Osaka, Japan, December-December (2013).

Kameda D., Kubo T.: "Search for new isotopes and new isomers using in-flight fission of a 345 MeV/nucleon ^{238}U beam at RIKEN RI Beam Factory", 16th ASRC International Workshop on Nuclear Fission and Structure of Exotic Nuclei, (Japan Atomic Energy Agency (JAEA)), Tokai, Japan, March–March, (2014).

(Domestic Conference)

南方亮吾, 中村隆司, 近藤洋介, Achouri N.L., Aumann T., 馬場秀忠, Delaunay F., Doornenbal P., 福田直樹, Gibelin J., Huang J., 稲辺尚人, 磯部忠昭, 亀田大輔, 簡野大輝, Kim S., 小林信之, 小林俊雄, 久保敏幸, Leblond S., Lee J., Marques M., 本林透, 村井大地, 村上哲也, 武藤琴美, 中嶋丈嘉, 中塚徳継, Navin A., 西征爾郎, 生越駿, Orr N.A., 大津秀暁, 佐藤広海, 佐藤義輝, 清水陽平, 鈴木宏, 高橋賢人, 竹田浩之, 武内聡, 田中隆己, 栂野泰宏, Tuff A.G., Vandebrouck M., 米田健一郎.: "^{22}C のクーロン分解反応", 日本物理学会第 69 回年次大会, (東海大学), 神奈川, 3 月 (2014).

生越駿, 中村隆司, 近藤洋介, Achouri N.L., Aumann T., 馬場秀忠, Delaunay F., Doornenbal P., 福田直樹, Gibelin J., Huang J., 稲辺尚人, 磯部忠昭, 亀田大輔, 簡野大輝, Kim S., 小林信之, 小林俊雄, 久保敏幸, Leblond S., Lee J., Marques M., 南方亮吾, 本林透, 村井大地, 村上哲也, 武藤琴美, 中嶋丈嘉, 中塚徳継, Navin A., 西征爾郎, Orr N.A., 大津秀暁, 佐藤広海, 佐藤義輝, 清水陽平, 鈴木宏, 高橋賢人, 竹田浩之, 武内聡, 田中隆己, 栂野泰宏, Tuff A.G., Vandebrouck M., 米田健一郎.: "^{19}B のクーロン分解反応", 日本物理学会第 69 回年次大会, (東海大学), 神奈川, 3 月 (2014).

近藤洋介, 中村隆司, Achouri N.L., Aumann T., 馬場秀忠, Delaunay F., Doornenbal P., 福田直樹, Gibelin J., Huang J., 稲辺尚人, 磯部忠昭, 亀田大輔, 簡野大輝, Kim S., 小林信之, 小林俊雄, 久保敏幸, Leblond S., Lee J., Marques M., 南方亮吾, 本林透, 村井大地, 村上哲也, 武藤琴美, 中嶋丈嘉, 中塚徳継, Navin A., 西征爾郎, 生越駿, Orr N.A., 大津秀暁, 佐藤広海, 佐藤義輝, 清水陽平, 鈴木宏, 高橋賢人, 竹田浩之, 武内聡, 田中隆己, 栂野泰宏, Tuff A.G., Vandebrouck M., 米田健一郎.: "^{25}C,^{26}C 非束縛状態の探索", 日本物理学会第 69 回年次大会, (東海大学), 神奈川, 3 月 (2014).

小林信之, 中村隆司, 近藤洋介, Tostevin J.A., 宇都野穣, 青井考, 馬場秀忠, Barthelemy R., 福田直樹, Lee G., Lee H.S., 稲辺尚人, 石原正泰, Kanungo r., 久保敏幸, Kim S.J., Famiano M., 松下昌史, 本林透, 大西哲哉, Orr N.A., 大津

秀暁, 大塚孝治, 櫻井博儀, 佐古貴行, 炭竃聡之, 佐藤義輝, 高橋好太郎, 竹田浩之, 武内聡, 田中隆己, 栂野泰宏, 米田健一郎.: “分解反応を用いた中性子過剰な Mg 同位体の研究”, 日本物理学会第 69 回年次大会, (東海大学), 神奈川, 3 月 (2014).

川瀬頌一郎, 上坂友洋, 下浦享, 矢向謙太郎, 大田晋輔, 道正新一郎, 時枝紘史宮裕之, Leung T.T., 木佐森慶一, 高木基伸, 久保田悠樹, 李清秀, 横山輪, 藤井俊彦, 小林幹, 笹野匡紀, 銭廣十三, 松原礼明, 堂園昌伯, Lee J., 酒井英行, 久保敏幸, 吉田光一, 稲辺尚人, 柳澤善行, 竹田浩之, 日下健祐, 福田直樹, 亀田大輔, 鈴木宏, 河原朋美, 涌井崇志, 坂口聡志, 野呂哲夫, 若狭智嗣, 安田淳平, 福永拓, 前田幸重, Kim W.Y., Hwang S.H., Stepanyan S., Obertelli A., Galindo-Uribarri A., Padilla-Rodal E., Beaumel D.: “準弾性 ^{A}O(p,2p) 反応による窒素同位体の陽子一空孔状態の核分光”, 日本物理学会第 69 回年次大会, (東海大学), 神奈川, 3 月 (2014).

西隆博, Berg G.P.A., 堂園昌伯, 福田直樹, 古野達也, 藤岡宏之, Geissel H., 早野龍五, 稲辺尚人, 板橋健太, 伊藤聖, 亀田大輔, 久保敏幸, 松原礼明, 道正新一郎, 三木謙二郎, 宮裕之, 中村祐喜, 村上洋平, 中塚徳継, 野地俊平, 大河内公太, 大田晋輔, 鈴木宏, 鈴木謙 高木基伸, 竹田浩之, 田中良樹, 轟孔一, 塚田暁, 上坂友洋, 渡辺珠以, Weick H., 山田裕之, 吉田光一.: “(d,^{3}He) 反応を用いた π 中間子原子の精密分光 (10)“, 日本物理学会第 69 回年次大会, (東海大学), 神奈川, 3 月 (2014).

宮崎卓也, 大津秀暁, Nikolskii E.Y., 志賀慶明, 西村美月, 武内聡, 佐藤義輝, 黒川明子, 馬場秀忠, Lorusso G., 磯部忠昭, 新倉潤, Kuzmin E.A., Korsheninnikov A.A., Ogloblin A.A., Krupko S.A., Golovkov M.S., Bezbakh A.A, Slepnev R.S., Fomichev A.S., Sidorchuk S.I., Gorshkov A.V., Knyazev A.G., Papka P., JinØ.H., Kim S. Hwang J., Choi S., Chae H., Kim E., Kim Y., Lubos D., Beaumel D., Söderström P.A., 坂口聡志, 久保野茂, Perrevoort A.K., Milman E., Chebotaryov S., Powell W., 本林透, 米田健一郎, 櫻井博儀.: “欠損質量核分光による ^{8}C 核励起状態の探索”, 日本物理学会第 69 回年次大会, (東海大学), 神奈川, 3 月 (2014).

西隆博, Berg G.P.A., 堂園昌伯, 福田直樹, 古野達也, 藤岡宏之, Geissel H., 早野龍五, 稲辺尚人, 板橋健太, 伊藤聖, 亀田大輔, 大河内公太, 久保敏幸, 松原礼明, 道正新一郎, 三木謙二郎, 宮裕之, 中村祐喜, 村上洋平, 中塚徳継, 野地俊平, 大田晋輔, 鈴木宏, 鈴木謙 高木基伸, 竹田浩之, 田中良樹, 轟孔一, 塚田暁, 上坂友洋, 渡辺珠以, Weick H., 山田裕之, 吉田光一.: “(d,^{3}He) 反応を用いた π 中間子原子の精密分光 (9)“, 日本物理学会 2013 年秋季大会, (高知大学), 高知, 9 月 (2013).

宮裕之, 下浦享, 木佐森慶一, 馬場秀忠, 馬場辰雄, 堂園昌伯, 福田直樹, 藤井俊彦, 郷慎太郎, 井手口栄治, 稲辺尚人, 伊藤正俊, 亀田大輔, 川畑貴裕, 川瀬頌一郎, 久保敏幸, 久保田悠樹, 小林幹, 近藤洋介, 李清秀, 前田幸重, 松原礼明, 三木謙二郎, 道正新一郎, 西隆博, 西村美月, 大田晋輔, 坂口聡志, 酒井英行, 笹野匡紀, 佐藤広海, 清水陽平, 鈴木宏, 高木基伸, 民井淳, 竹田浩之, 武内聡, 時枝紘史, 村美保, 上坂友洋, 柳沢善行, 矢向謙太郎, 横山輪, 吉田光一, Assie M., Beaumel D., Fariouz H., Stolz A.: “発熱型荷電交換反応 (^{8}He,^{8}Li γ) を用いた ^{4}He 核のスピン・アイソスピン応答の研究”, 日本物理学会 2013 年秋季大会, (高知大学), 高知, 9 月 (2013).

木佐森慶一, 下浦享, 宮裕之, 馬場秀忠, 馬場辰彦, 堂園昌伯, 福田直樹, 藤井俊彦, 郷慎太郎, 井手口栄治, 稲辺尚人, 伊藤正俊, 亀田大輔, 川畑貴裕, 川瀬頌一郎, 久保敏幸, 久保田悠樹, 小林幹, 近藤洋介, 李清秀, 前田幸重, 松原礼明, 三木謙二郎, 道正新一郎, 西隆博, 西村美月, 大田晋輔, 坂口聡志, 酒井英行, 笹野匡紀, 佐藤広海, 清水陽平, 鈴木宏, 高木基伸, 民井淳, 竹田浩之, 武内聡, 時枝紘史, 津村美保, 上坂友洋, 柳沢善行, 矢向謙太郎, 横山輪, 吉田光一, Assie M., Beaumel D., Fariouz H., Stolz A.: “二重荷電交換反応をもちいた 4 中性子系質量欠損核分光実験”, 日本物理学会 2013 年秋季大会, (高知大学), 高知, 9 月 (2013).

園田哲, 和田道治, 飯村秀紀, 上野秀樹, 富田英生, 足立義貴, 高塚卓旦, Wendt K., 久保敏幸, 若杉昌徳, 日下健祐, 眞家武士, 山澤秀行, 藤縄雅, 片山一郎, 新井郁也, Schury P., 篠塚勉, 涌井崇志, 松尾由賀利, 古川武, 宮武宇也, 石山博恒, 今井伸明, 平山賀一, 渡辺裕, 鄭淳讃, 岡田邦宏, 伊藤由太, 中尾愛子, “RIBF-SLOWRI 共鳴イオン化レーザーイオン源 (PALIS) の開発とレーザー核分光への応用”, 日本物理学会 2013 年秋季大会, (高知大学), 高知, 9 月 (2013).

石元茂, 小澤顕, 小林俊雄, 鈴木祥仁, 田中純貴, 谷畑勇夫, 森本喜三夫, Sanetullaev A., Kanungo R.: “TRIUMF-IRIS 実験用窓なし固体水素ターゲットの開発”, 日本物理学会 2013 年秋季大会, (高知大学), 高知, 9 月 (2013).

南方亮吾, 中村隆司, 近藤洋介, Achouri N.L., Aumann T., 馬場秀忠, Delaunay F., Doornenbal P., 福田直樹, Gibelin J., Huang J., 稲辺尚人, 磯部忠昭, 亀田大輔, 簡野大輝, Kim S., 小林信之, 小林俊雄, 久保敏幸, Leblond S., Lee J., Marques M., 本林透, 村井大地, 村上哲也, 武藤琴美, 中嶋丈嘉, 中塚徳継, Navin A., 西征爾郎, 生越駿, Orr N.A., 大津秀暁, 佐藤広海, 佐藤義輝, 清水陽平, 鈴木宏, 高橋賢人, 竹田浩之, 武内聡, 田中隆己, 栂野泰宏, Tuff A.G., Vandebrouck M., 米田健一郎.: “^{22}C の分解反応 II”, 日本物理学会 2013 年秋季大会, (高知大学), 高知, 9 月 (2013).

大道理恵, 渡邉寛, 八木彩祐未, 小田原厚子, 方一帆, 西畑洸希, 下田正, 西村俊二, Lorusso G., 炭竃聡之, Söderström P.A., Wu J., Brown D.F., 徐正宇, 磯部忠昭, 馬場秀忠, 鈴木宏, 稲辺尚人, 亀田大輔, 福田直樹, 竹田浩之, 久保敏幸, Bruce A., Regan P., Podolyak Z., Roberts O., the EURICA collaborators: “LaBr3 検出器を用いた中性子過剰核の励起状態の寿命測定”, 日本物理学会 2013 年秋季大会, (高知大学), 高知, 9 月 (2013).

井手口栄治, Simpson G., 横山輪, 田中まな, 青井考, 馬場秀忠, Bello F., Browne F., 大道理恵, Doornenbal P., Fang Y., 福田直樹, Gey G., 郷慎太郎, 稲辺尚人, 磯部忠昭, 亀田大輔, 小林和馬, 小林幹, 小松原哲郎, 久保敏幸, Kuri I., Li Z., Lorusso G., 松下昌史, 道正新一郎, Moon C.-B., 西畑洸希, 西村俊二, 西塚一平, 小田原厚子, Patel Z., Rice S., Sahin E., Sinclair L., Söderström P.A., 炭竃聡之, 鈴木宏, 竹田浩之, Taprogge J., Vajra Z., 渡邉寛, Wu J., 徐正宇, 八木彩祐未.: “中性子過剰領域 Z∼60 原子核における K ア

イソマーの探索”, 日本物理学会 2013 年秋季大会, (高知大学), 高知, 9 月 (2013).

田中まな, 井手口栄治, Simpson G., 横山輪, 青井考, 馬場秀忠, Bello F., Browne F., 大道理恵, Doornenbal P., Fang Y., 福田直樹, Gey G., 郷慎太郎, 稲辺尚人, 磯部忠昭, 亀田大輔, 小林和馬, 小林幹, 小松原哲郎, 久保敏幸, Kuri I., Li Z., Lorusso G., 松下昌史, 道正新一郎, Moon C.-B., 西畑洸希, 西村俊二, 西塚一平, 小田原厚子, Patel Z., Rice S., Sahin E., Sinclair L., Söderström P.A., 炭竃聡之, 鈴木宏, 竹田浩之, Taprogge J., Vajra Z., 渡邉寛, Wu J., 徐正宇, 八木彩祐未.: “中性子過剰 Nd 同位体におけるアイソマー分光”, 日本物理学会 2013 年秋季大会, (高知大学), 高知, 9 月 (2013).

方一帆, 小田原厚子, Lozeva R., Moon C., 八木彩祐未, 大道理恵, 西畑洸希, 下田正, 西村俊二, Doornenbal P., Lorusso G., 炭竃聡之, 渡辺寛, Söderström P.A., Wu J., Brown F., 徐正宇, 横山輪, 磯部忠昭, 馬場秀忠, 櫻井博儀, 鈴木宏, 稲辺尚人, 亀田大輔, 福田直樹, 竹田浩之, 安得順, 清水陽平, 佐藤広海, 久保敏幸, 石垣知樹, 森本翔太, 井手口栄治, 小松原哲郎, 新倉潤, the EURICA collaborators: “Study of beta decay of neutron-rich I isotopes at RIKEN RIBF using a stack of Si-strip detectors WASA3Bi combined with a cluster-Ge array EURICA”, 日本物理学会 2013 年秋季大会, (高知大学), 高知, 9 月 (2013).

八木彩祐未, 小田原厚子, Lozeva R., Moon C., 方一帆, 大道理恵, 西畑洸希, 下田正, 西村俊二, Doornenbal P., Lorusso G., 炭竃聡之, 渡辺寛, Söderström P.A., Wu J., Brown F., 徐正宇, 横山輪, 磯部忠昭, 馬場秀忠, 櫻井博儀, 鈴木宏, 稲辺尚人, 亀田大輔, 福田直樹, 竹田浩之, 安得順, 清水陽平, 佐藤広海, 久保敏幸, 石垣知樹, 森本翔太, 井手口栄治, 小松原哲郎, 新倉潤, the EURICA collaborators: “理研 RIBF の EURICA を用いた中性子過剰な Cs 同位体 (A 150) のアイソマーの研究”, 日本物理学会 2013 年秋季大会, (高知大学), 高知, 9 月 (2013).

横山 輪, 井手口 栄治, Simpson G., 田中 まな, 西村 俊二, Lorusso G., 炭竃 聡之, Doornenbal P., 馬場 秀忠, 磯部忠昭, Söderström P.A., Wu J., Xu Z., Browne F., Patel Z., Rice S., Sinclair L., Li Z., 渡邉 寛, Gey G., Sahin E., Bello F., Vajra Z., Kuri I., Taprogge J., 小田原厚子, Fang Y., 大道理恵, 八木彩祐未, 西畑洸希, 青井考, 小林和馬, 道正新一郎, 松下昌史, 小林幹, 郷慎太郎, 久保敏幸, 亀田大輔, 稲辺尚人, 竹田浩之, 福田直樹, 鈴木宏, 西塚一平, 小松原哲郎, Moon C.-B.: “過剰変形領域の Pm 同位体における新アイソマーの発見”, 日本物理学会 2013 年秋季大会, (高知大学), 高知, 9 月 (2013).

堂園昌伯, 上坂友洋, 笹野匡紀, 銭廣十三, 松原礼明, 下浦享, 矢向謙太郎, 道正新一郎, 大田晋輔, 時枝紘史, 宮裕之, 川瀬頌一郎, Tang R., 木佐森慶一, 高木基伸, 久保田悠樹, 李清秀, 藤井俊彦, 横山輪, 酒井英行, 久保敏幸, 吉田光一, 柳沢善行, 福田直樹, 竹田浩之, 亀田大輔, 稲辺尚人, 若狭智嗣, 藤田訓裕, 坂口聡志, 市村宗武, 佐川弘幸.: “パリティ移行核反応による原子核の 0^- 状態の研究”, 日本物理学会 2013 年秋季大会, (高知大学), 高知, 9 月 (2013).

佐藤優樹, 稲辺尚人, 亀田大輔, 久保敏幸, 熊谷秀和, 鈴木宏, 竹田浩之, 福田直樹, 吉田光一.: “位置敏感型平行平板雪崩検出器の基礎特性に関する考察”, 日本物理学会 2013 年秋季大会, (高知大学), 高知, 9 月 (2013).

BigRIPS Team

Publications

[Journal]

(Original Papers) *Subject to Peer Review

Suzuki H., Kubo T., Fukuda N., Inabe N., Kameda D., Takeda H., Yoshida K., Kusaka K., Yanagisawa Y., Ohtake M., Sato H., Shimizu Y., Baba H., Kurokawa M., Ohnishi T., Tanaka K., Tarasov O.B., Bazin D., Morrissey D.J., Sherrill B.M., Ieki K., Murai D., Iwasa N., Chiba A., Ohkoda Y., Ideguchi E., Go S., Yokoyama R., Fujii T., Nishimura D., Nishibata H., Momota S., Lewitowicz M., DeFrance G., Celikovic I., Steiger K.: "Production cross section measurement of radioactive isotopes by BigRIPS separator at RIKEN RI Beam Factory", Nucl. Instr. Meth. B **317**, 756–768 (2013). *

Fukuda N., Kubo T., Ohnishi T., Inabe N., Takeda H., Kameda D., Suzuki H.: "Identification and separation of radioactive isotope beams by the BigRIPS separator at the RIKEN RI Beam Factory", Nucl. Instr. Meth. B **317**, 323–332 (2013). *

Yoshida K., Fukuda N., Yanagisawa Y., Inabe N, Mizoi Y., Kubo T.: "High-power beam dump system for the BigRIPS fragment separator at RIKEN RI Beam Factory", Nucl. Instr. Meth. B **317**, 373–380 (2013). *

Kumagai H., Ohnishi T., Fukuda N., Takeda H., Kameda D., Inabe N., Yoshida K., Kubo T.: "Development of Parallel Plate Avalanche Counter (PPAC) for BigRIPS fragment separator", Nucl. Instr. Meth. B **317**, 717–727 (2013). *

Takeda H,, Kubo T., Kusaka K., Suzuki H., Inabe N., Nolen J.A.: "Extraction of 3D field maps of magnetic multipoles from 2D surface measurements with applications to the optics calculations of the large-acceptance superconducting fragment separator BigRIPS" Nucl. Instr. Meth. B **317**, 798–809 (2013). *

Tanaka K., Inabe N., Yoshida K, Kusaka K., Kubo T.: "Pillow seal system at the BigRIPS separator", Nucl. Instr. Meth. B **317**, 734–738 (2013). *

Nishi T., Berg G.P.A., Dozono M., Fujioka H., Fukuda N., Furuno T., Geissel H., Hayano R.S., Inabe N., Itahashi K., Itoh S., Kameda D., Kubo T., Matsubara H., Michimasa S., Miki K., Miya H., Murakami Y., Nakamura M., Nakatsuka N., Noji S., Okochi K., Ota S., Suzuki H., Suzuki K., Takaki M., Takeda H., Tanaka Y.K., Todoroki K., Tsukada K., Uesaka T., Watanabe Y.N., Weick H., Yamada H., Yoshida K.: "BigRIPS as a high resolution spectrometer for pionic atoms", Nucl. Instr. Meth. B **317**, 290–293 (2013). *

Ichikawa Y., Ueno H., Ishii Y., Furukawa T., Yoshimi A., Kameda D., Watanabe H., Aoi N., Asahi K., Balabanski D.L., Chevrier R., Daugas J.M., Fukuda N., Georgiev G., Hayashi H., Iijima H., Inabe N., Inoue T., Ishihara M., Kubo T., Nanao T., Ohnishi T., Suzuki K., Tsuchiya M., Takeda H., Rajabali M.M.: "Spin-aligned RI beams via two-step fragmentation reactions", Nucl. Instr. Meth. B **317**, 769–773 (2013). *

Michimasa S., Takaki M., Sasamoto Y., Dozono M., Nishi T., Kawabata T., Ota S., Baba H., Fujii T., Go S., Kawase S., Kikuchi Y., Kisamori K., Kobayashi M., Kubota Y., Lee C.S., Matsubara H., Miki K., Miya H., Noji S., Tokieda H., Tsumura M., Yako K., Yokoyama R., Takeda H., Yanagisawa Y., Kubo T., Inabe N., Fukuda N., Kameda D., Suzuki H., Shimizu Y., Sato H., Ichihara T., Stolz A., Zegers R.G.T., Sakai H., Uesaka T., Shimoura S.: "SHARAQ spectrometer for high-resolution studies for RI-induced reactions", Nucl. Instr. Meth. B **317**, 305–310 (2013). *

Yamaguchi Y., Wakasugi M., Uesaka T., Ozawa A., Abe Y., Fujinawa T., Kase M., Komiyama M., Kubo T., Kumagai K., Maie T., Nagae D., Ohnishi J., Suzuki F., Tokuchi A., Watanabe Y., Yoshida K., Yamada K., Yamaguchi T., Yamasawa H., Yanagisawa Y., Zenihiro J., Yano Y.: "Construction of rare-RI ring at RIKEN RI Beam Factory", Nucl. Instr. Meth. B **317**, 629–635 (2013). *

Yoshida A., Kambara T., Nakao A., Uemoto R., Uno H., Nagano A., Yamaguchi H., Nakao T., Kahl D., Yanagisawa T., Kameda D., Ohnishi T., Fukuda N., Kubo T.: "Wear diagnostics of industrial material using RI beams of ^{7}Be and ^{22}Na", Nucl. Instr. Meth. B **317**, 785–788 (2013). *

Kusaka K., Ohtake M., Ohnishi T., Yoshida K., Kubo T., Ito H., Tsuchihashi T.: "Long-Term Operation of the Superconducting Triplet Quadrupoles With Small Cryocoolers for BigRIPS In-Flight Separator and RI-Beam Delivery Line at RIKEN" IEEE Trans. Appl. Supercond. **vol. 23, No.3**, 4101305 (2013). *

Watanabe H., Lorusso G., Nishimura S., Xu Z.Y., Sumikama T., Söderström P.-A., Doornenbal P., Browne F., Gey G., Jung H.S., Taprogge J., Vajta Zs., Wu J., Yagi A., Baba H., Benzoni G., Chae K.Y., Crespi F.C.L., Fukuda N., Gernhäuser R., Inabe N., Isobe T., Jungclaus A., Kameda D., Kim G.D., Kim Y.K., Kojouharov I., Kondev F.G., Kubo T., Kurz N., Kwon Y.K., Lane G.J., Li Z., Moon C.-B., Montaner-Pizá A., Moschner K., Naqvi F., Niikura M., Nishibata H., Nishimura D., Odahara A., Orlandi R., Patel Z., Podolyák Zs., Sakurai H., Schaffner H., Simpson G.S., Steiger K., Suzuki H., Takeda H., Wendt A., Yoshinaga K.: "Isomers in ^{128}Pd and ^{126}Pd: Evidence for a Robust Shell Closure at the Neutron Magic Number 82 in Exotic Palladium Isotopes", Phys. Rev. Lett. **111**, 152501 (2013). *

Söderström P.A., Lorusso G., Watanabe H., Nishimura S., Doornenbal P., Thiamova G., Browne F., Gey G., Jung H.S., Sumikama T., Taprogge J., Vajta Zs., Wu J., Xu Z.Y., Baba H., Benzoni G., Chae K.Y., Crespi F.C.L., Fukuda N., Gernhäuser R., Inabe N., Isobe T., Jungclaus A., Kameda D., Kim G.D., Kim Y.K., Kojouharov I., Kondev F.G., Kubo T., Kurz N., Kwon Y.K., Lane G.J., Li Z., Montaner-Pizá A., Moschner K., Naqvi F., Niikura M., Nishibata H., Odahara A., Orlandi R., Patel Z., Podolyák Zs., Sakurai H., Schaffner H., Simpson G.S., Steiger K., Suzuki H., Takeda H., Wendt A., Yagi A., Yoshinaga K.: "Shape evolution in ^{116,118}Ru: Triaxiality and transition between the O(6) and U(5) dynamical symmetries", Phys. Rev. C **88**, 024301 (2013). *

Steppenbeck D., Takeuchi S., Aoi N., Doornenbal P., Matsushita M., Wang H., Baba H., Fukuda N., Go S., Honma M., Lee J., Matsui K., Michimasa S., Motobayashi T., Nishimura D., Otsuka T., Sakurai H., Shiga Y., Sumikama T., Suzuki H., Taniuchi T., Utsuno Y., Valiente-Dobon J.J., Yoneda K.: "Evidence for a new nuclear 'magic number' from the level structure of ^{54}Ca" Nature **502**, 207 (2013). *

Ichikawa Y., Ueno H., Ishii Y., Furukawa T., Yoshimi A., Kameda D., Watanabe H., Aoi N., Asahi K., Balabanski D.L., Chevrier R., Daugas J.M., Fukuda N., Georgiev G., Hayashi H., Iijima H., Inabe N., Inoue T., Ishihara M., Kubo T., Nanao T., Ohnishi T., Suzuki K., Tsuchiya M., Takeda H., Rajabali M.M.: "Novel method for the production of spin-aligned RI beams in projectile fragmentation reaction with the dispersion matching technique", Hyperfine Interact **220**, 47–51 (2013). *

(Review)

吉田光一, 久保敏幸, 日下健祐, 福田直樹, 柳澤善行, 竹田浩之, 稲辺尚人, 大竹政雄, 亀田大輔, 田中鐘信, 鈴木宏.: "理研の超伝導 RI ビーム生成装置 BigRIPS について", 加速器 **Vol. 10**, 93–100 (2013).

Oral Presentations

(International Conference etc.)

Kameda K.: "Observation of 18 new microsecond isomers among fission products from in-flight fission of 345 MeV/nucleon ^{238}U" International workshop on radiation effects in superconducting magnet materials, (KEK), Tsukuba, Japan, Feb. (2013).

Kusaka K.: "Beam heat loads to superconducting quadrupoles for BigRIPS In-flight separator at RIKEN" International workshop on radiation effects in superconducting magnet materials, (KEK), Tsukuba, Japan, April (2013).

Kameda D., Kubo T.: "Search for new isotopes and new isomers using in-flight fission of a 345 MeV/u ^{238}U beam", RIBF Users Meeting, (RIKEN), Wako, Japan, June (2013).

Suzuki H.: "Production cross section measurements of radioactive isotopes by BigRIPS separator at RIKEN RI Beam Factory", RIBF Users Meeting, (RIKEN), Wako, Japan, June (2013).

Kameda D., Kubo T.: "New isomers in the neutron-rich rare earth region by in-flight fission of 345 MeV/nucleon ^{238}U" RCNP international workshop on Physics Opportunities using Compton Suppressed Ge Clover Array (CAGRA13), (RCNP), Osaka, Japan, Dec. (2013).

Takeda H.: "Extraction of 3D Field Maps of Magnetic Multipoles from 2D Surface Measurements with Applications to Optics Calculations" 5th Expert Meeting on Challenging Issues of Next-generation High-intensity Inflight Separators, (RIKEN), Wako, Japan, Dec. (2013).

Fukuda N.: "RI-beam Production at BigRIPS: Optimization of Particle Identification" 5th Expert Meeting on Challenging Issues of Next-generation High-intensity Inflight Separators, (RIKEN), Wako, Japan, Dec. (2013).

Kusaka K.: "Status and Operational Experiences of Magnets and Cryogenic System at BigRIPS" 5th Expert Meeting on Challenging Issues of Next-generation High-intensity In-flight Separators, (RIKEN), Wako, Japan, Dec. (2013).

Kusaka K.: "Magnetic Field mapping at BigRIPS" 5th Expert Meeting on Challenging Issues of Next-generation High-intensity In-flight Separators, (RIKEN), Wako, Japan, Dec. (2013).

Suzuki H.: "Measurement of Production Yields and Cross sections and Comparison with Models" 5th Expert Meeting on Challenging Issues of Next-generation High-intensity In-flight Separators, (RIKEN), Wako, Japan, Dec. (2013).

Yoshida K.: "Status of High Power Issues at BigRIPS" 5th Expert Meeting on Challenging Issues of Next-generation High-intensity In-flight Separators, (RIKEN), Wako, Japan, Dec. (2013).

Tanaka K.: "Evaluation of Radiation Issues and Comparison with PHITS Calculations for BigRIPS Separator in RIBF " 5th Expert Meeting on Challenging Issues of Next-generation High-intensity In-flight Separators, (RIKEN), Wako, Japan, Dec. (2013).

Kameda D., Kubo T.: "Search for new isotopes and new isomers using in-flight fission of a 345 MeV/nucleon ^{238}U beam at RIKEN RI Beam Factory", 16th ASRC International Workshop on Nuclear Fission and Structure of Exotic Nuclei, (Japan Atomic Energy Agency (JAEA)), Tokai, Japan, Mar., (2014).

(Domestic Conference)

南方亮吾, 中村隆司, 近藤洋介, Achouri N.L., Aumann T., 馬場秀忠, Delaunay F., Doornenbal P., 福田直樹, Gibelin J., Huang J., 稲辺尚人, 磯部忠昭, 亀田大輔, 簡野大輝, Kim S., 小林信之, 小林俊雄, 久保敏幸, Leblond S., Lee J., Marques M., 本林透, 村井大地, 村上哲也, 武藤琴美, 中嶋丈嘉, 中塚徳継, Navin A., 西征爾郎, 生越駿, Orr N.A., 大津秀暁, 佐藤広海, 佐藤義輝, 清水陽平, 鈴木宏, 高橋賢人, 竹田浩之, 武内聡, 田中隆己, 栂野泰宏, Tuff A.G., Vandebrouck M., 米田健一郎.: "^{22}C のクーロン分解反応", 日本物理学会第 69 回年次大会, (東海大学), 神奈川, 3 月 (2014).

生越駿, 中村隆司, 近藤洋介, Achouri N.L., Aumann T., 馬場秀忠, Delaunay F., Doornenbal P., 福田直樹, Gibelin J., Huang J., 稲辺尚人, 磯部忠昭, 亀田大輔, 簡野大輝, Kim

S., 小林信之, 小林俊雄, 久保敏幸, Leblond S., Lee J., Marques M., 南方亮吾, 本林透, 村井大地, 村上哲也, 武藤琴美, 中嶋丈嘉, 中塚徳継, Navin A., 西征爾郎, Orr N.A., 大津秀暁, 佐藤広海, 佐藤義輝, 清水陽平, 鈴木宏, 高橋賢人, 竹田浩之, 武内聡, 田中隆己, 栂野泰宏, Tuff A.G., Vandebrouck M., 米田健一郎.: "^{19}B のクーロン分解反応", 日本物理学会第 69 回年次大会, (東海大学), 神奈川, 3 月 (2014).

近藤洋介, 中村隆司, Achouri N.L., Aumann T., 馬場秀忠, Delaunay F., Doornenbal P., 福田直樹, Gibelin J., Huang J., 稲辺尚人, 磯部忠昭, 亀田大輔, 簡野大輝, Kim S., 小林信之, 小林俊雄, 久保敏幸, Leblond S., Lee J., Marques M., 南方亮吾, 本林透, 村井大地, 村上哲也, 武藤琴美, 中嶋丈嘉, 中塚徳継, Navin A., 西征爾郎, 生越駿, Orr N.A., 大津秀暁, 佐藤広海, 佐藤義輝, 清水陽平, 鈴木宏, 高橋賢人, 竹田浩之, 武内聡, 田中隆己, 栂野泰宏, Tuff A.G., Vandebrouck M., 米田健一郎.: "^{25}C,^{26}C 非束縛状態の探索", 日本物理学会第 69 回年次大会, (東海大学), 神奈川, 3 月 (2014).

小林信之, 中村隆司, 近藤洋介, Tostevin J.A., 宇都野穣, 青井考, 馬場秀忠, Barthelemy R., 福田直樹, Lee G., Lee H.S., 稲辺尚人, 石原正泰, Kanungo r., 久保敏幸, Kim S.J., Famiano M., 松下昌史, 本林透, 大西哲哉, Orr N.A., 大津秀暁, 大塚孝治, 櫻井博儀, 佐古貴行, 炭竃聡之, 佐藤義輝, 高橋好太郎, 竹田浩之, 武内聡, 田中隆己, 栂野泰宏, 米田健一郎.: "分解反応を用いた中性子過剰な Mg 同位体の研究", 日本物理学会第 69 回年次大会, (東海大学), 神奈川, 3 月 (2014).

川瀬頌一郎, 上坂友洋, 下浦享, 矢向謙太郎, 大田晋輔, 道正新一郎, 時枝紘史宮裕之, Leung T.T., 木佐森慶一, 高木基伸, 久保田悠樹, 李清秀, 横山輪, 藤井俊彦, 小林幹, 笹野匡紀, 銭廣十三, 松原礼明, 堂園昌伯, Lee J., 酒井英行, 久保敏幸, 吉田光一, 稲辺尚人, 柳澤善行, 竹田浩之, 日下健祐, 福田直樹, 亀田大輔, 鈴木宏, 河原朋美, 涌井崇志, 坂口聡志, 野呂哲夫, 若狭智嗣, 安田淳平, 福永拓, 前田幸重, Kim W.Y., Hwang S.H., Stepanyan S., Obertelli A., Galindo-Uribarri A., Padilla-Rodal E., Beaumel D.: "準弾性 ^{A}O(p,2p) 反応による窒素同位体の陽子一空孔状態の核分光", 日本物理学会第 69 回年次大会, (東海大学), 神奈川, 3 月 (2014).

西隆博, Berg G.P.A., 堂園昌伯, 福田直樹, 古野達也, 藤岡宏之, Geissel H., 早野龍五, 稲辺尚人, 板橋健太, 伊藤聖, 亀田大輔, 久保敏幸, 松原礼明, 道正新一郎, 三木謙二郎, 宮裕之, 中村祐喜, 村上洋平, 中塚徳継, 野地俊平, 大河内公太, 大田晋輔, 鈴木宏, 鈴木謙 高木基伸, 竹田浩之, 田中良樹, 轟孔一, 塚田暁, 上坂友洋, 渡辺珠以, Weick H., 山田裕之, 吉田光一.: "(d,^{3}He) 反応を用いたπ中間子原子の精密分光 (10)", 日本物理学会第 69 回年次大会, (東海大学), 神奈川, 3 月 (2014).

西隆博, Berg G.P.A., 堂園昌伯, 福田直樹, 古野達也, 藤岡宏之, Geissel H., 早野龍五, 稲辺尚人, 板橋健太, 伊藤聖, 亀田大輔, 大河内公太, 久保敏幸, 松原礼明, 道正新一郎, 三木謙二郎, 宮裕之, 中村祐喜, 村上洋平, 中塚徳継, 野地俊平, 大田晋輔, 鈴木宏, 鈴木謙 高木基伸, 竹田浩之, 田中良樹, 轟孔一, 塚田暁, 上坂友洋, 渡辺珠以, Weick H., 山田裕之, 吉田光一.: "(d,^{3}He) 反応を用いたπ中間子原子の精密分光 (9)", 日本物理学会 2013 年秋季大会, (高知大学), 高知, 9 月 (2013).

宮裕之, 下浦享, 木佐森慶一, 馬場秀忠, 馬場辰雄, 堂園昌伯, 福田直樹, 藤井俊彦, 郷慎太郎, 井手口栄治, 稲辺尚人, 伊藤正俊, 亀田大輔, 川畑貴裕, 川瀬頌一郎, 久保敏幸, 久保田悠樹, 小林幹, 近藤洋介, 李清秀, 前田幸重, 松原礼明, 三木謙二郎, 道正新一郎, 西隆博, 西村美月, 大田晋輔, 坂口聡志, 酒井英行, 笹野匡紀, 佐藤広海, 清水陽平, 鈴木宏, 高木基伸, 民井淳, 竹田浩之, 武内聡, 時枝紘史, 村美保, 上坂友洋, 柳沢善行, 矢向謙太郎, 横山輪, 吉田光一, Assie M., Beaumel D., Fariouz H., Stolz A.: "発熱型荷電交換反応 (^{8}He,^{8}Li γ) を用いた ^{4}He 核のスピン・アイソスピン応答の研究", 日本物理学会 2013 年秋季大会, (高知大学), 高知, 9 月 (2013).

木佐森慶一, 下浦享, 宮裕之, 馬場秀忠, 馬場辰彦, 堂園昌伯, 福田直樹, 藤井俊彦, 郷慎太郎, 井手口栄治, 稲辺尚人, 伊藤正俊, 亀田大輔, 川畑貴裕, 川瀬頌一郎, 久保敏幸, 久保田悠樹, 小林幹, 近藤洋介, 李清秀, 前田幸重, 松原礼明, 三木謙二郎, 道正新一郎, 西隆博, 西村美月, 大田晋輔, 坂口聡志, 酒井英行, 笹野匡紀, 佐藤広海, 清水陽平, 鈴木宏, 高木基伸, 民井淳, 竹田浩之, 武内聡, 時枝紘史, 津村美保, 上坂友洋, 柳沢善行, 矢向謙太郎, 横山輪, 吉田光一, Assie M., Beaumel D., Fariouz H., Stolz A.: "二重荷電交換反応をもちいた 4 中性子系質量欠損核分光実験", 日本物理学会 2013 年秋季大会, (高知大学), 高知, 9 月 (2013).

園田哲, 和田道治, 飯村秀紀, 上野秀樹, 富田英生, 足立義貴, 高塚卓旦, Wendt K., 久保敏幸, 若杉昌徳, 日下健祐, 眞家武士, 山澤秀行, 藤縄雅, 片山一郎, 新井郁也, Schury P., 篠塚勉, 涌井崇志, 松尾由賀利, 古川武, 宮武宇也, 石山博恒, 今井伸明, 平山賀一, 渡辺裕, 鄭淳讃, 岡田邦宏, 伊藤由太, 中尾愛子, "RIBF-SLOWRI 共鳴イオン化レーザーイオン源 (PALIS) の開発とレーザー核分光への応用", 日本物理学会 2013 年秋季大会, (高知大学), 高知, 9 月 (2013).

南方亮吾, 中村隆司, 近藤洋介, Achouri N.L., Aumann T., 馬場秀忠, Delaunay F., Doornenbal P., 福田直樹, Gibelin J., Huang J., 稲辺尚人, 磯部忠昭, 亀田大輔, 簡野大輝, Kim S., 小林信之, 小林俊雄, 久保敏幸, Leblond S., Lee J., Marques M., 本林透, 村井大地, 村上哲也, 武藤琴美, 中嶋丈嘉, 中塚徳継, Navin A., 西征爾郎, 生越駿, Orr N.A., 大津秀暁, 佐藤広海, 佐藤義輝, 清水陽平, 鈴木宏, 高橋賢人, 竹田浩之, 武内聡, 田中隆己, 栂野泰宏, Tuff A.G., Vandebrouck M., 米田健一郎.: "^{22}C の分解反応 II", 日本物理学会 2013 年秋季大会, (高知大学), 高知, 9 月 (2013).

大道理恵, 渡邉寛, 八木彩祐未, 小田原厚子, 方一帆, 西畑洸希, 下田正, 西村俊二, Lorusso G., 炭竃聡之, Söderström P.A., Wu J., Brown D.F., 徐正宇, 磯部忠昭, 馬場秀忠, 鈴木宏, 稲辺尚人, 亀田大輔, 福田直樹, 竹田浩之, 久保敏幸, Bruce A., Regan P., Podolyak Z., Roberts O., the EURICA collaborators: "LaBr3 検出器を用いた中性子過剰核の励起状態の寿命測定", 日本物理学会 2013 年秋季大会, (高知大学), 高知, 9 月 (2013).

井手口栄治, Simpson G., 横山輪, 田中まな, 青井考, 馬場秀忠, Bello F., Browne F., 大道理恵, Doornenbal P., Fang Y.,

福田直樹, Gey G., 郷慎太郎, 稲辺尚人, 磯部忠昭, 亀田大輔, 小林和馬, 小林幹, 小松原哲郎, 久保敏幸, Kuri I., Li Z., Lorusso G., 松下昌史, 道正新一郎, Moon C.-B., 西畑洸希, 西村俊二, 西塚一平, 小田原厚子, Patel Z., Rice S., Sahin E., Sinclair L., Söderström P.A., 炭竃聡之, 鈴木宏, 竹田浩之, Taprogge J., Vajra Z., 渡邉寛, Wu J., 徐正宇, 八木彩祐未.: "中性子過剰領域 Z〜60 原子核における K アイソマーの探索", 日本物理学会 2013 年秋季大会, (高知大学), 高知, 9 月 (2013).

田中まな, 井手口栄治, Simpson G., 横山輪, 青井考, 馬場秀忠, Bello F., Browne F., 大道理恵, Doornenbal P., Fang Y., 福田直樹, Gey G., 郷慎太郎, 稲辺尚人, 磯部忠昭, 亀田大輔, 小林和馬, 小林幹, 小松原哲郎, 久保敏幸, Kuri I., Li Z., Lorusso G., 松下昌史, 道正新一郎, Moon C.-B., 西畑洸希, 西村俊二, 西塚一平, 小田原厚子, Patel Z., Rice S., Sahin E., Sinclair L., Söderström P.A., 炭竃聡之, 鈴木宏, 竹田浩之, Taprogge J., Vajra Z., 渡邉寛, Wu J., 徐正宇, 八木彩祐未.: "中性子過剰 Nd 同位体におけるアイソマー分光", 日本物理学会 2013 年秋季大会, (高知大学), 高知, 9 月 (2013).

方一帆, 小田原厚子, Lozeva R., Moon C., 八木彩祐未, 大道理恵, 西畑洸希, 下田正, 西村俊二, Doornenbal P., Lorusso G., 炭竃聡之, 渡辺寛, Söderström P.A., Wu J., Brown F., 徐正宇, 横山輪, 磯部忠昭, 馬場秀忠, 櫻井博儀, 鈴木宏, 稲辺尚人, 亀田大輔, 福田直樹, 竹田浩之, 安得順, 清水陽平, 佐藤広海, 久保敏幸, 石垣知樹, 森本翔太, 井手口栄治, 小松原哲郎, 新倉潤, the EURICA collaborators: "Study of beta decay of neutron-rich I isotopes at RIKEN RIBF using a stack of Si-strip detectors WASA3Bi combined with a cluster-Ge array EURICA", 日本物理学会 2013 年秋季大会, (高知大学), 高知, 9 月 (2013).

八木彩祐未, 小田原厚子, Lozeva R., Moon C., 方一帆, 大道理恵, 西畑洸希, 下田正, 西村俊二, Doornenbal P., Lorusso G., 炭竃聡之, 渡辺寛, Söderström P.A., Wu J., Brown F., 徐正宇, 横山輪, 磯部忠昭, 馬場秀忠, 櫻井博儀, 鈴木宏, 稲辺尚人, 亀田大輔, 福田直樹, 竹田浩之, 安得順, 清水陽平, 佐藤広海, 久保敏幸, 石垣知樹, 森本翔太, 井手口栄治, 小松原哲郎, 新倉潤, the EURICA collaborators: "理研 RIBF の EURICA を用いた中性子過剰な Cs 同位体 (A 150) のアイソマーの研究", 日本物理学会 2013 年秋季大会, (高知大学), 高知, 9 月 (2013).

横山 輪, 井手口 栄治, Simpson G., 田中 まな, 西村 俊二, Lorusso G., 炭竃 聡之, Doornenbal P., 馬場 秀忠, 磯部忠昭, Söderström P.A., Wu J., Xu Z., Browne F., Patel Z., Rice S., Sinclair L., Li Z., 渡邉 寛, Gey G., Sahin E., Bello F., Vajra Z., Kuri I., Taprogge J., 小田原厚子, Fang Y., 大道理恵, 八木彩祐未, 西畑洸希, 青井考, 小林和馬, 道正新一郎, 松下昌史, 小林幹, 郷慎太郎, 久保敏幸, 亀田大輔, 稲辺尚人, 竹田浩之, 福田直樹, 鈴木宏, 西塚一平, 小松原哲郎, Moon C.-B.: "過剰変形領域の Pm 同位体における新アイソマーの発見", 日本物理学会 2013 年秋季大会, (高知大学), 高知, 9 月 (2013).

堂園昌伯, 上坂友洋, 笹野匡紀, 銭廣十三, 松原礼明, 下浦享, 矢向謙太郎, 道正新一郎, 大田晋輔, 時枝紘史, 宮裕之, 川瀬頌一郎, Tang R., 木佐森慶一, 高木基伸, 久保田悠樹, 李清秀, 藤井俊彦, 横山輪, 酒井英行, 久保敏幸, 吉田光一, 柳沢善行, 福田直樹, 竹田浩之, 亀田大輔, 稲辺尚人, 若狭智嗣, 藤田訓裕, 坂口聡志, 市村宗武, 佐川弘幸.: "パリティ移行核反応による原子核の 0^- 状態の研究", 日本物理学会 2013 年秋季大会, (高知大学), 高知, 9 月 (2013).

佐藤優樹, 稲辺尚人, 亀田大輔, 久保敏幸, 熊谷秀和, 鈴木宏, 竹田浩之, 福田直樹, 吉田光一.: "位置敏感型平行平板雪崩検出器の基礎特性に関する考察", 日本物理学会 2013 年秋季大会, (高知大学), 高知, 9 月 (2013).

SAMURAI Team

Publications

[Journal]

(Original Papers) *Subject to Peer Review

Kobayashi T., Chiga N., Isobe T., Kondo Y., Kubo T., Kusaka K., Motobayashi T., Nakamura T., Ohnishi J., Okuno H., Otsu H., Sato T., Sato H., Shimizu Y., Sekiguchi K., Takahashi K., Tanaka R., Yoneda K.: "SAMURAI spectrometer for RI beam experiments" Nucl. Instrum. Methods B **317**, 294–304 (2013).*

Shimizu Y., Otsu H., Kobayashi T., Kubo T., Motobayashi T., Sato H., Yoneda K.: "Vacuum system for the SAMURAI spectrometer", Nucl. Instrum. Methods B **317**, 739–742 (2013).*

Suzuki H., Kubo T., Fukuda N., Inabe N., Kameda D., Takeda H., Yoshida K., Kusaka K., Yanagisawa Y., Ohtake M., Sato H., Shimizu Y., Baba H., Kurokawa M., Ohnishi T., Tanaka K., Tarasov O.B., Bazin D., Morrissey D.J., Sherrill B.M., Ieki K., Murai D., Iwasa N., Chiba A., Ohkoda Y., Ideguchi E., Go S., Yokoyama R., Fujii T., Nishimura D., Nishibata H., Momota S., Lewitowicz M., DeFrance G., Celikovic I., Steiger K.: "Production cross section measurement of radioactive isotopes by BigRIPS separator at RIKEN RI Beam Factory", Nucl. Instr. Meth. B **317**, 756–768 (2013).*

Matsuda Y., Sakaguchi H., Takeda H., Terashima S., Zenihiro J., Kobayashi T., Murakami T., Iwao Y., Ichihara T., Suda T., Ohnishi T., Watanabe Y., Otsu H., Yoneda K., Satou Y., Ozeki K., Kanazawa M.: "Elastic scattering of protons from ^{9}C with a 290 MeV/nucleon ^{9}C beam", Phys. Rev. C **87**, 034614(8 pages) (2013).*

Wang H., Aoi N., Takeuchi S., Matsushita M., Doornenbal P., Motobayashi T., Steppenbeck D., Yoneda K., Baba H., Caceres L., Dombradi Zs., Kobayashi K., Kondo Y. Lee J., Li K., Liu H., Minakata R., Nishimura D., Otsu H., Sakaguchi S., Sakurai H., Scheit H., Sohler D., Sun Y., Tian Z., Tanaka R., Togano Y., Vajta Zs., Yang Z., Yamamoto T., Ye Y., Yokoyama R.: "Collectivity evolution in the neutron–rich Pd isotopes toward the N=82 shell closure", Phys. Rev. C **88**, 054318(5 pages) (2013).*

Doornenbal P., Scheit H., Takeuchi S., Aoi N., Li K., Matsushita M., Steppenbeck D., Wang H., Baba H., Crawford H., Hoffman C.R., Hughes R., Ideguchi E., Kobayashi N., Kondo Y., Lee J., Michimasa S., Motobayashi T., Sakurai H., Takechi M., Togano Y., Winkler R., Yoneda K.: "In-Beam γ–Ray Spectroscopy of ^{34,36,38}Mg: Merging the N=20 and N=28 Shell Quenching", Phys.Rev.Lett.**111**, 212502(5 pages) (2013).*

Steppenbeck D., Takeuchi S., Aoi N., Doornenbal P., Lee J., Matsushita M., Wang H., Baba H., Fukuda N., Go S., Honma M., Matsui K., Michimasa S., Motobayashi T., Nishimura D., Otsuka T., Sakurai H., Shiga Y., Soderstrom P.-A., Sumikama T., Suzuki H., Taniuchi R., Utsuno Y., Valiente-Dobon J.J., Yoneda K.: "Investigating the strength of the N = 34 subshell closure in ^{54}Ca" J.Phys.:Conf.Ser. **445**, 012012(4 pages) (2013).*

Steppenbeck D., Takeuchi S., Aoi N., Doornenbal P., Matsushita M., Wang H., Baba H., Fukuda N., Go S., Honma M., Lee J., Matsui K., Michimasa S., Motobayashi T., Nishimura D., Otsuka T., Sakurai H., Shiga Y., Soderstrom P.-A., Sumikama T., Suzuki H., Taniuchi R., Utsuno Y., Valiente-Dobon J.J., Yoneda K.: "Evidence for a new nuclear 'magic number' from the level structure of ^{54}Ca", Nature(London)502, 207–210 (2013).*

Ueno H. Miyatake H. Yamamoto Y. Tanimoto S. Shimoda T. Aoi N. Asahi K. Ideguchi E. Ishihara M. Izumi H. Kishida T. Kubo T. Mitsuoka S. Mizoi Y. Notani M. Ogawa H. Ozawa A. Sasaki M. Shirakura T. Takahashi N. Yoneda K: "β–delayed neutron and γ–ray spectroscopy of ^{17}C utilizing spin-polarized ^{17}B", Phys.Rev. C87,034316(17 pages)(2013).*

Oral Presentations

(International Conference etc.)

Yoneda K: "Unbound-state physics with the SAMURAI spectrometer in RIKEN RIBF" The Gordon Research Conference on Nuclear Chemistry, New London, NH, USA, June 9–14, 2013.*

(Domestic Conference)

南方亮吾, 中村隆司, 近藤洋介, Achouri N.L., Aumann T., 馬場秀忠, Delaunay F., Doornenbal P., 福田直樹, Gibelin J., Huang J., 稲辺尚人, 磯部忠昭, 亀田大輔, 簡野大輝, Kim S., 小林信之, 小林俊雄, 久保敏幸, Leblond S., Lee J., Marques M., 本林透, 村井大地, 村上哲也, 武藤琴美, 中嶋丈嘉, 中塚徳継, Navin A., 西征爾郎, 生越駿, Orr N.A., 大津秀暁, 佐藤広海, 佐藤義輝, 清水陽平, 鈴木宏, 高橋賢人, 竹田浩之, 武内聡, 田中隆己, 栂野泰宏, Tuff A.G., Vandebrouck M., 米田健一郎.: "^{22}C のクーロン分解反応", 日本物理学会第 69 回年次大会, (東海大学), 神奈川, 3 月 (2014).

生越駿, 中村隆司, 近藤洋介, Achouri N.L., Aumann T., 馬場秀忠, Delaunay F., Doornenbal P., 福田直樹, Gibelin J., Huang J., 稲辺尚人, 磯部忠昭, 亀田大輔, 簡野大輝, Kim S., 小林信之, 小林俊雄, 久保敏幸, Leblond S., Lee J., Marques M., 南方亮吾, 本林透, 村井大地, 村上哲也, 武藤琴美, 中嶋丈嘉, 中塚徳継, Navin A., 西征爾郎, Orr N.A., 大津秀暁, 佐藤広海, 佐藤義輝, 清水陽平, 鈴木宏, 高橋賢人, 竹田浩之, 武内聡, 田中隆己, 栂野泰宏, Tuff A.G., Vandebrouck M., 米田健一郎.: "^{19}B のクーロン分解反応", 日本物理学会第 69 回年次大会, (東海大学), 神奈川, 3 月 (2014).

近藤洋介, 中村隆司, Achouri N.L., Aumann T., 馬場秀忠, Delaunay F., Doornenbal P., 福田直樹, Gibelin J., Huang J., 稲辺尚人, 磯部忠昭, 亀田大輔, 簡野大輝, Kim S., 小林信之, 小林俊雄, 久保敏幸, Leblond S., Lee J., Marques M., 南方亮吾, 本林透, 村井大地, 村上哲也, 武藤琴美, 中嶋

丈嘉, 中塚徳継, Navin A., 西征爾郎, 生越駿, Orr N.A., 大津秀暁, 佐藤広海, 佐藤義輝, 清水陽平, 鈴木宏, 高橋賢人, 竹田浩之, 武内聡, 田中隆己, 栂野泰宏, Tuff A.G., Vandebrouck M., 米田健一郎.: "^{25}C,^{26}C 非束縛状態の探索", 日本物理学会第 69 回年次大会, (東海大学), 神奈川, 3 月 (2014).

宮崎卓也, 大津秀暁, Nikolskii E.Y., 志賀慶明, 西村美月, 武内聡, 佐藤義輝, 黒川明子, 馬場秀忠, Lorusso G., 磯部忠昭, 新倉潤, Kuzmin E.A., Korsheninnikov A.A., Ogloblin A.A., Krupko S.A., Golovkov M.S., Bezbakh A.A, Slepnev R.S., Fomichev A.S., Sidorchuk S.I., Gorshkov A.V., Knyazev A.G., Papka P., JinØ.H., Kim S. Hwang J., Choi S., Chae H., Kim E., Kim Y., Lubos D., Beaumel D., Soederstroem P.A., 坂口聡志, 久保野茂, Perrevoort A.K., Milman E., Chebotaryov S., Powell W., 本林透, 米田健一郎, 櫻井博儀.: "欠損質量核分光による ^{8}C 核励起状態の探索", 日本物理学会第 69 回年次大会, (東海大学), 神奈川, 3 月 (2014).

石元茂, 小澤顕, 小林俊雄, 鈴木祥仁, 田中純貴, 谷畑勇夫, 森本喜三夫, Sanetullaev A., Kanungo R.: "TRIUMF-IRIS 実験用窓なし固体水素ターゲットの開発", 日本物理学会, (高知大学), 高知, 9 月 (2013).

南方亮吾, 中村隆司, 近藤洋介, Achouri N.L., Aumann T., 馬場秀忠, Delaunay F., Doornenbal P., 福田直樹, Gibelin J., Huang J., 稲辺尚人, 磯部忠昭, 亀田大輔, 簡野大輝, Kim S., 小林信之, 小林俊雄, 久保敏幸, Leblond S., Lee J., Marques M., 本林透, 村井大地, 村上哲也, 武藤琴美, 中嶋丈嘉, 中塚徳継, Navin A., 西征爾郎, 生越駿, Orr N.A., 大津秀暁, 佐藤広海, 佐藤義輝, 清水陽平, 鈴木宏, 高橋賢人, 竹田浩之, 武内聡, 田中隆己, 栂野泰宏, Tuff A.G., Vandebrouck M., 米田健一郎.: "^{22}C の分解反応 II", 日本物理学会, (高知大学), 高知, 9 月 (2013).

Computing and network Team

Oral Presentations

(International Conference etc.)

Baba H., Ichihara T., Isobe T., Houarner C., Maugeais C., Raine B., Saillant F., Wittwer G., Kurz N., Schaffner H., Gernhäuser R., Anvar S., Calvet D., Château F., Pollacco E.: "DAQ Coupling in RIKEN RIBF", 19th REAL TIME CONFERENCE (RT2014) , (RCNP, RIKEN, KEK), Nara, Japan, May (2014).

Baba H.: "Development of FPGA-based NIM logic circuits", 4th Joint Meeting of the APS Division of Nuclear Physics and the Physical Society of Japan , Waikoloa, Hawaii, October (2014).

(Domestic Conference)

馬場秀忠, 市原卓, 大西哲哉, 武内聡, 渡邊康, 吉田光一, 大田晋介, 下浦享: "モジュールマウント型 VME コントローラの開発", 日本物理学会, (日本物理学会), 平塚, 3 月 (2014).

Detector Team

Publications

[Journal]

(Original Papers) *Subject to Peer Review

Sato Y., Taketani A., Fukuda N., Takeda H., Kameda D., Suzuki H., Shimizu Y., Nishimura D., Fukuda M., Inabe N., Murakami H., Yoshida K., Kubo T.: "Energy Resolution of Gas Ionization Chamber for High-Energy Heavy Ions", Jpn. J. Appl. Phys. **53**, 016401 (2014). *

Sato Y., Shimaoka T., Kaneko H. J., Murakami H., Miyazaki D., Tsubota M., Chayahara A., Umezawa H., Shikata S.: "Pulse height reduction effects of single-crystal CVD diamond detector for low-energy heavy ions", Euro. Phys. Let. **104**, 22003 (2013). *

Sato Y., Morita Y., Kanno I., "Performance estimation of InSb compound semiconductor detectors as a function of active area using alpha particles", Nucl. Instr. and Meth. A **737**, 1–4 (2014). *

Oral Presentations

(International Conference etc.)

Sato Y.: "Status of Beam Profile, Tracking and Particle Identification Detectors at BigRIPS: Issues on High Rates and Resolution", 5th Expert Meeting on Challenging Issues of Next-generation High-intensity In-flight Separators, (RIKEN), Wako, Japan, December (2013).

(Domestic Conference)

佐藤優樹 : " 位置敏感型平行平板雪崩検出器の基礎特性に関する考察 ", 日本物理学会 2013 年秋季大会 , (高知大学), 高知 , 9 月 (2013).

Radiation Biology Team

Publications

[Journal]

(Original Papers) *Subject to Peer Review

Ma L., Kazama Y., Inoue H., Abe T., Hatakeyama S. and Tanaka S.: "The type of mutations induced by carbon-ion beam irradiation of the filamentous fungus Neurospora crassa", Fungal Biology **117**, 227-238 (2013).*

Kazama Y., Hirano T., Nishihara K., Ohbu S., Shirakawa Y., and Abe T.: "Effect of high-LET Fe-ion beam irradiation on mutation induction in Arabidopsis thaliana", Genes Genet. Syst. **88**, 189-197 (2013). *

Ota S., Matsuda T., Yamazaki T., Kazama Y., Abe T., and Kawano S.: "Phenotypic spectrum of *Parachlorella kessleri* (Chlorophyta) mutants produced by heavy-ion irradiation", Bioresour. Technol. **149**, 432-438 (2013). *

Tahira C., Shitsukawa N., Kazama Y., Abe T., and Murai K.: "The Wheat Plastochron Mutant, *fushi-darake*, Shows Transformation of Reproductive Spikelet Meristem into Vegetative Shoot Meristem", Am. J. Plant Sci. **4**, 28-36 (2013).*

Murai K., Nishiura A., Kazama Y., and Abe T.: "A large-scale mutant panel in wheat developed using heavy-ion beam mutagenesis and its application to genetic research", Nucl. Instrum. Meth. B **314**, 59-62 (2013). *

Ishii K., Nishiyama R., Shibata F., Kazama Y., Abe T., and Kawano S.: "Rapid degeneration of noncoding DNA regions surrounding *SlAP3X/Y* after recombination suppression in a dioecious plant, *Silene latifolia*", G3: Genes, Genomes, Genetics. **3**: 2121-2130. (2013) *

Shirao T., Ueno K., Abe T. and Matsuyama, T. : "Development of DNA markers for identifying chrysanthemum cultivars generated by ion-beam irradiation", Mol. Breeding **31**, 729-735 (2013).*

Nakano Y., Takano Y., Ikeda T., Kanai Y., Suda S., Azuma T., Bräuning H., Bräuning-Demian A., Dauvergne D., Stöhlker Th., and Yamazaki Y.: "Resonant coherent excitation of the lithiumlike uranium ion: A scheme for heavy-ion spectroscopy", Phys. Rev. A **87**, 060501(R) (2013). *

Zhou C. L., Simon M., Ikeda T., Guillous S., Iskandar W., Méry A., Rangama J., Lebius H., Benyagoub A., Grygiel C., Müller A., Döbeli M., Tanis J. A., and Cassimi A.: "Transmission of slow highly charged ions through glass capillaries: Role of the capillary shape", Phys. Rev. A **88**, 050901(R) (2013). *

Wickramarachchi S.J., Ikeda T., Keerthisinghe D., Dassanayake B.S., and Tanis J.A.: "Angular dependence of electron transmission through a microsized tapered glass capillary", Nucl. Instrum. Methods Phys. Res. B 317, Part A, P.101-104 (2013). *

Nakai Y., Nakano Y., Ikeda T., Kanai Y., Kambara T., Fukunishi N., Kondo C., Azuma T., Komaki K., and Yamazaki Y.: "Stark effect in resonant coherent excitation of 2s electron of Li-like Fe^{23+} ions channeling in a Si crystal", Nucl. Instrum. Methods Phys. Res. B **315**, P.94-98 (2013). *

Wickramarachchi S. J., Dassanayake B. S., Keerthisinghe D., Ikeda T., and Tanis J. A.: "Dependence of electron transmission on charge deposited in tapered glass macrocapillaries at a tilt angle of 5.0°", Phys. Scr. **T156**, 014057 (2013). *

Jin W-G., Katoh K., Minowa T., and Ikeda T.: "Light Microbeams by Tapered Glass Capillaries for Biological Irradiation", J. Comput. Comm. **1**, 5-8 (2013). *

Mäckel V., Meissl W., Ikeda T., Clever M., Meissl E., Kobayashi T., Kojima T. M., Imamoto N., Ogiwara K., and Yamazaki Y.: "A novel facility for 3D micro-irradiation of living cells in a controlled environment by MeV ions", Rev. Sci. Instrum. **85**, 014302 (2014). *

仲條眞介，長谷川聡，吉田宏，漆原昌二，阿部陽，阿部知子，福西暢尚，龍頭啓充，大清水保見る："短稈・低アミロースヒエ新品種「ねばりっこ１号」,「ねばりっこ２号」,「ねばりっこ３号」の育成"，岩手農研センター研究報告　12, 43-60 (2013)

(Review)

池田時浩: "総説 ガラスキャピラリー光学系のビーム通過特性とマイクロビーム応用"，原子衝突学会誌 Vol.10, Issue 5, P.125-144 (2013).

[Book・Proceedings]

(Review)

阿部知子，平野智也：" 突然変異（イオンビーム）育種"，農業技術大系　花卉編（追録第 15 号），農山漁村文化協会，東京. pp. +124-2～12（2013）

(Proceedings)

Furukawa K., Abe T., Tabata S., and Matsuyama T.: " Heavy Ion-Beam Breeding and Cultivar Identification by 'DNA marking' in Cymbidium", The 11th Asia Pacific Orchid Conference, Okinawa, Japan, Vol.11, pp.230-234 (2013).

Oral Presentations

(International Conference etc.)

Onda Y., Tsuchiya Y., Kazama Y., Abe T., Mochida K., and Shinozaki K.: "Analysis of heavy ion beam mutants in *Brachypodium distachyon*", Plant and Animal Genome XXI, San Diego, USA, Jan. (2013)

Sato Y., Yamaguchi M., Hirano T., Hayashi Y., Fukunishi N., and Abe T.: "The development of new tank system for mutation breeding in *Undaria pinnatifida*", 21st International Seaweed Symposium, Bali, Indonesia, April (2013).

Masuyama F., Hokura A., Abe T., Hirano T., Terada Y., and Sano T.: "Study on accumulation mechanism of cadmium in Tobacco BY-2 cells by SR-XRF analysis", 4th International Symposium on Metallomics, Oviedo, Spain, July (2013).

Katoh K., Jin W-G., Minowa T., and Ikeda T.: "Propagation of visible light through tapered glass capillaries for microbeams", ICPEAC2013 (XXVIII International Conference on Photonic, Electronic and Atomic Collisions), Lanzhou, China, July (2013).

Wickramarachchi S., Ikeda T., Keerthisinghe D., Dassanayake B. S., and Tanis J. A.: "Broadening in the energy distribution of electron beams transmitted through a micrometer-sized tapered glass capillary", ICPEAC2013 (XXVIII International Conference on Photonic, Electronic and Atomic Collisions), Lanzhou, China, July (2013).

Cassimi A., Simon M. J., Zhou C. L., Döbeli M., Ikeda T., Müller A. M., Benyagoub A., Grygiel C., Guillous S., Lebius H., Mery A., Monnet I., Ropars F., and Shiromaru H.: "Simulation of MeV ion transmission through glass micro-capillaries", ICPEAC2013 (XXVIII International Conference on Photonic, Electronic and Atomic Collisions), Lanzhou, China, July (2013).

Ikeda T.: "Ion-beam guiding in insulators Dynamic features of slow highly charge ion beam guided with a glass surface", ICPEAC2013 (XXVIII International Conference on Photonic, Electronic and Atomic Collisions), Lanzhou, China, July (2013).

Ikeda T. and Kojima T. M.: "Dynamic features of slow highly charge ion beam guided with a glass surface" ICPEAC2013 (XXVIII International Conference on Photonic, Electronic and Atomic Collisions), Lanzhou, China, July (2013).

Ikeda T.: "Application of ion microbeams through tapered glass capillary optics", The 21st International Conference on Ion-Surface Interactions, Yaroslavl, Russia, Aug. (2013).

Ikeda T.: "Application of ion microbeams produced by tapered glass capillary optics", Seminar in Institute of Physics, Moscow State University, Moscow, Russia, Aug. (2013).

Ishii K., Morita R., Kogure S., Shibukawa T., Nagamura Y., and Abe T.: "Cyclopedic analysis of rice genes induced by heavy-ion beam irradation", 7th International Rice Genetics Symposium, Manila, Philippines, Nov. (2013).

Morita R., Takehisa H., Ishii K., Hayashi Y., Kogure S., Ichinose K., Tokairin H., Sato T., Saito H., Okumoto Y., and Abe T.: "Exome resequencing reveals mutations induced by heavy-ion beam with LETmax in rice", 7th International Rice Genetics Symposium, Manila, Philippines, Nov. (2013).

Hirano T.: "Heavy ion beam applications in microbes and plant mutation breeding: modifying bio-informatics and bio-sciences", Seminar in Hasanuddin University. Makassar, Indonesia. Dec. (2013).

Ikeda T.: "Transmission Characteristics of keV Highly Charged Ions and MeV Light Ions Through Single Tapered Glass Capillaries", 20th International Workshop on Inelastic Ion-Surface Collisions (IISC-20), Wirrina Cove, South Australia, Feb. (2014).

(Domestic Conference)

池田時浩, 加藤幹男, Meissl W., 梅澤憲司,山崎泰規: "ガラスキャピラリーによる大腸菌へのマイクロビーム照射法", 日本物理学会第 68 回年次大会, 広島, 3 月 (2013).

小暮祥子, 森田竜平, 林依子, 一瀬勝紀, 若菜妙子, 東海林英夫, 石井公太郎, 佐藤雅志, 阿部知子: "重イオンビームで誘発されたイネわい性突然変異体集団の解析", 日本育種学会第 123 回講演会, 東京, 3 月 (2013).

古川浩二, 阿部知子, 田畑哲之, 松山知樹:" シンビジウム品種内判別のための DNA マーク開発", 日本育種学会第 123 回講演会, 東京, 3 月 (2013).

安井康夫, 林依子, 阿部知子: "重イオンビーム照射を利用したソバ S-supergene への突然変異誘導の試み", 第 9 回イオンビーム育種研究会大会, 福井県, 5 月 (2013).

風間裕介, 平野智也, 大部澄江, 白川有希, 阿部知子: "重イオンビーム照射において LET が突然変異の種類や規模へ与える影響", 第 9 回イオンビーム育種研究会大会, 福井県, 5 月 (2013).

高原学, 蝦名真澄, 森田竜平, 風間裕介, 阿部知子, 高溝正, 中川仁: "重イオンビーム照射によるギニアグラスのアポミクシス領域欠失変異体の解析", 第 9 回イオンビーム育種研究会大会, 福井県, 5 月 (2013).

松田尚大, 竹下毅, 三木弥名子, 吉澤有子, 大田修平, 山崎誠和, 風間裕介, 阿部知子, 河野重行: "クロレラ類 *Parachlorella kessleri* の重イオン照射の効果とデンプン・オイル蓄積の動態" 第 9 回イオンビーム育種研究会大会, 福井県, 5 月 (2013).

阿部知子, 風間裕介, 平野智也: "Mutagenesis から Mutagenomics へ", 第 52 回ガンマーフィールドシンポジウム「次世代育種の可能性:環境、食糧、エネルギー問題解決へのストラテジー」, 水戸, 7 月(2013).

風間裕介, 平野智也, 石井公太郎, 大部澄江, 白川侑希, 林祐子, 阿部知子: "高 LET 精密制御照射によるシロイヌナズナのタンデム重複遺伝子破壊技術の確立", 第 52 回ガンマーフィールドシンポジウム 「次世代育種の可能性:環境、食糧、エネルギー問題解決へのストラテジー」, 水戸, 7 月(2013).

森田竜平, 竹久妃奈子, 石井公太郎, 林依子, 小暮祥子, 一瀬勝紀, 東海林英夫, 佐藤雅志, 齊藤大樹, 奥本裕, 阿部知子: "重イオンビーム照射によるイネ突然変異体の Exome 解析", 第 52 回ガンマーフィールドシンポジウム 「次世代育種の可能性:環境、食糧、エネルギー問題解決へのストラテジー」, 水戸, 7 月(2013).

中野道治, 山本浩史, 阿部知子, 林依子, 草場信: "イネ stay-green 突然変異体 *fsg1* の高精度マッピング", 第 52 回ガンマーフィールドシンポジウム 「次世代育種の可能性:環境、食糧、エネルギー問題解決へのストラテジー」, 水戸, 7 月(2013).

遠藤貴司, 佐藤雅志, 阿部知子, 佐伯研一, 佐藤浩子, 酒井球絵: "宮城県水稲奨励品種における塩害耐性の評価", 日本作物学会東北支部会第 56 回講演会, 福井, 8 月 (2013).

池田時浩: "ガラスキャピラリーによるマイクロビーム生成と細胞照射への応用", 第 1 回放射線総合センター タンデム加速器共同利用シンポジウム プログラム, 東京, 9 月 (2013).

森田竜平, 竹久妃奈子, 石井公太郎, 林依子, 小暮祥子, 一瀬勝紀, 東海林英夫, 佐藤雅志, 齊藤大樹, 奥本裕, 阿部知子: "イネ Exome 解析による LETmax での重イオンビーム突然変異の特徴", 第 31 回日本植物細胞分子生物学会, 北海道, 9 月 (2013).

平野智也, 風間裕介, 石井公太郎, 大部澄江, 白川侑希, 阿部知子: "シロイヌナズナにおける重イオンビーム誘発突然変異の全ゲノム解析", 第31回日本植物細胞分子生物学会, 北海道, 9 月 (2013).

増山文博, 保倉明子, 阿部知子, 平野智也, 寺田靖子, 佐野俊夫: "放射光蛍光 X 線分析によるタバコ BY-2 培養細胞におけるカドミウム蓄積機構の解明", 第 31 回日本植物細胞分子

生物学会, 北海道, 9 月 (2013).

石井公太郎, 風間裕介, 阿部知子:“川本法を利用したヒロハノマンテマ蕾のレーザーマイクロダイセクション” 日本植物形態学会第 25 回総会・大会, 北海道, 9 月 (2013).

青沼航, 川元寛章, 石井公太郎, 風間裕介, 阿部知子, 河野重行: “雌雄異株植物ヒロハノマンテマの両性花突然変異体における開花同調性と雌雄離熟の出現”, 日本植物形態学会第 25 回総会・大会, 北海道, 9 月 (2013).

風間裕介, 平野智也, 石井公太郎, 大部澄江, 白川侑希, 阿部知子: “高 LET 重イオンビームの変異誘発作用とそれを利用したタンデム重複遺伝子の破壊”, 日本植物学会第 77 回大会, 北海道, 9 月 (2013).

青沼航, 川元寛章, 石井公太郎, 風間裕介, 阿部知子, 河野重行: “ヒロハノマンテマ XY 性染色体にある B クラス遺伝子 S1AP3X/Y の欠失変異”, 日本植物学会第 77 回大会, 北海道, 9 月 (2013).

山﨑誠和, 大田修平, 佐藤聖樹, 竹下毅, 風間裕介, 阿部知子, 河野重行: “微細藻類への重イオンビーム照射による突然変異率の算出と凍結保存法による変異体の安定性評価”, 第 65 回日本生物工学会大会, 広島, 9 月 (2013).

池田時浩, 小島隆夫: “ガラス板表面の帯電による低速多価イオンビームガイド”, 日本物理学会 2013 年秋季(第 69 回年次)大会, 徳島, 9 月 (2013).

阿部知子, 平野智也, 風間裕介: “加速器施設の生物利用 - 品種改良技術の開発と普及”, 日本育種学会第 124 回講演会, 鹿児島, 10 月 (2013).

風間裕介, 平野智也, 阿部知子: “重イオンビームによるオンデマンド照射技術の開発”, 日本育種学会第 124 回講演会, 鹿児島, 10 月 (2013).

石井公太郎, 森田竜平, 竹久妃奈子, 林依子, 小暮祥子, 一瀬勝紀, 東海林英夫, 佐藤雅志, 阿部知子: “イネ重イオンビーム突然変異体の Exome 解析”, 日本育種学会第 124 回講演会, 鹿児島, 10 月 (2013).

高原学, 蝦名真澄, 森田竜平, 風間裕介, 阿部知子, 高溝正, 中川仁: “重イオンビーム照射によりアポミクシス遺伝子領域に欠失を生じた変異体の解析”, 日本育種学会第 124 回講演会, 鹿児島, 10 月 (2013).

風間裕介, 石井公太郎, 青沼航, 川元寛章, 池田時浩, 松永杏樹, 河野重行, 阿部知子: “巡回セールスマン問題を応用したヒロハノマンテマ Y 染色体欠失マッピング”, 日本育種学会第 124 回講演会, 鹿児島, 10 月 (2013).

小林有里奈, 風間裕介, Manickavelu A., 阿部知子, 坂 智広: “野生オオムギ Hordeum bulbosum L. の球茎形成過程におけるフィトクロム遺伝子発現解析と重イオンビームによる変異体作出”, 日本育種学会第 124 回講演会, 鹿児島, 10 月 (2013).

西浦愛子, 風間裕介, 阿部知子, 水野信之, 那須田周平, 村井耕二: “一粒系コムギ極早生突然変異体 *extra early-flowering 1* (*exe1*) および *exe3* は *Wheat PHYTOCLOCK 1* 遺伝子の欠失突然変異体である”, 日本育種学会第 124 回講演会, 鹿児島, 10 月 (2013).

阿部知子: “加速器が生んだ吟醸酒 理研ブランド清酒「仁科誉」”, 日本化学会秋季事業 第 3 回 CSJ 化学フェスタ 2013, 東京, 10 月 (2013).

阿部知子: “重イオン加速器(サイクロトロン)を用いた品種改良技術の開発”, アグリビジネス創出フェア 2013, 東京, 10 月 (2013).

小暮祥子, 森田竜平, 林依子, 一瀬勝紀, 若菜妙子, 山田美恵子, 東海林英夫, 石井公太郎, 佐藤雅志, 阿部知子: “重イオンビームで誘発されたイネ矮性変異体集団を用いた DNA 変異の解析”, 植物化学調節学会第 48 回大会, 新潟, 10 月-11 月 (2013).

阿部知子: “重イオンビーム育種技術で「日本ブランド」の花を創る”, 花き新品種育成研修会, 静岡, 11 月 (2013).

阿部知子: “量子ビームを用いて「東北ブランド」の新しい農林水産物を創る”, 第 126 回東北大学金属材料研究所講演会, 宮城, 11 月 (2013).

阿部知子: “高速重イオンビーム照射による品種改良技術の開発”, 2013 植物科学シンポジウム 持続可能資源の開発に向けた植物科学, 東京, 12 月 (2013).

佐藤陽一, 山口正希, 平野智也, 福西暢尚, 阿部知子, 河野重行: “大型褐藻類の選抜育種に使用する新型水槽設備の開発”, 日本藻類学会第 38 回大会, 船橋, 3 月 (2014).

森田竜平, 石井公太郎, 竹久妃奈子, 林依子, 小暮祥子, 一瀬勝紀, 東海林英夫, 佐藤雅志, 阿部知子: “エキソーム解析によるイネ変異遺伝子の迅速決定”, 日本育種学会第 125 回講演会, 仙台, 3 月 (2014).

平野智也, 風間裕介, 石井公太郎, 大部澄江, 白川侑希, 阿部知子: “全ゲノム解析で明らかとなった重イオンビーム誘発染色体再編成”, 日本育種学会第 125 回講演会, 仙台, 3 月 (2014).

風間裕介, 石井公太郎, 青沼航, 川元寛章, 河野重行, 阿部知子: “川本法 LMD と Y 染色体発現アレイを用いたヒロハノマンテマ性決定遺伝子の絞込み”, 日本育種学会第 125 回講演会, 仙台, 3 月 (2014).

道坂怜生, 増岡千裕, 津山睦, 阿部知子, 田中朋之: “イネ突然変異系統 13-45 における白未熟粒発生機構の解析”, 日本作物学会第 237 回講演会, 千葉, 3 月 (2014).

RI Applications Team

Publications

[Journal]

(Original Papers) *Subject to Peer Review

Khandaker M. U., Haba H., Kanaya J., and Otuka N.: "Excitation functions of (d,x) nuclear reactions on natural titanium up to 24 MeV", Nucl. Instr. and Meth. B **296**, 14 (2013).*

Asai M., Tsukada K., Sakama M., Haba H., Ichikawa T., Ishii Y., Toyoshima A., Ishii T., Nishinaka I., Nagame Y., Kasamatsu Y., Shibata M., Kojima Y., and Hayashi H.: "Ground-state configuration of the N = 157 nucleus ^{259}No", Phys. Rev. C **87**, 014332 (2013).*

Sumita T., Morimoto K., Kaji D., Haba H., Ozeki K., Sakai R., Yoneda A., Yoshida A., Hasebe H., Katori K., Sato N., Wakabayashi Y., Mitsuoka S., Goto S., Murakami M., Kariya Y., Tokanai F., Mayama K., Takeyama M., Moriya T., Ideguchi E., Yamaguchi T., Kikunaga H., Chiba J., and Morita K.: "New result on the production of ^{277}Cn by the ^{208}Pb + ^{70}Zn reaction", J. Phys. Soc. Jpn. **82**, 024202 (2013).*

Motomura S., Kanayama Y., Hiromura M., Fukuchi T., Ida T., Haba H., Watanabe Y., and Enomoto S.: "Improved imaging performance of a semiconductor Compton camera GREI makes for a new methodology to integrate bio-metal analysis and molecular imaging technology in living organisms", J. Anal. At. Spectrom. **28**, 934 (2013).*

Kasamatsu Y., Toyoshima A., Toume H., Tsukada K., Asai M., Haba H., and Nagame Y.: "Adsorption behavior of ^{95}Nb and ^{179}Ta as homologues of element 105, Db, on cation exchanger in HF/HNO_3 solution", J. Nucl. Radiochem. Sci. **13**, 9 (2013).*

Murakami M., Goto S., Murayama H., Kojima T., Kudo H., Kaji D., Morimoto K., Haba H., Kudou Y., Sumita T., Sakai R., Yoneda A., Morita K., Kasamatsu Y., Kikunaga H., and Sato T. K.: "Excitation functions for production of Rf isotopes in the ^{248}Cm + ^{18}O reaction", Phys. Rev. C **88**, 024618 (2013).*

Khandaker M. U., Haba H., Kanaya J., and Otuka N.: "Activation cross-sections of deuteron-induced nuclear reactions on natural iron up to 24 MeV", Nucl. Instr. and Meth. B **316**, 33 (2013).*

Toyoshima A., Li Z., Asai M., Sato N., Sato T., Kikuchi T., Kaneya Y., Kitatsuji Y., Tsukada K., Nagame Y., Schädel M., Ooe K., Kasamatsu Y., Shinohara A., Haba H., and Even J.: "Measurement of the Md^{3+}/Md^{2+} reduction potential studied with flow electrolytic chromatography", Inorg. Chem. **52**, 12311 (2013).*

Schury P., Wada M., Ito Y., Naimi S., Sonoda T., Mita H., Takamine A., Okada K., Wollnik H., Chon S., Haba H., Kaji D., Koura H., Miyatake H., Morimoto K., Morita K., and Ozawa A.: "A multi-reflection time-of-flight mass spectrograph for short-lived and super-heavy nuclei", Nucl. Instr. and Meth. B **317**, 537 (2013).*

Hirata J., Takahashi K., and Tanaka M.: "Determination method of multi elements in ferromanganese samples by LA-ICP-MS", Anal. Sci. **29**, 151 (2013).*

Tanaka M. and Takahashi K.: "Ionised silica in the estuary of a river as supply to seawater: Identification and ionization efficiency of silica species by FAB-MS", Estuar. Coast. Shelf Sci. **121**, 1 (2013).*

Tanaka M., Takahashi K., Nemoto M., and Horimoto N.: "Selectivity of silica species in ocean observed from seasonal and local changes", Spectrochim. Acta Part A Mol. Biomol. Spectrosc. **104**, 423 (2013).*

南武志，今津節生，北川路子，牧田碧夏，西川恵祐，永松剛，田中龍彦，卜部達也，木寺正憲，石塚香織，高久雄一，高橋和也："鉛同位体比測定に基づく遺跡から出土した朱（水銀朱）の産地の解析"，分析化学 **62**, 825 (2013).*

南武志，河野摩耶，古川登，高橋和也，武内章記，今津節生："硫黄同位体分析による西日本日本海沿岸の弥生時代後期から古墳時代の墳墓における朱の産地同定の試み"，地球化学 **47**, 237 (2013).*

Gan Z. G., Ma L., Yu L., Yang H. B., Huang T. H., Li G. S., Tian Y. L., Wang Y. S., Xu X. X., Wu X. L., Huang M. H., Luo C., Ren Z. Z., Zhou S. G., Zhou X. H., Xu H. S., and Xiao G. Q.: "α decay of the new neutron-deficient isotope ^{205}Ac", Phys. Rev. C **89**, 014308 (2014).*

Urabe T., Takahashi K., Kitagawa M., Sato T., Kondo T., Enomoto S., Kidera M., and Seto Y.: "Development of portable mass spectrometer with electron cyclotron resonance ion source for detection of chemical warfare agents in air", Spectrochim. Acta Part A Mol. Biomol. Spectrosc. **120**, 437 (2014).*

Haba H., Huang M., Kaji D., Kanaya J., Kudou Y., Morimoto K., Morita K., Murakami M., Ozeki K., Sakai R., Sumita T., Wakabayashi Y., Yoneda A., Kasamatsu Y., Kikutani Y., Komori Y., Nakamura K., Shinohara A., Kikunaga H., Kudo H., Nishio K., Toyoshima A., and Tsukada K.: "Production of ^{262}Db in the ^{248}Cm(^{19}F,5n)^{262}Db reaction and decay properties of ^{262}Db and ^{258}Lr", Phys. Rev. C **89**, 024618 (2014).*

Sato N., Sato T. K., Asai M., Toyoshima A., Tsukada K., Li Z. J., Nishio K., Nagame Y., Schädel M., Haba H., Ichikawa S., and Kikunaga H.: "Production of ^{256}Lr in the ^{249,250,251}Cf + ^{11}B, ^{243}Am + ^{18}O, and ^{248}Cm + ^{14}N reactions", Radiochim. Acta **102**, 211 (2014).*

[Book · Proceedings]

(Original Papers) *Subject to Peer Review

Khandaker M. U., Haba H., Kanaya J., Otuka N., Kassima H. A., and Amina Y. M.: "Investigations of ^{nat}Ti(d,x)^{48}V nuclear reactions for beam monitoring purposes", AIP Conf. Proc. **1528**, 433 (2013).*

(Others)

高橋和也："ベーシックマスター 分析化学 第 14 章 質量分析"，オーム社 (2013).

Oral Presentations

(International Conference etc.)

Urabe T., Kidera M., Kitagawa M., Nagamatsu T., Toda M., Makita M., and Takahashi K.: "New method for comprehensive detection of trace elements in environmental or biochemical materials using an electron-cyclotron-resonance ion-source mass spectrometer", 5th International Congress of the Federation of the European Societies for Trace Elements and Materials, (Federation of the European Societies for Trace Elements and Minerals), Avignon, France, May (2013).

Haba H.: "Chemistry of superheavy elements", RIKEN–CAS IMP Joint Workshop, (RIKEN), Wako, Japan, April (2013).

Even J., Yakushev A., Düllmann Ch. E., Haba H., Asai M., Sato T., Brand H., Di Nitto A., Eichler R., Fangli F., Hartmann W., Huang M., Jäger E., Kaji D., Kanaya J., Kaneya Y., Khuyagbaatar J., Kindler B., Kratz J. V., Krier J., Kudou Y., Kurz N., Lommel B., Miyashita S., Morimoto K., Morita K., Nagame Y., Nitsche H., Ooe K., Schädel M., Steiner J., Sumita T., Tanaka K., Toyoshima A., Tsukada K., Türler A., Usoltsev I., Wakabayashi Y., Wang Y., Wiehl N., Yamaki S., and Qin Z.: "$Sg(CO)_6$ – First organometallic complex of a superheavy element", XXXIII Mazurian Lakes Conference on Physics, Frontiers in Nuclear Physics, (National Centre for Nuclear Research and University of Warsaw), Piaski, Poland, Sept. (2013).

Di Nitto A., Even J., Yakushev A., Düllmann Ch. E., Haba H., Asai M., Sato T., Brand H., Eichler R., Fangli F., Hartmann W., Huang M., Jäger E., Kaji D., Kanaya J., Kaneya Y., Khuyagbaatar J., Kindler B., Kratz J. V., Krier J., Kudou Y., Kurz N., Lommel B., Miyashita S., Morimoto K., Morita K., Nagame Y., Nitsche H., Ooe K., Schädel M., Steiner J., Sumita T., Tanaka K., Toyoshima A., Tsukada K., Türler A., Usoltsev I., Wakabayashi Y., Wang Y., Wiehl N., Yamaki S., and Qin Z.: "Decay spectroscopy of ^{265}Sg after combined physical and chemical separation", XXXIII Mazurian Lakes Conference on Physics, Frontiers in Nuclear Physics, (National Centre for Nuclear Research and University of Warsaw), Piaski, Poland, Sept. (2013).

Haba H.: "Coupling superheavy element chemistry to recoil separators", 8th Workshop on the Chemistry of the Heaviest Elements (CHE 8), (Japan Atomic Energy Agency), Takayama, Japan, Sept. (2013).

Ooe K., Tsukada K., Asai M., Sato T. K., Toyoshima A., Miyashita S., Nagame Y., Schädel M., Kaneya Y., Lerum H. V., Omtvedt J. P., Kratz J. V., Haba H., Wada A., and Kitayama Y.: "Development of new degasser with a hydrophobic membrane for SISAK system", 8th Workshop on the Chemistry of the Heaviest Elements (CHE 8), (Japan Atomic Energy Agency), Takayama, Japan, Sept. (2013).

Yokokita T., Kino A., Nakamura K., Komori Y., Toyomura K., Kasamatsu Y., Takahashi N., Yoshimura T., Kudou Y., Haba H., Kanaya J., Huang M., and Shinohara A.: "Extraction of group 4 and 5 elements and development of rapid extraction apparatuses for Rf and Db experiments", 8th Workshop on the Chemistry of the Heaviest Elements (CHE 8), (Japan Atomic Energy Agency), Takayama, Japan, Sept. (2013).

Tsukada K., Toyoshima A., Asai M., Kasamatsu Y., Li Z. J., Ishii Y., Haba H., Sato T. K., Nagame Y., and Schädel M.: "Studies of ion-exchange chromatographic behavior of Rf and Db using automated rapid chemical separation apparatuses in JAEA", 8th Workshop on the Chemistry of the Heaviest Elements (CHE 8), (Japan Atomic Energy Agency), Takayama, Japan, Sept. (2013).

Toyoshima A., Li Z. J., Asai M., Sato N., Sato T. K., Kikuchi T., Kaneya Y., Kitatsuji Y., Tsukada K., Nagame Y., Schädel M., Ooe K., Kasamatsu Y., Kogama Y., Shinohara A., Haba H., and Evan J.: "Electrolytic reduction of mendelevium using a flow electrolytic column", 8th Workshop on the Chemistry of the Heaviest Elements (CHE 8), (Japan Atomic Energy Agency), Takayama, Japan, Sept. (2013).

Kitayama Y., Shigeyoshi Y., Yokoyama A., Toyoshima A., Tsukada K., Ooe K., Maeda E., Kimura H., Kikunaga H., Kudou Y., Kanaya J., Huang M., and Haba H.: "Adsorption behavior of Zr and Hf to TTA-resin in microcolumn for determining the forming ability of Rf monofluoride complex", 8th Workshop on the Chemistry of the Heaviest Elements (CHE 8), (Japan Atomic Energy Agency), Takayama, Japan, Sept. (2013).

Murakami M., Goto S., Murayama H., Kojima T., Kaji D., Morimoto K., Haba H., Kudou Y., Sumita T., Sakai R., Yoneda A., Morita K., Kasamatsu Y., Kikunaga H., Sato T. K., and Kudo H.: "Excitation functions for production of Rf isotopes in ^{248}Cm + ^{18}O reaction", 8th Workshop on the Chemistry of the Heaviest Elements (CHE 8), (Japan Atomic Energy Agency), Takayama, Japan, Sept. (2013).

Komori Y., Yokokita T., Nakamura K., Toyomura K., Masashi M., Kikunaga H., Kasamatsu Y., Takahashi N., Yoshimura T., Haba H., Kanaya J., Huang M., Kudou Y., Toyoshima A., and Shinohara A.: "Development of liquid scintillation α/SF detection system for aqueous chemical studies of Sg", 8th Workshop on the Chemistry of the Heaviest Elements (CHE 8), (Japan Atomic Energy Agency), Takayama, Japan, Sept. (2013).

Miyashita S., Toyoshima A., Ooe K., Sato T. K., Asai M., Tsukada K., Nagame Y., Schädel M., Kaneya Y., Haba H., Kanaya J., Huang M., Wada A., Akiyama K., Kitayama Y., Yokoyama A., Kratz J. V., Lerum H. V., and Omtvedt J. P.: "Extraction behavior of hexavalent and reduced Mo and W with 4-isopropyltropolone (Hinokitiol)", 8th Workshop on the Chemistry of the Heaviest Elements (CHE 8), (Japan Atomic Energy Agency), Takayama, Japan, Sept. (2013).

Kasamatsu Y., Toyomura K., Yokokita T., Haba H., Kanaya J., Kudou Y., Morita K., Kikunaga H., Ohtsuki T., Mitsugashira T., and Shinohara A.: "Hydroxide coprecipitation with Sm investigated for various elements using multitracer –For the application of precipitation method to superheavy element chemistry–", 8th Workshop on the Chemistry of the Heaviest Elements (CHE 8), (Japan Atomic Energy Agency), Takayama, Japan, Sept. (2013).

Even J., Yakushev A., Düllmann Ch. E., Haba H., Asai M., Sato T., Brand H., Di Nitto A., Eichler R., Fangli F., Hartmann W., Huang M., Jäger E., Kaji D., Kanaya J., Kaneya Y., Khuyagbaatar J., Kratz J. V., Krier J., Kuboki Y. K., Lommel B., Kurz N., Miyashita S., Morimoto K., Morita K., Nagame Y., Nitsche H., Ooe K., Schädel M., Steiner J., Sumita T., Tanaka K., Toyoshima A., Tsukada K., Türler A., Usoltsev I., Wakabayashi Y., Wang Y., Wiehl N., Yamaki S., and Qin Z.: "$Sg(CO)_6$ – The first organometallic transactinide complex opening a window to a new compound class", 8th Workshop on the Chemistry of the Heaviest Elements (CHE 8), (Japan Atomic Energy Agency), Takayama, Japan, Sept. (2013).

Kaji D., Morimoto K., Haba H., Wakabayashi Y., Kudou Y., Huang M., Goto S., Murakami M., Goto N., Koyama T., Tamura N., Tsuto S., Sumita T., Tanaka K., Takeyama M., Yamaki S., and Morita K.: "Startup of a new gas-filled recoil separator GARIS-II", The 5th Asia-Pacific Symposium on Radiochemistry '13 (APSORC13), (The Japan Society of Nuclear and Radiochemical Sciences), Kanazawa, Japan, Sept. (2013).

Kasamatsu Y., Yokokita T., Kino A., Nakamura K., Toyomura K., Komori Y., Takahashi N., Haba H., Kanaya J., Huang M., Kudou Y., Yoshimura T., and Shinohara A.: "Development of a batch-type solid-liquid extraction apparatus for repetitive extraction experiment of element 104, Rf", The 5th Asia-Pacific Symposium on Radiochemistry '13 (APSORC13), (The Japan Society of Nuclear and Radiochemical Sciences), Kanazawa, Japan, Sept. (2013).

Toyomura K., Kasamatsu Y., Shiohara N., Yokokita T., Komori Y., Nakamura K., Takahashi N., Yoshimura T., Haba H., Kudou Y., Kikunaga H., Ohtsuki T., Takamiya K., Mitsugashira T., and Shinohara A.: "Coprecipitation of Zr, Hf and Th with Sm hydroxide for chemical study of Rf", The 5th Asia-Pacific Symposium on Radiochemistry '13 (APSORC13), (The Japan Society of Nuclear and Radiochemical Sciences), Kanazawa, Japan, Sept. (2013).

Haba H.: "Production and decay studies of transactinide nuclides with GARIS at RIKEN", The 5th Asia-Pacific Symposium on Radiochemistry '13 (APSORC13), (The Japan Society of Nuclear and Radiochemical Sciences), Kanazawa, Japan, Sept. (2013).

Even J., Yakushev A., Düllmann Ch. E., Haba H., Asai M., Sato T., Brand H., Di Nitto A., Eichler R., Fangli F., Hartmann W., Huang M., Jäger E., Kaji D., Kanaya J., Kaneya Y., Khuyagbaatar J., Kindler B., Kratz J. V., Krier J., Kudou Y., Kurz N., Lommel B., Miyashita S., Morimoto K., Morita K., Nagame Y., Nitsche H., Ooe K., Schädel M., Steiner J., Sumita T., Tanaka K., Toyoshima A., Tsukada K., Türler A., Usoltsev I., Wakabayashi Y., Wang Y., Wiehl N., Yamaki S., and Qin Z.: "$Sg(CO)_6$ – The first organometallic transactinide complex opening a window to a new compound class", The 5th Asia-Pacific Symposium on Radiochemistry '13 (APSORC13), (The Japan Society of Nuclear and Radiochemical Sciences), Kanazawa, Japan, Sept. (2013).

Murakami M., Tsuto S., Ooe K., Haba H., Kanaya J., Goto S., and Kudo H.: "Extraction behavior of Nb and Ta in HF solutions with tributyl phosphate", The 5th Asia-Pacific Symposium on Radiochemistry '13 (APSORC13), (The Japan Society of Nuclear and Radiochemical Sciences), Kanazawa, Japan, Sept. (2013).

Huang M., Asai M., Haba H., Kaji D., Kanaya J., Kasamatsu Y., Kikunaga H., Kikutani Y., Komori Y., Kudo H., Kudou Y., Morimoto K., Morita K., Murakami M., Nakamura K., Ozeki K., Sakai R., Shinohara A., Sumita T., Tanaka K., Toyoshima A., Tsukada K., Wakabayashi Y., and Yoneda A.: "Production of ^{88}Nb and ^{170}Ta for chemical studies of element 105 Db using the GARIS gas-jet system", The 5th Asia-Pacific Symposium on Radiochemistry '13 (APSORC13), (The Japan Society of Nuclear and Radiochemical Sciences), Kanazawa, Japan, Sept. (2013).

Toyoshima A., Miyashita S., Asai M., Sato T. K., Kaneya Y., Tsukada K., Kitatsuji Y., Nagame Y., Schädel M., Lerum H. V., Omtvedt J. P., Oshimi Y., Ooe K., Kitayama Y., Yokoyama A., Wada A., Oura Y., Haba H., Kanaya J., Huang M., Komori Y., Yokokita T., Kasamatsu Y., Shinohara A., Pershina V., and Kratz J. V.: "Chemical studies of Mo and W in preparation of a seaborgium (Sg) reduction experiment using MDG, FEC, and SISAK", The 5th Asia-Pacific Symposium on Radiochemistry '13 (APSORC13), (The Japan Society of Nuclear and Radiochemical Sciences), Kanazawa, Japan, Sept. (2013).

Ooe K., Tsukada K., Asai M., Sato T. K., Toyoshima A., Miyashita S., Nagame Y., Schädel M., Kaneya Y., Lerum H. V., Omtvedt J. P., Kratz J. V., Haba H., Wada A., and Kitayama Y.: "Development of a new continuous dissolution apparatus with a hydrophobic membrane for superheavy element chemistry", The 5th Asia-Pacific Symposium on Radiochemistry '13 (APSORC13), (The Japan Society of Nuclear and Radiochemical Sciences), Kanazawa, Japan, Sept. (2013).

Koyama T., Goto N., Murakami M., Ooe K., Haba H., Kaneya J., Goto S., and Kudo H.: "Development of a rapid solvent extraction technique with flow injection analysis for superheavy element chemistry", The 5th Asia-Pacific Symposium on Radiochemistry '13 (APSORC13), (The Japan Society of Nuclear and Radiochemical Sciences), Kanazawa, Japan, Sept. (2013).

Komori Y., Yokokita T., Toyomura K., Nakamura K., Kasamatsu Y., Haba H., Kanaya J., Huang M., Kudou

Y., Toyoshima A., Takahashi N., and Shinohara A.: "Solid-liquid extraction of Mo and W by Aliquat 336 from HF and HCl solutions towards extraction chromatography experiments of Sg", The 5th Asia-Pacific Symposium on Radiochemistry '13 (APSORC13), (The Japan Society of Nuclear and Radiochemical Sciences), Kanazawa, Japan, Sept. (2013).

Tsukada K., Toyoshima A., Asai M., Kasamatsu Y., Li Z. J., Ishii Y., Haba H., Sato T. K., Nagame Y., and Schädel M.: "Chemical studies of Rf and Db in liquid-phases using automated rapid chemical separation apparatuses at JAEA", The 5th Asia-Pacific Symposium on Radiochemistry '13 (APSORC13), (The Japan Society of Nuclear and Radiochemical Sciences), Kanazawa, Japan, Sept. (2013).

Miyashita S., Toyoshima A., Ooe K., Asai M., Sato T. K., Tsukada K., Nagame Y., Schädel M., Kaneya Y., Haba H., Kanaya J., Huang M., Kitayama Y., Yokoyama A., Wada A., Oura Y., Kratz J. V., Lerum H. V., and Omtvedt J. P.: "Solvent extraction of hexavalent Mo and W using 4-isopropyltropolone (Hinokitiol) for seaborgium (Sg) reduction experiment", The 5th Asia-Pacific Symposium on Radiochemistry '13 (APSORC13), (The Japan Society of Nuclear and Radiochemical Sciences), Kanazawa, Japan, Sept. (2013).

Even J., Yakushev A., Düllmann Ch. E., Haba H., Asai M., Sato T. K., Ackermann D., Block M., Brand H., Di Nitto A., Eichler R., Fangli F., Hartmann W., Hessberger F. P., Huang M., Jäger E., Kaji D., Kanaya J., Kaneya Y., Khuyagbaatar J., Kindler B., Kratz J. V., Krier J., Kudou Y., Kurz N., Lommel B., Maurer J., Miyashita S., Morimoto K., Morita K., Nagame Y., Nitsche H., Ooe K., Schädel M., Steiner J., Sumita T., Tanaka K., Toyoshima A., Tsukada K., Türler A., Usoltsev I., Wakabayashi Y., Wang Y., Wiehl N., Yamaki S., and Qin Z.: "In-situ synthesis of volatile carbonyl complex with short-lived isotopes", The Third International Conference on Application of RadiotraCers and Energetic Beams in Sciences (ARCEBS-14), (Saha Institute of Nuclear Physics), Kolkata, India, Jan. (2014).

Khandaker M. U., Haba H., Murakami M., Otuka N., and Kassim H. A.: "Activation cross sections of deuteron-induced reactions on natural copper up to 24 MeV", The Third International Conference on Application of RadiotraCers and Energetic Beams in Sciences (ARCEBS-14), (Saha Institute of Nuclear Physics), Kolkata, India, Jan. (2014).

Haba H.: "Present status and perspectives of superheavy element nuclear chemistry at RIKEN GARIS", The Third International Conference on Application of RadiotraCers and Energetic Beams in Sciences (ARCEBS-14), (Saha Institute of Nuclear Physics), Kolkata, India, Jan. (2014).

Haba H.: "Production of ^{261}Rf, ^{262}Db, and ^{265}Sg for chemical studies using the gas-jet transport system coupled to GARIS", Fifth Symposium on Nuclear Analytical Chemistry (NAC-V), (Bhabha Atomic Research Centre), Mumbai, India, Jan. (2014).

Haba H.: "Production and decay studies of ^{261}Rf, ^{262}Db, and ^{265}Sg at GARIS@RIKEN", 16th ASRC International Workshop "Nuclear Fission and Structure of Exotic Nuclei", (Japan Atomic Energy Agency), Tokai, Japan, Mar. (2014).

(Domestic Conference)

高橋和也: "鉛同位体測定に基づく弥生時代後期から古墳時代前期にかけての遺跡から出土した水銀朱の産地同定の試み", 日本分析化学会第62年会, (日本分析化学会), 大阪, 9月 (2013).

笠松良崇, 豊村恵悟, 横北卓也, 羽場宏光, 金谷淳平, 工藤祐生, 森田浩介, 菊永英寿, 大槻勤, 三頭聰明, 篠原厚: "マルチトレーサーを用いた様々な元素の水酸化サマリウム共沈", 日本化学会第94春季年会, (日本化学会), 名古屋市, 3月 (2014).

豊村恵悟, 笠松良崇, 横北卓也, 塩原直也, 小森有希子, 重河優大, 吉村崇, 高橋成人, 菊永英寿, 大槻勤, 三頭聰明, 羽場宏光, 金谷淳平, 黄明輝, 村上昌史, 工藤祐生, 森田浩介, 高宮幸一, 篠原厚: "104番元素Rfの希アンモニア水中での水酸化サマリウム共沈挙動", 日本化学会第94春季年会, (日本化学会), 名古屋市, 3月 (2014).

Industrial Cooperation Team

Publications

[Journal]

(Original Papers) *Subject to Peer Review

Yoshida A., Kambara T., Nakao A., Uemoto R., Uno H., Nagano A., Yamaguchi H., Nakao T., Kahl D., Yanagisawa Y., Kameda D., Ohnishi T., Fukuda N., Kubo T., "Wear diagnostics of industrial material using RI beams of ^{7}Be and ^{22}Na", Nucl. Instrum. Methods Phys. Res. B **317**, 785-788(2013).

Oral Presentations

(International Conference etc.)

Yoshida A., et al., "Wear diagnostics of industrial material using RI beams of ^{7}Be and ^{22}Na", 16th International Conference on Electromagnetic Iso-tope Separators and Techniques Related to their Applications (EMIS2012), Matsue, Dec.(2012)

(Domestic Conference)

吉田敦: "RI ビームの工業応用－表面摩耗量検査法の開発－", 理研シンポジウム第 16 回「トライボコーティングの弁城と将来」, (トライボコーティング技術研究会), 和光, 2 月(2014).

Safety Management Group

Publications

[Journal]

(Original Papers)　*Subject to Peer Review

Iimoto T., Uwamino Y., Kawano T.: "Fundamentals of Radiation Measurement", Journal of Plasma and Fusion Research **89**, No. 9, pp. 629–634 (2013).

Uwamino Y.: "Relation between Surface Dose Rate and Induced Radioactivity", Japanese Journal of Radiation Safety Management **12**, No. 1, pp. 36–40 (2013). *

Tanaka K., Inabe N., Yoshida K., Kusaka K., and Kubo T.: "Pillow seal system at the BigRIPS separator", Nuclear Instruments and Methods in Physics Research B **317**, pp. 734–738 (2013). *

[Book · Proceedings]

(Review)

高淵雅廣, 上蓑義朋, 小木曽洋一, 桧垣正吾: 5 版 やさしい放射線とアイソトープ, 公益社団法人 日本アイソトープ協会, 東京都, (2014).

Oral Presentations

(International Conference etc.)

Tanaka K., Inabe N., Yoshida K., Kusaka K., and Kubo T.: "Evaluation of radiation level and comparison with PHITS calculation for BigRIPS separator in RIBF", ANS(American nuclear society) winter meeting 2013, (米国原子力学会), Washington D.C., USA, Nov. (2013).

(Domestic Conference)

上蓑義朋: "加速器施設におけるサーベイメータを用いた放射化物判断の可能性", 日本原子力学会「2013 年秋の大会」, (日本原子力学会), 八戸市, 9 月 (2013).

上蓑義朋: "サーベイメータを用いた放射化物の評価", 日本放射線安全管理学会第 12 回学術大会, (日本放射線安全管理学会), 札幌市, 11 月 (2013).

上蓑義朋: "加速器施設における安全管理の経験と課題", 加速器施設安全シンポジウム, (高エネルギー加速器研究機構、日本原子力研究開発機構、J-PARC センター), 東京都, 12 月 (2013).

向井弘樹, 上蓑義朋: "ドラム缶に収納した放射化物の定量方法の検討", 平成 25 年度放射線安全取扱部会年次大会 (第 54 回放射線管理研修会), (日本アイソトープ協会放射線安全取扱部会), 鹿児島市, 11 月 (2013).

CNS (Center for Nuclear Study, Graduate School of Science, University of Tokyo)

Publications

[Journal]

(Original Papars) *Subject to Peer Review

Adare A., *et al.* [PHENIX Collaboration], "Azimuthal anisotropy of π^0 and eta mesons in Au+Au collisions at $\sqrt{s_{NN}}$=200 GeV", Phys. Rev. C **88**, 064910 (2013)

Abelev B. B., *et al.* [ALICE Collaboration]. "K^0_S and Λ production in Pb-Pb collisions at $\sqrt{s_{NN}} = 2.76$ TeV", Phys. Rev. Lett. **111**, no. 22, 222301 (2013)

Abelev B. B., *et al.* [ALICE Collaboration], "Long-range angular correlations of pi, K and p in p–Pb collisions at $\sqrt{s_{NN}} = 5.02$ TeV", Phys. Lett. B **726**, 164 (2013)

Abelev B. B.,*et al.* [ALICE Collaboration], "Multiplicity dependence of two-particle azimuthal correlations in pp collisions at the LHC", JHEP **1309**, 049 (2013)

Abelev B. B., *et al.* [ALICE Collaboration], "Multiplicity dependence of the average transverse momentum in pp, p-Pb, and Pb-Pb collisions at the LHC", Phys. Lett. B **727**, 371 (2013)

Abelev B. B.,*et al.* [ALICE Collaboration], "Energy Dependence of the Transverse Momentum Distributions of Charged Particles in pp Collisions Measured by ALICE", Eur. Phys. J. C **73**, 2662 (2013)

Abelev B. B. *et al.* [ALICE Collaboration], "Directed Flow of Charged Particles at Midrapidity Relative to the Spectator Plane in Pb-Pb Collisions at $\sqrt{s_{NN}}$=2.76 TeV", Phys. Rev. Lett. **111**, no. 23, 232302 (2013)

Abbas E., *et al.* [ALICE Collaboration], "Performance of the ALICE VZERO system", JINST **8**, P10016 (2013)

Adare A., *et al.* [PHENIX Collaboration], "Nuclear Modification of ψ', χ_c, and J/ψ Production in d+Au Collisions at $\sqrt{s_{NN}}$=200 GeV", Phys. Rev. Lett. **111**, no. 20, 202301 (2013)

Abelev B., *et al.* [ALICE Collaboration], "D meson elliptic flow in non-central Pb-Pb collisions at $\sqrt{s_{NN}}$ = 2.76TeV", Phys. Rev. Lett. **111**, 102301 (2013)

Abbas E. *et al.* [ALICE Collaboration], "Mid-rapidity anti-baryon to baryon ratios in pp collisions at $\sqrt{s}$ = 0.9, 2.76 and 7 TeV measured by ALICE", Eur. Phys. J. C **73**, 2496 (2013)

Abbas E., *et al.* [ALICE Collaboration], "Charmonium and e^+e^- pair photoproduction at mid-rapidity in ultra-peripheral Pb-Pb collisions at $\sqrt{s_{NN}} = 2.76$ TeV", Eur. Phys. J. C **73**, 2617 (2013)

Adare A., *et al.* [PHENIX Collaboration], "Spectra and ratios of identified particles in Au+Au and d+Au collisions at $\sqrt{s_{NN}} = 200$ GeV", Phys. Rev. C **88**, no. 2, 024906 (2013)

Abbas E., *et al.* [ALICE Collaboration] "Centrality dependence of the pseudorapidity density distribution for charged particles in Pb-Pb collisions at $\sqrt{s_{NN}} = 2.76$ TeV", Phys. Lett. B **726**, 610 (2013)

Abbas E., *et al.* [ALICE Collaboration], "J/ψ Elliptic Flow in Pb-Pb Collisions at $\sqrt{s_{NN}} = 2.76$ TeV", Phys. Rev. Lett. **111**, 162301 (2013)

Adare A., *et al.* [PHENIX Collaboration], "Quadrupole Anisotropy in Dihadron Azimuthal Correlations in Central d+Au Collisions at $\sqrt{s_{NN}}$=200 GeV", Phys. Rev. Lett. **111**, no. 21, 212301 (2013)

Abelev B., *et al.* [ALICE Collaboration], "Centrality dependence of π, K, p production in Pb-Pb collisions at $\sqrt{s_{NN}} = 2.76$ TeV", Phys. Rev. C **88**, no. 4, 044910 (2013)

Abelev B., *et al.* [ALICE Collaboration], "Centrality determination of Pb-Pb collisions at $\sqrt{s_{NN}} = 2.76$ TeV with ALICE", Phys. Rev. C **88**, no. 4, 044909 (2013)

Abelev B., *et al.* [ALICE Collaboration], "Charge correlations using the balance function in Pb-Pb collisions at $\sqrt{s_{NN}} = 2.76$ TeV", Phys. Lett. B **723**, 267 (2013)

Abelev B., *et al.* [ALICE Collaboration], "Measurement of the inclusive differential jet cross section in *pp* collisions at $\sqrt{s} = 2.76$ TeV", Phys. Lett. B **722**, 262 (2013)

He J.J., Zhang L.Y., Parikh A., Xu S.W., Yamaguchi H., Kahl D., Kubono S., Hu J., Ma P., Chen S.Z., Wakabayashi Y., Sun B.H., Wang H.W., Tian W.D., Chen R.F., Guo B., Hashimoto T., Togano Y., Hayakawa S., Teranishi T., Iwasa N., Yamada T., Komatsubara T., "The ^{18}Ne(α, p)^{21}Na breakout reaction in x-ray bursts: Experimental determination of spin-parities for α resonances in ^{22}Mg via resonant elastic scattering of ^{21}Na+p", Phys. Rev. C **88** 012801(R) (2013).

Jin S.J., Wang Y.B., Su J., Yan S.Q., Li Y.J., Guo B., Li Z.H., Zeng S., Lian G., Bai X.X., Liu W.P., Yamaguchi H., Kubono S., Hu J., Kahl D., Jung H.S., Moon J.Y., Lee C.S., Teranishi T., Wang H.W., Ishiyama H., Iwasa N., Komatsubara T., Brown B.A., "Resonant scattering of ^{22}Na + p studied by the thick-target inverse-kinematic method", Phys. Rev. C **88**, 035801 (2013).

Muto H., Ohshiro Y., Yamaka S., Watanabe S., Oyaizu M., Kubono S., Yamaguchi H., Kase M., Hattori T., Shimoura S., "Grating monochromator for electron cyclotron resonance ion source operation", Review of Scientific Instruments **84** 073304 (2013).

Ohshiro Y., Yamaka S., Watanabe S., Kobayashi K., Kotaka Y., Nishimura M., Kase M., Muto H., Yamaguchi H., Shimoura S., "Production of beams from solid materials at center for nuclear study electron cyclotron resonance ion source", Rev. of Sci. Instrum. **85** 02A912 (2013).

Duy N., Kubono S., Yamaguchi H., Kahl D., Wakabayashi Y., Teranishi T., Iwasa N., Kwon Y., Khiem L., Kim Y., Song J., Hu J., Ayyad Y., "Low-energy radioactive ion beam production of ^{22}Mg", Nucl. Instr. and Meth. in Phys. Res. A, **723** 99–101 (2013).

He J.J., Zhang L.Y., Parikh A., Xu S.W., Yamaguchi H., Kahl D., Kubono S., Hu J., Ma P., Chen

S.Z., Wakabayashi Y., Sun B.H., Wang H.W., Tian W.D., Chen R.F., Guo B., Hashimoto T., Togano Y., Hayakawa S., Teranishi T., Iwasa N., Yamada T., Komatsubara T., "The ^{18}Ne(α,p)^{21}Na breakout reaction in x-ray bursts: Experimental determination of spin-parities for α resonances in ^{22}Mg via resonant elastic scattering of ^{21}Na+p", Phys. Rev. C **88**, 012801(R) (2013).

Zhang L.Y., He J.J., Parikh A., Xu S.W., Yamaguchi H., Kahl D., Kubono S., Mohr P., Hu J., Ma P., Chen S.Z., Wakabayashi Y., Wang H.W., Tian W.D., F. R., Guo B., Hashimoto T., Togano Y., Hayakawa S., Teranishi T., Iwasa N., Yamada T., Komatsubara T., Zhang Y.H., Zhou X.H., "Investigation of the thermonuclear ^{18}Ne(α,p)^{21}Na reaction rate via resonant elastic scattering of ^{21}Na+p" Phys. Rev. C **89** (2014) 015804.

Satou Y., Hwang J.W., Kim S., Tshoo K., Choi S., Nakamura T., Kondo Y., Matsui N., Hashimoto Y., Nakabayashi T., Okumura T., Shinohara M., Fukuda N., Sugimoto T., Otsu H., Togano Y., Motobayashi T., Sakurai H., Yanagisawa Y., Aoi N., Takeuchi S., Gomi T., Ishihara M., Kawai S., Ong H.J., Onishi T.K., Shimoura S., Tamaki M., Kobayashi T., Matsuda Y., Endo N., Kitayama M., "One-neutron knockout reaction of 17C on a hydrogen target at 70 MeV/nucleon ", Phys. Lett. B **728** (2014) 462–466.

Muto H., Ohshiro Y., Yamaka S., Watanabe S., Oyaizu M., Kubono S., Yamaguchi H., Kase M., Hattori T., Shimoura S., "Plasma spectroscopy of metal ions for hyper-electron cyclotron resonance ion source", Rev. Sci. Instrum. **85** (2014) 02A905.

Ohshiro Y., Yamaka S., Watanabe S., Kobayashi K., Kotaka Y., Nishimura M., Kase M., Muto H., Yamaguchi H., Shimoura S., "Production of beams from solid materials at Center for Nuclear Study electron cyclotron resonance ion source", Rev. Sci. Instru. **85** (2014) 02A912.

Suzuki H., Aoi N., Takeshita E., Takeuchi S., Ota S., Baba H., Bishop S., Fukui T., Hashimoto Y., Ideguchi E., Ieki K., Imai N., Ishihara M., Iwasaki H., Kanno S., Kondo Y., Kubo T., Kurita K., Kusaka K., Minemura T., Motobayashi T., Nakabayashi T., Nakamura T., Nakao T., Niikura M., Okumura T., Ohnishi T.K., Ong H.J., Sakurai H., Shimoura S., Sugo R., Suzuki D., Suzuki M.K., Tamaki M., Tanaka K., Togano Y., Yamada K., "Collectivity of neutron-rich Ti isotopes", Phys. Rev. C **88** (2013) 024326.

Michimasa S., Takaki M., Dozono M., Go S., Baba H., Ideguchi E., Kisamori K., Matsubara H., Miya H., Ota S., Sakai H., Shimoura S., Stolz A., Tang T.L., Tokieda H., Uesaka T., Zegers R.G.T., " Development of CVD diamond detector for time-of-flight measurements", Nucl. Instru Meth. B **317** (2013) 710–713.

Miya H., Ota S., Fujii T., Kawase S., Kubota Y., Lee C.S., Matsubara H., Miki K., Saito A., Michimasa S., Uesaka T., Sakai H., Shimoura S., "Development of low-pressure multi-wire drift chambers for high-resolution spectroscopy with radioactive isotope beams", Nucl. Instru Meth. B **317** (2013) 701–704.

Hwang J.W., Satou Y., Nakamura T., Kondo Y., Matsui N., Hashimoto Y., Nakabayashi T., Okumura T., Shinohara M., Fukuda N., Sugimoto T., Otsu H., Togano Y., Motobayashi T., Sakurai H., Yanagisawa Y., Aoi N., Takeuchi S., Gomi T., Ishihara M., Kawai S., Ong H.J., Onishi T.K., Shimoura S., Tamaki M., Kobayashi T., Matsuda Y., Endo N., Kitayama M., "Discovery of the First 2- State in 16C via Neutron Knockout Reaction", Few-Body Syst (2013) **54** 1469-1472.

Michimasa S., Takaki M., Sasamoto Y., Dozono M., Nishi T., Kawabata T., Ota S., Baba H., Baba T., Fujii T., Go S., Kawase S., Kikuchi Y., Kisamori K., Kobayashi M., Kubota Y., Lee C.S., Matsubara H., Miki K., Miya H., Noji S., Tokieda H., Tsumura M., Yako K., Yokoyama R., Takeda H., Yanagisawa Y., Kubo T., Inabe N., Fukuda N., Kameda D., Suzuki H., Shimizu Y., Ichihara T., Stolz A., Zegers R.G.T., Sakai H., Uesaka T., Shimoura S., "SHARAQ spectrometer for high-resolution studies for RI-induced reactions", Nucl. Instru Meth. B **317** (2013) 305–310.

Otsuka T., Shimoura S., Onda Y., Shinohara A., Shibata T., "Soil Radioactivity of ^{131}I Measured by"Pilot Investigation"", RADIOISOTOPES, 62 (2013) 752–760

Shimoura S., "Activities of Center for Nuclear Study (CNS), The University of Tokyo", RADIOISOTOPES, 62 (2013) 810–816

Doornenbal P., Scheit H., Takeuchi S., Aoi N., Li K., Matsushita M., Steppenbeck D., Wang H., Baba H., Crawford H., Hoffman C.R., Hughes R., Ideguchi E., Kobayashi N., Kondo Y., Lee J., Michimasa S., Motobayashi T., Sakurai H., Takechi M., Togano Y., Winkler R., Yoneda K., "In-Beam γ-Ray Spectroscopy of ^{34,36,38}Mg: Merging the N=20 and N=28 Shell Quenching", Phys. Rev. Lett. **111**, 212502 (2013).

Steppenbeck D., Takeuchi S., Aoi N., Doornenbal P., Lee J., Matsushita M., Wang H., Baba H., Fukuda N., Go S., Honma M., Matsui K., Michimasa S., Motobayashi T., Nishimura D., Otsuka T., Sakurai H., Shiga Y., Soderstrom P.A., Sumikama T., Suzuki H., Taniuchi R., Utsuno Y., Valiente-Dobon J.J., Yoneda K., "Investigating the strength of the N = 34 subshell closure in ^{54}Ca", J. Phys. Conf. Ser. **445**, 012012 (2013).

Steppenbeck D., Takeuchi S., Aoi N., Doornenbal P., Matsushita M., Wang H., Baba H., Fukuda N., Go S., Honma M., Lee J., Matsui K., Michimasa S., Motobayashi T., Nishimura D., Otsuka T., Sakurai H., Shiga Y., Soderstrom P.A., Sumikama T., Suzuki H., Taniuchi R., Utsuno Y., Valiente-Dobon J.J., Yoneda K., "Evidence for a new nuclear 'magic number' from the level structure of ^{54}Ca", Nature (London) **502**, 207

(2013).

Utsuno Y., Shimizu N., Otsuka T., Abe T., "Efficient computation of Hamiltonian matrix elements between nonorthogonal Slater determinants", Comp. Phys. Comm. **184**, (2013) 102.

Papuga J., Bissell M.L., Kreim K., Blaum K., Brown B.A., De M., GarciaRuiz R.F., Heylen H., Kowalska M., Neugart R., Neyens G., Nortershauser W., Otsuka T., Rajabali M.M., Sanchez R., Utsuno Y., Yordanov D.T., "Spins and Magnetic Moments of 49K and 51K: Establishing the 1/2+ and 3/2+ Level Ordering Beyond N=28", Physical Review Letters **110**, 172503 (2013).

Tsunoda Y., Otsuka T., Shimizu N., Honma M., Utsuno Y., "Novel shape evolution in exotic Ni isotopes and configuration-dependent shell structure", Physical Review C **89** (2014) 031301(R).

Otsuka T., "原子核物理学者による環境放射線の大規模緊急測定とそこから学べること", RADIOISOTOPES (日本アイソトープ協会), **62** (2013) 746.

[Book・Proceedings]

(Original Papers) *Subject to Peer Review

Duy N., Kubono S., Yamaguchi H., Kahl D., Wakabayashi Y., Teranishi T., Iwasa N., Kwon Y., Khiem L., Kim Y., Song J., Hu J., Ayyad Y., "Low-energy radioactive ion beam production of ^{22}Mg", Nuclear Instruments and Methods in Physics Research Section A **723** 99–101 (2013).

Kubono S., Binh D.N., Hayakawa S., Hashimoto T., Kahl D.M., Yamaguchi H., Wakabayashi Y., Teranishi T., Iwasa N., Komatsubara T., Kato S., Chen A., Cherubini S., Choi S.H., Hahn I.S., He J.J., Khiem L.H., Lee C.S., Kwon Y.K., Wanajo S., Janka H.T., "Experimental challenge to nucleosynthesis in core-collapse supernovae - Very early epoch of type II SNe -", AIP Conf. Proc. **1533** 70 (2013).

Ohshiro Y., Yamaka S., Watanabe S., Kobayashi K., Kotaka Y., Nishimura M., Kase M., Muto H., Yamaguchi H., Shimoura S., "Production of beams from solid materials at center for nuclear study electron cyclotron resonance ion source", Rev. of Sci. Instrum. **85** 02A912 (2013).

Yamaguchi H., Kahl D., Nakao T., Wakabayashi Y., Kubono S., Hashimoto T., Hayakawa S., Kawabata T., Iwasa N., Teranishi T., Kwon Y.K., Binh D.N., Khiem L.H., Duy N.N., "Recent developments and research projects at the low-energy RI beam facility CRIB", Nucl. Instr. and Meth. B, **317** 664–667 (2013).

Gulino M., Cherubini S., Rapisarda G.G., Kubono S., Lamia L., Cognata M.La., Yamaguchi H., Hayakawa S., Wakabayashi Y., Iwasa N., Kato S., Komatsubara H., Teranishi T., Coc A., DeSéréville N., Hammache F., Spitaleri C., "Trojan Horse method and radioactive ion beams: study of ^{18}F$(p,\alpha)^{15}$O reaction at astrophysical energies", 11th International Conference on Nucleus-Nucleus Collisions (NN2012), Journal of Physics: Conference Series **420** 012149 (2013).

Yamaguchi H., Kahl D., Nakao T., Wakabayashi Y., Kubono S., Hashimoto T., Hayakawa S., Kawabata T., Iwasa N., Teranishi T., Kwon Y.K., Lee P.S., Binh D.N., Khiem L.H., Duy N.N., "Studies on alpha-induced astrophysical reactions using the low-energy RI beam separator CRIB" EPJ Web of Conferences **66**, 07027 (2014).

Kobayashi M., Yako K., Shimoura S., Dozono M., Kawase S., Kisamori K., Kubota Y., Lee C.S., Michimasa S., Miya H., Ota S., Sakai H., Sasano M., Takaki M., "Measurement of the ^{8}He$(p,n)^8$Li reaction at intermediate energy in inverse kinematics", Proceedings of the 12th Asia Pacific Physics Conference (APPC12), Jul. 14–19, 2013, Makuhari, Japan, JPS Conf. Proc. 1, 013034 (2014)

Kubota Y., Sasano M., Uesaka T., Dozono M., Itoh M., Kawase S., Kobayashi M., Lee C.S., Matsubara H., Miya H., Ota S., Sekiguchi K., Taguchi T., Tang T.L., Tokieda H., Wakui T., "A new neutron detector with a high position resolution for the study of the (p,pn) reaction on rare isotopes", EPJ Web of Conferences Vol. 66, No. 11022 (2014).

Matsushita M., Takeuchi S., Aoi N., Doornenbal P., Lee J., Li K., Motobayashi T., Scheit H., Steppenbeck D., Wang H., Baba H., Bazin D., C ≒ ceres, L., Crawford H., Fallon P., Gernh ∽ user R., Gibelin J., Go S., Gr・vy, S., Hinke C., Hoffman C.R., Hughes R., Ideguchi E., Ieki K., Jenkins D., Kobayashi N., Kondo Y., Kr ◯ cken, R., Le T., Lee G., Matta A., Michimasa S., Nakamura T., Ota S., Petri M., Sako T., Sakurai H., Shimoura S., Steiger K., Takahashi K., Takechi M., Togano Y., Winkler R., Yoneda K., "In-beam γ-ray spectroscopy of ^{38,40,42}Si", EPJ Web of Conferences Vol. 66, No. 02070 (2014).

Shimizu N., Otsuka T., Utsuno Y., Mizusaki T., Honma M., Abe T., "History and future perspectives of the Monte Carlo shell model -from Alphleet to K computer-", J. Phys.: Conf. Ser. **445** (2013) 012004.

Yoshida T., Shimizu N., Abe T., Otsuka T., " Density profiles of the intrinsic frame of light nuclei obtained from Monte Carlo shell model calculation", J. Phys.: Conf. Ser. **445** (2013) 012038.

Tsunoda Y., Otsuka T., Shimizu N., Honma M., Utsuno Y., " Study of nuclei around Z = 28 by large-scale shell model calculations", J. Phys.: Conf. Ser. **445** (2013) 012028.

Oral Presentations

(International Conference etc.)

Hamagaki H. (invited), "ALICE Experiment", at PHENIX Workshop on Physics Prospects with Detector and Accelerator Upgrades; from 29 July 2013 to 2 August 2013 at RIKEN

Gunji T. (invited), "ALICE Physics Perspectives and GEM-TPC upgrade", Heavy Ion Meeting, Nov 2, 2013, Inha University, Korea

Gunji T. (invited), “Probing the hot and dense QCD medium with hard probes at RHIC and LHC”, Pioneering Symposium for heavy ion collisions, in Korean Physical Society Meeting, Oct 30, 2013, Pusan, Korea.

Gunji T. (invited), “RHIC-LHC の広範エネルギー重イオン衝突によるクォーク物質物性の系統性”, シンポジウム講演「高温クォーク物質研究の最前線：発見から精密研究へ」, 日本物理学会 (9/20-9/23)

Gunji T. (invited), “LHC-ALICE 実験の第一次運転成果と今後の展” Heavy Ion Pub, May 31, 2013, Osaka, Japan

Terasaki K. for the ALICE Collaboration (poster), “Study of Ion Back Flow suppression with thick COBRA GEM”, The 3rd International Conference on Micro Pattern Gaseous Detectors (MPGD203), July 1-4, 2013, Zaragoza, Spain.

Yamaguchi Y. for the ALICE Collaboration (oral), “ALICE 実験における GEM-TPC 開発”, 第 10 回 Micro-Pattern Gas Detector 研究会 Dec. 12–13, 2013, Kyoto, Japan

Terasaki K. for the ALICE Collaboration (oral), “Thick COBRA GEM によるイオンバックフロー抑制 ”, 第 10 回 Micro-Pattern Gas Detector 研究会, Dec. 12–13, 2013, Kyoto, Japan

Yukawa K. (oral), “スペースチャージによるイオンバックフローへの影響の研究 ”, 第 10 回 Micro-Pattern Gas Detector 研究会, Dec. 12–13, 2013, Kyoto, Japan

Hamagaki H. (invited), “Study of hadron properties in QCD medium using the high-energy heavy-ion collisions”, workshop on Hadrons in Nucleus, Oct. 31 – Nov. 2, 2013, Kyoto, Japan

Terasaki K. (oral), “R & D of Thick COBRA GEM for the application of the GEM-based TPC”, 2013 IEEE Nuclear Science Symposium and Medical Imaging Conference (2013 NSS/MIC), Oct 27 – Nov 02, 2013, Seoul, Korea

Sekiguchi Y. (poster), “Basic performance of SoI pixel detector for radiation monitor”, 2013 IEEE Nuclear Science Symposium and Medical Imaging Conference (2013 NSS/MIC), Oct 27 – Nov 02, 2013, Seoul, Korea

Yamaguchi Y. for the PHENIX Collaboration (oral), “A Search for Beyond the Standard Model Particles with the PHENIX detector at RHIC”, APS Division of Nuclear Physics, Fall Meeting, October 23-26, 2013, Newport News, VA,

Yamaguchi Y. for the PHENIX Collaboration (oral), “Dark photon search at the PHENIX experiment”, at the JPS Fall meeting, Sep. 20–23, 2013, Kochi University, Japan

Terasaki K. (oral), “COBRA GEM を用いたイオンバックフロー抑制の研究 ”, at the JPS Fall meeting, Sep. 20–23, 2013, Kochi University, Japan

Hayashi S. for the ALICE Collaboration (oral), “Dielectron measurement in $\sqrt{s_{NN}} = 5.02$ TeV $p{-}$Pb collisions at LHC-ALICE, at the JPS Fall meeting, Sep. 20–23, 2013, Kochi University, Japan

Sekiguchi Y. (oral), “放射線モニターのための SOI ピクセル検出器の性能評価 ”, at the JPS Fall meeting, Sep. 20–23, 2013, Kochi University, Japan

Tsuji T. for the ALICE collabotation (oral), ”Neutral pion production in Pb-Pb collisions at $\sqrt{s_{NN}} = 2.76$ TeV with the ALICE experiment”, JPS 2013 Spring Meeting, March 26-29, 2013, Hiroshima University, Hiroshima, Japan.

Hayashi S., Hamagaki H., Gunji T., Tanaka M., Ikeda H. (oral), “LHC-ALICE における前方方向カロリメータ用読み出し ASIC の性能評価”, at the JPS Spring Meeting, Mar. 26–29, 2013, Hiroshima University, Hiroshima, Japan

Sekiguchi Y., Hamagaki H., Gunji T., Arai Y., Imamura T., Ohmoto T., Iwata A. (oral), “SOI ピクセル技術を用いた環境放射線モニターの基本動作評価 ”at the JPS Spring Meeting, Mar. 26–29, 2013, Hiroshima University, Hiroshima, Japan

Terasaki K., Hamagaki H., Gunji T., Yamaguchi Y. (oral), “Development of Thick COBRA GEM for Ion Back Flow Suppression”, at the JPS Spring Meeting, Mar. 26–29, 2013, Hiroshima University, Hiroshima, Japan

Yamaguchi H. (oral,invited), “Nuclear astrophysics and structure studies using low-energy RI beams”, Pioneering Symposium: “The Third Generation of RIB Facilities” in Korean Physical Society Meeting, Apr 24–26, 2013, Daejeon, Korea.

Yamaguchi H. (oral), “Studies on nuclear reaction and structure using low-energy RI beams at CRIB”, Workshop on the INFN-RIKEN collaboration on nuclear physics activities May 17, 2013, Istituto Italiano di Cultura di Tokyo, Sala “G Puccini” 2-1-30 Kudan Minami, Chiyoda-ku, Tokyo

Yamaguchi H. (oral), “Studies on alpha-induced astrophysical reactions using the low-energy RI beam separator CRIB” The 25th International Nuclear Physics Conference (INPC 2013), June 2–7 2013, Florence, Italy.

Yamaguchi H. (oral), “Recent activities at CRIB - nuclear astrophysics, reaction, and structure studies with low-energy RI beam” RIBF Users Meeting 2013, June 26–27, 2013, RIKEN, Wako, Saitama, Japan.

Yamaguchi H. (oral), “Studying alpha-cluster structure using low-energy RI beam”, RCNP Workshop; Clustering phenomena in multi nucleon and hyperon system, Jul 26–27 2013, Kansai Gakuin University, Yokohama, Japan.

Yamaguchi H. (oral), “Studies on astrophysical reactions using low-energy RI beam at CRIB”, SKKU Symposium on Astrophysics and Cosmology: from Particle to Universe, Oct. 4 and December 2-4, 2013, SKKU Natural Sciences Campus, Suwon, Korea.

Yamaguchi H. (oral), “Recent status of the low-enrgy RI beam separator CRIB”, 1st RIKEN-RISP Joint Workshop, Nov. 7–8, 2013, IBS, Daejeon, Korea

Yamaguchi H. (oral), “Alpha resonant scattering for astrophysical reaction studies", The 12th International Symposium on Origin of Matter and Evolution of the Galaxies (OMEG12), Nov 18–22, 2013, Epochal Tsukuba, Tsukuba, Ibaraki, Japan.

Yamaguchi H. (oral), "The low-energy RI beam facility CRIB for astrophysics and nuclear structure studies", JUSTIPEN-JUSEIPEN Workshop, Dec. 9–12, 2013, RIKEN, Wako, Saitama, Japan

Yamaguchi H. (oral), "Recent status and technical aspects of RI Beam separator CRIB", Nuclear physics seminar at RISP, Feb. 28, 2014, IBS, Daejeon, Korea.

Lee C.S. (oral), "Properties of thick GEM in low-pressure deuterium", The 3rd International Conference on Micro Pattern Gaseous Detectors (MPGD203), July 1-4, 2013, Zaragoza, Spain.

Ota S. (oral), "CNS Active Target", French-Japanese SYmposeium on Nuclear Structure Problems, Sep. 30 - Oct. 3, 2013, Paris, France.

Ota S. (oral), "Active Target", The 1st RIBF-RISP Joint Workshop, Nov. 7-8, 2013, Daejeon, Korea

Matsushita M., Takeuchi S., Aoi N., Doornenbal P., Lee J., Li K., Motobayashi T., Scheit H., Steppenbeck D., Wang H., Baba H., Bazin D., C ≒ ceres, L., Crawford H., Fallon P., Gernh ∽ user R., Gibelin J., Go S., Gr・vy, S., Hinke C., Hoffman C.R., Hughes R., Ideguchi E., Ieki K., Jenkins D., Kobayashi N., Kondo Y., Kr ◯ cken, R., Le T., Lee G., Matta A., Michimasa S., Nakamura T., Ota S., Petri M., Sako T., Sakurai H., Shimoura S., Steiger K., Takahashi K., Takechi M., Togano Y., Winkler R., Yoneda K. (oral): "In-beam γ-ray spectroscopy of ^{38,40,42}Si", International Nuclear Physics Conference (INPC2013), June 2-7, 2013, Firenze, Italy

Michimasa S., Yanagisawa Y., Inafuku K., Aoi N., Elekes Z., Fulop Zs., Ichikawa Y., Iwasa N., Kurita K., Kurokawa M., Machida T., Motobayashi T., Nakamura T., Nakabayashi T., Notani M., Ong H.J., Onishi T.K., Otsu H., Sakurai H., Shinohara M., Sumikama T., Takeuchi S., Tanaka K., Togano Y., Yamada K., Yamaguchi M., Yoneda K. (poster), "Proton inelastic scattering study on ^{30}Ne and ^{34,36}Mg isotopes" International Nuclear Physics Conference (INPC2013), June 2-7, 2013, Firenze, Italy.

Go S., Kameda D., Kubo T., Inabe N., Fukuda N., Yokoyama R., Fujii T., Ideguchi E., Takeda H., Suzuki H., Yoshida K., Kusaka K., Yanagisawa Y., Ohtake M., Sato H., Shimizu Y., Baba H., Kurokawa M., Nishimura D., Ohnishi T., Iwasa N., Chiba A., Yamada T., Nishibata H., Ieki K., Murai D., Momota S., Sato Y., Hwang J., Kim S., Tarasov O.B., Morrissey D.J., Sherrill B.M., Simpson G. (poster), "Observation of new isomers in N=100 neutron-rich rare-earth nuclei" International Nuclear Physics Conference (INPC2013), June 2-7, 2013, Firenze, Italy

Kubota Y., Sasano M., Uesaka T., Dozono M., Itoh M., Kawase S., Kobayashi M., Lee C.S., Matsubara H., Miya H., Ota S., Sekiguchi K., Taguchi T., Tang T.L., Tokieda H., Wakui T. (poster), "A new neutron detector with a high position resolution for the study of the (p,pn) reaction on rare isotopes", The 25th International Nuclear Physics Conference (INPC2013), July 2-7, 2013, Florence, Italy

Shimoura S. (oral), "Experimental opportunities for the high-resolution spectroscopy using GRAPE and/or SHARAQ", Sunflower Workshop, Sept. 10-11, 2014, Darmstadt, Germany

Yako K. (invited): "(p,n) measurements in inverse kinematics at SHARAQ-WINDS", JUSTIPEN-JUSEIPEN Workshop, Dec. 9–12, 2013, RIKEN.

Shimoura S. (invited), "Energy degrading project for RI beams in CNS", JUSTIPEN-JUSEIPEN Workshop, Dec. 9-12, 2013, Wako

Shimoura S. (invited), "Energy degrading project of RI beams in CNS – OEDO project", Workshop on Physics Opportunities using Compton Supressed Ge Clover Array (CAGRA13), Dec. 16-17, 2013, Osaka University

Shimoura S. (oral), "Physics Oppotunity via transfer reaction measurements with gamma-ray detectors" Workshop on Physics Research with Grand Raiden Forward-mode Beam Line, Nov. 28-29, 2013, RCNP, Osaka University.

Dozono M. (oral), "Research for 0^- states via (^{16}O,^{16}Nγ) reaction" Workshop on Physics Research with Grand Raiden Forward-mode Beam Line, Nov. 28-29, 2013, RCNP, Osaka University.

Takaki M. (oral), "Research for double GT states via (^{12}C,^{12}Beγ) reaction" Workshop on Physics Research with Grand Raiden Forward-mode Beam Line, Nov. 28-29, 2013, RCNP, Osaka University.

Shimoura S. (invited), "OEDO project" 長寿命核分裂核廃棄物の核変換データとその戦略」ワークショップ, 2014 年 3 月 6 日 (木)〜3 月 8 日 (土), 理化学研究所

Kobayashi M., Yako K., Shimoura S., Dozono M., Kawase S., Kisamori K., Kubota Y., Lee C.S., Michimasa S., Miya H., Ota S., Sakai H., Sasano M., Takaki M. (oral), "Measurement of the ^{8}He$(p,n)^8$Li reaction at intermediate energy in inverse kinematics", APPC12, Jul. 14–19, 2013, Makuhari, Japan

Yako K. (oral), "Recent physics programs at SHARAQ spectrometer", RIBF Users Meeting 2013, Jun. 26–27, 2013, RIKEN.

Lee C.S., Ota S., Tokieda H., Kojima R., Watanabe Y., Uesaka T. (oral), "Properties of Thick GEM in Low-pressure Deuterium", Micro-Pattern Gaseous Detector (MPGD) 2013, Jul.1–4, 2013, Zaragoza, Spain.

Go S., Ideguchi E., Kobayashi M., Yokoyama R., Kisamori K., Michimasa S., Shimoura S., Niikura M., Yagi A., Nishibata H., Matea I., Verney D., Azaiez F., Koizumi M., Toh Y., Kimura A., Harada H., Furukata K., Nakamura S., Kitatani F., Hatsukawa Y., Ohshima M. (oral), "Study of high spin states in ^{35,36}S" 2nd Workshop on the physics at the Tandem-ALTO facility, May 14–15, 2013, Orsay, France

Go S., Ideguchi E., Yokoyama R., Kobayashi M., Kisamori K., Michimasa S., Shimoura S., Niikura M., Yagi A., Nishibata H., Matea I., Verney D., Azaiez F., Koizumi M., Toh Y., Kimura A., Harada H., Furukata K., Nakamura S., Kitatani F., Hatsukawa Y. (oral), “Study of high spin states in ^{35}S” French-Japanese Symposium on Nuclear Structure Problems, Sep. 30–Oct. 3, 2013, Paris, France

Kobayashi M., Yako K., Shimoura S., Dozono M., Kawase S., Kisamori K., Kubota Y., Lee C.S., Michimasa S., Miya H., Ota S., Sakai H., Sasano M., Takaki M. (oral), “Spin-isospin response of a neutron rich nucleus ^{8}He via (p, n) reactions in inverse kinematics”, at the JPS Fall meeting, Sep. 20–23, 2013, Kochi University, Japan

Miya H., Shimoura S., Kisamori K., Baba H., Baba T., Dozono M., Fukuda N., Fujii T., Go S., Ideguchi E., Inabe N., Ito M., Kameda D., Kawabata T., Kawase S., Kubo T., Kubota Y., Kobayashi M., Konodo Y., Lee C.S., Maeda Y., Matsubara H., Miki K., Michimasa S., Nishi T., Nishimura M., Ota S., Sakaguchi S., Sakai H., Sasano M., Sato H., Shimizu Y., Suzuki H., Takaki M., Tamii A., Takeda H., Takeuchi S., Tokieda H., Tsumura M., Uesaka T., Yanagisawa Y., Yako K., Yokoyama R., Yoshida K., Assie M., Beaumel D., Fariouz H., Stolz A. (oral), “Study of spin-isospin response via exothermic charge exchange (^{8}He, ^{8}Liγ) for ^{4}He nuclei” at the JPS Fall meeting, Sep. 20–23, 2013, Kochi University, Japan

Kisamori K., Shimoura S., Miya H., Baba H., Baba T., Dozono M., Fukuda N., Fujii T., Go S., Ideguchi E., Inabe N., Ito M., Kameda D., Kawabata T., Kawase S., Kubo T., Kubota Y., Kobayashi M., Konodo Y., Lee C.S., Maeda Y., Matsubara H., Miki K., Michimasa S., Nishi T., Nishimura M., Ota S., Sakaguchi S., Sakai H., Sasano M., Sato H., Shimizu Y., Suzuki H., Takaki M., Tamii A., Takeda H., Takeuchi S., Tokieda H., Tsumura M., Uesaka T., Yanagisawa Y., Yako K., Yokoyama R., Yoshida K., Assie M., Beaumel D., Fariouz H., Stolz A. (oral), “二重荷電交換反応をもちいた 4 中性子系質量欠損核分光実験” at the JPS Fall meeting, Sep. 20–23, 2013, Kochi University, Japan

Go S., Ideguchi E., Kobayashi M., Yokoyama R., Kisamori K., Michimasa S., Shimoura S., Niikura M., Yagi A., Nishibata K., Matea I., Suzuki D., Verney D., Azaiez F., Sugawara M., Koizumi M., Fuji Y., Shizuma T., Kimura A., Harada H., Furutaka K., Yakamura S., Kitatani F., Hatsukawa Y., Oshima M. (oral), “35S における高スピン状態の研究” at the JPS Fall meeting, Sep. 20–23, 2013, Kochi University, Japan

Dozono M., Uesaka T., Sasano M., Zenihiro J., Matsubara H., Shimoura S., Yako K., Michimasa S., Ota S., Tokieda H., Miya H., Kawase S., Tang R., Kisamori K., Takaki M., Kubota Y., Lee C.S., Fujii T., Yokoyama R., Sakai H., Kubo T., Yoshida K., Yanagisawa Y., Fukuda N., Takeda H., Kameda D., Inabe N., Wakasa T., Fujita K., Sakaguchi S., Ichimura M., Sagawa H., “パリティ移行核反応による原子核の 0-状態の研究” at the JPS Fall meeting, Sep. 20–23, 2013, Kochi University, Japan

Yokoyama R., Ideguchi E., Simpson G., Tanaka M., Nishimura S., Lorusso G., Sumikama H., Doornenbal P., Baba H., Isobe T., Wu J., Xu Z., Browne R., Patel Z., Rice S., Sinclair L., Li Z., Watanabe H., Gey G., Sahin E., Bello F., Vajra Z., Kuri I., Taprogge J., Odahara A., Fang Y., Daido R., Yagi A., Nishibata K., Aoi N., Kobayashi K., Michimasa S., Matsushita M., Kobayashi M., Go S., Kubo T., Kameda D., Inabe N., Takeda H., Fukuda N., Suzuki H., Nishiduka I., Komatsubara T., Moon C.B. (oral), “過剰変形領域の Pm 同位体における新アイソマーの発見” at the JPS Fall meeting, Sep. 20–23, 2013, Kochi University, Japan

Lee C.S., Ota S., Tokieda H., Kojima R., Watanabe Y., Uesaka T. (oral), “重水素アクティブ標的の大強度重イオンビーム照射に向けた開発” at the JPS Spring meeting, Mar. 27–30, 2014, Tokai University, Japan.

Kawase S., Uesaka T., Shimoura S., Yako K., Ota S., Michimasa S., Tokieda H., Miya H., Leung T.T., Kisamori K., Takaki M., Kubota Y., Lee C.S., Yokoyama R., Fujii T., Kobayashi M., Sasano M., Zenihiro J., Matsubara H., Dozono M., Lee J., Sakai H., Kubo T., Yoshida K., Inabe N., Yanagisawa Y., Takeda H., Kusaka K., Fukuda N., Kameda D., Suzuki H., Kawahara T., Wakui T., Sakaguchi S., Noro T., Wakasa T., Yasuda J., Fukunaga T., Maeda Y., Kim. W., Hwang S., Stepanyan S., Obertelli A., Galind-Uribarri A., Padilla-Rodal E., Beaumel D. (oral), “準弾性 AO(p,2p) 反応による窒素同位体の陽子一空孔状態の核分光” at the JPS Spring meeting, Mar. 27–30, 2014, Tokai University, Japan

Ota S., Corsi A., Dozono M., Hashimoto T., Ito M., Kawabata T., Kawase S., Kojima R., Kubota Y., Lee C.S., Maeda Y., Matta J., Matsuda Y., Michimasa S., Obertelli A., Otsu H., Patel D., Santamaria C., Sasano M., Takaki M., Terashima T., Tokieda H., Uesaka T., Yamaguchi H., Zenihiro J. and H307 collaboration (oral), “重水素ガスアクティブ標的を用いた錫領域不安定核における巨大単極共鳴の測定計画” at the JPS Spring meeting, Mar. 27–30, 2014, Tokai University, Japan

Tokieda H., Ota S., Dozono M., Gunji T., Hamagaki H., Hashimoto T., Kawabata T., Kawase S., Kojima R., Kubono S., Kubota Y., Lee C.S., Maeda Y., Matsubara H., Michimasa S., Otsu H., Sako M., Uesaka T., Yamaguchi H., Watanabe Y. (oral), “重水素ガスアクティブ標的の反跳粒子飛跡再構成と性能評価” at the JPS Spring meeting, Mar. 27–30, 2014, Tokai University, Japan

Yako K. (oral), ”Study of nuclear matrix element of the double-beta decay by charge-exchange reactions”, JPS Spring meeting, Mar. 27–30, 2014, Tokai University.

Kubota Y., Sasano M., Uesaka T., Dozono M., Itoh M., Kawase S., Kobayashi M., Lee C.S., Matsubara H., Miki K., Miya H., Ota S., Sekiguchi K., Shima T., Taguchi T., Tamii A., Tang T.L., Tokieda H., Wakasa T., Wakui T., Yasuda J., Zenihiro J. (oral), "不安定核研究のための高位置分解能ファイバーシンチ中性子検出器の開発" at the JPS Spring meeting, Mar. 27–30, 2014, Tokai University, Japan

Yoshida T., Shimizu N., Abe T., Otsuka T. (oral), "Density of ligh nuclei obtained from Monte Carlo shell model", HPCI Strategic Program Field 5 Symposium, Fujisoft Akiba Plaza, Tokyo, Japan, March 5-6, 2013.

Ebata S., Nakatsukasa T., Inakura T. (oral), "Density functional approaches to nuclear dynamics", HPCI Strategic Program Field 5 Symposium, Fujisoft Akiba Plaza, Tokyo, Japan, March 5-6, 2013.

Otsuka T. (oral), "Ultra large-scale Simulations of quantum many-body systems for nuclear properties and its applications", HPCI Strategic Program Field 5 Symposium, Fujisoft Akiba Plaza, Tokyo, Japan, March 5-6, 2013.

Iwata Y., Otsuka T., Heinz S. (oral), "Fission dynamics of superheavy compound nuclei", Fission 2013, Caen, France, May 2013.

Utsuno Y., Otsuka T., Shimizu N., Honma M., Mizusakia T., Tsunoda Y., Abe T. (oral), "Recent shell-model results for exotic nuclei", 25th International Nuclear Physics Conference (INPC 2013), Florence, Italy, June 3-7, 2013.

Iwata Y., Otsuka T., Heinz S. (oral), "Fission dynamics of superheavy compound nucle", International Nuclear Physics Conference 2013 (INPC2013), Florence, Italy, June 3-7, 2013.

Iwata Y., Otsuka T., Heinz S. (oral), "Fission dynamics of superheavy compound nuclei", The 12th Asia Pacific Physics Conference of AAPPS (APPC 12), Chiba, Japan, July 14-19, 2013.

Yoshida T., Shimizu N., Abe T., Otsuka T. (poster), "Density profiles of light nuclei in Monte Carlo shell-model calculation", International Nuclear Physics Conference 2013 (INPC2013), Florence, Italy, June 3-7, 2013.

Yoshida T., Shimizu N., Abe T., Otsuka T. (poster), "Density profiles of light nuclei in Monte Carlo shell-model calculation", The 12th Asia Pacific Physics Conference, Chiba, Japan, July 14-19, 2013.

Iwata Y. (oral), "Fission dynamics of superheavy compound nuclei", The 12th Asia Pacific Physics Conference, Chiba, Japan, July 14-19, 2013.

Otsuka T. (invited), "Monte Carlo Shell Model and shape phase transitions in exotic nuclei", Int. Conf. on Nuclear Theory in the Supercomputing Era - 2013, Ames, USA, May 13-17, 2013.

Otsuka T. (invited), "Fukushima Nuclear Power Plant Accident and Nuclear Physicists", International Nuclear Physics Conference 2013 (INPC2013), Florence, Italy, June 3-7, 2013.

Otsuka T. (invited), "Driving forces of shell evolution and shapes of exotic nuclei", Gordon Conference on Nuclear Chemistry, Colby-Sawyer College, New London, USA, June 9-14, 2013.

Otsuka T. (invited), "Structure Evolutions in Exotic Nuclei", 12th Asia Pacific Physics Conference, Makuhari, Chiba, Japan, July 15-19, 2013.

Iwata Y. (invited), "The TDDFT calculations for low-energy heavy-ion collisions", French-Japanese Symposium on Nuclear Structure Problems, Paris, France, September 30, 2013.

Otsuka T. (invited), "Perspectives beyond the Shell Evolution", French-Japanese Symposium on Nuclear Structure Problems -Organized in the framework of FJNSP LIA-, CNRS, Paris, September 30-Oct. 3, 2013.

Otsuka T. (invited), "Structure Evolutions in Exotic Nuclei", Mini-Symposium on Experiment and Theory for Nuclei Close to the Driplines, 2013 Fall Meeting of the APS DNP, Newport News, USA, October 23-26, 2013.

Otsuka T. (invited), "Perspectives of physics of exotic nuclei beyond the shell evolution", First African Symposium on Exotic Nuclei (IASEN-2013), Cape Town, South Africa, December 2-6, 2013.

Utsuno Y. (invited), "Shell evolution along the Sn isotopes", 10th ASRC International Workshop "Nuclear Fission and Decay of Exotic Nuclei", JAEA Nuclear Science Research Institute, Tokai, Japan, March 21-22, 2013.

Ebata S., Nakatsukasa T. (oral), "Pairing effects in fusion phenomena utilizing a time-dependent mean field theory", 10th ASRC International Workshop "Nuclear Fission and Decay of Exotic Nuclei", JAEA Nuclear Science Research Institute, Tokai, Japan, March 21-22, 2013.

Iwata Y., Otsuka T., Heinz S. (oral), "Fission dynamics of superheavy compound nuclei", The 10th ASRC International Workshop "Nuclear Fission and Decay of Exotic Nuclei", JAEA Nuclear Science Research Institute, Tokai, Japan, March 21-22, 2013.

Utsuno Y., Otsuka T., Shimizu N., Mizusaki T., Honma M. (oral), "Tensor-force driven shell evolution studied with large-scale shell-model calculations", RCNP Workshop on the Importance of Tensor Interactions in Nuclear and Hadron Structures, Osaka, Japan, July, 2013.

Yoshida T. (oral), "Density distributions of Be isotopes based on Monte Carlo shell model", RCNP 研究会「核子・ハイペロン多体系におけるクラスター現象」, Kanagawa, Japan, July 26-27, 2013.

Iwata Y. (invited), "TDDFT calculations for the symmetry energy research", RIBF-ULIC Mini Workshop 027 "Nuclear symmetry-energy and nucleus-nucleus collision simulation", Saitama, Japan, July 2-4, 2013.

Iwata Y., Otsuka T., Heinz S. (oral), "Fission dynamics of superheavy compound nuclei", Fission 2013, Caen, France "Fifth International Workshop on Nuclear Fission and Fission Product Spectroscopy", May 28-31, 2013.

Utsuno Y. (invited), “Shell-model approach to shape coexistence in light nuclei”, IOP Workshop “Shape Coexistence Across the Chart of Nuclides”, York, UK, April, 2013.

Otsuka T. (invited), “Tensor force and shell structure - A personal history - ”, RCNP Workshop on the Importance of Tensor Interactions in Nuclei and Hadron structure, RCNP, Osaka, Japan, July 11-12, 2013.

Shimizu N. (oral), “Large-scale shell-model calculations and Monte Carlo shell model”, JUSTIPEN-JUSEIPEN Workshop, Saitama, Japan, December 9-12, 2013.

Otsuka T. (oral), “ICN status”, JUSTIPEN-JUSEIPEN Workshop, Saitama, Japan, December 9-12, 2013.

Iwata Y. (invited), “Charge equilibration and its application to symmetry energy research”, ECT* workshop “Advances in time-dependent methods for quantum many-body systems”, Trento, Italy, October, 2013.

Iwata Y. (invited), “A study of nuclear reaction mechanism based on TDDFT calculations”, 3 回 HPCI 戦略プログラム分野 2 分野 5 異分野交流研究会, Institute for Molecular Science, Aichi, Japan, November 2013.

Otsuka T. (invited), “Shell model calculations with more than one shell”, INT workshop “Computational and Theoretical Advances for Exotic Isotopes in the Medium Mass Region”, INT, Seattle, USA, March 25-Aprl 19, 2013.

Otsuka T. (invited), “Shape coexistence and shell evolution in exotic Ni isotopes”, International Workshop on “Shape Coexistence Across the Chart of the Nuclides”, Kings Manor, York, UK, April 15-16, 2013.

Otsuka T. (invited), “Shapes of medium-mass exotic nuclei and MCSM calculations”, ECT*/HIC for FAIR workshop “From Few-Nucleon Forces to Many-Nucleon Structure”, ECT*, Trento, Italy, June 10-14, 2013.

Utsuno Y., Otsuka T., Shimizu N., Mizusaki T., Honma M. (oral), “Energy levels and shell evolution for neutron-rich Ca isotopes”, JPS 2013 Spring Meeting, March 26-29, 2013, Hiroshima University, Hiroshima, Japan.

Yoshida T., Shimizu N., Abe T., Otsuka T. (oral), “Study of light-nuclei density measured from body-fixed frame in Monte Carlo shell model”, JPS 2013 Spring Meeting, March 26-29, 2013, Hiroshima University, Hiroshima, Japan.

Ebata S., Nakatsukasa T., Inakura T. (oral), “Systematic study of low-lying E1 mode”, JPS 2013 Spring Meeting, March 26-29, 2013, Hiroshima University, Hiroshima, Japan.

Ebata S., (oral): “Approaches to nuclear dynamics by time dependent mean field theory”, JPS 2013 Spring Meeting, March 26-29, 2013, Hiroshima University, Hiroshima, Japan.

Shimizu N., Utsuno Y., Ebata S., Honma M., Mizusaki T., Otsuka T. (oral), “Study of E1 excitations for neutron-rich Ca isotopes”, JPS 2013 Spring Meeting, March 26-29, 2013, Hiroshima Univ, Hiroshima, Japan.

Utsuno Y., Shimizu N., Otsuka T., Yoshida T., Tsunoda Y. (oral), “Structure of neutron excess S isotopes”, JPS 2013 Autumn Meeting, September 20-23, 2013, Kochi University, Kochi, Japan.

Togashi T., Shimizu N., Utsuno Y., Tsunoda Y., Otsuka T., Honma M., Mizusaki T. (oral), “A study of high-spin excited states for Cr isotopes based on shell-model calculations”, JPS 2013 Autumn Meeting, September 20-23, 2013, Kochi University, Kochi, Japan.

Yoshida T., Shimizu N., Abe T., Otsuka T. (oral), “A study of Be nuclei based on Monte Carlo shell model”, JPS 2013 Autumn Meeting, September 20-23, 2013, Kochi University, Kochi, Japan.

Iwata Y., Ichikawa T., Itagaki N., Maruhn J.A., Otsuka T. (oral), “Existence of 6 alpha linear chain state based on systematic Cranking-Hartree-Fock calculations”, JPS 2013 Autumn Meeting, September 20-23, 2013, Kochi University, Kochi, Japan.

Shimizu N., Utsuno Y., Ebata S., Honma M., Mizusaki T., Otsuka T. (oral), “Large-scale shell-model calculations for E1 excitations of Ca isotopes”, JPS 2013 Autumn Meeting, September 20-23, 2013, Kochi University, Kochi, Japan.

Niigata University

Publications

[Journal]

(Original Papars) *Subject to Peer Review

Saraya Y., Izumikawa T., Goto J., Kawasaki T., Kimura T.: "Study of spatial resolution of proton computed tomography using a silicon strip detector", Nucl. Instr. Methods Phys. Res. A **735** (2014) 485–489.*

Koizumi M., Goto J., Matsuki S., Nakamura S.: "Dynamic nuclear self-polarization for measurements of nuclear magnetic moments", Nucl. Instr. Methods Phys. Res. B **317** (2013) 689–692.*

Moriguchi T., Ozawa A., Ishimoto S., Abe Y., Fukuda M., Hachiuma I., Ishibashi Y., Ito Y., Kuboki T., Lantz M., Nagae D., Namihira K., Nishimura D., Ohtsubo T., Ooishi H., Suda T., Suzuki H., Suzuki T., Takechi M., Tanaka K., Yamaguchi T.: "Density distributions of Li-11 deduced from reaction cross-section measurements", Phys. Rev. C **88** (2013) 024610.*

Hirayama Y., Mihara M., Watanabe Y., Jeong S., Miyatake H., Momota S., Hashimoto T., Imai N., Matsuta K., Ishiyama H., Ichikawa S., Ishii T., Izumikawa T., Katayama I., Kawakami H., Kawamura H., Nishinaka I., Nishio K., Makii H., Mitsuoka S., Osa A., Otokawa Y., Sato T., Wakabayashi Y.: "Spin-polarized radioactive isotope beam produced by tilted-foil technique", Phys. Rev. C **88** (2013) 024618.*

Momota S., Mihara M., Nishimura D., Fukuda M., Kamisho Y., Wakabayashi M., Matsuta K., Suzuki S., Nagashima M., Shengyun Zhu, Daqing Yuan, Yongnan Zheng, Zuo Yi, Ping Fan, Izumikawa T., Kitagawa A., Sato S., Kanazawa M., Torikoshi M., Minamisono T., Nakamura Y., Tashiro K., Honma A., Yoshida N., Shirai H., Ohtsubo T., Nagatomo T., Uenishi H., Iwamoto K., Yaguchi M., Ogura T., Ito T., Yamamura K., Ichikawa Y., Nojiri Y., Alonso J.R., Symons T.J.M.: "Momentum dependence of spin polarization for beta emitting nuclei produced through charge exchange reaction at intermediate energy", Hyperfine Interact. **220** (2013) 53–58.*

Mihara M., Matsuta K., Nishimura D., Fukuda M., Yaguchi M., Iwamoto K., Wakabayashi M., Kamisho Y., Ohno J., Morita Y., Izumikawa T., Ohtsubo T., Suzuki S., Nagashima M., Abe K., Sakai T., Momota S., Ozawa A., Nagae D., Ishibashi Y., Abe Y., Niwa T., Nagatomo T., Minamisono T., Kubo M.K., Kitagawa A., Torikoshi M., Kanazawa M., Sato S., Watanabe Y., Minamisono K.: "Production of spin polarized ^{12}N through heavy ion reactions", Hyperfine Interact. **220** (2013) 83–88.*

Matsuta K., Minamisono T., Mihara M., Fukuda M., Shengyun Zhu, Masuda Y., Hatanaka K., Daqing Yuan, Yongnan Zheng, Yi Zuo, Ping Fang, Dongmei Zhou, Ohtsubx T., Izumikawa T., Momota S., Nishimura D., Matsumiya R., Kitagawa A., Sato S., Kanazawa M., Torikoshi M., Nagatomo T., Nojiri Y., Suzuki T., Xizhen Zhang, Alonso J.R., Symons T.J.M, Kawasaki S., Jeong S.C.: "Nuclear moments as a probe of electronic structure in material, exotic nuclear structure and fundamental symmetry", Hyperfine Interact. **220** (2013) 21–28.*

Yamaguchi T., Suzaki F., Izumikawa T., Miyazawa S., Morimoto K., Suzuki T., Tokanai F., Furuki H., Ichihashi N., Ichikawa C., Kitagawa A., Kuboki T., Momota S., Nagae D., Nagashima M., Nakamura Y., Nishikiori R., Niwa T., Ohtsubo T., Ozawa A., Sato K., Sato S., Suzuki S.: "Performance of high-resolution position-sensitive detectors developed for storage-ring decay experiments", Nucl. Instr. Methods Phys. Res. B **317** (2013) 697–700.*

Yamaki S., Yamaguchi T., Kouno J., Sato K., Ichihashi N., Suzuki T., Abe K., Abe Y., Fukuda M., Furuki H., Inaba N., Iwamoto K., Izumikawa T., Kamisho Y., Kikuchi N., Kitagawa A., Mihara M., Miyazawa S., Momota S., Morita Y., Nagae D., Nagashima M., Nakamura Y., Nishikiori R., Nishimura D., Nishizuka I., Ohtsubo T., Ohno J., Ozawa A., Sakai T., Sato S., Sera D., Suzaki F., Suzuki S., Suzuki S., Wakabayashi M., Yaguchi M., Yasumoto S.: "Systematic study of individual charge-changing cross sections of intermediate-energy secondary beams", Nucl. Instr. Methods Phys. Res. B **317** (2013) 774–778.*

Murakami M., Goto S., Murayama H., Kojima T., Kudo H., Kaji D., Morimoto K., Haba H., Kudou Y., Sumita T., Sakai R., Yoneda A., Morita K., Kasamatsu Y., Kikunaga H., Sato T.: "Excitation functions for production of Rf isotopes in the ^{248}Cm $+^{18}$ O reaction", Prog. Theor. Exp. Phys. (2013) 113D02.*

Toyoshima A., Li Z., Asai M., Sato N., Sato T., Kikuchi T., Kaneya Y., Kitatsuji Y., Tsukada, K., Nagame Y., Schädel M., Ooe K., Kasamatsu Y., Shinohara A., Haba H., Even J.: "Measurement of the Md^{3+}/Md^{2+} Reduction Potential Studied with Flow Electrolytic Chromatography", Inorg. Chem. **52** (2013) 12311–12313.*

Sato T., Sato N., Asai M., Tsukada K., Toyoshima A., Ooe K., Miyashita S., Schädel M., Kaneya Y., Nagame Y., Osa A., Ichikawa S., Stora T., Kratz J.: "First successful ionization of Lr (Z = 103) by a surface-ionization technique", Rev. Sci. Instrum. **85** (2013) 023304.*

Yoshida K., Nakatsukasa T.: "Shape evolution of giant resonances in Nd and Sm isotopes", Phys. Rev. C **88** (2013) 034309.*

Yoshida K.: "Spin-isospin response of deformed neutron-rich nuclei in a self-consistent Skyrme energy-density-functional approach", Prog. Theor. Exp. Phys. (2013) 113D02.*

Shimoyama H., Matsuo M.: "Di-neutron correlation in monopole two-neutron transfer modes in Sn isotope chain", Phys. Rev. C **88** (2013) 054308.*

[Book Proceedings]

(Original Papars) *Subject to Peer Review

Yoshida K.: "Skyrme energy-density functional approach to collective modes of excitation in exotic nuclei", J. Phys.: Conf. Ser. **445** (2013) 012027.*

Oral Presentations

(International Conference etc.)

Takechi M., Suzuki S., Nishimura D., Fukuda M., Ohtsubo T., Nagashima M., Suzuki T., Yamaguchi T., Ozawa A., Moriguchi T., Ohishi H., Sumikama T., Geissel H., Ishihara M., Aoi N., Rui-Jiu Chen, De-Qing Fang, Fukuda N., Fukuoka S., Furuki H., Inabe N., Ishibashi Y., Itoh T., Izumikawa T., Kameda D., Kubo T., Lee C.S., Lantz M., Yu-Gang Ma, Matsuta K., Mihara M., Momota S., Nagae D., Nishikiori R., Niwa T., Ohnishi T., Okumura K., Ogura T., Sakurai H., Sato K., Shimbara Y., Suzuki H., Takeda H., Takeuchi S., Tanaka K., Uenishi H., Winkler M., Yanagisawa Y., Watanabe S., Minomo K., Tagami S., Shimada M., Kimura M., Matsumoto T., Shimizu Y.R., Yahiro M. (Oral): "Search for halo nucleus in Mg isotopes through the measurements of reaction cross sections towards the vicinity of neutron drip line", International Nuclear Physics Conference (INPC 2013), Jun. 2–7, 2013, Firenze, Italy.

Suzuki S., Takechi M., Ohtsubo T., Nishimura D., Fukuda M., Kuboki T., Nagashima M., Suzuki T., Yamaguchi T., Ozawa A., Ohishi H., Moriguchi T., Sumikama T., Geissel H., Aoi N., Rui-Jiu Chen, De-Qing Fang, Fukuda N., Fukuoka S., Furuki H., Inabe N., Ishibashi Y., Ito T., Izumikawa T., Kameda D., Kubo T., Lantz M., Lee C.S., Yu-Gang Ma, Mihara M., Momota S., Nagae D., Nishikiori R., Niwa T., Ohnishi T., Okumura K., Ogura T., Sakurai H., Sato K., Shimbara Y., Suzuki H., Takeda H., Takeuchi S., Tanaka K., Uenishi H., Winkler M., Yanagisawa Y., Yanagisawa Y., Watanabe S., Minomo K., Tagami S., Shimada M., Kimura M., Matsumoto T., Shimizu Y.R., Yahiro M. (Oral): "Measurements of interaction cross sections for $^{22--35}$Na isotopes", International Nuclear Physics Conference (INPC 2013), Jun. 2–7, 2013, Firenze, Italy.

Nagashima} M., Ohtsubo T., Suzuki S., Nishimura D., Takechi M., Fukuda M., Suzuki T., Yamaguchi T., Ozawa A., Moriguchi T., Ohishi H., Sumikama T., Geissel H., Aoi N., Rui-Jiu Chen, De-Qing Fang, Fukuda N., Fukuoka S., Furuki H., Inabe N., Ishibashi Y., Itoh T., Izumikawa T., Kameda D., Kubo T., Lantz M., Yu-Gang Ma, Matsuta K., Mihara M., Momota S., Nishikiori R., Niwa T., Ohnishi T., Okumura K., Ohtake M., Ogura T., Sakurai H., Shimbara Y., Suzuki H., Takeda H., Takeuchi S., Tanaka K., Uenishi H., Winkler M., Yanagisawa Y. (Oral): "Interaction cross section measurement of Al isotopes", International Nuclear Physics Conference (INPC 2013), Jun. 2–7, 2013, Firenze, Italy.

Murakami M., Goto S., Murayama H., Kojima T., Kaji D., Morimoto K., Haba H., Kudou Y., Sumita T., Sakai R., Yoneda A., Morita K., Kasamatsu Y., Kikunaga H., Sato T.: Kudo H. (Poster): "Excitation functions for production of Rf isotopes in the ^{248}Cm$+^{18}$O reaction", Eighth Workshop on the Chemistry of the Heaviest Elements (CHE8), Sep. 19–21, 2013, Takayama, Gifu, Japan.

Goto S., Oshimi Y., Tomitsuka T., Murakami M., Tsuto S., Yatsu Y., Ooe K., Sato T., Tsukada K., Asai M., Toyoshima A., Miyashita S., Kaneya Y., Nagame Y., Kudo H. (Poster): "Gas phase chemistry of the volatile chloride compound of Hf isotopes", Eighth Workshop on the Chemistry of the Heaviest Elements (CHE8), Sep. 19–21, 2013, Takayama, Gifu, Japan.

Oshimi Y., Goto S., Taguchi T., Tomitsuka T., Ooe K., Kudo H. (Poster): "Off-line isothermal gas chromatography of Zr and Hf compounds", 5th Asia-Pacific Symposium on Radiochemistry '13 (APSORC13), Sep. 22–27, 2013, Kanazawa, Ishikawa, Japan.

Koyama T., Goto N., Murakami M., Ooe K., Haba H., Kanaya J., Goto S., Kudo H. (Poster): "Development of a rapid solvent extraction technique with flow injection analysis for superheavy element chemistry", 5th Asia-Pacific Symposium on Radiochemistry '13 (APSORC13), Sep. 22–27, 2013, Kanazawa, Ishikawa, Japan.

Ooe K., Tsukada K., Asai M., Sato T., Toyoshima A., Miyashita S., Nagame Y., Schädel M., Kaneya Y., Lerum H. V., Omtvedt J. P., Kratz J. V., Haba H., Wada A., Kitayama Y. (Poster): "Development of a new degasser with a hydrophobic membrane for the SISAK system", Eighth Workshop on the Chemistry of the Heaviest Elements (CHE8), Sep. 19–21, 2013, Takayama, Gifu, Japan.

Ooe K., Tsukada K., Asai M., Sato T., Toyoshima A., Miyashita S., Nagame Y., Schädel M., Kaneya Y., Lerum H. V., Omtvedt J. P., Kratz J. V., Haba H., Wada A., Kitayama Y. (Poster): "Development of a new continuous dissolution apparatus with a hydrophobic membrane for superheavy element chemistry", 5th Asia-Pacific Symposium on Radiochemistry '13 (APSORC13), Sep. 22–27, 2013, Kanazawa, Ishikawa, Japan.

Sato D., Murakami M., Ooe K., Goto S., Kudo H. (Poster): "Extraction behavior of Nb and Ta with Aliquat 336 in HF solution", The 3rd International Congress on Natural Sciences with Sisterhood Universities (ICNS2013), Oct. 12–14, 2013, Niigata, Niigata, Japan.

Yoshida K. (Oral): "Shape evolution in Skyrme energy-density-functional method", IN2P3-BLTP Workshop "Recent Achievements in Nuclear Theory", Jul. 22–27, 2013, Bogoliubov Laboratory of Theoretical Physics, JINR, Dubna, Russia.

Yoshida K. (Oral): "Collective mass parameters in Skyrme EDF", INT program on Quantitative Large Amplitude Shape Dynamics: fission and heavy ion fusion, Sep. 23–Oct. 4, 2013, Institute for Nuclear Theory, University of Washington, USA.

Yoshida K. (Oral): “Spin-isospin modes of excitation and beta-decay properties of neutron-rich Zr isotopes”, JUSTIPEN-JUSEIPEN Workshop, Dec. 9–12, 2013, RIKEN Nishina Center, Wako, Saitama, Japan.

Yoshida K. (Oral): “Low-lying spin-isospin modes of excitation and isoscalar pairing”, YITP International Molecule-type Workshop on New correlations in exotic nuclei and advances of theoretical models, Mar. 10–23, 2014, Yukawa Institute for Theoretical Physics, Kyoto University, Kyoto, Japan.

Matsuo M. (Oral): “Quadrupole shape dynamics in view from a theory of large amplitude collective motion”, 20th Nuclear Physics Workshop “Marie & Pierre Curie”, Sep. 25–29, 2013, Kazimierz Dolny, Poland.

Matsuo M. (Oral): “Exotic aspects of pair correlation in neutron-rich nuclei”, French-Japanese Symposium on Nuclear Structure Problems, Sep. 39–Oct.3, 2013, CNRS, Paris, France.

Matsuo M. (Oral): “Two-neutron transfer amplitudes having extended tail: from the pair rotation to the giant pair vibration in Sn isotopic chain”, Workshop “From nuclear structure to particle-transfer reactions and back”, Nov. 4–8, 2013, European Center for Theoretical Studies in Nuclear Physics and Related Areas (ECT*), Trento, Italy.

Matsuo M. (Oral): “Asymptotics of neutron Cooper pair in weakly bound nuclei”, JUSTIEPN-JUSEIPEN Workshop, Dec. 9–12, 2013, RIKEN Nishina Center, Wako, Saitama, Japan.

Matsuo M. (Oral): “Spatial two-neutron correlation in the Hartree-Fock-Bogoliubov description of weakly bound nuclei”, International Molecule-type Workshop on New Correlations in exotic nuclei and advances of theoretical models, Mar. 10–23, 2014, Yukawa Institute for Theoretical Physics, Kyoto University, Kyoto, Japan.

(Domestic Conference)

Yoshida K. (Oral): “Fully-selfconsistent deformed proton-neutron QRPA with Skyrme EDF”, 日本物理学会第 69 回年次大会, (日本物理学会), 2014 年 3 月 27–30 日, 東海大学（湘南キャンパス）.

Shimoyama H., Yoshida K., Nakatsukasa T. (Oral): “2 次元座標表示拘束条件付き HFB 法による大変形状態の記述”, 日本物理学会第 69 回年次大会, (日本物理学会), 2014 年 3 月 27–30 日, 東海大学（湘南キャンパス）.

Radioactive nuclear beam group
IPNS (Institute for Particle and Nuclear Studies)
KEK (High Energy Accelerator Research Organization)

Publications

[Journal]

(Original Papers) *Subject to Peer Review

Watanabe Y.X., Hirayama Y., Imai N., Ishiyama H., Jeong S.C., Miyatake H., Clement E., de France G., Navin A., Rejmund M., Schmit C., Pollarolo G., Corradi L., Fioretto E., Motanari D., Choi S.H., Kim Y.H., Song J.S., Niikura M., Suzuki D., Nishibata H., Takatsu J., "Study of collisons of ^{136}Xe + ^{198}Pt for the KEK isotope separator", Nucl. Instrum. Meth. B **317** (2013) 752-755, *

Mukai M., Hirayama Y., Jeong S.C., Imai N., Ishiyama H., Miyatake H., Oyaizu M., Watanabe Y.X., Kim Y.H., "In–gas–cell laser ion source for KEK isotope separation system", Rev. Sci. Instrum. **85** (2014) 02B906, *

Hirayama Y., Mihara M., Watanabe Y.X., Jeong S.C., Miyatake H., Momota S., Hashimoto T., Imai N., Matsuta K., Ishiyama H., Ichikawa S., Ishii T., Izumikawa T., Katayama I., Kawakami H., Kawamura H., Nishinaka I., Nishio K, Makii H., Mitsuoka S., Osa A., Otokawa Y., Sato T.K., Wakabayashi Y., "Spin–polarized radioactive isotope beam produced by tilteld–foil technique", Nucl. Instrum. Meth. B. **317** (2013) 693–696, *

Hirayama Y., Watanabe Y.X., Imai N., Ishiayma H., Jeong S.C., Miyatake H., Oyaizu M., Kim Y.H., Mukai M., Matsuo Y., Sonoda T., Wada M., Mark H., Kudryavstev Y., Piet V.D., "Off–line test of the KISS gas cell", Nucl. Instrum. Meth. **317** (2013) 480–483, *

Ishiyama H., Jeong S.C., Watanabe Y.X., Hiryatama Y., Imai N., Miyatake H., Oyaizu M., Katayama I., Sataka M., Osa A., Otokawa Y., Matsuda M., Makii H., Nishio K., Sato T.K., Nakao A., "In situ diffusion measurements in solids using short-lived radioactive tracers of ^{8}Li and ^{20}Na", Nucl. Instrum. Meth. **317** (2013) 789–792, *

Suzuki H., Aoi N., Takeshita E., Takeuchi S., Ota S., Baba H., Bishop S., Fukui T., Hashimoto Y., Ideguchi E., Ieki K., Imai N., Ishihara M., Iwasaki H., Kanno S., Kondo Y., Kubo T., Kurita K., Kusaka K., Minemura T., Motobayashi T., Nakayabayashi T., Nakamura T., Nakao T., Niikura M., Okumura T., Ohnishi T.K., Ong H.J., Sakurai H., Shimoura S., Sugo R., Suzuki D., Suzuki M.K., Tamaki M., Tanaka K., Togano Y., Yamada K. " Collectivity of neutron-rich Ti isotopes", Phys.Rev. C 88, 024326 (2013),*

Rothe S., Andreyev A.N., Antalic S., Borschevsky A., Capponi L., Cocolios T.E., Witte H. De., Eliav E., Fedorov D.V., Fedosseev V.N., Fink D.A., Fritzsche S., Ghys L., Huyse M., Imai N., Kaldor U., Kudryavtsev Yuri., Köster U., Lynch K.M., Marsh B.A., Nishio K., Pauwels D., Pershina V., Popescu L., Radulov D., Raeder S., Rajabali M.M., Rapisarda E., Rossel R.E., Sandhu K., Seliverstov M.D., Sjördin A.M., Bergh P. Van den, Duppen P. Van., Venhart M., Wakabayashi Y., Went K.D.A., "Measurement of the first ionization potential of astatine by laser ionization spectroscopy." Nature Communications 05/2013; 4:1835.

[Book・ Proceedings]

(Original Papers) *Subject to Peer Review

Watanabe Y.X., Miyatake H., Jeong S.C., Ishiyama H., Imai N., Hirayama Y., Oyaizu M., Niki K., Okada M., Wada M., Sonoda T., "KEK Isotope Separation System for β Deacy Spectroscopy of R-Process Nuclei", NUCLEAR STRUCTURE PROBLEMS Proceeding of the French–Japanese Symposium, World Scientific Publishing Co. (2013) 167-172. ,*

Sonoda T., Wada M., Tomita H., Sakamoto C., Takatsuka T., Noto T., Iiumra H., Matsuo Y., Kubo T., Shinozuka T., Wakui T., Mita H., Naimi S., Furukawa T., Itou Y., Schury P., Miyatake H., Jeong S.C., ishiyama H., Watanabe Y.X., Hirayama Y., "Development of a gas cell–based laser ion source for RIKEN PALIS", Hyper fine Interract Proceedings of the 6th International Conference on Laser Probing (LAP 2012), DOI 10.1007/s10751-013-0817-6, *

Oral Presentations

(International Conference etc.)

Hirayama Y., "beta–decay spectroscopy of r–process nuclei with N=126 at Kiss", The 12th international symposium on Origin of Matter and Evoltion of Galaxies (OMEG12), 17–21 November, 2013, Tsukuba, Japan

Watanabe Y.X., Miyatake H., Jeong S.C., Ishiyama H., Imai N., Hirayama Y., Oyaizu M., Mukai M., Kim Y.H., "Present status of KEK isotope separation system", French–Japanese International Assoiciated Laboratory for Nuclear Structure Problems (LIA 2013), 30 September–3 October, 2013, Paris, JFrench

Miyatake H., "RNB KISS Project", KEK–TRIUMF Scientific Symposium, 10–11 October, 2013, TRIUMF, Canada

Mukai M., Hirayama Y., Jeong S.C., Imai N., Ishiyama H., Miyatake H., Oyaizu M., Watanabe Y.X., Kim Y.H., "In–gas–cell laser ion source for KEK isotope separation system", The 15th International Conference on Ion Sources (ISIS'13), 9–13 September, 2013, Chiba, Japan

Kim Y.H., "Study of the Multi–Nucleon Transfer Reactions of ^{136}Xe + ^{198}Pt for producing Exotic Heavy Nuclei", The 12th Asia Pacific Physics Conference ASEPS Asia–Europe Physics Summit (APPC12), 14–19 July, 2013, Makuhari, Japan

Hirayama Y., "Development of the KISS gas cell", 11th IGISOL Workshop, 11–13 June, 2013, Jyvaskyla, Finland

VIII. LIST OF PREPRINTS

List of Preprints (April 2013 - March 2014)

RIKEN NC-NP

101	Feasibility of the finite amplitude method in covariant density functional theory	H. Liang, T. Nakatsukasa et al.	Apr., 2013
102	Deformation and cluster structures in 12C studied with configuration mixing using Skyrme interactions	Y. Fukuoka, S. Shinohara et al.	Apr., 2013
105	Giant dipole resonance in ^{88}Mo from phonon damping model's strength functions averaged over temperature and angular momentum distributions	N. Dinh Dang, M. Ciemala et al.	Apr., 2013
106	Nuclear β+/EC decays in covariant density functional theory and the impact of isoscalar proton-neutron pairing	Z. M. Niu, Y. F. Niu et al.	Apr., 2013
107	Shape evolution of giant resonances in Nd and Sm isotopes	K. Yoshida, T. Nakatsukasa	Jun., 2013
108	Low-energy E1 strength in select nuclei: Possible constraints on the neutron skins and the symmetry energy	T. Inakura, T. Nakatsukasa et al.	Jun., 2013
109	Single-reference high-precision mass measurement with a multi-reflection time-of-flight mass spectrograph	Y. Ito, P. Schury et al.	Jul., 2013
110	On the importance of using exact pairing in the study of pygmy dipole resonance	N. Dinh Dang, N. Quang Hung	May, 2013
111	A Novel Ion Cooling Trap for Multi-Reflection Time-of-Flight Mass Spectrograph	Y. Ito, P. Schury et al.	Aug., 2013
112	Pseudospin symmetry in supersymmetric quantum mechanics. II. Spin-orbit effects	S. Shen, H. Liang et al.	May, 2013
113	Pairing effects in nuclear fusion reaction	S. Ebata, T. Nakatsukasa	Aug., 2013
114	Wide-band mass measurements with a multi-reflection time-of-flight mass spectrograph	P. Schury, Y. Ito et al.	Sep., 2013
115	Nuclear charge-exchange excitations in localized covariant density functional theory	H.Z. Liang, J. Meng et al.	Aug., 2013
116	Pseudospin symmetry: Recent progress with supersymmetric quantum mechanics	H. Liang, J. Meng et al.	Oct., 2013
117	Production cross section measurements of radioactive isotopes by BigRIPS separator at RIKEN RI Beam Factory	H. Suzuki, T. Kubo et al.	Oct., 2013
118	Identification and Separation of Radioactive Isotope Beams by the BigRIPS Separator at the RIKEN RI Beam Factory	N. Fukuda, T. Kubo et al.	Oct., 2013
119	Extraction of 3D field maps of magnetic multipoles from 2D surface measurements with applications to the optics calculations of the large-acceptance superconducting fragment separator BigRIPS	H. Takeda, T. Kubo et al.	Nov., 2013
120	Development of Parallel Plate Avalanche Counter PPAC for BigRIPS fragment separator	H. Kumagai, T. Ohnishi et al.	Nov., 2013
121	Finite-amplitude method: An extension to the covariant density functionals	H. Liang, T. Nakatsukasa et al.	Oct., 2013
122	Pure collective precession motion of a high-spin torus isomer	T. Ichikawa, K. Matsuyanagi et al.	Jan., 2014
123	Structure of 136Sn and the Z=50 magicity	H. Wang, N. Aoi et al.	Nov., 2013
124	Probing the critical behavior in the evolution of GDR width at very low temperatures in A ~ 100 mass region	B. Dey, D. Mondal et al.	Oct., 2013
125	Current status of the "Hybrid Kurotama model" for total reaction cross sections	L. Sihver, A. Kohama et al.	Mar., 2014
126	An improved parameterization of the transparency parameter in Kox and Shen models of total reaction cross sections	L. Sihver, M. Lantz et al.	Mar., 2014
127	DALI2: A NaI(Tl) detector array for measurements of $¥gamma$ rays from	S. Takeuchi, T. Motobayashi et al.	Feb., 2014
128	Giant dipole resonance in highly excited nuclei	N. Dinh Dang	Jul., 2013
129	Oblate deformation of light neutron-rich even-even nuclei	I. Hamamoto	Feb., 2014
130	Treating Coulomb exchange contributions in relativistic mean field calculations: why and how	N. Van Giai, H. Liang et al.	Nov., 2013
131	Energy-density-functional calculations including proton-neutron mixing	K. Sato, J. Dobaczewski et al.	Aug., 2013

RIKEN NC- AC

	Not Applicable		

RIKEN MP

69	Towards Holographic Spintronics	K. Hashioto, N. Iizuka et al.	Apr., 2013
71	Superconformal Indices and M2 Branes	R. Eager, J. Schmude	May, 2013
73	Primordial spectra from sudden turning trajectory	T. Noumi, M. Yamaguchi	Jul., 2013
74	Laplace operators on Sasaki-Einstein manifolds	J. Schmude	Aug., 2013
75	Vacuum Instability in Electric Fields via AdS/CFT: Euler-Heisenberg Lagrangian and Planckian Thermalization	K. Hashimoto, T. Oka	July, 2013
76	Effective gravitational interactions of dark matter axions	T. Noumi, K. Saikawa et al.	Oct., 2013
77	From the Berkovits formulation to the Witten formulation in open superstring field theory	Y. Iimori, T. Noumi et al.	Dec., 2013
78	Non-Lagrangian Theories from Brane Junctions	L. Baoa, V. Mitevb et al.	Oct., 2013
79	Notes on Enhancement of Flavor Symmetry and 5d Superconformal Index	M. Taki	Oct., 2013
80	Phase structure of topological insulators by lattice strong-coupling expansion	Y. Araki, T. Kimura et al.	Nov., 2013
81	General conditions ensuring relativistic causality in an effective field theory based on the derivative expansion	Y. Minami, Y. Hidaka	Jan., 2014
82	Note on intersecting branes in topological strings	T. Kimura	Jan., 2014
83	Seiberg duality, and 5d SCFTs and Nekrasov Partition Functions	M. Taki	Jan., 2014
84	Current Reflection and Transmission at Conformal Defects	T. Kimura, M. Murata	Feb., 2014
85	Non-Gaussianities of primordial perturbations and tensor sound speed	T. Noumi, M. Yamaguchi	Mar., 2014
86	Magnetic instability in AdS/CFT : Schwinger effect and Euler-Heisenberg Lagrangian of Supersymmetric QCD	K. Hashimoto, T. Oka et al.	Mar., 2014
87	On AGT-W Conjecture and q-Deformed W-Algebra	M. Taki	Mar., 2014

RIKEN QHP

50	Neutrino spectral density at electroweak scale temperature	K. Miura, Y. Hidaka et al.	Jun., 2013
77	Strangeness and charmness content of nucleon from overlap fermions on 2+1-flavor domain-wall fermion configurations	M. Gong, A. Alexandru et al.	Apr., 2013
81	Nambu-Goldstone modes and the Josephson supercurrent in the bilayer quantum Hall system	Y. Hama, G. Tsitsishvili et al.	Apr., 2013
82	Energy-momentum tensor from the Yang-Mills gradient flow	H. Suzuki	Apr., 2013
83	Flow equation of functional renormalization group for three-body scattering problems	Y. Tanizaki	Apr., 2013
84	Phase shifts in I=2 ¥pi¥pi-scattering from two lattice approaches	T. Kurth, N. Ishii et al.	May, 2013
86	Spin-Orbit Force from Lattice QCD	K. Murano, N. Ishii et al.	May, 2013

87	Dynamical Mass Generation of Light-vector Mesons from QCD Trace Anomaly	T. Hayata	Jun., 2013
88	Equation of State for Nucleonic Matter and its Quark Mass Dependence from the Nuclear Force in Lattice QCD	T. Inoue, S. Aoki et al.	Jul., 2013
89	SUSY breaking by nonperturbative dynamics in a matrix model for 2D type IIA superstrings	M.G. Endres, T. Kuroki et al.	Aug., 2013
90	Rotating lattice	A. Yamamoto, Y. Hirono	Aug., 2013
91	Vortices and Other Topological Solitons in Dense Quark Matter	M. Eto, Y. Hirono et al.	Aug., 2013
92	Temporal Chiral Spiral in Strong Magnetic Fields	T. Hayata, Y. Hidaka et al.	Aug., 2013
93	Fermionic Functional Renormalization Group Approach to Superfluid Phase Transition	Y. Tanizaki, G. Fejos et al.	Oct., 2013
94	Sign problem and the chiral spiral on the finite-density lattice	R. Fukuda, K. Fukushima et al.	Sep., 2013
95	Domain Walls and Vortices in Chiral Symmetry Breaking	M. Eto, Y. Hirono et al.	Sep., 2013
96	First Numerical Simulations of Anomalous Hydrodynamics	M. Hongo, Y. Hirono et al.	Sep., 2013
98	On the symmetry improved CJT formalism in the \$O(4)\$ linear sigma model	H. Mao	Sep., 2013
100	Broken spacetime symmetries and elastic variables	T. Hayata, Y. Hidaka	Dec., 2013
101	Fermionic Functional Renormalization Group Approach to Bose-Einstein Condensation of Dimers	Y. Tanizaki	Nov., 2013
102	Cutoff effects on lattice nuclear forces	T. Doi (HAL QCD Collaboration)	Nov., 2013
103	Functional renormalization group approach to conventional theory of superfluidity and beyond	Y. Tanizaki, G. Fejős et al.	Nov., 2013
104	General conditions ensuring relativistic causality in an effective field theory based on the derivative expansion	Y. Minami, Y. Hidaka	Jan., 2014
105	Charmed Tetraquarks Tcc and Tcs from Dynamical Lattice QCD Simulations	Y. Ikeda, B. Charron et al.	Nov., 2013
106	Universal physics of three bosons with isospin	T. Hyodo, T. Hatsuda et al.	Nov., 2013
107	Fermionic functional renormalization group with multiple regulators and the BCS-BEC crossover	Y. Tanizaki	Feb., 2014
108	A comparative study of two lattice approaches to two-body systems	B. Charron (HAL QCD Collaboration)	Nov., 2013
109	A Lattice Study of Quark and Glue Momenta and Angular Momenta in the Nucleon	M. Deka, T. Doi et al.	Dec., 2013
110	Thermodynamics of SU(3) Gauge Theory from Gradient Flow	M. Asakawa, T. Hatsuda et al.	Dec., 2013
111	Ultrasoft fermionic excitation at finite chemical potential	J.-P. Blaizot, D. Satow	Feb., 2014
113	Lattice QCD with mismatched Fermi surfaces	A. Yamamoto	Feb., 2014
114	Phase structure of SU(3) gauge-Higgs unification models at finite temperature	K. Kashiwa, Y. Tanizaki	Mar., 2014
115	Schwinger Mechanism with Stochastic Quantization	K. Fukushima, T. Hayata	Mar., 2014
116	Momentum transport away from jet in expanding medium	Y. Tachibana, T. Hirano	Feb., 2014
117	Massive Hybrid Stars with Strangeness	T. Takatsuka, T. Hatsuda et al.	Feb., 2014
120	Spin-2 N Omega Dibaryon from Lattice QCD	F. Etminan, H. Nemura et al.	Mar., 2014
123	Chiral dynamics in a magnetic field from the functional renormalization group	K. Kamikado, T. Kanazawa	Dec., 2013
124	Real-time correlation functions in the O(N) model from the functional renormalization group	K. Kamikado, N. Strodthoff et al.	Feb., 2014
125	Microscopic Origin and Universality Classes of the Efimov Three-Body Parameter	P. Naidon, S. Endo et al.	Dec., 2013

126	Rabi Oscillations between Atomic and Molecular Condensates Driven with Coherent One-Color Photoassociation	M. Yan, B.J. DeSalvo et al.	Aug., 2013
128	Complex 2D Matrix Model and Its Application to Nc-dependence of Hadron Structures	K. Nawa, S. Ozaki et al.	Jan., 2014
131	Double-spin asymmetry A_{LT} in open charm production.	Y. Hatta, K. Kanazawa et al.	May, 2014
132	Three-gluon contribution to the single spin asymmetry for light hadron production in pp collision	H. Beppu, K. Kanazawa et al.	Dec., 2013
133	Sine Square Deformation and String Theory	T. Tada	Jul., 2013
140	Search for possible bound Tcc and Tcs on the lattice	Y. Ikeda (HAL QCD Coll.)	Oct., 2013
142	QCD effective potential with strong U(1)_{¥em} magnetic fields	S. Ozaki	Nov., 2013
145	Hybrid Monte Carlo on Lefschetz thimbles - A study of the residual sign problem	H. Fujii, D. Honda et al.	Sep., 2013

CNS-REP

91	Mixed harmonic azimuthal correlations in $\sqrt{s_{NN}}$=2.76TeV Pb-Pb collisions measured by ALICE at LHC	Y. Hori	Apr., 2013

Nishina Center Preprint server (not including Partner Institution) can be found at
http://nishina-preprints.riken.jp/

IX. LIST OF SYMPOSIA & WORKSHOPS

List of Symposia & Workshops (April 2013 - March 2014)

RNC

1	The 6th RIBF discussion "Nuclear mass" http://indico2.riken.jp/indico/conferenceDisplay.py?confId=1165	RNC	May 24
2	MINOS collaboration meeting http://indico2.riken.jp/indico/conferenceDisplay.py?confId=1196	RNC	Jun. 25
3	SAMURAI Collaboration meeting http://indico2.riken.jp/indico/conferenceDisplay.py?confId=1164	RNC	Jun. 25
4	RIBF Users Meeting 2013 http://indico2.riken.jp/indico/conferenceDisplay.py?confId=1142	RNC	Jun. 26-27
5	The 7th RIBF discussion "Exotic modes of nuclear rotation" http://indico2.riken.jp/indico/conferenceDisplay.py?confId=1236	RNC	Jul. 24
6	PHENIX Workshop on Physics Prospects with Detector and Accelerator Upgrade http://indico2.riken.jp/indico/conferenceDisplay.py?confId=1221	RNC	Jul. 29 - Aug. 2
7	2nd BRIKEN Workshop http://indico.ific.uv.es/indico/conferenceDisplay.py?ovw=True&confId=1938	RNC	Jul. 30 - 31
8	The 1st JCPRG-RNC Joint Workshop on Nuclear Data http://indico2.riken.jp/indico/conferenceDisplay.py?confId=1235	RNC	Aug. 8-9
9	SAMURAI International Collaboration Workshop http://indico2.riken.jp/indico/conferenceDisplay.py?confId=1144	Tokyo Tech.	Sep. 9 - 10
10	HPCI Joint Workshop: "Multi-particle resonances and astrophysical reaction problems in few-body systems" http://www.jicfus.jp/jp/131021-25few-body/	RNC	Oct. 21 – 25
11	Todai/Riken joint workshop on Super Yang-Mills, solvable systems and related subjects https://sites.google.com/site/workshop235/home/	Univ. of Tokyo	Oct. 23 - 24
12	Japan-Korea PHENIX Collaboration Workshop 2013 http://indico2.riken.jp/indico/conferenceDisplay.py?confId=1327	SungKyunKwan Univ.	Nov. 4 – 5
13	Hadron2013 http://hadron2013.kek.jp/	Nara prefectural New Public Hall	Nov. 4 - 8
14	Workshop on Nuclear equation of state with strangeness http://www.jicfus.jp/field5/jp/131111-15hpci/	RIKEN	Nov. 11 - 15
15	Lattice Meets Experiment 2013: Beyond the Standard Model http://www.bnl.gov/lme2013/	BNL	Dec. 5 - 6
16	JUSTIPEN-JUSEIPEN Workshop http://indico2.riken.jp/indico/conferenceDisplay.py?confId=1263	RNC	Dec. 9 - 12
17	The Investigation of Hot QCD Matter http://indico2.riken.jp/indico/conferenceDisplay.py?confId=1291	RNC	Dec. 10
18	Nuclear matter in neutron stars investigated by experiments and astronomical observations http://indico2.riken.jp/indico/conferenceDisplay.py?confId=1296	RNC	Dec. 25
19	K Computer, Post K Computer and Fundamental Physics http://indico2.riken.jp/indico/conferenceDisplay.py?confId=1393	RIKEN	Jan. 7
20	7th Workshop on Nuclear Spectroscopy using Slow & Stopped RI beams (SSRI) http://indico2.riken.jp/indico/conferenceDisplay.py?confId=1411	RNC	Mar. 3 - 4
21	The 8th RIBF discussion "Nuclear EOS probed by direct reaction" http://indico2.riken.jp/indico/conferenceDisplay.py?confId=1409	Kyushu Univ.	Mar. 4

22	[RIBF ULIC mini-workshop 027] Nuclear symmetry-energy and nucleus-nucleus collision simulation http://indico2.riken.jp/indico/conferenceDisplay.py?confId=1175	RNC	Jul. 2 – 4
23	[RIBF ULIC mini-workshop 028] An investigation into multi-neutron detection via NEBULA and new neutron detectors http://indico2.riken.jp/indico/conferenceDisplay.py?confId=1311	RNC	Oct. 10 - 11
24	[RIBF-ULIC mini-workshop 029] Progress and Future Plans of the Research Group for Reaction Cross Sections http://indico2.riken.jp/indico/conferenceDisplay.py?confId=1454	RNC	Mar. 11
25	[RIBF-ULIC mini-workshop 030] RIBF Users Executive Committee http://indico2.riken.jp/indico/conferenceDisplay.py?confId=1456	RNC	Mar. 18

CNS

1	The 12th international symposium on Origin of Matter and Evolution of Galaxies (OMEG12) http://kekrnb.kek.jp/omeg12/	Tsukuba	Nov. 18 - 22

Niigata Univ.

1	原子核密度汎関数理論ミーティング（DFT ミーティング）	Niigata Univ.	Feb. 10
2	Progress and Future Plans of the Research Group for Reaction Cross Sections	RNC	Mar. 11

KEK

1	The 12th International Symposium on Origin of Matter and Evolution of Galaxies	Tsukuba	Nov. 18 - 22

X. LIST OF SEMINARS

List of Seminars (April 2013 - March 2014)

Nuclear Physics Monthly Colloquium

1	Hirohiko Shimizu (Nagoya Univ.)	Particle and Nuclear Physics using Slow Neutrons http://indico2.riken.jp/indico/conferenceDisplay.py?confId=1047	May 14
2	Junichiro Makino (Tokyo Tech.)	Dark matter halo simulation using the Kei computer http://indico2.riken.jp/indico/conferenceDisplay.py?confId=1295	Oct. 8
3	Emiko Hiyama (RNC)	Exotic nuclei with strangeness from viewpoint of few-body problem http://indico2.riken.jp/indico/conferenceDisplay.py?confId=1309	Nov. 26
4	Kazunori Itakura (KEK)	Strong field physics and its application to hadron physics http://indico2.riken.jp/indico/conferenceDisplay.py?confId=1371	Jan. 14

RIBF Nuclear Physics Seminar

1	Haozhao Liang (RNC)	Pseudospin symmetry in nuclear single-particle spectra and its perturbative interpretation http://indico2.riken.jp/indico/conferenceDisplay.py?confId=1091	Apr. 9
2	UENO Hideki (RNC)	Spin-oriented RI beams at RIBF and their applications http://indico2.riken.jp/indico/conferenceDisplay.py?confId=1157	Jun. 11
3	Yoshimasa Hidaka (RNC)	Generalization of the Nambu-Goldstone theorem http://indico2.riken.jp/indico/conferenceDisplay.py?confId=1185	Jun. 18
4	Shigehiro Nagataki (Astrophysical Big Bang Lab., RIKEN)	RIBF Nuclear Physics Seminars 167th: Nuclear Astrophysics in Astrophysical Big Bang Laboratory http://indico2.riken.jp/indico/conferenceDisplay.py?confId=1222	Jul. 9
5	Valerii Panin (GSI)	Exclusive Measurements of Proton-Induced Quasi-Free Scattering Reactions in Inverse and Complete Kinematics http://indico2.riken.jp/indico/conferenceDisplay.py?confId=1250	Aug. 12
6	Yoshihiro Aritomo (Tokyo Tech.)	Dynamics approach to synthesis of superheavy elements http://indico2.riken.jp/indico/conferenceDisplay.py?confId=1326	Oct. 29
7	Yasuro Funaki (RNC)	Imaginary time theory for triple-alpha reaction rate http://indico2.riken.jp/indico/conferenceDisplay.py?confId=1348	Nov. 22
8	Hiroshi Suzuki (RNC)	Production cross section measurements and New isotope searches by BigRIPS separator at RIKEN RI Beam Factory http://indico2.riken.jp/indico/conferenceDisplay.py?confId=1410	Jan. 28
9	Lembit Sihver (Chalmers Univ. of Tech.)	Charged Particle Transport Simulations for Radiotherapy and Space Dosimetry http://indico2.riken.jp/indico/conferenceDisplay.py?confId=1419	Feb. 6
10	Nobuyuki Kobayashi (Univ. of Tokyo)	Spectroscopy of p-wave neutron halo nuclei via neutron removal reactions http://indico2.riken.jp/indico/conferenceDisplay.py?confId=1427	Feb. 18
11	Stefano Gandolfi (Los Alamos National Lab.)	Microscopic Calculations of Homogeneous and Inhomogeneous Neutron Matter http://indico2.riken.jp/indico/conferenceDisplay.py?confId=1425	Feb. 26
12	Kenichiro Tateishi (RNC)	Dynamic nuclear polarization - from polarized target to NMR spectroscopic applications http://indico2.riken.jp/indico/conferenceDisplay.py?confId=1440	Mar. 11
13	Bijay Kumar Agrawal (Saha Inst. of Nuclear Physics)	Nuclear symmetry energy from nuclear observables http://indico2.riken.jp/indico/conferenceDisplay.py?confId=1444	Mar. 25
14	Attila Krasznahorkay (MTA Atomki)	Constraining the EoS of neutron-rich matter by studying giant resonances http://indico2.riken.jp/indico/conferenceDisplay.py?confId=1469	Mar. 31

Lecture Series on Nuclear Physics

1	Tatsuyuki Takatsuka (Iwate Univ.)	X-2: Baryonic Matter and Neutron Stars http://indico2.riken.jp/indico/conferenceDisplay.py?confId=1117	May 9
2	Tatsuyuki Takatsuka (Iwate Univ.)	X-3: Baryonic Matter and Neutron Stars http://indico2.riken.jp/indico/conferenceDisplay.py?confId=1192	Jul. 26

Special Seminar

	not held in FY2013		

Seminar by Each Laboratory

Theoretical Research Division

1	Shigehiro Nagataki (Astrophysical Big Bang Lab., RIKEN)	Take off of Our New Lab. "Astrophysical Big Bang Laboratory" http://indico2.riken.jp/indico/conferenceDisplay.py?confId=1122	Apr. 10
2	Charles Melby-Thompson (IPMU, Univ. of Tokyo)	Anisotropic Conformal Symmetry and Gravity http://indico2.riken.jp/indico/conferenceDisplay.py?confId=1123	Apr. 15
3	Jens Hoppe (Sogang Univ.)	Noncommutative Surfaces	Apr. 22
4	Takashi Nakatsukasa (RNC)	Introduction of Theoretical Nuclear Physics Laboratory http://indico2.riken.jp/indico/conferenceDisplay.py?confId=1131	Apr. 24
5	Takashi Nakatsukasa (RNC)	Real-time calculations of many-body quantum dynamics (II) http://indico2.riken.jp/indico/conferenceDisplay.py?confId=1160	May 15
6	Kantaro Omori (Univ. of Tokyo)	Superstring theory and integration over moduli space http://indico2.riken.jp/indico/conferenceDisplay.py?confId=1159	May 20
7	Nodoka Yamanaka (Kyoto Univ.)	Electric dipole moments and supersymmetric CP violation http://indico2.riken.jp/indico/conferenceDisplay.py?confId=1176	May 27
8	Akihisa Kohama (RNC)	Systematic studies of nuclear total reaction cross sections and related topics http://indico2.riken.jp/indico/conferenceDisplay.py?confId=1177	May 29
9	Kosuke Yoshioka (Univ. of Tokyo)	Quantum degenerate phases of electron-hole systems in photoexcited semiconductors http://indico2.riken.jp/indico/conferenceDisplay.py?confId=1181	May 31
10	Shin Nakamura (Nagoya Univ.)	Non-equilibrium Phase Transitions and Non-equilibrium Critical Point from AdS/CFT	Jun. 3
11	Etsuko Itou (KEK)	Conformal fixed point of Nf=12 SU(3) gauge theory	Jun. 10
12	Kouhei Washiyama (RNC)	Fusion and dynamical potential in heavy systems http://indico2.riken.jp/indico/conferenceDisplay.py?confId=1195	Jun. 19
13	Atsushi Nakamura (Hiroshima Univ.)	HPCI 主催素核宇宙融合レクチャーシリーズ第 9 回「ゼロからの格子 QCD 入門-有限バリオン密度系の研究を目指して」	Jun. 26-27
14	Shuhrat Kalandarov (JINR / Tokyo Tech.)	Production of doubly magic nucleus 100Sn in fusion reactions via particle and cluster emission channels http://indico2.riken.jp/indico/conferenceDisplay.py?confId=1200	Jul. 5
15	Hiroto So (Ehime Univ.)	Criteria of Lattice Supersymmetry: Cyclic Leibniz Rule	Jul. 8
16	Hiroshi Suzuki (RIKEN)	Energy-momentum tensor from the Yang-Mills gradient flow	Jul. 22

17	Ellena Botta (INFN - Sezione di Torino and Torino Univ.)	Highlights on n-rich $¥Lambda$-Hypernuclei from the FINUDA experiment http://indico2.riken.jp/indico/conferenceDisplay.py?confId=1270	Aug. 28
18	Nguyen Dinh Dang (RNC)	Giant dipole resonance in 88-Mo from phonon damping model's strength functions averaged over temperature and angular momentum http://indico2.riken.jp/indico/conferenceDisplay.py?confId=1275	Sep. 4
19	Jiangming Yao (Tohoku Univ. / Southwest Univ.)	Description of Nuclear Collective Excitations with Multi-Reference Covariant Density Functional Theory (The 41st Nuclear Theory Seminar)	Oct. 9
20	Masato Taki (RIKEN)	Junction of 5d CFT, 5-branes and AGT relation	Oct. 21
21	Seiji Terashima (YITP)	Exact results in supersymmetric field theories on manifolds with boundaries	Oct. 28
22	Akio Hosoya (Tokyo Tech.)	Black Holes and Quantum Information http://indico2.riken.jp/indico/conferenceDisplay.py?confId=1332	Oct. 30
23	Y. Taniguchi (Univ. of Tsukuba)	Cluster correlations in deformed states http://indico2.riken.jp/indico/conferenceDisplay.py?confId=1345	Nov. 8
24	Shinichi Sasa (Kyoto Univ)	An Introduction to Modern Non-Equilibrium Statistical Mechanics	Nov. 14
25	Marcus Werner (IPMU)	Mathematical properties of gravitational lensing theory	Nov. 18
26	Koichi Sato (RNC)	Energy-density-functional calculations including the proton-neutron mixing http://indico2.riken.jp/indico/conferenceDisplay.py?confId=1351	Nov. 20
27	Nguyen Dinh Dang (RNC), Maria Dainotti, and Herman Lee (Astrophysical Big Bang Lab., RIKEN)	Viscosity: From air to hot nuclei/ The Luminosity-time correlation (Lx-Ta) in GRB afterglows as a cosmological tool/ Supernova Remnants --- Active Retirement Life of Stars http://indico2.riken.jp/indico/conferenceDisplay.py?confId=1365	Nov. 27
28	Jiangming Yao (Tohoku Univ. & Southwest Univ.)	Beyond mean - field description of impurity effect of Lambda hyperon on nuclear collective excitations http://snp.riken.jp/abstract_pdf/abstract_RIKEN2013_yao.pdf	Dec. 3
29	Hitoshi Murayama (Kavli IPMU, Univ. of Tokyo)	The Quantum Universe http://indico2.riken.jp/indico/conferenceDisplay.py?confId=1378	Dec. 4
30	Yasuhiro Yamaguchi (RCNP)	Exotic baryons from a heavy meson and a nucleon http://indico2.riken.jp/indico/conferenceDisplay.py?confId=1373	Dec. 10
31	Mitsuhiro Kato (Univ. of Tokyo)	Extending string field theory for massless higher spin fields	Dec. 10
32	Takahiro Tanaka (YITP)	Field theory in de Sitter space	Dec. 12
33	Hyun-Chul Kim (Inha Univ.)	Transverse charge and spin structures of the pion and the nucleon	Dec. 17
34	Akinori Ogawa (KIAS)	Basic issues of entanglement entropy in AdS/CFT	Jan. 6
35	Akihiro Ishibashi (Kinki Univ.)	Black Holes in Higher Dimensions http://indico2.riken.jp/indico/conferenceDisplay.py?confId=1396	Jan. 8
36	Kosuke Sumiyoshi (Numazu National College of Tech.)	素核宇宙融合レクチャーシリーズ第 10 回「重力崩壊型超新星の爆発メカニズム：核物理と天文数値シミュレーションの連携」	Jan. 10-11
37	Haozhao Liang (RNC)	Nuclear beta-decay half-lives and the impact of isoscalar proton-neutron pairing http://indico2.riken.jp/indico/conferenceDisplay.py?confId=1405	Jan. 15
38	Shigeru Kubono (RNC)	Study of explosive hydrogen burning process for type II supernovae http://indico2.riken.jp/indico/conferenceDisplay.py?confId=1408	Jan. 22

39	Yoshimasa Hidaka (RNC)	Spacetime Symmetry Breaking, Elastic Variables and Nambu-Goldstone Modes	Jan. 29
40	Daigo Honda (Univ. of Tokyo)	Classical Liouville Three-point Functions from Riemann-Hilbert Analysis	Feb. 3
41	Maxim Barkov (Astrophysical Big Bang Lab., RIKEN)	Magnetically driven gamma-ray bursts http://indico2.riken.jp/indico/conferenceDisplay.py?confId=1431	Feb. 12
42	Jirong Mao (Astrophysical Big Bang Lab., RIKEN)	Gamma-ray Burst: A Possible Site to Detect R-process Elements? http://indico2.riken.jp/indico/conferenceDisplay.py?confId=1431	Feb. 12
43	Haozhao Liang (RNC)	Nuclear collective excitations and r-process nucleosynthesis http://indico2.riken.jp/indico/conferenceDisplay.py?confId=1431	Feb. 12
44	Avraham Gal (The Hebrew Univ.)	Pion-assisted Nucleon-Delta and Delta-Delta dibaryons	Feb. 26
45	Kengo Maeda (Shibaura tech.)	Application of AdS/CFT beyond Linear Response Theory and Construction of New Static Black Holes Solutions	Mar. 10
46	Taro Kimura (RIKEN/CEA Saclay)	Current reflection and transmission at conformal defects	Mar. 17
47	Kazuyuki Ogata (RCNP)	素核宇宙融合レクチャーシリーズ 第 11 回「離散化チャネル結合法を軸とする原子核反応研究の進展と応用」	Mar. 24-25

Sub Nuclear System Research Division

1	Jinfeng Liao (Indiana Univ. & CEEM, RBRC)	Jet Quenching at RHIC vs LHC in Light of Recent dAu vs pPb Controls Workshop: Opaqueness Evolution from Color Liberation	Apr. 16
2	Bernd Kniehl (Hamburg Univ.)	Theoretical Physics Seminar at BNL: Heavy-quarkonium theory in the LHC era	Jun. 18
3	Shu Lin (SUNY Stony Brook)	Theoretical Physics Seminar at BNL: Out of equilibrium chiral magnetic conductivity and chiral magnetic wave	Jul. 25
4	Michael Lublinsky (Ben-Gurion Univ.)	Theoretical Physics Seminar at BNL: QCD Reggeon Field Theory from the JIMWLK/KLWMIJ evolution	Jul. 26
5	Robert Lohmayer (Florida International Univ.)	Theoretical Physics Seminar at BNL: Many-flavor Schwinger model at finite chemical potential	Aug. 8
6	Denis Molnar	Theoretical Physics Seminar at BNL	Aug. 30
7	Anna Stasto (Penn State)	Nuclear Physics & RIKEN Theory Seminar at BNL: Forward particle production in proton(deutron)-nucleus collisions at higher order accuracy	Sep. 6
8	Zheng Li (RBRC)	Novel Silicon Detector Development and Processing for Nuclear and High Energy Physics and Photon Science at BNL http://indico2.riken.jp/indico/conferenceDisplay.py?confId=1265	Sep. 9
9	Isao Watanabe (RNC)	muSR Applications Seminar (UI/Indonesia)	Sep. 10-11
10	Tilman Plehn (Univ. of Heidelberg)	High-Energy Physics & RIKEN Theory Seminar at BNL: Higgs Physics for the LHC	Sep. 11
11	Naoki Yamamoto (Univ. of Maryland)	Nuclear Physics & RIKEN Theory Seminar: Kinetic theory with quantum anomalies and its applications	Sep. 13
12	Isao Watanabe (RNC)	Muon Site Esimation Seminar (USM/Malaysia)	Sep. 13

13	Isao Watanabe (RNC)	μSR Applications to Materials Science (Kyutech)	Sep. 17
14	Luca Vecchi (Univ. of Maryland)	High-Energy Physics & RIKEN Theory Seminar at BNL: Dark Matter in Un Natural Composite Higgs Models	Sep. 18
15	V. Parameswaran Nair (CUNY City College)	Nuclear Physics & RIKEN Theory Seminar at BNL: Anomalies and Fluid dynamics: A group-theoretic approach	Sep. 20
16	Yu Maezawa (BNL)	RIKEN Theory Seminar at BNL: Spatial meson correlations and screening masses at finite temperature in lattice simulations with HISQ	Sep. 26
17	Taku Izubuchi (BNL)	Theoretical Physics Seminar at BNL	Sep. 27
18	Daisuke Satow (RNC/BNL)	RIKEN Theory Physics Seminar at BNL: (Quasi) Nambu-Goldstone Fermion in QGP and Cold Atom System	Oct. 3
19	Gokce Basar (Stony Brook)	Nuclear Physics & RIKEN Theory Seminar at BNL Resurgence theory, ghost instantons and analytical continuation of path integrals	Oct. 4
20	Akihiko Monnai (RBRC)	RIKEN Theory Seminar at BNL: Non-equilibrium collective dynamics in high-energy heavy ion collisions	Oct. 10
21	Isao Watanabe (RNC)	μSR Applications at the RIKEN-RAL and RAON(Chung-ang Univ./ Korea)	Oct. 10
22	Amarjit Soni (BNL)	Theoretical Physics Seminar at BNL	Oct. 11
23	Shinsuke Yoshida (RNC)	RIKEN Theory Seminar at BNL: Application of the twist-3 framework to the high energy spin physics	Oct. 17
24	Isao Watanabe (RNC)	μSR Applications at the RIKEN-RAL(National Tsing Hua Univ./Taiwan)	Oct. 17
25	Denes Molnar (Purdue)	Nuclear Physics & RIKEN Theory Seminar at BNL: Radiative ggg<->gg transport and thermalization	Oct. 18
26	Isao Watanabe (RNC)	μSR Applications at the RIKEN-RAL(National Cheng Kung Univ./Taiwan)	Oct. 18
27	Gabe Shaughnessy (Univ. of Wisconsin)	Theoretical Physics Seminar at BNL	Oct. 23
28	Anna Hasenfratz (Univ. of Colorado)	RIKEN Theory Seminar at BNL: Strongly coupled gauge theories in and out of the conformal window	Oct. 24
29	Chris Monahan (College of William and Mary)	High-Energy Physics & RIKEN Theory Seminar at BNL: B physics from the lattice: m_b and f_B	Oct. 30
30	Jose Wudka (UC Riverside)	High-Energy Physics & RIKEN Theory Seminar at BNL: Effective Theories and Some Applications	Nov. 6
31	Keitaro Nagata (KEK)	RIKEN Theory Seminar at BNL: Baryon number distribution in lattice QCD simulations	Nov. 7
32	Azwindinni Muronga (Johannesburg)	Nuclear Physics & RIKEN Theory Seminar at BNL: Beyond second-order dissipative fluid dynamics	Nov. 8
33	Teiichiro Matsuzaki, Katsuhiko Ishida & Isao Watanabe (RNC)	Applications and Researches at the RIKEN-RAL (ITS/Indonesia)	Nov. 11
34	James Gainer (Univ. of Florida)	High-Energy Physics & RIKEN Theory Seminar at BNL: The Higgs Boson in the Golden Channel	Nob. 13
35	Shigemi Ohta (KEK/RBRC)	RIKEN Theory Seminar at BNL: Nucleon structure from 2+1-flavor dynamical DWF lattice QCD at nearly physical pion mass	Nov. 14

36	Tseh Liou (Columbia)	Nuclear Physics & RIKEN Theory Seminar at BNL: Radiative pT-broadening of high energy quarks and gluons in QCD matter	Nov. 15
37	Axel Cortes Cubero (CUNY)	RIKEN Theory Seminar at BNL: The Integrable Bootstrap Program at Large N and its Applications in Gauge Theory	Nov. 21
38	Timo Alho (Jyvaskyla)	Nuclear Physics & RIKEN Theory Seminar at BNL: Thermodynamics of holographic models for QCD in the Veneziano limit	Nov. 22
39	Berndt Mueller (BNL)	The Investigation of Hot QCD Matter	Dec. 10
40	Jared Evans (Rutgers Univ.)	Joint HET/RIKEN/YITP Seminar at BNL: Under the Lens of RPV: An Examination of the LHC Program	Dec. 11
41	Ethan Neil (Univ. of Colorado / RBRC)	RIKEN Theory Seminar at BNL: Composite Bosonic Dark Matter	Dec. 12
42	Vladimir Skokov (Western Michigan Univ.)	Nuclear Physics & RIKEN Theory Seminar at BNL: Collectivity in proton-nucleus collisions at LHC	Dec. 13
43	Isao Watanabe (RNC)	µSR Facility at RAON(Osaka Univ.)	Dec. 18
44	Sergey Syritsyn (RBRC)	RIKEN Theory Seminar at BNL: Nucleon structure on a lattice near the physical point	Dec. 19
45	Taichi Kawanai (BNL)	Theoretical Physics Seminar at BNL	Dec. 20
46	Yasumichi Aoki (KMI, Nagoya Univ.)	RIKEN Theory Seminar at BNL: Physics near the conformal boundary in SU(3) gauge theory	Jan. 9
47	Heikki Mantysaari (Jyvaskyla Univ.)	Nuclear Physics & RIKEN Theory Seminar at BNL: Particles from the Colored Glass: diffraction, DIS and hadron production	Jan. 10
48	Maxwell T. Hansen (Univ. of Washington)	Nuclear Physics & RIKEN Theory Seminar at BNL: Mapping the finite-volume spectrum to the S-matrix	Jan. 15
49	Isao Watanabe (RNC)	µSR Applications at RCNP, RIKEN-RAL and RAON (ibs／Korea)	Jan. 15
50	Soeren Schlichting (BNL)	Theoretical Physics Seminar at BNL: Turbulent thermalization process in heavy-ion collisions at ultrarelativistic energies	Jan. 16
51	Jinfeng Liao (Indiana Univ.)	Nuclear Physics & RIKEN Theory Seminar at BNL: Opaqueness evolution and hard probe of fluctuating geometry from RHIC to LHC	Jan. 17
52	Gabe Shaughnessy	RIKEN Theory Seminar at BNL: Exploring Higgs Doublet Models With Future Colliders	Jan. 22
53	Isao Watanabe (RNC)	µSR Applications at the RIKEN-RAL (NTNU／Norway)	Jan. 28
54	Sergei Dubovsky (New York Univ.)	RIKEN Theory Seminar at BNL: Integrable Quantum Gravity and the Hierarchy Problem	Jan. 29
55	Hiroshi Ohno (BNL)	RIKEN Theory Seminar at BNL: Dirac spectrum and chiral and U_A(1) symmetries at finite temperature with the highly improved staggered quarks	Jan. 30
56	Chris Kelly (RBRC)	Theoretical Physics Seminar at BNL	Jan. 31
57	Yuji Koike (Niigata Univ.)	第１回高エネルギーQCD・核子構造勉強会：摂動ＱＣＤに基づくシングルスピン非対称研究の現状 http://indico2.riken.jp/indico/conferenceDisplay.py?confId=1417	Feb. 4
58	Yuji Goto (RNC)	第１回高エネルギーQCD・核子構造勉強会：RHIC-PHENIX 実験の高度化計画 http://indico2.riken.jp/indico/conferenceDisplay.py?confId=1417	Feb. 4

59	Matt Buckley (Rutgers, The State Univ. of New Jersey)	High-Energy Physics & RKEN Theory Seminar at BNL : Searching for new electroweak particles with superrazor variables	Feb. 5
60	Kouji Kashiwa (RBRC)	RIKEN Theory Seminar at BNL: Investigation of QCD phase structure from imaginary chemical potential	Feb. 6
61	Christoph Lehner (BNL)	High-Energy Physics & RKEN Theory Seminar at BNL: Perspectives in lattice B physics	Feb. 7
62	Ioannis Iatrakis	Nuclear Physics & RKEN Theory Seminar at BNL: The Chern-Simons diffusion rate in improved Holographic QCD	Feb. 14
63	Stefan Meinel (MIT)	High-Energy Physics & RKEN Theory Seminar at BNL: Hadron structure calculations in lattice QCD: from flavor physics to the proton radius	Feb. 19
64	Mike Creutz (BNL)	High-Energy Physics & RKEN Theory Seminar at BNL: Chiral symmetry and lattice fermions	Feb. 21
65	Isao Watanabe (RNC)	Muon Site Estimations by Computational Methods (USM/Malaysia)	Feb. 25
66	Aaron Pierce (Univ. of Michigan)	Joint HET/RIKEN/YITP Seminar at BNL: Exotic Top Partners and Little Higgs	Feb. 26
67	Daniel Pitonyak (RBRC)	RIKEN Theory Seminar at BNL: The transverse single-spin asymmetry "spin crisis" in proton-proton collisions	Feb. 27
68	Yi Yin (Univ. of Illinois at Chicago)	Nuclear Physics & RKEN Theory Seminar at BNL : Exploring Quark Gluon Plasma with Realistic Hydrodynamic Evolution	Feb. 28
69	Yuya Tanizaki (Univ. of Tokyo)	RIKEN Theory Seminar at BNL : Functional renormalization group method for ultra cold fermions	Mar. 6
70	Aian Dumitru (Baruch)	Nuclear Physics & RIKEN Theory Seminar at BNL: Azimuthal anisotropies in collisions of protons with a holographic shock wave	Mar. 7
71	Claudia Frugiuele (Fermilab)	RIKEN Theory Seminar at BNL: Dirac gauginos, R symmetry and the 125 GeV Higgs	Mar. 12
72	Pedroo Jimenez-Delgado (Jefferson Lab.)	Nuclear Physics & RIKEN Theory Seminar at BNL : Delineating polarized and unpolarized parton distribution functions	Mar. 14
73	Isao Watanabe (RNC)	Workshop on Muon Site Estimations (RAL/UK)	Mar. 15
74	Matthew Sievert (Ohio State Univ.)	RIKEN Theory Seminar at BNL : Sivers Function in the Quasi-Classical Approximation	Mar. 20
75	Gokce Basar (Stony Brook)	Nuclear Physics & RIKEN Theory Seminar at BNL : Resurgence theory in quantum mechanics and analytical continuation of path integrals	Mar. 21
76	Yan-Qing Ma (BNL)	RIKEN Theory Seminar at BNL: QCD factorization and Parton Distribution Functions on Lattice	Mar. 27
77	Meifeng Lin (BNL)	High-Energy Physics & Theoretical Physics Seminar at BNL: Nucleon structure on the lattice: Approaching the physical limit	Mar. 28

RIBF Research Division

1	Masaharu Okano (RNC)	環境放射線１００年を振返る http://indico2.riken.jp/indico/conferenceDisplay.py?confId=1125	May 9
2	Andrei Andreyev (Univ. of York)	Shape coexistence and fission in the lead region studied by in-source laser spectroscopy at RILIS-ISOLDE http://indico2.riken.jp/indico/conferenceDisplay.py?confId=1179	May 27

3	Masaomi Tanaka (NAO)	Optical observations of supernova explosions http://indico2.riken.jp/indico/conferenceDisplay.py?confId=1166	May 31
4	Wataru Iwakiri (RNC)	Observational Study of Radiative Transfer under Strong Magnetic Fields on Neutron Stars http://indico2.riken.jp/indico/conferenceDisplay.py?confId=1189	Jun. 12
5	Kumi Ishikawa (RNC)	Systematic Search for Solar Wind Charge Exchange X-Ray Emission from the Earth's Exosphere with Suzaku http://indico2.riken.jp/indico/conferenceDisplay.py?confId=1194	Jun. 19
6	Takayuki Kotani (NAO)	Search for extra-solar Earth-like planets around nearby M-type stars by Infrared Doppler Instrument (IRD) http://indico2.riken.jp/indico/conferenceDisplay.py?confId=1201	Jun. 26
7	Taro Matsuo (Kyoto Univ.)	Direct Imaging of Earth-like Exoplanets with Extremely Large Telescope http://indico2.riken.jp/indico/conferenceDisplay.py?confId=1202	Jun. 26
8	Gregory Pang (LBL)	Direct Measurement of Superheavy Element Z & A at the Berkeley Gas-Filled Separator http://indico2.riken.jp/indico/conferenceDisplay.py?confId=1210	Jul. 1
9	Yuri A Litvinov (GSI)	Precision experiments with stored exotic nuclides for nuclear structure and astrophysics http://indico2.riken.jp/indico/conferenceDisplay.py?confId=1232	Jul. 10
10	Mikio Morii (MAXI team, RIKEN)	Discovery of an ignition of a nova on MAXI J0158-744 http://indico2.riken.jp/indico/conferenceDisplay.py?confId=1267	Aug. 29
11	Alexey P. Severyukhin (JINR)	Gamow-Teller transitions and a separable approximation for Skyrme interactions http://indico2.riken.jp/indico/conferenceDisplay.py?confId=1272	Sep. 5
12	Dao Tien Khoa (Inst. for Nuclear Sci. & Tech.)	Charge-exchange scattering to IAS and implication for the nuclear symmetry energy http://indico2.riken.jp/indico/conferenceDisplay.py?confId=1290	Sep. 13
13	Shiu-Hang (Herman) Lee (Astrophysical Big Bang Lab., RIKEN)	Unraveling the Many Facets of Supernova Remnants in High-energy and Their Link to Galactic Cosmic Rays http://indico2.riken.jp/indico/conferenceDisplay.py?confId=1318	Oct. 10
14	Habil. M.I.Faley (Peter Grünberg Inst., Forschungszentrum Jülich GmbH)	Technology, properties and applications of graphoepitaxial high-Tc SQUIDs http://indico2.riken.jp/indico/conferenceDisplay.py?confId=1328	Oct. 29
15	Lucio Rossi (CERN)	Advanced technology at the LHC of CERN: Higgs boson and more http://indico2.riken.jp/indico/conferenceDisplay.py?confId=1343	Nov. 19
16	Jiancheng Yang (IMP, CAS)	Introduction to HIAF project (High-Intensity Heavy Ion Accelerator Facility-HIAF) http://indico2.riken.jp/indico/conferenceDisplay.py?confId=1377	Dec. 16
17	Sudip Bhattacharyya (Tata Inst. of Fundamental Research)	Burst oscillations from neutron star LMXBs http://indico2.riken.jp/indico/conferenceDisplay.py?confId=1376	Dec. 19
18	Fabio Acero (NASA / GSFC)	From GeV to TeV: a SNR overview http://indico2.riken.jp/indico/conferenceDisplay.py?confId=1401	Jan. 16

CNS

1	Shinya Wanajo (NAO)	重元素の起源:超新星爆発 vs. 中性子星合体	July 23
2	Haozhao Liang (RNC)	Nuclear charge-exchange excitations in covariant density functional theory	Oct. 31
3	Toshiyuki Sumikama (Tohoku Univ.)	中性子過剰 Zr および Mo 同位体の質量数 110 近傍での形状変化	Nov. 7
4	Jirina Stone (Univ. of Oxford / Univ. of Tennessee-Knoxville)	Neutron Rich Matter in Stellar Processes	Nov. 22
5	Bruce R. Barrett (Univ. of Arizona, Tucson)	The No Core Shell Model within an Effective Field Theory framework	Nov. 27
6	Michio Kohno (Kyushu Dental Univ.),	カイラル有効理論の 3 体力に基づく核子多体系の微視的理解	Nov. 28

7	Kosuke Nomura (GANIL)	Interacting boson model and nuclear mean field	Dec. 26

Niigata Univ.

1	Fumiharu Kobayashi (Kyoto Univ.)	軽い原子核におけるダイニュートロン相関の系統的研究	Apr. 18
2	Yusuke Tanimura (Tohoku Univ.)	Application of the inverse Hamiltonian method to relativistic point coupling model calculations on 3D mesh	Jun. 4
3	Jinniu Hu (Peking Univ.)	The relativistic Brueckner-Hartree-Fock theory for finite nuclei system	Aug. 26
4	Kazuyuki Ogata (RCNP)	核子系非束縛状態の存在形態と崩壊様式に対する動力学的研究	Oct. 11
5	Toshitaka Tatsumi (Kyoto Univ.)	高温・高密度クォーク物質での非一様カイラル相	Oct. 22

KEK

	not held in FY2013		

AUTHOR INDEX

D

E

F

G

L

M

P

Q

R

S

T

RIKEN Accelerator Progress Report *vol.* **47**

独立行政法人理化学研究所加速器年次報告　第47巻 (2014)

印　刷　平成 27 年（2015）2 月　2 日
発　行　平成 27 年（2015）2 月 27 日

発行者　独立行政法人理化学研究所　仁科加速器研究センター
代表者　延　與　秀　人
〒351-0198　埼玉県和光市広沢2番1号
progress@ribf.riken.jp

編集者　独立行政法人理化学研究所　仁科加速器研究センター
加速器年次報告編集委員会

印刷所　松枝印刷株式会社
〒303-0034　茨城県常総市水海道天満町2438